Geology of the Blue Mountains Region of Oregon, Idaho, and Washington:

Petrology and Tectonic Evolution of Pre-Tertiary Rocks of the Blue Mountains Region

U.S. GEOLOGICAL SURVEY PROFESSIONAL PAPER 1438

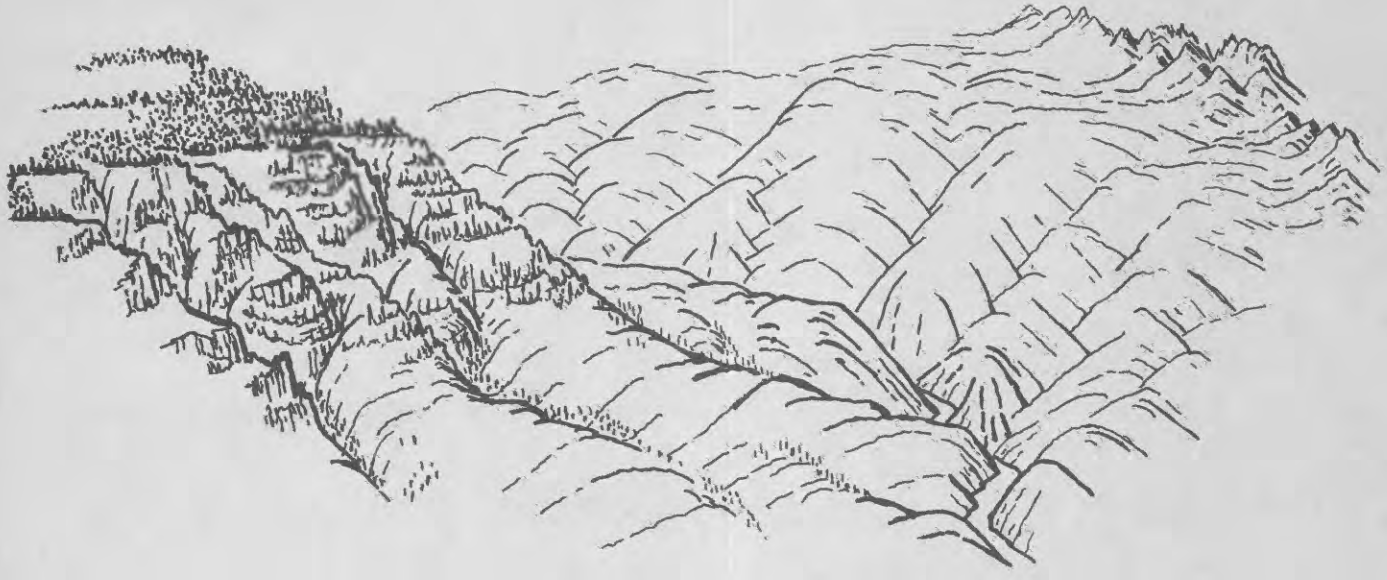

AVAILABILITY OF BOOKS AND MAPS OF THE U.S. GEOLOGICAL SURVEY

Instructions on ordering publications of the U.S. Geological Survey, along with prices of the last offerings, are given in the current-year issues of the monthly catalog "New Publications of the U.S. Geological Survey." Prices of available U.S. Geological Survey publications released prior to the current year are listed in the most recent annual "Price and Availability List." Publications that are listed in various U.S. Geological Survey catalogs (**see back inside cover**) but not listed in the most recent annual "Price and Availability List" are no longer available.

Reports released through the NTIS may be obtained by writing to the National Technical Information Service, U.S. Department of Commerce, Springfield, VA 22161; please include NTIS report number with inquiry.

Order U.S. Geological Survey publications **by mail** or **over the counter** from the offices given below.

BY MAIL

Books

Professional Papers, Bulletins, Water-Supply Papers, Techniques of Water-Resources Investigations, Circulars, publications of general interest (such as leaflets, pamphlets, booklets), single copies of Earthquakes & Volcanoes, Preliminary Determination of Epicenters, and some miscellaneous reports, including some of the foregoing series that have gone out of print at the Superintendent of Documents, are obtainable by mail from

U.S. Geological Survey, Information Services
Box 25286, Federal Center
Denver, CO 80225

Subscriptions to periodicals (Earthquakes & Volcanoes and Preliminary Determination of Epicenters) can be obtained ONLY from the

Superintendent of Documents
Government Printing Office
Washington, DC 20402

(Check or money order must be payable to Superintendent of Documents.)

Maps

For maps, address mail orders to

U.S. Geological Survey, Map Distribution
Box 25286, Bldg. 810, Federal Center
Denver, CO 80225

Residents of Alaska may order maps from

U.S. Geological Survey, Earth Science Information Center
101 Twelfth Ave., Box 12
Fairbanks, AK 99701

OVER THE COUNTER

Books and Maps

Books and maps of the U.S. Geological Survey are available over the counter at the following U.S. Geological Survey offices, all of which are authorized agents of the Superintendent of Documents.

- **ANCHORAGE, Alaska**—4230 University Dr., Rm. 101
- **LAKEWOOD, Colorado**—Federal Center, Bldg. 810
- **MENLO PARK, California**—Bldg. 3, Rm. 3128, 345 Middlefield Rd.
- **RESTON, Virginia**—National Center, Rm. 1C402, 12201 Sunrise Valley Dr.
- **SALT LAKE CITY, Utah**—Federal Bldg., Rm. 8105, 125 South State St.
- **SPOKANE, Washington**—U.S. Post Office Bldg., Rm. 135, W. 904 Riverside Ave.
- **WASHINGTON, D.C.**—Main Interior Bldg., Rm. 2650, 18th and C Sts., NW.

Maps Only

Maps may be purchased over the counter at the U.S. Geological Survey offices:

- **FAIRBANKS, Alaska**—New Federal Building, 101 Twelfth Ave.
- **ROLLA, Missouri**—1400 Independence Rd.
- **STENNIS SPACE CENTER, Mississippi**—Bldg. 3101

Geology of the Blue Mountains Region of Oregon, Idaho, and Washington:

Petrology and Tectonic Evolution of Pre-Tertiary Rocks of the Blue Mountains Region

TRACY L. VALLIER *and* HOWARD C. BROOKS, *editors*

U.S. GEOLOGICAL SURVEY PROFESSIONAL PAPER 1438

UNITED STATES GOVERNMENT PRINTING OFFICE, WASHINGTON : 1995

U.S. DEPARTMENT OF THE INTERIOR

BRUCE BABBITT, *Secretary*

U.S. GEOLOGICAL SURVEY

Gordon P. Eaton, *Director*

Any use of trade, product, or firm names
in this publication is for descriptive purposes only and
does not imply endorsement by the U.S. Government

Text and illustrations edited by
Helen Gibbons and Andrea C. Eddy

Library of Congress Cataloging-in-Publication Data

Petrology and tectonic evolution of pre-Tertiary rocks of the Blue Mountains region / Tracy L. Vallier and Howard C. Brooks, editors.
p. cm. — (Geology of the Blue Mountains region of Oregon, Idaho, and Washington) (U.S. Geological Survey professional paper ; 1438)
Includes bibliographical references.
Supt. of Docs. no.: I19.16: 1438
1. Geology, Structural—Blue Mountains Region (Or. and Wash.) 2. Island arcs—Blue Mountains Region (Or. and Wash.) 3. Rocks—Blue Mountains Region (Or. and Wash.) I. Vallier, T. L. (Tracy L.) II. Brooks, Howard C. III. Series. IV. Series: U.S. Geological Survey professional paper ; 1438.
QE747.B58P48 1995
551.7'009795—dc20 94-48560
CIP

For sale by U.S. Geological Survey, Information Services
Box 25286, Federal Center, Denver, CO 80225

PREFACE

U.S. Geological Survey Professional Paper 1438 is one volume of a five-volume series on the geology, paleontology, and mineral resources of the Blue Mountains region in eastern Oregon, western Idaho, and southeastern Washington. This professional paper deals specifically with petrology and tectonic evolution. Other professional papers in the series include Professional Paper 1435 on paleontology and biostratigraphy, Professional Paper 1436 on the Idaho Batholith and its border zone, Professional Paper 1437 on Cenozoic geology, and Professional Paper 1439 on stratigraphy, physiography, and mineral resources. The purpose of these volumes is to familiarize readers with work that has been completed in the Blue Mountains region and to emphasize the region's importance for understanding island-arc processes and the accretion of an allochthonous terrane to a continent. These professional papers provide current interpretations of a complex island-arc terrane that was accreted to ancient North America in the late Mesozoic Era, of a large batholith that was emplaced after accretion had occurred, and of overlying Cenozoic volcanic rocks that were subsequently uplifted and partly stripped off the older rocks by erosion.

Modern island arcs are not well understood, and even less so are ancient arcs that have been deformed, metamorphosed, and subsequently accreted to continents. We have learned that characteristics of modern arcs change significantly both along and across the arcs' axes and that studies of arc fragments are less than satisfactory because they generally do not characterize an entire arc. For example, the landward trench slopes of arcs can differ greatly, depending on whether materials from the descending slab are being accreted or the slope is being tectonically eroded; which process dominates apparently is related to the volume of sediment in the adjacent trench and the vector of plate convergence. In addition, some arcs (Aleutian) have broad, long, and sediment-filled fore-arc basins, whereas in others (Tonga-Kermadec) the fore-arc insular slopes descend precipitously to trench depths and are only interrupted in places by narrow fault-bounded terraces. Moreover, some arcs (Tonga-Kermadec) have erupted primarily tholeiitic igneous products throughout their histories, and others (Aleutian) have a long history of both calc-alkaline and tholeiitic eruptive activity. Ridge axes of island arcs may be narrow or broad, and in some arcs (Solomons and Vanuatu), the axial regions have extended to form deep bathymetric and sedimentary basins. Even back-arc basins have different origins and histories of development. Some (Mariana Trough and Lau Basin) have active spreading ridges, whereas others (Aleutian basin) are floored by ancient oceanic crust that was trapped behind the arc.

Because our knowledge of the diverse processes within modern arcs is limited, it becomes even more important to study ancient analogs. Just by the nature of their on-land exposures, ancient arcs can provide insights into sedimentary facies, magmatic evolution, and deep crustal processes that can only be studied in modern arcs by geophysical methods, dredging, and drilling. Few ancient island arcs have exposures as well developed and as extensive as those in the Blue Mountains region. Particularly spectacular and helpful are outcrops provided by intensive stream erosion, which has left some canyon walls more than 2 km deep (Snake River canyon west of the Seven Devils Mountains).

Most earth scientists who have worked in the Blue Mountains region agree that pre-Tertiary rocks there form one or more allochthonous terranes. The importance of such terranes in the evolution of circum-Pacific continental margins has been recognized for more than a decade, but many complex questions remain. For example, how, when, and where did most of the circum-Pacific allochthonous terranes form? How did they accrete to continents? What are the mechanisms of amalgamation processes during terrane formation and transport? And, perhaps most importantly, what are the effects of these processes on mineral and hydrocarbon resources? While these volumes provide some answers, the data and interpretations contained in them will no doubt raise new and equally intriguing questions for future generations of earth scientists.

CONTENTS

[Numbers indicate chapters]

Page

1. Petrology of the Canyon Mountain Complex, eastern Oregon ---------- 1
   William P. Leeman, Hans G. Avé Lallemant, David C. Gerlach, John F. Sutter, and Richard J. Arculus
2. A closer look at the Bald Mountain batholith, Elkhorn Mountains, and some comparisons with the Wallowa batholith, Wallowa Mountains, northeastern Oregon ---------- 45
   William H. Taubeneck
3. Petrology of pre-Tertiary igneous rocks in the Blue Mountains region of Oregon, Idaho, and Washington: Implications for the geologic evolution of a complex island arc ---------- 125
   Tracy L. Vallier
4. High-pressure, low-temperature schistose rocks of the Baker terrane, northeastern Oregon ---------- 211
   Ellen M. Bishop
5. Mafic and ultramafic rocks of the Baker terrane, eastern Oregon, and their implications for terrane origin ---------- 221
   Ellen M. Bishop
6. Tectonic implications of U-Pb zircon ages of the Canyon Mountain Complex, Sparta complex, and related metaplutonic rocks of the Baker terrane, northeastern Oregon ---------- 247
   Nicholas W. Walker
7. Pre-Cretaceous tectonic evolution of the Blue Mountains province, northeastern Oregon ---------- 271
   Hans G. Avé Lallemant
8. Pre-Tertiary deformation in the Desolation Butte quadrangle, northeastern Oregon ---------- 305
   James G. Evans
9. The Bourne and Greenhorn subterranes of the Baker terrane, northeastern Oregon: Implications for the evolution of the Blue Mountains island-arc system ---------- 331
   Mark L. Ferns and Howard C. Brooks

10. An $^{40}Ar/^{39}Ar$ chronicle of the tectonic development of the Salmon River suture zone, western Idaho ---------- 359

Lawrence W. Snee, Karen Lund, John F. Sutter, David E. Balcer, and Karl V. Evans

11. Geology of the northern part of the Ironside Mountain inlier, northeastern Oregon ------ 415

Peter R. Hooper, Michel D. Houseman, John E. Beane, Gregory M. Caffrey, Kenneth R. Engh, James V. Scrivner, and A. John Watkinson

12. Petrology and deformation history of the Burnt River Schist and associated plutonic rocks in the Burnt River Canyon area, northeastern Oregon ---------- 457

Roger P. Ashley

13. Gravity studies of an island-arc/continent suture zone in west-central Idaho and southeastern Washington ---------- 497

Gregory B. Mohl and Richard L. Thiessen

14. Metamorphic and structural development of island-arc rocks in the Slate Creek-John Day Creek area, west-central Idaho ---------- 517

Karen Lund

1. PETROLOGY OF THE CANYON MOUNTAIN COMPLEX, EASTERN OREGON

By WILLIAM P. LEEMAN,[1] HANS G. AVÉ LALLEMANT,[1] DAVID C. GERLACH,[2] JOHN F. SUTTER,[3] and RICHARD J. ARCULUS[4]

CONTENTS

	Page
Abstract	1
Introduction	1
Acknowledgments	2
Regional geologic setting	2
Geochronology	5
Canyon Mountain Complex	5
Sparta complex	6
Geology of the Canyon Mountain Complex	6
Previous investigations	6
Geologic descriptions of units	9
Ultramafic member	9
Gabbroic member	10
Sheeted (sill-like) member	10
Structure	11
Petrography and mineralogy	11
Paleothermometry and paleobarometry	12
Geochemistry and petrology	12
Analytical methods	13
General geochemical characteristics	13
Comparative geochemistry and evaluation of tectonic setting	20
Petrogenetic models	30
Plagiogranite suite	30
Mafic rocks	32
Summary	37
Tectonic implications	38
References cited	39

ABSTRACT

The Permian Canyon Mountain Complex of northeastern Oregon has many attributes of ophiolites, including a stratified structure and characteristic lithologic succession. The stratigraphic sequence consists of a basal harzburgite tectonite overlain successively by an ultramafic-to-mafic cumulate member (penetratively deformed in the eastern part of the complex and undeformed in the western part), and an upper sheeted member (plagiogranites, mafic dikes and sills, and keratophyres). The majority of the keratophyres appear to have formed prior to the sheeted member and may represent part of a Permian island arc. The tectonite and metamorphosed cumulate rocks are cut by undeformed isotropic gabbro, which may be cogenetic with the layered cumulate gabbros and possibly some of the mafic dikes. However, because clinopyroxenes from basaltic rocks of the sheeted member differ (lower Ca contents and higher Fe/Mg ratios) from those in the gabbros, it is probable that most of the mafic dikes were emplaced during a separate event. Field relations and $^{40}Ar/^{39}Ar$ age determinations demonstrate that the plagiogranites, mafic dikes, and some keratophyres were emplaced in the sheeted member more or less contemporaneously at about 260 Ma. U-Pb zircon geochronology for a single high-level cumulate gabbro (Walker, 1986) suggests a time interval of perhaps 15 m.y. between formation of the gabbro and emplacement of the sheeted member. The mafic dikes, sills, and minor flows apparently formed by partial melting of a source that was strongly depleted with respect to incompatible trace elements. A source resembling that for midocean-ridge basalt (MORB) from which melts had been previously extracted is plausible. The plagiogranite suite appears to have been derived by hydrous partial melting of a mafic source rock (such as amphibolite), possibly representing subducted oceanic crust. Thus, the Canyon Mountain Complex appears to be a composite body whose members formed over a significant period of time, possibly in different tectonic settings; there is no compelling reason to propose a cogenetic relation between magmas of the sheeted member and other rocks of the complex. For the mafic magmas, discriminant diagrams indicate transitional affinities between ocean-floor and primitive island-arc basalts. However, striking depletions in Ta and Hf, relative to other incompatible elements, suggest a subduction-related volcanic-arc (or possibly fore-arc or marginal-basin) setting for their origin.

INTRODUCTION

Participants at a Penrose Field Conference concluded that ophiolites are pseudostratified rock assemblages (Anonymous, 1972) comprising four diagnostic lithologic units or members—from bottom to top, an ultramafic member, a gabbroic member, a mafic sheeted-dike complex, and a mafic volcanic complex—as

[1]Department of Geology and Geophysics, Rice University, Houston, TX 77251
[2]Charles Evans and Associates, 301 Chesapeake Dr., Redwood City, CA 94063
[3]U.S. Geological Survey, Reston, VA 22092
[4]Present address: Department of Geology, Australian National University, Canberra ACT 0200, Australia

Manuscript approved for publication February 18, 1994.

well as associated minor rock types that commonly are found in ophiolites. These associated rock types include chromitites, sodic felsic intrusive and extrusive rocks (such as trondhjemites, keratophyres), and sedimentary rocks (such as chert, shale, limestone). Although no genetic significance was intended in the Penrose Conference definition, many geologists consider ophiolites to have formed at midocean spreading centers (see Coleman, 1981). In recent years, the recognition that ophiolites have quite varied characteristics has led to alternative interpretations of their tectonic settings and processes of formation.

One or more of the four key lithologic members may be absent in surface exposures of some ophiolites as a result of tectonic disruption. However, many apparently intact ophiolite complexes lack one or more of these units, or have units that are similar but occur in uncharacteristic style. For example, the Point Sal ophiolite (southern California) has a sill member but no dike member (Hopson and Frano, 1977). The (informal) Sparta (ophiolite) complex of eastern Oregon is characterized by an unusually large proportion of silicic intrusive rocks (Prostka and Bateman, 1962; Phelps, 1978, 1979); in fact, nontrivial volumes of felsic igneous rocks are associated with most so-called ophiolites in Oregon and California (Bailey and Blake, 1974). Coleman and Peterman (1975) designated such silicic intrusive rocks as "oceanic plagiogranites" and proposed that they formed by extensive fractional crystallization of basaltic magmas at midocean ridges.

Alternative tectonic environments proposed to account for the now-recognized ophiolite variants include actively spreading back-arc basins such as the Marianas (Karig, 1971), leaky transform faults such as the Cayman Trough (Thompson and others, 1980; Holcombe and Sharman, 1983), and island arcs such as Tonga (Ewart and Bryan, 1972). The uncertainty over tectonic setting is well illustrated by the various interpretations of the Troodos ophiolite (Cyprus); an island-arc origin is suggested on the basis of geochemical and petrologic data (see Miyashiro, 1973; McCulloch and Cameron, 1983; Robinson and others, 1983), but this model has been widely contested (for example, Hynes, 1975; Moores, 1975; Church and Coish, 1976). Multiple magmatic suites that may have originated in different tectonic settings and (or) at different times have been recognized in some cases (see Coleman, 1977; Thayer, 1977b), including the Betts Cove (Coish and others, 1982), New Caledonia (Dupuy and others, 1981), Troodos (Robinson and others, 1983; Schminke and others, 1983), Vourinos (Noiret and others, 1981; Beccaluva and others, 1979), Pindos (Capedri and others, 1980), and Oman ophiolites (Alabaster and others, 1982). Juxtaposition of coherent stratal sequences formed in distinct settings may be more the rule than an exception in convergent-margin tectonic zones (Moores and others, 1984).

The Canyon Mountain Complex, Sparta complex, and several other possible ophiolite fragments occur in the Blue Mountains province of northeastern Oregon (see Mullen, 1985). This province consists of five tectonostratigraphic terranes (Silberling and Jones, 1984) believed to have formed at indeterminate distances from the North American craton and then to have been accreted to the craton at later times (see Coney and others, 1980). In order to reconstruct the plate tectonic evolution of these terranes, it is necessary to understand the original tectonic settings of ophiolite remnants preserved in suture zones separating the terranes.

The Canyon Mountain Complex is the best exposed and most completely preserved ophiolite in the province. Herein, we review published petrologic, geochemical, and structural data, and present new geochemical data for this body, especially for the basaltic components. We specifically address the petrogenesis of felsic and mafic magmas associated with the sheeted member and late-stage intrusions, and the geochemical constraints on the type of tectonic setting in which these rocks formed. To further elucidate ages of formation, we also present new radiometric ages for samples from the Canyon Mountain Complex and Sparta complex.

ACKNOWLEDGMENTS

We are grateful to Bruce Chappell, Mike Rhodes, Ben Powell, Doug Blanchard, and Roman Schmitt for access to analytical facilities. Lisanne Pearcy and Tracy Vallier provided thorough and constructive reviews. This work was supported by the National Science Foundation through grants GA-25894, EAR-76-13372, EAR-79-04829, and EAR-82-06531.

REGIONAL GEOLOGIC SETTING

Postulated remnants of ophiolites occur throughout the Blue Mountains province of northeastern Oregon and adjacent areas of Idaho. Their bearing on regional tectonic interpretations is discussed within the context of four of the five tectonostratigraphic terranes of the province. From north to south, these are the Wallowa, Baker, Izee, and Olds Ferry terranes (Silberling and Jones, 1984; the fifth terrane, the Grindstone, will not be discussed in this chapter). An

oceanic affinity is inferred for these terranes on the basis of their internal geology and the fact that the igneous rocks within each terrane are characterized by initial Sr isotopic compositions ($^{87}Sr/^{86}Sr$) at or below 0.704 (Armstrong and others, 1977). There is no compelling evidence for the presence of old continental crust within the province.

The Wallowa terrane (formerly called the Seven Devils terrane by Dickinson, 1979) consists of Permian and Upper Triassic volcaniclastic and volcanic rocks with affinity to low-K_2O basalt-andesite-dacite-rhyolite suites typical of present-day island arcs (Vallier and Batiza, 1978). In three areas in the Snake River canyon (Vallier, 1974), the volcanic rocks overlie gabbro, plagiogranite, and diabase of Permian to Triassic age (Balcer, 1980; Walker, 1981, 1982); contacts between the plutonic and volcanic rocks are intrusive or tectonic. The supposed basement exposures in the Snake River canyon are lithologically similar to the Late Triassic Sparta complex (fig. 1.1), which is usually included in the Baker terrane. Phelps (1978, 1979) and Avé Lallemant and others (1980) concluded that the Sparta complex is the plutonic equivalent of a low-K_2O island-arc volcanic suite; they suggested that it is a part of the root of the Wallowa arc. Volcanic rocks of the Wallowa terrane are overlain by Upper Triassic limestone and Upper Triassic to lower Upper Jurassic clastic sedimentary rocks (Morrison, 1964; Nolf, 1966; Vallier, 1974, 1977).

The Baker terrane (formerly called the Central Melange terrane by Dickinson, 1979) consists of disrupted fragments of oceanic crust, including local melange deposits, large coherent tectonic slices of ophiolitic and volcanic assemblages, and Triassic to possibly Lower Jurassic chert-argillites (Dickinson and Vigrass, 1965; Blome and others, 1983; Nestell, 1983; Blome and others, 1986). Analyses of basaltic and gabbroic blocks (Mullen, 1985; Bishop, chap. 5, this volume) indicate that they are varied in composition and include tholeiitic (that is, midocean-ridge), calc-alkaline, and rare alkalic basalt types. Late Triassic blueschists occur near Mitchell (fig. 1.1; Hotz and others, 1977), and somewhat lower pressure schistose rocks occur in serpentine-matrix melange elsewhere in the Baker terrane (Bishop, chap. 5, this volume). The Canyon Mountain Complex is by far the largest and most complete ophiolite fragment in this terrane.

The Olds Ferry terrane (formerly called the Huntington terrane by Dickinson, 1979) is a poorly exposed Late Triassic volcanic arc (Brooks and Vallier, 1978). It consists of Upper Triassic volcanic (basalt, andesite, and rhyolite) and volcaniclastic rocks and rare limestone (Brooks and Vallier, 1978; Brooks, 1979). Gabbro and plagiogranite plutons were emplaced locally during the Late Triassic (Henricksen, 1975). Lower Jurassic volcanogenic flysch-like deposits, tectonically overlying the Triassic rocks (Avé Lallemant, 1984a), were previously included in the Mesozoic Clastic terrane of Dickinson (1979).

The Izee terrane (formerly called the Mesozoic Clastic terrane by Dickinson, 1979) comprises Upper Triassic to Upper Jurassic turbidites deposited on the Baker terrane. Volcanic tuff beds occur mainly in its lower parts. Dickinson (1979) proposed that the turbidites were deposited in a fore-arc basin associated with the Olds Ferry arc to the south; however, the upper units of Jurassic age may represent an overlap sequence. Fault-bounded lenses and blocks of chert-argillite, gabbro, and serpentinite occur throughout this terrane.

Two major orogenic events apparently affected the rocks in the Blue Mountains province (Avé Lallemant and others, 1980; Avé Lallemant, chap. 7, this volume). First, during Triassic and Early Jurassic time, south to southeastward subduction of an oceanic plate beneath the Olds Ferry volcanic arc caused the formation of the melange and blueschists of the Baker terrane, and resulted in tectonic imbrication and folding of the melange into Upper Triassic and earliest Jurassic forearc-basin turbidites (Brown and Thayer, 1966; Dickinson and Thayer, 1978; Avé Lallemant, chap. 7, this volume). Exposed rocks of the Olds Ferry terrane do not appear to be affected by the Late Triassic deformation. However, a Late Triassic to Early Jurassic depositional hiatus signifies uplift of the terrane at that time (Brooks and Vallier, 1978). Neither unconformities nor folds of this age are apparent in the Wallowa terrane; Late Triassic deformation there seems to be confined to three major northeast-trending left-lateral shear zones (Vallier, 1974; Avé Lallemant, 1983; Avé Lallemant and others, 1985).

The second orogenic event was manifested by short-lived north-south shortening that affected all terranes (Avé Lallemant, 1984a, chap. 7, this volume). Timing of this event is well constrained in the Wallowa terrane, where the youngest deformed sediments are of early Oxfordian age (Morrison, 1964) and the oldest post-tectonic granitic intrusion is 160 Ma or late Oxfordian in age (Armstrong and others, 1977). This deformation may correspond to the collision of the Wallowa (or Blue Mountains) arc with the other four terranes. Subsequently, between 160 and 120 Ma (Armstrong and others, 1977), a number of granitic intrusions were emplaced in all four terranes, and locally these Jurassic and Cretaceous plutons crosscut contacts between terranes. No penetrative structures younger in age than Late Jurassic have been recognized in the Blue Mountains province of Oregon, but they are developed

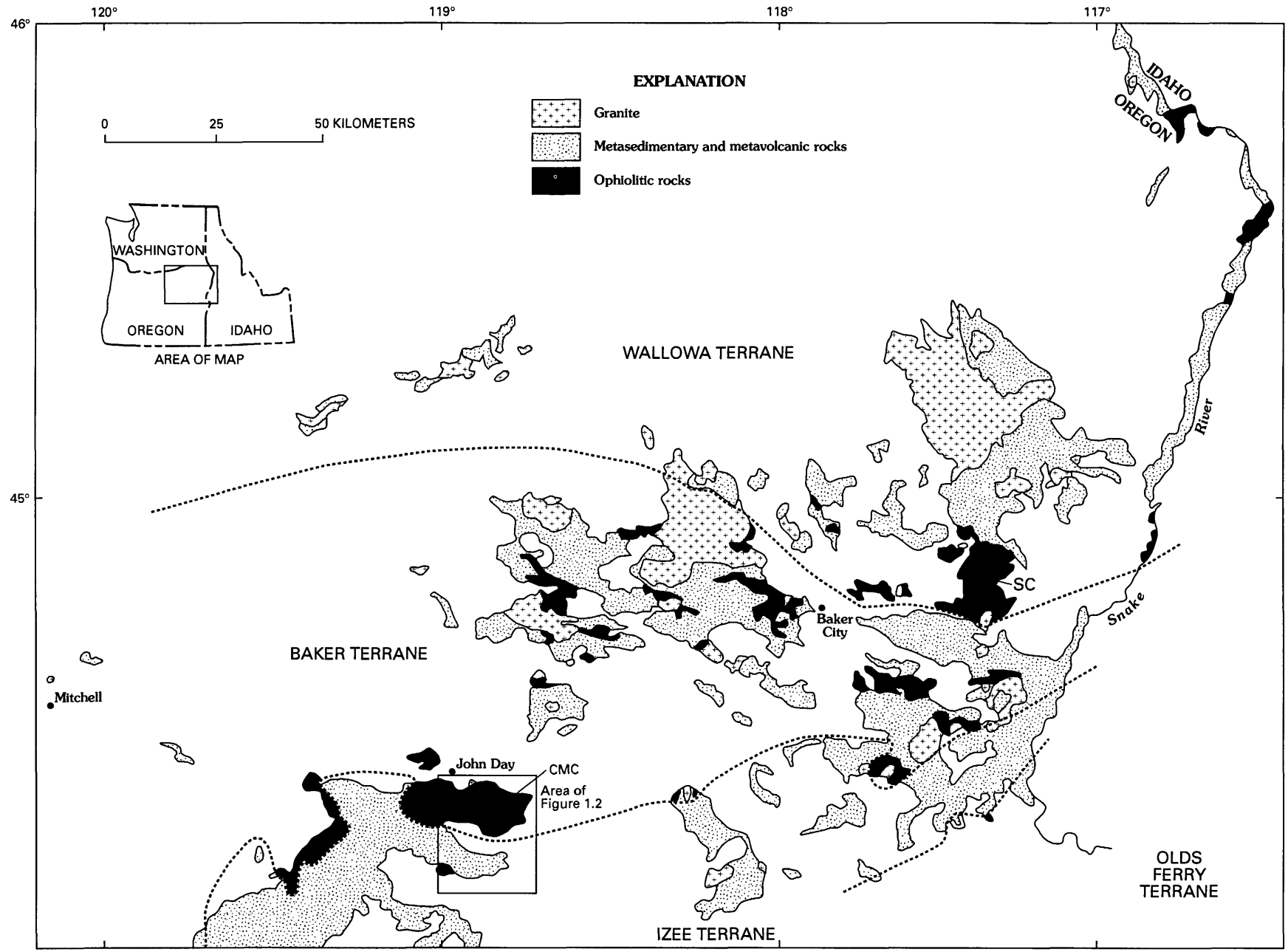

FIGURE 1.1.—Simplified geology of Blue Mountains province (modified from Walker, 1977), showing four tectonostratigraphic terranes of Silberling and Jones (1984): Wallowa, Baker, Izee, and Olds Ferry terranes. Ophiolitic rocks include the Canyon Mountain Complex (CMC) and the (informal) Sparta complex (SC) of Phelps (1979). Other basement rock types include Permian to Jurassic metasedimentary and metavolcanic rocks and predominantly Cretaceous granitoid intrusions. Dotted lines indicate terrane boundaries.

TABLE 1.1.—*$^{40}Ar/^{39}Ar$ age determinations using hornblende separates from hornblende diorites of the Canyon Mountain Complex and from hornblende gabbro of the Sparta complex*

[Error estimates in Age column reflect analytical precision and are calculated following methods of Cox and Dalrymple (1967) and Dalrymple and others (1981). Monitor mineral was MMhb-1, which has an accepted age of 519.4 Ma. Samples were irradiated in U.S. Geological Survey's TRIGA (Training Research Isotope General Atomic) reactor in Denver, Colo. Corrections for Ca- and K-derived Ar isotopes were made using constants suggested by Dalrymple and others (1981); decay constants used in age calculations are from Steiger and Jäger (1977). J, irradiation parameter; pct, percent; T, temperature]

T (°C)	$^{40}Ar/^{39}Ar$	$^{37}Ar/^{39}Ar$	$^{36}Ar/^{39}Ar$	^{39}Ar (pct)	^{40}Ar (pct)	^{39}Ar (moles)	K/Ca (molar)	Age (Ma)
Sample CMG-190A, hornblende diorite, Canyon Mountain Complex [44°18'59" N., 118°51'44" W.; J=0.006618±0.000033; sample weight=0.9740 g]								
800	352.7	64.00	1.125	3.0	7.1	0.294	0.00777	276.5±12.8
950	77.17	41.59	.1916	15.2	30.8	1.50	.0122	263.5 ±1.8
1150	43.87	60.93	.0849	62.4	53.6	6.08	.00818	260.6±1.3
Fuse	109.8	61.22	.3096	19.4	21.0	1.89	.00814	255.7±2.6
Total gas age								260.6
Plateau age (950 and 1150 °C steps)								261.2±1.6
Sample CMG-190B, hornblende diorite, Canyon Mountain Complex [44°18'59" N., 118°51'44" W.; J=0.006349±0.000032; sample weight=1.0376 g]								
950	116.2	41.92	0.3188	20.1	21.7	1.90	0.0121	267.7±1.5
1150	94.80	71.97	.2563	58.2	26.0	5.39	.00688	261.9±3.3
Fuse	315.0	69.80	.9922	21.6	8.7	2.01	.00710	287.6±21.4
Total gas age								268.7
Preferred age (1150 °C step)								261.9±3.3
Sample SP-96A, hornblende gabbro, Sparta complex [44°48'35" N., 117°22'45" W.; J=0.006614±0.000033; sample weight=1.0039 g]								
550	221.8	26.02	0.7090	0.9	6.4	0.448	0.0196	162.5±13.3
650	157.2	24.33	.4971	.1	7.8	.0073	.0210	140.4±67.3
750	72.72	16.09	.1891	.7	24.9	.249	.0320	203.6±10.5
850	26.68	12.02	.02433	12.8	76.5	6.68	.0429	228.5±1.2
950	23.30	11.72	.01288	28.2	87.6	14.7	.0440	228.3±1.2
1050	22.62	11.93	.01140	44.5	89.2	23.1	.0432	225.9±1.2
1150	28.05	12.56	.02980	9.8	72.1	5.09	.0410	226.3±1.5
Fuse	115.3	16.91	.3281	3.0	17.1	1.57	.0304	220.7±4.6
Total gas age								226.0
Plateau age (950 and 1150 °C steps)								227.0±1.3

in Idaho along the North America-Blue Mountains suture between Orofino and McCall (Sutter and others, 1984). However, post-Cretaceous 65° clockwise rotation of the Blue Mountains province (Wilson and Cox, 1980; Hillhouse and others, 1982) may be responsible for many faults and long-wavelength, low-amplitude folds that affect the Canyon Mountain Complex and overlying Eocene rocks (Thayer, 1956).

GEOCHRONOLOGY

A major question about the origin of the Oregon ophiolites concerns relationships between the associated mafic rocks (gabbros, basalts) and silicic rocks (plagiogranites, keratophyres). Thus, absolute ages for these different rock types constitute an important constraint on their formation. Because reliable age determinations for ophiolites of the Blue Mountains province are sparse, we have determined three new $^{40}Ar/^{39}Ar$ ages using hornblende separates from rocks of the Canyon Mountain Complex and Sparta complex (table 1.1). These are discussed within the context of other available data.

CANYON MOUNTAIN COMPLEX

Previous age determinations include concordant zircon U-Pb ages of 278 Ma for an undeformed intrusive

gabbro from Canyon Mountain, and 278 Ma for a plagiogranite that cuts cumulate gabbro; U-rich zircon (with 5–10 times more U than zircons from the plagiogranite) from a quartz diorite yielded slightly discordant U-Pb ages of about 268 Ma (Walker and Mattinson, 1980; Walker, 1981, 1986). Hornblende from a late-stage hornblende pegmatite yielded a $^{40}Ar/^{39}Ar$ plateau age of 262±14 Ma (Avé Lallemant and others, 1980).

New $^{40}Ar/^{39}Ar$ hornblende ages are reported herein (table 1.1) for two relatively late-stage hornblende diorite intrusions. One of these samples yields a $^{40}Ar/^{39}Ar$ plateau age of 261.2±1.6 Ma (for 78 percent of the argon released). The other sample may be slightly disturbed as it did not yield a plateau age. However, more than 58 percent of the argon released (the 1,150°C step) yielded an age of 261.9±3.3 Ma; the total-gas age obtained is about 269 Ma. The ages for these samples are analytically indistinguishable.

From the available geochronological data, it can be argued that all intrusive phases of the Canyon Mountain Complex are older than 260 Ma but probably no older than about 280 Ma. The data appear to resolve a small but significant difference in age between the gabbroic and sheeted members of the complex. Considering the uncertainties of these ages, we cannot preclude that the magmas of the gabbroic and sheeted members of the complex were coeval and possibly cogenetic; at the least they may have formed in the same general tectonic environment.

SPARTA COMPLEX

Although some investigators previously included both the Sparta complex and the Canyon Mountain Complex in the Baker terrane, this interpretation is questionable because of the similarity between rocks in the Sparta complex and those in the Wallowa terrane. Also, the Sparta complex differs from the Canyon Mountain Complex in that it lacks an ultramafic member, owing to faulting (Prostka and Bateman, 1962). The structurally lowest member of the Sparta complex consists mainly of cumulate pyroxenites, which grade upward into cumulate gabbros; the highest gabbros are massive and contain primary amphibole and quartz (Phelps, 1978). Overlying and intruding the gabbros is a composite trondhjemite-quartz diorite pluton. It also intrudes volcanic rocks that were considered to be part of the Wallowa terrane by Vallier (1977). The apparently large proportion of felsic magmas supports the idea that the Sparta complex is part of the Wallowa terrane (Phelps, 1978, 1979; Phelps and Avé Lallemant, 1980). Phelps (1979) interpreted the gabbro-plagiogranite association to be cogenetic.

Published ages for the quartz diorite include (1) a K-Ar biotite age of 213±5 Ma (Marvin and Cole, 1978), (2) hornblende $^{40}Ar/^{39}Ar$ plateau ages of 223.0±3.3 and 223.2±5.5 Ma and a $^{40}Ar/^{39}Ar$ total-gas biotite age of 212.1 Ma (Avé Lallemant and others, 1980), and (3) a concordant U-Pb zircon age of 223 Ma (Walker, 1983, 1986). The reasonably close agreement among these ages suggests that the plagiogranite unit was emplaced about 223 Ma. Walker (1986) also reported a concordant U-Pb zircon age of 253 Ma for an albite granite unit within the plagiogranite member. These data indicate that silicic magmatism occurred over a relatively wide range in time.

Because no age information was available to ascertain the relationship of the cumulate gabbro member to the silicic units, we dated a hornblende separate from the massive hornblende-quartz gabbro unit; a $^{40}Ar/^{39}Ar$ plateau age of 227.0±1.3 Ma was obtained (table 1.1). Thus, the formation of the gabbro was nearly coeval with that of most(?) of the plagiogranite. The sole Permian plagiogranite must be part of an older basal complex, possibly a part of the Permian segment of the Wallowa arc or perhaps an allochthonous fragment of older basement (see Walker, 1982; T.L. Vallier, oral commun., 1987). It seems unlikely that the gabbro is as old as Permian. The exact relationship between the albite granite and the gabbro-plagiogranite assemblage remains unresolved.

GEOLOGY OF THE CANYON MOUNTAIN COMPLEX

PREVIOUS INVESTIGATIONS

The first detailed map of the Canyon Mountain Complex (Thayer, 1956) showed it as an almost rectangular east-trending body about 22 km in length and 8 km in width (fig. 1.2). An ultramafic member in the northern part is overlain successively southward by an ultramafic-mafic layered zone, a gabbroic member, a sheeted sill-like (multiply intruded) zone, and a volcanic sequence. Plagiogranite intrusions occur locally throughout the complex but are concentrated near the contact between the gabbroic and sill-like members. Thayer (1963a) interpreted the Upper Permian and (or) Lower Triassic volcanic rocks in the southern part of the complex (keratophyre, quartz keratophyre, and spilite) to be hosts to the younger ultramafic and gabbroic intrusions of the complex. Apparently, emplacement of late-stage plagiogranite (quartz diorite to albite granite) magmas in the upper part of the complex caused metasomatism of the gabbroic and volcanic wallrocks. The ultramafic and gabbroic rocks were believed to have formed at upper-mantle and lower-

crustal depths, respectively, in a large stratiform complex (analogous to the Stillwater intrusion) and to have been remobilized as a crystal mush and emplaced into higher structural levels (Thayer, 1963a, b; Thayer and Himmelberg, 1968; Thayer, 1969a). According to Thayer (1963b), layering in these rocks formed due to flow differentiation; primary structures were largely destroyed except for nodular structures in the podiform chromitite deposits (Thayer, 1969b).

On the basis of detailed structural and petrofabric studies, it has been demonstrated that the Canyon Mountain Complex consists of two distinct mantle diapirs that were emplaced at relatively high temperatures (Avé Lallemant, 1976; Misseri and Boudier, 1985). To account for the disproportionately large volumes of plagiogranite and silicic volcanic rocks, Avé Lallemant (1976) suggested that these diapirs ascended either beneath a volcanic island arc or at least proximal to such an arc in a marginal basin. Thayer (1977a) briefly accepted this model but later in the same year stated that the ultramafic-mafic rocks of the complex formed in a stratiform intrusion beneath a midoceanic ridge, that these rocks were deformed during ascent as a crystal mush, and that they were subsequently intruded by diabase and plagiogranite magmas and then covered by equivalent volcanic rocks (Thayer, 1977b).

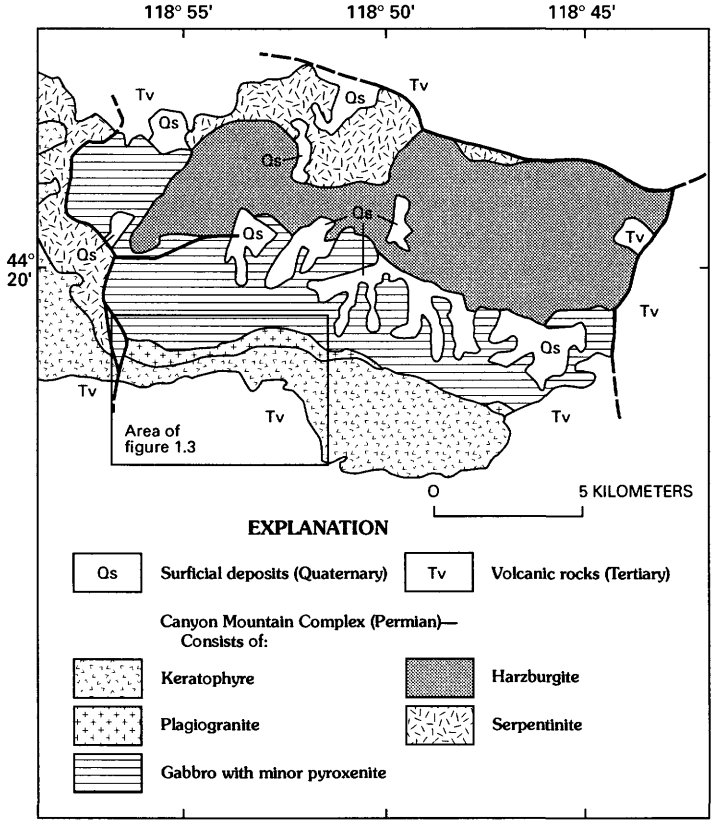

FIGURE 1.2.—Simplified geology of the Canyon Mountain Complex (modified from Thayer, 1977b). Heavy lines represent faults, dashed where covered. Area of map shown in figure 1.1.

On the basis of petrologic and geochemical studies of the ultramafic and gabbroic rocks, Himmelberg and Loney (1980) concluded that (1) the major harzburgitic component of the ultramafic member represents residual upper-mantle material that had been subjected to a previous partial-melting event unrelated to the formation of the remainder of the ophiolite, (2) the podiform chromitite found only in dunite bodies represents cumulate material in the basal harzburgite unit, (3) the gabbroic member formed by fractional crystallization of basaltic magma that had been emplaced into depleted mantle wallrocks, and (4) the large volume of silicic rocks implies an island-arc setting for the formation of the Canyon Mountain Complex.

Detailed geologic mapping of the sheeted member (Gerlach, 1980) confirmed the abundance of silicic magmas (fig. 1.3) and provided information on relative timing for the emplacement of its respective magma types. On the basis of petrologic and geochemical studies, Gerlach, Avé Lallemant, and Leeman (1981) and Gerlach, Leeman, and Avé Lallemant (1981) interpreted the plagiogranites as the products of partial melting of hydrated mafic rocks at relatively shallow depths within an island arc; emplacement of basaltic magmas was invoked to provide the necessary heat.

Further detailed mapping and petrologic studies of the ultramafic and gabbroic rocks led E.M. Bishop (Mullen, 1983a, b; Bishop, chap. 5, this volume) to conclude that (1) several generations of gabbros (some of which are penetratively deformed) intruded the depleted harzburgite tectonite member, and (2) the most primitive gabbros were tholeiitic whereas the more evolved gabbros were calc-alkalic. Considering the regional geology, she proposed that the Canyon Mountain Complex formed in a fore-arc setting. On the basis of regional tectonic constraints, Avé Lallemant (1984b) suggested that it formed in an intra-arc extensional basin produced by en echelon strike-slip faulting related to oblique subduction.

Despite uncertainties concerning details of the original setting for the Canyon Mountain Complex, the overall evidence indicates that the ultramafic rocks (plus some of the mafic rocks in the eastern part of the complex) ascended diapirically, that early mafic magmas were intruded syntectonically or pretectonically, and that post-tectonic mafic and felsic intrusions cut the ultramafic rocks and led to formation of high-level magma chambers, dike and sill complexes, and possibly lava flows as well.

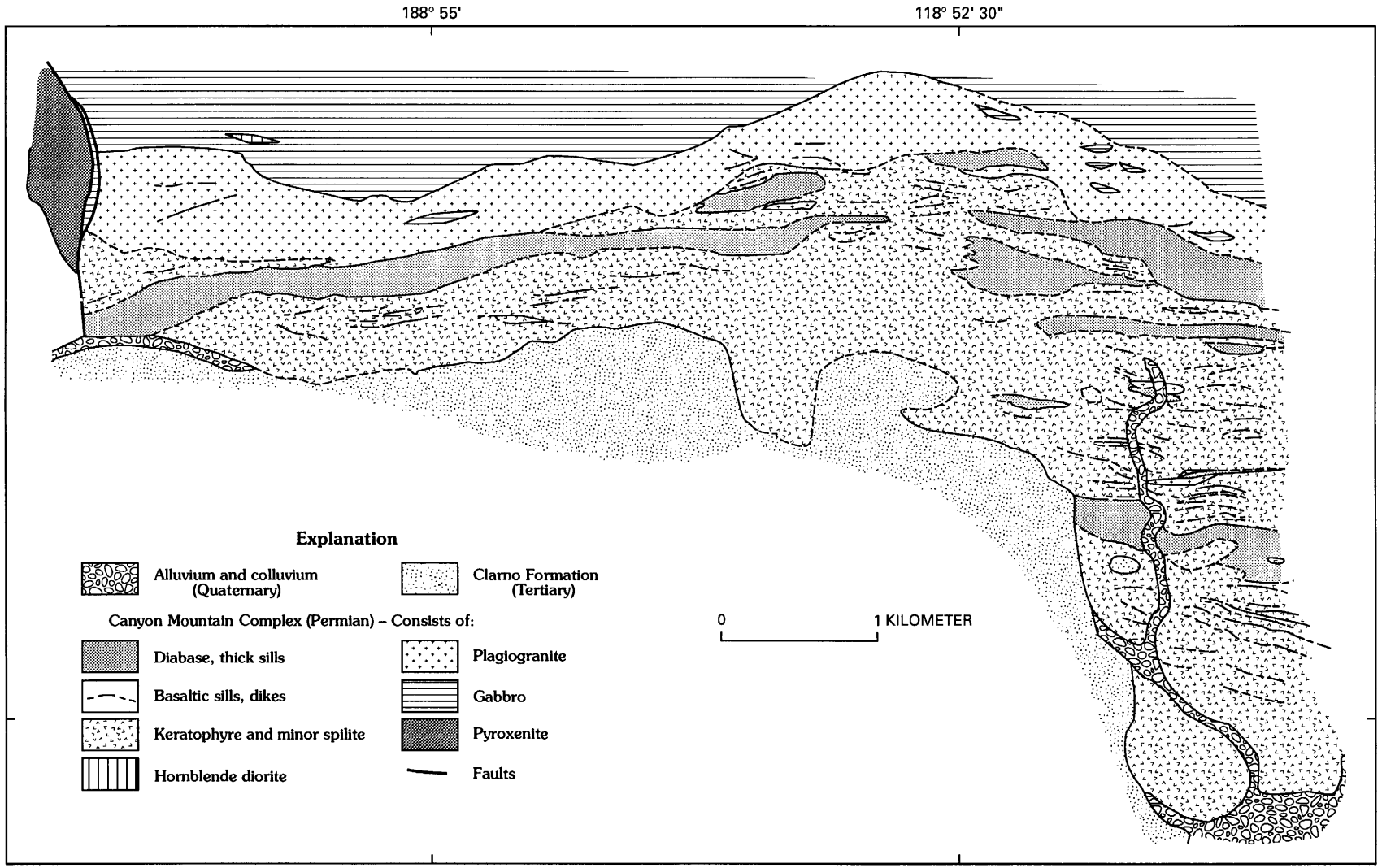

FIGURE 1.3.—Geology of sheeted member and keratophyre unit of the Canyon Mountain Complex showing major dikes and sill-like intrusive lenses (modified from Gerlach, 1980). Contacts, faults, and sills or dikes are dashed where covered. Area of map shown in figure 1.2.

GEOLOGIC DESCRIPTIONS OF UNITS

In general, the lithologic units (or members) of the Canyon Mountain Complex (fig. 1.4) are characteristic of many ophiolites; they are described individually later. E.M. Bishop (Mullen, 1983a, b; Bishop, chap. 5, this volume) presents additional details of the geology and mineralogy of the ultramafic and mafic members of the complex. Contacts between lithologic units trend approximately east-southeast to west-northwest and are near vertical. On the east, north, and west the ophiolite is fault bounded; on the south it is overlain by Eocene conglomerates and volcanic rocks (Thayer, 1956).

ULTRAMAFIC MEMBER

The ultramafic member consists mostly of harzburgite with rare lherzolite. In a few areas, the peridotites show faint layering due to orthopyroxene concentrations along foliation planes. Large irregular dunite bodies occur throughout, and these commonly include layers of nodular and disseminated chromitite. Pretectonic or syntectonic (diapiric) gabbro, gabbro pegmatite, and pyroxenite dikes crosscut the peridotites. Clearly post-tectonic dunite occurs in veinlike layers and as dikes in the peridotites. Interstitial plagioclase occurs in rocks toward the top of the ultramafic member and locally near dikes of gabbro.

All rock types in the ultramafic member are penetratively deformed and have well-developed foliation and lineation (Avé Lallemant, 1976). The chromitites have relict cumulate textures (Thayer, 1969b); Himmelberg and Loney (1980) suggested that the chromitites and the enclosing dunite bodies together represent the basal part of the overlying gabbroic member, which was folded into the tectonite harzburgite. The dunite dikes and veins are not folded,

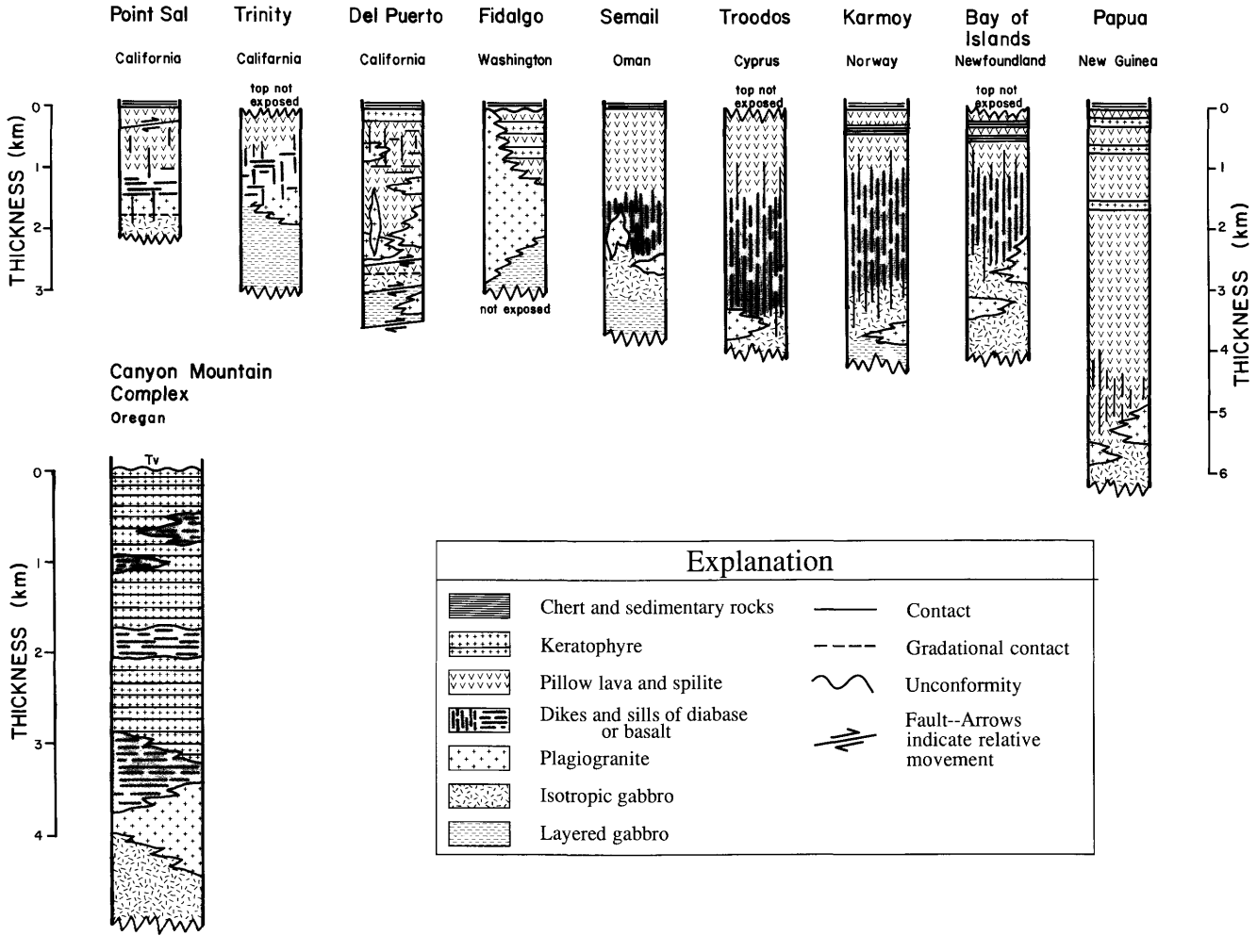

FIGURE 1.4.—Comparative stratigraphic sections of upper parts of selected ophiolites worldwide (from Gerlach, Avé Lallemant, and Leeman, 1981). Tv, Tertiary volcanic rocks.

but have a tectonite fabric; they appear to have formed by metasomatic transformation of harzburgite (Dungan and Avé Lallemant, 1977). Subsequent to dunite formation, gabbro, pyroxenite, rare diabase, and very rare plagiogranite dikes and sills intruded the ultramafic rocks. Most of the peridotites, particularly those exposed near the bounding fault along the north margin of the complex, locally are serpentinized and sheared to various extents.

GABBROIC MEMBER

Unlike the petrographically and structurally homogeneous harzburgite tectonites of the ultramafic member, the gabbroic member is very heterogeneous. Most primary igneous textures in the eastern part of the complex have been obliterated by intense penetrative deformation, whereas in the west primary textures are preserved.

Cyclical igneous layering in the western massif is consistent with crystal fractionation by gravitational settling within a periodically refilled basaltic-magma chamber. The lowermost units are dunites and chromitites, which are overlain by olivine pyroxenites. Relict cumulate textures are ubiquitous, and rocks are not penetratively deformed. The olivine pyroxenites in turn are overlain by layered gabbroic rocks that locally contain lenses of wehrlite or olivine pyroxenite. The gabbroic rocks comprise various proportions of plagioclase, clinopyroxene, olivine, and rare orthopyroxene; corresponding rock types include gabbro, troctolite, norite, and anorthosite. Depositional structures such as slumps and trough banding are rare. Diabase dikes occur throughout this unit but are more numerous southward toward the contact with the sheeted member. At Canyon Mountain, they form a northeast-trending swarm and locally form coarse-grained stocks (the ophitic gabbros of Avé Lallemant, 1976).

In contrast, the gabbroic member of the eastern massif represents a number of small independent intrusive bodies. The main rock type is coarse-grained gabbro containing relict cumulate structures. This gabbro in turn contains inclusions of fine-grained gabbro and is cut by gabbro pegmatite, olivine pyroxenite, and several other gabbroic intrusions (Avé Lallemant, 1976; Mullen, 1983a, b; Bishop, chap. 5, this volume). Penetrative deformation overprinted all of these rocks as they were partly folded into the tectonite harzburgites of the ultramafic member. This deformation was followed by intrusion of isotropic gabbro, pyroxenite, diabase, hornblende pegmatite, and plagiogranite bodies.

SHEETED (SILL-LIKE) MEMBER

The sheeted member consists of east-west-striking, steeply dipping layers of gabbro, keratophyre, basalt, basaltic andesite, diabase, and plagiogranite. The contact with the underlying gabbroic member is gradational. Gabbro, diabase, and plagiogranite are mostly concentrated in the structurally lower northern part, and keratophyre, basalt, and basaltic andesite are more abundant at structurally higher levels to the south. The largest plagiogranite bodies occur near the contact between the sheeted and gabbroic members. Field relations indicate that gabbros, keratophyres, and basalts are the oldest rocks in the sheeted member and that they were intruded by diabase and plagiogranite. Rocks of the plagiogranite suite were emplaced in the general sequence hornblende diorite, quartz diorite, and trondhjemite; these rocks were intruded by later basalts and diabases. Rare banded keratophyre lenses apparently represent one of the latest magmatic phases. Relative timing and duration of intrusive events as deduced from crosscutting relations in the sheeted member are shown in figure 1.5.

Because neither pillow basalts nor cherts were found in the sheeted member, Thayer (1977b) interpreted it to be a dike complex. However, some keratophyres display fine lamination, which Avé Lallemant (1976) previously interpreted as pyroclastic layering. Also, the presence of vesicles in some basalt and basaltic andesite units suggest that they are lava flows. If these rocks are indeed extrusive, then conformable attitudes between them and the diabase and plagio-

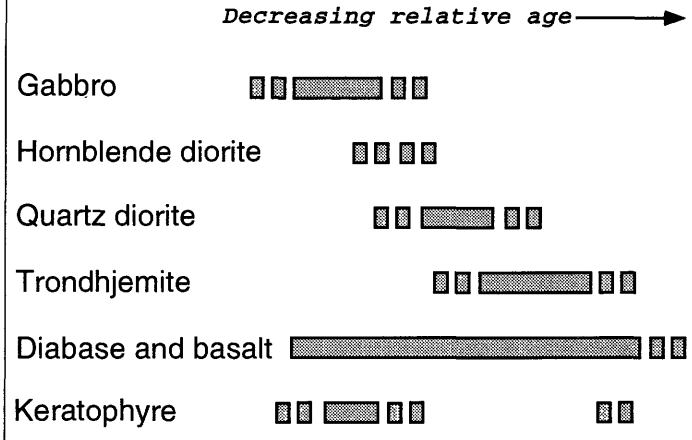

FIGURE 1.5.—Relative timing and duration of magmatic pulses that produced sheeted member in upper part of the Canyon Mountain Complex. Evidence is based on field relations including intrusive contacts, crosscutting dikes and lenses, and presence of xenoliths and intrusion breccias. Segments are dashed where uncertain.

granite lenses imply that the sheeted member is a sill rather than a dike complex.

STRUCTURE

The penetrative-deformation structure in the ultramafic member and in the eastern part of the gabbroic member is manifested by well-developed foliation, lineation, and strong preferred orientation of all constituent minerals (Avé Lallemant, 1976). As deduced from the preferred orientations, the major principal extension direction (X) is vertical. This inference and the overall structural style led to the conclusion that the Canyon Mountain Complex was emplaced as two separate massifs by diapiric flow in the upper mantle (Avé Lallemant, 1976). In the western massif, the extension axis (X) is vertical in the north, but rotated and even overturned to the south near the contact with the gabbroic member, where the cumulate layering is vertical to slightly overturned. These data indicate that the ophiolite is folded into a large asymmetric east-west-trending anticline (Avé Lallemant, 1976; Thayer and others, 1981). The contact between the gabbroic and sheeted members is steep, but aeromagnetic data (Thayer and others, 1981) suggest that at depth the contact rotates toward a more southerly dip of about 45° and that the ophiolite extends southward for some distance beneath surface cover. If this anticline is unfolded, the cumulate layering in the gabbroic member, layering in the keratophyre units, and the intrusive layers of diabase and plagiogranite all become subhorizontal. Rotation of the sheeted member is poorly constrained in time; it may have occurred during Late Triassic subduction, during Triassic subduction, during Jurassic collision, or possibly in Eocene or later time. Because Eocene conglomerates overlying the southern part of the ophiolite also have a steep southward dip (average is about 45°, but locally as high as 70°), folding of the Canyon Mountain Complex cannot be dated closely (Thayer, 1956). Although we consider the sheeted member to be a stack of rotated sills and minor flows (Gerlach, Avé Lallemant, and Leeman, 1981), others (for example, Thayer, 1963a; Misseri and Boudier, 1985) favor emplacement of this member as steeply dipping dikes because elsewhere in the complex most dikes are steeply dipping.

PETROGRAPHY AND MINERALOGY

The peridotite of the ultramafic member is generally harzburgite of uniform composition consisting of olivine (Fo_{88-91}) with 10 to 25 percent orthopyroxene (En_{90-92}), 3 to 5 percent clinopyroxene (0.8–1.0 percent Cr_2O_3), and 1 to 2 percent chrome spinel (Himmelberg and Loney, 1980). Pargasitic amphiboles commonly border or enclose pyroxene grains. Only rarely does the peridotite contain enough clinopyroxene (as much as 10 percent) to make it a true lherzolite. The texture is xenoblastic-granular; most grains are slightly flattened and elongate parallel to foliation and lineation, respectively. Olivines and orthopyroxenes in the dunites in which chromitite deposits occur are slightly enriched in Mg (Fo_{92-96}, En_{92-95}), and rare clinopyroxenes contain 1 to 2 percent Cr_2O_3 (Mullen, 1983a, b); textures in the dunites are similar to those in the harzburgites, except for the chromitite layers, which contain subhedral to euhedral chromite grains. Dunite veins and dikes have textures similar to those in the harzburgite, although the olivines are coarser. All peridotites and dunites are somewhat serpentinized.

Ultramafic and gabbroic rocks in the eastern part of the gabbroic member are mostly tectonites that display the same penetrative-deformation structures as found in harzburgites of the ultramafic member. Although these gabbroic rocks have relict primary banding, their overall texture is xenoblastic-granular; only rarely are cumulate textures preserved (Avé Lallemant, 1976). Himmelberg and Loney (1980) found evidence of a slight Fe-enrichment trend in going from dunites to gabbros, on the basis of compositions of olivine (Fo_{93} in dunites to Fo_{68} in gabbros), orthopyroxenes (En_{88} to En_{73}), and clinopyroxenes ($Ca_{49}Mg_{49}Fe_2$ to $Ca_{46}Mg_{42}Fe_{12}$); plagioclases in the same rocks range in composition from An_{96} in dunites to An_{70} in gabbros. Pearcy (1987) observed that such compositional trends are not necessarily regular.

The mafic cumulates of the western massif are folded but not penetratively deformed. Cumulate textures are generally preserved except where the rocks are altered near diabase and plagiogranite intrusions and near brecciated zones. Mineral compositions for these rocks are similar to those given for the tectonite metacumulates in the eastern part of the complex (Himmelberg and Loney, 1980).

Both the ultramafic and gabbroic members contain gabbro, gabbro pegmatite, and pyroxenite dikes that were emplaced prior to penetrative deformation. Their textures are similar to those described above for compositionally equivalent rocks. Post-tectonic dikes and veins have igneous textures. For example, in some gabbro dikes, euhedral plagioclase crystals are aligned parallel to the dike walls; this texture may reflect flow alignment of crystals parallel to conduit walls. Pyroxenite, gabbro pegmatite, and hornblende pegmatite

dikes are very coarse grained and have allotriomorphic to hypidiomorphic textures. Diabase dikes display subophitic textures but vary in grain size.

The gabbroic rocks have undergone subsolidus alteration of at least two different types. Proximal to intrusions of hornblende pegmatite or plagiogranite or near mylonite zones, clinopyroxenes are partly to completely amphibolitized. In contrast, gabbroic rocks in permeable zones are commonly altered to greenschist-facies assemblages, including hydrogrossular, chlorite, prehnite, calcite, and serpentine.

The sheeted member consists of screens of cumulate gabbros in the lower (more northerly) part and keratophyres and basaltic rocks in the upper (more southerly) part; these rocks are intruded by many sills, dikes, and stocks of plagiogranite, diabase, and minor basalt. The keratophyres are porphyritic, bearing phenocrysts of quartz and plagioclase in a fine-grained felty, spherulitic, or trachytic groundmass; quartz phenocrysts tend to be embayed but commonly display high-temperature bipyramidal morphology. Basalts are fine grained with intergranular to intersertal textures, and consist of plagioclase, clinopyroxene, and opaque minerals. A few vesicular basaltic andesites contain elongate plagioclase phenocrysts in a groundmass containing abundant microlites of plagioclase and oxides. Diabases contain diopsidic to subcalcic augite, plagioclase, magnetite, and ilmenite and have characteristic ophitic texture. Plagiogranites consist of plagioclase, quartz, hornblende, and small amounts of biotite and opaque minerals; their textures include hypidiomorphic-granular, granophyric, and porphyritic. Plagioclase phenocrysts display oscillatory zoning in some samples. Modal green hornblende varies from less than 10 percent in trondhjemites to more than 50 percent in some diorites; it occurs as an interstitial phase, as euhedra, and rarely as poikilitic grains with inclusions of plagioclase and quartz. Severe local alteration of rocks in the sheeted member produced secondary albite, chlorite, epidote, and calcite.

Electron-microprobe analyses of fresh clinopyroxenes in selected mafic rocks mainly from the sheeted member (fig. 1.6) display a marked difference in composition from those of clinopyroxenes in the cumulate and tectonite members. These data suggest that the basaltic magmas that intruded different parts of the complex do not represent cogenetic liquids.

PALEOTHERMOMETRY AND PALEOBAROMETRY

Information on pressures and temperatures of formation for rocks of the Canyon Mountain Complex is sparse. Himmelberg and Loney (1980) estimated temperatures of about 880 to 975 °C for the harzburgite tectonites and cumulate pyroxenites using analyses of coexisting orthopyroxenes and clinopyroxenes and the geothermometer of Wells (1977). These temperature estimates are unreasonably low for near-liquidus conditions, and it is probable that the mineral compositions have readjusted to subsolidus conditions due to low cooling rates or to recrystallization.

Mercier (1980; oral commun., 1982) applied his own geothermometer-barometer to seven harzburgites and obtained apparent equilibration temperatures of 1,000 to 1,100 °C and rather high pressures of 15 to 25 kb for samples from the deformed eastern part of the complex, and 900 to 1,000 °C and 8 to 15 kb for the western part. Because Mercier's method is based largely on empirical relationships, the calculated temperatures and pressures may not be correct in an absolute sense; however, they are internally consistent and suggest at least relative pressure-temperature conditions for recrystallization of the two structurally distinct parts of the complex.

GEOCHEMISTRY AND PETROLOGY

Reconnaissance geochemical investigations were undertaken to characterize all common rock types of the

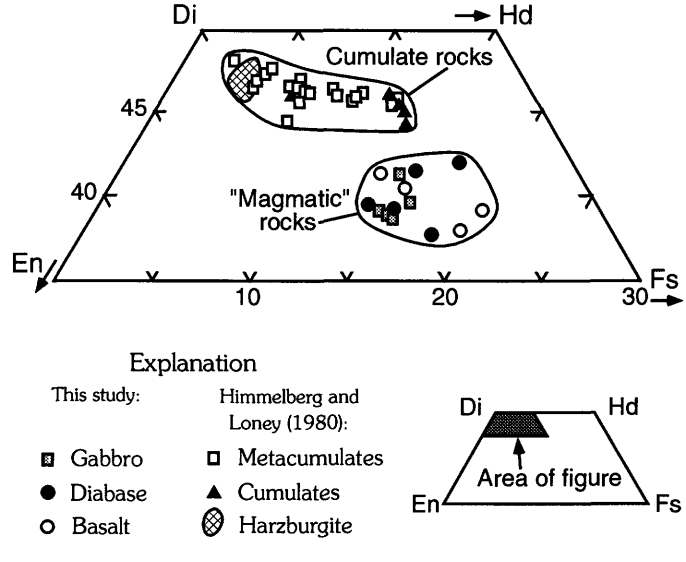

FIGURE 1.6.—Compositions of clinopyroxenes from mafic rocks of the Canyon Mountain Complex projected onto the pyroxene quadrilateral. Data from Himmelberg and Loney (1980) are representative of clinopyroxenes from the tectonite and cumulate members (see also Mullen, 1983a; Bishop, chap. 5, this volume). Note distinction between pyroxenes from cumulate rocks and those from gabbro, diabase, and basaltic rocks that have near-liquidus or "magmatic" compositions. Di, diopside; En, enstatite; Fs, ferrosilite; Hd, hedenbergite.

Canyon Mountain Complex. Representative samples have been analyzed for major and (or) trace elements using a variety of methods (see section "Analytical Methods," below). These samples include the plagiogranite and keratophyre suites previously described in detail by Gerlach, Leeman, and Avé Lallemant (1981). Of primary concern here are the volcanic and hypabyssal rocks that most closely represent magmatic liquids; relatively little emphasis has been placed on the cumulate gabbros or the various ultramafic tectonites, the chemical and (or) mineralogical compositions of which have been described by others (Thayer and Himmelberg, 1968; Himmelberg and Loney, 1980; Mullen, 1983a, b; Bishop, chap. 5, this volume). Analytical results as well as brief descriptions of the analyzed samples are given in tables 1.2 through 1.6. Specific sample locality information is available from the authors.

Most of the rocks selected for geochemical study are relatively fresh and have retained their original mineral compositions and textures. However, because many of our samples exhibit at least some alteration or low-grade metamorphic recrystallization, it is necessary to carefully assess those geochemical parameters that supposedly reflect primary petrogenetic processes. The problems of evaluating the effects of element mobility in altered rocks and of deciphering tectonic setting and petrogenetic history of ophiolitic rocks have been summarized by Pearce and Cann (1973), Winchester and Floyd (1977), Pearce (1982, 1983), and others. Most attention has focused on geochemical comparisons with modern basaltic associations such as midocean-ridge basalt (MORB), oceanic-island or within-plate basalt (WPB), and island-arc basalt (IAB) suites, which have diagnostic geochemical features. To facilitate such a comparison, it is first necessary to identify those samples that retain or closely approach their original magmatic compositions.

ANALYTICAL METHODS

Representative samples were analyzed in two batches as follows: Group I (CM-prefix samples) and Group II (CMG- and OC-prefix samples). Major-element analyses were determined for Group II samples by combined electron microprobe analysis (EMPA) of fused glasses and atomic absorption spectrophotometry (AAS) (Gerlach, Leeman, and Avé Lallemant, 1981), and for Group I samples by X-ray fluorescence (XRF) analysis of flux-fused samples (see Jacques and Chappell, 1980). Trace-element analyses were obtained on Group II samples by instrumental neutron activation analysis (INAA) at Oregon State University and at the National Aeronautic and Space Administration (NASA) Johnson Space Center (Gerlach, Leeman, and Avé Lallemant, 1981), and by XRF analysis of pressed powder disks at the University of Massachusetts (Frey and others, 1984). Group I samples were analyzed for a few trace elements by the latter method at the Australian National University. For selected Group II samples, Sr, Ba, Sc, V, Cr, Ni, Zn, and Zr were determined by inductively coupled plasma (ICP) spectroscopy at Rice University.

Analytical uncertainties are generally within 1 to 5 percent of the amount present for the major elements and 5 to 10 percent for most trace elements. Uncertainties may be somewhat larger for elements with low abundance or low sensitivity, such as Th, Ta, Ba, and Nb; the results for these elements (and especially for Nb) are reported to indicate the extremely low abundances in most samples. Dashes in tables indicate that abundances either were not determined or were below detection limits.

Analysts included the following: XRF, D.C. Gerlach at the University of Massachusetts and Bruce Chappell at the Australian National University; INAA, W.P. Leeman at Oregon State University and D.C. Gerlach at NASA; AAS, D.C. Gerlach at NASA; EMPA, D.C. Gerlach at Rice University; ICP, W.P. Leeman at Rice University.

Data are presented in separate tables (tables 1.2 – 1.6) according to rock type. However, we have arbitrarily included gabbroic samples with greater than 0.7 weight percent TiO_2 in table 1.4 with diabase, dolerite, and basaltic rocks because all of these rocks are believed to approximate original magmatic liquids in composition. Throughout this paper, all samples in table 1.4 have been plotted together as "magmatic" samples. Inspection of figures 1.7 and 1.8, for example, shows that the compositions of these samples do indeed resemble basaltic compositions and define coherent geochemical trends. All major-element data shown in diagrams are based on analyses recalculated to 100 percent totals on an anhydrous basis.

GENERAL GEOCHEMICAL CHARACTERISTICS

Major-element characteristics of the rocks of the Canyon Mountain Complex generally resemble those of most ophiolites. The main lithologic groups are easily distinguished in SiO_2 variation diagrams (fig. 1.7). The ultramafic rocks define a restricted grouping (low SiO_2, alkalis, TiO_2, P_2O_5, and Al_2O_3, and high MgO) consistent with their dominantly olivine and pyroxene mineral assemblages. With exception of the cumulate gabbros, which have relatively high

TABLE 1.2.—*Analyses of major-element oxides and selected trace elements in ultramafic rocks (peridotite, harzburgite, pyroxenite) of the Canyon Mountain Complex*

Sample	CM65	CM37	CM38	CM60	CM54	CM64	CM61	CM62	CM63
Rock type	Serpentinized peridotite	Tectonite harzburgite	Tectonite harzburgite	Pyroxenite	Pyroxenite	Pyroxenite	Cumulate olivine pyroxenite	Plagioclase-bearing pyroxenite	Olivine-plagioclase pyroxenite
Major-element oxides, in weight percent									
SiO_2	37.43	42.71	43.78	47.32	51.27	49.77	42.30	41.24	41.33
TiO_2	0.09	0.01	0.01	0.04	0.16	0.15	0.11	0.08	0.07
Al_2O_3	5.70	1.19	0.80	1.19	3.33	2.82	2.73	6.23	6.21
Fe_2O_3	4.33	2.10	1.45	2.35	1.23	1.19	4.28	2.30	2.75
FeO	4.85	5.56	6.42	2.36	4.47	4.53	5.66	6.14	5.77
MnO	0.15	0.13	0.14	0.10	0.15	0.14	0.16	0.15	0.16
MgO	32.73	42.25	42.97	26.56	19.44	20.51	26.85	26.01	25.76
CaO	3.11	1.10	0.79	13.08	17.77	18.49	9.42	9.72	9.42
Na_2O	0.04	0.02	0.01	0.08	0.17	0.14	0.10	0.16	0.13
K_2O	0.08	0.02	0.01	0.08	0.03	0.03	0.03	0.03	0.03
P_2O_5	0.01	0.01	0.01	0.01	0.01	0.01	0.01	0.01	0.01
H_2O^+	11.09	4.44	0.01	6.07	1.19	1.52	7.41	6.98	7.41
H_2O^-	0.30	0.31	0.31	0.30	0.20	0.17	0.30	0.39	0.38
CO_2	0.18	0.32	3.01	0.18	0.21	0.14	0.28	0.23	0.20
Total	100.09	100.17	99.72	99.72	99.63	99.61	99.64	99.67	99.63
Trace elements, in parts per million									
V	62	41	38	70	262	228	125	93	84
Cr	4,325	2,960	3,300	2,985	2,255	4,360	1,495	1,895	1,785

MgO and Al_2O_3, the remaining rocks define what appear to be coherent trends more or less typical of igneous liquid lines of descent. A plot of Al_2O_3 versus SiO_2 (fig. 1.7) is particularly effective in discriminating those rocks with compositions appropriate for magmatic liquids (that is, non-cumulate gabbro, diabase, basaltic rocks, and the more siliceous plagiogranite and keratophyre suites) from rocks having high proportions of cumulate minerals (cumulate gabbro and pyroxenite) and rocks from which melt may have been extracted (harzburgitic peridotites). Solely on the basis of petrography or field relations, it is often difficult to differentiate coarse-grained, dominantly cumulate gabbroic rocks from gabbros that represent magmatic liquids. For example, many dolerites and coarse-grained diabases have higher contents of incompatible elements (such as K, Ti, P) than expected for purely cumulate gabbros. Also, because the cumulate rocks represent concentrates of plagioclase, olivine, and pyroxenes, they are relatively enriched in Al, Mg, and Ca. A plot of the relatively immobile components Al_2O_3 versus TiO_2 (fig. 1.8) clearly discriminates a group of mafic rocks that resemble modern oceanic basalts (see Melson and others, 1976; Bryan and others, 1981) from the other lithologic groups. In this chapter we rely mainly on these presumably magmatic or near-magmatic samples to understand petrogenetic processes.

The basaltic to felsic rocks of the intrusive complex and the extrusive keratophyres are characterized by a relatively strong covariation between SiO_2 and the oxides CaO, MgO, FeO* (total Fe as FeO), Na_2O, and TiO_2 (fig. 1.7)—not unlike that expected for magmatic liquid lines of descent. However, considerable scatter for contents of K_2O and possibly P_2O_5 may reflect alteration. Alteration effects are more clearly seen in plots of various elements against TiO_2 (fig. 1.8), which tends to be one of the least mobile constituents of igneous rocks under conditions of alteration (Pearce, 1983).

The possible effects of crystal-liquid fractionation must be considered in evaluating overall compositional variations for both the felsic and mafic rocks. The mafic rocks alone display strong positive correlations between TiO_2 and P_2O_5, Ce, and Hf (fig. 1.8), as well as between TiO_2 and Zr (see fig. 1.14). Weaker posi-

TABLE 1.3.—*Analyses of major-element oxides and selected trace elements in gabbroic rocks (with less than 0.7 weight percent TiO_2) of the Canyon Mountain Complex*

[---, not determined or below detection limit]

Sample	CM55	CM56	CM57	CM58	CM28	CM34	CM35	OC277
Rock type	Anorthositic gabbro	Foliated anorthositic gabbro	Foliated gabbroic anorthosite	Foliated gabbroic anorthosite	Cumulate gabbro	Cumulate anorthositic gabbro	Cumulate anorthositic gabbro	Olivine-plagioclase cumulate (troctolite)
Major-element oxides, in weight percent								
SiO_2	45.54	44.31	44.07	43.93	47.05	45.19	45.82	47.50
TiO_2	0.09	0.09	0.05	0.08	0.18	0.16	0.27	0.01
Al_2O_3	20.57	14.86	26.00	22.21	18.00	23.76	20.69	24.40
Fe_2O_3	0.61	0.64	0.56	0.65	0.96	1.09	2.08	---
FeO	2.51	5.08	1.89	3.08	3.51	2.63	3.98	5.70
MnO	0.06	0.11	0.04	0.07	0.10	0.07	0.09	0.08
MgO	11.90	16.77	6.42	8.85	10.06	6.70	7.80	9.54
CaO	13.08	11.60	16.47	15.08	17.11	16.83	15.49	11.90
Na_2O	1.82	1.47	1.22	1.17	0.90	1.00	1.14	1.46
K_2O	0.06	0.04	0.06	0.09	0.06	0.05	0.03	0.02
P_2O_5	0.01	0.01	0.01	0.01	0.01	0.01	0.01	---
H_2O^+	2.87	4.31	2.76	3.92	2.03	2.03	2.07	---
H_2O^-	0.19	0.12	0.30	0.30	0.17	0.21	0.25	---
CO_2	0.30	0.19	0.14	0.15	0.01	0.06	0.01	---
Total	99.61	99.60	99.99	99.59	100.15	99.79	99.73	100.61
Trace elements, in parts per million								
Sc	---	---	---	---	---	---	---	2.1
V	47	79	50	87	146	114	150	---
Cr	1,130	1,085	496	357	429	354	86	6
Co	---	---	---	---	---	---	---	47.4
Ni	---	---	---	---	---	---	---	53
Th	---	---	---	---	---	---	---	0.03
La	---	---	---	---	---	---	---	0.11
Sm	---	---	---	---	---	---	---	0.05
Eu	---	---	---	---	---	---	---	0.17
Tb	---	---	---	---	---	---	---	0.012
Yb	---	---	---	---	---	---	---	0.062
Lu	---	---	---	---	---	---	---	0.007

tive correlations between TiO_2 and Th, Ba, and possibly K_2O in the mafic rocks (fig. 1.8) may reflect alteration of some samples, because normally these incompatible elements are coherently enriched in evolving mafic liquids. Negative correlations between TiO_2 and Mg number (fig. 1.8) and between TiO_2 and abundances of Sc, Co, Cr, and Ni (table 1.4) and the positive correlations just mentioned are consistent with differentiation involving removal of Fe-Ti-oxide-poor mineral assemblages from the evolving mafic liquids. Under such conditions Ti behaves as an essentially incompatible element, and its abundance correlates with that of other incompatible trace elements (see Cann, 1970; Saunders and others, 1980).

On some of the TiO_2 variation diagrams (see fig. 1.8), the plagiogranites and keratophyres show trends that preclude their derivation by simple fractionation from mafic precursor magmas. In the felsic rocks, TiO_2 and Mg number decrease together—along with other transition metals (tables 1.5 and 1.6)—in accord with fractionation of Fe-Ti oxides and ferromagnesian minerals. Fractionation of such minerals is consistent with the small degree of Fe enrichment (fig. 1.9) and the strong alkali-enrichment trend (fig. 1.10) observed

TABLE 1.4.—*Analyses of major-element oxides and selected trace elements in mafic rocks (diabase, dolerite,*

[---, not determined or

Sample	CM26	CM27	CM19	CM20	CM21	CM39	CM40	CMG124A	CMG49	OC244	OC256	OC259
Rock type	Olivine gabbro	Olivine gabbro	Hornblende-plagioclase dolerite	Gabbro	Cumulate gabbro	Gabbro	Gabbro	Porphyritic plagioclase-clinopyroxene diabase	Quartz diabase	Diabase	Diabase	Diabase
Major-element oxides,												
SiO_2	48.56	49.52	49.75	49.54	50.83	49.99	47.29	50.80	56.30	53.90	52.20	54.30
TiO_2	1.29	1.22	1.89	2.14	2.34	1.20	2.12	1.44	1.73	0.84	1.61	1.05
Al_2O_3	15.19	15.52	14.87	14.62	14.59	15.17	15.13	15.10	14.90	16.70	15.50	15.10
Fe_2O_3	2.22	2.03	0.75	0.63	1.16	2.58	3.64	---	---	---	---	---
FeO	7.81	7.27	10.53	11.54	10.93	6.94	7.92	10.20	9.59	8.68	9.57	10.20
MnO	0.19	0.18	0.20	0.22	0.23	0.18	0.22	0.21	0.24	0.15	0.19	0.16
MgO	8.04	7.76	5.72	4.85	4.67	6.58	6.94	7.78	5.79	6.25	8.81	6.93
CaO	11.16	10.81	10.05	9.10	7.36	9.03	8.13	10.10	6.09	9.74	7.21	7.99
Na_2O	2.45	3.07	3.91	4.24	4.89	4.21	3.98	2.70	3.79	3.49	3.98	4.49
K_2O	0.15	0.13	0.20	0.19	0.29	0.19	0.40	0.22	0.29	0.03	0.13	0.32
P_2O_5	0.06	0.09	0.16	0.20	0.21	0.07	0.17	---	---	---	---	---
H_2O^+	2.43	1.96	1.92	1.78	2.31	3.12	3.34	---	---	---	---	---
H_2O^-	0.17	0.24	0.08	0.09	0.16	0.28	0.35	---	---	---	---	---
CO_2	0.08	0.01	0.07	0.53	0.04	0.09	0.29	---	---	---	---	---
Total	99.80	99.81	100.10	99.67	100.01	99.63	99.92	98.55	98.72	99.78	99.20	100.54
Trace elements,												
Sr	---	---	---	---	---	---	---	132	109	72	125	83
Ba	15	30	30	35	20	15	30	12	27	---	20	31
Sc	---	---	---	---	---	---	---	36.5	31.1	40.5	35.9	41.1
V	329	278	370	396	430	286	356	236	174	244	262	293
Cr	272	262	86	38	26	113	133	173	124	60	220	71
Co	---	---	---	---	---	---	---	41.6	26.6	30.4	36.8	37.1
Ni	---	---	---	---	---	---	---	106	47	22	96	36
Zn	---	---	---	---	---	---	---	102	121	88	114	104
Ta	---	---	---	---	---	---	---	---	0.06	---	---	---
Nb	---	---	---	---	---	---	---	0.1	0.2	---	0.1	0.2
Hf	---	---	---	---	---	---	---	2.99	3.79	1.19	2.41	2.04
Th	---	---	---	---	---	---	---	0.54	0.60	---	---	---
Zr	---	---	---	---	---	---	---	102	138	44	102	74
La	---	---	---	---	---	---	---	2.62	3.06	1.15	2.83	2.00
Ce	7	9	18	18	16	7	11	9.0	11.2	3.7	9.0	6.4
Nd	---	---	---	---	---	---	---	7.3	10.7	4.0	9.8	7.2
Sm	---	---	---	---	---	---	---	3.40	4.39	1.77	3.56	2.76
Eu	---	---	---	---	---	---	---	1.32	1.48	0.74	1.26	0.97
Tb	---	---	---	---	---	---	---	0.97	0.96	0.52	0.83	0.72
Yb	---	---	---	---	---	---	---	3.69	4.41	1.92	2.88	2.85
Lu	---	---	---	---	---	---	---	0.53	0.68	0.30	0.52	0.42

in these rocks. A small number of samples described as basaltic andesites and spilites, and probably some so-called epidiorites, display significant alkali enrichment that in part is due to alteration; these rocks have been lumped in with the plagiogranite suite in fig. 1.10.

The positive correlation between TiO_2 and P_2O_5 in the mafic rocks is consistent with concurrent fractionation of apatite and Fe-Ti oxides (see fig. 1.8). Negative correlations of TiO_2 with Ce, Hf, and Zr simply indicate that Ti is not incompatible in the more evolved magmas, whereas Ce, Hf, and Zr are (tables 1.4–1.6).

basaltic rocks, and gabbroic rocks with more than 0.7 weight percent TiO_2) of the Canyon Mountain Complex

below detection limit]

CMG-162	CMG-166	CMG-211	CMG-207	CMG-43C	CM8	CM6	CM25	CMG32	CMG81	CMG-227	OC216	CMG18A	CMG146B
Diabase	Diabase	Diabase	Diabase	Hornblende epidiorite	Gabbro	Plagioclase phyric basalt	Basalt	Basalt	Basalt	Spilite	Spilite	Porphyritic basaltic andesite	Porphyritic basaltic andesite
in weight percent													
51.30	52.40	52.50	55.90	51.90	48.65	50.91	50.07	53.00	54.90	61.00	61.50	57.80	59.10
1.00	1.23	1.86	1.32	0.72	1.49	1.55	1.21	1.39	1.57	1.04	1.23	1.30	1.00
15.50	16.30	14.90	14.80	15.90	15.97	14.84	15.56	15.40	15.10	15.10	15.70	15.20	15.1
---	---	---	---	---	1.87	1.84	1.18	---	---	---	---	---	---
9.57	10.10	11.50	10.00	9.64	8.18	8.53	8.71	10.90	11.90	9.71	7.68	8.38	10.00
0.19	0.19	0.18	0.18	0.18	0.20	0.30	0.18	0.19	0.18	0.18	0.23	0.13	0.14
7.75	7.42	6.95	6.15	8.46	7.91	7.33	6.69	7.02	5.97	3.48	2.83	5.62	6.43
10.20	8.63	8.29	7.55	9.15	8.41	5.89	9.01	7.64	5.65	4.19	2.12	5.16	2.59
2.68	3.33	3.33	4.36	2.81	3.21	4.19	3.60	4.43	5.18	5.58	6.64	5.45	4.92
0.10	0.12	0.60	0.20	0.68	0.55	0.46	0.77	0.20	0.09	0.04	0.15	0.89	0.42
---	---	---	---	---	0.12	0.10	0.07	---	---	---	---	---	---
---	---	---	---	---	3.08	3.23	2.56	---	---	---	---	---	---
---	---	---	---	---	0.24	0.34	0.09	---	---	---	---	---	---
---	---	---	---	---	0.21	0.10	0.14	---	---	---	---	---	---
98.29	99.72	100.11	100.46	99.44	100.09	99.61	99.84	100.17	100.54	100.32	98.08	99.93	99.70
in parts per million													
167	197	---	79	---	---	---	---	129	78	45	---	91	83
7	9	---	22	---	50	50	40	19	1	---	---	141	33
42.8	40.1	41.3	37.4	42.4	---	---	---	39.8	40.4	29.4	20.4	34.9	33.5
289	288	---	214	---	332	325	321	303	349	---	---	7	248
162	124	80	138	121	267	240	123	162	15	2	4	250	26
37.6	38.2	40.3	31.4	38.9	---	---	---	36.3	33.0	21.1	8.8	27.6	26.9
66	49	---	44	---	---	---	---	67	17	8	---	32	17
82	91	---	109	---	---	---	---	98	117	106	---	76	95
---	0.09	0.09	---	---	---	---	---	---	---	---	0.09	---	---
0.2	0.4	---	0.8	---	---	---	---	---	---	---	---	0.2	---
1.50	2.09	3.28	2.40	1.31	---	---	---	2.65	2.01	2.00	4.04	2.27	1.58
0.28	0.28	0.68	0.21	0.37	---	---	---	0.63	0.45	0.38	0.19	0.55	0.54
55	77	---	85	---	---	---	---	90	69	68	---	84	51
1.57	1.77	2.86	2.86	1.10	---	---	---	2.19	1.71	1.75	3.62	2.09	1.34
5.2	7.5	10.2	8.3	2.5	8	7	9	7.9	5.0	5.4	14.2	6.6	5.4
5.3	6.4	8.8	8.2	3.4	---	---	---	6.9	6.8	6.0	17.1	7.0	8.4
2.18	2.79	4.03	3.41	0.96	---	---	---	3.77	2.85	2.45	6.16	3.08	4.08
0.80	0.97	1.40	1.02	0.43	---	---	---	1.47	1.18	0.98	1.78	1.09	1.84
0.50	0.71	1.03	0.82	0.26	---	---	---	0.87	0.73	0.57	1.43	0.72	0.99
2.15	2.65	3.88	3.10	1.25	---	---	---	3.16	2.74	2.37	4.95	2.81	3.12
0.34	0.43	0.60	0.49	0.18	---	---	---	0.50	0.44	0.40	0.74	0.42	0.45

The scatter observed for some elements or oxides may reflect alteration (Ba, K_2O) and possibly analytical uncertainties (Th) at low concentration levels. More importantly, the significant decrease in contents of many incompatible elements (Ce, Hf, Zr, Th) and the retention of comparable levels for others (K_2O, Th, Ba) observed in going from the basaltic rocks to the felsic ones is inconsistent with a comagmatic relationship between these two groups of rocks. Further comparisons of covariations between other expectedly incompatible elements (fig. 1.11) reveal that, among the mafic rocks, La (like Ce) correlates strongly with Ti,

TABLE 1.5.—*Analyses of major-element oxides and selected trace*

[---, not determined or

Sample -------	CM17	CM15	CM51	CM41	CM42	CM11	CM10	CM18	CM44
Rock type ----	Feldspathic diorite	Diorite with cumulate clinopyroxene plagioclase	Diorite	Hornblende diorite pegmatite	Hornblende diorite	Hornblende diorite	Diorite (xenolith in keratophyre)	Quartz diorite (chloritized)	Hornblende plagiogranite
Major-element oxides,									
SiO_2----------	53.64	55.01	55.44	52.70	58.11	54.15	59.58	71.46	75.95
TiO_2----------	0.69	0.68	0.94	0.57	0.80	1.17	1.10	0.30	0.14
Al_2O_3 -------	17.39	16.14	16.66	16.67	14.86	15.49	15.38	14.61	11.95
Fe_2O_3 -------	1.38	4.56	2.14	2.36	1.57	2.74	1.97	0.50	0.73
FeO ----------	5.80	4.80	6.29	4.59	6.20	8.19	6.38	0.45	1.63
MnO---------	0.15	0.17	0.16	0.17	0.18	0.19	0.15	0.02	0.07
MgO ---------	5.33	4.45	4.10	5.04	4.45	4.12	3.00	0.56	0.73
CaO ----------	6.32	6.41	4.36	10.14	5.72	6.33	6.19	3.72	0.85
Na_2O -------	4.86	3.81	5.49	3.62	4.76	3.87	3.94	6.35	6.24
K_2O ---------	0.84	0.31	0.28	0.15	0.43	0.38	0.32	0.25	0.07
P_2O_5---------	0.07	0.08	0.13	0.04	0.05	0.08	0.10	0.05	0.01
H_2O^+ --------	2.75	3.38	3.01	3.08	2.35	2.67	1.67	1.12	0.91
H_2O^---------	0.25	0.31	0.37	0.62	0.26	0.27	0.19	0.15	0.13
CO_2 ----------	0.11	0.05	0.38	0.34	0.15	0.09	0.01	0.05	0.18
Total -----	99.58	100.16	99.75	100.09	99.89	99.74	99.98	99.59	99.59
Trace elements,									
Sr----------	---	---	---	---	---	---	---	---	---
Ba ----------	85	35	35	15	40	55	50	30	20
Sc----------	---	---	---	---	---	---	---	---	---
V----------	155	185	216	223	166	371	164	6	5
Cr----------	17	13	7	113	76	5	3	1	2
Co ----------	---	---	---	---	---	---	---	---	---
Ni----------	---	---	---	---	---	---	---	---	---
Zn ----------	---	---	---	---	---	---	---	---	---
Ta ----------	---	---	---	---	---	---	---	---	---
Nb----------	---	---	---	---	---	---	---	---	---
Hf----------	---	---	---	---	---	---	---	---	---
Th ----------	---	---	---	---	---	---	---	---	---
Zr----------	---	---	---	---	---	---	---	---	---
La ----------	---	---	---	---	---	---	---	---	---
Ce ----------	5	2	7	6	8	9	6	4	13
Nd----------	---	---	---	---	---	---	---	---	---
Sm ----------	---	---	---	---	---	---	---	---	---
Eu----------	---	---	---	---	---	---	---	---	---
Tb ----------	---	---	---	---	---	---	---	---	---
Yb ----------	---	---	---	---	---	---	---	---	---
Lu ----------	---	---	---	---	---	---	---	---	---

Hf, and Zr, and slightly less so with Th. Thus, it seems reasonable that all of these elements and probably Ta and Nb as well (see Wood, Joron, and Treuil, 1979) are controlled mainly by magmatic processes and are not significantly affected by alteration or weathering processes (see Menzies and others, 1977). On the other hand, the alkalis (K, Na, Ba) usually display poor correlations with the other determined incompatible elements, and it appears that they may be unreliable as petrogenetic indicators (see Pearce, 1983). Despite the wide range in bulk composition and the apparent influence of alkali metasomatism, it is notable that K_2O contents are generally low (<1 weight percent) in all of the rocks studied.

elements in rocks from plagiogranite suite of the Canyon Mountain Complex

below detection limit]

CM12	CM43	CMG174C	CMG190B	OC314	CMG137	CMG2	CMG55A	CMG191	OC114
Plagiogranite	Hornblende plagiogranite	Epidiorite (altered gabbro)	Hornblende diorite	Hornblende diorite	Tonalite	Tonalite	Trondhjemite	Trondhjemite	Trondhjemite
in weight percent									
74.45	77.42	59.40	62.30	59.40	61.10	67.30	69.70	71.90	76.00
0.30	0.10	0.44	0.65	0.90	0.65	0.55	0.50	0.36	0.21
12.45	11.72	15.10	14.20	14.90	16.30	16.10	15.80	15.50	13.80
1.27	0.85	---	---	---	---	---	---	---	---
1.96	1.06	6.06	7.67	7.26	8.30	5.54	4.22	3.31	1.56
0.07	0.04	0.13	0.16	0.18	0.18	0.18	0.10	0.07	0.06
0.85	0.34	7.91	4.90	4.84	3.71	0.94	1.12	0.60	0.38
2.37	1.16	6.62	5.47	6.28	5.31	3.30	3.29	3.65	1.04
5.49	6.01	3.62	4.54	4.71	4.41	5.00	4.40	3.91	5.99
0.17	0.08	0.11	0.56	0.40	0.26	0.40	0.98	0.48	0.15
0.04	0.01	---	---	---	---	---	---	---	---
1.30	0.68	---	---	---	---	---	---	---	---
0.15	0.12	---	---	---	---	---	---	---	---
0.01	0.08	---	---	---	---	---	---	---	---
100.88	99.67	99.39	100.45	98.87	100.22	99.31	100.11	99.78	99.19
in parts per million									
---	---	---	146	---	---	107	148	100	49
15	20	---	28	---	---	57	63	46	23
---	---	22.0	33.8	31.3	28.4	15.8	12.5	4.7	4.5
16	3	---	164	---	---	8	45	28	6
1	1	206	73	72	10	7.4	13	13	3
---	---	29.7	23.8	21.8	20.7	6.2	7.5	4.8	1.8
---	---	---	32	47	---	1	4	4	10
---	---	---	87	---	---	76	57	38	19
---	---	---	---	---	---	---	0.09	0.11	0.10
---	---	---	0.2	---	---	---	---	0.6	---
---	---	1.57	2.29	2.20	1.71	3.12	2.99	4.65	5.83
---	---	0.63	0.49	0.12	0.46	0.35	0.42	0.42	0.29
---	---	---	63	---	---	100	108	153	198
---	---	3.44	1.88	1.95	1.74	3.42	3.07	2.34	4.21
10	20	9.2	7.0	6.2	5.7	10.4	9.3	6.7	14.0
---	---	3.9	6.5	8.9	5.2	9.6	8.3	4.9	11.1
---	---	1.25	2.56	2.82	2.14	3.39	2.68	1.80	3.84
---	---	0.47	0.84	0.83	0.91	0.83	0.80	0.59	0.97
---	---	0.20	0.60	0.63	0.65	0.86	0.70	0.53	0.91
---	---	0.84	2.68	2.87	2.26	4.03	2.90	2.68	4.74
---	---	0.15	0.44	0.49	0.36	0.63	0.49	0.41	0.77

Considering the more reliable elements, it is clear that the least fractionated felsic rocks with the highest TiO_2 contents have lower incompatible-element contents than many of the basaltic rocks. This point is well illustrated in comparing chondrite-normalized rare-earth-element (REE) profiles for rocks of the Canyon Mountain Complex (fig. 1.12). This figure contrasts REE contents for a variety of mafic to felsic rocks, including the basaltic andesites and spilites. Despite evidence for selective alteration of some of these rocks, REE contents and relative abundances are broadly similar for the mafic rocks. From this observation, it appears that the REE have not been significantly mobilized and they should be useful for

TABLE 1.6.—*Analyses of major-element oxides and selected trace elements*

[---, not determined or

Sample	CMG15	CMG157A	OC214	OC224	OC241	OC243	CM1
Rock type	Quartz keratophyre	Plagioclase keratophyre	Plagioclase keratophyre	Quartz keratophyre	Keratophyre	Quartz keratophyre	Keratophyre
							Major-element oxides,
SiO_2	75.80	75.00	73.20	79.40	76.60	76.10	77.92
TiO_2	0.14	0.27	0.59	0.16	0.18	0.18	0.14
Al_2O_3	14.20	12.60	12.60	11.00	12.80	12.70	11.47
Fe_2O_3	---	---	---	---	---	---	1.17
FeO	2.70	3.94	5.75	1.73	3.21	3.82	0.60
MnO	0.10	0.07	0.15	0.04	0.04	0.10	0.02
MgO	0.25	0.49	2.56	1.01	0.24	0.52	0.31
CaO	0.56	0.83	0.77	0.97	1.50	0.52	0.82
Na_2O	6.23	6.19	5.09	5.10	5.49	6.07	5.85
K_2O	0.11	0.06	0.03	0.09	0.09	0.09	0.10
P_2O_5	---	---	---	---	---	---	0.02
H_2O^+	---	---	---	---	---	---	0.78
H_2O^-	---	---	---	---	---	---	0.23
CO_2	---	---	---	---	---	---	0.21
Total	100.09	99.45	100.74	99.50	100.15	100.10	99.64
							Trace elements,
Sr	72	49	23	83	---	27	---
Ba	20	10	8	38	---	7	10
Sc	9.7	13.3	18.4	8.7	11.9	15.0	---
V	2	---	72	8	---	11	6
Cr	19	15	44	4	3	22	2
Co	0.8	1.6	12.0	1.9	1.4	3.1	---
Ni	4	7	22	13	---	9	---
Zn	46	70	107	25	---	73	---
Ta	0.12	0.08	---	0.09	0.07	---	---
Nb	---	---	0.2	0.1	---	0.1	---
Hf	6.47	3.04	3.41	3.71	3.65	3.30	---
Th	0.16	0.18	0.16	0.39	0.16	0.21	---
Zr	225	98	123	120	---	108	---
La	4.25	2.57	2.11	1.93	3.04	3.29	---
Ce	14.3	7.8	8.2	7.8	11.5	10.4	10
Nd	14.9	7.9	8.6	6.9	---	11.3	---
Sm	5.07	2.99	3.42	2.71	3.58	3.67	---
Eu	0.72	0.82	0.77	0.38	0.85	1.08	---
Tb	1.37	1.00	0.96	0.89	0.88	0.98	---
Yb	6.80	3.86	4.04	4.08	3.48	4.37	---
Lu	1.02	0.58	0.64	0.64	0.64	0.68	---

petrogenetic purposes. Another striking feature of the data is the strong similarity between REE profiles for the mafic and the felsic rocks, with the exception that the latter have marginally higher La/Sm ratios and conspicuous Eu anomalies. The most unusual REE pattern obtained is for an altered gabbroic rock (the so-called epidiorite, sample CMG-174C) that displays significant depletion of heavy REEs.

COMPARATIVE GEOCHEMISTRY AND EVALUATION OF TECTONIC SETTING

Having established that most of the analyzed incompatible trace elements are likely to be representative of original magmatic abundances, it is of interest to determine the affinity of the mafic rocks of the Canyon Mountain Complex to other present-day

in keratophyres and quartz keratophyres of the Canyon Mountain Complex

below detection limit]

CM3	CM7	CM9	CM45	CM47	CM49	CM50	CM46
Keratophyre	Keratophyre	Keratophyre	Keratophyre	Quartz keratophyre	Quartz keratophyre	Quartz keratophyre	Quartz keratophyre
in weight percent							
75.98	73.62	75.98	74.82	78.52	75.72	74.32	77.22
0.14	0.22	0.15	0.17	0.10	0.16	0.21	0.10
11.53	12.94	12.12	12.44	11.13	11.91	12.18	11.83
1.12	1.77	1.36	1.14	0.74	0.80	1.36	0.65
2.27	1.52	1.19	1.98	0.89	1.73	2.05	1.08
0.07	0.04	0.03	0.08	0.02	0.06	0.08	0.04
0.53	0.68	0.40	0.45	0.52	1.02	0.50	0.64
0.74	1.64	1.49	1.64	0.61	0.32	1.63	0.29
5.58	5.89	5.63	5.81	6.07	6.44	5.38	6.39
0.43	0.32	0.25	0.06	0.06	0.09	0.08	0.07
0.05	0.05	0.01	0.01	0.01	0.01	0.02	0.01
0.94	0.78	0.85	0.98	0.68	1.01	1.36	0.72
0.17	0.15	0.16	0.14	0.14	0.20	0.19	0.17
0.07	0.04	0.23	0.18	0.23	0.14	0.24	0.36
99.62	99.66	99.85	99.90	99.72	99.61	99.60	99.57
in parts per million							
---	---	---	---	---	---	---	---
10	10	30	---	10	10	15	15
---	---	---	---	---	---	---	---
12	9	3	3	4	15	5	4
2	3	1	3	2	2	2	1
---	---	---	---	---	---	---	---
---	---	---	---	---	---	---	---
---	---	---	---	---	---	---	---
---	---	---	---	---	---	---	---
---	---	---	---	---	---	---	---
---	---	---	---	---	---	---	---
---	---	---	---	---	---	---	---
---	---	---	---	---	---	---	---
---	---	---	---	---	---	---	---
---	---	---	---	---	---	---	---
8	2	19	8	36	8	10	13
---	---	---	---	---	---	---	---
---	---	---	---	---	---	---	---
---	---	---	---	---	---	---	---
---	---	---	---	---	---	---	---
---	---	---	---	---	---	---	---
---	---	---	---	---	---	---	---

basaltic associations. Unfortunately, a similar comparison cannot yet be attempted either for the cumulate and ultramafic members of the complex, owing to insufficient data and because these rocks do not approximate magmatic liquids in composition, or for the felsic rocks, because of limited data and ambiguity of the available petrogenetic discriminators for such rock types (see Pearce and others, 1984).

Direct comparison of representative diabases and a basaltic andesite of the Canyon Mountain Complex with basaltic rocks from other environments is illustrated in figure 1.13, which shows incompatible-element abundances normalized to Wood's (1979) estimated primordial-mantle composition. Similar profiles are obtained by normalizing to estimated midocean ridge basalt (MORB) abundances (see Sun and Nesbitt,

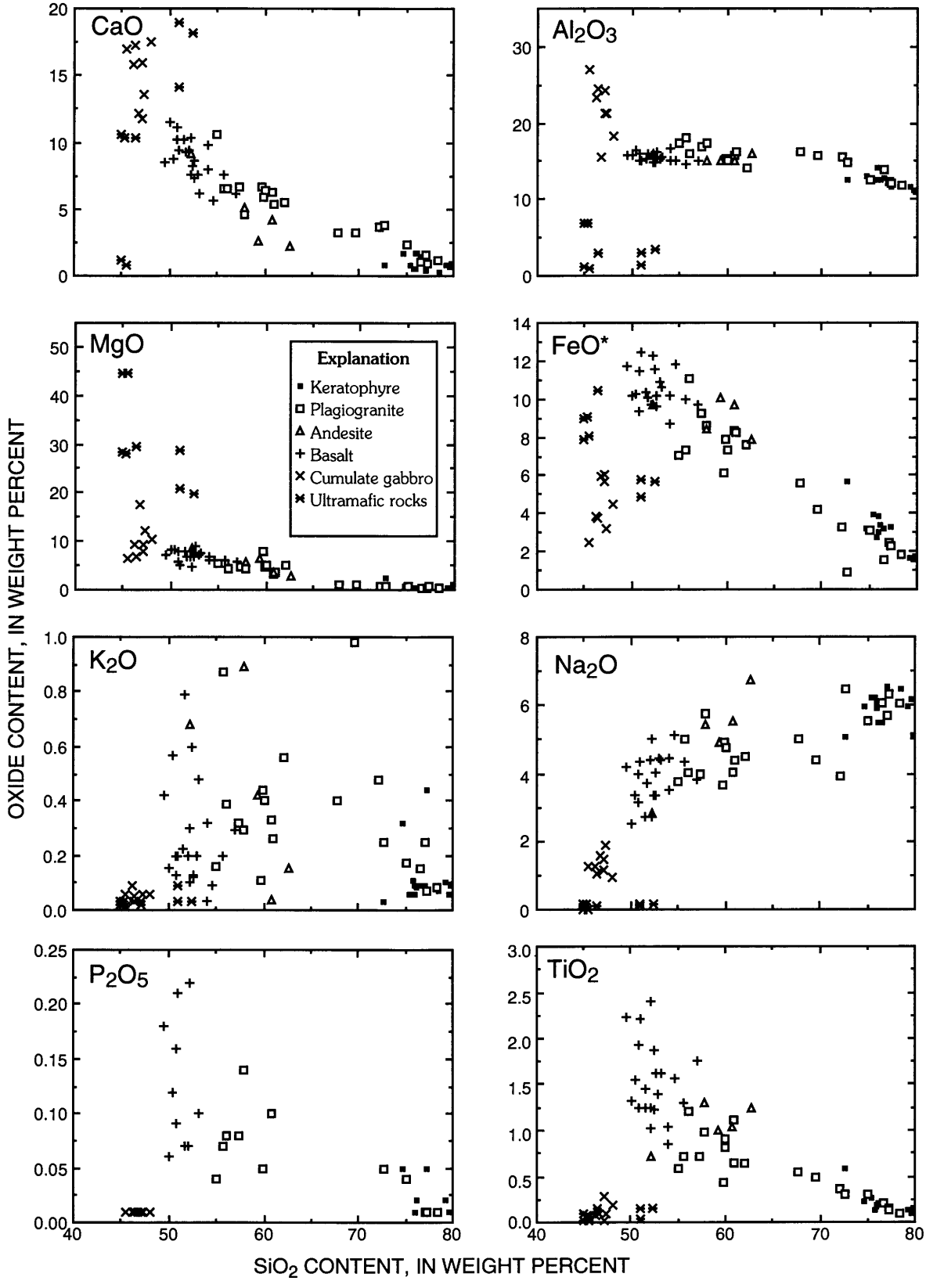

FIGURE 1.7.—SiO_2 variation diagrams for all analyzed rock samples of the Canyon Mountain Complex. FeO*, total iron as FeO.

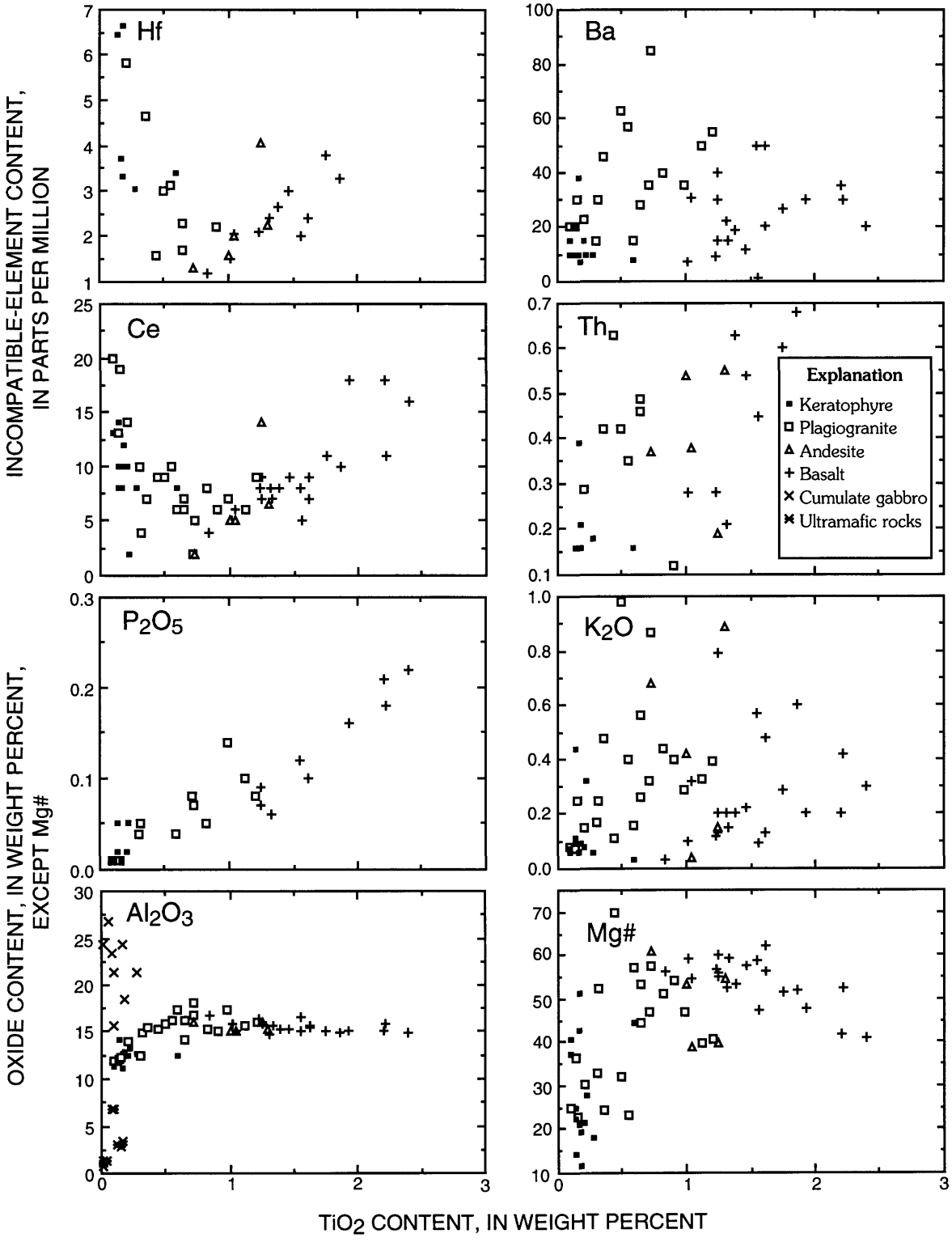

FIGURE 1.8.—TiO_2 variation diagrams for rocks of the Canyon Mountain Complex. Note that ultramafic rocks and cumulate gabbros are shown only in the Al_2O_3 plot to illustrate their distinction from the other rock types, which have near-liquidus or "magmatic" compositions. For clarity the ultramafic rocks and cumulate gabbros are omitted in all other plots. Mg# is percent of MgO/(MgO+FeO*) on molar basis.

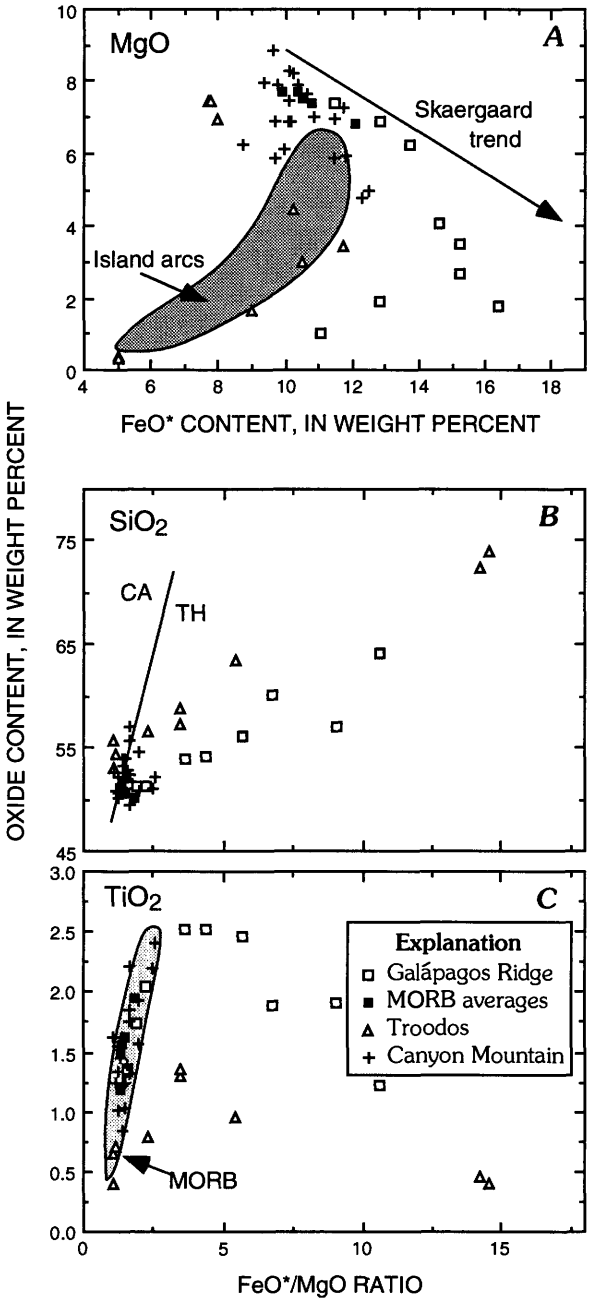

FIGURE 1.9.—Fe-Mg variations in basaltic rocks of the Canyon Mountain Complex compared to trends for average midocean-ridge basalts (MORB; Melson and others, 1976), lavas from the Galápagos Ridge (Perfit and others, 1983), and glasses from upper pillow lavas of the Troodos ophiolite (Robinson and others, 1983). FeO*, total iron as FeO. *A*, MgO versus FeO*. Canyon Mountain Complex and Troodos ophiolites both show only moderate Fe enrichment relative to Galápagos and Skaergaard rocks. Island-arc data field (stippled) and Skaergaard trend (arrow) are from Robinson and others (1983). *B*, SiO_2 versus FeO*/MgO ratio. Samples from all suites display only limited increase in FeO*/MgO ratio with increasing SiO_2; Canyon Mountain Complex samples straddle the calc-alkalic (CA)/tholeiitic (TH) boundary of Miyashiro (1973). *C*, TiO_2 versus FeO*/MgO ratio. Mafic samples of all suites, including the Canyon Mountain Complex, plot within the MORB data field (from Casey and others, 1985).

1977; Sun and others, 1979; Pearce, 1983). Other than anomalous spikes in Ba and K, the Canyon Mountain Complex basaltic andesite has a profile similar to those of the diabases (fig. 1.13*A*). Furthermore, excluding the epidiorite, all Canyon Mountain Complex mafic rocks display striking relative depletions in the light REEs, Nb, and Ta relative to the heavy REEs. All analyzed samples have relatively high ratios of K, Th, or Ba to Nb (or Ta), and the Hf-Zr-Sm segments of their profiles are slightly convex upward. Except for the Ba-Th-K-Nb segments, these profiles are similar to those of many MORBs as exemplified by a sample from the Ecuador Rift in the East Pacific (fig. 1.13*B*). For comparison, a sample of the Geotimes basaltic unit of the well-studied Semail ophiolite (Oman) closely resembles the MORB profile shown (except for a K spike). This particular basaltic unit has been interpreted as a fragment of oceanic crust; its K spike is explained by extensive

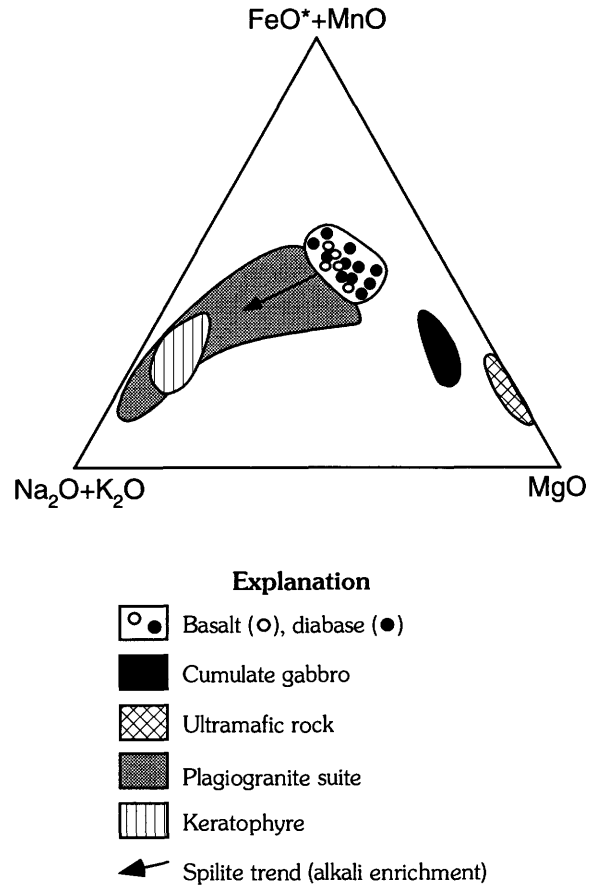

FIGURE 1.10.—A (Na_2O+K_2O)–F (FeO*+MnO)–M (MgO) ternary diagram for samples of the Canyon Mountain Complex. Basaltic and equivalent intrusive rocks (diabases, dolerites) overlap in composition and display only moderate Fe enrichment. Relatively evolved rocks (including basaltic andesite) and slightly altered rocks (spilite, epidiorite) plot in plagiogranite field; alkali enrichment trend (arrow) indicates effect of alteration.

alteration (Alabaster and others, 1982). The relative depletions of Nb (and Ta) seen in the Canyon Mountain Complex samples are uncharacteristic of MORB samples (Noiret and others, 1981) and suggest that the Oregon ophiolite perhaps formed in a setting other than near a midocean ridge.

Oceanic-island basaltic rocks (such as those found in Hawaii or Iceland) or intracontinental (within-plate) basaltic rocks generally are quite distinct in composition from ophiolitic basalts (see fig. 1.13*D*). The Salahi basalt unit, also part of the Semail ophiolite, is a possible exception (fig. 1.13*B*). This unit is interpreted as having formed at a seamount by Alabaster and others (1982), who viewed the Semail ophiolite as a composite body formed as tectonic conditions changed with time. Commonly characterized by low relative abundances of

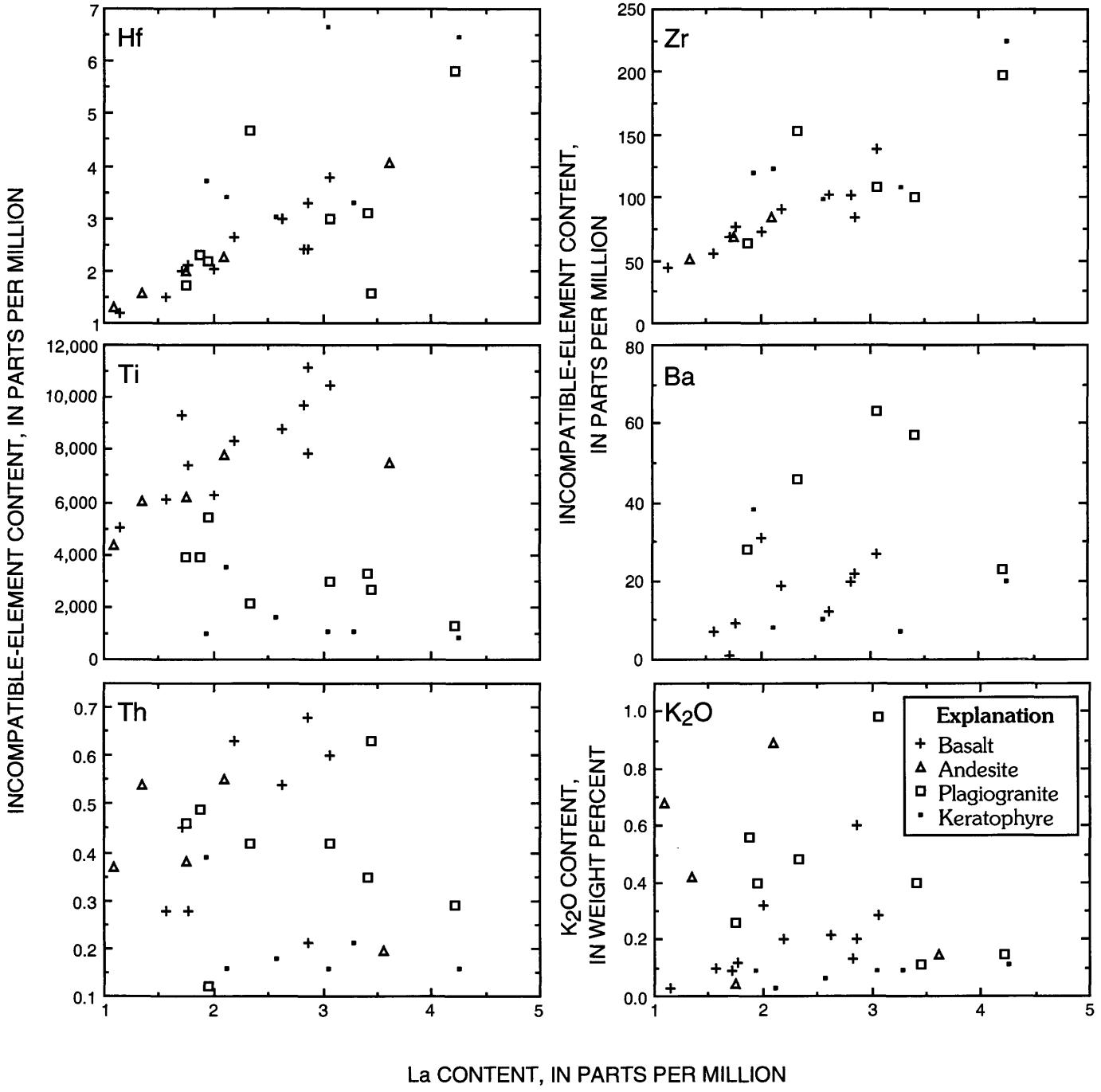

FIGURE 1.11.—La-variation diagrams for incompatible elements in magmatic rocks of the Canyon Mountain Complex.

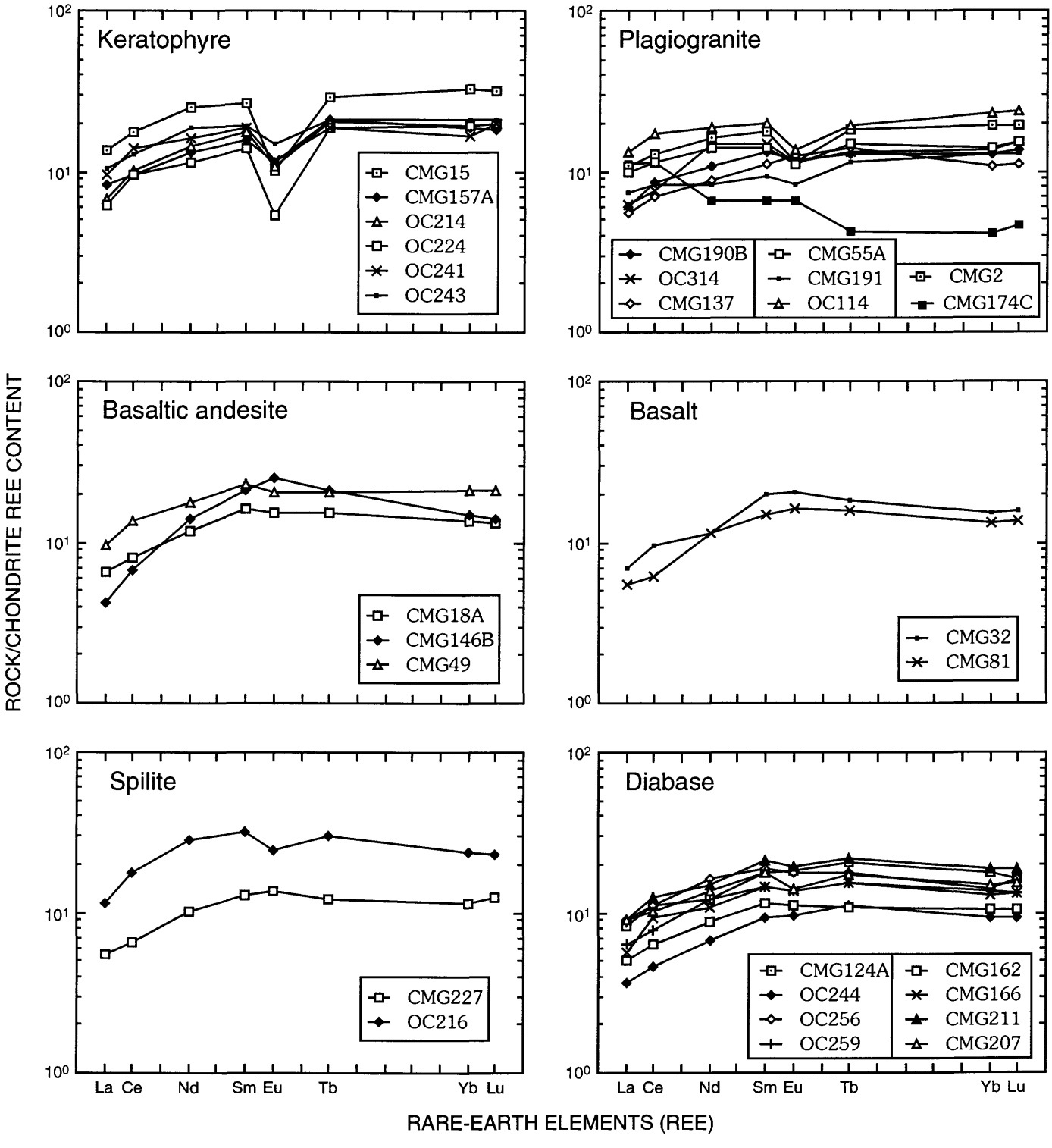

FIGURE 1.12.—Plots of rare-earth element (REE) contents of magmatic rocks of the Canyon Mountain Complex normalized to REE contents of chondrite meteorites; normalization values are from Sun and Nesbitt (1977). Note similarity of profiles for all mafic rock types (including basalt, diabase, basaltic andesite, and spilite). Most felsic rocks (plagiogranite and keratophyre) display significant negative Eu anomalies, and plagiogranites are slightly enriched in light REEs compared to the mafic rocks. Sample numbers are listed in explanation at lower right corner of each graph.

Nb and Ta, basalts from volcanic arcs associated with subduction processes appear to be the strongest analogs for basaltic magmas of the Canyon Mountain Complex; these are exemplified (fig. 1.13*C*) by samples from the Andean (Laguna Maule, Chile) and Aeolian (Salina, Italy) volcanic arcs, and similar rocks occur in some potassic volcanic provinces such as Vulsini (Italy).

Various other discriminant diagrams (figs. 1.14–1.16) have been proposed to elucidate the origin of basaltic magmas from different tectonic settings (see Pearce and Cann, 1973; Beccaluva and others, 1979; Wood, Joron, and Treuil, 1979; Noiret and others, 1981; Pearce, 1982; Shervais, 1982; Mullen, 1983b); these emphasize some of the details of the normalized abundance profiles seen in figure 1.13. Although these diagrams have little applicability to silicic magmas, data for both the mafic and felsic rocks of the Canyon Mountain Complex are plotted for comparison. In figure 1.14, the mafic rocks of the Canyon Mountain Complex plot within the island-arc basalt field of the Th/Yb–Ta/Yb plot, overlap both the MORB and island-arc basalt fields in the Ti–Zr plot, and lie largely within the MORB field of the V–Ti plot. Similar ambiguity is seen in figure 1.15, in which Canyon Mountain Complex samples resemble island-arc basalts in the Hf/Th–Ta/Th plot, but are transitional between island-arc basalts and MORB in the Cr–Yb and Ti/Cr–Ni plots.

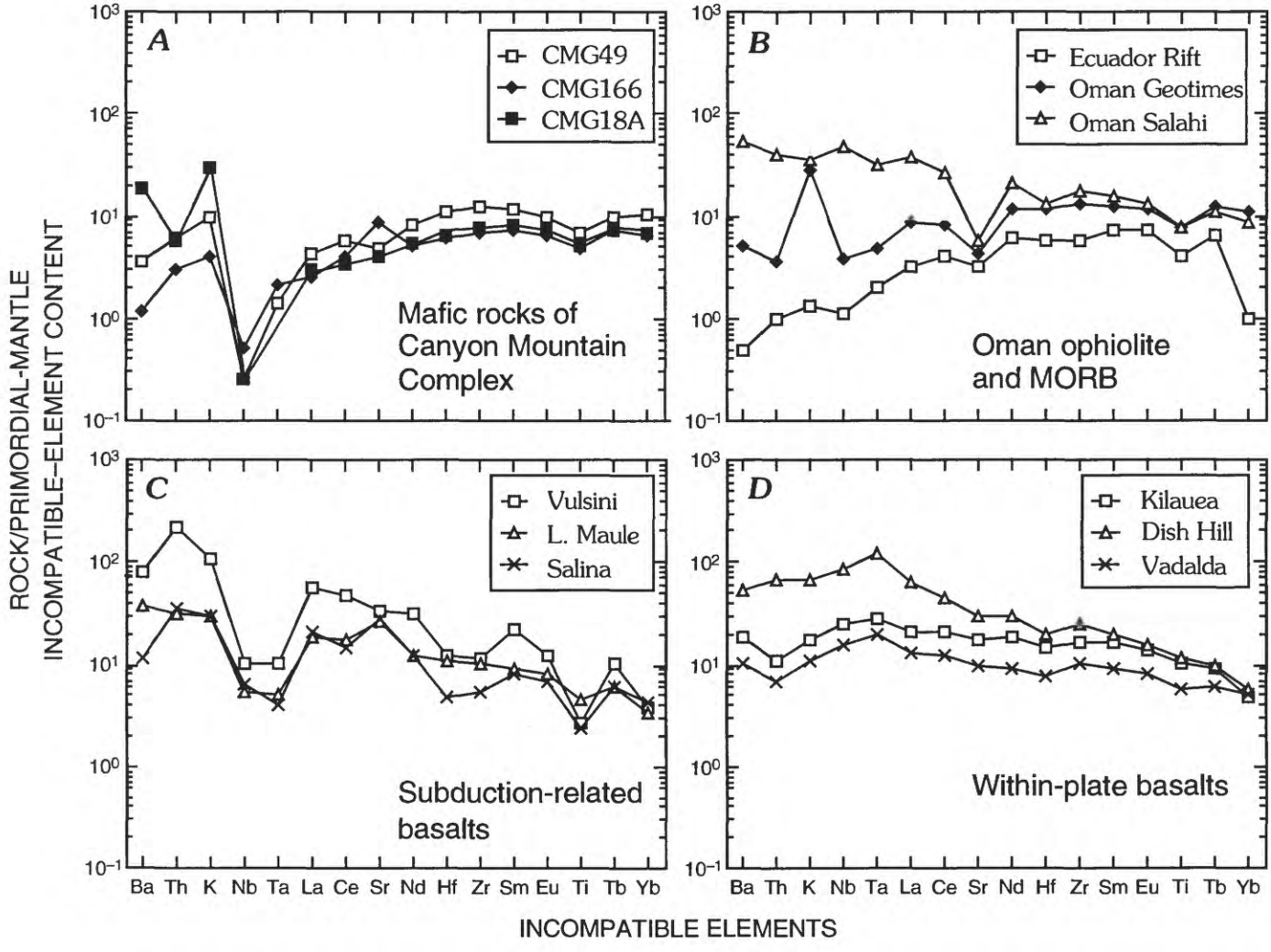

FIGURE 1.13.—Plots of incompatible-element contents normalized to incompatible-element contents estimated for primordial mantle (Wood, 1979). *A*, Mafic rocks from the Canyon Mountain Complex, including two diabases (CMG49, CMG166) and a basaltic andesite (CMG18A). Samples plotted for other tectonic settings: *B*, Oceanic basalts from Ecuador Rift midocean-ridge basalt (MORB) (Perfit and others, 1983) and Geotimes and Salahi basalts from Semail ophiolite, Oman (Alabaster and others, 1982). *C*, Subduction-related basalts from Vulsini (Rogers and others, 1985) and Salina Island (Ellam, 1986), Italy, and from Laguna del Maule (L. Maule), Chile (Frey and others, 1984). *D*, Within-plate basalts from Kilauea, Hawaii, and Dish Hill, California (Thompson and others, 1984), and from Vadalda, Iceland (Wood, Joron, Treuil, Norry, and Tarney, 1979).

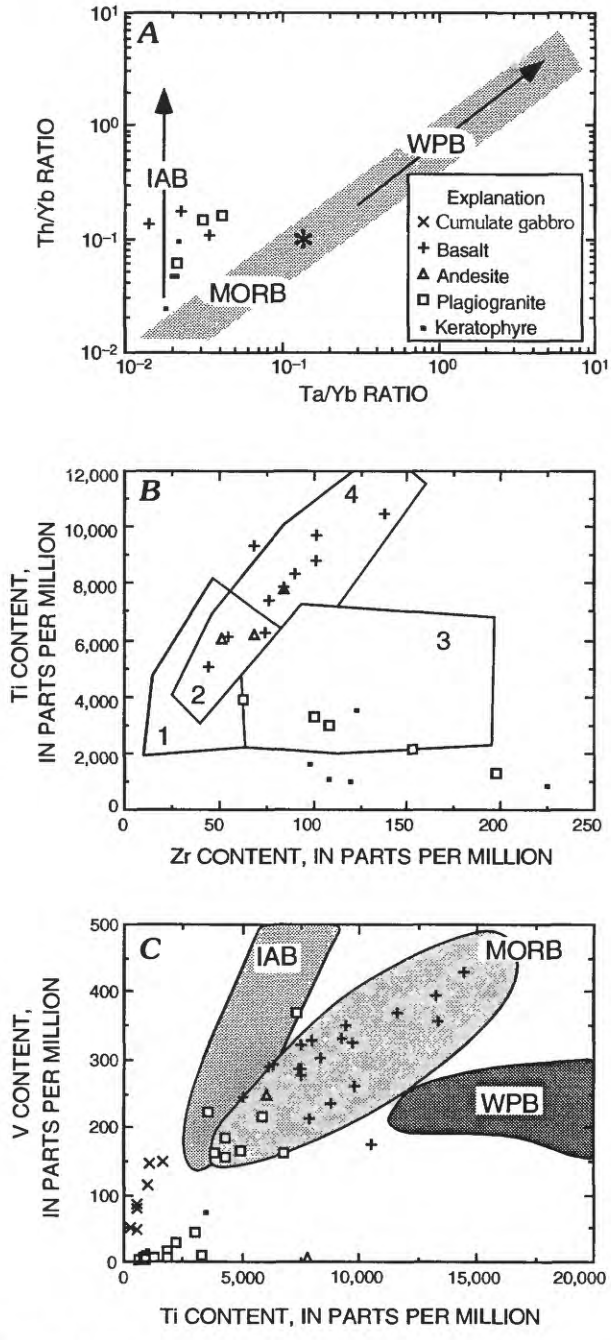

FIGURE 1.14.—Discriminant diagrams showing compositions of magmatic rocks of Canyon Mountain Complex relative to present-day volcanic suites: IAB, island-arc basalts; WPB, within-plate basalts; MORB, midocean-ridge basalts. *A*, Th/Yb versus Ta/Yb plot (from Pearce, 1982) shows estimated primordial-mantle composition (asterisk) and composition field for non-arc basalts (stippled band). Arrow labelled "WPB" indicates mantle enrichment trend typical of ocean-island (within-plate) magmatism; arrow labelled "IAB" indicates enrichment of Th relative to Ta characteristic of subduction-zone (island-arc) magmatism. *B*, Ti versus Zr plot (from Pearce and Cann, 1973); fields discriminate basalts from various tectonic settings: 1, island-arc tholeiites; 2, island-arc basalts and MORB; 3, calc-alkalic basalts; 4, MORB. *C*, V versus Ti plot (from Shervais, 1982).

The ternary discriminant diagrams shown in figure 1.16 again suggest that the basalts of the Canyon Mountain Complex are transitional in character. They

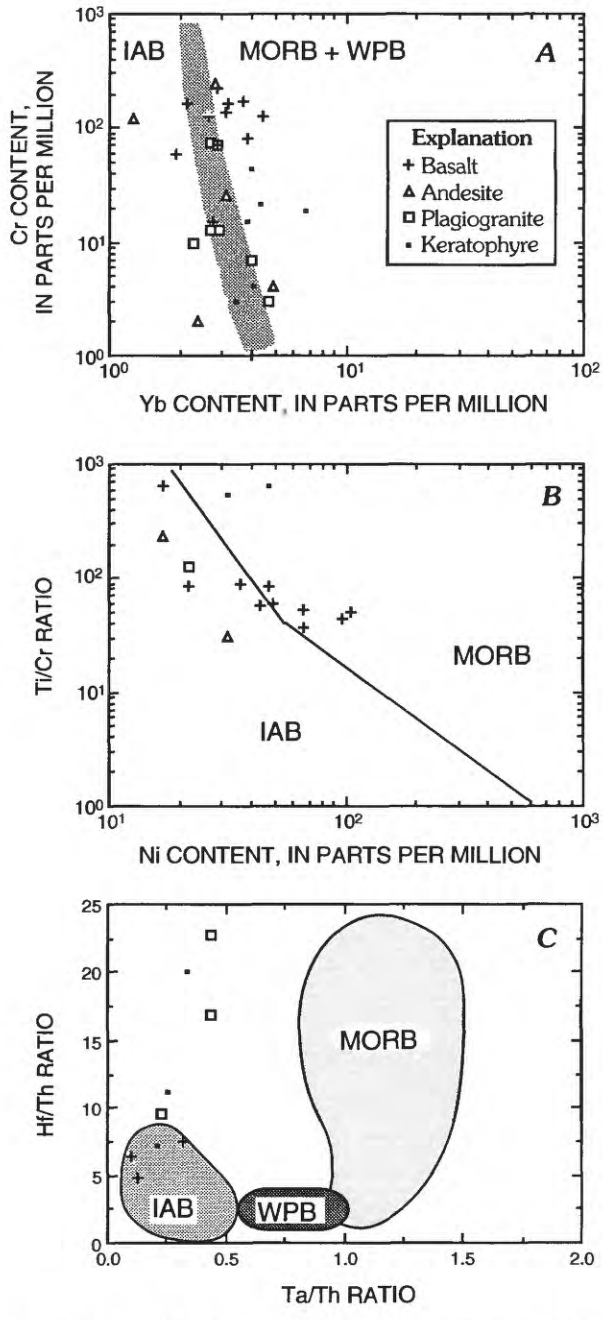

FIGURE 1.15.—Discriminant diagrams showing compositions of magmatic rocks of Canyon Mountain Complex relative to present-day volcanic suites. IAB, island-arc basalt; MORB, midocean-ridge basalt; WPB, within-plate basalt. *A*, Cr versus Yb plot adapted from Cr-Y diagram of Pearce (1982) assuming Y/Yb=10, which is typical of most basalts. Stippled area corresponds to overlap between IAB and MORB+WPB fields. *B*, Ti/Cr versus Ni plot (from Beccaluva and others, 1979). *C*, Hf/Th versus Ta/Th plot (from Noiret and others, 1981).

lie within the island-arc basalt field in the Th-Ta-Hf diagram but also partly overlap with MORB fields in the Zr-Yb-Ti and MnO-P_2O_5-TiO_2 diagrams. Despite the uncertainty of assigning specific tectonic settings solely on geochemical grounds, the distinct Nb-Ta depletion characteristic of rocks of the Canyon Mountain Complex is analogous to that documented in volcanic-arc rocks. Fortunately, this apparent affinity is compatible with geologic criteria, particularly with the large relative abundance of silicic hypabyssal rocks.

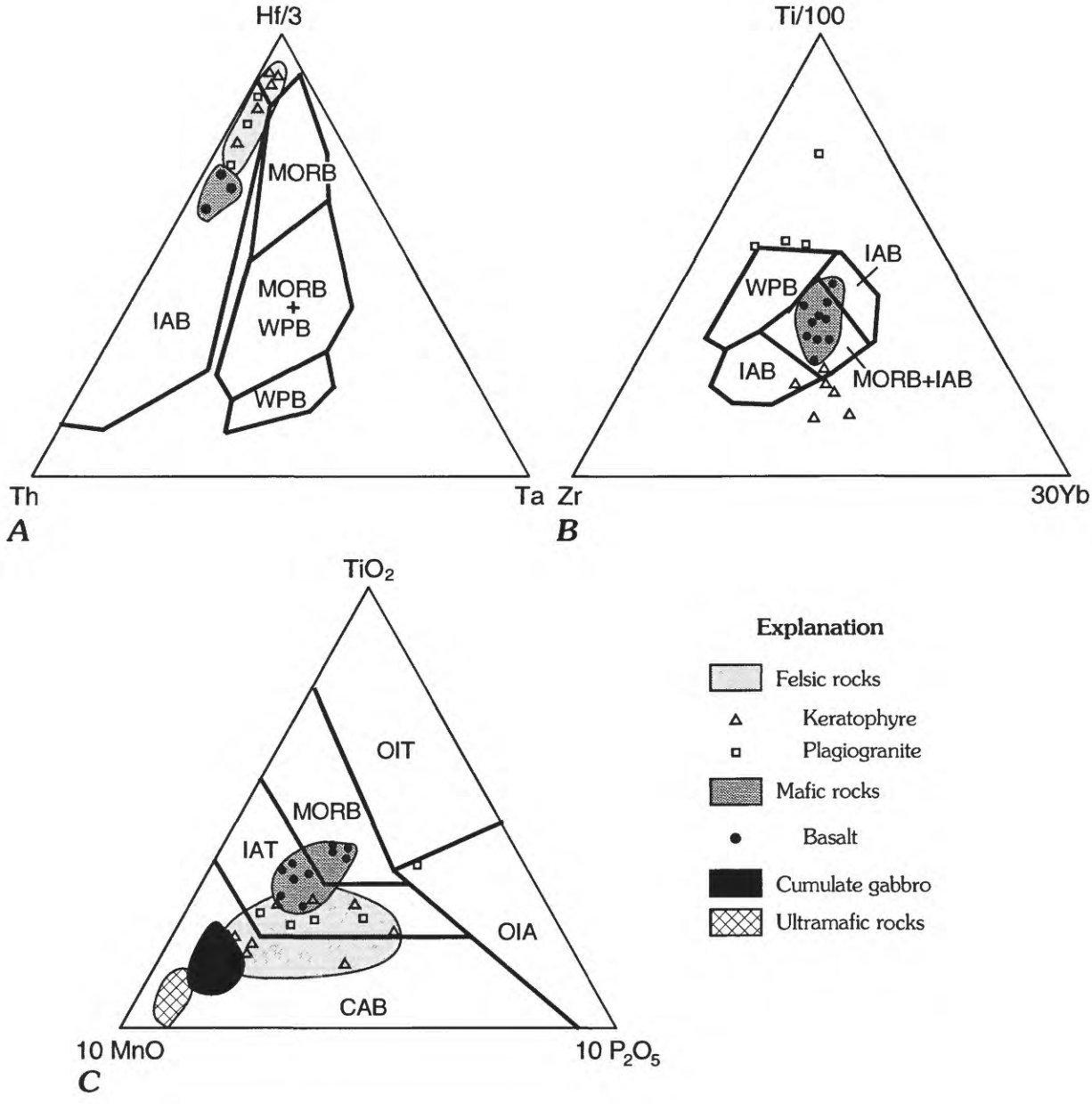

FIGURE 1.16.—Ternary discriminant diagrams for Canyon Mountain Complex magmatic rocks compared to basaltic rocks from other tectonic settings. CAB, calc-alkalic basalt; IAB, island-arc basalt; IAT, island-arc tholeiite; MORB, midocean-ridge basalt; WPB, within-plate basalt; OIT, ocean-island tholeiite; OIA, ocean-island alkalic basalt. *A*, Th-Ta-Hf diagram (from Wood, Joron, and Treuil, 1979). *B*, Zr-Ti-Yb diagram, modified from Pearce and Cann's (1973) similar diagram that used Y instead of Yb (see fig. 1.15). *C*, TiO_2-MnO-P_2O_5 diagram (from Mullen, 1983b). Ocean-island basalts are subdivided into OIT and OIA fields. Note that data fields for Canyon Mountain Complex cumulate gabbros and ultramafic rocks, used alone, can lead to confusion in assigning tectonic setting.

PETROGENETIC MODELS

Further insights into the origin and history of the Canyon Mountain Complex may be gleaned from consideration of the petrogenetic processes that produced its lithologic members. Very little detail is known about the petrogenesis of the tectonite and metacumulate members, but published information on mineral compositions (Himmelberg and Loney, 1980) and the general characteristics of these units suggest that they may well represent a partial section of oceanic lithosphere. There is also relatively little information on the cumulate and intrusive gabbros. They clearly represent a phase of magmatism that occurred after deformation of the structurally lower parts of the complex. On the basis of clinopyroxene analyses (Himmelberg and Loney, 1980) and mineral-melt partition coefficients (see Elthon and Casey, 1985), the magmas that precipitated the cumulates apparently had Na_2O and TiO_2 contents not unlike those of some of the mafic dikes in the sheeted member. Nevertheless, as pointed out earlier, the phenocrysts in these dikes differ substantially in composition from the minerals in the cumulate rocks. Thus, it is probable that these two members are unrelated, in which case the basaltic magmas of the sheeted member must represent a distinct phase of magmatism.

Finally, there is the problem of the plagiogranite-keratophyre suite. The majority of keratophyres appear to have formed as a hypabyssal sequence, probably in an island arc, prior to emplacement of the Canyon Mountain Complex (Gerlach, Avé Lallemant, and Leeman, 1981). However, published $^{40}Ar/^{39}Ar$ age determinations (Avé Lallemant and others, 1980; this chapter) and our field studies suggest that the diverse magmas of the sheeted member formed as part of the same magmatic phase at approximately 262 Ma. In contrast, the maximum U-Pb zircon age of about 278 Ma for an intrusive gabbro high in the cumulate-gabbro sequence (Walker, 1986) suggests that they formed during an earlier magmatic phase. Thus, available data imply that the Canyon Mountain Complex consists of at least two mafic-ultramafic magmatic suites separated by a significant time interval (perhaps as much as 15 m.y.). Furthermore, the geochemical data summarized earlier demonstrate that the plagiogranites (and minor keratophyres) are unlikely to be strictly cogenetic with the contemporaneous basaltic magmas despite their mutually intrusive relations in the sheeted member. Examination of the petrogeneses of these two roughly coeval groups of magmas provides insight into the conditions under which they formed.

PLAGIOGRANITE SUITE

The origin of the plagiogranites and keratophyres of the Canyon Mountain Complex was discussed by Gerlach, Leeman, and Avé Lallemant (1981), so only their essential arguments are repeated here. Silicic lavas (low-K_2O dacites to rhyodacites) are found at certain oceanic spreading centers; in some cases these appear to be extreme differentiates of MORB-like magmas (Sinton and Byerly, 1980; Clague and others, 1981; Perfit and others, 1983). It has been proposed that plagiogranites in ophiolites represent hypabyssal equivalents of such magmas (Coleman and Peterman, 1975; Kay and Senechal, 1976; Pallister and Knight, 1981). Whereas this may be a reasonable model in many cases, the fact that mafic and felsic rocks of the Canyon Mountain Complex have overlapping REE profiles and contents of several other incompatible elements such as Hf, Th, Ta, and Nb (figs. 1.8, 1.11, 1.12, 1.17; tables 1.4–1.6) effectively precludes such a simple cogenetic link between the two magma types. Figure 1.17 illustrates REE variations that result from fractionation of basaltic magmas to rhyodacitic differentiated liquids at the Galápagos spreading center (Clague and others, 1981; Perfit and others, 1983) and in the Troodos ophiolite (Kay and Senechal, 1976). In contrast, in the Canyon Mountain Complex $(La/Yb)_n$ and Yb_n values are similar in the basaltic and felsic rocks.

Compositional variations for relatively immobile major and trace elements appear to be coherent within both the mafic and silicic suites (figs. 1.7, 1.8), and are somewhat consistent with the operation of fractional-crystallization processes. However, as discussed earlier in this chapter, inconsistencies in incompatible-trace-element abundances and compositional trends for the two suites indicate that they cannot have been derived from a common parental magma. Alternatively, on the basis of experimental studies, Dixon and Rutherford (1979) proposed that some plagiogranites form by means of liquid immiscibility. We consider this process to be insignificant for the Canyon Mountain Complex because the required element partitioning between mafic and felsic liquids is inconsistent with that actually observed (Gerlach, Leeman, and Avé Lallemant, 1981). Furthermore, the dominance of felsic rocks in the Canyon Mountain Complex is inconsistent with either fractional crystallization or liquid immiscibility.

It was proposed instead that the felsic magmas formed as a result of extensive partial melting of hydrated (that is, amphibole-bearing) mafic rocks in the underlying crust (Gerlach, Leeman, and Avé Lallemant, 1981). Although this model cannot be uniquely

quantified, it is consistent with available experimental studies on melting of various basaltic compositions in the presence of high water contents (Holloway and Burnham, 1972; Helz, 1976; Spulber and Rutherford, 1983; Rapp and others, 1991) in that compositions of the experimentally produced liquids approximate those of natural plagiogranites. Assuming single-stage batch melting at low to moderate pressure (<5 kb) and at partial water pressure less than or equal to total pressure, Gerlach, Leeman, and Avé Lallemant (1981) demonstrated by inverse modeling that REE profiles in the required plagiogranite sources are likely to resemble those in the mafic rocks of the Canyon Mountain Complex and in many other ophiolites. This process presumably is driven by convective heating associated with the emplacement of basaltic magmas. The availability of aqueous fluids is a critical feature of the model and can be accommodated either by hydrothermal convection in the shallow crust in areas of crustal extension (Gregory and Taylor, 1979) or by subduction processes that provide access of fluids or water-bearing magmas (see Pearce, 1982). The depth of partial melting is uncertain but, judging from the exposed stratigraphic section, the main plagiogranite bodies were emplaced at a minimum depth of 5 km. Although

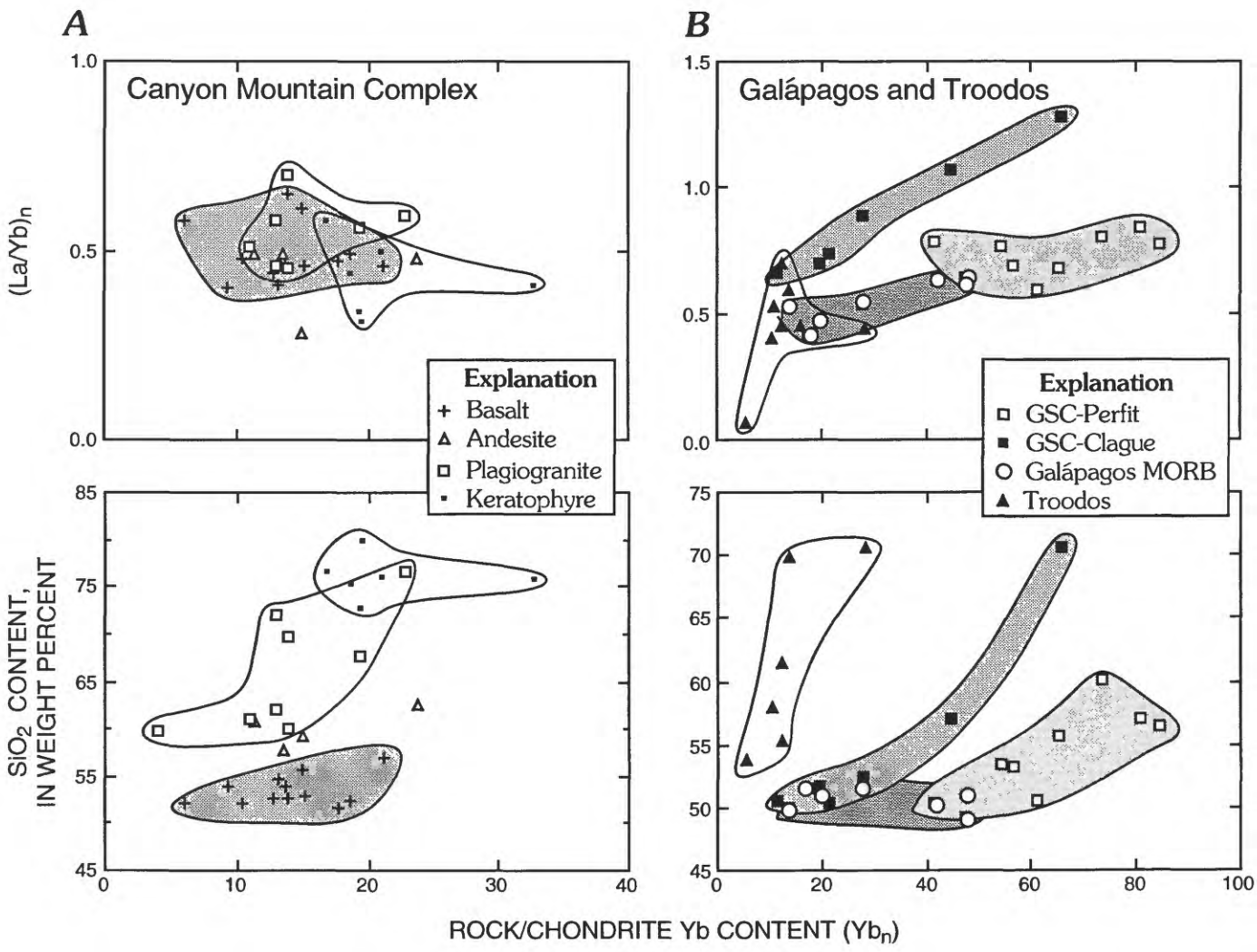

FIGURE 1.17.—Rare-earth element (REE) fractionation in *A*, magmatic rocks of the Canyon Mountain Complex and *B*, Troodos ophiolite (Kay and Senechal, 1976) and midocean-ridge basalt (MORB) and differentiated lavas from Galápagos spreading center (GSC) (Clague and others, 1981; Perfit and others, 1983). Plots of chondrite-normalized La/Yb and Yb abundances illustrate REE fractionation; values of $(La/Yb)_n=1$ and $Yb_n=1$ correspond to chondritic relative abundances of REE (that is, flat profiles). Variation of SiO_2 with Yb_n illustrates the range in bulk rock compositions. Yb_n may be variably enriched depending upon details of crystallization process. Because La is more incompatible than Yb in such magma suites, $(La/Yb)_n$ ratio should increase significantly during fractionation, as is the case in both Troodos and Galápagos rocks. Note difference in scale for both $(La/Yb)_n$ and SiO_2 in parts *A* and *B* of figure.

there is field evidence for hydrothermal alteration of wallrocks near these bodies and even for limited in situ melting (for instance, leucocratic segregations in hornblende-rich rocks that may be altered basalt or gabbro), the primary partial-melting zone must have been at a greater structural depth than is presently exposed. An attractive feature of this model is that it can account for the contemporaneity of the mafic and felsic magmas and the common observance of plagiogranite intruding gabbro and basalt in the upper part of the complex.

The thick section of keratophyres in the uppermost part of the Canyon Mountain Complex is believed to represent a slightly older or possibly coeval subvolcanic pile into which the plagiogranites and associated mafic magmas were emplaced (Gerlach, Avé Lallemant, and Leeman, 1981). Because the keratophyres are compositionally and mineralogically similar to the most evolved rocks of the plagiogranite suite (trondhjemites), it is possible that keratophyre magmas (or their precursors) had a similar origin. Allowing for metasomatic effects (Na gain or K loss), the geochemical features of these rocks (such as low Ta and Nb despite their evolved compositions), their porphyritic texture, and the common occurrence of plagioclase and quartz phenocrysts (indicative of originally dacitic to rhyodacitic magmas) suggest that the keratophyres formed in an island-arc environment.

MAFIC ROCKS

Mafic rocks of the sheeted member are dominantly basaltic. Their major-element compositions may be compared in some detail with those of volcanic rocks from the Galápagos Ridge (Perfit and others, 1983), average MORB compositions (Melson and others, 1976), and fresh glasses from the Troodos ophiolite (Robinson and others, 1983) by juxtaposing SiO_2 and MgO variation diagrams (figs. 1.18, 1.19) for these rocks. Although there is some scatter in the Canyon Mountain Complex analyses, many clearly resemble MORB analyses with respect to MgO, P_2O_5, TiO_2, FeO* (total Fe as FeO), and Al_2O_3. The relative depletion in CaO and variable enrichment in Na_2O and K_2O compared to MORB averages are attributed to postemplacement alteration. Such patterns of alteration are not unusual for ophiolitic basalts (see Hopson and Frano, 1977; Vallier and Batiza, 1978; Schminke and others, 1983). Unfortunately, even minor modification of major-element compositions precludes use of detailed mass-balance methods of petrogenetic modeling. We can, however, use data for the more immobile trace elements to evaluate the relative importance of fractional crystallization and partial-melting processes in producing these magmas.

Two fundamental questions concern (1) whether the various mafic magmas are cogenetic, and (2) whether they are related to the lower parts of the complex (such as the undeformed isotropic or layered gabbros). The first question can be assessed through inspection of figures 1.8, 1.11, and 1.20. In general, the basaltic rocks define strong coherent trends among such elements as Ti, P, Zr, Hf, LREEs, and to a lesser extent Th. For some of the analyzed samples, even Ba and K correlate well with these other incompatible elements. This correlation is notably poorer for some of the basaltic andesites and spilites, which are presumably altered to varying degrees. Although not shown in detail, there is antithetic depletion of compatible transition elements with increasing incompatible-element contents throughout the suite of rocks composing the Canyon Mountain Complex (see figs. 1.18 and 1.19).

A simple test of coherent fractionation involves comparison of relative enrichment factors for the immobile trace elements (Saunders and others, 1980), which should correlate systematically with degree of fractionation in a cogenetic magma suite. Because phenocryst-magma distribution coefficients (D) for the incompatible trace elements are very low in magnitude (much less than 0.1), during crystallization in closed magma systems these elements tend to be enriched in the residual liquids in inverse proportion to the fraction of original liquid remaining at any given stage. Thus, for a suite of cogenetic derivative liquids, if the incompatible-trace-element abundances are normalized to those in a relatively primitive liquid, such normalized ratios should be highly correlated for equally incompatible elements (that is, those with similar D values). Such relationships for representative elements in the Canyon Mountain Complex mafic rocks (normalized to elemental abundances in a relatively unfractionated diabase, sample CMG162) are shown in figure 1.20. Normalized Ce values (Ce_n) are comparable to those for other light REEs, Zr, and Hf. Ce appears to be slightly enriched relative to TiO_2, Eu, and Yb; this behavior is consistent with the relative D values characteristic of these elements (see Frey and others, 1978). Similar plots are shown for Ba and K_2O to illustrate their anomalously large (alteration-related) enrichments relative to those expected for closed-system fractionation. Finally, the surprisingly unsystematic behavior of Th may partly reflect analytical uncertainties. In general, the behavior of the immobile incompatible elements implies cogenetic relations among most of the mafic rocks. In detail, however, there are inconsistencies and irregularities

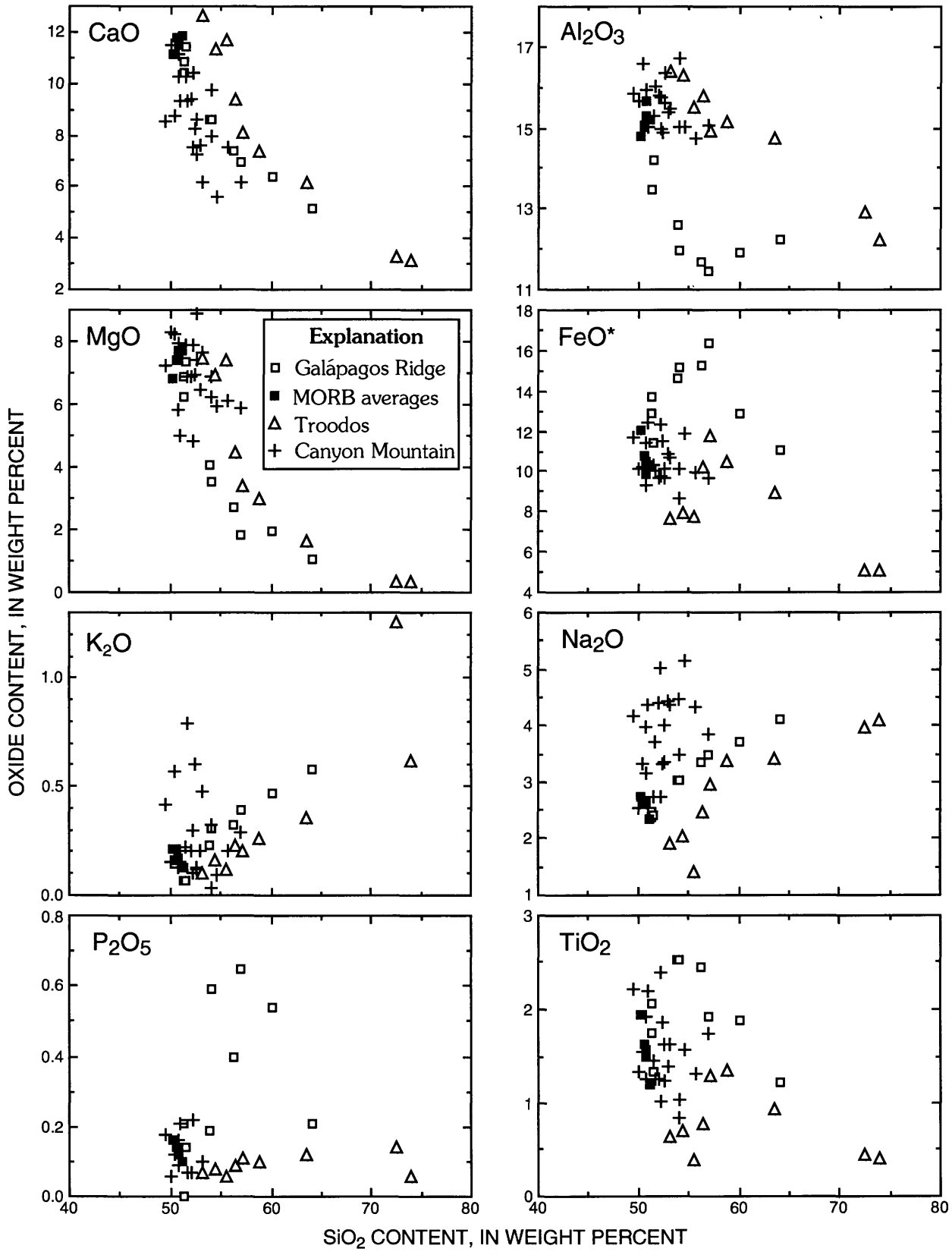

FIGURE 1.18.—Silica variation diagrams for basaltic rocks from the Canyon Mountain Complex contrasted with average mid-ocean-ridge basalt (MORB) compositions (Melson and others, 1976), glasses from the Troodos ophiolite (Robinson and others, 1983), and selected lavas from the Galápagos Ridge spreading center (Perfit and others, 1983). FeO*, total Fe as FeO.

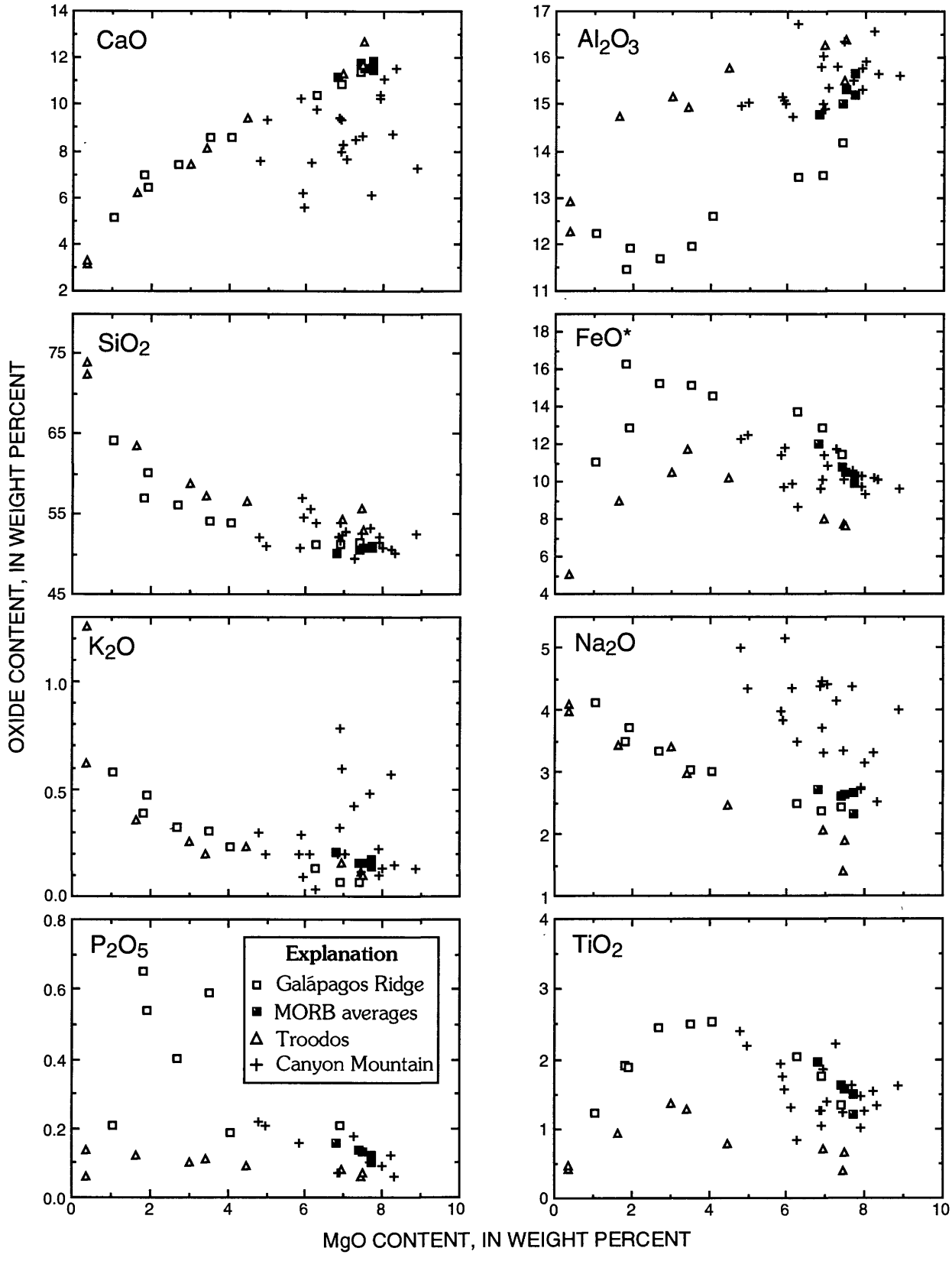

FIGURE 1.19.—MgO variation diagrams for basaltic rocks from the Canyon Mountain Complex; other samples as given in previous figure. FeO*, total Fe as FeO.

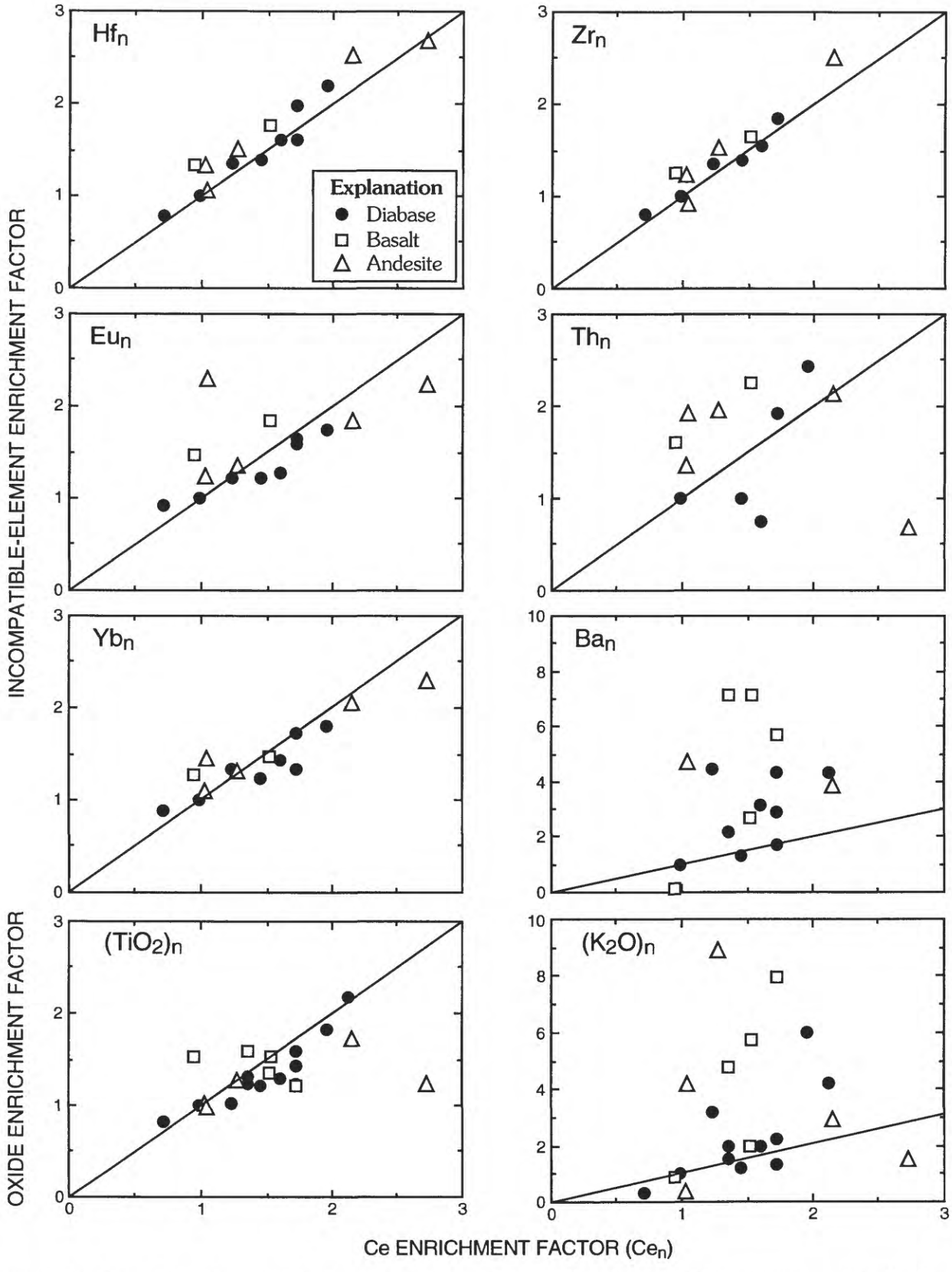

FIGURE 1.20.—Covariation of incompatible elements in mafic rocks of the Canyon Mountain Complex; incompatible-element contents of each sample are normalized to their abundances in diabase sample CMG162. Closed-system fractionation of liquidus phases (olivine, pyroxenes, plagioclase) from basaltic magmas causes equivalent enrichment of these elements such that normalized abundances will theoretically follow the equiline in each plot. (See section "Mafic Rocks" for discussion.)

between the behavior of these and the more compatible (such as transition metal) elements. It is not clear to what extent these reflect varied metasomatic and (or) alteration effects as opposed to the emplacement of distinct and unrelated batches of magma within the sheeted member.

The second question, concerning possible relations between Canyon Mountain Complex mafic magmas and gabbroic rocks, cannot be resolved definitively in this study due to insufficient data. Trace-element data for a single cumulate troctolitic gabbro (approximate mode is $plag_{75}ol_{25}opx_5$; sample OC277, table 1.3), show that it is characterized by very low REE abundances except for a striking positive Eu anomaly (fig. 1.21). Assuming that this rock is a cumulate cognate to typical basaltic rocks of the sheeted member, we used the method of Shaw (1970) to model REE profiles of hypothetical parental liquids required for compositional mass balance between the troctolite and several basaltic rocks chosen as possible fractionated liquids. The choice of liquid composition is not very critical because REE profiles are rather uniform for the basalts. Representative model profiles are shown in figure 1.21. Despite the latitude in choice of model parameters, we conclude that the parental liquids had significant positive Eu anomalies if the troctolite precipitated from the sheeted member basaltic magmas. On the other hand, Bishop (chap. 4, this volume) analyzed several intrusive noncumulate gabbros that have REE profiles roughly subparallel to, but less enriched than, those of the basalts. The gabbros she analyzed clearly have no cumulate relation to the basaltic rocks. They could possibly represent more primitive precursor magmas, but to test this hypothesis requires a combination of data not yet available to us. For example, the discrepancy in pyroxene compositions between analyzed basalts and gabbros must somehow be resolved before cogenetic links can be demonstrated.

Another question related to the petrology of the mafic rocks (or their parental magmas) concerns their ultimate source. We consider an origin by partial melting within the mantle to be quite reasonable, but inverse modeling of the REE data can provide more specific constraints on the required characteristics of the mantle source rocks. Using both equilibrium- and fractional-melting equations (Shaw, 1970) and a reasonable range in partition coefficients (Leeman and others, 1977; Frey and others, 1978), we have estimated the compositions of a variety of possible source rocks. We considered three bulk lithologies: spinel lherzolite (mode: $ol+opx_{75-85}cpx_{25-15}$), feldspathic lherzolite ($ol+opx_{65-75}cpx_{15-20}plag_{10-20}$), and garnet lherzolite ($ol+opx_{75}cpx_{20-22}gt_{5-3}$). Other aspects of the calculations follow Leeman (1976) and Leeman and others (1977).

A representative set of models is illustrated in figure 1.22. In these models it was assumed that the analyzed basaltic rock had undergone as much as 25 percent fractionation of olivine between the melt-extraction stage and emplacement in the sheeted member. Corrections for this effect lower the REE contents of the hypothetical parental magma, but have no effect on its relative REE abundances. From this assumed range of liquid compositions, we calculated

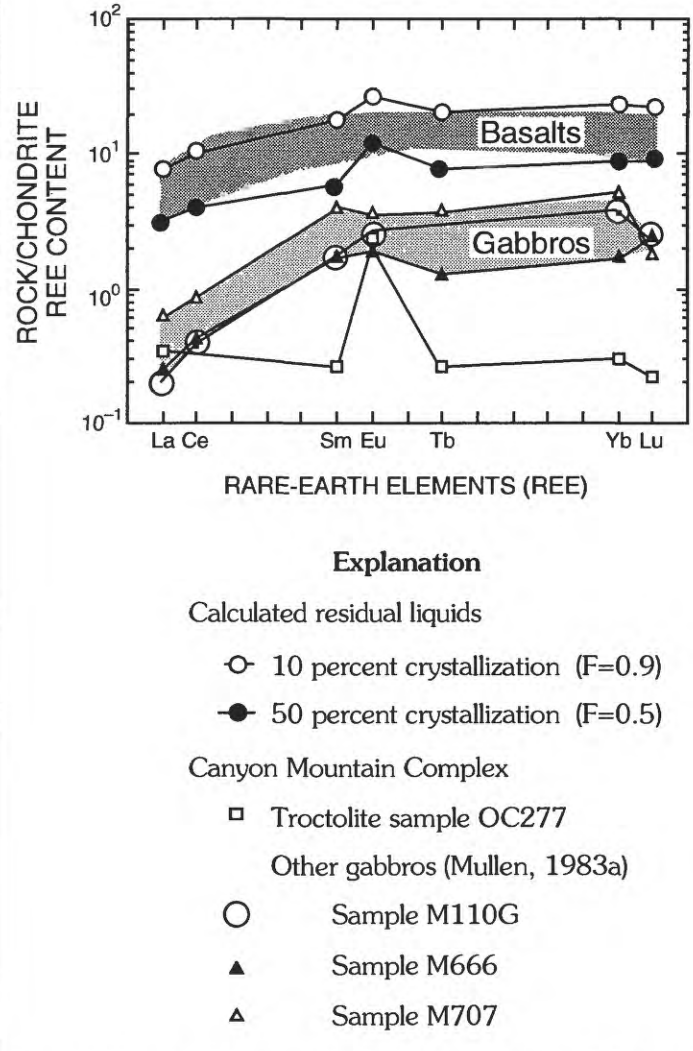

FIGURE 1.21.—Chondrite-normalized rare-earth element (REE) plot showing patterns for calculated parental magmas that can produce troctolite cumulate (such as sample OC277) by either 10 percent or 50 percent fractional crystallization. Except for their positive Eu anomalies, these patterns are similar to the range for basaltic rocks of the Canyon Mountain Complex (stippled band). Shown for comparison are three gabbro samples analyzed by Mullen (1983a). F, fraction of original liquid remaining.

REE profiles required for the sources and residues corresponding to formation of between 2 and 25 percent melt. Ranges in these compositions, shown in figure 1.22, illustrate that the source for the basaltic magmas was strongly depleted in light REEs, regardless of which model peridotite lithology is adopted; details of the modeling have only second-order influence on this conclusion. It appears that this source essentially resembles that which produces MORB and that this source has heavy-REE contents of about 1 to 5 times chondritic abundances.

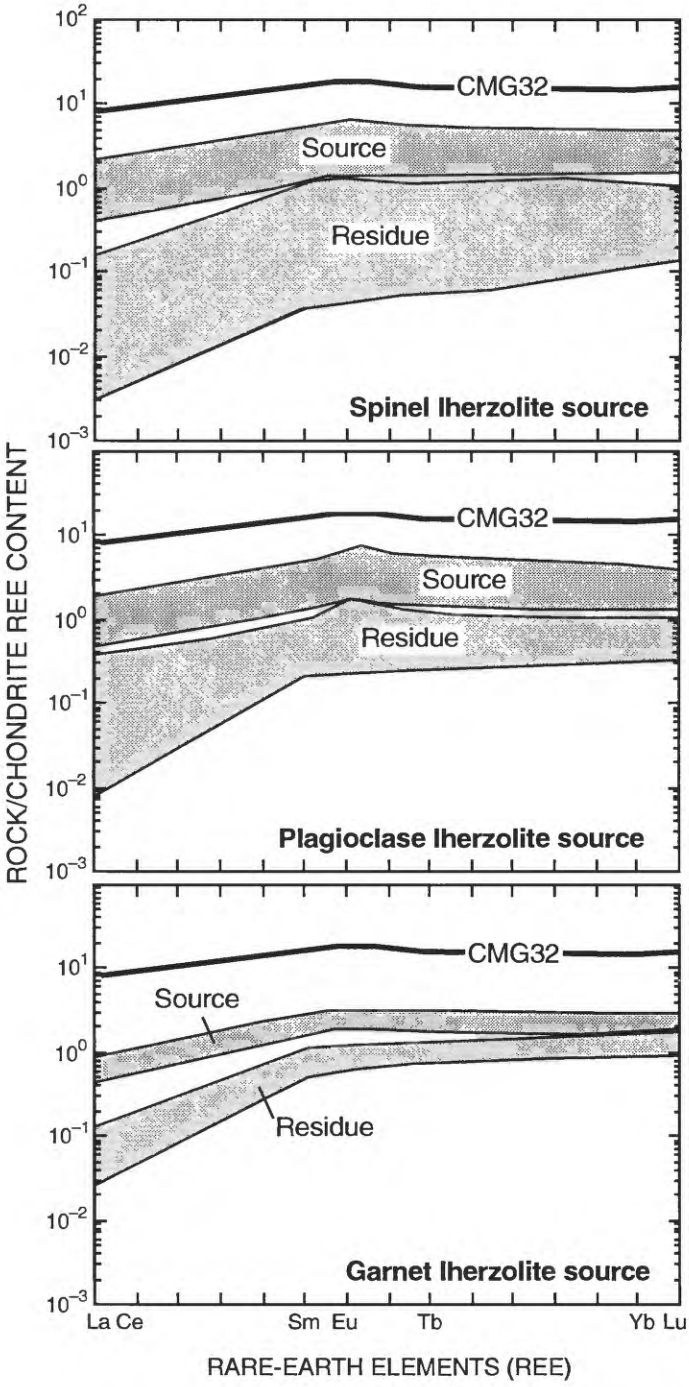

◄ FIGURE 1.22.—Chondrite-normalized rare-earth element (REE) plot (heavy solid line) for representative basalt sample (CMG32) from the Canyon Mountain Complex, and results (shaded areas) of partial melting calculations. Reasonable ranges are shown for calculated hypothetical source rocks (Source) and ultramafic residue (Residue) after melt extraction (see Shaw, 1970). Model spinel, plagioclase, and garnet lherzolites were used to represent source-rock mineralogy at a range of depths appropriate to melting. Shaded areas represent range in calculated REE contents resulting from varied degrees of melting (2–25 percent) and a range in partition coefficients (see Leeman and others, 1977; Frey and others, 1978). As degree of melting increases, source composition approaches that of the liquid. Despite wide latitude in these calculations, a source strongly depleted in light REEs is required to produce the REE profiles characteristic of mafic rocks from the Canyon Mountain complex.

SUMMARY

The principal results and conclusions derived from our petrogenetic and geochemical studies are listed below. They should be considered with the caveats that we have focused our studies primarily on the upper parts of the Canyon Mountain Complex and that much remains to be learned about the petrogenesis of the ultramafic and gabbroic parts of the complex.

(1) The effects of chemical alteration in Canyon Mountain Complex rocks are sufficiently minor (when care is taken to obtain good samples) that for many elements significant information is retained concerning original magmatic compositions.

(2) The basalts underwent different degrees of fractionation and were derived from distinct batches of unrelated magma emplaced at different times. For the Canyon Mountain Complex as a whole, a minimum of three phases of basaltic magmatism can be recognized on the basis of field and (or) geochemical criteria; these magmatic phases separately produced the deformed metacumulates (earliest phase), the undeformed (or only partly deformed) layered cumulate gabbros, and the intrusive isotropic gabbros. The sheeted member may also represent distinct phases of magmatism.

(3) A cogenetic relationship between sheeted-member basaltic rocks and the gabbros of the undeformed part of the complex is tenuous and unresolved at this time because of limited mineralogical and geochemical constraints.

(4) Basalts in the upper part of the complex crystallized from magmas formed by partial melting of a light-REE-depleted source like that which produces

MORB, except for the notable depletion of both Nb and Ta (whose concentrations approach analytical detection limits). Such depletion is very unusual for MORB and suggests, instead, an island-arc petrogenesis. Light-REE-depleted arclike rocks are indeed found in other ophiolites (such as Vourinos, Troodos) and in fore-arc regions (for example Japan, Marianas).

(5) Separate petrogeneses are required for the basaltic rocks and for the plagiogranite suite (diorite to trondhjemite) to explain the absence of normal fractionation trends and specifically the similar abundances of many immobile incompatible elements.

(6) The plagiogranites most likely represent partial melts of hydrated mafic rocks with compositions similar to those of gabbroic rocks in many ophiolites, such as those that are analogous to parts of oceanic or marginal-basin crust. Coexistence with the upper basalts suggests that the basaltic magmas may have provided the necessary heat source to drive crustal-level melting. Thus, magma probably was produced concurrently from two or more, different-depth sources.

(7) The keratophyres into which the Canyon Mountain Complex was emplaced indicate an island-arc association judging from the mineralogy and geochemistry of these rocks. They so closely resemble the trondhjemites of the plagiogranite suite that a similar model of crustal anatexis is considered reasonable. Presumably the keratophyre parent magmas formed by melting in the deep-crustal root of a volcanic arc.

TECTONIC IMPLICATIONS

Studies of the Canyon Mountain Complex offer some interesting perspectives on the formation of ophiolites and on the nature of convergent tectonic processes in general. The complex appears to comprise a variety of lithotectonic units that are not strictly related to one another in a cogenetic sense. Specifically, the tectonite harzburgite and metacumulate members together have characteristics similar to those envisaged for oceanic lithosphere. Diapiric ascent of these rocks in one or more stages (Avé Lallemant, 1976; Misseri and Boudier, 1985) is possibly analogous to diapirism inferred at spreading centers (Casey and Dewey, 1984; Casey and others, 1985; Rabinowitz and others, 1987), or in fore-arc regions (Bloomer, 1983). The deformation in these rocks could be related to primary flowage in an extensional setting or to tectonic factors associated with convergence and accretion in a fore-arc region. The undeformed isotropic and layered gabbros represent a second magmatic phase that did not necessarily occur in the same place or manner as the first. Primarily on the basis of their respective mineral compositions, Mullen (1983a, 1985) suggested that these rocks have calc-alkaline affinities, whereas the earlier gabbros have tholeiitic affinities. These distinctions are rather tenuous, and further work would certainly be useful to elucidate the associated tectonic history. Nevertheless, magmas of the sheeted member have definite island-arc affinities, although the basalts are relatively primitive. The combined geochemical characteristics of these rocks suggest that they may form by fusion of fundamentally MORB source material but that the distinctive Ta and Nb depletion is related to hydrous conditions of melting proximal to a subduction zone (Saunders and others, 1980; Wood and others, 1980; Pearce, 1982, 1983). The close association of these transitional basalts with plagiogranites and keratophyres also suggests proximity to an island arc (Gerlach, Avé Lallemant, and Leeman, 1981) onto which the remainder of the complex was accreted. Another notable feature of the Canyon Mountain Complex is the absence of a well-developed sheeted-dike complex, a pillow lava sequence, and pelagic sedimentary rocks. Although such units could have been removed tectonically, it is possible that they were never present. Our interpretation of the sheeted member as a sill-like unit (Gerlach, Avé Lallemant, and Leeman, 1981), if correct, is consistent with development of the latest magmatic phase under conditions of tectonic convergence, which would have favored the stagnation of magma at crustal levels and the formation of sills (see Leeman, 1983).

Based on the foregoing discussion, our general impression is that the Baker terrane, of which the Canyon Mountain Complex is a part, resembles a fore-arc region to which a variety of unrelated oceanic lithotectonic blocks accreted during Triassic to Early Jurassic convergence. This accretionary phase resulted in telescoping part of an oceanic or marginal basin and juxtaposition of unrelated fragments of oceanic lithosphere, seamounts, and remnants of island arcs.

This situation is reminiscent of many other ophiolite complexes in which the mafic rocks define two or more distinct magma series. Examples include the Troodos (McCulloch and Cameron, 1983; Robinson and others, 1983; Schminke and others, 1983; Dilek and others, 1990), Vourinos (Noiret and others, 1981; Beccaluva and others, 1984), Pindos (Capedri and others, 1980), New Caledonia (Dupuy and others, 1981), Betts Cove (Coish and others, 1982), Bay of Islands (Casey and others, 1985), Papua (Jacques and Chappell, 1980), Oman (McCulloch and others, 1981; Alabaster and others, 1982), and southern Chile (Stern, 1980) ophiolites. Multiple stratigraphic sequences

that represent distinct accreted lithotectonic blocks (including seamounts, oceanic crust, island-arc edifices) are recognized in some of the better studied complexes (such as Troodos and Oman). It has been proposed that some of these sequences formed in diverse tectonic settings and were emplaced adjacent to one another during accretion of different ophiolites (or fragments thereof) in a common collision zone (see Capedri and others, 1980). In Papua, New Guinea, local geologic evolution was complicated by primitive island-arc magmatism that postdated and is unrelated to the main ophiolite complex. Good geochronologic control is essential to fully understand the accretionary history of such compound ophiolites.

Despite the inferred polyphase magmatic and tectonic evolution of the Canyon Mountain Complex, exclusive of the basal ultramafic unit, the overall bulk composition of the complex is similar to basaltic andesite (Pearcy and others, 1990). This relatively mafic composition is consistent with our interpretation that the complex represents a section of immature oceanic to island-arc crust.

The application of geochemical studies to ophiolite petrogenesis provides another tool that can help in unraveling some of the problems of ophiolite formation. Nd or Hf isotopic studies may be particularly useful because these elements are resistant to mobilization during weathering and alteration. Interestingly, Nd data suggest non-MORB affinities for many ophiolites: $\varepsilon_{Nd}<+8$ for Troodos (McCulloch and Cameron, 1983), Oman (McCulloch and others, 1981), Vourinos (Noiret and others, 1981), and other ophiolite complexes. As we have learned in our work on the Canyon Mountain Complex, geochemical studies need to be integrated with comprehensive geologic and geochronologic studies to appreciate the complexities of ophiolite evolution.

REFERENCES CITED

Alabaster, T., Pearce, J.A., and Malpas, J., 1982, The volcanic stratigraphy and petrogenesis of the Oman ophiolite complex: Contributions to Mineralogy and Petrology, v. 81, p. 168-183.

Anonymous, 1972, Penrose Field Conference—Ophiolites: Geotimes, v. 17, no. 12, p. 24-25.

Armstrong, R.L., Taubeneck, W. R., and Hales, P.O., 1977, Rb-Sr and K-Ar geochronometry of Mesozoic granitic rocks and their Sr isotopic composition, Oregon, Washington, and Idaho: Geological Society of America Bulletin, v. 88, p. 397-411.

Avé Lallemant, H.G., 1976, Structure of the Canyon Mountain (Oregon) ophiolite complex and its implication for sea-floor spreading: Geological Society of America Special Papers 173, 49 p.

———1983, The pre-Tertiary tectonics of the Blue Mountains region, NE Oregon [abs.]: Geological Society of America Abstracts with Programs, v. 15, p. 372.

———1984a, The kinematic insignificance of mineral lineations in a Late Jurassic thrust and fold belt in eastern Oregon: Tectonophysics, v. 100, p. 389-404.

———1984b, Speculations on the origin of the ophiolites of northeastern Oregon (U.S.A.): Geologie en Mijnbouw, v. 63, p. 151-158.

Avé Lallemant, H.G., Phelps, D.W., and Sutter, J.F., 1980, ^{40}Ar-^{39}Ar ages of some pre-Tertiary plutonic and metamorphic rocks of eastern Oregon and their tectonic relationships: Geology, v. 8, p. 371-374.

Avé Lallemant, H.G., Schmidt, W.J., and Kraft, J.L., 1985, Major Late-Triassic strike-slip displacement in the Seven Devils terrane, Oregon and Idaho—A result of left-oblique plate convergence?, *in* Carter, N.L., and Uyeda, S., eds., Collision tectonics: Tectonophysics, v. 119, p. 299-328.

Bailey, E.H., and Blake, M.C., Jr., 1974, Major chemical characteristics of Mesozoic Coast Range ophiolite in California: Journal of Research of the U.S. Geological Survey, v. 2, p. 637-656.

Balcer, D.E., 1980, ^{40}Ar-^{39}Ar ages and REE geochemistry of selected basement terranes, Snake River canyon, Oregon-Idaho: Columbus, Ohio State University, M.S. thesis, 111 p.

Beccaluva, L., Ohnenstetter, D., and Ohnenstetter, M., 1979, Geochemical discrimination between ocean-floor and island-arc tholeiite—Application to some ophiolites: Canadian Journal of Earth Sciences, v. 16, p. 1874-1882.

Beccaluva, L., Ohnenstetter, D., Ohnenstetter, M., and Paupy, A., 1984, Two magmatic series with island arc affinities within the Vourinos ophiolite: Contributions to Mineralogy and Petrology, v. 85, p. 253-271.

Blome, C.D., Jones, D.L., and Murchey, B.L., 1983, Paleogeographic implications of radiolarian-rich rocks from eastern Oregon [abs.]: Geological Society of America Abstracts with Programs, v. 15, p. 371.

Blome, C.D., Jones, D.L., Murchey, B.L., and Liniecki, M., 1986, Geologic implications of radiolarian-bearing Paleozoic and Mesozoic rocks from the Blue Mountains province, eastern Oregon, chap. 8 *in* Vallier, T.L., and Brooks, H.C., eds., Geology of the Blue Mountains region of Oregon, Idaho, and Washington—Geologic implications of Paleozoic and Mesozoic paleontology and stratigraphy, Blue Mountains Province, Oregon and Idaho: U. S. Geological Survey Professional Paper 1435, p. 79-101.

Bloomer, S.H., 1983, Distribution and origin of igneous rocks from the landward slopes of the Mariana Trench—Implications for its structure and evolution: Journal of Geophysical Research, v. 88, p. 7411-7428.

Brooks, H.C., 1979, Geologic map of the Huntington and part of the Olds Ferry quadrangles, Baker and Malheur Counties, Oregon: Oregon Department of Geology and Mineral Industries Geologic Map Series Map GMS-13, 1:62,500.

Brooks, H.C., and Vallier, T.L., 1978, Mesozoic rocks and tectonic evolution of eastern Oregon and western Idaho, *in* Howell, D.G., and McDougall, K.A., eds., Mesozoic paleogeography of the Western United States (Pacific Coast Paleogeography Symposium 2): Los Angeles, Society of Economic Paleontologists and Mineralogists, Pacific Section, p. 133-145.

Brooks, H.C., McIntyre, J.R., and Walker, G.W., 1976, Geology of the Oregon part of the Baker 1° by 2° quadrangle: Oregon Department of Geology and Mineral Industries Geologic Map Series Map GMS-7, scale 1:250,000.

Brown, C.E., and Thayer, T.P., 1966, Geologic map of the Mount Vernon quadrangle, Grant County, Oregon: U.S. Geological Survey Geologic Quadrangle Map GQ-548, scale 1:62,500.

Bryan, W.B., Thompson, G., and Ludden, J.N., 1981, Compositional variation in normal MORB from 22°–25°N—Mid-Atlantic

Ridge and Kane fracture zone: Journal of Geophysical Research, v. 86, p. 11,815-11,836.

Cann, J.R., 1970, Rb, Sr, Y, Zr, and Nb in some ocean-floor basaltic rocks: Earth and Planetary Science Letters, v. 10, p. 7-11.

Capedri, S., Venturelli, G., Bocchi, G., Dostal, J., Garuti, G., and Rossi, A., 1980, The geochemistry and petrogenesis of an ophiolitic sequence from Pindos, Greece: Contributions to Mineralogy and Petrology, v. 74, p. 189-200.

Casey, J.F., and Dewey, J.F., 1984, Initiation of subduction zones along transform and accreting-plate boundaries, triple-junction evolution, and forearc spreading centers—Implications for ophiolite geology and obduction, *in* Gass, I.G., Lippard, S.J., and Shelton, A.W., eds., Ophiolites and oceanic Lithosphere: Blackwell, London, p. 269-290.

Casey, J.F., Elthon, D.L., Siroky, F.X., Karson, J.A., and Sullivan, J., 1985, Geochemical and geological evidence bearing on the origin of the Bay of Islands and Coastal Complex ophiolites of western Newfoundland: Tectonophysics, v. 116, p. 1-40.

Church, W.R., and Coish, R.A., 1976, Oceanic versus island arc origin of ophiolites: Earth and Planetary Science Letters, v. 31, p. 8-14.

Clague, D.A., Frey, F.A., Thompson, G., and Ringe, S., 1981, Minor and trace element geochemistry of volcanic rocks dredged from the Galápagos spreading center—Role of crystal fractionation and mantle heterogeneity: Journal of Geophysical Research, v. 86, p. 9469-9482.

Coish, R.A., Hickey, R., and Frey, F.A., 1982, Rare earth element geochemistry of the Betts Cove ophiolite, Newfoundland—Complexities in ophiolite formation: Geochimica et Cosmochimica Acta, v. 46, p. 2117-2134.

Coleman, R.G., 1977, Ophiolites: New York, Springer-Verlag, 229 pp.

———1981, Tectonic setting for ophiolite obduction in Oman: Journal of Geophysical Research, v. 86, p. 2497-2508.

Coleman, R.G., and Peterman, Z.E., 1975, Oceanic plagiogranites: Journal of Geophysical Research, v. 80, p. 1099-1108.

Coney, P.J., Jones, D.L., and Monger, J.W.H., 1980, Cordilleran suspect terranes: Nature, v. 288, p. 329-333.

Cox, A., and Dalrymple, G.B., 1967, Statistical analysis of geomagnetic reversal data and the precision of potassium-argon dating: Journal of Geophysical Research, v. 72, p. 2603-2614.

Dalrymple, G.B., Alexander, E.C., Jr., Lanphere, M.A., and Kraker, G.P., 1981, Irradiation of samples for $^{40}Ar/^{39}Ar$ dating using the Geological Survey TRIGA reactor: U.S. Geological Survey Professional Paper 1176, 55 p.

Dickinson, W.R., 1979, Mesozoic forearc basin in central Oregon: Geology, v. 7, p. 166-170.

Dickinson, W.R., and Thayer, T.P., 1978, Paleogeographic and paleotectonic implications of Mesozoic stratigraphy and structure in the John Day inlier of Central Oregon, *in* Howell, D.G., and McDougall, K.A., eds., Mesozoic paleogeography of the Western United States (Pacific Coast Paleogeography Symposium 2): Los Angeles, Society of Economic Paleontologists and Mineralogists, Pacific Section, p. 147-161.

Dickinson, W.R., and Vigrass, L.W., 1965, Geology of the Suplee-Izee area, Crook, Grant, and Harney Counties, Oregon: Oregon Department of Geology and Mineral Industries Bulletin 58, 109 p.

Dilek, Y., Thy, P., Moores, E.M., and Ramsden, T.W., 1990, Tectonic evolution of the Troodos ophiolite within the Tethyan framework: Tectonics, v. 9, p. 811-823.

Dixon, S., and Rutherford, M.J., 1979, Plagiogranites as late-stage immiscible liquids in ophiolite and mid-ocean ridge suites—An experimental study: Earth and Planetary Science Letters, v. 45, p. 45-60.

Dungan, M.A., and Avé Lallemant, H.G., 1977, Formation of small dunite bodies by metasomatic transformation of harzburgite in the Canyon Mountain ophiolite, northeast Oregon, *in* Dick, H.J.B., ed., Magma genesis: Oregon Department of Geology and Mineral Industries Bulletin 96, p. 109-128.

Dupuy, C., Dostal, J., and LeBlanc, M., 1981, Geochemistry of an ophiolitic complex from New Caledonia: Contributions to Mineralogy and Petrology, v. 76, p. 77-83.

Ellam, R.M., 1986, The transition from calc-alkaline to potassic volcanism in the Aeolian Islands, southern Italy: Milton Keynes, The Open University, Ph.D. dissertation, 210 p.

Elthon, D., and Casey, J.F., 1985, The very depleted nature of certain primary mid-ocean ridge basalts: Geochimica et Cosmochimica Acta, v. 49, p. 289-298.

Ewart, A., and Bryan, W.B., 1972, Petrography and geochemistry of the igneous rocks from Eua, Tongan Islands: Geological Society of America Bulletin, v. 83, p. 3281-3298.

Frey, F.A., Gerlach, D.C., Hickey, R.L., Lopez-Escobar, L., and Munizaga-Villavicendo, F., 1984, Petrogenesis of the Laguna del Maule volcanic complex, Chile (36° S): Contributions to Mineralogy and Petrology, v. 88, p. 133-149.

Frey, F.A., Green, D.H., and Roy, S.D., 1978, Integrated models of basalt petrogenesis—A study of quartz tholeiites to olivine melilitites from southeastern Australia, utilizing geochemical and experimental petrological data: Journal of Petrology, v. 19, p. 463-513.

Gerlach, D.C., 1980, Petrology and geochemistry of plagiogranite and related basic rocks of the Canyon Mountain ophiolite complex, Oregon: Houston, Rice University, M.A. thesis, 203 p.

Gerlach, D.C., Avé Lallemant, H.G., and Leeman, W.P., 1981, An island arc origin for the Canyon Mountain ophiolite complex, eastern Oregon, U.S.A.: Earth and Planetary Science Letters, v. 53, p. 255-265.

Gerlach, D.C., Leeman, W.P., and Avé Lallemant, H.G., 1981, Petrology and geochemistry of plagiogranite in the Canyon Mountain ophiolite, Oregon: Contributions to Mineralogy and Petrology, v. 77, p. 82-92.

Gregory, R.T., and Taylor, H.P., 1980, Oxygen isotope and field studies applied to the origin of oceanic plagiogranites [abs.], *in* Panayiotou, A., ed., International Ophiolite Symposium, 1979 [Proceedings]: Nicosia, Cyprus Geological Survey, p. 117-118.

Helz, R.T., 1976, Phase relations of basalts in their melting ranges at P_{H_2O}=5 kb—Pt. II, Melt compositions: Journal of Petrology, v. 17, p. 139-193.

Henricksen, T.A., 1975, Geology and mineral deposits of the Mineral-Iron Mountain District, Washington County, Idaho, and of a metallized zone in western Idaho and eastern Oregon: Corvallis, Oregon State University, Ph.D. dissertation, 260 p.

Hillhouse, J.W., Grommé, C.S., and Vallier, T.L., 1982, Paleomagnetism and Mesozoic tectonics of the Seven Devils volcanic arc in northeastern Oregon: Journal of Geophysical Research, v. 87, p. 3777-3794.

Himmelberg, G.R., and Loney, R.A., 1980, Petrology of ultramafic and gabbroic rocks of the Canyon Mountain ophiolite, Oregon: American Journal of Science, v. 280-A, p. 232-268.

Holcombe, T.L., and Sharman, G.F., 1983, Post-Miocene Cayman Trough evolution—A speculative model: Geology, v. 11, p. 714-717.

Holloway, J.R., and Burnham, C.W., 1972, Melting relations of basalt with equilibrium water pressure less than total pressure: Journal of Petrology, v. 13, p. 1-30.

Hopson, C.A., and Frano, C.J., 1977, Igneous history of the Point Sal ophiolite, Southern California, *in* Coleman, R.G., and Irwin, W.P., eds., North American ophiolites: Oregon Department of Geology and Mineral Industries Bulletin 95, p. 161-183.

Hotz, P.E., Lanphere, M.A., and Swanson, D.A., 1977, Triassic blueschist from northern California and north-central Oregon: Geology, v. 5, p. 659-663.

Hynes, A., 1975, Comment on "The Troodos ophiolite complex was probably formed in an island arc" by A. Miyashiro: Earth and Planetary Science Letters, v. 25, p. 213-216.

Jacques, A.L., and Chappell, B.W., 1980, Petrology and trace element geochemistry of the Papuan ultramafic belt: Contributions to Mineralogy and Petrology, v. 75, p. 55-70.

Karig, D.E., 1971, Origin and development of marginal basins in the western Pacific: Journal of Geophysical Research, v. 76, p. 2542-2561.

Kay, R.W., and Senechal, R.G., 1976, The rare earth geochemistry of the Troodos ophiolite complex: Journal of Geophysical Research, v. 81, p. 964-970.

Leeman, W.P., 1976, Petrogenesis of McKinney (Snake River) olivine tholeiite in light of rare-earth element and Cr/Ni distributions: Geological Society of America Bulletin, v. 87, p. 1582-1586.

———1983, The influence of crustal structure on subduction-related magmas: Journal of Volcanology and Geothermal Research, v. 18, 561-588.

Leeman, W.P., Murali, A.V., Ma, M.-S., and Schmitt, R.A., 1977, Mineral constitution of mantle source regions for Hawaiian basalts—Rare-earth evidence for mantle heterogeneity, *in* Dick, H.J.B., ed., Magma genesis, Oregon Department of Geology and Mineral Industries Bulletin 96, p. 169-184.

Marvin, R.F., and Cole, J.C., 1978, Radiometic ages—Compilation A, U.S. Geological Survey: Isochron/West, no. 22, p. 3-14.

McCulloch, M.T., and Cameron, W.E., 1983, Nd-Sr isotopic study of primitive lavas from the Troodos ophiolite, Cyprus—Evidence for a subduction-related setting: Geology, v. 11, p. 727-731.

McCulloch, M.T., Gregory, R.T., Wasserburg, G.J., and Taylor, H.P., Jr., 1981, Sm-Nd, Rb-Sr, and $^{18}O/^{16}O$ isotopic systematics in an oceanic crustal section—Evidence from the Semail ophiolite: Journal of Geophysical Research, v. 86, p. 2721-2735.

Melson, W.G., Vallier, T.L., Wright, T.W., Byerly, G.R., and Nelson, J., 1976, Chemical diversity of abyssal volcanic glasses erupted along Pacific, Atlantic, and Indian Ocean sea-floor spreading centers: American Geophysical Union Monograph 19, p. 351-367.

Menzies, M.A., Blanchard, D., and Jacobs, R., 1977, Rare-earth and trace-element geochemistry of metabasalts from the Point Sal ophiolite, California: Earth and Planetary Science Letters, v. 37, p. 203-215.

Mercier, J-C.C., 1980, Single-pyroxene thermobarometry: Tectonophysics, v. 70, p. 1-37.

Misseri, M., and Boudier, F., 1985, Structures in the Canyon Mountain ophiolite indicate an island-arc intrusion: Tectonophysics, v. 120, p. 191-209.

Miyashiro, Akiho, 1973, The Troodos ophiolitic complex was probably formed in an island arc: Earth and Planetary Science Letters, v. 19, p. 218-224.

Moores, E.M., 1975, Discussion of "Origin of Troodos and other ophiolites—A reply to Hynes," by Akiho Miyashiro: Earth and Planetary Science Letters, v. 25, p. 223-226.

Moores, E.M., Robinson, P.T., Malpas, J., and Xenophontos, C., 1984, Model for the origin of the Troodos massif, Cyprus, and other Mideast ophiolites: Geology, v. 12, p. 500-503.

Morrison, R.F., 1964, Upper Jurassic mudstone unit named in Snake River canyon, Oregon-Idaho boundary: Northwest Science, v. 38, p. 83-87.

Mullen, E.D., 1983a, Petrology and regional setting of peridotite and gabbro of the Canyon Mountain Complex, northeast Oregon: Corvallis, Oregon State University, Ph.D. dissertation, 277 p.

———1983b, $MnO/TiO_2/P_2O_5$—A minor element discriminant for basaltic rocks of oceanic environments and its implications for petrogenesis: Earth and Planetary Science Letters, v. 62, p. 53-62.

———1985, Petrologic character of Permian and Triassic greenstones from the melange terrane of eastern Oregon and their implications for terrane origin: Geology, v. 13, p. 131-134.

Nestell, M.K., 1983, Permian foraminiferal faunas of central and eastern Oregon [abs.]: Geological Society of America Abstracts with Programs, v. 15, p. 371.

Noiret, G., Montigny, R., and Allegre, C.J., 1981, Is the Vourinos Complex an island arc ophiolite?: Earth and Planetary Science Letters, v. 56, p. 375-386.

Nolf, B.O., 1966, Structure and stratigraphy of part of the northern Wallowa Mountains, Oregon: Princeton, N.J., Princeton University, Ph.D. dissertation, 193 p.

Pallister, J.S., and Knight, R.J., 1981, Rare-earth element geochemistry of the Semail ophiolite near Ibra, Oman: Journal of Geophysical Research, v. 86, p. 2673-2697.

Pearce, J.A., 1982, Trace element characteristics of lavas from destructive plate boundaries, *in* Thorpe, R.S., ed., Orogenic andesites: New York, John Wiley, p. 525-548.

———1983, Role of sub-continental lithosphere in magma genesis in active continental margins, *in* Hawkesworth, C.J., and Norry, M.J., eds. Continental basalts and mantle xenoliths, Nantwich, U.K., Shiva, p. 230-249.

Pearce, J.A., and Cann J.R., 1973, Tectonic setting of basic volcanic rocks determined using trace element analyses: Earth and Planetary Science Letters, v. 19, p. 290-300.

Pearce, J.A., Harris, N.B.W., and Tindle, A.G., 1984, Trace-element discrimination diagrams for the tectonic interpretation of granitic rocks: Journal of Petrology, v. 25, p. 956-983.

Pearcy, L.G., 1987, Clinopyroxene compositions and petrogenesis of the mantle-crust transition zone—Canyon Mountain Complex, Oregon [abs.]: Geological Society of America Abstracts with Programs, v. 19, p. 439.

Pearcy, L.G., DeBari, S.M., and Sleep, N.H., 1990, Mass balance calculations for two sections of island arc crust and implications for the formation of continents: Earth and Planetary Science Letters, v. 96, p. 427-442.

Perfit, M.R., Fornari, D.J., Malahoff, A., and Embley, R.W., 1983, Geochemical studies of abyssal lavas recovered by DSRV Alvin from eastern Galápagos Rift, Inca Transform, and Ecuador Rift—Pt. 3, Trace element abundances and petrogenesis: Journal of Geophysical Research, v. 88, p. 10,551-10,572.

Phelps, D.W., 1978, Petrology, geochemistry, and structural geology of Mesozoic rocks in the Sparta quadrangle and Oxbow and Brownlee Reservoir areas, eastern Oregon and western Idaho: Houston, Rice University, Ph.D. dissertation, 229 p.

———1979, Petrology, geochemistry, and origin of the Sparta quartz diorite-trondhjemite complex, northeastern Oregon, *in* Barker, F., ed., Trondhjemites, dacites and related rocks, New York, Elsevier, p. 547-580.

Phelps, D.W., and Avé Lallemant, H.G., 1980, The Sparta ophiolite complex, northeast Oregon—A plutonic equivalent to low K_2O island-arc volcanism: American Journal of Science, v. 280-A, p. 345-358.

Prostka, H.J., and Bateman, R.L., 1962, Geologic map of the Sparta quadrangle: Oregon Department of Geology and Mineral Industries Geologic Map Series Map GMS-1, scale 1:62,500.

Rabinowitz, M., Ceuleneer, G., and Nicolas, A., 1987, Melt segregation and flow in mantle diapirs below spreading centers—Evidence from the Oman ophiolite: Journal of Geophysical Research, v. 92, p. 3475-3486.

Rapp, R.P., Watson, E.B., and Miller, C.F., 1991, Partial melting of amphibolite/eclogite and the origin of Archean trondhjemites and tonalites: Precambrian Research, v. 51, p. 1-25.

Robinson, P.T., Melson, W.G., O'Hearn, T., and Schmincke, H.-U., 1983, Volcanic glass compositions of the Troodos ophiolite, Cyprus: Geology, v. 11, p. 400-404.

Rogers, N.W., Hawkesworth, C.J., Parker, R.J., and Marsh, J.S., 1985, The geochemistry of potassic lavas from Vulsini, central Italy and implications for mantle enrichment processes beneath the Roman region: Contributions to Mineralogy and Petrology, v. 90, p. 244-257.

Saunders, A.D., Tarney, J., Marsh, N.G., and Wood, D.A., 1980, Ophiolites as ocean crust or marginal basin crust—A geochemical approach, *in* Panayiotou, A., ed., International Ophiolite Symposium, 1979 [Proceedings]: Nicosia, Cyprus Geological Survey, p. 193-204.

Schmincke, H.-U., Rautenschlein, M., Robinson, P.T., and Mehegan, J.M., 1983, Troodos extrusive series of Cyprus—A comparison with oceanic crust: Geology, v. 11, p. 405-409.

Shaw, D.M., 1970, Trace element fractionation during anatexis: Geochimica et Cosmochimica Acta, v. 34, p. 237-243.

Shervais, J.W., 1982, Ti-V plots and the petrogenesis of modern and ophiolitic lavas: Earth and Planetary Science Letters, v. 59, p. 101-118.

Silberling, N.J., and Jones, D.L., 1984, Tectonic terrane map of the northern Cordillera: U. S. Geological Survey Open-File Report OFR-84-523.

Sinton, J.M., and Byerly, G.R., 1980, Silicic differentiates of abyssal oceanic magmas—Evidence for late-magmatic vapor transport of potassium: Earth and Planetary Science Letters, v. 47, p. 423-430.

Spulber, S.D., and Rutherford, M.J., 1983, The origin of rhyolite and plagiogranite in oceanic crust—An experimental study: Journal of Petrology, v. 24, p. 1-25.

Steiger, R.H., and Jäger, E., 1977, Subcommission on geochronology—Convention on the use of decay constants in geo- and cosmochronology: Earth and Planetary Science Letters, v. 36, p. 359-362.

Stern, C.R., 1980, Geochemistry of Chilean ophiolites—Evidence for the compositional evolution of the mantle source of back-arc basin basalts: Journal of Geophysical Research, v. 85, p. 955-966.

Sun, S.S., and Nesbitt, R.W., 1977, Chemical heterogeneity of the Archean mantle, composition of the Earth, and mantle evolution: Earth and Planetary Science Letters, v. 35, p. 429-448.

Sun, S.S., Nesbitt, R.W., and Sharaskin, A.Y., 1979, Geochemical characteristics of mid-ocean ridge basalts: Earth and Planetary Science Letters, v. 44, p. 119-138.

Sutter, J.F., Snee, L.W., and Lund, K., 1984, Metamorphic, plutonic, and uplift history of a continent-island-arc suture zone, west-central Idaho [abs.]: Geological Society of America Abstracts with Programs, v. 16, p. 670.

Thayer, T.P., 1956, Preliminary geologic map of the John Day quadrangle, Oregon: U.S. Geological Survey Mineral Investigations Field Studies Map MF 51, scale 1:62,500.

———1963a, The Canyon Mountain Complex, Oregon, and the alpine mafic magma stem, *in* U.S. Geological Survey Research 1963: U.S. Geological Survey Professional Paper 475-C, p. 82-85.

———1963b, Flow-layering in alpine peridotite-gabbro complexes, *in* Symposium on Layered Intrusions: Mineralogical Society of America Special Paper 1, p. 55-61.

———1969a, Peridotite-gabbro complexes as keys to petrology of mid-oceanic ridges: Geological Society of America Bulletin, v. 80, p. 1515-1522.

———1969b, Gravity differentiation and magmatic re-emplacement of podiform chromite deposits, *in* Symposium on Magmatic Ore Deposits: Economic Geology Monograph 4, p. 132-146.

———1977a, Some implications of sheeted dike swarms in ophiolitic complexes: Geotectonics, v. 11, p. 419-426.

———1977b, The Canyon Mountain Complex, Oregon, and some problems of ophiolites, *in* Coleman, R.G., and Irwin, W.P., eds., North American ophiolites: Oregon Department of Geology and Mineral Industries Bulletin 95, p. 93-105.

Thayer, T.P., Case, J.E., and Stottelmeyer, R.B., 1981, Mineral resources of the Strawberry Mountain Wilderness and adjacent areas, Grant County, Oregon: U.S. Geological Survey Bulletin 1498, 67 p.

Thayer, T.P., and Himmelberg, G.R., 1968, Rock succession in the alpine-type mafic complex at Canyon Mountain, Oregon: International Geological Congress, 23rd, Prague, 1968 [Proceedings], v. 1, p. 175-186.

Thompson, G., Bryan, W.B., and Melson, W.G., 1980, Geological and geophysical investigation of the mid-Cayman Rise spreading center—Geochemical variation and petrogenesis of basalt glasses: Journal of Geology, v. 88, p. 41-55.

Thompson, R.N., Morrison, M.A., Hendry, G.L., and Parry, S.J., 1984, An assessment of the relative roles of crust and mantle in magma genesis—An elemental approach: Royal Society of London Philosophical Transactions, ser. A, v. A310, p. 549-590.

Vallier, T.L., 1974, A preliminary report on the geology of part of the Snake River Canyon, Oregon and Idaho: Oregon Department of Geology and Mineral Industries Geological Map Series Map GMS-6, 1 map sheet and 15 p. of text, scale 1:125,000.

———1977, The Permian and Triassic Seven Devils Group, western Idaho and northeastern Oregon: U.S. Geological Survey Bulletin 1437, 58 p.

Vallier, T.L., and Batiza, R., 1978, Petrogenesis of spilite and keratophyre from a Permian and Triassic volcanic arc terrane, eastern Oregon and western Idaho, U.S.A.: Canadian Journal of Earth Sciences, v. 15, p. 1356-1369.

Walker, G.W., 1977, Geologic map of Oregon east of the 121st meridian: U.S. Geological Survey Miscellaneous Investigations Series Map I-902, scale 1:500,000.

Walker, N.W., 1981, U-Pb geochronology of ophiolitic and volcanic-plutonic arc terranes, northeastern Oregon and westernmost-central Idaho [abs.]: Eos (American Geophysical Union Transactions), v. 62, p. 1087.

———1982, Pre-Tertiary plutonic rocks in the Snake River Canyon, Oregon/Idaho—Intrusive roots of a Permo-Triassic arc complex [abs.]: Geological Society of America Abstracts with Programs, v. 14, p. 242-243.

———1983, Pre-Tertiary tectonic evolution of northeastern Oregon and west-central Idaho—Constraints based on U/Pb ages of zircons [abs.]: Geological Society of America Abstracts with Programs, v. 12, p. 544.

———1986, U/Pb geochronologic and petrologic studies in the Blue Mountains Terrane, northeastern Oregon and westernmost-central Idaho—Implications for pre-Tertiary tectonic evolution: Santa Barbara, University of California, Ph.D. dissertation, 224 p.

Walker, N.W., and Mattinson, J.M., 1980, The Canyon Mountain Complex, Oregon—U-Pb ages of zircons and possible tectonic correlations [abs.]: Geological Society of America Abstracts with Programs, v. 12, p. 544.

Wells, P.R.A., 1977, Pyroxene thermometry in simple and complex systems: Contributions to Mineralogy and Petrology, v. 62, p. 129-139.

Wilson, D., and Cox, A., 1980, Paleomagnetic evidence for tectonic rotation of Jurassic plutons in Blue Mountains, eastern Oregon: Journal of Geophysical Research, v. 85, p. 3681-3689.

Winchester, J.A., and Floyd, P.A., 1977, Geochemical discrimination of different magma series and their differentiation products using immobile elements: Chemical Geology, v. 20, p. 325-343.

Wood, D.A., 1979, A variably veined suboceanic upper mantle—Genetic significance for mid-ocean ridge basalts from geochemical evidence: Geology, v. 7, p. 499-503.

Wood, D.A., Joron, J.L., Marsh, N.G., Tarney, J., and Treuil, M., 1980, Major and trace element variations in basalts from the northern Philippine Sea drilled during Deep Sea Drilling Project Leg 58—A comprehensive study of back-arc basin basalts, *in* Klein, G.D., and Kobayashi, K., eds., Initial Reports of the Deep Sea Drilling Project, v. 58, Washington, D.C., U.S. Government Printing Office, p. 873-894.

Wood, D.A., Joron, J.L., and Treuil, M., 1979, A reappraisal of the use of trace elements to classify and discriminate between magma series erupted in different tectonic settings: Earth and Planetary Science Letters, v. 45, p. 326-336.

Wood, D.A., Joron, J.L., Treuil, M., Norry, M., and Tarney, J., 1979, Elemental and Sr isotope variations in basic lavas from Iceland and the surrounding ocean floor: Contributions to Mineralogy and Petrology, v. 70, p. 319-339.

2. A CLOSER LOOK AT THE BALD MOUNTAIN BATHOLITH, ELKHORN MOUNTAINS, AND SOME COMPARISONS WITH THE WALLOWA BATHOLITH, WALLOWA MOUNTAINS, NORTHEASTERN OREGON

By WILLIAM H. TAUBENECK[1]

CONTENTS

	Page
Abstract	46
Introduction	47
Acknowledgments	52
Age relations and distribution of rocks near Bald Mountain batholith	53
Geographic names	54
Metamorphic aureole of Bald Mountain batholith	54
Ribbon chert	54
Cherty argillite	54
In the Belleview wedge	54
South of the Elkhorn pluton	56
Argillite and tuffaceous argillite	57
Limestone	58
Metagabbro	59
Ultramafic rocks	61
Structure of Elkhorn pluton	62
Peripheral contacts and associated foliation in margins of pluton	62
Internal foliation	64
Intraplutonic contact	68
Rocks of Bald Mountain batholith	70
Norite of Badger Butte	70
Setting and general description	70
Microscopic description	70
Tonalite of Bald Mountain and granodiorite of Anthony Lake	71
Setting and general description	71
Comparative modal compositions and crystallization of augite	72
Assimilation of graphite-bearing metasedimentary rocks in Elkhorn pluton	82
Distinctive petrographic features of rocks of Elkhorn pluton	83
Specific gravity of rocks of Elkhorn pluton	84
Compositions of cores of oscillatory-zoned plagioclase in Elkhorn pluton and other granitic intrusions of northeastern Oregon	84
Rocks of Bald Mountain batholith—Continued	
Tonalite of Bald Mountain and granodiorite of Anthony Lake—Continued	
Volume percent and origin of calcic cores in plagioclase of Elkhorn pluton	85
Interludes: A newly described feature of oscillatory-zoned plagioclase in granitic rocks	85
Pegmatites and aplites of Elkhorn pluton	87
Xenoliths of country rocks and inclusions of unknown origin in Elkhorn pluton	87
Quartz diorite of Limber Creek	91
Setting and general description	91
Microscopic description	92
Leucogranodiorite of Trail Creek	94
Setting and general description	94
Microscopic description	94
Granite of Clear Creek	94
Setting and general description	94
Microscopic description	95
Quartz diorite of Wolf Creek	95
Setting and general description	95
Microscopic description	95
Distinguishing features	96
Boundary quartz diorite unit	96
Setting and general description	96
Microscopic description	96
Distinguishing features	98
Granodiorite of Indiana Mine Road	98
Setting and general description	98
Microscopic description	98
Distinguishing features	98
Granodiorite of Beaver Meadow	99
Setting and general description	99
Microscopic description	99
Distinguishing features	100
Granite of Anthony Butte	100
Setting and general description	100
Microscopic description	101
Distinguishing features	102
Leucogranite of Dutch Creek	102
Setting and general description	102
Microscopic description	102
Distinguishing features	102
Satellitic bodies east of granite of Anthony Butte	103
Tonalite of North Fork	103

[1]Department of Geosciences, Oregon State University, Corvallis, OR 97331-5506

Satellitic bodies east of granite of Anthony Butte—Continued
Tonalite of North Fork—Continued
Setting and general description ---- 103
Microscopic description ---- 103
Distinguishing features ---- 104
Granite of Isham Spring ---- 104
Setting and general description ---- 104
Microscopic description ---- 104
Distinguishing features ---- 104
Granitic rocks of the Guard Station inlier ---- 105
Overview of granitic rocks ---- 105
Method of emplacement of Elkhorn pluton ---- 108
Volatiles contents of granitic magmas in relation to interstitial zeolites and potassium feldspar in granitic rocks of the Bald Mountain and Wallowa batholiths ---- 113
Major-element compositions ---- 118
Conclusions ---- 121
References cited ---- 121

ABSTRACT

The Late Jurassic Bald Mountain batholith, about 450 km^2 in area, is in the Elkhorn Mountains of northeastern Oregon. It intrudes a melange terrane (Baker terrane) that consists of the Devonian to Triassic Elkhorn Ridge Argillite—which is a heterogeneous assortment of metasedimentary rocks—as well as scattered masses of metagabbro and serpentinized ultramafic rocks of uncertain age. Contact-metamorphic effects, evident as a wide thermal aureole that includes high-temperature minerals characteristic of the pyroxene hornfels facies, overprint a regional (greenschist-facies) metamorphism, characterized by green biotite. The most widespread pyroxene hornfels-facies rocks are argillites and metagabbros with two-pyroxene assemblages, and cherty argillites with metapelitic assemblages characterized by cordierite and orthoclase, with or without one or more other minerals such as sillimanite and garnet. One notable high-temperature aureole rock is a rare pargasitic hornblende-peridotite hornfels that contains small amounts of green spinel and plagioclase. The grain size of recrystallized quartz in bedded chert near the batholith is a good approximation of the intensity of thermal metamorphism.

Forceful intrusion apparently was the dominant process responsible for the emplacement of the batholith. Much wallrock yielded by plastic flow. Segregation banding in intensely deformed metagabbro resembles the bedding in some metasedimentary rocks. Intensely deformed salients of country rock that project far into the batholith are commonly gneissic and include the Archean gneiss unit of Lindgren (1901). Scattered boudins in the gneiss indicate extreme plastic deformation. Much of the gneiss apparently is underlain by the batholith.

An assessment of stoping as a significant emplacement mechanism is severely hampered by the absence of critical field evidence within the batholith. However, the size differential between xenoliths in the margin and in the interior of the major unit of the batholith combined with size relations in the upper parts of small cupolas of granitic rocks alongside the batholith imply that stoping played a more important role than is commonly recognized in mesozonal plutons.

In the area south of lat 45° N. at least nine discrete intrusive units of the Bald Mountain batholith were emplaced in a mafic-to-felsic sequence that commenced with three small gabbroic bodies and a small unit of quartz diorite, continued with the very large compositionally zoned Elkhorn pluton (tonalite and granodiorite) that constitutes most of the batholith, and ended with four small felsic units. The tonalite and granodiorite of the compositionally zoned Elkhorn pluton are separated for about 9 km on the north and 4 km on the northwest by an intraplutonic contact, concealed for about 4 km between the north and northwest exposures by Tertiary volcanic rocks. Microscopic evidence indicates that augite crystallized initially throughout much of the tonalite but only in some of the granodiorite in the Elkhorn pluton. The small volume percent of calcic cores in oscillatory-zoned plagioclase of the Elkhorn pluton indicates that the granitic rocks crystallized from a melt that contained only a comparatively minor amount of solid constituents. An interlude is the name herein applied to concentrations of one or several mafic minerals of small size in a distinct layer of plagioclase between consecutive oscillations in oscillatory-zoned plagioclase. Heretofore, interludes apparently have not been reported in the plagioclase of granitic rocks.

Good to excellent planar structure characterizes most margins of the Elkhorn pluton except near much of the southern contact. Faint to fairly good planar structure that generally is difficult to detect occurs sporadically in parts of the interior of the pluton. New procedures that take into account realistic (rather than idealized) field relations facilitate recognition of planar structure on smooth joint surfaces, exposures controlled by steep diagonal joints, and exposures shaped by exfoliation.

Xenoliths of metagabbroic and metasedimentary rocks throughout the central and southwestern parts of the Elkhorn pluton are more abundant than xenoliths of country rocks in most batholiths. The scarcity of xenoliths of argillaceous rocks as compared to chert is attributed to a more rapid rate of assimilation. Granitic rocks in the Elkhorn Mountains with reddish-brown to red biotite and little or no iron oxide are attributed to assimilation of graphite-bearing metasedimentary rocks.

Far more abundant than xenoliths of country rocks are mafic inclusions of uncertain origin (see, for example, Pabst, 1928). No mafic synplutonic dikes occur in the Bald Mountain batholith at the present level of erosion. On the basis of field observations and petrographic data, most of the derivations postulated for mafic inclusions in circum-Pacific granitic intrusions can be questioned or discounted for mafic inclusions in the Bald Mountain batholith.

A distinct zone in which microcline twinning characterizes the potassium feldspar extends for 19 km across the Elkhorn pluton and is related to deformation rather than to the concentration of volatiles.

Much of this report concerns the part of the Bald Mountain batholith that lies north of lat 45° N. in the Anthony Butte 7½-minute quadrangle. Here many small intrusive units of the batholith occur, and deformation features of the rocks are more pronounced than in the southern part of the batholith. The plutons commonly are separated in part by dismembered screens. One granodiorite body contains small amounts of orthopyroxene and is notable for reaction relations between orthopyroxene, cummingtonite, hornblende, and biotite. This body is one of two intrusions that contain red-brown biotite and little or no iron oxide. Another pluton in the study area is the largest granite body in northeastern Oregon and contains traces of orthopyroxene and garnet. Several intrusions are composed of silica-rich granitic rocks. Both satellitic intrusions in metasedimentary rocks near this part of the batholith contain either red-brown or red biotite and almost no iron oxide.

The mineralogy of the granitic rocks coupled with the pyroxene hornfels-facies thermal metamorphism of the wallrocks indicates that much of the batholith crystallized from relatively hot and water-undersaturated magmas.

Rocks of the Bald Mountain batholith range in composition from norite that contains about 52 weight percent SiO_2 to leucogranite that contains about 77 weight percent SiO_2. The rocks are metaluminous to weakly peraluminous. The compositionally zoned Elkhorn pluton ranges inward from border rocks that contain

about 61 weight percent SiO_2 and 0.5 weight percent K_2O to core rocks that contain about 69 weight percent SiO_2 and 2.1 weight percent K_2O.

Rocks of the Bald Mountain batholith show a typical calc-alkaline compositional trend on an Al_2O_3-FeO-MgO (AFM) diagram. They also show marked late-stage iron enrichment on diagrams used to distinguish calc-alkaline from tholeiitic rocks.

INTRODUCTION

The name "Bald Mountain batholith" originated, according to Hewett (1931), with Lindgren (1901), who derived it at the turn of the century from the local designation "Bald Mountain" for a prominent peak of tonalite in the Elkhorn Mountains of northeastern Oregon. In 1917 the U.S. Board on Geographic Names officially designated the peak "Ireland Mountain," and the local usage of the term "Bald Mountain" gradually was discontinued. The new name "Ireland Mountain" was soon changed to "Mount Ireland" (fig. 2.1). However, the name that Lindgren informally used for the batholith was retained by Taubeneck (1957) mostly in recognition of Lindgren's many pioneering contributions, including a remarkable geologic map of much of northeastern Oregon and closely adjacent parts of Idaho. Lindgren's (1901) classic reconnaissance map, based on approximately three months of field work, encompasses about 17,550 km^2, has a contour interval of 500 ft, accurately indicates the peak then known as Bald Mountain, and shows much of the associated batholith. The accomplishments of Lindgren in the Blue Mountains region strongly suggest that he is among the most perceptive of the great American reconnaissance geologists.

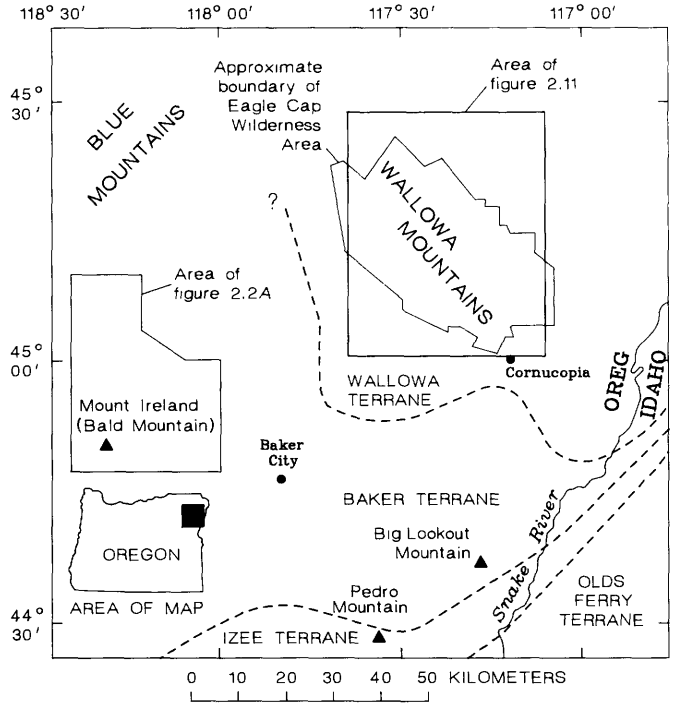

FIGURE 2.1.—Index map showing major geographic features of northeastern Oregon. Dashed lines are terrane boundaries (from Vallier, chap. 3, this volume), queried where uncertain.

The 450-km^2 Bald Mountain batholith (figs. 2.2 and 2.3) is mostly in the central part of the Elkhorn Mountains. About 78 percent of the batholith is south of lat 45° N.; here exposures generally are good to excellent except in some of the westernmost and easternmost parts of the batholith. Contacts of the batholith north and east of Mount Ireland (fig. 2.2) commonly are concealed by glacial deposits. The batholith is mountainous south of lat 45° N. with elevations commonly greater than 2,375 m; total relief is 1,555 m. Prior to 1965, no map was available for the area north of lat 45° N. and only a 1901 map (of the Sumpter 30-minute quadrangle) at a scale of 1:125,000, was available for the area south of lat 45° N. Modern 1:24,000-scale topographic maps for the Elkhorn Mountains and adjacent areas were not available until the 1960's and 1970's when the U.S. Geological Survey published the Anthony Butte (1965), Limber Jim Creek (1965), Little Beaver Creek (1965), Marley Creek (1965), Tucker Flat (1965), Anthony Lakes (1972), Bourne (1972), Crawfish Lake (1972), Elkhorn Peak (1972), Granite (1972), Mt. Ireland (1972), Rock Creek (1972), and Trout Meadows (1972) 7½-minute quadrangles (fig. 2.2A).

South of lat 45° N., the composite Bald Mountain batholith consists of at least nine discrete intrusive units emplaced in a mafic-to-felsic sequence. Intrusive activity commenced with the emplacement of three small gabbroic bodies and a small unit of quartz diorite, continued with the intrusion of a tonalite and granodiorite body herein called the Elkhorn pluton, which constitutes most of the batholith, and ended with the injection of four small felsic units. The three gabbroic plutons consist of the norite of Willow Lake, the norite of Badger Butte, and the quartz gabbro of Black Bear; the small unit of quartz diorite is the quartz diorite of Limber Creek (fig. 2.4). The Elkhorn pluton is compositionally zoned from a mafic margin (tonalite of Bald Mountain) to a felsic core (granodiorite of Anthony Lake). The four felsic units are the leucogranodiorite of Mount Ruth, the leucogranodiorite of Red Mountain, the leucogranite of Elk Peak, and the leucogranodiorite of Trail Creek. Seven of the units listed above were identified in an earlier report (Taubeneck, 1957), and the names used here are modified from that report. Two of the

units—the quartz diorite of Limber Creek and the leucogranodiorite of Trail Creek—are newly mapped and named. The rock name for the Elk Peak unit has been changed from leucocratic quartz monzonite

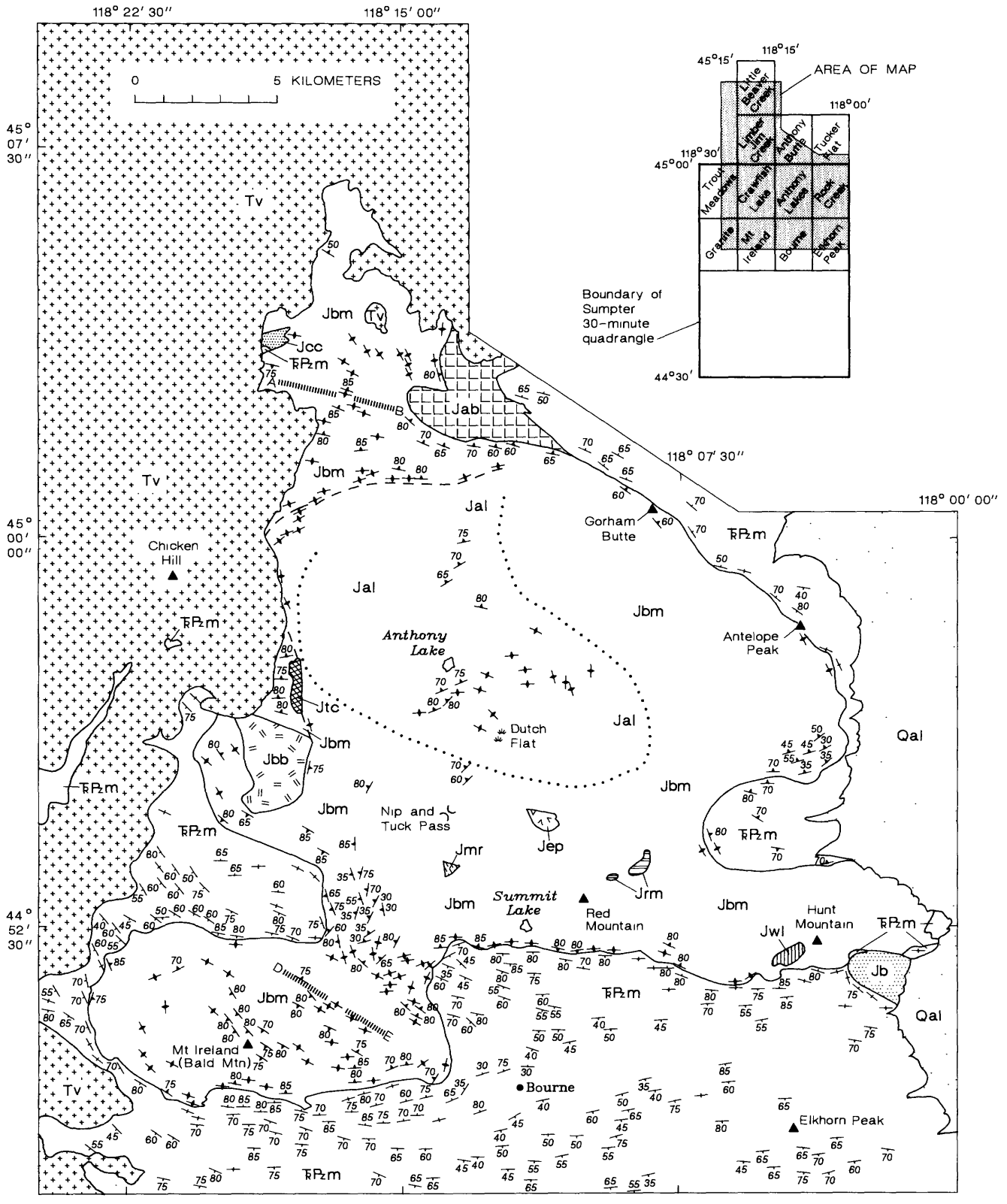

A

(Taubeneck, 1957) to leucogranite in accordance with the classification of Streckeisen (1973).

This chapter describes the metamorphic aureole and structure of the Elkhorn pluton, then updates

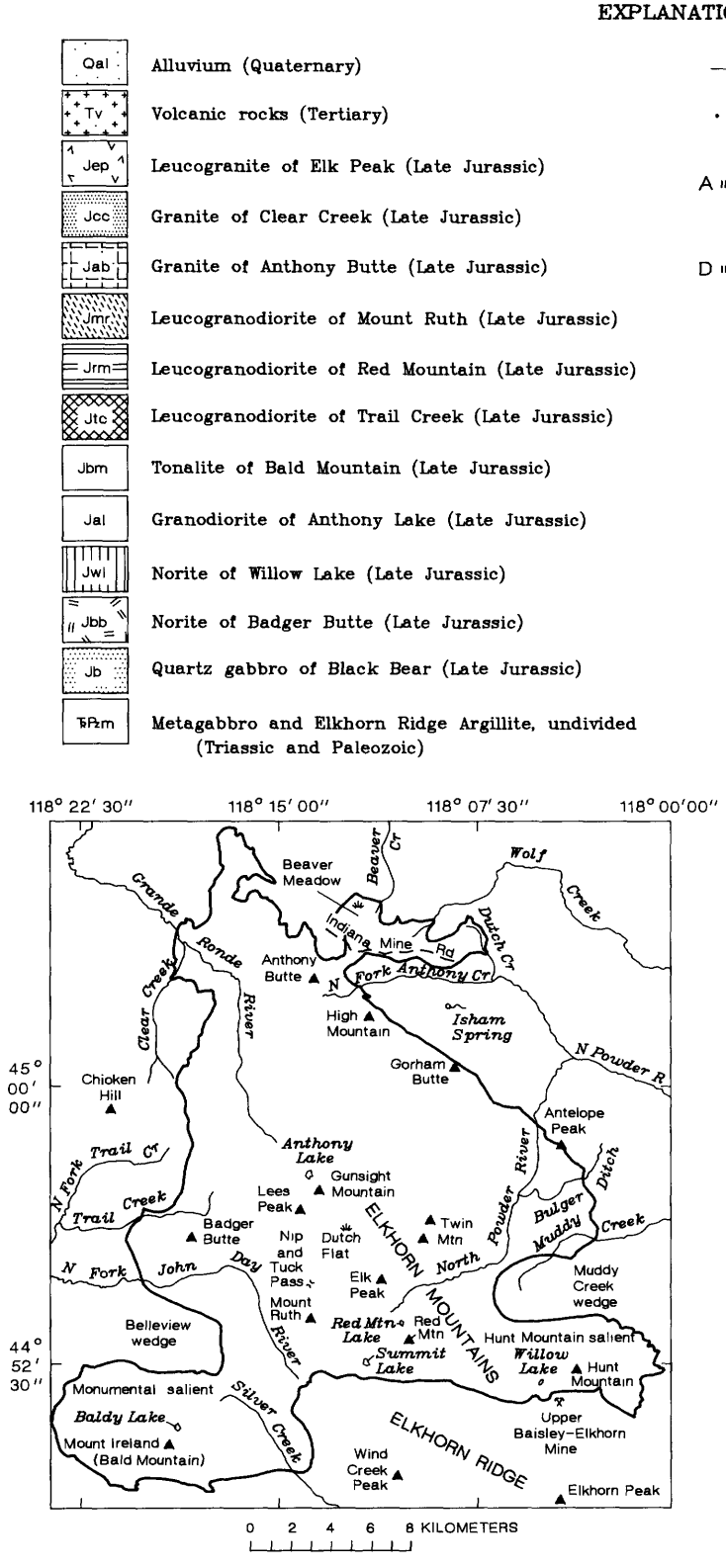

FIGURE 2.2.—Bald Mountain batholith. *A*, Generalized geology of all but northeastern part of Bald Mountain batholith. Except in area south and southwest of Hunt Mountain, contacts of the batholith with country rocks were mapped anew (since 1950's) on 7½-minute quadrangles shown in upper right corner. Within batholith, contacts of small intrusions south and southeast of Anthony Lake were mapped in 1950's on Sumpter 30-minute quadrangle (1901) and are only approximate. *B*, Topographic and cultural features of Elkhorn Mountains and extent of Bald Mountain batholith (heavy line is contact between batholith and country rocks). Also shown are named salients and wedges in southern part of Bald Mountain batholith.

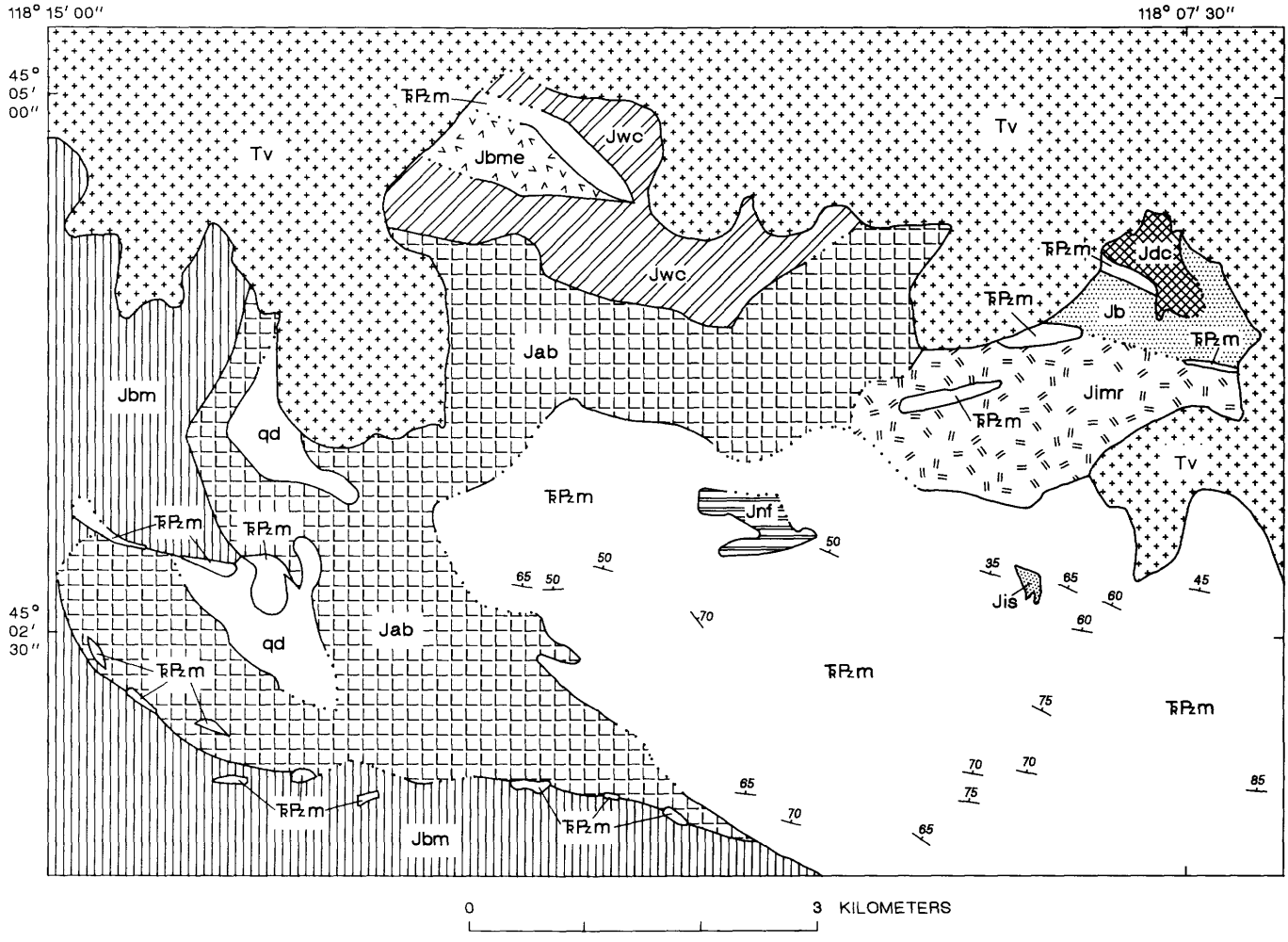

EXPLANATION

Volcanic rocks (Tertiary)

ROCKS OF CENTRAL PART OF BALD MOUNTAIN BATHOLITH

Tonalite of Bald Mountain (Late Jurassic)

ROCKS OF PERIPHERAL PART OF BALD MOUNTAIN BATHOLITH

Leucogranite of Dutch Creek (Late Jurassic)

Granite of Anthony Butte (Late Jurassic)
—Locally contains large quartz diorite inclusions (qd)

Granodiorite of Beaver Meadow (Late Jurassic)

Granodiorite of Indiana Mine Road (Late Jurassic)

Boundary quartz diorite unit (Late Jurassic)

Quartz diorite of Wolf Creek (Late Jurassic)

SATELLITIC ROCKS OF BALD MOUNTAIN BATHOLITH

Granite of Isham Spring (Late Jurassic)

Tonalite of North Fork (Late Jurassic)

PREBATHOLITHIC ROCKS

Metagabbro and Elkhorn Ridge Argillite, undivided (Triassic and Paleozoic)

Contact—Dotted where concealed

70 Strike and dip of bedding

FIGURE 2.3.—Geology of northeastern part of Bald Mountain batholith.

petrographic data for the norite of Badger Butte, the tonalite of Bald Mountain, and the granodiorite of Anthony Lake before describing the newly identified quartz diorite of Limber Creek and leucogranodiorite of Trail Creek.

The batholith north of lat 45° N. was not suitable for field studies until the 1960's because of dense timber that concealed the limited exposures, poor access, and the lack of topographic maps. About 80 km^2 of forest in the Anthony Butte quadrangle (fig. 2.2*A*) burned during 1960 in a wildfire known as the Anthony Burn. Moss and lichens that originally covered most exposures could not survive direct sunlight and reduced moisture. Formerly concealed exposures within the burn became apparent. In addition, much new bedrock was exposed along more than 180 km of

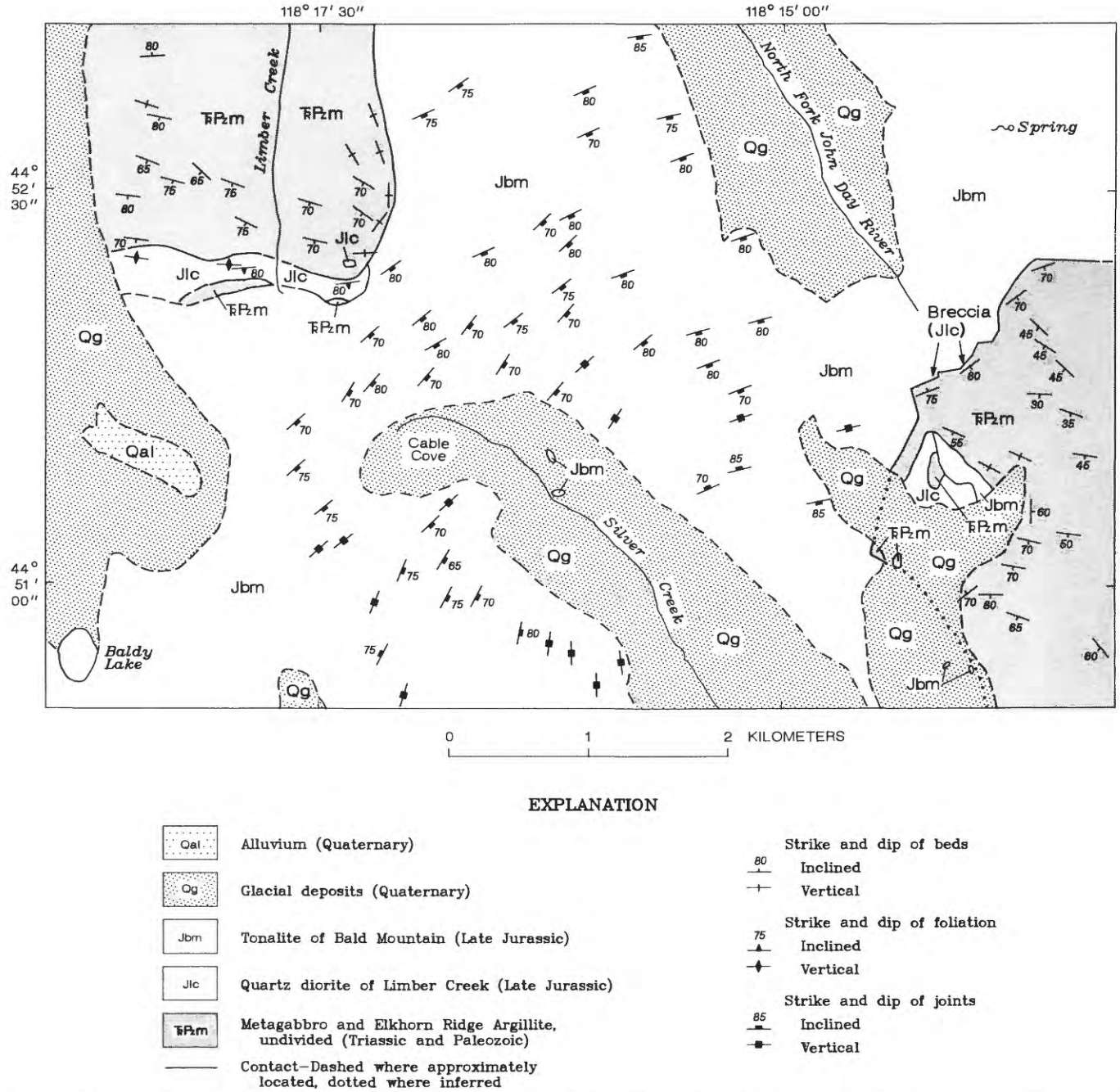

FIGURE 2.4.—Geology of area between Monumental salient (see fig. 2.2*B*) and central part of Bald Mountain batholith. Arrows pointing toward breccia indicate east and west extent of brecciated quartz diorite of Limber Creek.

roads that were constructed during and after the fire for purposes of firefighting, reforestation, erosion control, and timber salvage. Areas outside the Anthony Burn remain in timber and are poorly exposed, especially the southeastern part of the Limber Jim Creek quadrangle (fig. 2.2*A*), where at least 95 percent of the scattered exposures in an area of 20 km^2 are covered with moss and lichen. Thus, the fire and new roads were critical factors in creating adequate exposures to determine many geologic relations.

Much of this chapter concerns an area (fig. 2.3) in the Anthony Butte quadrangle where many heretofore-unreported intrusive units of the Bald Mountain batholith occur within and near the Anthony Burn. These units are mostly felsic; some have a high quartz content. The largest pluton consists of the hereinnamed granite of Anthony Butte, which is by far the most extensive granite in northeastern Oregon.

A major purpose of this chapter is to increase the data base for rocks of the batholith and to provide a reference for future studies. Ten new major-element analyses are included, but petrogenetic interpretations for the array of rocks in the batholith are not possible without additional data from trace elements and isotope geochemistry.

Mineral proportions (by volume) were determined by the point-counter method (Chayes, 1949), tallying at least 2,400 points for each of two or three large thin sections (generally 800–960 mm^2) of each analyzed rock. Two thin sections each were used for modal analysis of norite, quartz diorite, the granodiorite of Anthony Lake, and all tonalite except in the inlier 1.5 to 2 km southeast of the Grande Ronde Guard Station; three thin sections each were used for all other rocks. Classification of the rocks is based on the IUGS system (Streckeisen, 1973), except that a distinction between tonalite and quartz diorite was not made in the border rocks of the tonalite of Bald Mountain.

Specific-gravity determinations for rocks of the tonalite of Bald Mountain and the granodiorite of Anthony Lake were made on a beam balance by balancing the specimen in air and in water and measuring the change in length of the lever arm. Measurements are reproducible with ±0.01 precision.

Refractive indices of minerals in the metamorphic aureole were determined on suitably oriented grains by the immersion method using a sodium vapor lamp. After each determination, the immersion liquid was tested on a refractometer. The accuracy of refractive-index measurements is regarded as ±0.002.

Optic-axial angles for potassium feldspar were obtained (except where stated as estimates) with a four-ring universal stage by direct rotation (from one optic axis to the other) of crystals showing nearly centered acute-bisectrix figures.

Granitic rocks of the Bald Mountain batholith commonly are compared in this chapter with those of the Wallowa batholith. The Wallowa batholith is within the Wallowa Mountains (fig. 2.1), called in Oregon the "Swiss Alps of America." The peaks of the Wallowa Mountains and intervening glaciated canyons as much as 1,375 m in depth contribute to many superior exposures of granitic and metasedimentary rocks. The two batholiths and the Cornucopia stock, the major satellite of the Wallowa batholith, dominate the Late Jurassic granitic rocks of northeastern Oregon. Almost all of the Wallowa batholith and most of the Cornucopia stock are within the approximately 1,450-km^2 Eagle Cap Wilderness Area (fig. 2.1).

Fieldwork totaling 14.5 months in the Elkhorn Mountains was done in 1955, 1956, 1966, 1970, 1971, and 1983 through 1987. Fieldwork totaling 24 months in the Wallowa Mountains was done from 1956 through 1964 and from 1966 through 1969. The work in both mountain ranges was done alone.

ACKNOWLEDGMENTS

The writer thanks the Department of Geosciences of Oregon State University for office space and clerical support.

Tracy L. Vallier, Howard C. Brooks, Ellen M. Bishop, and Keith F. Oles provided many helpful suggestions for improving the manuscript.

A.J. Piwinskii provided indispensable analytical assistance at the University of Chicago in 1967 in microprobe determination of the composition of cores of oscillatory-zoned plagioclase feldspars. Additional core compositions were determined by Ellen M. Bishop at Washington University in St. Louis in 1983.

The writer also gratefully acknowledges the many courtesies of Howard C. Brooks and Mark L. Ferns of the Baker City office of the Oregon Department of Geology and Mineral Industries. During recent years these courtesies have ranged from the temporary storage of rock specimens and field equipment to discussions of the nineteenth- and early twentieth-century history of the Elkhorn Mountains and adjoining areas of northeastern Oregon.

Support for studies in the Elkhorn Mountains during 1970 and 1971 from National Science Foundation Research Grant GA-31852 is acknowledged with special gratitude. Studies of granitic rocks in the Wallowa Mountains were supported during the period 1956 through 1969 by National Science Foundation Grants G2415, G14553, GP-472, and GA-427.

AGE RELATIONS AND DISTRIBUTION OF ROCKS NEAR BALD MOUNTAIN BATHOLITH

The Bald Mountain batholith intrudes a widespread and heterogeneous assortment of metasedimentary rocks that compose the Elkhorn Ridge Argillite (Gilluly, 1937) as well as scattered masses of metagabbro with small amounts of serpentinized ultramafic rocks.

The Elkhorn Ridge Argillite consists of predominant argillite, tuffaceous argillite, cherty argillite, and ribbon chert with small amounts of tuff, graywacke, massive chert, limestone, and rare conglomerate. Fossils of Pennsylvanian, Permian, and Triassic age occur within limestone pods in the Elkhorn Ridge Argillite (Brooks and others, 1982) and indicate that the different limestones are parts of a complex lithologic mix of similar-appearing rocks. The Elkhorn Ridge Argillite has persistently defied attempts to stratigraphically subdivide it. Its most northerly exposures, heretofore unmapped, are located in the northern part of the inlier of pre-Tertiary rocks (fig. 2.5) in the Little Beaver Creek quadrangle (fig. 2.2*A*) and are part of the Baker terrane (Silberling and others, 1984).

The ages of the metagabbro and associated ultramafic rocks within the aureole are uncertain. Metagabbro exposed 50 km southeast of the batholith is at least 241 Ma (Brooks and others, 1982), whereas gabbroic rocks about 70 km southwest of the batholith are at least 278 Ma (Walker and Mattinson, 1980).

Small masses of previously unreported ultramafic rocks are associated with metagabbro and schistose amphibolite north of lat 45° N. in the Tucker Flat and Anthony Butte quadrangles (fig. 2.2*A*). These masses, mostly in country rocks near the southeast part of the granite of Anthony Butte (fig. 2.3), are among the northernmost exposures of ultramafic rocks in Oregon and are part of the Baker terrane.

K-Ar and Rb-Sr ages and Sr isotopic compositions (Armstrong and others, 1977) of rocks from the Bald Mountain batholith suggest emplacement of the batholith about 160 Ma in a volcanic-arc environment.

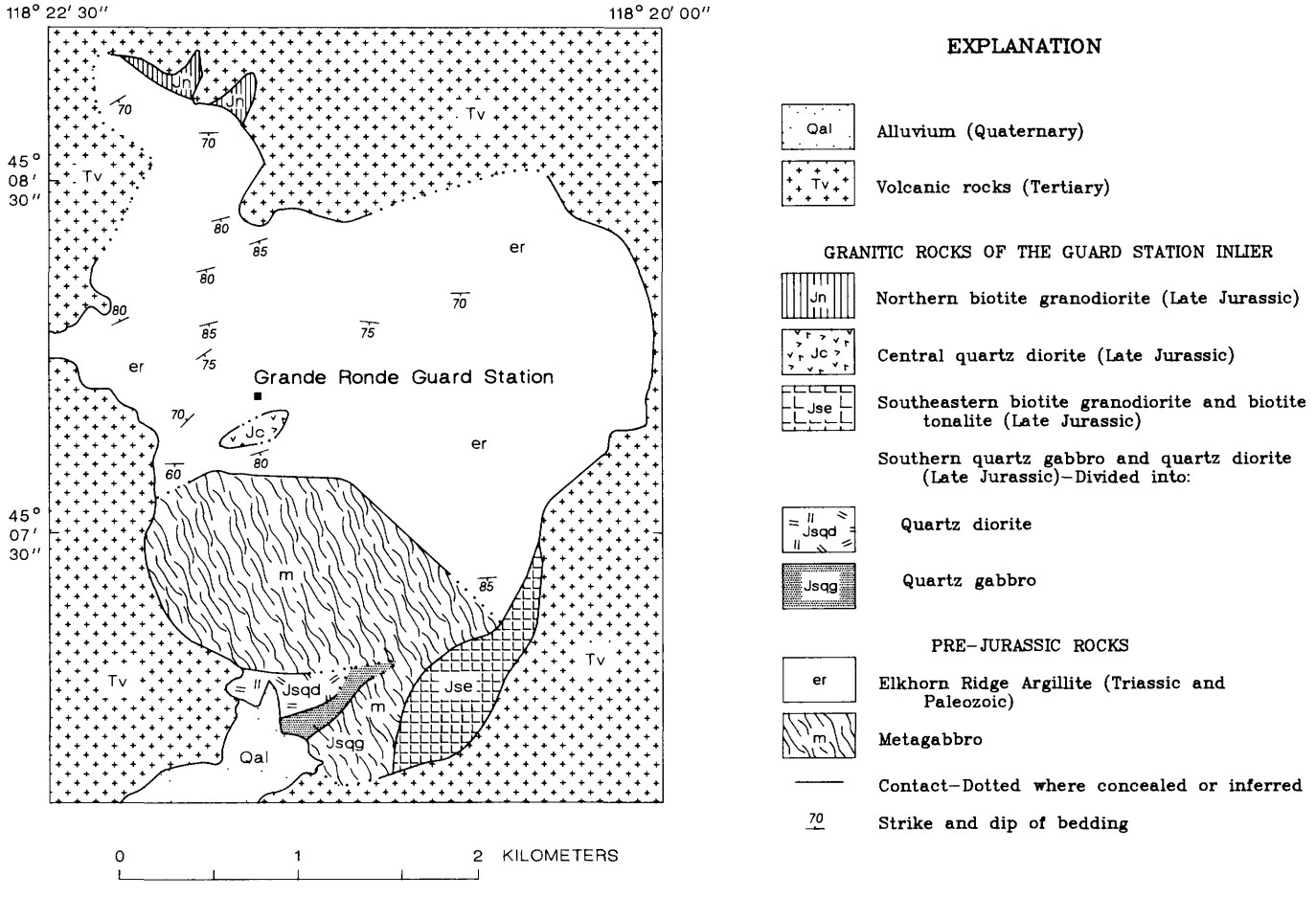

FIGURE 2.5.—Reconnaissance geology of Guard Station inlier. Many very small granitic bodies, including at least two consisting of granite, are not shown on map.

The northern part of the batholith is overlain by Miocene Grande Ronde Basalt in the Tucker Flat and Anthony Butte quadrangles (fig. 2.2*A*) and by older Tertiary volcanic rocks (Walker, 1973) to the west in the Limber Jim Creek quadrangle. The older volcanic rocks extend south of lat 45° N. into the Crawfish Lake quadrangle, where they conceal the west contact of the batholith with country rocks for about 6.5 km.

GEOGRAPHIC NAMES

For reference purposes certain parts of the batholith and adjacent country rocks have been assigned geographic names (fig. 2.2*B*). The westward-projecting mass of tonalite in the southwestern part of the batholith is known as the Monumental salient (Hewett, 1931). The wedge of country rocks that separates the north side of the Monumental salient from the central part of the batholith herein is called the Belleview wedge. The eastward-projecting mass of tonalite in the southeastern part of the batholith is designated the Hunt Mountain salient (Taubeneck, 1957). The wedge of country rocks that separates the north side of the Hunt Mountain salient from the central mass of the batholith is called the Muddy Creek wedge (Taubeneck, 1957).

METAMORPHIC AUREOLE OF BALD MOUNTAIN BATHOLITH

The well-developed contact aureole of the Bald Mountain batholith includes thermally metamorphosed ultramafic rocks, metagabbro, metadiorite, greenstone, graywacke, limestone, and chert. Argillaceous rocks of the Elkhorn Ridge Argillite—metamorphosed to pyroxene hornfels facies and including argillite, cherty argillite, and tuffaceous argillite (Pardee and Hewett, 1914)—are the predominant type of country rock. Ribbon chert and cherty argillite are the main rock types in the Belleview wedge, whereas metagabbro composes nearly all of the Muddy Creek wedge (fig. 2.2*B*). The widespread high-temperature assemblages in argillaceous rocks, impure limestone, metagabbro, and serpentinite near the contact of the batholith are attributed to the emplacement of hot and relatively dry tonalitic magmas.

Aureole rocks are considered in the order of ribbon chert, cherty argillite, argillite and tuffaceous argillite, limestone, metagabbro, and ultramafic rocks. The metamorphic mineralogy of cherty argillite is characteristic of pelitic assemblages, whereas the mineralogy of argillite and tuffaceous argillite is representative of basic assemblages. Field and laboratory data are mostly a summary of work done in the 1950's.

RIBBON CHERT

The grain size of recrystallized quartz in ribbon chert near the batholith generally is a good field approximation of the intensity of thermal metamorphism. Ribbon chert is moderately common throughout much of the aureole and locally is the dominant rock type. The rhythmic layers, mostly less than 7 cm thick, are separated by thin argillaceous partings. Quartz crystals in chert within 150 m of the contact are glassy and commonly 1 to 3 mm across in hand specimens. Grain size progressively decreases away from the batholith and generally is less than 0.5 mm in rocks more than 350 m from the contact.

Rocks of the Belleview wedge provide an example of the correlation of grain size in ribbon chert with intensity of thermal metamorphism. Ribbon chert and cherty argillite that are plastically deformed and intensively recrystallized characterize all but the southwestern part of the Belleview wedge. The grain size of most of the chert exceeds 0.5 mm and suggests metamorphism at temperatures of and above hornblende hornfels facies.

The correlation of grain size in ribbon chert and intensity of thermal metamorphism is evident elsewhere in northeastern Oregon in rocks of the Baker terrane. For example, the grain size of recrystallized quartz in ribbon chert is a useful guide to the proximity of the west and southwest contacts of the Big Lookout Mountain stock, which is about 68 km east-southeast of Hunt Mountain, and of the south and southeast contacts of the Pedro Mountain stock, which is about 64 km southeast of Hunt Mountain (figs. 2.1 and 2.2).

CHERTY ARGILLITE

High-temperature mineral assemblages in metamorphosed cherty argillite in the Belleview wedge differ in mineralogy from assemblages in cherty argillite south of the Elkhorn pluton. Moreover, gneiss derived primarily from cherty argillite extends throughout most of the Belleview wedge, whereas the distribution of metasedimentary gneiss is restricted elsewhere in the aureole. Accordingly, metamorphosed cherty argillite of the Belleview wedge and of the aureole south of the batholith are described separately.

IN THE BELLEVIEW WEDGE

Metasedimentary rocks in an 18-km^2 area of intense metamorphism comprising most of the Belleview

wedge were justifiably regarded as Archean gneiss by Lindgren (1901, p. 577), who correctly reported that the rocks have no counterparts in northeastern Oregon. Lindgren (1901, p. 594) rejected "the supposition of contact-metamorphic origin" for the gneiss because "it is completely recrystallized over a large area." The rock type and age assignment of Lindgren (1901) underscore the unique features of the metasedimentary rocks. The gneiss is mostly an intensely metamorphosed cherty argillite but includes some very argillaceous ribbon chert that also was converted into gneissic rocks. Metamorphosed ribbon chert typically is composed of more than 90 to 95 percent quartz and therefore occurs either as small and distinct quartz-rich areas within the gneiss or as much larger areas, many meters in width, that alternate with gneiss. The visible difference in quartz content between areas of metamorphosed ribbon chert and gneiss is accentuated by the common retention of very crude bedding (the original argillaceous partings) in the ribbon chert, in contrast to the obliteration of sedimentary bedding in the gneiss. Foliation in the gneiss is mostly defined by wispy streaks and lenticular concentrations of biotite as much as 3 cm long. Assorted boudins in the gneiss commonly intensify the foliation. The gneiss is not migmatitic or cut by leucocratic veins, except locally by small pegmatites that contain tourmaline.

Modal analyses of ten rock specimens of gneiss gave the following range in volume percent for the five major minerals: quartz, 41.1 to 74.5; plagioclase, 7.1 to 29.6; biotite, 8.0 to 23.4; orthoclase, 0.3 to 8.8; and cordierite, 2.1 to 7.3. Significant minerals present in some but not all rock specimens are sillimanite, andalusite, and garnet. Muscovite (from 0.3 to 2.4 percent by volume) occurs in eight rocks and is mostly a replacement of cordierite and andalusite, as well as of orthoclase and plagioclase. Some muscovite in three rocks could be primary. Accessory minerals generally include fairly constant amounts of apatite, tourmaline, monazite, and iron oxides, but widely variable quantities of graphite (from 0.1 to 4.2 percent by volume).

The overall grain size of the gneiss is approximately 1 mm; quartz and cordierite have maximum dimensions of about 3 mm, whereas biotite and plagioclase have maximum dimensions of only about 1.5 mm. Biotite and cordierite in strongly deformed rocks exhibit marked parallelism to foliation, as do most of the small aggregates of graphite (as much as 0.25 mm in length) that typically occur along grain boundaries. The most extreme elongation of cordierite is about 10 to 1. In strongly deformed rocks some quartz that is 2 to 3 mm in greatest dimension and parallel to foliation has length-to-width ratios of as much as 4 to 1 and rarely 5 to 1.

All 21 rock specimens of gneiss were collected from about 9 to 360 m from the batholith. The diagnostic high-temperature pair of cordierite and orthoclase occurs with quartz, plagioclase, and red-brown biotite in each of the 21 rock specimens. The potassium feldspar is orthoclase, as determined on the flat stage by estimated optic-axial angles ($2V$) of about 55° for nearly centered acute-bisectrix figures. Zoning in the plagioclase is a clear indicator of disequilibrium. Rather strong normal zoning predominates, but locally as many as four oscillations occur.

Sillimanite, fibrolite, garnet, and andalusite occur in two or more of the 21 rock specimens of gneiss. Sillimanite is the name applied here to prisms that are approximately 0.01 mm or more in width, whereas fibrolite denotes much thinner prisms that occur mostly as fibrous bundles, sprays, and mats. Sillimanite is present in two rocks, 9 and 30 m from the batholith. Garnet and fibrolite each occur in six rocks from 9 to about 360 m from the batholith; two of the rocks contain both minerals. Garnets are mostly from 0.05 to 0.5 mm across; a few are as much as 1.0 mm across. Crystals less than about 0.1 mm are commonly euhedral to subhedral, whereas larger garnets are mostly irregular, commonly perforated, and frequently characterized by a core of opaque inclusions. Andalusite, present in eight rocks from 20 to about 345 m from the batholith, is a relict mineral generally composing not more than 0.2 percent by volume of each rock. Simultaneous extinction of relicts in three thin sections indicates that andalusite originally occurred as crystals of at least 0.5 to 1.0 mm in size. The relicts also suggest that andalusite was of wide occurrence during the early history of the gneiss. Significantly, in the extreme southwestern part of the Belleview wedge, beyond the area of gneiss, euhedral porphyroblasts of andalusite occur about 1 km from the batholith.

No specimens of gneiss were collected farther than 360 m from the contact with the batholith, so no report of metapelitic assemblages in the interior of the Belleview wedge is possible in this chapter. Some specimens of basic metasedimentary rocks, however, provide information about metamorphic intensities in the interior of the wedge. Basic metasedimentary rocks containing amphibole and (or) pyroxene are rare in the Belleview wedge, but they do occur very near the center of the wedge, approximately 1.9 km from both the south and north contacts of the batholith. The rocks are well foliated and contain hornblende commonly from 0.5 to 1.0 mm in greatest dimension. Among five rock specimens that were collected, one contains brown hornblende, plagioclase, diopside, and quartz, whereas three contain brown hornblende and plagioclase with

small amounts of both biotite and quartz. The fifth rock specimen contains cummingtonite, plagioclase, and biotite with minor quartz and brown hornblende. The five rock specimens from the center of the Belleview wedge are very similar to cummingtonite and brown hornblende schists found within 100 m of the contact on the south side of the batholith where they are in the upper part of the hornblende hornfels facies.

SOUTH OF THE ELKHORN PLUTON

Contact metamorphism of cherty argillite south of the Elkhorn pluton is superimposed on a regional greenschist-facies metamorphism characterized by green biotite. The aureole is exposed in its entirety only on the south side where country rocks extend outward for 14 km from the contact of the pluton without being concealed by Cenozoic volcanic rocks or wide alluvial valleys. The outer limit of the aureole is difficult to determine in argillaceous rocks because the distinction between green and brown biotite is not optically possible in very fine grained metasedimentary rocks. Brown biotite is much easier to identify in metagabbro near the aureole boundary; it occurs in chlorite in metagabbro 6.5 km from the Elkhorn pluton.

Proceeding toward the batholith in the zone of brown biotite, garnet is present about 2,500 m from the contact but is not common within the aureole, whereas cordierite is common and occurs at least 1,320 m from the contact. Orthoclase is found at least 1,270 m from the contact. Inadequate rock specimens of cherty argillite prevent a more precise determination of the first appearance in the aureole of garnet, cordierite, and orthoclase.

Grain size in metamorphosed cherty argillite south of the batholith varies considerably even within the same thin section. Within a given thin section, grain size is determined by the ratio between quartz and argillaceous material, including graphite. For example, a quartz-rich layer or lens in a thin section commonly will have a grain size several times larger than that of associated argillaceous layers and lenses. Grain size decreases as the amount of biotite and graphite increases. Thus grain size in the metapelitic cherty argillite cannot be correlated as closely with distance from the batholith as can the size of quartz crystals in metamorphosed ribbon chert. The general range in grain size for most rock specimens of cherty argillite within 15 m of the contact is 1 to 2 mm for quartz, 0.2 to 0.5 mm for biotite, and 0.4 to 1.3 mm for orthoclase, plagioclase, and cordierite.

Petrographic data in this paragraph apply to 71 aureole specimens of cherty argillite, all collected approximately S. 10° E. of Summit Lake (fig. 2.2) along a traverse of 1,090 m that commenced at the contact of the batholith. Orthoclase, cordierite, quartz, and biotite are the major rock components. Plagioclase is present only in small amounts, if at all, and exhibits good normal zoning as far from the intrusive contact as 125 m. The potassium feldspar is orthoclase as determined (for samples from contact outward for 410 m) on the flat stage by estimated $2V$ from about 50° to 60° for nearly centered acute-bisectrix figures. Cordierite is elongated parallel to foliation; elongation ratios are most pronounced in schists between 240 and 620 m from the batholith. Four very strongly foliated schists contain cordierite with elongation ratios ranging from 5 to 1 to as much as 10 to 1; ratios of as much as 12 to 1 occur in two other schists. Within about 575 m of the batholith, muscovite occurs only in small amounts, but it is much more abundant farther from the intrusive contact. Most muscovite within half a kilometer of the batholith is an alteration of cordierite, whereas many flakes of muscovite farther than 575 m from the contact are independent of cordierite. Muscovite not associated with cordierite commonly crosscuts foliation; this relation implies a retrograde origin for the muscovite.

Biotite is widely distributed throughout the aureole and allows investigation of the possibility that the mineral composition of biotite changes progressively with increasing metamorphism. Pitcher and Sinha (1957) showed that changes in composition of biotite in the aureole of the Ardara pluton, Northern Ireland, coincide with systematic variations in refractive index. Biotite from the aureole of the Bald Mountain batholith was concentrated from 72 rocks that were collected south of the batholith from within 950 m of the contact. The β index for biotite from rocks within 230 m of the contact is generally between 1.637 and 1.655, whereas the index is mostly between 1.607 and 1.637 for rocks farther from the contact. The index for biotite from 12 of the 72 rocks is inconsistent with these values. Therefore, the data show only an approximate correlation between refractive index of biotite and metamorphic intensity. The higher indices that characterize most biotite within 230 m of the batholith presumably denote increases in ferrous iron and titanium in the biotite (Pitcher and Sinha, 1957).

Graphite is much more abundant in the aureole rocks than is apparent from the examination of thin sections because it occurs as small flakes along grain boundaries. The mineral commonly is rather inconspicuous partly because the thin sections are made at right angles to the planes of schistosity and bedding in which the flakes lie. Accordingly, the small crystals in general show the minimum cross-sectional area

and are easily overlooked in many rocks that contain comparatively small amounts of graphite. An estimated 20 percent of the argillaceous rocks (argillite as well as cherty argillite) collected south and southeast of Summit Lake contain more than 2 percent graphite. The presence of graphite in argillaceous rocks can be verified by placing –100-mesh powder of crushed rock in a large glass beaker and vigorously introducing tap water, allowing the larger grains to settle from the suspended minute particles, and decanting and repeating the process. Where graphite is present, a grayish-black scum of the mineral will collect on the top of the water in the beaker.

Rutile also is more abundant than apparent in thin sections, in which it is discerned as small crystals that mostly appear opaque in ordinary light and commonly are masked by flakes of associated biotite. The crystals of rutile are best seen petrographically in convergent light. The abundance of rutile became evident after the heavy minerals were extracted from the 72 rocks that were crushed for the separation of biotite. Knee-shaped twins of rutile are common among the heavy minerals; rutile probably is more widespread in metamorphosed argillaceous rocks than has been realized.

Sporadic tourmaline is seen in thin sections of rocks from near the contact of the Elkhorn pluton to beyond the aureole. Much of the tourmaline is in biotite-rich horizons within cherty argillite. The mineral was seen neither in microfractures (in thin sections) nor as megascopic crystals in veins and along joints. Concentrations of tourmaline were obtained from 21 rocks within 20 to 2,400 m of the contact, but no pattern was recognized in the indices of refraction, distribution, or color of tourmaline throughout this part of the aureole. The distribution and occurrence of tourmaline suggest that it is not a metasomatic byproduct of granitic emanations. Presumably boron in the argillaceous sediments contributed to the growth of tourmaline.

Remarkable concentrations of apatite occur in a thin section of a cherty argillite collected southeast of Summit Lake and about 20 m from the near-vertical contact of the batholith. The largest concentration of apatite is confined to a quartz-rich area of 24 mm^2 that contains 451 apatite crystals mostly 0.01 to 0.20 mm across. Apatite constitutes 16.2 modal percent of the rock within the quartz-rich area. Two hundred ninety-three crystals of apatite occur along three chainlike stringers that represent annealed fractures. The other 158 crystals are restricted to grain boundaries between quartz. The second eye-catching occurrence of apatite is a lens-shaped pod packed with 93 crystals; the pod is about 1.0 mm long and as much as 0.35 mm wide. Two more concentrations of apatite are associated with continuous sequences of biotite that define recrystallized argillaceous material. One occurrence consists of 23 closely spaced crystals within 2.0 mm, whereas the other has 9 chainlike crystals within a distance of 0.5 mm.

Two additional concentrations of apatite are present in a thin section of a cherty argillite also collected southeast of Summit Lake but about 35 m from the batholith. Both occurrences are veinlike and parallel to the foliation, and they extend mostly along grain boundaries of quartz. Locally, however, one or more comparatively large crystals of quartz are crossed by the veins. One vein containing about 560 small crystals of apatite extends from the edge of the thin section for about 12 mm into the interior of the section. The second vein contains an estimated 700 crystals of apatite and extends across the width of the thin section for about 16 mm. All concentrations of apatite in the two rock specimens are interpreted as of pneumatolytic origin.

Index determinations for apatite from 26 aureole rocks within 1,000 m of the batholith range from 1.633 to 1.640 for n_e and from 1.637 to 1.643 for n_w; these values are essentially the same as indices for apatite extracted from four widely scattered tonalite specimens from the batholith. All indices are characteristic of fluorapatite.

Garnet, from about 0.02 mm to rarely as much as 0.5 mm across, occurs in 12 rock specimens from 3 to about 2,500 m from the batholith. Much of the garnet is irregular, but nearly all crystals less than about 0.1 mm in four rock specimens are subhedral. Crystals in half of the rock specimens are commonly perforated with voids as much as 0.02 mm across; many crystals in two rock specimens contain opaque inclusions.

Andalusite as partly resorbed porphyroblasts is present in two rock specimens from an area about 780 m from the batholith. The embayed and scalloped crystals, from 0.5 to 0.9 mm in greatest dimension, are separated from the graphitic groundmass by a clear rim of quartz as much as 0.2 mm wide. Andalusite, which also was recovered as a heavy mineral from one rock specimen that was crushed for the separation of biotite, clearly was unstable during the late crystallization history of the aureole rocks southeast of Summit Lake.

ARGILLITE AND TUFFACEOUS ARGILLITE

Argillite and tuffaceous argillite within 670 m of the south contact of the batholith occur mostly as rocks of the hornblende hornfels facies, but a narrow

zone of pyroxene hornfels-facies rocks is present near the batholith. The outward extent of hornblende hornfels-facies rocks beyond 670 m is unknown.

Rocks of both facies are well exposed for almost 8 km near the contact west of Hunt Mountain (fig. 2.2). The rocks are contact schists rather than hornfelses. Orthopyroxene was found as far as 38 m from the batholith, but common replacement by cummingtonite suggests that the original outward distribution of orthopyroxene was greater. Typical assemblages containing orthopyroxene are (1) orthopyroxene-plagioclase-quartz, (2) orthopyroxene-plagioclase-biotite-quartz, and (3) orthopyroxene-plagioclase-diopside-quartz with or without hornblende. Refractive-index determinations of α and γ for orthophyroxene separated from six specimens gave compositions of En_{48} to En_{52}. Determinations of α and γ indices for plagioclase separated from the same six specimens gave compositions of An_{34} to An_{44}.

Both cummingtonite and hornblende are common in the hornblende hornfels-facies rocks. The two amphiboles occur together in some rocks but separately in other rocks. Cummingtonite is common from the contact outward for about 200 m but occurs as far outward as 650 m. Both brown and green hornblende are present; most brown hornblende occurs within about 100 m of the batholith. Some brown hornblende contains cores of cummingtonite. The typical assemblage containing either cummingtonite or hornblende as the only amphibole includes plagioclase and quartz with or without biotite. Diopside may occur as an additional mineral in rocks that contain hornblende as the only amphibole.

Eight rock samples of argillite were collected from the dismembered screen between the herein-named granodiorite of Indiana Mine Road (fig. 2.3) and the boundary quartz diorite unit for comparison with metamorphic assemblages in argillaceous rocks near the south contact of the Elkhorn pluton. Five of these samples are pyroxene hornfels-facies rocks that contain variable amounts of orthopyroxene, diopside, hornblende, plagioclase, and quartz; biotite is an additional mineral in two of the five samples. The remaining three samples are hornblende hornfels-facies rocks that contain hornblende, plagioclase, and quartz, with or without diopside.

LIMESTONE

Scattered xenoliths of calc-silicate rocks occur throughout much of the batholith, but wallrock contacts with metacarbonate rocks are rare at the present levels of exposure. Metamorphosed limestone near the batholith occurs either as marble, as bedded calc-silicate rocks, or locally as garnet skarns. Nearly all exposures of these rocks within 30 m of the contact are poor and discontinuous. Wollastonite is the highest temperature index mineral in the metacarbonate rocks. The best and most accessible examples of both a garnet skarn and bedded calc-silicate rocks containing wollastonite are about 1.2 km S. 55° E. of Antelope Peak (fig. 2.2).

Abandoned prospect pits southeast of Antelope Peak aid in following the garnet skarn along the contact of the batholith. Minor quartz and epidote occur with the garnet. A narrow zone of scheelite as much as 1.5 cm wide commonly extends along the garnet-marble contact; smaller amounts of scheelite occur within the massive garnet. The garnet-marble contact, several meters or more from the edge of the batholith, is sharp and irregular and has extensions of garnet projecting into the marble in a manner consistent with metasomatism of a pure limestone.

Tonalite as much as 4 m from the contact of the garnet skarn on the southeast slopes of Antelope Peak contains diopside instead of hornblende and biotite. Considerable sphene is characteristic of diopside tonalite. Thin sections of 2 of 11 rocks show associations of diopside and hornblende that suggest replacement of amphibole by pyroxene. Formation of diopside is attributed to reaction of the solidifying magma with limestone and enrichment of CaO with concomitant loss of Al_2O_3, (Mg,Fe)O, and SiO_2 to the wallrocks. In the tonalite, TiO_2 freed by cessation of crystallization of hornblende and biotite combined with CaO to form sphene. However, the volume of garnet skarn requires the transfer of much more material than could have been derived from the apparent volume of diopside tonalite as exposed at the surface.

Bedded calc-silicate rocks near the contact southeast of Antelope Peak occur as fine-layered sequences mostly from 5 to 20 mm in width but also in layered sequences more than 20 mm wide. Only the wide layers were sampled. Assemblages in seven rock specimens are wollastonite-diopside-plagioclase and wollastonite-garnet-diopside. Plagioclase separated from three rocks is An_{93-96}. The four minerals in the two assemblages have random orientations except where wollastonite is aligned between two or more closely spaced crystals of garnet. Preferential deformation of plagioclase is evident by recrystallized shear zones, bent twinning lamellae, and microfaults with offset twin lamellae.

Wollastonite in the Belleview wedge occurs in four small lenses of bedded calc-silicate rocks at distances of about 100, 250, 310, and 1,300 m from the batholith. The lenses are from 0.5 to 3.0 m in maximum width and from about 4 to 7 m in length. The most conspic-

uous feature of the four metamorphosed carbonate lenses is repetitious sequences of apparently monomineralic zones of red-brown garnet, green diopside, and white wollastonite. Some layers are as much as 20 mm across, but most are less than 8 mm; many layers are less than 3 mm, and some are less than 1 mm. Sawed surfaces (45 to 65 cm^2) of hand specimens clearly reveal that the calc-silicate layers interfinger. Layers commonly are less than about 0.3 mm wide where they terminate. Coarsely crystalline marble occurs with the calc-silicate sequences in two of the metacarbonate lenses. Zones of pure marble contain no calc-silicate minerals, whereas marble zones with minor impurities contain either scattered silicate crystals or crystals concentrated in laminae that commonly are very thin. For example, some layers of garnet in marble do not exceed 1 mm in width and 25 mm in length.

Two thin sections of fine-layered calc-silicate rocks from each of the four metacarbonate lenses disclose that the layering consists primarily of alternating sequences of wollastonite-diopside, garnet-diopside, and plagioclase-diopside. Two or more layers that contain the same minerals commonly differ in modal proportions, but no true monomineralic zones were detected, except for short distances of not more than about 8 mm. However, zones of wollastonite with only about 4 volume percent diopside extend across the width (24 mm) of thin sections, as do both zones of garnet with only about 10 volume percent diopside and zones of diopside with only about 10 volume percent plagioclase. The metacarbonate lens farthest (1,300 m) from the batholith differs from the other lenses in the presence of minor quartz in some layers of both diopside-plagioclase and garnet-diopside.

Foliation in the calc-silicate layers is mostly defined by elongated crystals of wollastonite; the other minerals are more or less equigranular and generally less than 0.5 mm across. Many crystals of wollastonite are almost 1 mm in length and rarely as much as 3 mm. In strongly foliated rocks many wollastonite crystals have elongation ratios from 7:1 to as much as 9:1. Polysynthetic twinning in plagioclase in strongly deformed rocks commonly is parallel to bedding. Twinning lamellae in plagioclase are deformed both by plastic deformation and by rupture. Maximum deformation of plagioclase occurs in crystals more than 1 mm across that exhibit common differences in directions of twinning lamellae from 15° to 20°.

METAGABBRO

Thermal metamorphism of metagabbro without a dynamic component is characterized by the random crystallization of amphibole needles that penetrate original plagioclase in a decussate fashion. The gabbroic texture is somewhat modified but never obliterated. Most metagabbro within 1,000 m of the batholith, however, is dark amphibolite that commonly shows only traces of the original gabbroic texture. Many of the metagabbros are schistose. Intensely deformed metagabbros commonly show gneissic layering with alternating light and dark layers that resembles the bedding in some metasedimentary rocks (fig. 2.6). The difficulty in recognizing intensely metamorphosed metagabbro is underscored by a small inlier of pre-Tertiary rocks about 2.5 km due south of Chicken Hill (fig. 2.2). Throughout this inlier, metagabbro with gneissic layering is shown as "argillite series" on an otherwise excellent map by Pardee (1941). Good exposures of the misinterpreted metagabbro are on either side of the North Fork of Trail Creek (fig. 2.2*B*). The light layers are plagioclase, whereas the dark layers are mostly hornblende and diopside. In some metagabbroic rocks near the batholith the light layers are elongated lenses. Much less commonly the metagabbros contain so little plagioclase that on weathered surfaces they are a uniform greenish-black to coal black. Some metagabbro at the contact of the batholith at an elevation of about 2,578 m and 0.59 km S. 15° E. of Summit Lake (fig. 2.2) shows contorted layering that suggests plastic deformation.

Strongly foliated amphibolite occurs mostly within 200 m of the batholith, throughout much of the Muddy Creek and Belleview wedges (fig. 2.2*B*), and as screens and inclusions within the batholith. Foliation generally dips within 20° of vertical. At least a few unequivocal vestiges of gabbroic texture (fig. 2.7) survive in all bodies of metagabbro outside of the batholith except one small mass in the Belleview wedge. Although most gabbroic relics in the amphibolites are lens-shaped (fig. 2.7), some are small knotlike masses, commonly from 0.5 to 2.5 cm across; locally, two or more closely spaced knots resemble boudins or even large rolled garnets.

The typical foliated amphibolite is characterized by a simple assemblage of plagioclase, hornblende, iron oxide, and apatite. Plagioclase compositions range from An_{62} to An_{86}, as determined by refractive indices of crystals separated from nine samples of amphibolite. Minor quantities of quartz and green diopside are present in some amphibolites. Plagioclase in many amphibolites has been completely recrystallized to equant xenoblastic grains that are water-clear and commonly untwinned. Rounded and lens-shaped relics of the original plagioclase persist in some amphibolites. Recrystallization is accompanied by reduction in average grain size from considerably more than 1.0 mm to slightly less than 0.1 mm. The average grain size of

hornblende in rock specimens of strongly foliated amphibolite ranges from 0.35 to 0.10 mm. The foliated amphibolite is indicative of directed pressure associated with the forceful injection of granitic magma.

A notable feature of some schistose amphibolites north of lat 45° N. is the presence of so-called segregation veins and lenses that are leucocratic except for central concentrations of garnet. Locally, where extreme deformation and recrystallization have occurred, the garnet-filled veins and lenses provide evidence of the metagabbroic origin of the amphibolite.

Pyroxene hornfels-facies amphibolites occur in the northern and western parts of the batholith as judged by samples collected near (1) Gorham Butte (fig. 2.2), (2) from a dismembered screen along the southwest contact of the herein-named granite of Clear Creek (fig. 2.2) with the Elkhorn pluton, (3) from a dismembered screen between the herein-named leucogranite

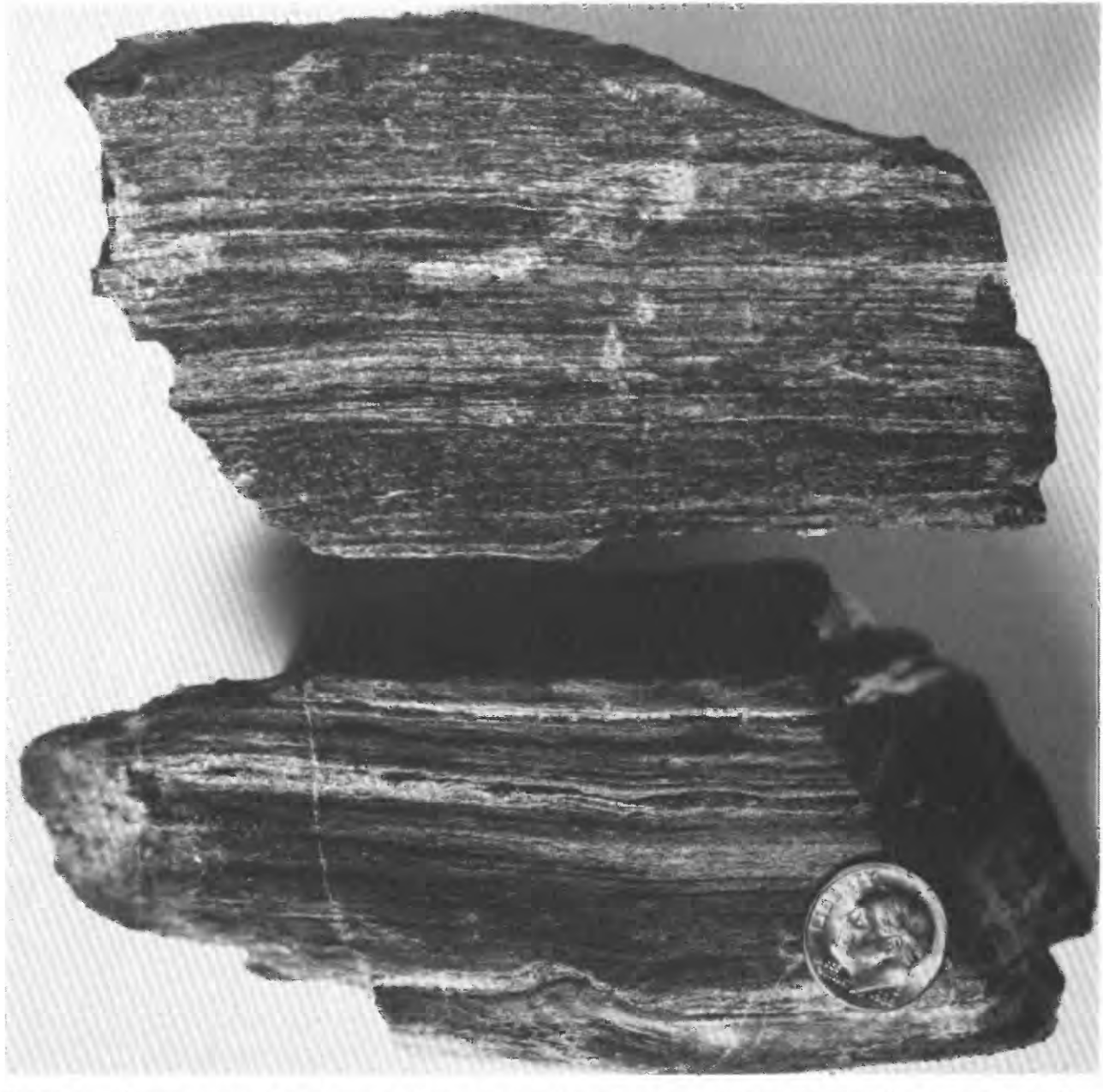

FIGURE 2.6.—Gneissic layering in intensely deformed metagabbro. Such layering can be mistaken for metasedimentary bedding. Lower rock specimen is from small inlier of metagabbro about 2.5 km south of Chicken Hill (fig. 2.2). Upper specimen was collected about 125 m from Bald Mountain batholith near westernmost part of Muddy Creek wedge (fig. 2.2*B*). Coin is about 18 mm in diameter.

of Dutch Creek and the boundary quartz diorite unit (fig. 2.3), and (4) from a large inclusion at least 3 m long in the Elkhorn pluton. This inclusion is 1.65 km N. 31° E. of Badger Butte, about 60 m due west of Trail Creek (fig. 2.2*B*), on the west side of a dirt road that closely parallels Trail Creek; it is just north of a conspicuous xenolith of layered calc-silicate rock at least 12 m long. The consistent assemblage for the pyroxene hornfels-facies amphibolites from all four localities is orthopyroxene-diopside-plagioclase, with or without hornblende.

ULTRAMAFIC ROCKS

Serpentinized ultramafic rocks are present in the aureole as small lenses commonly less than 25 m wide that constitute about 1.5 percent of the country rock within 2 km of the batholith. According to Evans (1977), the following minerals in serpentinite indicate progressive zones of increasingly intense thermal metamorphism: (1) tremolite, (2) talc, (3) anthophyllite, (4) enstatite, (5) spinel, (6) pargasitic hornblende, and (7) plagioclase. The first mineral in the series, tremolite, marks the transition from greenschist to hornblende hornfels facies, and the next-to-last mineral, pargasitic hornblende, denotes the transformation to pyroxene hornfels facies. Tremolite occurs in nearly all ultramafic rocks within 1.6 km of the Bald Mountain batholith. Green spinel appears before enstatite, but otherwise the progressive sequence of index minerals closely parallels the parageneses of Evans (1977).

Green spinel (n=1.756 to 1.767) is present in most ultramafic rock specimens collected within 200 m of the batholith. Specimens from near the contact commonly contain 4.0 to 11.3 volume percent spinel. Grain size increases and crystals become more nearly euhedral as the batholith is approached. Subhedral to euhedral spinel crystals between 0.3 and 0.5 mm across are common in thermally metamorphosed serpentinite within about 30 m of the contact. Some green spinel is enclosed or adjacent to chlorite and less commonly phlogopite. The chlorite apparently is clinochlore, as suggested by birefringence of about 0.08, distinct polysynthetic twinning, biaxial + figure, and estimated $2V$ of 25°. Chlorite in the aureole rocks overlaps the stability field of enstatite.

The highest temperature metamorphic assemblage in ultramafic rocks in the Elkhorn Mountains is near the apex of the Belleview wedge (fig. 2.2*B*), where metaperidotite contains olivine, clinopyroxene, enstatite, pargasitic hornblende, and commonly plagioclase with small amounts of phlogopite, green spinel, and uncommon chlorite. The assemblage, which indicates pyroxene hornfels facies, is rare in high-grade contact-metamorphic aureoles; plagioclase peridotite hornfels were first reported by Frost (1976) near the contact of a gabbro that is an early unit of the Mount Stuart batholith, Washington. In the Elkhorn Mountains the high-grade plagioclase peridotite hornfels are exposed at elevations between 2,225 and 2,270 m in a lens as much as 30 m wide near the crest of the ridge about 4.3 km N. 31° E. from the summit of Mount Ireland. These exceedingly tough rocks can only be adequately sampled with a long-handled rock hammer such as those available in England and Germany or with a somewhat heavier American sledge hammer.

Pargasitic hornblende, olivine, and clinopyroxene are the most abundant of the major minerals in the

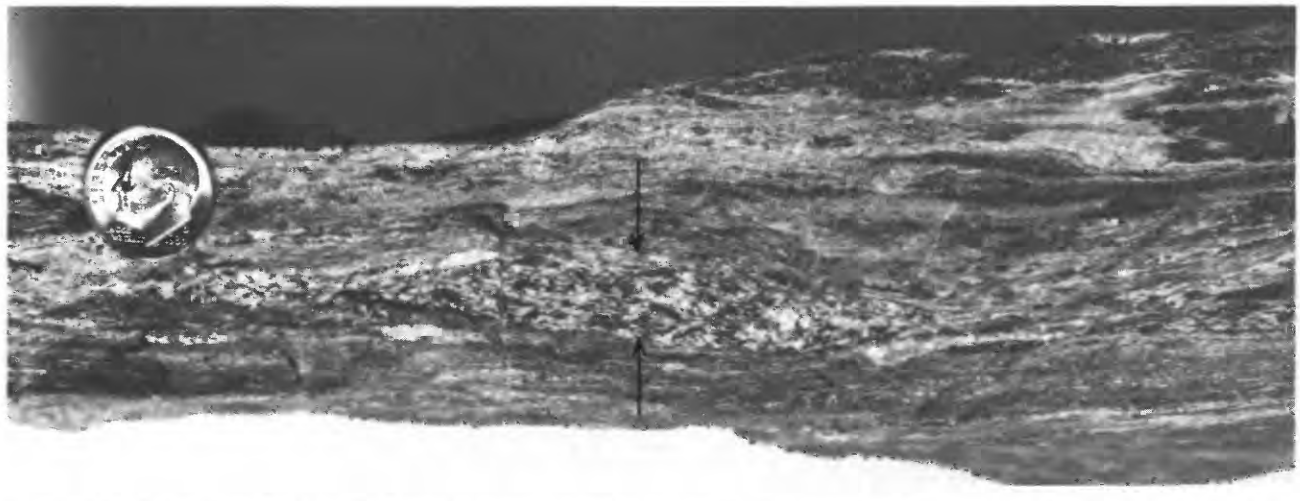

FIGURE 2.7.—Lens-shaped relic of metagabbro (arrows point to top and bottom margins) in sheared and recrystallized amphibolite. Coin is about 18 mm in diameter. Specimen from small inlier south of Chicken Hill.

pyroxene hornfels-facies rocks northeast of Mount Ireland. The hornblende is either almost colorless, pale brown, or light reddish brown. Very small amounts of phlogopite occur in all rock specimens. Chlorite is rare and apparently has been removed by reactions (Fawcett and Yoder, 1966) that formed forsterite, enstatite, spinel, and H_2O. Most rock specimens contain green spinel but in much less abundance than in lower temperature assemblages. Much of the spinel may have reacted with one or more Ca-Mg-silicate minerals to form calcic plagioclase and forsterite (Evans, 1977). Plagioclase is present in small amounts in most rock specimens but does not exceed 3 percent by volume in contrast to from 20 to 25 percent by volume in rocks described by Frost (1976).

STRUCTURE OF ELKHORN PLUTON

PERIPHERAL CONTACTS AND ASSOCIATED FOLIATION IN MARGINS OF PLUTON

The Elkhorn pluton constitutes about 93 percent of the batholith and is a single intrusion that ranges outward from a felsic core composed of the potassium-poor granodiorite of Anthony Lake to a margin composed of the mafic tonalite of Bald Mountain. The complexity of contacts of the tonalite of Bald Mountain with country rocks differs from south to north as does the intensity and distribution of foliation in the tonalite.

The south contact of the tonalite of Bald Mountain is best exposed near the serrated crest of a glaciated ridge south and southeast of Summit Lake (fig. 2.2); here, along about 4 km of its length, the contact is sharp and simple with few inclusions of country rock. The mafic inclusions (Pabst, 1928) of uncertain origin that characterize most circum-Pacific plutons of tonalite and granodiorite compose about 0.26 volume percent (range, 0.18–0.35 volume percent) of the tonalite of Bald Mountain as determined at eight localities near the contact by measurement of inclusions exposed across areas ranging in size from 56 to 70 m^2. In comparison, mafic inclusions of unknown origin in a 12-km^2 area near Anthony Lake in the interior of the pluton (fig. 2.8) average 0.35 volume percent (range, 0.17–0.56 volume percent) of the rock as determined at 58 localities by measuring inclusions across areas ranging in size from 47 to 187 m^2. Thus, mafic inclusions of unknown origin are not as abundant in mafic tonalite south and southeast of Summit Lake as they are in granodiorite near Anthony Lake in the interior of the pluton. Near some peripheral contacts south and southeast of Summit Lake, the mafic inclusions are randomly oriented. However, they commonly are elongated (fig. 2.9) within 350 m of the contact, with some elongation ratios as much as 5 to 1. Planar structure in two areas southeast of Summit Lake extends at least as far as 425 m from the contact. Planar structure roughly parallels the contact and dips either north or south, mostly within 10° of vertical.

Foliation in tonalite in the south-central and southeastern parts of the batholith is mostly localized near contacts. In the Monumental salient, to the southwest (fig. 2.2*B*), foliation is absent in tonalite near many contacts. The absence of planar structure near many contacts of the Monumental salient and the restricted occurrence of planar structure near most other contacts in the southern parts of the batholith are anomalous in a mesozonal pluton and contrast with widespread foliation in the tonalite in the northern part of the batholith.

The zone of foliation along the east contact of the batholith near Antelope Peak (fig. 2.2) is wider and more pronounced than the zone along the southern contact of the batholith. Elongated mafic inclusions of unknown origin occur as far inward from the contact as 500 m before the shapes become rounded and irregular. Elongation ratios commonly are 6 to 1 and many are 8 to 1. Inclusions are much more abundant here than along the south contact of the batholith. Mafic inclusions of unknown origin in most exposures constitute between 0.5 and 2.2 volume percent of the tonalite, but only a few recognizable inclusions of country rocks occur. Near Antelope Peak the contact of the Elkhorn pluton is sharp and relatively simple. The foliated border zone of the batholith southeast of Antelope Peak is well exposed in the minichasm of the Bulger Ditch (fig. 2.2*B*). Since the turn of the century the irrigation waters have cut an almost vertical trench as deep as 12 m through most of the border-zone rocks.

Contact relations northwest of Antelope Peak are more complex near Gorham Butte (fig. 2.2). Here the contact consists of a zone as much as 60 m wide of foliated and crudely interlayered country rocks and tonalite, commonly alternating in a large-scale lit-par-lit fashion. Planar structure extends inward as far as 900 m from the zone of interlayered rocks. Foliation parallels the contact and generally dips 60°–75° NE. Recognizable inclusions of country rocks occur inward from the zone of interlayered rocks, but inclusions of all types generally constitute less than 2 percent of the tonalite. Numerous elongated mafic inclusions of unknown origin are present in tonalite as far as 500 m from the zone of interlayered rocks; some inclusions near the contact have elongation ratios exceeding 25 to 1 (fig. 2.10). One extreme exam-

ple is 132 cm long and only 4 cm wide. Locally, small lensoid concentrations of mafic inclusions make up as much as 20 percent of the tonalite.

From Gorham Butte the contact of the batholith continues northwestward for about 3 km as a mixed zone of tonalite and foliated country rocks as much as 80 m wide. Foliated tonalite strikes about N. 60° W. and dips mostly 50°–70° NE. Farther west, where the contact zone is intruded by the granite of Anthony Butte (fig. 2.3), a dismembered screen represented by large inclusions (as long as 0.5 km) and numerous smaller country-rock xenoliths occurs along and near the tonalite-granite contact. From Gorham Butte northwestward along the tonalite contact for about 5 km, small inclusions of country rocks and mafic inclusions of unknown origin make up as much as 5 percent of the tonalite. The country rock inclusions contain many calc-silicate xenoliths, which suggest that emplacement of the tonalite in this part of the batholith proceeded alongside a large limestone lens.

Throughout an area slightly larger than 45 km^2 that lies west, southwest, and northwest of the granite of Anthony Butte (figs. 2.2 and 2.3), nearly all tonalite is foliated, in marked contrast to the restricted distribution of peripheral foliation in tonalite south of lat 45° N. Foliated tonalite west of the granite of Anthony Butte extends south to an intraplutonic contact with granodiorite (fig. 2.2), located just north of lat 45° N. and described in a later part of this chapter. Elongation ratios of mafic inclusions commonly are between 6 to 1 and 17 to 1. Concentrations of mafic inclusions occur in lens-shaped zones as much as 2 m wide and 35 m long; the mafic inclusions constitute as much as 40 percent of the rock in several zones.

FIGURE 2.8.—Granodiorite of Anthony Lake near center of Elkhorn pluton. View to west. Anthony Lake is 2 km north of the two peaks on central skyline. Granodiorite in this part of Elkhorn pluton averages 0.35 percent inclusions, mostly of unknown origin but including some of recognizable country rocks as much as 0.9 m across. Some granodiorite is characterized by a faint to fairly good planar structure. Northernmost sampled granodiorite showing evidence of early crystallization of augite was collected on ridge extending northeastward from prominent unnamed peak on left horizon.

In general, the complexity of contacts of tonalite with country rocks correlates with the dip of the contact. Most vertical to near-vertical plutonic contacts in northeastern Oregon are relatively simple in comparison with contacts that dip outward from the pluton at about 60° or less. Magma commonly crosscuts and (or) intrudes along several or more bedding planes where it ascends beneath outward-dipping contacts but not where contacts are essentially vertical. The lens-shaped concentrations of mafic inclusions north of lat 45° N. are interpreted as relatively large slabs of wallrock that were gradually fragmented into many closely spaced inclusions as they were incorporated into the magma.

In northeastern Oregon the most accessible outward-dipping contact with well-exposed sequences of alternating tonalite and country rocks is along the north contact of the Cornucopia stock (Taubeneck, 1964, fig. 2). The pertinent exposures, visible from distances of several hundred meters, are in open terrain about 5.3 km N. 38° W. of Cornucopia (fig. 2.1). Ready access from Cornucopia is by a trail to Pine Lakes, which lie nearly 6 km northwest of Cornucopia. Within the stock the trail crosses a small stream at an elevation of about 1,850 m and roughly parallels the intrusive contact at higher elevations to the north. West-northwest of the stream crossing, at an elevation of about 2,160 m, are alternating sequences of bedded metasedimentary rocks and tonalite that extend northward to an elevation of about 2,260 m. Most of the alternating sequences of metasedimentary rocks are less than 4.5 m wide. Commonly the relative volumes of metasedimentary rocks and tonalite in the larger exposures are about equal. Bedding dips mostly between 50° to 65° outward (north) but locally as shallowly as 30°. The metasedimentary rocks consist of a variety of rock types including calc-silicate rocks, mafic rocks of amphibolitic composition, and rare cherty beds (as much as 15 cm wide). Many of the small-scale features commonly associated with contacts of granitic intrusions, as reported in the literature worldwide, occur in this vicinity.

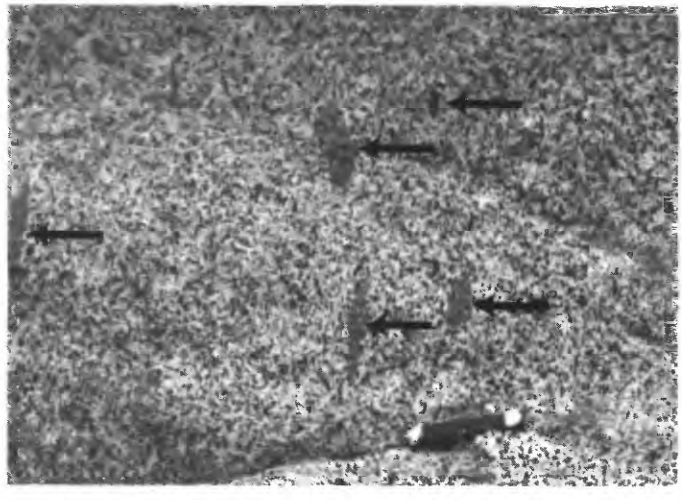

FIGURE 2.9.—Cluster of five elongated mafic inclusions (arrows) of unknown origin about 90 m from contact of Elkhorn pluton southeast of Summit Lake (fig. 2.2). Elongation ratios from 2:1 to 5:1 are common for inclusions near south contact of Elkhorn pluton but are much lower than ratios for mafic inclusions along north contact. Knife is 10 cm long.

INTERNAL FOLIATION

The Elkhorn pluton is distinctive among the zoned intrusions of tonalite and granodiorite in northeastern Oregon in the occurrence of sporadic planar structure in the granodiorite of Anthony Lake that forms the core of the pluton and also in the tonalite of Bald Mountain that composes the interior of the Monumental salient. The structural relations generally are elusive but locally are clear for distances of

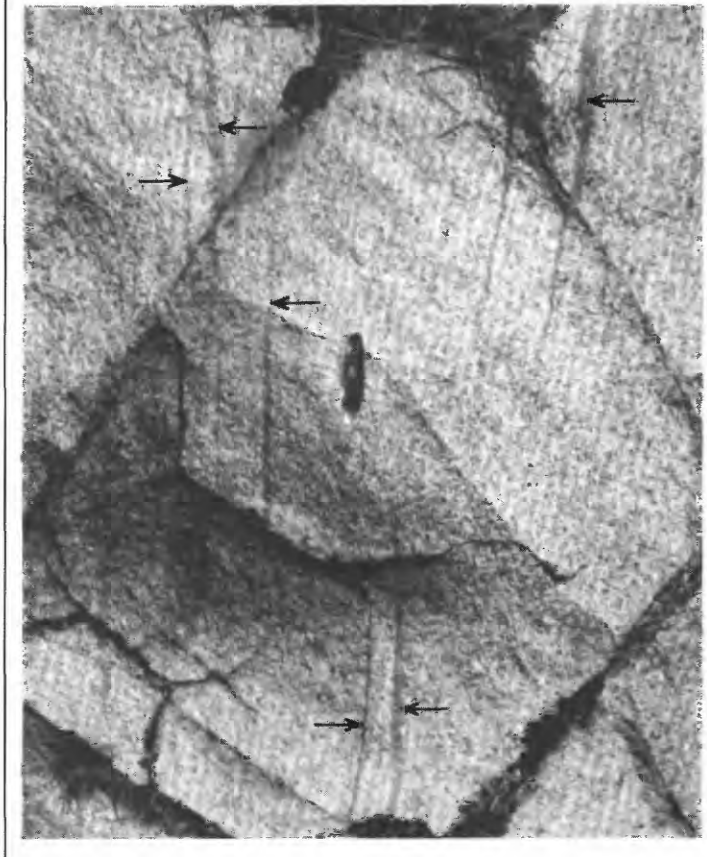

FIGURE 2.10.—Extreme elongation of mafic inclusions (arrows) in tonalite near Gorham Butte (fig. 2.2). Elongation ratios of all inclusions here exceed 25:1. Knife is 10 cm long.

100 m and more. The sporadic structures are indicative of numerous magma surges and pulses during the consolidation phase of emplacement of the granodiorite core and the interior of the tonalite in the Monumental salient.

Examination of the granodiorite core was mostly confined to a 12-km^2 area south to east of Anthony Lake; the greatest number of continuous exposures of the granodiorite core occur here. The area is characterized by sharp peaks and cirque basins. The southeastern part of the core, deeply dissected by a major glaciated valley that includes Dutch Flat (fig. 2.2), remains to be studied.

Textbooks, field manuals, and the nonetheless highly commendable memoir of Balk (1937) provide little guidance for the recognition of planar structure throughout much of the interior of the Elkhorn pluton. Therefore, field procedures and observations are detailed herein because the Bald Mountain batholith is not unique in its elusive planar structure, rocks with relatively smooth joint surfaces, and common exposures either controlled by steep diagonal joints or shaped by exfoliation.

Diagonal joints warrant primary consideration. Serrate ridges as well as notched or V-shaped peaks are common physiographic expressions of diagonal joints in recently glaciated granitic terrains. Gunsight Mountain (fig. 2.2*B*) is merely one example of a notched peak south of Anthony Lake. Much of the Wallowa batholith also is dominated by diagonal joints. Excellent examples of sawtooth ridges occur in unit 3 of the Wallowa batholith about 9.8 km S. 25° W. of the south end of Wallowa Lake (fig. 2.11).

Most exposures south to east of Anthony Lake are controlled by two prominent northeast-striking diagonal-joint sets that dip 35°–45° NW and 60° SE, respectively. Faintly to even moderately delineated planar structure is difficult to detect because (1) the relatively smooth joint surfaces obscure the structure, (2) the diagonal joints restrict the interval for recognition across outcrops, and (3) the glaring reflection of the sun from the dominant diagonal surfaces (the northwest-dipping set) makes further structural elucidation nearly impossible.

The character of the exposed rock surface is an important factor in the recognition of planar structure; with increasing roughness of the rock surface, planar structure is increasingly discernible. The most favorable surfaces are those created by dynamite blasting done by the U.S. Forest Service in making trails. Weak planar structure that is visible in massive rock on large surfaces exposed by blasting generally cannot be seen on adjacent smooth-jointed natural exposures. Large talus blocks at the base of cliffs, especially blocks 1 m or larger in size, as well as natural exposures with rough surfaces commonly reveal structure that is obscure on relatively smooth surfaces.

Diagonal-joint surfaces south to east of Anthony Lake are among the most difficult in the pluton to examine with any degree of success. On these surfaces, traces of planar structures mostly trend at angles within 45° to 75° of joint strikes. Even fairly well delineated planar structure is not easy to recognize looking downdip along surfaces that are inclined at 35° to 45°, because the observer is looking at an acute angle at a surface that is rapidly becoming too distant for inspection. Therefore the surface area that can be viewed at the proper distance or proper angle is inadequate. Any structure in the rocks is much easier to detect if the observer turns 180° and then scans a surface that is at a roughly uniform radial distance. Viewing an exposure from several different angles and different distances is essential to the recognition of any poorly defined planar structure. The angle of recognition of elusive planar structure on diagonal-joint surfaces commonly is as low as 20°.

The diagonal-joint set that dips 35°–45° NW. exposes the largest continuous surface areas amenable to the identification of planar structure. As noted previously, however, even fairly well defined planar structure is generally difficult to recognize looking downdip at angles of 35° to 45°. But looking updip is also difficult because in this area it necessitates facing southeast, toward the sun. The constant reflection of sunlight from the white surfaces of granodiorite is an almost insuperable obstacle; however, in October, before the arrival of the winter snows, many areas of northwest-dipping diagonal joints (especially where angles are near 45°) are in shade for as many as four consecutive hours and some throughout the day.

Taking advantage of smoke from wildfires and using artificial-shading devices are two means of facilitating the recognition of planar structure. Major wildfires are fairly common during August and September in northeastern Oregon and generally burn for 15 to 25 days. Smoke from wildfires as much as 130 km away can reduce midday visibility to a distance of 6 to 10 km. Planar structure is more easily detected in the Elkhorn pluton on any day when smoke reduces visibility to less than about 25 km. Thus very good to excellent field observations are possible throughout the day when visibility is only 6 to 10 km.

Artificial-shading devices permit the detection of fairly to moderately well delineated planar structure. The devices are almost always practical on south-facing slopes, and they also are useful during July and August for most north-facing slopes. Examples of effective artificial-shading devices are pieces of cardboard

and a standard collapsible umbrella. An advantage of cardboard is its availability in a wide range of sizes. An unopened umbrella's compact size means that it is small enough to fit inside a day pack, but recognition

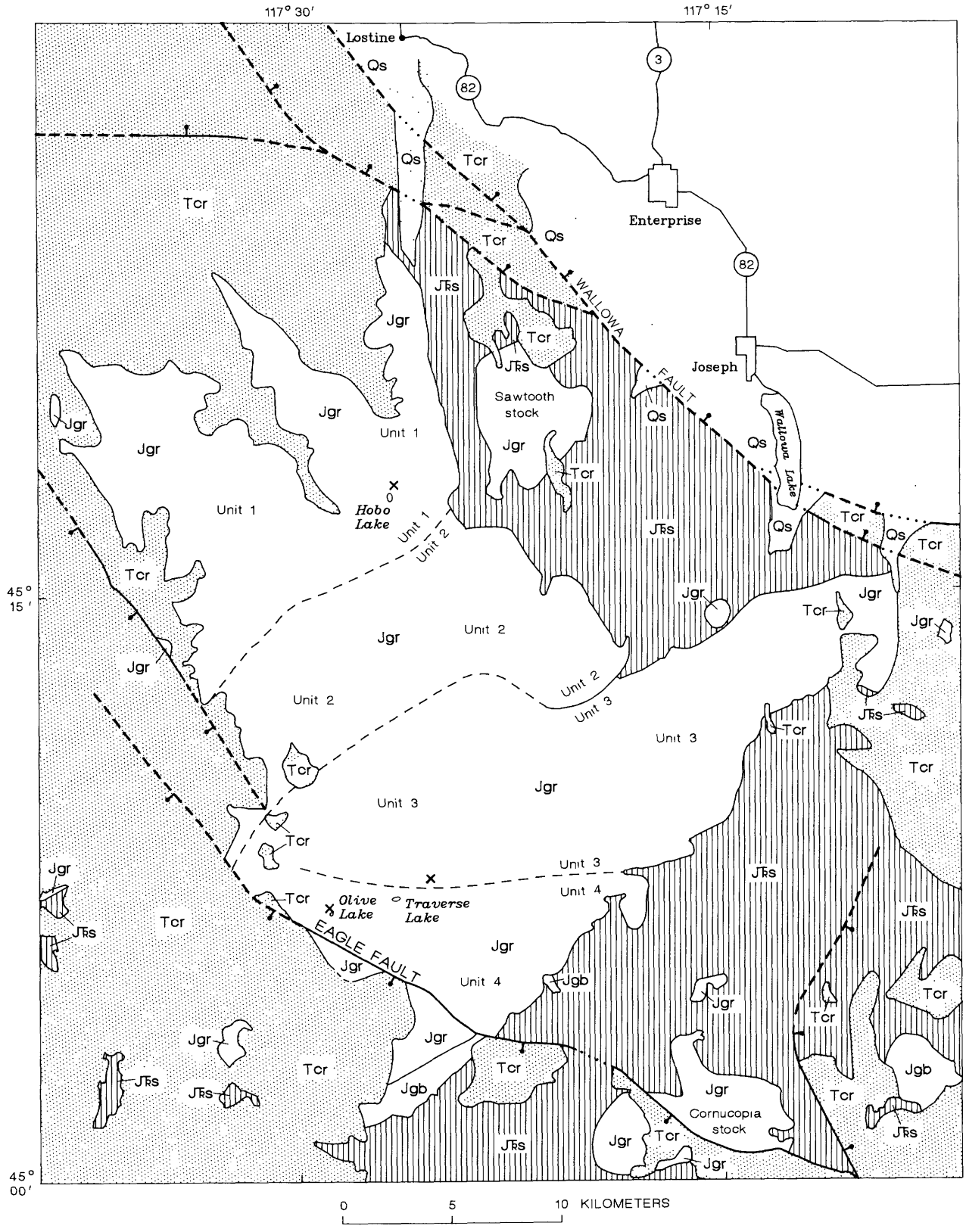

of weak structure commonly requires a larger shadow than that provided by an umbrella (depending in part on the hour of day, month of year, and latitude of the area). For example, even at high noon on October 15 at lat 45° N., a 6-ft (~1.8-m) person standing on a horizontal surface will cast a 2-m shadow that rapidly lengthens within 90 minutes. The shadow at noon on June 15 is only about 0.7 m, but it is 4 m long at noon on December 15. Therefore, the effectiveness of the same artificial-shading device for revealing weak structures varies according to time and place.

Examination of most exposures south and southeast of Anthony Lake indicates respectively that east and northeast structural trends and west-northwest trends dominate (fig. 2.2). About 4 to 5 km east and east-southeast of the lake, trends have changed to N. 0°–25° W. Overall, including areas not previously mentioned to the north and southwest of the lake, the apparent pattern of structural trends in the interior of the Elkhorn pluton crudely defines an arc of about 130°. The arcuate pattern is consistent with upward surges of magma during the progressive inward consolidation of the core.

Planar structure where present within the interior of the Monumental salient varies from faint to well defined. Tonalite in the western one-fourth of the salient occurs as exfoliation knobs. Such rounded surfaces complicate the recognition of planar structures and the determination of their orientations, but the extent of the complications depends on many factors. For example, structure in exfoliation knobs north of the intraplutonic contact (fig. 2.2) is comparatively easy to recognize partly because the structure is accentuated by the large size, pronounced elongation, and relative abundance of mafic inclusions. In contrast, the relative scarcity, smaller size, and absence of pronounced elongation of mafic inclusions in the western part of the Monumental salient contribute to the difficulty of recognizing planar structures there. The contrast is intensified by weaker fabrics in rocks from the salient due, for instance, to their containing less than half as much hornblende, which is important in defining the fabric. Structural definition in the western part of the salient is, at best, only fair to fairly good.

Exfoliation knobs in the salient commonly are surrounded at ground level by spalled slabs and rinds. The most instructive slabs are more than 0.6 m^2, at least 7 cm thick on two adjoining sides, and comparatively fresh; have originated from the central and lower parts of knobs that are more than 2.5 m high; and provide rock surfaces for inspection in three different directions. Planar structure can be determined more readily in such slabs than in the knobs themselves. Rotating a slab in the air is essential in searching for unknown structure but is more important in confirming and documenting the attitude of suspected structures. The confirmed attitude is marked on each slab. A larger slab's original position on the knob generally is apparent and may be verified by lifting and then moving a slab until the respective curved surfaces of knob and slab coincide precisely.

Many knobs do not yield even one suitable exfoliation slab for the possible detection and measurement of planar structures. Furthermore, some appropriate slabs cannot be convincingly restored to their original position. Examination of the knobs commonly discloses incipient to well-developed exfoliation cracks, many of which permit the breaking of large pieces of rock for inspection. Massive exfoliation surfaces are best broken with a heavy, long-handled rock hammer such as a 2-kg German hammerhead on a hickory handle or a 6-lb American sledge. Large specimens broken from exfoliation knobs facilitate the recognition of fair to moderately well defined planar structure, but the surface areas are inadequate for the recognition of weak structures.

Joint surfaces rather than exfoliation surfaces characterize the well-exposed rock at higher elevations in the central and eastern parts of the Monumental salient. The tonalite throughout most of the salient is distinctive compared to tonalite elsewhere in northeastern Oregon in its relatively large number of xenoliths composed of country rocks. Oriented xenoliths are the best indicators of otherwise weak fabrics. Xenoliths

EXPLANATION

- Qs — Surficial deposits (Quaternary)—Shown only near Wallowa fault
- Tcr — Columbia River Basalt Group (Miocene)
- Jgr — Granitic intrusive rocks (Jurassic)
- Jgb — Gabbroic intrusive rocks (Jurassic)
- JTrs — Sedimentary rocks (Jurassic and Triassic) —Includes some mafic volcanic rocks
- Contact—Short dashed where approximately located
- Gradational unit boundary
- High-angle fault—Dashed where approximately located; dotted where concealed. Bar and ball on downthrown side
- Aplite body

FIGURE 2.11.—Generalized geologic map showing units 1 through 4 of Wallowa batholith; these four compositionally zoned plutons, composed of tonalite and granodiorite, constitute most of the Wallowa batholith. Locations of three large aplite bodies are also shown.

of foliated country rocks, mostly metagabbro, commonly occur as elongated inclusions many of which are small slivers less than 5 cm long. The slender dark slivers that contain abundant hornblende are readily visible and, where aligned, accentuate or confirm a weak planar structure. Some narrow inclusions of ribbon chert also are arranged with their longest axes parallel to enclosing foliation planes. It is notable that aligned xenoliths are not everywhere accompanied by foliation planes. However, aligned xenoliths without associated foliation planes generally are parallel to planar structure in nearby areas.

A representative axis of planar structure in the interior of the Monumental salient trends west-northwest at an angle across the salient (fig. 2.2) rather than parallel to the length of the salient, which runs east-west. This structural axis closely parallels a line drawn through the narrowest part of the neck of the salient and coincides with the overall west-northwest trends of country rocks on either side of the neck. These gross relations suggest that the salient initially was an independent, satellitic intrusion that subsequently coalesced with the main part of the batholith.

Planar structure within the neck of the salient varies from faint to well defined but is absent in many exposures. Trends in the neck are much more variable than in the interior of the salient and locally arc as much as 45° within 245 m. In the northwest part of the neck, structures generally trend north-northwest to north-northeast (fig. 2.2*A*). In the southeast part of the neck, structures trend northeast. However, in the restricted exposures of the northern part of the border area between the neck and the salient, structures are mostly west-northwest, parallel to both the long direction of the neck and structures to the southwest in the interior of the salient. These west-northwest trends are contrary to the structural pattern that would be expected as a result of magma passing through the neck between the batholith and the salient, and support the interpretation that the salient originally was a satellite of the batholith. The lack of structural symbols on figure 2.2 in the important 1-km-wide zone just south-southwest of the neck is caused by a glacial valley (fig. 2.4) that contains only a small number of iron-stained roches moutonnees, each without discernible planar structure.

Extensive limonitic alteration along closely spaced joints associated with gold-quartz mineralization (Lindgren, 1901; Ferns and others, 1982) greatly complicates the recognition of planar structure throughout much of the neck. The principal joint set includes one major and many minor zones of atypical joints that are very closely spaced (2.5 to 20 cm apart), hydrothermally altered, and accompanied by gold-quartz veins that mostly parallel the jointing. In areas outside of the zones of atypical jointing, joints of the principal joint set are less regular, mostly spaced from 0.3 to 2.4 m apart, and generally parallel to the trend of the nearest zone of atypical joints. The principal joint set commences about 5 km S. 78° E. of Mount Ireland (fig. 2.2), strikes about N. 10° W. for almost two km, and then gradually arcs to the northeast through the neck. In the area of figure 2.4, the major zone of atypical joints extends northward from the southernmost vertical joint symbol (striking N. 20° E.), then arcs through Cable Cove and the two roches moutonnees on the north side of Silver Creek before continuing northeast to the vicinity of the spring east of the North Fork John Day River. Rock near the spring is a limonitic-stained grus peppered with many century-old prospect pits that assist in confirming the northeast continuation of the mineralization and closely spaced joints. The major zone of atypical joints has a maximum width of about 1,200 m within 0.5 km north and northeast of Cable Cove. Minor zones of atypical joints, to either side of the major zone, are mostly from 2 to 15 m wide. Of the 64 joint symbols shown on figure 2.4, 51 represent the atypical closely spaced joints. Associated quartz veins are mostly 3 to 50 mm wide; a few are as much as 60 cm wide.

The gaping joints and gold-quartz veins are the result of pronounced upward expansion and arching of the granitic rocks on both sides of the neck. Whatever the earlier emplacement history of the tonalite, the dominant joint set indicates that the neck and salient reacted as a coherent unit during the final episode in the emplacement of the Elkhorn pluton.

INTRAPLUTONIC CONTACT

The gradational zoning within the Elkhorn pluton from tonalite in the margin to granodiorite in the core is disrupted 6.5 km north to 8 km northwest of Anthony Lake and again about 6 km west of Anthony Lake by an intraplutonic contact (fig. 2.2) where core magma on the south and east sides intruded already solidified tonalite on the north and west sides. Tonalite north and west of the intraplutonic contact has a color index of 17 to 30, whereas younger core rocks south and east of the intraplutonic contact have an index of 9 to 16. Rocks on either side of the intraplutonic contact in most areas also can be distinguished by the presence or absence of planar structure. Older tonalite north and west of the contact is strongly foliated, whereas younger core rocks south and east of the contact are generally unfoliated. The foliation that occurs in core rocks near the intraplutonic con-

tact (mostly about 8 km N. 50° W. of Anthony Lake) is faint to fairly good.

The intraplutonic contact invariably separates rocks of different color index and fabric, but the younger core rocks are not everywhere of uniform composition. Nearly all core rocks on the north are granodiorite, whereas those northwest and west of Anthony Lake are either granodiorite or rocks transitional between granodiorite and tonalite; core rocks near the intraplutonic contact about S. 67° W. of Anthony Lake are tonalite. Locally, the intraplutonic contact north to northwest of Anthony Lake is accentuated by small intrusions of leucogranodiorite that, in outcrop, are elongate parallel to the contact. The best exposed and most accessible intrusion of leucogranodiorite, about N. 9° E. of Anthony Lake, is approximately 600 m long and as much as 80 m wide.

Relations near the intraplutonic contact north and northwest of Anthony Lake can be readily determined for only about 2.5 km in the general vicinity of where the contact changes in strike from almost east-west to about N. 75° E. Tonalite in this area has a color index of about 25, whereas the granodiorite (core) has an index of about 12. Just east of the directional change in the contact, foliated tonalite (on the north-northwest side) with elongated inclusions is within 6 m of nonfoliated granodiorite (on the south-southeast side) containing a few rounded inclusions of strongly foliated tonalite. Inclusions of tonalite are rare or absent elsewhere in core rocks near the intraplutonic contact.

From due north of Anthony Lake the intraplutonic contact extends roughly westward for about 7 km before disappearing beneath Cenozoic volcanic rocks. Elongated inclusions and faint to fairly good planar structure are found in core rocks near the contact for about 1.5 km east of the Cenozoic volcanic rocks in notable contrast to their absence in core rocks farther east.

A fundamental consideration is whether the intraplutonic contact turns southward beneath the Cenozoic volcanic rocks and reappears somewhere north of the norite of Badger Butte (fig. 2.2). Planar structure and associated elongated inclusions in core rocks curve from about N. 45° E. on the north at lat 45° N. to S. 20° E. about 2.5 km to the south. Virtually all foliation in core rocks near the intraplutonic contact occurs in a relatively small area near and just south of lat 45° N. and apparently formed only where the core magma was most closely constricted during emplacement. The curving foliation in the core rocks suggests that the intraplutonic contact continues, concealed, beneath the Cenozoic volcanic rocks and reappears to the south.

Relations near the north end of the elongated leucogranodiorite of Trail Creek (fig. 2.2) indicate that the intraplutonic contact reappears in a poorly exposed area about 1 km north-northwest of the elongated leucogranodiorite. Mafic tonalite, strongly foliated, outcrops for about 500 m northwest of the leucogranodiorite and extends eastward at least as far as the intraplutonic contact as mapped on figure 2.2. The nearest exposures of nonfoliated granodiorite are about 75 m farther east. Almost due south, near the east contact of the leucogranodiorite of Trail Creek, nonfoliated granodiorite with a color index of 10 to 14 is exposed intermittently southward for about two-thirds of the length of the leucocratic intrusion. Strongly foliated tonalite with a color index of 19 to 30 is on both the west and south sides of the leucogranodiorite. The relations indicate that the intraplutonic contact extends southward along the east margin of the leucogranodiorite (fig. 2.2).

Most bedrock between 300 to 900 m south-southeast of the leucogranodiorite of Trail Creek is concealed by widespread glacial deposits, but a solitary exposure of the intraplutonic contact occurs in a driftless area almost midway between the southern extremity of the leucogranodiorite and the northeast corner of the norite of Badger Butte. At this locality the intraplutonic contact separates a strongly foliated mafic tonalite on the west with a color index in a representative rock specimen of 23.8 and a quartz content of 15.3 from a nonfoliated felsic tonalite on the east with a color index in a typical rock specimen of 13.2 and a quartz content of 27.8.

Metasedimentary xenoliths in the driftless area occur in core tonalite near the exposure of the intraplutonic contact. Relict bedding in the xenoliths, where preserved, strikes about N. 15° W. and dips vertically. The largest xenolith is almost 1 m long and as much as 0.35 m wide. Much larger metasedimentary xenoliths occur in core rocks about 300 m to the north-northwest, including a banded calc-silicate xenolith more than 12 m long that strikes roughly N. 15° W. and dips 80° NE.; weak planar structure in the core rocks strikes roughly north and dips about 75° E. The source of the metasedimentary xenoliths (which include pyroxene hornfels-facies rocks with two-pyroxene assemblages) is unknown, but their restricted distribution near the south end of the intraplutonic contact suggests that in this general vicinity an earlier wallrock contact of the batholith with metasedimentary rocks was obliterated during the emplacement of core magma. No trace of this probable former contact occurs to the south at the present level of erosion. Core tonalite to the south is in sharp contact with the norite of Badger Butte with no intervening metasedimentary rocks.

The intraplutonic contact, concealed within 450 m of the norite of Badger Butte, terminates at the northeast corner of the norite as determined by the contrasting

fabric and modal compositions of granitic rocks on the north (border rocks) and east (core rocks) sides of the norite. Strongly foliated tonalite north of the norite has in three specimens a color index of 24.9 to 30.6, a quartz content of 12.6 to 15.3 volume percent, and only trace amounts of potassium feldspar, whereas nonfoliated or weakly foliated (one locality) tonalite within 90 m of the east side of the norite has in three specimens a color index of 13.9 to 16.0, a quartz content of 23.2 to 27.5 volume percent, and a potassium feldspar content of 0.6 to 1.9 volume percent.

The dip of the intraplutonic contact, whether outward as in classical cauldron subsidence or inward, can only be indirectly approximated from attitudes of limited planar structure in core rocks and even more restricted bedding in local metasedimentary inclusions near the norite of Badger Butte. A nearly vertical dip for the intraplutonic contact is suggested by planar structure in core rocks near the concave side of the contact in the vicinity of lat 45° N. (fig. 2.2). Near the southern extremity of the intraplutonic contact, bedding in metasedimentary xenoliths in core rocks is vertical or dips about 80° E. Poor planar structure in associated tonalite also dips steeply eastward. In review, field evidence for the outward or inward dip of the intraplutonic contact is inconclusive.

ROCKS OF BALD MOUNTAIN BATHOLITH

For convenience, rocks of the Bald Mountain batholith are divided into those of the central area that constitutes most of the batholith (fig. 2.2) and those of a northeastern peripheral area (fig. 2.3) that is small but encompasses diverse rock types and includes most of the heretofore-unmapped intrusive units. Rocks of the two areas are described separately in two mafic-to-felsic sequences commencing with the intrusive-rock units (fig. 2.2) that have been restudied or discovered since 1957. The reexamined units are the norite of Badger Butte and the two units of the compositionally zoned Elkhorn pluton, the tonalite of Bald Mountain and the granodiorite of Anthony Lake (names modified from Taubeneck, 1957). Herein-named additional units within the Elkhorn pluton are the quartz diorite of Limber Creek, leucogranodiorite of Trail Creek, and granite of Clear Creek. The mafic-to-felsic intrusive sequences were established on the basis of field relations.

The newly named units in the northeastern peripheral area (fig. 2.3) are the quartz diorite of Wolf Creek, boundary quartz diorite unit, granodiorite of Indiana Mine Road, granodiorite of Beaver Meadow, granite of Anthony Butte, and leucogranite of Dutch Creek. Granitic rock units mapped in figure 2.3 are distinctly different from other granitic intrusive rocks in northeastern Oregon. Accordingly, the format used in describing each rock unit concludes with a section in which the distinguishing features of the unit are summarized.

NORITE OF BADGER BUTTE

SETTING AND GENERAL DESCRIPTION

The norite of Badger Butte (Taubeneck, 1957) is the largest of the three small gabbroic bodies that are the earliest intrusive units in the batholith. Limited access, poor exposures in most areas, and contacts that were almost entirely concealed by extensive deposits of glacial drift restricted fieldwork during the 1950's (Taubeneck, 1957). Modern roads with deep roadcuts, and clear-cut logging of dense forests of lodgepole pine have disclosed much bedrock since about 1970. A new study of the norite of Badger Butte was motivated by the desire to more accurately determine its distribution, to collect specimens from a larger area than was originally possible, and to obtain specimens that contain few or no metamorphic minerals.

The dark color of the norite of Badger Butte is caused primarily by the grayish plagioclase, which is the dominant mineral. The rock is medium grained with plagioclase and pyroxene as much as 4.0 mm in length. Poikiloblastic biotite is commonly 10 cm across and rarely 20 cm. The norite generally exhibits a parallelism of plagioclase and a less pronounced alignment of pyroxene, but the dark color of the rock tends to obscure the foliation. Seventeen specimens were collected for petrographic study. Modal data given in table 2.1 are for the five rocks with the lowest amounts of postconsolidation biotite and amphiboles; the new data constitute a much closer approximation of the composition of the original norite than did previously published modes (Taubeneck, 1957).

The norite of Badger Butte, about 6 km^2 in areal distribution, is surrounded by the tonalite of Bald Mountain (fig. 2.2). Deep roadcuts that expose the tonalite-norite contact both to the northeast and to the southeast of Badger Butte reveal that the norite was intruded by the tonalite. Also, dikes of tonalite within the norite contain inclusions of norite.

MICROSCOPIC DESCRIPTION

The general petrographic features of the norite of Badger Butte were given by Taubeneck (1957). Additional descriptive data recorded herein pertain exclusively to deformation and crystallization histories.

Deformation features in plagioclase are more pronounced in the norite of Badger Butte than in any

TABLE 2.1.—*Modes of the norite of Badger Butte*

[Values in volume percent. Each analysis represents at least 2,400 point counts for each of two thin sections; ---, not present]

Specimen number	Quartz	Plagioclase	Hypersthene	Augite	Hornblende	Biotite	Opaque minerals	Nonopaque accessory minerals
83 ------	0.9	65.5	18.5	9.1	3.5	0.7	1.4	0.4
84 ------	.6	67.5	19.7	9.4	1.0	---	1.5	.3
85 ------	4.3	69.6	11.1	3.9	5.8	4.2	.8	.3
98 ------	4.6	66.5	10.8	7.2	4.5	4.4	1.4	.6
99 ------	.2	67.8	17.7	9.3	3.2	---	1.4	.4
Average	2.1	67.4	15.6	7.8	3.6	1.8	1.3	.4

other unit of the batholith. Plagioclase is recrystallized into groups of small and nearly equant crystals at pressure points along margins of crystals where plagioclase contacts other plagioclase or pyroxene. Twinning lamellae of plagioclase commonly are bent as much as 10°, less commonly as much as 20°, and rarely more than 25°. Some plagioclase crystals in 3 of the 17 rocks studied are deformed into S shapes in which bending generally is most extreme near the ends of crystals. More intense plastic deformation occurs in a few crystals that show three curve reversals in the trends of twin lamellae. Whereas plagioclase shows the effects of strong plastic deformation, pyroxene commonly is fractured; an exception is one 2.1-mm-long prism of hypersthene that is bent 24°.

Hypersthene crystallized early; many small crystals (0.1 to 0.5 mm) are enclosed within plagioclase. Augite surrounds or partly surrounds hypersthene, but inclusions of augite in plagioclase are not common. Hypersthene commonly is replaced partly by cummingtonite, whereas augite is replaced partly by actinolite. Some rocks contain no fibrous amphibole, but others contain only relics of pyroxene.

Hornblende and biotite are present as undeformed, poikiloblastic crystals that commonly continue as narrow extensions along grain boundaries between plagioclase (original or recrystallized), pyroxene, quartz, iron oxide, and apatite. In some thin sections, either hornblende or biotite along a microfracture is in optical continuity respectively with hornblende or biotite that is intersected by the same microfracture. Relations along microfractures support a postconsolidation origin for hornblende and biotite.

TONALITE OF BALD MOUNTAIN AND GRANODIORITE OF ANTHONY LAKE

SETTING AND GENERAL DESCRIPTION

Rocks in the margin and the core of the compositionally zoned Elkhorn pluton were named the tonalite of Bald Mountain and the granodiorite of Anthony Lake, respectively (Taubeneck, 1957). Except along the intraplutonic contact, the two rock units represent gradational facies of the same intrusion (fig. 2.2), and the only major distinction between the rock types is a difference in mineral proportions. Accordingly, one general description of both lithologies is given.

The tonalite and granodiorite are medium-grained pale-gray rocks containing from 9 to 30 modal percent biotite and hornblende. Granodiorite and much tonalite in the field are almost white in the glare of the sun. Granodiorite near Anthony Lake has a color index of 11, whereas the two ferromagnesian minerals commonly constitute as much as 25 modal percent of the tonalite in the north and near contacts of the Elkhorn pluton.

The crystal habit and maximum size of the major rock-forming minerals were recorded in the field by examining more than 100 large exposures of both the tonalite and granodiorite. Most hornblende occurs in euhedral prisms that commonly are as long as 8 mm and rarely 14 mm. The euhedral form of the hornblende indicates crystallization from a melt. Only in some tonalite in the margin of the pluton does the hornblende have megascopic features that might suggest an origin as restite (White and Chappell, 1977), that is, unmelted solid residue in granitic rocks that originated as partial melts in the deep crust. Much biotite occurs as euhedral books commonly as much as 5 mm across and rarely 8 mm across. Tabular plagioclase commonly is as long as 6 mm with some larger crystals present in nearly all exposures. Plagioclase crystals as long as 10 mm occur in many outcrops; the largest one measured was 14 mm. Quartz is interstitial with common maximum dimensions of 5 mm and rarely 8 mm. Potassium feldspar is interstitial with poikilitic crystals in granodiorite commonly 10 mm across and rarely 16 mm. Detailed petrographic descriptions of the tonalite of Bald

Mountain and granodiorite of Anthony Lake are given in Taubeneck (1957).

COMPARATIVE MODAL COMPOSITIONS AND CRYSTALLIZATION OF AUGITE

New modal analyses for the tonalite of Bald Mountain and granodiorite of Anthony Lake have provided a basis for comparing rock units or subgroups of rocks throughout the Elkhorn pluton in terms of their petrographic characteristics. Much of the new data is for tonalite north and west of the intraplutonic contact where relatively few specimens were collected during the early 1950's (Taubeneck, 1957). Special attention is paid to augite, which is generally rare or uncommon in tonalite and granodiorite in western North America.

Tonalite north of the intraplutonic contact can be geographically divided into a distinct subgroup of northern rocks that generally contain a small amount of augite and a southern subgroup without augite. Rocks with augite occur in an 18-km^2 area in the northwesternmost part of the tonalite of Bald Mountain (north of line A-B, fig. 2.2), whereas rocks without augite are to the south. Modal analyses of 18 rocks of the northern subgroup and 12 rocks of the southern subgroup are given in table 2.2.

The most notable mineralogical feature of the northern tonalite (table 2.2) is the widespread occurrence of augite cores in hornblende, whereas augite is uncommon or absent in most tonalite elsewhere in the batholith. The augite cores within hornblende are generally 0.3 to 1.5 mm across, but two cores exceed 3.0 mm in greatest dimension. The augite is sufficiently abundant to indicate that it was the dominant early mafic mineral to crystallize. Accordingly, the tonalitic magma must have been water-undersaturated during the early crystallization history of the rocks.

Augite originally was much more abundant in the crystallizing tonalite than the small modal percentage shown in table 2.2 implies. The formerly larger amounts of augite within hornblende in each of the 18 rocks is indicated by hornblende with bleached cores that enclose minute crystals of quartz (fig. 2.12; Taubeneck, 1964). The bleached cores in hornblende represent an advanced stage in the replacement of augite by hornblende (Taubeneck, 1967), and the common quartz inclusions represent silica liberated during the conversion of pyroxene to amphibole. The small inclusions of quartz in some cores are almost vermicular in shape rather than mostly oval, elliptical, or elongated as shown in figure 2.12. Generally the sieve-like areas of quartz in hornblende are distinctly bleached; some are only faintly bleached; a few are not associated with a change in color of the amphibole.

The original crystal habit of augite is best seen in longitudinal sections rather than in nearly equidimensional cross sections, in which the crystal faces are blurred by even comparatively minor growth of hornblende. The 36 thin sections used for modal analysis of rocks of the northern subgroup (2 thin sections of each of the 18 rock samples) contain six prismatic crystals of augite ranging from 2.3 to 3.2 mm in length, surrounded by 0.03- to 0.15-mm rims of hornblende. The thinnest rims of hornblende invariably are along the prismatic faces; the rims are sufficiently thin to conclude that four of the augite crystals were initially bounded by euhedral prisms. None of the original faces that terminated the six prismatic crystals are clearly defined, but the approximate location of the faces that bounded two of the crystals is apparent. The two augite crystals that most nearly retain their original shape were either euhedral or almost euhedral before replacement by hornblende commenced.

Nine small inclusions of augite in plagioclase in the 36 thin sections also verify the early crystallization of augite. The largest inclusions are about 0.3 mm across; all inclusions are either subhedral or euhedral.

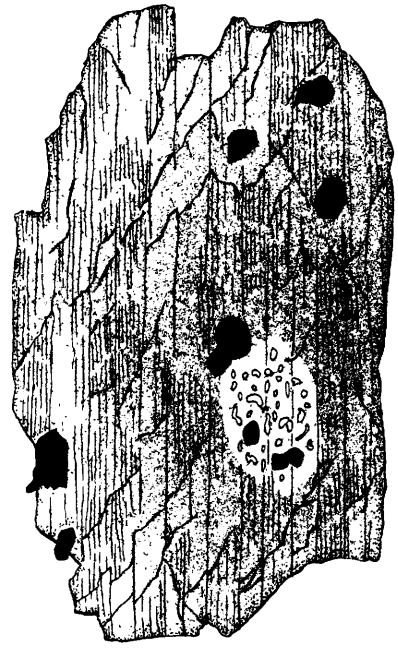

FIGURE 2.12.—Sketch of hornblende crystal with bleached core enclosing minute inclusions of quartz (white); black areas represent magnetite inclusions. Width of hornblende crystal is 0.8 mm.

TABLE 2.2.—*Modes of the tonalite of Bald Mountain north of the intraplutonic contact*

[Values in volume percent. Each analysis represents at least 2,400 point counts for each of two thin sections; 0.0, <0.05; ---, not present]

Specimen number	Quartz	Potassium feldspar	Plagioclase	Biotite	Hornblende	Augite	Opaque minerals	Nonopaque accessory minerals
Tonalite of northern subgroup								
R13 -----	17.7	1.3	54.8	11.9	13.1	0.3	0.5	0.4
R126 ----	17.5	.0	58.4	10.4	13.0	.1	.5	.1
R138 ----	20.6	.9	57.1	10.6	10.1	.2	.2	.3
R139 ----	21.7	2.5	56.2	10.0	9.1	.0	.2	.3
R140 ----	18.1	1.0	54.3	12.0	13.7	.3	.3	.3
R141 ----	23.4	2.3	52.8	10.7	10.2	.2	.2	.2
R148 ----	22.8	3.1	50.0	10.1	13.5	.3	.1	.1
R152 ----	20.6	1.1	59.5	12.9	5.0	.0	.7	.2
R155 ----	23.5	2.6	50.2	11.7	11.0	.6	.2	.2
R156 ----	24.7	.4	50.4	13.3	10.4	.0	.5	.3
R157 ----	17.3	.2	56.2	11.4	14.1	.4	.3	.1
R158 ----	21.2	2.4	53.4	11.3	11.2	.2	.1	.2
R164 ----	20.1	2.2	50.6	12.0	14.7	.1	.1	.2
R165 ----	23.2	2.1	52.6	9.6	12.2	.1	.1	.1
R166 ----	20.7	1.1	52.4	11.9	13.3	.0	.3	.3
R167 ----	20.4	.3	53.8	11.3	13.5	.3	.3	.1
R170 ----	20.5	2.4	53.4	10.8	12.3	.1	.3	.2
R760 ----	16.4	.3	58.4	8.8	15.0	.5	.4	.2
Average	20.5	1.5	54.1	11.2	12.0	.2	.3	.2
Tonalite of southern subgroup								
R10 -----	24.8	2.0	55.8	10.5	6.4	---	0.3	0.2
R11 -----	18.9	.3	55.3	8.9	15.8	---	.6	.2
R39 -----	22.3	3.7	54.7	8.9	10.1	---	.2	.1
R40 -----	17.6	.9	56.7	9.4	15.0	---	.2	.2
R41 -----	19.8	.2	55.2	9.0	15.2	---	.5	.1
R42 -----	22.2	3.2	52.3	10.5	11.3	---	.4	.1
R43 -----	18.9	1.4	53.1	17.2	8.9	---	.4	.1
122 -----	22.9	1.0	54.4	10.5	10.5	---	.5	.2
133 -----	22.2	3.4	54.6	8.5	10.9	---	.3	.1
134 -----	22.6	1.6	50.3	12.5	12.4	---	.5	.1
137 -----	20.3	2.2	56.5	8.1	12.4	---	.4	.1
220 -----	23.8	.7	59.9	9.3	6.0	---	.2	.1
Average	21.4	1.7	54.9	10.3	11.2	---	.4	.1
Tonalite near line A-B								
R150 ----	14.8	0.0	55.2	12.1	17.3	0.1	0.3	0.2
R151 ----	14.4	.0	55.3	11.1	18.6	.0	.4	.2
R171 ----	13.5	.1	54.7	11.4	19.7	.1	.4	.1
Average	14.2	.0	55.1	11.5	18.5	.1	.4	.2

The volume percentage of augite in the crystallizing magma can be crudely approximated by point counting the areas of bleached cores, the local sieved areas that are not bleached, the areas of hornblende between two or more augite relicts that extinguish simultaneously, and all relict augite as well as inclusions of augite in plagioclase. This method indicates the presence of from 0.4 to 2.3 volume percent augite during the early crystallization history of the northernmost subgroup of tonalites in the Elkhorn pluton.

Unit 1 of the Wallowa batholith (fig. 2.11) provides the most complete documentation for comparative purposes of the early crystallization of augite in the tonalitic magmas of northeastern Oregon. Augite relicts in hornblende are common in 78 thin sections of 39 rock specimens, as are small inclusions of euhedral to

subhedral augite in plagioclase. Inclusions of augite in plagioclase in unit 1 commonly are larger than any in the Elkhorn pluton; 11 inclusions are from 0.3 to 0.7 mm in greatest dimension, and one is 0.9 mm across. The procedure used to determine the original content of augite in the northern tonalites of the Elkhorn pluton indicates that six tonalites of unit 1 of the Wallowa batholith initially contained from 1.9 to 3.1 volume percent augite.

Augite cores in hornblende were not seen in thin sections of the southern subgroup of tonalites (table 2.2), but the former presence of augite is disclosed in most rocks by hornblende with bleached cores that enclose minute crystals of quartz. Accordingly, augite was the first mafic mineral to crystallize throughout the southern area of tonalite as well as in the northern area. Lack of augite cores in the southern rocks could be a function of earlier water saturation than in the northern rocks and consequent replacement of augite by hornblende.

The average modal compositions of the northern and southern subgroups of tonalites (table 2.2) show an abnormally small increase in the felsic components of the rocks southward toward the intraplutonic contact (or toward the central area of the Elkhorn pluton). An explanation for the small change in modal composition inward is complicated by overlying Cenozoic volcanic rocks on the north and west that conceal both interior and peripheral tonalites. Border tonalites on the east were mostly removed during intrusion of the granite of Anthony Butte. In addition, an explanation for the small change in modal composition inward is hindered by poor exposures throughout the area of tonalite.

The northern subgroup of tonalites may consist of an earlier pulse of magma that slightly preceded the emplacement of the southern subgroup of tonalites. This possibility requires an internal intrusive contact (approximating line A-B, fig. 2.2) and derives modal support from low contents of quartz and potassium feldspar and high contents of hornblende in the three rock samples (R150, R151, and R171, table 2.2) collected nearest the postulated contact. The northern subgroup of tonalites, in addition to containing augite, is characterized by plagioclase that is antiperthitic as seen in at least a few crystals in nearly all thin sections. Moreover, the plagioclase in many thin sections is clouded (Poldervaart and Gilkey, 1954). Distinctions between the plagioclase in the northern and southern tonalites are consistent with the probability of two tonalitic intrusions separated by an intrusive contact near the line A-B.

The systematic changes in modal mineralogy that typically occur inward from wallrock contacts of the Elkhorn pluton are well defined in the triangular area of tonalite west of the intraplutonic contact and north of the norite of Badger Butte (fig. 2.2). Tonalites in this area can be divided, from south to north, into three subgroups (table 2.3) that are at distances from the norite contact of 0.3 to 0.5 km, 1.0 to 2.0 km, and 2.2 to 3.2 km. The most apparent systematic modal changes (table 2.3) northward in the three subgroups are an increase in potassium feldspar from trace amounts to several volume percent, an increase in quartz from about 14 to 21 volume percent, and a decrease in hornblende from about 18.5 to 10.5 volume percent. Similar changes typically occur inward from the margins of other tonalitic intrusions in northeastern Oregon, although the changes are not necessarily as pronounced for an equivalent horizontal distance as those north of the norite of Badger Butte. Moreover, in the Cornucopia tonalite unit in the Wallowa Mountains, the inward increase in quartz and decrease in hornblende is accompanied by almost no increase in potassium feldspar (Taubeneck, 1967).

Outcrops of tonalite near the south contact of the Elkhorn pluton were sampled where the contact is best exposed to determine the modal composition of border tonalite in contrast to other tonalite and also in contrast to granodiorite in the core of the pluton. Eight specimens from within 40 m of the contact were collected westward for 12 km from Hunt Mountain (fig. 2.2). Previously published modal analyses (Taubeneck, 1957) for tonalite sampled throughout most of the Elkhorn pluton indicate that the eight border-rock samples (table 2.4) contain minimum amounts of quartz and potassium feldspar and high amounts of hornblende. Augite cores in hornblende occur in three of the eight rock samples (table 2.4); four of the five remaining rock samples contain hornblende with bleached cores that enclose minute crystals of quartz.

The augite cores (in three samples) and the indirect evidence of former augite (in four samples) prompted an attempt to more nearly determine the original distribution of augite in the crystallizing magma south of the intraplutonic contact. Reexamination of thin sections of rocks collected during the early 1950's (Taubeneck, 1957) disclosed small cores of augite in 3 rock samples, as well as bleached cores (indicative of former augite) in the hornblende of 21 other rock samples. The 24 rock samples are confined to the southern and eastern parts of the batholith. Forty-six additional rock samples were collected to increase sampling density in and near this part of the batholith. Four rock specimens in this group have augite cores in hornblende, whereas 16 other rock specimens contain

TABLE 2.3.—*Modes of the tonalite of Bald Mountain west of the intraplutonic contact and north of the norite of Badger Butte*

[Values in volume percent. Each analysis represents at least 2,400 point counts for each of two thin sections; 0.0, <0.05]

Specimen number	Quartz	Potassium feldspar	Plagioclase	Biotite	Hornblende	Augite	Opaque minerals	Nonopaque accessory minerals
Tonalite 0.3 to 0.5 km north of norite								
77	15.3	0.1	58.6	6.2	17.6	1.1	0.8	0.3
79	12.6	.1	55.8	10.6	19.7	.3	.6	.3
80	13.7	.0	55.8	10.2	18.3	1.2	.5	.3
Average	13.9	.1	56.7	9.0	18.5	.9	.6	.3
Tonalite 1.0 to 2.0 km north of norite								
74	17.9	0.3	57.4	11.2	12.8	0.1	0.2	0.1
75	18.3	.4	55.7	10.8	13.9	.3	.3	.3
76	17.2	.0	53.4	12.4	16.2	.2	.4	.2
Average	17.8	.2	55.5	11.5	14.3	.2	.3	.2
Tonalite 2.2 to 3.2 km north of norite								
68	19.4	1.3	53.9	12.1	11.9	1.1	0.2	0.1
68B	20.1	2.0	53.2	11.4	12.7	.0	.2	.4
69	23.1	3.5	51.4	10.9	10.4	.2	.2	.3
70	20.8	3.3	56.6	11.9	7.0	.0	.2	.2
72	22.6	2.4	51.1	12.5	10.6	.3	.3	.2
Average	21.2	2.5	53.2	11.8	10.5	.3	.2	.3

TABLE 2.4.—*Modes of the tonalite of Bald Mountain near the south contact of the Elkhorn pluton*

[Values in volume percent. Each analysis represents at least 2,400 point counts for each of two thin sections; ---, not present]

Specimen number	Quartz	Potassium feldspar	Plagioclase	Biotite	Hornblende	Augite	Opaque minerals	Nonopaque accessory minerals
B1	7.6	---	65.4	9.5	16.4	0.3	0.7	0.1
B2	19.4	---	62.6	11.2	7.5	---	.2	.1
B3	17.2	---	62.4	7.9	12.2	.1	.2	.1
B4	18.4	---	63.7	9.1	8.1	---	.6	.1
B5	20.1	---	65.3	7.0	6.8	---	.6	.2
B6	15.2	0.2	65.8	5.6	12.5	.1	.4	.2
B7	19.5	---	61.7	10.4	8.0	---	.2	.2
B8	18.7	1.2	55.8	11.3	11.4	---	.3	.3
Average	17.0	.2	62.8	9.0	10.3	.1	.4	.2

the diagnostic bleached cores in hornblende that denote the former presence of augite.

Tonalite in which augite is known to have crystallized extends west from Hunt Mountain and southwest from Antelope Peak to about 5 km N. 80° W. of Summit Lake. Early augite crystallization is also evident in rocks that extend northward from near Summit Lake to within about 2 km of Anthony Lake, including the southeastern part (about 35 km^2) of the granodiorite of Anthony Lake (fig. 2.2). Thus, all tonalite south and southeast of the granodiorite (except in and very near the Monumental salient) is within the area of augite crystallization. Additional sampling of tonalite would surely enlarge the area of known

augite crystallization throughout the general area from 5 to 13 km N. 50°–75° W. of Summit Lake. However, sampling density in the granodiorite is adequate to conclude that any appreciable extension of the area of augite crystallization farther northward in granodiorite is unlikely.

Tonalites of the Monumental salient (table 2.5) are distinctly more siliceous than tonalites elsewhere in the Elkhorn pluton at equivalent distances from peripheral contacts (tables 2.2–2.4). A precise comparison of modal data for different subgroups of border tonalites would necessitate that each group be sampled at identical distances from wallrocks. Accordingly, no exact comparison of modal data is feasible; some contacts of the Elkhorn pluton are overlain by Cenozoic volcanic rocks, whereas other contacts are not exposed within distances of 15 to 60 m. General comparisons of modal data are adequate, however, in substantiating the conspicuous compositional differences between tonalite in the salient and tonalite elsewhere in the Elkhorn pluton. The average modal content of quartz in border rocks (0.0 to 0.5 km from contact) of the salient is roughly between 4 and 11 volume percent more than in other parts of the pluton. The average modal content of hornblende in border rocks of the salient is between 4 and 12 volume percent less than in border rocks elsewhere in the pluton. Interior tonalite (0.5 to 3.0 km from nearest contact) of the salient contains about 3 volume percent more quartz than tonalite from 1.5 to 3.5 km north of the south contact of the pluton in the general area north of Summit Lake.

The high modal quartz and low modal hornblende contents of border tonalite of the salient could have originated from the peripheral crystallization of a separate tonalitic magma that was more siliceous than tonalitic magmas elsewhere in the Elkhorn pluton. This possibility is supported indirectly by the interpretation from structural data that the salient originally was a satellite of the Elkhorn pluton.

Direct support for the crystallization of a more siliceous magma in the Monumental salient is derived from the absence of any evidence in hornblende for the former presence of augite, in contrast to evidence for the presence of augite in tonalite from nearby parts of the Elkhorn pluton. For example, in tonalite west of the Muddy Creek wedge and at least 3 km north of the south contact of the Elkhorn pluton, bleached cores containing minute crystals of quartz occur in hornblende in eight rocks containing 23.1 to 25.6 volume percent quartz. One specimen containing 23.6 volume percent quartz also contains augite relicts. Farther west, specimen 482 (table 2.5, fig. 2.13) containing 24.1 volume percent quartz is the nearest tonalite to the Monumental salient showing evidence in hornblende for the former presence of augite. The salient constitutes the largest area of tonalite in the Elkhorn pluton showing no evidence for the former presence of augite. At least a few rocks of the salient containing less than 25.6 volume percent quartz should show such evidence if the salient crystallized from the same magma as the tonalite to the north and northeast in the main part of the pluton.

Mafic tonalite along the southwest, south, east, and northeast contacts of the Elkhorn pluton grades inward, across a wide transitional zone, to granodiorite in the central part of the exposed pluton. On the north and northwest the intraplutonic contact abruptly separates tonalite on the north from a more felsic rock on the south that generally is granodiorite. Pertinent relations are defined in figure 2.13 by the content of potassium feldspar in specimens of tonalite, granodiorite, and rocks transitional between typical tonalite and typical granodiorite. Corresponding modal analyses are given in tables 2.5, 2.6, and 2.7.

An arbitrary unit boundary between the tonalite of Bald Mountain and the granodiorite of Anthony Lake is shown in figures 2.2 and 2.13; a more precise boundary would require the collection of additional samples, especially from north and northeast of Nip and Tuck Pass (fig. 2.2), east and northeast of Chicken Hill, and west of Antelope Peak. Moreover, the present study reveals that modal analyses of only two thin sections of specimens that are borderline in composition between tonalite and granodiorite will introduce significant errors for the purposes of nomenclature in perhaps as many as a third of the specimens. Potassium feldspar contents in two thin sections of the same rock differ by less than 15 percent of the smaller value in about half of the rock samples but by more than 45 percent in a quarter of the rock samples. Trial and error shows that variations by even 45 to 95 percent in potassium feldspar content from one thin section to another are of little consequence in a mode that is the average of tabulations from five thin sections. Therefore, a rigorous determination of the geographic distribution of the tonalite of Bald Mountain and the granodiorite of Anthony Lake would require perhaps as many as five thin sections for all specimens in the gradational zone between tonalite and granodiorite. Other considerations pertaining to modal variations in thin sections of granitic rocks were reviewed by Emerson (1964).

Distinct mineralogic and textural differences occur in rocks along the south side of the intraplutonic contact. Granodiorite predominates, and most textural differences occur within 250 m of the contact. Some

TABLE 2.5.—*Modes of the tonalite of Bald Mountain in the border and interior of the Monumental salient, in the area of the neck between the salient and the main part of the Elkhorn pluton, and in the remaining parts of the Elkhorn pluton*

[Values in volume percent. Each analysis represents at least 2,400 point counts for each of two thin sections; 0.0, <0.05; ---, not present]

Specimen number	Quartz	Potassium feldspar	Plagioclase	Biotite	Hornblende	Opaque minerals	Nonopaque accessory minerals
Border tonalite (0.0 to 0.5 km from contact) of the Monumental salient							
404 -----	21.5	0.8	62.8	9.9	4.8	0.1	0.1
411 -----	25.5	1.3	60.6	7.0	5.4	.1	.1
412 -----	25.5	.1	62.8	5.7	5.2	.5	.2
413 -----	23.9	---	61.3	4.5	10.0	.2	.1
414 -----	27.9	---	54.7	11.5	5.7	.0	.2
415 -----	25.4	.4	56.0	11.7	6.4	---	.1
416 -----	26.0	.2	56.9	10.5	6.0	.3	.1
417 -----	26.7	.8	59.2	8.3	4.6	.3	.1
418 -----	24.7	.8	55.7	11.2	7.4	.1	.1
419 -----	27.3	1.9	57.6	8.3	4.2	.5	.2
460 -----	19.6	---	62.5	8.9	8.7	.2	.1
469 -----	20.6	---	61.2	8.8	9.2	.1	.1
490 -----	24.9	---	60.4	9.1	5.3	.1	.2
491 -----	28.0	.1	55.7	9.7	6.3	.1	.1
493 -----	24.3	---	57.3	10.6	7.5	.1	.2
Average	24.8	.4	59.0	9.1	6.4	.2	.1
Interior tonalite (more than 0.5 km from contact) of the Monumental salient							
400 -----	25.7	0.2	59.9	8.9	5.0	0.2	0.1
401 -----	26.6	1.5	59.6	8.7	3.1	.4	.1
402 -----	27.4	1.0	57.6	9.4	3.6	.7	.3
403 -----	28.5	1.4	56.8	9.6	3.3	.3	.1
405 -----	28.1	.2	58.2	8.9	4.1	.4	.1
406 -----	27.5	1.2	61.0	6.5	3.2	.5	.1
407 -----	27.2	1.2	59.8	7.2	3.8	.6	.2
408 -----	28.0	.8	60.1	7.2	3.4	.3	.2
409 -----	24.9	1.9	61.5	7.6	3.7	.3	.1
410 -----	22.7	.1	58.8	10.1	7.7	.4	.2
422 -----	25.5	.4	60.6	7.5	5.2	.7	.1
423 -----	28.4	.7	60.3	5.0	5.2	.3	.1
425 -----	27.2	1.0	60.8	7.5	3.3	.1	.1
426 -----	25.3	1.6	59.3	7.4	5.8	.5	.1
427 -----	24.4	.8	60.5	9.1	4.7	.4	.1
428 -----	29.0	.5	59.4	7.3	3.6	.1	.1
429 -----	27.3	.6	58.7	8.1	5.2	.0	.1
463 -----	27.3	.5	58.9	8.2	5.0	.0	.1
464 -----	23.2	1.1	58.1	10.0	7.5	---	.1
467 -----	29.8	.7	56.4	6.7	5.5	.7	.2
468 -----	28.7	3.1	57.5	8.4	2.1	.1	.1
483 -----	26.1	2.7	54.6	9.2	7.3	---	.1
492 -----	26.9	.6	57.5	10.0	4.7	.1	.2
Average	26.8	1.1	58.9	8.2	4.6	.3	.1
Tonalite in the area of the neck between the salient and the main part of the Elkhorn pluton							
431 -----	24.5	1.5	61.2	8.1	4.7	---	0.0
442 -----	24.0	.9	60.2	8.9	6.0	.0	.0
443 -----	27.3	2.0	59.4	7.5	3.7	---	.1
444 -----	25.1	1.4	60.2	8.2	5.1	---	.0
446 -----	24.3	1.8	56.1	7.9	9.7	.1	.1
449 -----	20.7	1.5	59.9	7.7	10.0	.1	.1
462 -----	24.2	.1	61.2	6.5	7.9	.0	.1
475 -----	23.9	2.1	61.6	7.9	3.8	.6	.2
Average	24.2	1.4	60.0	7.8	6.4	.1	.1

Table continued on next page.

TABLE 2.5.—*Modes of the tonalite of Bald Mountain in the border and interior of the Monumental salient, in the area of the neck between the salient and the main part of the Elkhorn pluton, and in the remaining parts of the Elkhorn pluton*—Continued

[Values in volume percent. Each analysis represents at least 2,400 point counts for each of two thin sections; 0.0, <0.05; ---, not present]

Specimen number	Quartz	Potassium feldspar	Plagioclase	Biotite	Hornblende	Opaque minerals	Nonopaque accessory minerals
Tonalite in the remaining parts of the Elkhorn pluton							
31 ------	27.1	3.2	53.6	9.6	6.0	0.4	0.1
32 ------	20.1	.8	57.4	5.7	15.3	.5	.2
34 ------	23.7	3.4	58.3	8.6	5.2	.5	.3
35 ------	25.4	2.4	60.7	6.7	4.1	.5	.2
37 ------	26.0	3.5	56.6	6.8	6.2	.6	.3
38 ------	24.4	3.2	56.3	8.3	7.1	.5	.2
45 ------	19.8	1.8	58.6	7.5	11.4	.6	.3
46 ------	23.9	2.3	55.4	8.4	9.0	.7	.3
62 ------	22.9	2.8	55.9	11.0	6.4	.7	.3
78 ------	27.3	1.4	57.4	10.4	3.1	.2	.2
89 ------	23.5	3.1	57.4	9.1	6.0	.7	.2
90 ------	23.2	.6	60.6	8.3	6.7	.4	.2
98 ------	27.5	1.9	53.3	9.2	6.6	1.0	.5
100 -----	25.6	1.4	58.2	7.5	6.4	.5	.4
116 -----	19.7	.6	55.9	9.2	14.3	.2	.1
158 -----	24.4	1.8	54.6	9.5	9.2	.4	.1
167 -----	26.7	2.2	55.4	8.7	6.3	.6	.1
169 -----	26.4	3.1	57.5	7.9	4.5	.4	.2
174 -----	10.6	---	59.8	10.9	17.9	.6	.2
220 -----	23.8	.7	59.9	9.3	6.0	.2	.1
246 -----	21.3	1.2	61.2	6.7	9.2	.3	.1
247 -----	20.3	1.3	56.7	10.1	10.9	.6	.1
248 -----	26.3	1.4	59.2	7.2	5.2	.5	.2
250 -----	21.3	.8	62.1	8.3	7.4	.0	.1
251 -----	21.6	3.6	55.8	10.1	8.0	.8	.1
252 -----	22.5	1.6	59.7	7.9	8.0	.2	.1
254 -----	19.2	1.8	58.9	8.2	11.2	.6	.1
255 -----	19.8	.4	57.2	10.4	11.4	.7	.1
256 -----	19.6	.2	57.0	9.4	13.0	.6	.2
257 -----	20.5	.7	59.7	9.3	9.4	.2	.2
258 -----	20.6	.7	58.6	10.7	8.9	.4	.1
259 -----	21.5	1.7	57.0	9.4	9.9	.3	.2
264 -----	21.2	1.5	58.7	8.1	9.9	.5	.1
265 -----	17.8	1.1	60.2	9.0	11.5	.3	.1
271 -----	20.9	.3	57.1	9.5	11.2	.8	.2
470 -----	25.9	2.3	56.5	8.4	6.3	.4	.2
471 -----	26.1	1.6	57.4	7.2	7.3	.3	.1
472 -----	19.4	.5	58.4	9.1	12.0	.4	.2
473 -----	18.1	---	50.0	11.9	19.5	.4	.1
482 -----	24.1	3.7	59.2	7.8	4.1	.9	.2
530 -----	24.1	4.1	59.8	5.9	4.9	.9	.3
Average	22.5	1.7	57.6	8.7	8.8	.5	.2

rocks are considerably finer in grain size than normal granodiorite, whereas others are slightly coarser. Mineralogic differences are less obvious, but well-defined megascopic variations in color index and, especially, hornblende content occur at least as far as 450 m from the contact, and variations in mineral proportions not recognized in the field are apparent by modal analysis. For example, 3 of 10 specimens from a 4-km^2 area just south of the intraplutonic contact are tonalites containing 2.0, 2.4, and 3.0 volume percent potassium feldspar, respectively (specimens 160, 111, 213, table 2.7, fig. 2.13). Specimen 111 was collected only 15 m from specimen 110 (7.3 volume percent potassium feldspar) and could not be separately shown at the scale of figure 2.13. Five thin sections were used to obtain modal data for each of the three aberrant tonalite samples as well as for specimen 110. Therefore, the low values for potassium feldspar in the three tonalite samples were adequately verified, as was the absolute difference of about 5 percent modal potassium feldspar between specimens 110 and 111 collected within 15 m of each other.

A disproportionately large amount of quartz is a further mineralogic variation in some specimens of granodiorite from within 1.5 km of the intraplutonic contact. Modal percentages for quartz that are an average of analyses of five thin sections for each of three rock samples are 32.5, 31.6, and 32.6 volume percent, respectively (specimens 110, 159, 212, table 2.7, fig. 2.13). The very high values for modal percentages of

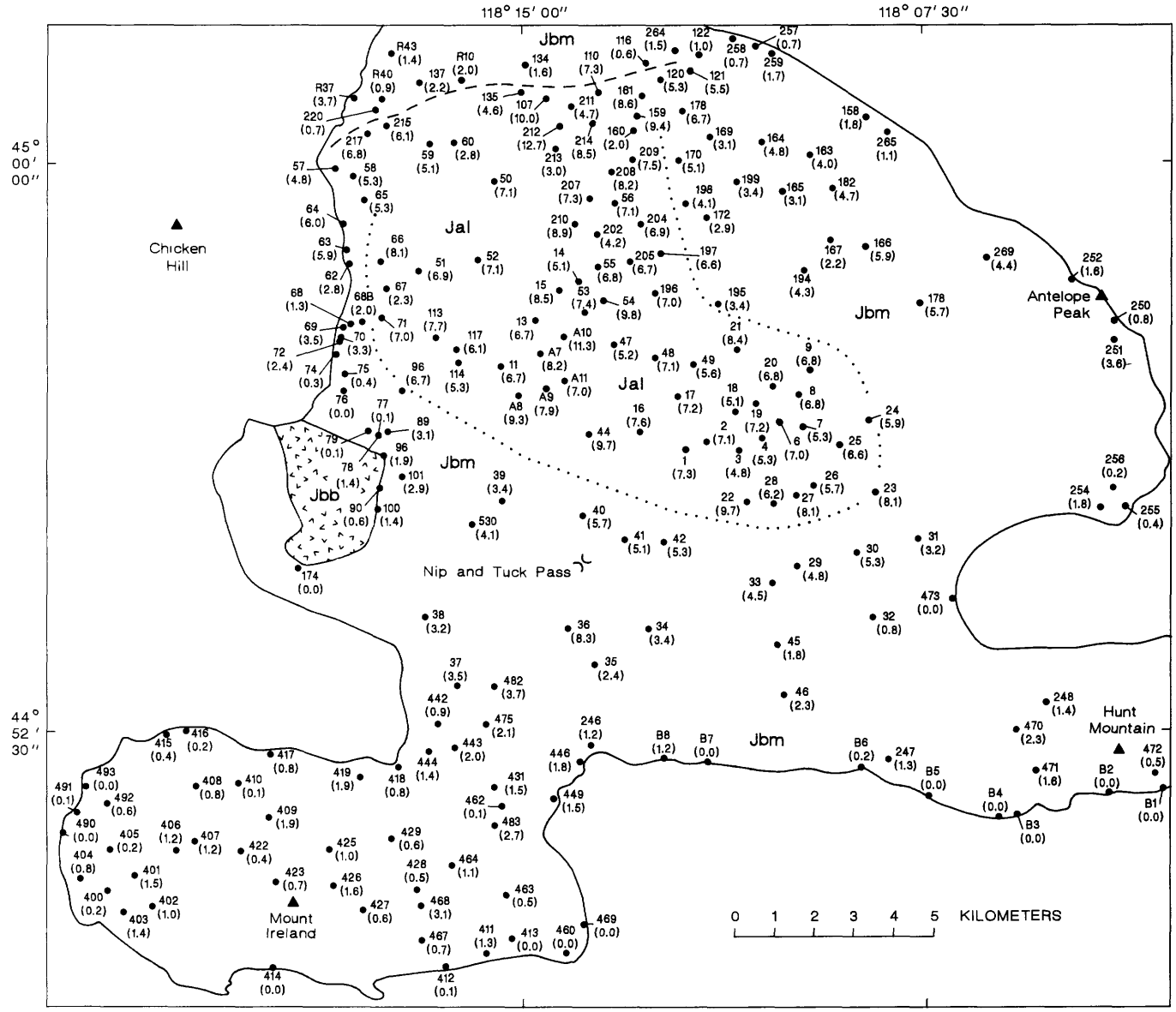

FIGURE 2.13.—Sample localities and potassium feldspar contents for rock specimens of the granodiorite of Anthony Lake and the tonalite of Bald Mountain.

TABLE 2.6.—*Modes of rocks transitional between the tonalite of Bald Mountain and the granodiorite of Anthony Lake*

[Values in volume percent. Each analysis represents at least 2,400 point counts for each of two thin sections]

Specimen number	Quartz	Potassium feldspar	Plagioclase	Biotite	Hornblende	Opaque minerals	Nonopaque accessory minerals
29 ------	23.6	4.8	51.4	9.8	9.4	0.7	0.3
30 ------	22.8	5.3	55.2	8.3	8.0	.3	.1
33 ------	24.1	4.5	55.9	9.7	5.0	.6	.2
36 ------	24.6	6.3	54.8	10.3	3.2	.6	.2
39 ------	29.1	3.4	54.7	7.4	4.4	.7	.3
40 ------	29.1	5.7	53.7	6.8	3.9	.6	.2
41 ------	26.5	5.1	57.5	6.9	3.4	.4	.2
42 ------	27.0	5.3	57.1	5.8	4.1	.5	.2
57 ------	26.7	4.8	54.9	7.4	5.9	.2	.1
58 ------	27.5	5.3	50.4	7.9	8.3	.4	.2
59 ------	29.2	5.1	51.1	11.0	2.9	.5	.2
60 ------	22.2	2.8	62.0	6.7	5.2	.7	.4
63 ------	28.0	5.9	48.6	8.9	8.1	.4	.1
64 ------	28.0	6.0	53.5	7.9	4.1	.4	.1
65 ------	28.3	5.3	54.2	6.8	4.7	.5	.2
101 -----	25.5	2.9	59.2	7.3	4.5	.4	.2
120 -----	27.7	5.3	54.9	7.8	3.7	.4	.2
121 -----	29.7	5.5	52.5	5.9	5.5	.7	.2
135 -----	26.2	4.6	53.4	9.9	4.9	.7	.3
162 -----	26.3	4.7	54.7	8.5	5.2	.4	.2
163 -----	26.3	4.0	53.8	9.9	5.6	.3	.1
164 -----	29.2	4.8	52.7	8.6	4.0	.6	.1
165 -----	30.0	3.1	51.8	9.7	4.7	.4	.3
166 -----	29.4	5.9	50.2	7.9	6.2	.3	.1
170 -----	28.2	5.1	48.3	10.0	7.5	.6	.3
172 -----	28.8	2.9	51.4	9.4	6.4	.9	.2
173 -----	28.8	6.7	53.0	7.2	3.8	.4	.1
178 -----	26.1	5.7	52.2	9.8	5.6	.5	.1
194 -----	28.7	4.3	51.9	8.6	6.0	.4	.1
195 -----	30.6	3.4	51.9	7.5	5.9	.5	.2
198 -----	24.7	4.1	55.8	8.3	6.2	.6	.3
199 -----	27.2	3.4	52.3	8.1	8.3	.5	.2
215 -----	27.6	6.1	52.4	7.1	6.2	.5	.1
217 -----	27.3	6.8	50.3	8.1	7.1	.3	.1
269 -----	27.9	4.4	53.5	8.9	4.8	.3	.2
Average	27.2	4.8	53.5	8.3	5.5	.5	.2

quartz in rock specimens such as these and the low values for potassium feldspar in other specimens are not understood, but general proximity to the intraplutonic contact suggests that the variations are related to this intrusive contact. Careful sampling and detailed field studies near the contact are essential before relations can be adequately appraised. The variations may result from perturbations in magma chemistry that resulted from surging and mixing prior to crystallization.

The most felsic rocks of the granodiorite core of the Elkhorn pluton occur in an area of about 2 km^2 just west and southwest of Anthony Lake. Modal analyses of five rock samples from this area are given in table 2.8. The average content of both potassium feldspar and quartz for these five samples is generally from 1 to 3 volume percent higher than in rocks from other areas near Anthony Lake, whereas the content of hornblende is from 0.5 to 2.5 volume percent lower. Many crystals of hornblende throughout most of the Elkhorn pluton south of the intraplutonic contact are strongly corroded where they are in contact with either quartz or potassium feldspar; resorption is greatest where hornblende is completely surrounded by one or both minerals. Obviously, hornblende was not stable in the rest magma of rocks that contain a relatively high content of quartz and potassium feldspar. The low average content of hornblende for the five specimens (table 2.8) near Anthony Lake together with the high average contents of quartz and potassium feldspar suggests that the low content of hornblende may be partly a function of greater resorption in this area rather than less crystallization of hornblende.

The most felsic rocks (table 2.8) of the granodiorite core contain more quartz than equivalent parts of the four similarly zoned units that grade from mafic tonalite to granodiorite in the Wallowa batholith (fig. 2.11), which is about 70 km to the northeast of the northern

TABLE 2.7.—*Modes of the granodiorite of Anthony Lake and the three aberrant rock specimens of tonalite (111, 160, 213) just south of the intraplutonic contact*

[Values in volume percent. Table includes all rock specimens collected inside approximate boundary between granodiorite of Anthony Lake and tonalite of Bald Mountain (fig. 2.13). Rock specimen 111 was collected 15 m from specimen 110 and could not be shown separately at scale of figure 2.13. Modal analyses for rock specimens 110, 111, 159, 160, 212, and 213 represent at least 2,400 point counts for each of five thin sections; all other analyses represent at least 2,400 point counts for each of two thin sections]

Specimen	Quartz	Potassium feldspar	Plagioclase	Biotite	Hornblende	Opaque minerals	Nonopaque accessory minerals
1 -------	27.5	7.3	50.4	9.8	3.9	0.8	0.3
2 -------	26.2	7.1	53.8	7.6	4.7	.4	.2
3 -------	24.2	4.8	55.7	9.5	4.8	.8	.2
4 -------	25.1	5.3	55.6	9.5	3.5	.8	.2
6 -------	28.9	7.0	52.1	6.9	4.2	.5	.4
7 -------	29.2	5.3	52.9	7.5	4.3	.5	.3
8 -------	25.5	6.8	51.4	9.6	5.7	.8	.2
9 -------	26.4	6.8	54.1	7.2	4.8	.6	.1
11 ------	29.2	6.7	53.5	6.1	3.5	.7	.3
13 ------	29.4	6.7	53.6	7.1	2.7	.3	.2
14 ------	27.0	5.1	56.3	6.1	4.7	.5	.3
15 ------	26.5	8.5	53.9	7.4	3.1	.5	.1
16 ------	26.7	7.6	51.8	7.9	4.7	1.1	.2
17 ------	27.1	7.2	52.8	8.1	4.1	.5	.2
18 ------	26.3	5.1	55.2	7.4	4.8	.8	.4
19 ------	24.1	7.2	55.3	8.3	4.4	.4	.3
20 ------	26.2	6.8	53.9	8.7	3.8	.4	.2
21 ------	25.8	8.4	55.3	6.9	2.9	.6	.1
22 ------	26.8	9.7	53.2	7.3	2.4	.4	.2
23 ------	28.7	6.1	53.3	8.9	2.4	.4	.2
24 ------	24.6	5.9	59.5	6.4	2.7	.7	.2
25 ------	28.8	6.6	52.3	6.6	4.7	.7	.3
26 ------	26.9	5.7	56.6	6.9	3.1	.5	.3
27 ------	27.6	8.1	53.8	7.3	2.1	.9	.2
28 ------	27.8	6.2	56.4	4.8	4.1	.6	.1
44 ------	29.4	9.7	47.2	7.1	5.7	.6	.3
47 ------	25.6	5.2	55.1	7.2	5.7	.8	.4
48 ------	24.7	7.1	56.1	7.2	3.9	.7	.3
49 ------	26.6	5.6	54.3	7.5	5.3	.5	.2
50 ------	28.6	7.1	51.8	6.4	5.3	.6	.2
51 ------	27.3	6.9	49.3	9.8	5.7	.7	.3
52 ------	27.6	7.1	49.8	8.6	6.1	.6	.2
53 ------	28.7	7.4	50.6	5.9	6.6	.6	.2
54 ------	28.9	9.8	48.8	7.8	3.7	.7	.3
55 ------	29.7	6.8	52.4	6.3	4.1	.5	.2
66 ------	23.6	8.1	56.7	7.1	3.9	.4	.2
71 ------	29.0	7.0	51.8	7.7	3.8	.5	.2
96 ------	27.5	6.7	55.6	6.0	3.5	.5	.2
103 -----	25.1	5.9	55.0	7.2	5.8	.8	.2
107 -----	29.8	10.0	51.2	5.5	3.0	.3	.2
110 -----	32.5	7.3	49.2	8.0	2.4	.5	.1
113 -----	29.7	7.7	51.3	7.9	2.3	.8	.3
114 -----	28.3	5.3	55.3	5.6	4.7	.5	.3
117 -----	26.9	8.1	52.5	7.3	4.5	.5	.2
159 -----	31.5	9.4	48.5	7.7	2.4	.4	.1
161 -----	27.7	8.6	50.6	7.4	5.0	.5	.2
171 -----	31.1	8.4	47.6	8.6	3.8	.4	.1
196 -----	28.8	7.0	47.9	9.1	6.4	.6	.2
197 -----	29.8	6.6	51.3	8.0	3.6	.5	.2
202 -----	27.5	4.2	55.6	6.0	5.6	.8	.3
204 -----	27.9	6.9	50.4	8.9	5.0	.7	.2
205 -----	28.4	6.7	51.4	7.8	5.0	.5	.2
207 -----	31.8	7.3	47.6	6.9	5.7	.5	.2
208 -----	27.8	8.2	50.1	8.1	4.9	.6	.3
209 -----	26.5	7.5	54.9	6.5	4.1	.3	.2
210 -----	29.2	6.9	51.2	6.6	5.8	.2	.1
211 -----	30.3	4.7	54.5	6.4	3.6	.4	.1
212 -----	32.6	12.7	45.3	6.5	2.4	.3	.2
214 -----	30.0	8.5	49.8	7.4	3.6	.5	.2
A7 ------	31.0	8.2	49.7	7.7	2.7	.5	.2
A8 ------	28.1	9.3	51.3	8.1	2.6	.5	.1
A9 ------	30.4	7.9	49.1	7.8	4.2	.5	.1
A10 -----	28.2	11.3	49.5	6.3	4.2	.4	.1
A11 -----	31.2	7.0	50.2	7.3	3.2	.8	.3
Average	28.0	7.2	52.4	7.4	4.2	.6	.2
Aberrant specimens of tonalite just south of the intraplutonic contact							
111 -----	25.7	2.4	59.2	7.6	4.7	0.3	0.1
160 -----	28.5	2.0	52.5	9.6	6.7	.5	.2
213 -----	26.7	3.0	58.3	7.6	3.8	.4	.2
Average	26.9	2.5	56.6	8.3	5.1	.4	.2

TABLE 2.8.—*Modes of the granodiorite of Anthony Lake in the Bald Mountain batholith near Anthony Lake compared with modes of core granodiorite of units 2 and 4 of the Wallowa batholith, northeastern Oregon*

[Values in volume percent. Each analysis represents at least 2,400 point counts for each of two thin sections]

Specimen number	Quartz	Potassium feldspar	Plagioclase	Biotite	Hornblende	Opaque minerals	Nonopaque accessory minerals
Core granodiorite (near Anthony Lake), Bald Mountain batholith							
A7 ------	31.0	8.2	49.7	7.7	2.7	0.5	0.2
A8 ------	28.1	9.3	51.3	8.1	2.6	.5	.1
A9 ------	30.4	7.9	49.1	7.8	4.2	.5	.1
A10 -----	28.2	11.3	49.5	6.3	4.2	.4	.1
A11 -----	31.2	7.0	50.2	7.3	3.2	.8	.3
Average	29.8	8.7	50.0	7.4	3.4	.5	.2
Core granodiorite of unit 2, Wallowa batholith							
116 -----	24.5	9.4	49.4	8.9	6.8	0.7	0.3
272 -----	24.1	9.1	52.7	9.0	4.6	.3	.2
273 -----	25.5	12.2	48.9	8.3	4.5	.4	.2
289 -----	26.4	8.4	47.9	8.9	7.6	.6	.2
290 -----	24.6	11.2	48.7	9.3	5.6	.4	.2
Average	25.0	10.1	49.5	8.9	5.8	.5	.2
Core granodiorite of unit 4, Wallowa batholith							
765 -----	29.6	15.0	45.2	6.5	2.8	0.6	0.3
766 -----	28.0	18.0	41.7	6.9	4.7	.4	.3
767 -----	27.7	14.6	45.1	7.5	4.5	.3	.3
768 -----	27.0	10.9	47.5	8.4	5.7	.3	.2
779 -----	25.0	10.7	49.5	6.1	7.6	.6	.5
Average	27.5	13.8	45.8	7.1	5.1	.4	.3

part of the Elkhorn pluton. For example, five rock samples from the granodiorite core near Anthony Lake contain an average of 29.8 volume percent quartz, whereas five samples from the core of unit 2 of the Wallowa batholith (Taubeneck, 1987) contain an average of 25.0 volume percent quartz, and five samples from the core of unit 4 contain an average of 27.5 volume percent quartz (table 2.8). The comparatively high content of quartz in both the granodiorite of Anthony Lake and the younger felsic intrusions of the Bald Mountain batholith suggests a genetic relationship between these silica-rich granitic units.

ASSIMILATION OF GRAPHITE-BEARING METASEDIMENTARY ROCKS IN ELKHORN PLUTON

The higher content of modal quartz in tonalite of the Monumental salient (table 2.5) than in tonalite elsewhere in the Elkhorn pluton apparently resulted from the intrusion of a separate and more siliceous magma (see previous section, "Comparative Modal Compositions and Crystallization of Augite"). Assimilation of siliceous metasedimentary rocks may also have contributed to the high content of modal quartz in rocks of the Monumental salient. Xenoliths of siliceous metasedimentary rocks are relatively common throughout most of the salient, and the rounded shapes of many xenoliths indicate assimilation.

Thin sections of tonalite containing red-brown biotite and low amounts of modal iron oxide support the interpretation that metasedimentary rocks were assimilated into the Monumental salient, as well as into many other granitic intrusions in the Elkhorn Mountains. Both the red-brown biotite and the low modal iron oxide content indicate that the rocks are reduced; assimilation of graphite-bearing metasedimentary wallrocks is the logical way to explain the reduction (Flood and Shaw, 1975, p. 162). Notably, the most continuous graphite-bearing sequences of metasedimentary wallrocks in contact with the Elkhorn pluton

occur west and southwest of Summit Lake in the vicinity of the Monumental salient.

Much of the tonalite in and near the Monumental salient contains evidence of reduction: Including rock specimens collected during the 1950's (Taubeneck, 1957), 14 of 23 tonalite samples collected within 400 m of the contact of the salient contain red-brown biotite and have an average of 0.09 volume percent iron oxide, and 10 of 15 tonalites from within the area of the neck contain red-brown biotite and have an average of 0.06 volume percent iron oxide. In contrast, modal iron oxide is much more abundant—constituting 0.26 to 1.10 volume percent—in nearly all tonalite bodies in northeastern Oregon that do not contain red-brown or red biotite.

Further evidence of reduced rocks in the Elkhorn pluton is provided by an analysis of a border tonalite containing red-brown biotite and collected southwest of Summit Lake. This tonalite was analyzed for selected oxides using classical wet methods (C.O. Ingamells, analyst, 1966, Pennsylvania State University); the analysis yielded values for Fe_2O_3 and FeO of 0.39 and 3.39 weight percent, respectively. These iron oxide values and the red-brown color of biotite are typical of S-type granitic rocks (Hine and others, 1978; White and Chappell, 1983; Whalen and Chappell, 1988), which are derived from the melting of sedimentary source rocks.

The granitic rocks of northeastern Oregon, even the cordierite-bearing trondhjemites of the Wallowa Mountains, are I-type granitoids on the basis of their low initial $^{87}Sr/^{86}Sr$ ratios (Armstrong and others, 1977), low K_2O/Na_2O ratios, high Fe_2O_3 /FeO ratios, and the unrefutable evidence for the magmatic crystallization of cordierite in the trondhjemites (Taubeneck, 1987). Accordingly, granitic rocks in the Elkhorn pluton with red-brown biotite and minor amounts of iron oxide crystallized from I-type magmas that acquired their low Fe_2O_3 /FeO ratios by assimilation of graphite-bearing metasedimentary rocks.

Tonalite with red-brown biotite—that is, reduced tonalite—is present not only within the Monumental salient, but also, sporadically, eastward from the salient to the contact south of Hunt Mountain and northward to tonalite west of the norite of Badger Butte (fig. 2.2). Some of the tonalite in the Monumental salient lacks red-brown biotite and contains moderate amounts of iron oxide. The distribution of xenoliths in the salient indicates that even this unreduced tonalite assimilated metasedimentary rocks; presumably tonalite that is not reduced assimilated metasedimentary rocks that contained little or no graphite. No assessment of the importance of assimilation during the emplacement and crystallization of the Elkhorn pluton is possible without trace-element data and oxygen-isotope compositions for both metasedimentary rocks and associated border and interior tonalite.

DISTINCTIVE PETROGRAPHIC FEATURES OF ROCKS OF ELKHORN PLUTON

Three petrographic features that distinguish rocks of the Elkhorn pluton from many other granitic rocks are (1) very strong oscillatory zoning in plagioclase, (2) magnetite concentrations as much as 2 mm across, and (3) general absence of rutile needles in quartz.

Zoning in plagioclase in plutonic rocks south of the intraplutonic contact is sharp and strongly oscillatory: Except in the two salients, at least one crystal in every two thin sections of each rock sample generally exhibits 48 or more distinct oscillations. As many as 82 oscillations occur, but more than 65 is uncommon. Delicate rhythmic oscillations especially characterize the most strongly zoned crystals. Zoning in the Monumental salient is slightly less intense than throughout the main part of the pluton, although nearly all rocks contain some plagioclase with 44 or more oscillations and one crystal has 72 oscillations. Zoning throughout the Hunt Mountain salient is less uniform than elsewhere in the pluton, but about one-half of the rocks contain some plagioclase with at least 40 oscillations.

The very strong oscillatory zoning in plagioclase of the Elkhorn pluton is not confined to rocks well within the batholith but commonly persists to within less than 100 m of peripheral contacts with country rocks. For example, the maximum of 22 oscillations in plagioclase in specimen 250 (fig. 2.13), collected 6.5 m from the contact at Antelope Peak (fig. 2.2), is greater than the number of oscillations in crystals throughout many plutons of batholithic dimensions.

The character of the oscillatory zoning in plagioclase is a significant feature in distinguishing between different plutonic environments as well as between individual plutons (Hutchison, 1970). The four major units of the Wallowa batholith (fig. 2.11) provide a convenient basis for contrasting oscillatory zoning in four compositionally zoned plutons that grade inward from peripheral tonalite to core granodiorite. Each of the four units is large enough to qualify as a small batholith. Oscillatory zoning in plagioclase of 76 rock specimens from unit 1 ranges from less than 20 oscillations in rocks in the east to as many as 45 in rocks in the extreme west. Zoning in different parts of unit 2, as studied in 70 rock samples, ranges from 10 oscillations to as many as 36. Seventeen or fewer oscillations occur in plagioclase in 84 rock samples from unit 3 and in most of

90 rock samples of unit 4. Thus, oscillatory zoning in plagioclase from the Elkhorn pluton is much more pronounced and uniform than in other compositionally zoned plutons in northeastern Oregon; it is also more conspicuous than in other granitic bodies such as those of the Prince Rupert region of British Columbia (Hutchison, 1970).

Concentrations of magnetite in large clots that contain many crystals is a second distinctive feature of most rocks of the Elkhorn pluton. Clots are absent or rare in tonalite that has assimilated adequate graphite in metasedimentary rocks to reduce the modal iron oxide content to less than about 0.2 volume percent. Clots of magnetite in most thin sections are about 1 mm across, but many are about 2 mm across. Individual crystals of magnetite mostly are less than 0.1 mm across. Therefore, some clots contain more than 100 crystals. Many crystals retain their euhedral outline, but others commonly have coalesced, obliterating most faces. Open spaces in compact aggregates of magnetite fairly commonly are filled with sphene.

Clots of magnetite are not numerous enough to occur in every thin section, but they are present in most rocks throughout the Elkhorn pluton. In contrast, other granitic plutons in northeastern Oregon contain few or no clusters of magnetite. Some concentrations similar to those in the Elkhorn pluton are present in units 3 and 4 of the Wallowa batholith (fig. 2.11) and in cordierite trondhjemite of the Cornucopia stock (Taubeneck, 1964).

A third distinctive feature of rocks of the Elkhorn pluton is the general absence of needles of rutile in quartz in comparison to other intrusions of tonalite and hornblende-bearing granodiorite in northeastern Oregon. (Data are insufficient to make a comparison with plutons outside of northeastern Oregon). Rutile needles in quartz in the Elkhorn pluton are estimated to occur in only about 3 percent of the rock samples. The slender needles generally are not more than 0.2 mm long, lack birefringence, and were not mentioned in previous reports (see Taubeneck, 1957). In contrast, long hairlike needles of rutile generally are common in quartz in granitic rocks elsewhere in northeastern Oregon. Quartz in some of these rocks contains needles as much as 1 mm long, and a few needles are considerably longer; birefringence is commonly discernible in the longer needles; scores of hairlike needles commonly occur in a single crystal of quartz; and many groups of needles are oriented.

SPECIFIC GRAVITY OF ROCKS OF ELKHORN PLUTON

The specific gravity of rocks of the Elkhorn pluton decreases inward in accordance with the compositional variations indicated by modal analyses. Specific-gravity determinations for 109 specimens yielded values of 2.78 to 2.67. Border rocks near the southern contact of the Elkhorn pluton and most mafic tonalite north of the intraplutonic contact have densities of 2.75 to 2.78, whereas those of other tonalites are 2.70 to 2.75. Densities of granodiorite are 2.67 to 2.70.

COMPOSITIONS OF CORES OF OSCILLATORY-ZONED PLAGIOCLASE IN ELKHORN PLUTON AND OTHER GRANITIC INTRUSIONS OF NORTHEASTERN OREGON

Limited compositional data for calcic cores in oscillatory-zoned plagioclase in the Elkhorn pluton, Cornucopia stock (Taubeneck, 1964), and Wallowa batholith (Taubeneck, 1987) were obtained with the assistance of A.J. Piwinskii at the University of Chicago in 1967. The focus of that study was to determine the maximum anorthite content of cores of oscillatory-zoned plagioclase. Compositions of plagioclase feldspar were measured with an Applied Research Laboratory (ARL) electron microprobe analyzer, following the methods described by Smith (1965) and by Ribbe and Smith (1966). The pertinent plagioclase compositional data are recorded in the following six paragraphs, together with data for the cordierite trondhjemite of Crater Lake (Taubeneck, 1964) obtained by E.M. Bishop in 1983 at Washington University in St. Louis.

In specimens of five border rocks of the tonalite of Bald Mountain, the anorthite content in cores of eight crystals ranged from $An_{47.2}$ to $An_{51.0}$. The most calcic spot compositions were found in three other crystals from the same group of rocks: $An_{51.5}Ab_{47.2}Or_{1.0}$, $An_{53.5}Ab_{44.8}Or_{1.0}$, and $An_{57.2}Ab_{41.0}Or_{1.3}$.

In four rock samples (six crystals) of the granodiorite of Anthony Lake, the anorthite content ranged from $An_{46.9}$ to $An_{50.1}$. The most calcic composition found was $An_{50.1}Ab_{48.5}Or_{1.2}$.

The anorthite content ranged from $An_{49.0}$ to $An_{53.5}$ for six crystals in five rock specimens from the interior of the Cornucopia tonalite unit (Taubeneck, 1967, p. 6). Analysis of a seventh crystal yielded an even more calcic (spot) composition: $An_{59.4}Ab_{39.6}Or_{0.7}$.

Core compositions for 10 crystals from five border rocks (Taubeneck, 1967, p. 6) of the Cornucopia tonalite unit ranged from $An_{49.2}$ to $An_{60.0}$. The most calcic compositions found, local spots in each of three other crystals, were $An_{63.1}Ab_{35.3}Or_{0.7}$, $An_{64.0}Ab_{34.2}Or_{0.8}$, and $An_{69.0}Ab_{29.6}Or_{0.3}$.

Eight crystals in two border-rock samples of unit 4 of the Wallowa batholith (Taubeneck, 1987) ranged in composition from $An_{49.6}$ to $An_{55.5}$; five crystals in three core-rock samples yielded a similar range of composition, from $An_{49.0}$ to $An_{54.8}$, indicating an in-

significant difference between core- and border-rock plagioclase.

The most calcic composition detected in four crystals in two specimens of the Tramway trondhjemite unit (Taubeneck, 1964), the oldest trondhjemite of the Cornucopia stock, was $An_{54.2}Ab_{45.0}Or_{0.6}$. $An_{39.7}$ was the most calcic composition detected by E.M. Bishop in nine crystals from six specimens of the cordierite trondhjemite of Crater Lake (Taubeneck, 1964), the youngest trondhjemite of the Cornucopia stock.

VOLUME PERCENT AND ORIGIN OF CALCIC CORES IN PLAGIOCLASE OF ELKHORN PLUTON

In the restite model, granitic magmas are visualized as crystal mushes that incorporate as much as about 60 percent of restite as single crystals (rather than refractory rock inclusions) of cordierite, sillimanite, garnet, zircon, and calcic cores of plagioclase (Chappell and others, 1987). Only zircon and calcic cores of plagioclase occur in the granitic rocks of the Elkhorn pluton. The euhedral habit of the zircon (Taubeneck, 1957, p. 216) indicates that the crystals are of magmatic origin, except for possible zircon cores too small to be seen with a petrographic microscope. A major linchpin of the restite model is that calcic cores of plagioclase in granitic rocks that contain less than 70 weight percent SiO_2 (such as granitic rocks of the Elkhorn pluton) are residuals of restite that have been overgrown by magmatic, oscillatory-zoned plagioclase of more sodic compositions (Chappell and others, 1987).

Seventeen rock specimens of the granodiorite of Anthony Lake and 11 specimens of the tonalite of Bald Mountain (from near the contact south and east of Summit Lake) were used for this exploratory study of the volume percent and origin of calcic cores in plagioclase of the Elkhorn pluton. The volume percent of calcic core was determined for crystals that show a large number of oscillations and apparently were cut through the center. To select appropriate crystals for examination, one must view many random slices of plagioclase in thin section (see Dowty, 1980). Some of the most favorable orientations occur in one or more crystals of synneusis aggregates (see Vance, 1969, figs. 10–14), but aggregates of two or more crystals were excluded from consideration in this study because of interference during growth. Commonly not more than a few suitable crystals occur in a thin section. Point counts for each plagioclase were tabulated for the core and the remainder of the crystal. In each case, the remainder of the crystal consists of oscillatory-zoned andesine bordered by rim oligoclase. The rim oligoclase is restricted volumetrically in peripheral tonalite but is as abundant as 35 percent by volume for some crystals in the granodiorite of Anthony Lake. For all volume percent determinations, a mechanical stage was adjusted to record 20,491 points for an area of 920 mm^2.

Calcic cores in 36 crystals of the granodiorite of Anthony Lake range from 0.8 to 5.9 volume percent of the plagioclase. The average volume of core is 2.4 volume percent. The crystals examined are from 0.9 to 5.2 mm in maximum dimensions. The average core volume of 23 plagioclase crystals from the tonalite of Bald Mountain is 3.7 volume percent in a range from 1.7 to 7.8 volume percent. The crystals examined are from 1.1 to 4.9 mm in maximum dimensions.

Biotite did not commence to crystallize in the Elkhorn pluton until just before growth of the plagioclase rim of oligoclase; quartz and potassium feldspar are interstitial. Therefore, irrespective of the origin of the cores of plagioclase in the granodiorite of Anthony Lake and the tonalite of Bald Mountain, the small core volumes indicate a magma that was emplaced as a near-liquid rather than as a crystal mush.

The following considerations were instrumental in the conclusion that calcic cores in the plagioclase of the Elkhorn pluton are of magmatic origin: The cores are not separated by higher birefringence from the surrounding oscillatory-zoned plagioclase or by an encircling corrosion rim. Polysynthetic twinning, where present, extends through oscillatory-zoned plagioclase into cores. The two-dimensional shape (mostly rectangular or squarish) of the cores closely approximates in gross outline the outer configuration of the plagioclase crystals. Furthermore, in a simple twin that exhibits considerable disparity in size, that part of the core within the longer individual is proportionally longer than the part within the shorter individual.

INTERLUDES: A NEWLY DESCRIBED FEATURE OF OSCILLATORY-ZONED PLAGIOCLASE IN GRANITIC ROCKS

Significant features of the oscillatory zoning in plagioclase of the Elkhorn pluton are interruptions in the rhythmic crystallization that herein are called "interludes." An interlude in oscillatory-zoned plagioclase is a concentration of either one or several different mafic minerals of small size in a concentric zone of plagioclase between consecutive oscillations. No descriptions of interludes were found during a literature search focused on oscillatory zoning in plagioclase of granitic rocks. A hint that interludes may occur in the Tokuwa batholith, central Japan, is the statement of Shimizu (1986, p. 63) that some plagioclase crystals have "lines of tiny inclusions along the crystal growth lines." In northeastern Oregon, examples of interludes occur in plagioclase of the Wallowa batholith and Cornucopia

stock, as well as in plagioclase of the Elkhorn pluton. It is illogical to assume that interludes are restricted to the plagioclase of granitic intrusions in northeastern Oregon, especially considering the common worldwide occurrence of oscillatory zoning in the plagioclase of granitic rocks containing less than about 70 weight percent SiO_2.

Interludes are subdivided for discussion into complete interludes, which are continuous and extend between oscillations around the circumference of a plagioclase crystal, and incomplete interludes, which are discontinuous and do not extend around the circumference. Incomplete interludes pinch out parallel to either one or two crystal faces. In this study of 20 rock specimens (40 thin sections) of the granodiorite of Anthony Lake, only six interludes are complete. In two of the complete interludes, the only mafic mineral is an iron oxide, whereas in four of the complete interludes, both iron oxide and hornblende are present. The complete interludes contain from 41 to 168 mafic crystals. Twenty-one incomplete interludes are present; four contain inclusions of iron oxide only. The proportions of iron oxide and hornblende inclusions in incomplete interludes range from entirely iron oxide in some interludes to almost as many crystals of hornblende as of iron oxide in other interludes. The 21 incomplete interludes contain from 6 to 69 mafic crystals.

Concentrations of iron oxide and hornblende in plagioclase also occur in the cores of 121 crystals in the 40 thin sections; 10 additional cores contain concentrations of iron oxide only. Cores that contain both mafic minerals have from 6 to 149 mafic crystals; cores that contain only iron oxide have from 7 to 21 mafic crystals. Almost invariably the cores of plagioclase that contain mafic inclusions are mottled, in contrast to cores that contain no mafic inclusions. Mottling consists of spots and blotches that exhibit different intensities of light under crossed nicols as the plagioclase is rotated on the stage of a microscope. A few mottled cores also contain small areas (square and rectangular in shape) of a more sodic plagioclase that is sufficiently different in composition to produce a distinct Becke line. Six of the 121 cores that contain both hornblende and iron oxide locally show resorption along as much as about 35 percent of the core periphery. Resorption was not detected, however, around the circumference of any core with concentrated mafic inclusions or any core without mafic inclusions.

Complete interludes differ from incomplete interludes in greater overall thickness, larger size of mafic inclusions, conspicuous mottling of plagioclase, and the common occurrence of microcracks localized within or adjacent to the interlude. The four complete interludes containing inclusions of both hornblende and iron oxide are from about 0.3 to 0.5 mm in width, whereas the two complete interludes with inclusions only of iron oxide are about 0.05 and 0.10 mm in width. In comparison, each incomplete interlude is less than 0.05 mm in maximum width; some have a maximum width of less than about 0.02 mm.

Most hornblende crystals in the complete interludes are subhedral to euhedral prisms of stubby habit with maximum dimensions from about 0.02 to 0.08 mm. Crystals larger than 0.12 mm are rare. Overall, the hornblende crystals are slightly larger than very similar inclusions of hornblende in the 121 cores of plagioclase that contain concentrated inclusions of iron oxide and hornblende. Cubic crystals of iron oxide in the complete interludes commonly are about 0.02 mm on an edge. Some crystals are 0.03 mm; a few are as much as about 0.04 mm. Similarities in size and habit between the mafic minerals in the plagioclase cores and those in the complete interludes suggest a genetic relationship that is much less apparent in the incomplete interludes, where crystallization was relatively short-lived. Crystals of both iron oxide and hornblende in the incomplete interludes are an estimated one-third to two-fifths as large as those in the complete interludes.

Point counts (20,491 points for an area of 920 mm^2) for hornblende confirm that collectively, the smallest crystals occur in the incomplete interludes rather than in the plagioclase cores or any other part of the plagioclase. One hundred sixteen counts were tabulated for the 1,511 hornblende crystals in the 121 plagioclase cores, whereas only 4 points were recorded for the 126 crystals of hornblende in the incomplete interludes. Much larger crystals of hornblende occur in plagioclase outside of the interludes and between the calcic cores and outer margins of the oligoclase rims. The largest inclusion of hornblende between a core and an incomplete interlude is a euhedral prism about 0.65 mm long and 0.15 mm wide. Larger crystals of hornblende (including resorbed crystals) occur between the incomplete interludes and the oligoclase margins. In review, the small overall size of hornblende in the incomplete interludes is explained by a more restricted period of growth after nucleation than in either the complete interludes, the calcic cores, or elsewhere within the plagioclase.

Each complete interlude is characterized by mottled plagioclase that commonly extends in an irregular manner beyond the interlude for a short distance into adjoining oscillations. The mottling obscures detailed examination of adjacent oscillations and therefore prevents a close determination of possible fine-scale resorption along the borders of interludes. However, no wholesale resorption is apparent. Locally, the mottled

interludes are further distinguished by small areas (square and rectangular in shape) of a more sodic plagioclase, as is also observed in some of the mottled cores of plagioclase that are characterized by concentrations of mafic inclusions. Mottling occurs in the incomplete interludes only where they are widest and hence generally does not obscure detailed relations along the margins of the interludes. No resorption was detected along the margin of any incomplete interlude.

Mottling in both complete interludes and the cores of plagioclase that contain concentrated mafic inclusions undermines the suggestion of Presnall and Bateman (1973) that mottled cores of plagioclase are evidence of restite. The cause for the local mottling of plagioclase in the granodiorite of Anthony Lake remains unknown, but the common occurrence of a mafic inclusion centered in a light blotched area repeatedly suggests that mottling is actuated by the presence of mafic inclusions. However, this interpretation is not entirely satisfactory because many blotches contain no inclusion, at least not in the plane of the thin section.

Three of the six complete interludes exhibit microcracks that are confined mostly to the interlude but also extend for short distances into adjacent oscillations. The microcracks possibly represent differential strain induced during cooling of layers of different plagioclase composition, enhanced perhaps by the numerous mafic inclusions within each interlude.

About three-quarters of the interludes occur within 15 percent of the midpoint of the total number of oscillations in each plagioclase. The most consistent position of interludes relative to oscillations occurs about 4 km east-southeast of Anthony Lake where interludes in specimens 18, 19, and 20 (fig. 2.13) are within about 10 percent of the midpoint of the total oscillations in each plagioclase, with each interlude closer to the rim than to the core. The lateral extent of the interludes beyond the locations of these three rock specimens is unknown, but the distribution of interludes is sufficiently widespread to imply a significant event, or events, in the solidification of the magma before crystallization of quartz, biotite, potassium feldspar, and much of the plagioclase.

This survey of interludes in the granodiorite of Anthony Lake also suggests that interludes might be useful in studies of the progressive compositional changes in mafic minerals during crystallization of granitic rocks, as well as the crystallization histories of plagioclase, both locally and throughout a pluton.

PEGMATITES AND APLITES OF ELKHORN PLUTON

Pegmatites are rare except in the interior of the Elkhorn pluton, where they occur as small dikes less than 0.7 m wide. Some pegmatites are less than 1.0 m long and not more than 10 cm wide. South and southeast of Anthony Lake a few of the larger aplite dikes, from 20 to 60 cm wide, contain either a continuous or discontinuous narrow core of pegmatite. Almost all pegmatites have a simple mineralogy: feldspar, quartz, and minor biotite. Scattered crystals of black tourmaline occur in two pegmatites.

Twenty-three pegmatites containing tourmaline, mostly in the Belleview wedge, were noted in country rocks near the contact of the Elkhorn pluton. With one exception, these pegmatites are small or very small.

Aplite dikes are not common in the tonalite of Bald Mountain except in the northeast; they are much more abundant in the granodiorite core of the pluton. The dikes generally are 2 to 10 cm wide in the tonalite of Bald Mountain and commonly as much as 17 cm near the center of the exposed pluton. Some aplite dikes in the granodiorite core are as much as 70 cm wide. The dikes mostly are flesh-colored and composed of feldspar, quartz, and a small amount of biotite.

The overall scarcity of pegmatite and aplite dikes in the Elkhorn pluton is consistent with the crystallization of a relatively dry magma. Moreover, almost no quartz veins occur in the core area, where aplites and pegmatites are most abundant. Only one small group of closely associated quartz veins was found in a 5-km^2 area south and southeast of Anthony Lake. The small veins contain as much as about 2 volume percent chalcopyrite and are confined within a zone less than 20 m in length.

XENOLITHS OF COUNTRY ROCKS AND INCLUSIONS OF UNKNOWN ORIGIN IN ELKHORN PLUTON

The scarcity of metasedimentary xenoliths except near contacts with metasedimentary wallrocks is characteristic of many batholiths in the Western United States, ranging from the small Snoqualmie batholith (Erikson, 1969) to the larger Boulder batholith (Grout and Balk, 1934; Becraft and others, 1963) to the immense Sierra Nevada batholith (Bateman, 1983; Noyes and others, 1983).

The Elkhorn pluton is unique among the zoned intrusions in northeastern Oregon in the comparative abundance of xenoliths of country rocks in the interior of the pluton. Elsewhere in northeastern Oregon xenoliths of country rocks are relatively rare except near contacts such as in the Wallowa batholith (Taubeneck, 1987) and Cornucopia stock (Taubeneck, 1964).

Field studies of the xenoliths in the Elkhorn pluton commenced in 1987 with the goal of determining their character, relative abundance, and distribution. The studies ultimately should provide insight concerning

emplacement mechanisms, extent of assimilation, and the origin of the comparatively numerous mafic inclusions of unknown origin that cannot be visibly correlated with known country rocks. Mafic inclusions of unknown origin in granitic rocks commonly have been interpreted as restite of deep-seated origin, carried upward from its source by the granitic magma. General field studies are well advanced in the Monumental salient and in an area of about 12 km^2 south and east of Anthony Lake. The ensuing discussion of field observations refers to these areas, respectively, as the "salient" and the "lakes area."

Xenoliths of country rock in the two areas consist of (in order of increasing abundance) rare calc-silicate rocks, cherty argillite, ribbon chert, and mafic foliated rocks (mostly foliated metagabbro). Xenoliths of country rock constitute substantially less than 0.01 volume percent of the granodiorite in the lakes area and an estimated 0.02 volume percent of the tonalite in the salient. The xenoliths are more easily seen and sampled in the many accumulations of large talus blocks in cirque basins than in massive outcrops. Counts of metasedimentary xenoliths observed each day during the examination of talus are as follows: calc-silicate rocks, 0 to 1 in the lakes area and 0 to 2 in the salient; cherty argillite, 0 to 3 in the lakes area and 6 to 13 in the salient; ribbon chert, 3 to 8 in the lakes area and 19 to 34 in the salient.

Xenoliths of mafic foliated rocks in the lakes area are three to four times as abundant as all other xenoliths of country rock as judged mostly by counts in four large accumulations of talus. Initial attempts to count the number of mafic foliated xenoliths were abandoned because of their great abundance, especially in much of the salient area where many thousands of very small foliated-rock slivers occur. Counts in the salient exceeded 300 such xenoliths per day before tabulations were terminated.

The greatest dimensions of xenoliths for each of the four types are calc-silicate rocks, as much as 22 cm in the lakes area and 15 cm in the salient; cherty argillite, as much as 45 cm in the lakes area and 51 cm in the salient; ribbon chert, as much as 70 cm in the lakes area and 89 cm in the salient; and mafic foliated rocks, as much as 29 cm in the lakes area and 31 cm in the salient. The smaller size of the mafic foliated xenoliths is attributed to fragmentation along the sharply defined planes of foliation in contrast to much less well defined foliation in chert and most cherty argillite.

Xenoliths of chert range in shape and size from rare blocks and slabs to very small circular relicts. Some xenoliths more than about 14 cm in smallest dimensions lack bedding and are derivatives either of very coarse ribbon chert or conceivably of massive chert which constitutes less than about 0.03 volume percent of country rocks within 3 km of the batholith. A few xenoliths in the salient area (but not in the lakes area) are slender ribbons up to 15 cm long. The irregular to subrounded shape of many xenoliths indicates magmatic resorption. Some xenoliths less than 20 cm in greatest dimension are almost elliptical, whereas a few less than 3 cm are circular. The xenoliths are not rimmed by a mafic corona as in the Ballachulish granodiorite, Argyllshire, Scotland (Muir, 1953). The shapes of the smaller xenoliths in particular indicate assimilation.

The grain size of recrystallized quartz in the xenoliths is no larger than in bedded chert near contacts of the Elkhorn pluton or in much chert throughout the Belleview wedge. Therefore, either the grain size in high-temperature aureole rocks does not continue to increase at magmatic temperatures, or the temperatures of aureole rocks and crystallizing granitic magma were too close to produce any additional increase in grain size.

The light-colored xenoliths of chert are difficult to detect in the granitic rocks. Consequently, the search for inclusions is more successful from a stationary position than while moving. The inclusions of chert are best seen in the Monumental salient near the headwall in the cirque basin just north of Mount Ireland (fig. 2.2) and along the crests of the three ridges that enclose this basin.

Cherty argillite composes the large number of rocks in the Elkhorn Mountains that are gradational between ribbon chert and argillite (Pardee and Hewett, 1914). Most xenoliths of cherty argillite are surrounded by an eye-catching halo of iron oxide that is visible for appreciable distances. Cherty argillite is common in the aureole but is disproportionately uncommon among xenoliths of country rocks. Assimilation of cherty argillite is much more prevalent than assimilation of ribbon chert, as is apparent along and near contacts with wallrocks. Accordingly, the relative scarcity of xenoliths of cherty argillite is consistent with the comparatively rapid rate of assimilation of pelitic rocks in contrast to that of ribbon chert.

Mafic foliated xenoliths, generally less than 18 cm long, are mostly metagabbro that is moderately fine grained and strongly foliated. Some mafic schistose xenoliths could be meta-argillite; no unequivocal megascopic distinction is possible. Many moderate to large xenoliths are transected by finer grained shear zones such as are conspicuous in metagabbro in the aureole. Xenoliths vary from uncommon, almost-black rocks with sparse visible plagioclase to common, lighter rocks with approximately equal amounts of horn-

blende and plagioclase. Many xenoliths are angular or somewhat rectangular, whereas some are subrounded. Substantially less than 1 percent of the xenoliths have reacted with the magma to produce a halo of recrystallized but nonfoliated rock surrounding a foliated-rock core. Otherwise, the xenoliths exhibit no or only rare indication of reaction with the magma.

A distinct decrease in the number of xenoliths occurs in the Monumental salient east and northeast of a boundary shown as line D-E in figure 2.2. Xenoliths increase again farther east, commencing slightly more than 1 km from the east contact of the salient. The distribution of xenoliths must be related to source regions and magmatic-flow directions. However, the xenoliths are distributed randomly and cannot be followed along zones of inclusions to a source in peripheral wallrocks, as in the Donegal granite in Northern Ireland (Pitcher and others, 1959).

The Monumental salient is mostly in contact with metagabbro for about 2.5 km along its east side. Elsewhere metagabbro constitutes less than 2 percent of wallrock, which is almost entirely ribbon chert and cherty argillite with small amounts of argillite. Xenoliths of ribbon chert and cherty argillite occur throughout the salient, although less commonly east of the line D-E in figure 2.2. The distribution of mafic foliated xenoliths, however, shows a closer relation to the line D-E and the distance to metagabbroic wallrock. Most of the mafic foliated xenoliths east of line D-E are of larger size and can be correlated with metagabbro along the east side of the salient. The thousands of small slivers of foliated metagabbro are mostly west of line D-E and presumably were derived largely from a western source. The scarcity of metagabbro in the aureole west of line D-E suggests a source for the slivers at a different level or levels from those now exposed by erosion. Whatever the source or sources, a thorough mixing of magma is required to explain the distribution of xenoliths.

Mafic inclusions of uncertain origin constitute more than 99 percent of all inclusions in the lakes area and an estimated 95 percent in the salient. In the lakes area, the mafic inclusions average 0.35 volume percent of the granodiorite; in the salient, they average 0.32 volume percent of tonalite in the interior of the salient to the west of line D-E (fig. 2.2). Nearly all inclusions are less than 0.6 m in greatest dimension; a few in the lakes area are slightly more than 1 m across, and one is 2.1 by 1.6 m.

The mafic inclusions exhibit notable variations in color, grain size, texture, mineral proportions, and shape. Color ranges from grayish black to gray, grain size from fine to medium grained, and texture from equigranular to heterogranular. The heterogranular inclusions contain large crystals of hornblende and (or) plagioclase. It is not known whether many of these large crystals are phenocrysts or porphyroblasts. Many mafic inclusions of unknown origin contain few (if any) large crystals of hornblende or few (if any) of plagioclase; some contain no large crystals of either mineral. Modal contents of hornblende and plagioclase vary significantly. Haloes of hornblende rim some inclusions but not more than 5 percent of the inclusions in any area. Most inclusions are subrounded, some have one or more angular corners, some are angular with no rounded surfaces, and a few appear almost spherical. Scalloped margins are rare. According to Didier (1987, p. 47), inclusions with angular shapes "prove the proximity" of their source, whereas inclusions with ellipsoidal shapes originated "much farther away."

The inclusions are sufficiently scattered that two or more of them generally cannot be closely examined and compared from one vantage point; swarms of inclusions are extremely rare. For comparative purposes, specimens of some inclusions can be carried throughout the day, but most inclusions are in massive rock that defies sampling even with a heavy sledge. In the ensuing discussion, one of only three known clusters containing more than 10 inclusions is described.

The swarm occurs at an elevation of 2,225 m, approximately 0.5 km N. 2° W. of the summit of Mount Ireland. The inclusions are in an area of about 1.4 m^2 on a large and conspicuous diagonal joint face that dips 25° N. The cluster is 2 m west of an aplite dike that strikes about N. 20° E; the aplite is extremely wide (about 20 cm) compared to relatively few others within 500 m.

The cluster contains four xenoliths of ribbon chert, one xenolith of cherty argillite, two metagabbro xenoliths and two probable metagabbro xenoliths (one 7 cm long, spear-shaped; the other, about 1 by 2 cm, rectangular), and 23 mafic inclusions of uncertain origin from 2 to 30 cm in greatest dimension. Three of the 23 inclusions are angular to very angular, whereas six have one or more pointed corners but are mostly subrounded. The remaining 14 inclusions are subrounded. Of the 23 inclusions, 21 contain large crystals of hornblende, but some of these 21 have almost no large crystals of plagioclase. The two other inclusions contain no large crystals of either hornblende or plagioclase. The inclusions range considerably in color from almost light gray to dark gray, reflecting differences in the amount of hornblende and plagioclase. Many of the 21 inclusions with large crystals of hornblende differ from their neighbors, but some appear almost identical.

Exceptional numbers of closely associated xenoliths of metasedimentary wallrocks together with mafic inclusions of unknown origin occur near the contact of the Monumental salient near elevation 2,089 m about 5.2 km S. 77° E. of the summit of Mount Ireland (near summit 6,853 on the Mount Ireland 7½-minute quadrangle). Inclusions of all the types commonly total about 35 percent of the rock by volume. Roughly one-half of all inclusions are metasedimentary xenoliths, and the remainder are mafic inclusions of uncertain origin. The derivation of the inclusions of uncertain origin cannot be determined by megascopic observations, but observations do trigger a few thoughts. If the mafic inclusions of uncertain origin are restite, why are they 50 times more abundant near a wallrock contact than throughout the interior of the salient? What is the significance of the positive correlation between excessive numbers of inclusions of unknown origin and excessive numbers of xenoliths of country rocks?

Exceptional numbers of closely associated xenoliths of country rocks together with mafic inclusions of unknown origin occur in a small satellitic intrusion about 5.1 km S. 65° E. of the summit of Mount Ireland and roughly 0.7 km south of the south contact of the salient. The inclusions are in an offshoot of tonalite (at elevations from 1,920 to 1,972 m) that intrudes metasedimentary rocks of the Elkhorn Ridge Argillite on either side of the boundary between T. 8 S. and T. 9 S, R. 36 E. At least one-half of the outcrops within 60 m of the west contact of the offshoot contain 20 to 35 percent inclusions. An estimated 12 to 15 percent of the inclusions are xenoliths of country rocks, including metagabbro that does not crop out within 3 km of the offshoot of tonalite. Some mafic inclusions of unknown origin are elongated and angular, but most are subrounded. Some contain no large crystals of either hornblende or plagioclase. Why is the concentration of supposed restite in a small satellitic offshoot of tonalite between 50 and 100 times greater than throughout the main part of the Monumental salient? Why are so many xenoliths of country rocks concentrated with the supposed restite? Have excessive numbers of xenoliths of country rocks been mixed in one small offshoot with an excessive amount of supposed restite? Or have all inclusions in the offshoot been derived from mesozonal levels near the south side of the Monumental salient?

In the Elkhorn Mountains there are too many disquieting field relations, including the overall diversity among the inclusions of uncertain origin, to allow acceptance of the restite model without question.

Four other explanations for the origin of the mafic inclusions are (1) disaggregated and dispersed synplutonic mafic dikes, (2) genetically related plutonic rocks, (3) xenoliths of reconstituted mafic country rocks, and (4) globules of either basic or intermediate magmas that intruded granitic magma in the lower crust. Assessment of all explanations is not feasible merely from field observations and examination of thin sections of three norite and six metagabbro xenoliths. However, sufficient overall information is available to question all but the fourth explanation for the derivation of the mafic inclusions.

No synplutonic dikes occur at the present level of erosion in any granitic intrusion in the Elkhorn Mountains. Accordingly, the possibility that mafic to intermediate inclusions of unknown origin in the Elkhorn pluton are dismembered fragments of synplutonic dikes is remote. The absence of synplutonic dikes is another feature that distinguishes the Bald Mountain batholith from most circum-Pacific batholiths.

Three inclusions of genetically related noritic rocks were found in an area about 12 km^2 south to east of Anthony Lake. The norite xenoliths possess the unmistakable features of the norite of Badger Butte, such as local recrystallization of plagioclase into small grains at pressure points and the postconsolidation extension of hornblende along grain boundaries of plagioclase and quartz. Thin sections reveal no further reduction in grain size beyond that which occurred at plagioclase pressure points during emplacement of the norite. The xenoliths have maintained their integrity, despite traveling at least several kilometers from their point of origin. Accordingly, evidence in the Elkhorn pluton does not support the possibility that the mafic inclusions of uncertain origin were derived from genetically related plutonic rocks.

The possibility that the mafic inclusions of unknown origin represent reconstituted mafic country rocks is considered mostly from field observations, supplemented by thin sections of six xenoliths of metagabbro. The largest xenolith of metagabbro seen in the lakes area is 29 cm in maximum dimension; the xenoliths generally are less than 18 cm long. In comparison, many mafic inclusions of unknown origin in the lakes area exceed 29 cm in greatest dimension; a few exceed even 100 cm. Clearly, the larger inclusions of unknown origin were not derived from the smaller xenoliths of metagabbro. Field observations of xenoliths of metagabbro reveal little or no mineralogical or textural reaction with the magma, other than the uncommon hornblende rims that border a small number of the xenoliths. Metagabbro xenoliths are foliated in contrast to the nonfoliated mafic inclusions of unknown origin. The grain size of plagioclase and hornblende in the mafic inclusions of unknown origin is quite variable; most inclusions contain large

crystals of hornblende; many also contain large crystals of plagioclase. In contrast, nearly all plagioclase and hornblende in the six xenoliths of metagabbro are restricted to a grain size from 0.05 to 0.5 mm. No large crystals of plagioclase or hornblende that qualify as either phenocrysts or porphyroblasts occur in the six xenoliths. Accordingly, reconstituted xenoliths of metagabbro are an improbable source for the mafic inclusions of uncertain origin.

In summary, the diversity of textures and compositions as observed during field observations of the mafic inclusions of uncertain origin suggests a multiple source that possibly includes the intrusion in granitic magma at depth of basic to intermediate magmas.

QUARTZ DIORITE OF LIMBER CREEK

SETTING AND GENERAL DESCRIPTION

The quartz diorite of Limber Creek, represented by four small intrusions near the neck of the Monumental salient, is herein named for rocks that crop out in the headwaters of Limber Creek (fig. 2.4). Rocks of the four intrusions are medium grained and have a color index of about 18 to 46, in sharp contrast to the nearby tonalite of Bald Mountain which has an index of 10 to 18. The quartz diorite in the upper drainage of Limber Creek is part of the largest intrusion, exposed as an elongated east-west mass of 0.4 km^2 and designated for location purposes as the western quartz diorite. This elongated body is concealed on the west by glacial deposits and does not reappear west of the map area (fig. 2.4). The western quartz diorite is sharply truncated on the east by the tonalite of Bald Mountain and is partly separated from the tonalite on the south by a dismembered screen of country rocks.

Planar structure in the western quartz diorite, absent in numerous exposures, is fair to fairly good at some locations; strikes are approximately east-west and dips are mostly vertical to 70° S. Favorable sites for viewing the planar structure are the numerous small cliffs from 1 to 5 m high that are 150 to 400 m west of Limber Creek. Only three elongated mafic inclusions of unknown origin were noted in the area of small cliffs during a search of 90 minutes. Elongation ratios are from 2.5:1 to 4.0:1. Good planar structure in the quartz diorite is confined to a small area of perhaps 1,000 m^2 in the extreme west, about 75 m south of the contact with country rocks and near the glacial deposits (fig. 2.4). Here, mafic inclusions of uncertain origin have elongation ratios of as much as 8:1.

Xenoliths of country rocks are common in the western quartz diorite. West of Limber Creek they are concentrated within 50 m of both the north and the south contacts of the quartz diorite; the xenoliths occur mostly as slices of metasedimentary rocks as much as 3 m wide and 7 m long. In contrast, xenoliths are much smaller and less abundant in the interior of the western quartz diorite, where maximum dimensions of xenoliths rarely exceed 0.7 m. The relatively flat crest of a north-northwest-trending ridge roughly 0.5 km west of Limber Creek provides a convenient cross section for observing the distribution and size variations of the xenoliths within the quartz diorite, the features of the intruded metasedimentary rocks of the screen, and, just to the south, the peripheral exposures of the tonalite of Bald Mountain. Metasedimentary xenoliths in the tonalite are comparatively few in comparison with those within the western quartz diorite; they also are relatively small with one conspicuous exception. The largest metasedimentary xenolith found (18 m long and as much as 2 m wide) in the tonalite of the Monumental salient is just south of the screen and about 0.3 km west of Limber Creek.

A second of the four intrusions of quartz diorite in the neck area is a very small exposure of about 0.003 km^2, approximately 0.5 km east of Limber Creek and 80 m north of the western quartz diorite (fig. 2.4). The rocks are well exposed, except on the east, and probably connect at depth to the western quartz diorite. This small intrusion was not sampled and will receive no further consideration.

A third body of the quartz diorite of Limber Creek, on the east side of the neck, is exposed in a 0.13-km^2 area (fig. 2.4) about 5 km S. 75° E. from the headwaters of Limber Creek. This mass (designated for location purposes as the eastern quartz diorite) is intruded on the northeast by a small body of tonalite containing red-brown biotite and minor iron oxide, separated on the northwest from the batholith by a narrow screen of ribbon chert, and concealed on the south by glacial deposits. The quartz diorite is well exposed in the east half of the intrusion but poorly exposed throughout much of the west half. Many xenoliths of metasedimentary rocks, as much as 6.5 m in maximum dimension, occur in the east-central part of the eastern quartz diorite, together with xenoliths of metagabbro that do not exceed 1 m across. Distance from source is a plausible explanation for the disparity in size between xenoliths of the two rock types; the eastern quartz diorite is in contact with metasedimentary wallrocks (fig. 2.4), whereas the nearest surface exposures of metagabbro are 0.55 km to the southeast.

The eastern quartz diorite is cut by leucocratic granitic dikes (as much as 8 m wide) that contain no hornblende and only minor biotite. Dikes on the west intrude the screen of ribbon chert that separates the quartz diorite from the tonalite of the batholith. Two

TABLE 2.9.—*Modes of the quartz diorite of Limber Creek*

[Values in volume percent. Each analysis represents at least 2,400 point counts for each of two thin sections; 0.0, <0.05]

Specimen number	Quartz	Plagioclase	Biotite	Hornblende	Augite	Opaque minerals	Nonopaque accessory minerals
Western quartz diorite							
233 -----	6.2	45.0	2.5	45.8	0.2	0.1	0.2
234 -----	14.2	48.7	8.4	27.9	.4	.2	.2
235 -----	21.2	46.0	12.6	19.7	.3	.1	.1
236 -----	14.4	46.2	11.6	27.5	.1	.1	.1
441 -----	14.2	51.6	11.9	22.1	.1	.0	.1
476 -----	23.6	47.3	12.1	16.6	.2	.1	.1
Average	15.6	47.5	9.9	26.6	.2	.1	.1
Eastern quartz diorite							
447 -----	11.9	45.1	13.4	29.3	0.2	0.0	0.1
448 -----	15.8	43.4	7.4	32.6	.6	.1	.1
470 -----	11.3	54.2	11.5	22.7	.0	.0	.3
Average	13.0	47.5	10.8	28.2	.3	.0	.2
Brecciated quartz diorite							
445 -----	14.9	45.6	6.1	32.5	0.6	0.1	0.2
472 -----	11.1	46.3	4.6	37.5	.2	.1	.2
Average	13.0	45.9	5.4	35.0	.4	.1	.2

excellent examples of partial assimilation of ribbon chert occur in the granitic dikes near the east contact of the screen. As much as 3 m of ribbon chert in a thicker sequence has been partly assimilated in a 5-m-wide dike at an elevation near 2,160 m, about 20 to 30 m east of a prominent gulch. The location is roughly N. 40° E. of a conspicuous prospect dump at an elevation of about 2,100 m. Dikes to the northeast, at an elevation of about 2,260 m, exhibit many small-scale examples of the partial assimilation of pieces of ribbon chert as much as 0.5 m in greatest dimension. Thus even leucocratic granitic dikes can assimilate some refractory chert; assimilation commenced along the argillaceous partings. More extensive assimilation of refractory ribbon chert occurs within the western quartz diorite, as well as in those parts of the screen south of the western quartz diorite that were intruded by the quartz diorite in a crude lit-par-lit fashion.

A fourth occurrence of the quartz diorite of Limber Creek is along a restricted part of the east contact of the neck of the Monumental salient where the quartz diorite in contact with the tonalite of Bald Mountain is mostly a giant breccia. The quartz diorite (including breccia) is not more than about 30 m wide and is merely a remnant of a larger mass that was intruded, brecciated, and dispersed during emplacement of the tonalite. The breccia is as much as 20 m wide and contains blocks of quartz diorite as large as 6.4 by 4.6 m. For identification purposes this small body is designated as the brecciated quartz diorite. As is true of both the western and eastern quartz diorites, the brecciated quartz diorite contains more xenoliths of metasedimentary rocks than the tonalite of Bald Mountain. Modal analyses of six rock specimens of the western quartz diorite, three rock specimens of the eastern quartz diorite, and two rock specimens of the brecciated quartz diorite are given in table 2.9.

MICROSCOPIC DESCRIPTION

Rocks of the western quartz diorite, eastern quartz diorite, and brecciated quartz diorite (table 2.9) crystallized from magmas sufficiently alike to warrant a single petrographic description. In addition to the overall petrographic description, a discussion of several late-stage features of the brecciated quartz diorite will be presented.

Augite occurs in hornblende as relict crystals as much as 2.1 mm in greatest dimension. Replacement of augite generally is advanced, and commonly only bleached areas in hornblende with small grains of quartz signify the former presence of augite. Nearly all larger relicts of augite are composed of many isolated parts that extinguish simultaneously. For example, eight cores of augite that range in greatest dimension from 1.1 to 1.9 mm are composed of from 5 to 12 detached (in plane of thin section) parts that extinguish in unison. No augite relicts contain inclusions of plagioclase, but one large relict is in reaction relation to a core of hypersthene about 0.1 by 0.3 mm. Orthopyroxene and subsequently clinopyroxene apparently were the earliest major minerals to crystallize.

Primary hornblende is brown and generally between 0.5 and 5.0 mm in greatest dimension, whereas recrystallized hornblende is light green and mostly about 0.1 mm across. Many smaller crystals of brown hornblende, mostly less than 1.0 mm in greatest dimension, are subhedral, but larger crystals are commonly irregular and even poikilitic. From some massive crystals, narrow fingers of hornblende extend outward along grain boundaries and, rarely, along fractures in plagioclase. One poikilitic hornblende roughly 2 by 4 mm encloses nine small laths of plagioclase; a few poikilitic crystals surround tabular plagioclase as much as 0.7 mm in length. However, during the overlapping crystallization histories of the two minerals, several hornblende crystals as much as 0.8 mm by 0.4 mm were enclosed in plagioclase. Late-stage deformation and recrystallization of hornblende is much more prevalent than in any other quartz diorite or tonalite in northeastern Oregon. Hornblende in the quartz diorite of Limber Creek commonly has recrystallized into a mosaic of nearly equidimensional grains. For example, after recrystallization, one original crystal of hornblende about 1.1 by 0.8 mm consists of 97 grains, each about 0.1 mm across.

Tabular plagioclase is mostly between 0.3 and 4.0 mm in greatest dimension. The bulk of the plagioclase is andesine, but core compositions are as calcic as about An_{53}. Some plagioclase shows oscillatory zoning, generally from three to seven broad and rather indistinct bands; a few crystals exhibit as many as 12 oscillations. Polysynthetic twinning fairly commonly is bent as much as 7° and infrequently from 8° to 16°. Locally, at least a few crystals in every rock specimen except 476 (table 2.9) have recrystallized along contacts with adjacent plagioclase to form a mosaic of xenoblastic grains mostly 0.1 to 0.04 mm across; recrystallization of plagioclase is not as extensive as recrystallization of hornblende. Slender needles of rutile (mostly less than 0.1 mm long) that are aligned crystallographically in plagioclase are a distinctive feature of the quartz diorite. The interior of a few of the larger plagioclase crystals is mottled in some thin sections. The mottling is characterized either by imperfect square or rectangular areas that are interconnected and extinguish simultaneously or by discontinuous patches. Mild clouding of the plagioclase is attributed to thermal metamorphism (MacGregor, 1931). Clouding in some thin sections consists of very fine particles that are concentrated toward the central part of plagioclase, whereas in other thin sections larger particles are aligned along twinning planes.

Quartz is interstitial. Some crystals in every thin section show wavy extinction, but they extinguish within a relatively small rotation of 3°. Quartz alongside bent plagioclase or recrystallized plagioclase commonly shows almost no wavy extinction. Apparently quartz crystallized after the mechanical stress that was responsible for the recrystallization of hornblende and plagioclase. Two examples were noted of narrow quartz veins that cross plagioclase but cannot be traced into areas of interstitial quartz. Rutile needles mostly less than 0.15 mm long are characteristic of the quartz. Orientation of the needles generally is evident where more than 12 to 15 needles occur in a relatively small area.

Biotite crystallized late, as is demonstrated by a common reaction relation to hornblende, by general occurrence along grain boundaries, by some poikilitic crystals, and by thin stringers of biotite that extend along fractures that cross plagioclase. The striking red-brown to red color of the biotite as seen microscopically is also megascopically visible in thin sections. Biotite fairly commonly is bent from 7° to 12°, infrequently from 13° to 17°, and rarely as much as 26°.

Accessory minerals are allanite, zircon (mostly euhedral), apatite, and iron oxide. The allanite replaces hornblende, as is commonly true in northeastern Oregon in granitic rocks such as quartz diorite, tonalite, and granodiorite. Much of the apatite occurs as relatively large crystals more than 0.08 mm in cross section. The rocks are notable for the small amount of iron oxide.

The brecciated quartz diorite is distinguished petrographically from the western and eastern quartz diorites by resorption of hornblende and resorption of plagioclase that is not recrystallized. Resorption is minor in rock specimen 445 but strong in specimen 472 (table 2.9).

Resorption of hornblende is denoted by irregular and embayed contacts with quartz, rounded appendages of hornblende that extend into quartz, and isolated pieces of hornblende in quartz that extinguish simultaneously

TABLE 2.10.—*Modes of the leucogranodiorite of Trail Creek*

[Values in volume percent. Each analysis represents at least 2,400 point counts for each of three thin sections; 0.0, <0.05]

Specimen number	Quartz	Potassium feldspar	Plagioclase	Biotite	Opaque minerals	Nonopaque accessory minerals
93 ------	39.5	14.0	42.1	4.3	0.1	0.0
97 ------	34.6	13.8	46.3	4.8	.5	.0
104 -----	36.6	13.3	48.5	1.5	.1	.0
Average	36.9	13.7	45.6	3.6	.2	.0

with neighboring crystals of hornblende. Resorbed plagioclase generally occurs as an irregular core separated by a sharp Becke line from a clear rim that constitutes as much as 60 percent by volume of some crystals. Cores commonly show higher birefringence than rims and always are darker from clouding than the rims, which never display clouding. Fractures in the cores as much as 0.01 mm wide do not extend into either the rims or the quartz adjacent to the plagioclase. Many of the larger fractures contain chlorite.

Perhaps heat from the younger tonalite of Bald Mountain generated an interstitial melt phase in the brecciated quartz diorite to produce the unique features of the plagioclase and the resorption of hornblende. This possibility cannot be assessed without a systematic sampling of several large blocks of breccia (from margin to center), as well as the sampling of the brecciated quartz diorite farthest from the tonalite of Bald Mountain.

LEUCOGRANODIORITE OF TRAIL CREEK

SETTING AND GENERAL DESCRIPTION

The leucogranodiorite of Trail Creek (fig. 2.2) is herein named for exposures in the headwaters area of Trail Creek, along the crest of a north-south-trending ridge extending from about 1.7 to about 3.4 km north of Badger Butte. It underlies an area about 1 km^2 and is the largest leucogranodiorite body in the batholith. The leucogranodiorite intrudes the tonalite of Bald Mountain on the northwest, but elsewhere its contacts with the tonalite and the granodiorite of Anthony Lake are concealed.

The leucogranodiorite is medium grained and contains widely scattered crystals of dark biotite from 3 to 5 mm across. Fresh specimens are light gray, but nearly all outcrops are weathered to various shades of yellow. The rock disintegrates readily into a sandy grus; most good exposures are restricted to steep slopes near the south and north extremities of the Trail Creek body. Modal analyses of three rock specimens of the leucogranodiorite are given in table 2.10.

Notable quantities of aplite are associated with the leucogranodiorite. The dimensions of the largest aplite dikes—15 to 18 m wide—greatly exceed the dimensions of aplite dikes in other parts of the batholith. Some large aplite dikes extend or occur outside the leucogranodiorite; one is as far as 0.6 km from the nearest surface exposure of leucogranodiorite.

MICROSCOPIC DESCRIPTION

Plagioclase (An_{16-42}) occurs as subhedral to anhedral crystals throughout most of the leucogranodiorite of Trail Creek. Oscillatory zoning in the core is surrounded by a wide mantle of progressively more sodic oligoclase. Potassium feldspar is orthoclase and mostly interstitial; some anhedral to subhedral crystals as much as 5 mm show exsolution lamellae and Carlsbad twinning. Orthoclase that is not interstitial may contain euhedral crystals of both quartz and plagioclase. Myrmekite occurs in limited amounts as narrow fringes about 0.02 mm wide between plagioclase and orthoclase. Strong undulatory extinction and local recrystallization characterize the interstitial quartz. Biotite is subhedral to anhedral except for small crystals in orthoclase. Most biotite occurs as flakes, less than 0.7 mm across, that commonly are along grain boundaries. The leucogranodiorite shows considerable alteration of biotite to chlorite and minor amounts of epidote. Accessory minerals are iron oxide, apatite, and zircon.

GRANITE OF CLEAR CREEK

SETTING AND GENERAL DESCRIPTION

The granite of Clear Creek (fig. 2.2) is herein named for rocks exposed in an area about 0.67 km^2

TABLE 2.11.—*Modes of the granite of Clear Creek*

[Values in volume percent. Each analysis represents at least 2,400 point counts for each of three thin sections; 0.0, <0.05]

Specimen number	Quartz	Potassium feldspar	Plagioclase	Biotite	Hornblende	Opaque minerals	Nonopaque accessory minerals
R147 ----	31.7	21.9	39.7	6.6	0.1	0.0	0.0
R148 ----	33.5	20.9	39.8	5.3	.5	.0	.0
Average	32.6	21.4	39.7	6.0	.3	.0	.0

near the junction of Clear Creek and the Grande Ronde River. The unit intrudes the tonalite of Bald Mountain but is overlain on the west by Cenozoic volcanic rocks. A dismembered screen of country rocks extends along the southwest contact between the granite and the tonalite.

The granite is medium grained and light gray to slightly pinkish where fresh; it contains scattered dark biotite. Many outcrops are covered with lichens; some of the best exposures form bluffs on the north side of the Grande Ronde River opposite Clear Creek. Foliation is shown by aligned biotite and varies from faint to strong with mostly east-northeast trends. The modes of two rock specimens are given in table 2.11.

MICROSCOPIC DESCRIPTION

Most plagioclase is anhedral, but small subhedral crystals, not more than 0.8 mm long, occur enclosed within quartz and potassium feldspar. The plagioclase is antiperthitic oligoclase with cores, in larger crystals, of sodic andesine. In most crystals zoning is normal, but in some large crystals normal zoning encloses several faint oscillatory zones. Twinning lamellae in a few crystals are bent as much as 5°; fractured crystals also occur with twinning planes in adjoining pieces at angles as much as 14°. The potassium feldspar is anhedral and mostly a fine microperthitic orthoclase; some crystals show faint microcline gridiron twinning. Myrmekite is common as a narrow fringe between plagioclase and potassium feldspar, but the intergrowths are not prominent. Quartz shows strong undulatory extinction and local recrystallization. Biotite occurs as subhedral crystals as much as 1 mm across in potassium feldspar, as irregular flakes along grain boundaries, and as very small stringers along a few fractures. Some biotite along grain boundaries is bent. Hornblende is present as strongly corroded relicts that commonly are surrounded by quartz.

Accessory minerals are apatite, zircon, monazite, allanite, and iron oxide. The iron oxide occurs as small cubic crystals that commonly are in aggregates of two or more intergrown cubes. Alteration products are restricted to uncommon chloritization of biotite and a slight kaolinitization of potassium feldspar.

QUARTZ DIORITE OF WOLF CREEK

SETTING AND GENERAL DESCRIPTION

The quartz diorite of Wolf Creek is herein named for rocks that crop out on the north side of the canyon of Wolf Creek (fig. 2.2*B*). The rock is exposed in an east-west-trending zone about 3.25 km^2 (fig. 2.3) that extends westward into the headwaters of Beaver Creek, where the unit is divided by a wedge-shaped body composed of the presumably younger granodiorite of Beaver Meadow and a dismembered screen of country rock about 0.1 km wide. Not all contacts are exposed. The quartz diorite is intruded along its south contact by the granite of Anthony Butte and elsewhere is overlain by the Columbia River Basalt Group.

The quartz diorite is a gray, medium-grained rock with a color index of about 27. An alignment of tabular plagioclase is typical. Conspicuous crystals of poikilitic biotite, commonly between 10 and 15 mm in greatest dimension, contribute to a foliation that generally is good to excellent. Mafic inclusions help to define the foliation but commonly constitute less than 1 percent of the rock. Foliation trends from about east-west to west-northwest with northward, mostly steep dips. Modal analyses of six quartz diorite rock specimens are given in table 2.12.

MICROSCOPIC DESCRIPTION

The plagioclase consists of subhedral laths of slightly zoned calcic andesine. The margins of many crystals show slight normal zoning, whereas the interiors of some crystals have as many as eight oscillatory zones. Plagioclase in rock specimens from near the contact with the granite of Anthony Butte is moderately clouded by dustlike particles, probably as a result of thermal metamorphism (MacGregor, 1931). Some plagioclase

TABLE 2.12.—*Modes of the quartz diorite of Wolf Creek*

[Values in volume percent. Each analysis represents at least 2,400 point counts for each of two thin sections; 0.0, <0.05; ---, not present]

Specimen number	Quartz	Potassium feldpsar	Plagioclase	Biotite	Hypersthene	Augite	Hornblende	Opaque minerals	Nonopaque accessory minerals
R9 ------	15.3	3.5	59.3	14.9	1.2	5.3	0.3	0.2	0.0
R17 -----	16.3	4.9	56.1	14.6	1.7	5.9	---	.4	.1
R18 -----	5.1	---	61.3	4.6	6.1	1.3	20.5	1.0	.1
R21 -----	19.4	2.4	48.8	16.8	0.0	3.7	8.7	.1	.1
R122 ----	18.6	0.1	51.1	22.6	.2	6.1	1.1	.1	.1
R125 ----	17.8	1.6	50.4	17.6	.3	3.7	8.4	.1	.1
Average	15.4	2.1	54.5	15.2	1.6	4.3	6.5	.3	.1

encloses small crystals of hypersthene and augite (generally less than 0.1 mm across), but crystals of hypersthene as large as 0.9 mm also occur in plagioclase. Twinning lamellae in plagioclase commonly are bent 8° and rarely as much as 12°. Bent twinning lamellae in plagioclase adjacent to quartz in which strain shadows are the maximum deformation effects suggest late-stage deformation of plagioclase before crystallization of quartz. Recrystallization of plagioclase to a fine mosaic occurs along two microfractures as well as at grain boundaries where plagioclase crystals impinge on one another. Twinning lamellae on opposite sides of microfractures commonly are offset or trend in slightly different directions. Microfractures that do not extend into adjacent quartz suggest protoclastic deformation of plagioclase before crystallization of quartz.

Hypersthene is subhedral and generally not more than 2.0 mm in length. Discrete crystals of augite are of similar size, but much of the augite either surrounds or partly rims hypersthene. Small crystals of hypersthene and augite enclosed in plagioclase are evidence that pyroxene began to appear in the magma at an early stage of crystallization. Hornblende and biotite are in reaction relation to both pyroxenes but also occur as discrete crystals. Hornblende and biotite crystallized very late and conceivably are poikiloblastic. For example, narrow fringes of biotite and hornblende extend along boundaries between plagioclase crystals, between plagioclase and quartz, and between crystals of quartz. Biotite also extends along several microfractures that offset twinning lamellae of plagioclase.

Quartz and potassium feldspar are interstitial. Some quartz shows strong undulatory extinction, and local recrystallization has occurred in two rock samples. The potassium feldspar is orthoclase as indicated by (flat-stage) estimates of $2V$ of less than 60° for nearly centered acute-bisectrix figures. Iron oxide, apatite, and stubby crystals of zircon are the main accessory minerals.

DISTINGUISHING FEATURES

The quartz diorite is unique among the granitic intrusions of northeastern Oregon in containing hypersthene and augite. Poikiloblastic(?) texture of biotite and hornblende also is distinctive, as well as the deformational features of plagioclase.

BOUNDARY QUARTZ DIORITE UNIT

SETTING AND GENERAL DESCRIPTION

A quartz diorite that occurs in a timbered area about 0.8 km^2 along the boundary between the Anthony Butte quadrangle and the Tucker Flat quadrangle (fig. 2.2*A*) is herein informally designated the boundary quartz diorite unit (fig. 2.3). Most of the unit's better outcrops are located in the eastern third of the body. Farther west, much of the quartz diorite has disintegrated into a greenish-gray grus, which is well exposed along several abandoned logging roads. The quartz diorite is locally intruded on the north by the leucogranite of Dutch Creek, but the two rock types are mostly separated by a dismembered screen of metasedimentary rocks. A fragmented screen on the south separates the quartz diorite from the granodiorite of Indiana Mine Road. The relationship between these two granitic rock units is unknown, but presumably the quartz diorite is older than the granodiorite. The Columbia River Basalt Group overlies the quartz diorite on the west and east.

The quartz diorite is a gray, medium-grained rock ranging from massive to slightly foliated. In nearly all outcrops, a few crystals of plagioclase, hornblende, and biotite are as much as 10 mm across, but most crystals are 1.5 to 4.0 mm across. Modal analyses of two rock specimens are given in table 2.13.

MICROSCOPIC DESCRIPTION

The plagioclase is subhedral andesine that shows as many as 16 oscillatory zones surrounded by a nar-

TABLE 2.13.—*Modes of granitic rocks of the northeastern (peripheral) part of the Bald Mountain batholith*

[Values in volume percent. Each analysis of the boundary quartz diorite unit represents at least 2,400 point counts for each of two thin sections; all other analyses represent at least 2,400 point counts for each of three thin sections; 0.0, <0.05; ---, not present]

Specimen number	Quartz	Potassium feldspar	Plagioclase	Biotite	Muscovite	Orthopyroxene	Augite	Hornblende	Cummingtonite	Opaque minerals	Nonopaque accessory minerals
Boundary quartz diorite unit											
R115	18.2	1.8	52.0	13.1	---	---	0.2	14.6	---	0.1	0.1
R116	13.0	.0	56.0	11.8	---	---	.3	18.6	---	.2	.1
Average	15.6	.9	54.0	12.4	---	---	.2	16.6	---	.2	.1
Granodiorite of Indiana Mine Road											
R187	33.3	5.5	52.9	8.3	---	---	---	---	---	0.0	0.0
R188	34.5	11.7	44.9	8.9	---	---	---	---	---	.0	.0
R189	36.9	6.7	49.5	6.6	---	---	---	0.2	---	.0	.1
R190	31.1	11.9	50.2	6.1	---	---	---	.7	---	.0	.0
Average	34.0	8.9	49.4	7.5	---	---	---	.2	---	.0	.0
Granodiorite of Beaver Meadow											
R118	31.1	20.6	42.4	5.7	---	---	---	0.2	---	---	0.0
R119	32.8	11.2	46.5	7.8	---	0.4	---	.6	0.6	---	.1
R127	33.8	19.1	40.1	6.2	---	.2	---	.3	.3	---	.0
Average	32.5	17.0	43.0	6.6	---	.2	---	.4	.3	---	.0
Granite of Anthony Butte											
R120	32.7	28.2	36.4	2.6	---	---	---	---	---	0.0	0.1
R121	32.9	23.4	38.0	5.7	---	---	---	---	---	.0	.0
R123	32.8	23.6	37.2	4.3	---	0.2	---	---	1.8	.0	.1
R128	31.4	28.4	36.0	4.1	---	---	---	---	---	---	.1
R129	31.2	25.4	37.5	5.9	---	---	---	---	---	---	.0
Average	32.3	25.8	37.0	4.5	---	.0	---	---	.4	.0	.1
Leucogranite of Dutch Creek											
R22	38.4	29.1	30.5	1.6	0.4	---	---	---	---	0.0	0.0
R24	38.2	26.8	33.6	1.1	.1	---	---	---	---	.2	.0
R25	37.2	28.6	31.9	2.1	.1	---	---	---	---	.1	.0
Average	37.9	28.2	32.0	1.6	.2	---	---	---	---	.1	.0

row mantle that is progressively more sodic toward the periphery. The cores of some plagioclase crystals contain small inclusions (<0.1 mm) of augite and hornblende. The margins of a few adjacent plagioclase crystals are recrystallized at pressure points to a fine-grained mosaic of nearly equant crystals less than 0.1 mm across. Twinning lamellae in plagioclase are bent as much as 12°. Bent twinning lamellae are

common at the ends of plagioclase crystals where they impinge on one another. Quartz is interstitial and commonly shows strong undulatory extinction; at least a few sutured contacts indicative of recrystallization under stress are present in every thin section. Hornblende occurs as subhedral and anhedral crystals; some that are poikilitic are of late origin. Relicts of augite as large as 1.6 mm occur within some hornblende. The former presence of augite in other crystals of hornblende is indicated by bleached cores that enclose minute crystals of quartz (Taubeneck, 1964). Biotite occurs in reaction relation to hornblende and commonly as irregular crystals ≥2 mm across. Late crystallization of biotite is indicated commonly by biotite along grain boundaries and rarely by biotite as small flakes along fractures in plagioclase. Interstitial potassium feldspar is orthoclase, as verified on the flat stage by estimated $2V$ of 50°–55°for nearly centered acute-bisectrix figures. Accessory minerals are iron oxide, apatite, zircon, and sphene.

DISTINGUISHING FEATURES

The boundary quartz diorite unit is characterized by small crystals of augite within plagioclase and by millimeter-size cores of augite in hornblende. Both occurrences of augite confirm the early crystallization of clinopyroxene. The deformation features of the plagioclase distinguish this quartz diorite from other quartz diorites in the Bald Mountain batholith, with the exception of the quartz diorite of Wolf Creek.

GRANODIORITE OF INDIANA MINE ROAD

SETTING AND GENERAL DESCRIPTION

The granodiorite of Indiana Mine Road is herein named for the Indiana Mine Road (fig. 2.2*B*) that extends across the western part of the intrusion. The unit consists of an elongated mass about 3 km^2 (fig. 2.3) that extends westward for about 3 km from Dutch Creek (fig. 2.2*B*). The granodiorite intrudes country rocks along its southwestern margin and contains several sizable inclusions of wallrocks in its western part. By far the largest inclusion extends nearly east-west for about 1 km and dips steeply north. The granodiorite's west contact with the granite of Anthony Butte and its north contact with the boundary quartz diorite unit are concealed. A dismembered screen on the north partly separates the granodiorite from the boundary quartz diorite unit. The normal mafic-to-felsic sequence occurring in the composite batholiths and stocks of northeastern Oregon suggests that the granodiorite is younger than the boundary quartz diorite unit but older than the granite of Anthony Butte. The eastern and southeastern parts of the granodiorite are overlain by the Columbia River Basalt Group.

The granodiorite is a light-colored, medium-grained rock with scattered relatively small crystals of biotite that generally define a strong east-west-striking, steeply north-dipping foliation. The rock tends to crumble and is poorly exposed; much of it has disintegrated into a distinctive yellowish grus, which is best seen along several abandoned logging roads. Modal analyses of four rock specimens of the granodiorite are given in table 2.13.

MICROSCOPIC DESCRIPTION

Plagioclase (An_{25-34}) is subhedral to anhedral and only slightly zoned. Resorption of plagioclase is common where it contacts potassium feldspar; some plagioclase in quartz also has irregular borders that appear corroded. Much of the plagioclase is antiperthitic. Deformation of the crystals is pronounced and twinning lamellae commonly are bent as much as 8°. The quartz is strongly strained and sutured boundaries indicate considerable recrystallization. The potassium feldspar is orthoclase microperthite; at least a few Carlsbad twins occur in almost every thin section. Biotite, generally less than 1.0 mm in largest dimension, is mostly anhedral and restricted to grain boundaries. Cleavage traces of some biotite are bent. Late crystallization of biotite is verified by small crystals along microfractures in plagioclase. Small amounts of resorbed hornblende in two rock samples (R189 and R190 in table 2.13) indicate that hornblende originally was more abundant. Accessory minerals are apatite, zircon, allanite, monazite, and iron oxide, but they generally are not abundant enough (<0.05 volume percent) to be recorded in modal analyses.

DISTINGUISHING FEATURES

The granodiorite of Indiana Mine Road is distinguished mineralogically by a very high content of quartz, almost no hornblende, and very little iron oxide (0.01 volume percent). The high content of quartz and paucity of iron oxide clearly suggest assimilation of graphite-bearing cherty argillite and ribbon chert. However, the biotite in each of the four rock specimens (table 2.13) exhibits no trace of the red-brown (typical) to reddish (atypical) color of biotite in other contaminated granitic rocks in this part

of the Bald Mountain batholith. The deformation fabric of this rock unit is almost unique among the granodiorite bodies of northeastern Oregon in the comparatively abundant deformed plagioclase, bent biotite, and recrystallized quartz.

GRANODIORITE OF BEAVER MEADOW

SETTING AND GENERAL DESCRIPTION

The name "granodiorite of Beaver Meadow" is herein applied to a body of granodiorite that is exposed in a 0.35-km^2 area in the Anthony Burn east of Beaver Meadow (fig. 2.2*B*). The granodiorite is a wedge-shaped mass situated between the quartz diorite of Wolf Creek to the north (beyond country rock screen) and south and overlain to the west by alluvium in Beaver Meadow and farther west by the Columbia River Basalt Group (fig. 2.3). Contacts with the quartz diorite are concealed, but the granodiorite presumably is younger as judged from the typical mafic to felsic intrusive sequence in composite batholiths.

The granodiorite is medium grained, light gray where fresh, and mottled with dark biotite. Scattered megacrysts of potassium feldspar are common and are as much as 2.5 cm across. These megacrysts generally constitute less than 2 percent of the rock by volume. Foliation is well developed and shown by aligned biotite and commonly also by plagioclase and megacrysts of potassium feldspar. The foliation is somewhat variable but strikes approximately N. 70° W. and has a steep northeastward dip. Modes of three rock specimens are given in table 2.13.

MICROSCOPIC DESCRIPTION

The plagioclase ranges from sodic andesine to calcic oligoclase and commonly shows slight zoning. The mineral occurs as anhedral crystals mostly 0.5 to 4.0 mm long and as smaller subhedral to euhedral crystals within potassium feldspar. A small number of resorbed crystals are present within quartz. Anhedral plagioclase is antiperthitic, and twin planes are commonly bent 5° to 8°. Some microfractures offset twinning lamellae that differ in trend on opposite sides of the microfracture. Almost every thin section contains at least one example of the recrystallization of plagioclase to a fine-grained (0.05–0.20 mm) mosaic along contacts where two crystals directly impinge on each other.

Potassium feldspar is present as small interstitial crystals and also as subhedral, commonly Carlsbad-twinned crystals more than 1 mm across. Many of the larger crystals are microperthitic. The potassium feldspar is exclusively orthoclase in rock specimen R119, but some microcline also is present in specimen R127; microcline is more abundant than orthoclase in rock specimen R118 (table 2.13).

Myrmekite is mostly inconspicuous and nearly always occurs as a very narrow fringe between plagioclase and potassium feldspar. Only a few of the typical cauliflower-like protuberances are present in any thin section, and they are absent in some sections. Quartz occurs generally as interstitial crystals up to 4 mm across, but some euhedral crystals, mostly less than 0.5 mm across, are present in potassium feldspar. The quartz shows weak to strong undulatory extinction as well as some recrystallization.

Orthopyroxene has been mostly replaced by fibrous cummingtonite and typically is present only as small cores within aggregates of cummingtonite. Pseudomorphs after orthopyroxene suggest that it originally occurred as stout subhedral prisms mostly 0.3 to 0.6 mm long; the largest prism was 0.9 mm long. Relatively early crystallization of orthopyroxene is indicated by three unreplaced crystals that occur inside plagioclase. A slight to moderate alteration to a reddish iron oxide is associated with nearly all orthopyroxene.

Cummingtonite is characterized by polysynthetic twinning and extinction angles between 14° to 18°. Small quantities of green hornblende occur in reaction relation to cummingtonite and also as independent crystals along grain boundaries. Hornblende associated with cummingtonite commonly occurs as a very narrow fringe around the cummingtonite. This replacement is always peripheral and never extensive. The interstitial hornblende consists of thin stringers and fingers, commonly less than 0.03 mm wide, that locally are poikilitic.

Biotite occurs as (1) poikilitic crystals as much as 2.5 mm across, (2) small flakes along grain boundaries, (3) small subhedral crystals as much as 0.5 mm long within quartz and potassium feldspar, (4) reaction rims on both cummingtonite and hornblende, and (5) very small flakes, mostly less than 0.2 mm long, within microfractures in plagioclase and potassium feldspar. All occurrences except the subhedral crystals in quartz and potassium feldspar indicate late to very late crystallization. Cleavage traces of biotite commonly are bent between 5° to 10° and, rarely, more than 30°. Deformation of biotite generally is most intense at the corners of plagioclase and between closely adjacent crystals of plagioclase that are at high angles to each other. Biotite is red-brown in rock specimens R119 and R127 but not in specimen R118 (table 2.13).

Alteration products are relatively uncommon. Some biotite shows chloritization, and potassium feldspar

commonly is dusted by kaolin. Flakes of muscovite as much as 0.1 mm long are visible on some potassium feldspar crystals and also along a few grain boundaries. Trace amounts of calcite occur interstitially and also in association with hornblende. Accessory minerals are apatite, zircon, allanite, and very small amounts of iron oxide. The virtual absence of iron oxide indicates that the granodiorite of Beaver Meadow crystallized under more reducing conditions than prevailed in most granitic plutons in northeastern Oregon.

DISTINGUISHING FEATURES

Foliation and megacrysts of potassium feldspar are the two distinguishing megascopic features of the granodiorite of Beaver Meadow. Nearly all other granodiorite bodies in northeastern Oregon lack foliation, and no other granodiorite contains megacrysts of potassium feldspar.

The presence of orthopyroxene is an even more notable distinction. Furthermore, the reaction relations between orthopyroxene, cummingtonite, hornblende, and biotite are exceptional. A literature search failed to disclose any reference to a similar reaction sequence in granitic rocks.

Another distinction of the granodiorite is the scarcity of iron oxide. Iron oxide occurs in such small amounts that it was not recorded during the modal analysis of three samples (26,727 points, across nine thin sections) of the granodiorite (R118, R119, and R127 in table 2.13). In contrast, iron oxide constitutes, respectively, 0.23, 0.23, 0.27, and 0.30 volume percent of the four small intrusions of granodiorite in the batholith south of lat 45° N., and 0.27, 0.30, 0.31, and 0.36 volume percent of the four small intrusions of granodiorite in the Wallowa batholith extending from about 45 to about 70 km to the northeast. Each of the other eight intrusions of granodiorite contains more than 60 times as much iron oxide as the Beaver Meadow unit.

Red-brown biotite in rock specimens R119 and R127 (table 2.13) is petrographic evidence of reduction, here attributed to the assimilation of graphite-bearing metasedimentary rocks. However, a chemical analysis (Ken-ichiro Aoki, 1973, Tohoku University, Japan) of rock specimen R118 (table 2.13) which does not contain red-brown biotite yielded values for Fe_2O_3 and FeO of 0.26 and 2.13 weight percent, respectively, indicating that R118 also is reduced. The absence of red-brown biotite in R118 is difficult to interpret without additional whole-rock chemical analyses, each accompanied by a mineral analysis of biotite, including biotite from R118.

GRANITE OF ANTHONY BUTTE

SETTING AND GENERAL DESCRIPTION

The granite on either side of the major ridge in the northern part of the batholith is herein called the granite of Anthony Butte. This rock unit is exposed over an irregular area approximately 14 km^2 (fig. 2.3); in size it greatly exceeds any other granite body in northeastern Oregon. The granite notably contains two very large inclusions of quartz diorite and country rock; xenoliths probably constitute at least 20 percent of the volume of the intrusion, as indicated by surface exposures. The granite of Anthony Butte intrudes the tonalite of Bald Mountain on the south and west, the quartz diorite of Wolf Creek on the north, and country rocks on the east. The granite's contact with the granodiorite of Indiana Mine Road is concealed, but the granite is probably younger than the granodiorite according to the typical mafic-to-felsic sequence. A fragmented screen on the south and southwest partly separates the granite from the tonalite of Bald Mountain.

Fresh specimens of the granite of Anthony Butte have about 5 percent dark biotite scattered throughout a white matrix of feldspar and quartz. Weathered specimens are discolored and dominated by various shades of yellow. Exposures are generally poor, partly because the rock tends to disintegrate. Some relatively fresh outcrops occur locally as rounded knobs that stand 2 to 5 m above the surrounding ground level.

The granite is a predominantly medium-grained rock; most crystals of plagioclase and quartz are 2 to 6 mm across. Twinned megacrysts of potassium feldspar occur in many parts of the intrusion and constitute as much as 2.3 percent of the rock by volume. The volume percentage of megacrysts was determined by placing a transparent grid across large exposures and counting the grid squares and parts of squares that cover each megacryst. Megacrysts commonly are 2.0 to 2.5 cm long, but some are as much as 3.5 cm. The megacrysts apparently crystallized from the magma and thus are phenocrysts rather than porphyroblasts.

Foliation is well developed in many parts of the intrusion and is shown both by biotite and by aligned megacrysts of potassium feldspar. Some foliation is almost gneissic and is locally accentuated by elongated inclusions and schlieren of nearly assimilated metasedimentary rocks. Intricate swirled foliation occurs locally. Foliation generally closely parallels external contacts as well as internal contacts with large inclusions and dips more than 65° N. to NE. Modal analyses of five rock specimens are given in table 2.13.

MICROSCOPIC DESCRIPTION

Plagioclase is present as anhedral crystals about 1 to 4 mm long and as much smaller euhedral to subhedral crystals in potassium feldspar. The plagioclase is oligoclase that shows slight normal zoning. Some highly resorbed crystals of plagioclase occur in both quartz and potassium feldspar. Antiperthite is common in rock specimens R121 and R123 (table 2.13). Twinning lamellae in many larger crystals are bent 5° and rarely 12°. Microfractures are fairly common in most thin sections, and some plagioclase shows minor crushing. Trends of twinning planes in adjacent pieces of broken plagioclase differ by as much as 13°. Local recrystallization of plagioclase to a mosaic of small grains, commonly less than 0.1 mm across, occurs along some microfractures and also at some pressure points where crystals impinge on each other.

Potassium feldspar is microperthitic, and many of the larger crystals show Carlsbad twinning. Excellent microcline gridiron twinning is common in rock specimens R120 and R123, (table 2.13), but much of the potassium feldspar in both rocks is orthoclase, as revealed by the relatively small $2V$ of many acute-bisectrix figures. Microcline occurs locally in rock specimen R121, but potassium feldspar in rock specimens R128 and R129 is exclusively orthoclase. Alteration of potassium feldspar to kaolin is ubiquitous in all rock samples; flakes of muscovite as much as 0.5 mm across occur within the orthoclase of rock specimen R128.

Myrmekite in small amounts is present in all the rock samples, mostly as a very narrow fringe between plagioclase and potassium feldspar. Conspicuous myrmekite is restricted to rock specimen R123 (table 2.13), in which myrmekite occurs as cauliflower-like protuberances that project as far as 0.4 mm into adjacent potassium feldspar.

Quartz occurs as large crystals from 3 to 8 mm across, as smaller interstitial crystals, and as much smaller euhedral to subhedral crystals in potassium feldspar. The large areas of quartz generally are devoid of other minerals and are believed to have crystallized relatively early. Some are egg- or lens-shaped. Large crystals generally show weak to strong undulatory extinction, but sutured boundaries indicate that some recrystallization has occurred. However, unstrained crystals as much as 4 to 6 mm across occur in the same thin section with strongly strained quartz and recrystallized quartz.

In rock specimen R123 (table 2.13), orthopyroxene occurs with iron oxide and cummingtonite as small relicts and as remnant cores of subhedral crystals of orthopyroxene; in the partially replaced crystals, the pyroxene is surrounded by cummingtonite. Orthopyroxene is rarely found in true granites; the small (about 0.4 km^2) leucogranite of Mt. Rubidoux (Larsen, 1948) in southern California is the best known orthopyroxene-bearing granite in North America. The orthopyroxene crystals in specimen R123 are 0.15 to 0.9 mm long and are characterized by pale-pink to greenish pleochroism and by alteration to dark-red, apparently nearly opaque iron oxide. However, in thin section most of the iron oxide appears translucent when viewed with the upper condenser inserted. Patches of iron oxide as large as 0.5 mm across compose as much as 60 volume percent of a few pseudomorphs. Orthopyroxene in felsic granitic rocks typically is iron-rich and commonly is ferrohypersthene. The iron oxide associated with the orthopyroxene in the granite of Anthony Butte strengthens the probability of an iron-rich composition for this pyroxene. Moreover, the small amount of iron oxide in the rock (table 2.13) and consequent implication of low oxygen fugacity during crystallization also strengthens the probability of an iron-rich orthopyroxene. Most of the orthopyroxene typically is replaced by fibrous cummingtonite that generally occurs as compact aggregates and clusters of small crystals. In contrast to the cummingtonite that is associated with iron oxide in obvious pseudomorphs after orthopyroxene, some cummingtonite in interstitial areas without iron oxide appears to have formed as a primary mineral of magmatic crystallization. Of possible significance in this respect is the report by Sams and Saleeby (1988, p. 876) of cummingtonite in the southernmost Sierra Nevada in a hornblende quartz diorite that contains neither orthopyroxene nor clinopyroxene. Irrespective of origin, cummingtonite in the granite of Anthony Butte commonly is fringed by biotite in reaction relation.

Most biotite is anhedral and generally occurs along grain boundaries as small crystals 0.1 to 0.8 mm long. Cleavage in some crystals is bent. Small flakes of biotite also occur along a few microfractures in plagioclase. Some biotite in rocks that show comparatively little foliation occurs as clusters of as many as a dozen flakes as much as 1.5 mm across. Biotite also is present as subhedral crystals enclosed within either potassium feldspar or quartz. Biotite crystallized before some potassium feldspar and quartz, but much of the biotite along grain boundaries is very late, as is the biotite along microfractures in plagioclase.

Biotite in rock specimens R123 and R128 is red-brown, but this indicator color, typical of biotite in reduced rocks, is absent in specimens R120, R121, and R129 (table 2.13). Chemical analyses (Ken-ichiro Aoki, 1973, Tohoku University, Japan) for rock specimens

R121, R123, and R128 (table 2.13) yielded, respectively, the following values in weight percent: Fe_2O_3 =0.74, FeO=1.80; Fe_2O_3 =0.52, FeO=1.93; and Fe_2O_3 =0.17, FeO=1.91. Ratios of the iron values for the three rocks correlate with the absence of red-brown biotite in rock specimen R121, a moderate red-brown color in the biotite of specimen R123, and a strong red-brown color in the biotite of specimen R128.

Accessory minerals are garnet, apatite, allanite, zircon, monazite, and iron oxide. The garnet occurs only in rock specimen R128 (table 2.13) in which it constitutes 0.1 volume percent of the rock. Garnet is present as subhedral to euhedral crystals 0.05 to 0.80 mm in diameter, is faint pink, and locally is fringed by biotite. The garnet either is a primary magmatic mineral or occurs as xenocrysts from assimilated metasedimentary rocks. More than 99 percent of the garnets in 21 metapelitic rocks from the aureole are 0.03 to 0.50 mm across; garnets showing well-developed crystal habit commonly occur as crystals as much as about 0.1 mm in diameter. Crystals larger than about 0.2 mm invariably are irregular, commonly contain a core of opaque inclusions, and generally are perforated. In contrast, the numerous garnets larger than 0.2 mm in the granite contain no inclusions, are not perforated, and have subhedral to euhedral borders. Therefore, features of the garnet in the granite suggest crystallization from a melt.

DISTINGUISHING FEATURES

The granite body is distinct in the common strong foliation, abundance of large igneous and metasedimentary inclusions, and relative size which exceeds that of other granite bodies in northeastern Oregon by at least 20 times. Mineralogical distinctions are common megacrysts of potassium feldspar, low content of iron oxide (0.02 volume percent), red-brown biotite in two specimens, and local occurrence of garnet, orthopyroxene, and cummingtonite.

LEUCOGRANITE OF DUTCH CREEK

SETTING AND GENERAL DESCRIPTION

A poorly exposed leucogranite in a heavily wooded area about 0.25 km^2 in the headwaters of Dutch Creek (fig. 2.2*B*) is herein called the leucogranite of Dutch Creek (fig. 2.3). It intrudes the boundary quartz diorite unit on the south and east, is overlain on the north and west by rocks of the Columbia River Basalt Group, and is in contact with a dismembered screen of country rocks on the southwest. Throughout much of the area, the leucogranite has disintegrated into a grus; rock specimens can be obtained from only a few outcrops. However, it is unexpectedly common as float, which typically shows faint to moderate foliation.

Fresh leucogranite is pale gray with sparsely scattered dark biotite. Most rock specimens, however, are discolored by weathering and are dominated by shades of yellow and yellow orange. The grain size might best be characterized as fine to medium because most crystals are 0.5 to 2.0 mm. Modes of three rock specimens of the leucogranite are given in table 2.13.

MICROSCOPIC DESCRIPTION

Plagioclase in the xenomorphic-granular leucogranite is a weakly zoned oligoclase that is partly altered to small flakes of white mica. The potassium feldspar is mostly orthoclase, as verified in many crystals by $2V$ of less than 60°. Indistinct microcline gridiron twinning occurs in a few crystals. The orthoclase shows faint exsolution and minor development of small (0.05–0.1 mm) secondary albite granules at the margins of larger potassium feldspar crystals. Myrmekite in minor amounts occurs both as bulbous protuberances and as narrow fringes along contacts between plagioclase and potassium feldspar.

Quartz is characterized by strong undulatory extinction and considerable recrystallization that ranges from strong in rock specimen R22 to moderate in specimen R24 to minor in specimen R25 (table 2.13). The grain size of crystals in rock specimen R22 commonly has been reduced by recrystallization from grains more than 1 mm across to about 0.5 mm and locally to less than 0.1 mm.

Biotite is present mostly along grain boundaries as irregular flakes less than 0.5 mm long. A few flakes are found along microfractures in plagioclase and potassium feldspar. Muscovite occurs mostly associated with potassium feldspar as flakes as much as 0.8 mm across, but also in small quantities intergrown with biotite. Accessory minerals are iron oxide, apatite, and zircon.

No field or petrographic evidence was noted to suggest that the character of the leucogranite of Dutch Creek has been modified by assimilation of country rocks. Rock specimens R22, R24, and R25 (table 2.13) contain, respectively, 0.04, 0.18, and 0.07 volume percent iron oxide. These iron oxide contents would be considered low for tonalites and granodiorites, but not for leucogranite, such as the leucogranite of Dutch Creek.

DISTINGUISHING FEATURES

The leucogranite is distinct in having a grain size that is intermediate between aplite and normal medi-

TABLE 2.14.—*Modes of satellitic granitic rocks northeast of the Bald Mountain batholith*

[Values in volume percent. Each analysis represents at least 2,400 point counts for each of two thin sections of the tonalite of North Fork or for each of three thin sections of the granite of Isham Spring; 0.0, trace amount; ---, not present]

Specimen number	Quartz	Potassium feldspar	Plagioclase	Biotite	Hornblende	Opaque minerals	Nonopaque accessory minerals
Tonalite of North Fork							
R133 ----	29.0	0.3	56.5	11.8	2.3	0.0	0.1
R134 ----	30.8	1.5	55.4	11.5	.7	.0	.1
Average	29.9	.9	55.9	11.7	1.5	.0	.1
Granite of Isham Spring							
R136 ----	36.3	25.7	33.6	4.4	---	0.0	0.0
R137 ----	36.0	26.5	33.3	4.2	---	.0	.0
Average	36.1	26.1	33.5	4.3	---	.0	.0

um-grained granitic rocks. Moreover, the leucogranite has the highest average content of both quartz and potassium feldspar of any unit in the Bald Mountain batholith. The modal composition of the leucogranite closely resembles that of aplite, except for the leucogranite's higher content of biotite. Recrystallization of quartz is notable, especially in rock specimen R22 (table 2.13).

SATELLITIC BODIES EAST OF GRANITE OF ANTHONY BUTTE

TONALITE OF NORTH FORK

SETTING AND GENERAL DESCRIPTION

A somewhat irregular body of tonalite that occupies a 0.4-km^2 area surrounded by country rocks just north of the North Fork of Anthony Creek is called the tonalite of North Fork (fig. 2.3). The country rocks are mostly schistose metasedimentary rocks but include amphibolites derived from metagabbro. The tonalite is medium grained with a color index of about 12. Biotite commonly is concentrated within moderately distinct planes that accentuate a well-defined foliation that strikes from due west to N. 60° W. and dips 35°–60° N. Modal analyses of specimens of tonalite from two widely separated outcrops are given in table 2.14.

MICROSCOPIC DESCRIPTION

The plagioclase is andesine and occurs mostly as subhedral crystals that are only weakly zoned. The crystals are antiperthitic, and some are markedly embayed by quartz. Twinning lamellae are commonly bent 6° and rarely as much as 14°. Local recrystallization has occurred along the contact of some plagioclase where it is in contact with another plagioclase crystal. Quartz is characterized by moderate to strong undulatory extinction, and about half of the quartz shows one or more sutured contacts. Features of quartz are best viewed with low-power magnification.

Biotite ranges from fairly well-formed plates to ragged grains and aggregates. It generally is independent of hornblende, and only a few examples of a reaction relation were observed. The biotite in both specimens (table 2.14) is pleochroic from grayish yellow (X-axis direction) to either reddish brown or, more generally, red (Z axis), in contrast to the brownish color of biotite (Z) in most other granitic rocks of northeastern Oregon. The pronounced reddish coloration of the biotite in thin sections is readily visible megascopically. Both megascopically and microscopically, colors of biotite in the tonalite of North Fork (as in all reduced rocks in the Elkhorn Mountains) are best seen in crystals more than 0.5 mm in maximum dimension. In the tonalite of North Fork the occurrence of much biotite along grain boundaries, including those between adjacent crystals of quartz, indicates late crystallization. The cleavage of some biotite is bent. A conspicuous feature of the biotite is numerous enclosed crystals of apatite. For example, one flake about 0.6 mm long contains 11 small crystals of apatite.

Hornblende occurs mostly as euhedral to subhedral crystals less than 2.5 mm long, but much hornblende

that is enclosed within quartz is partly resorbed. Early crystallization of some hornblende is implied by crystals as large as 0.3 mm enclosed within plagioclase. Interstitial potassium feldspar is orthoclase as judged from estimated $2V$ (flat stage) of about 55° for nearly centered acute-bisectrix figures. Accessory minerals are ubiquitous apatite and zircon as well as uncommon allanite and iron oxide. Local alteration products are white mica (on plagioclase) and chlorite (after biotite).

DISTINGUISHING FEATURES

The tonalite of North Fork is distinctive in modal composition, texture, and mineralogic features and has no known counterpart in northeastern Oregon. Nearly all other granitic rocks in northeastern Oregon with 30 percent modal quartz contain less biotite, more hornblende, and considerably more orthoclase than this tonalite. Trondhjemites in northeastern Oregon with 30 percent quartz contain less biotite and hornblende and commonly slightly more orthoclase than this tonalite. The core of the Cornucopia tonalite unit in the Wallowa Mountains (Taubeneck, 1967, fig. 1) most nearly approximates the tonalite of North Fork, but the Cornucopia core rocks contain only about 60 percent as much biotite and essentially no hornblende.

The tonalite of North Fork has a distinctive fabric characterized by deformed plagioclase, strained and recrystallized quartz, and bent biotite. Other distinctive features are the reddish biotite and the numerous enclosed crystals of apatite. The virtual absence of iron oxide (0.01 volume percent) in the tonalite also is noteworthy. The reddish biotite and dearth of iron oxide in the tonalite of North Fork are evidence of the assimilation of graphite-bearing metasedimentary rocks.

GRANITE OF ISHAM SPRING

SETTING AND GENERAL DESCRIPTION

A small (about 0.04 km^2) mass of granite that crops out just south of the North Fork of Anthony Creek and about 1.1 km north of Isham Spring is herein called the granite of Isham Spring (fig. 2.3). The granite is a tabular body that was emplaced concordantly between schistose metasedimentary rocks that strike roughly east-west and dip 35°–50° north. The granite is a medium-grained light-gray rock with scattered, small crystals of biotite that define a distinct foliation. The granite is well exposed and contains no megacrysts of potassium feldspar. Modal analyses of two rock specimens are given in table 2.14.

MICROSCOPIC DESCRIPTION

The plagioclase is weakly zoned oligoclase that shows some corrosion by both quartz and potassium feldspar. Plastic deformation of plagioclase is not as common as fracturing, but twinning lamellae in one crystal are bent 14°. Microfractures are common, and a few crystals are composed of annealed pieces of plagioclase in which the twinning planes trend in different directions by about 10°. The potassium feldspar is orthoclase microperthite ($2V<60°$). The commonly Carlsbad-twinned crystals are as much as 8 mm across and anhedral; some enclose subhedral to euhedral quartz. Conspicuous myrmekite occurs predominantly as cauliflower-like protuberances that extend as far as 0.3 mm inside the orthoclase. Quartz is interstitial and exhibits very strong extinction and considerable recrystallization. Nearly all areas of interstitial quartz reveal some recrystallization, especially as viewed with low-power magnification. Red-brown biotite (both rock specimens, table 2.14) generally occurs along grain boundaries as small and irregular flakes that commonly show deformation effects. Cleavage planes in biotite are bent as much as 21°. Biotite locally extends along fractures in plagioclase. Accessory minerals are zircon, monazite, allanite, apatite, and a very small amount of iron oxide. Much of the zircon and monazite occurs in clusters of two or more crystals. The largest cluster consists of 27 crystals of monazite. Alteration products include small amounts of chlorite associated with biotite and minor kaolinitic alteration of orthoclase.

DISTINGUISHING FEATURES

Recrystallized quartz is the most distinctive feature of the major minerals of the granite. The only other granitic rock body in the Elkhorn Mountains with as much recrystallized quartz is the leucogranite of Dutch Creek. The granite of Isham Spring also is characterized by conspicuous myrmekite as bulbous and wartlike masses. The scarcity of iron oxide, only 0.005 volume percent, and the presence of red-brown biotite are other distinctive features of this rock. The clusters of zircon and monazite are unique among the granitic rocks of northeastern Oregon. Intrusions of cordierite trondhjemite in the Cornucopia stock (Taubeneck, 1964) and Wallowa batholith are characterized by concentrations of zircon but not of monazite.

GRANITIC ROCKS OF THE GUARD STATION INLIER

The northern part of the Bald Mountain batholith is concealed by Cenozoic volcanic rocks, and only two small exposures of tonalite occur near the bottoms of canyons incised in rocks of the Columbia River Basalt Group about 3 to 4 km north and northeast of the leucogranite of Dutch Creek (fig. 2.3). More widespread and significant exposures of granitic rocks are present about 18 km west on either side of the Grande Ronde River (fig. 2.2*B*) in an area about 6.5 km^2 (fig. 2.5) that is partly in the northwest corner of the Limber Jim Creek quadrangle but mostly in the southwest corner of the Little Beaver Creek quadrangle (fig. 2.2*A*). For purposes of reference the area of pre-Tertiary rocks shown in figure 2.5 is called the Guard Station inlier after a U.S. Forest Service building, the Grande Ronde Guard Station, that is located well within the area. Most and possibly all granitic rocks in the inlier are satellitic to the batholith rather than an integral part of the batholith. Biotite granodiorite and biotite tonalite in the southeastern part of the inlier could be peripheral components of the batholith.

Country rocks in the Guard Station inlier are metasedimentary rocks and metagabbro that have their counterparts in the aureole of the batholith south of lat 45° N. The metasedimentary rocks are mostly ribbon chert, cherty argillite, and argillite that are correlative with the Elkhorn Ridge Argillite and are a northward extension of the Baker terrane. Strata in the east half of the inlier strike approximately east-west and dip steeply southward, whereas most metasedimentary rocks to the west strike about N. 70° E. and dip ≥70° SE. or (less commonly) NW. Whether the contact between metagabbro on the south and metasedimentary rocks on the north (fig. 2.5) is tectonic or intrusive is debatable.

OVERVIEW OF GRANITIC ROCKS

For purposes of discussion the granitic rocks of the Guard Station inlier have been divided geographically and lithologically into four units (fig. 2.5): (1) a northern biotite granodiorite, (2) a central quartz diorite, (3) a southeastern biotite granodiorite and biotite tonalite, and (4) a southern quartz gabbro and quartz diorite. Many very small granitic intrusions, including at least two consisting of granite, are not shown in figure 2.5; several larger intrusions could not be sampled because of ubiquitous grus. The Guard Station inlier is a unique area in northeastern Oregon in the large number and great diversity of its small granitic intrusions. Moreover, petrographic evidence indicates that the granitic magma of nearly every intrusion assimilated graphite-bearing metasedimentary rocks. The rock types are considered briefly by geographic distribution commencing in the north.

The northern biotite granodiorite (fig. 2.5) crops out for about 250 m along each of two small tributaries of the Grande Ronde River. The granodiorite intrudes metasedimentary rocks on the southwest and is overlain by Cenozoic volcanic rocks elsewhere. Modal analyses of three rock specimens are given in table 2.15.

Discrete crystals of muscovite as much as 1 mm long are the most distinctive feature of the northern biotite granodiorite. Some muscovite is intergrown with biotite, but most occurs as irregular crystals on either plagioclase or orthoclase. Muscovite is rare in granitic rocks in northeastern Oregon and is not known to occur in granodiorite bodies except within the Guard Station inlier. Another notable feature in each rock specimen (table 2.15) of the northern biotite granodiorite is the distinctive reddish-brown biotite. Other significant features of the northern biotite granodiorite are scarcity of iron oxide (only 0.016 modal percent), traces of garnet (in rock specimen R592, table 2.15), and a relatively high content of quartz. Zircon commonly is zoned.

Many small and poorly exposed granitic intrusions occur in the central part of the Guard Station inlier near the contact between metasedimentary rocks and metagabbro. Most of the intrusions are in metasedimentary rocks, are elongated in an approximate east-west direction, are medium grained, and contain hornblende. The largest of the elongated bodies is an unmapped mass of grus extending from about 0.5 to 1.5 km east of the Guard Station. No specimens could be obtained because of poor exposures and deep weathering. The best exposed intrusion into the metasedimentary rocks is the central quartz diorite, which crops out in an area about 0.04 km^2 approximately 200 m south of the Grand Ronde Guard Station. Modal analyses of two rock specimens are given in table 2.15.

The central quartz diorite is characterized by crystals mostly less than 1 mm across, by cloudy plagioclase, and by evidence of early crystallization of abundant augite. Approximately one-half of the hornblende crystals contain bleached cores enclosing minute grains of quartz (Taubeneck, 1964), and some of the original augite is preserved as cores in hornblende. The largest augite is a core about 0.7 mm across surrounded by a rim of hornblende between 0.1 and 0.2 mm wide. The abundance of augite as the early mafic phase in the fine-grained quartz diorite supports the general conclusion that granitic rocks in the Elkhorn Mountains crystallized from relatively hot and water-undersaturated magmas.

TABLE 2.15.—*Modes of plutonic rocks of the Guard Station inlier*

[Values in volume percent. Each analysis represents at least 2,400 point counts for each of three thin sections; 0.0, trace amount; ---, not present]

Specimen number	Quartz	Potassium feldspar	Plagioclase	Biotite	Muscovite	Augite	Hornblende	Opaque minerals	Nonopaque accessory minerals
Northern biotite granodiorite									
R590 ----	36.2	10.1	47.0	6.2	0.5	---	---	0.0	0.0
R591 ----	36.9	7.3	48.4	7.3	.1	---	---	.0	.0
R592 ----	33.9	16.8	44.5	3.6	1.2	---	---	.0	.0
Average	35.7	11.4	46.6	5.7	.6	---	---	.0	.0
Central quartz diorite									
R55 -----	8.1	3.0	65.5	14.5	---	0.6	8.2	0.1	0.0
R56 -----	8.3	2.8	64.7	12.3	---	1.0	10.6	.3	.0
Average	8.2	2.9	65.1	13.4	---	.8	9.4	.2	.0
Leucogranite from central part of inlier									
R54 -----	33.6	27.2	34.9	3.8	0.5	---	---	---	0.0
Southeastern biotite granodiorite									
R594 ----	39.1	16.3	40.3	4.2	0.1	---	---	0.0	0.0
R595 ----	38.0	12.7	44.0	4.9	.4	---	---	.0	.0
Average	38.5	14.5	42.1	4.6	.3	---	---	.0	.0
Southeastern biotite tonalite									
R596 ----	39.6	1.5	52.9	6.0	---	---	---	0.0	0.0
R597 ----	35.7	1.9	53.4	9.0	---	---	---	.0	.0
Average	36.7	1.7	53.1	7.5	---	---	---	.0	.0
Southern quartz gabbro									
R46 -----	11.0	---	25.4	---	---	0.6	62.3	0.2	0.5
R47 -----	11.8	---	31.9	---	---	1.3	54.4	.1	.5
Average	11.4	---	28.6	---	---	1.0	58.3	.2	.5
Southern quartz diorite									
R49 -----	9.7	---	52.7	5.8	---	---	31.4	0.1	0.3
R50 -----	13.8	---	49.2	5.6	---	---	30.2	.9	.3
Average	11.8	---	50.9	5.7	---	---	30.8	.5	.3
Biotite tonalite dike from southern part of inlier									
R51 -----	34.3	---	58.6	7.1	---	---	0.0	0.0	0.0
Granite from southern part of inlier									
R45 -----	31.5	24.6	38.7	4.8	0.4	---	---	0.0	0.0

Granitic intrusions in the central part of the Guard Station inlier also occur in metagabbro near the contact with the metasedimentary rocks. The intrusions are less abundant than those into the metasedimentary rocks, smaller in size, and generally contain no hornblende. Only one of these intrusions was sampled: a medium-grained leucogranite (specimen number R54, table 2.15) about 12 m wide on the east side of the Grande Ronde River about 900 m south of the Guard Station. The leucogranite is distinguished by muscovite in irregular crystals as much as 1.5 mm across, bent cleavage traces in some of the red-brown biotite, quartz showing strong undulatory extinction and some recrystallization, and near absence of iron oxide.

The southeastern biotite granodiorite and biotite tonalite make up a rather poorly exposed mass that extends for about 1.4 km along the southeast contact of the inlier. These granitic rocks intrude both the metagabbro and the metasedimentary rocks and are overlain on the east, southeast, and south sides by Cenozoic volcanic rocks (fig. 2.5). The foliation strikes mostly N. 20° E. to N. 60° E., approximately parallel to the contact with country rocks. The northern part of the mass is a biotite granodiorite, whereas the southern part is a biotite tonalite. Relations between the tonalite and granodiorite are unknown; presumably the granodiorite is younger. Modal analyses of two rock samples of the biotite granodiorite and two of the biotite tonalite are given in table 2.15.

The most distinctive feature of the biotite granodiorite is the unusual amount of strongly corroded plagioclase. In contrast, only minor corrosion of plagioclase occurs in the biotite tonalite. The granodiorite also is distinguished by muscovite in flakes as much as 0.8 mm across, by a very high content of quartz, and by such small amounts of iron oxide that none was tabulated during the point counting of six thin sections (16,462 points). Both rock specimens of biotite granodiorite (table 2.15) are characterized by red-brown biotite.

Many features of the biotite tonalite duplicate characteristics of other granitic rocks in the Elkhorn Mountains north of lat 45° N. but are distinct from most granitic rocks elsewhere in northeastern Oregon. These features are local recrystallization of plagioclase at pressure points, mild bending of twinning lamellae in plagioclase, stringers of biotite and orthoclase along fractures in plagioclase, high content of quartz, and a dearth of iron oxide (0.02 volume percent). Biotite is red-brown in rock specimen R596 (table 2.15) but apparently not in specimen R597.

The southern quartz gabbro and quartz diorite (fig. 2.5) are the dominant intrusions into metagabbro in this part of the inlier. Presumably the quartz gabbro is older than the quartz diorite, according to the common mafic-to-felsic intrusive sequence. Near the north contact of the quartz diorite with the metagabbro is a banded gneiss with sharply defined layers of plagioclase and hornblende. The gneiss is more than 12 m wide and is interpreted as a regional east-west-trending shear zone that controlled the emplacement of the quartz diorite. Modal analyses of the southern quartz gabbro and quartz diorite are given in table 2.15.

The quartz gabbro is a medium-grained melanocratic rock dominated by many nearly equant crystals of hornblende mostly 3 to 6 mm across. Slender extensions of amphibole that project into adjacent plagioclase from well-defined crystal faces of hornblende are a notable microscopic feature of the gabbro. The extensions are in optical continuity with the large primary crystals of hornblende and are regarded as a product of thermal metamorphism. Another characteristic of the quartz gabbro is the preservation of most of the original augite within plagioclase rather than within hornblende. Subhedral to euhedral augite 0.1 to 0.5 mm across is fairly common within plagioclase. In contrast, only small, irregular, and scattered relicts of augite remain enclosed within hornblende. Features of deformation are widespread. Twinning lamellae of plagioclase are bent as much as 12°; locally, plagioclase is crushed and, along most shears, annealed or recrystallized. Some hornblende has crystallized along fractures within plagioclase and also along a few crush zones. Quartz shows strong strain shadows and local recrystallization. Clouded crystals of apatite are another earmark of the quartz gabbro.

The quartz diorite is almost fine grained; most crystals are either slightly larger or smaller than 1 mm. Poikilitic crystals of biotite as much as 5 mm across distinguish the rock megascopically by contrasting markedly with the relatively small crystal size of the remainder of the rock. The quartz diorite is characterized by a very large amount of hornblende but a comparatively low content of biotite. The absence of augite is surprising in a mafic quartz diorite having a color index of 37 and a quartz content of only about 10 volume percent.

A medium-grained dike of biotite tonalite (table 2.15) without chilled contacts cuts the quartz diorite and locally confirms the assumption that the quartz diorite is older than the more felsic granitic rocks in the Guard Station inlier. Felsic granitic rocks north of lat 45° N. typically show deformation features, and the dike is no exception. Twinning lamellae in plagioclase are bent as much as 8°, and sutured contacts in quartz are relatively common. In addition, biotite extends along fractures in plagioclase. The dike contains small amounts of apatite, zircon, iron oxide,

and unresorbed hornblende. The low content of iron oxide (0.03 volume percent) and abundant quartz (table 2.15) suggest assimilation of siliceous components of the Elkhorn Ridge Argillite, but the brown of the larger biotite crystals has only a slight, if any, reddish tint.

The quartz diorite in the extreme southwestern part of the inlier is intruded by a medium-grained granite (table 2.15); this small body, exposed over an area only about 10 m across, is concealed to the south by alluvium and Cenozoic volcanic rocks. The granite is either an east-west-striking dike or the northernmost part of a concealed pluton. Deformation features in the granite are twinning lamellae bent as much as 5° and quartz showing strong wavy extinction as well as some recrystallized contacts. The red-brown color of biotite is sufficiently intense to recognize readily even in most crystals no more than 0.1 mm across. Accessory minerals (not recorded in 8,431 point counts) are apatite, zircon, monazite, and iron oxide.

METHOD OF EMPLACEMENT OF ELKHORN PLUTON

Studies of the emplacement of even small batholiths such as the Bald Mountain batholith involve formidable structural problems that invite an integrated team investigation. Only prolonged field studies in areas of favorable exposures can provide evidence of long-distance effects of emplacement (Balk, 1937). Unfortunately, most of the area surrounding the Bald Mountain batholith is not suitable for studies of emplacement mechanisms. Many pertinent rock exposures in the east are concealed by valley alluvium (fig. 2.2). Cenozoic volcanic rocks are within 1 km of the batholith on the southwest, and they overlie the granitic rocks on the north and northwest. Furthermore, major structural features have not been recognized in the Elkhorn Ridge Argillite (Gilluly, 1937; Pardee, 1941). The absence of established fold axes and well-defined marker horizons restricts the discussion of regional structural features to strike-and-dip patterns displayed by hundreds of individual beds.

In the Elkhorn Mountains the regional trend is essentially east-west and the strata commonly dip south at angles steeper than 50°. As intrusive contacts are approached, the regional trend becomes progressively disrupted. In most parts of the world, including the Elkhorn Mountains, structural patterns that surround small stocks are more straightforward than the pattern around a nearby batholith. Located 3 to 8 km south of the Bald Mountain batholith, the satellitic Lake Creek and Grays Peak stocks mostly are concordant, with strikes of surrounding strata approximately parallel to intrusive contacts (Taubeneck, 1957, figs. 4 and 5). The strong deflection of the regional trend around the two stocks implies that emplacement was by forceful intrusion.

The earliest intrusive units of the batholith are the three small gabbroic bodies (fig. 2.2). The forceful intrusion of the tonalite of Bald Mountain, which surrounds the norite of Badger Butte, left almost no trace of the norite's host rock. Therefore, little proof remains regarding the emplacement mechanism of the norite. Adequate metasedimentary rocks occur within and near the norite of Willow Lake (Taubeneck and Poldervaart, 1960, fig. 3) to suggest that this body was emplaced by forceful intrusion. Unlike the two norite bodies, only part of the quartz gabbro of Black Bear (fig. 2.2) is in contact with the tonalite of Bald Mountain. Accordingly, considerable evidence pertaining to the emplacement of this mass survives in country rocks. A dismembered screen between the quartz gabbro and the tonalite provides additional evidence. The strike of ribbon chert changes progressively in a clockwise direction from east-west at the southeast corner of the quartz gabbro (fig. 2.2) to N. 25° W. on the west side. The strike of ribbon chert further changes within the dismembered screen from north-south on the southwest side to east-west on the east side. The eastern part of the quartz gabbro is concealed by alluvium. This 180° change in strike of the ribbon chert around the exposed contacts of the quartz gabbro of Black Bear is consistent with emplacement by forceful intrusion.

Gabbroic units in composite batholiths commonly occur as comagmatic mafic forerunners around large granitic plutons. The mafic rocks of the Bald Mountain batholith mostly were the products of high-alumina basaltic magma that was fundamental in transferring heat and mass into the crust. Accordingly, subsequent emplacement of the Elkhorn pluton was facilitated by intrusion of the three peripheral masses of gabbroic rocks, as well as by the intrusion of the quartz diorite of Limber Creek.

The zoned Elkhorn pluton that constitutes the largest part of the batholith is broadly concordant along about 85 percent of the exposed contacts (fig. 2.2). The two major areas of discordance are at the neck of the Monumental salient and along the northwest contact of the salient (fig. 2.2). Some major discordances are almost inevitable in a forcefully emplaced intrusion with the dimensions of the Elkhorn pluton. Observations of salt domes (Trusheim, 1960) and experiments on diapirism (Ramberg, 1981) show that mature dia-

pirs commonly crosscut the structures that they induced during their forceful intrusion.

Tertiary volcanic rocks west and northwest of Anthony Lake overlie the contact of the Elkhorn pluton and prevent an evaluation of emplacement mechanisms for this part of the pluton. However, limited exposures of metagabbro shown in figure 2.2 about 2.5 km south of Chicken Hill indicate that the general concordancy of the pluton continues from the vicinity of the norite of Badger Butte northward under the Tertiary volcanic rocks. Nearly vertical gneissic layering in the metagabbro south of Chicken Hill strikes about N. 10° W. as is consistent with a north-striking concealed contact. The intensity of metamorphism in the metagabbro implies that the concealed contact of the Elkhorn pluton is not more than a few hundred meters to the east.

The area encompassed by figure 2.2 does not extend far enough to the west and south of the Elkhorn pluton to reveal the prevailing east-west regional trend that occurs in areas not concealed by Tertiary volcanic rocks. Maps by Evans (1986) and Elfrink (1987) show that trends are essentially east-west in country rocks more than 6 km west of the Monumental salient. The east-west trend in most of the area south of the Elkhorn pluton is shown on maps by Pardee (1941) and by Ferns and others (1987). Conspicuous disruption of the regional trend near the Elkhorn pluton is compatible with forceful intrusion of the largest unit of the batholith.

Emplacement of the Elkhorn pluton along the southeast side of the Belleview wedge and through the neck of the Monumental salient was preceded by intrusion of the quartz diorite of Limber Creek. The dike-like western quartz diorite (see section "Quartz Diorite of Limber Creek") extends eastward along the southeast side of the Belleview wedge where it is truncated at the neck by the tonalite of Bald Mountain (fig. 2.4). The original eastward dimensions of the western quartz diorite are unknown; speculation suggests that this quartz diorite extended continuously or discontinuously eastward through much of the neck and perhaps to the general location of the brecciated quartz diorite. The basis for this speculation is the occurrence of scattered xenoliths of the quartz diorite of Limber Creek in the tonalite. The largest xenolith, exposed on a flat surface, is a slab that tapers almost to a point at one end; dimensions are 1.7 m long with a maximum width of 0.6 m near the wide end but only 0.04 m at the narrow end.

Intrusions of the quartz diorite of Limber Creek are localized on either side of the neck of the Monumental salient. The brecciated quartz diorite is clearly a remnant of a larger intrusion that was mostly removed during emplacement of the tonalite of Bald Mountain. The western quartz diorite unmistakably exerted a structural control on the emplacement of the Monumental salient, initially or ultimately, by confining tonalitic magma to the south (fig. 2.4). The tonalite of the salient probably also was confined south of the neck, at least in part, by extensions of the western quartz diorite and the brecciated quartz diorite. Country rock originally within the area of the neck is envisioned as being squeezed and dragged upward during extreme plastic deformation as is characteristic of rocks of the Belleview wedge. Subsequently, or very late in the severing of the country rock partition between rocks of the salient and those of the main batholith, most wallrock very near the contacts of the neck was bent aside into a crude concordance (fig. 2.4).

Two major discordances in metasedimentary rocks occur within about 75 m of the east contact of the neck and one on the west side of the neck. One marked discordance along the east contact of the neck is southwest of the brecciated quartz diorite where cherty argillite on the ridge crest at 2,347 m dips 75° NW. and strikes S. 65° W. (fig. 2.4) at right angles to the contact. The second discordance along the east contact occurs farther south at the corner of the neck where an almost rectangular area of ribbon chert is surrounded on the northeast and southeast by glacial deposits (fig. 2.4). Most strikes in this small area vary from N. 65° E. to N. 85° W. with dips from vertical to 50° south. On the west side of the neck the only highly discordant strata are just north of where the western quartz diorite is cut off by the tonalite of Bald Mountain. For slightly more than 200 m (mostly north of the vertical attitude with east-west strike on fig. 2.4) the metasedimentary rocks strike into the contact at high angles.

Isolated boudins of chert and less common boudins of ribbon chert in Lindgren's (1901) Archean gneiss unit demonstrate extreme plastic deformation of country rock in the Belleview wedge during forceful emplacement of the Elkhorn pluton. Nearly all boudins in the gneiss occur as randomly scattered lens-shaped to ellipsoidal masses without stratigraphic continuity. Each dismembered boudin originally was part of one or more continuous beds. Most boudins are relicts of lamellae of ribbon chert originally interbedded with more extensive sequences of cherty argillite. Less commonly the boudins are relicts of layers of massive chert. Some boudins are pieces of ribbon chert that contain two or more chert lamellae. Lenticular to blocklike boudins of ribbon chert rarely exceed 1 m in length. The dimensions of most single-ribbon-wide boudins are less than 20 by 10 cm; many are less than 8 cm in greatest dimension.

The boudins are revealing vestiges of extreme plastic deformation. Rocks of the wedge flowed upward as they were confined by intruding magma. The extreme plastic deformation and recrystallization require an exceptional heat source and thus imply that granitic magma must have underlain much of the wedge. Some planar structure in tonalite east of the Belleview wedge dips westward at angles of no more than 30° (fig. 2.2). The low dips, if projected westward, would extend under the eastern part of the wedge. The topography is such that all planar structure near the wedge may decrease in dip at depths of less than 300 m. Extreme metamorphism of the Belleview wedge rocks suggests that the three-dimensional form of much of the wedge very crudely resembles an almost flat-bottomed boat. Such a configuration for the wedge at depth is consistent with deformation and recrystallization features of the metasedimentary rocks, although it is probably an oversimplified proposal for this dilemma, which was faced first by Lindgren (1901).

Folding in metasedimentary rocks in the Belleview wedge represents the compressional stresses on wallrock by incoming magma. Many folds with planar limbs and very angular hinges are chevron folds. The folds are tightly appressed (fig. 2.14*A*), and some are almost isoclinal. Layers are attenuated along limbs and thickened at hinges. One of the best exposures is of a 48-m-thick sequence of tightly folded ribbon chert (fig. 2.14*B*) on a ridge at an elevation of 2,246 m almost 3.6 km due south of Badger Butte and 1.2 km from the nearest exposed contact of the Elkhorn pluton. The strongest folding in the wedge mostly occurs in the interior rather than along contacts with the tonalite of Bald Mountain. Concentration of the most-intense folding well within the wedge adds credibility to the idea that Belleview wedge rocks were confined by rising magma everywhere but on the west side. Country rocks unable to flow downward and compressed laterally could explain the internal folding.

Other structural features of rocks near and within the Elkhorn pluton suggest that forceful intrusion was the dominant process responsible for the emplacement of the pluton.

Peripheral joints and upthrusts occur in granitic rocks near many contacts of the Elkhorn pluton. The joints and upthrusts dip inward, generally at angles of 20° to 40°. Narrow aplite dikes fairly commonly fill and accentuate the peripheral joints and upthrusts. Two accessible localities for observing peripheral joints are near the summit of Gorham Butte and in the minichasm of the Bulger Ditch (fig. 2.2*B*). Good examples of the much less common peripheral upthrusts are near the contact southeast of Summit Lake. The peripheral joints represent the tension produced by the upward flow of semisolid magma past steep confining walls. The Elkhorn pluton made additional room for itself along the peripheral upthrusts by crowding the walls outward as well as upward.

Pulled-apart lenses of ribbon chert in an argillaceous matrix denote the plastic deformation that occurred in wallrock south of the Elkhorn pluton to accommodate intruding magma. The shape and regularity of the lenses are related to the amount of argillaceous material in the rocks. Excellent examples of these lenses occur as much as 600 m south of the Elkhorn pluton, but they are well developed only in rocks that contain at least 20 percent argillaceous matrix. In strongly deformed rocks with considerable argillaceous material, most lenses range from 2.5 to 18 cm in length and commonly are 0.3 to 1.4 cm wide; evidence of bedding survives because biotite shows minimum deflection around the lenses. Bedded chert with all lamellae 5 cm or more in width commonly includes only a small amount of argillaceous material. Plastically deformed lamellae are more oblong than lens shaped; some are sausage shaped. Dismembered ribbon chert with very little argillaceous matrix consists of tightly packed cylindrical chunks of chert totally unlike angular pieces of sedimentary or igneous breccias. Biotite conspicuously winds between the dismembered cylinders of chert. No bedding survives.

Another point worthy of consideration is that argillaceous wallrocks of the Elkhorn pluton are schists, whereas ribbon cherts and cherty argillites of the Belleview wedge are gneissic rather than massive hornfelses. Foliated wallrocks along and near contacts of the pluton are consistent with the outward compression and upward drag of a forcefully intruded magma.

A review of the field evidence indicates that forceful intrusion was the dominant process in the emplacement of the Elkhorn pluton. Xenoliths entrained throughout the granitic rocks of the pluton at the present level of erosion suggest that stoping of country rocks was of minor overall importance. The space taken by pieces of wallrock represents only a fraction of 1 percent of the total volume of granitic rocks in nearly all surface exposures of the pluton. However, a field observer sees in the granitic rocks evidence of only the final stages of intrusion at the present level of erosion; stoping may have taken place on a larger scale during the early stages of intrusion. Evidence for such stoping is discussed below.

Structures within the Elkhorn pluton indicate that major stoping occurred along at least part of the intraplutonic contact. In the vicinity of the leucogranodior-

ite of Trail Creek, the intraplutonic contact is essentially at right angles to the structure of the foliated tonalite on the west (fig. 2.2). Most exposures near the intraplutonic contact are poor, but the only reasonable conclusion is that the foliated tonalite is abruptly truncated by the intraplutonic contact. Much foliated tonalite to the east must have been removed by stoping along a semicircular fracture that now is the intraplutonic contact. On a much smaller scale, the brecciated quartz diorite of Limber Creek (fig. 2.4) is a convincing example of stoping. The quartz diorite was emplaced in country rocks, but the only remaining contact with

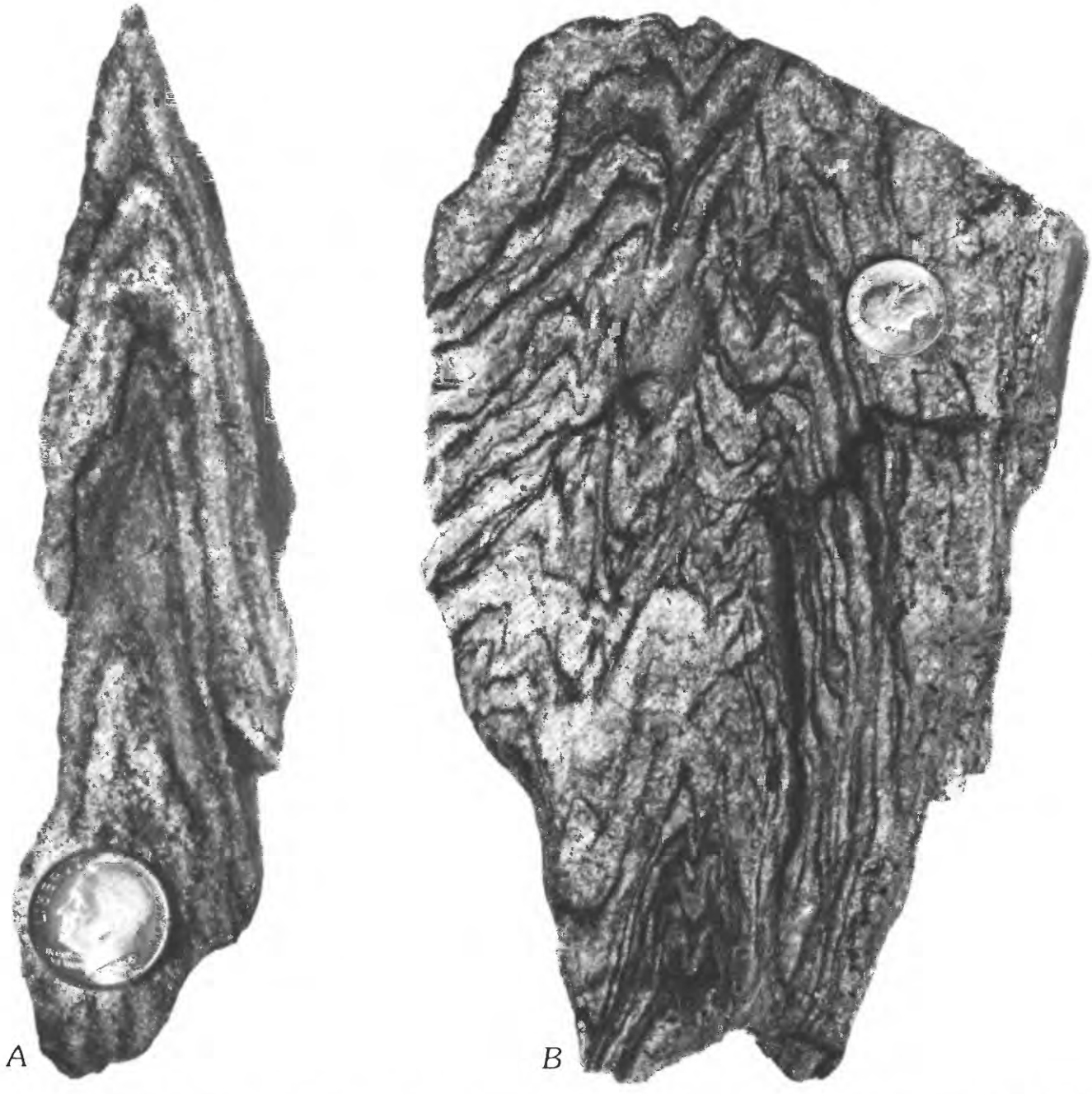

FIGURE 2.14.—Folding in metasedimentary rocks in Belleview wedge. *A*, Typical tightly appressed fold in bedded chert. Similar small-scale folds are present in metasedimentary rocks in most other areas near Elkhorn pluton, but nowhere is folding as widespread as within Belleview wedge. Coin is about 18 cm in diameter. *B*, Rock specimen from 48-m thick sequence of folded chert in Crawfish Lake quadrangle (fig. 2.2*A*) about 1.3 km from contact of Elkhorn pluton. Attenuation and thickening of layers is common. Coin is about 24 mm in diameter.

wallrocks is along the southeast side. Stoping must have removed the other wallrock contacts, as well as an unknown volume of the shattered quartz diorite.

The removal by stoping of a large volume of foliated tonalite east of the leucogranodiorite of Trail Creek, together with the field relations between the brecciated quartz diorite of Limber Creek and adjacent rocks, prompts a closer consideration of stoping as a significant emplacement mechanism throughout the Elkhorn pluton. A rigorous and direct assessment of stoping is possible only by comparing the sizes of xenoliths near wallrocks with the sizes of xenoliths in the interior of the pluton and by examining the upper parts of cupolalike extensions of granitic rocks near the margin of the Elkhorn pluton.

The largest xenolith along the contact south to east of Summit Lake (fig. 2.2) is a slice of ribbon chert 60 m long and as much as 9 m wide. This inclusion, about 40 m from the contact of the pluton, verifies that some xenoliths near their source are much larger than any xenoliths within the central part of the pluton, which do not exceed 1 m in greatest dimension. Three larger xenoliths, all of metagabbro, occur in peripheral tonalite near the contact with the granite of Anthony Butte. The larger of the two xenoliths shown in figure 2.3 is nearly 300 m long and as much as 80 m wide. The notable discrepancy in size between peripheral xenoliths and interior xenoliths suggests that larger xenoliths originally within the central parts of the pluton sank rapidly enough in the region of slower cooling to leave only small xenoliths behind as an incomplete testimony of piecemeal stoping.

The roof and upper part of the Elkhorn pluton were removed by erosion before Albian time (Taubeneck, 1960). Accordingly, roof rocks can be examined only in the upper part of cupolalike extensions of tonalite near the margin of the pluton. If several of the dissected cupolas in country rocks near the contact of the Elkhorn pluton provide accurate small-scale models of the former roof of the pluton, stoping of as much as 15 percent of the roof rocks was in progress during consolidation of the magma.

A readily accessible cupola occurs at an elevation of about 2,225 m approximately 0.45 km N. 35° W. of the Upper Baisley-Elkhorn Mine (fig. 2.2*B*) and approximately 1.7 km S. 45° W. from the summit of Hunt Mountain. At this locality a precipitous stream has cut down through overlying metagabbro to reveal the top of a small cupola. The contact of the metagabbro and tonalite, exposed for about 12 m along its length, dips 30° to 35° SW. Southwest of the stream in the immediate vicinity of the contact, xenoliths of metagabbro range from 2 cm to almost 2 m across. An inclusion of metagabbro about 4 m in greatest dimension occurs on the northeast side of the stream. The xenoliths constitute 10 to 15 volume percent of the cupola.

Roof rocks in the small cupola southwest of Hunt Mountain probably are a small-scale replica of the long-vanished roof of the Elkhorn pluton. Xenoliths in the cupola are as much as four times as large as any xenolith in the interior of the Elkhorn pluton. Furthermore, the size differential between xenoliths in the margin and those in the interior of the pluton suggests that large xenoliths with comparatively small surface areas and rapid sinking velocities have disappeared into the interior parts of the pluton. Therefore, the size differential of xenoliths within the Elkhorn pluton combined with relations exhibited in small cupolas implies that stoping was a significant emplacement mechanism, but the magnitude of the stoping process can never be closely appraised in mesozonal batholiths such as those of northeastern Oregon because the critical field evidence is gone.

Northeast of the Elkhorn pluton and north of lat 45° N. is a concentrated group of six intrusions within the batholith (fig. 2.3). The units are the quartz diorite of Wolf Creek, boundary quartz diorite unit, granodiorite of Indiana Mine Road, granodiorite of Beaver Meadow, granite of Anthony Butte, and leucogranite of Dutch Creek. The problem concerning the mechanism of emplacement is to determine how six different magmas successively acquired space for themselves to build up the composite batholith. No conclusive answer is possible partly because of the widespread distribution of overlying Tertiary volcanic rocks (fig. 2.3).

Significantly, each of these six units is elongated in an approximate east-west direction subparallel to the Monumental and Hunt Mountain salients (figs. 2.2*B*) of the Elkhorn pluton. By analogy with the two salients of the Elkhorn pluton, these six units probably were emplaced mostly by forceful intrusion. The dismembered screens in figure 2.3 reveal that a preferred route for intrusion of each successive unit was near a contact between an earlier intrusion and country rock. The pattern of the dismembered screens as well as the common strong planar structure and deformation features of the granitic rocks imply that emplacement was by forceful intrusion.

Two very large inclusions in the granite of Anthony Butte suggest that the emplacement of this unit was more complex than that of other units of the batholith. The southeastern part of the granite of Anthony Butte tapers to a narrow wedge (fig. 2.3) between the tonalite of Bald Mountain and country rock. The granite is strongly foliated as if forcefully intruded into a restricted space. Within the granite to the northwest are

two very large northwest-trending inclusions composed mostly of earlier foliated quartz diorite, some country rocks, and local hybrid rocks that nearly all occur as part of the large northern inclusion. Each inclusion is approximately 1.5 km long. Foliation and bedding in the inclusions strike dominantly northwestward. The two large inclusions are in the western and southwestern parts of the granite body; field relations suggest that magma in this area initially was intruded along three elongated conduits that subsequently coalesced. The characteristic mafic-to-felsic intrusive sequence in composite batholiths suggests that except for the leucogranite of Dutch Creek, the granite of Anthony Butte was the last intrusive unit emplaced within the area of figure 2.3. Earlier granitic rocks that surround the granite of Anthony Butte on nearly all sides should have restricted the forceful emplacement of yet another magma, whereas the two large inclusions of quartz diorite (relatively massive) might have favored multiple intrusion along paralleling channels rather than major intrusion along a solitary channel. In any event the features of the granite of Anthony Butte and associated rocks seem best interpreted as resulting from the forceful emplacement of tightly constricted magma that initially intruded along three more or less parallel passageways.

Likewise, the elongated, east-northeast-trending inclusion of country rock almost 1 km long in the granodiorite of Indiana Mine Road (fig. 2.3) almost surely is a clue to the growth of the magma body. The inclusion suggests that early in the emplacement history the granodioritic magma intruded along at least two east-west-trending channels before coalescing.

Thus these six units' overall strong planar structure and deformation features, their general east-west configuration controlled by so-called basement rocks, and the features of their dismembered screens and large inclusions are consistent with forceful intrusion as the dominant emplacement mechanism for this part of the batholith.

The five other units of the batholith are small intrusions in the Elkhorn pluton. Any statement regarding the emplacement mechanism of the leucogranodiorite of Red Mountain and the leucogranite of Elk Peak (fig. 2.2) is necessarily inconclusive, but emplacement of the granite of Clear Creek and the leucogranodiorite of Trail Creek was definitely controlled by structure. The granite of Clear Creek was emplaced alongside an inclusion of country rock in the tonalite of Bald Mountain, whereas the leucogranodiorite of Trail Creek intruded along the intraplutonic contact.

The leucogranodiorite of Mount Ruth (Taubeneck, 1957) is the smallest and best exposed of these five small units that intrude the Elkhorn pluton. The leucogranodiorite, which crops out over a triangular area about 0.15 km^2 at the summit of Mount Ruth (fig. 2.15), is a sheetlike intrusion; its subhorizontal contact with the underlying tonalite of Bald Mountain dips 10° to 15° NE. The leucogranodiorite is moderately fine grained (0.5 to 1.0 mm) with scattered phenocrysts (about 4.0 mm across) of biotite and plagioclase. The resemblance of the texture of the leucogranodiorite to that of some epizonal rocks suggests that emplacement occurred after the batholith was deroofed or partly deroofed. In any event, presumably the subhorizontal walls of the intrusion moved apart because the hydrostatic pressure exerted by the leucogranodiorite magma exceeded the lithostatic pressure associated with the tonalite of Bald Mountain.

VOLATILES CONTENTS OF GRANITIC MAGMAS IN RELATION TO INTERSTITIAL ZEOLITES AND POTASSIUM FELDSPAR IN GRANITIC ROCKS OF THE BALD MOUNTAIN AND WALLOWA BATHOLITHS

Interstitial zeolites in granitic rocks were reported in the Cornucopia tonalite unit (Taubeneck, 1967) and now are known to occur in many granitic plutons in northeastern Oregon, westernmost Idaho, and northwest Nevada. The maximum known content of interstitial zeolite in any specimen of these granitic rocks is 0.63 volume percent but few contain more than 0.15 volume percent. Heulandite is by far the dominant interstitial zeolite; chabazite is comparatively rare.

Interstitial heulandite in the Cornucopia tonalite unit characteristically contains many small apatite crystals. However, the association of apatite with heulandite is much less common in other granitic intrusions, including the Elkhorn pluton. The heulandite-apatite association represents hydrothermal crystallization of a residual fluid rich in volatiles.

Interstitial heulandite and chabazite are easily overlooked and superficially resemble very small amounts of interstitial orthoclase such as may occur locally between plagioclase crystals in tonalites and granodiorites. Interstitial zeolites in the tonalite of Bald Mountain and granodiorite of Anthony Lake were incorrectly tabulated as orthoclase in earlier modal analyses (Taubeneck, 1957).

Heulandite in granitic rocks also occurs along fractures and as a selective replacement of one or more zones of oscillatory-zoned plagioclase. Both occurrences in the Elkhorn pluton are relatively unimportant. For example, only two fractures containing heulandite were seen during a close examination of 437 thin sections.

The following summary of zeolite distribution in granitic rocks of northeastern Oregon is restricted to interstitial zeolite in the Elkhorn pluton and in the four major units of the Wallowa batholith (fig. 2.11). The Elkhorn pluton contains the smallest amount of interstitial zeolite of these five compositionally zoned intrusions of tonalite and granodiorite. On the average, the Elkhorn pluton (number of samples (n)=193) contains 0.0054 volume percent interstitial zeolite. In contrast, unit 1 (n=76) of the Wallowa batholith (fig. 2.11) contains 0.011 volume percent interstitial zeolite, unit 2 (n=70) contains 0.0073 volume percent, unit 3 (n=124) contains 0.0294 volume percent, and unit 4 (n=90) contains 0.0087 volume percent. All four major units of the Wallowa batholith contain more interstitial zeolite than the Elkhorn pluton, but unit 3 contains in excess of 400 percent more zeolite.

Paucity of interstitial zeolite in the Elkhorn pluton is consistent with crystallization of a relatively dry magma. Because aplites are generally believed to represent late-stage residual liquids remaining after extensive crystallization of a granitic magma, the general abundance of aplites and pegmatites associated with a granitic intrusion may correlate with the relative abundance of interstitial zeolite in some plutons. The possibility of such a correlation is strengthened in northeastern Oregon by the occurrence of several times as much aplite and pegmatite in unit 3 of the Wallowa batholith as in either the Elkhorn pluton or the other Wallowa units.

Interstitial zeolites are present in such small amounts in granitic rocks that their possible use as a general guide to the volatiles content of a magma seems very limited. A more common mineral with di-

FIGURE 2.15.—View across Dutch Flat (lower left foreground) toward Mount Ruth, highest peak on left skyline. Solid line near summit of Mount Ruth denotes subhorizontal contact between overlying leucogranodiorite of Mount Ruth and underlying tonalite of Bald Mountain, as viewed from well within granodiorite of Anthony Lake (fig. 2.2). Contact dips toward observer, but sheetlike intrusion does not intersect any peaks in foreground nor higher peaks to left of photograph. View looking S. 25° W. from a point 3.6 km S. 65° E. of Anthony Lake.

agnostic properties that vary systematically—such as potassium feldspar—would be much more suitable in attempting to gauge the relative volatiles contents of granitic magmas.

Emeleus and Smith (1959) and many subsequent authors suggested that volatiles have a catalytic effect on the ordering of potassium feldspar. If so, potassium feldspar that crystallized from relatively dry magmas presumably should be characterized by little or no evidence of exsolution, a relatively small $2V$, and no microcline twinning. As both orthoclase and microcline occur in different parts of the Elkhorn pluton, changes in properties such as exsolution textures, size of $2V$, and distribution of crosshatch twinning might provide useful data regarding the relative water content of the crystallizing magma.

Exsolution lamellae are absent from potassium feldspar in the Hunt Mountain salient and rare in the Monumental salient but relatively common elsewhere south of the intraplutonic contact. The lamellae occur as straight and very narrow stringlike lines about 0.001 mm wide and as much as 0.6 mm long. The microperthite threads are so narrow that in thin section (plane-polarized light) they resemble cleavage traces and can scarcely be detected at low magnifications. The stringers commonly are confined to the interior of larger crystals. Individual members of a swarm of exsolution lamellae are generally rigidly parallel to each other, and the stringers are estimated to constitute as much as 15 volume percent of some crystals. Stringers do not cross grain boundaries but may extend to within less than 0.1 mm of boundaries. The scarcity of aplite and pegmatite dikes in the Hunt Mountain and Monumental salients is consistent with the absence or rarity of exsolution lamellae in both salients. Elsewhere in the Elkhorn pluton, however, the relative abundance of aplite and pegmatite dikes, such as near Anthony Lake, does not correlate locally with a greater number or width of exsolution lamellae.

Significant differences in the volatiles content of crystallizing magma in the Elkhorn pluton might be expressed by inward-increasing values of $2V$ for orthoclase and orthoclase microperthite. Average values of $2V$ for potassium feldspar vary from about 49° in each of the two salients to about 52° for most of the remainder of the pluton. Higher values of $2V$ occur in a diagonal zone that crosses the pluton approximately midway between Summit Lake and Anthony Lake (fig. 2.16). In the Hunt Mountain salient, determinations of $2V$ for 12 crystals in 7 rock samples range from 47.0° to 51.0° and average 49.2°; in the Monumental salient, determinations of $2V$ for 14 crystals in 6 rock samples range from 43.0° to 51.5° and average 49.3°; in the remainder of the pluton, excluding the diagonal microcline zone that crosses the batholith, determinations of $2V$ for 27 crystals in 14 rock samples range from 50.5° to 53.5° and average 52.2°.

The restricted range in values of $2V$ implies that potassium feldspar has a nearly uniform structural state and bulk chemical composition throughout most of the pluton. Average values of $2V$ for samples from an area near Anthony Lake where aplite and pegmatite dikes are concentrated are only about 3° higher than in the two salients where aplite and pegmatite dikes are uncommon. Accordingly, only a tenuous correlation is evident between the value of $2V$ in potassium feldspar and the abundance of aplite and pegmatite dikes in the Elkhorn pluton.

The occurrence of much microcline in a diagonal zone (fig. 2.16) that crosses the Elkhorn pluton suggests that the structural state of the crosshatched feldspar is not directly linked to the volatiles content of the Elkhorn magma. Crosshatched twinning occurs in most rock samples from within the zone but in only 3 of 197 rock samples from outside the zone. An assessment of the significance of the distribution of microcline requires consideration of the general textural features of rock types that contain this distinctive feldspar in contrast to rock types that lack microcline.

Rock types that lack microcline almost invariably contain quartz with moderate to strong undulatory extinction but little or no recrystallization. Parts of a single crystal of quartz commonly extinguish at angles that differ by several degrees and rarely by as much as 8°. Potassium feldspar, however, generally extinguishes simultaneously, and nearly all biotite is undeformed. In contrast, significantly different properties of quartz, potassium feldspar, and biotite characterize the various rock types within the zone of microcline (fig. 2.16). Quartz commonly shows very strong undulatory extinction, with parts of one crystal extinguishing at angles that differ by 5° to 12° and, rarely, as much as 16°. Sutured contacts are relatively common, and some zones of fine-grained (0.03–0.05 mm) recrystallized quartz extend through what originally was a single crystal. In a few rock types such narrow zones of fine-grained quartz may subdivide an original crystal into as many as seven or eight parts.

Much potassium feldspar shows wavy extinction with as much as an 11° difference in the extinction position of parts of one crystal. Many crystals show a dramatic change in $2V$ from core to rim. Angle changes in three examples are from 51.5° near the center of one large crystal to 68° near the edge, from 53.0° near one side of a second crystal to 72.0° near the other side,

and from 52.5° near the center of a third crystal to 67.0° near a corner of a plagioclase that projects into the potassium feldspar. In each example the highest value of $2V$ is close to the crystal margin and near a pressure point associated with a corner of plagioclase.

The three examples of widely varying optic-axial angles are in different rock samples from within the outer part of the zone of microcline (fig. 2.16). Near the center of the zone many, commonly small, crystals show pervasive crosshatched twinning. Some large crystals, however, show microcline twinning everywhere except in their cores.

Deformation effects are less pronounced in biotite than in quartz or potassium feldspar, but crystals of biotite in rock samples from the microcline zone are much more likely to show bent cleavage traces than those in rock samples from outside the zone. Fracturing in some biotite accompanied plastic deformation. For example, one large biotite lath is crossed nearly at right angles to cleavage by slightly irregular fractures

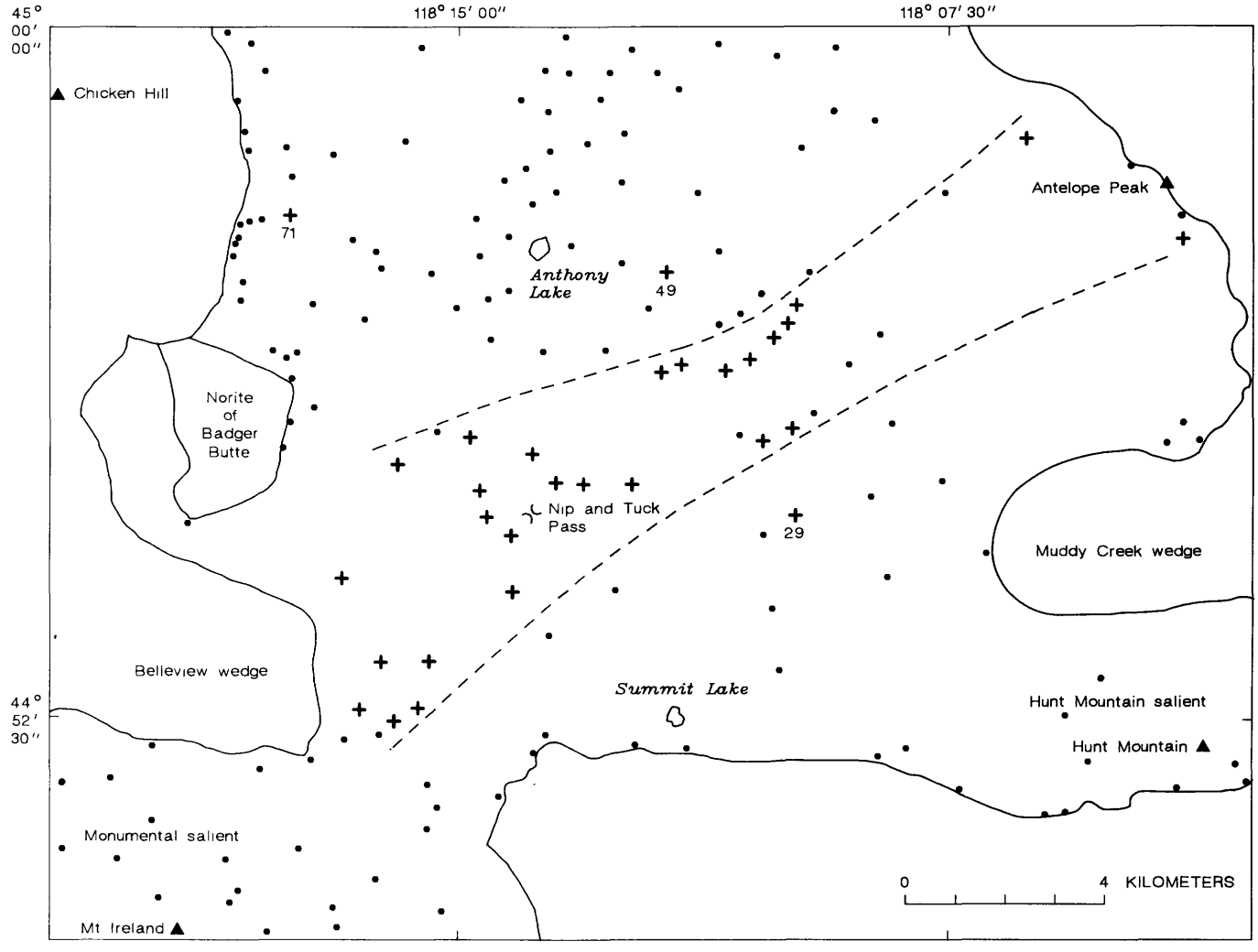

FIGURE 2.16.—Location of rocks of Elkhorn pluton with and without microcline twinning in potassium feldspar. Solid-line contacts surround the norite of Badger Butte and divide the Elkhorn pluton from wallrocks.

that contain small (0.02–0.04 mm) fragments of biotite with cleavage directions rotated as much as 23°.

Exsolution lamellae within the zone of microcline (fig. 2.16) are significantly different from lamellae in rock samples outside the zone. Lamellae within the zone commonly are coarser, lens shaped, slightly curved, continuous to crystal boundaries, and only approximately parallel. In addition, some en echelon sequences occur. A few lens-shaped lamellae are as much as 0.03 mm wide near a midpoint and gradually taper in both directions to a sharp termination. Lens-shaped lamellae are mostly 0.05 to 0.30 mm long. Some lamellae gradually curve as much as 10° or rarely even 15° throughout their length, whereas others change direction only in a restricted part of the lamellae near one termination. Lamellae that extend to a crystal boundary commonly are noticeably coarser at the boundary than within the crystal. The corner of a plagioclase crystal that is surrounded by potassium feldspar is a favored locality for one or more lamellae to extend into the potassium feldspar. Most en echelon sequences involve three or more lamellae each less than 0.1 mm long. In summary, features of lamellae within the zone of microcline support the conclusion that the occurrence of microcline is a byproduct of deformation rather than a function of the volatiles content of the crystallizing magma.

Crosshatched twinning in three rock samples (fig. 2.16) outside the diagonal zone of microcline occurs in a small part (0.03 mm^2) of one crystal in specimen 71, in two small crystals in specimen 49, and in many crystals of different size in specimen 29. Petrographic features indicate limited deformation in rock specimen 71, moderate deformation in specimen 49, and strong deformation in rock specimen 29. A second zone of microcline-bearing rocks may occur in the vicinity of rock specimen 29, but such a zone, if present, must be comparatively minor in extent. Additional minor zones of microcline are conceivable near rock specimens 71 and 49 (fig. 2.16).

The leucogranodiorite of Trail Creek has the most aplite and pegmatite dikes of any unit that intrudes the Elkhorn pluton. Therefore, the leucogranodiorite has high potential for a possible occurrence of microcline that can be related to a relatively high volatiles content. However, no crosshatched twinning occurs in any thin sections of the leucogranodiorite. Determinations of 2*V* for four crystals in three rock samples (table 2.10) range from 47° to 56°. Some exsolution lamellae that are several times as wide as those in undeformed orthoclase in the Elkhorn pluton provide the only strong suggestion of a magma with a higher volatiles content.

Aplite dikes are generally regarded as having crystallized from late-stage residual liquids of granitic magmas. Each of four aplite dikes from widely separated parts of the Elkhorn pluton has exsolution lamellae in potassium feldspar. Lamellae are approximately 0.001 mm or less in width. The presence of exsolution lamellae in four small dikes of aplite, each less than 15 cm wide, is consistent with an increased volatiles content in the aplitic melts. In contrast, no lamellae occur in the tonalite of Bald Mountain throughout the 31-km^2 Hunt Mountain salient and only rarely throughout the larger Monumental salient.

Microcline in two of the aplites, however, is not unequivocal evidence of increased volatiles because of the uncertainty of the magnitude of deformation effects. A small percentage of the microcline clearly is associated with healed microfractures that cross crystals of potassium feldspar. Narrow zones of delicate and incipient crosshatched twinning faithfully follow the microfractures. In addition, crystals of quartz with extinction positions that differ by 5° and, rarely, 6° occur in both aplite dikes and suggest that all microcline is related to deformation. A definitive study of the occurrence of microcline in aplite dikes of the Elkhorn pluton would require many additional specimens.

The Wallowa batholith (fig. 2.11) is composed of a more diverse array of granitic intrusions, including sizable bodies of aplite, than the Bald Mountain batholith and hence has greater possibilities for rocks in which microcline can be attributed to a volatile-rich magma. Microcline occurs in parts of each of the four major units of the batholith as well as in nearly all small units (not shown on fig. 2.11) of granodiorite and granite. Some microcline in the various intrusions may be unrelated to tectonism, but the evidence is inconclusive. Accordingly, the focus turns to the three largest known aplite bodies in northeastern Oregon. One of these aplites is within unit 1 of the Wallowa batholith, about 0.55 km north of Hobo Lake (fig. 2.11); this intrusion is quadrilateral in plan view, with longest and shortest boundaries about 125 m and 55 m, respectively. The second of the three aplites is in unit 3, about 1.75 km northeast of Traverse Lake. Estimated dimensions are 250 m long and as much as 125 m wide. The third aplite, in unit 4 and slightly northwest of Olive Lake, is irregular with an estimated maximum dimension of 300 m. Each of the three aplitic units contains less than 1.5 volume percent biotite; has an average grain size that ranges in most rock specimens from 0.5 to 1.0 mm; is composed of nearly equal amounts of quartz, plagioclase, and potassium feldspar; and contains about 77 weight percent SiO_2 (C.O. Ingamells, analyst, 1962, Pennsylvania State University).

Microcline is the only potassium feldspar in the aplite near Hobo Lake, whereas orthoclase constitutes at least 60 percent of the potassium feldspar in each of the other aplites. Petrographic characteristics of the aplite near Hobo Lake support the conclusion that the microcline crystallized from a volatile-rich magma. Of the three intrusions, the aplite near Hobo Lake has by far the strongest alteration of potassium feldspar to kaolinite, the most extensive distribution of flakes of muscovite (as much as 0.5 mm long) associated with plagioclase, and the coarsest exsolution lamellae (as much as about 0.025 mm wide). In addition, the aplite near Hobo Lake contains the only micropegmatite in thin sections of the three intrusions. Perhaps the relative abundance of needles of rutile in quartz is another indication of a high volatiles concentration. A crude correlation has been recognized in northeastern Oregon between the occurrence of rutile needles and the presence of hydrous alteration minerals. In any event, the aplite near Hobo Lake seemingly is an unequivocal example of a rock whose potassium feldspar is exclusively microcline and a product of crystallization of a magma with a high volatiles content. In contrast to their presence (locally) in the other two large aplites, neither annealed microfractures in potassium feldspar nor pressure points are present to suggest that any of the microcline is pressure induced.

MAJOR-ELEMENT COMPOSITIONS

Major-element compositions of 10 rock specimens from units of the Bald Mountain batholith are presented in table 2.16 to augment 11 analyses reported earlier (Taubeneck, 1957), which are not repeated here. The following discussion incorporates all analyses given earlier except that of the rhyolite porphyry dike (Taubeneck, 1957).

Most specimens of the norite of Badger Butte contain biotite and amphiboles that are regarded as postconsolidation. The specimen of the norite analyzed earlier (Taubeneck, 1957) contained only 1.9 volume percent pyroxene but 9 volume percent biotite and 22.7 volume percent amphibole. A new analysis (specimen 99, table 2.16) is a much closer approximation of the composition of the original magma, and the analyzed specimen contains 27 volume percent pyroxene, no biotite, and 3.2 volume percent amphibole. This analysis plots in the field of high-alumina basalt on both an alkali-silica diagram and an alumina-alkali diagram (Kuno, 1968), as does the single analysis of the norite of Willow Lake (Taubeneck, 1957).

The role of basaltic magmas in the petrogenesis of the granitic rocks of the Bald Mountain batholith cannot be assessed within the framework of available data, but the noritic components of the batholith suggest the involvement of magmas that had the composition of high-alumina basalt.

The major unit of the batholith ranges inward from mafic border rocks of quartz diorite and tonalite to a core of granodiorite. The chemical change inward, however, was not documented earlier (Taubeneck, 1957) in the absence of an analysis of a sample of the border rocks. Rock specimen B6 (table 2.16) is a representative border-rock sample collected about 40 m from the south contact of the batholith, whereas rock specimens 15 and 27 (table 2.16) are granodiorites from the interior of the compositionally zoned intrusion. Analyses recalculated to 100 percent H_2O-free show that silica ranges from about 61 weight percent in the border rock to about 69 weight percent in the core rocks. K_2O, the only other major oxide to increase inward, ranges from 0.54 weight percent in the border rock to about 2.1 weight percent in the core rocks.

The leucogranite of Dutch Creek (rock specimen R22) is the most felsic unit in the batholith. Its silica content is 77.92 weight percent after recalculating the analysis to 100 percent, in comparison to 76.4 weight percent silica in a 7.5-cm-wide aplite dike (Taubeneck, 1957) in the granodiorite of Anthony Lake. Normative quartz is 39.75 percent in the leucogranite but only 34.0 percent in the aplite. The differentiation index for the aplite, however, is 94.36, essentially the same as the value 94.22 for the leucogranite of Dutch Creek.

The analysis of the leucogranite of Dutch Creek closely approximates the compositions of the three large bodies of aplite (see previous section) in units 1, 3, and 4 of the Wallowa batholith (fig. 2.11). Silica contents for the aplite bodies are 77.15, 77.05, and 77.04 weight percent; normative quartz percentages are, respectively, 38.39, 36.71, and 37.26. Differentiation indexes are, respectively, 94.81, 94.42, and 92.95.

The leucogranite of Dutch Creek as well as the three large aplite intrusions indicate that the compositions of the last intrusive units within both the Bald Mountain and the Wallowa batholiths are those of minimum melts, irrespective of the manner in which these melts may have originated.

One important criterion for classification of granitic rocks involves the molecular ratio of $Al_2O_3/(CaO+Na_2O+K_2O)$, abbreviated A/CNK. Tonalites of the batholith are metaluminous, whereas most granodiorites and all granites are weakly peraluminous (A/CNK = 1.0 to 1.1). The values of A/CNK imply that the granitic

TABLE 2.16.—*Chemical analyses and corresponding norms and modes of selected specimens from the Bald Mountain batholith*

[Specimens B6, 15, and 27 analyzed at Pennsylvania State University in 1966 by C.O. Ingamells using wet chemical methods. Specimens R118, R121, R123, and R128 analyzed at Tohoku University, Japan, in 1973 by Ken-ichiro Aoki using wet chemical methods. Specimens 99, R22, and R125 analyzed in 1985 in laboratories of U.S. Geological Survey using X-ray fluorescence. LOI, loss on ignition; n.d., not determined; 0.0, <0.05; ---, not present]

Specimen No.[1]	99	B6	R125	15	27	R118	R121	R123	R128	R22
Major-element oxides (weight percent)										
SiO_2	51.3	60.70	62.0	68.59	68.79	74.51	73.06	72.95	74.39	77.0
Al_2O_3	19.1	17.83	16.3	15.23	16.09	12.71	13.44	13.76	12.81	12.4
TiO_2	1.07	.75	.63	.35	.32	.24	.27	.27	.23	.07
Fe_2O_3	3.32	2.11	.45	1.46	1.38	.26	.74	.52	.17	.39
FeO	5.18	3.31	4.62	1.95	1.60	2.13	1.80	1.93	1.91	.18
MnO	.15	.09	.09	.08	.07	.07	.06	.06	.09	<.02
MgO	5.91	2.98	3.10	1.71	1.26	.49	.67	.43	.39	.15
CaO	9.74	6.58	6.53	3.83	3.77	1.84	2.04	1.62	1.14	.78
SrO	n.d.	.09	n.d.	.05	.06	n.d.	n.d.	n.d.	n.d.	n.d.
BaO	n.d.	.05	n.d.	.10	.11	n.d.	n.d.	n.d.	n.d.	n.d.
Na_2O	3.28	4.01	3.34	3.82	3.89	3.01	3.22	3.74	3.67	2.90
K_2O	.17	.53	1.72	2.08	2.14	3.77	3.76	3.69	4.12	4.95
H_2O^+	n.d.	.40	n.d.	.04	.50	.58	.63	.51	.58	n.d.
H_2O^-	n.d.	.13	n.d.	.19	.00	.09	.10	.08	.09	n.d.
P_2O_5	.31	.15	.20	.13	.07	.06	.07	.04	.05	<.05
LOI	.42	n.d.	.51	n.d.	n.d.	n.d.	n.d.	n.d.	n.d.	.44
Total	99.95	99.71	99.49	99.61	100.05	99.76	99.86	99.60	99.64	99.33
CIPW norms (weight percent, water free)										
Quartz	2.40	16.46	16.50	27.35	27.75	36.85	33.99	32.13	33.30	39.75
Orthoclase	1.00	3.16	10.16	12.39	12.72	22.48	22.42	22.02	24.60	29.60
Albite	27.91	34.26	24.69	32.57	33.12	25.70	27.48	31.96	31.38	24.86
Anorthite	27.37	29.36	28.58	18.29	18.36	8.82	9.75	7.85	5.38	3.92
Corundum	—	—	—	.04	.69	.48	.53	.77	.36	.81
Wollastonite	7.36	1.09	5.57	—	—	—	—	—	—	—
Enstatite	12.15	7.49	6.30	4.29	3.16	1.23	1.68	1.08	.98	.38
Ferrosilite	4.29	3.29	5.61	1.96	1.41	3.46	2.38	2.81	3.19	.01
Magnetite	4.82	3.09	0.95	2.13	2.01	.38	1.08	.76	.25	.53
Ilmenite	1.94	1.44	1.21	.67	.61	.46	.52	.52	.44	.14
Apatite	.74	.36	.43	.31	.17	.14	.17	.10	.12	—
Modes (volume percent) [0.0, <0.05]										
Quartz	0.2	15.2	17.8	26.5	27.6	31.1	32.9	32.8	31.4	38.4
Potassium feldspar	—	.2	1.6	8.5	8.1	20.6	23.4	23.6	28.4	29.1
Plagioclase	67.8	65.8	50.4	53.9	53.8	42.4	38.0	37.2	36.0	30.5
Biotite	—	5.6	17.6	7.4	7.3	5.7	5.7	4.3	4.1	1.6
Muscovite	—	—	—	—	—	—	—	—	—	.4
Hornblende	3.2	12.5	8.4	3.1	2.1	.2	—	—	—	—
Augite	9.3	.1	3.7	—	—	—	—	—	—	—
Hypersthene	17.7	—	.3	—	—	—	—	.2	—	—
Cummingtonite	—	—	—	—	—	—	—	1.8	—	—
Opaque oxides	1.4	.4	.1	.5	.9	—	.0	.0	—	.0
Nonopaque accessory minerals	.4	.2	.1	.1	.2	.0	.0	.1	.1	.0

[1]Specimens are from the following units:

99	Norite of Badger Butte	R118	Granodiorite of Beaver Meadow
B6	Tonalite of Bald Mountain	R121	Granite of Anthony Butte
R125	Quartz diorite of Wolf Creek	R123	Granite of Anthony Butte
15	Granodiorite of Anthony Lake	R128	Granite of Anthony Butte
27	Granodiorite of Anthony Lake	R22	Leucogranite of Dutch Creek

rocks of the batholith are I-type in the classification of Chappell and White (1974). I-type geochemistry is verified by all analyses' plotting in the Na_2O field on a diagram of Na_2O versus K_2O (White and Chappell, 1983).

The alkali-lime index of Peacock (1931) is the silica value at which curves on variation diagrams intersect for CaO and total alkalies (Na_2O+K_2O). Peacock arbitrarily distinguished calc-alkaline rocks as those with an index between 56 and 61, and calcic rocks as those with an index greater than 61. The alkali-lime index for rocks of the Bald Mountain batholith is about 63.5 in comparison to about 62 for the Mount Stuart batholith in Washington (Erikson, 1977), about 63 for widely scattered granitic rocks in the Klamath Mountains of Oregon and California (Hotz, 1971), about 61.5 for the Wooley Creek batholith in northern California (Barnes, 1983), about 63 for the western Sierra Nevada (Ross, 1972), and about 64.5 for the southern California batholith (Larsen, 1948). By the chemical classification of Peacock, nearly all granitic suites in the Western United States west of the quartz diorite line (Moore, 1959) are calcic rather than calc-alkaline. Moreover, many tholeiitic suites, whether on continental margins or in oceanic islands, are calc-alkaline by the alkali-lime index. The Peacock index is useful in the comparison of regional data but does not define calc-alkaline suites as this term has been increasingly used since the work of Wager and Deer (1939) on the Skaergaard intrusion. In contemporary petrogenetic studies, the (Na_2O+K_2O)-FeO-MgO (AFM) plot has become widely adopted as a discriminant diagram to identify calc-alkaline trends.

An AFM diagram (fig. 2.17) for rocks of the Bald Mountain batholith has the typical calc-alkaline trend of little or no iron enrichment for intermediate compositions. Also, a Na_2O-K_2O-CaO diagram (Taubeneck, 1957, fig. 18) indicates that the rocks have a trend similar to the common calc-alkaline trend found by Nockolds and Allen (1953).

The calc-alkaline trend also is clearly distinguished in a diagram showing the rate of iron enrichment relative to silica (fig. 2.18). Consistent with calc-alkaline suites, rocks of the Bald Mountain batholith show essentially no iron enrichment for compositions with less than 70 weight percent SiO_2. However, marked enrichment occurs at higher percentages of silica because the relative percent decrease in MgO as it approaches zero on the abscissa of a Harker diagram progressively exceeds any corresponding absolute decrease in FeO* (total iron as FeO). The sharp increase shown in figure 2.18 in the FeO*/(FeO*+MgO) ratio for compositions with more than 70 percent SiO_2 is graphically visualized from general Harker variation diagrams for contents of FeO and MgO throughout the spectrum of granitic rocks.

Relative iron enrichment in late calc-alkaline plutonic units is responsible for many analyses of granites plotting in the tholeiitic field of Miyashiro (1974). For example, at least 32 of the 497 chemical analyses of batholithic rock samples of southern California (Baird and Miesch, 1984) are tholeiitic on Miyashiro's diagram. Most of these 32 rock samples have more than 74 weight percent SiO_2, and many are undoubtedly leucogranites or alaskites.

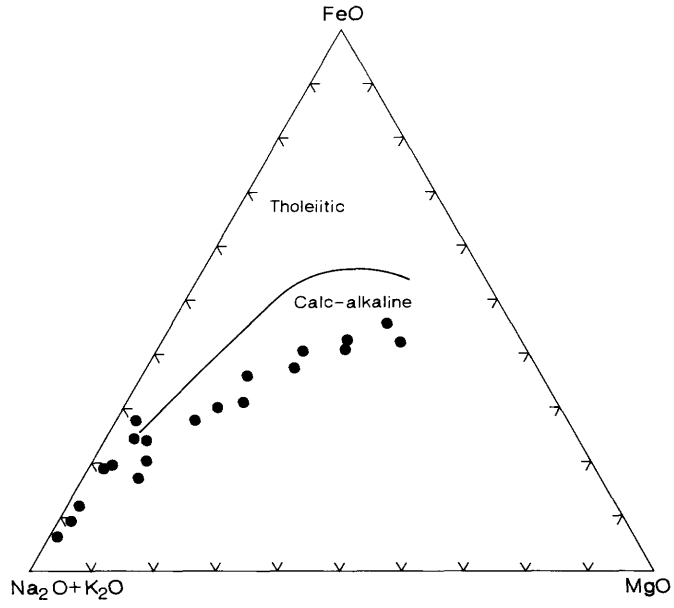

FIGURE 2.17.—Alkali-iron-magnesium (AFM) ternary diagram for rocks of Bald Mountain batholith. Boundary between tholeiitic and calc-alkaline fields is from Kuno (1968).

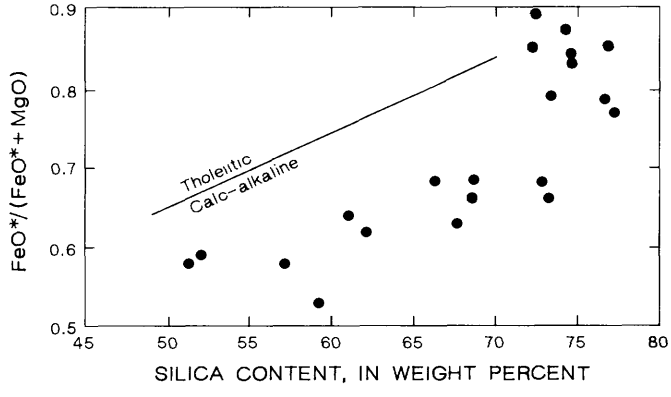

FIGURE 2.18.—Graph showing rate of iron enrichment, as FeO*/(FeO*+MgO), with increasing silica for rocks of Bald Mountain batholith. FeO* is total iron as FeO. Boundary between tholeiitic and calc-alkaline fields is modified from McBirney (1984, p. 307) by extending the termination of the original line from about 63 percent SiO_2 to 70 percent SiO_2.

CONCLUSIONS

The principal conclusions of this study are as follows:

(1) All units of the Bald Mountain batholith except some small felsic bodies mostly south of lat 45° N. have the overall features of mesozonal (Buddington, 1959) plutons. Contacts with country rocks are mostly concordant in the broad sense with much of the discordance on the scale of outcrops. Relations with country rocks along the contact of the batholith range from relatively simple in the south to relatively complex in the north.

(2) The batholith is characterized by an extensive metamorphic aureole that includes widespread pyroxene hornfels-facies rocks. Salients of country rock that project far into the batholith are intensely deformed and commonly gneissic; they include the Archean gneiss unit of Lindgren (1901). Intense contact metamorphism of metagabbro produced a rock with gneissic layering that resembles some well-bedded metasedimentary rocks. The relative grain size of recrystallized quartz in ribbon chert near the batholith is a good approximation of the intensity of thermal metamorphism.

(3) The general concordance of structural trends in country rocks adjacent to the contact of the batholith and especially in dismembered screens between units of the batholith is strong evidence for forceful emplacement. Much wall rock yielded by plastic flow. Planar structure and deformation textures in granitic rocks are more pronounced in the northern one-fourth of the batholith than elsewhere. Some tonalite in the north is gneissoid; the granite of Anthony Butte locally is almost gneissic. Structural style in the north is characterized by dismembered screens between intrusive units. The Elkhorn pluton is distinctive among the zoned intrusions of tonalite and granodiorite composition in northeastern Oregon in the occurrence of planar structure and inclusions of country rocks in the granodiorite core. The major structural feature within the Elkhorn pluton is an intraplutonic contact where core magma, mostly of granodioritic composition, intruded outer solidified tonalite. The intraplutonic contact provided the structural control for the emplacement of leucogranodiorite as elongated intrusions.

(4) Augite was the dominant early mafic mineral to crystallize throughout much of the tonalite and some of the granodiorite of the Elkhorn pluton. The small volume percent of calcic core in oscillatory-zoned plagioclase indicates that the granitic rocks crystallized from a melt that contained only a comparatively minor amount of solid constituents. An interlude is a concentration of one or several different mafic minerals of small size in a distinct layer of plagioclase between consecutive oscillations in oscillatory-zoned plagioclase. The larger interludes are characterized by mottled plagioclase; similar mottling in cores of plagioclase cannot be cited as an unequivocal petrographic criterion for a restite origin of plagioclase cores in the Elkhorn pluton or elsewhere.

(5) Granitic rocks in the Elkhorn Mountains with reddish-brown to red biotite and minor or no iron oxide crystallized from magmas that assimilated graphite-bearing metasedimentary rocks. These rocks are characterized by a much lower Fe_2O_3 /FeO ratio than the normal I-type granitic rocks of northeastern Oregon.

(6) The granodiorite of Beaver Meadow is notable for a reaction relation between orthopyroxene, cummingtonite, hornblende, and biotite.

(7) Much of the batholith crystallized from hot and relatively dry magmas as judged by early crystallization of pyroxene and by aureole rocks that include pyroxene hornfels facies. The general scarcity of pegmatite and aplite dikes in the Elkhorn pluton is consistent with the crystallization of a relatively dry magma, as is the paucity of interstitial zeolites in the tonalite and granodiorite.

(8) The zone of microcline that extends for 19 km across the Elkhorn pluton is attributed to deformation during final crystallization of the magma rather than to increased volatiles content.

(9) Early intrusive units in both the Bald Mountain batholith and the nearby Wallowa batholith are very similar norites with the composition of high-alumina basalt. However, compositionally zoned plutons of tonalite and granodiorite of the two batholiths differ in the decidedly higher content of quartz in rocks of the Bald Mountain batholith. The compositions of the last intrusive units of the two batholiths are those of minimum melts.

(10) Rocks of the Bald Mountain batholith show an exceptionally well defined calc-alkaline trend on an AFM diagram. The Peacock index does not identify the calc-alkaline trend of most granitic suites west of the quartz diorite line in Washington, Oregon, and California.

REFERENCES CITED

Armstrong, R.E., Taubeneck, W.H., Hales, P.O., 1977, Rb-Sr and K-Ar geochronometry of Mesozoic granitic rocks and their Sr isotopic composition, Oregon, Washington, and Idaho: Geological Society of America Bulletin, v. 88, p. 397–411.

Baird, A.K., and Miesch, A.T., 1984, Batholithic rocks of southern California—A model for the petrochemical nature of their source materials: U.S. Geological Survey Professional Paper 1284, 42 p.

Balk, Robert, 1937, Structural behavior of igneous rocks: Geological Society of America Memoir 5, 177 p.

Barnes, C.G., 1983, Petrology and upward zonation of the Wooley Creek batholith, Klamath Mountains, California: Journal of Petrology, v. 24, p. 495–537.

Bateman, P.C., 1983, A summary of critical relations in the central part of the Sierra Nevada batholith, California, U.S.A., *in* Roddick, J.A., ed., Circum-Pacific plutonic terranes: Geological Society of America Memoir 159, p. 241–254.

Becraft, G.B., Pinckney, D.M., and Rosenblum, Sam, 1963, Geology and mineral deposits of the Jefferson City quadrangle, Jefferson and Lewis and Clark Counties, Montana: U.S. Geological Survey Professional Paper 428, 101 p.

Brooks, H.C., Ferns, M.L., Coward, R.I., Paul, E.K., and Nunlist, M., 1982, Geology and gold deposits of the Bourne quadrangle, Baker and Grant Counties, Oregon: Oregon Department of Geology and Mineral Industries, Geologic Map Series GMS–19 scale 1:24,000.

Buddington, A.F., 1959, Granite emplacement with special reference to North America: Geological Society of America Bulletin, v. 70, p. 671–747.

Chappell, B.W., and White, A.J.R., 1974, Two contrasting granite types: Pacific Geology, v. 8, p. 173–174.

Chappell, B.W., White, A.J.R., and Wyborn D., 1987, The importance of residual source material (restite) in granite petrogenesis: Journal of Petrology, v. 28, p. 1111–1138.

Chayes, Felix, 1949, A simple point counter for thin-section analysis: American Mineralogist, v. 34, p. 1–11.

Didier, Jean, 1987, Contribution of enclave studies to the understanding of origin and evolution of granitic magmas: Geologische Rundschau, v. 76, p. 41–50.

Dowty, Eric, 1980, Synneusis reconsidered: Contributions to Mineralogy and Petrology, v. 74, p. 75–84.

Elfrink, N.M., 1987, Geology of the east central Desolation Butte quadrangle, Grant County, Oregon: Corvallis, Oregon State University, M.S. thesis, 123 p.

Emeleus, C.H., and Smith, J.V., 1959, The alkali feldspars—Sanidine and orthoclase perthites from the Slieve Gullion area, northern Ireland: American Mineralogist, v. 44, p. 1187–1209.

Emerson, D.O., 1964, Modal variations within granitic outcrops: American Mineralogist, v. 49, p. 1224–1233.

Erikson, E.H., 1969, Petrology of the composite Snoqualmie batholith, central Cascade Mountains, Washington: Geological Society of America Bulletin, v. 80, p. 2213–2236.

———1977, Petrology and petrogenesis of the Mount Stuart batholith—Plutonic equivalent of the high-alumina basalt association: Contributions to Mineralogy and Petrology, v. 60, p. 183–207.

Evans, B.W., 1977, Metamorphism of alpine peridotite and serpentinite: Annual Reviews of Earth and Planetary Sciences, v. 5, p. 397–447.

Evans, J.G., 1986, Geologic map of the North Fork John Day River Roadless Area, Grant County, Oregon: U.S. Geological Survey Miscellaneous Field Studies Map MF–1581–C, scale 1:48,000.

Fawcett, J.J., and Yoder, H.S., 1966, Phase relationships of chlorite in the system MgO-Al_2O_3-SiO_2-H_2O: American Mineralogist, v. 51, p. 353–380.

Ferns, M.L., Brooks, H.C., Avery, D.G., and Blome, C.D., 1987, Geology and mineral resources map of the Elkhorn Peak quadrangle, Baker County, Oregon: Oregon Department of Geology and Mineral Industries Geologic Map Series GMS–41, scale 1:24,000.

Ferns, M.L., Brooks, H.C., Doucette, John, 1982, Geology and mineral resources map of the Mt. Ireland quadrangle, Baker and Grant Counties, Oregon: Oregon Department of Geology and Mineral Industries Geologic Map Series GMS–22, scale, 1:24,000.

Flood, R.H., and Shaw, S.E., 1975, A cordierite-bearing granite suite from the New England batholith, N.S.W., Australia: Contributions to Mineralogy and Petrology, v. 52, p. 157–164.

Frost, B.R., 1976, Limits to the assemblage forsterite-anorthite as inferred from peridotite hornfelses, Icicle Creek, Washington: American Mineralogist, v. 61, p. 732–750.

Gilluly, James, 1937, Geology and mineral resources of the Baker quadrangle, Oregon: U.S. Geological Survey Bulletin 879, 119 p.

Grout, F.F., and Balk, Robert, 1934, Internal structures in the Boulder batholith: Geological Society of America Bulletin, v. 45, p. 877–896.

Hewett, D.F., 1931, Zonal relations of the lodes of the Sumpter quadrangle: American Institute of Mining and Metallurgical Engineers Transactions, p. 305–346.

Hine, R., Williams, I.S., Chappell, B.W., and White, A.J.R., 1978, Contrasts between I- and S-type granitoids of the Kosciusko batholith: Journal of Geological Society of Australia, v. 25, p. 219–234.

Hotz, P.E., 1971, Plutonic rocks of the Klamath Mountains, California and Oregon: U.S. Geological Survey Professional Paper 684–B, 20 p.

Hutchison, W.W., 1970, Metamorphic framework and plutonic styles in the Prince Rupert region of the central Coast Mountains, British Columbia: Canadian Journal of Earth Sciences, v. 7, p. 376–405.

Kuno, Hisashi, 1968, Differentiation of basalt magmas, *in* Hess, H.H., and Poldervaart, Arie, eds., Basalts, v. 2: New York, John Wiley and Sons, p. 623–688.

Larsen, E.S., Jr., 1948, Batholith and associated rocks of Corona, Elsinore, and San Luis Rey quadrangles, southern California: Geological Society of America Memoir 29, 182 p.

Lindgren, Waldemar, 1901, The gold belt of the Blue Mountains of Oregon: U.S. Geological Survey Twenty-Second Annual Report, pt. 2, p. 551–776.

MacGregor, A.G., 1931, Clouded feldspars and thermal metamorphism: Mineralogical Magazine, v. 22, p. 524–538.

McBirney, A.R., 1984, Igneous petrology: San Francisco, Freeman, Cooper and Co., 509 p.

Miyashiro, Akiho, 1974, Volcanic rock series in island arcs and active continental margins: American Journal of Science, v. 274, p. 321–355.

Moore, J.G., 1959, The quartz diorite boundary line in the Western United States: Journal of Geology, v. 67, p. 198–210.

Muir, I.D., 1953, Quartzite xenoliths from the Ballachulish Granodiorite: Geological Magazine, v. 40, p. 409–427.

Nockolds, S.R., and Allen, R., 1953, The geochemistry of some igneous rock series: Geochimica et Cosmochimica Acta, v. 4, p. 105–142.

Noyes, H.J., Wones, D.R., and Frey, F.A., 1983, A tale of two plutons—Petrographic and mineralogic constraints on the petrogenesis of the Red Lake and Eagle Peak plutons, central Sierra Nevada, California: Journal of Geology, v. 91, p. 353–377.

Pabst, Adolf, 1928, Observations on inclusions in the granitic rocks of the Sierra Nevada: University of California Publications in Geological Sciences, v. 17, p. 325–368.

Pardee, J.T., 1941, Preliminary geologic map of the Sumpter quadrangle, Oregon: State Department of Geology and Mineral Industries, scale 1:96,000.

Pardee, J.T., and Hewett, D.F., 1914, Geology and mineral resources of the Sumpter quadrangle, Oregon: Oregon Bureau of Mines and Geology, Mineral Resources of Oregon, v. 1, no. 6, p. 3–128.

Peacock, M.A., 1931, Classification of igneous rock series: Journal of Geology, v. 39, p. 54–67.

Pitcher, W.S., Read, H.H., Cheesman, R.L., Pande, I.C., and Tozer, C.F., 1959, The main Donegal granite: Quarterly Journal of Geological Society of London, v. 114, p. 259–305.

Pitcher, W.S., and Sinha, R.C., 1957, The petrochemistry of the Ardara aureole: Quarterly Journal of Geological Society of London, v. 113, p. 393–408.

Poldervaart, Arie, and Gilkey, A.K., 1954, On clouded plagioclase: American Mineralogist, v. 39, p. 75–91.

Presnall, D.C., and Bateman, P.C., 1973, Fusion relationships in the system $NaAlSi_3O_8$-$CaAl_2Si_2O_8$-$KAlSi_3O_8$-SiO_2-H_2O and generation of granitic magmas in the Sierra Nevada batholith: Geological Society of America Bulletin, v. 84, p. 3181–3202.

Ramberg, Hans, 1981, Gravity, deformation, and the Earth's crust: London, Academic Press, 452 p.

Ribbe, P.H., and Smith, J.V., 1966, X-ray emission microanalysis of rock-forming minerals, Pt. 4, Plagioclase feldspars: Journal of Geology, v. 74, p. 217–233.

Ross, D.C., 1972, Petrographic and chemical reconnaissance study of some granitic and gneissic rocks near the San Andreas fault from Bodega Head to Cajon Pass, California: U.S. Geological Survey Professional Paper 698, 92 p.

Sams, D.B., and Saleeby, J.B., 1988, Geology and petrotectonic significance of crystalline rocks of the southernmost Sierra Nevada, California, *in* Ernst, W.G., ed., Metamorphism and crustal evolution of the Western United States (Rubey Volume VII): Englewood Cliffs, N.J., Prentice-Hall, p. 865–893.

Shimizu, Masaaki, 1986, The Tokuwa batholith, central Japan: The University Museum, University of Tokyo, Bulletin No. 28, 143 p.

Silberling, N.J., Jones, D.L., Blake, M.C., Jr., and Howell, D.G., 1984, Lithotectonic terrane map of the western conterminous United States, Pt. C *of* Silberling, N.J., and Jones, D.L., eds., Lithotectonic terrane maps of the North American Cordillera: U.S. Geological Survey Open-File Report 84–523, 43 p.

Smith, J.V., 1965, X-ray emission microanalysis of rock-forming minerals, Pt. 1, Experimental techniques: Journal of Geology, v. 73, p. 830–864.

Streckeisen, A.L., 1973, Plutonic rocks—Classification and nomenclature recommended by the IUGS subcommission on the systematics of igneous rocks: Geotimes, v. 18, p. 26–30.

Taubeneck, W.H., 1957, Geology of the Elkhorn Mountains, northeastern Oregon—Bald Mountain batholith: Geological Society of America Bulletin, v. 68, p. 181–238.

———1960, Emplacement of granitic magmas in northeastern Oregon: Geological Society of America Bulletin, v. 71, p. 2026.

———1964, Cornucopia stock, Wallowa Mountains, northeastern Oregon: Geological Society of America Bulletin, v. 75, p. 1093–1116.

———1967, Petrology of the Cornucopia tonalite unit, Cornucopia stock, Wallowa Mountains, northeastern Oregon: Geological Society of America Special Paper 91, 56 p.

———1987, The Wallowa Mountains, northeast Oregon, *in* Hill, M.L., ed., Cordilleran Section of the Geological Society of America Centennial Field Guide, v. 1, p. 327–332.

Taubeneck, W.H., and Poldervaart, Arie, 1960, Geology of the Elkhorn Mountains, northeastern Oregon—Pt. 2, Willow Lake intrusion: Geological Society of America Bulletin, v. 71, p. 1295–1322.

Trusheim, F., 1960, Mechanism of salt migration in northern Germany: American Association of Petroleum Geologists Bulletin, v. 44, p. 1519–1540.

Vance, J.A., 1969, On synneusis: Contributions to Mineralogy and Petrology, v. 24, p. 7–29.

Wager, L.R., and Deer, W.A., 1939, Geological investigations in East Greenland, Pt. III, The petrology of the Skaergaard intrusion, Kangerdlugssuaq, East Greenland: Meddelelser om Grønland, v. 105, no. 4, 352 p.

Walker, G.W., 1973, Reconnaissance geologic map of the Pendleton quadrangle, Oregon and Washington: U.S. Geological Survey Miscellaneous Geologic Investigations Map 1–727, scale 1:250,000.

Walker, N.W., and Mattinson, J.M., 1980, The Canyon Mountain complex, Oregon: U-Pb ages of zircons and possible tectonic correlations: Geological Society of America Abstracts with Programs, v. 12, no. 7, p. 544.

Whalen, J.B., and Chappell, B.W., 1988, Opaque mineralogy and mafic mineral chemistry of I- and S-type granites of the Lachlan fold belt, southeast Australia: American Mineralogist, v. 73, p. 281–296.

White, A.J.R., and Chappell, B.W., 1977, Ultrametamorphism and granitoid genesis: Tectonophysics, v. 43, p. 7–22.

———1983, Granitoid types and their distribution in the Lachlan fold belt, southeastern Australia, *in* Roddick, J.A., ed., Circum-Pacific plutonic terranes: Geological Society of America Memoir 159, p. 21–34.

———1988, Some supracrustal (S-type) granites of the Lachlan fold belt: Transactions of Royal Society of Edinburgh, Earth Sciences, v. 79, p. 169–181.

3. PETROLOGY OF PRE-TERTIARY IGNEOUS ROCKS IN THE BLUE MOUNTAINS REGION OF OREGON, IDAHO, AND WASHINGTON: IMPLICATIONS FOR THE GEOLOGIC EVOLUTION OF A COMPLEX ISLAND ARC

By TRACY L. VALLIER

CONTENTS

	Page
Abstract	125
Introduction	126
Acknowledgments	126
Methods	127
Field and laboratory methods	127
Rock classification and data presentation	130
Interpretations of petrogenesis and tectonic setting	131
Geologic framework	132
Baker terrane	138
Grindstone terrane	138
Wallowa terrane	138
Olds Ferry terrane	139
Izee terrane	139
Age and field characteristics of pre-Tertiary igneous rocks in the Blue Mountains region	140
Late Paleozoic and Triassic igneous rocks of the Baker terrane	140
Plutonic rocks of the Baker terrane	141
Canyon Mountain Complex	141
Other plutonic rocks of the Baker terrane	143
Petrogenesis of plutonic rocks of the Baker terrane	145
Volcanic rocks of the Baker terrane	145
Late Paleozoic and Triassic igneous rocks of the Wallowa terrane	149
Plutonic and associated hypabyssal rocks of the Wallowa terrane	150
Sparta complex	150
Oxbow Complex	161
Cougar Creek Complex	163
Wolf Creek-Deep Creek and Imnaha plutonic rocks	165
Sheep Creek plutonic rocks	166
Plutonic rocks of the southern Seven Devils Mountains	166
Plutonic rocks of the Salmon River canyon	167
Plutonic rocks associated with the Blue Mountains anticline	167
Wildhorse River dike	167
Petrogenesis of plutonic rocks of the Wallowa terrane	168
Volcanic (flow) and associated hypabyssal intrusive rocks of the Wallowa terrane	170
Late Paleozoic and Triassic igneous rocks of the Wallowa terrane—Continued	
Volcanic (flow) and associated hypabyssal intrusive rocks of the Wallowa terrane—Continued	
Permian volcanic (flow) and associated hypabyssal intrusive rocks	170
Triassic volcanic (flow) and associated hypabyssal intrusive rocks	175
Petrogenesis of Permian and Triassic volcanic (flow) and associated hypabyssal intrusive rocks	178
Triassic and Early Jurassic(?) igneous rocks of the Olds Ferry terrane	180
Plutonic rocks	181
Volcanic (flow) and associated hypabyssal intrusive rocks	183
Petrogenesis of igneous rocks of the Olds Ferry terrane	185
Jurassic igneous rocks associated with the Coon Hollow Formation of the Wallowa terrane	186
Description of the igneous rocks	186
Petrogenesis	187
Jurassic to Cretaceous plutonic rocks of Blue Mountains region	188
Description of the plutonic rocks	190
Petrogenesis of the Jurassic to Cretaceous plutonic rocks	193
Tectonic implications of petrologic and other data	193
Tectonic setting of igneous rocks of the Baker terrane	194
Tectonic setting of igneous rocks of the Wallowa terrane	194
Tectonic setting of igneous rocks of the Olds Ferry terrane	195
Tectonic setting of Jurassic to Cretaceous igneous rocks	196
Plate tectonic evolution of Blue Mountains island arc	197
Paleomagnetic and faunal evidence for latitudinal movement	197
Plate movements and terrane tectonism	198
Seven-stage model for plate tectonic evolution of Blue Mountains island arc	199
References cited	204

ABSTRACT

Pre-Tertiary rocks in the Blue Mountains region of Oregon, Idaho, and Washington constitute a complex multi-generation intraoceanic volcanic arc, the Blue Mountains island arc, consisting of five

terranes: the Baker, Grindstone, Izee, Olds Ferry, and Wallowa terranes. The known igneous history of the Blue Mountains island arc extends from Pennsylvanian(?) to Early Cretaceous time. The oldest isotopically dated igneous rocks, Pennsylvanian(?) in age, are exposed in the Wallowa and Baker terranes. The largest volumes of igneous rocks formed in the Early Permian in the Wallowa and Baker terranes, in the Middle and Late Triassic in the Wallowa and Baker terranes, in the Late Triassic and Early Jurassic in the Olds Ferry terrane, and in the Late Jurassic and Early Cretaceous in all terranes except the Grindstone terrane.

Chemical data are used to assign the igneous rocks to tholeiitic- and calc-alkaline-magma series and to interpret plate tectonic settings, magmatic-source rocks, and processes of melting, magma mixing, assimilation of older rocks, differentiation, and metamorphism. Erupted in an intraoceanic-arc setting, almost all late Paleozoic and Triassic igneous rocks of the Blue Mountains island arc are tholeiitic. The Jurassic to Cretaceous intrusive rocks are calc-alkaline. The change from tholeiitic- to calc-alkaline-magma series had occurred by the Middle Jurassic.

The Baker terrane is petrologically and tectonically distinct. The Paleozoic and Triassic igneous rocks are tholeiitic, alkaline, and calc-alkaline, and crystallized in a large variety of oceanic tectonic settings (spreading ridge, ocean island or seamount, and volcanic arc). Most occur in fault-bounded blocks and as blocks or knockers in serpentinite-matrix melange. Many probably were accreted along the inner wall of one or more trenches and subsequently were deformed and tectonically shuffled extensively within the fore-arc regions of the Blue Mountains island arc.

Igneous rocks of the Wallowa terrane are related to magmatic-axis (volcanic-front) activity of an island arc. Most of the Permian and Triassic rocks belong to the island-arc tholeiite magma series. Siliceous flows are dominant volcanic rocks in the Permian sequence, whereas the Triassic flows are mafic, intermediate, and siliceous. Calc-alkaline hypabyssal rocks intrude the Middle and Upper Jurassic Coon Hollow Formation. The plutonic and volcanic (flow) rocks of the Olds Ferry terrane are mostly tholeiitic. The flow rocks are chemically similar to tholeiitic rocks of the Tonga and Kermadec island arcs of the southwest Pacific, except for higher concentrations of K-group elements (K, Rb, Cs, Ba, and Sr) in rocks from the Olds Ferry terrane. Calc-alkaline plutonic bodies of Late Jurassic and Early Cretaceous age occur in all terranes of the Blue Mountains island arc except the Grindstone. Some Jurassic to Cretaceous plutonic bodies were emplaced along terrane boundaries.

Paleomagnetic data indicate that the Wallowa terrane and, by inference, the other terranes in the Blue Mountains island arc were always in the northern hemisphere. Southward movement occurred in the Late Permian and Early Triassic and northward movement occurred in the Late Triassic to Late Jurassic. Final accretion of the arc to the North American craton occurred in the Early Cretaceous. The volumes and compositions of igneous rocks reflect major changes in plate motions.

Characteristics of the igneous rocks are strongly related to tectonic setting. Changes in tectonic setting and associated igneous rock characteristics probably occurred in the (1) late Paleozoic, especially during voluminous Early Permian siliceous volcanism, (2) Late Permian to Early Triassic during relative igneous quiescence and probable southward transport of the island arc, (3) Middle and early Late Triassic during igneous activity in the Wallowa and Baker(?) terranes, (4) Late Triassic through the Early Jurassic during igneous activity in the Olds Ferry terrane, (5) Middle and Late Jurassic during relative quiescence and northward transport of the island arc, (6) Late Jurassic to Early Cretaceous when calc-alkaline plutonic bodies intruded at least four terranes, and (7) mid- and Late Cretaceous during accretion of the Blue Mountains island arc to North America.

INTRODUCTION

The origins of metamorphosed pre-Tertiary plutonic and volcanic rocks in the Blue Mountains region (fig. 3.1) of eastern Oregon, western Idaho, and southeastern Washington have long puzzled and intrigued geologists. The close affinity of these rocks to a volcanic arc was first suggested by Hamilton (1963), who compared the chemistry of volcanic rocks from the Seven Devils Mountains and closely adjacent areas with those from the Aleutian island arc of Alaska. Most geologists who have worked in the Blue Mountains region now agree that it contains fragments of a pre-Tertiary island arc. In this chapter I refer to that arc as the Blue Mountains island arc. In general, all late Paleozoic and Triassic igneous rocks of the Blue Mountains island arc either formed directly within the arc or were accreted to it along subduction zones. Interpretation of the plate tectonic setting of Jurassic to Cretaceous plutonic rocks is less constrained, and I refer to those rocks within the broader context of the Blue Mountains region. The term "Blue Mountains region," as used in this chapter, includes parts of the Blue Mountains, Columbia Intermontane, Deschutes-Umatilla Plateau, and Joseph Upland provinces (fig. 3.2; Walker, 1990).

Volcanic arcs may lie within an ocean basin (intraoceanic island arc), be built on a continent (continental arc), or be a combination of the two. Studies of modern volcanic arcs show that there are significant petrologic and tectonic differences both within and between arcs. Some of the factors contributing to the differences include (1) age of the arc (maturity), (2) characteristics of subducting lithosphere, including age and evolution, (3) physical and chemical characteristics of the mantle and crust in which the magmas form and through which they ascend, (4) fractionation processes, (5) relative movements of the converging plates, (6) subduction angles, and (7) processes such as collisions of volcanic arcs with oceanic spreading ridges, oceanic plateaus, continents, and other arcs.

In this chapter, I (1) describe the pre-Tertiary igneous rocks of the Blue Mountains region using field, petrographic, and chemical data, (2) interpret the petrology of the igneous rocks, (3) discuss the implications of the petrology for specific tectonic settings within the Blue Mountains island arc, and (4) propose a plate tectonic model for the arc's geologic evolution on the basis of igneous petrology, rock ages, and paleomagnetic data.

ACKNOWLEDGMENTS

I am indebted to many scientific colleagues for help with this and associated studies. I particularly appre-

ciate the intellectual stimulation and friendship of H.C. Brooks, D.L. White, and D.W. Scholl, who have been patient mentors and associates. I thank W.H. Taubeneck for introducing me to many of the geologic problems in the Blue Mountains region and for his continued encouragement. I thank E.M. Bishop, H.C. Brooks, M.L. Ferns, and N.W. Walker for providing thoughtful reviews of an early draft of this manuscript. I am very grateful to the chemists within the U.S. Geological Survey for their painstaking efforts of providing high-quality data. I thank Jim Pearl and Leda Beth Gray for providing previously unreported radiometric ages using K-Ar methods. Without the willing and capable assistance of my wife and field companion, Trudy Vallier, I would not have completed the research for this chapter.

METHODS

FIELD AND LABORATORY METHODS

Beginning in 1963, I spent several complete summer field seasons and parts of many others in the Blue Mountains region, mostly in the Snake River canyon and adjacent areas of the Wallowa and Seven Devils Mountains (figs. 3.1–3.3). Thin sections of more than 300 igneous rocks collected throughout the region were studied to select appropriate samples for chemical analyses. Vallier (1967a) and Vallier and Batiza (1978) gave petrographic descriptions of some of the rocks that were chemically analyzed for this chapter.

The chemical data presented here are results of analyses completed during the 1967–1987 interval at

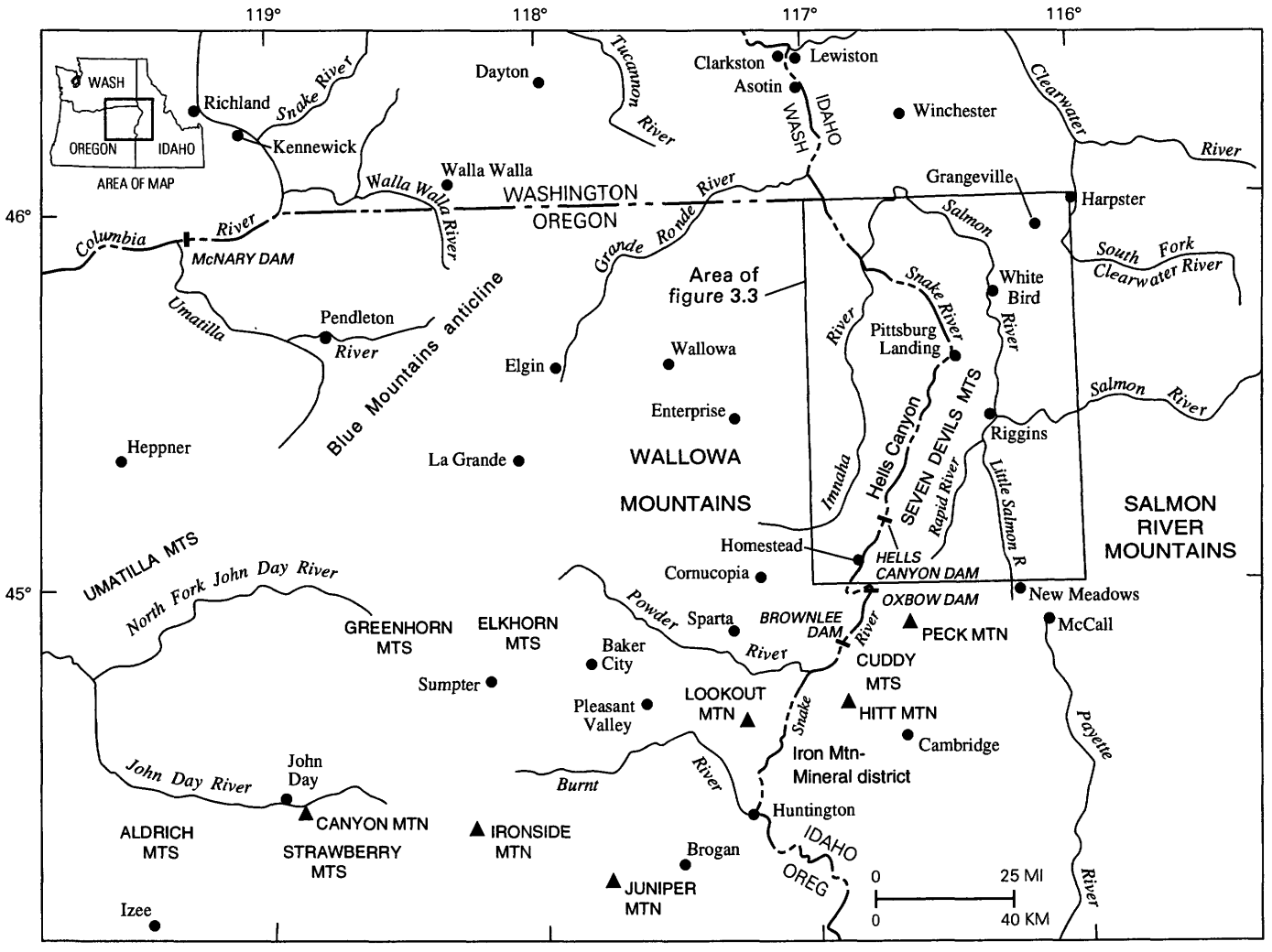

FIGURE 3.1.—Map of Blue Mountains region of Oregon, Idaho, and Washington showing major features mentioned in text. For more detail refer to figure 3.3 and to quadrangles shown in figure 3.2.

the U.S. Geological Survey. During that time, changes in procedures and instrumentation increased the precision and accuracy of some techniques. Because some already published major- and minor-element oxide analyses (Vallier and Batiza, 1978) were not completed in U.S. Geological Survey laboratories, the rocks were reanalyzed to provide consistency in the data set; the new analyses are included in the tabulated data. The analyzed samples generally are typical of a given outcrop. Volcanic-rock samples were

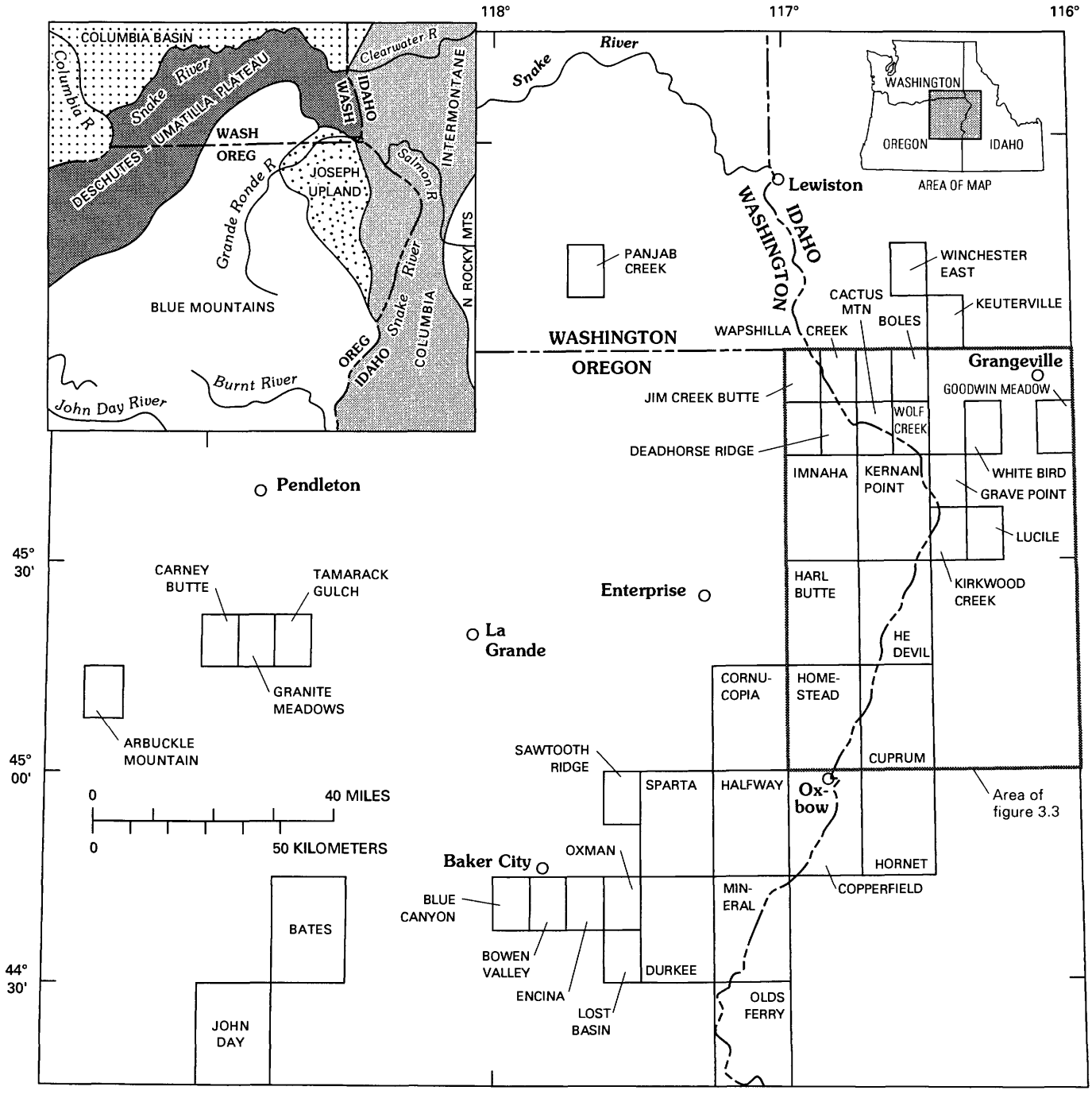

FIGURE 3.2.—Map of Blue Mountains region showing quadrangle maps referred to in tables. Inset map shows physiographic provinces (modified from Walker, 1990). Grindstone, Baker, and Izee terranes (see fig. 3.8) are almost entirely within Blue Mountains province, whereas Olds Ferry terrane is split between Blue Mountains and Columbia Intermontane provinces. Wallowa terrane is in Blue Mountains, Columbia Intermontane, and Joseph Upland provinces.

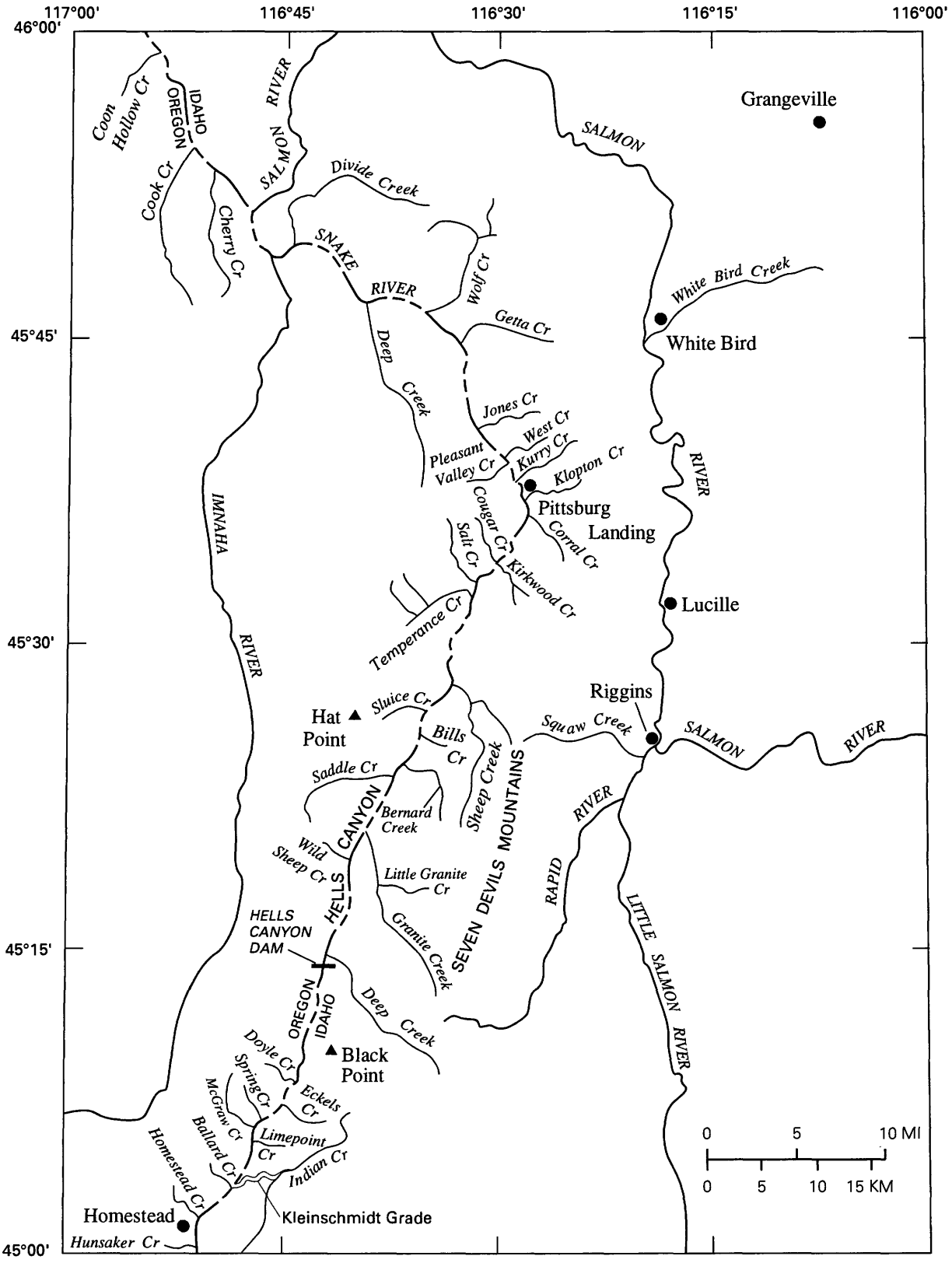

FIGURE 3.3.—Major rivers, creeks, and towns of Snake River and Salmon River areas that are referred to in tables and text. For specific locations, see appropriate quadrangle map (fig. 3.2).

TABLE 3.1.—*Classification scheme used for most igneous rocks in the Blue Mountains island arc*

[Names granodiorite and granite are used only for unaltered high-K_2O, high-SiO_2 Jurassic to Cretaceous plutonic rocks. Quartz keratophyre is high-Na_2O, low-K_2O rhyolite]

SiO_2 content (weight percent)	Plutonic rock	Volcanic rock
<52	Gabbro or norite; diabase	Basalt
52–56	Meladiorite	Basaltic andesite
56–62	Diorite	Andesite
62–70	Quartz diorite; tonalite; granodiorite	Dacite
>70	Trondhjemite; granite	Rhyolite; quartz keratophyre

selected mainly from aphyric flows; rocks with abundant phenocrysts were avoided.

Methods used for chemical analyses were X-ray fluorescence spectrometry, both wavelength-dispersive (Taggart and others, 1981, 1987) and energy-dispersive (Johnson and King, 1987), for eight major- and two minor-element oxides and selected trace elements (particularly Rb, Sr, Ba, Y, Zr, and Nb); wet chemical and gravimetric analysis for ferrous iron, water (H_2O^+ and H_2O^-), and carbon dioxide (Peck, 1964; Kolthoff and others, 1969; Tillman, 1977); direct-current arc-emission and optical-emission spectrometry (Golightly and others, 1987; Wilson and others, 1987) for a few trace elements; and instrumental neutron activation analysis for the remaining trace elements including the rare-earth elements (Baedecker, 1979; Baedecker and McKown, 1987). Some trace elements were determined by more than one method; the value used here depends on the presumed precision and accuracy of the data. Initial strontium isotope ratios were determined using methods that are discussed by Fleck and Criss (1985). Previously unreported K-Ar radiometric ages were determined using standard methods.

ROCK CLASSIFICATION AND DATA PRESENTATION

Most igneous rocks described in this chapter are classified by texture and chemical composition. The use of mineral modes for classification is hampered because of metamorphic effects. For example, regional metamorphism to the greenschist or amphibolite facies and contact metamorphism to the albite-epidote or hornblende hornfels facies caused extensive replacement of primary minerals in rocks older than Late Jurassic. Plagioclase feldspars have been partly to wholly replaced by albite. Mafic minerals are extensively replaced by chlorite and epidote. Primary textures in shear zones of some plutonic complexes were obliterated during deformation and metamorphism; some of the resultant foliated rocks are schist, amphibolite, mylonite, and gneissic mylonite.

The lava flows are both phyric and aphyric; the groundmasses of mafic and intermediate volcanic rocks (basalt, basaltic andesite, and some andesite) mostly have intersertal, intergranular, and hyalopilitic textures, whereas siliceous volcanic rocks (dacite and rhyolite) have felty groundmasses. Most rocks selected from large intrusive bodies have hypidiomorphic-granular textures.

A simple igneous-rock classification (table 3.1), based on texture and silica content, is used throughout this chapter, except for the Jurassic to Cretaceous plutons; the classification of rocks from them depends in part on the amount of K_2O (for example, K_2O content is used to distinguish granodiorite from granite). Igneous rocks older than the Late Jurassic are variably metamorphosed, and the prefix "meta" should be added to the rock name, but "meta" is omitted in this chapter in order to simplify descriptions and discussions. Some massive mafic-rock bodies in the Baker terrane have been so deformed and metamorphosed that original colors, textures, and minerals are destroyed. These mostly green rocks are referred to as greenstones.

Classification of metamorphosed siliceous igneous rocks is a problem. Many low-K_2O trondhjemites and quartz diorites are Na_2O rich and have been referred to by others as plagiogranite, soda granite, metatrondhjemite, and albite granite. I generally refer to those rocks as Na_2O-rich trondhjemite and Na_2O-rich quartz diorite. Low-K_2O siliceous volcanic rocks containing abundant Na_2O have been referred to as quartz keratophyre, soda rhyolite, and plagiorhyolite. In this chapter, the name quartz keratophyre is used because it is recognized by most igneous petrologists. The name spilite is not used, although metamorphosed basalt and basaltic andesite with Na_2O contents greater than 4.5 weight percent occur in Permian and Triassic mafic rocks throughout the Blue Mountains region.

Igneous rocks are separated into tholeiitic-, alkalic-, and calc-alkaline-magma series. Gill (1981) explained the history of this classification and commented on the difficulties in assigning volcanic rocks to a specific magma series. Particular problems arose in separating the igneous rocks of the Blue Mountains island arc into magma series because of the metamorphic effects. Selected major-element plots, such as AFM ($[Na_2O + K_2O]$–FeO_{total}–MgO) and FeO_{total}/MgO ratio versus SiO_2 content diagrams, and certain trace-element plots, such as rare-earth element (REE), Ti-Zr-Y and Ti-Zr, and FeO_{total}/MgO versus Ce_n/Yb_n ratio diagrams, serve to distinguish calc-alkaline from tholeiitic rocks; and some trace-element plots, such as Ti-Zr-Y, Ti-Zr, and REE diagrams, distinguish alkalic basalt. The FeO_{total}/MgO ratio versus SiO_2 content diagram is helpful for distinguishing tholeiitic and calc-alkaline rocks for SiO_2 contents between about 53 and 70 percent. The FeO_{total}/MgO versus Ce_n/Yb_n ratio diagram is used to distinguish calc-alkaline from tholeiitic rocks because it shows both the iron enrichment and the flatness of the chondrite-normalized-REE diagram. Ce (rather than La) and Yb (instead of Lu) are used in the diagram because of suspected greater mobility of La during weathering and metamorphism and the better precision of Yb measurements. An arbitrary line at the Ce_n/Yb_n ratio of 2.5 is used to divide tholeiitic and calc-alkaline rocks in the FeO_{total}/MgO versus Ce_n/Yb_n ratio diagrams.

There are some difficulties in using the diagrams mentioned above for distinguishing tholeiitic from calc-alkaline rocks. Some rocks show neither flat REE patterns nor conclusive iron enrichment; for example, rocks whose REE patterns show LREE (light REE) contents as 15 to 20 times chondrite abundances and HREE (heavy REE) contents as 8 to 12 times chondrite values and whose FeO_{total}/MgO ratio versus SiO_2 content diagram is not diagnostic are difficult to assign to a specific magma series. Herein, those rocks are referred to as transitional between the tholeiitic and calc-alkaline series. High-Al_2O_3 basalts (greater than 18 weight percent Al_2O_3) are rare in the analyzed rock suites, in part because of the mostly aphyric nature of the rocks selected for chemical analyses.

Metasomatism has affected most pre-Jurassic rocks. In particular, sodium metasomatism was extensive. Some of the Permian volcanic rocks would be classified as alkalic if only major-element diagrams, such as the Na_2O versus SiO_2 content diagram (MacDonald and Katsura, 1964), were used. REE diagrams are not entirely conclusive because the LREE's may have been mobilized. The HREE's, on the other hand, probably were immobile during metamorphism. Reviews of suspected REE mobility in metamorphosed basalt are given by Frey and others (1974), Hermann and others (1974), Hellman and Henderson (1977), Menzies and others (1977, 1980), and Humphris and others (1978).

Most chemical data discussed in this chapter are new. A few of the analyses have also been reported by Ferns and others (1983, 1987), Walker (1986), and Ferns and Brooks (chap. 9, this volume); the rocks analyzed by Vallier and Batiza (1978) were reanalyzed for consistency and the new analyses are presented here. White and Vallier (1994) briefly discuss the chemistry of rocks in the Pittsburg Landing area of Oregon and Idaho. In general, except for the Baker terrane rocks, my samples seem to adequately characterize the pre-Tertiary igneous rocks of the Blue Mountains region. Additional chemical analyses and (or) comments on the igneous petrology are given in this volume (see Ashley, chap. 12; Bishop, chaps. 4 and 5; Leeman and others, chap. 1; Hooper and others, chap. 11; Taubeneck, chap. 2; and Walker, chap. 6). Dissertations, theses, and journal articles that contain chemical analyses of igneous rocks and (or) discuss important field relations and petrography of igneous rocks from the Blue Mountains region are those by Huntting (1942), Taubeneck (1957, 1967); White (1973); Skurla (1974); Trauba (1975); Shorey (1976); Almy (1977); Armstrong and others (1977); Phelps (1978, 1979); Mullen (1978, 1983, 1985); Gerlach (1980); Himmelberg and Loney (1980); Phelps and Avé Lallemant (1980); Gerlach and others (1981); Brooks, Ferns, Coward and others (1982); Brooks, Ferns, and Mullen (1982); Sarewitz (1982, 1983); Scheffler (1983); Brooks and others (1983, 1984); Ferns and others (1983, 1987); Hunt (1985); Goldstrand (1987); and LaPierre and others (1988). The isotope ratios and isotopic ages determined and compiled by Hendricksen and others (1972), Armstrong and others (1977), Walker (1986), and Criss and Fleck (1987) are helpful for interpretations of the region's petrologic and tectonic evolution. For comparisons of plutonic rocks from the Blue Mountains region with Cretaceous plutonic rocks of the Idaho batholith, refer to Hyndman (1983) and to individual chapters in the volume by Vallier and Brooks (1987). Chemical and petrographic data for Eocene plutonic rocks of the Idaho batholith were reported by Motzer (1986).

INTERPRETATIONS OF PETROGENESIS AND TECTONIC SETTING

It is not easy to interpret igneous-rock data from modern volcanic arcs, let alone those from ancient arcs that have undergone several thermal and tectonic

events. Furthermore, volcanic arcs are notorious for showing large differences in rock chemistry both across and along magmatic axes and within individual volcanoes themselves (Gill, 1981; Kay and Kay, 1994). In this chapter, comparison between igneous rocks of the Blue Mountains island arc and those of modern island arcs use as models the calc-alkaline and tholeiitic rocks from the Aleutian island arc (Kay and others, 1990; Kay and Kay, 1994) and tholeiitic rocks from the Tonga and Kermadec island arcs of the southwestern Pacific Ocean (Ewart and others, 1973; Vallier and others, 1985; Ewart and Hawkesworth, 1987; Vallier and others, 1991).

Source rocks of volcanic-arc parent magmas are a subject of major debate (see reviews by Gill, 1981; Kay, 1984). Data presented in this paper are not adequate for a detailed treatment of source rocks and source areas.

Differentiation processes in arc magmas are thoroughly discussed by Grove and Baker (1983, 1984) and Grove and Kinzler (1986), who used experimentally determined phase equilibria of mafic melts at low pressure to study processes of fractionation, assimilation, and magma mixing. They showed that both calc-alkaline- and tholeiitic-series magmas can be generated from a common parent and that composition of the parent magma, pressure of fractionation, fugacity of water, extent of magma mixing, and crustal contamination are all important in determining differentiation paths.

Grove and Baker (1984) concluded that the proportions of olivine, plagioclase, and pyroxene crystallizing from a parent magma during fractionation are important compositional controls in determining whether a crystallizing magma follows a tholeiitic or calc-alkaline trend. They did not discuss the roles of magnetite and amphibole fractionation, although they believed that in some cases both are important. The fractionation of plagioclase, olivine or orthopyroxene, clinopyroxene (generally augite), and magnetite has the greatest effect on the final rock compositions, according to Gill (1981). Kay and Kay (1985a, b, 1994) discussed the important role of amphibole fractionation in the generation of calc-alkaline volcanic rocks. Garnet crystallization may also play a role in the evolution of calc-alkaline magmas, and particularly may account for the prominent HREE depletion.

The tholeiitic trend, according to Grove and Baker (1984), is produced by low-pressure fractionation of a basalt magma, characterized by the sequential crystallization of olivine, plagioclase, and augite, with plagioclase continuously dominating the assemblage. Crystallization continues until the remaining magma reaches a reaction point, where olivine reacts with the liquid to form augite, plagioclase, and pigeonite. A dramatic increase in total Fe and a mild decrease in SiO_2 occur in the liquid at the reaction point.

The calc-alkaline trend (Grove and Baker, 1984), in contrast, develops when olivine, calcic plagioclase, and augite crystallize in nearly equal mass proportions. This phase assemblage precipitates under conditions of moderate pressure and water undersaturation in the middle to upper crust. The crystallization process is characterized by a small increase in total Fe, an increase in SiO_2, and a decrease of MgO in derivative liquids. Assimilation of a crustal component and mixing of basaltic liquids with siliceous residual melts are additional processes in the calc-alkaline-crystallization sequence. Relative proportions and types of crystallizing phases change in response to an increase in total pressure and an increase in P_{H_2O}. Crystallization can occur at elevated pressure if basalt magma is slowed during its ascent or held in a crystallizing magma chamber.

I use three diagrams to separate rocks into magma series or trends and to compare rocks from different arcs: (1) the FeO_{total}/MgO ratio versus SiO_2 content diagram of Miyashiro (1974) that shows iron-enrichment trends (fig. 3.4) to distinguish tholeiitic from calc-alkaline fields; (2) the FeO_{total}/MgO versus Ce_n/Yb_n ratio diagram (fig. 3.5), which is used not only to distinguish calc-alkaline and tholeiitic series but also to show differences between the tholeiitic suites, such as Tongan versus Aleutian (Okmok Caldera) tholeiitic suites; and (3) REE diagrams for both plutonic rocks (figs. 3.6*A*, 3.6*B*) and lavas (fig. 3.7), which show relative LREE enrichment and HREE depletion for calc-alkaline igneous rocks and relatively flat patterns for tholeiitic igneous rocks. The FeO_{total}/MgO versus Ce_n/Yb_n ratio diagram is a new method of portraying these magma series and may be applicable in other petrologic investigations.

Chemical and other geological data can be combined to interpret petrogenesis and tectonic settings of the igneous rocks (table 3.2). Almost all pre-Tertiary rocks in the Blue Mountains region, except for a few alkalic flows in the Baker terrane, are interpreted using the tholeiitic/calc-alkaline classification scheme. Rocks that do not fit solidly within specific fields of the diagrams or that have REE patterns between the flat tholeiitic trend and the sloping calc-alkaline trend are called transitional. I follow many of Gill's (1981) interpretations of tectonic settings.

GEOLOGIC FRAMEWORK

Important to understanding the geologic framework of pre-Tertiary (particularly the Permian and Triassic)

rocks in the Blue Mountains region are the concepts that (1) they formed in a volcanic arc (Hamilton, 1963), and (2) major tectonostratigraphic terranes compose the arc (Brooks and others, 1976; Vallier and others, 1977; Brooks and Vallier, 1978; Dickinson, 1979; Brooks, 1979a; Mullen and Sarewitz, 1983; Silberling and others, 1984). The tectonostratigraphic-terrane concept, used to explain complex geologic relations in western North America (see Davis and others, 1978; Coney and others, 1980; Howell and others, 1985), has been particularly helpful in understanding the evolution of the Blue Mountains island arc. The early-proposed names for terranes (oceanic crust terrane, arc terrane, and so on) became unacceptable because they had genetic connotations that did not hold up as processes responsible for the terranes' geologic evolution became better understood. Silberling and others (1984) renamed the terranes for localities rather than for interpreted origins. Vallier and Brooks (1986) recommended that those terrane names be used when discussing the pre-Tertiary rocks of the Blue Mountains region. Therefore, the terrane names of Baker, Grindstone, Izee, Olds Ferry, and Wallowa (Silberling and others, 1984) are used in this chapter. Some boundaries between the terranes (fig. 3.8) have been slightly modified and should be compared with the boundaries proposed by Silberling and others (1984).

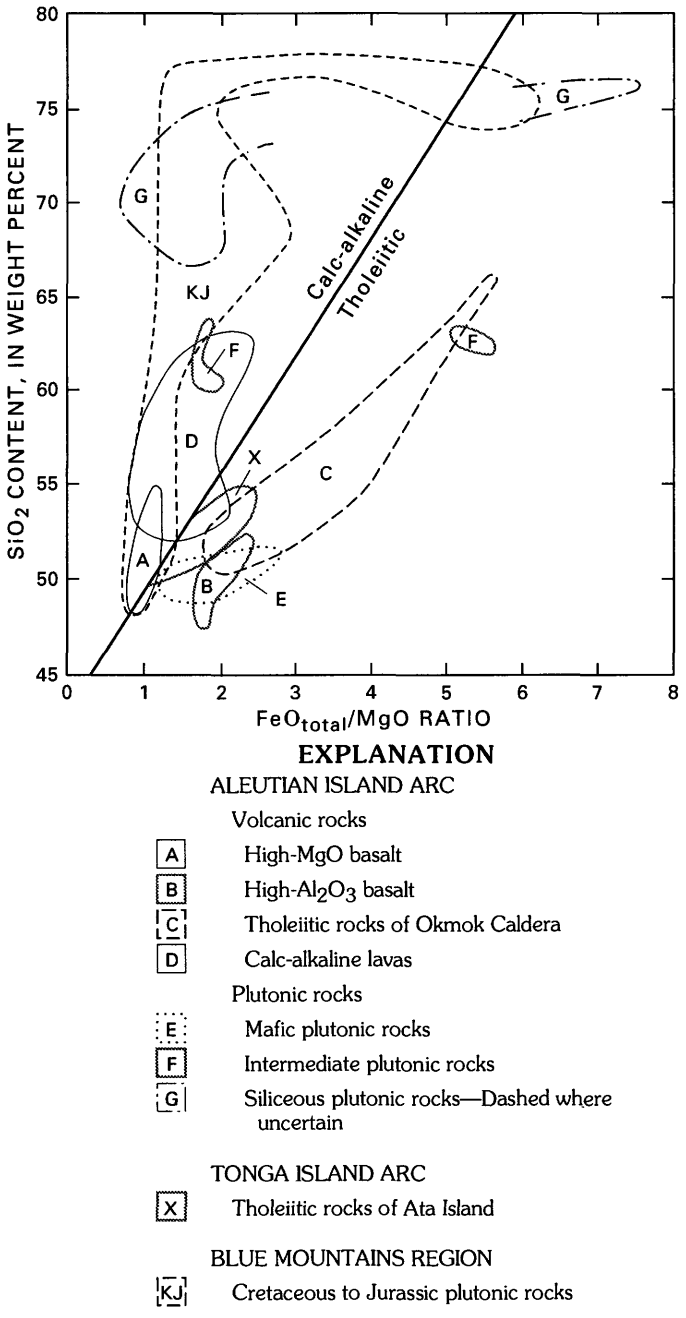

FIGURE 3.4.—FeO_{total}/MgO ratio versus SiO_2 content for volcanic and plutonic rocks of Aleutian island arc (Kay and others, 1990; Kay and Kay, 1994) and volcanic rocks of Ata Island of Tonga island arc (Vallier and others, 1985). Area KJ, representing plutonic rocks of Blue Mountains region, was constructed from analyses of rocks of the Wallowa and Bald Mountain batholiths (W.H. Taubeneck, written commun., 1987). Calc-alkaline–tholeiitic compositional boundary from Miyashiro (1974).

In describing the terranes, I suggest a few new interpretations, some of which are dealt with in more detail elsewhere (see Ferns and Brooks, chap. 9, this volume). The basic premises are the following:

(1) All terranes in the Blue Mountains region are kindred. Since becoming coherent terranes, they have always been part of the same complex island arc.

(2) The Grindstone and Baker terranes are parts of the same terrane (or tectonic region) that formed within a late middle Paleozoic to Late Triassic island arc (Morris and Wardlaw, 1986). Their differences partly reflect multiple deformations within the fore-arc region or regions.

(3) Rocks within the inliers that occur in the Blue Mountains anticline of north-central Oregon and along the Tucannon River tributaries in Washington are more similar to rocks of the Baker terrane than to those of the Wallowa terrane. Igneous rocks from those areas, however, are discussed in sections concerning the Wallowa terrane. The small number of samples preclude a definitive terrane assignment.

(4) The highly metamorphosed and deformed rocks near New Meadows, Idaho (Bonnichsen, 1987), have protoliths of chert and ultramafic rocks that are more similar to rocks in the Baker terrane than to those in any other terrane of the Blue Mountains region.

(5) The Wallowa and Olds Ferry terranes are parts of volcanic edifices and subjacent intrusions built on, and within, a more ancient arc framework (or basement).

(6) The (informal) Sparta complex is part of the Wallowa terrane rather than the Baker terrane as mapped by Silberling and others (1984).

(7) The Izee terrane is part of an extensive belt that includes the Weatherby Formation (Brooks, 1979a) and presumably parts of the Squaw Creek Schist (Brooks and Vallier, 1978). This belt extends from east-central Oregon into western Idaho, where it turns northward and merges with the border zone of the Idaho batholith.

(8) Rocks from both the Izee and Olds Ferry terranes compose parts of the Squaw Creek Schist (Hamilton, 1963) in the Riggins, Idaho, area and probably some of the rocks (for example, amphibolites and

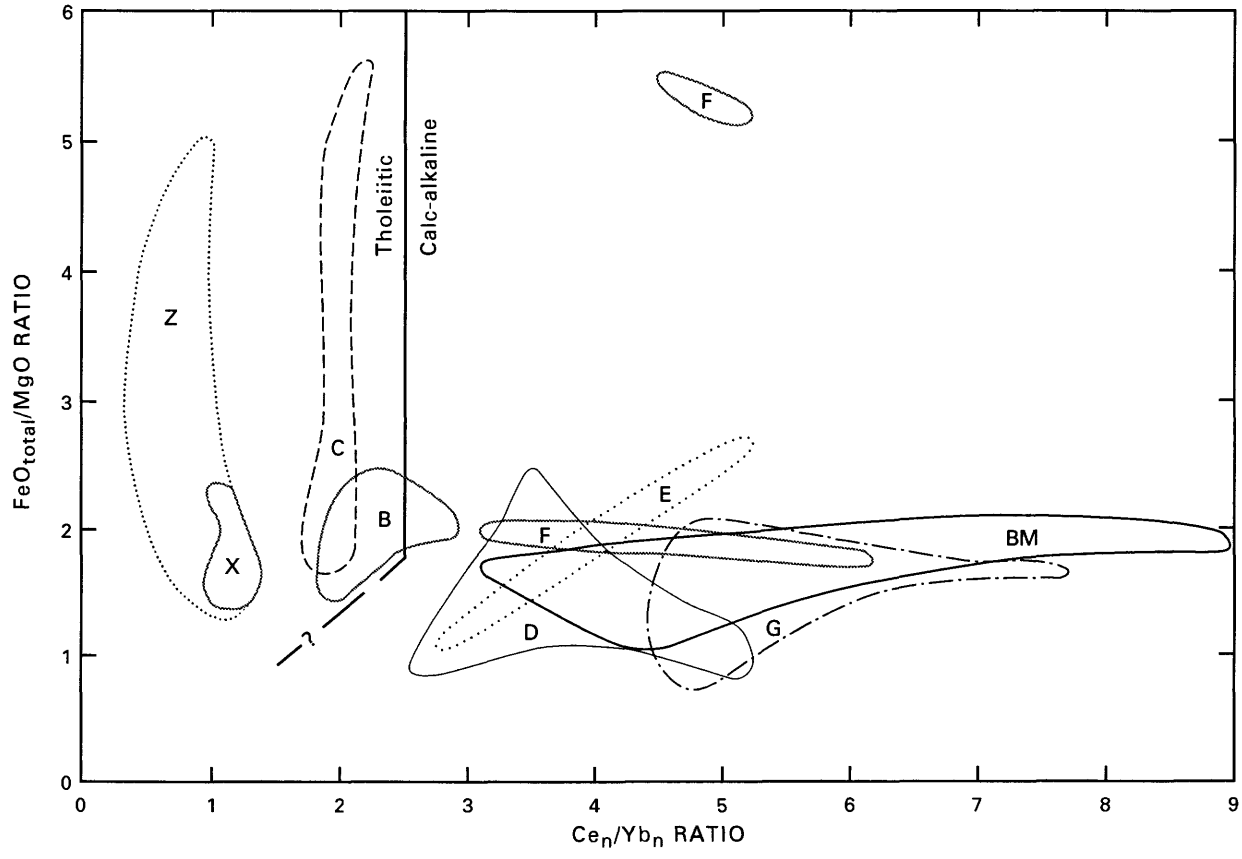

EXPLANATION

ALEUTIAN ISLAND ARC

Volcanic rocks

- B — High-Al_2O_3 basalt
- C — Tholeiitic rocks of Okmok Caldera
- D — Calc-alkaline lavas

Plutonic rocks

- E — Mafic plutonic rocks
- F — Intermediate plutonic rocks
- G — Siliceous plutonic rocks

TONGA ISLAND ARC

- X — Tholeiitic rocks of Ata Island, Tonga
- Z — Tonga-Kermadec island arc lavas

BLUE MOUNTAINS REGION

- BM — Bald Mountain batholith

FIGURE 3.5.—FeO_{total}/MgO versus Ce_n/Yb_n ratios for igneous rocks of the Aleutian and Tonga-Kermadec island arcs. Data fields correspond to similarly designated fields in figure 3.4, with addition of Tonga-Kermadec island arc lavas. In this plot, Jurassic to Cretaceous plutonic rocks of Blue Mountains region are represented by data field for Late Jurassic Bald Mountain batholith (BM). Line, dashed and queried where uncertain, divides tholeiitic from calc-alkaline fields. Tholeiitic fields show increasing iron content with relatively constant chondrite-normalized rare-earth-element ratios. Calc-alkaline fields show relatively constant iron content with increasing chondrite-normalized rare-earth-element ratios. n, chondrite normalized.

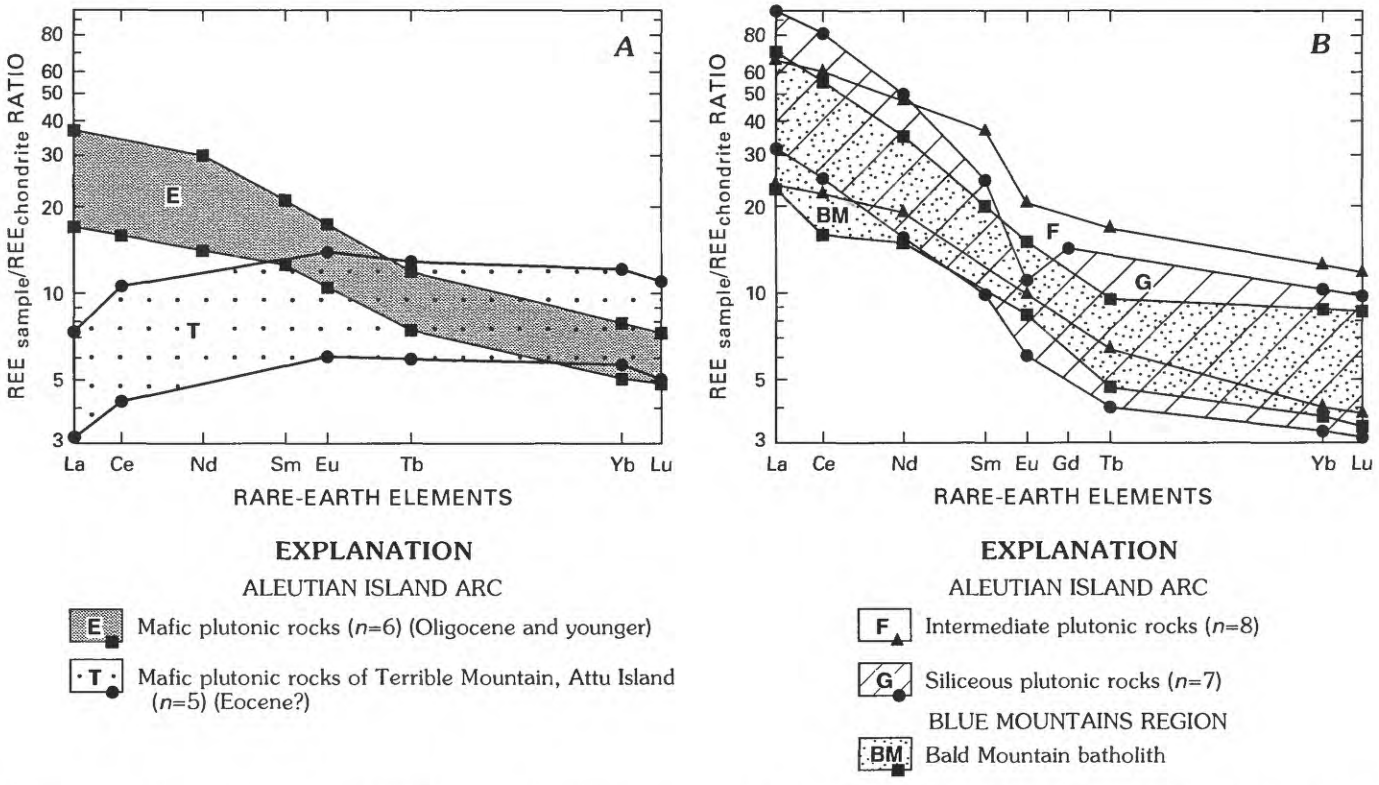

FIGURE 3.6.—Rare-earth element (REE) diagrams for Aleutian island arc plutonic rocks and Bald Mountain batholith. Normalizing values (Masuda and others, 1973) used for this diagram and for other REE diagrams in this chapter: La, 0.378; Ce, 0.976; Nd, 0.716; Sm, 0.230; Eu, 0.0866; Tb, 0.589; Yb, 0.249; Lu, 0.0387. *A*, Mafic plutonic rocks of Aleutian island arc, including five rocks from Terrible Mountain on Attu Island (Vallier, unpub. data, 1984) and plutonic rocks from Adak and other islands (Kay and others, 1990). Missing data points for Nd and Sm indicate elements that were below detection limit of the analytical instrument, were not determined, or had large coefficient of variation. *B*, Aleutian island arc intermediate and siliceous plutonic rocks and Late Jurassic Bald Mountain batholith of Blue Mountains region.

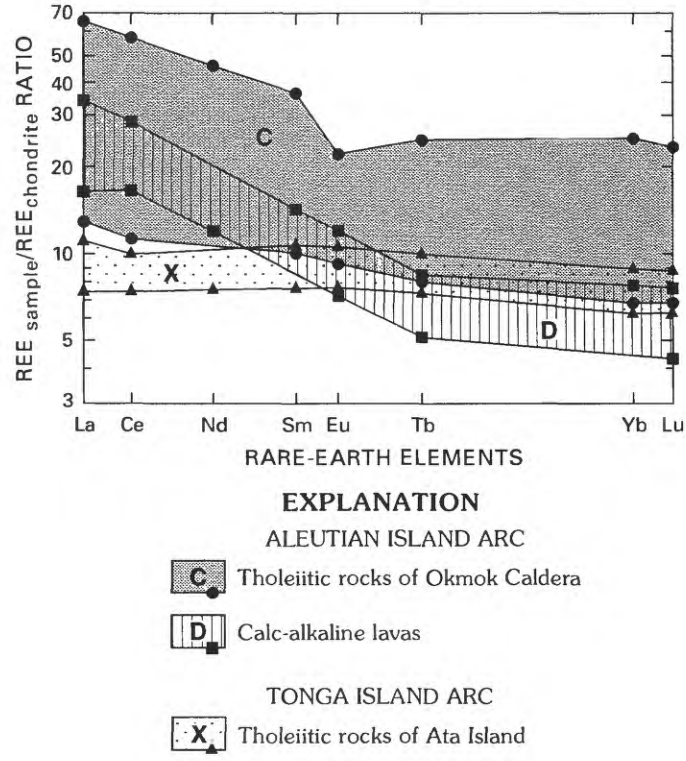

FIGURE 3.7.—Rare-earth element (REE) diagram for Aleutian calc-alkaline (n=8) and tholeiitic (n=6) lavas and Tongan (Ata Island) tholeiite (n=12). Note spread of Okmok Caldera data, reflecting broad range of differentiated lavas, and relative increase in light rare-earth element contents among Aleutian island arc calc-alkaline lavas (n=8). For normalizing values used, see figure 3.6. Missing Sm and Nd data points indicate that the elements were below detection limit of the analytical instrument, were not determined, or had large coefficient of variation.

TABLE 3.2.—*Chemical characteristics, petrogenetic interpretations, and tectonic implications of tholeiitic- and calc-alkaline-magma series in the Blue Mountains island arc*

[amph, amphibole; cpx, clinopyroxene; gt, garnet; mt, magnetite; ol, olivine; opx, orthopyroxene; plag, plagioclase]

	Tholeiitic series	Calc-alkaline series
Chemical characteristics		
K-group elements[1]	Low to intermediate	Intermediate to high.
Ti-group elements[2]	Variable (low to high)	Low.
FeO_{total}/MgO ratio	High (1 to 6+; increases with increasing SiO_2).	Low (1 to 2; remains about constant with increasing SiO_2).
Ce_n/Yb_n ratio	Low (remains about constant with increasing SiO_2).	High (increases with increasing SiO_2).
$^{87}Sr/^{86}Sr$ ratio	Low	Low.
Petrogenetic interpretations		
Sources and melting	Partial melting of mantle wedge ± material from subducting slab ± crustal material.	Partial melting of mantle wedge ± material from subducting slab ± crustal material.
Parental magma	Island-arc tholeiite	High-Al_2O_3 basalt.
Dominant form of differentiation	Fractionation	Fractionation.
Type of fractionation	Plag, ol, ±opx, cpx, mt	Plag, ol, ±opx, cpx, mt, ±amph, ±gt.
Degree of mixing	Low	Low to intermediate.
Water content	Low	High.
Crustal assimilation	Low	Intermediate.
Pressure for fractionation	Low	High.
Temperature of eruption	High	Low.
Tectonic implications		
Setting	Island arc[3]	Island and continental arcs.[4]
Crustal thickness	Thin (≤ 20 km)	Thick (>30 km).
Relative age of subducting slab	Old	Old to young.
Convergence rates	>7 cm/yr	<7 cm/yr.
Angle of Benioff zone	High	Intermediate to low.

[1]K-group includes K, Rb, Cs, Ba, and Sr.
[2]Ti-group includes Ti, Zr, Hf, Nb, and Ta.
[3]Intraoceanic volcanic arc; volcanic activity occurs mostly along the magmatic axis or volcanic front.
[4]Volcanic activity is not necessarily along the magmatic axis or volcanic front.

FIGURE 3.8.—Terranes of Blue Mountains region showing some differences from terranes designated by Silberling and others (1984). Major differences and suggested changes are (1) continuation of Izee terrane as narrow belt into western Idaho to include Weatherby Formation and Squaw Creek Schist, (2) change in contact between Baker and Wallowa terranes to include (informal) Sparta complex of Phelps (1979) in Wallowa terrane, (3) continuation of Baker terrane into Cuddy Mountains area of western Idaho (see fig. 3.1 for geographic locations), (4) assignment of border zone near McCall, Idaho, to Olds Ferry terrane in this figure, although it may belong to Baker terrane, (5) pre-Tertiary rock inliers in Blue Mountains anticline of northern Oregon are assigned to Baker terrane, and (6) small inliers in Tucannon River area of southern Washington can be assigned to either Wallowa terrane or Baker terrane.

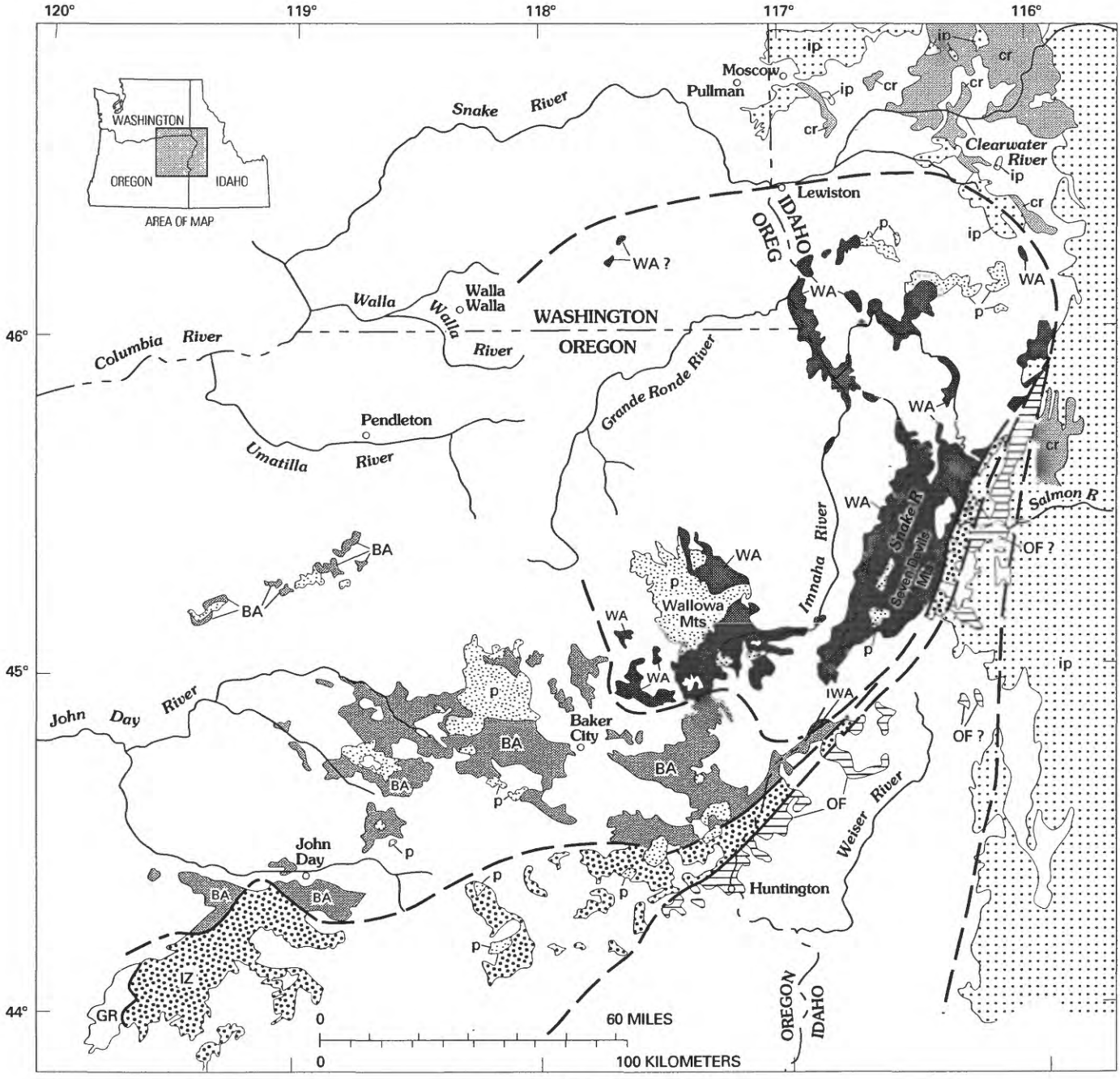

EXPLANATION

TERRANES OF THE BLUE MOUNTAINS REGION

- IZ — Izee terrane
- OF — Olds Ferry terrane
- WA — Wallowa terrane
- BA — Baker terrane
- GR — Grindstone terrane
- Boundary between terranes—Dashed where covered or uncertain

ROCKS NOT ASSOCIATED WITH TERRANES

- Cenozoic volcanic and sedimentary rocks
- ip — Late Cretaceous Idaho batholith and related plutonic rocks
- p — Cretaceous to Jurassic plutonic rocks of the Blue Mountains region
- cr — Paleozoic and Precambrian North American cratonal rocks

gneisses) that occur within the border zone of the Idaho batholith south of Riggins (Aliberti, 1988; Manduca, 1988).

BAKER TERRANE

The Baker and Grindstone terranes are structurally the most complex of the five recognized terranes in the Blue Mountains region. The Baker terrane is by far the most extensive (fig. 3.8). It had been called fragmented oceanic crust (Brooks and others, 1976), the oceanic crust terrane (Vallier and others, 1977), the dismembered oceanic crust terrane (Brooks and Vallier, 1978; Brooks, 1979a), and the central melange terrane (Dickinson and Thayer, 1978; Dickinson, 1979) before being named the Baker terrane by Silberling and others (1984).

The Baker terrane is a seemingly chaotic assemblage of Devonian through Late Triassic igneous and sedimentary rocks that have undergone varying, but pervasive, metamorphism, mostly to greenschist facies. Small amounts of amphibolite- and blueschist-facies rocks are present. Locally, hornfels-facies rocks surround Jurassic to Cretaceous intrusions. The Canyon Mountain Complex has many characteristics of an island-arc ophiolite (Bishop, chap. 5, this volume; Leeman and others, chap. 1, this volume).

Large parts of the Baker terrane probably formed in the fore-arc region, or regions, of the Blue Mountains island arc (Mullen, 1985; Bishop, chaps. 4 and 5, this volume; Leeman and others, chap. 1, this volume; Avé Lallemant, chap. 7, this volume). Most structural deformation apparently occurred in the Late Triassic and Early Jurassic(?). A complicating factor, however, is that volcanic and plutonic rocks in the Burnt River Schist, in the Canyon Mountain Complex, and in some parts of the Baker terrane (Mullen, 1985; Ferns and Brooks, chap. 9, this volume; Ashley, chap. 12, this volume; Bishop, chap. 5, this volume; Leeman and others, chap. 1, this volume; Peter Hooper, oral commun., 1987) have many chemical characteristics similar to those of rocks that form along the magmatic axis of a volcanic arc; this similarity suggests that the tectonic setting changed over time (for example, from magmatic axis to fore-arc or from fore-arc to magmatic axis). Another possibility is that some magmatism occurred within the fore-arc region itself (for example, see Marlow and others, 1988).

GRINDSTONE TERRANE

Reviews of structure, paleontology, and evolution of the Grindstone terrane were given by Buddenhagen (1967), Blome and others (1986), Morris and Wardlaw (1986), Miller (1987), and Blome and Nestell (1991). Blome and Nestell (1991) reported differences in faunas, lithology, and metamorphic grade that suggest that the Grindstone terrane is a tectonic block that is separate from other terranes in the Blue Mountains region; the terranes probably were juxtaposed in the latest Triassic or Early Jurassic. Ferns and Brooks (chap. 9, this volume), however, showed that the southern part of the Baker terrane has Paleozoic faunal affinities with the Grindstone terrane; thus, at least in the late Paleozoic, the Baker and Grindstone terranes may have been kindred (see Morris and Wardlaw, 1986). Miller (1987) suggested that the Grindstone terrane is the continuation of similar terranes in the northern Klamath Mountains.

Blome and Nestell (1991) adequately explained some of the complex structural relationships. Briefly, they hypothesized that Paleozoic blocks slid and slumped into Permian and Lower Triassic base-of-slope and basinal sediments from shelf and other relatively shallow-water environments; these blocks and basinal sediments subsequently were covered by Upper Triassic and Lower Jurassic debris- and turbidity-flow deposits. Reshuffling along some of the faults mapped by Buddenhagen (1967) also must have occurred.

Long-distance transport of an exotic terrane-sized block probably is not necessary to explain either the geologic relationships in the Grindstone terrane or the differences between the Baker and Grindstone terranes. Lithological and chronological heterogeneities reported from fore-arc regions of the Tongan (Bloomer and Fisher, 1987), Marianas (Bloomer, 1983; Fryer and others, 1985), and Aleutian (Vallier and others, 1994) island arcs indicate that fore-arc regions are very complex entities, particularly the parts that form along the inner trench wall. The Grindstone terrane probably is related to the Baker terrane in both time and space; upper Mesozoic sedimentary rocks were deposited in local basins that formed during and after deformation of the outer fore-arc region (including the inner trench wall) of the Blue Mountains island arc during the Late Triassic and Early Jurassic.

WALLOWA TERRANE

The Wallowa terrane (Silberling and others, 1984) was previously called the volcanic arc terrane (Vallier and others, 1977), the Wallowa Mountains-Seven Devils Mountains volcanic arc terrane (Brooks and Vallier, 1978), and the Seven Devils terrane (Dickinson and Thayer, 1978). The terrane includes the Wallowa

and Seven Devils Mountains in addition to the Snake River canyon north of Brownlee Dam (figs. 3.1, 3.8).

Wallowa terrane rocks are Pennsylvanian(?) through Early Cretaceous in age. A Permian stratified sequence of siliceous volcanic rocks (flows and associated volcaniclastic rocks) seemingly overlies an upper Paleozoic basement that probably was part of an ancient arc terrane. Permian stratified and intrusive rocks of the Wallowa terrane are overlain unconformably by Middle and Upper Triassic (Ladinian and Karnian) mafic to intermediate volcanic flow rocks and related volcaniclastic rocks; both the Permian and Triassic rocks were cut by intrusions of Middle and Late Triassic age. Massive carbonate and sandstone-mudstone flysch units of Late Triassic (mostly Norian) and Early Jurassic age unconformably cap the upper Paleozoic and Triassic (Ladinian and Karnian) sequences. Middle Jurassic conglomerate, sandstone, shale, and tuff and Middle and Upper Jurassic flysch-type turbidites occur in fault-bounded inliers in the Snake River canyon. Late Jurassic and Early Cretaceous intrusions cut the older rocks.

The Wallowa terrane is believed by some workers to be part of the Wrangellia superterrane (hereafter called Wrangellia for brevity), which extends from the Blue Mountains of Oregon to southeastern Alaska (Jones and others, 1977; Hillhouse and others, 1982). This interpretation was questioned by Mullen and Sarewitz (1983), Sarewitz (1983), and Scheffler (1983) on the basis of geochemical data for Triassic volcanic rocks of the Wallowa terrane; these rocks are very different from lavas of the same age in undisputed parts of Wrangellia. Vallier (1986) suggested that Triassic volcanic rocks in the Wrangellia superterrane (specifically in the Wallowa terrane and in the Vancouver Island area of British Columbia) may have evolved in different parts of the same island arc, the Wallowa terrane rocks forming along the magmatic axis and the Vancouver Island rocks forming in the back-arc region during a rifting event in the Middle and Late Triassic. The chemistry of the Triassic volcanic rocks on Vancouver Island, however, do not support an island-arc origin.

OLDS FERRY TERRANE

The Olds Ferry terrane, as mapped by Silberling and others (1984), is part of the volcanic arc terrane of Vallier and others (1977) and the Juniper Mountain-Cuddy Mountains volcanic arc terrane of Brooks and Vallier (1978). Although Silberling and others (1984) included the Weatherby Formation (Brooks, 1979a) in the Olds Ferry terrane, it is interpreted in this chapter to be part of the extensive clastic belt that includes the Izee terrane.

The Olds Ferry terrane is in part lithologically similar to, but chronologically distinct from, the Wallowa terrane. Like the rocks in the Wallowa terrane, those in the Olds Ferry terrane evolved along the magmatic axis of an island arc. The Olds Ferry terrane volcanic rocks are Late Triassic (late Karnian and Norian) in age, and the intrusive rocks, exclusive of the Jurassic to Cretaceous plutons, range in age from Middle Triassic to Early Jurassic(?). In contrast, volcanic rocks of the Wallowa terrane range in age from Early Permian to Late Triassic (early Karnian), and intrusive rocks, exclusive of the Jurassic to Cretaceous plutons, are late Paleozoic (mostly Permian) to Late Triassic. Additional radiometric ages of plutonic rocks are needed from both terranes, particularly the Olds Ferry terrane.

IZEE TERRANE

The Izee terrane contains a thick coherent sequence of clastic sedimentary rocks with subordinate limestone and volcanic rocks of Late Triassic to Middle Jurassic age (Dickinson, 1979; Blome and others, 1986). It is the flysch terrane of Brooks and Vallier (1978).

The Izee terrane (fig. 3.8) is here considered to be part of the long belt of clastic rocks that includes the Weatherby Formation of eastern Oregon and western Idaho (Brooks, 1979a, b; Mann, 1988) and parts of the Squaw Creek Schist (Hamilton, 1963) of the Riggins Group. As previously defined (Silberling and others, 1984), the Izee terrane was more limited in extent. Rocks of the Izee terrane along the west boundary as defined by Silberling and others (1984) overlie an unconformity that was cut across rocks of the Grindstone and Baker terranes. Rocks of the Izee terrane that are exposed along the east boundary as defined by Silberling and others (1984) lie beneath Tertiary volcanic rocks. Rocks lithologically similar to those of the Izee terrane of Silberling and others (1984) crop out a short distance east of that east boundary, in the Ironside Mountain area, and form a wide but coherent belt that can be traced eastward in Oregon and thence northeastward across the Snake River into Idaho. These flyschlike rocks, called the Weatherby Formation in Oregon (Brooks, 1979a, b), are Jurassic in age (Imlay, 1986), in part the same age as most rocks in the Izee terrane of Silberling and others (1984).

As pointed out by Avé Lallemant (chap. 7, this volume), the Weatherby Formation is generally separated from the Olds Ferry terrane by a thrust fault

(Bruce, 1971; Hendricksen, 1974; Skurla, 1974; Mann, 1988). On the north, the Baker terrane is faulted over the Weatherby Formation along the Connor Creek fault in eastern Oregon and western Idaho, but near Riggins, Idaho, the Squaw Creek Schist (probably in part correlative with the Weatherby Formation) is faulted over the Wallowa terrane, the probable result of thrusting during the Early Cretaceous accretion of the Blue Mountains island arc to North America. It is evident that sediments in the Weatherby Formation were derived in large part from the erosion of the Olds Ferry terrane (Brooks, 1979a, b).

The Izee terrane, as defined here, includes the Weatherby Formation and Squaw Creek Schist and forms a coherent belt of clastic rocks that extends into easternmost Oregon and westernmost Idaho. This belt narrows along the northwest side of the Cuddy Mountains and disappears to the northeast beneath the Columbia River Basalt Group; it reappears along the Little Salmon River south of Riggins, Idaho (fig. 3.8). Rocks with characteristics of the Squaw Creek Schist have been mapped north of Riggins along the Idaho batholith border zone (Myers, 1982; Lund, 1984; Lund and Snee, 1988; Lund, chap. 14, this volume; Snee and others, chap. 15, this volume), but because of the map scale in figure 3.8, the belt is not shown north of Riggins.

AGE AND FIELD CHARACTERISTICS OF PRE-TERTIARY IGNEOUS ROCKS IN THE BLUE MOUNTAINS REGION

Intrusive bodies in the Blue mountains region can be separated by age into three major groups: (1) late Paleozoic and Triassic (mostly in the Wallowa and Baker terranes), (2) Middle Triassic to Early Jurassic(?) (mostly in the Olds Ferry terrane), and (3) Late Jurassic to Early Cretaceous (in all terranes except the Grindstone).

Plutonic rocks of the oldest group are generally metamorphosed to the greenschist facies; some have no primary mafic minerals remaining, whereas others have pyroxene (commonly two pyroxenes) and blue-green actinolitic amphibole as major primary minerals. Plagioclase feldspars have been replaced wholly, or in part, by albite. Almost all of these plutonic rocks are K-poor and have tholeiitic chemical affinities. The youngest plutonic rocks, in contrast, are not metamorphosed, have pyroxene, amphibole, and biotite as primary mafic minerals in their modes, are K-rich compared to rocks of the oldest group, and have calc-alkaline chemical affinities. The Middle Triassic to Early Jurassic(?) plutonic rocks, mostly of the Olds Ferry terrane, are generally tholeiitic and have field relations and petrographic characteristics that are similar to both other groups.

The geologic field relations of the group of Jurassic to Cretaceous plutonic bodies differ from those of the two older groups. The Jurassic to Cretaceous plutonic bodies, which include the large Bald Mountain and Wallowa batholiths, intrude all terranes except the Grindstone. Some of these younger intrusive masses were emplaced along terrane boundaries. Such intrusion between established terranes is apparent along the border between the Baker and Izee terranes. In contrast, the oldest (late Paleozoic and Triassic) intrusions do not intrude terrane boundaries, although parts of them have been incorporated into some terrane boundaries by faulting.

Late Paleozoic and Triassic plutonic rocks (group 1) are widespread in the Blue Mountains region, particularly in the Baker and Wallowa terranes. Although several papers have been written about the Canyon Mountain Complex (see reviews by Mullen, 1983; Leeman and others, chap. 1, this volume) and the (informal) Sparta complex (Gilluly, 1933; Prostka, 1962, 1963; Almy, 1977; Phelps, 1978; Avé Lallemant and others, 1980), those two well-described igneous complexes make up only a small percentage of the exposed late Paleozoic and Triassic plutonic rocks. Many in the Baker terrane occur in fault blocks and irregular fault slivers and locally as knockers within serpentinite-matrix melange (see maps by Brooks and others, 1976; 1983; Brooks, Ferns, Coward, and others, 1982; Brooks, Ferns, and Mullen, 1982; Ferns and others, 1982, 1983, 1987).

Volcanic (flow) rocks of late Paleozoic and Triassic age in the Baker terrane generally are exposed in fault-bounded and discontinuous outcrops. Pillow lavas occur in places. In contrast, flows in the Wallowa and Olds Ferry terranes are stratigraphically more continuous. Pillowed flows are abundant in some areas along the Snake River and in the Seven Devils Mountains of the Wallowa terrane. Flows and associated volcaniclastic rocks are stratigraphically stacked to thicknesses greater than 1,000 m in places along the walls of Snake River canyon (Vallier, 1977).

LATE PALEOZOIC AND TRIASSIC IGNEOUS ROCKS OF THE BAKER TERRANE

Late Paleozoic and Triassic igneous rocks of the Baker terrane constitute only a small percentage of its total rock volume. These igneous rocks are fragments representing several tectonic regimes. The wide range in crystallization ages for these rocks, from the

TABLE 3.3.—*Lithology, sample locality, and field description of late Paleozoic and Triassic plutonic rocks of the Baker terrane*

[Rocks within each group arranged by increasing SiO_2 content to correspond to chemical analyses in tables 3.4 and 3.5]

Sample	Rock type	Sample locality	Field description and remarks
		Plutonic rocks of the Canyon Mountain Complex	
CM-79-3	Quartz diorite ------	Southeast ridge of Canyon Mountain; elevation 2,274 m (7,460 ft); NW1/4 NE1/4NW1/4 sec. 28, T. 14 S., R. 32 E.; John Day quadrangle; Oreg.	Quartz-rich cumulate layer within gabbroic rocks. Permian U-Pb radiometric age (Walker, 1986).
CM-79-1	Trondhjemite -------	North side of Berry Creek; elevation 1,417 m (4,650 ft); NE1/4SW1/4 sec. 31, T. 14 S., R. 32 E.; John Day quadrangle; Oreg.	Coarse-grained dike in dike complex of varied lithology (diabase, basalt, quartz keratophyre, quartz diorite).
CM-79-4	Trondhjemite -------	On ridge north of Sheep Gulch; elevation 1,661 m (5,450 ft); NE1/4 SE1/4 sec. 24, T. 14 S., R. 31 E.; John Day quadrangle; Oreg.	Large dike, one of small quartz-rich intrusions that cut gabbro.
CM-79-2	Trondhjemite -------	On ridge about 200 m from gravel pit that is north of Berry Creek; elevation 1,567 m (5,140 ft); SE1/4 SE1/4SE1/4 sec. 25, T. 14 S., R. 31 E.; John Day quadrangle; Oreg.	Large dike, one of small quartz-rich intrusions that cut gabbro.
		Other plutonic rocks of the Baker terrane	
BR-79-1	Diorite ----------	About 5 km up Burnt River canyon (near "Y" split in canyon); along Burnt River road, elevation 900 m (2,950 ft); unsurveyed; Lost Basin quadrangle; Oreg.	Small irregular intrusion associated with volcanic breccia. Intrudes Burnt River Schist.
V-1-79	Trondhjemite -------	Along U.S. Highway 30 in Pleasant Valley; elevation 1,161 m (3,810 ft); NW1/4NW1/4 sec. 30, T. 10 S., R. 42 E.; Oxman quadrangle; Oreg.	Dike rock in classic association with serpentinite and gabbro.

Pennsylvanian to the Late Triassic, combined with an extraordinary diversity of igneous rock types indicates a long and complex pre-Jurassic evolution.

Several metamorphic facies are represented in rocks of the Baker terrane (Kays and others, 1988; Evans, chap. 8, this volume; Bishop, chap. 4, this volume). The metamorphic-rock diversity is related to a broad range of pressure and temperature (P/T) conditions. Both low-P/T greenschist and actinolite facies and high-P amphibolite and blueschist facies have been recognized. In addition, Jurassic to Cretaceous plutons produced wide contact aureoles that overprinted older metamorphic facies.

PLUTONIC ROCKS OF THE BAKER TERRANE

The six plutonic rocks described in this section (tables 3.3–3.5) include (1) quartz diorite (sample CM-79-3) and trondhjemite (samples CM-79-1, CM-79-2, and CM-79-4) from the Canyon Mountain Complex and (2) diorite (sample BR-79-1) and trondhjemite (sample V-1-79) from other parts of the Baker terrane.

CANYON MOUNTAIN COMPLEX

The Canyon Mountain Complex is a dismembered ophiolitic body composed of peridotite, gabbro, and subordinate amounts of siliceous, intermediate, and diabasic intrusive bodies (Thayer, 1956, 1963, 1977; Thayer and Himmelberg, 1968; Avé Lallemant, 1976; Dungan and Avé Lallemant, 1977; Himmelberg and Loney, 1980; Gerlach, 1980; Gerlach and others, 1981; Mullen, 1983; Walker, 1986 and chap. 6, this volume; Pearcy, 1991; Bishop, chap. 5, this volume; and Leeman and others, chap. 1, this volume).

TABLE 3.4.—*Major- and minor-element oxides of late Paleozoic and Triassic plutonic rocks of the Baker terrane*

[Oxides in weight percent, normalized to 100 percent; prenormalization volatile contents included to indicate amount of alteration. ---, not determined or below instrumental detection limit]

	Plutonic rocks of the Canyon Mountain Complex				Other plutonic rocks of the Baker terrane	
Sample	CM-79-3	CM-79-1	CM-79-4	CM-79-2	BR-79-1	V-1-79
SiO_2	69.10	76.39	78.15	79.17	57.31	74.55
TiO_2	.63	.16	.20	.08	.74	.38
Al_2O_3	13.56	12.81	12.18	11.87	19.51	12.80
Fe_2O_3	1.63	1.27	.78	1.22	1.15	2.42
FeO	3.43	2.04	1.17	.65	3.98	.42
MgO	2.08	.31	.59	.29	2.79	.50
MnO	.07	.04	.03	---	.08	.03
CaO	6.56	1.84	1.24	1.12	5.15	4.25
Na_2O	2.83	4.82	5.50	5.56	6.29	4.62
K_2O	.06	.32	.16	.04	.79	.01
P_2O_5	.05	---	---	---	.21	.02
H_2O^+	1.35	0.94	0.76	0.73	2.54	0.59
H_2O^-	.31	.16	.17	.14	.14	.10
CO_2	.06	.16	.05	.07	.22	.04
FeO_{total}/MgO	2.35	2.20	3.17	6.02	1.80	5.20

The Canyon Mountain Complex is of Early Permian (intrusive) age, as shown by concordant $^{206}Pb/^{238}U$ ages on zircon of 276 and 268 Ma (Walker, 1986 and chap. 6, this volume) and $^{40}Ar/^{39}Ar$ ages as young as 262 Ma (Avé Lallemant and others, 1980; Mullen, 1983). On the basis of the concordant $^{206}Pb/^{238}U$ ages, Walker concluded that at least two separate crystallization events are represented in the complex, one at or before 276 Ma and the other about 268 Ma. One sample analyzed by Walker (1986 and chap. 6, this volume) yielded discordant ages on zircon of 314±29 Ma ($^{206}Pb/^{207}Pb$) and 278 Ma ($^{206}Pb/^{238}U$), leading Walker to speculate that 278 Ma may be a minimum age and that part of the Canyon Mountain Complex may be as old as 314±29 Ma, or Pennsylvanian(?). However, Walker did not extend the formal age of the Canyon Mountain Complex to Pennsylvanian(?) on the basis of these data.

The siliceous intrusive bodies sampled for this study (table 3.3) include a quartz diorite (sample CM-79-3) within the large gabbro body, two small trondhjemite intrusions (samples CM-79-2 and CM-79-4) that cut upper parts of the same gabbro, and a trondhjemite dike (sample CM-79-1) in the sheeted member of the ophiolitic body. All rock samples have hypidiomorphic-granular textures with cloudy plagioclase, quartz, blue-green amphibole, and rare clinopyroxene as primary minerals. Chlorite and epidote are common secondary minerals.

The siliceous rocks have low K_2O contents (table 3.4). Three of the rocks have high Na_2O contents and low amounts of CaO, suggesting extensive soda metasomatism. High Na_2O contents also occur in other siliceous intrusive bodies in the Canyon Mountain Complex (Leeman and others, chap. 1, this volume). A FeO_{total}/MgO versus SiO_2 diagram (fig. 3.9) shows the large range in silica content for Baker terrane plutons (mostly the Canyon Mountain Complex; Thayer, 1977; Leeman and others, chap. 1, this volume) and the trend towards Fe-enrichment, particularly if compared to the calc-alkaline Jurassic to Cretaceous plutons.

Trace-element data (table 3.5) are similar to those from other siliceous intrusive bodies in the Canyon Mountain Complex (Gerlach and others, 1981; Leeman and others, chap. 1, this volume). Samples CM-79-3 (quartz diorite) and CM-79-1 (trondhjemite dike rock) have similar trace-element concentrations with relatively high Sr contents and depleted REE contents (for example, subtotals of seven REE's are 21.61 and 23.96 parts per million for samples CM-79-3 and CM-79-1, respectively, compared to subtotals of 46.28 parts per million for sample CM-79-4 and 43.69 parts per million for sample CM-79-2).

TABLE 3.5.—*Trace elements of late Paleozoic and Triassic plutonic rocks of the Baker terrane*

[Results in parts per million. Analysis by neutron activation unless otherwise noted. ---, not determined or below detection limit or discarded because of high coefficient of variation]

	Plutonic rocks of the Canyon Mountain Complex				Other plutonic rocks of the Baker terrane	
Sample	CM-79-3	CM-79-1	CM-79-4	CM-79-2	BR-79-1	V-1-79
Rb	---	---	---	---	---	---
Sr	170	126	[1]90	77	386	[2]160
Ba	---	---	[1]36	[1]27	301	67
Th	---	.21	.55	.60	.16	.9
U	.16	.17	.29	.27	.19	.7
La	2.8	2.6	7.2	6.1	5	9
Ce	8.7	8.3	24.1	22.0	13.7	21
Sm	3.5	4.1	5.6	5.4	2.2	3.7
Eu	1.20	1.15	.90	.84	.78	1.11
Gd	6.04	---	---	---	---	3.5
Tb	.93	1.16	1.25	1.40	.24	.61
Tm	---	---	---	---	---	---
Yb	3.88	5.75	6.26	6.90	.67	2.8
Lu	.60	.90	.97	1.05	.11	.42
Y	[2]55	[2]77	[2]75	[2]80	[2]6	[2]27
Zr	163	138	192	200	[2]60	120
Hf	5.03	3.52	5.54	5.58	1.38	4.5
Ta	.073	---	---	.14	.07	.23
Nb	---	---	---	---	---	---
Ni	[2]20	---	---	---	[2]10	8
Co	13	.4	2.2	1.5	13.5	1.8
Cr	42	2	.9	1.4	12.4	1
Sc	18	13	9	11	11	10
Zn	---	---	---	---	[2]140	---

[1]Analysis by X-ray fluorescence.
[2]Analysis by emission and optical spectroscopy.

An FeO_{total}/MgO versus Ce_n/Yb_n diagram (fig. 3.10) shows that most rocks of the Canyon Mountain Complex (Leeman and others, chap. 1, this volume) plot in a tholeiitic field (strong FeO_{total} enrichment and flat REE pattern) near the Tonga-Kermadec field. Only the diorites (Leeman and others, chap. 1, this volume) show a LREE-enrichment trend. Plots of REE's (fig. 3.11), normalized against the chondrite values of Masuda and others (1973), show patterns that are characteristic of other rocks sampled from the Canyon Mountain Complex (for example, Leeman and others, chap. 1, this volume). Samples CM-79-2 and CM-79-4 show a fractionated-tholeiitic pattern with a large negative Eu anomaly, indicating extensive plagioclase fractionation.

OTHER PLUTONIC ROCKS OF THE BAKER TERRANE

Two other intrusive rock bodies in the Baker terrane were sampled (tables 3.3-3.5). Both are from more easterly outcrops in the terrane and include diorite (sample BR-79-1) associated with the Burnt River Schist and trondhjemite (sample V-1-79) from serpentinite-gabbro-trondhjemite outcrops near Pleasant Valley, Oreg. (table 3.3). Zircons from sample BR-79-1 have slightly discordant $^{206}Pb/^{238}U$ ages of 233 and 230 Ma; zircons from sample V-1-79 yielded concordant ages of 244 Ma (Walker, 1986, p. 80). Another trondhjemite intrusive body from the Greenhorn Mountains area yielded a U-Pb age of 243 Ma (Brooks, Ferns, Coward, and others, 1982; Walker, 1986). All of these intrusive bodies are younger than

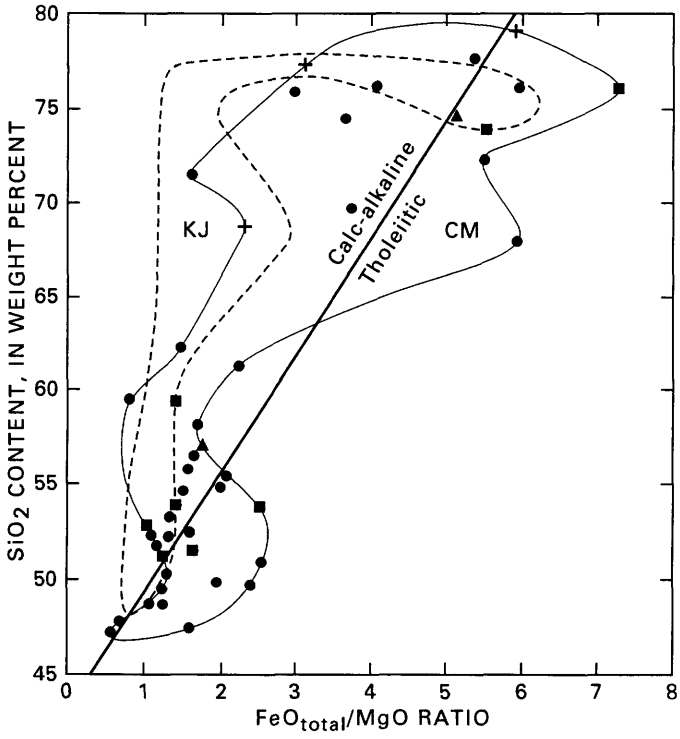

FIGURE 3.9.—FeO_{total}/MgO ratio versus SiO_2 content for plutonic rocks of Canyon Mountain Complex (CM) and other plutonic rocks of Baker terrane. Many mafic plutonic rocks show tholeiitic affinities, whereas some siliceous plutons have decidedly calc-alkaline characteristics. Dots, data from Leeman and others (chap. 1, this volume); squares, data from Thayer (1977); crosses, new data for the Canyon Mountain Complex (this chapter); triangles, data for other plutonic rocks of Baker terrane (this chapter). Compare with area (KJ) representing Jurassic to Cretaceous plutonic rocks of Blue Mountains region (see fig. 3.4). Calc-alkaline–tholeiitic compositional boundary from Miyashiro (1974).

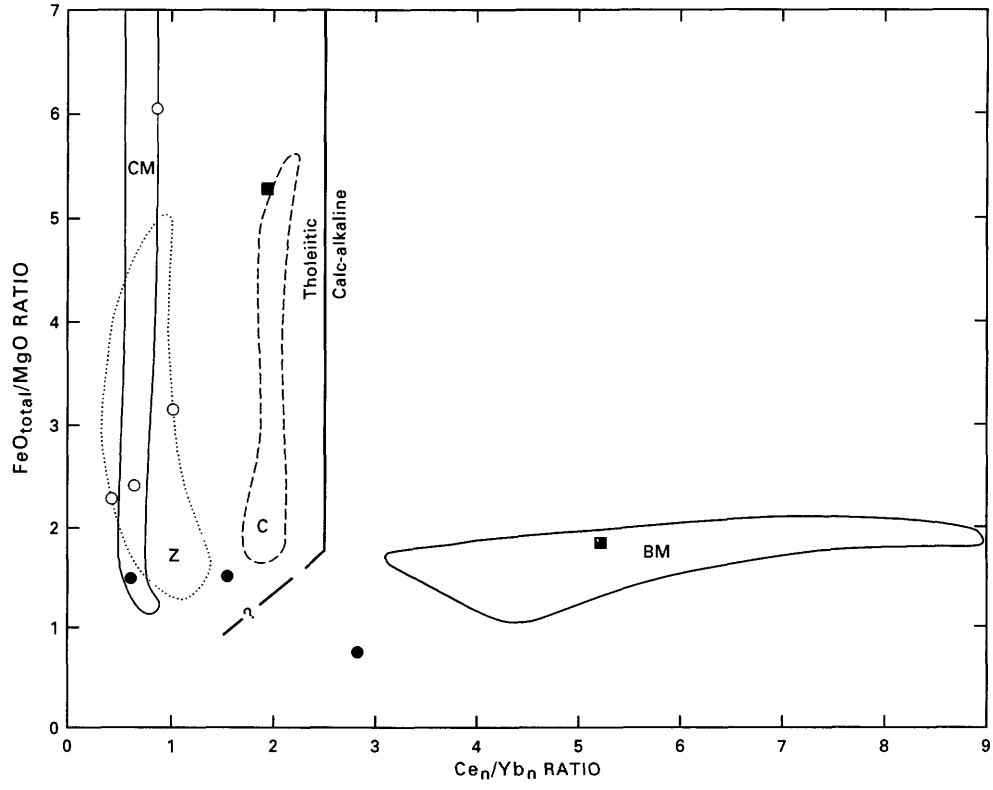

FIGURE 3.10.—FeO_{total}/MgO versus Ce_n/Yb_n ratios for plutonic rocks of Baker terrane. Data field for Canyon Mountain Complex (CM) from Leeman and others (chap. 1, this volume). Squares, diorite of Canyon Mountain Complex (Leeman and others, chap. 1, this volume); open circles, Canyon Mountain Complex (this chapter); solid circles, other plutonic rocks (this chapter). Data fields for Tonga-Kermadec island arc lavas (Z), tholeiitic rocks of Okmok Caldera of Aleutian island arc (C), and Bald Mountain batholith of Blue Mountains region (BM; see fig. 3.5) are shown for comparison. Line, dashed and queried where uncertain, divides tholeiitic and calc-alkaline fields. n, chondrite normalized.

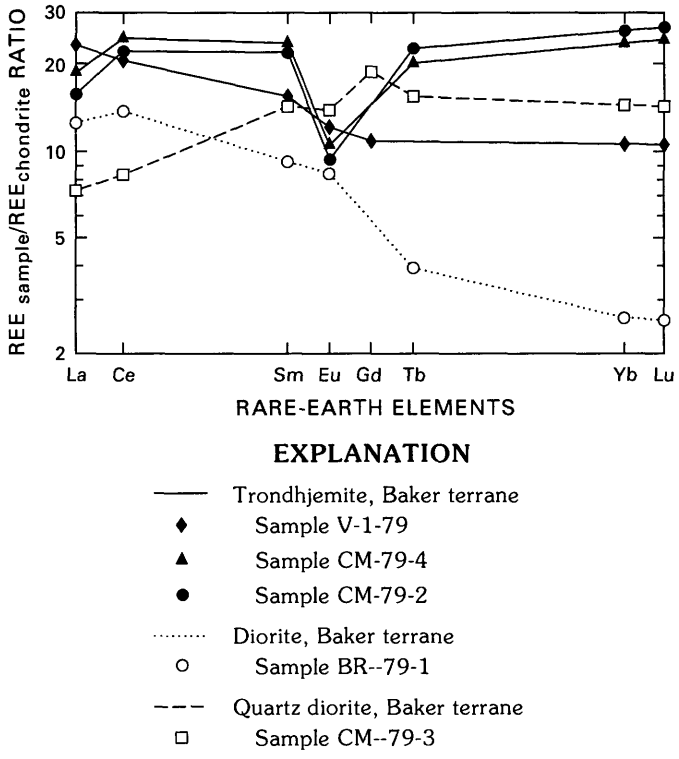

FIGURE 3.11.—Rare-earth element (REE) diagram for plutonic rocks of Baker terrane. Sample numbers correspond to those in tables 3.3 through 3.5; for normalizing values used, see figure 3.6.

the isotopically dated rocks of the Canyon Mountain Complex. These isotopic ages indicate an Early and Middle Triassic phase of igneous activity in the Baker terrane.

The diorite and trondhjemite samples (BR-79-1 and V-1-79) show important differences from samples of the Canyon Mountain Complex on the basis of trace-element contents (table 3.5) and diagrams (figs. 3.10 and 3.11). For example, both samples show LREE enrichment; sample V-1-79 plots in the Aleutian Okmok Caldera tholeiitic field and sample BR-79-1 plots in the Bald Mountain batholith calc-alkaline field on the FeO_{total}/MgO versus Ce_n/Yb_n plots (fig. 3.10). REE plots of the two samples (fig. 3.11) also show relative enrichment in LREE's compared to granitoids of the Canyon Mountain Complex; the HREE's are extremely depleted in sample BR-79-1 (Yb, about 3 times chondrite; $Ce_n/Yb_n \approx 6$), which indicates a calc-alkaline fractionation history. The geologic evolution of the Burnt River Schist, from which this sample was collected, is problematical; most igneous rocks from that unit are of volcanic-arc (magmatic-axis) origin (P.R. Hooper, oral commun., 1987) and therefore may be related to the igneous evolution of either the Wallowa terrane or the Olds Ferry terrane.

PETROGENESIS OF PLUTONIC ROCKS OF THE BAKER TERRANE

The diversity of plutonic rocks in the Baker terrane suggests more than one petrogenetic (and tectonic) environment. The plutonic rocks of the Canyon Mountain Complex definitely are different, both in age and composition, from many other plutonic rocks of the terrane.

The siliceous rocks of the Canyon Mountain Complex are classified as metamorphosed I-type granitoids (White and Chappell, 1983) mostly on the basis of their low K_2O/Na_2O ratios and Cr contents. An average analysis of I-type granitoids, however, shows higher concentrations of Sr, Ba, Rb, Th, U, Zr, and REE's (White and Chappell, 1983, p. 32) relative to granitoid plutonic rocks of the Canyon Mountain Complex. Melts that fractionated to yield siliceous plutonic rocks of the Canyon Mountain Complex had an igneous source and must have been derived from a very depleted mantle similar to mantle that produces plagiogranites under midocean spreading ridges and plagiogranites associated with many onland ophiolites (Coleman and Peterman, 1975; Coleman, 1977).

On the basis of chemical analyses of ultramafic and gabbroic rocks in the Canyon Mountain Complex, Mullen (1983) concluded that although most gabbros and so-called transitional rocks are tholeiitic, some calc-alkaline gabbros also occur, and that parent magma (or magmas) for the calc-alkaline gabbros originated by partial melting of a hydrous source. Also, she speculated that the origin of felsic plutons (plagiogranites) was by partial fusion of altered oceanic gabbro upon intrusion by the younger gabbro magma. Mullen (1983) related the origin of the Canyon Mountain Complex to early fore-arc magmatism generated by hydration and melting of depleted mantle adjacent to the leading edge of a subducting slab.

VOLCANIC ROCKS OF THE BAKER TERRANE

The upper Paleozoic and Triassic volcanic rocks of the Baker terrane are more diverse than those in any other terrane of the Blue Mountains region. Work by E.M. Bishop (Mullen, 1978, 1985; Bishop, chap. 5, this volume), for example, clearly pointed out the petrologic diversity of the volcanic rocks and led to the conclusion that the rocks have volcanic-arc, within-plate, and midocean-ridge petrotectonic affinities and are part of a complex fore-arc terrane. My data in part duplicate the work by Mullen (1985) and Ferns and Brooks (chap. 9, this volume) and provide additional analyses (tables 3.6–3.8).

In the Baker terrane, all volcanic rocks that were sampled for this study are metamorphosed to the greenschist or amphibolite facies and are deeply

TABLE 3.6.—*Lithology, sample locality, and field description of Paleozoic and Triassic volcanic (flow) and hypabyssal (dike and sill) rocks of the Baker terrane*

[Rocks arranged by increasing SiO_2 content to correspond to chemical analyses in tables 3.7 and 3.8. Do. and do., ditto]

Sample	Rock type	Sample locality	Field description and remarks
V-3-82	Basalt	Secondary pinnacle on Vinegar Hill; elevation 2,301 m (7,550 ft); NE1/4 SE1/4NW1/4 sec. 12, T. 9 S., R. 35 E.; Bates quadrangle, Oreg.	Flow rock.
V-2-82	---- do ----	Main pinnacle of Vinegar Hill; elevation 2,335 m (7,660 ft); NE1/4SE1/4NW1/4 sec. 12, T. 9 S., R. 35 E.; Bates quadrangle, Oreg.	Pillow lava.
B133A1	---- do ----	North side of State Highway 220; elevation 1,189 m (3,900 ft); SE1/4NW1/4 sec. 29, T. 10 S., R. 39 E.; Blue Canyon quadrangle, Oreg.	Flow rock.
BB135B	---- do ----	North side of State Highway 220; elevation 1,229 m (4,030 ft); SE1/4SE1/4 sec. 24, T. 10 S., R. 38 E.; Blue Canyon quadrangle, Oreg.	Flow rock, probably pillow lava.
V-1-82	---- do ----	Vinegar Hill; elevation 2,274 m (7,460 ft); NE1/4NW1/4 sec. 12, T. 9 S., R. 35 E.; Bates quadrangle, Oreg.	Sill or flow within chert-clast sandstone unit.
VB-31	Amphibolite	Above and west of road along Lodge Creek; elevation 1,219 m (4,000 ft); SW1/4NE1/4 sec. 20, T. 10 S., R. 41 E.; Encina quadrangle, Oreg.	Probable metamorphosed flow cutting breccia, chert, and argillite.
VB-30	---- do ----	Above and west of road along Lodge Creek; elevation 1,204 m (3,950 ft); SW1/4NE1/4 sec. 20, T. 10 S., R. 41 E.; Encina quadrangle, Oreg.	Do.
BM8001	Basaltic andesite	South side of road between Richland, Oreg., and Snake River, north of cattle guard; elevation 960 m (3,150 ft); SW1/4SE1/4 sec. 29, T. 11 S., R. 46 E.; Mineral quadrangle, Oreg.	Pillow lava.

weathered, as shown by high water contents (table 3.7). Several are pillow lavas (table 3.6). Where the flows are intercalated with metasedimentary rocks they can be traced laterally for only a few tens of meters; most exposures are bounded by faults. Greenstone derived from volcanic rocks occurs in places as blocks or knockers in a serpentinite-matrix melange.

A (Na_2O+K_2O)–FeO_{total}–MgO diagram (fig. 3.12) shows the characteristic Fe-enrichment and Na- and K-depletion of most Baker terrane volcanic rocks. No coherent fields are apparent on the diagram, in part because of the suspected mobility of the alkali elements and the small number of samples. However, the rocks plot in the Fe-enriched (tholeiitic) and Mg-Fe-enriched (alkalic) fields. Plots on an FeO_{total}/MgO ratio versus SiO_2 content diagram (fig. 3.13) also indicate that most are Fe-enriched. High TiO_2 contents are characteristic of alkalic rocks (see samples V-1-82 and BM8001 in table 3.7), and the low TiO_2 concentrations in samples V-2-82, B133A1, and BB135B suggest volcanic-arc affinities.

A REE diagram (fig. 3.14) shows a wide range of trends similar to those discussed by Mullen (1985); it strengthens her conclusion that the basaltic rocks crystallized in different tectonic settings. Samples V-1-82 and BM8001 have alkalic basalt trends (high LREE abundances with HREE contents about 10

TABLE 3.7.—*Major- and minor-element oxides of Paleozoic and Triassic volcanic (flow) and hypabyssal (dike and sill) rocks of the Baker terrane*

[Oxides in weight percent, normalized to 100 percent; prenormalization volatiles contents included to indicate amount of alteration. ---, not determined]

Sample	V-3-82	V-2-82	B133A1	BB135B	V-1-82	VB-31	VB-30	BM8001
SiO_2	46.07	47.76	50.05	50.16	50.27	52.03	52.30	52.71
TiO_2	1.78	1.03	1.26	1.39	2.45	1.71	1.68	2.53
Al_2O_3	15.73	15.41	16.02	17.13	15.21	15.43	14.85	18.76
Fe_2O_3	4.56	1.99	3.06	2.39	1.61	2.17	---	3.39
FeO	6.67	10.77	5.28	6.95	9.45	8.67	11.22	9.30
MgO	9.09	8.64	6.48	6.64	8.38	7.14	7.24	2.87
MnO	.20	.21	.15	.15	.21	.32	.19	.29
CaO	10.52	11.29	14.24	11.66	9.11	8.33	7.90	2.67
Na_2O	3.50	2.37	3.16	3.10	2.57	3.75	4.11	5.14
K_2O	1.60	.36	.17	.25	.35	.34	.37	1.65
P_2O_5	.28	.17	.13	.18	.39	.11	.14	.69
H_2O^+	4.10	2.23	2.13	2.35	2.25	3.13	---	3.98
H_2O^-	.27	.17	.12	.38	.38	.34	---	.50
CO_2	4.79	.08	1.51	.17	.01	.20	---	.02
FeO_{total}/MgO	1.19	1.45	1.24	1.37	1.30	1.49	1.55	4.30

TABLE 3.8.—*Trace elements of selected Paleozoic and Triassic volcanic (flow) and hypabyssal (dike and sill) rocks of the Baker terrane*

[Results in parts per million. Analysis by neutron activation unless otherwise noted. ---, not determined or below detection limit or discarded because of high coefficient of variation]

Sample	V-3-82	V-2-82	B133A1	BB135B	V-1-82	VB-31	BM8001
Rb[1]	21	10	2	4	13	4	38
Sr[1]	188	172	223	162	373	142	125
Ba[1]	99	189	32	56	677	126	646
Th	.96	.50	.5	.9	2.61	---	1.7
U	.59	.45	---	---	.73	---	.4
La	10.4	3.54	7	11	22.5	4	20
Ce	21.6	8.0	15	20	44.7	12	39
Sm	4.0	---	---	---	6.3	3.4	5.6
Eu	1.31	.89	1.04	1.17	1.7	1.23	2.05
Gd	---	---	3.2	3.9	5.5	4.6	---
Tb	.70	.70	.71	.65	.85	.99	1.22
Tm	---	---	---	---	.42	.53	---
Yb	2.41	3.42	2.5	2.1	2.26	4.3	4.1
Lu	.37	.52	.41	.32	.33	.60	.66
Y[1]	26	30	23	22	27	34	44
Zr[1]	133	60	95	97	212	82	165
Hf	2.89	1.54	2.3	2.2	4.74	2.9	4.0
Ta	.72	---	.48	.84	1.75	---	1.58
Nb[1]	16	9	7	13	25	---	23
Ni[1]	---	96	73	---	---	26	
Co	66	57	37	36	47	39	49
Cr	679	320	310	121	295	165	56
Sc	33	62	35	34	21	37	36
Zn	104	134	72	75	100	130	237

[1]Analysis by X-ray fluorescence.

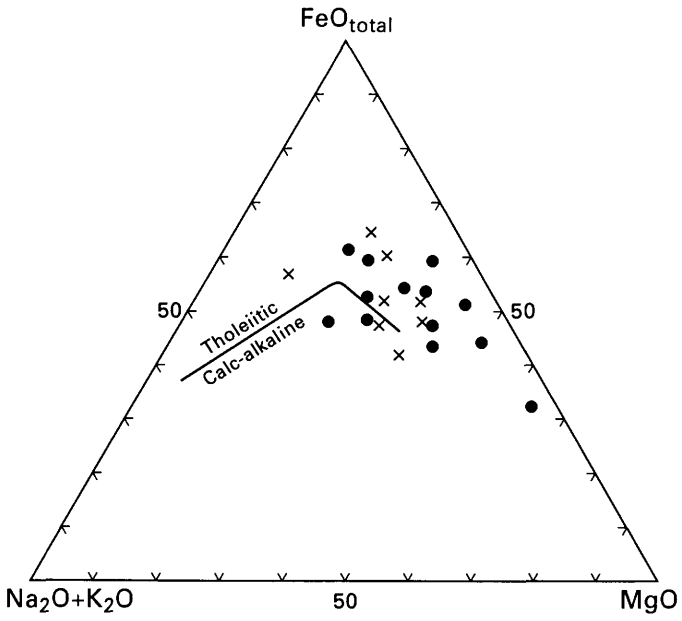

FIGURE 3.12.—(Na_2O+K_2O)–FeO_{total}–MgO (AFM) diagram for volcanic (flow) rocks of Baker terrane, showing iron enrichment in most rocks. Dots, data from Mullen (1978, 1985); crosses, data from this chapter. Curved line (from Kuno, 1968) approximately separates calc-alkaline field from tholeiitic field. This diagram generally is not useful for distinguishing alkalic from tholeiitic basaltic rocks.

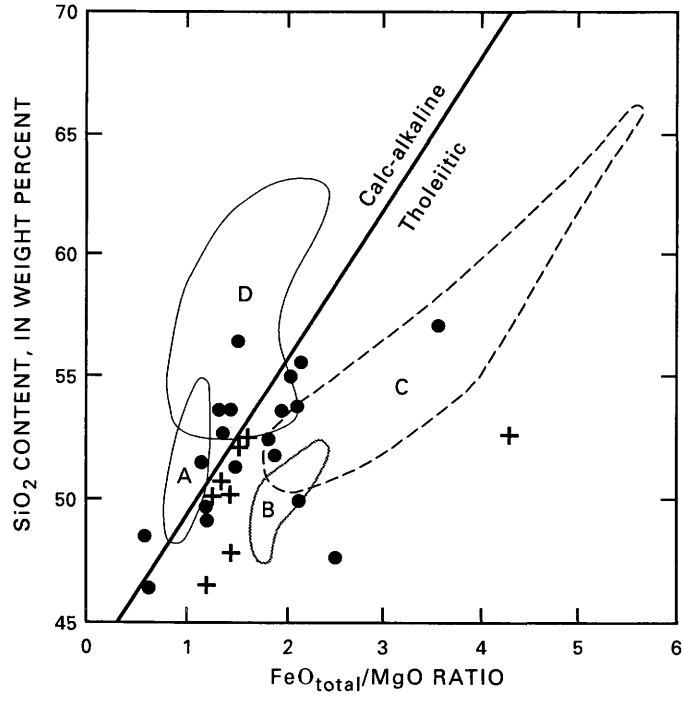

FIGURE 3.13.—FeO_{total}/MgO ratio versus SiO_2 content for volcanic rocks of Baker terrane. Dots, data from E.M. Bishop (Mullen, 1978, 1985; Bishop, chap. 5, this volume); crosses, new data (this chapter). Data fields A through D represent volcanic rocks of Aleutian island arc and correspond to those in figure 3.4. Note strong Fe enrichment in most Baker terrane volcanic rocks. Calc-alkaline–tholeiitic compositional boundary from Miyashiro (1974).

times chondrite values). The other samples have either flat tholeiitic or upward-sloping transitional (between tholeiitic and calc-alkaline) REE trends.

Discrimination diagrams (Pearce and Cann, 1973) using Y, Ti, and Zr data (figs. 3.15 and 3.16) also show the chemical diversity of basaltic rocks in the Baker terrane. Two rocks (samples V-1-28 and BM8001) are alkalic on the basis of high contents of Ti and closely associated elements (Zr, Hf, and Ta), relatively high quantities of alkali and alkaline-earth elements, high concentrations of Th, and enriched-LREE patterns. In addition, two of Mullen's (1985) samples of basaltic rocks of the Baker terrane (BRS and V27) are alkalic. Three basalts (samples V-2-82, B133A1, and VB-31) are tholeiitic (midocean-ridge basalt or island-arc basalt affinities) on the basis of their relatively flat and

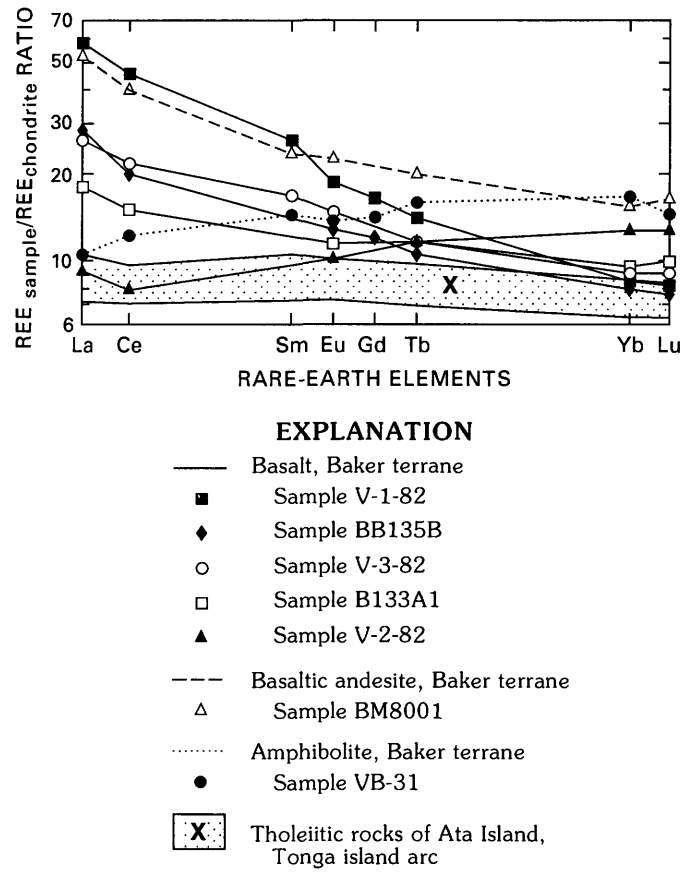

FIGURE 3.14.—Rare-earth element (REE) diagram for volcanic rocks of Baker terrane. Sample numbers correspond to those in tables 3.6 to 3.8; for normalizing values used, see figure 3.6. Ata Island field (Vallier and others, 1985) shows island-arc tholeiite trend for mafic lavas. Samples V-1-82 and BM8001 show alkalic basalt trends; samples V-3-82, V-2-82, B133A1, BB135B, and VB- 31 are tholeiitic. Some light rare-earth element enrichment may have occurred in samples V-3-82 and BB135B. Nd, Sm, and Gd data are missing for some samples either because element was not analyzed, there was a high coefficient of variation, or content was below detection limit of instrument.

(or) depleted-LREE patterns (fig. 3.14), relatively low Ti contents, and plotted positions (within "OFB+LKT +CAB" field) on the discrimination diagrams (figs. 3.15 and 3.16). Sample B133A1, especially, has very low amounts of Rb and Ba, which are compatible with a midocean-ridge basalt setting, although ion mobility during metamorphism may have affected some elemental concentrations. The relatively high quantities of Ti in these rocks are more similar to midocean-ridge basalt than to island-arc basalt. Ocean island (seamount) tholeiites are difficult to distinguish, but sample V-3-82 is the best candidate, although it could represent a high-K island-arc transitional basalt. The samples from Vinegar Hill (V-1-82, V-2-82, and V-3-82; table 3.6) in the Greenhorn Mountains, selected from knockers within serpentinite-matrix melange, are both alkalic and tholeiitic; their great compositional diversity and present positions must represent a mixing of rocks during melange formation, probably in the fore-arc region of the Blue Mountains island arc (Mullen, 1985; Bishop, chap. 5, this volume).

The petrogenesis of volcanic rocks in the Baker terrane has been discussed in more detail by E.M. Bishop (Mullen, 1985; Bishop, chap. 5, this volume). According to her interpretation, all of the major oceanic tectonic settings (midocean ridge, seamount or oceanic island, and volcanic arc) are represented. The Baker terrane apparently has been involved in several tectonic episodes, not only during the convergence of oceanic plates, but also during, and subsequent to, the accretion of the Blue Mountains island arc to North America.

LATE PALEOZOIC AND TRIASSIC IGNEOUS ROCKS OF THE WALLOWA TERRANE

The lithologies and chemistries of igneous rocks of the Wallowa terrane suggest that it is part of the late Paleozoic (mainly Early Permian) and Triassic magmatic axis (volcanic front) of the Blue Mountains island arc. The terrane is very small (fig. 3.8) when compared with modern arcs. The magmatic axes of modern island arcs have volcanoes (counting submarine edifices) spaced at distances of 50 to 70 km (Aleutian island arc) or 20 to 30 km (Tonga island arc). The Aleutian and Tonga arcs are long and wide; volcanoes along the Aleutian Islands, for example, extend for about 1,200 km, and the entire arc, from the trench inner wall to the abyssal depths in the back-arc region, is generally about 150 to 200 km wide. If the Alaska Peninsula is included in the Aleutian arc, then the length of the magmatic axis is greater than 2,000 km. The Wallowa terrane, as mapped, is about 150 by 200 km in size. As such, that terrane alone would have supported only a few volcanoes at any one time during its geologic evolution. In the Middle (Ladinian) and Late (Karnian) Triassic, for example, the Wallowa terrane would have supported no more than ten (analogy to the Tonga arc), and probably five or fewer (analogy with the Aleutian arc), volcanoes. Therefore, it is evident that a large part (probably at least 50 percent and possibly as much as 70 percent) of the Wallowa terrane is missing from the immediate area. The missing parts of the Wallowa terrane were either translated northward to become part of western Canada and

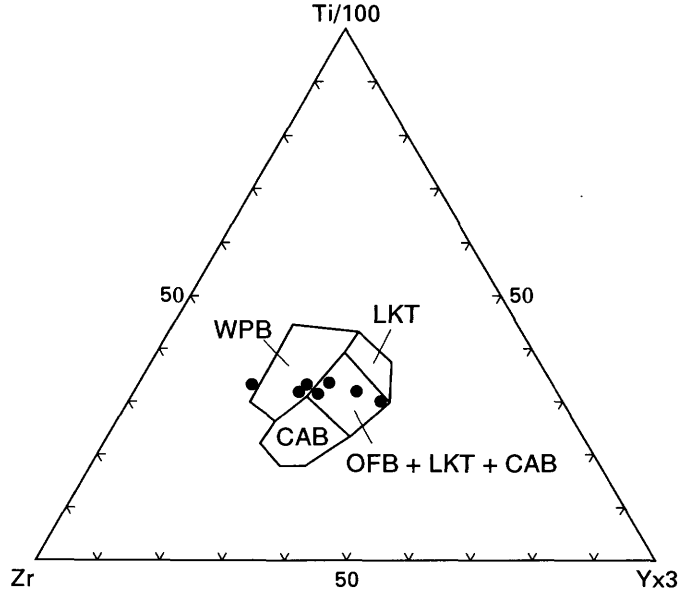

FIGURE 3.15.—(Zr)-(Ti/100)-(Yx3) discrimination diagram (Pearce and Cann, 1973). CAB, calc-alkaline basalt; LKT, low-potassium tholeiite; OFB, ocean-floor basalt; and WPB, within-plate basalt. Dots represent lavas of Baker terrane.

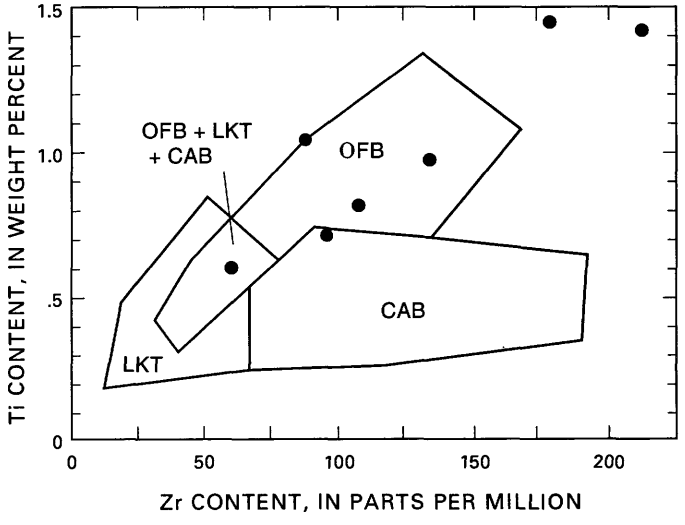

FIGURE 3.16.—Ti versus Zr content (Pearce and Cann, 1973), showing ocean-floor affinity of volcanic rocks of Baker terrane. CAB, calc-alkaline basalt; LKT, low-potassium tholeiite; and OFB, ocean-floor basalt. High Ti contents in upper part of OFB field suggest seamount alkalic basalt.

southeastern Alaska or were overridden during tectonic convergence. Processes of tectonic convergence were (1) subduction during the times when the Wallowa terrane was part of an intraoceanic island arc and (2) accretion (overthrusting and wrench faulting) when the North American craton was in direct contact with the terranes.

Although most of the shallow crustal rocks of the Wallowa terrane are composed of Permian and Triassic volcano-root plutons, volcanic flow rocks, and volcaniclastic rocks, there is an overlying carapace of Upper Triassic limestone and Upper Triassic to Middle Jurassic siliciclastic rocks (Vallier, 1977). Furthermore, Jurassic to Cretaceous plutons intrude the older rocks. The Permian and Triassic volcanic strata comprise the Seven Devils Group (Vallier, 1977). A composite geologic column for the Wallowa terrane and local variants across that terrane are shown schematically in figure 3.17. This schematic diagram, in contrast to a stratigraphic column by Vallier (1977), shows the Windy Ridge Formation as a lithofacies equivalent of the lower part of the Hunsaker Creek Formation and shows the Doyle Creek Formation as a lithofacies equivalent of the upper part of the Wild Sheep Creek Formation.

PLUTONIC AND ASSOCIATED HYPABYSSAL ROCKS OF THE WALLOWA TERRANE

Plutonic rocks of the Wallowa terrane were emplaced mostly in late Paleozoic (mostly Permian), Middle and Late Triassic, and Jurassic to Cretaceous time intervals. Only the late Paleozoic and Triassic plutonic rocks are discussed in this section. A total of 39 samples of plutonic and hypabyssal rocks from the Wallowa terrane were analyzed (table 3.9), all 39 for major- and minor-element oxides (table 3.10), and 36 for trace elements (table 3.11). These igneous rocks of the Wallowa terrane are separated into specific rock masses and (or) grouped by geographic area (table 3.9; figs. 3.1, 3.2, 3.3): the (informal) Sparta complex; Oxbow Complex; Cougar Creek Complex; Wolf Creek-Deep Creek and Imnaha plutonic rocks; Sheep Creek plutonic rocks; plutonic rocks of the southern Seven Devils Mountains; plutonic rocks of the Salmon River canyon; plutonic rocks associated with the Blue Mountains anticline; and Wildhorse River dike.

The compositional range of coarse-grained plutonic rocks of late Paleozoic (mostly Permian) and Triassic age includes norite and gabbro, meladiorite and diorite, and tonalite (quartz diorite and trondhjemite). K-rich plutonic rocks (granodiorite and granite) of Permian and Triassic age are extremely rare. In addition, dikes of quartz keratophyre and keratophyre porphyries, diabase, and aplite were collected and analyzed where field relations indicated that they are offshoots of larger plutonic bodies. One orthogneiss associated with the Blue Mountains anticline was analyzed.

Na_2O-rich siliceous plutonic bodies are common in the Wallowa terrane. They are characterized by abundant blue-colored bipyramidal quartz phenocrysts, high contents of albite (and hence Na_2O), and low amounts of K_2O-bearing minerals. Quartz keratophyre dikes are common in the Oxbow Complex and the (informal) Sparta complex and generally are closely associated with mafic dikes. In the Oxbow Complex, the felsic and mafic dikes occur together in sheetlike sequences.

The FeO_{total}/MgO ratios versus SiO_2 contents (figs. 3.18*A*, 3.18*B*), FeO_{total}/MgO versus Ce_n/Yb_n ratios (fig. 3.19), and REE diagrams (figs. 3.20*A*–3.20*E*) show the broad compositional diversity of plutonic rocks in the Wallowa terrane. Tholeiitic, transitional, and calc-alkaline late Paleozoic and Triassic plutonic rocks all occur within the terrane.

SPARTA COMPLEX

The (informal) Sparta complex was thoroughly studied by Prostka (1962), Almy (1977), Phelps (1978, 1979), and Phelps and Avé Lallemant (1980) and will not be discussed in detail here. Chemical analyses given in tables 3.10 and 3.11 complement the previously published work. Phelps (1979) presented analyses of 34 rocks from the Sparta complex. He separated out the quartz diorite unit, which, according to Prostka (1962, 1963) is the youngest plutonic unit from the trondhjemite unit (older plutonic sequence), and speculated that they might be co-magmatic. On the basis of recent isotopic age data (Walker, 1986 and chap. 6, this volume), however, it is apparent that the two plutonic masses represent separate events.

Walker (1986 and chap. 6, this volume) reviewed previous isotopic age determinations for the younger

FIGURE 3.17.—Schematic geologic columns for Wallowa terrane. *A*, Four localities (see fig. 3.1) within Wallowa terrane. Stratigraphy interpreted mostly from Nolf (1966), Vallier (1977), Follo (1994), and White and Vallier (1994). Lines joining columns indicate time correlations, queried where uncertain. Queries below Trws in right-hand columns indicate that the stratigraphic unit beneath the Wild Sheep Creek Formation is unknown. *B*, Composite column for Wallowa terrane. Circled "1" labels area of undivided Permian and Triassic Cougar Creek Complex of Vallier (1968), Oxbow Complex of Vallier (1967a, b), and (informal) Sparta complex of Phelps (1979).

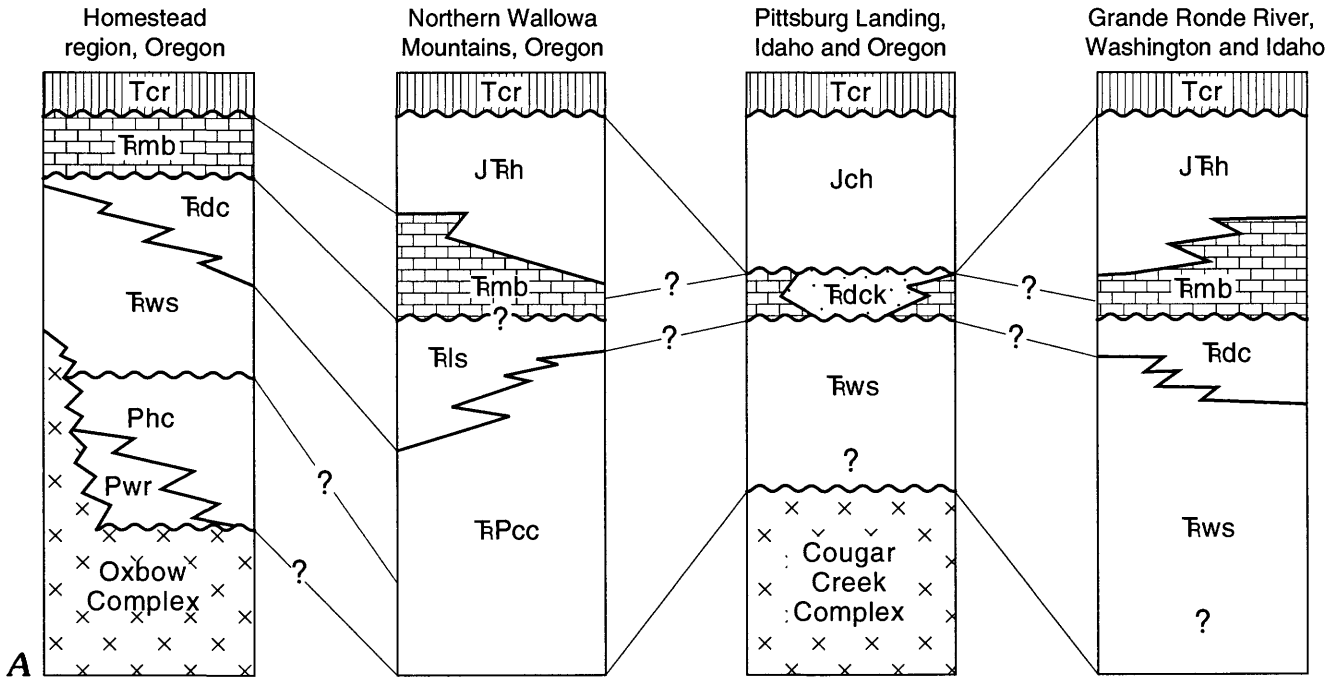

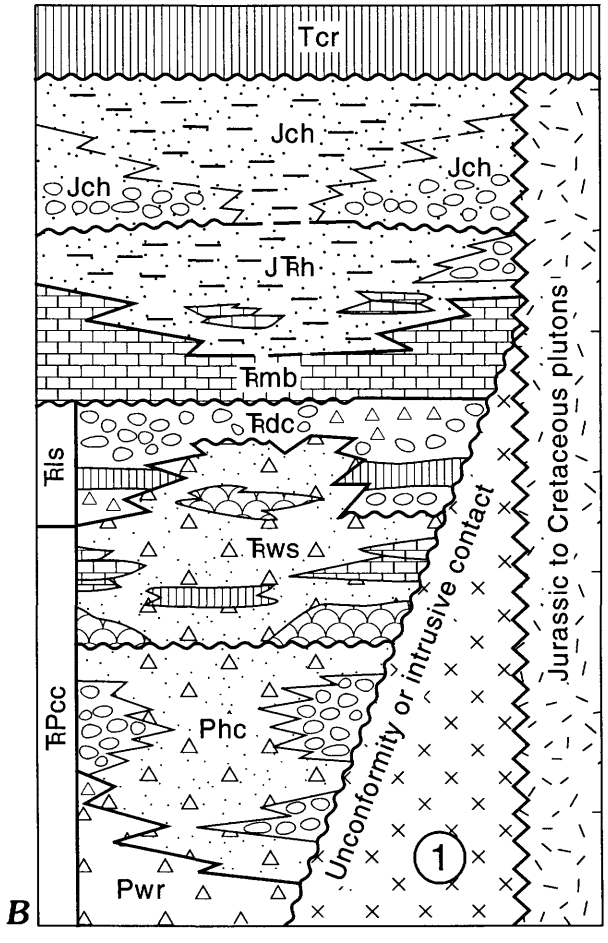

EXPLANATION

Tcr	Columbia River Basalt Group (Miocene)
Jch	Coon Hollow Formation (Upper and Middle Jurassic)
JTrh	Hurwal Formation (Lower Jurassic and Upper Triassic)
Trmb	Martin Bridge Limestone (Upper Triassic)
Trls	"Lower Sedimentary Series" of Prostka (1962) (Upper Triassic)
Trdc	Doyle Creek Formation (Upper and Middle Triassic)—Includes:
Trdck	Kurry unit (Upper Triassic)
Trws	Wild Sheep Creek Formation (Upper and Middle Triassic)
TrPcc	Clover Creek Greenstone (Triassic and Permian)
Phc	Hunsaker Creek Formation (Lower Permian)
Pwr	Windy Ridge Formation (Lower Permian)

Volcanic flows
Sandstone, siltstone, and shale
Conglomerate
Sandstone
Limestone
Breccia
Breccia and sandstone
Pillow lava
Interfingering contact
Intrusive contact
Unconformity

TABLE 3.9.—*Lithology, sample locality, and field description of late Paleozoic and Triassic plutonic and hypabyssal (dike) rocks of the Wallowa terrane*

[Rocks within each group arranged by increasing SiO_2 content to correspond to chemical analyses in tables 3.10 and 3.11. Do. and do., ditto]

Sample	Rock type	Sample locality	Field description and remarks
		Sparta complex	
SP-79-1	Trondhjemite	Bishop Springs, along State Highway 86; elevation 777 m (2,550 ft); NW1/4NW1/4 sec. 6, T. 9 S., R. 44 E.; Sparta quadrangle; Oreg.	Youngest pluton (stock) that cuts older suite (gabbro) of the Sparta complex. Late Triassic in age (Walker, 1986).
V-8-79	do	Ridge west of road to Sparta; elevation 1,036 m (3,400 ft); SE1/4NW1/4 sec. 23, T. 8 S., R. 45 E.; Sparta quadrangle; Oreg.	Dike rock from sequence of trondhjemite and diabasedikes, probably associated with the older suite (gabbro) of the Sparta complex.
V-100-79	Quartz keratophyre	Ridge east of Clover Creek; elevation 982 m (3,220 ft); NW1/4NW1/4 sec. 1, T. 8 S., R. 42 W.; Sawtooth Ridge quadrangle; Oreg.	Dike rock from sequence of quartz keratophyre, trondhjemite, and diabase dikes, probably associated with older suite (gabbro).
		Oxbow Complex	
V-4-73	Gabbro	North side of small tributary near prospect; elevation 1,000 m (3,280 ft); SE1/4NW1/4 sec. 2, T. 19 N., R. 4 W.; Homestead quadrangle; Idaho.	Small intrusion; several textures, mostly massive.
V-67-33	Diabase porphyry	Along old road that parallels Snake River; elevation 537 m (1,760 ft); NW1/4SW1/4 sec. 3, T. 7 S., R. 48 E.; Copperfield quadrangle, Oreg.	Mafic dike crosscut by trondhjemite. Some fluxion structure.
VC-184	Trondhjemite	Below major switchback along old road west of Indian Creek; elevation 774 m (2,540 ft); NW1/4SE1/4 sec. 9, T. 19 N., R. 4 W.; Copperfield quadrangle; Idaho.	Cataclastic rock from wide zone of dikes.
VC-45	do	North side of Scorpion Creek; elevation 817 m (2,600 ft); NW1/4SE1/4 sec. 21, T. 19 N., R. 4 W.; Copperfield quadrangle; Idaho.	Dike cutting gabbroic body.
LC-48	do	North side of Scorpion Creek; elevation 677 m (2,200 ft); SE1/4NW1/4 sec. 21, T. 19 N., R. 4 W.; Copperfield quadrangle; Idaho.	Dike rock from sequence of gabbro, diabase, and trondhjemite dikes.
CO-79-1	do	West side of Oxbow dam; elevation 560 m (1,840 ft); SE1/4NW1/4 sec. 10, T. 7 S., R. 49 E.; Copperfield quadrangle; Oreg.	Dike rock in sequence of diabase and trondhjemite dikes; Late Permian U-Pb age (Walker, 1986).
		Cougar Creek Complex	
T-68-14	Gabbro	South edge of Cougar Creek complex along trail that parallels Snake River; elevation 396 m (1,300 ft); SE1/4 NW1/4 sec. 36, T. 26 N., R. 1 W.; Kernan Point quadrangle; Idaho.	Small pluton that cuts metamorphosed and sheared sedimentary and volcanic rocks.

TABLE 3.9.—*Lithology, sample locality, and field description of late Paleozoic and Triassic plutonic and hypabyssal (dike) rocks of the Wallowa terrane*—Continued

[Rocks within each group arranged by increasing SiO_2 content to correspond to chemical analyses in tables 3.10 and 3.11. Do. and do., ditto]

Sample	Rock type	Sample locality	Field description and remarks
		Cougar Creek Complex—Continued	
V-61-79	---- do ----------	South edge of Cougar Creek Complex along trail that parallels Snake River about 60 m south of sample locality T-68-14; elevation 396 m (1,300 ft).	Do.
V-5-73	---- do ----------	North side of Klopton Creek along ridge; elevation 1,479 m (4,850 ft); SE1/4SE1/4 sec. 26, T. 27 N., R. 1 W.; Grave Point quadrangle; Idaho.	Massive outcrops of pluton cut by Klopton Creek fault. Forms the northern rock unit of the Cougar Creek Complex.
T-68-26	---- do ----------	Along trail that parallels Snake River about 400 m south of Corral Creek; elevation 369 m (1,210 ft); NW1/4SE1/4 sec. 9, T. 26 N., R. 1 W.; Kirkwood Creek quadrangle; Idaho.	Dike rock from sequence of mafic dikes striking about N. 65° E.
V-12-73	Diorite----------	Along road between White Bird and Pittsburg Landing, Idaho; elevation 1,037m (3,400 ft); extreme southwest corner of SW1/4SE1/4 sec. 24, T. 27 N., R. 1 W.; Grave Point quadrangle; Idaho.	Greatly altered and sheared; prehnite and calcite zones indicate extreme calcium mobilization.
V-6-73	---- do ----------	North side of Klopton Creek along ridge; elevation 1,256 m (4,120 ft); SE1/4SW1/4 sec. 26, T. 27 N., R. 1 W.; Grave Point quadrangle; Idaho.	Associated with gabbro sampled at same locality as V-5-73. Minor part of mostly gabbroic pluton.
V-37-79	Quartz diorite---------	North of White Bird Creek-Salmon River confluence; elevation 550 m (1,800 ft); NE1/4SE1/4 sec. 34, T. 29 N., R. 1 E.; White Bird quadrangle; Idaho.	From series of dikes and small stocks (trondhjemite, quartz diorite, and diabase).
KC-79-1	---- do ----------	Ridge south of Corral Creek; elevation 885 m (2,900 ft); NE1/4SW1/4NE1/4 sec. 16, T. 26 N., R. 1 W.; Kirkwood Creek quadrangle; Idaho.	Pluton that cuts across mafic sequence. Probably among youngest rocks in Cougar Creek Complex. Permian U-Pb age(Walker, 1986).
T-68-11	Trondhjemite ---------	Along trail that parallels Snake River about 400 m north of Cougar Creek; elevation 397 m (1,300 ft); T. 1 N., R. 50 E. (unsurveyed); Kirkwood Creek quadrangle; Oreg.	Dike rock from sequence of trondhjemite and mafic dikes.
T-68-23	---- do ----------	Along trail that parallels Snake River; elevation 390 m (1,280 ft); NW1/4 NE1/4 sec. 36, T. 26 N., R. 2 W.; Kernan Point quadrangle; Idaho.	Dike rock from sequence of dikes that range from gabbro to trondhjemite in composition.
V-66-79	---- do ----------	Along trail that parallels Snake River; elevation 385 m (1,260 ft); NE1/4 sec. 30, T.26 N., R. 1 W.; Kirkwood Creek quadrangle; Idaho.	Sheared, partly mylonitized dike rock from sequence of dikes striking about N. 50° E.
V-35-79	---- do ----------	North of White Bird Creek-Salmon River confluence; elevation 543 m (1,780 ft); NE1/4SE1/4 sec. 34, T. 29 N., R. 1 E.; White Bird quadrangle; Idaho.	Dike rock from series of dikes and small stocks (trondhjemite, quartz diorite, and diabase).

Table continued on next page.

TABLE 3.9.—*Lithology, sample locality, and field description of late Paleozoic and Triassic plutonic and hypabyssal (dike) rocks of the Wallowa terrane*—Continued

[Rocks within each group arranged by increasing SiO_2 content to correspond to chemical analyses in tables 3.10 and 3.11. Do. and do., ditto]

Sample	Rock type	Sample locality	Field description and remarks
		Cougar Creek Complex—Continued	
TP-l3	Diorite	Pittsburg Landing area; elevation 565 m (1,850 ft); SW1/4SE1/4 sec. 28, T. 27 N., R. 1 W.; Grave Point quadrangle; Idaho.	Clast typical of well-rounded igneous rock clasts in conglomerate of the Coon Hollow Formation; all 29 igneous rock clasts collected at this locality apparently were eroded from the nearby Cougar Creek Complex.
TP-l5	Quartz diorite	do	Do.
TP-l8	do	do	Do.
		Wolf Creek-Deep Creek and Imnaha plutonic rocks	
V-70-79	Gabbro	Near mouth of Wolf Creek; elevation 320 m (1,050 ft); SEl/4 sec. 9, T. 28 N., R. 2 W.; Wolf Creek quadrangle; Idaho.	Part of basement intrusive complex. Most outcrops are massive; sampled gabbro shows rare rough layering.
DR-SR-79-1	Trondhjemite	Along Snake River near confluence with Imnaha River l00 m upstream from "Mile l92" and near old mine; elevation 305 m (1,000 ft); unsurveyed part of canyon; Deadhorse Ridge quadrangle; Oreg.	From outcrops that are mostly quartz diorite and diorite in composition. Associated with rugged outcrops of gabbro upstream.
V-72-79	Aplite	Near mouth of Deep Creek; elevation 310 m (1,020 ft); near south boundary of T. 4 N., R. 49 E. (unsurveyed); Cactus Mountain quadrangle; Oreg.	Dike rock from abundant mostly vertical white to buff dikes that cut gabbro.
		Sheep Creek pluton	
T-68-2	Meladiorite	North side of Bills Creek in Snake River Canyon; elevation 442 m (1,450 ft); NE1/4NW1/4 sec. 16, T. 24 N., R. 2 W.; He Devil quadrangle; Idaho.	Mafic part of Sheep Creek pluton. Contact zone with country rock is sheared.
HD-79-1	Quartz diorite	North side of Sheep Creek near trail; elevation 500 m (1,640 ft); NE1/4SE1/4 sec. 35, T. 25 N., R. 2 W.; He Devil quadrangle; Idaho.	Permian U-Pb age (Walker, 1986). Light gray rocks contain blue quartz. Coarse grained.
T-68-3	do	North side of Sheep Creek near trail 200 m downstream from sample site HD-79-1; elevation 482 m (1,580 ft); NE1/4SE1/4 sec. 35, T. 25 N., R. 2 W.; He Devil quadrangle; Idaho.	Probably same age as dated sample HD-79-1. Similar texture and mineralogy.
T-68-1	Trondhjemite	North side of Bills Creek; elevation 450 m (1,480 ft); NE1/4NW1/4 sec. 16, T. 24 N., R. 2 W.; He Devil quadrangle; Idaho.	Silicic part of Sheep Creek pluton at Bills Creek. Coarse grained.

TABLE 3.9.—*Lithology, sample locality, and field description of late Paleozoic and Triassic plutonic and hypabyssal (dike) rocks of the Wallowa terrane*—Continued

[Rocks within each group arranged by increasing SiO_2 content to correspond to chemical analyses in tables 3.10 and 3.11. Do. and do., ditto]

Sample	Rock type	Sample locality	Field description and remarks
		Plutons of southern Seven Devils Mountains	
V-2-84	Gabbro	Along trail near Joe's Gap; elevation 2,440 m (8,000 ft); SW1/4NW1/4 sec. 4, T. 21 N., R. 2 W.; Cuprum quadrangle; Idaho.	Permian(?) or Early Triassic(?) White Mountain pluton of White (1968). Probably related to Cougar Creek and Oxbow Complexes.
V-4-84	Diorite	Along trail near Black Lake Fork; elevation 1,982 m (6,500 ft); NW1/4NE1/4 sec. 2, T. 21 N., R. 2 W.; Cuprum quadrangle; Idaho.	Pactolian pluton of White (1968). Probably Permian or Early Triassic in age and related to Cougar Creek and Oxbow Complexes.
V-3-84	---- do	Along trail east of Joe's Gap; elevation 2,395 m (7,850 ft); extreme northwest corner NW1/4NW1/4SW1/4 sec. 3, T. 21 N., R. 2 W.; Cuprum quadrangle; Idaho.	Horse Pasture pluton of White (1968). Probably Permian or Early Triassic in age and related to Cougar Creek and Oxbow Complexes.
V-1-84	Quartz diorite	Along trail northwest of Joe's Gap; elevation 2,250 m (7,380 ft); NE1/4NE1/4 sec. 5, T. 21 N., R. 2 W.; Cuprum quadrangle; Idaho.	Big Lake pluton of White (1968). Probably Permian or Early Triassic in age and related to Cougar Creek and Oxbow Complexes.
		Salmon River canyon plutonic rocks	
V-39-79	Diorite	North side of Salmon River; elevation 780 m (2,560 ft); SW1/4NW1/4 sec. 3, T. 31 N., R. 2 W.; Boles quadrangle; Idaho.	Relatively massive diorite and quartz diorite pluton; altered and mineralized, particularly along shear zones.
V-57-79	Trondhjemite	In Box Canyon along U.S. Highway 95 and the Salmon River; elevation 512 m (1,680 ft); SW1/4SE1/4 sec. 1, T. 26 N., R. 1 E.; Lucile quadrangle; Idaho.	Dike rock from sequence of silicic and mafic dikes. Permian U-Pb age (Walker, 1986).
		Plutons within the Blue Mountains anticline	
V-20-79	Hornblende gneiss	Along road that parallels Stanley Creek; elevation 1,073 m (3,520 ft); NE1/4NE1/4 sec. 32, T. 25 N., R. 32 E.; Granite Meadows quadrangle; Oreg.	Within Blue Mountains anticline; probably part of metagabbro unit mapped by Trauba (1975).
V-17-79	Trondhjemite	At major turn along road that parallels Pearson Creek; elevation 1,073 m (3,520 ft); SE1/4NE1/4NE1/4 sec. 9, T. 3 S., R. 33 E.; Tamarack Gulch quadrangle; Oreg.	Small pluton that cuts volcanic sequence (silicic and mafic flows and volcaniclastic rocks).

Table continued on next page.

TABLE 3.9.—*Lithology, sample locality, and field description of late Paleozoic and Triassic plutonic and hypabyssal (dike) rocks of the Wallowa terrane*—Continued

[Rocks within each group arranged by increasing SiO_2 content to correspond to chemical analyses in tables 3.10 and 3.11. Do. and do., ditto]

Sample	Rock type	Sample locality	Field description and remarks
		Wildhorse River dike	
V-5-84	Trondhjemite	North side of bridge that crosses Wildhorse River (northwest of Cuddy Mountains); elevation 738 m (2,420 ft); SE1/4NE1/4NE1/4 sec. 33, T. 18 N., R/ 4 W.; Brownlee quadrangle, Idaho.	Dike rock along major fault separating Wallowa and Baker terranes.

TABLE 3.10.—*Major- and minor-element oxides of late Paleozoic and*

[Oxides in weight percent, normalized to 100 percent; prenormalization volatile contents included

	Sparta complex			Oxbow Complex					
Sample	S-79-1	V-8-79	V-100-79	V-4-73	V-67-33	VC-184	VC-45	LC-48	CO-79-1
SiO_2	70.07	74.54	79.85	51.49	53.60	71.40	73.63	74.73	75.56
TiO_2	.59	.36	.29	1.35	1.23	.58	.43	.39	.33
Al_2O_3	14.40	12.97	12.67	16.68	18.20	14.44	14.67	13.99	13.27
Fe_2O_3	2.36	1.67	.13	5.88	2.37	2.12	1.62	1.42	.95
FeO	2.48	1.74	.11	6.00	7.61	1.62	.93	1.12	1.15
MgO	1.22	.88	.29	4.74	4.12	1.21	.84	.81	.64
MnO	.06	.05	---	.19	.23	.12	.07	.06	.03
CaO	3.89	3.26	.39	9.14	8.33	2.63	1.11	1.42	1.90
Na_2O	3.56	3.67	5.73	3.61	3.29	4.14	6.57	4.56	4.41
K_2O	1.25	.79	.54	.72	.79	1.62	.05	1.42	1.70
P_2O_5	.12	.07	---	.20	.23	.12	.08	.08	.06
H_2O^+	0.84	0.75	0.52	3.10	2.60	1.00	0.85	1.00	0.85
H_2O^-	.09	.09	.26	.84	.17	.12	.15	.14	.11
CO_2	.04	.07	.04	.02	.02	.32	.03	.04	.21
FeO_{total}/MgO	3.77	3.70	.78	2.38	2.37	2.92	2.84	2.96	3.13

	Cougar Creek Complex—Continued				Wolf Creek-Deep Creek and Imnaha plutonic rocks			Sheep Creek pluton	
Sample	V-35-79	TP-13	TP-15	TP-18	V-70-79	DR-SR-79-1	V-72-79	T-68-2	HD-79-1
SiO_2	76.47	56.66	65.78	69.07	50.65	72.31	78.68	53.80	68.22
TiO_2	.30	.80	1.44	1.18	.78	.40	.17	.75	.56
Al_2O_3	12.86	22.07	14.31	17.48	18.40	14.64	11.79	17.87	14.88
Fe_2O_3	1.43	1.10	1.74	1.07	2.64	.77	.89	2.87	2.47
FeO	.64	1.44	2.00	2.99	6.44	1.27	.18	5.02	2.45
MgO	.58	2.22	1.19	1.35	6.65	1.34	.21	5.04	1.95
MnO	.08	.03	.12	.07	.17	---	---	.14	.10
CaO	2.95	8.11	6.56	2.10	11.42	4.75	4.07	10.81	4.65
Na_2O	3.96	5.76	6.03	3.69	2.64	4.09	3.96	3.04	4.13
K_2O	.73	1.50	.39	.69	.15	.43	.05	.57	.49
P_2O_5	---	.31	.44	.31	.06	---	---	.09	.10
H_2O^+	0.76	2.00	1.30	1.70	1.00	0.93	0.42	1.31	1.12
H_2O^-	.04	.63	.34	.44	.11	.16	.04	.10	.11
CO_2	.03	.02	3.10	.68	.07	.04	---	.10	.04
FeO_{total}/MgO	3.01	1.10	3.00	2.93	1.33	1.47	4.41	1.51	2.40

plutonic rocks. Earlier work gave K-Ar and $^{40}Ar/^{39}Ar$ ages of 223 to 212 Ma. U-Pb studies by Walker (1986) yielded a $^{206}Pb/^{238}U$ age of 215 Ma for the younger plutonic suite, in good agreement with the K-Ar and $^{40}Ar/^{39}Ar$ age determinations. Zircons in trondhjemite from the older plutonic suite have a $^{206}Pb/^{238}U$ age of 252 Ma. On the basis of these new data, field relations, and a regional understanding of similar plutonic complexes, it is apparent that there are at least two separate plutonic suites in the Sparta complex: the older plutonic rocks are Late Permian in age and the younger plutonic rocks crystallized in the Late Triassic. Good outcrops of both suites are along State Highway 86 in the Powder River canyon west of Richland, Oreg.; particularly good outcrops of the younger plutonic rocks are near Bishop Springs along State Highway 86 in the Sparta quadrangle (table 3.9; fig. 3.2).

Some obvious compositional differences between the two plutonic suites are shown in tables 3.10 and 3.11 and in figure 3.18*A*. The older suite is composed mostly of gabbro, trondhjemite, quartz diorite, quartz keratophyre, and diabase and is very similar to parts of the Canyon Mountain, Oxbow, and Cougar Creek Complexes; rare ultramafic rocks occur along the southern border of the Sparta complex and rocks of intermediate compositions are uncommon. In places, the rocks are variably sheared and metamorphosed. Included in the older suite are abundant Na-rich felsic plutonic bodies, particularly albite-rich trondhjemite (albite granite of Gilluly, 1933). The younger suite

Triassic plutonic and hypabyssal (dike) rocks of the Wallowa terrane

to indicate amount of alteration. ---, not determined or below instrumental detection limit]

Cougar Creek Complex										
T-68-14	V-61-79	V-5-73	T-68-26	V-12-73	V-6-73	V-1-37-79	KC-79-1	T-68-11	T-68-23	V-66-79
49.35	49.98	50.62	51.76	53.25	54.51	62.81	69.36	71.67	74.90	76.44
1.03	1.10	.83	.51	.98	.45	.70	.36	.41	.28	.28
21.50	18.21	19.51	9.67	18.50	24.21	15.22	15.80	14.16	13.18	13.11
2.46	3.37	3.30	2.81	3.08	2.06	3.37	1.93	2.01	1.84	1.09
5.89	6.81	7.41	7.40	6.89	2.30	3.39	1.53	2.02	1.42	1.16
5.05	6.58	4.92	13.64	4.77	1.46	3.80	1.16	1.22	.89	.76
.15	.19	.23	.21	.23	.07	.13	.12	.08	.03	---
11.73	11.13	10.11	12.19	8.19	10.80	6.41	4.19	4.95	2.87	3.15
2.51	2.38	2.81	1.29	3.27	3.66	3.81	4.05	3.15	4.35	3.78
.23	.20	.18	.45	.60	.36	.25	1.36	.23	.18	.23
.10	.05	.08	.07	.24	.12	.11	.14	.10	.06	---
0.13	1.02	0.68	1.40	2.30	0.21	2.48	0.63	0.97	0.67	0.83
.91	.10	.28	.30	.32	.32	.16	.11	.17	.30	.14
.08	.03	.02	.20	.16	.03	.01	.05	.02	.20	.02
1.61	1.50	2.11	.73	2.03	2.85	1.69	2.82	3.14	3.46	2.82

Sheep Creek pluton—Continued		Plutons of southern Seven Devils Mountains				Salmon River canyon plutonic rocks		Plutons within Blue Mountains anticline		Wildhorse River dike
T-68-3	T-68-1	V-2-84	V-4-84	V-3-84	V-1-84	V-39-79	V-57-79	V-20-79	V-17-79	V-5-84
68.93	70.74	51.66	59.31	59.39	69.60	57.34	74.60	44.22	77.69	77.08
.53	.45	.50	1.27	1.20	.57	.93	.29	1.03	.38	.26
14.54	14.94	19.89	16.42	15.71	14.72	17.39	13.65	21.07	12.09	12.16
2.53	.63	1.78	3.95	3.57	1.93	2.07	1.70	3.03	1.06	.86
2.01	1.66	4.57	4.55	4.61	2.43	5.91	.55	9.65	.91	.70
1.67	1.49	6.66	2.67	2.92	1.30	4.92	.49	6.90	.53	.55
.09	.03	.10	.18	.19	.09	.18	---	.23	.03	.04
5.05	4.30	10.97	5.88	6.41	2.80	5.39	2.85	12.30	2.94	1.57
4.08	4.98	2.67	4.05	4.62	4.11	4.55	5.32	1.34	4.19	4.53
.52	.71	1.20	1.38	1.07	2.32	1.18	.50	.17	.12	2.20
.05	.07	---	.34	.31	.13	.14	.05	.06	.06	.05
1.12	1.28	2.33	1.40	2.01	0.860	2.48	0.63	3.51	0.40	0.68
.18	.20	.16	.06	.04	.07	.16	.04	.21	.14	.06
.25	.04	.20	.06	2.00	.07	.01	.10	.28	.03	1.01
2.57	1.50	.93	3.04	2.68	3.20	1.58	4.24	1.79	3.52	2.66

TABLE 3.11.—*Trace elements of selected late Paleozoic and Triassic*

[Results in parts per million. Analysis by neutron activation unless otherwise noted. ---, not

	Sparta complex			Oxbow Complex		Cougar Creek Complex		
Sample-----	S-79-1	V-8-79	V-100-79	V-4-73	CO-79-1	T-68-14	V-61-79	V-5-73
Rb ----------	[1]29	---	---	[1]15	21	---	[1]3	[1]9
Sr----------	172	[1]169	[1]94	[1]311	127	[2]410	[1]367	[1]392
Ba ----------	26	[1]349	117	[1]143	440	94	[1]69	[1]117
Th ----------	2.94	---	1.06	.38	2.13	---	---	---
U----------	2.04	---	.65	---	1.02	---	---	---
La ----------	9.6	---	5.3	5.1	11.4	3	1	1.7
Ce ----------	19.6	---	11.3	12.4	25.5	7	5	4
Sm----------	3.1	---	1.4	---	3.4	2	1.2	1.3
Eu ----------	.92	---	.63	1.11	.81	.76	.64	.61
Gd ----------	3.42	---	---	---	3.4	1.8	2.6	---
Tb ----------	.56	---	---	.63	.61	.43	.33	.29
Tm----------	---	---	---	---	---	---	---	.22
Yb ----------	2.04	---	1.53	2.17	3.21	3.0	---	1.49
Lu ----------	.33	---	.29	.33	.53	.48	.19	.21
Y ----------	[2]34	[2]45	[2]8	[1]25	[2]28	[2]22	[1]10	[1]15
Zr----------	234	[1]170	187	[1]84	164	---	[1]4	[1]33
Hf----------	7.11	---	5.57	1.76	4.63	1.0	.6	.4
Ta ----------	.254	---	.41	---	.35	---	---	---
Nb ----------	---	---	---	[1]9	---	---	---	9
Ni----------	[2]6	---	---	---	---	[2]35	---	---
Co ----------	7.6	[2]6	.4	30	3	26	33	29
Cr----------	8.2	[2]4	---	13	2	49	99	---
Sc----------	9	[2]17	5	31	7	27	35	34
Zn ----------	----	[2]30	---	91	---	[2]74	[2]83	[2]98

	Cougar Creek Complex—Continued		Wolf Creek-Deep Creek and Imnaha plutonic rocks			Sheep Creek pluton			
Sample-----	TP-15	TP-18	V-70-79	DR-SR-79-1	V-72-79	T-68-2	HD-79-1	T-68-3	T-68-1
Rb ----------	---	[1]19	[1]8	---	[1]3	7	---	6	10
Sr----------	[1]154	[1]238	[1]357	266	[1]211	[2]360	198	[2]150	[2]160
Ba ----------	[1]92	[1]138	[1]60	[1]63	[1]26	140	154	210	150
Th ----------	2.48	2.63	---	.88	1.0	.90	1.68	1.50	1.4
U----------	1.19	.90	---	.36	---	---	.77	.80	.7
La ----------	13.1	9.5	2	2.9	3	7	8.9	8	5
Ce ----------	31.5	22.8	4	.4	6	22	21.1	19	15
Sm----------	8.4	---	1.2	2.0	---	---	3.4	3.1	3.1
Eu ----------	1.85	1.51	.65	.37	.43	1.11	.90	.85	.72
Gd ----------	---	---	---	2.1	---	6.4	3.70	---	3.5
Tb ----------	---	1.20	.34	.37	---	1.25	.73	.55	.52
Tm----------	.99	.60	---	---	---	---	---	---	---
Yb ----------	6.95	4.79	1.4	1.65	1.00	4.70	3.51	3.0	2.5
Lu ----------	.89	.66	.20	.26	.14	.69	.57	.48	.38
Y ----------	[1]54	[1]41	[1]10	[2]12	[1]8	[2]54	[2]39	[2]31	[2]27
Zr----------	[1]206	[1]187	[1]32	107	[1]112	---	124	150	130
Hf----------	7.04	6.19	.6	3.13	4.6	1.50	3.81	4.3	3.9
Ta ----------	.47	.38	---	.22	.30	.24	.38	.33	.32
Nb ----------	[1]5	[1]8	---	---	---	---	---	---	---
Ni----------	---	---	---	7	---	[2]26	[2]6	[2]6	[2]8
Co ----------	6	8	32	2.6	.7	22	10	6	3
Cr----------	2	5	117	3.7	7.4	56	12	7	---
Sc----------	15	21	38	3	4	32	18	13	9
Zn ----------	37	127	78	---	---	83	69	35	12

[1]Analysis by X-ray fluorescence.
[2]Analysis by emission spectroscopy.

plutonic and hypabyssal (dike) rocks of the Wallowa terrane

determined or below detection limit or discarded because of high coefficient of variation]

Cougar Creek Complex—Continued									
T-68-26	V-12-73	V-6-73	V-37-79	KC-79-1	T-68-11	T-68-23	V-66-79	V-35-79	TP-13
[1]12	[1]15	[1]19	[1]6	[1]27	[1]6	---	---	---	[1]40
[1]117	[1]308	[1]478	[1]233	377	[1]206	[1]179	[1]239	[1]304	[1]317
[1]63	[1]192	[1]173	[1]99	230	[1]71	[1]124	[1]215	[1]197	[1]231
.42	.29	.24	0.6	1.57	.34	.79	---	---	.52
.20	---	---	---	.97	---	.36	---	---	.48
4.1	5	2.9	7	15.4	3.4	5.1	---	---	4.7
10.6	12.1	6.6	17	34.9	6.5	9.5	---	---	11.9
1.9	---	1.7	3.3	4.0	1.4	1.6	---	---	2.8
.39	.83	.93	1.05	1.11	.6	.6	---	---	1.02
---	---	---	---	3.5	---	2.0	---	---	---
.31	.63	.26	.74	---	---	---	---	---	.50
---	.30	---	---	---	---	---	---	---	.30
---	2.56	1.04	3.0	2.5	1.36	1.38	---	---	2.35
.31	.39	.16	.45	.41	.22	.21	---	---	.34
[1]17	[1]25	[1]13	[1]22	24	[1]16	[1]17	13	---	[1]24
[1]39	[1]41	[1]51	[1]103	110	[1]98	[1]116	[1]255	[1]255	[1]125
.73	1.0	.97	2.7	3.1	2.55	3.15	---	---	3.56
---	---	---	.12	.24	---	.14	---	---	.21
8	8	6	---	---	[1]6	[1]6	---	---	[1]6
---	---	---	---	---	---	---	---	---	---
45	27	9	20	5	7	6.1	---	[2]3	5
964	7	2	23	1	3	4	[2]9	4	4
85	31	12	23	5	13	9	[2]10	---	18
[2]125	[2]115	[2]39	[2]64	[2]150	[2]48	[2]29	---	---	26

Plutons of southern Seven Devils Mountains				Salmon River canyon plutonic rocks		Rocks within Blue Mountains anticline		Wildhorse River dike
V-2-84	V-4-84	V-3-84	V-1-84	V-39-79	V-57-79	V-20-79	V-17-79	V-5-84
33	26	24	42	[1]24	---	11	[1]4	33
250	260	150	200	[1]183	[1]220	817	[1]171	[2]85
194	350	208	552	[1]316	[1]197	35	[1]143	386
.15	1.11	1.86	2.87	.40	---	---	1.5	3.12
---	.52	.94	1.14	---	---	---	.6	.81
1.27	8.62	10.50	15.40	7	---	1	7	9.40
4.35	23.60	29.50	36.90	21	---	4	14	20.30
1.37	5.20	5.89	4.78	4.2	---	1.7	2.5	2.12
.72	1.66	1.69	1.14	.85	---	.77	1.12	.48
---	6.03	7.10	5.28	6.1	---	---	3.3	2.00
.30	.96	1.12	.86	1.04	---	.48	.66	.35
.19	.63	.71	.60	---	---	---	---	.30
1.18	3.99	4.49	3.88	---	---	---	3.99	1.96
.18	.61	.67	.57	.70	---	.37	.58	.30
---	35	40	35	[1]37	249	12	[1]26	[2]20
23	217	215	166	[1]65	[1]170	38	[1]114	73
.48	6.33	6.03	4.97	2.6	---	.6	3.3	2.73
.03	.24	.31	.39	.61	---	---	.27	.36
---	---	---	---	---	---	---	---	---
---	---	---	---	---	---	23	---	---
22	16	17	7	23	[2]4	36	1.5	3
240	139	14	4	44	[2]4	13	1.4	14
37	25	27	12	29	27	47	13	5
---	91	94	51	[2]115	---	104	2	33

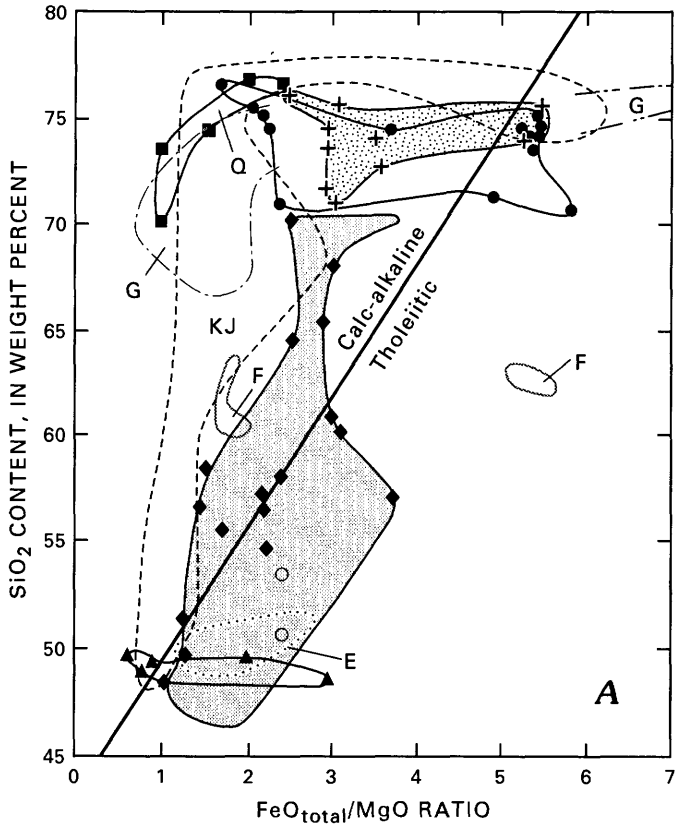

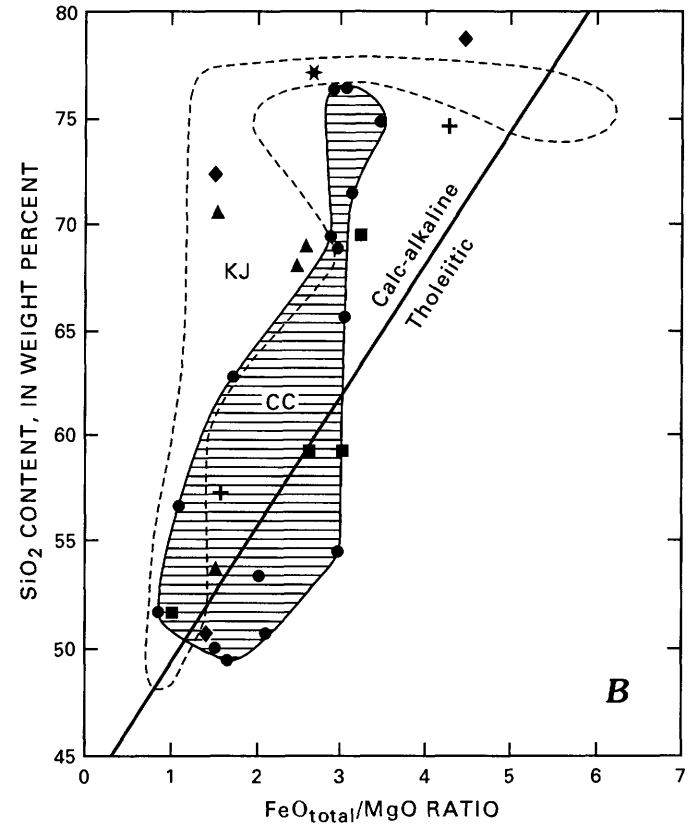

EXPLANATION

(Informal) Sparta complex of Phelps (1979)

Bishop Springs plutonic rocks

Gabbro, diorite, tonalite—Data field represents compositional range; diamonds, separate samples

Older plutonic rocks—Heavy line encloses range of samples for each composition

Gabbro

Trondhjemite

Quartz keratophyre

Oxbow Complex of Vallier (1967a, b)

Trondhjemite—Data field represents compositional range; crosses, separate samples

Amphibolite

EXPLANATION

Cougar Creek Complex of Vallier (1968)—Data field (CC) represents compositional range; dots, separate samples

Sheep Creek plutonic rocks

Wolf Creek-Deep Creek and Imnaha plutonic rocks

Southern Seven Devils Mountains plutonic rocks

Salmon River canyon plutonic rocks

Wildhorse River dike

FIGURE 3.18.—FeO_{total}/MgO ratio versus SiO_2 content for plutonic rocks of Wallowa terrane. Calc-alkaline–tholeiitic compositional boundary from Miyashiro (1974). *A*, (Informal) Sparta complex of Phelps (1979) and Oxbow Complex of Vallier (1967a, b). New data (this chapter) supplemented by data from Almy (1977) and Phelps (1978). Note Fe-enriched compositions of almost all plutonic rocks. Quartz keratophyre samples (data field Q) show calc-alkaline affinity on the basis of this diagram only. Strongly fractionated igneous rocks (SiO_2 contents above approximately 70 percent) generally show calc-alkaline affinities on this diagram as explained in text. For comparison, areas representing Aleutian plutonic rocks (E, F, G) and Jurassic to Cretaceous plutonic rocks of Blue Mountains region (KJ) are shown (see fig. 3.4). *B*, Cougar Creek Complex of Vallier (1968) and other Permian and Triassic plutonic rocks of Wallowa terrane. Note calc-alkaline affinities of many plutonic rocks. For comparison, area (KJ) representing Jurassic to Cretaceous plutons (see fig. 3.18*A*) is shown. Also, compare with plots of plutonic rocks of Oxbow Complex and (informal) Sparta complex (fig. 3.18*A*).

consists of gabbro, diorite, and quartz diorite (tonalite); highly siliceous trondhjemite is rare or absent. These younger rocks, compared to rocks in the older suite, are less felsic, are less metamorphosed, and have undergone less shearing. Biotite is common in some of the younger plutonic rocks, whereas it is absent in the older plutonic rocks.

The chemical differences between the older and younger suites are well shown in figure 3.18*A*. Highly fractionated trondhjemite and quartz keratophyre, mostly of the older group, occupy data fields in the upper part of the figure and overlap both Aleutian siliceous plutonic rocks and the more siliceous Jurassic to Cretaceous plutons of the Blue Mountains region. The data field for the (undivided) Sparta complex and Oxbow Complex on the FeO_{total}/MgO versus Ce_n/Yb_n ratio diagram (fig. 3.19) overlaps parts of the field for the Aleutian Okmok Caldera tholeiite. Rocks of these two complexes are more enriched in LREE's than most rocks of the Canyon Mountain Complex.

OXBOW COMPLEX

The Oxbow Complex was described by Vallier (1967a, b, 1974) and named for rocks exposed near the Oxbow Dam and in the Indian Creek canyon northeast of the dam. Geology of the Oxbow region also has been studied by Phelps (1978), Balcer (1980), Schmidt (1980), Walker (1986), and Avé Lallemant (chap. 7, this volume).

Rocks in the Oxbow Complex are similar to many in the Sparta complex and in the Cougar Creek Complex (figs. 3.18*A*, 3.18*B*, 3.19, 3.20*A*, 3.20*B*). Rock types are amphibolite, mylonite, gneissic mylonite, gneiss, diabase, quartz keratophyre, gabbro, diorite, quartz diorite, and trondhjemite. Rocks in a wide shear zone consist of mylonite, gneissic mylonite, and amphibolite; protomylonite and ultramylonite also occur. The shear-zone unit is extremely foliated. The foliation planes strike approximately parallel to the strike of the dikes (about N. 35°–60° E.); dips on foliation planes vary from about 60° NW to vertical to

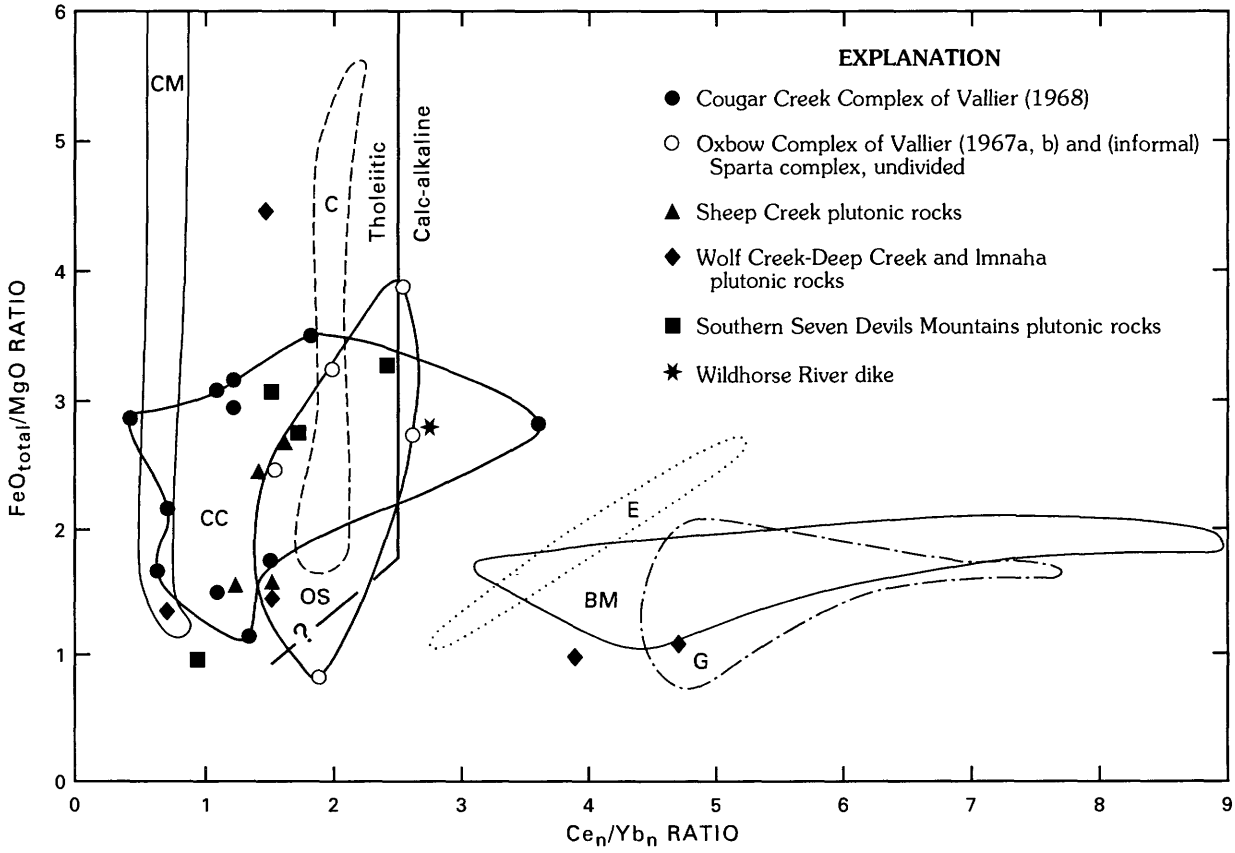

FIGURE 3.19.—FeO_{total}/MgO versus Ce_n/Yb_n ratios for late Paleozoic and Triassic plutonic rocks of Wallowa terrane. Data fields for Bald Mountain batholith (BM), tholeiitic rocks of Okmok Caldera (C), Canyon Mountain Complex (CM), and Aleutian island arc plutonic rocks (E and G) are shown for comparison. Diagram also includes plutonic rocks of Cougar Creek Complex of Vallier (1968) (data field CC) and the undivided Oxbow Complex of Vallier (1967a, b) and (informal) Sparta complex of Phelps (1979) (data field OS). Line, dashed and queried where uncertain, separates tholeiitic from calc-alkaline fields. n, chondrite normalized.

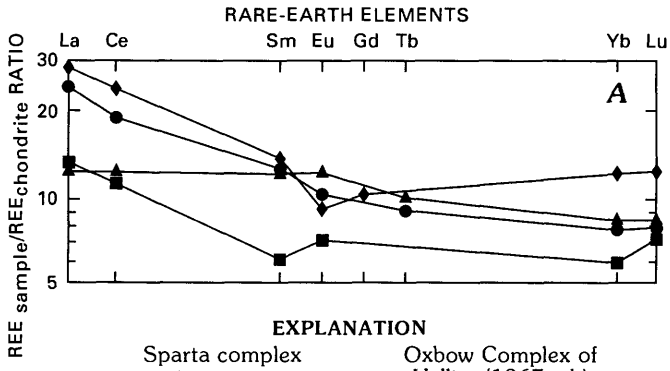
RARE-EARTH ELEMENTS
La Ce Sm Eu Gd Tb Yb Lu
REE sample/REE chondrite RATIO
30
20
10
5
A
EXPLANATION
Sparta complex (informal)
Sample V-100-79
Sample SP-79-1
Oxbow Complex of Vallier (1967a, b)
Sample V-4-73
Sample CO-79-1

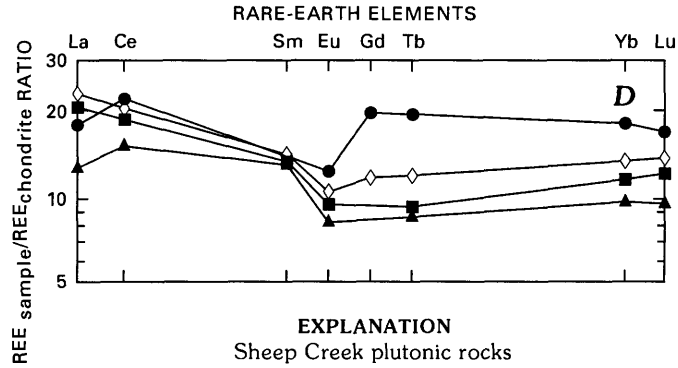
RARE-EARTH ELEMENTS
La Ce Sm Eu Gd Tb Yb Lu
REE sample/REE chondrite RATIO
30
20
10
5
D
EXPLANATION
Sheep Creek plutonic rocks
Sample T-68-1
Sample T-68-3
Sample HD-79-1
Sample T-68-2

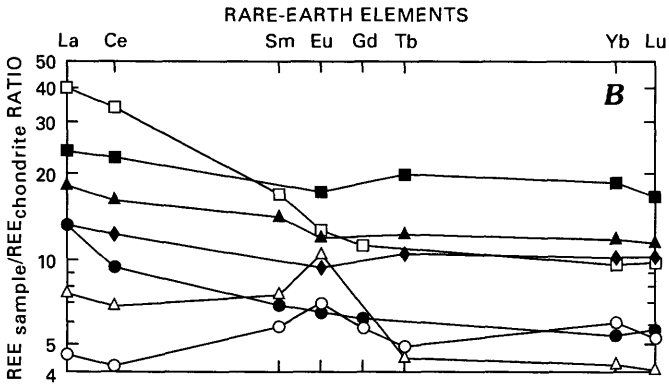
RARE-EARTH ELEMENTS
La Ce Sm Eu Gd Tb Yb Lu
REE sample/REE chondrite RATIO
50
40
30
20
10
5
4
B
EXPLANATION
Cougar Creek Complex of Vallier (1968)
Sample V-5-73
Sample V-6-73
Sample T-68-23
Sample V-12-73
Sample V-37-79
Sample TP-18
Sample KC-79-1

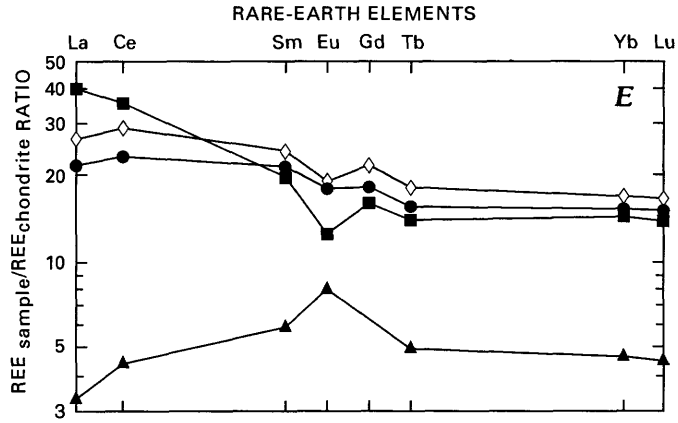
RARE-EARTH ELEMENTS
La Ce Sm Eu Gd Tb Yb Lu
REE sample/REE chondrite RATIO
50
40
30
20
10
5
3
E
EXPLANATION
Southern Seven Devils plutonic rocks
Sample V-2-84
Sample V-1-84
Sample V-4-84
Sample V-3-84

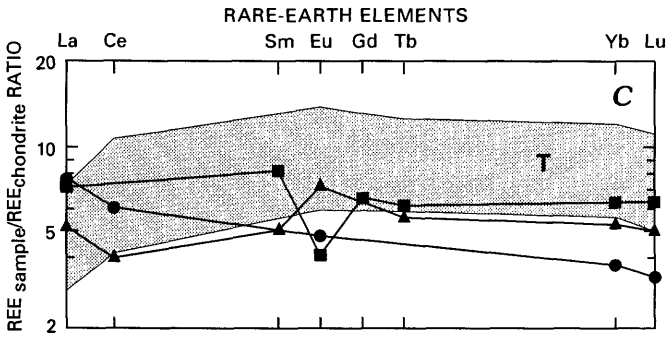
RARE-EARTH ELEMENTS
La Ce Sm Eu Gd Tb Yb Lu
REE sample/REE chondrite RATIO
20
10
5
2
C
T
EXPLANATION
Wolf Creek-Deep Creek and Imnaha plutonic rocks
Sample V-72-79
Sample V-70-79
Sample DRSR-79-1
Aleutian island arc
T
Mafic plutonic rocks of Terrible Mountain, Attu Island (n=5) (Eocene?)

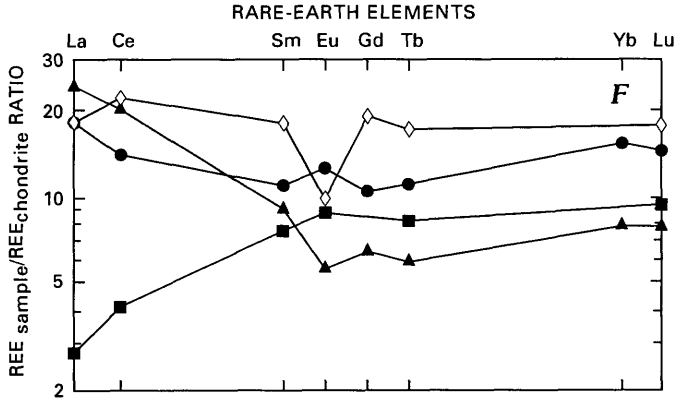
RARE-EARTH ELEMENTS
La Ce Sm Eu Gd Tb Yb Lu
REE sample/REE chondrite RATIO
30
20
10
5
2
F
EXPLANATION
Wildhorse River dike
Sample V-5-84
Salmon River canyon plutonic rocks
Sample V-39-79
Blue Mountains anticline plutonic rocks
Sample V-20-79
Sample V-17-79

60° SE. Lineations of stretched quartz and amphibole crystals are nearly horizontal; some have shallow plunges.

Mapped field relations show that the oldest units in the Oxbow Complex are gabbro, trondhjemite, meladiorite, and diabase that crop out in Idaho near the mouth of Indian Creek. Dikes whose predeformation compositions include quartz keratophyre, diabase, gabbro, and basalt occur in the wide shear zone, which subsequently was intruded by quartz diorite, trondhjemite, and diabase. All gradations of mechanical deformation are evident in the Oxbow Complex: unsheared plutonic and hypabyssal rocks through cataclasites, mylonites, mylonite gneisses, and ultramylonites. Rare tachylite in some shear zones suggests postmetamorphic movement. The history of tectonic movement, however, is not simple. There is good evidence for Triassic sinistral movement (Avé Lallemant, chap. 7, this volume).

U-Pb radiometric ages (Walker, 1986) of rocks in the Oxbow Complex are 249 Ma ($^{206}Pb/^{238}U$ on mylonite sample CO-80-1) and 225 to 222 Ma ($^{206}Pb/^{238}U$ on two zircon fractions from trondhjemite sample CO-79-1). An $^{40}Ar/^{39}Ar$ age of 214 Ma on hornblende from an amphibolite in the shear zone is interpreted as the time of Ar retention in the hornblende after metamorphism (Phelps, 1978). Avé Lallemant and others (1980) reported an $^{40}Ar/^{39}Ar$ age of 220 Ma for an amphibolite of the Oxbow Complex. Balcer (1980) reported weighted-average $^{40}Ar/^{39}Ar$ plateau ages of 227.8±5.3 Ma and 219.2±7.6 Ma for two hornblende cooling ages and interpreted them as "a minimum age for deformation and peak regional metamorphism in this terrane" (p. 49). Events interpreted from these isotopic ages are (1) Late Permian (about 249 Ma) dike injections, probably into an older (or comagmatic) gabbro-trondhjemite complex, (2) Late Triassic (225–222 Ma) injection of trondhjemite, and (3) Late Triassic (228–219 Ma) shearing and metamorphism that occurred during sinistral movement (Avé Lallemant, chap. 7, this volume). An unsheared lamprophyre dike with an $^{40}Ar/^{39}Ar$ age of 197.4 Ma cuts the mylonites (Avé Lallemant and others, 1985), thereby indicating that most deformation in the Oxbow Complex had ceased by middle Early Jurassic time.

The petrography of most rock types in the Oxbow Complex was discussed by Vallier (1967a). In general, the older protoliths are metamorphosed to the amphibolite (and hornblende hornfels) facies and to the greenschist (and albite-epidote hornfels) facies. Mafic rocks were more susceptible to metamorphism than the felsic rocks. Most siliceous plutonic rocks have an assemblage of albite, chlorite, blue-green hornblende, epidote and, locally, secondary quartz, sphene, leucoxene, white mica, and (or) pyrite as the metamorphic phases. Amphibolite-grade mafic rocks have feldspar (andesine and oligoclase) and blue-green amphibole as major minerals, with chlorite and epidote and possibly also sphene, pyrite, and (or) quartz as minor minerals.

Most rocks selected for chemical analyses (tables 3.9–3.11) are siliceous, although mafic and intermediate rocks compose as much as 50 percent of the exposures. The gabbro (sample V-4-73) lies close to the contact between the Hunsaker Creek Formation and the Oxbow Complex and may cut both rock bodies; field relations are not clear. Except for sample VC-45, K_2O values are higher than those from many other trondhjemitic plutonic bodies in the Wallowa terrane (table 3.10). Sample VC-45 also has a high Na_2O value. The FeO_{total}/MgO ratios versus SiO_2 contents and FeO_{total}/MgO versus Ce_n/Yb_n ratios (figs. 3.18*A*, 3.19) show an Fe-enrichment trend in both the mafic and silicic rocks. The isotopically dated siliceous sample (CO-79-1) has relatively high REE contents (figs. 3.20*A*, 3.20*B*) compared to rocks from the Cougar Creek Complex and the (informal) Sparta complex.

◀ FIGURE 3.20.—Rare-earth element (REE) diagrams of late Paleozoic and Triassic plutonic and hypabyssal rocks of Wallowa terrane. Sample numbers correspond to those in tables 3.9 to 3.11; for normalizing values used, see figure 3.6. *A*, Oxbow Complex of Vallier (1967a, b) and (informal) Sparta complex of Phelps (1979). *B*, Cougar Creek Complex of Vallier (1968). All samples yield nearly flat REE patterns (excluding Eu), except sample KC-79-1, whose trend is transitional to calc-alkaline. *C*, Wolf Creek-Deep Creek and Imnaha plutonic rocks. These plutonic rocks are strongly tholeiitic. Note negative europium anomaly for sample DRSR-79-1. Data field (n=5) for Terrible Mountain (Attu Island of Aleutian island arc; see fig. 3.6) is shown for comparison. *D*, Sheep Creek plutonic rocks. This diagram shows that Sheep Creek plutonic rocks are derived from tholeiitic magma by extreme fractionation with some light rare-earth element (LREE) enrichment. *E*, Southern Seven Devils Mountains plutonic rocks. Big Lake pluton (sample V-1-84) has so-called transitional pattern shown by some LREE enrichment. *F*, Miscellaneous plutonic rocks. Note strong LREE depletion of hornblende orthogneiss (sample V-20-79) from Blue Mountains anticline. Sample V-5-84 trend is transitional to calc-alkaline.

COUGAR CREEK COMPLEX

The Cougar Creek Complex (Vallier, 1968, 1974; Balcer, 1980; Walker, 1986) is best exposed for about 10 km along the Snake River canyon between Temperance Creek and Pittsburg Landing (fig. 3.3), but it

apparently extends northeasterly beneath Tertiary basalt and crops out again in the Salmon River canyon north of Whitebird, Idaho. Furthermore, exposures along the South Fork of the Clearwater River east of Grangeville, Idaho, are strikingly similar to, and essentially on structural trend with, the Cougar Creek Complex. The area between the Salmon River near Whitebird and the South Fork of the Clearwater River east of Grangeville has a Tertiary basalt cover. If the Cougar Creek Complex does extend from Temperance Creek on the Snake River northeasterly about 65 km to the South Fork of the Clearwater River, then the complex is a major structural feature within the Wallowa terrane. The Cougar Creek Complex in its type area near Pittsburg Landing has been faulted against sheared Permian and Triassic stratified rocks along the southeast side and is faulted over rocks of the Jurassic Coon Hollow Formation on the northwest.

The Cougar Creek Complex is structurally and petrologically diverse. Most shear zones composed of mylonite and amphibolite are deformed dike (or sill) sequences. The dike/shear zones trend about N. 60°–70° E. and dip steeply. In places the mylonitic foliation itself is folded, indicating more than one deformation. Individual dikes range in width from a few centimeters to as much as 10 m. A marked foliation, resulting from mylonitization, parallels the preexisting dike (or sill) trends in most outcrops. A distinct subhorizontal lineation is formed by stretched quartz porphyroblasts and long axes of amphibole crystals.

The wide range of igneous rock compositions is shown in tables 3.9 to 3.11. The coarse-grained plutonic rocks comprise gabbro, norite, meladiorite, diorite, quartz diorite, and trondhjemite; finer grained diabase, quartz keratophyre, basalt, and andesite also occur, particularly in dike (or sill) zones. Protoliths of the mylonite, gneissic mylonite, and amphibolite in dike zones probably include most of the rock types just mentioned; in places plagioclase-rich dikes are similar to plagioclase cumulates.

Chlorite schist and hornblende schist are locally abundant, particularly along the Oregon side of the Snake River canyon near Salt Creek. Metasedimentary rocks are faulted into the complex; metasedimentary rock outcrops along the trail just south of Suicide Point are composed of stretched-clast conglomerate and breccia, sandstone, and argillite.

The effects of metamorphism are variable in rocks of the Cougar Creek Complex; most dike rocks and rocks within wide zones of shearing are in the greenschist and amphibolite facies. Many plutonic rocks (samples T-68-14, V-61-79, V-5-73, V-6-73, and KC-79-1), however, are not intensely altered. Primary minerals (calcic plagioclase, orthopyroxene, clinopyroxene, hornblende, and biotite) are relatively unaffected in some samples selected several meters from fractures and shears. In the amphibolite bodies, however, high-temperature metamorphic minerals such as hornblende and andesine show retrograde metamorphic effects, indicated by rims of albite surrounding the andesine and rims of chlorite and (or) epidote surrounding hornblende.

Plutonic rocks of the Cougar Creek Complex are mildly Fe-enriched, as shown on the FeO_{total}/MgO ratio versus SiO_2 content diagram (fig. 3.18*B*), and somewhat more calc-alkaline—or transitional—than most other pre-Jurassic plutonic rocks of the Blue Mountains island arc. Most have low K_2O contents (table 3.10). Trace-element concentrations (table 3.11) indicate a wide range of rock types and diverse crystallization histories. Plots of FeO_{total}/MgO versus Ce_n/Yb_n ratios and chondrite-normalized REE diagrams (figs. 3.19 and 3.20*B*) indicate that most plutonic rocks of the Cougar Creek Complex are tholeiitic, marked by relatively flat REE patterns. Only sample KC-79-1 (fig. 3.20*B*) has a trend that appears to be transitional between calc-alkaline and tholeiitic.

Balcer (1980) determined $^{40}Ar/^{39}Ar$ ages on amphiboles from a deformed gneissic unit; the ages, based on Ar-release spectra, range from 239.2 to 225.8 Ma and average 233.6 Ma. Balcer (1980, p. 48) suggested that the average age "is the time at which this area of the Cougar Creek shear zone cooled below 500±50° C and as such represents an upper limit to the time of peak metamorphism and deformation." Further work by Walker (1986) on rocks from a similar gneissic unit, using two zircon fractions and a Tera-Wasserburg diagram, suggests a late Carboniferous (Middle Pennsylvanian) age of 309(?) Ma for magmatic crystallization. Younger siliceous plutonic bodies cut the older gneissic and sheared-dike units. One of these younger bodies, a hornblende-biotite quartz diorite (sample KC-79-1), contained two zircon fractions that yielded the concordant latest Permian $^{206}Pb/^{238}U$ age of 246 Ma. Walker (1986) subsequently sampled a similar intrusive body of the Cougar Creek Complex and determined a Late Permian $^{206}Pb/^{238}U$ age of 256 Ma. A siliceous protomylonite collected from the dike zone near the mouth of Two Corral Creek yielded a U-Pb age 262 Ma (Walker, 1986).

The Cougar Creek Complex had a long history of igneous activity that may have started as early as 309 Ma. The 262-Ma age of the mylonitized silicic dike analyzed by Walker (1986) is about the same as the age of the Lower Permian tuffaceous rocks of the

Hunsaker Creek Formation. This similarity in age suggests that the rocks are related. The younger, and relatively unmetamorphosed, plutonic bodies with ages of 256 and 246 Ma probably mark the end of Permian igneous activity. These Late Permian rocks are about the same age as the older plutonic rocks in the Sparta complex and the Oxbow Complex. The average 233.6-Ma amphibole age that was determined by Balcer (1980) is strikingly close to the fossil age of the Middle Triassic (Ladinian) volcanic rocks of the Wild Sheep Creek Formation in the Wallowa terrane.

The 309(?)-Ma rocks of the Cougar Creek Complex may be the oldest rocks in the Wallowa terrane. If some of the rocks of the Canyon Mountain Complex are as old as 314 Ma, as suspected by Walker (chap. 6, this volume), then the two plutonic units may have been spatially linked during the late Carboniferous and Permian. These old plutonic rocks may represent parts of an ancient arc terrane that later hosted Permian and Triassic igneous intrusions and volcanic eruptions.

Recent mapping (T.L. Vallier, unpub. data, 1992) of the Cougar Creek Complex suggests that the rock body is a tilted fragment of island-arc crust that formed at deep to intermediate depths (probably 5–15 km). The rocks occur in distinct bands or layered units. Mylonite zones both occur within and separate some of the layered units. The older rocks to the north consist of gabbro, norite, and diabase that have been deformed and recrystallized into amphibolite and gneissic gabbro. The igneous rocks become more fractionated and siliceous to the south (shallower depth), ending in mostly trondhjemite, quartz diorite, rhyolite, diabase, and rare gabbro intrusive bodies. The igneous rocks of the Cougar Creek Complex are overlain by volcanic flow rocks, conglomerate, breccia, and sandstone.

WOLF CREEK-DEEP CREEK AND IMNAHA PLUTONIC ROCKS

A plutonic-rock complex crops out in places beneath Tertiary basalt in the Snake River canyon east of the mouth of the Imnaha River (Morrison, 1963; Vallier, 1974). These rocks are herein informally referred to as the Wolf Creek-Deep Creek plutonic rocks in the eastern outcrops and the Imnaha plutonic rocks in the west near the mouth of the Imnaha River (figs. 3.2, 3.3). The two areas are separated by an inlier of the Columbia River Basalt Group that reaches river level and covers the older plutonic rock bodies (Vallier, 1974). The plutonic rock bodies are bordered on the northeast by a northwest-trending shear zone (Morrison, 1963; Chen, 1985), which is well exposed in the lower parts of Divide Creek. The metamorphosed and structurally deformed rocks in the shear zone are similar to many rocks of the Cougar Creek Complex.

An initial $^{87}Sr/^{86}Sr$ ratio of 0.70311±0.00001 was obtained for a gabbro (sample V-70-79, table 3.9) near the mouth of Wolf Creek. The rock is relatively unaltered (tables 3.10 and 3.11) and has very low REE contents (fig. 3.20*C*) that show a flat tholeiitic trend, a positive Eu anomaly, and depletion in LREE's. The initial Sr-isotope ratio is low even for midocean-ridge basalt and island-arc basalt (Gill, 1981); chemically, it is the most primitive gabbro yet analyzed from the Wallowa terrane.

A striking feature of the Wolf Creek-Deep Creek plutonic rocks is the abundance of pegmatitic and aplitic dikes. The pegmatite dikes are composed predominantly of large feldspar and quartz crystals (some have lengths of 5 cm or more), with or without muscovite. The pegmatite dikes crop out mostly in the eastern parts of the inlier along the Snake River; they range from a few centimeters to tens of meters in width and anastomose irregularly within the host rocks. The aplite dikes crop out mostly in the western part of the inlier; these steeply dipping white to buff dikes are thin (all are less than 50 cm wide, and most are 10 to 20 cm wide) and cut sharply across a gabbro host. The aplite dikes protrude like slivers from the gabbro host; from a distance, the sheer black canyon walls appear to be broken by thin, nearly vertical white lines.

An aplite selected for chemical analyses (sample V-72-79) contains mostly plagioclase and quartz and, as expected, has relatively high amounts of SiO_2, Al_2O_3, CaO, and Na_2O. K_2O content is extremely low (table 3.10). Trace-element analyses (table 3.11) show low amounts of REE's and Y, and relatively high concentrations of Zr and Hf. The Ce_n/Yb_n ratio is about 1.5 (fig. 3.19). From field relations and chemistry, it appears that the aplite is a late-stage differentiation product of the host gabbro. As the gabbro cooled, extension-induced fractures developed, thereby allowing volatile-charged fluids to be injected into the fractures, where they crystallized as dikes.

Walker (1986) selected a trondhjemite sample from a plutonic body near the mouth of Deep Creek for isotopic dating using the U-Pb method. Three zircon fractions had concordant $^{206}Pb/^{238}U$ ages of 231 Ma (late Ladinian on the time scale of Palmer, 1983).

A sample selected for chemistry from the Imnaha plutonic bodies (DR-SR-79-1) is petrographically and chemically similar to many of the other Permian and Triassic trondhjemites in the Wallowa and Baker terranes. It has notably high SiO_2 and low K_2O contents.

Its tholeiitic affinity is indicated by both a low Ce_n/Yb_n ratio (fig. 3.19) and the REE plot (fig. 3.20*C*), which is relatively flat with a strong negative Eu anomaly. This sample gave slightly discordant $^{206}Pb/^{238}U$ ages (Walker, 1986) of 228 and 225 Ma (Karnian). Balcer (1980) used the $^{40}Ar/^{39}Ar$ dating technique on hornblende from four samples of plutonic bodies exposed near the mouth of the Imnaha River and determined ages of 225.0±2.3 Ma, 223.3±5.9 Ma, 215.6±3.6 Ma, and 213.0±2.0 Ma (Karnian and Norian Stages of the Triassic).

Rocks from the Imnaha and Wolf Creek-Deep Creek plutonic bodies apparently crystallized in the Middle and Late Triassic (late Ladinian and Karnian, with some crystallization occurring possibly as late as the Norian). The ages are the same as, and slightly younger than, those of the major Triassic volcanic units in the Wallowa terrane (Ladinian and Karnian Wild Sheep Creek and Karnian Doyle Creek Formations). The plutonic and volcanic events, therefore, are related in time and space. The plutonic bodies probably are the crystallized magma chambers that fed one or more Middle and Late Triassic volcanoes in the Wallowa terrane.

Sheared rock bodies (Morrison, 1963; Chen, 1985; Avé Lallemant, chap. 7, this volume) in the Divide Creek area north of the Imnaha plutonic bodies probably are composed of Permian and Triassic rocks that were deformed prior to and during intrusion of the plutons. Foliated rocks in the Imnaha plutonic bodies (Morrison, 1963) imply that some deformation occurred during crystallization.

SHEEP CREEK PLUTONIC ROCKS

Plutonic bodies in the Sheep Creek area of the Snake River canyon (fig 3.3) have a broad compositional range, but the contacts between the bodies have not been well mapped. A gabbro and diorite body crosses the river near the mouth of Bills Creek and parallels the river for about 12 km in Idaho along the hanging wall of a thrust fault. In the Sheep Creek canyon, the intrusive bodies are mostly trondhjemite and quartz diorite. Four rocks were sampled for chemical analyses (tables 3.9–3.11); one, a quartz diorite sample (HD-79-1), was dated isotopically using the U-Pb method (Walker, 1986). This sample is similar, both petrographically and in outcrop characteristics, to many of the Permian and Triassic plutonic rocks in other parts of the Wallowa terrane. Where mapped north of Sheep Creek, the quartz diorite body is both in structural contact with and overlain unconformably by Triassic rocks of the Wild Sheep Creek Formation. Trondhjemite and quartz diorite clasts in overlying conglomerate of the Wild Sheep Creek Formation indicate erosion of the plutonic rocks during the Middle Triassic (Vallier, 1977).

The Sheep Creek plutonic rocks are calc-alkaline on the basis of the FeO_{total}/MgO ratios versus SiO_2 contents (fig. 3.18*B*), but are definitely tholeiitic on the basis of the FeO_{total}/MgO versus Ce_n/Yb_n ratios (fig. 3.19) and REE patterns (fig. 3.20*D*). The REE patterns are nearly flat. Ce_n/Yb_n ratios range from 1.3 to 1.6. All samples have negative Eu anomalies. Sr contents are lower than in many other Permian and Triassic plutonic rocks in the Wallowa terrane; Hf, Zr, Ba, and Ta values are within the range of those for other Permian and Triassic plutonic rocks in the terrane.

Two zircon fractions from sample HD-79-1 yielded concordant Early Permian U-Pb ages of 263 Ma (Walker, 1986). Clasts of Sheep Creek plutonic rocks in overlying strata of the Wild Sheep Creek Formation indicate significant tectonic uplift and erosion from about 263 to 235 Ma (the latter is the probable oldest age of the Wild Sheep Creek Formation).

PLUTONIC ROCKS OF THE SOUTHERN SEVEN DEVILS MOUNTAINS

Plutonic rock bodies in the southern Seven Devils Mountains are well described by White (1968) who mapped six plutons in an "old mafic suite," three in an "older granitic suite," and two in a "younger granitic suite." I selected samples from four separate plutonic bodies for chemical analysis (tables 3.9–3.11): gabbro (V-2-84) from the White Mountain pluton; diorite (V-4-84) from the Pactolian pluton; diorite (V-3-84) from the Horse Pasture pluton; and quartz diorite (V- 1-84) from the Big Lake pluton. The first three belong to White's (1968) "old mafic suite," and sample V-1-84 belongs to his "older granitic suite."

Three of the four samples are Fe-enriched (fig. 3.18*B*). Their K_2O contents are higher than those of most other late Paleozoic and Triassic plutonic rocks in the Wallowa terrane; P_2O_5 and Rb also are enriched (tables 3.10 and 3.11). In the more siliceous samples (diorite and quartz diorite), Th, U, Zr, and Hf abundances also are greater than in most other Permian and Triassic plutonic rocks of the Wallowa terrane. The FeO_{total}/MgO versus Ce_n/Yb_n ratios (fig. 3.19) and REE patterns (fig. 3.20*E*) show that the plutonic rocks are tholeiitic to transitional in composition.

Crystallization ages are unknown. White (1968) suggested that the two older suites are most likely Late Triassic to Late Jurassic in age. Some of the plutonic bodies are in fault contact with Permian stratified rocks on the west and are on trend with

the Oxbow Complex, which is Late Permian and Triassic in age. On the basis of chemistry, mineralogy (mostly greenschist-facies minerals), and field relations—all of which are similar to those of known Permian and Triassic plutonic rocks in the Wallowa terrane—I infer that the "old mafic suite" and "older granitic suite" of White (1968) are also Permian and Triassic in age.

PLUTONIC ROCKS OF THE SALMON RIVER CANYON

There is a broad assortment of plutonic bodies in the Salmon River canyon between Riggins, Idaho, and the mouth of the Salmon River (figs. 3.1, 3.3). Some are dike units and are very similar to Permian dike rocks in the Cougar Creek Complex. Other plutonic bodies, from field relations and mineralogy, are similar to known Permian and Triassic plutonic bodies in other parts of the Wallowa terrane. Still others are nearly unaltered and may be as young as Late Cretaceous in age.

A trondhjemite sample (V-57-79, table 3.9) was taken from one of several plutonic bodies exposed in the Salmon River canyon north of Riggins, Idaho. This sample is from the same outcrop as Walker's (1986) sample LU 8-1, which was radiometrically dated. Sample V-57-79 was chemically analyzed (tables 3.10–3.11), and an initial Sr-isotope ratio of 0.70425±0.00003 was determined. Two zircon fractions yielded concordant $^{206}Pb/^{238}U$ ages of 260 Ma (sample LU 8-1; Walker, 1986). The U-Pb age of 260 Ma (Early Permian) suggests that the pluton may have crystallized from a magma that had served as a source for some of the siliceous flows and tuffs of the Hunsaker Creek Formation.

PLUTONIC ROCKS ASSOCIATED WITH THE BLUE MOUNTAINS ANTICLINE

Along the Blue Mountains anticline (fig. 3.1; Trauba, 1975; Shorey, 1976), igneous rocks have similarities to rocks from both the Baker and Wallowa terranes. For example, ultramafic rocks are abundant along the Blue Mountains anticline (Trauba, 1975); this abundance is more characteristic of the Baker terrane than of the Wallowa terrane. In the Tucannon River area of southern Washington (fig. 3.1), four inliers expose pre-Tertiary rocks (Huntting, 1942) that are similar to those found in both terranes. The largest and most central inlier (Huntting, 1942, fig. 4) has argillite, chert, and greenstone that are very similar to many rocks composing the Elkhorn Ridge Argillite of the Baker terrane. The southernmost exposures along Panjab Creek (a tributary of the Tucannon River), however, have volcanic (flow) and volcaniclastic rocks similar to those of the Seven Devils Group (Vallier, 1977) in the Wallowa terrane. Huntting (1942) mapped a small amount of supposed diorite that is similar to metagabbro common to both terranes. Therefore, rocks in those inliers along the Tucannon River may have been part of either the Baker or Wallowa terrane.

The rocks analyzed for this study have been placed in the Wallowa terrane. My most recent work suggests they should instead be assigned to the Baker terrane; however, sufficient justification for such a reassignment is beyond the purpose and scope of this chapter.

Hornblende gneiss and trondhjemite of probable Permian and possible Triassic age from the inlier south of Pendleton, Oreg. (Trauba, 1975), were sampled for chemical analyses (V-20-79 and V-17- 79, tables 3.9–3.11) and strontium isotopic analysis (sample V-21-79). Major-, minor-, and trace-element chemistry of sample V-20-79, a hornblende gneiss, suggests that it was derived from a primitive gabbro. Its extremely low REE contents, especially the extremely depleted LREE's (fig. 3.20*F*), and a La_n/Lu_n ratio of about 0.3 (Yb was not determined) indicate its tholeiitic affinity. Another hornblende gneiss sample, V-21-79, has an initial $^{87}Sr/^{86}Sr$ ratio of 0.70367±0.00006, which suggests a depleted mantle source.

Sample V-17-79, a Na_2O-rich trondhjemite (albite granite), contains quartz (light blue) and albite as the major minerals, with some epidote, chlorite, and sphene as secondary minerals. High amounts of Na_2O and low K_2O contents (table 3.10) show its similarity to some of the older trondhjemitic plutonic rocks in the Wallowa and Baker terranes. The FeO_{total}/MgO versus Ce_n/Yb_n ratios (fig. 3.19) and REE patterns (fig 3.20*F*) strongly suggest a tholeiitic classification. This trondhjemite is very similar to siliceous plutonic rocks of the Canyon Mountain Complex and to some in the (informal) Sparta complex. Although trondhjemite sample V-17-79 has a higher initial $^{87}Sr/^{86}Sr$ ratio (0.70418±0.00005) than sample V-21-79, described above, its ratio is well within the range expected of igneous rocks from an intraoceanic island arc (Gill, 1981).

WILDHORSE RIVER DIKE

A trondhjemite dike sample (V-5-84) was collected in the Wildhorse River canyon (table 3.9). This metamorphosed dike is near, and may be within, a major shear zone that separates the Baker and Wallowa terranes (Mann, 1988). The dike most likely was emplaced

during Permian to Late Triassic time. Compared to most other Permian and Triassic intrusive bodies in the Wallowa terrane, this dike rock has unusually high amounts of K_2O and Rb, a relatively high amount of Ba, and a low Sr content (tables 3.10 and 3.11). The FeO_{total}/MgO versus Ce_n/Yb_n ratios (fig. 3.19) and REE patterns (fig. 3.20*F*) show characteristics that are transitional between tholeiitic and calc-alkaline. It has one of the highest Ce_n/Yb_n ratios (about 2.7) of all Wallowa terrane Permian and Triassic plutonic rocks (fig. 3.19). High contents of LREE's, Rb, and Ba parallel the K_2O content. Metasomatism may have been important in producing the dike rock's unusual chemistry.

PETROGENESIS OF PLUTONIC ROCKS OF THE WALLOWA TERRANE

Plutonism was active throughout most of the Permian and Triassic in the Wallowa terrane (fig. 3.21). Isotopic ages indicate Permian and Middle to Late Triassic plutonic pulses. The Permian ages of plutonic rocks in the Wallowa terrane are about the same

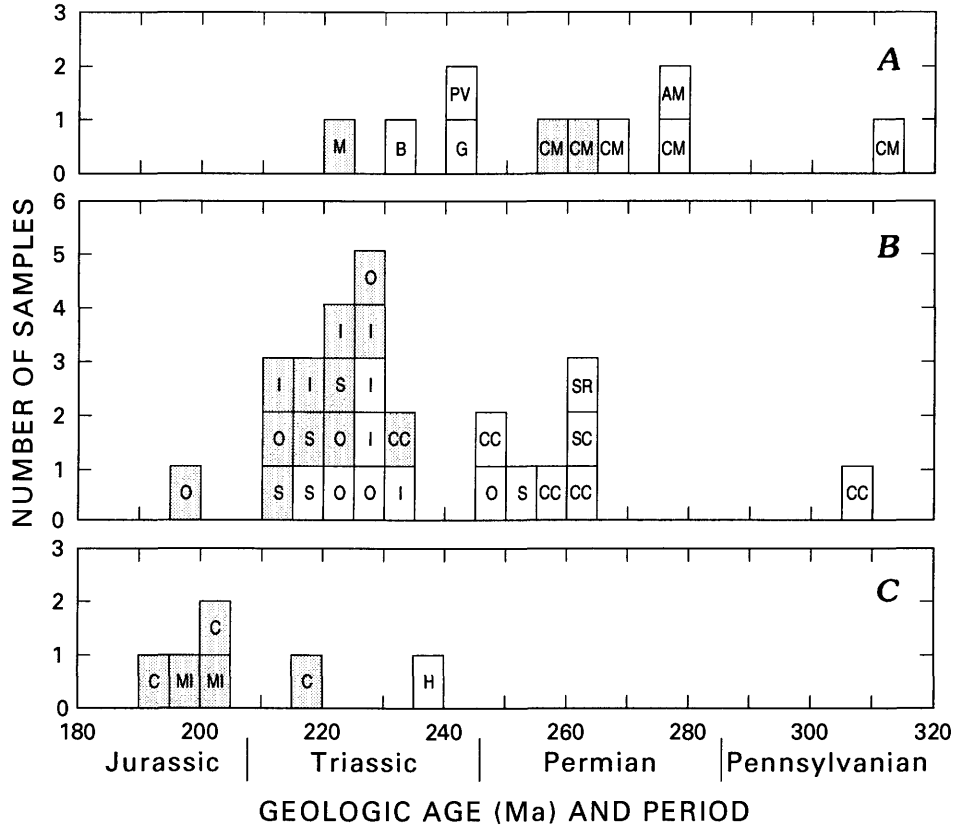

FIGURE 3.21.—Isotopic ages ranging from Pennsylvanian(?) to Early Jurassic for plutonic rock samples from Baker, Wallowa, and Olds Ferry terranes of Blue Mountains island arc. Shading indicates ages determined by K-Ar methods; other ages were determined by U-Pb methods (Walker, 1986). Where a large range is reported in K-Ar ages for a particular sample or group of samples from the same plutonic body, the oldest age was used in compiling the histograms. Palmer's (1983) time scale is followed in this diagram. See text for specific age determinations and data sources. *A*, Baker terrane. AM, melange of Aldrich Mountain; B, dike or sill cutting Burnt River Schist; CM, samples from Canyon Mountain Complex; G, trondhjemite of Granite Creek; M, blueschist near Mitchell, Oreg., which is about 50 km west-northwest of John Day, Oreg. (fig. 3.1); PV, trondhjemite at Pleasant Valley in Oxman quadrangle, Oreg. *B*, Wallowa terrane. CC, Cougar Creek Complex of Vallier (1968); I, plutonic rocks of Imnaha-Deep Creek area; O, Oxbow Complex of Vallier (1967a, b) (youngest age is for crosscutting lamprophyre dike reported by Avé Lallemant, chap. 7, this volume); S, (informal) Sparta complex of Phelps (1979); SC, plutonic rocks of Sheep Creek; SR, Salmon River plutonic rocks; *C*, Olds Ferry terrane. C, Cuddy Mountains plutonic rocks; H, Brownlee Reservoir plutonic body exposed near Huntington, Oreg.; MI, plutonic rocks of Mineral-Iron Mountain mining district.

as the youngest ages of dated rocks in the Canyon Mountain Complex in the Baker terrane (fig. 3.21*A*); these age relations suggest a comagmatic series. The Middle to Late Triassic plutonic pulse is particularly distinct in the Wallowa terrane (fig. 3.21*B*).

Plutonic rocks of the Permian and Triassic suites in the Wallowa terrane are similar. Na_2O-rich trondhjemites occur in both suites, but they are more common in the Permian plutonic rocks. Almost all of the larger complexes have gabbro, diorite, quartz diorite, and trondhjemite plutonic bodies with diabase-quartz keratophyre-trondhjemite dike sequences. I presume that the Permian plutonic bodies served as zones of weakness for the intrusion of Middle and Late Triassic plutons; a good example is the Late Triassic diorite-quartz diorite unit (exposed along State Highway 86 near Bishop Springs), which apparently was emplaced into older Permian rocks of the (informal) Sparta complex. Quartz keratophyre dikes and associated trondhjemite plutonic bodies of Permian age are no doubt related to the Na_2O-rich and K_2O-poor Permian volcanic rocks (flows and tuffs) of the Wallowa terrane.

In the following numbered paragraphs, interpretations summarized in table 3.2 and conclusions made by Phelps (1979), Phelps and Avé Lallemant (1980), and Leeman and others (chap. 1, this volume) are used to discuss the petrogenesis and possible tectonic significance of Permian and Triassic plutonism in the Wallowa terrane.

(1) The plutonic rocks are mostly tholeiitic in composition, although a few, such as those from the Sheep Creek plutons, are transitional between calc-alkaline and tholeiitic. Most have low Ce_n/Yb_n ratios, low initial Sr-isotope ratios, and low quantities of K and Ti. Fractional crystallization of plagioclase, olivine, orthopyroxene (not always present), augite, and magnetite (with or without amphibole removal) at relatively low pressures and high temperatures (Gill, 1981; Grove and Baker, 1984) was most likely the dominant differentiation process.

(2) Regional geologic relations, isotopic ages, and rock chemistries suggest that all late Paleozoic and Triassic plutonic bodies were emplaced in a volcanic arc, most likely along the magmatic axis.

(3) A Pennsylvanian(?) U-Pb age for a sample from the Cougar Creek Complex suggests pre-Permian magmatism. The presence of plutonic rock clasts in Lower Permian conglomerates indicates plutonism in the Early Permian, but does not rule out the possibility of older igneous activity. The amount of pre-Permian igneous activity is not known, but it may have been extensive.

(4) The oldest well-documented major plutonic suite crystallized in the interval from 265 to 245 Ma. Rocks from three of the plutonic bodies have U-Pb isotopic ages in the 265- to 260-Ma range, approximately synchronous with the Early Permian eruptions of tuffs and lavas that formed the Hunsaker Creek Formation. Some of the plutons may be crystallized magma chambers that fed the volcanic eruptions.

(5) The plutonic rock samples from the Canyon Mountain Complex of the Baker terrane and the Cougar Creek Complex of the Wallowa terrane that yielded Pennsylvanian(?) radiometric ages may be part of the magmatic axis of an ancient arc associated with the early evolution of the Blue Mountains island arc.

(6) It is clear that trondhjemite with characteristics of oceanic plagiogranite can form in tectonic settings other than midocean spreading centers (Hawkins, 1988). Wherever depleted mantle is partially melted and the resultant melt is not mixed with abundant sediment and (or) liquids derived from the subducting slab, then similar magmas should be expected.

(7) The excess Na_2O in the Na_2O-rich trondhjemites (such as the so-called albite granite of the older plutonic suite of the Sparta complex) may have an entirely igneous origin (Phelps, 1978). If so, the magma chambers probably maintained open systems with free seawater interchange. Spooner and Fyfe (1973) and Coleman (1977) discussed the characteristics of hydrothermal alteration in subsea geothermal (spreading-center) systems; similar effects probably occur in island-arc settings. In an extensional setting, such as that at spreading centers (and in subsea parts of island arcs), circulation of hot seawater is probably voluminous. Tholeiitic magmas are hot and crystallize at relatively shallow levels in the crust; their high temperature and shallow depth can account for both the driving thermal energy and seawater accessibility. Seawater, by directly mixing with the magma during late stages of crystallization through a system of fractures in the upper parts of the chamber, probably has a significant role in Na_2O metasomatism. Furthermore, in volcanic arcs, seawater brine probably can be trapped in the thick piles of subducted sediments; this process would increase the quantity of Na_2O available for metasomatic exchange. In many places within the Na_2O-rich trondhjemite plutons, Na_2O contents of rocks increase in fractures and shear zones; the fractures probably served as conduits for hot seawater. A double diffusive model, such as that proposed by J.L. Bischoff (oral commun., 1989), may be necessary to account for a brine that contains sufficient Na_2O for the extensive metasomatism evident in these altered rocks.

(8) Quartz keratophyre dikes are genetically related to the Na_2O-rich trondhjemites; both rock types are late-stage differentiation products.

(9) Diorite and quartz diorite (younger Triassic plutonic suite) and trondhjemite (older Permian plutonic suite) in the (informal) Sparta complex may be cogenetic, but are not related through the process of magmatic differentiation, as proposed by Phelps (1978, 1979). On the basis of available age and field data, it is evident that separate melting and crystallization took place. The source rocks were either the same or very similar, and the same processes of differentiation occurred.

(10) Liquids with REE concentrations similar to those of the trondhjemite and quartz diorite samples could be generated by partial melting of an oceanic tholeiite (Phelps, 1978; Phelps and Avé Lallemant, 1980). Just as possible, and probably more likely, is that the magmas resulted from partial melting of a depleted mantle with some assimilation of crustal rocks; influences from the downgoing slab probably were minimal. This problem, however, is difficult to sort out in modern arcs (Gill, 1981; Kay, 1984) let alone in ancient arcs, where even the arc polarities are difficult to determine.

(11) Similarities in ages and compositions of many plutonic bodies within the Wallowa terrane suggest a cogenetic relationship. On the basis of the high volume of these rocks, the plutonic rocks appear to underlie and to have intruded a large part of the Wallowa terrane. The older plutons with associated dike sequences (Cougar Creek Complex) probably are either basement or (and) volcano-root magma chambers for the Lower Permian Hunsaker Creek and Windy Ridge Formations; the younger Triassic plutons probably are crystallized magma chambers that evolved beneath Triassic volcanoes.

VOLCANIC (FLOW) AND ASSOCIATED HYPABYSSAL INTRUSIVE ROCKS OF THE WALLOWA TERRANE

Almost all volcanic (flow) and hypabyssal intrusive rocks in the Wallowa terrane are of Permian and Triassic age. Lava flows of Permian age are relatively easy to separate from Triassic flows, both in the field and in the laboratory. The Permian flows are more siliceous, have a near-equilibrium greenschist-facies mineralogy, are extremely Na_2O-rich and K_2O-poor, and are associated with thick sequences of siliceous tuffs. Reflecting both their original petrologic settings and subsequent metamorphism, the Triassic rocks are more mafic, are metamorphosed to different intensities (although mostly in the greenschist facies), and contain variable amounts of Na_2O and K_2O.

PERMIAN VOLCANIC (FLOW) AND ASSOCIATED HYPABYSSAL INTRUSIVE ROCKS

Permian rocks are particularly well exposed in the southern Wallowa Mountains and the Homestead, Oreg., area of the Snake River canyon between Oxbow, Oreg., and the Kleinschmidt grade (Lindgren, 1901; Livingston and Laney, 1920; Anderson, 1930; Gilluly, 1937; Cook, 1954, Wetherell, 1960; Bostwick and Koch, 1962; Vallier, 1967a, b, 1974, 1977; Vallier and others, 1977; Scheffler, 1983; La Pierre and others, 1988). Some reconnaissance studies farther north along the Snake and Salmon River canyons and in the Seven Devils Mountains indicate that Permian rock outcrops are much more extensive than previously realized. Volcanic (flow) rocks and associated hypabyssal intrusive rocks are relatively rare, however, and compose no more than five percent of the Permian sequences.

Vallier (1977) divided the Permian rocks into the Windy Ridge and Hunsaker Creek Formations (fig. 3.17). Best exposures of the Windy Ridge Formation are along the Idaho Power and Light Company road in Idaho immediately north of The Oxbow of the Snake River (Vallier, 1974). The Windy Ridge Formation is composed almost entirely of stratigraphically coherent quartz keratophyre (and keratophyre) pyroclastic rocks and rare lava flows, all of which are cut by mafic dikes. In the siliceous volcanic flows, phenocrysts of quartz and plagioclase feldspar (albite) are set in a felty quartz-albite groundmass. Quartz phenocrysts generally are either bipyramidal or rounded by magmatic resorption. Primary magnetite is uncommon. Penninite and epidote replace the other, originally very rare primary mafic minerals, which were ortho- and clinopyroxenes. In addition to quartz and albite, penninite, sphene, white mica, epidote, calcite, hematite, and pyrite occur in the groundmasses. The mafic dikes are basalt and basaltic andesite porphyries, gabbro, and diabase; in these dikes most mafic minerals have been replaced by epidote and chlorite and the primary plagioclase is replaced by albite. Pumice and other glassy debris in the pyroclastic rocks are entirely recrystallized to quartz and albite; vague outlines of the original fragments can be observed on some slabbed surfaces and in a few thin sections.

The Windy Ridge Formation, originally designated as Early Permian(?) in age (Vallier, 1977) is now considered to be a lithofacies equivalent of the lower part of the Hunsaker Creek Formation (fig. 3.17). Such lithofacies equivalence supports an Early Permian age for the Windy Ridge Formation. The lithologic similarity between this formation and the tuffaceous lower part of the Hunsaker Creek Formation, as well as the poorly exposed contact between the units, makes it reasonable to correlate the units. However, the presence of abundant mafic dikes, the dominance of pyroclastic debris, an absence of epiclastic sedimentary rocks, and the siliceous composi-

tion of the Windy Ridge Formation distinguish it from most parts of the Hunsaker Creek Formation.

The rock types of the Hunsaker Creek Formation (Vallier, 1967a, 1977) are more diverse than those of the Windy Ridge Formation. Most are fragmental (pyroclastic and epiclastic) rocks, many of which are siliceous tuffs that were deposited in a submarine environment. Locally abundant and thick conglomerate and sandstone units indicate close proximity to one or more major landmasses, probably islands. The rocks are dominantly pyroclastic breccia and tuff and epiclastic conglomerate, breccia, sandstone, and siltstone. Although flows are rare, in places dikes are abundant; concentrations of siliceous dikes near Homestead, Oreg., and in the lower parts of Deep Creek canyon in Idaho near the Hells Canyon Dam may mark proximity to volcanic vents. These dikes and sills are part of the Hunsaker Creek Formation. The presence of trondhjemite, quartz diorite, and gabbro clasts in conglomerate units (Wetherell, 1960; Vallier, 1967a, b, 1977) of the Hunsaker Creek Formation indicates not only that the Permian source area was lithologically diverse, but also that the islands were high; erosion of the older plutonic rocks indicates substantial uplift. Furthermore, the islands were eroding contemporaneously with the outpourings of siliceous lavas and tuffs.

Three samples from the Windy Ridge Formation and nine from the Hunsaker Creek Formation were selected for chemical analysis (tables 3.12–3.14). The mineralogy and chemistry of siliceous rocks from the two units are similar. High H_2O and CO_2 contents (table 3.13) reflect both extensive weathering and large amounts of secondary calcite.

Sample VB-79 is from a dike that cuts the Windy Ridge Formation, and samples VS5-1 and VS5-7 are from rhyolite (quartz keratophyre) flows from the Windy Ridge Formation. Sample VB-79 is a low-K basaltic andesite (classification of Gill, 1981). Compared to a representative low-K tholeiitic basaltic andesite from modern arcs as defined by Gill (1981, p. 100), sample VB-79 has relatively high amounts of TiO_2 (2.00 percent for VB-79 versus 0.57 percent for modern arcs), Na_2O (6.73 percent versus 1.8 percent), P_2O_5 (0.41 percent versus 0.08 percent), MnO (0.42 percent versus 0.19 percent), Y (40 parts per million versus 17 parts per million), Zr (140 versus 28 parts per million), Hf (3.4 versus 0.8 parts per million), Nb (7 versus 0.6 parts per million), Zn (1,070 versus 89 parts per million), and relatively high REE contents (tables 18.13 and 18.14). However, it has significantly lower amounts of K_2O (0.04 percent for sample VB-79 versus 0.40 percent for basaltic andesite of modern arcs), CaO (4.27 percent versus 11.0 percent), and Sr (106 parts per million versus 235 parts per million). The abundance of the high-field-strength elements Ti, Zr, Hf, and Nb is more similar to that of alkalic basalt than of island-arc low-K basalt or basaltic andesite. Samples VS5-1 and VS5-7 are quartz keratophyres (low-K rhyolites). These siliceous rocks have abundant Na_2O and low CaO and K_2O contents (table 3.13). Furthermore, sample VS5-7 is enriched in LREE's with a Ce_n/Yb_n ratio of about 2; Sr and Ba contents are depleted and Nb and Y are enriched compared to most modern arc rhyolites.

Volcanic (flow) rocks and associated hypabyssal intrusive rocks in the Hunsaker Creek Formation include rare basalt, basaltic andesite, and andesite with more abundant dacite and rhyolite (quartz keratophyre). No basalt flow was sampled although some of the intraformational dikes and sills are microgabbro, diabase, or basalt porphyry. All rocks have near-equilibrium greenschist-facies mineralogies. Albite replaced most calcic plagioclase, and chlorite and epidote replaced almost all mafic minerals (predominantly pyroxene); the secondary groundmass minerals epidote, chlorite, sphene, calcite, and white mica are ubiquitous. Rare relict clinopyroxene phenocrysts occur (for example in sample VC-197).

Basalt sample VB-88 (tables 3.12 and 3.13) from the Hunsaker Creek Formation has high amounts of TiO_2, Na_2O, and P_2O_5 and a low K_2O content compared to other island-arc basalt (Ewart and others, 1973; Vallier and others, 1985; Kay and Kay, 1991). Ba, Zr, Y, Hf, and the REE contents (table 3.14) also are relatively high. Basaltic andesite samples (VC-131 and VC-197) have relatively high Na_2O contents compared to lavas from modern island arcs. K_2O contents are extremely low. Andesite samples (VB-91 and LS7-32b) have some chemical variability in the amounts of TiO_2 and K_2O, but are consistently high in Na_2O. Rhyolite (quartz keratophyre) samples (VC-225 and VC-15) also have high Na_2O and variable K_2O contents; trace-element contents of sample VC-225 (table 3.14) are similar to those of sample VS5-7 from the Windy Ridge Formation.

Relatively high Na_2O, TiO_2, P_2O_5, Hf, Zr, Y, Ba, and REE contents, compared to those of modern island-arc rocks (for example, see Ewart and others, 1973; Gill, 1981; Vallier and others, 1985; Ewart and Hawkesworth, 1987; Kay and Kay, 1994), and high FeO_{total}/MgO ratios along with low K_2O contents and low Ce_n/Yb_n ratios suggest that the petrogenesis of these Permian rocks is different from that of most igneous rocks of present-day island arcs. According to FeO_{total}/MgO ratios versus SiO_2 contents (fig. 3.22), the rocks are both tholeiitic and calc-alkaline. The Ce_n/Yb_n ratios (fig. 3.23) indicate a tholeiitic trend between those of the Tonga arc and Okmok Caldera in the Aleutians. The REE patterns indicate fractionated-tholeiitic trends and slight LREE enrichment (fig. 3.24). The petrogenesis of these rocks is problematical.

TABLE 3.12.—*Lithology, sample locality, and field description of volcanic (flow) and associated hypabyssal intrusive rocks from the Lower Permian Windy Ridge and Hunsaker Creek Formations*

[Samples arranged by increasing SiO_2 content to correspond to chemical analyses in tables 3.13 and 3.14. Do. and do., ditto]

Sample	Rock type[1]	Sample locality	Field description and remarks
VB-88	Basalt	Along road south of Ballard Creek; elevation 543 m (1,780 ft); SE1/4SW1/4 sec. 11, T. 6 S., R. 48 E.; Homestead quadrangle; Oreg.	Sill in bedded-tuff unit; Hunsaker Creek Formation.
VC-131	Basaltic andesite	Ridge between Homestead Creek and Whiskey Gulch; elevation 975 m (3,200 ft); center of SE1/4 sec. 16, T. 6 S., R. 48 E.; Homestead quadrangle; Oreg.	Lava flow about 4 m thick in tuff breccia sequence; Hunsaker Creek Formation.
VC-197	do	Ridge between Irondyke and Holbrook Creeks; elevation 598 m (1,960 ft); SE1/4SW1/4 sec. 21, T. 6 S., R. 48 E.; Homestead quadrangle; Oreg.	Lava flow about 5 to 6 m thick in mafic tuff breccia; Hunsaker Creek Formation.
VB-79	do	Idaho Power and Light Company road; elevation 550 m (1,820 ft); NE1/4 NW1/4 sec. 17, T. 20 N., R. 4 W.; Homestead quadrangle; Idaho.	Mafic dike that cuts the Windy Ridge Formation.
VB-91	Andesite	North side of Ballard Creek; elevation 732 m (2,400 ft); SW1/4NW1/4 sec. 11, T. 6 S., R. 48 E.; Homestead quadrangle; Oreg.	Lava flow about 3 m thick in tuff-and-sandstone sequence; Hunsaker Creek Formation.
LS7-32b	do	North side of Hunsaker Creek; elevation 869 m (2,850 ft); east edge of SE1/4 NE1/4 sec. 6, T. 7 S., R. 48 E.; Homestead quadrangle; Oreg.	Large clast about 70 cm indiameter from breccia; Hunsaker Creek Formation.
LS9-12	Dacite	North side of Ballard Creek; elevation 747 m (2,450 ft); SW1/4NS1/4 sec. 11, T. 6 S.; R. 48 E.; Homestead quadrangle; Oreg.	Clast about 15 cm in diameter from breccia;Hunsaker Creek Formation.
LS7-36	do	North side of Hunsaker Creek; elevation 900 m (2,950 ft); SE1/4NE1/4 sec. 6, T. 7 S., R. 48 E.; Homestead quadrangle; Oreg.	Lava flow in flow-and-breccia sequence; Hunsaker Creek Formation.
VC-225	Rhyolite	Near top of Grassy Ridge about 1.6 km west of Kinney Point; elevation 1,905 m (6,250 ft); NW1/4SE1/4 sec. 10, T. 21 N., R. 3 W.; Cuprum quadrangle; Idaho.	Sill(?) or flow(?); poor outcrop; Hunsaker Creek(?) Formation.
VS5-7	do	Idaho Power and Light Company road; elevation 550 m (1,820 ft); NW1/4 SW1/4 sec. 17, T. 20 N., R. 4 W.; Homestead quadrangle; Idaho.	Flow in thick sequence of tuff breccia; Windy Ridge Formation.
VS5-1	do	Idaho Power and Light Company road; elevation 550 m (1,820 ft); NW1/4 SW1/4 sec. 17, T. 20 N., R. 4 W.; Homestead quadrangle; Idaho.	Do.
VC-15	do	Ridge between forks of Homestead Creek; elevation 1,310 m (4,300 ft); NE1/4SE1/4 NW1/4 sec. 17, T. 6 S., R. 48 E.; Homestead quadrangle; Oreg.	Flow(?) in tuff-and-sandstone sequence; Hunsaker Creek Formation.

[1]Rocks are metamorphosed to the greenschist facies; Na_2O-rich rock can be classified either as spilite (metabasalt and metabasaltic andesite), keratophyre (meta-andesite), or quartz keratophyre (metadacite and metarhyolite).

TABLE 3.13.—*Major- and minor-element oxides of Permian volcanic (flow) and associated hypabyssal intrusive rocks from the Lower Permian Windy Ridge and Hunsaker Creek Formations*

[Oxides in weight percent, normalized to 100 percent; prenormalization volatile contents included to indicate amount of alteration. ---, not determined]

Sample	VB-88	VC-131	VC-197	VB-79	VB-91	LS7-32b	LS9-12	LS7-36	VC-225	VS5-7	VS5-1	VC-15
SiO_2	51.95	54.36	54.49	54.74	59.81	60.04	62.38	62.94	68.18	76.42	76.98	79.97
TiO_2	2.55	1.89	.93	2.00	1.77	1.22	.47	1.31	.85	.35	.36	.24
Al_2O_3	16.21	16.65	17.39	15.73	16.44	16.40	13.92	14.47	15.00	12.78	13.21	12.09
Fe_2O_3	5.81	4.50	2.97	5.52	3.92	8.18	---	---	4.98	.61	.55	1.02
FeO	7.92	5.34	5.30	6.21	4.20	1.35	7.46	7.95	.85	1.65	1.63	.16
MgO	5.79	3.47	7.85	3.93	2.74	1.96	4.43	2.58	.51	2.15	1.12	.24
MnO	.23	.21	.17	.42	.25	.05	.13	.22	---	.08	.12	.16
CaO	3.13	10.05	6.37	4.27	3.58	2.83	4.40	3.46	1.61	.45	.00	.00
Na_2O	5.90	3.14	4.24	6.73	6.84	7.02	5.01	5.93	6.99	4.71	5.80	5.89
K_2O	.08	.02	.08	.04	.13	.74	.10	.73	.83	.80	.18	.15
P_2O_5	.43	.37	.21	.41	.32	.21	1.20	.41	.20	---	.05	.08
H_2O^+	3.79	3.10	4.10	2.20	2.49	1.71	2.77	---	0.59	1.67	1.10	0.57
H_2O^-	.64	.36	.79	.27	.31	.65	---	---	.26	.27	.11	.15
CO_2	1.46	.05	.08	.08	2.24	1.20	1.51	---	1.04	.18	.02	.06
FeO_{total}/MgO	2.27	2.71	1.02	2.84	2.82	4.45	1.68	3.08	10.45	1.02	1.90	4.49

TABLE 3.14.—*Trace elements of selected volcanic (flow) and associated hypabyssal intrusive rocks from the Lower Permian Windy Ridge and Hunsaker Creek Formations*

[Results in parts per million. Analysis by neutron activation unless otherwise noted. ---, not determined or below instrumental detection limit or discarded because of high coefficient of variation]

Sample	VB-88	VB-79	VB-91	LS7-32b	VC-225	VS5-7
Rb[1]	3	---	2	4	14	19
Sr[1]	68	106	116	130	147	40
Ba[1]	989	160	136	168	304	112
Th	---	---	---	.7	1.7	1.2
U	---	---	---	---	---	---
La	9	9	9	5	13	13
Ce	26	---	---	12	33	33
Sm	5.2	4.8	4.5	2.6	6.2	5.1
Eu	1.80	1.62	1.48	.43	1.66	1.21
Gd	---	---	---	---	6.7	---
Tb	1.30	1.07	1.06	.45	1.10	.92
Tm	.66	.47	.56	---	---	.53
Yb	4.4	4.1	4.6	1.9	4.6	4.4
Lu	.67	.60	.66	.30	.65	.65
Y[1]	43	40	44	21	45	46
Zr[1]	223	140	217	68	192	176
Hf	4.6	3.4	5.2	2.2	4.5	4.6
Ta	---	---	.56	.94	3.45	2.54
Nb[1]	---	7	---	15	---	19
Ni	---	---	---	---	---	---
Co	31	25	15	13	8	6
Cr	---	---	---	---	11	21
Sc	35	32	25	36	16	10
Zn	168	1,070	168	82	39	88

[1]Analysis by X-ray fluorescence.

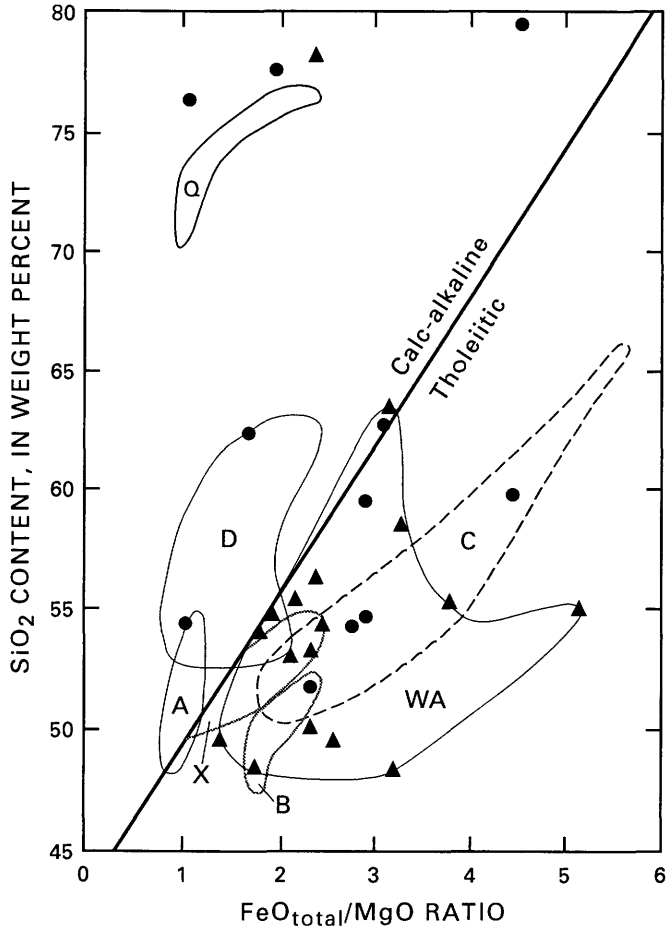

FIGURE 3.22.—FeO_{total}/MgO ratio versus SiO_2 content for Permian and Triassic lavas and dikes of Wallowa terrane. Dots, Permian rocks; triangles, Triassic rocks. (Two samples, one with an FeO_{total}/MgO ratio of 1.71 and an SiO_2 content of 48.2 weight percent and the other with an FeO_{total}/MgO ratio of 2.37 and an SiO_2 content of 78.29 weight percent, are plotted as Triassic but may be otherwise.) Main data field for Triassic rocks, WA, shows that they are strongly tholeiitic. Data fields A through D represent Aleutian island arc volcanic rocks (fig. 3.4), X represents tholeiitic rocks of Ata Island (Tonga island arc; fig. 3.4), and Q represents quartz keratophyre of (informal) Sparta complex of Phelps (1979) (fig. 3.18*A*). Calc-alkaline–tholeiitic compositional boundary from Miyashiro (1974).

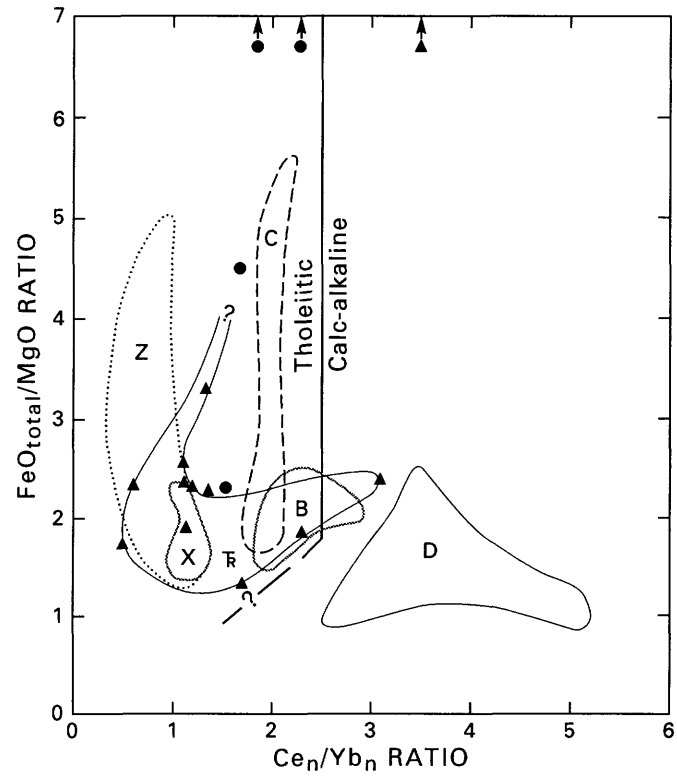

FIGURE 3.23.—FeO_{total}/MgO versus Ce_n/Yb_n ratios for Permian (dots) and Triassic (triangles) lavas and dikes of Wallowa terrane. Ŧ, data field for Triassic lavas, extent uncertain where queried. Three data points plot off scale, as indicated by arrows: Values of FeO_{total}/MgO ratio for two Permian lavas are both 10.4, and for one Triassic lava, 15.2. Two samples (basalt, FeO_{total}/MgO=1.71; rhyolite, FeO_{total}/MgO=2.37) are plotted as Triassic lavas, although they may not be Triassic in age (see text). Data fields B, C, and D represent Aleutian island arc volcanic rocks, and fields X and Z, Tonga island arc volcanic rocks (fig. 3.5). Line, dashed and queried where uncertain, separates tholeiitic and calc-alkaline fields. n, chondrite normalized.

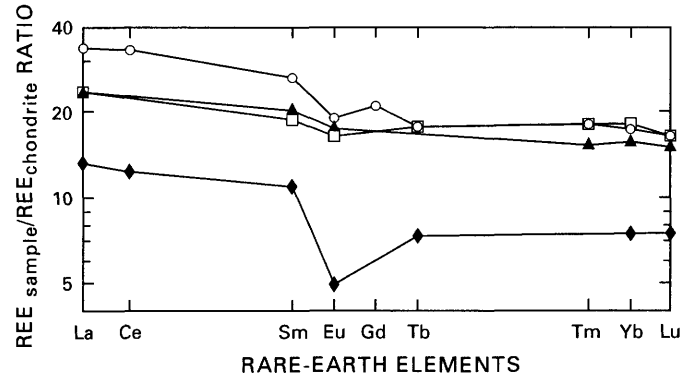

FIGURE 3.24.—Rare-earth element (REE) diagram for Early Permian lavas and dikes. Note relatively flat patterns (excluding Eu anomaly) for all samples. Sample numbers correspond to those in tables 3.12 through 3.14; for normalizing values used, see figure 3.6.

TRIASSIC VOLCANIC (FLOW) AND ASSOCIATED HYPABYSSAL INTRUSIVE ROCKS

The Triassic volcanic (flow) and associated hypabyssal intrusive rocks in the Wallowa terrane occur in the upper part of the Clover Creek Greenstone (Gilluly, 1937; Nolf, 1966) and in the Wild Sheep Creek and Doyle Creek Formations of the Seven Devils Group (Vallier, 1977). There are striking differences between the Permian and Triassic sequences in outcrop characteristics, field relations, petrography, and chemistry (Vallier, 1967a, 1977; Vallier and Batiza, 1978; Scheffler, 1983; La Pierre and others, 1988). Compared to Permian lavas, compositions of Triassic lavas are more similar to those from present-day island arcs.

Middle (Ladinian) and Late (Karnian) Triassic flows and dikes of the Wallowa terrane range in composition from basalt to rhyolite (tables 3.15–3.17). Except for samples V-26-79, V-51-79, and V-10-79, the samples were collected from outcrops in the Snake and Imnaha River canyons and closely adjacent areas.

Sample V-26-79, a basalt, was collected from outcrops along the road paralleling the Tucannon River in Washington. Its age could be other than Triassic, and its association with chert, argillite, gabbro, and greenstone (Huntting, 1942) suggests that those outcrops could easily be assigned to the Baker terrane (fig. 3.8) and not to the Wallowa terrane. The chemistry supports assignment to the Baker terrane. For consistency with previous terrane assignments (Silberling and others,1984), however, I have tabulated data for this basalt with other Wallowa terrane lavas, although it is not included in the diagrams and discussions dealing with the Triassic rocks of the Wallowa terrane.

Stratigraphic relations between the mostly marine Wild Sheep Creek Formation (green or greenish, pillow lavas, thick debris-flow breccia units, carbonate lenses) and the partly subaerial and partly marine Doyle Creek Formation (red or reddish, abundant silicic tuff units, few pillow lavas, large vesicles in flows) need further clarification (fig. 3.17). In many places the two formations are difficult to separate. On the basis of work completed subsequent to the initial stratigraphic synthesis (Vallier, 1977), it is apparent that parts of the Doyle Creek Formation are subaerial or shallow-marine-lithofacies equivalents of the Wild Sheep Creek Formation. However, in many places it is evident that strata of the Doyle Creek Formation overlie the Wild Sheep Creek Formation. The Doyle Creek Formation is considered to be, in total, a lithofacies equivalent of both the Wild Sheep Creek Formation and the overlying unit. On the basis of composition and depositional character (Doyle Creek rocks are more siliceous and tuffaceous), the more oxidized rocks in the Doyle Creek Formation may merely represent the final products of volcano maturation, growth above sea level, and erosion. Ladinian fossils have been recovered from red marine beds of the formation. No fossils, however, have been found in the younger and mainly subaerial parts of the Doyle Creek Formation near its type area. At Pittsburg Landing, Karnian *Halobia* sp. were recovered in beds (newly named Kurry unit) that overlie the Wild Sheep Creek Formation; these strata of the Kurry unit have been recently reassigned to the Doyle Creek Formation (White and Vallier, 1994). To further confuse age relationships, Karnian *Halobia* sp. were recovered from the Wild Sheep Creek Formation from northern parts of the Snake River canyon (Grant, 1980). Thus, the ages of both the Wild Sheep Creek and the Doyle Creek Formations are now considered to be Middle (Ladinian) and Late (Karnian) Triassic; this is a change in age assignment for the Doyle Creek Formation, which was previously thought to be no older than Late Triassic (Vallier, 1977).

Metamorphic grades and the extent of metamorphism are lower in the Triassic sequences than in the Permian rocks of the Wallowa terrane. Triassic volcanic rocks range in metamorphic facies from lower greenschist to zeolite, whereas Permian rocks are in the lower to middle greenschist facies. Higher temperature facies occur in contact aureoles near the Late Triassic and the Jurassic to Cretaceous plutonic bodies.

Samples of 19 Triassic igneous rocks of the Wallowa terrane were analyzed for major and minor elements (table 3.16), and 14 were analyzed for trace elements (table 3.17). The analyses complement those of Scheffler (1983) and Goldstrand (1987, 1994).

Discounting samples V-26-79 (problem with age and terrane assignments) and V-10-79 (may be Permian in age), the SiO_2 contents (n=17) range from 48.29 percent to 75.67 percent. TiO_2 content is relatively high in two basalts (samples VC-265 and VB-85), three basaltic andesites (samples VC-135, VS6-5, and VC-224), and one andesite (sample VB-105) compared to mafic rocks of modern island arcs (Gill, 1981; Kay and Kay, 1991). High Fe contents are reflected in relatively high FeO_{total}/MgO ratios in most of these volcanic and hypabyssal intrusive rocks (table 3.16 and fig. 3.22). Al_2O_3 contents vary greatly; three basaltic andesites have Al_2O_3 concentrations greater than 18 percent, probably related to a higher volume of plagioclase in the modes. On the basis of the K_2O versus SiO_2 content diagram (Gill, 1981, p. 6), the rocks are

TABLE 3.15.—*Lithology, sample locality, and field description of analyzed volcanic (flow) rocks and associated hypabyssal intrusive rocks, mostly from the Middle and Upper Triassic Wild Sheep Creek and Doyle Creek Formations of the Wallowa terrane*

[Rocks arranged by increasing SiO_2 content to correspond to chemical analyses in tables 3.16 and 3.17. do., ditto; BM, bench mark]

Sample	Rock type	Sample locality	Field description and remarks
V-26-79	Basalt	Along road paralleling Tucannon River; elevation 960 m (3,150 ft); NW1/4NW1/4 sec. 15, T. 9 N., R. 41 E.; Panjab Creek quadrangle; Wash.	Probably northernmost exposure of Wallowa terrane (but possibly Baker terrane) rocks. Flow within sequence of argillite, cherty argillite, and greenstone.
VC-265	do	Ridge north of Hibbles Gulch; elevation 975 m (3,200 ft); SE1/4 sec. 31, T. 2l N., R. 3. W.; Cuprum quadrangle; Idaho.	Flow about 5 m thick; may be either the Wild Sheep Creek or Doyle Creek Formation.
VB-85	do	Idaho Power and Light Company road, about 0.8 km south of Hells Canyon Dam; elevation 580 m (1,900 ft); eastern boundary, sec. 2l, T. 22 N., R. 3 W.; Cuprum quadrangle; Idaho.	Coarse-grained porphyritic flow; Wild Sheep Creek Formation.
VC-413	do	North side of Imnaha River canyon, about 0.8 km N. 30° E. of Indian Crossing; elevation 1,440 m (4,720 ft); unsurveyed part of T. 5 S., R. 47 E.; Cornucopia quadrangle; Oreg.	Flow (6 m thick) in sequence of flows and breccias; Wild Sheep Creek Formation.
VC-335	do	North side of Imnaha River canyon, l.6 km N. 70° E. of BM 4521; elevation 1,452 m (4,900 ft); unsurveyed part of T. 5 S., R. 47 E.; Homestead quadrangle; Oreg.	Flow of unknown thickness; Wild Sheep Creek Formation.
V-51-79	Basaltic andesite	Cottonwood Butte, near radio facility; elevation 1,738 m (5,700 ft); NE1/4SW1/4 sec. 33, T. 32 N., R. l W.; Keuterville quadrangle; Idaho.	Porphyritic lava flow, probably correlative with the Wild Sheep Creek Formation.
VC-269	do	North side of unnamed creek between Azurite Gulch and Limepoint Creek; elevation 884 m (2,900 ft); SE1/4SW1/4NWl/4 sec. 13, T. 20 N., R. 3 W.; Homestead quadrangle; Idaho.	Flow unit (about 10 m thick) in sequence of flows; Triassic age, most likely part of the Wild Sheep Creek Formation.
VC-135	do	Northeast flank of Grassy Ridge; elevation l,006 m (3,300 ft); NEl/4NWl/4 sec. l6, T. 22 N., R. 3 W.; Cuprum quadrangle; Idaho.	Flow unit about 3 m thick, Wild Sheep Creek Formation.
VC-302	do	Near Lynes Saddle; elevation 1,555 m (5,100 ft); NW1/4NWl/4 sec . 9, T. 20 N., R. 3 W.; Cuprum quadrangle; Idaho.	Flow of unknown thickness; Doyle Creek Formation.
VS3-1	do	North side of Doyle Creek near Snake River; elevation 497 m (1,630 ft), unsurveyed area across river from center of sec. 17, T. 2l N., R. 3 W. (Idaho); Cuprum quadrangle; Oreg.	Flow unit about 5 m thick; lower part of the Doyle Creek Formation or upper part of the Wild Sheep Creek Formation.
VC-224	do	Southwest side of Black Point; elevation 1,723 m (5,650 ft); NE1/4NW1/4 sec. 10, T. 21 N., R. 3 W.; Cuprum quadrangle; Idaho.	Wild Sheep Creek Formation near stratigraphic contact with the Permian Hunsaker Creek Formation. Thick flow unit among alternating flows and breccias.

TABLE 3.15.—*Lithology, sample locality, and field description of analyzed volcanic (flow) rocks and associated hypabyssal intrusive rocks, mostly from the Middle and Upper Triassic Wild Sheep Creek and Doyle Creek Formations of the Wallowa terrane*—Continued

[Rocks arranged by increasing SiO_2 content to correspond to chemical analyses in tables 3.16 and 3.17. do., ditto; BM, bench mark]

Sample	Rock type	Sample locality	Field description and remarks
VS6-5	------ do ----------	North side of McGraw Creek, about 50 m below contact with the Martin Bridge Limestone; elevation 865 m (2,840 ft); unsurveyed area directly across Snake River from NW1/4NW1/4 sec. 1, T. 20 N., R. 4 W. (Idaho); Homestead quadrangle; Oreg.	Red flow of unknown thickness; Doyle Creek Formation.
VB-87	------ do ----------	Idaho Power and Light Company road about 0.8 km south of Eagle Bar, parallel to Snake River; elevation 613 m (2,010 ft); SW1/4SE1/4 sec. 28, T. 22 N., R. 3. W.; Cuprum quadrangle; Idaho,	Clast in flow breccia; Wild Sheep Creek Formation.
VB-103	Andesite ----------	North side of Hibbles Gulch, along Idaho Power and Light Company road parallel to Snake River, about 150 m below contact with the Martin Bridge Limestone, elevation 576 m (1,890 ft); center of NW1/4 sec. 3l, T. 2l N., R. 3 W.; Cuprum quadrangle; Idaho.	Red flow about 5 m thick; Doyle Creek Formation.
VB-105	------ do ----------	South side of Hibbles Gulch, along Idaho Power and Light Company road parallel to Snake River; elevation 580 m (1,900 ft); center of NW1/4 sec. 3l, T. 2l N., R. 3 W.; Cuprum quadrangle; Idaho.	Banded flow about 3 m thick; Doyle Creek Formation.
VS3-6	Dacite ----------	North side of Doyle Creek near Snake River; elevation 510 m (1,670 ft); unsurveyed area across Snake River from center of sec. 17, T. 21 N., R. 3 W. (Idaho); Cuprum quadrangle; Oreg.	Flow about 8 m thick; Doyle Creek Formation.
VC-218	------ do ----------	First spur south of McCraw Creek; elevation 854 m (2,800 ft); unsurveyed area across Snake River from center of sec. 1, T. 20 N., R. 4 W. (Idaho) Homestead quadrangle; Oreg.	Porphyritic flow about 6 m thick; Doyle Creek Formation.
VC-262	Rhyolite ----------	Along trail that parallels Snake River, north of Spring Creek; elevation 585 m (1,920 ft); unsurveyed area directly across Snake River from NE1/4SE1/4 sec. 36, T. 21 N., R. 4 W. (Idaho); Homestead quadrangle; Oreg.	Dark-brown flow; Doyle Creek Formation.
V-10-79	------ do ----------	Along road to Sparta, Oreg., parallel to Torchlight Creek; elevation 1,250 m (4,100 ft); unsurveyed part of T. 7 S., R. 44 E.; Sparta quadrangle; Oreg.	Clover Creek Greenstone; age here presumed to be Permian on basis of surrounding lithologies.

intermediate-K and low-K lavas. The wide range in Na_2O and K_2O contents may in part reflect metamorphic influences on ion mobility rather than just igneous processes. Correlations of K_2O content and tectonic setting (for example, Mortimore, 1986) are suspect where metamorphic effects are not well understood (Vallier and Batiza, 1978).

In these Triassic rocks, trace elements (table 3.17) are more helpful than major elements (table 3.16) for petrologic interpretations. Sr content in some samples

TABLE 3.16.—*Major- and minor-element oxides of Middle and Late Triassic volcanic (flow) rocks and associated hypabyssal intrusive rocks of the Wallowa terrane*

[Oxides in weight percent, normalized to 100 percent; prenormalization volatile contents included to indicate amount of alteration. ---, not determined

Sample	V-26-79	VC-265	VB-85	VC-413	VC-335	V-51-79	VC-269	VC-135	VC-302	VS3-1
SiO_2	48.17	48.29	49.84	49.87	50.29	53.09	53.16	54.28	54.30	54.97
TiO_2	1.45	2.23	2.22	1.05	1.49	.81	1.02	1.77	.82	.88
Al_2O_3	15.55	17.48	15.99	17.63	16.48	20.15	18.07	16.97	18.52	16.04
Fe_2O_3	1.37	---	3.85	2.98	4.94	4.47	5.67	4.48	4.44	5.24
FeO	9.50	11.34	9.61	7.45	8.70	4.54	4.06	5.31	4.38	4.84
MgO	6.28	3.65	5.25	7.61	5.63	4.06	4.05	3.86	4.65	5.10
MnO	.18	.20	.22	.20	.22	.12	.20	.22	.23	.17
CaO	13.57	14.99	8.03	9.52	8.81	10.33	8.26	6.35	7.69	9.03
Na_2O	3.56	1.45	4.46	2.92	2.71	2.21	4.36	5.42	3.31	3.12
K_2O	.25	.03	.22	.56	.63	.09	1.05	.90	1.35	.51
P_2O_5	.12	.34	.31	.21	.10	.13	.10	.44	.31	.10
H_2O^+	3.51	4.74	3.35	4.08	1.89	2.11	2.74	2.00	3.14	2.80
H_2O^-	.21	---	.23	.35	.33	.12	.30	.19	.24	.34
CO_2	.28	.34	.08	.19	.11	.01	.21	.05	.12	.25
FeO_{total}/MgO	1.71	3.11	2.49	1.33	2.34	2.11	2.26	2.42	1.80	1.87

Sample	VC-224	VS6-5	VB-87	VB-103	VB-105	VS3-6	VC-218	VC-262	V-10-79
SiO_2	55.40	55.48	55.56	56.32	58.69	63.65	67.86	75.67	78.29
TiO_2	1.90	1.91	1.20	1.17	1.62	1.24	.59	.32	.25
Al_2O_3	14.79	14.22	15.79	14.70	14.65	15.56	16.81	13.32	12.50
Fe_2O_3	---	10.16	---	8.96	8.08	3.61	3.03	1.09	.90
FeO	11.51	.42	8.58	2.57	2.50	3.91	.32	1.11	.66
MgO	5.07	1.88	3.95	4.62	3.01	2.27	.20	.20	.62
MnO	.27	.13	.19	.17	.25	.14	.03	.05	---
CaO	6.05	14.18	7.81	7.04	6.49	3.09	.81	.58	.54
Na_2O	3.61	1.25	5.77	4.11	3.12	6.08	7.85	6.81	6.12
K_2O	1.18	.06	1.15	0.24	1.38	.21	2.30	.81	.12
P_2O_5	.22	.31	---	.10	.21	.24	.20	.04	---
H_2O^+	3.04	3.26	---	2.55	2.62	1.80	0.47	0.54	0.71
H_2O^-	---	.24	---	.30	.42	.17	.17	.14	.11
CO_2	.14	.27	---	.09	1.13	.03	.15	.29	.02
FeO_{total}/MgO	3.75	5.10	2.17	2.30	3.24	3.15	15.23	10.45	2.37

correlates with CaO content. REE contents are similar to those of many other island-arc lavas. The Ce_n/Yb_n ratios have a wide range (fig. 3.23). Basalt, basaltic andesite, and andesite samples have nearly flat REE signatures, whereas dacite and rhyolite samples show patterns that are more enriched in LREE's (fig. 3.25); Ce_n/Yb_n ratios in the more siliceous rocks are as large as 3.1 (fig. 3.23). None of the lavas has the distinct calc-alkaline REE signature of Aleutian lavas (fig. 3.25; Kay and Kay, 1994); they are more similar to the tholeiitic lavas from Okmok Caldera in the Aleutians and to tholeiitic lavas from the Tonga and Kermadec island arcs.

PETROGENESIS OF PERMIAN AND TRIASSIC VOLCANIC (FLOW) AND ASSOCIATED HYPABYSSAL INTRUSIVE ROCKS

The Permian and Triassic lavas and associated hypabyssal intrusive rocks of the Wallowa terrane formed within an island arc. On the basis of criteria used in this chapter, most are tholeiitic in composition and are assigned to the island-arc tholeiite series (IAT). They formed in both marine and subaerial settings on and near island and seamount volcanoes above a subduction zone. LaPierre and others (1988) reported both tholeiitic and calc-alkaline Triassic lavas, according to their classification.

TABLE 3.17.—*Trace elements of selected Middle and Upper Triassic volcanic (flow) rocks and associated hypabyssal intrusive rocks of the Wallowa terrane*

[Results in parts per million. Analysis by neutron activation unless otherwise noted. ---, not determined or below detection limit or discarded because of high coefficient of variation]

Sample----	V-26-79	VB-85	VC-413	VC-335	V-51-79	VC-269	VC-302	VS3-1	VS6-5	VB-103	VB-105	VC-218	VC-262	V-10-79
Rb[1]-------	5	6	6	6	3	17	34	8	---	5	26	26	8	---
Sr[1]-------	192	124	308	210	498	194	436	202	132	213	214	92	78	94
Ba[1]-------	82	38	172	152	112	184	309	200	---	78	281	607	236	74
Th --------	---	---	.3	---	.3	---	1.1	---	---	---	1.6	2.2	1.7	2.8
U ---------	---	.7	---	---	---	---	.9	---	---	---	.8	1.2	---	.7
La --------	2	8	5	4	3	5	12	4	10	4	9	16	23	18
Ce --------	7	23	12	13	7	14	23	11	24	9	24	30	48	33
Sm -------	2.5	6.0	3.0	3.5	1.5	3.0	3.5	2.7	6.2	2.8	5.5	4.3	6.8	2.8
Eu --------	.98	1.65	.89	1.05	.63	.95	1.1	.76	1.55	.95	1.49	1.15	1.82	.61
Gd --------	---	---	---	---	2.0	---	---	---	4.8	---	---	4.0	---	3.6
Tb --------	.84	1.42	.51	.74	.33	.67	.60	.67	.89	.66	1.27	.56	1.16	---
Tm -------	---	.63	---	---	---	---	---	---	---	---	.63	---	---	---
Yb --------	3.4	5.3	1.8	3.0	1.4	3.0	2.6	2.6	3.3	3.8	4.9	2.2	5.5	2.7
Lu --------	.54	.78	.28	.47	.21	.45	.39	.39	.45	.64	.72	.31	.82	.38
Y[1] --------	30	48	16	26	9	18	26	20	30	30	42	22	48	22
Zr[1]-------	81	122	27	53	40	62	79	49	182	46	126	117	304	123
Hf --------	2.1	4.1	1.2	1.7	.9	2.2	2.3	1.8	4.0	1.8	4.0	3.0	6.9	3.7
Ta --------	.19	---	---	---	---	---	.5	1.13	3.4	.77	.54	5.0	3.6	.35
Nb--------	---	6	---	---	---	---	---	---	15	---	---	8	---	---
Ni --------	153	---	---	---	28	---	---	---	---	---	---	---	---	10
Co --------	41	39	38	45	28	31	19	32	28	33	31	19	13	2
Cr --------	400	55	174	21	21	45	35	33	49	132	15	23	25	2
Sc --------	41	46	32	38	26	34	19	38	24	42	31	8	12	7
Zn --------	95	147	90	153	83	111	127	110	99	92	136	41	85	37

[1]Analysis by X-ray fluorescence.

The petrogenesis of the Triassic lavas and related hypabyssal rocks of the Wallowa terrane is very similar to that of Cenozoic and modern island-arc tholeiitic rocks (Gill, 1981). The petrogenesis of the Permian lavas and related dikes and sills, however, is puzzling. On the basis of several chemical characteristics (FeO_{total}/MgO ratios, REE contents and trends, and low-K group chemistry), they can be classified as island-arc tholeiites, and interpretations of petrology and tectonic settings can be invoked on the basis of the compilation in table 3.2. There are several mineralogical and chemical characteristics, however, that distinguish these Permian rocks from most arc lavas.

(1) They are very siliceous; dacite and rhyolite are the dominant rock types.

(2) The siliceous lava flows have a phenocryst assemblage of bipyramidal quartz and albite, which contrasts greatly with the assemblages of most Cenozoic island-arc lavas. Quartz keratophyre flows and dikes with similar field, petrographic, and chemical characteristics occur in the Eocene sequences of the Komandorsky Islands of the Aleutian island arc (Andrei Tsvetkov, oral commun., 1987).

(3) These rocks are characterized by high Na_2O contents, and most are depleted in K_2O. Is this chemistry the result of igneous processes only or of igneous processes in conjunction with extensive seawater interaction? Is it purely a metamorphic effect? Is there a tectonic significance?

(4) Most of these Permian rocks have high FeO_{total}/MgO ratios and relatively flat to slightly LREE-enriched REE patterns. These characteristics suggest that most rocks result from the fractionation of a tholeiitic basalt parent magma.

(5) In comparison with other volcanic-arc rocks, these Permian rocks are particularly enriched in high-field-strength elements; such enrichment is more characteristic of alkalic seamount and alkalic ocean-island (Hawaiian Islands, for example) rocks than of tholeiitic rocks from Cenozoic island arcs. Calc-alkaline rocks are almost always depleted in these elements. Either a locally atypical (for example, highly metasomatized) mantle rock served as source rock, partial melting took place at great depths where mantle is not as depleted, significant crustal contamination of the magmas occurred, or these elements were concentrated by extreme fractionation of magma in

high-level chambers that were accessible to seawater brine.

(6) On the basis of field relations, mineralogy, and chemistry, some of the Permian Na_2O-rich plutonic bodies apparently are the crystallized magma chambers that fed the Permian lavas and hypabyssal intrusive rocks.

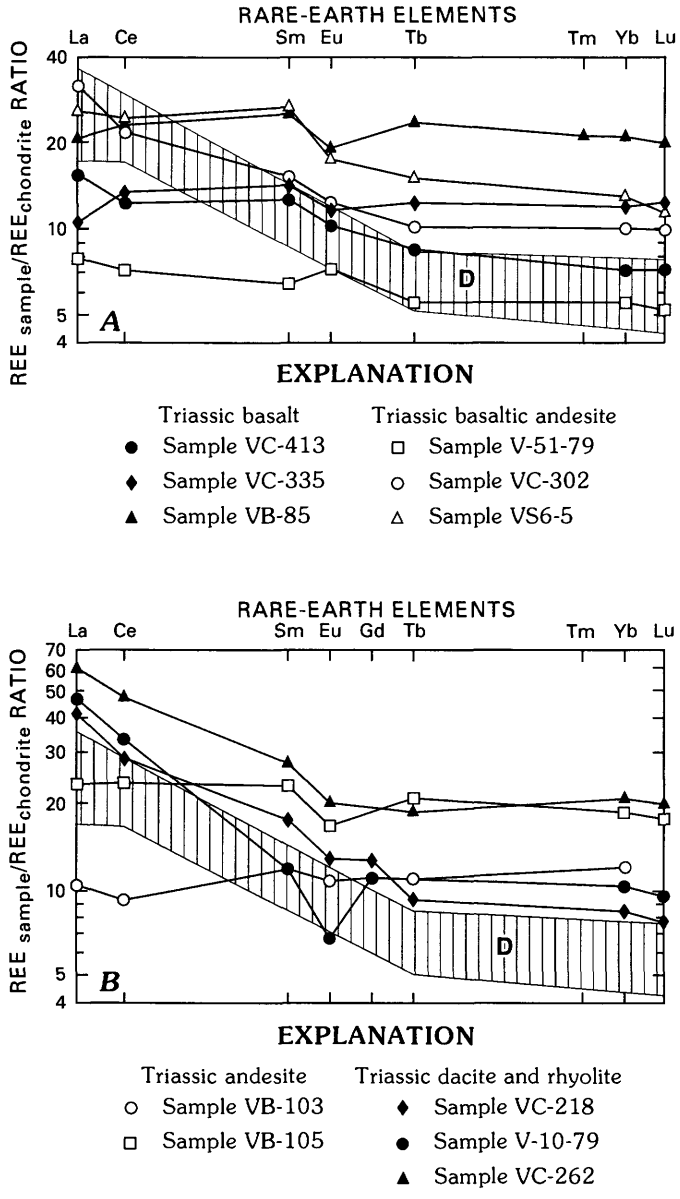

FIGURE 3.25.—Rare-earth element (REE) diagrams for Triassic lavas and dikes of Wallowa terrane. Patterned area (D) is data field for Aleutian calc-alkaline lavas (fig. 3.7), shown for comparison. Sample numbers correspond to those in tables 3.15 through 3.17; for normalizing values used, see figure 3.6. *A*, Basalt and basaltic andesite. *B*, Andesite, dacite, and rhyolite. (Rhyolite sample V-10-79 may be Permian.) Note strong light-REE enrichment in samples VC-218 and VC-262; heavy-REE contents for those samples, however, are not depleted.

Higher grade metamorphic facies in Permian rocks than in Triassic rocks can be attributed to one or more of the following: (1) deeper burial, (2) a period of higher heat flow during eruption and intrusion of Triassic lavas and plutonic bodies, (3) higher temperature regimes over a longer period of time (and two or more magmatic events), and (or) (4) higher susceptibility of Permian siliceous glassy rocks to the effects of temperature, pressure, and fluids.

The most likely source for magmas of both ages was the mantle wedge; fluids from the downgoing slab where oceanic crust and associated sediments were being subducted also had some influence on the magma's composition (see Kay, 1984). Partial melting of the mantle was succeeded by migration of magma upward into chambers at upper-mantle and (or) lower-crust depths. The fractionation of plagioclase, olivine, orthopyroxene (not always present), augite, and magnetite was the major differentiation mechanism, although some magma mixing and crustal assimilation probably occurred. The fractionating magmas were at relatively low pressures and high temperatures.

TRIASSIC AND EARLY JURASSIC(?) IGNEOUS ROCKS OF THE OLDS FERRY TERRANE

Exposures of the Olds Ferry terrane, as defined in this chapter, extend from Juniper Mountain west of Brogan, Oreg., toward the east and northeast through the Cuddy Mountains and Peck Mountain, and possibly as far as Riggins, Idaho (figs. 3.2 and 3.8). Some of the rocks along the west border of the Idaho batholith north of McCall, Idaho (Aliberti, 1988; Manduca, 1988), may belong to the Olds Ferry terrane. The Weatherby Formation (Brooks, 1979a) was placed in the Olds Ferry terrane by Silberling and others (1984). However, in this chapter I place that formation in the Izee terrane.

The terrane is composed mostly of volcanic (flow) and volcaniclastic (pyroclastic and epiclastic) rocks of the Huntington Formation (Brooks, 1979b). Siliceous plutonic bodies occur locally. Volcanic (flow) rocks and hypabyssal intrusive rocks range in composition from basalt to rhyolite with andesite being the most prevalent. Fossils from the Huntington Formation are of late Karnian and early Norian ages. Isotopic ages from pre-Late Jurassic plutonic bodies include one 235-Ma U-Pb age (Walker, 1986) and five K-Ar ages (Hendricksen and others, 1972) that range from 216 (middle Norian) to 190 Ma (Toarcian). The 235-Ma isotopic age of the small plutonic body exposed along the Brownlee Reservoir (see section "Plutonic Rocks," below) overlaps isotopic ages of Triassic rocks in the Baker and Wallowa terranes.

TABLE 3.18.—*Lithology, sample locality, and field description of Triassic and Early Jurassic(?) plutonic rocks of the Olds Ferry terrane*

[Rocks arranged by increasing SiO_2 content to correspond to chemical analyses in tables 3.19 and 3.20]

Sample	Rock type	Sample locality	Field description and remarks
		Plutons of northern Cuddy Mountains	
V-7-84	Diorite	Upper reaches of Hornet Creek near Cuddy Mine; elevation 2,225 m (7,300 ft); SW1/4NW1/4 sec. 17, T. 17 N., R. 3 W.; Hornet quadrangle; Idaho.	Relatively fresh rock; light colored in part.
V-6-84	Quartz diorite	Johnson Creek Park near U.S. Forest Service quarters; elevation 1,845 m (6,050 ft); SW1/4NW1/4 sec. 31, T. 17 N., R. 2 W.; Hornet quadrangle; Idaho.	Relatively fresh rock; light colored.
		Brownlee pluton	
HU-79-1	Trondhjemite	In Snake River canyon, along road from Huntington to Richland, at Brownlee Reservoir; elevation 590 m (1,935 ft); extreme west edge of NW1/4 sec. 32, T. 13 S., R. 45 E.; Olds Ferry quadrangle; Oreg.	Small silicic pluton. Middle Triassic age (Walker, 1986).

PLUTONIC ROCKS

Three plutonic bodies were sampled for chemistry (tables 3.18–3.20). Sample HU-79-1 is from a small plutonic body exposed along the road that parallels the Brownlee Reservoir, which extends along the Snake River southward from Brownlee Dam (fig. 3.1); the outcrops are about 5 km north of Huntington, Oreg. Samples V-6-84 and V-7-84 are from plutonic bodies exposed in the Cuddy Mountains of western Idaho.

The plutonic body exposed along the Brownlee Reservoir has the minimum U-Pb age of 235 Ma (Walker, 1986) and is the oldest plutonic body thus far recognized in the Olds Ferry terrane. Contact relationships are obscure; Brooks (written commun., 1989) suggested that it may unconformably underlie the Huntington Formation. Furthermore, the plutonic body is older than the late Karnian and early Norian Huntington Formation (Brooks, 1979a) and also much older than the isotopically dated plutonic rocks in the Cuddy Mountains and in the Mineral-Iron Mountain mining district (Hendricksen and others, 1972).

Five pre-Late Jurassic plutonic bodies exposed in the Cuddy Mountains and the Mineral-Iron Mountain mining district, gabbro to trondhjemite in composition, range in age (K-Ar methods on hornblende and biotite) from about 216 to 190 Ma (Hendricksen and others, 1972; Cyrus Field, written commun., 1988). Four of the five plutonic bodies are significantly younger than the pre-Jurassic plutonic bodies in the Baker and Wallowa terranes (fig. 3.21). N.W. Walker (written commun., 1989), cautioned, however, that the K-Ar ages may have been reset by argon release, which would produce younger apparent ages.

Two Jurassic to Cretaceous plutonic bodies in the Olds Ferry terrane, one exposed at Peck Mountain and the other at Hitt Mountain, have K-Ar ages of Late Jurassic (161 Ma) and Early Cretaceous (120 Ma), respectively (Cyrus Field, written commun., 1988). These plutonic bodies were not sampled for this study.

There are notable petrographic differences among plutonic rocks sampled for this study. The rock sampled from the plutonic body exposed along the Brownlee Reservoir (sample HU-79-1) is a metamorphosed trondhjemite; both in hand specimen and in thin section the rock is similar to trondhjemites from the Oxbow Complex and the (informal) Sparta complex of the Wallowa terrane and from the Canyon Mountain Complex of the Baker terrane. Feldspars are mostly albitized and hornblende is partly replaced by actinolite and chlorite; white mica is common. The other two samples (V-6-84 and V-7-84) are not as metamorphosed as sample HU-79-1. They

TABLE 3.19.—*Major- and minor-element oxides of Triassic and Early Jurassic(?) plutonic rocks of the Olds Ferry terrane*

[Oxides in weight percent, normalized to 100 percent; prenormalization volatile contents included to indicate amount of alteration]

	Plutons of northern Cuddy Mountains		Brownlee pluton
Sample	V-7-84	V-6-84	HU-79-1
SiO_2	56.83	62.88	74.28
TiO_2	.83	.57	.35
Al_2O_3	17.73	16.37	13.28
Fe_2O_3	3.17	2.72	2.01
FeO	5.15	3.76	1.36
MgO	3.85	2.64	.94
MnO	.14	.13	.09
CaO	7.99	6.74	2.20
Na_2O	2.76	2.94	3.55
K_2O	1.40	1.14	1.88
P_2O_5	.15	.11	.06
H_2O^+	1.19	0.70	1.04
H_2O^-	.06	.03	.08
CO_2	.08	.07	.17
FeO_{total}/MgO	2.08	2.35	3.37

TABLE 3.20.—*Trace elements of Triassic and Early Jurassic(?) plutonic rocks of the Olds Ferry terrane*

[Results in parts per million. Analysis by neutron activation unless otherwise noted. ---, not determined or below detection limit or discarded because of high coefficient of variation]

	Plutons of northern Cuddy Mountains		Brownlee pluton
Sample	V-7-84	V-6-84	HU-79-1
Rb	48	41	26
Sr	350	290	[1]129
Ba	664	640	466
Th	2.65	4.47	1.26
U	.99	1.22	.84
La	7.41	9.15	5.2
Ce	18.00	21.00	14.4
Sm	3.00	3.59	3.3
Eu	.91	.86	.78
Gd	3.28	3.93	4.05
Tb	.56	.68	.78
Tm	.31	.44	---
Yb	1.96	2.77	4.08
Lu	.28	.41	.63
Y	20	10	46
Zr	79	99	170
Hf	2.52	3.02	3.8
Ta	.16	.16	---
Co	22	15	15
Cr	26	13	13
Sc	26	23	19
Zn	87	68	110

[1]Analysis by X-ray fluorescence.

have plagioclase, hornblende, and quartz as dominant primary minerals; orthoclase is an uncommon constituent. Metamorphic minerals are mostly epidote and chlorite; albite is rare.

Major- and minor-element contents (table 3.19) are compatible with an island-arc origin. Although FeO_{total}/MgO ratios are higher for these three samples than for both the Aleutian intrusive rocks and the Jurassic to Cretaceous plutonic rocks of the Blue Mountains region (fig. 3.26), they plot within the data fields of late Paleozoic and Triassic plutonic rocks of the Wallowa terrane (fig. 3.18). TiO_2 contents are low. K_2O contents are generally higher than in the late Paleozoic and Triassic plutonic rocks of the Wallowa and Baker terranes. Quantities of Zr and Y are low; Rb, Sr, and Ba contents are high (table 3.20). LREE's are enriched in the Cuddy Mountains samples (V-7-84 and V-6-84) with Ce_n/Yb_n ratios of about 2 (fig. 3.27). The LREE's are not enriched in sample HU-79-1

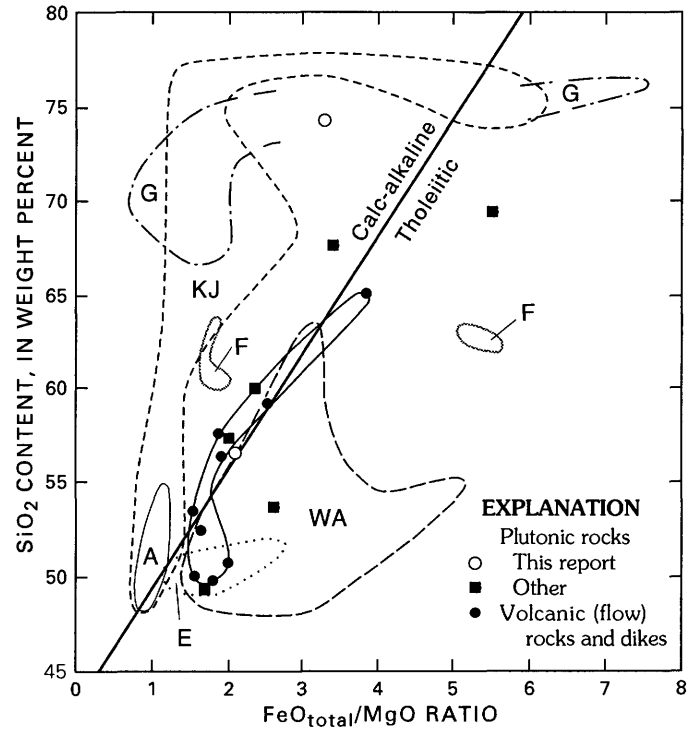

FIGURE 3.26.—FeO_{total}/MgO ratio versus SiO_2 content for plutonic, volcanic (flow), and hypabyssal (dike) rocks of Olds Ferry terrane. Heavy line encloses volcanic rock and dike data for Olds Ferry terrane. Data field A represents Aleutian island arc volcanic rocks; fields E, F, and G represent Aleutian island arc plutonic rocks; and field KJ represents Jurassic to Cretaceous plutonic rocks of Blue Mountains region (fig. 3.4). Field WA represents Triassic flows of Wallowa terrane (fig. 3.22). Includes some data (squares) compiled by C.W. Field (written comm., 1988). Calc-alkaline–tholeiitic compositional boundary from Miyashiro (1974).

from the plutonic body exposed along the Brownlee Reservoir, whose Ce_n/Yb_n ratio is less than 1 (fig. 3.27). REE patterns have a nearly flat tholeiitic trend (fig. 3.28).

Four of the six isotopically dated samples of the Olds Ferry terrane intrusive bodies are younger than pre-Jurassic plutonic rocks of both the Baker and Wallowa terranes (fig. 3.21). The age of the intrusive body exposed along the Brownlee Reservoir (sample HU-79-1) is similar to ages of several intrusive rocks from the Wallowa and Baker terranes. The intrusive body along the Brownlee Reservoir may be basement upon which strata of the Huntington Formation were deposited; the plutonic bodies exposed in and near the Cuddy Mountains are probably volcano-root plutons.

VOLCANIC (FLOW) AND ASSOCIATED HYPABYSSAL INTRUSIVE ROCKS

Lava flows from the Upper Triassic (late Karnian and early Norian) Huntington Formation are well exposed along the road that parallels Brownlee Reservoir in Oregon (table 3.21). Interbedded fossiliferous marine sedimentary rocks indicate that most of the lavas were erupted in a submarine environment. Red and maroon tuffaceous rocks (V-17-85 and V-18-85) near the upper part of the exposed section suggest nearby subaerial or shallow-marine eruptions, and reversed grading of pumice clasts in some beds suggests subaqueous deposition.

Most rocks of the Huntington Formation are regionally metamorphosed to the upper greenschist facies. The flows have a wide range in textures, including pilotaxitic, intersertal, and intergranular. Primary minerals are plagioclase, clinopyroxene, and magnetite. Clinopyroxene is abundant in some lavas. The replacement of calcic plagioclase by albite is variable but ubiquitous; primary orthoclase is rare. In some thin sections clinopyroxene is replaced by chlorite and epidote. Besides albite, chlorite, and epidote, white mica and calcite are common secondary minerals; less common accessory and secondary minerals are sphene, leucoxene, pyrite, prehnite, and hematite.

Major- and minor-element oxides indicate a wide range of rock compositions for the Huntington

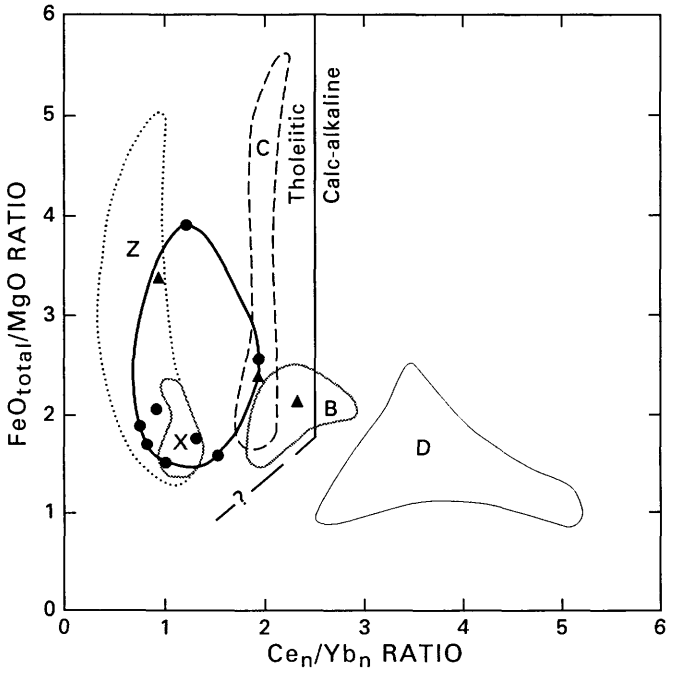

FIGURE 3.27.—FeO_{total}/MgO versus Ce_n/Yb_n ratios for plutonic, volcanic (flow), and hypabyssal (dike) rocks of Olds Ferry terrane. Dots, Late Triassic flows and dikes; triangles, Triassic to Jurassic plutonic rocks. Heavy line encloses field for Late Triassic volcanic (flow) and hypabyssal (dike) rocks of Olds Ferry terrane. Data fields B, C, and D represent Aleutian island arc volcanic rocks, and X and Z, Tonga island arc volcanic rocks (fig. 3.5). Note overlap of data field (heavy outline) that includes all Late Triassic flows with data field (X) for tholeiitic rocks of Ata Island. Line, dashed and queried where uncertain, separates tholeiitic and calc-alkaline fields. n, chondrite normalized.

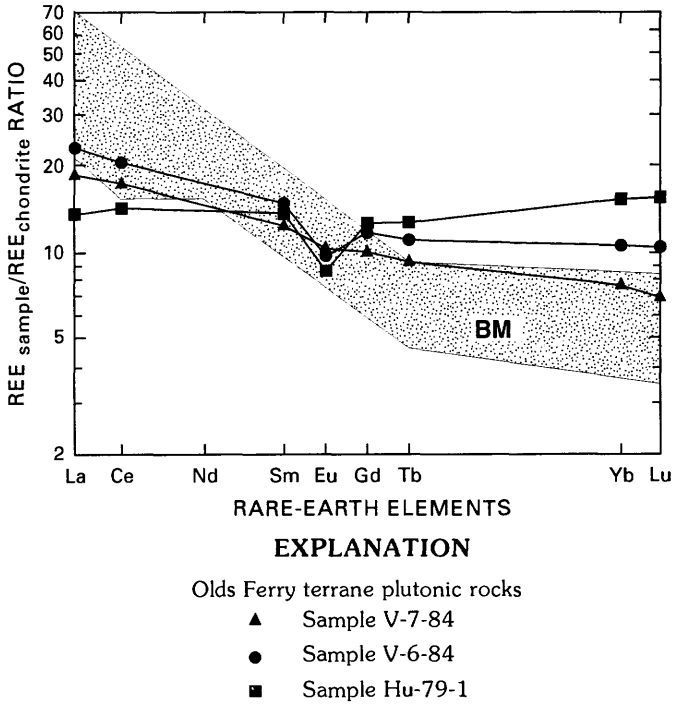

FIGURE 3.28.—Rare-earth element (REE) diagram for plutonic rocks of Olds Ferry terrane. Patterned area (BM) is data field for Jurassic Bald Mountain batholith of Blue Mountains region (fig. 3.6*B*), which has a strong calc-alkaline trend. In contrast, plutonic rocks of Olds Ferry terrane are tholeiitic. Sample numbers correspond to those in tables 3.18 through 3.20; for normalizing values used, see figure 3.6.

TABLE 3.21.—*Lithology, sample locality, and field description of Late Triassic volcanic (flow) and hypabyssal (dike) rocks of the Olds Ferry terrane, collected along Brownlee Reservoir road, eastern Oregon*

[Rocks arranged by increasing SiO_2 content to correspond to chemical analyses in tables 3.22 and 3.23. Do. and do., ditto; BM, bench mark]

Sample	Rock type	Sample locality	Field description and remarks
VB-62	Diabase	Along road that parallels Brownlee Reservoir on the west side; NW1/4 sec. 32, T. 13 S., R. 45 E.; Olds Ferry quadrangle, Oreg.	Dike cutting trondhjemite (see HU-79-1, tables 3.18–3.20).
VB-56	Basalt	Near bridge that crosses Burnt River east of Huntington, Oreg.; NE1/4SE1/4 sec. 8, T. 14 S., R. 45 E.; Olds Ferry quadrangle, Oreg.	Flow rock; Huntington Formation.
V-13-85	--- do	Near confluence of Burnt and Snake Rivers; SE1/4NE1/4 sec. 8, T. 14 S., R. 45 E.; Olds Ferry quadrangle, Oreg.	Do.
V-14-85	Basaltic andesite	North of confluence of Burnt and Snake Rivers; SE1/4NE1/4 sec. 8, T. 14 S., R. 45 E.; Olds Ferry quadrangle, Oreg.	Do.
V-16-85	--- do	Near BM 2017; NE1/4SW1/4 sec. 16, T. 13 S., R. 45 E.; Olds Ferry quadrangle, Oreg.	Do.
V-12-85	Andesite	Near confluence of Burnt and Snake Rivers; SE1/4NE1/4 sec. 8, T. 14 S., R. 45 E.; Olds Ferry quadrangle, Oreg.	Do.
VB-59	--- do	0.8 km east of bridge that crosses Burnt River; NE1/4SE1/4 sec. 8, T. 14 S., R. 45 E.; Olds Ferry quadrangle, Oreg.	Do.
V-15-85	--- do	Near BM 2022; SE1/4SE1/4NW1/4 sec. 21, T. 13 S., R. 45 E.; Olds Ferry quadrangle, Oreg.	Do.
V-17-85	Dacite	Near BM 2006; NE1/4SW1/4 sec. 9, T. 13 S., R. 45 E.; Olds Ferry quadrangle, Oreg.	Clast in tuff breccia of the Huntington Formation.
V-18-85	Rhyolite	Near BM 2006 and about 30 m north of site for V-17-85; NE1/4SW1/4 sec. 9, T. 13 S., R. 45 E.; Olds Ferry quadrangle, Oreg.	Do.

Formation (table 3.22), including basalt, basaltic andesite, and andesite as flows, and dacite and rhyolite as clasts (in tuff breccias). The flows have low TiO_2 contents; Al_2O_3 concentrations are high, mostly reflecting the amount of plagioclase. Fe enrichment is characteristic of the more mafic lavas; the plot of FeO_{total}/MgO ratios versus SiO_2 contents indicates that these rocks are tholeiitic and transitional (fig. 3.26). K_2O contents are high compared to those of most island-arc lavas (Gill, 1981). Na_2O contents are variable and reflect albitization of plagioclase, particularly in the more mafic rocks, in which Na_2O ranges from 3.19 to 5.41 percent; these are high values compared to those for unaltered mafic lavas from island arcs (Gill, 1981).

Trace-element contents may be more useful for interpreting the petrogenesis of these rocks and the extent of ion mobility during metamorphism (table 3.23). Rb, Sr, Ba, Cs, Th, and U contents can be correlated with K_2O content, strengthening the interpretation that high amounts of these trace elements as well as the high K_2O concentrations are related to magmatic rather than metamorphic processes. Zr and Y contents are low and correlate with the low abundance of TiO_2. The high concentrations of K, Rb, Sr, and Ba in sample VB-56 and the high Rb content of sample V-13-85, however, are perplexing; thin-section analyses suggest that the K_2O is in the plagioclase; no orthoclase phenocrysts or xenocrysts were observed. The FeO_{total}/MgO versus Ce_n/Yb_n ratios and REE patterns (figs. 3.27 and 3.29) indicate that most of the rocks are tholeiitic. The similarities with plots of Ata Island (Tonga) flows are noteworthy, implying a somewhat similar island-arc tholeiite petrogenesis.

TABLE 3.22.—*Major- and minor-element oxides of Late Triassic volcanic (flow) and hypabyssal (dike) rocks of the Olds Ferry terrane*

[Oxides in weight percent, normalized to 100 percent; prenormalization volatile contents included to indicate amount of alteration]

Sample	VB-62	VB-56	V-13-85	V-14-85	V-16-85	V-12-85	VB-59	V-15-85	V-17-85	V-18-85
SiO_2	49.91	50.10	50.82	52.65	53.44	56.41	57.75	59.24	65.08	72.06
TiO_2	.86	.77	.81	.76	1.01	.93	.93	1.26	.87	.67
Al_2O_3	17.32	19.78	21.90	20.10	19.60	17.80	17.69	14.47	16.27	14.46
Fe_2O_3	5.09	3.35	3.82	3.19	3.05	3.19	3.65	5.50	2.65	4.18
FeO	6.63	6.95	5.32	6.93	5.71	7.09	5.96	5.98	2.82	.16
MgO	6.41	6.35	4.35	5.90	5.47	5.42	4.95	4.16	1.35	.18
MnO	.27	.23	.24	.32	.16	.32	.22	.38	.15	.04
CaO	8.12	7.04	6.90	3.84	4.44	2.12	1.87	4.12	2.21	.46
Na_2O	5.09	3.19	4.54	5.41	4.73	5.75	6.00	4.67	7.68	5.33
K_2O	.24	2.20	1.23	.82	2.23	.87	.91	.48	.71	2.24
P_2O_5	.06	.04	.07	.08	.16	.10	.07	.19	.21	.22
H_2O^+	3.33	3.99	4.37	4.11	3.28	3.58	3.31	2.52	0.81	1.13
H_2O^-	.42	.66	.29	.23	.52	.29	.48	.27	.20	.23
CO_2	3.16	.08	.29	.06	.56	1.12	.87	.15	4.03	.09
FeO_{total}/MgO	1.75	1.57	2.02	1.66	1.54	1.84	1.87	2.53	3.85	21.80

TABLE 3.23.—*Trace elements of Late Triassic volcanic (flow) and hypabyssal (dike) rocks of the Olds Ferry terrane*

[Results in parts per million. Analysis by neutron activation unless otherwise noted. ---, not determined or below detection limit or discarded because of high coefficient of variation]

Sample	VB-62	VB-56	V-13-85	V-14-85	V-16-85	V-12-85	VB-59	V-15-85	V-17-85	V-18-85
Rb	[1]6	[1]58	23	---	59	17	[1]9	15	---	46
Sr	[1]134	[1]218	[2]120	[2]160	[2]340	[2]120	[1]164	[2]150	[2]150	[2]12
Ba	[1]70	[1]397	193	151	689	214	[1]275	254	220	637
Cs	---	---	.91	2.16	16.90	1.33	---	1.47	.63	4.42
Th	---	.3	.22	.19	1.87	.28	---	.65	2.41	2.91
U	---	---	.16	.20	.63	.18	---	.36	.65	.89
La	4	2	1.74	1.71	6.63	2.51	3	4.55	6.83	14.30
Ce	8	5	4.93	5.42	14.70	6.23	6	11.30	17.10	34.00
Sm	1.9	1.4	1.46	1.54	2.65	1.95	2.0	3.00	3.09	5.30
Eu	.69	.50	.63	.76	.96	.91	.75	1.20	1.22	1.59
Gd	---	---	---	2.07	3.30	2.62	---	4.23	4.71	6.08
Tb	.45	.32	.38	.39	.61	.52	.59	.75	.87	1.07
Tm	---	---	---	.27	.40	.34	.31	.48	.61	.74
Yb	1.6	1.3	1.46	1.75	2.50	2.20	---	3.05	3.68	4.55
Lu	.25	.21	.23	.26	.36	.35	.35	.45	.55	.68
Y	[1]18	[1]12	---	[2]10	[2]20	[2]15	[1]24	[2]20	[2]25	[2]35
Zr	[1]24	[1]25	37	[2]30	67	58	[1]39	94	92	114
Hf	1.0	.7	.72	.80	1.78	1.03	1.0	1.75	2.42	3.54
Ta	---	---	---	.03	.11	.03	---	.08	.16	.18
Nb	---	[1]15	---	---	---	---	[1]6	---	---	---
Co	36	28	23	26	23	22	21	23	7	3
Cr	20	20	19	17	20	50	---	4	24	5
Sc	41	36	34	34	34	40	40	42	26	17
Zn	130	114	125	182	90	184	154	216	183	361

[1]Analysis by X-ray fluorescence.
[2]Analysis by optical spectroscopy.

PETROGENESIS OF IGNEOUS ROCKS OF THE OLDS FERRY TERRANE

The chemically analyzed igneous rocks from the Olds Ferry terrane formed in an intraoceanic island arc. The major characteristics of Olds Ferry lavas are the ubiquitous presence of plagioclase and clinopyroxene in the modes, Fe enrichment, flat REE patterns, low quantities of high-field-strength elements,

and intermediate but variable amounts of K-group elements. These rocks have higher contents of the K-group elements than most igneous rocks in the Blue Mountains island arc older than the Jurassic to Cretaceous intrusive rocks.

K_2O contents are particularly interesting because Mortimore (1986) used them to conclude that the Olds Ferry rocks were part of a high-K arc that bordered the North American continent. On the basis of a plot of K_2O versus SiO_2 contents (see Gill, 1981, p. 6), the rocks are high- to intermediate-K basalt and basaltic andesite, and intermediate- to low-K andesite. Relatively high K_2O content, in comparison with that of most Cenozoic tholeiitic island-arc lavas, could be explained by one or more of the following: (1) It may be related to a large amount of sediments that were added to the magma source region above a subduction zone, particularly if the sediments had been eroded from a continent; (2) it may be related to tectonic setting, such as the depth to the dipping subduction zone (Gill, 1981); (3) it may merely reflect abnormal fractionation of magma beneath a single volcano and (or) K mobility during metamorphism.

Parent magmas probably were derived from partial melting of a depleted mantle source above a dipping subduction zone. The fractionation of plagioclase, olivine and (or) orthopyroxene, augite, and magnetite must have been the dominant differentiation process, although assimilation of older arc crust and magma mixing cannot be ruled out. The magmas differentiated in relatively high-temperature and low-pressure environments.

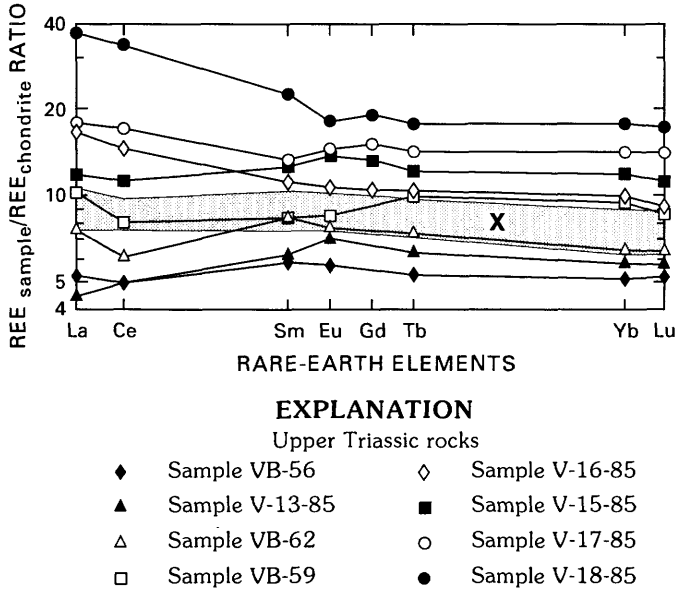

FIGURE 3.29.—Rare-earth element (REE) diagram for volcanic (flow) and hypabyssal (dike) rocks of Olds Ferry terrane; these rocks are strongly tholeiitic. Patterned area (X) is data field for tholeiitic rocks of Ata Island (fig. 3.7), shown for comparison. Most samples are from Upper Triassic Huntington Formation of Brooks (1979a, b); sample numbers correspond to those in tables 3.21 through 3.23. For normalizing values used, see figure 3.6. Missing data points for Gd indicate that element was not determined, contents were below detection limit, or data were discarded because of high coefficient of variation.

JURASSIC IGNEOUS ROCKS ASSOCIATED WITH THE COON HOLLOW FORMATION OF THE WALLOWA TERRANE

I sampled dikes and sills within the Middle and Upper Jurassic Coon Hollow Formation of the Wallowa terrane (Morrison, 1963; White, 1972; White, 1985; Goldstrand, 1987, 1994; White and Vallier, 1994; White, 1994) and a partially welded tuff that is interbedded with the oldest strata in that formation (table 3.24). Middle (Bajocian and Callovian) and Late (Oxfordian) Jurassic marine fossils from the Coon Hollow Formation were identified by Imlay (1986) and Stanley and Beauvais (1990).

DESCRIPTION OF THE IGNEOUS ROCKS

The diabase (sample V-1-85, table 3.24) is metamorphosed to the upper greenschist facies; abundant chlorite and epidote have replaced clinopyroxene and groundmass glass, and some albite has replaced calcic plagioclase. The microdiorite (sample V-58-79) has undergone very low grade metamorphism; most primary minerals are unaltered. Estimated modal mineralogy of sample V-58-79 is plagioclase, 50 percent; hornblende, 30 percent; augite, 10 percent; Fe-oxide minerals, 1 percent; and epidote+chlorite, 9 percent. White mica is rare. In the metamorphosed andesite porphyry (sample T-68-16), albite has replaced calcic plagioclase, and chlorite and epidote have replaced the mafic minerals. The andesite porphyry occurs in several places within the Coon Hollow Formation in the Pittsburg Landing area.

The rhyolite tuff (sample V-11-85), described in more detail by White and Vallier (1994), crops out over a very small area and is associated with abundant alluvial-fan channel deposits of cobble and pebble conglomerate. In the more welded parts of the tuff, unaltered feldspar and lithic fragments are set in a eutaxitic matrix of altered glass and pumice.

These igneous rocks have low amounts of TiO_2 and, except for sample V-11-85, relatively low FeO_{total}/MgO ratios (table 3.25). K_2O contents are low for samples V-1-85, T-68-16, and V-11-85, and relatively

TABLE 3.24.—*Lithology, sample locality, and field description of Jurassic hypabyssal intrusive rocks and a welded tuff interbedded in lowest part of the Coon Hollow Formation, Wallowa terrane*

[Rocks arranged by increasing SiO_2 content to correspond to chemical analyses in tables 3.25 and 3.26]

Sample	Rock type	Sample locality	Field description and remarks
V-58-79	Microdiorite	North side Coon Hollow Creek; elevation 365 m (1,200 ft); SE1/4SE1/4 sec. 26, T. 6 N., R. 47 E.; Jim Creek Butte quadrangle; Oreg.	Sill that cuts the Coon Hollow Formation.
V-1-85	Diabase	East side, north fork of West Creek; elevation 870 m (2,850 ft); SW1/4NE1/4 sec. 21, T. 27 N., R. 1 W; Grave Point quadrangle; Idaho.	Large dike that cuts the Coon Hollow Formation.
T-68-16	Andesite porphyry	Along road that parallels Kurry Creek near Pittsburg Landing; elevation 518 m (1,700 ft); SE1/4 sec. 28, T. 27 N., R. 1 W.; Grave Point quadrangle; Idaho.	Irregular pluton that cuts the Coon Hollow Formation.
V-11-85	Rhyolite	Ridge south of West Creek; elevation 457 m (1,500 ft); extreme NW1/4NW1/4 sec. 27, T. 27 N., R. 1 W.; Grave Point quadrangle; Idaho.	Welded tuff; near base of the Coon Hollow Formation. Prominent ledge.

TABLE 3.25.—*Major- and minor-element oxides of Jurassic hypabyssal intrusive rocks and a welded tuff interbedded in lowest part of the Coon Hollow Formation, Wallowa terrane*

[Oxides in weight percent, normalized to 100 percent; prenormalization volatile contents included to indicate amount of alteration]

Sample	V-58-79	V-1-85	T-68-16	V-11-85
SiO_2	54.74	55.02	60.15	74.14
TiO_2	1.02	.96	.72	.43
Al_2O_3	16.79	16.54	17.81	12.20
Fe_2O_3	2.13	1.51	.96	1.07
FeO	5.10	6.95	4.11	4.01
MgO	6.73	6.66	4.24	1.53
MnO	.10	.11	.06	.07
CaO	7.71	6.38	4.37	2.58
Na_2O	3.90	5.30	6.79	3.76
K_2O	1.41	.35	.43	.15
P_2O_5	.37	.22	.26	.06
H_2O^+	2.51	3.85	2.20	2.26
H_2O^-	.21	.27	.48	.42
CO_2	.12	3.53	1.80	2.08
FeO/MgO	1.04	1.25	1.17	3.25

high for sample V-58-79. The plot of FeO_{total}/MgO ratios versus SiO_2 contents (fig. 3.30) clearly shows the similarities between samples V- 58-79, V-1-85, and T-68-16 and the large Jurassic to Cretaceous plutons of the Blue Mountains region; the tuff sample is more Fe enriched and lies outside the data field for Jurassic to Cretaceous plutons.

Trace-element contents show strong enrichments in Rb, Sr, and Ba for samples V-58-79 and T-68-16, but lower contents were found in the other samples (table 3.26). Th and U contents are consistently high in all four samples. Zr and Y are depleted in parallel with the depletion of TiO_2. Ce_n/Yb_n ratios of three of the four samples are within or close to the data field for the Bald Mountain batholith (fig. 3.31); the tuff (sample V-11-85) has a low ratio and plots within the tholeiitic field. The REE diagram (fig. 3.32) shows calc-alkaline affinities for all samples except the tuff, which has a flat tholeiitic pattern.

PETROGENESIS

The composition, size, degree of metamorphism, and field relationships separate the small intrusive bodies associated with the Coon Hollow Formation from the large Jurassic to Cretaceous plutons of the Blue Mountains region. The strongly calc-alkaline character of the intrusive rocks has several petrologic implications (table 3.2): fractionation of amphibole (and garnet?), abundant water in the magma, greater mixing in the source region, and a higher pressure (deeper) fractionation regime. These possibilities in turn have tectonic implications, including slower convergence rates, a shallower dip of the subducting slab, and possibly a thicker crust. The important point is that there must have been a change in tectonic setting within the Wallowa terrane between the

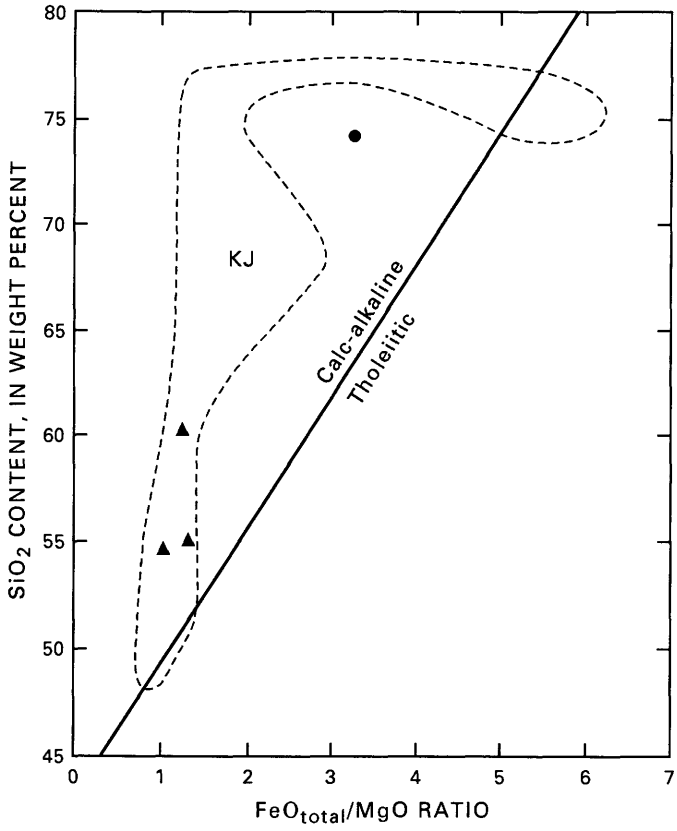

FIGURE 3.30.—FeO_{total}/MgO ratio versus SiO_2 content for hypabyssal rocks (dikes and plugs) that cut strata of Coon Hollow Formation and for a welded tuff interbedded in lowest part of Coon Hollow Formation. Note that dikes and plugs (triangles) lie entirely within area (KJ) representing Jurassic to Cretaceous (calc-alkaline) plutons of Blue Mountains region (fig. 3.4) and that welded tuff (dot) is more Fe-enriched. Calc-alkaline–tholeiitic compositional boundary from Miyashiro (1974).

eruption of the youngest (Karnian) flows of the Doyle Creek Formation and the intrusion of the small intrusive bodies (Bajocian or younger in age at Pittsburg Landing and Oxfordian or younger in age in the northern Snake River canyon).

The presence of a low-K rhyolite tuff in the lower part of the Coon Hollow Formation may signal the last gasp of a tholeiitic magmatic regime before a change in tectonic setting led not only to the calc-alkaline hypabyssal intrusive rocks within the Coon Hollow Formation but also to the voluminous Jurassic to Cretaceous calc-alkaline plutons of the entire Blue Mountains region.

JURASSIC TO CRETACEOUS PLUTONIC ROCKS OF BLUE MOUNTAINS REGION

The Jurassic to Cretaceous plutons are only briefly discussed in this chapter. Taubeneck (1957, 1967, chap. 2 of this volume and references cited therein) is most familiar with the field relations and petrology of this large group of rocks. Armstrong and others (1977) compiled and discussed a significant number of isotopic (mostly K-Ar) ages and Sr-isotope data for Jurassic to Cretaceous plutons in the Blue Mountains region. They concluded that most of these plutons crystallized in the interval from 160 to 115 Ma. However, on the basis of U-Pb isotopic age dating of zircons, Walker (1989; oral commun., 1990) concluded that almost all of the plutons were emplaced within the interval from 145 to 120 Ma.

In this section, I describe several small Jurassic to Cretaceous plutonic bodies that are widely separated geographically from the Wallowa and Bald Mountain batholiths. Major- and trace-element data, four initial Sr-isotope ratios, and two new K-Ar isotopic ages are given. These data certainly are not sufficient for thorough study of all Jurassic to Cretaceous plutons in the Blue Mountains region, but the data warrant some discussion of the petrology and tectonic setting of these plutons.

TABLE 3.26.—*Trace elements of Jurassic hypabyssal intrusive rocks and a welded tuff interbedded in lowest part of the Coon Hollow Formation, Wallowa terrane*

[Results in parts per million. Analysis by neutron activation unless otherwise noted. ---, not determined or below detection limit or discarded because of high coefficient of variation]

Sample ------	V-58-79	V-1-85	T-68-16	V-11-85
Rb	[1]29	9	[1]23	---
Sr	[1]884	[2]290	[1]505	[2]170
Ba	[1]935	86	[1]280	105
Cs	---	1.02	---	.35
Th	1.70	1.12	1.20	1.29
U	.60	.65	.51	.93
La	16	9.93	11.5	4.56
Ce	34	23.50	21.7	11.10
Sm	3.6	3.02	2.7	2.28
Eu	1.21	1.08	.73	.85
Gd	---	3.21	---	2.95
Tb	.41	.44	---	.55
Tm	---	.22	.10	.40
Yb	1.2	1.40	.69	2.70
Lu	.20	.18	.11	.41
Y	7	10	13	20
Zr	[1]100	[2]80	[1]90	114
Hf	2.2	2.02	1.9	3.28
Ta	.4	.28	.19	.20
Nb	8	---	8	---
Ni	118	---	---	---
Co	29	32	18	9
Cr	225	207	113	24
Sc	20	24	13	13
Zn	75	92	44	61

[1]Analysis by X-ray fluorescence.
[2]Analysis by optical spectroscopy.

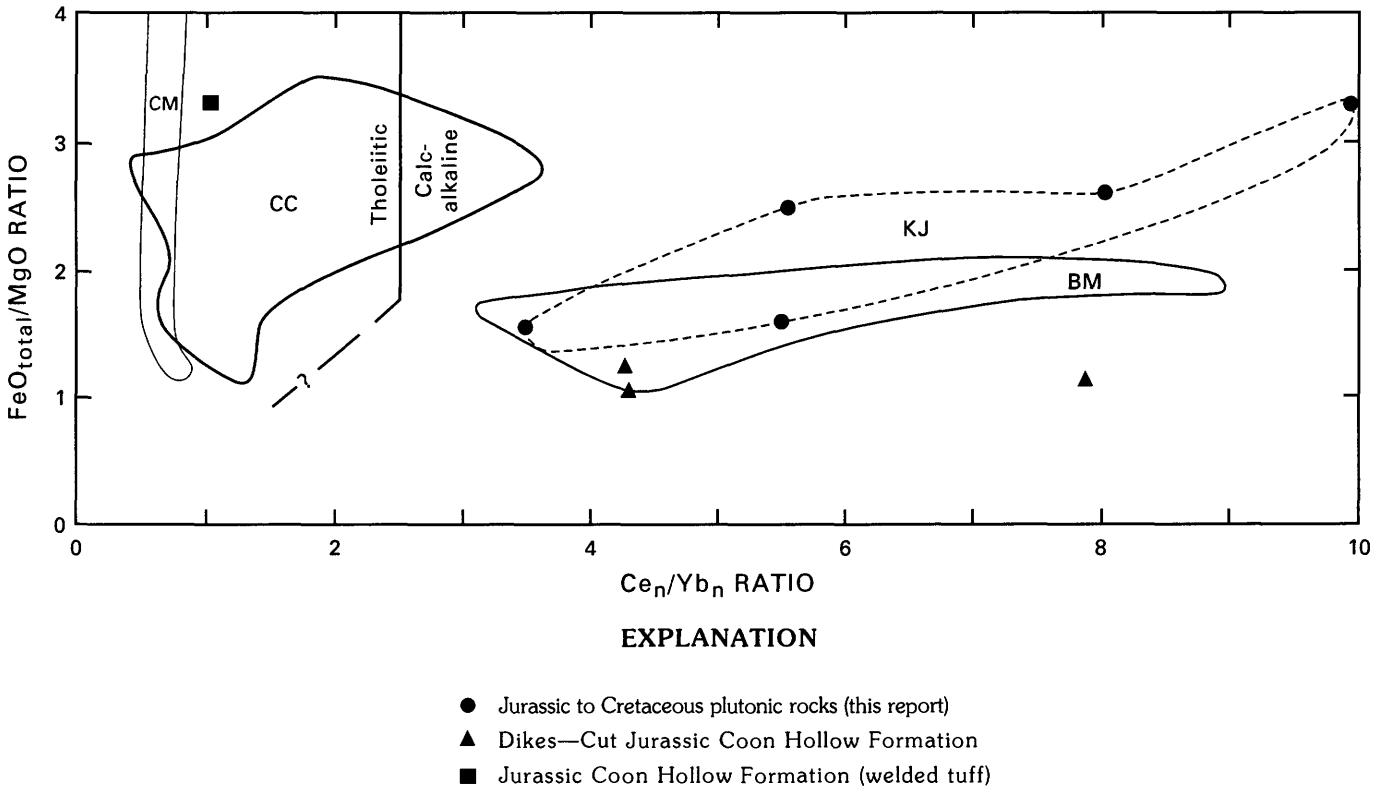

FIGURE 3.31.—FeO_{total}/MgO versus Ce_n/Yb_n ratios for Jurassic and Cretaceous rocks in Blue Mountains region. Line, dashed and queried where uncertain, separates tholeiitic and calc-alkaline fields. Note that among Jurassic and Cretaceous rocks, only tuff in Coon Hollow Formation shows tholeiitic affinity. Data field KJ corresponds only to those Jurassic to Cretaceous plutonic rocks analyzed for this chapter (see table 3.29). For comparison, plot also includes Cougar Creek Complex of Vallier (1968) (data field CC; fig. 3.19), Canyon Mountain Complex (CM; fig. 3.10), and Bald Mountain batholith (BM; fig. 3.5). n, chondrite normalized.

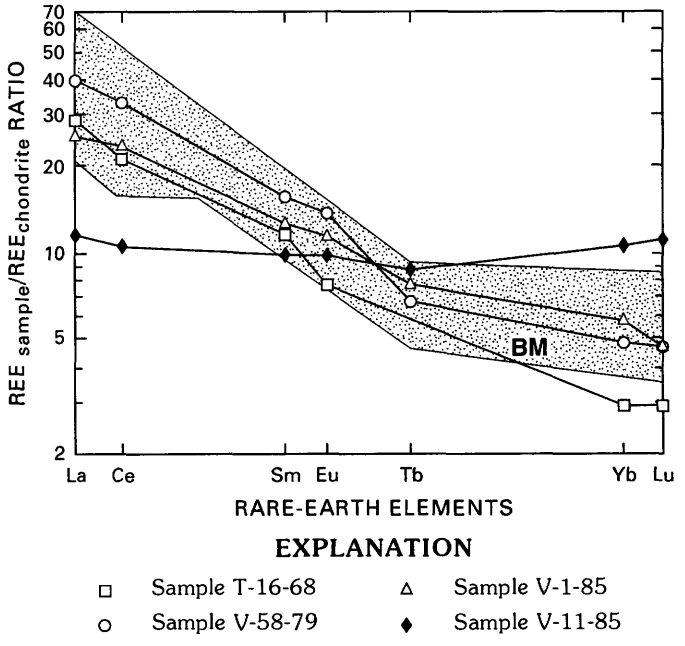

FIGURE 3.32.—Rare-earth element (REE) diagram for Jurassic welded tuff of Coon Hollow Formation (sample V-11-85) and for sill and dike rocks that cut Coon Hollow Formation (samples T-16-68, V-58-79, and V-1-85). Patterned area (BM) is data field for Late Jurassic Bald Mountain batholith of Blue Mountains region (fig. 3.6*B*), shown for comparison. Note flat pattern for sample V-11-85. Sample numbers correspond to those in tables 3.24 through 3.26; for normalizing values used, see figure 3.6. Missing Tb data point indicates no analysis, content below detection limit, or large coefficient of variation.

TABLE 3.27.—*Lithology, sample locality, and field description of analyzed Jurassic to Cretaceous plutonic rocks of the Blue Mountains region*

[Rocks arranged by increasing SiO_2 content to correspond to chemical analyses in tables 3.29 and 3.30. Do. and do., ditto]

Sample	Rock type	Sample locality	Field description and remarks
V-12-79	Gabbro	Cutsforth County Park along stream near small lake; elevation 1,275 m (4,185 ft); T. 4 S., R. 28 E.; Arbuckle Mountain quadrangle; Oreg.	Near contact with granodiorite (sample V-11-79).
V-24-79	Diorite	Carney Butte north of lookout tower; elevation 1,503 m (4,930 ft); NE1/4NW1/4 sec. 28, T. 3 S., R. 31 E.; Carney Butte quadrangle; Oreg.	Melanocratic pluton; some cumulate texture.
V-23-79	---- do	--------do	Do.
V-54B-79	---- do	Along trail, west side of Seven Devils Mountains south of Baldy Lake; elevation 2,335 m (7,660 ft); unsurveyed part of T. 23 N., R. 2 W.; He Devil quadrangle; Idaho.	Melanocratic pluton that extends irregularly along west side of Seven Devils Mountains.
V-46-79	Quartz diorite	Outcrop along road near entrance; Winchester State Park; elevation 1,175 m (3,850 ft); T. 33 N., R. 2 W; Winchester East quadrangle; Idaho.	Small inlier within the Columbia River Basalt Group.
V-11-79	Granodiorite	Cutforth County Park along stream near small lake; elevation 1,280 m (4,200 ft); T. 4 S., R. 28 E.; Arbuckle Mountain quadrangle; Oreg.	Poor outcrops, near contact with gabbro (sample V-12-79).
V-75-79	---- do	Blacktail stock, along road east of Mt. Idaho; elevation 745 m (2,445 ft); SE1/4SE1/4 sec. 26, T. 30 N., R. 3 E.; Grangeville East quadrangle; Idaho.	Pluton that apparently cuts both the Seven Devils Group and the Riggins Group.
VC-295	Granite	Small ridge south of Eckels Creek; elevation 1,396 m (4,580 ft); NW1/4NE1/4 sec. 4, T. 20 N., R. 3 W.; Cuprum quadrangle; Idaho.	Small pluton; intrudes rocks of the Hunsaker Creek Formation.

DESCRIPTION OF THE PLUTONIC ROCKS

The Jurassic to Cretaceous plutonic rocks sampled (table 3.27) represent a wide range of rock types. Ages of most are unknown, but field relationships and compositions, including the small amount of alteration, were used to assign them Jurassic to Cretaceous ages. Sample V-75-79 from the Blacktail stock, which is along the South Fork of the Clearwater River in Idaho (fig. 3.1), has been isotopically dated at 78 Ma by K-Ar methods (Criss and Fleck, 1987), and the plutonic body at Winchester State Park in Idaho (sample V-46-79) has a K-Ar hornblende age of about 141 Ma (same as sample 719 of Armstrong and others, 1977). Sample VC-295 is a two-mica granite that cuts Permian rocks in the upper reaches of Eckels Creek in Idaho south of Hells Canyon Dam (fig. 3.3). The absence of granite from known late Paleozoic and Triassic intrusive bodies in the Blue Mountains region and the lack of appreciable alteration suggest a Jurassic to Cretaceous age.

Two previously unreported K-Ar radiometric ages (samples V-47-79 and V-3-86, table 3.28), complement the age data already available for the Jurassic to Cretaceous plutons of eastern Oregon and western Idaho (Armstrong and others, 1977; Goldstrand, 1987). Armstrong and others (1977) cautioned that many of the ages are minima; for example, they stated that 136 Ma may be the minimum age for all or nearly all of the granitic plutons within the Wallowa Mountains (Armstrong and others, 1977, p. 402). In contrast, N.W. Walker (oral commun., 1989) stated that his U-Pb isotopic age data indicate that 137 Ma (for his Pole Bridge unit) is the maximum age determined for the Wallowa batholith.

The consistent K-Ar isotopic ages (about 115 Ma) on both biotite and hornblende mineral separates from a diorite exposed along Little Granite Creek

TABLE 3.28.—*K-Ar ages of selected Jurassic to Cretaceous plutonic rocks of the Blue Mountains region*

[Apparent ages, calculated using two or more replicate determinations on each mineral separate, listed as averages of replicate data (weighted by inverse of variance) or as minimum age. Error values for ages are estimates of the standard deviation of analytical precision. Half-lives used in calculations: λ_e=0.581×10^{-10}/yr and λ_β=4.96×10^{-10}/yr. Abundance ratio: ^{40}K/K=1.167×10^{-4} atom percent. rad, radiogenic; do., ditto. Analysts, L.B. Gray and J.E. Pearl, U.S. Geological Survey]

Sample	Locality	Rock type	Mineral	K_2O (weight percent)	$^{40}Ar_{rad}$ (moles per gram)	$^{40}Ar_{rad}/^{40}Ar_{total}$	Apparent age (Ma): Replicate determination	Apparent age (Ma): Average or minimum age
7-18H	Intersection of Dry and Cook Creeks, unsurveyed part, southeast corner of Jim Creek Butte quadrangle, Oreg.	Diorite[1]	Biotite	9.00	1.866x10^{-9}	0.979	139.1	139.5±2.1 (average)
			-- do.	8.93	1.879x10^{-9}	.902	140.0	
V-47-79	Extreme southeast corner of Washington along Snake River; SE 1/4SW 1/4 sec. 9, T. 6 N. R. 47 E.; Lime Kiln Rapids quadrangle; Wash.	Quartz diorite.	Biotite	7.24				
			-- do.	7.16	1.417x10^{-9}	.897	None	133.8±4.0 (minimum)
			-- do.	6.86	(average)			
V-3-86	Little Granite Creek, along trail; elevation 1,160 m (3,800 ft); unsurveyed part, T. 23 N., R. 2 W.; He Devil quadrangle; Idaho.	-- do.	Biotite	9.31	1.599x10^{-9}	.829	115.5	115.3±2.5 (average)
			-- do.	9.32	1.601x10^{-9}	.797	115.6	
			Hornblende	.412	6.967x10^{-9}	.584	115.3	
			-- do.	.401	(average)	(average)	(average)	

[1]Dry Creek stock.

TABLE 3.29.—*Major- and minor-element oxides of Jurassic to Cretaceous plutonic rocks of the Blue Mountains region*

[Oxides in weight percent, normalized to 100 percent; prenormalization volatile contents included to indicate amount of alteration. ---, not determined]

Sample	V-12-79	V-24-79	V-54B-79	V-46-79	V-11-79	V-75-79	VC-295
SiO_2	47.07	53.58	54.41	64.43	66.54	68.52	75.57
TiO_2	3.08	.31	.82	.59	.35	.28	.05
Al_2O_3	15.69	7.46	19.53	16.60	16.89	17.43	14.89
Fe_2O_3	3.32	1.70	3.02	1.60	1.76	1.43	.58
FeO	11.09	10.24	4.13	2.87	2.33	.96	.24
MgO	5.76	15.19	4.55	2.65	1.57	.86	.23
MnO	.23	.23	.14	.07	.15	.06	---
CaO	10.32	9.98	8.70	5.14	5.63	4.52	.85
Na_2O	3.39	1.14	3.88	4.03	3.18	4.45	4.35
K_2O	.05	.17	.65	1.86	1.45	1.37	3.14
P_2O_5	---	---	.17	.16	.15	.12	.10
H_2O^+	1.30	0.57	1.53	0.65	1.05	0.55	0.35
H_2O^-	.13	.12	.10	.09	.07	.11	.31
CO_2	.01	.01	---	.01	.01	---	1.02
FeO_{total}/MgO	2.44	.78	1.51	1.63	2.49	2.61	3.31

(sample V-3-86, table 3.28) are the youngest thus far reported for granitoid plutonic bodies in the Hells Canyon-Seven Devils Mountains region. This diorite crops out less than 16 km from the 133-Ma Deep Creek stock (White, 1973; Armstrong and others, 1977).

A gabbro and a diorite (samples V-12-79 and V-24-79, table 3.27) were collected from layered sequences and probably are crystal cumulates. Augite, hypersthene, hornblende, Fe-oxide minerals, and plagioclase are present in both samples. The remaining plutonic rocks sampled have hypidiomorphic-granular textures and have pyroxene, hornblende, and biotite as the primary mafic phases and plagioclase, quartz, and orthoclase as the dominant felsic phases. Muscovite occurs in samples V-75-79 and VC-295.

Some major-element contents (table 3.29) closely reflect mineral modes. For example, high MgO contents

TABLE 3.30.—*Trace elements of Jurassic to Cretaceous plutonic rocks of the Blue Mountains region*

[Results in parts per million. Analysis by neutron activation unless otherwise noted. ---, not determined or below detection limit or discarded because of high coefficient of variation]

Sample -----	V-12-79	V-24-79	V-54B-79	V-46-79	V-11-79	V-75-79	VC-295
Rb[1]	2	5	23	57	37	41	50
Sr[1]	201	212	592	452	600	726	205
Ba[1]	13	78	232	467	647	548	2,360
Th	---	.5	.6	6.4	4.2	1.0	3.77
U	---	---	---	1.2	1.4	.8	2.29
La	1	3	10	14	23	10	16.5
Ce	2	9	21	34	37	19	31.5
Sm	1.1	2.4	2.6	3.9	2.6	1.7	2.77
Eu	.92	.65	1.00	.94	.85	.61	.53
Gd	---	---	3.3	---	2.5	---	2.2
Tb	.34	.53	.42	.65	---	.19	---
Tm	.16	.30	---	---	.24	---	.13
Yb	---	---	1.5	1.6	1.7	.6	.8
Lu	.16	.41	.24	.23	.24	.10	.11
Y[1]	12	19	11	15	11	5	17
Zr[1]	26	43	45	147	75	102	75
Hf	.3	1.2	1.4	4.2	1.8	2.6	2.4
Ta	---	---	.19	.03	.22	.41	.64
Nb[1]	---	---	---	6	5	9	12
Ni[1]	32	302	15	35	5	---	---
Co	38	55	19	14	6	3	1
Cr	63	903	63	32	3	2	1
Sc	38	54	19	13	7	3	2
Zn	98	168	63	57	39	53	17

[1]Analyses by X-ray fluorescence.

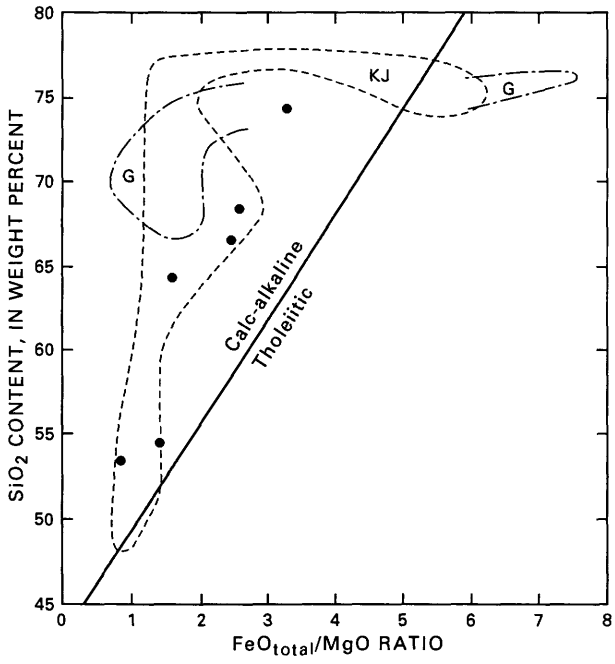

FIGURE 3.33.—FeO_{total}/MgO ratio versus SiO_2 content of Jurassic to Cretaceous plutonic rocks. Data field KJ represents most of the analyzed Jurassic to Cretaceous plutonic rocks of Blue Mountains region. Data field G represents Aleutian island arc siliceous plutonic rocks (fig. 3.4). Dots, new data. Calc-alkaline–tholeiitic compositional boundary from Miyashiro (1974).

correlate directly with pyroxene abundances in sample V-24-79. The higher K_2O contents reflect abundances of orthoclase and (or) muscovite. With the exception of sample V-12-79, FeO_{total}/MgO ratios increase with increasing SiO_2 content, but most samples still plot within the data field of Jurassic to Cretaceous plutonic rocks on a FeO_{total}/MgO ratio versus SiO_2 content diagram (fig. 3.33).

Rb, Sr, Ba, Th, and U contents correlate reasonably well with the amount of K_2O in the samples (tables 3.29 and 3.30). Ba content is extremely high in sample VC-295. The high-field-strength elements are strongly depleted in all samples; Zr contents range from 26 to 147 parts per million, and Y contents range from 5 to 19 parts per million. Plots of FeO_{total}/MgO versus Ce_n/Yb_n (fig. 3.31) and normalized REE (fig. 3.34) satisfactorily show the calc-alkaline character of these samples and their similarities to both the Bald Mountain batholith of eastern Oregon and the siliceous plutonic rocks of the Aleutian island arc (Kay and others, 1990).

Four new initial Sr-isotope ratios (table 3.31) range from a low of 0.70335±0.00002 to a high of 0.70422± 0.00004. They are within the range of values reported by Armstrong and others (1977) for other Jurassic to Cretaceous plutons in the Blue Mountains region, including plutons (such as the Deserette and Council

TABLE 3.31.—*$^{87}Sr/^{86}Sr$ ratios for selected Jurassic to Cretaceous plutonic rocks of the Blue Mountains region*

[Sample localities listed in table 3.27. Sr and Rb contents in parts per million, determined by X-ray fluorescence; analyst, R.J. Fleck, U.S. Geological Survey. Measured ratios normalized to $^{86}Sr/^{87}Sr=0.1194$. Mean (n=76) of $^{87}Sr/^{86}Sr$ ratio obtained on standard (NBS SRM-987) is 0.71023±0.00003. Error values for ratios are standard deviations (2σ) and represent analytical uncertainty for split]

Sample	Rock type	Rb	Sr	Rb/Sr	$^{87}Sr/^{86}Sr$
V-11-79	Granodiorite --------	35	608	0.057	0.70335±.00002
V-75-79	Granodiorite --------	34	729	.046	.70381±.00003
V-23-79	Diorite ----------	4	608	.007	.70406±.00001
V-46-79	Quartz diorite ------	54	436	.121	.70422±.00004

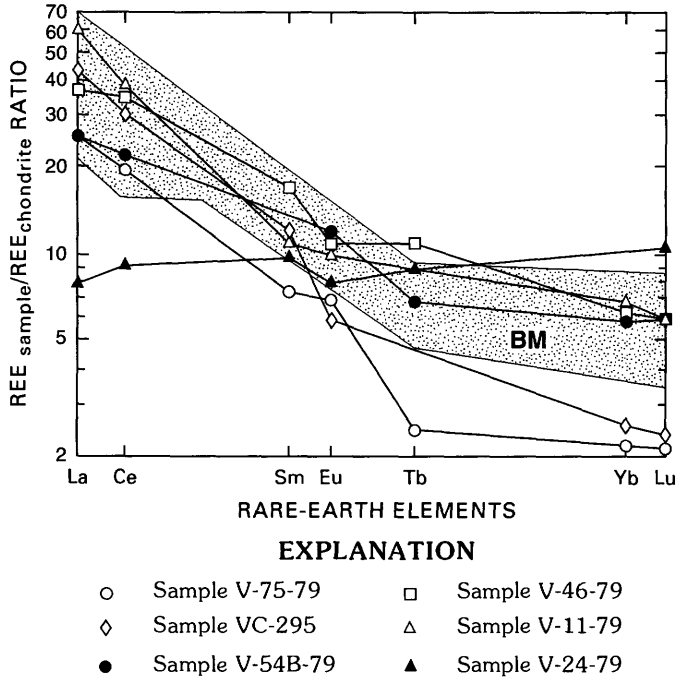

FIGURE 3.34.—Rare-earth element (REE) diagram showing calc-alkaline trends of Jurassic to Cretaceous plutonic rocks of Blue Mountains region. Sample with anomalous trend (number V-24-79) has cumulate texture and abundant hornblende. Patterned area (BM) is data field for Late Jurassic Bald Mountain batholith (fig. 3.6*B*), shown for comparison. Sample numbers correspond to those in tables 3.27 through 3.30; for normalizing values used, see figure 3.6.

Mountain plutons) that are very near the suture zone between the Blue Mountains island arc and the ancient North American craton. The average of 62 Sr-isotope ratios (table 3.31; Armstrong and others, 1977), calculated after eliminating the extremely high ratios associated with aplites and pegmatites, is 0.70392. The Bald Mountain batholith (13 samples) has the highest average of 0.70441, and the Deep Creek stock (10 samples) has the lowest average of 0.70350.

PETROGENESIS OF THE JURASSIC TO CRETACEOUS PLUTONIC ROCKS

The Jurassic to Cretaceous intrusive bodies in the Blue Mountains region are I-type plutons (Armstrong and others, 1977; White and Chappell, 1983). These plutons' characteristics and implied tectonic settings are important for understanding the last pre-Cenozoic igneous stage in the evolution of the Blue Mountains region.

The abrupt change in petrologic character of igneous rocks in the Blue Mountains island arc that occurred after about 180 Ma probably can be linked to one or more tectonic events. The strongly calc-alkaline affinity of the Jurassic to Cretaceous intrusive rocks points to such factors as different depths and temperatures of differentiation, fractionation of additional crystallizing phases (or different proportions of the same ones), and perhaps the addition of water, mixing of magmas, and assimilation of older crust (table 3.2). Source magmas probably were derived by partial melting of depleted mantle, followed by some crustal assimilation. The crust of the region must have been thicker than at any time prior to the Middle Jurassic.

TECTONIC IMPLICATIONS OF PETROLOGIC AND OTHER DATA

Igneous petrology is a helpful tool for interpreting the geologic evolution of tectonostratigraphic terranes (table 3.2). However, it is the integration of igneous petrology with geochronology (both isotopic and paleontologic data), paleomagnetism, stratigraphy, and structure that promotes better interpretive endeavors.

In this section I discuss the petrogenetic-tectonic association in each terrane and conclude with a plate tectonic model for the pre-Cenozoic evolution of the Blue Mountains region. The model is preliminary and no doubt will be greatly modified as better understanding of Cordilleran tectonics is achieved. For

example, the model does little to correlate terranes of the Blue Mountains island arc with those in Washington (Tabor and others, 1987), British Columbia (Monger and others, 1982), and southern Alaska (Silberling and others, 1984). Furthermore, the possible correlation of the Blue Mountain island arc terranes with those of the Klamath Mountains and the Sierra Nevada (Davis and others, 1978; Saleeby, 1983) are not integrated into this approach. Rather, I concentrate only on the Blue Mountains region.

TECTONIC SETTING OF IGNEOUS ROCKS OF THE BAKER TERRANE

The Baker terrane is structurally and petrologically the most diverse and the most complicated part of the Blue Mountains island arc. Previous studies (see Davis and others, 1978; Saleeby, 1983) adequately pointed out that the Baker terrane is probably a fragment of a much larger tectonic belt that can be connected to terranes in British Columbia and southern Alaska and possibly to terranes in the Klamath Mountains and the Sierra Nevada of the Western United States.

The petrology and ages of igneous rocks within the Baker terrane have the following tectonic implications:

(1) The Baker terrane was part of an extensive elongate belt within (or bordering) an intraoceanic island arc that was tectonically and magmatically active during the late Paleozoic and Triassic. After amalgamation with other terranes in the island arc, it was intruded by Late Jurassic to Early Cretaceous plutons.

(2) Many igneous rocks of the Baker terrane originated in an ocean basin (or basins) in conjunction with sea-floor spreading, rifting, and the growth of seamounts and oceanic islands and were subsequently accreted to the fore arc of the Blue Mountains island arc, possibly along the inner wall of a trench (Mullen, 1985; Bishop, chap. 5, this volume).

(3) Rocks with volcanic arc characteristics that occur in the Baker terrane probably formed along one or more magmatic axes of an island arc. They were subsequently faulted, sheared, and shuffled with rocks from the oceanic plate during tectonic processes that are known to occur in fore-arc regions of long-lasting and geologically complex island arcs (Bloomer, 1983; Fryer and others, 1985; Bloomer and Fisher, 1987). Active fore-arc volcanism in island arcs is extremely rare (Marlow and others, 1988); almost all isotopically dated igneous rocks from fore-arc regions are older than igneous rocks of an associated magmatic axis or volcanic front.

(4) The Canyon Mountain Complex formed within an island arc. A possible explanation for its present position in the Baker terrane is that it crystallized near the magmatic axis of the ancestral (Pennsylvanian to Permian) Blue Mountains island arc and subsequently was incorporated within serpentinite-matrix melange during Middle and Late Triassic activity along the inner trench wall (outer-arc high) of a subduction zone.

(5) Many of the exotic (not directly associated with arc volcanism) igneous rocks occur within serpentinite-matrix melange. Serpentinite-matrix melange is common in the Baker terrane, but the entire terrane is not melange. Rather, the terrane is composed of relatively coherent units that are chaotically mixed in structural zones, some of which are serpentinite-matrix melange. Serpentinite diapirs, like those reported from the Marianas Islands fore arc (Fryer and others, 1985), may have been important contributors to Baker terrane serpentinite-matrix melanges (Mullen, 1983). The regions of serpentinite-matrix melange probably mark fault zones (within the old fore-arc region of the Blue Mountains island arc) where highly pressurized and water-rich mantle and crust materials were diapirically emplaced. These diapirs could easily incorporate high-pressure amphibolites and blueschist-facies rocks from deep levels beneath the arc (Bishop, chap. 4, this volume).

(6) The Burnt River Schist is an enigmatic unit in the Baker terrane. Many of its somewhat rare volcanic rocks have arc affinities (Ashley, chap. 12, this volume; Bishop, chap. 5, this volume; P.R. Hooper, oral commun., 1987); the age of the Burnt River Schist is not well known, but its protolith probably formed mostly during the Permian or Triassic (Ashley, 1967; Ashley, chap. 12, this volume).

TECTONIC SETTING OF IGNEOUS ROCKS OF THE WALLOWA TERRANE

The Wallowa terrane was the site of an active volcanic front during the Early Permian as well as during the Middle and Late Triassic. There is a noteworthy gap in both plutonism and volcanism in the Early Triassic, although some rocks of that age are present in the Baker terrane. $^{40}Ar/^{39}Ar$ isotopic ages indicate that limited igneous activity occurred as late as about 215–210 Ma—evident in the (informal) Sparta complex, the Oxbow Complex, and in the intrusive body at the mouth of the Imnaha River; U-Pb isotopic age data confirmed a Late Triassic (215 Ma) age for the youngest pluton of the Sparta complex (Walker, 1986). The bulk of the U-Pb ages lie in the

265- to 245-Ma and 235- to 215-Ma intervals (Walker, 1986), which overlap the ages of the two major volcanic episodes (Vallier, 1977).

Petrologic and tectonic interpretations for the late Paleozoic and Triassic igneous rocks of the Wallowa terrane are as follows:

(1) The igneous rocks are mostly tholeiitic; rare plutonic rocks have transitional or calc-alkaline affinities. Plutonic bodies are I-type and exhibit no apparent evidence for mixing with continental crust. The igneous rocks most likely formed from fractionation of a parental tholeiitic basalt magma that had been derived from partial melting of the mantle wedge, with or without significant input from the subducting slab. Magma chambers were relatively shallow (probably less than 10 km), and magma temperatures were high. Plagioclase, olivine, orthopyroxene (not always present), augite, and magnetite were the major fractionating minerals. Mixing may have occurred, but most likely with magmas of similar composition. Water content was relatively low.

(2) The Permian and Triassic igneous rocks were erupted along the magmatic axis of an intraoceanic island arc. This setting implies a separation of 100 to 150 km, depending on the angle of the subducting slab, between the trench and volcanic front. Outcrops of high-pressure blueschist (Hotz and others, 1977; Bishop, chap. 4, this volume) now lie west of the Wallowa terrane and probably mark the location of the ancient trench. A sample from one of these outcrops, near Mitchell, Oreg. (about 50 km west-northwest of John Day, Oreg.; fig. 3.1), yielded an isotopic age of 225 Ma (Hotz and others, 1977). Considering the suspected clockwise rotation (Wilson and Cox, 1980), the trench was probably southwest of the Wallowa terrane in the Late Triassic.

(3) The Permian volcanic rocks are siliceous and dominated by pyroclastic debris. A notable characteristic of the Permian volcanic and plutonic rocks is high Na_2O content, most likely the result of metasomatism associated with the free interchange of seawater brine during crystallization. The abundance of high-field-strength elements suggests a tectonic environment different from those of modern island arcs. The high concentrations may reflect tectonic and (or) magmatic processes similar to those associated with the development of alkalic lavas in extensional (deeply rifted) settings. The Triassic lavas are more mafic than the Permian lavas and evolved from predominantly submarine flows and coarse breccias in early eruptions to subaerial and more tuffaceous deposits during later eruptions.

(4) The Wallowa terrane, as now recognized, may have shared its basement rocks with the Baker terrane in the early history (older than late Early Permian) of the Blue Mountains island arc. If this is true, then a change in implied plate tectonic relationships promoted volcano growth (formation of Wallowa terrane) in the Permian upon a preexisting terrane.

(5) The Jurassic hypabyssal intrusive rocks that cut strata of the Middle and Upper Jurassic Coon Hollow Formation are calc-alkaline. The petrologic change from mostly tholeiitic to calc-alkaline igneous rocks implies a change, some time after about 180 Ma, in factors such as relative lithosphere thickness, the tectonic setting with respect to a subduction zone, the depth to the subducting slab, and processes of differentiation.

(6) On the basis of what we understand about Cenozoic intraoceanic island arcs, a large part of the Wallowa terrane (in fact, probably much of the entire Blue Mountains island arc) is missing. Particularly noteworthy is the missing sea floor that must have existed between the arc and the North American continent. Several mechanisms can be called upon to account for the small size of the Wallowa terrane, the missing materials, and the present configuration of the terranes. These mechanisms include double subduction zones with attendant tectonic erosion, westward subduction and tectonic erosion during part of the arc's evolution, tectonic overriding of the Wallowa terrane by North America, extensive overthrusting during amalgamation of terranes within the Blue Mountains island arc and during its accretion to North America, and northward translation of large blocks into Washington, British Columbia, and southern Alaska (Jones and others, 1977; Saleeby, 1983; Wernicke and Klepacki, 1988).

TECTONIC SETTING OF IGNEOUS ROCKS OF THE OLDS FERRY TERRANE

Most of the igneous rocks of the Olds Ferry terrane are different from those of the Wallowa terrane in age and chemistry. From the available data, it appears that the Olds Ferry magmatic front became active at about the same time that igneous activity in the Wallowa terrane quieted down. The following paragraphs present major petrologic and tectonic interpretations of the igneous rocks of the Olds Ferry terrane.

(1) The igneous rocks are tholeiitic. They are more similar lithologically to Tongan island-arc tholeiites than to igneous rocks from the Wallowa terrane. The igneous rocks most likely formed in an intraoceanic island arc. The tholeiitic affinity implies a mantle wedge source, shallow and hot magma chambers, small amounts of magma mixing and crustal assimilation,

and fractionation predominantly by crystallization of plagioclase, olivine, orthopyroxene (may or may not be present), augite, and magnetite (table 3.2).

(2) A major difference between Olds Ferry terrane and Wallowa terrane volcanic rock chemistries is the greater abundance of most incompatible elements (particularly K, Rb, Ba, and Sr) in the Olds Ferry terrane rocks. This greater abundance of the incompatible elements in the Olds Ferry terrane might be related to a greater distance from the subduction zone (Gill, 1981) and hence, for example, a shallower dip on the subducting slab. A possible explanation for a change in subduction-zone geometry would be a change in plate-convergence direction and velocity with a resultant decrease in subduction angle and the eventual formation of a new magmatic axis at a greater distance from the trench. Changes in differentiation processes, however, might also account for the higher concentrations of the incompatible elements.

(3) A large part of the Olds Ferry terrane, like the other terranes of the Blue Mountains island arc, is either missing or covered by Tertiary rocks. A 60-degree counterclockwise rotation of the Olds Ferry terrane, to compensate for the clockwise rotation suspected by Wilson and Cox (1980) to have taken place since Early Cretaceous time, would orient the terrane nearly north-south, parallel and very close to the probable cratonal boundary. This position would suggest that during accretion much of the terrane may have been overridden by the craton. I assume, in this reconstruction, that the terrane was not rotated prior to the Early Cretaceous.

(4) The Olds Ferry terrane probably was built on rocks lithologically similar to those of the Baker terrane. The lavas probably were erupted onto the older terrane after a Late Triassic (late Karnian to early Norian) change in convergence direction between the oceanic and the Blue Mountains island-arc plates. At that time, the Wallowa and Baker terranes became part of the Olds Ferry terrane fore-arc region. Mortimore (1986) concluded that the Olds Ferry terrane was part of an extensive, highly potassic volcanic arc that formed along the margin of the North American continent. I would modify his conclusion somewhat because lavas in the Olds Ferry terrane were erupted in an intraoceanic island-arc setting. It is likely that the Olds Ferry terrane was an offshore part of the extensive Late Triassic continental-margin volcanic arc of Mortimore (1986).

TECTONIC SETTING OF JURASSIC TO CRETACEOUS IGNEOUS ROCKS

The Jurassic dikes and sills intruding the Coon Hollow Formation are significant because they are calc-alkaline in character. Different from the older, mostly tholeiitic rocks, they are similar in chemistry to the Jurassic to Cretaceous plutonic bodies. There may have been a significant change in the plate tectonic setting of the Wallowa terrane (and probably all of the Blue Mountains island arc) after about 180 Ma.

The Jurassic to Cretaceous igneous rocks were emplaced after terranes of the Blue Mountains island arc had been amalgamated and, in part, after the arc had been accreted to North America. In fact, as pointed out by Snee and others (chap. 15, this volume), some of the intrusive bodies along the border zone between ancestral North America and the Blue Mountains island arc probably formed during the final stages of accretion.

The chemistry of these Jurassic to Cretaceous calc-alkaline intrusive bodies implies the following tectonic setting (table 3.2):

(1) The crust was thicker in the Jurassic than in the Permian and Triassic. The crust of the arc had a long period of time in which to thicken, from the Pennsylvanian (or earlier) to the Middle Jurassic, or as many as 140 to 150 m.y. To put this in perspective, changes in plate motions within the ancestral Pacific Ocean during that time interval may have been comparable to changes that the present-day ocean floors have undergone since the beginning of the Early Cretaceous. There were many opportunities for the crust to thicken, not only through magmatic activity, but also through sedimentation, tectonic stacking, and underplating. I speculate that the crustal thickness of Blue Mountains island arc in the Middle Jurassic was at least as great as in the modern Aleutian island arc, where it has been measured in places as more than 20 km.

(2) Initial strontium isotope ratios indicate that evolved continental crust was not assimilated, nor did it serve as a principal source for magmas (Armstrong and others, 1977).

(3) These calc-alkaline magmas crystallized at relatively high pressures and contained more water than is typical of tholeiitic magmas. Fractionation took place predominantly by crystallization of plagioclase, olivine, orthopyroxene (not always present), augite, and magnetite, with amphibole and garnet possibly playing minor roles. Magma mixing and assimilation of older arc crust may have been important processes.

(4) Calc-alkaline magmatism in an oceanic setting implies converging tectonic plates. Thermal conditions leading to calc-alkaline magmatism may be related to a difference in ages of the converging plates. The subducting slab may have been younger and therefore much warmer. Young crust being subducted

would cause a much higher heat flow and probably more melting above the subducting slab. Paralleling the tectonic setting of the present-day Pacific Ocean floor off northern California, Oregon, and Washington, a spreading ridge near the west coast of North America during the Late Jurassic and Early Cretaceous may have led to suitable conditions for forming large calc-alkaline plutons.

(5) The dip of the subducting slab may have had a significant influence on the locations of the Jurassic to Cretaceous plutons. A low-angle dip could have put the magmatic axis at a greater distance from the trench. Some outer-arc terranes, if they existed, may have been ripped away from the margin during the Early Cretaceous and transported northward by wrench faulting for a rendezvous with British Columbia and southern Alaska.

PLATE TECTONIC EVOLUTION OF BLUE MOUNTAINS ISLAND ARC

PALEOMAGNETIC AND FAUNAL EVIDENCE FOR LATITUDINAL MOVEMENT

Paleomagnetism is a powerful tool for determining paleolatitudes of so-called exotic or suspect terranes and their positions relative to the North American craton through time. Paleomagnetic data have been gathered for the Jurassic to Cretaceous plutons of the Blue Mountains region (Wilson and Cox, 1980), Middle and Upper Triassic lavas of the Wallowa and Olds Ferry terranes (Hillhouse and others, 1982), and Lower Permian strata of the Wallowa terrane (Harbert and others, 1988, 1995). Assuming that terranes of the Blue Mountains island arc are kindred, then these paleomagnetic data can be used to describe the movement of the island arc relative to its site of accretion to the North American craton. Reconstructing this movement is difficult because the North American craton also was moving during the Permian through Late Jurassic interval, particularly in the Late Jurassic as North America began separating from Europe.

Contrary to earlier speculations (for example, Vallier and Engebretson, 1984), it is now evident that parts of the Blue Mountains island arc have been in the northern latitudes since the Early Permian (Hillhouse and others, 1982; Harbert and others, 1988, 1995). Some of the blocks associated with melange and disrupted units in the Baker and Grindstone terranes, however, are probably parts of an accretionary wedge and may have been scraped off a downgoing oceanic plate (or plates) that had formed in southern latitudes. Unfortunately, paleomagnetic data cannot be used to determine paleolongitudes, so they shed no light on the arc's distance west of the North American craton; The Permian island arc may have formed very close to the North American craton or it may have formed in the northwestern parts of the ancestral Pacific Ocean.

Harbert and others (1988, 1995) concluded that Lower Permian strata (the Hunsaker Creek Formation) of the Wallowa terrane were deposited in the northern hemisphere at a paleolatitude of about 28° N. According to the apparent polar wander path of Irving and Irving (1982) and studies of the North American craton by Gordon and others (1984) and Symons (1990), the site of accretion of the Wallowa terrane to the North American craton (that is, the site now at 45° N., 116° W.) was at a paleolatitude of about 11° to 19° N. during the Permian. Thus, during Permian time, the island arc on which the Hunsaker Creek Formation sediments were deposited lay about 9° to 17° north of the site of accretion on the North American craton.

Hillhouse and others (1982) concluded that Middle and Late Triassic volcanic rocks from both the Wallowa and Olds Ferry terranes were at a paleolatitude of 20° N. or 20° S. in the Middle and Late Triassic. Because the work by Harbert and others (1995) shows that the Wallowa terrane was probably in the northern hemisphere during the Permian, it follows that the Triassic lavas probably erupted in the northern hemisphere as well. According to the apparent polar wander path of Irving and Irving (1982), the site of accretion was at a paleolatitude of about 15° to 20° N. in the Middle and Late Triassic (230-210 Ma). This paleolatitude implies that by Late Triassic time the Blue Mountains island arc was at about the same latitude relative to the North American craton as when the arc finally accreted to the continent in the Early Cretaceous. Thus the island arc moved south as much as 1,000 to 2,000 km between the Early Permian and the Late Triassic.

In the Late Triassic, both the site of eventual accretion to the North American craton and the Blue Mountains island arc itself were at about 20° N. latitude. In other words, the latitude of most of the Blue Mountains island arc relative to the site of accretion on the North American craton has not changed significantly since the Late Triassic; both the continent and the arc moved northward to their present positions. Furthermore, paleomagnetic measurements for the Jurassic to Cretaceous plutons in the Blue Mountains region (Wilson and Cox, 1980) indicate very little latitudinal movement, but do suggest clockwise rotation of up to 60° since crystallization. Apparently, both the Blue Mountains island arc and the site of

accretion to the North American craton had reached their present positions by the Late Jurassic. Faunal studies by Pessagno and Blome (1986) showed a northward progression of the Izee terrane in the Early and Middle Jurassic from a southerly Tethyan region to a more northerly boreal zone. By Bajocian time (approximately 180 Ma) a faunal link had been established between the Blue Mountains island arc (Wallowa terrane) and the North American craton (Stanley and Beauvais, 1990).

These data suggest southward transport of the island arc between the late Early Permian and Late Triassic (about 15° of latitude in 30 m.y., which is an average of roughly 50 km/m.y.) and northward transport of about the same distance in the Jurassic (the island arc now moving with North America, with most movement occurring in the Early and Middle Jurassic). Because North America also was moving northward during the Jurassic and because the North American site of accretion and the island arc were at about the same latitude by the Late Triassic, it is probable that the Blue Mountains island arc has not moved a significant distance latitudinally relative to the North American craton since the Late Triassic.

PLATE MOVEMENTS AND TERRANE TECTONISM

A comprehensive discussion of the Grindstone terrane has not been attempted here. Buddenhagen (1967), Miller (1987), Blome and Nestell (1991), and Ferns and Brooks (chap. 9, this volume) have presented and interpreted critical data pertinent to the original tectonic setting and evolution of the Grindstone terrane. At least in part its history is probably very similar to that of the Baker terrane. There are data, however, that tie the Grindstone terrane to the northern part of the Klamath Mountains (Miller, 1987); interpretations of the original tectonic setting of the terrane, its relations to both the Klamath and the Blue Mountains, and its particular dynamics should remain open until additional data are collected.

The Baker terrane is probably kindred to all other terranes in the Blue Mountains island arc; for instance, some of the Baker terrane formed in the fore-arc regions of the Wallowa and Olds Ferry terranes, and other parts (including pieces of an ancient arc terrane) probably underlie the Wallowa, Olds Ferry, and Izee terranes. It is not a so-called exotic terrane that formed elsewhere and then collided with the other terranes of the arc, although fragments of oceanic crust from the downgoing slab were caught up in the arc's subduction zone (or zones). To account for the diversity of rock types in the Baker terrane and the occurrence of the many distinct structural or melange zones (Evans, chap. 8, this volume; Ferns and Brooks, chap. 9, this volume; Bishop, chaps. 4 and 5, this volume), the relation between the Blue Mountains island arc and the Baker terrane must be considered in both time and space.

If a long interval of time is combined with the changing of tectonic and magmatic locations within an island arc, then the mixing of arc and nonarc (for example, oceanic-crust, including seamount and mid-ocean-ridge) igneous rocks should be expected. What is now the Baker terrane undoubtedly shifted position relative to other parts of the maturing island arc; furthermore, during its long and complex evolution, parts of the Baker terrane probably were tectonically eroded and either subducted or translated subparallel to the arc axis by strike-slip faulting, similar to the present translation of fore-arc materials in the western part of the Aleutian island arc Vallier and others, 1994). For example, what originally had been the magmatic axis and fore arc(?) of the Blue Mountains island arc in the late Paleozoic may have become mostly fore arc in the Middle and Late Triassic. Therefore, parts that were related to the late Paleozoic magmatic axis, such as the Canyon Mountain Complex, were reshuffled along—and incorporated within—the Middle and Late Triassic fore-arc region. Some of the oldest parts (for example, an ancient pre-Permian arc terrane) of what is now the Baker terrane could thereby become basement to the Wallowa and Olds Ferry terranes. Exotic fragments of ocean-floor rocks, probably from more southerly latitudes, that occur as knockers in serpentinite-matrix melange and as possible olistoliths within the Elkhorn Ridge Argillite probably were scraped off an ancient oceanic plate (or plates) during subduction. The high-pressure rocks would be brought to the surface from beneath the arc framework along major fractures, some of which were greased by serpentinite diapirs like those discovered in the Marianas fore-arc region (Fryer and others, 1985; Bishop, chap. 5, this volume).

A major change in plate-convergence vectors probably occurred between the last major igneous activity in the Late Permian (about 260 Ma) and the Middle Triassic (about 235 Ma). This is the time of suspected southward transport of the Blue Mountains island arc. Fragmentation and eastward transport of the Melanesian island arc (Kroenke, 1984) in the late Eocene to early Miocene interval (approximately 3,000 km in 20–25 m.y.) may be an analogous situation.

Differences in ages and petrologic characteristics of the Wallowa and Olds Ferry terranes suggest that another major change in plate vectors occurred in the late Karnian, when the magmatic axis switched from the Wallowa terrane to the Olds Ferry terrane. The

Upper Triassic Huntington Formation formed along a magmatic axis in the Olds Ferry terrane. Igneous quiescence in the Wallowa terrane and in parts of the Baker terrane led to subsidence, the growth of large carbonate banks on the subsiding platforms, and the formation of rift basins. These conditions accompanied the deposition of the Martin Bridge Limestone and the Hurwal Formation in the Wallowa terrane and probably some of the Upper Triassic limestone bodies in the Baker terrane.

Rocks lithologically similar to those in the Baker terrane (chert, serpentinite, limestone, tuffaceous argillite) are faulted into the Weatherby Formation, herein considered part of the Izee terrane (see section "Izee Terrane"), near Huntington, Oreg. (Brooks and others, 1976; Brooks, 1979a); such rocks also crop out on strike with the Olds Ferry terrane near New Meadows, Idaho (Bonnichsen, 1987). Their presence suggests that parts of both the Izee and the Olds Ferry terranes are underlain by rocks of the Baker terrane or a similar (for example, an ancient arc) terrane. In addition, a Middle Triassic (235 Ma; Walker, 1986) intrusive body beneath (or intruding?) strata of the Huntington Formation suggests either that an older arc terrane existed prior to deposition of Upper Triassic strata in the Olds Ferry terrane or that the Huntington Formation includes rocks as old as 235 Ma. I prefer the former explanation because of field relations. If the Middle Triassic intrusive body is part of the Baker terrane or a lithologically similar ancient arc terrane, as I suspect, then it follows that the Olds Ferry terrane represents a Late Triassic (late Karnian and early Norian) and Early Jurassic(?) magmatic axis that grew on the Baker (or similar) terrane. A change in converging-plate vectors in the Late Triassic can explain the shift in magmatic axis from the Wallowa terrane to the Olds Ferry terrane. Such a change may have been analogous to the change in arc polarity proposed by Kroenke (1984) for the Solomon Islands during the Miocene.

An intra-arc (fore arc to the Olds Ferry terrane) Late Triassic to Late Jurassic basin evolved between the Olds Ferry and the (composite) Baker and Wallowa terranes and formed what is now the Izee terrane. Strata of the Izee terrane were deposited in that intra-arc basin and thus were deposited on parts of the Baker and Olds Ferry terranes. Late Cenozoic elongate basins in modern arcs, probably analogous to the basin that formed the Izee terrane, occur in the Solomon Islands and Vanuatu (Kroenke, 1984), where subduction polarity changes in the Miocene caused profound extension of the older arc frameworks and the formation of intra-arc basins. A Late Triassic (late Karnian) change in plate-convergence vectors between the ancestral oceanic plate (or plates) and the Blue Mountains island arc, proposed above, could have led to the formation of an intra-arc basin into which sediments poured from uplifted parts of the fore-arc region (parts of the Baker and Wallowa terranes) and the new magmatic axis (Olds Ferry terrane). The creation of such a basin would account for the formation of the Izee terrane within the Blue Mountains island arc. Upper Triassic to Upper Jurassic sediments deposited in the Wallowa terrane are correlative with those in the Izee terrane; this relation indicates that the Wallowa terrane did not merely subside, but experienced block faulting, subaerial erosion of the uplifted blocks, and marine transgression during block subsidence.

A new subduction zone (convergence between oceanic plate and combined Blue Mountains island arc and North American craton) apparently was initiated by 160 to 150 Ma. The continuity of Jurassic to Cretaceous plutonic bodies that have the same approximate age range and chemistry from California through Vancouver Island and into Alaska indicates that a volcanic arc was built along the newly formed continental margin. Considering the high amount of melting that must have occurred to form the plutonic bodies, the rarity of equivalent volcanic rocks is puzzling. Either the volcanic rocks were completely eroded or the magmas simply did not reach the surface to form volcanoes. Jurassic to Cretaceous plutonic bodies in the Blue Mountains cut across terrane boundaries and across major thrust faults, indicating that a significant deformational phase occurred in the time interval between deposition of the youngest Jurassic sediments (Callovian in the Izee terrane and Oxfordian in the Wallowa terrane, or about 165 to 155 Ma) and the crystallization of these large plutonic bodies (most are 145 Ma and younger according to N.W. Walker, written commun., 1989).

SEVEN-STAGE MODEL FOR PLATE TECTONIC EVOLUTION OF BLUE MOUNTAINS ISLAND ARC

A speculative plate tectonic model for the evolution of the Blue Mountains island arc from the late Paleozoic to the Late Cretaceous is shown in figure 3.35. Major assumptions are that (1) the Blue Mountains island arc has always been one complex island arc, (2) all terranes of the Blue Mountains island arc are kindred, (3) processes occurring in island arcs were the same in the late Paleozoic and Mesozoic as they are at present, and (4) the petrology of igneous rocks can be combined with other geologic data to interpret the evolution of a complex island arc. The proposed seven stages of arc evolution are as follows:

Stage 1, late Paleozoic and Early Permian, about 370(?) to 270 Ma (fig: 3.35A).—A complex island arc began to form in the pre-Early Permian. A magmatic axis of some kind had formed by the Pennsylvanian (about 310 Ma). The oldest parts (an ancient arc terrane) of what are now the Baker terrane and possibly the lower crustal parts of the Wallowa terrane may have formed even earlier. Many of these ancient rocks presumably have been covered, subducted, and (or) ripped away and transported elsewhere. The configuration of this postulated ancient arc, including its polarity, paleolatitude, and paleolongitude, are unknown.

Stage 2, Early Permian, about 270 to 260 Ma (fig. 3.35B).—The Early Permian interval is marked by extensive igneous activity and volcano growth. Siliceous arc volcanoes grew on part of the ancient arc terrane. This Permian arc (at least the Wallowa terrane) was in the northern hemisphere at about 28° N. latitude on the basis of paleomagnetic data (Harbert and others, 1988, 1995). The accretion site on the North American craton was at about 11° to 19° N. latitude on the basis of the apparent polar wander path of Irving and Irving (1982). The direction of plate convergence (arc polarity) is unknown. Figure 3.35*B* shows an ancient oceanic plate being subducted northwestward under the arc. Northwestward subduction (sea floor moving southeast to northwest, from equatorial to subpolar site) could account, in the Baker terrane, for the presence of Tethyan (warm-water) fusulinids in carbonate rocks that presumably had been scraped off the ancient oceanic plate during subduction to become part of an accretionary prism. Warm-water (subtropical) Permian fauna have not been reported from the Wallowa terrane; their absence tentatively supports the more northerly paleolatitude (G.D. Stanley, Jr., oral commun., 1990). The arc's paleolongitude and geographic relation to other terranes and continents are unknown.

Stage 3, Late Permian and Early Triassic, 260 to 235 Ma (fig. 3.35C).—Igneous activity of the arc quieted down during this time interval but did not stop altogether. The arc moved southward toward the latitude of the site of eventual accretion to the North American craton. During the proposed extensive transport, there probably were abundant opportunities for the fragmentation of the arc and the formation of terranes, in addition to the Baker and Wallowa terranes, that would ultimately end up along different parts of North America (and possibly eastern Siberia). In fact, the Blue Mountains island arc during this time interval may have been only a small part of an extensive offshore microcontinent. The ancient arc terrane (in stages 1 and 2 above) was changing into what is now the Baker terrane through the reworking of its rocks by tectonic and igneous processes. The eastward movement of the Melanesian and younger arcs away from Australia (Kroenke, 1984) since the early Eocene may be a good model to explain how the Blue Mountains island arc moved southward over the Pacific Ocean floor during the Late Permian and Early Triassic. Extensive strike-slip faulting, or movement along transform faults, would be the simplest method of transporting the arc, but no direct evidence for such movement has been found in the Blue Mountains rocks. In any scenario, the convergence of the ancient oceanic plate (or plates) with the Blue Mountains island arc probably was in a southeast-to-northwest direction.

Stage 4, late Middle and early Late Triassic, 235 to 225 Ma (fig. 3.35D).—The late Middle and early Late Triassic time interval (235–225 Ma) was one of voluminous magmatic activity in the Wallowa terrane and of minor, probably related, activity in what is now the Baker terrane. This magmatism may have been preceded by a change in converging-plate vectors. There must have been a well-developed subduction zone. The

FIGURE 3.35—Speculative model to explain geologic evolution of Blue Mountains island arc in seven stages, from late Paleozoic to mid-Cretaceous, based mainly on petrologic and paleomagnetic interpretations. Abbreviations are AA, ancient arc terrane (undivided); AOP, ancient oceanic plate; BA, Baker terrane (includes Grindstone terrane); IZ, Izee terrane; NA, North American craton; OF, Olds Ferry terrane; OT, other terranes; PP, Pacific (or Farallon) plate; and WA, Wallowa terrane. Schematic cross section (left side) and plan view (right side) are shown for each of seven evolutionary stages (*A–G*). In section and plan view, faults are dashed where approximately located, queried where speculative; single-barbed arrow indicates relative movement along fault or plate boundary. In section, sedimentary rocks are shown by conventional symbols and intrusive rocks by randomly oriented dashes. In plan view, paleonorth is up and double-barbed arrow indicates relative plate movement; at convergent-plate boundary, teeth are on upper plate; *, approximate site of future accretion of Wallowa terrane to North American craton. *A*, Stage 1, Late Devonian(?) to Early Permian (370?–270 Ma): Evolution of ancient arc terrane; spatial relationships are speculative; presence of landmass on left of plan view is suspected, but relative positions of arc, suspected landmass, and North American craton are unknown and therefore queried; note that the arc can migrate over the oceanic plate. Major topographic and structural features of an island arc are shown in cross-section view. *B*, Stage 2, Early Permian (270–260 Ma): Formation of siliceous volcanoes (Wallowa terrane) on ancient-arc framework; siliceous volcanic rocks erupt at approximately 30° N. latitude; fore-arc parts of ancient arc terrane become Baker terrane; question mark in plan view indicates that distance between arc and North America is unknown. *C*, Stage 3, Late Permian and Early Triassic (260–235 Ma): Relative igneous quiescence; southward transport of Blue Mountains island arc about 2,000 km relative to North American craton; what remains of ancient arc terrane has been incorporated into Baker terrane. Arc shown close to North America, but its position in ancestral Pacific is unknown; it could have been in western or eastern part.

A Late Devonian(?) to Early Permian (370?-270 Ma)

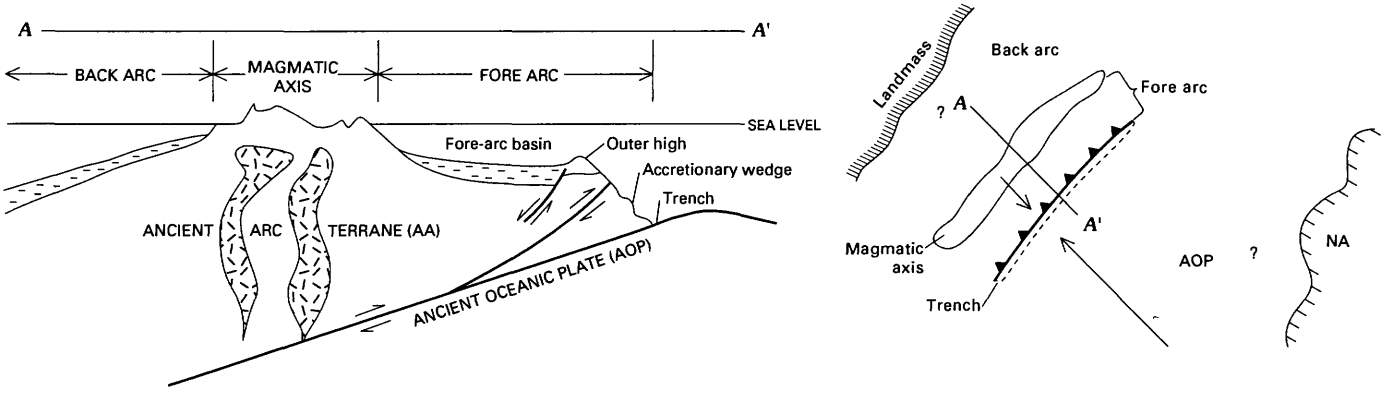

B Early Permian (270-260 Ma)

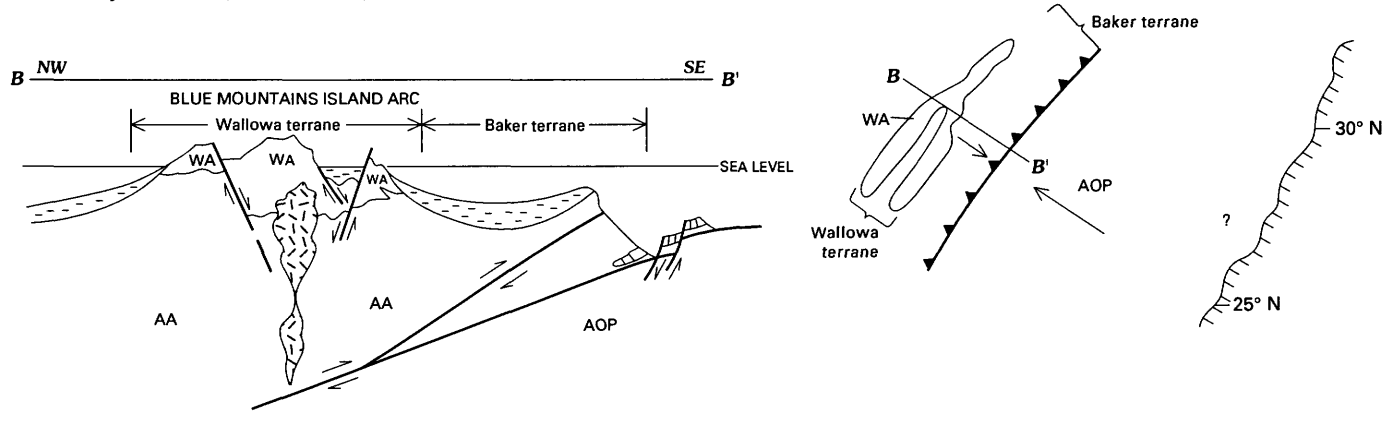

C Late Permian and Early Triassic (260-235 Ma)

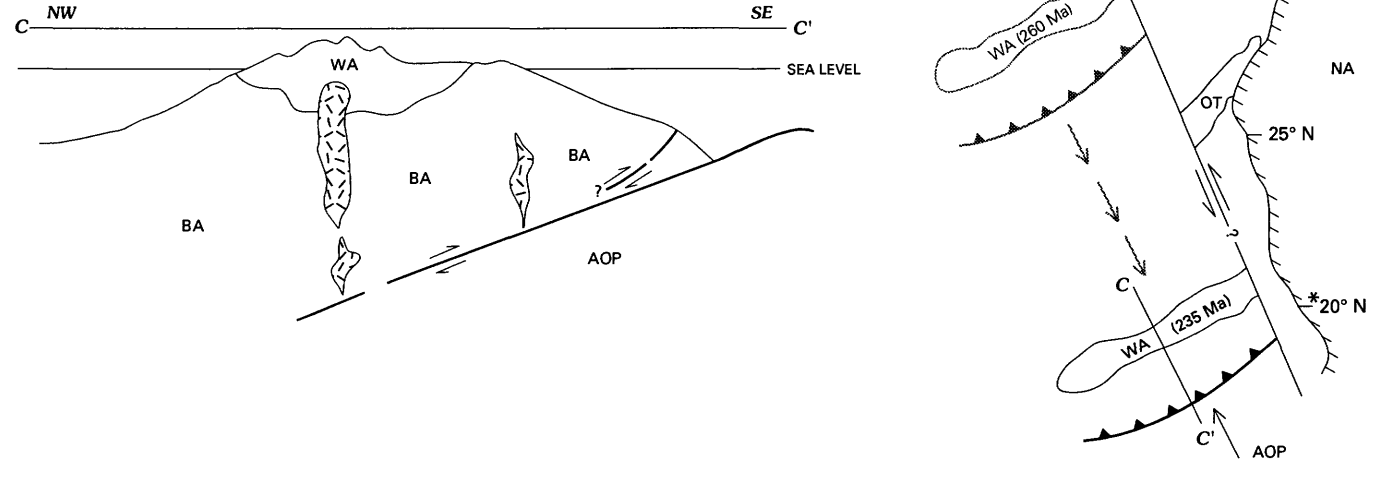

Figure continued on next page.

presence of blueschist in the western segments of the Baker terrane (Hotz and others, 1977; Bishop, chap. 4, this volume), and the 60° clockwise rotation of the arc since the Early Cretaceous suggest that the arc polarity was associated with south-to-north subduction (assuming that no rotation took place between the Late Triassic and the Early Cretaceous). The Blue Mountains island arc was at about 20° N. latitude, approximately directly offshore from its ultimate site of accretion. Sinistral movement along major shear zones in the Cougar Creek and Oxbow Complexes of the Wallowa terrane (Avé Lallemant, chap. 7, this volume) suggests extensive internal deformation of the arc and may account for some of its lateral movement. Formation of a fore-arc basin and irregular basins along the inner wall of the trench, olistostromal sliding of large blocks, intrusion of serpentinite diapirs, and accretion of materials from the oceanic plate probably all oc-

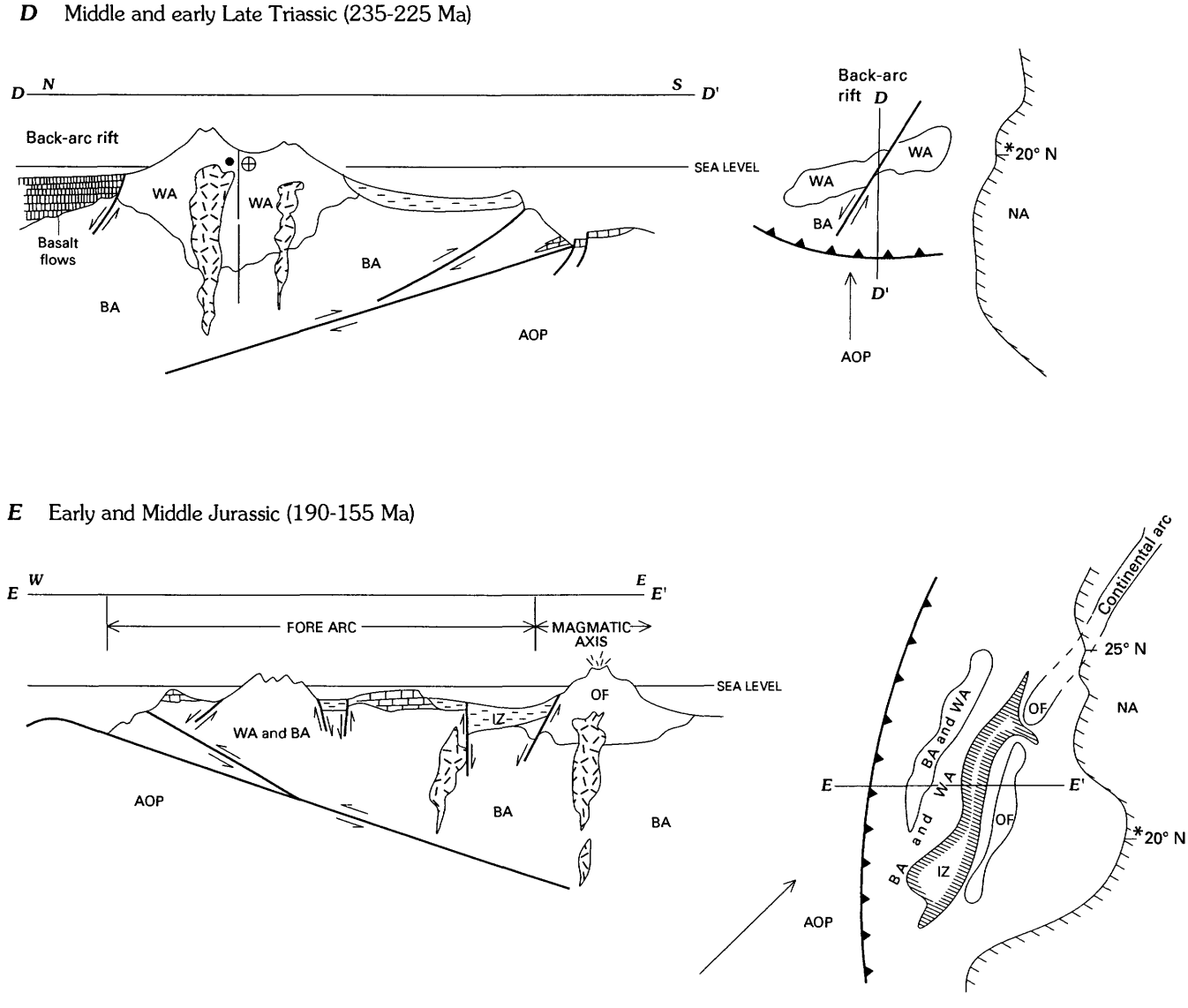

FIGURE 3.35—Continued. *D*, Stage 4, Middle and early Late Triassic (235–225 Ma): Volcanism in Wallowa terrane; well-developed subduction zone; Triassic volcanic rocks cool at approximately 20° N. latitude, about same latitude as accretion site on North American craton; left-lateral movement on northeast-striking faults (on section, movement toward reader shown by solid circle, away from reader, by circled cross); proposed oceanic plateau or rifted back-arc basin may account for extensive outpourings of Middle Triassic basalt now exposed in the Wrangellia and related terranes. *E*, Stage 5, Late Triassic and Early Jurassic (225–190 Ma): Shift of volcanic activity to Olds Ferry terrane; inception of intra-arc basin (Izee terrane); growth of carbonate banks (Martin Bridge Limestone and correlative strata) on volcanically quiescent parts of Wallowa and Baker terranes that had become fore arc to Olds Ferry volcanic arc. At this time, Blue Mountains island arc and North American continent began moving northward together.

curred in the Wallowa terrane fore-arc region, exemplified by parts of what are now called the Grindstone and Baker terranes. The Canyon Mountain Complex may have been exhumed at this time along the outer high (inner trench wall) of the Wallowa terrane's fore-arc region. Extensive outpourings of Middle Triassic basalt, now exposed as parts of the Wrangellia terrane on Vancouver and Queen Charlotte Islands (Canada) and southeast Alaska (Jones and others, 1977), probably formed near the Wallowa terrane, possibly in a back-arc environment (Vallier, 1986) or as an oceanic plateau (P.R. Hooper, oral commun., 1987).

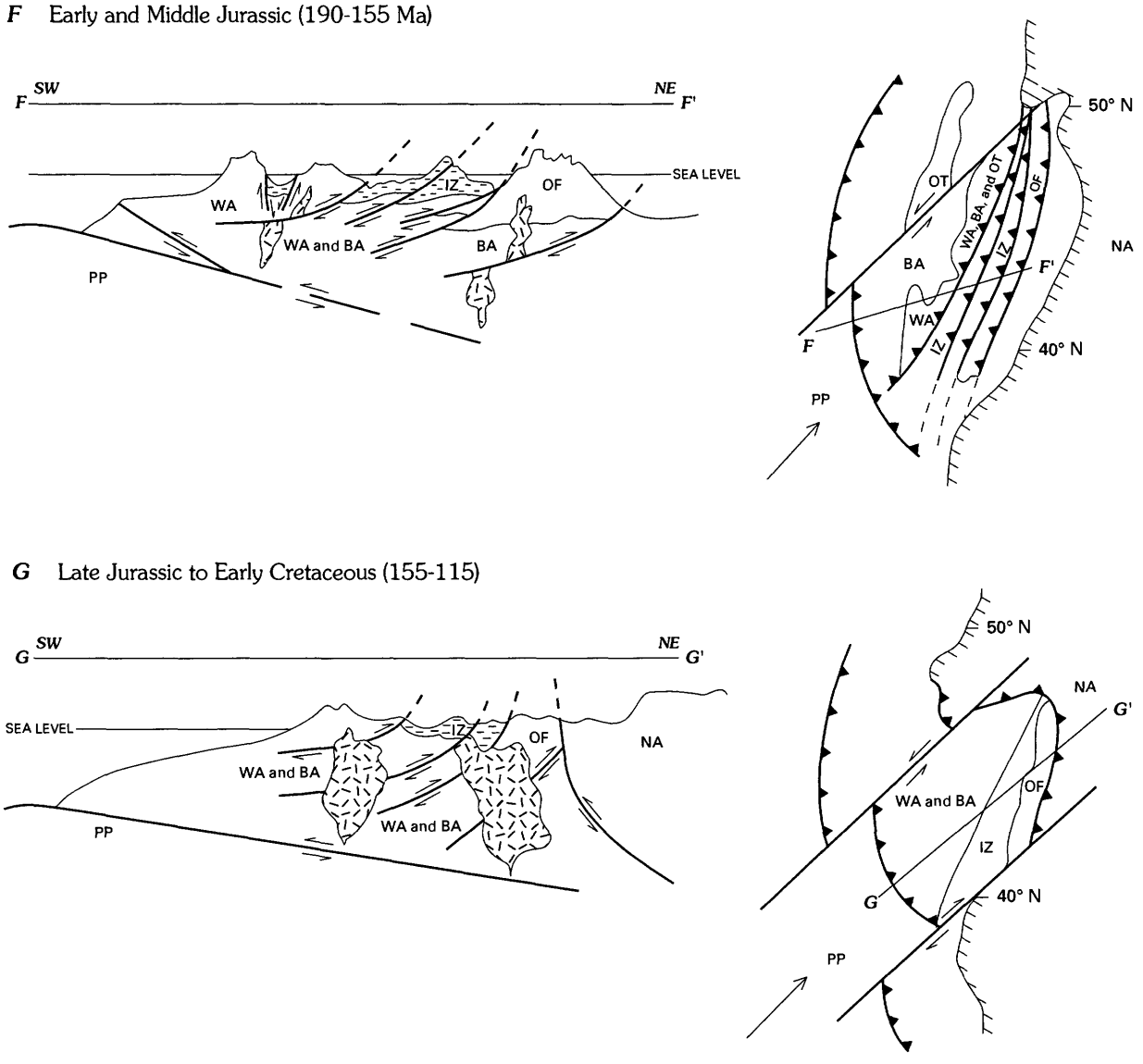

FIGURE 3.35—Continued. *F*, Stage 6, Early and Middle Jurassic (190–155 Ma): Voluminous sedimentation in Izee terrane as intra-arc basin subsided; figure shows configuration of Blue Mountains island arc during final stages of northward movement (155 Ma) when arc had already reached site of accretion; thrust-faulting in latter parts of interval telescoped terranes. Strike-slip faulting active during accretion process; fragments of the island arc presumably split off at this stage; Pacific (or Farallon) plate probable oceanic plate; some igneous activity, particularly in Wallowa and Olds Ferry terranes. *G*, Stage 7, Late Jurassic to Early Cretaceous (155–115 Ma): Intrusion of large calc-alkaline plutonic bodies throughout the island arc; collision of Blue Mountains island arc with North America; thrust faults within Blue Mountains island arc not shown in plan view because they were not active during this interval; strike-slip faults modified from Wernicke and Klepacki (1988).

Stage 5, Late Triassic and Early Jurassic, 225-190 Ma (fig. 3.35E).—The Olds Ferry terrane evolved mostly during the 225- to 190-Ma interval. It probably developed on old island-arc crust composed of fragments of the Baker terrane. A plate-motion change could account for the growth of the Olds Ferry terrane as a magmatic axis; this plate-motion change and consequent growth of the Olds Ferry terrane would make the Wallowa and Baker terranes parts of the Olds Ferry fore-arc region. An arc-reversal model like that proposed for the Solomon Islands arc (Kroenke, 1984, p. 47-61) could explain these relationships, although even a small change in converging-plate vectors could effect a similar result. Thus, igneous activity decreased in the Wallowa (and possibly Baker) terrane while it began building the Olds Ferry terrane. Carbonate banks (Martin Bridge Limestone and correlative strata) grew on slowly subsiding parts of the new fore-arc region, and horsts and grabens formed islands and basins, which filled with sediments such as those in the Hurwal Formation. A large intra-arc basin (between and on the Olds Ferry and the composite Baker and Wallowa terranes) formed and ultimately became the Izee terrane (herein considered to include the Weatherby Formation and Squaw Creek Schist; see section "Izee Terrane"). The Olds Ferry terrane probably was an oceanic part of the extensive volcanic arc that bordered North America in the Late Triassic and the Early Jurassic (Mortimore, 1986), some of which developed as a continental volcanic arc. Northward movement of the Blue Mountains island arc along with the North American craton (Irving and Irving, 1982) probably began by at least the latest Triassic or earliest Jurassic. It is possible that as early as 225 Ma, the North American craton and the Blue Mountains island arc were parts of the same tectonic (North American) plate.

Stage 6, latest Early to late Middle Jurassic, 190 to 155 Ma (fig. 3.35F).—Prolific sedimentation occurred during the 190- to 155-Ma interval in the intra-arc basin that ultimately became the Izee terrane. The Blue Mountains island arc continued to migrate northward with North America. Proximity to North America by about 180 Ma is indicated by an early Bajocian fauna in the Wallowa terrane that has North American affinities (Stanley and Beauvais, 1990). Although igneous activity was minor in all terranes during this time interval, a change from tholeiitic to calc-alkaline characteristics of igneous rocks is shown by the presence of small calc-alkaline intrusive rocks within the Coon Hollow Formation of the Wallowa terrane. Extensive thrust faulting occurred in the latter part of this time interval, probably along an oblique transpressive margin. A bulge in the North American craton north of the site of accretion, as shown in figure 3.35*F*, is suspected because of the present-day spatial relations. Right lateral strike-slip faulting is inferred to have begun the accretion process (Wernicke and Klepacki, 1988). Fragments of the complex island arc (and adjacent parts of the Wrangellia terrane) were possibly broken away to be subsequently transported northward along the cratonic margin. During the latter parts of this time interval, I suspect that either the Pacific plate or Farallon plate was the subducted oceanic plate.

Stage 7, Late Jurassic and Early Cretaceous, 155 to 115 Ma (fig. 3.35G).—Large calc-alkaline plutons were emplaced during the 155- to 115-Ma interval, beginning particularly around 145 Ma (N.W. Walker, written commun., 1989). By 155 Ma, the crust apparently had thickened; the onset of plutonism may be related to a major change in plate motions. The Blue Mountains island arc and the site of accretion on the North American craton probably reached their present approximate latitude by the earliest Cretaceous. Although most accretion of the island arc to the North American craton occurred during the latter part of this time interval, especially in the 120- to 115-Ma interval (Lund and Snee, 1988), the accretion process itself probably began somewhat earlier (fig. 3.35*F*). Accretionary events such as those outlined by Wernicke and Klepacki (1988), which were dominated by strike-slip faults, may have occurred and would account for the absence of rocks that must have existed between the North American craton and the Blue Mountains island arc. During accretion, the already telescoped and amalgamated terranes were probably overridden by the North American craton from the east, and extensive wrench faulting may have occurred along the suture zone between the arc and the North American craton. Following accretion, the Blue Mountains island arc was rotated clockwise (Wilson and Cox, 1980), covered by Tertiary volcanic rocks, and, since the late Miocene, differentially uplifted and eroded.

REFERENCES CITED

Aliberti, E.A., 1988, A structural, petrographic, and isotopic study of the Rapid River area and selected mafic complexes in the northwestern United States—Implications for the evolution of an abrupt island-arc-continent boundary: Cambridge, Mass., Harvard University, Ph.D. dissertation, 194 p.

Almy, R.B., III, 1977, Petrology and major element chemistry of albite granite near Sparta, Oregon: Bellingham, Western Washington State College, M.S. thesis, 100 p.

Anderson, A.L., 1930, The geology and mineral resources of the region about Orofino, Idaho: Idaho Bureau of Mines and Geology Pamphlet 34, 63 p.

Armstrong, R.L., Taubeneck, W.H., and Hales, P.O., 1977, Rb-Sr and K-Ar geochronometry of Mesozoic granitic rocks and their Sr isotopic composition, Oregon, Washington, and Idaho: Geological Society of America Bulletin, v. 88, p. 397-411.

Ashley, R.P., 1967, Metamorphic petrology and structure of the Burnt River Schist area, northeastern Oregon: Stanford, Calif., Stanford University, Ph.D. dissertation, 193 p.

Avé Lallemant, H.G., 1976, Structure of the Canyon Mountain (Oregon) ophiolite complex and its implication for seafloor spreading: Geological Society of America Special Paper 173, 49 p.

Avé Lallemant, H.G., Phelps, D.W., and Sutter, J.F., 1980, $^{40}Ar/^{39}Ar$ ages of some pre-Tertiary plutonic and metamorphic rocks of eastern Oregon and their tectonic relationships: Geology, v. 8, p. 371-374.

Avé Lallemant, H.G., Schmidt, W.J., and Kraft, J.L., 1985, Major Late-Triassic strike-slip displacement in the Seven Devils terrane, Oregon and Idaho—A result of left-oblique plate convergence?: Tectonophysics, v. 119, p. 299-328.

Baedecker, P.A., 1979, The INAA program of the U.S. Geological Survey (Reston, Virginia), *in* Carpenter, B.S., and others, eds., Computers in activation analysis and X-ray spectroscopy: Conference # 78042, U.S. Department of Energy, p. 373-385.

Baedecker, P.A., and McKown, D.M., 1987, Instrumental neutron activation analysis of geochemical samples, *in* Baedecker, P.A., ed., Methods for geochemical analysis: U.S. Geological Survey Bulletin 1770, p. H1-H14.

Balcer, D.E., 1980, $^{40}Ar/^{39}Ar$ ages and REE geochemistry of basement terranes in the Snake River canyon, northeast Oregon-western Idaho: Columbus, Ohio State University, M.S. thesis, 111 p.

Blome, C.D., Jones, D.L., Murchey, B.L., and Liniecki, Margaret, 1986, Geologic implications of radiolarian-bearing Paleozoic and Mesozoic rocks from the Blue Mountains province, eastern Oregon, *in* Vallier, T.L., and Brooks, H.C., eds., Geology of the Blue Mountains region of Oregon, Idaho, and Washington—Geologic implications of Paleozoic and Mesozoic paleontology and biostratigraphy, Blue Mountains province, Oregon and Idaho: U.S. Geological Survey Professional Paper 1435, p. 79-93.

Blome, C.D., and Nestell, M.K., 1991, Evolution of a Permo-Triassic sedimentary melange, Grindstone terrane, east-central Oregon: Geological Society of America Bulletin, v. 103, p. 1280-1296.

Bloomer, S.H., 1983, Structure and evolution of the inner slope of the Mariana Trench—Implications from geochemical studies: Journal of Geophysical Research, v. 88, p. 7411-7428.

Bloomer, S.H., and Fisher, R.L., 1987, Petrology and geochemistry of igneous rocks from the Tonga Trench—Implications for its structure: Journal of Geology, v. 95, p. 469-495.

Bonnichsen, Bill, 1987, Pre-Cenozoic geology of the West Mountain-Council Mountain-New Meadows area, west-central Idaho, *in* Vallier, T.L., and Brooks, H.C., eds., Geology of the Blue Mountains region of Oregon, Idaho, and Washington—The Idaho batholith and its border zone: U.S. Geological Survey Professional Paper 1436, p. 151-170.

Bostwick, D.A., and Koch, G.S., 1962, Permian and Triassic rocks of northeastern Oregon: Geological Society of America Bulletin, v. 73, p. 419-422.

Brooks, H.C., 1979a, Geologic map of the Huntington and part of the Olds Ferry quadrangles, Baker and Malheur Counties, Oregon: Oregon Department of Geology and Mineral Industries Geological Map Series GMS-13, scale 1:62,500.

———1979b, Plate tectonics and the geologic history of the Blue Mountains: Oregon Geology, v. 41, no. 5, p. 71-80.

Brooks, H.C., Ferns, M.L., and Avery, D.G., 1984, Geology and gold deposits map of the southwest quarter of the Bates quadrangle, Grant County, Oregon: Oregon Department of Geology and Mineral Industries Geological Map Series GMS-35, scale 1:24,000.

Brooks, H.C., Ferns, M.L., Coward, R.I., Paul, E.K., and Nunlist, M.A., 1982, Geology and gold deposits of the Bourne quadrangle, Baker and Grant Counties, Oregon: Oregon Department of Geology and Mineral Industries Geological Map Series GMS-19, scale 1:24,000.

Brooks, H.C., Ferns, M.L., and Mullen, E.D., 1982, Geology and gold deposits of the Granite quadrangle, Grant County, Oregon: Oregon Department of Geology and Mineral Industries Geological Map Series GMS-25, scale 1:24,000.

Brooks, H.C., Ferns, M.L., Wheeler, G.R., and Avery, D.G., 1983, Geology and gold deposits map of the northeast quarter of the Bates quadrangle, Baker and Grant Counties, Oregon: Oregon Department of Geology and Mineral Industries Geological Map Series GMS-29, scale 1:24,000.

Brooks, H.C., McIntyre, J.R., and Walker, G.W., 1976, Geology of the Oregon part of the Baker 1° by 2° quadrangle: Oregon Department of Geology and Mineral Industries Geological Map Series GMS-7, 29 p. of text, scale 1:250,000.

Brooks, H.C., and Vallier, T.L., 1978, Mesozoic rocks and tectonic evolution of eastern Oregon and western Idaho, *in* Howell, D.G., and McDougall, K.A., eds., Mesozoic paleogeography of the Western United States (Pacific Coast Paleogeography Symposium 2): Los Angeles, Society of Economic Paleontologists and Mineralogists, Pacific Section, p. 133-145.

Bruce, W.R., 1971, Geology, mineral deposits, and alteration of parts of the Cuddy Mountains district, western Idaho: Corvallis, Oregon State University, Ph.D. dissertation, 165 p.

Buddenhagen, H.J., 1967, Structure and orogenic history of the southwestern part of the John Day uplift: Ore Bin, v. 29, no. 7, p. 129-138.

Chen, S.-J., 1985, Structural geology of the Eureka complex in the Seven Devils terrane, eastern Oregon and western Idaho: Houston, Rice University, M.A. thesis, 94 p.

Coleman, R.G., 1977, Ophiolites—Ancient oceanic lithosphere?: New York, Springer-Verlag, 229 p.

Coleman, R.G., and Peterman, Z.E., 1975, Oceanic plagiogranites: Journal of Geophysical Research, v. 80, p. 1099-1108.

Coney, P.J., Jones, D.L., and Monger, J.W.H., 1980, Cordilleran suspect terranes: Nature, v. 288, p. 329-333.

Cook, E.F., 1954, Mining geology of the Seven Devils region: Idaho Bureau of Mines and Geology Pamphlet 97, 22 p.

Criss, R.E., and Fleck, R.J., 1987, Petrogenesis, geochronology, and hydrothermal systems of the northern Idaho batholith and adjacent areas based on $^{18}O/^{16}O$, D/H, $^{87}Sr/^{86}Sr$, K-Ar, and $^{40}Ar/^{39}Ar$ studies, *in* Vallier, T.L., and Brooks, H.C., eds., Geology of the Blue Mountains region of Oregon, Idaho, and Washington—The Idaho batholith and its border zone: U.S. Geological Survey Professional Paper 1436, p. 95-137.

Davis, G.A., Monger, J.W.H., and Burchfiel, B.C., 1978, Mesozoic construction of the Cordilleran "collage," central British Columbia to central California, *in* Howell, D.G., and McDougall, K.A., eds., Mesozoic paleogeography of the Western United States (Pacific Coast Paleogeography Symposium 2): Los Angeles, Society of Economic Paleontologists and Mineralogists, Pacific Section, p. 1-32.

Dickinson, W.R., 1979, Mesozoic fore-arc basin in central Oregon: Geology, v. 7, p. 166-170.

Dickinson, W.R., and Thayer, T.P, 1978, Paleogeographic and paleotectonic implications of Mesozoic stratigraphy and structure in the John Day inlier of central Oregon, *in* Howell, D.G., and McDougall, K.A., eds., Mesozoic paleogeography of the Western United States (Pacific Coast Paleogeography Symposium

2): Los Angeles, Society of Economic Paleontologists and Mineralogists, Pacific Section, p. 147-161.

Dungan, M.A., and Avé Lallemant, H.G., 1977, Formation of small dunite bodies by metasomatic transformation of harzburgite in the Canyon Mountain ophiolite, northeast Oregon, *in* Dick, H.J.B., ed., Magma genesis: Oregon Department of Geology and Mineral Industries Bulletin 96, p. 109-128.

Ewart, Anthony, Bryan, W.B., and Gill, J.B., 1973, Mineralogy and geochemistry of the younger volcanic islands of Tonga, S.W. Pacific: Journal of Petrology, v. 14, p. 429-465.

Ewart, Anthony, and Hawkesworth, C.J., 1987, The Pleistocene-Recent Tonga-Kermadec arc lavas—Interpretation of new isotopic and rare-earth data in terms of a depleted-mantle source model: Journal of Petrology, v. 28, p. 495-530.

Ferns, M.L., Brooks, H.C., and Avery, D.G., 1983, Geology and gold deposits map of the Greenhorn quadrangle, Baker and Grant Counties, Oregon: Oregon Department of Geology and Mineral Industries Geological Map Series GMS-28, map scale 1:24,000.

Ferns, M.L., Brooks, H.C., Avery, D.G., and Blome, C.D., 1987, Geology and mineral resources map of the Elkhorn Peak quadrangle, Baker County, Oregon: Oregon Department of Geology and Mineral Industries Geological Map Series GMS-41, scale 1:24,000.

Ferns, M.L., Brooks, H.C., and Ducette, J., 1982, Geology and mineral resources map of the Mt. Ireland quadrangle, Baker and Grant Counties, Oregon: Oregon Department of Geology and Mineral Industries Geological Map Series GMS-22, scale 1:24,000.

Fleck, R.J., and Criss, R.E., 1985, Strontium and oxygen isotopic variability in Mesozoic and Tertiary plutons of central Idaho: Contributions to Mineralogy and Petrology, v. 90, p. 291-308.

Follo, M.R., 1994, Sedimentology and stratigraphy of the Martin Bridge Limestone and Hurwal Formation (Upper Triassic to Lower Jurassic) from the Wallowa terrane, Oregon, *in* Vallier, T.L., and Brooks, H.C., eds., Geology of the Blue Mountains region of Oregon, Idaho, and Washington—Stratigraphy, physiography, and mineral resources: U.S. Geological Survey Professional Paper 1439, p. 1-27.

Frey, F.A., Bryan, W.B., and Thompson, G., 1974, Atlantic Ocean floor—Geochemistry and petrology of basalts from legs 2 and 3 of the Deep-Sea Drilling Project: Journal of Geophysical Research, v. 79, p. 5507-5527.

Fryer, Patricia, Ambos, E.L., and Hussong, D.M., 1985, Origin and emplacement of Mariana fore-arc seamounts: Geology, v. 13, p. 774-777.

Gerlach, D.C., 1980, Petrology and geochemistry of plagiogranite and related basic rocks of the Canyon Mountain ophiolite complex, Oregon: Houston, Rice University, M.S. thesis, 203 p.

Gerlach, D.C., Avé Lallemant, H.G., and Leeman, W.P., 1981, Petrology and geochemistry of plagiogranite in the Canyon Mountain ophiolite, Oregon: Contributions to Mineralogy and Petrology, v. 77, p. 88-92.

Gill, J.B., 1981, Orogenic andesites and plate tectonics: New York, Springer-Verlag, 390 p.

Gilluly, James, 1933, Replacement origin of the albite granite near Sparta, Oregon: U.S. Geological Survey Professional Paper 175-C, 16 p.

———1937, Geology and mineral resources of the Baker quadrangle, Oregon: U.S. Geological Survey Bulletin 879, 119 p.

Goldstrand, P.M., 1987, The Mesozoic stratigraphy, depositional environments, and tectonic evolution of the northern portion of the Wallowa terrane, northeastern Oregon and western Idaho: Bellingham, Western Washington State University, M.S. thesis, 200 p.

———1994, The Mesozoic geologic evolution of the northern Wallowa terrane, northeastern Oregon and western Idaho, *in* Vallier, T.L., and Brooks, H.C., eds., Geology of the Blue Mountains region of Oregon, Idaho, and Washington—Stratigraphy, physiography, and mineral resources: U.S. Geological Survey Professional Paper 1439, p. 29-53.

Golightly, D.W., Dorrzapf, A.F., Jr., Mays, R.E., Fries, T.L., and Conklin, N.M., 1987, Analysis of geologic materials by direct-current arc-emission spectrography and spectrometry, *in* Baedecker, P.A., ed., Methods for geochemical analysis: U.S. Geological Survey Bulletin 1770, p. A1-A13.

Gordon, R.G., Cox, Alan, and O'Hare, Scott, 1984, Paleomagnetic Euler poles and the apparent polar wander and absolute motion of North America since the Carboniferous: Tectonics, v. 3, p. 499-537.

Grant, P.R., 1980, Limestone units within the Triassic Wild Sheep Creek Formation, Snake River canyon: Pullman, Washington State University, M.S. thesis, 103 p.

Grove, T.L., and Baker, M.B., 1983, Effects of melt density on magma mixing in calc-alkaline series lavas: Nature, v. 305, p. 416-418.

———1984, Phase-equilibrium controls on the tholeiitic versus calc-alkaline differentiation trends: Journal of Geophysical Research, v. 89, p. 3253-3274.

Grove, T.L., and Kinzler, R.J., 1986, Petrogenesis of andesites: Annual Review of Earth and Planetary Sciences, v. 14, p. 417-454.

Hamilton, Warren, 1963, Metamorphism in the Riggins region, western Idaho: U.S. Geological Survey Professional Paper 436, 95 p.

Harbert, William, Hillhouse, John, and Vallier, Tracy, 1988, Leonardian paleolatitude of Wrangellia [abs.]: Eos (American Geophysical Union Transactions), v. 69, p. 1169.

———1995, Paleomagnetism of the Permian Wallowa terrane, Oregon—Implications for terrane migration and orogeny: Journal of Geophysical Research, v. 100, p. 12,573-12,588.

Hawkins, J.W., 1988, Silica-rich rocks of back-arc basins—A clue to the origin of the plagiogranite series of ophiolites [abs.]: Eos (American Geophysical Union Transactions), v. 69, p. 1471-1472.

Hellman, P.L., and Henderson, P., 1977, Are the rare-earth elements mobile during spilitization?: Nature, v. 267, p.38.

Hendricksen, T.A., 1974, Geology and mineral deposits of the Mineral-Iron Mountain district, Washington County, Idaho, and of a metallized zone in western Idaho and eastern Oregon: Corvallis, Oregon State University, Ph.D. dissertation, 205 p.

Hendricksen, T.A., Skurla, S.J., and Field, C.W., 1972, K-Ar dates for plutons from the Iron Mountain and Sturgill Peak areas of western Idaho: Isochron/West, no. 5, p. 13-16.

Hermann, A.G., Potts, M.J., and Knake, D., 1974, Geochemistry of the rare-earth elements in spilites from oceanic and continental crust: Contributions to Mineralogy and Petrology, v. 44, p. 1-16.

Hillhouse, J.W., Grommé, C.S., and Vallier, T.L., 1982, Paleomagnetism and Mesozoic tectonics of the Seven Devils volcanic arc in northeastern Oregon: Journal of Geophysical Research, v. 87, no. B5, p. 3777-3794.

Himmelberg, G.R., and Loney, R.A., 1980, Petrology of ultramafic and gabbroic rocks of the Canyon Mountain ophiolite, Oregon: American Journal of Science, v. 280-A, pt. 1, p. 232-268.

Hotz, P.E., Lanphere, M.A., and Swanson, D.A., 1977, Triassic blueschist from northern California and north-central Oregon: Geology, v. 5, p. 659-663.

Howell, D.G., Jones, D.L., and Schermer, E.R., 1985, Tectonostratigraphic terranes of the circum-Pacific region, *in* Howell, D.G., ed., Tectonostratigraphic terranes of the circum-Pacific region: Houston, Circum-Pacific Council for Energy and Mineral Resources Earth Science Series, v. 1, p. 3-30.

Humphris, S.E., Morrison, M.A., and Thompson, R.N., 1978, Influence of rock crystallization history upon subsequent lanthanide mobility during hydrothermal alteration of basalts: Chemical Geology, v. 23, p. 125-137.

Hunt, P.T., 1985, The metamorphic petrology and structural geology of the serpentinite-matrix melange in the Greenhorn Mountains, northeastern Oregon: Eugene, University of Oregon, M.S. thesis, 127 p.

Huntting, M.T., 1942, Geology of the middle Tucannon area: Pullman, State College of Washington, M.S. thesis, 35 p.

Hyndman, D.W., 1983, The Idaho batholith and associated plutons, Idaho and Montana: Geological Society of America Memoir 159, p. 213-240.

Imlay, R.W., 1986, Jurassic ammonites and biostratigraphy of eastern Oregon and western Idaho, *in* Vallier, T.L., and Brooks, H.C., eds., Geology of the Blue Mountains region of Oregon, Idaho, and Washington—Geologic implications of Paleozoic and Mesozoic paleontology and biostratigraphy, Blue Mountains province, Oregon and Idaho: U.S. Geological Survey Professional Paper 1435, p. 53-57.

Irving, E., and Irving, G.A., 1982, Apparent polar wander paths, Carboniferous through Cenozoic and the assembly of Gondwana: Geophysical Surveys, v. 5, p. 141-188.

Johnson, R.G., and King, B.-S.L., 1987, Energy-dispersive X-ray fluorescence spectrometry, *in* Baedecker, P.A., ed., Methods for geochemical analysis: U.S. Geological Survey Bulletin 1770, p. F1-F5.

Jones, D.L., Silberling, N.J., and Hillhouse, J.W., 1977, Wrangellia—A displaced terrane in northwestern North America: Canadian Journal of Earth Sciences, v. 14, p. 2565-2577.

Kay, R.W., 1984, Elemental abundances relevant to identification of magma sources: Royal Society of London Philosophical Transactions, ser. A, v. 310, p. 535-547.

Kay, S.M., and Kay, R.W., 1985a, Aleutian tholeiitic and calc-alkaline magma series—Pt. I, The mafic phenocrysts: Contributions to Mineralogy and Petrology, v. 90, p. 276-290.

———1985b, Role of crystal cumulates and the oceanic crust—The formation of the lower crust of the Aleutian arc: Geology, v. 13, p. 461-464.

———1994, Aleutian magmas in space and time, *in* Plafker, George, and Berg, H.C., eds., The Geology of Alaska: Boulder, Colorado, Geological Society of America, The Geology of North America [Decade of North American Geology], v. G–1, p. 687-722.

Kay, S.M., Kay, R.W., Citron, G.P., and Perfit, M.R., 1990, Calc-alkaline plutonism in the intra-oceanic Aleutian arc, Alaska, *in* Kay, S.M., and Rapela, C.W., eds., Plutonism from Antarctica to Alaska: Geological Society of America Special Paper 241, p. 233-255.

Kays, M.A., Ferns, M.L., and Brooks, H.C., 1988, Metamorphism of Triassic-Paleozoic belt rocks—A guide to field and petrologic relations in the oceanic melange, Klamath and Blue Mountains, California and Oregon, *in* Ernst, W.G., ed., Metamorphism and crustal evolution of the Western United States (Rubey Volume VII): Englewood Cliffs, N.J., Prentice-Hall, p. 1099-1142.

Kolthoff, I.M., Sandell, E.B., Meehan, E.J., and Bruckenstein, S., 1969, Quantitative chemical analysis (4th ed.): London, Collier-MacMillan, p. 573-579.

Kroenke, L.W., with a contribution by Peter Rodda, 1984, Cenozoic tectonic development of the southwest Pacific: Suva, Fiji, United Nations Economic and Social Commission for Asia and the Pacific, Committee for Co-ordination of Joint Prospecting for Mineral Resources in South Pacific Offshore Areas, Technical Bulletin 6, 122 p.

Kuno, H., 1968, Differentiation of basalt magmas, *in* Hess, H.H., and Poldevaart, Arie., eds., Basalts—The Poldervaart treatise on rocks of basaltic composition: New York, John Wiley, v. 2, p. 624-688.

LaPierre, H., Rouer, O., Charvet, J., Lecuyer, C., Gross, E., and Coulon, C., 1988, Les magmatismes tholeiitiques d'arc permotriasiques des Blue Mountains (Oregon oriental): correlations possibles avec les unites voisines de Californe: Compte Rendu, Academie des Sciences Paris, v. 396, Serie H, p. 1103-1108.

Lindgren, Waldemar, 1901, The gold belt of the Blue Mountains of Oregon: U.S. Geological Survey Annual Report 22, p. 560-776.

Livingston, D.C., and Laney, F.B., 1920, The copper deposits of the Seven Devils and adjacent districts (including Heath, Hornet Creek, Hoodoo, and Deer Creek): Idaho Bureau of Mines and Geology Pamphlet 13, 24 p.

Lund, Karen, 1984, Tectonic history of the continent-island arc boundary, west-central Idaho: University Park, Pennsylvania State University, Ph.D. dissertation, 207 p.

Lund, Karen, and Snee, L.W., 1988, Metamorphism, structural development, and age of the continent-island arc juncture in west-central Idaho, *in* Ernst, W.G., ed., Metamorphism and crustal evolution, western conterminous United States (Rubey Volume VII): Geological Society of America, p. 296-337.

MacDonald, G.A., and Katsura, T., 1964, Chemical composition of Hawaiian lavas: Journal of Petrology, v. 5, p. 82-113.

Manduca, C.A., 1988, Geology and geochemistry of the oceanic arc-continent boundary in western Idaho batholith near McCall [Idaho]: Pasadena, California Institute of Technology, Ph.D. dissertation, 272 p.

Mann, G.M., 1988, Geologic map of the Brownlee Dam and Cuddy Mountain 7.5-minute quadrangle: U.S. Geological Survey Open-File Report 88-657, 2 maps, scale 1:24,000.

Marlow, M.S., Exon, N.F., and Tiffin, D.L., 1988, Widespread lava flows and sediment deformation in a fore-arc setting north of Manus Island, northern Papua New Guinea, *in* Marlow, M.S., Dadisman, S.V., and Exon, N.F., eds., Geology and offshore resources of Pacific island arcs—New Ireland and Manus region, Papua New Guinea: Circum-Pacific Council for Energy and Mineral Resources Earth Science Series, v. 9, p. 221-237.

Masuda, A., Nakamura, N., and Tanaki, T., 1973, Fine structures of mutually normalized rare-earth patterns of chondrites: Geochimica et Cosmochimica Acta, v. 37, p. 239-248.

Menzies, M.A., Blanchard, D.P., and Jacobs, J.A., 1977, Rare-earth and trace-element geochemistry of metabasalts from the Point Sal ophiolite, California: Earth and Planetary Science Letters, v. 37, p. 203-215.

Menzies, M.A., Blanchard, D.P., and Xenophontos, C., 1980, Genesis of the Smartville arc-ophiolite, Sierra Nevada foothills, California: American Journal of Science, v. 280-A, pt. 1, p. 329-344.

Miller, M.M., 1987, Dispersed remnants of a northeast Pacific fringing arc—Upper Paleozoic terranes of Permian McCloud faunal affinities, Western U.S.: Tectonics, v. 6, p. 807-830.

Miyashiro, Akiho, 1974, Volcanic rock series in island arcs and active continental margins: American Journal of Science, v. 274, p. 321-355.

Monger, J.W.H., Price, R.A., and Tempelman-Kluit, D.J., 1982, Tectonic accretion and the origin of the two major metamorphic and plutonic welts in the Canadian Cordillera: Geology, v. 10, p. 70-75.

Morris, E.M., and Wardlaw, B.R., 1986, Conodont ages for limestones of eastern Oregon and their implications for pre-Tertiary melange terranes, *in* Vallier, T.L., and Brooks, H.C., eds., Geology of the Blue Mountains region of Oregon, Idaho, and Washington—Geologic implications of Paleozoic and Mesozoic paleontology and biostratigraphy, Blue Mountains province, Oregon and Idaho: U.S. Geological Survey Professional Paper 1435, p. 59-64.

Morrison, R.K., 1963, Pre-Tertiary geology of the Snake River canyon between Cache Creek and Dug Bar, Oregon-Idaho boundary: Eugene, University of Oregon, Ph.D. dissertation, 290 p.

Mortimore, Nicholas, 1986, Late Triassic, arc-related, potassic igneous rocks in the North American Cordillera: Geology, v. 14, p. 1035-1038.

Motzer, W.E., 1986, Tertiary epizonal plutonic rocks of the Selway-Bitterroot Wilderness, Idaho County, Idaho: Moscow, University of Idaho, Ph.D. dissertation, 467 p.

Mullen, E.D., 1978, Geology of the Greenhorn Mountains, northeastern Oregon: Corvallis, Oregon State University, M.S. thesis, 372 p.

———1983, Petrology and regional setting of peridotite and gabbro of the Canyon Mountain Complex, northeast Oregon: Corvallis, Oregon State University, Ph.D. dissertation, 277 p.

———1985, Petrologic character of Permian and Triassic greenstones from the melange terrane of eastern Oregon and their implications for terrane origin: Geology, v. 13, p. 131-134.

Mullen, E.D., and Sarewitz, D.M., 1983, Paleozoic and Triassic terranes of the Blue Mountains, northeast Oregon. Discussion and field trip guide, Part I. A new consideration of old problems: Oregon Geology, v. 45, p. 65-68.

Myers, P.E., 1982, Geology of the Harpster area, Idaho County, Idaho: Idaho Department of Lands/Idaho Bureau of Mines and Geology Bulletin 25, 46 p.

Nolf, Bruce, 1966, Geology and stratigraphy of part of the northern Wallowa Mountains, Oregon: Princeton, N.J., Princeton University, Ph.D. dissertation, 138 p.

Palmer, A.R., 1983, The Decade of North American Geology 1983 geologic time scale: Geology, v. 11, p. 503-504.

Pearce, J.A., and Cann, J.R., 1973, Tectonic setting of basic volcanic rocks determined using trace-element analyses: Earth and Planetary Science Letters, v. 19, p. 290-300.

Pearcy, L.G., 1991, Island-arc petrogenesis and crustal growth—Examples from Oregon and Alaska: Palo Alto, Calif., Stanford University, Ph.D. dissertation, 184 p.

Peck, D.C., 1964, Systematic analysis of silicates: U.S. Geological Survey Bulletin 1170, p. 39-42.

Pessagno, E.A., Jr., and Blome, C.D., 1986, Faunal affinities and tectonogenesis of Mesozoic rocks in the Blue Mountains province of eastern Oregon and western Idaho, *in* Vallier, T.L., and Brooks, H.C., eds., Geology of the Blue Mountains region of Oregon, Idaho, and Washington—Geologic implications of Paleozoic and Mesozoic paleontology and biostratigraphy, Blue Mountains province, Oregon and Idaho: U.S. Geological Survey Professional Paper 1435, p. 65-78.

Phelps, D.W., 1978, Petrology, geochemistry, and structural geology of Mesozoic rocks in the Sparta quadrangle and Oxbow and Brownlee Reservoir areas, eastern Oregon and western Idaho: Houston, Rice University, Ph.D. dissertation, 229 p.

———1979, Petrology, geochemistry, and origin of the Sparta quartz diorite-trondhjemite complex, northeastern Oregon, *in* Barker, Fred, ed., Trondhjemites, dacites, and related rocks: New York, Elsevier, p. 547-580.

Phelps, D.W., and Avé Lallemant, H.G., 1980, The Sparta ophiolite complex, northeast Oregon—A plutonic equivalent to low-K_2O island-arc volcanism: American Journal of Science, v. 280-A, pt. 1, p. 345-358.

Prostka, H.J., 1962, Geology of the Sparta quadrangle, Oregon: Oregon Department of Geology and Mineral Industries Geologic Map GMS-1, one map sheet, scale 1:62,500.

———1963, The geology of the Sparta quadrangle, Oregon: Baltimore, John Hopkins University, Ph.D. dissertation, 245 p.

Saleeby, J.B., 1983, Accretionary tectonics of the North American Cordillera: Annual Review of Earth and Planetary Sciences, v. 11, p. 45-73.

Sarewitz, D.R., 1982, Geology of part of the Heavens Gate quadrangle, Seven Devils Mountains, western Idaho: Corvallis, Oregon State University, M.S. thesis, 144 p.

———1983, Seven Devils terrane—Is it really a piece of Wrangellia?: Geology, v. 11, p. 634-637.

Scheffler, J.M., 1983, A petrologic and tectonic comparison of the Hells Canyon area, Oregon-Idaho, and Vancouver Island, British Columbia: Pullman, Washington State University, M.S. thesis, 98 p.

Schmidt, W.J., 1980, Structure of the Oxbow area, Oregon and Idaho: Houston, Rice University, M.S. thesis, 61 p.

Shorey, E.F., 1976, Geology of part of southern Morrow County, northeast Oregon: Corvallis, Oregon State University, M.S. thesis, 119 p.

Silberling, N.J., Jones, D.L., Blake, M.C., Jr., and Howell, D.G., 1984, Lithotectonic terrane map of the western conterminous United States, Pt. C *of* Silberling, N.J., and Jones, D.L., eds., Lithotectonic terrane maps of the North American Cordillera: U.S.Geological Survey Open-File Report 84-523, 43 p.

Skurla, S.J., 1974, The geology of the Sturgill Peak area, Washington County, Idaho: Corvallis, Oregon State University, M.S. thesis, 98 p.

Spooner, E.T.C, and Fyfe, W.S., 1973, Sub-sea-floor metamorphism, heat and mass transfer: Contributions to Mineralogy and Petrology, v. 42, p. 287-304.

Stanley, G.D., Jr., and Beauvais, L., 1990, Middle Jurassic corals from the Wallowa terrane, west-central Idaho: Journal of Paleontology, v. 64, p. 352-362.

Symons, D.T.A., 1990, Early Permian pole—Evidence from the Pictou red beds, Prince Edward Island, Canada: Geology, v. 18, p. 234-237.

Tabor, R.W., Zartman, R.E., and Frizzell, V.A., Jr., 1987, Possible tectonostratigraphic terranes in the North Cascades crystalline core, Washington, *in* Schuster, J.E., ed., Selected papers on the geology of Washington: Washington Division of Geology and Earth Resources Bulletin, v. 77, p.107-127.

Taggart, J.E., Jr., Lichte, F.E., and Wahlberg, J.S., 1981, Methods of analysis of samples using X-ray fluorescence and induction-coupled plasma spectroscopy: U.S. Geological Survey Professional Paper 1250, p. 683-687.

Taggart, J.E., Jr., Lindsay, J.R., Scott, B.A., Vivit, D.V., Bartel, A.J., and Stewart, K.C., 1987, Analysis of geologic materials by wavelength-dispersive X-ray fluorescence spectrometry, *in* Baedecker, P.A., ed., Methods for geochemical analysis: U.S. Geological Survey Bulletin 1770, p. E1-E19.

Taubeneck, W.H., 1957, Geology of the Elkhorn Mountains, northeastern Oregon—Bald Mountain batholith: Geological Society of America Bulletin, v. 68, p. 181-238.

———1967, Petrology of Cornucopia tonalite unit, Cornucopia stock, Wallowa Mountains, northeastern Oregon: Geological Society of America Special Paper 91, 56 p.

Thayer, T.P., 1956, Preliminary geologic map of the John Day quadrangle, Oregon: U.S. Geological Survey Mineral Investigations Field Studies Map MF-51, scale 1:62,500.

———1963, The Canyon Mountain Complex, Oregon, and the alpine mafic-magma stem, article 81 *of* Short papers in geology and hydrology: U.S. Geological Survey Professional Paper 475-C, p. 82-85.

———1977, The Canyon Mountain Complex, Oregon, and some problems of ophiolites, *in* Coleman, R.G., and Irwin, W.P., eds., North American ophiolites: Oregon Department of Geology and Mineral Industries Bulletin 95, p. 93-105.

Thayer, T.P., and Himmelberg, G.R., 1968, Rock succession in the alpine-type mafic complex at Canyon Mountain, Oregon: International Geological Congress, 23d, Prague, 1968 [Proceedings], v. 1, p. 175-186.

Tillman, J.H., 1977, A systematic method for determining the total carbon content of geologic materials: Journal of Research of the U.S. Geological Survey, v. 5, no. 5, p. 583-587.

Trauba, W.C., 1975, Petrography of pre-Tertiary rocks of the Blue Mountains, Umatilla County, northeastern Oregon: Corvallis, Oregon State University, M.S. thesis, 171 p.

Vallier, T.L., 1967a, Geology of part of the Snake River canyon and adjacent areas in northeastern Oregon and western Idaho: Corvallis, Oregon State University, Ph.D. dissertation, 267 p.

———1967b, The geology of part of the Snake River canyon and adjacent areas in northeastern Oregon and western Idaho [abs., Oregon State University dissertation]: Dissertation Abstracts, sec. B, v. 28, no.4, p. 1585.

———1968, Reconnaissance geology of the Snake River canyon between Granite Creek and Pittsburg Landing, Oregon and Idaho: Ore Bin, v. 30, no. 12, p. 233-252.

———1974, Preliminary report on the geology of part of the Snake River Canyon: Oregon Department of Geology and Mineral Industries Map GMS-6, 1 map sheet, 15 p. of text, scale 1:125,000.

———1977, The Permian and Triassic Seven Devils Group, western Idaho and northeastern Oregon: U.S. Geological Survey Bulletin 1437, 58 p.

———1986, Tectonic implications of arc-axis (Wallowa terrane) and back-arc (Vancouver Island) volcanism in Triassic rocks of Wrangellia [abs.]: Eos (American Geophysical Union Transactions), v. 67, no. 44, p.1233.

Vallier, T.L., and Batiza, Rodey, 1978, Petrogenesis of spilite and keratophyre from a Permian and Triassic volcanic-arc terrane, eastern Oregon and western Idaho: Canadian Journal of Earth Sciences, v. 15, p. 1356-1369.

Vallier, T.L., and Brooks, H.C., 1986, Paleozoic and Mesozoic faunas of the Blue Mountains province—A review of their geologic implications and comments on papers in the volume, *in* Vallier, T.L., and Brooks, H.C., eds., Geology of the Blue Mountains region of Oregon, Idaho, and Washington—Geologic implications of Paleozoic and Mesozoic paleontology and biostratigraphy, Blue Mountains province, Oregon and Idaho: U.S. Geological Survey Professional Paper 1435, p. 1-6.

———eds., 1987, Geology of the Blue Mountains region of Oregon, Idaho, and Washington—The Idaho batholith and its border zone: U.S. Geological Survey Professional Paper 1436, 196 p.

Vallier, T.L., Brooks, H.C., and Thayer, T.P., 1977, Paleozoic rocks of eastern Oregon and western Idaho, *in* Stewart, J.H., Stevens, C.H., and Fritsche, A.E., eds., Paleozoic paleogeography of the Western United States (Pacific Coast Paleogeography Symposium 1): Los Angeles, Society of Economic Paleontologists and Mineralogists, Pacific Section, p. 455-466.

Vallier, T.L., and Engebretson, D.C., 1984, The Blue Mountains island arc of Oregon, Idaho, and Washington—An allochthonous coherent terrane from the ancestral western Pacific Ocean?, *in* Howell, D.G., Jones, D.L., Cox, Allan, and Nur, Amos, eds., Circum-Pacific Terrane Conference, Stanford, Calif., 1983, Proceedings: Stanford University Publications/Geological Sciences, v. 18, p. 197-199.

Vallier, T.L., Jenner, G.A., Frey, F.A., Gill, J.B., Davis, A.S., Volpe, A.M., Hawkins, J.W., Morris, J.D., Cawood, P.A., Morton, J.L., Scholl, D.W., Rautenschlein, M., White, W.M., Williams, R.W., Stevenson, A.J., and White, L.D., 1991, Subalkaline andesite from Valu Fa Ridge, a back-arc spreading center in southern Lau Basin—Petrogenesis, comparative chemistry, and tectonic implications: Chemical Geology, v. 91, p. 227-256.

Vallier, T.L., Scholl, D.W., Fisher, M.A., Bruns, T.R., Wilson, F.H. von Huene, Roland, and Stevenson, A.J., 1994, Geologic framework of the Aleutian arc, Alaska, *in* Plafker, George, and Berg, H.C., eds., The Geology of Alaska: Boulder, Colorado, Geological Society of America, The Geology of North America [Decade of North American Geology], v. G–1, p. 367-388.

Vallier, T.L., Stevenson, A.J., and Scholl, D.W., 1985, Petrology of igneous rocks from Ata Island, Kingdom of Tonga, *in* Scholl, D.W., and Vallier, T.L., eds., Geology and offshore resources of Pacific island arcs—Tonga region: Houston, Circum-Pacific Council for Energy and Mineral Resources Earth Science Series, v. 2, p. 301-316.

Walker, G.W., 1990, Overview of the Cenozoic geology of the Blue Mountains region, *in* Walker, G.W., ed., Geology of the Blue Mountains region of Oregon, Idaho, and Washington—Cenozoic geology of the Blue Mountains region: U.S. Geological Survey Professional Paper 1437, p. 1-11.

Walker, N.W., 1986, U-Pb geochronologic and petrologic studies in the Blue Mountains terranes, northeastern Oregon and westernmost-central Idaho—Implications for pre-Tertiary tectonic evolution: Santa Barbara, University of California, Ph.D. dissertation, 224 p.

Wernicke, Brian, and Klepacki, D.W., 1988, Escape hypothesis for the Stikine block: Geology, v. 16, p. 461-464.

Wetherell, C.E., 1960, Geology of part of the southeastern Wallowa Mountains, northeastern Oregon: Corvallis, Oregon State University, MS thesis, 208 p.

White, A.J.R., and Chappell, B.W., 1983, Granitoid types and their distribution in the Lachlan fold belt, southeastern Australia, *in* Roddick, J.A., ed., Circum-Pacific plutonic terranes: Geological Society of America Memoir 159, p. 21-34.

White, D.L., 1972, The geology of the Pittsburg Landing area, Snake River canyon, Oregon and Idaho: Terre Haute, Indiana State University, M.S. thesis, 98 p.

White, D.L., and Vallier, T.L., 1994, Geologic evolution of the Pittsburg Landing area, Snake River canyon, Oregon and Idaho, *in* Vallier, T.L., and Brooks, H.C., eds., Geology of the Blue Mountains region of Oregon, Idaho, and Washington—Stratigraphy, physiography, and mineral resources of the Blue Mountains region: U.S. Geological Survey Professional Paper 1439, p. 55-73.

White, J.D.L., 1985, The Doyle Creek Formation (Seven Devils Group), Pittsburg Landing, Idaho—A study of intra-arc sedimentation: Columbia, University of Missouri, M.S. thesis, 151 p.

White, J.D.L., 1994, Intra-arc basin deposits within the Wallowa terrane, Pittsburg Landing area, Oregon and Idaho, *in* Vallier, T.L., and Brooks, H.C., eds., Geology of the Blue Mountains region of Oregon, Idaho, and Washington—Stratigraphy, physiography, and mineral resources of the Blue Mountains region: U.S. Geological Survey Professional Paper 1439, p. 75-89.

White, W.H., 1968, Plutonic rocks of the southern Seven Devils Mountains, Idaho: Corvallis, Oregon State University, Ph.D. dissertation, 177 p.

———1973, Flow structure and form of the Deep Creek stock, southern Seven Devils Mountains, Idaho: Geological Society of America Bulletin, v. 84, p. 199-210.

Wilson, Douglas, and Cox, Allan, 1980, Paleomagnetic evidence for the tectonic rotation of Jurassic plutons in the Blue Mountains, eastern Oregon: Journal of Geophysical Research, v. 85, no. B7, p. 3681-3689.

Wilson, S.A., Kane, J.S., Crock, J.G., and Hatfield, D.B., 1987, Chemical methods of separation for optical emission, atomic-absorption spectrometry, and colorimetry, *in* Baedecker, P.A., ed., Methods for geochemical analysis: U.S. Geological Survey Bulletin 1770, p. D1-D14.

4. HIGH-PRESSURE, LOW-TEMPERATURE SCHISTOSE ROCKS OF THE BAKER TERRANE, NORTHEASTERN OREGON

By ELLEN M. BISHOP[1]

CONTENTS

	Page
Abstract	211
Introduction: The Baker terrane	211
Acknowledgments	213
High-pressure, low-temperature schists of the Baker terrane	213
Blueschist near Mitchell, Oregon	213
Greenhorn Mountains	214
Aldrich Mountains (serpentinite-matrix) melange and Mount Vernon area	216
Schistose rocks of Mine Ridge	216
Schistose rocks of Rhea Creek	216
Discussion	217
Conclusions	218
References cited	218

ABSTRACT

Schistose rocks are present at widely separated localities within the serpentinite-matrix melange of the Baker terrane, northeastern Oregon. These schists vary in lithology and metamorphic grade, but most contain minerals whose compositions suggest initial metamorphism under conditions at or approaching blueschist-facies conditions. This high-pressure metamorphism was succeeded and overprinted by lower pressure metamorphism, usually in greenschist facies. Amphiboles in the high-pressure schists range from glaucophane to barroisite and winchite. Microprobe analyses of Na/Al relations in amphiboles from blueschists near Mitchell, Oreg. suggest initial metamorphism at greater than 7 kilobars (kb), with pressure subsequently decreasing to about 5 kb. At Pleasant Hill, south of Mount Vernon, blue amphiboles that are near crossite in composition suggest initial pressures of 5 kb, followed by pressures of 4 to 5 kb. Schists from the Greenhorn Mountains have a similar history, but the compositions indicate initial pressures of about 6 to 5 kb. Blue-green amphiboles from schistose rocks in the Mine Ridge area to the southeast suggest initial pressures of about 5 kb. Schists from the Rhea Creek area in north-central Oregon near Heppner contain no relict high-pressure minerals, but may have been strongly overprinted by contact metamorphism.

This study suggests that some schists of the Baker terrane originated at high pressures, most likely in a subduction zone, and were affected by later conditions at decreased pressures and elevated temperatures. The rarity of true glaucophane blueschists in the Baker terrane may indicate that fairly rapid, high shear-stress subduction was characteristic of the Blue Mountains island-arc subduction zone during the Permian and Early Triassic. Later retrograde greenschist metamorphism may have been related to long-term incorporation in a fore arc under greenschist conditions or a shift in the locus of volcanism and the direction of subduction.

[1]52040 Highway 203, Union, OR 97883

INTRODUCTION: THE BAKER TERRANE

The Blue Mountains of eastern Oregon contain a complex assemblage of tectonically emplaced and juxtaposed late Paleozoic and early Mesozoic terranes. These terranes are considered related to the Blue Mountains island arc (Vallier and Brooks, 1986) and are named the Wallowa, Baker, Grindstone, Izee, and Olds Ferry terranes (Silberling and Jones, 1984; fig. 4.1).

The Baker terrane is a disordered mixture of oceanic and island-arc sedimentary, volcanic, and plutonic rocks ranging from Devonian to Triassic in age. It has been characterized as an oceanic melange (Dickinson, 1979), a relatively coherent fore arc (Mullen, 1985), or possibly an ocean-floor environment (Vallier and others, 1977) associated with the Blue Mountains island arc. Most rocks in the terrane have been metamorphosed to greenschist facies; virtually all are deformed. The location and orientation of any subduction zone associated with the Blue Mountains island arc is still a matter of conjecture.

The rock types of the Baker terrane are diverse. Sedimentary rocks are dominantly chert or siliceous argillite. Graywacke and conglomerates, with clasts ranging from about 1 cm in fine-grained rocks to nearly 1 m in boulder conglomerates, are distributed throughout the terrane. Shales and quartz-rich sandstones are rare. Turbidite sandstones are unknown. Disrupted ophiolitic assemblages (greenstone, gabbro, layered gabbro, and serpentinized peridotite) and tectonic slices are present throughout the Baker terrane. Coherent ophiolitic blocks include the Canyon Moun-

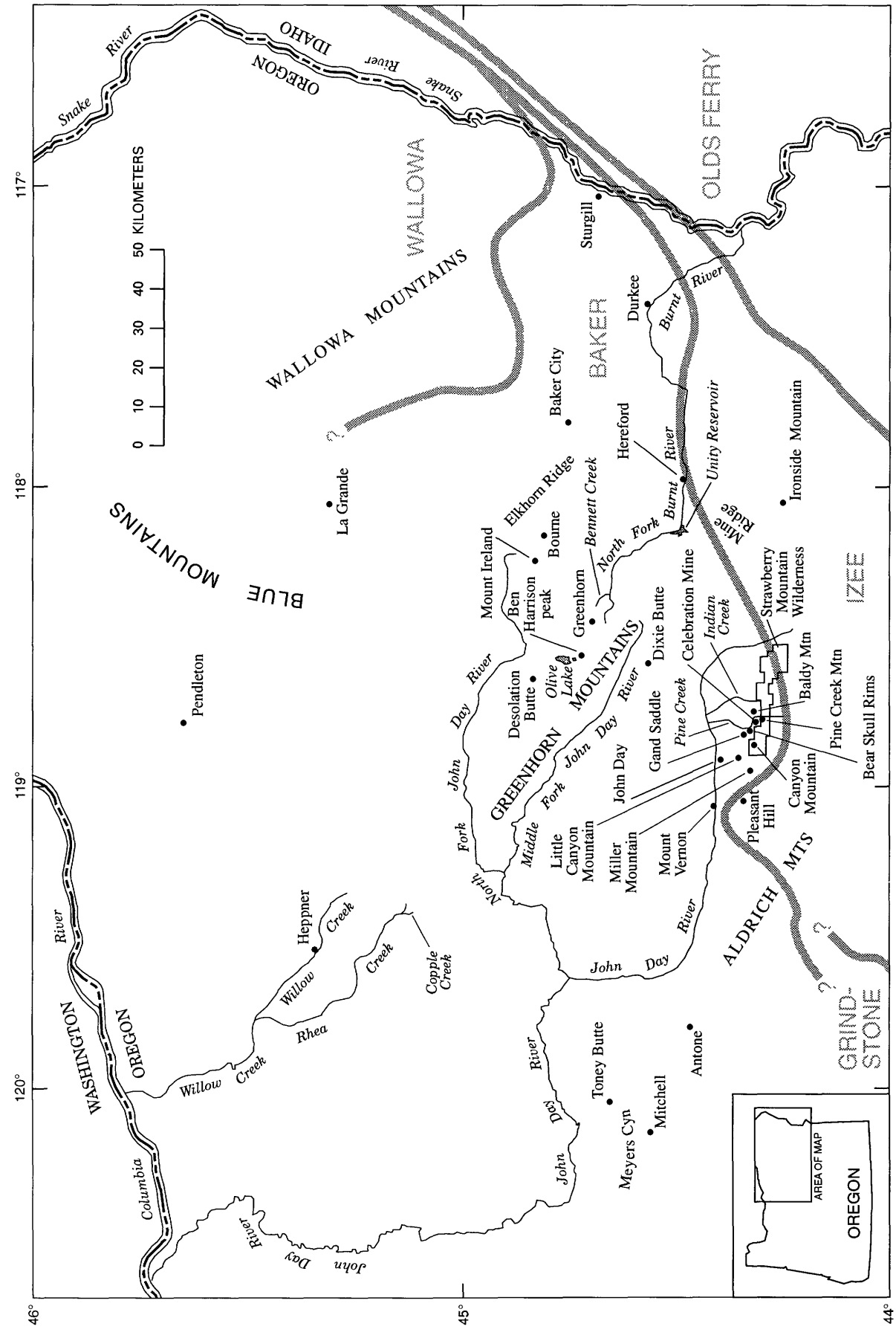

FIGURE 4.1.—Location map showing region of study and places mentioned in chapters 4 and 5 (Bishop, this volume). Broad gray lines are terrane boundaries (approximate) as modified from Silberling and Jones (1984) by Vallier (chap. 3, this volume); queried where location uncertain.

tain Complex (Thayer, 1963; Leeman and others, chap. 1, this volume; Bishop, chap. 5, this volume).

The igneous rocks have tholeiitic, calc-alkaline, and alkalic compositions. The Canyon Mountain Complex is interpreted as island-arc basement (Leeman and others, chap. 1, this volume; Bishop, chap. 5, this volume).

Sheared serpentinite serves as a matrix in melanges or mixed-rock zones that occur from Mitchell at the western extremity to the Burnt River on the east (fig. 4.1). The nature of these serpentinite-matrix melanges is unresolved. They have been interpreted as diapiric upwellings of hydrated peridotite in a fore-arc environment (Bishop, 1988) and as faulted zones of structural weakness (Kays and others, 1988). Knockers within the serpentinite-matrix melanges include all lithic components of the Baker terrane as well as a variety of amphibolites and high-pressure, low-temperature schists.

ACKNOWLEDGMENTS

This study was partly funded by Sigma Xi (82-256) and the Oregon Department of Geology and Mineral Industries. Discussions with Howard Brooks, M. Alan Kays, Mark Ferns, Tracy Vallier, and R.G. Coleman were helpful. Reviews by Mary Donato and Bernard Evans significantly improved the manuscript.

HIGH-PRESSURE, LOW-TEMPERATURE SCHISTS OF THE BAKER TERRANE

The high-pressure, low-temperature schistose rocks of the Baker terrane are important because they provide insight into the pressure and temperature regimes that affected the Baker terrane, whether fore arc or subduction zone. Blueschist and other high-pressure, low-temperature metamorphic rocks are associated with melange assemblages, subduction complexes, and accreted exotic terranes elsewhere, including the Franciscan Complex (California), the North Cascades (Washington), the Klamath Mountains (California and Oregon), the Sanbagawa terrane (Japan), and Otago, New Zealand. Thus, it is logical to expect blueschist or related rocks to occur in the Baker terrane, which represents a fore-arc or subduction complex for the island-arc-derived terranes of northeastern Oregon.

In this study, I examined a number of schistose rocks from the Baker terrane that contain blue amphiboles. The goal was to determine whether there are any blueschists in the Baker terrane beyond those at the already-defined localities near Mitchell and Toney Butte (fig. 4.1, Swanson, 1969). I also considered what limits of pressure and temperature could be estimated using amphibole compositions. This paper briefly describes schistose rocks of the Baker terrane and their mineral compositions, and speculates on their origins and possible significance.

Estimation of metamorphic pressure and temperature in this study is based upon amphibole chemistry. Coleman and Papike (1968) noted that with increasing metamorphic grade the Ca content of glaucophane increases. Brown (1977) found that Ca amphibole crystals from high-pressure terranes contain significantly more Na in $X(M_4)$ sites (octahedrally coordinated sites occupied by the relatively large cations Ca, Na, or K) than amphiboles from low-pressure terranes, and that where critical buffers are present, the Na/Ca ratio of amphibole is fixed by pressure. Ernst (1968), Liou and others (1975), and Brown (1977) observed that Al^{IV} (Al in $(Si,Al)O_4$ tetrahedra within the crystal) increases with temperature in amphiboles. This reaction uses the same buffers as the Na/Ca reaction and provides a relative geothermometer.

Progressive changes in metamorphic conditions can be determined from zonation in amphibole composition. On the basis of these estimates and the composition of other minerals, a metamorphic history is suggested for each locality.

BLUESCHIST NEAR MITCHELL, OREGON

The lawsonite blueschist of Meyers Canyon near Mitchell in central Oregon (fig. 4.1) was described by Swanson (1969). Exposures of Permian to Triassic rocks in Meyers Canyon include crystalline marble, pelitic schist, quartzite, chert, and mafic metavolcanic rocks, with exposure of serpentinite at the nearby blueschist location at Toney Butte. The blueschist at Meyers Canyon has been dated by Hotz and others (1977) at about 220 Ma using the K-Ar method.

The blueschist of Meyers Canyon contains feathery to idioblastic blue amphibole, with pleochroic colors ranging from light yellow to pale blue in the alpha optical direction and from light purple to pale blue in the gamma direction. On the basis of optics, Swanson (1969) classified these amphiboles as crocidolite to crossite with compositions close to glaucophane (see table 4.1). Very fine, slightly corroded prismatic lawsonite is dispersed throughout the rock and also forms fine aggregates. White mica (paragonite) also forms aggregates and occasional lenticular crystals. Chlorite occurs around amphiboles and micas. Quartz and albite are groundmass constituents. Small, prismatic crystals of Al-rich pumpellyite (see table 4.2) are present in mafic schists.

TABLE 4.1.—*Compositions of amphiboles in schistose rocks of the Baker terrane, northeastern Oregon*

[Values in weight percent. FeO*=FeO+Fe_2O_3; ---, not determined]

Location ----	Meyers Canyon, near Mitchell		Mount Vernon area (Aldrich Mountains)		Bennett Creek, in the Greenhorn Mountains		Mine Ridge		Rhea Creek	
Analyzed mineral--	Glaucophane core	Glaucophane rim	Amphibole core	Amphibole rim	Barroisite core	Barroisite rim	Amphibole in amphibole schist	Amphibole in mica schist, core	Hornblende in biotite schist	Blue magnesiogrunerite in graphite schist
SiO_2 ------	53.6	54.8	53.1	52.7	55.0	54.5	47.5	47.0	44.2	53.7
TiO_2 ------	.1	.1	.0	.2	.0	.0	.6	.3	.2	.0
Al_2O_3 -----	10.2	9.8	4.1	4.0	5.5	2.4	10.5	11.0	14.3	.7
FeO* ------	14.4	13.4	19.7	17.3	17.4	12.8	14.4	14.2	17.0	25.1
MnO ------	.2	.2	.2	.3	.3	.3	.2	.2	.0	.0
MgO ------	9.3	9.1	9.7	11.7	12.0	16.4	13.1	11.8	9.7	17.8
CaO -------	5.6	7.4	3.5	5.2	4.4	10.3	10.1	12.0	12.5	.6
Na_2O -----	4.9	4.4	5.5	4.4	4.7	1.6	2.7	1.3	1.1	.0
K_2O -------	.1	.1	.1	.1	.1	.6	.6	.6	.0	---
F ----------	.0	.0	.0	.1	.0	.1	.2	---	---	---
Cl ---------	.0	.0	.0	.0	.0	.0	.0	---	---	---
Total---	98.5	99.3	97.9	97.9	99.3	99.6	98.3	99.3	98.8	99.7

Large idioblastic amphiboles were selected for microprobe core and rim analysis. Results (table 4.1) show that amphiboles from the blueschist of Meyers Canyon are zoned from sodic cores to more calcic rims (fig. 4.2). Analyses of cores gave an average composition of $(Na_{1.7},Ca_{0.3})(Fe_{2.0},Mg_{1.8},Al_{1.2})Si_8O_{22}(OH)_2$ (crossite). Rim analyses vary widely in the amount of CaO—from 4.5 to 8.6 weight percent—which may be a function of the precise site analyzed. The average rim composition is $(Na_{1.3}Ca_{0.7})(Fe_{1.5}Mg_{1.7}Al_{0.7})Si_8O_{22}(OH)_2$, which is intermediate between actinolite and winchite (Leake, 1968). Al^{IV} is absent in all analyses.

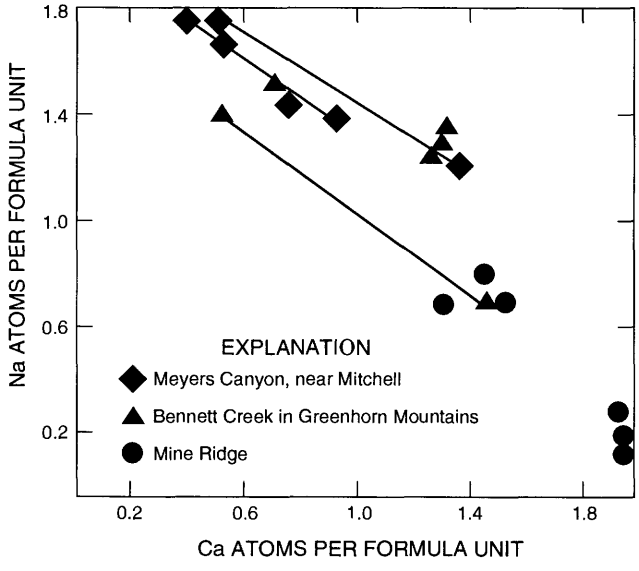

FIGURE 4.2.—Stoichiometric Na/Ca ratios for amphiboles from three eastern Oregon localities. Lines connect core (upper) and rim (lower) compositions.

The transition from low Ca content in the core to moderate Ca content in the rim suggests increased miscibility of amphiboles with time, and hence a probable increase in temperature (fig. 4.2). Plots of amphibole NaM_4 (Na in M_4 sites) versus Al^{IV} (Al in tetrahedral sites) after Brown (1977) indicate that pressures during growth of both core and rim exceeded 7 kb. The restriction of Al to six-fold coordination suggests that the temperatures of metamorphism were relatively low.

GREENHORN MOUNTAINS

The Greenhorn Mountains are midway between Mitchell at the western edge of the Baker terrane and the Burnt River on the east (fig. 4.1). Permian metasedimentary rocks and volcanic greenstones of tholeiitic, calc-alkaline, and alkalic compositions are juxtaposed with and tectonically intruded by metagabbros and serpentinized peridotites. An oceanic component is represented by chert of the Elkhorn Ridge Argillite and pillowed greenstones that occur as knockers. Alkalic pillowed greenstones that may be related to arc rifting are also intercalated with cherts (Mullen, 1985). Arc-derived metasedimentary rocks include fine-grained graywackes, shales, conglomerates, and tuffaceous pyroclastic rocks. Most greenstones associated with or adjacent to these metasedimentary rocks have calc-alkaline geochemical and mineralogical characteristics (Mullen, 1985). The serpentinite-matrix melange in the Greenhorn Mountains contains clasts of all lithic types and occurs in several broad zones.

TABLE 4.2.—*Compositions of minerals (excepting amphiboles) in schistose rocks of the Baker terrane, northeastern Oregon*

[Values in weight percent. FeO*=FeO+Fe_2O_3; ---, not determined]

Location	Meyers Canyon, near Mitchell	Mine Ridge	Bennett Creek, in the Greenhorn Mountains			
Analyzed mineral	Pumpellyite from blueschist	Epidote	Epidote	Garnet, rim	Garnet, intermediate zone	Garnet, core
SiO_2	37.00	38.82	38.20	38.77	37.81	38.31
Al_2O_3	29.03	24.28	23.31	22.12	21.69	21.36
TiO_2	.16	.15	.01	.04	.05	.07
FeO*	2.57	11.94	12.40	23.01	22.50	21.06
MnO	---	.01	.12	4.76	5.71	7.27
MgO	1.45	.05	.06	.80	.69	.59
CaO	21.73	23.64	23.43	11.02	11.69	11.76
Na_2O	.12	---	---	---	---	---
K_2O	.01	---	---	---	---	---
Total	92.08	99.01	97.47	100.52	100.14	100.15

The best known schists in the Greenhorn Mountains are restricted to an area of about one-half square kilometer at the head of Bennett Creek (fig. 4.1). There are two lithic types—a finely crystalline, highly foliated mica schist and a more massive blue-grey greenstone (Mullen, 1979a). The protolith of the mica schist was probably a pelitic sediment; the more massive rock contains relict pyroclastic fragments that suggest origin from a tuff.

The mica schist contains segregation bands of clear, granoblastic quartz and clouded, untwinned albite alternating with layers of white mica. The mica contains an average of 2 weight percent Na_2O (phengite). The micaceous bands include fine stringers and veins of iron oxides and discontinuous layers of graphite and chlorite. Pretectonic garnet and sphene are broken and stretched along axial planes. The garnets are small, corroded and embayed by quartz, jacketed by a thin rim of chlorite, and restricted to Al-rich quartz-albite layers. They are somewhat enriched in MnO (4 to 7 weight percent; table 4.2). Epidote has a high content of Al_2O_3 (table 4.2).

About 20 percent of the Bennett Creek outcrops are green tuffaceous schist. The schist contains chlorite, quartz, albite, epidote, and about 10 percent blue-green amphibole. Crystalloblasts of epidote commonly cluster around amphiboles. Sphene, paragonite, and apatite are accessory minerals.

The blue-green amphibole has prismatic basal sections that are light straw yellow in the alpha optical direction and purplish blue in the beta direction. Elongate grains parallel to the (001) plane are light greenish yellow to light green-blue in the gamma direction. Amphiboles are commonly bent, with broken segments rotated up to 35°.

Microprobe analyses of amphiboles from the Bennett Creek locality (table 4.1) indicate an average composition of $(NaCa)(Fe_2Mg_2Al)(Si_7Al)O_{22}(OH)_2$. This composition is similar to that of barroisites from the Ligurian Alps of Italy (Ernst, 1976) and the Sanbagawa II terrane of Japan (Toriumi, 1975). Extremes in composition are found at the core and rim. Core compositions are highly sodic, containing 4.7 weight percent Na_2O. The average core composition is $(Na_{1.4}Ca_{0.6})(Fe_2Mg_{2.2}Al_{0.8})(Si_{7.8}A_{l0.2})O_{22}(OH)_2$. This composition represents an intermediate solid solution of the glaucophane-hornblende series (Klein, 1969; Brown, 1974; Katagas, 1974) or winchite (Leake, 1968). Rim compositions are much less enriched in Na, with only 1.6 weight percent Na_2O. The average rim composition is $(Na_{0.4}Ca_{1.6})(Fe_{1.6}Mg_{0.4})(Si_{7.8}Al_{0.2})O_{22}(OH)_2$. Al^{IV} is absent in cores but enriched in rims. The rim composition of amphiboles in the schists of the Bennett Creek area resembles that of a sodic actinolite. Amphibole compositions suggest formation of cores at high pressures and low temperatures approaching or at blueschist-facies conditions. According to Brown's (1977) plot of NaM_4 versus Al^{IV} for calcic amphiboles, the schists of the Bennett Creek area were initially metamorphosed at 6 to 7 kb at relatively low temperatures (possibly 350°C) and later experienced conditions of 4 to 5 kb at slightly increased temperatures (possibly 400°C).

The compositions of other minerals support these conditions. Garnet is zoned from cores rich in MnO, suggesting low temperatures, to rims with less MnO, indicating increasing temperatures (Miyashiro, 1953). Phengitic micas are characteristic of high-pressure terranes in blueschist and lower greenschist facies (Velde, 1965).

ALDRICH MOUNTAINS (SERPENTINITE-MATRIX) MELANGE AND MOUNT VERNON AREA

Extensive serpentinite-matrix melanges occur across more than 1,000 km^2 in east-central Oregon south and southwest of the Greenhorn Mountains (fig. 4.1). They include serpentinite-matrix melange of Miller Mountain, west of the Canyon Mountain Complex (Brown and Thayer, 1966), and melange south of Mount Vernon, collectively and informally termed the Aldrich Mountains (serpentinite-matrix) melange by Carpenter and Walker (1992). Similar melange is found near the small community of Antone. The components of these serpentinite-matrix melanges include chert, limestone, greenstone of both tholeiitic and calc-alkaline composition, metagabbro, peridotite, and a variety of metamorphic rocks, including amphibolites. Metamorphic clasts in the Aldrich Mountains melange include epidote and garnet amphibolites with schistose fabrics, and greenstones in lower greenschist facies (Carpenter and Walker, 1992). The amphiboles in the amphibolites are blue-green barroisites to winchites or brown hornblende. Exchange thermometry data and amphibole Al^{IV}/Si ratios indicate that epidote amphibolites with blue-green barroisitic hornblende formed at temperatures of 550 to 650°C and pressures just below 5 kb, whereas garnet amphibolites with brown hornblendes formed at temperatures above 700°C and pressures of about 4 kb (Carpenter and Walker, 1992).

The Aldrich Mountains melange also contains schists not reported in Carpenter and Walker's (1992) work. These rocks are blue-gray schists exposed about 12 km south of Mount Vernon. They contain blue amphiboles with typical core compositions of $(Na_{1.4}Ca_{0.6})(Mg_{2.4}Fe_{0.6})(Al_{0.4}Fe_{1.6})(Al_{0.3}Si_{7.7})O_{22}(OH)_2$. These amphibole cores are high in Na_2O (5.5 weight percent) but low in Al^{IV}. They are chemically close to riebeckites, but have a pleochroic scheme and overall appearance more like those of glaucophane and crossite. Rim compositions of these blue amphiboles, and of small, euhedral amphiboles throughout the rock, are blue-green barroisite to winchite, with Na_2O of 3.5 to 4.5 weight percent and less Al^{IV} than the cores (table 4.1).

SCHISTOSE ROCKS OF MINE RIDGE

Schistose rocks at Mine Ridge (fig. 4.1) were mapped and described by Lowry (1968). They are described in some detail by Hooper and others (chap. 11, this volume). These rocks comprise a lithologically diverse assemblage of Permian to Triassic pelitic and mafic schists and minor chert included in or associated with serpentinite of probable Triassic age. The schistose rocks occur in serpentinite matrix and are exposed on the north and west sides of Mine Ridge as well as on low ridges about 5 mi south of Hereford (fig. 4.1).

Lowry (1968) obtained K-Ar whole-rock ages of 142 to 150 Ma for the Mine Ridge rocks. He attributed this relatively young age to the contact metamorphic effects of a nearby pluton (Grouse Creek pluton) that he believed to be Jurassic in age. However, recent work on this intrusion has shown that it is an epizonal body 33 to 36 Ma in age (Houseman, 1983). No contact effects are evident in the Mine Ridge rocks. Therefore, the 142- to 150-Ma age determination must be due to a factor other than contact metamorphism, and may reflect Ar loss from the Paleozoic to Triassic rocks heated to low temperatures by the adjacent intrusion. Alternatively, it may reflect a real, relatively young age of rocks entrained in a long-lived, high-shear-stress subduction-zone environment.

Mica schists contain alternating bands of quartz-albite and lenticular laths of chlorite cut by fine strings of graphite. Albite porphyroblasts are twinned and deformed. Blue to light-blue-green actinolite is also bent and fractured. Epidote is restricted to mafic-rich bands and is Al-rich (table 4.2). Small aggregates of green biotite were the last minerals to form.

Mafic amphibole schists contain coarse amphiboles with pleochroic colors ranging from blue to blue-green in the gamma direction and from blue to straw-yellow in the beta direction. These amphiboles contain inclusions of clear epidote, have rims altered to actinolite and chlorite, and are deformed. White mica is rare and phengitic and occurs as small, isolated fibrous crystals. Granular patches of small green biotite are found within interstitial chlorite.

Amphiboles from mica schists and mafic schists have significantly different compositions (table 4.1). Those from mica schists are intermediate between actinolite and hornblende, but are best characterized as actinolite because of generally low Al content and high Na content (fig. 4.3). The average formula is $(Na_{0.3}Ca_{1.7})(Mg_{2.7}Fe_{1.8}Al_{0.5})Si_8O_{22}(OH)_2$. The composition of these amphiboles is closest to that of barroisites reported from the Sanbagawa III terrane by Toriumi (1975)and Ernst and others (1970). On a diagram of NaM_4 versus Al^{IV} (after Brown, 1977), they plot in the same field as Sanbagawa barroisites, suggesting a pressure range of 5 to 6 kb (fig. 4.3). The complete buffering assemblage is present in the mafic amphibole schists, and thus this pressure may represent a maximum.

SCHISTOSE ROCKS OF RHEA CREEK

Schistose rocks associated with serpentine and metagabbro are exposed in a northeast-trending belt

of pre-Tertiary outcrops approximately 30 km southeast of Heppner, Oreg., along Rhea Creek and near Copple Creek (fig. 4.1). These metasedimentary rocks include phyllite, pelitic (mica) schists, graphite schists, amphibolite, biotite gneiss, marble, and metachert (quartzite) (Shorey, 1976). The schistose rocks of Rhea Creek are complexly deformed, containing evidence for at least two deformational events. In their area of exposure, these rocks seem to be interlayered with marbles and quartzites in coherent stratigraphic order. Similar and probably related schists are exposed along U.S. Highway 395 approximately 50 km south-southwest of Pendleton.

The mineral assemblages of the Rhea Creek metasedimentary rocks indicate high-grade-greenschist- (Shorey, 1976) to amphibolite-facies metamorphism. Pelitic schists contain varying amounts of biotite, hornblende, quartz, plagioclase (oligoclase), muscovite, almandine garnet, tourmaline, zircon, and carbonate minerals. Amphiboles in the mafic schists and amphibolites are hornblendes with 0.9 to 1.1 weight percent Na_2O. The average composition is $(Na_{0.3}Ca_{1.7})(Fe_{2.4}Mg_{1.7}Al)(Si_6Al_2)O_{22}(OH)_2$. Compositional zoning is not evident. A plot of NaM_4 versus Al^{IV} suggests metamorphism at 3 to 4 kb (fig. 4.3).

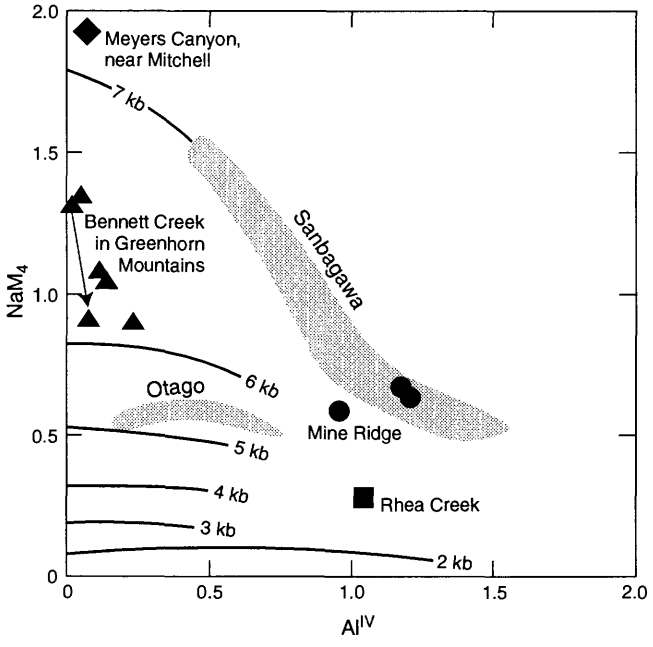

FIGURE 4.3.—NaM_4 (Na in M_4 sites) versus Al^{IV} (Al in tetrahedrally coordinated sites) for amphiboles from four eastern Oregon localities: Meyers Canyon, Bennett Creek, Mine Ridge, and Rhea Creek. Shaded areas show fields for amphiboles from the Sanbagawa terrane of Japan (Toriumi, 1975; Ernst and others, 1970) and from Otago, New Zealand (Brown, 1974). Pressures in kilobars (kb) as determined by Brown (1977). Arrow connects core (upper triangle) and rim (lower triangle) compositions in single amphibole from Bennett Creek area.

Schists that have a greater percentage of quartz, feldspar, and especially graphite contain a blue gruneriite rather than hornblende (table 4.1). The grunerite's average formula is $Ca_{0.1}(Fe_3Mg_4)Si_8O_{22}(OH)_2$. The uncharacteristic pleochroism—blue in the alpha direction and clear in the gamma direction—may be due to the extremely reduced character of the iron in the graphite schists. The blue color is more intense in amphiboles within graphite concentrations. Some of the Rhea Creek rocks are blue to steel-blue in outcrop because of the combination of graphite, muscovite, and blue gruneriite. Tourmalines in these rocks are also bluish, primarily because of the reduced iron.

Several factors suggest that the schistose rocks of Rhea Creek were initially formed by high-pressure, low-temperature metamorphism. The rocks occur along regional strike of the blueschists near Mitchell. Their fabric, deformational history, and lithic types are similar to those of the Mitchell rocks. They are associated with and probably enclosed by serpentinite-matrix melange. And contact metamorphism and metasomatism by adjacent plutons may have produced the mineralogy now observed.

However, despite extensive field, petrographic, and microprobe investigation, no relict high-pressure, low-temperature (blueschist-facies) minerals have been found. Thus, the correlation of the schistose rocks along Rhea Creek with the schistose rocks near Mitchell is very tentative, and the Rhea Creek rocks may have an entirely different origin or late history.

DISCUSSION

The schistose rocks at four localities examined in this study (Meyers Canyon near Mitchell, Bennett Creek in the Greenhorn Mountains, the Mount Vernon area, and Mine Ridge) have similar metamorphic histories: initial high-pressure metamorphism followed by deformation and a second metamorphism at higher temperatures and lower pressures. At Mitchell, metamorphic conditions remained at blueschist facies. Eastward, the rocks of Bennett Creek, the Mount Vernon area (Aldrich Mountains melange), and Mine Ridge suggest lower initial pressures and higher initial temperatures, with increasing temperatures and decreasing pressures through time. At Bennett Creek, schists underwent metamorphism at pressures near 6 kb, followed by greenschist-facies metamorphism. The Mine Ridge rocks initially underwent lower-greenschist-facies metamorphism at approximately 5 kb, followed by upper-greenschist-facies to amphibolite-facies metamorphism.

The schists most likely formed initially in a subduction-zone environment. The absence of glaucophane in most blue-amphibole-bearing schists of the

Baker terrane may indicate that subduction associated with these rocks was rapid and (or) that shear stresses were high. Where shear stresses exceed 100 megapascals (MPa) and subduction rates are faster than 10 cm/yr, amphibolite-facies metamorphism will occur (Peacock, 1992). Stability of glaucophane, whether epidote or lawsonite subfacies, requires either slow subduction and high shear stress or rapid subduction and low shear stress (Peacock, 1992).

A possible model for the formation of the schistose rocks of the Baker terrane would associate these rocks with subduction-zone metamorphism in a rapidly moving, high-shear-stress environment. Variations in core compositions of blue amphiboles across the terrane could reflect variations in subduction rates through time and space, variations in shear stress within the subduction zone, and (or) variations in the depth and conditions of subduction and accretion. Amphibolites of the Aldrich Mountains melange assigned to a "dynamothermal aureole" by Carpenter and Walker (1992), as well as amphibolites at Mine Ridge (Hooper and others, chap. 11, this volume) and amphibolite metagabbro in the Greenhorn Mountains may have been generated along shear boundaries within the same subduction zone by mechanisms elucidated by Peacock (1987). A separate episode of thrusting and tectonism may have affected these rocks, but is not required for their formation.

The later metamorphism of the schists in the Baker terrane—at higher temperatures and lower pressures—seems linked to the continuing history of the Blue Mountains island arc. The greenschist-facies rims of amphiboles and the rarity of blueschist-facies minerals indicate that higher temperatures and lower pressures affected the schistose rocks. Although the higher temperature and lower pressure minerals may simply indicate that these rocks were "stalled" under greenschist conditions, the deformed fabric of these rocks, including the later amphiboles, suggests that the higher temperature processes were dynamic.

Additional work, including dating of metamorphic episodes, fine-tuning of metamorphic petrology, use of exchange thermometry to calculate equilibrium temperatures (difficult for the early episodes), and structural studies are needed to further unravel the history of these rocks. In turn, this understanding is needed for a better understanding of the history of the Baker terrane.

CONCLUSIONS

The principal conclusions of this study are as follows:

(1) Most schistose rocks in the Baker terrane associated with serpentinite-matrix melange underwent initial blueschist- or near-blueschist-facies metamorphism. Later metamorphism occurred at higher temperatures and lower pressures.

(2) The schists were most likely initially produced in a subduction-zone environment and were incorporated in rising serpentinite diapirs.

(3) The lack of true glaucophane amphiboles in the schists east of Mitchell may indicate rapid subduction (greater than 10 cm/yr) and (or) high shear stress in the subduction zone.

(4) The temperature and intensity of continuing metamorphism that affected these rocks generally increased eastward across the Baker terrane.

(5) Metamorphism dated at about 255 to 268 Ma by Carpenter and Walker (1992) is possibly related to reversal of subduction-zone polarity or inception of a new subduction-zone, or to another process with high ductile shear. The blueschists at Mitchell (220 Ma; Hotz and others, 1977) did not experience this event and may be related instead to Triassic east-facing subduction (Vallier, 1992). The relevance of the 142- to 150-Ma event recorded in the schistose rocks of Mine Ridge (Lowry, 1968) is unclear.

(6) The schists of the Rhea Creek area are not clearly related to the other schists. However, factors such as their structure, location, and association suggest that they were initially high-pressure schists and may have an origin and history similar to those of the other schists in the Baker terrane, particularly the schists exposed near Mitchell.

REFERENCES CITED

Bishop, E.M., 1988, Igneous petrology of the Baker melange terrane and the Canyon Mountain complex, eastern Oregon: Geological Society of America Abstracts with Programs, v. 20, p. 407.

Brown, C.E., and Thayer, T.P., 1966, Geologic map of the Canyon City quadrangle, northeastern Oregon: U.S. Geological Survey Miscellaneous Geological Investigations Map I–477, scale 1:250,000.

Brown, E.H., 1974, Comparison of the mineralogy and phase relations of blueschists from North Cascades, Washington, and greenschists from Otago, New Zealand: Geological Society of America Bulletin, v. 85, p. 333-344.

———1977, The crossite content of Ca amphibole as a guide to the pressure of metamorphism: Journal of Petrology, v. 18, p. 53-72.

Carpenter, P.S., and Walker, N.W., 1992, Origin and tectonic significance of the Aldrich Mountains serpentinite matrix melange: Tectonics, v. 11, p. 690-708.

Coleman, R.G., and Papike, J.J., 1968, Alkali amphiboles from the blueschists of Cazadero, California: Journal of Petrology, v. 9, p. 105-122.

Dickinson, W.R., 1979, Mesozoic fore-arc basin in central Oregon: Geology, v. 7, p. 166-170.

Ernst, W.G., 1968, Amphiboles: New York, Springer-Verlag, 125 p.

———1976, Mineral chemistry of eclogite and related rocks from the Voltri group, western Liguria, Italy: Schweizerische Min-

eralogische und Petrographische Mitteilungen, v. 56, p. 293-343.

Ernst, W.G., Seki, Y., Onuki, H., and Gilbert, M.C., 1970, Comparative study of low-grade metamorphism in the California Coast Ranges and the outer metamorphic belt of Japan: Geological Society of America Memoir 124, 276 p.

Hotz, P.E., Lanphere, M.A., and Swanson, D.A., 1977, Triassic blueschist from northern California and north-central Oregon: Geology, v. 5, p. 659-663.

Houseman, M.D., 1983, Petrology and alteration of the Grouse Creek granodiorite porphyry: Pullman, Washington State University, M.S. thesis, 166 p.

Katagas, C., 1974, Alkali amphiboles intermediate between actinolite and riebeckite: Contributions to Mineralogy and Petrology, v. 46, p. 257-264.

Kays, M.A., Bishop, E.M., Walker, N.M., and Blackwell, D.L., 1988, Sodic amphibole-bearing schistose rocks of the Baker terrane: Geological Society of America Abstracts with Programs, v. 20, p. 423.

Klein, C., 1969, Two amphibole assemblage in the system actinolite-hornblende-glaucophane: American Mineralogist, v. 54, p. 212-237.

Leake, B., 1968, Classification of amphiboles: American Mineralogist, v. 63, p. 1023-1052.

Liou, J.C., Ho, C.O., and Ven, T.P., 1975, Petrology of some glaucophane schists and related rocks from Taiwan: Journal of Petrology, v. 16, p. 80-109.

Lowry, W.D., 1968, Geology of the Ironside, Oregon, quadrangle: Oregon Department of Geology and Mineral Industries Open File Report.

Miyashiro, A., 1953, Calcium-poor garnet in relation to metamorphism: Geochimica et Cosmochimica Acta, v. 4, p. 179-208.

Mullen, E.D., 1979a, Geology of the Greenhorn Mountains, northeastern Oregon: Corvallis, Oregon State University, M.S. thesis, 372 p.

———1979b, Temperature-pressure progression in high-pressure Permo-Triassic rocks of northeast Oregon: Eos (Transactions, American Geophysical Union), v. 51, p. 70.

———1985, Petrologic character of Permian and Triassic greenstones from the melange terrane of eastern Oregon and their implications for terrane origin: Geology, v. 13, p. 131-134.

Peacock, S.M., 1987, Creation and preservation of subduction-related inverted metamorphic gradient: Journal of Geophysical Research, v. 92, p. 12,763-12,781.

———1992, Blueschist-facies metamorphism, shear heating, and P-T-t paths in subduction shear zones: Journal of Geophysical Research, v. 97, p. 17,693-17,708.

Shorey, E.F., 1976, Geology of part of southern Morrow County, northeast Oregon: Corvallis, Oregon State University, M.S. thesis, 131 p.

Silberling, N.J., and Jones, D.L., 1984, Lithotectonic terrane maps of the North American Cordillera: U.S. Geological Survey Open File Report 84-523, 43 p.

Swanson, D.A., 1969, Lawsonite blueschist from north-central Oregon: U.S. Geological Survey Professional Paper 650-B, p. B8-B11.

Thayer, T.P., 1963, The Canyon Mountain Complex, Oregon, and the mafic magma stem: U.S. Geological Survey Professional Paper 475-C, p. C82-C85.

Toriumi, Mitsuhiro, 1975, Petrological study of the Sambagawa metamorphic rocks—the Kanto Mountains, central Japan: Tokyo, The University Museum, The University of Tokyo, 99 p.

Vallier, T.L., 1992, Late Triassic change in convergence direction, Blue Mountains island arc, Oregon and Washington: Geological Society of America Abstracts with Programs, v. 24, p. 88.

Vallier, T.L., and Brooks, H.C., 1986, Paleozoic and Mesozoic faunas of the Blue Mountains province—A review of their geologic implications and comments on papers in the volume, *in* Vallier, T.L., and Brooks, H.C., eds., Geology of the Blue Mountains region of Oregon, Idaho, and Washington—Geologic implications of Paleozoic and Mesozoic paleontology and biostratigraphy, Blue Mountains province, Oregon and Idaho: U.S. Geological Survey Professional Paper 1435, p. 1-7.

Vallier, T.L., Brooks, H.C., and Thayer, T.P., 1977, Paleozoic rocks in eastern Oregon and western Idaho, *in* Stewart, J.H., Stevens, C.H., and Fritsche, A.E., eds., Paleozoic paleogeography of the Western United States (Pacific Coast Paleogeography Symposium 1): Los Angeles, Society of Economic Paleontologists and Mineralogists, Pacific Section, p. 455-466.

Velde, B., 1965, Phengitic micas—Synthesis, stability, and occurrence: American Journal of Science, v. 263, p. 886-913.

5. MAFIC AND ULTRAMAFIC ROCKS OF THE BAKER TERRANE, EASTERN OREGON, AND THEIR IMPLICATIONS FOR TERRANE ORIGIN

By ELLEN M. BISHOP[1]

CONTENTS

	Page
Abstract	221
Introduction	221
Acknowledgments	223
Canyon Mountain Complex	223
Tectonite peridotite unit	223
Transition zone: Layered peridotites and gabbros unit	224
Gabbro units	227
Relations among gabbro units	229
Late intrusive gabbro: The zone of infiltration	229
Origin of the zone of infiltration	230
Migmatitic and recrystallized gabbro: Zone of plagiogranite genesis	231
Origin and significance of the migmatitic zone: Generation of plagiogranite	233
Geochemistry	236
Origin and tectonic setting	237
Other mafic and ultramafic components of the Baker terrane	238
Implications for the origin of the Baker terrane	243
References cited	244

ABSTRACT

The Baker terrane is a disordered assemblage of Paleozoic and Triassic metaigneous and metasedimentary rocks incorporated in serpentinite-matrix melange that occurs across more than 10,000 km^2 of eastern Oregon. Serpentinites, peridotites, gabbros, metagabbros, and volcanic greenstones are substantial components. Along with the Canyon Mountain Complex, these rocks provide petrologic and geochemical clues to the nature and origin of the Baker terrane and its relation to other eastern Oregon terranes of similar age.

The Permian Canyon Mountain Complex is the only coherent ophiolite associated with the Baker terrane. Its petrology and geochemistry suggest an island-arc (arc-tholeiite to calc-alkaline) affinity. The Canyon Mountain Complex contains two features not reported in ophiolites: gabbros that infiltrated into the tectonite peridotite, and well-defined migmatitic zones of partial melting and recrystallization of upper, hydrothermally altered gabbros that generated plagiogranite. These features suggest that the late- or post-magmatic history of the Canyon Mountain Complex included shear, pressure release, minor intrusions, and localized partial melting that produced the Canyon Mountain plagiogranites and keratophyres.

Mafic volcanic and plutonic rocks of lower greenschist to amphibolite facies occur as knockers and tectonic slivers throughout the Baker terrane. The mineralogy and geochemistry of the volcanic rocks indicate formation in a variety of tectonic settings, including midocean ridge, island arc, and rift or transform. Many plutonic rocks of the Baker terrane have characteristics of normal midocean-ridge basalt (NMORB); others have mineralogy and compositions similar to those of the arc-related Canyon Mountain Complex.

A fore arc and (or) erosive high-shear-stress subduction zone are the most likely petrotectonic settings for amalgamation of the igneous components of the Baker terrane.

INTRODUCTION

The Paleozoic and Triassic Baker terrane of eastern Oregon is a disordered assemblage of basaltic greenstone, silicic greenstone, argillite, chert, graywacke, conglomerate, Tethyan and North American limestone of Devonian to Triassic age, metadiorite, gabbro and metagabbro, and peridotite. These components, as well as amphibolites and high- to moderate-pressure schists (Bishop, 1988; Bishop, chap. 4, this volume; Hooper and others, chap. 11, this volume), are incorporated in serpentinite-matrix melanges throughout the terrane. Because of the lithologic and metamorphic heterogeneity of terrane components, the nature and origin of the Baker terrane have been major problems of eastern Oregon pre-Tertiary geology.

The Baker terrane is associated in space and time with the Wallowa terrane, the Olds Ferry terrane, the Grindstone terrane, and the Izee terrane, as delineated by Silberling and Jones (1984; fig. 5.1). These are generally considered to be arc-related tectonostratigraphic packages, collectively referred to as the Blue Mountains island arc (Vallier, chap. 3, this volume). The Wallowa terrane is related to Permian and Triassic arc volcanism. The Olds Ferry terrane is

[1] 52040 Highway 203, Union, OR 97883

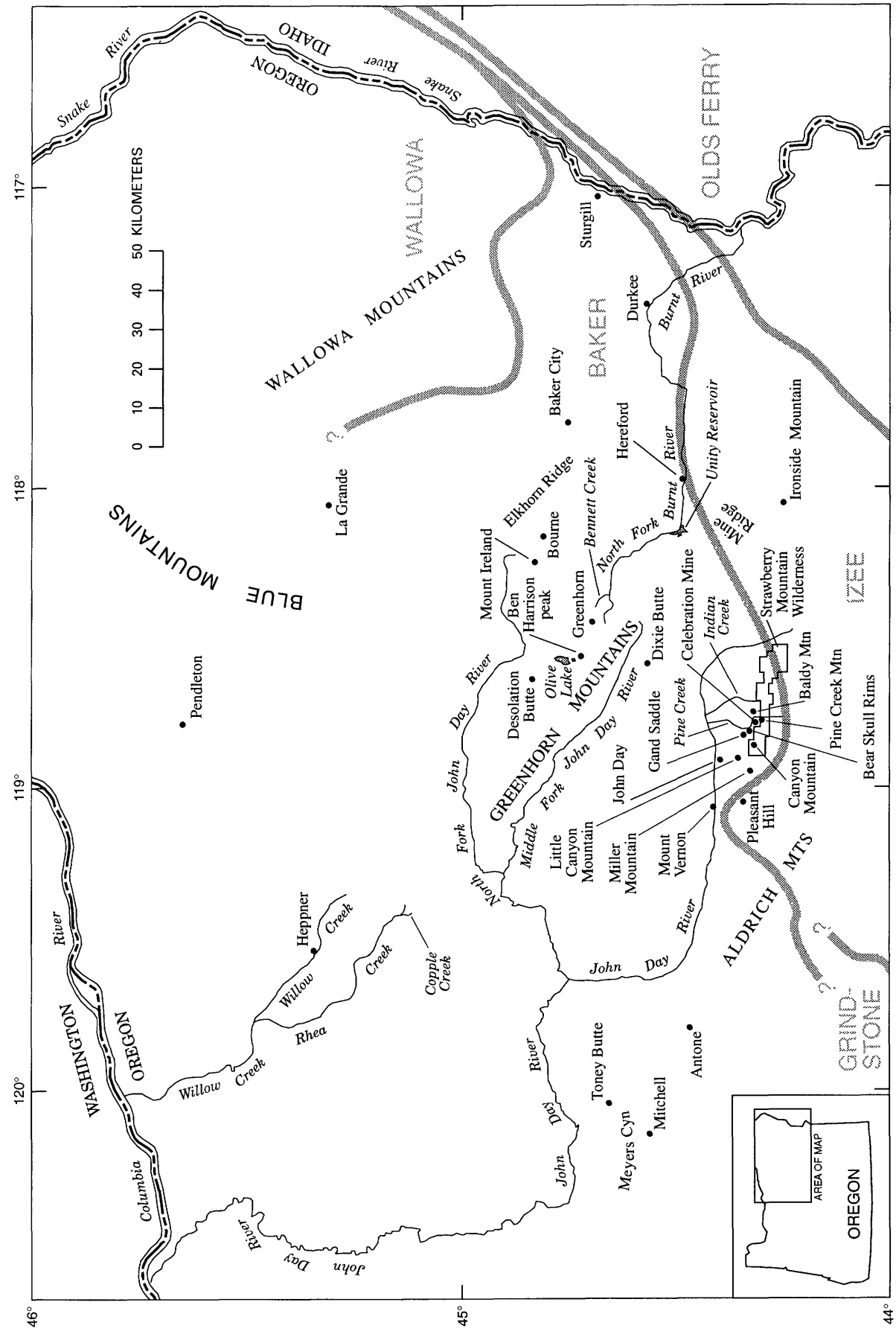

FIGURE 5.1.—Location map showing region of study and places mentioned in chapters 4 and 5 (Bishop this volume). Broad gray lines are terrane boundaries (approximate) as modified from Silberling and Jones (1984) by Vallier (chap. 3, this volume); queried where location uncertain.

a remnant of Late Triassic arc volcanism and sedimentation. The Grindstone terrane may represent an accretionary wedge (Blome and Nestell, 1992), and the Izee terrane records Triassic and Jurassic postmagmatic sedimentation in a fore-arc or related environment (Dickinson, 1979).

The Baker terrane has been interpreted as an oceanic basin (Brooks, 1979), a melange (Dickinson, 1979), and a relatively coherent fore arc associated with the magmatically and tectonically active Wallowa arc (Mullen, 1983a). Its rocks are substantially more deformed and older than those of the Izee terrane to the south, and can be distinguished from those of the Grindstone terrane by the preponderance in the Baker terrane of metaigneous and schistose metamorphic components in a largely serpentinite matrix. The Baker terrane sedimentary package includes voluminous cherts of the Elkhorn Ridge Argillite and sheared siliceous sedimentary rocks of the Burnt River Schist. Both are considered pelagic units, although they contain volcaniclastic sedimentary rocks and conglomerates.

Evaluation of the petrology, geochemistry, and character of the ultramafic and mafic rocks (for example, peridotite, gabbro, and volcanic greenstone) is one route to a better understanding of the Baker terrane. This paper discusses the nature of mafic and ultramafic igneous components and their implications for terrane origin, beginning with the largest and most complete component—the Canyon Mountain Complex.

ACKNOWLEDGMENTS

This work was funded in part by Geological Society of America Penrose grants 2271-77 and 2887-81, the Bowes Mining Co., and the Oregon Department of Geology and Mineral Industries. Discussions with H.C. Brooks, J.W. Hawkins, T.P. Thayer, and T.L. Vallier were helpful. The manuscript has benefited from reviews by Clifford Hopson, Cynthia Evans, W.P. Leeman, James Evans, and Lisanne Pearcy.

CANYON MOUNTAIN COMPLEX

The Canyon Mountain Complex is a 4-km-thick Permian sequence of ultramafic rocks, gabbros, plagiogranites, and keratophyres that is exposed over more than 150 km^2 in the Strawberry Mountain Wilderness, just south of John Day, Oreg. (figs. 5.1, 5.2). It has been dated at 278 to 261 Ma by K-Ar, U-Pb, and $^{40}Ar/^{39}Ar$ methods (Gerlach, and others, 1988; Leeman and others, chap. 1, this volume). Isotropic and layered gabbros have yielded Nd isochron ages of 267 to 274 Ma (Gerlach and others, 1988).

The Canyon Mountain Complex is an important component of the Baker terrane because it is a nearly complete ophiolite sequence and because it contains some features rarely reported from similar packages of oceanic or arc-related rocks. On the basis of chemistry and lithic types, previous workers (Thayer, 1977; Himmelberg and Loney, 1980; Gerlach, and others, 1981; Mullen, 1983a) have considered the Canyon Mountain Complex to have formed in an island-arc environment. Previous investigators examined the economic geology (Thayer, 1976), the structure (Avé Lallemant, 1976), the origin of the plagiogranite (Gerlach, 1980), the petrology of the peridotite and gabbro (Himmelberg and Loney, 1980; Mullen, 1983a), the petrogenesis of the gabbro units (Mullen, 1983b), and the origin of the layered igneous rocks (Pearcy, 1987, 1991), and have made detailed geochemical evaluations (Leeman and others, chap. 1, this volume).

TECTONITE PERIDOTITE UNIT

Tectonite peridotite constitutes the lowermost unit of the Canyon Mountain Complex. It grades upward from glossy green sheared serpentinite at the base to relatively fresh rock that is less than 10-percent serpentinized in some locations. Its overall thickness is approximately 1.5 km. The principal lithic type (>90 percent) is harzburgite, with olivine the dominant mineral phase (table 5.1). Mineral compositions are quite uniform throughout the tectonite peridotite (table 5.2). Elongated chrome spinel defines foliation in the harzburgite outcrops.

Lherzolite is rare in the Canyon Mountain Complex and constitutes less than 5 percent of the tectonite peridotite unit. It is in gradational contact with harzburgite and is most voluminous in the central part of the unit where gabbro dikes and veins are abundant.

Dunite most commonly occurs in lenses and elongate bodies from 1 to 100 m in length, but also occurs as veins, dikes, and small irregular blobs. Contacts of dunite with harzburgite are gradational. Foliation and structure defined in outcrop by chromite are parallel with structure in adjacent harzburgite. This finding supports a metasomatic origin for the dunite of the Canyon Mountain Complex as suggested by Dungan and Avé Lallemant (1977).

Dikes and sills of websterite, clinopyroxenite, and orthopyroxenite occur throughout the tectonite peridotite unit. Most are less than 20 cm wide. Several generations can be distinguished on the basis of crosscutting relations. Early dikes, commonly composed of clinopyroxene-rich websterite, are deformed conformably with the host peridotite. These dikes are crosscut by later, undeformed websterite or orthopyroxenite dikes. The adjacent peridotite is depleted in pyroxene within 2 to

10 cm of the early dikes. This relationship suggests that here, as well as in other ophiolites, the early websterite dikes are segregations of melt generated locally within the harzburgite (Boudier and Coleman, 1981; Nicolas and Jackson, 1982).

Podiform chromitite bodies occur throughout the tectonite peridotite unit. They are usually oblong to lensoidal in shape and range from less than 1 m to slightly more that 60 m in length. There are two different spinel compositions (table 5.3). Chrome-rich, aluminum-poor spinel occurs in chromitite pods that do not contain clinopyroxene and are generally deep within the tectonite peridotite unit, whereas more aluminum-rich chromite is found in chromitites that do contain clinopyroxene and are near the top of the tectonite peridotite unit. The two spinel compositions may be produced by fractionation, but the absence of intermediate compositions in the Canyon Mountain Complex suggests separate sources or interaction of Al-rich spinels with gabbroic magma (fig. 5.3).

TRANSITION ZONE: LAYERED PERIDOTITES AND GABBROS UNIT

A substantial thickness of interlayered, tectonized peridotite and gabbro forms the transition from tectonite peridotite to overlying cumulate and isotropic

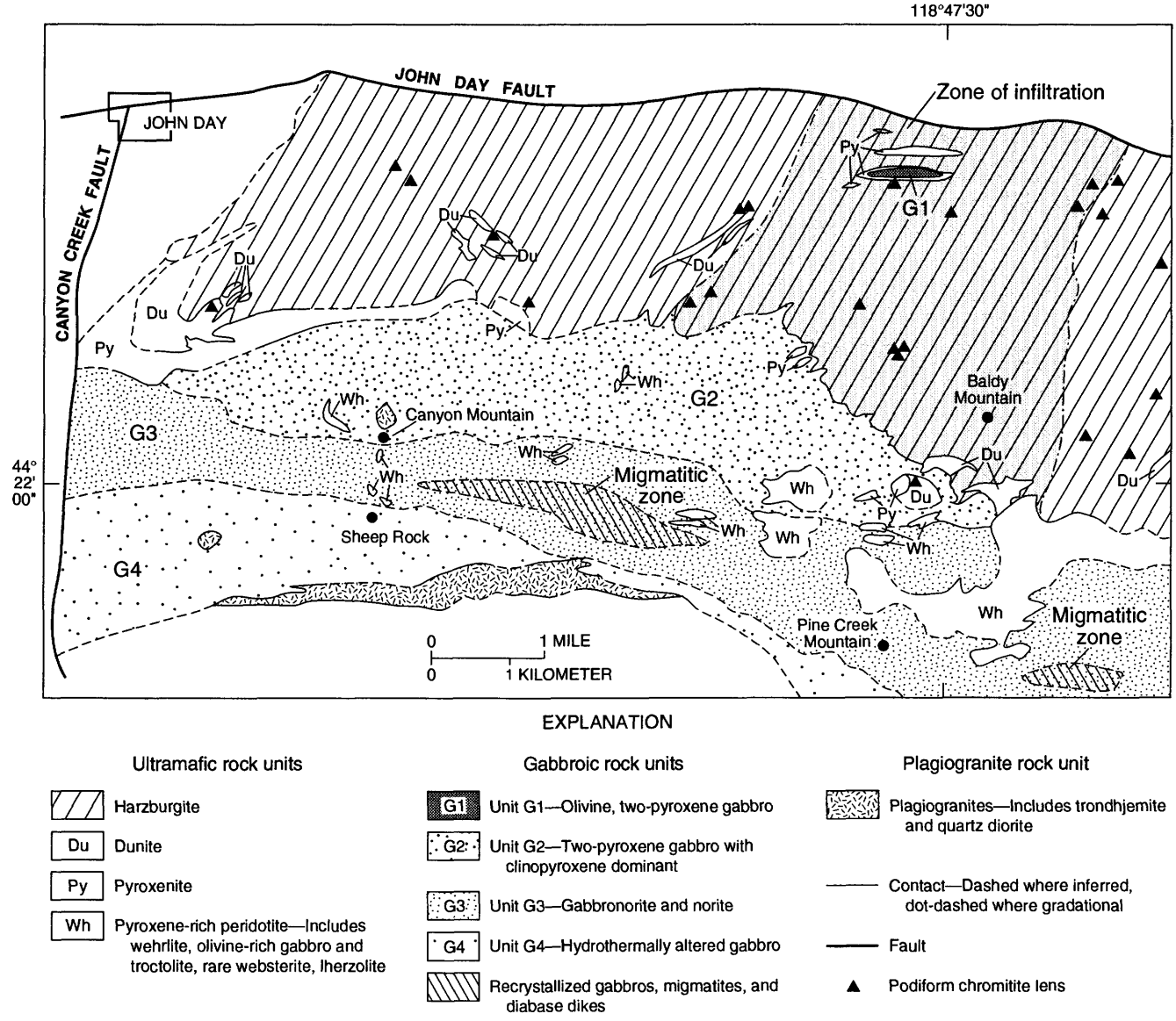

FIGURE 5.2.—Generalized map showing ultramafic, gabbroic, and plagiogranite rock units of the Canyon Mountain Complex. Scale is approximate.

TABLE 5.1.—*Modes of analyzed samples from the Canyon Mountain Complex*

[tr, trace; ---, not observed]

Sample	449A	563	664	579A	579B	110G	666	626	707	714
Lithic type	Harzburgite	Dunite	Wehrlite	Olivine websterite	Olivine gabbro	Gabbro dike	Unit G1 (gabbro)	Unit G2 (gabbro)	Unit G3 (gabbro)	Recrystallized gabbro
Olivine	39	78	7	15	---	1	12	---	---	---
Orthopyroxene	29	2	3	8	15	3	13	3	21	17
Clinopyroxene	2	---	87	61	20	29	47	32	20	15
Plagioclase	---	---	---	7	47	18	19	16	52	61
Hornblende	---	---	1	3	12	---	3	6	4	3
Actinolite	---	---	---	---	---	---	---	3	---	---
Chlorite	2	---	---	---	tr	28	---	13	2	2
Hydrogrossular	---	---	---	---	---	21	4	27	---	---
Serpentine	21	14	1	3	6	tr	1	---	---	---
Opaque minerals	6	6	1	2	tr	tr	1	---	tr	tr
Accessory minerals	1	---	---	1	---	---	---	---	1	tr
Total	100	100	100	100	100	100	100	100	100	100

TABLE 5.2.—*Compositions of silicate minerals from the tectonite peridotite unit of the Canyon Mountain Complex*

[FeO*=FeO+Fe_2O_3; ---, not applicable]

Sample	449A (harzburgite)					286 (lherzolite)					
Mineral	Olivine	Orthopyroxene		Clinopyroxene		Olivine		Orthopyroxene		Clinopyroxene	
Mineral grain	1	2	3	4	5	6	7	8	9	10	11
Major-element oxides (weight percent)											
SiO_2	42.02	58.30	57.66	53.15	54.36	40.34	40.33	57.11	56.24	53.22	53.25
TiO_2	.00	.10	.13	.29	.22	.00	.00	.10	.08	.10	.11
Al_2O_3	.00	1.19	1.18	1.99	1.97	.04	.01	2.05	1.75	2.28	2.38
FeO*	5.11	4.40	4.15	1.18	1.96	7.21	6.34	5.51	5.38	1.38	1.49
MnO	.02	.08	.07	.06	.08	.05	.07	.14	.07	.06	.03
MgO	52.17	35.34	35.33	17.34	17.38	52.20	52.58	34.47	35.22	17.44	16.98
CaO	.00	.47	.46	23.60	22.72	.00	.00	.46	.25	23.59	24.05
Na_2O	.00	.00	.00	.16	.34	.00	.00	.00	.00	.14	.19
Cr_2O_3	.04	.34	.46	1.03	1.14	.00	.00	.56	.47	.76	.80
NiO	.69	.07	.13	.08	.05	.45	.53	.09	.13	.11	.02
Total	100.05	100.26	99.57	98.88	100.19	100.29	99.92	100.50	99.58	99.10	99.30
Stoichiometry (number of ions per unit cell)[1]											
Si	0.995	1.985	1.978	1.946	1.963	0.978	0.978	1.954	1.942	1.944	1.930
Ti	.000	.003	.003	.008	.006	.000	.000	.002	.002	.002	.003
Al	.000	.048	.098	.086	.084	.000	.000	.080	.071	.098	.103
Fe	.110	.125	.119	.036	.059	.146	.128	.157	.155	.042	.045
Mn	.000	.002	.002	.002	.002	.000	.000	.004	.001	.001	.001
Mg	1.886	1.794	1.807	.947	.935	1.887	1.902	1.758	1.813	.950	.935
Ca	.000	.017	.017	.926	.879	.000	.000	.016	.009	.923	.951
Na	.000	.000	.000	.011	.024	.000	.000	.000	.001	.010	.013
Cr	.000	.009	.012	.030	.032	.000	.000	.015	.003	.021	.023
Ni	.080	.000	.004	.002	.001	.050	.050	.002	.003	.003	.000
Total	2.991	3.981	3.987	3.991	3.982	3.002	3.001	3.994	4.001	3.998	3.995
Relative proportions (percent)											
Fo	94.5	---	---	---	---	92.8	93.7	---	---	---	---
En[2]	---	93.5	93.8	---	---	---	---	93.4	92.1	---	---
Fs	---	---	---	2	3	---	---	---	---	2	1
En[3]	---	---	---	50	50	---	---	---	---	50	50
Wo	---	---	---	48	47	---	---	---	---	48	49

[1]Assuming 4 oxygen atoms per unit cell for olivine, 6 for orthopyroxene and clinopyroxene.
[2]Enstatite component of orthopyroxene.
[3]Enstatite component of clinopyroxene.

TABLE 5.3.—*Compositions of spinels from podiform chromitites, Canyon Mountain Complex*

[FeO*=FeO+Fe_2O_3]

Sample	410		74			82		149		169		667	
Mineral grain	1	2	1 Rim	1 Core	2	1	2	1	2	1	2	1	2
Major-element oxides (weight percent)													
SiO_2	0.10	0.13	0.10	0.20	0.12	0.13	0.04	0.07	0.09	0.12	0.06	0.07	0.01
Al_2O_3	13.21	12.60	14.00	13.67	13.71	13.38	13.84	18.24	17.90	28.49	27.13	28.75	28.21
TiO_2	.14	.14	.09	.01	.15	.10	.16	.75	.69	.29	.38	.36	.06
FeO*	14.27	14.75	14.57	14.28	13.78	14.82	14.71	17.27	17.67	16.65	17.19	14.46	12.81
MnO	.23	.18	.26	.24	.18	.24	.32	.21	.21	.16	.18	.20	.20
MgO	15.01	15.86	15.70	15.95	15.99	15.02	15.22	14.09	14.16	15.71	15.44	17.01	15.76
Cr_2O_3	56.27	56.13	55.24	55.79	54.81	53.23	55.72	48.49	48.36	37.25	37.39	38.09	37.16
NiO	.20	.22	.01	.01	.00	.12	.08	.18	.19	.09	.18	.21	.01
Total	99.43	100.01	99.97	100.15	98.74	97.04	100.09	99.30	99.27	98.76	97.95	99.15	94.22
Relative proportions (percent)													
Cr/(Cr+Al)	81.0	81.7	79.8	80.3	80.3	80.5	80.1	72.7	73.0	56.7	58.0	57.0	56.8
Mg/(Mg+Fe)	50.4	50.5	51.9	52.8	53.7	50.3	50.9	44.9	44.5	48.5	47.3	54.1	55.2

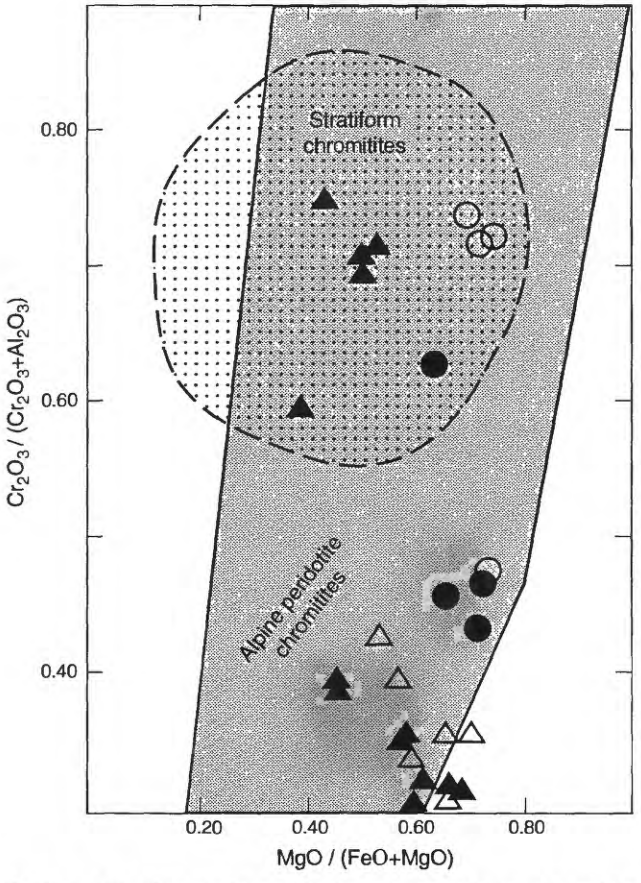

FIGURE 5.3.—Compositions of chrome spinels in chromitite bodies, Canyon Mountain Complex. Filled circles, spinels from chromitite bodies with clinopyroxene; open circles, spinels from chromitite bodies in harzburgite that contain no clinopyroxene; filled triangles, accessory spinels of layered peridotites of the transition zone; open triangles, accessory spinels of harzburgite.

gabbro. This transition unit is referred to as the layered peridotites and gabbros unit. The rocks are well exposed on sharp, barren ridges and constitute about 20 percent of the aerial exposure of the Canyon Mountain Complex. Their maximum thickness is less than 0.5 km.

Similar rocks in most ophiolite sequences are considered to be accumulations of early phases from fractional crystallization of basaltic magma. Such sequences are termed "metacumulates" by Coleman (1977). They achieve their distinctive textures and abrupt changes in composition through hypersolidus or subsolidus, metasomatic or metamorphic processes, including double diffusive convection (Irvine, 1980). Deformation at high-temperature, subsolidus conditions accounts for the glide twinning and other lattice defects common in minerals of such rocks.

The fabrics of the layered peridotites and gabbros of the Canyon Mountain Complex are dominantly deformed adcumulates, similar to other metacumulate sequences. Poikilitic textures are present, especially in the lower part of the unit. Diopside oikocrysts and the enclosed olivine are deformed. Layering is accentuated by deformation, especially in the gabbros.

The layered peridotites and gabbros unit shows no regularity in layer thickness or sequence. Layered sequences persist laterally over distances of only several tens of meters and cannot be traced from one ridge to the next. Harzburgite is absent. Clinopyroxene-rich peridotite constitutes about 70 percent of these rocks and is predominantly wehrlite. The wehrlite, with varying proportions of clinopyroxene and olivine, occurs in successions of layers whose thickness-

es vary from centimeters to several meters, and it constitutes about 70 percent of the layered peridotites and gabbros unit. Websterite, melagabbro, gabbro, troctolite, anorthosite, dunite, and rare lherzolite together constitute about 30 percent of the unit. Contacts between adjacent peridotite units are gradational over several centimeters. Contacts between gabbro and peridotite are generally sharp.

Although lithic types vary, mineral compositions are monotonously similar throughout the layered peridotites and gabbros unit (table 5.3). In the sequences examined along Celebration Ridge (a ridge that trends north from Pine Creek Mountain to Celebration Mine, fig. 5.1), there are only slight variations in mineral compositions, so lithic diversity is simply a function of different modal abundances.

Minerals are not compositionally zoned and are of nearly uniform composition throughout each layer (fig. 5.4). Olivine (Fo_{70-80}) is less Mg-rich than in the harzburgite, but exhibits ubiquitous deformation and twinning. Bronzitic orthopyroxene (En_{77-82}) commonly shows kink-banding as well as other evidence of deformation. Clinopyroxene is Ca-rich diopside, commonly with glide twins. Pearcy (1987, 1991) reports compositional ranges of approximately $Ca_{48}Mg_{45-48}Fe_{4-8}$ in wehrlite and websterite, and $Ca_{47-49}Mg_{44-45}Fe_{6-8}$ in gabbros of the layered peridotites and gabbros unit. Analyses of clinopyroxene for this investigation yielded similar compositions (table 5.4). Plagioclase of the gabbros, troctolites, and feldspathic wehrlites is extremely calcic (An_{92-97}) and typically has bent and (or) dislocated twins. In plagioclase-bearing peridotites the feldspar is rounded and interstitial, and commonly is rimmed by brown pargasitic amphibole.

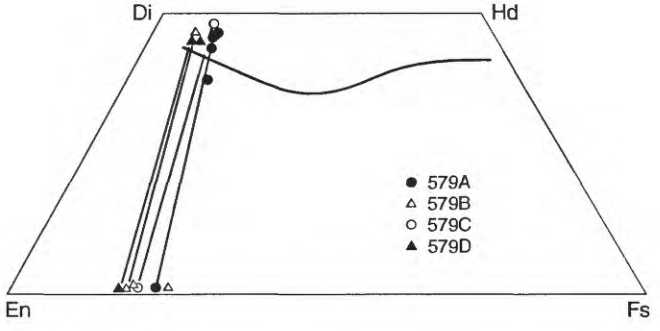

FIGURE 5.4.—Compositions of clinopyroxenes from four-layer sequence in layered peridotites and gabbros unit, which forms transition zone from tectonite peridotite to overlying cumulate and isotropic gabbro. Sample 579A is olivine melagabbro, 579B is websterite, 579C is olivine and plagioclase-bearing websterite, and 579D is olivine-bearing websterite. Di, diopside; En, enstatite; Fs, ferrosilite; Hd, hedenbergite. Lines connecting data points indicate pyroxenes from same sample; curve across top of diagram is Skaergaard pyroxene trend.

GABBRO UNITS

Gabbro constitutes approximately one-third of the Canyon Mountain Complex and can be divided into four units. Hydrothermal alteration has affected all units and to some degree obscures textures, mineral compositions, and geochemistry of the original rocks. The informal but mineralogically distinct gabbroic rock units recognized are G1, an olivine, two-pyroxene rock that occurs near the base of the harzburgite of the Canyon Mountain Complex and as dikes and sills within the harzburgite; G2, a two-pyroxene gabbro that overlies the layered peridotites and gabbros unit; G3, gabbronorite and norite that overly unit G2; and G4, hydrothermally altered gabbro (epidiorite) in which few original minerals remain.

Gabbro at the lowest stratigraphic level, unit G1, has the least evolved mineralogy and geochemistry. Unit G1 is exposed only as a 25-m-wide pod along Gwyn Creek (a tributary of Pine Creek whose source is on the northwest side of Baldy Mountain, fig. 5.1) within the lower part of the tectonite peridotite unit. Float of layered gabbro and wehrlite occur near, and apparently envelop, the isotropic gabbro in Gwyn Creek. Clinopyroxenite occurs between the gabbro and adjacent harzburgite. Unit G1 is an olivine, two-pyroxene gabbro with adcumulate to heteradcumulate textures. It displays subtle layering in its limited exposure at Gwyn Creek. Gabbro that is mineralogically and geochemically similar occurs as isotropic and layered gabbro dikes within the harzburgite (see section "Zone of Infiltration," below). In this gabbro unit, olivine (Fo_{85-89}) may be rimmed by clinopyroxene. Orthopyroxene (En_{80}) is interstitial to anhedral, with fine exsolution lamellae. The clinopyroxene is calcic augite; it encloses both olivine and orthopyroxene. Plagioclase (An_{92-85}) is subhedral, complexly twinned, and unzoned. Pargasitic hornblende replaces and rims mafic phases and some plagioclase.

Gabbro in which clinopyroxene is the dominant mafic phase occurs in the central and western parts of the Canyon Mountain Complex. This gabbro, unit G2, also called the gabbro of Bear Skull Rims, intrudes and overlies layered peridotites (layered peridotites and gabbros unit) near Gand Saddle (fig. 5.1).

Phase layering is common in unit G2 (fig. 5.5). In some locations, such as the northeast side of Bear Skull Rims, the layering is contorted. The absence of mineral deformation suggests that the contortion was caused by slumping or folding of layers prior to solidification. Pods and bands of melagabbro and clinopyroxene-rich peridotite are distributed throughout this unit and probably represent fragments of the layered peridotites and gabbros unit or local accumulations of mafic minerals resulting from the crystallization of the G2 gabbro unit.

TABLE 5.4.—*Compositions of silicate minerals from the upper part of the layered peridotites and gabbros unit of the Canyon Mountain Complex*

[FeO*=FeO+Fe_2O_3; ---, not applicable]

Mineral	Olivine		Orthopyroxene				Clinopyroxene				Plagioclase		
Sample	579A	579D	579A	579B	579C	579D	579A	579B	579C	579D	579A	579B	579C
Lithic type	Olivine websterite	Werhlite	Olivine websterite	Olivine gabbro	Metagabbro	Werhlite	Olivine websterite	Olivine gabbro	Metagabbro	Werhlite	Olivine websterite	Olivine gabbro	Metagabbro
Major-element oxides (weight percent)													
SiO_2	37.92	39.53	54.28	55.39	54.80	55.05	51.54	52.71	53.31	51.98	44.80	45.17	44.71
TiO_2	.00	.00	.16	.04	.00	.04	.56	.17	.15	.32	.00	.00	.00
Al_2O_3	.00	.00	2.25	1.80	2.32	2.26	3.81	2.54	2.92	2.97	36.11	35.52	36.32
FeO*	22.70	7.88	14.32	12.55	13.17	11.92	6.60	5.43	5.67	4.88	.30	.19	.20
MnO	.35	.26	.35	.24	.23	.24	.24	.08	.12	.09	.00	.00	.00
MgO	38.80	1.84	26.80	28.56	28.14	29.79	15.26	16.03	15.42	16.07	.02	.02	.02
CaO	.04	.04	.65	.80	.58	.63	21.00	22.01	22.04	22.08	18.71	19.21	18.99
Na_2O	.00	.01	.00	.00	.00	.00	.28	.16	.23	.19	.85	.66	.63
Cr_2O_3	.02	.00	.16	.11	.11	.22	.46	.15	.17	.46	.00	.00	.00
NiO	.21	.16	.12	.00	.00	.04	.04	.06	.00	.03	.00	.00	.00
Total	100.03	99.76	99.08	99.50	99.35	100.18	99.77	99.33	100.03	99.07	100.79	100.75	100.67
Stoichiometry (number of ions per unit cell)[1]													
Si	1.07	1.00	3.92	3.95	3.92	3.89	3.81	3.99	3.90	3.85	8.24	8.28	8.19
Ti	.00	.00	.01	.00	.00	.00	.03	.01	.01	.02	.00	.00	.00
Al	.00	.00	.19	.15	.20	.19	.33	.22	.25	.26	7.80	7.67	7.83
Fe	.50	.38	.87	.75	.78	.70	.41	.33	.35	.30	.05	.03	.08
Mn	.01	.33	.02	.01	.01	.01	.01	.00	.01	.01	.00	.00	.00
Mg	1.51	1.57	2.89	3.04	3.00	3.14	1.68	.00	.01	1.77	.00	.00	.00
Ca	.00	.00	.05	.06	.04	.05	1.66	1.74	1.73	1.75	3.67	3.77	3.70
Na	.00	.00	.00	.00	.00	.00	.04	.02	.03	.03	.30	.23	.22
Cr	.00	.00	.01	.01	.01	.00	.03	.01	.01	.03	.00	.00	.00
Ni	.01	.03	.01	.00	.00	.00	.00	.00	.00	.00	.00	.00	.00
Total	3.09	2.97	7.97	7.97	7.98	8.01	8.00	8.00	7.97	8.01	20.06	19.98	20.02
Relative proportions (percent)													
An	---	---	---	---	---	---	---	---	---	---	92	94	94
Fo	75	80	---	---	---	---	---	---	---	---	---	---	---
En[2]	---	---	77	80	79	82	---	---	---	---	---	---	---
Fs	---	---	---	---	---	---	11	8	9	8	---	---	---
En[3]	---	---	---	---	---	---	45	46	45	46	---	---	---
Wo	---	---	---	---	---	---	44	46	46	46	---	---	---

[1]Assuming 4 oxygen atoms per unit cell for olivine, 12 for orthopyroxene and clinopyroxene, and 32 for plagioclase.
[2]Enstatite component of orthopyroxene.
[3]Enstatite component of clinopyroxene.

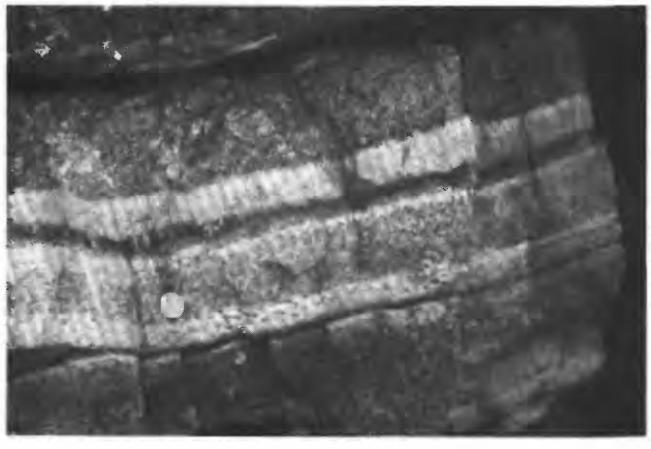

FIGURE 5.5.—Layering in unit G2 (gabbro of Bear Skull Rims). Coin is approximately 2 cm in diameter.

Two pyroxenes are commonly present and olivine is absent in the gabbro that forms unit G2. Clinopyroxene (calcic augite) is anhedral, and in deformed rocks may be pinched between grains of plagioclase. Orthopyroxene (En_{75-85}) is most abundant in layered rocks, seldom exceeds 10 modal percent, is subhedral to euhedral, and usually is altered to serpentine+chlorite+amphibole. Plagioclase (An_{70-75}) is unzoned and nearly always partly altered to chlorite+hydrogrossular.

The two-pyroxene gabbro that forms unit G2 grades upward into the more orthopyroxene-rich unit G3, also known informally as the gabbronorite of Pine Creek Mountain. Similar rocks extend east-west across most of the Canyon Mountain Complex. Most gabbros of unit G3 have heteradcumulate to adcumulate textures, and many display igneous lamination. The rocks are less deformed than those of the lower gabbro units; lattice defects in minerals are rare.

Olivine is absent in unit G3. Orthopyroxene is faintly pleochroic hypersthene (En_{65}). Clinopyroxene is augite. Pyroxenes are rimmed and replaced by late-magmatic to subsolidus pargasitic hornblende. Plagioclase (An_{60-65}) is unzoned. It is subhedral and lath-shaped in laminated gabbronorite, but anhedral in the uppermost, unlayered part of unit G3.

Gabbro that stratigraphically overlies unit G3 has been subjected to extensive hydrothermal alteration, and its original mineralogical and geochemical character is difficult to deduce. These rocks, which form unit G4, occupy the uppermost part of Canyon Mountain (fig. 5.1), which constitutes much of the western part of the Canyon Mountain Complex. Similar rocks are found on Little Canyon Mountain. This altered rock, strongly gabbroic in appearance, was termed "epidiorite" by Thayer (1972), meaning a hydrothermally altered rock in which chlorite and hornblende replace pyroxene, and plagioclase is largely altered to chlorite, hydrogrossular, and clays. Alteration of these rocks is so complete that igneous minerals cannot be identified, and geochemistry has been substantially changed from that of the original rock.

RELATIONS AMONG GABBRO UNITS

Lithologic, mineralogic, and stratigraphic relations in the gabbro units of the Canyon Mountain Complex support the origin of these rocks primarily by fractional crystallization of a single magma or as a rapidly intruded sequence of similar magmas. Although mineralogic units can be distinguished in the gabbro units of the Canyon Mountain Complex, their contacts are gradational and poorly defined; the lithic types progress upward from olivine gabbro to gabbro to gabbronorite, suggesting a fractionation sequence. Geochemical data support this interpretation. Although complex processes were undoubtedly involved in the generation and emplacement of the magma, field evidence supports the model of a single, fractionating magma chamber for the origin of the Canyon Mountain Complex.

LATE INTRUSIVE GABBRO: THE ZONE OF INFILTRATION

A 3.5-km-wide, northeast-trending zone of gabbroic veins and dikes, as well as feldspar-bearing harzburgite (fig. 5.6), occurs in the central part of the tectonite peridotite unit. It extends from the serpentinized base of the Canyon Mountain Complex upward to the layered peridotites and gabbros unit, and is 4 km wide. Unit G1, also called the gabbro Gwyn Creek, is included in this zone. The distribution and abundance of feldspar-bearing harzburgite and gabbroic dikes are remarkably symmetrical, changing from an outer subzone of feldspathic harzburgite and dikelets less than 1 cm wide (zone A), inward to a subzone of gabbroic dikelets 1 to 10 cm wide (zone B), inward to a subzone of gabbro dikes 10 cm or wider (zone C), and finally including some localities, such as the south face of Baldy Mountain, where gabbro dikes and pods occupy greater than 10 percent of the outcrop area (zone D). The textures, distribution, and compositions of the rocks suggest that basaltic magma intruded through the harzburgite to the overlying magma chamber along this zone. Textural evidence does not preclude the migration of gabbroic magma downward into the tectonite peridotite unit.

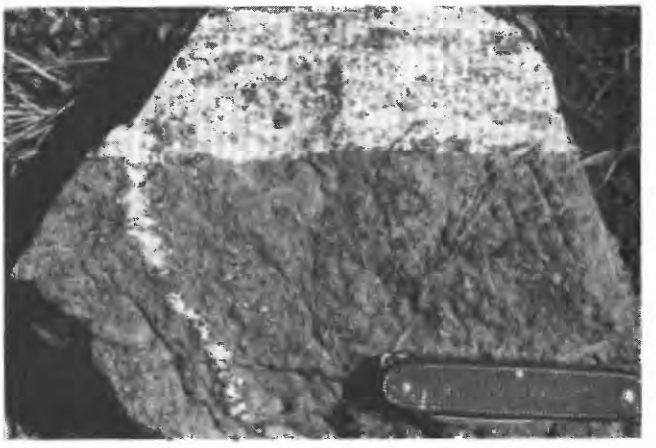

FIGURE 5.6.—Harzburgite of the Canyon Mountain Complex with plagioclase and gabbro dikes. Plagioclase-bearing harzburgite is found only adjacent to small gabbro veins in the central part of the Canyon Mountain Complex. Pocketknife, for scale, is approximately 6 cm long.

The dikes in all zones are principally melagabbro and olivine, two-pyroxene gabbro. Their coarse textures suggest formation and crystallization at depth, probably early in the history of the Canyon Mountain Complex. Where gabbro dikes are small or absent near the margins of the zone of infiltration, diffusion of basaltic melt through the host tectonite harzburgite has locally transformed the peridotite to plagioclase-bearing harzburgite, plagioclase lherzolite, troctolite, or even melagabbro.

Compositions of minerals in the intrusive gabbro are similar throughout the zone of infiltration. Feldspars are calcic plagioclase (An_{89-96}), olivine is Mg-rich (Fo_{85}). Clinopyroxene is calcic augite, and orthopyroxene is bronzite (En_{80}). These compositions are all slightly more evolved than those of minerals of the host harzburgite, and they are similar to those of both the layered peridotites and gabbros unit and unit G1, the gabbro of Gwyn Creek.

In the outermost subzone, zone A, dikelets of plagioclase, undeformed clinopyroxene, or olivine, two-pyroxene gabbro, are less than 1 cm wide. Harzburgite may contain as much as 50 percent undeformed plagioclase or as little as one plagioclase crystal in 10 m^2 of depleted harzburgite. This feldspar is undeformed and commonly surrounded by a magmatic reaction rim of pargasitic hornblende (fig. 5.7).

The transition from unaffected harzburgite of the tectonite peridotite unit to the feldspathic harzburgite and gabbroic dikelets of zone A is gradational. Blobs of feldspar and thin gabbroic dikelets increase in abundance inward. Early dikelets are contorted. Some are oblique to foliation in the host harzburgite, but many are parallel to host-harzburgite foliation or are offset parallel to it. Later veins are straight and crosscut early gabbro veins as well as structure in the host harzburgite. These relations suggest that early gabbro dikelets were emplaced before or during plastic deformation of the harzburgite, and later gabbro was emplaced after the last plastic deformation.

FIGURE 5.7.—Isolated plagioclase (dark, rounded form in middle of picture) in harzburgite is rimmed by pargasite reaction rim and is undeformed, indicating that plagioclase and gabbro infiltration postdated deformation of harzburgite. Field of view is about 1 mm across.

Field relations in zone A strongly suggest that gabbroic magma moved from veins and small dikes into the host harzburgite, rather than being a result of partial melting of a fertile peridotite, that is, a peridotite that will produce basaltic magma by partial melting. Gabbroic constituents decrease rapidly with distance from a vein, suggesting infiltration of fluid from the vein into depleted peridotite. There is no plagioclase, and only small (5 percent) amounts of clinopyroxene, in the harzburgite of the Canyon Mountain Complex outside the zone of infiltration.

A subzone containing broader gabbro dikes, 1 to 10 cm wide, occurs inward from zone A and is denoted as zone B. The gabbro dikes in zone B have been altered to rodingite. Larger dikes have broad serpentinized contacts with the host tectonite peridotite unit. Feldspar-bearing harzburgite is less abundant than in zone A.

Tectonite peridotite that was intruded by gabbro dikes greater than 10 cm wide was designated zone C. Zone C is exposed in the north-central part of the tectonite peridotite unit. It constitutes about 25 percent of the area mapped in the gabbroic zone. Significantly, unit G1 (gabbro of Gwyn Creek) is enclosed by zone C. This gabbro is very similar to the dike gabbros in mineralogy, mineral composition, and whole-rock geochemistry.

In zone D, gabbro forms at least 10 percent of the visible outcrops. The dikes are as much as 3 m wide. They crosscut foliation of the host tectonite peridotite unit and also crosscut one another. Some broader dikes, especially those exposed on the south face of Baldy Mountain, are banded or layered parallel to their borders. The banding may have resulted from flow segregation during magma movement or from pulses of magma flowing through an expanding fracture.

ORIGIN OF THE ZONE OF INFILTRATION

The zone of infiltration of the Canyon Mountain Complex is interpreted as a zone of depleted upper-mantle tectonite peridotite that was infiltrated and intruded by the chemically and mineralogically evolved gabbroic magmas that fed an overlying magma chamber, or were forced downward from that chamber. Similar rocks and relations in the Oman

ophiolite, in the Trinity (Calif.) ophiolite, and in ophiolites elsewhere have been interpreted as various stages in the partial to complete segregation and expulsion of a melt fraction from a rising mantle diapir (Clifford Hopson, oral commun., 1986). However, the infiltration/intrusion model is favored for the Canyon Mountain Complex for the following reasons:

(1) Feldspathic harzburgite does not occur elsewhere in the Canyon Mountain Complex. Depleted harzburgite, with low modal clinopyroxene and no other fertile components, occupies 95 percent of the tectonite peridotite unit of the Canyon Mountain Complex. Lherzolite also has low modal abundances of clinopyroxene. Hence, it is unlikely that the tectonite peridotite unit of the Canyon Mountain Complex was the source of the comparatively voluminous gabbro in the zone of infiltration.

(2) Plagioclase in harzburgite within the zone of infiltration is undeformed. Hence plagioclase was not present during the principal deformation of the harzburgite in the upper mantle.

(3) Plagioclase has magmatic reaction rims of pargasitic amphibole at its contacts with enstatite. These rims suggest magmatic or fluid emplacement of the plagioclase rather than subsolidus crystallization by phase change from spinel.

(4) Plagioclase and augitic clinopyroxene are abundant adjacent to small veins in zone A and decrease rapidly with distance from the veins. This strongly suggests that the veins are the source of the fertile components, rather than the plagioclase and clinopyroxene being contributed to the veins from partial melting in fertile peridotite. There is no plagioclase in the harzburgite of the Canyon Mountain Complex except in the zone of infiltration.

(5) The mineralogical and chemical compositions of the larger dikes (zone D) are somewhat evolved, as shown by their relatively high Fe and Na contents. Hence, it is unlikely that they represent a primary melt.

MIGMATITIC AND RECRYSTALLIZED GABBRO: ZONE OF PLAGIOGRANITE GENESIS

Elongate areas of unit G3 (the gabbronorite of Pine Creek Mountain) show evidence of generating the plagiogranites of the Canyon Mountain Complex. These zones, designated as migmatitic zones on figure 5.2, are more than 200 m wide and characteristically have a core of migmatitic textures (fig. 5.8), an intermediate band of granoblastic or granulitic fabrics, and an outer zone where lineated poikiloblastic hornblende is well developed in gabbronorite. The distinctive character of the migmatitic zones was first recognized by T.P. Thayer (written commun., 1980), who considered

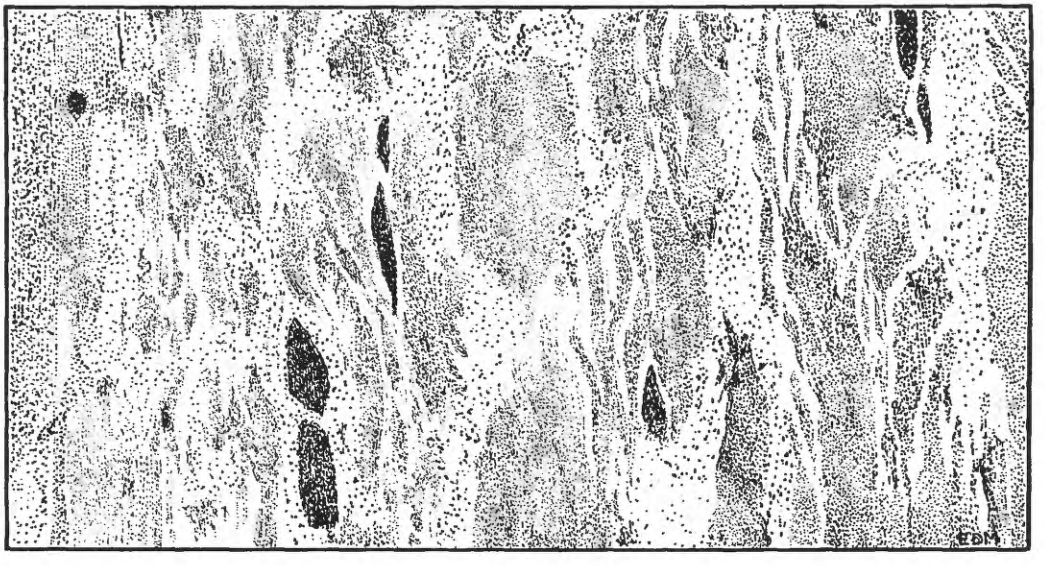

FIGURE 5.8.—Drawing of textures in the zone of infiltration, West Fork Pine Creek. Darkest areas are amphibolized diabase, intermediate are recrystallized gabbronorite, and lightest areas are plagiogranite. Contacts between plagiogranite and gabbronorite are gradational. Relict cumulate layering (vertical in this view) is shown at left.

the oddly textured rocks in the West Fork of Pine Creek (which flows between Gand Saddle and Bear Skull Rims, fig. 5.1) and the West Fork of Indian Creek (which flows along the southeast flank of Baldy Mountain, fig. 5.1) to be zones of penecontemporaneous diabase and plagiogranite intrusion and brecciation. Thayer indicated that these zones are important to the history of the Canyon Mountain Complex.

These zones of migmatitic and recrystallized rocks trend east-west and are parallel to diabase dikes and plagiogranite bodies. Gabbroic rocks in the narrow, migmatitic central zone are intimately mixed with plagiogranites (fig. 5.8). Gabbronorite grades into mafic diorite, which grades texturally and mineralogically into plagiogranite on scales ranging from meters to millimeters. Fabrics are migmatitic. Layered gabbro is plastically deformed into irregular, patchy mixtures of fine-grained and medium-grained gneissic rock. Angular to subrounded xenoliths of amphibolized diabase, up to 3 m in length, are contained within the migmatitic gabbros (figs. 5.9, 5.10). Diabase dikes, from less than 1 m to about 10 m in width, are crosscut and brecciated by plagiogranite. Mafic clots and fine-grained, amphibolized schlieren of gabbronorite also occur in the inner zones (figs. 5.9, 5.10).

Although gabbro immediately outside this migmatitic zone appears unaffected, in thin section these

FIGURE 5.9.—Gabbronorite schlieren in matrix that is mixture of quartz gabbro and plagiogranite. West Fork Indian Creek. Ruler is approximately 10 cm long. Photograph by T.P. Thayer, 1966.

rocks have a granuloblastic to xenomorphic-granular texture (fig. 5.11). Triple-point (120°-angle) junctions are well developed. Relicts of euhedral plagioclase and subhedral augite are present in a matrix of granuloblastic albite. Clinopyroxene commonly is recrystallized into aggregates of small clinopyroxene crystals with triple-point junctions, or has a sieve texture. Orthopyroxene appears largely unaffected by recrystallization.

Poikiloblastic hornblende up to 2 cm in length appears in an outer zone, where granulitic textures are not apparent (fig. 5.12). In some outcrops the hornblende is lineated obliquely to the trend of the zone. Plagiogranite intrudes this outer zone, but no migmatitic textures are developed in the host gabbro. The hornblende commonly has clinopyroxene cores and appears to be a product of high-temperature hydration of clinopyroxene.

ORIGIN AND SIGNIFICANCE OF THE MIGMATITIC ZONE: GENERATION OF PLAGIOGRANITE

Zones of recrystallization and migmatitic textures similar to that of the Canyon Mountain Complex are rare. Annealed fabrics attributed to strain-enhanced recrystallization are present in the Gosse Pile stratiform intrusion, central Australia (Moore, 1973).

FIGURE 5.10.—Migmatitic fabrics and brecciated diabase, migmatitic zone, West Fork Pine Creek. *A*, Light-colored plagiogranite is segregated into some poorly defined veins. Metal field stereoscope is 18 cm wide. Photograph by T.P. Thayer, 1966. *B*, See next page.

Other occurrences of fine-grained, granular-textured rocks have been attributed to supercooling and release of volatile pressure (Fonger-Hyllingen complex, Norway; Thy and Esbensen, 1982), and to recrystallization along slip planes (Josephine peridotite, Oreg.; Jorgenson, 1979). Generation of plagiogranite by amphibolite anatexis has been recognized in the Fournier ophiolite, Prince Edward Island, New Brunswick (Flager and Spray, 1991).

The extensive migmatitic textures and recrystallization in unit G3 (gabbronorite) of the Canyon Mountain Complex represent a significant postmagmatic event. These zones of partial melting and recrystallization appear to be related to the production of plagiogranites of the Canyon Mountain Complex by partial melting of altered (hydrated, greenschist-facies) gabbro. Gerlach (1980) used trace-element data to calculate that the plagiogranites of the Canyon Mountain Complex were produced by partial melting of altered oceanic (tholeiitic) gabbro. The migmatitic zones appear to be the locations where this partial melting and plagiogranite generation occurred. They are spatially associated with plagiogranites near the top of the gabbro section of the Canyon Mountain Complex. Although plagiogranites of the migmatitic zone cannot be traced directly to the overlying plagiogranite bodies due to lack of appropriate bedrock exposure, the abundance of plagiogranite in the

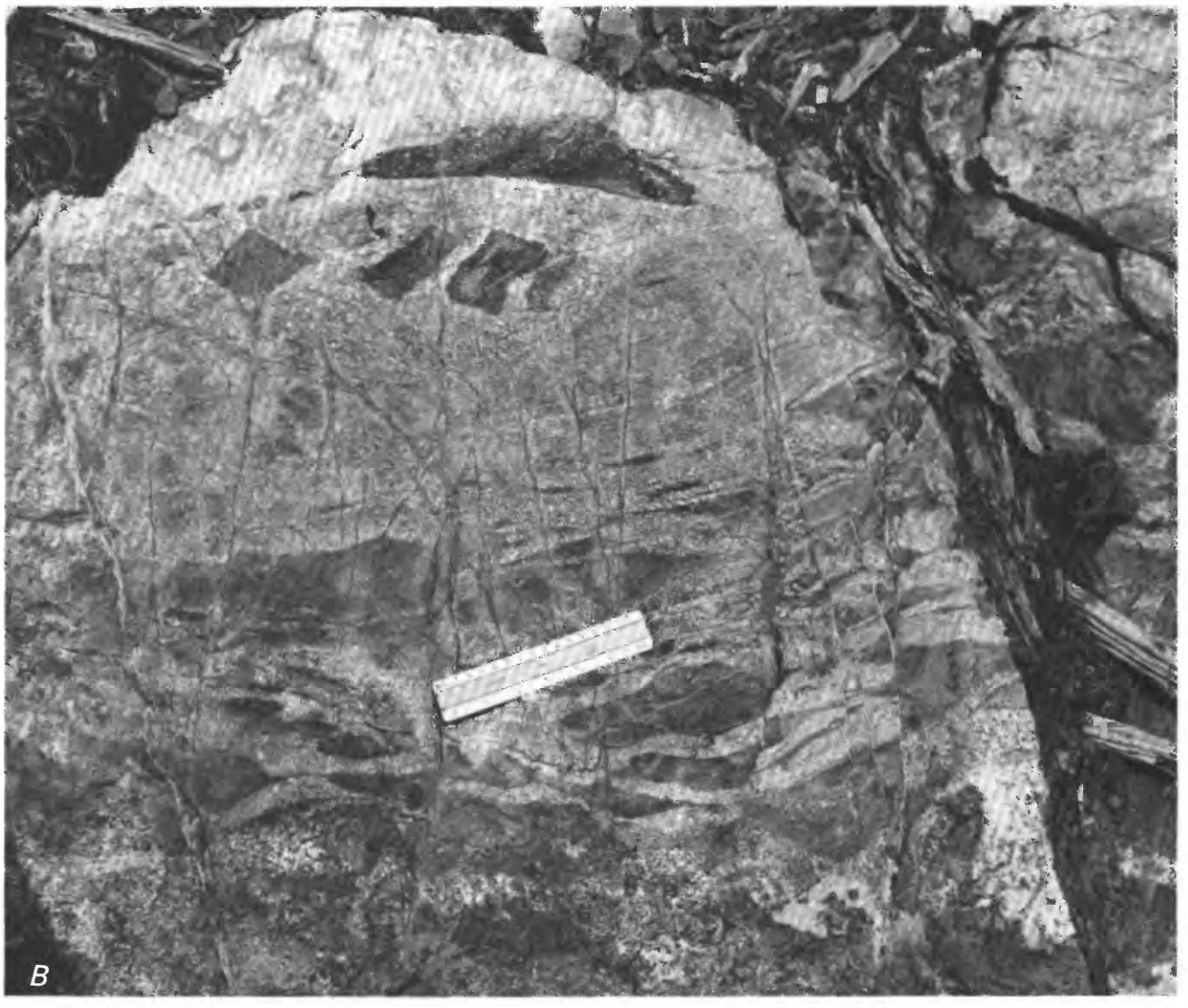

FIGURE 5.10.—Continued. *B*, Detail of migmatitic zone. Note complex mixture of diabase (very dark), recrystallized gabbro (dark), plagiogranite (coarse-grained and light), and mixed rock. Postmagmatic brittle deformation has offset some parts of this outcrop. Ruler is approximately 10 cm long. Photograph by T.P. Thayer, 1966.

migmatitic zone and the presence of plagiogranite dikes and veins leading upward indicate that this is a viable model.

The role of diabase dikes in this scenario is unclear. However, crosscutting field relations, the incorporation of diabase xenoliths within the plagiogranite, and the brecciation of diabase by plagiogranite dikes and stringers suggest that diabase dikes intruded the zone prior to plagiogranite generation.

Previously, the triple-point junctions and other granuloblastic to granulitic textures of the upper gabbros—as well as their anomalously dry, or unaltered and fresh, character—were attributed to adcumulate crystallization (Himmelberg and Loney, 1980). There is a marked resemblance between adcumulate texture and granuloblastic texture (Vernon, 1970). Both are characterized by straight grain boundaries and triple-point junctions. However, the reorganization of clinopyroxene into small, clustered crystals with triple-point boundaries and the absence of any intergranular phases throughout the recrystallized zone indicate that the texture of the Canyon Mountain Complex is due to recrystallization.

The presence of similar granuloblastic textures in the Fonger-Hyllingen complex, where they have been attributed to release of volatile pressure, and the association of similar textures in the Josephine peridotite with shear along slip planes suggest that shearing or some other tectonic event may have played a role in the creation of these zones during the late-magmatic or post-magmatic history of the Canyon Mountain Complex. Shear is recognized as an essential component of plagiogranite generation in the Fournier ophiolite.

The plagiogranites of the migmatitic zone of the Canyon Mountain Complex were produced by partial melting of altered Canyon Mountain gabbros; they are not the product of fractional crystallization nor the product of intrusion of a separate magma.

All the plagiogranite of the Canyon Mountain Complex is likely to have originated from this same mechanism and source. Field and geochemical evidence suggest that plagiogranites were generated during an event that released volatiles (H_2O) from altered gabbros and concentrated these volatiles in a central area under shear stress. Altered gabbros in the middle of the zone partly melted, producing plagiogranite magma, in accordance with Gerlach's (1980) geochemical modeling for plagiogranite genesis. If the partial melting occurred close to the surface, then small eruptions of keratophyres probably followed.

The production of the two other textural and mineralogical zones (granuloblastic fabrics and hornblende-gabbro) are also linked to this process. Altered gabbros outside this zone lost water and recrystallized with dry, granuloblastic textures. Volatiles (water) not directed inward or captured by partial melting would continue outward into gabbros cooled further by volatile release and expansion, producing amphiboles and amphibole reaction rims on clinopyroxenes. The alignment of hornblende in the zone strongly suggests crystallization under stress.

The operation of these processes is evident in the field and in thin section. Detailed work is needed to quantify the stress, water vapor pressures, and other parameters under which these processes occurred, and to elucidate the relation of diabase dikes. This

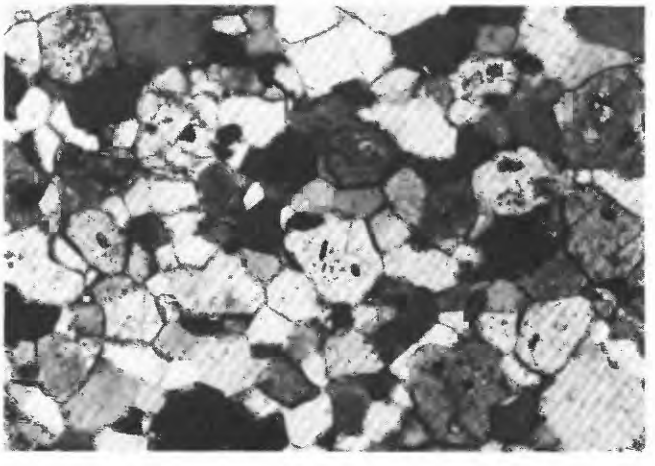

FIGURE 5.11.—Photomicrograph of granulite textures, migmatitic zone. Orthopyroxene, clinopyroxene, and albite in recrystallized gabbro, West Fork Pine Creek. Field of view, 2.5 mm.

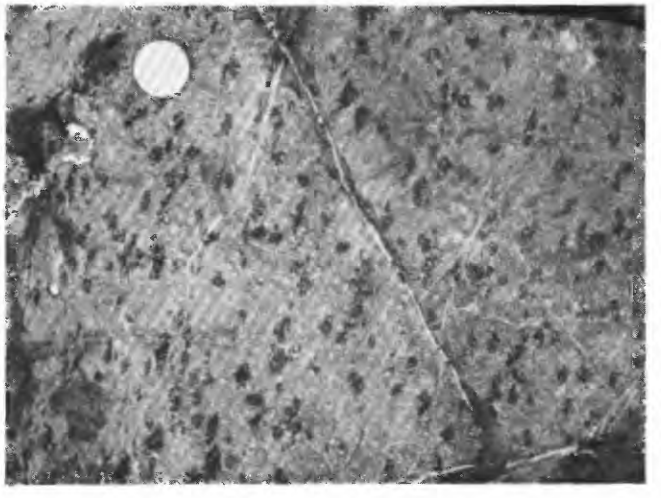

FIGURE 5.12.—Poikiloblastic hornblende in altered gabbro. Rim of migmatitic zone. West Fork Pine Creek. Coin is approximately 2 cm in diameter.

TABLE 5.5.—*Major- and trace-element analyses of rocks of the Canyon Mountain Complex*

[FeO*=FeO+Fe_2O_3; ---, not determined]

Lithic type ---	Dunite	Harzburgite	Lherzolite	Lherzolite, zone of infiltration	Olivine websterite, transition zone	Gabbro, upper transition zone, Celebration Ridge	Gabbro, lower transition zone, Baldy Mountain	Unit G1 (gabbro of Gwyn Creek)	Unit G2 (gabbro of Bear Skull Rims)	Unit G3 (gabbro-norite of Pine Creek Mountain)	Gabbro dike, zone of infiltration, Baldy Mountain
Sample	1	2	3	4	5	6	7	8	9	10	11
Major-element oxides (weight percent)											
SiO_2	36.1	44.3	42.5	42.7	48.3	49.8	50.3	45.7	48.6	50.6	---
Al_2O_3	.1	1.8	1.1	1.5	4.6	24.9	17.9	11.6	19.6	16.6	---
TiO_2	.0	.0	.0	.0	.4	.1	.2	.2	.2	.2	---
FeO*	9.1	8.3	8.6	8.6	11.1	3.5	6.6	9.9	5.0	8.5	---
MnO	.1	.1	.1	.1	.2	.1	.1	.2	.1	.1	---
MgO	35.2	32.8	35.8	33.8	17.5	5.1	10.7	17.3	8.8	8.9	---
CaO	.2	1.7	1.5	1.7	13.4	13.6	12.2	10.3	14.4	12.8	---
Na_2O	.1	.6	.3	.1	1.4	2.7	2.5	1.2	2.3	1.7	---
K_2O	.0	.0	.1	.1	.1	.1	.1	.1	.1	.1	---
P_2O_5	.0	.0	.0	.0	.0	.0	.0	.0	.0	.0	---
Total	80.9	89.6	90.0	88.6	97.0	99.9	100.6	96.5	99.1	99.5	---
Trace elements (parts per million)											
Sr	---	---	44	450	84	190	366	---	---	88	329
Co	---	43	40	44	26	42	30	90	42	31	25
Sc	---	11	11	6	36	54	24	24	40	44	40
Ni	---	2800	2800	2750	50	100	190	300	200	20	370
Cr	---	3700	3800	5800	3500	8000	2700	4850	2700	1050	1300
La	---	---	---	.06	.12	.20	.08	.08	.06	.20	.02
Ce	---	---	---	---	.41	.59	.39	.34	.28	.71	.13
Nd	---	---	---	---	.53	.54	.67	.53	.81	1.35	.42
Sm	---	.06	.01	.35	.13	.28	.32	.34	.39	.78	.25
Eu	---	---	.08	.19	.18	.29	.58	.14	.29	.26	.59
Yb	---	---	.09	.41	.20	.40	1.30	.36	.59	1.09	.40
Lu	---	.03	.03	.12	.06	.09	.06	.08	.17	.28	.09

information could prove vital for understanding the late history of the Canyon Mountain Complex and the Baker terrane.

The generation of plagiogranite from shear stress applied to the Canyon Mountain Complex fits with several dates in Baker terrane history. The postmagmatic, metasomatic generation of plagiogranite in the gabbros of the Canyon Mountain Complex would explain the 10-m.y. hiatus between the age of the gabbros (278 Ma) and the age of the plagiogranites (268 Ma)(Gerlach and others, 1988). Metagabbro amphibolites dated at 269 Ma, with a range of dynamothermal metamorphic ages between 255 and 269 Ma, are reported in the serpentinite-matrix melange in the Baker terrane just west of the Canyon Mountain Complex (Carpenter and Walker, 1992). These rocks are related to a "dynamothermal aureole" created by "emplacement of a young arc over mafic crust" (Carpenter and Walker, 1992).

The nature of the event that produced this significant increase in shear stress and "emplacement of a young arc over oceanic crust" is enigmatic. Volcanic activity in the Wallowa terrane peaked at about 270 Ma. Activity in the Olds Ferry terrane began at about 240 Ma. One possibility is that the high shear stresses and generation of amphibolites may be related to a change in arc polarity and (or) the inception of east-facing subduction at about 270 Ma that would eventually generate the Olds Ferry terrane (Vallier, chap. 3, this volume).

GEOCHEMISTRY

Geochemical studies of gabbro and peridotite of the Canyon Mountain Complex (table 5.5) suggest that the Canyon Mountain Complex is related to a calc-alkaline trend. The AFM plot is not diagnostic for gabbro and peridotite, as these units plot at the base of both calc-alkaline and tholeiitic trends. However, cumulate gabbros, as well as unit G3 (gabbronorite), are more calcic than in most ophiolites and plot in a

field of alkalic to calc-alkaline cumulates rather than in the field for oceanic ophiolites on an Al_2O_3/MgO/CaO diagram. These discriminants must be used with caution because all the units of the Canyon Mountain Complex are altered to some degree, and discriminants may not be as accurate for cumulate sections as for liquid compositions. The overall geochemistry of the complex is arc tholeiite to calc-alkaline.

The rare-earth-element (REE) compositions of rocks of the Canyon Mountain Complex are similar to those of analogous units of other arc-related ophiolites, including the Troodos (Cyprus) and Point Sal (Calif.) ophiolites. Light rare-earth elements (LREE's) increase and the positive europium anomaly is more pronounced upward through the cumulate units. Fractionation modeling of REE's from the lower gabbro units (G1, G2, G3) suggests that fractionation, with only very limited replenishment by more primitive magma, can account for the composition of the lower gabbros. On the basis of this model, the Canyon Mountain Complex appears to have been a nearly closed magmatic system with limited influx of new magma, rather than the open magmatic system characteristic of midocean ridges. However, the extreme alteration of the uppermost, isotropic gabbro units, in concert with the cumulate nature of (lower) unit G2 (gabbro of Bear Skull Rims), precludes reliable fractionation modeling of the gabbros of the Canyon Mountain Complex. The general requisites for a fractionating magma chamber are present.

Sr and Nd isotopic work by Gerlach and others (1988) indicates that the lower parts of the Canyon Mountain Complex were derived from an isotopically homogeneous, depleted source. Isotropic and layered gabbros of the Canyon Mountain Complex have initial $^{87}Sr/^{86}Sr$ ratios of 0.7024 to 0.7031. Keratophyres and rocks from the alternating diabase-keratophyre sill sequence that overlies the gabbros of the Canyon Mountain Complex have $^{87}Sr/^{86}Sr$ ratios of 0.7031 to 0.7037, within the average range of values for arc-derived basalts and andesites.

ORIGIN AND TECTONIC SETTING

The mineralogy and geochemistry of the Canyon Mountain Complex are more characteristic of island-arc magmas than of oceanic tholeiites or oceanic alkalic rocks. The gabbros of the Canyon Mountain Complex are more enriched in CaO and Al_2O_3 than are oceanic tholeiites; they are more like calc-alkaline to mildly alkalic continental intrusive bodies such as the Kiglapait (Morse, 1969) in this respect. The pyroxenes of the layered peridotites and gabbros unit and the gabbro units Canyon Mountain Complex are also enriched in CaO and Al_2O_3, and are quite low in TiO_2 and alkalis compared to pyroxenes from equivalent units in mid-ocean-ridge ophiolites such as the Oman ophiolite. These traits are characteristic of arc-derived magmas. Other discriminants, including TiO_2/Fe*O:MgO and $MnO/TiO_2/P_2O_5$, further suggest calc-alkaline to arc-tholeiite affinity for gabbro of the Canyon Mountain Complex. The initial $^{87}Sr/^{86}Sr$ ratios of cumulate gabbro from modern island arcs is not known. However, the ratios of 0.7024 to 0.7031 are within the range of ratios reported from arc basalts, as well as from normal midocean-ridge basalts (NMORB), and an arc origin cannot be ruled out on the basis of initial $^{87}Sr/^{86}Sr$ ratios. Thus, the geochemical signatures of the gabbros of the Canyon Mountain Complex support the complex's affiliation with an island arc.

The mineralogy and chemistry of the Canyon Mountain Complex also suggest that it is a remnant magmatic system produced immediately above upper-mantle peridotite in much the same setting where we might expect to find midocean-ridge magma chambers. This setting is also appropriate for early island-arc magmatism. The scale of the Canyon Mountain Complex is smaller than that of ophiolites related to midocean-ridge basalt (MORB). Its transition zone of layered peridotites and gabbros averages less than 1 km thick and is less than 100 m thick in the western part of the complex. Its gabbros and small transition zone suggest fractionation with a fairly limited rate of magma replenishment, which is consistent with early island-arc magmatism.

The dominantly arc-tholeiite geochemical signature of the gabbros of the Canyon Mountain Complex, its setting as a relatively small and quiet magma chamber perched directly above mantle harzburgite, and the presence of the Canyon Mountain Complex as the only coherent ophiolite in a sea of serpentinite-matrix melange suggest that this ophiolite may have originated as part of the fore-arc system or prior to the inception of significant arc-related magmatism. Limited arc-tholeiite magmatism occurs in the Marianas fore arc (in the western Pacific Ocean) more than 100 km from the active arc (Marlow and others, 1992). However, fore-arc magmatism, in general, is rare. A source directly beneath Marianas fore-arc basalts would require partial melting at depths of 20 to 30 km; partial melting at such shallow depths would not be possible without extraordinary amounts of hydration (Marlow and others, 1992). The source of Marianas fore-arc magmas is therefore assumed to be larger chambers beneath the active arc.

Pearcy (1991) has suggested that the Canyon Mountain Complex is a nascent island arc related to

Olds Ferry terrane volcanism. The generally arc-tholeiite geochemistry supports this hypothesis. However, Olds Ferry volcanism is Triassic in age, 235 to 216 Ma, and possibly as young as 181 Ma (Vallier, chap. 3, this volume), whereas the plagiogranites and gabbros of the Canyon Mountain Complex are Early Permian in age, 278 to 268 Ma (Gerlach and others, 1988).

Age and chemistry suggest that the Canyon Mountain Complex may be closely related to the Wallowa terrane. It may represent the early roots of arc volcanism, or it may represent fore-arc volcanism on a larger scale than we currently know and understand.

Two periods of igneous activity may be represented in the Canyon Mountain Complex. The first period of activity produced the bulk of the transition zone and gabbroic rocks of the Canyon Mountain Complex, ending about 278 Ma. The second period of activity involved relatively minor volumes of intrusion (zone of infiltration) and partial melting (migmatitic zones). This episode, at about 270 to 265 Ma, generated the plagiogranites of the Canyon Mountain Complex (268 Ma; Gerlach and others, 1988). Walker (chap. 6, this volume) has found evidence for two ages of igneous activity in discordant U-Pb ages. The second episode of activity may have been related more to tectonics than to igneous processes.

OTHER MAFIC AND ULTRAMAFIC COMPONENTS OF THE BAKER TERRANE

The diverse volcanic and plutonic components of the Baker terrane include a variety of volcanic greenstones and metagabbros (Mullen, 1985). Many are thoroughly altered to greenschist-facies assemblages and pervasively sheared. However, some contain relict clinopyroxenes and (or) well-preserved textures. Such rocks provide valuable mineralogical and geochemical insights into their petrotectonic affinities, and reasonable clues to the nature of the Baker terrane.

On the basis of rock textures, trace-element data, and the compositions of relict clinopyroxenes, volcanic greenstones from several locations have island-arc affinities (fig. 5.13). Metabasalts with relict intergranular textures occur within the Burnt River Schist near Durkee, Oreg. (fig. 5.1). They contain low-Ti augite (TiO_2<0.5 percent) (samples BR-52, BR-61, table 5.6). The pyroxene compositions are characteristic of low-K, early arc tholeiites (Nesbitt and Pearce, 1977). Whole-rock compositions (table 5.7) fall within arc fields on discriminant diagrams (fig. 5.14). Basaltic greenstones that occur in melange near the town of Greenhorn also have intergranular texture and is-

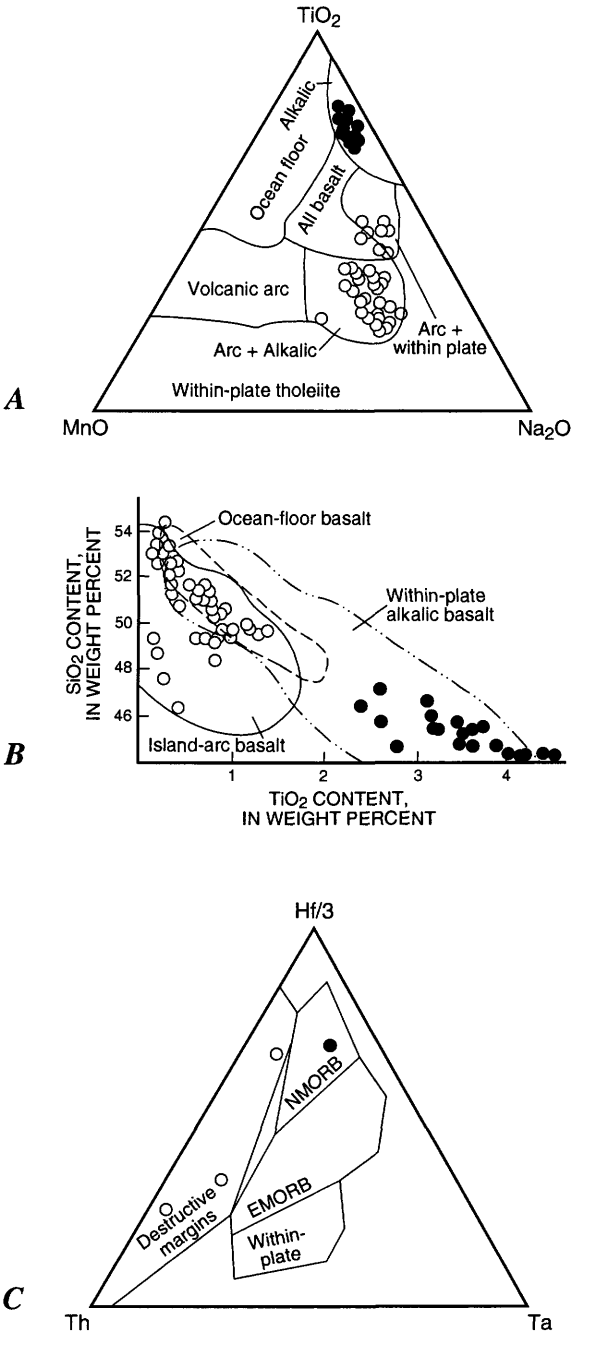

FIGURE 5.13.—Discriminant diagrams for greenstones of Baker terrane. Filled circles, pillowed greenstone samples V-27 (Greenhorn Mountains) and BRS (Sturgill); open circles, all other greenstones of Baker terrane. Compositions of relict clinopyroxenes are shown on *A*, $MnO/TiO_2/Na_2O$ diagram, and *B*, graph of SiO_2 versus TiO_2 content. Fields of basalt compositions modified from Pearce and others, 1977. *C*, Whole-rock trace-element analyses plotted on Th/Hf/Ta diagram. Fields of basalt compositions modified from Wood and others (1979). NMORB, normal midocean-ridge basalt; EMORB, enriched midocean-ridge basalt.

TABLE 5.6.—*Compositions of clinopyroxene and olivine from greenstones of the Baker terrane, northeastern Oregon*

[FeO*=FeO+Fe_2O_3; n.a., not applicable; ---, not determined]

Sample ----	Clinopyroxenes from MV-48A													
Mineral grain ---	1	2	3	4	5	6	7	8	9	10	11	12	13	14
Major-element oxides (weight percent)														
SiO_2 -------	51.33	49.02	53.58	51.17	52.08	52.33	52.27	53.78	51.19	51.26	50.88	49.91	50.25	48.59
TiO_2 -------	.94	1.21	.46	.84	.86	.47	.81	.73	.82	.80	1.13	1.18	.93	1.46
Al_2O_3 -----	3.61	4.50	2.01	4.14	3.94	3.15	4.34	3.97	4.05	3.84	4.26	3.77	3.78	3.62
FeO* -------	6.41	7.93	7.82	6.40	7.20	5.51	6.82	7.79	6.46	5.86	7.99	9.95	7.03	12.08
MnO -------	.14	.16	.23	.15	.21	.12	.12	.15	.14	.17	.22	.23	.15	.19
MgO -------	17.60	16.56	19.52	16.51	17.06	17.25	17.31	17.70	17.10	17.00	16.32	15.98	16.91	12.58
CaO --------	19.18	18.09	16.86	19.41	19.15	19.95	19.16	17.60	19.37	19.86	18.31	17.34	19.04	17.84
Na_2O ------	.25	.30	.22	.28	.27	.28	.25	.27	.30	.30	.27	.34	.32	.38
Cr_2O_3 -----	.10	.00	.43	.39	.15	.55	.05	.15	.22	.66	.00	.00	.10	.00
NiO ---------	.04	.06	.00	.00	.00	.00	.13	.03	.08	.14	.00	.06	.09	.09
Total -------	99.11	97.85	100.74	99.28	100.91	99.62	101.24	102.70	99.74	99.90	99.37	98.75	98.595	96.85
Stoichiometry (number of ions per unit cell)[1]														
Si ----------	1.896	1.85	1.941	1.888	1.893	1.918	1.889	1.920	1.882	1.882	1.883	1.876	1.876	1.88
Ti ----------	.026	.03	.012	.023	.023	.012	.002	.019	.022	.02	.031	.033	.024	.042
Al ----------	.157	.19	.085	.179	.168	.136	.184	.166	.175	.17	.185	.167	.166	.165
Fe ----------	.198	.25	.236	.197	.218	.168	.206	.232	.198	.18	.247	.312	.219	.392
Mn ----------	.004	.005	.007	.004	.006	.003	.008	.004	.004	.01	.006	.007	.004	.006
Mg ----------	.942	.931	1.054	.908	.924	.942	.933	.942	.397	.93	.901	.895	.94	.729
Ca ----------	.759	.731	.654	.767	.746	.783	.741	.673	.763	.78	.726	.698	.761	.743
Na ----------	.018	.021	.015	.020	.019	.019	.017	.018	.021	.02	.018	.024	.023	.029
Cr ----------	.002	.000	.001	.011	.004	.015	.001	.004	.006	.02	.000	.000	.003	.000
Ni ----------	.001	.001	.000	.000	.000	.000	.003	.000	.002	.01	.000	.001	.002	.002
Total -------	4.006	4.026	4.010	4.002	4.006	4.002	4.004	3.984	4.015	4.013	4.001	4.018	4.025	4.000
Relative proportions (percent)														
Fs ----------	10	13	12	11	12	9	11	13	10	10	13	16	11	21
En ----------	50	49	54	49	49	50	50	51	49	49	48	47	49	39
Wo ----------	40	38	34	40	40	41	39	36	40	41	39	37	40	40

Sample ----	Clinopyroxenes from BR-52													
Mineral grain ---	1	2	3	4	5	6A	6B	6C	7	8A	8B	9		
												Core	Intermediate	Rim
Major-element oxides (weight percent)														
SiO_2 -------	53.99	53.46	52.23	53.28	53.04	51.65	52.62	51.19	53.43	52.47	52.09	53.70	52.95	52.46
TiO_2 -------	.24	.26	.31	.26	.29	.41	.42	.56	.19	.35	.33	.23	.33	.31
Al_2O_3 -----	1.68	1.67	2.19	2.34	2.73	3.89	3.47	3.33	1.90	2.93	3.13	1.87	3.39	2.91
FeO* -------	6.07	5.34	5.69	6.08	5.99	6.70	6.06	6.20	6.01	5.04	4.42	5.74	6.07	6.17
MnO -------	.15	.12	.13	.20	.13	.10	.11	.12	.13	.15	.13	.13	.12	.16
MgO -------	18.91	19.03	18.14	18.29	18.25	17.07	17.42	16.59	19.12	18.12	17.46	19.17	17.03	18.55
CaO --------	18.09	18.73	19.83	17.95	18.46	19.21	19.54	19.54	18.49	18.96	20.50	17.62	19.30	18.46
Na_2O ------	.14	.14	.19	.17	.19	.32	.18	.24	.17	.19	.22	.17	.17	.23
Cr_2O_3 -----	.04	.24	.09	.10	.16	.03	.99	.00	.06	.32	.57	.12	.19	.16
NiO ---------	.06	.16	.03	.11	.08	.00	.27	.04	.09	.04	.05	.07	.05	.12
Total -------	99.38	99.00	98.82	98.69	99.35	99.40	99.96	97.79	99.61	98.62	99.15	98.82	99.62	99.52
Stoichiometry (number of ions per unit cell)[1]														
Si ----------	1.97	1.959	1.931	1.959	1.941	1.902	1.920	1.915	1.95	1.931	1.914	1.967	1.936	1.922
Ti ----------	.006	.007	.008	.007	.007	.011	.011	.015	.005	.009	.009	.006	.009	.003
Al ----------	.072	.071	.095	.101	.117	.169	.149	.146	.081	.127	.135	.08-	.146	.125
Fe ----------	.185	.163	.175	.186	.183	.206	.185	.194	.183	.155	.145	.175	.185	.189
Mn ----------	.004	.003	.003	.006	.004	.003	.003	.003	.004	.004	.003	.003	.003	.004
Mg ----------	1.03	1.040	.999	1.002	.996	.937	.947	.925	1.040	.994	.957	1.046	.928	1.013
Ca ----------	.707	.735	.785	.707	.724	.758	.764	.783	.723	.747	.807	.691	.756	.724
Na ----------	.009	.010	.014	.011	.013	.023	.013	.017	.012	.013	.015	.011	.012	.016
Cr ----------	.001	.006	.002	.003	.004	.000	.002	.000	.001	.009	.016	.003	.005	.004
Ni ----------	.001	.000	.001	.000	.002	.000	.000	.001	.002	.001	.001	.002	.001	.003
Total -------	3.990	3.944	4.018	3.987	3.996	4.013	3.998	4.004	4.007	3.997	4.008	3.990	3.985	4.012
Relative proportions (percent)														
Fs ----------	10	8	9	10	10	11	10	10	9	8	8	9	10	10
En ----------	54	54	51	53	52	49	50	49	53	52	50	55	50	53
Wo ----------	37	38	40	37	38	40	40	41	37	39	42	36	40	38

[1]Assuming 6 oxygen atoms per unit cell.

Table continued on next page.

TABLE 5.6.—*Compositions of clinopyroxene and olivine from greenstones of the Baker terrane, northeastern Oregon*—Continued

Sample	Clinopyroxenes from BR-61							Clinopyroxenes from V-252					
Mineral grain	1	2	3	4	5	6	7	Groundmass V252-1	Phenocryst Rim	Phenocryst Intermediate	Phenocryst Core	Phenocryst Intermediate	Phenocryst Rim
Major-element oxides (weight percent)													
SiO_2	52.84	53.89	52.50	52.71	52.37	51.58	51.64	48.8	50.7	50.0	50.6	50.1	50.2
TiO_2	.31	.23	.31	.27	.31	.26	.26	.9	.9	.6	.9	.7	.9
Al_2O_3	2.75	3.03	2.90	2.62	2.64	3.00	2.07	2.8	3.9	2.9	4.5	4.2	3.9
FeO	4.12	4.24	4.24	4.57	4.81	3.95	4.29	18.4	12.7	12.9	13.0	13.3	12.7
MnO	.11	.12	.11	.14	.10	.10	.01	.0	.0	.0	.0	.0	.0
MgO	17.84	18.62	18.01	18.17	18.69	17.35	17.55	.5	.3	.5	.4	.4	10.3
CaO	20.54	20.37	20.55	19.95	20.22	20.08	20.53	9.0	14.1	14.4	14.2	13.8	14.1
NaO	.25	.21	.19	.19	.20	.22	.49	15.8	17.6	16.5	17.6	17.5	17.6
Cr_2O_3	.56	.47	.47	.32	.81	.85	.27	1.6	.3	.2	.2	.3	.2
NiO	.00	.03	.38	.13	.13	.04	.01	.0	.1	.0	.0	.0	.2
Total	99.31	101.21	99.32	99.05	99.77	97.45	97.20	97.9	97.5	97.9	101.5	100.2	100.0
Stoichiometry (number of ions per unit cell)[1]													
Si	1.932	1.930	1.922	1.934	1.914	1.923	1.936	---	1.95	1.92	1.88	1.88	1.88
Ti	.008	.006	.008	.007	.008	.007	.007	---	.03	.02	.02	.02	.03
Al	.118	.127	.125	.113	.113	.132	.091	---	.12	.13	.20	.18	.17
Fe	.125	.126	.129	.140	.146	.123	.134	---	.40	.42	.40	.42	.40
Mn	.003	.003	.003	.004	.002	.003	.003	---	.02	.01	.01	.01	.01
Mg	.972	.994	.983	.993	1.018	.964	.98	---	.73	.83	.79	.76	.77
Ca	.804	.781	.806	.784	.791	.802	.824	---	.71	.67	.70	.71	.71
Na	.017	.014	.013	.013	.014	.015	.035	---	.02	.02	.01	.02	.04
Cr	.016	.013	.013	.009	.008	.025	.008	---	.00	.00	.00	.00	.00
Ni	.000	.000	.001	.003	.003	.001	.000	---	.00	.00	.00	.00	.00
Total	4.000	4.000	4.007	4.004	4.023	3.998	4.024	---	3.98	4.02	4.01	4.00	4.01
Relative proportions (percent)													
Fs	7	7	7	7	7	7	7	---	22	22	21	22	21
En	51	52	51	52	52	51	51	---	39	43	42	41	41
Wo	42	41	42	41	40	42	42	---	39	35	37	37	37

Sample	Clinopyroxenes from V-27A					Clinopyroxenes from BRS										
Mineral grain	1	2	3	4	5	1	2	3	4	5	6	7	8	9	10	11
Major-element oxides (weight percent)																
SiO_2	45.3	44.5	46.1	44.6	46.6	46.2	46.9	46.1	43.9	43.7	44.6	44.8	45.0	47.8	46.7	48.3
TiO_2	3.5	4.6	3.4	4.1	3.3	3.7	2.8	3.6	4.5	4.4	4.4	4.1	3.9	2.4	3.5	2.4
Al_2O_3	5.4	6.9	6.2	5.9	6.3	5.4	5.0	5.9	6.2	5.5	6.1	5.9	5.8	4.3	5.1	4.1
FeO*	13.2	13.6	12.3	13.5	11.4	12.5	12.1	11.7	11.6	12.3	11.6	11.9	12.3	12.9	12.2	12.5
Cr_2O_3	.6	.2	.1	.0	.0	.0	.0	.1	.0	.0	.0	.1	.0	.0	.0	.0
MnO	.3	.3	.2	.3	.2	.3	.3	.2	.2	.2	.3	.2	.3	.3	.3	.3
MgO	9.9	9.2	10.0	9.5	8.8	10.9	11.3	11.5	10.8	10.4	10.2	10.3	10.7	10.8	10.9	11.3
CaO	21.0	21.2	21.6	21.4	20.1	20.7	20.7	21.1	21.0	21.6	21.6	21.1	21.4	20.3	20.7	20.0
Na_2O	.6	.7	.6	.7	.8	.5	.5	.5	.5	.5	.5	.5	.5	.4	.4	.4
K_2O	.0	.0	.0	.0	.0	.0	.0	.2	.01	.0	.0	.0	.0	.0	.0	.0
Total	99.4	101.1	100.5	100.0	97.7	100.3	99.8	100.6	98.8	98.8	99.5	99.1	100.1	99.4	99.7	99.4
Stoichiometry (number of ions per unit cell)[1]																
Si	1.75	1.70	1.75	1.72	---	1.76	1.79	1.75	1.70	1.71	1.72	1.73	1.73	1.84	1.79	1.84
Ti	.10	.13	.10	.12	---	.11	.08	.10	.13	.13	.13	.12	.11	.07	.10	.07
Al	.25	.31	.28	.27	---	.24	.23	.26	.28	.26	.27	.27	.26	.20	.23	.18
Fe	.43	.44	.39	.57	---	.40	.38	.37	.38	.40	.38	.39	.40	.42	.39	.40
Mn	.01	.01	.01	.02	---	.01	.01	.01	.01	.01	.01	.01	.01	.01	.01	.10
Mg	.58	.52	.57	.87	---	.62	.65	.65	.63	.61	.59	.60	.66	.62	.62	.65
Ca	.87	.87	.88	.56	---	.85	.85	.86	.87	.90	.89	.87	.84	.84	.85	.82
Na	.05	.05	.05	.68	---	.04	.4	.04	.04	.04	.04	.03	.03	.03	.03	.31
K	.02	.00	.00	.00	---	.00	.01	.00	.00	.00	.00	.00	.00	.00	.01	.02
Total	4.06	4.03	4.03	4.81	---	4.03	4.40	4.04	4.04	4.06	4.03	4.02	4.04	4.03	4.03	4.39
Relative proportions (percent)																
Fs	23	24	21	29	---	21	20	20	20	21	20	21	21	22	21	21
En	31	28	31	44	---	33	35	35	34	32	32	32	35	33	33	35
Wo	46	48	48	28	---	45	45	46	46	47	48	47	44	45	46	45

[1]Assuming 6 oxygen atoms per unit cell.

Table continued on next page.

TABLE 5.6.—*Compositions of clinopyroxene and olivine from greenstones of the Baker terrane, northeastern Oregon*—Continued

Sample	Clinopyroxenes from M-42 (cumulate)													
Mineral grain	1							2			3	4	5	6
	Rim	Intermediate	Intermediate	Core	Intermediate	Intermediate	Rim	Rim	Core	Rim				
SiO_2	50.6	49.6	48.9	47.3	47.9	51.8	49.3	48.7	50.0	51.5	49.5	49.9	49.7	48.8
TiO_2	.7	.6	.3	.6	.7	.3	.6	.5	.7	.5	.8	.9	.8	.8
Al_2O_3	5.2	4.9	5.2	7.8	6.3	3.9	6.2	4.6	5.2	4.0	1.8	5.4	5.8	6.9
FeO*	9.1	7.5	8.3	12.5	8.6	8.0	10.6	8.1	8.5	8.7	12.0	8.4	8.3	9.4
Cr_2O_3	.0	.0	.0	.0	.3	.0	.0	.0	.0	.0	.0	.0	.0	.0
MnO	.3	.3	.3	.3	.3	.3	.3	.3	.3	.3	.4	.3	.3	.3
MgO	13.4	13.4	12.6	13.7	13.5	13.5	13.1	13.2	12.9	13.6	12.9	12.8	12.9	12.7
CaO	21.0	22.0	22.1	16.5	22.3	21.5	19.2	22.0	22.5	22.0	22.3	21.6	22.3	20.5
Na_2O	.4	.5	.4	.4	.4	.3	.4	.4	.4	.5	.5	.5	.4	.5
K_2O	.0	.0	.0	.0	.0	.0	.0	.0	.0	.0	.0	.0	.0	.0
Total	100.7	98.9	98.2	99.1	100.0	99.6	99.6	97.9	100.5	101.1	100.2	99.9	100.6	100.1
Stoichiometry (number of ions per unit cell)[1]														
Si	1.87	1.87	1.86	1.79	1.80	1.93	1.85	1.86	1.86	1.90	1.88	1.86	---	1.82
Ti	.02	.02	.01	.02	.02	.01	.02	.01	.02	.01	.02	.02	---	.02
Al	.23	.22	.23	.35	.28	.17	.27	.21	.23	.17	.08	.24	---	.31
Fe	.28	.24	.26	.90	.27	.25	.33	.26	.26	.27	.38	.26	---	.29
Mn	.00	.01	.01	.01	.01	.01	.08	.01	.01	.01	.01	.01	---	.01
Mg	.74	.75	.71	.77	.75	.75	.73	.75	.72	.75	.74	.71	---	.71
Ca	.83	.89	.90	.67	.90	.86	.77	.90	.89	.87	.91	.86	---	.82
Na	.04	.04	.03	.03	.03	.02	.03	.03	.03	.04	.04	.04	---	.04
K	.01	.00	.00	.00	.00	.00	.001	.00	.00	.00	.00	.00	---	.00
Total	4.02	4.04	4.01	4.54	4.06	4.00	4.081	4.03	4.02	4.02	4.06	4.00	---	4.02
Relative proportions (percent)														
Fs	15	13	14	22	14	13	18	14	14	14	19	14	---	17
En	40	40	38	42	39	40	40	39	39	40	36	39	---	39
Wo	45	47	48	36	47	46	42	47	47	46	45	47	---	45

Sample	Clinopyroxenes from M-46 (mafic gabbro)				Clinopyroxenes from M80b3 (layered ultramafic rock)			Clinopyroxenes from M-91				Olivines from M-91			
Mineral grain	1	2	3	4	1	2	3	1	2			1	2	3	4
									Rim	Core	Rim				
Major-element oxides (weight percent)															
SiO_2	47.9	46.4	47.5	54.8	53.4	53.0	52.8	54.9	53.8	54.2	54.5	40.6	40.6	40.1	40.5
TiO_2	.8	.7	1.4	.1	.1	.01	.20	.22	.18	.21	.10	.11	.03	.08	.04
Al_2O_3	11.6	10.8	8.6	2.0	3.1	4.7	4.3	1.48	1.7	1.2	1.5	.03	.00	.03	.04
FeO*	12.2	11.7	11.7	8.3	2.9	2.1	3.2	2.0	2.4	2.1	1.9	12.2	14.8	12.5	14.3
Cr_2O_3	.03	.03	.10	.02	.33	.13	.48	.14	.17	.17	.17	.0	.0	.03	.00
MnO	.2	.3	.2	.20	.1	.11	.10	.04	.10	.08	.10	.8	.20	.6	.4
MgO	14.7	13.7	14.6	17.5	15.7	18.2	15.7	17.0	16.7	16.7	17.0	45.9	44.1	46.0	44.72
CaO	11.6	12.4	12.0	14.5	23.6	21.0	24.2	24.7	23.7	23.7	24.0	.0	.0	.0	.0
Na_2O	1.7	2.1	1.9	.44	.07	.01	.09	.07	.08	.06	.02	.0	.0	.0	.0
K_2O	.04	.06	.20	.00	.01	.00	.00	.00	.02	.01	.01	.0	.0	.0	.0
Total	100.9	98.1	98.1	98.0	99.2	99.2	101.0	100.5	98.8	99.0	99.2	99.6	99.7	100.3	100.0
Stoichiometry (number of ions per unit cell)[2]															
Si	3.50	3.51	3.59	4.00	3.91	3.84	3.81	3.96	3.95	3.96	3.97	---	---	---	---
Ti	.04	.04	.08	.01	.01	.001	.01	.01	.01	.01	.01	---	---	---	---
Al	1.00	.96	.76	.98	.27	.40	.37	.13	.15	.14	.13	---	---	---	---
Fe	.75	.74	.74	.52	.17	.13	.19	.12	.15	.13	.11	---	---	---	---
Mn	.014	.02	.01	.01	.01	.01	.01	.00	.01	.01	.01	---	---	---	---
Mg	1.60	1.55	1.64	1.55	1.71	1.96	1.69	1.83	1.83	1.82	1.85	---	---	---	---
Ca	.91	1.00	.97	.70	1.85	1.63	1.87	1.91	1.86	1.86	1.87	---	---	---	---
Na	.24	.31	.29	.063	.01	.00	.01	.01	.01	.01	.01	---	---	---	---
K	.00	.01	.02	.00	.00	.00	.00	.00	.002	.00	.01	---	---	---	---
Cr	.02	.00	.01	.001	.019	.01	.03	.01	.01	.01	.01	---	---	---	---
Total	8.074	8.14	8.11	7.834	7.959	7.981	7.99	7.98	7.982	7.95	7.98	---	---	---	---
Relative proportions (percent)															
Fo	n.a.	n.a.	n.a.	n.a.	n.a.	n.a.	n.a.	n.a.	n.a.	n.a.	n.a.	89	85	90	84
Fs	23	22	22	29	5	3	5	3	4	4	3	n.a.	n.a.	n.a.	n.a.
En	49	47	49	31	46	53	45	47	48	48	48	n.a.	n.a.	n.a.	n.a.
Wo	28	30	29	40	50	44	50	49	48	48	49	n.a.	n.a.	n.a.	n.a.

[1]Assuming 6 oxygen atoms per unit cell of clinopyroxene.
[2]Assuming 12 oxygen atoms per unit cell of clinopyroxene.

TABLE 5.7.—*Major-element analyses of greenstones of the Baker terrane, northeastern Oregon*

[Values in weight percent; ---, not determined]

Sample	PH-76	MV-48	MV-48A	DXB-17	DXB-19	DXB-20	V-252	NF-64	NF-65	BR-49
SiO_2	47.5	52.2	51.6	55.4	53.4	53.6	57.1	55.0	53.3	51.2
Al_2O_3	22.0	16.0	16.2	21.5	17.5	18.1	16.0	21.6	18.8	18.6
TiO_2	1.1	1.5	1.4	1.0	1.5	1.3	1.1	.9	.9	.7
Fe_2O_3	4.5	5.0	5.5	3.2	5.4	3.8	5.3	3.9	4.4	4.1
FeO	5.1	5.8	6.3	3.6	6.2	4.4	6.0	4.5	5.1	4.7
MnO	.16	.16	.14	.11	.26	.18	.18	.11	.17	.25
MgO	3.6	6.2	6.1	3.0	5.4	5.9	3.5	3.9	4.7	5.8
CaO	11.9	7.8	8.3	7.8	6.4	7.8	6.9	4.9	8.3	11.2
Na_2O	3.5	3.3	3.0	3.3	2.8	2.8	3.3	4.6	3.4	3.2
K_2O	.01	1.57	1.07	.54	.54	1.43	.02	.06	.32	.01
P_2O_5	.13	.16	.16	.18	.26	.36	.13	.11	.13	.11
Total	99.5	99.7	99.8	99.6	99.7	99.7	99.5	99.6	99.5	99.9

Sample	BR-52	BR-59	BR-59A	V-27	BR-5	M-42	M-46	M-208	M-213	M-240
SiO_2	53.4	52.3	56.4	47.9	49.8	49.27	51.55	45.87	48.19	43.63
Al_2O_3	16.4	17.7	16.4	16.1	18.5	18.92	19.90	12.53	20.13	17.63
TiO_2	.9	.8	.9	2.0	3.2	.29	.21	.32	.22	.46
Fe_2O_3	4.6	4.2	4.2	4.5	5.1	1.3	1.76	1.52	1.16	3.37
FeO	5.5	4.8	4.8	7.1	8.2	6.5	4.21	7.02	3.16	5.63
MnO	.18	.13	.14	---	.2	---	---	---	---	---
MgO	5.8	6.6	5.7	9.5	6.2	6.57	6.40	14.40	7.90	12.72
CaO	8.7	9.8	6.9	9.0	4.3	15.62	15.10	15.95	17.35	15.80
Na_2O	3.7	3.2	4.1	3.1	3.5	.61	.58	.21	.61	.41
K_2O	.02	.02	.03	.04	.03	.09	.11	.06	.05	.05
P_2O_5	.09	.09	.08	.3	.4	---	---	---	---	---
Total	99.3	99.6	99.7	99.9	99.6	99.15	99.82	97.88	99.77	99.70

land-arc to island-arc-tholeiite geochemical signatures. Silicic metavolcanic rocks (53–55 percent SiO_2) are present along the North Fork of the John Day River. These rocks are strongly deformed, but in some localities an intergranular texture is preserved. They plot in the destructive-margin field on a Hf-Ta-Th discriminant diagram (Wood and others, 1979) and in fields for island-arc tholeiite and MORB on a MnO/TiO_2/P_2O_5 discriminant diagram (Mullen, 1983b). These rocks have a slightly LREE-depleted REE pattern, with a substantially negative Eu anomaly. The fairly silicic composition of these greenstones, their intergranular character, and the geochemical discriminants suggest an island-arc origin for these rocks as well.

Metavolcanic rocks that may have MORB affinity occur as knockers of pillowed greenstone in serpentinite-matrix melange near Mount Vernon, Oreg. (fig. 5.1). They fall within MORB fields on geochemical discriminant diagrams, and have flat 10×chondrite REE patterns. Relict clinopyroxenes have compositions typical of clinopyroxene from midocean-ridge basalts or arc tholeiites (sample MV-48A, table 5.6). Similar compositions have been reported for the same area by Carpenter and Walker (1992).

Alkalic mineralogy and geochemistry characterize pillowed metabasalts at two widely separated localities. Well-preserved titanaugite has nearly identical compositions in the pillowed basalts from both the Greenhorn Mountains (sample V-27A, table 5.6) and Sturgill, Oreg., on the west bank of the Snake River (fig. 5.1; sample BRS, table 5.6). Pyroxene compositions indicate alkalic affinity for these rocks. The metabasalts are high in TiO_2 (2–3.4 weight percent) and are mildly LREE-enriched. They are similar in petrography and geochemistry to oceanic transform basalts, as well as to many basalts recently reported from rifted-arc environments.

Fragments of plutonic ophiolitic rocks, principally gabbro, occur throughout the Baker terrane. They range in dimension from meter-sized knockers in serpentinite matrix to masses several kilometers square. They are usually deformed and metamorphosed to lower greenschist facies. Metagabbro exposed in the North Fork of the John Day River (fig. 5.1) is so strongly sheared that its phaneritic character is vir-

tually obliterated. Other gabbro, especially south-southeast of Olive Lake in the Greenhorn Mountains, has been locally transformed into flaser gneiss. Most plutonic rocks are metamorphosed to greenschist facies. Amphibolite and garnet amphibolite facies rocks are also present, mostly in the western part of the terrane. There is little apparent stratigraphic order to mafic and ultramafic plutonic blocks within the Baker terrane. Recognizable lithic types include isotropic clinopyroxene-rich gabbro, cumulate clinopyroxene-rich gabbro, layered two-pyroxene gabbro, layered peridotite and gabbro, clinopyroxenite (wehrlite), dunite, and harzburgite.

Clinopyroxenes from plutonic ophiolitic rocks of the Baker terrane plot in a broad scatter on a pyroxene quadrilateral. Immediately west of the Canyon Mountain Complex, these rocks resemble the complex in composition (Carpenter and Walker, 1992). Elsewhere, the chemistry and pyroxene compositions of the examined blocks do not overlap those of the Canyon Mountain Complex. Pyroxene samples from the Greenhorn Mountains, near Olive Lake (fig. 5.1; sample M42, table 5.6), are low-Cr augite, are enriched in TiO_2 and Al_2O_3, and plot in alkalic or island-arc fields on discriminant diagrams. Gabbro from Ben Harrison peak (sample M46, table 5.6), also in the Greenhorn Mountains, yields low-Ti augite similar to arc-tholeiite clinopyroxene. Clinopyroxenes from ultramafic rocks in the Baker terrane (samples M80, M91, table 5.6) are less calcic than clinopyroxene from lithically equivalent units in the Canyon Mountain Complex, and are subalkalic. On pyroxene discriminant diagrams, clinopyroxenes from the plutonic rocks plot in island-arc fields (fig. 5.13).

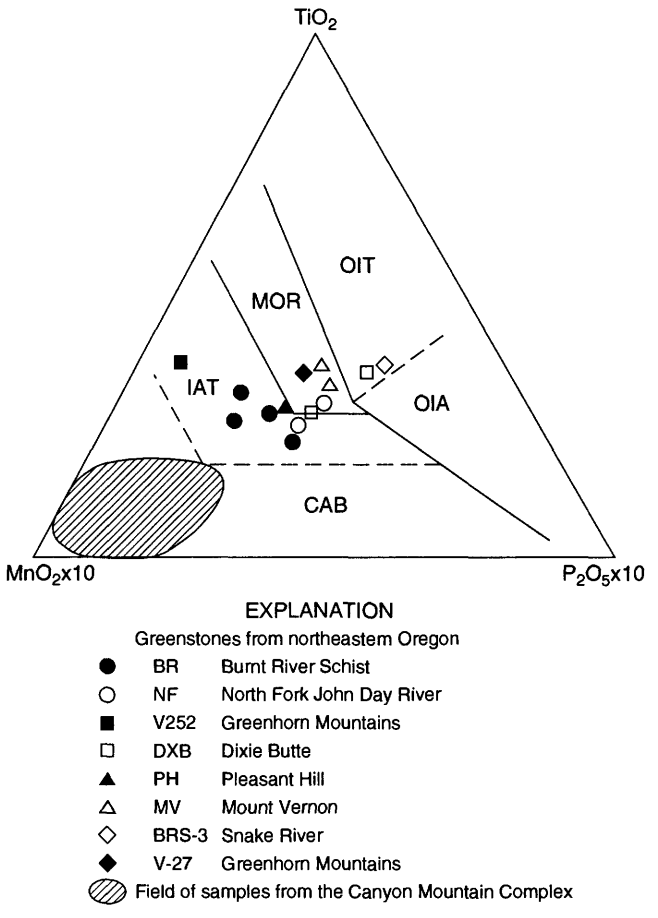

FIGURE 5.14.—$MnO/TiO_2/P_2O_5$ plot for mafic and ultramafic rocks of the Canyon Mountain Complex (shaded area) and greenstones of northeastern Oregon (data points). Abbreviations for fields of basalt compositions are as follows: CAB, calc-alkaline basalt; IAT, island-arc tholeiite; MOR, midocean ridge; OIA, ocean-island alkalic; OIT, ocean-island tholeiite. Modified from Mullen, 1983b.

Whole-rock geochemistry of the gabbros and peridotites in the Baker terrane is of dubious value as a tectonic discriminant because the rocks are thoroughly altered and deformed. On a plot of SiO_2 versus FeO*/MgO and on an AFM diagram, several compositions are apparently more tholeiitic than those of rocks of the Canyon Mountain Complex. However, this difference could be due simply to greater mobilization of MgO in the Baker terrane samples.

Trace-element data also show some differences between the Canyon Mountain Complex and lithically equivalent plutonic fragments from the Baker terrane. The gabbro that contains clinopyroxene with compositions characteristic of arc tholeiite has a relatively flat 4–12×chondrite REE pattern with slight LREE depletion and a small positive Eu anomaly, similar to the REE pattern of oceanic cumulate gabbro (Tiezzi and Scott, 1980). Peridotites of the Baker terrane analyzed in this study are far more REE-enriched and especially LREE-enriched than lithically equivalent units of the Canyon Mountain Complex. Although this enrichment may be due to alteration or to limited metasomatism from nearby granitic intrusions, it may also be related to original differences.

IMPLICATIONS FOR THE ORIGIN OF THE BAKER TERRANE

The origin of the Baker terrane can be read in the lithic types, geochemistry, and metamorphic facies of its components. The greenstones of the Baker terrane come from arc, midocean-ridge, and rift or seamount environments. The greenstones are incorporated into serpentinite-matrix melange with moderate- to high-pressure schists, allochthonous limestones, and diverse clastic sedimentary rocks. The environment

that best fits this assemblage is a subduction zone or deep fore-arc setting.

The Canyon Mountain Complex clearly carries an island-arc signature. Its gabbros have arc-tholeiite affinities. Its overall stratigraphy, including the upper plagiogranites and keratophyres with calc-alkaline geochemistry, is more characteristic of arc than of oceanic crust. The timing and nature of later magmatic events (gabbro infiltration, migmatitic melting and recrystallization) need further clarification. However, high shear stress may have played a role in them.

The greenstones represent environments that fit well in a subduction zone or deep fore-arc environment. The most abundant greenstones in the Baker terrane have island-arc geochemical affinities and contain early-crystallizing clinopyroxenes with intergranular textures generally characteristic of island-arc basalts. These rocks probably represent the early, basal material of arc volcanoes, rather than volcanic cones or segments of stratovolcanoes. Alkalic greenstones may be related to intra-arc rifting, transform (enriched-MORB, or EMORB) basalts, or oceanic-island environments. MORB affinities are most abundant in the western part of the terrane, fitting well with a model of east-facing subduction, at least in the Triassic.

Many plutonic components of the Baker terrane, aside from the Canyon Mountain Complex, seem to be more tholeiitic than the volcanic greenstones. They are distinct from the arc-related Canyon Mountain Complex in mineralogy and geochemistry. They may represent oceanic crust or primitive arc magmas.

The data presented above indicate that the Baker terrane contains many petrotectonic units that formed in or could have been associated with a subduction-zone or deep fore-arc environment. Detailed studies of fore arcs in the Marianas, Tonga, and Kermadec active arc systems in the western Pacific Ocean (Bloomer, 1983; Bloomer and others, 1988) have revealed that a combination of calc-alkaline and arc-tholeiite affinities in volcanic and plutonic components is characteristic of the submarine parts of fore arcs. Additional components of the erosive, active Marianas fore arc reported by Bloomer and Hawkins (1983) are fragments of oceanic crust, serpentinite diapirs, and alkalic basalts. Plutonic rocks are deformed. Siliceous sedimentary rocks, cherts, and allochthonous shallow-water limestones are also recognized by Bloomer (1983). Coarse sediments recognized in Deep Sea Drilling Project (DSDP) cores from the Marianas fore arc include conglomerates and breccias. All these components are present in the Baker terrane, along with a seemingly coherent ophiolite that represents early island-arc or fore-arc magmatism.

Thus, a reasonable model for the Baker terrane, based upon the mineralogy and geochemistry of its mafic and ultramafic components, the variety of its incorporated igneous, sedimentary, and metamorphic lithic types, and the preponderance of sheared serpentinites, is an erosive fore arc and remnant subduction zone. The rarity of glaucophane blueschists in the Baker terrane (Bishop, chap. 4, this volume; Mullen, 1978) suggests that shear stresses in the subduction zone were high, exceeding 50 megapascals (about 5 kilobars), and that subduction rates were high (greater than about 10 cm/yr) according to amphibole stability work by Peacock (1992). Subduction rates and shear stress may have been lower in the Triassic, during eastward-directed subduction proposed by Vallier (1992), if the blueschists near Mitchell reflect lower shear stresses related to Triassic subduction and formation of the Olds Ferry terrane. The mostly Permian to Early Triassic age of rocks in the Baker terrane suggests that the Baker terrane began as a fore arc and subduction zone related to the Wallowa arc and that it underwent a complex history of rapid subduction, high shear stresses, internal mixing, and a possible subduction-zone polarity reversal (Vallier, 1992). Generation of plagiogranites of the Canyon Mountain Complex at about 268 Ma, and the dynamothermal metamorphic ages of 255 to 269 Ma from melange just west of the Canyon Mountain Complex, may be related to a tectonic or petrotectonic event such as subduction-zone polarity reversal, or to the inception of a different subduction zone. This event may also be tied to slower subduction in the Triassic and eventual generation of the Olds Ferry terrane.

REFERENCES CITED

Avé Lallemant, H.G., 1976, Structure of the Canyon Mountain (Oregon) ophiolite complex and its implication for seafloor spreading: Geological Society of America Special Paper 173, 49 p.

Bishop, E.M., 1988, Igneous petrology of the Baker Melange Terrane and the Canyon Mountain complex, eastern Oregon: Geological Society of America Abstracts with Programs, v. 20, p. 407.

Blome, C., and Nestell, M., 1992, Field guide to the geology and paleontology of pre-Tertiary volcanic arc and melange rocks, Grindstone, Izee, and Baker terranes, east-central Oregon: Oregon Geology, v. 554, p. 123-141.

Bloomer, S., 1983, Distribution and origin of igneous rocks from the landward side of the Mariana trench—Implications for its structure and evolution: Journal of Geophysical Research, v. 88, p. 7411-7428.

Bloomer, S.H., and Hawkins, J.W., 1983, Gabbroic and ultramafic rocks from the Mariana Trench—An island arc ophiolite, *in* Hayes, D.E., ed., The tectonic and geologic evolution of Southeast Asia seas and islands, Part II: American Geophysical Union Monograph 27, p. 294-317.

Bloomer, S.H., Parsons, L., Huggett, Q., and Pearce, J., 1988, GLORIA Surveys of the Tonga and Kermadec trenches: Eos (Transactions, American Geophysical Union), v. 69, p. 1442.

Boudier, F., and Coleman, R.G., 1981, Cross section through the peridotite of the Samail ophiolite, southeastern Oman Mountains: Journal of Geophysical Research, v. 86, p. 2573-2592.

Brooks, H.G., 1979, Plate tectonics and the geologic history of the Blue Mountains: Oregon Geology, v. 41, p. 71-80.

Carpenter, P.S., and Walker, N.W., 1992, Origin and tectonic significance of the Aldrich Mountain serpentinite matrix melange, northeastern Oregon: Tectonics, v. 11, p. 690-708.

Coleman, R.G., 1977, Ophiolites: New York, Springer Verlag, 229 p.

Dickinson, W.R., 1979, Mesozoic forearc basin in central Oregon: Geology, v. 7, p. 166-170.

Dungan, M.A., and Avé Lallemant, H.G., 1977, Formation of small dunite bodies by metasomatic transformation of harzburgite in the Canyon Mountain ophiolite, northeast Oregon, *in* Dick, H.J.B, ed., Magma genesis: Oregon Department of Geology and Mineral Industries Bulletin 96, p. 109-128.

Flager, P.A., and Spray, J.G., 1991, Generation of plagiogranite by amphibolite anatexis in oceanic shear zones: Geology, v. 19, p. 70-73.

Gerlach, D., 1980, Petrology and geochemistry of plagiogranite and related basic rocks of the Canyon Mountain ophiolite, Oregon: Houston, Rice University, M.S. thesis, 198 p.

Gerlach, D., Avé Lallemant, H.G., and Leeman, W.P., 1981, An island arc origin for the Canyon Mountain complex, eastern Oregon, USA: Earth and Planetary Science Letters, v. 53, p. 255-265.

Gerlach, D., Leeman, W.P., Bishop, E.M., and Pearcy, L.A., 1988, Isotopic and trace element constraints on timing and the nature of magmatism in the Canyon Mt. Ophiolite, Oregon: Geological Society of America Abstracts with Programs, v. 20, p. A158.

Himmelberg, G.H., and Loney, R.A., 1980, Petrology of ultramafic and gabbroic rocks of the Canyon Mountain ophiolite, Oregon: American Journal of Science, v. 280A, p. 232-268.

Irvine, T.N., 1980, Magmatic infiltration metasomatism, double-diffusive fractional crystallization, and adcumulus growth in the Muskox intrusion and other layered intrusions, *in* Hargraves, R.B., ed., Physics of magmatic processes: Princeton, N.J., Princeton University Press, p. 325-383.

Jorgenson, D.B., 1979, Textural banding in igneous rocks—An example from SW Oregon: American Mineralogist, v. 64, p. 527-530.

Marlow, M.S., Johnson, L.E., Pearce, J.A., Fryer, P.B., Pickthorn, L.B., and Murton, B.J., 1992, Upper Cenozoic volcanic rocks in the Mariana forearc recovered from drilling at Ocean Drilling Program site 781—Implications for forearc magmatism: Journal of Geophysical Research, B, Solid Earth and Planets, v. 97, no. 11, p. 15,085-15,097.

Moore, A.C., 1973, Studies of igneous and tectonic textures and layering in rocks of the Gosse Pile intrusion, central Australia: Journal of Petrology, v. 14, p. 49-79.

Morse, S.A., 1969, The Kiglapait layered intrusion, Labrador: Geological Society of America Memoir 112, 204 p.

Mullen, E.D., 1978, Geology of the Greenhorn Mountains, northeastern Oregon: Corvallis, Oregon State University, M.S. thesis, 372 p.

———1983a, Petrology and regional setting of peridotite and gabbro of the Canyon Mountain Complex, northeast Oregon: Corvallis, Oregon State University, Ph.D. dissertation, 277 p.

———1983b, $MnO/TiO_2/P_2O_5$—A minor element discriminant for basaltic rocks of oceanic environments and its implications for petrogenesis: Earth and Planetary Science Letters, v. 62, p. 53-62.

———1985, Petrologic character of Permian and Triassic greenstones from the Melange terrane of eastern Oregon, and their implications for terrane origin: Geology, v. 13, p. 131-134.

Nesbitt, E.G., and Pearce, J., 1977, Clinopyroxene composition in mafic lavas from different tectonic settings: Contributions to Mineralogy and Petrology, v. 63, p. 149-160.

Nicolas, A., and Jackson, M., 1982, High temperature dikes in peridotites—Origin by hydraulic fracturing: Journal of Petrology, v. 23, p. 568-582.

Peacock, S.M., 1992, Blueschist-facies metamorphism, shear heating, and P-T-t paths in subduction zones: Journal of Geophysical Research, v. 97, p. 17,693-17,708.

Pearce, T.H., Gorman, B.E., and Birkett, T.C., 1977, The relationship between major element geochemistry and tectonic environment of basic and intermediate volcanic rocks: Earth and Planetary Science Letters, v. 36, p. 121-132.

Pearcy, L.G., 1987, Clinopyroxene compositions and petrogenesis of the mantle-crust transition zone: Geological Society of America Abstracts with Programs, v. 19, p. 439.

———1991, Nascent island arc petrogenesis for the basal crustal cumulates of the Canyon Mountain Complex, northeastern Oregon: Geological Society of America Abstracts with Programs, v. 23, no. 5, p. A272.

Silberling, N.J., and Jones, D.L., 1984, Lithotectonic terrane maps of the North American Cordillera: U.S. Geological Survey Open File Report 84-523, 43 p.

Thayer, T.P., 1972, Gabbro and epidiorite versus granulite and amphibolite—A problem in the ophiolite assemblage: Sixth Caribbean Geological Conference, Margarita, Venezuela, p. 315-320.

———1976, Metallogenic contrasts in the plutonic and volcanic rocks of the ophiolite assemblage: Geological Association of Canada Special Paper No. 14, p. 211-219.

———1977, The Canyon Mountain complex, Oregon, and some problems of ophiolites, *in* Coleman, R.G., and Irwin, W.P., eds., North American ophiolites: Oregon Department of Geology and Mineral Industries Bulletin 95, p. 93-105.

Thy, P., and Esbensen, K.H., 1982, Origin of fine-grained granular rocks in layered intrusions: Geological Magazine, v. 119, p. 405-412.

Tiezzi, L.J., and Scott, R.B., 1980, Crystal fractionation in a cumulate gabbro, mid-Atlantic ridge, 26 N: Journal of Geophysical Research, v. 85, p. 5454-5488.

Vallier, T.L., 1992, Late Triassic change in convergence direction, Blue Mountains island arc, Oregon and Washington: Geological Society of America Abstracts with Programs, v. 24, p. 88.

Vernon, R.H., 1970, Comparative grain boundary studies of some basic and ultrabasic granulites: Scottish Journal of Geology, v. 6, p. 337-351.

Wood, D.A., Jordon, J.L., and Treuil, M., 1979, A re-appraisal of the usage of trace elements to classify and discriminate between magma series erupted at different tectonic settings: Earth and Planetary Science Letters, v. 45, p. 326-336.

6. TECTONIC IMPLICATIONS OF U-Pb ZIRCON AGES OF THE CANYON MOUNTAIN COMPLEX, SPARTA COMPLEX, AND RELATED METAPLUTONIC ROCKS OF THE BAKER TERRANE, NORTHEASTERN OREGON

By NICHOLAS W. WALKER[1]

CONTENTS

	Page
Abstract	247
Introduction	247
Acknowledgments	248
Description of terranes	250
U-Pb geochronology	250
Analytical methods	250
Mass spectrometry	251
Procedural Pb blanks	251
Analytical uncertainty	251
Geochronologic results	251
Elkhorn Ridge argillite	251
Burnt River schist	256
Ultramafic-mafic-silicic ophiolitic igneous suites	256
Canyon Mountain Complex	256
Previous geochronologic investigations	259
U-Pb zircon geochronologic results	259
Sparta complex	260
Previous geochronologic investigations	261
U-Pb zircon geochronologic results	263
Serpentinite-matrix melange	263
Melange in the Aldrich Mountains	263
Timing of melange formation	265
Paleotectonic setting of the Baker terrane	265
Summary and conclusions	267
References cited	267

ABSTRACT

The Baker terrane consists of plutonic, metamorphic, and sedimentary rocks of oceanic origin that now are the components of kilometer-scale tracts of melange and broken formation. The structural character of the terrane resulted from the breaking and mixing of Permian to Triassic volcanic-plutonic arc crust and sediment cover. Plutonic and metaplutonic constituents of this terrane represent this volcanic-plutonic arc crust and include the ophiolitic Canyon Mountain Complex, the Sparta complex, and other tectonic blocks in melange and broken formation. U-Pb zircon ages for separate intrusive phases in the Canyon Mountain Complex vary from 276 to 268 Ma; this age range indicates an Early Permian multistage magmatic history for the complex. The Sparta complex exhibits a two-stage igneous history that involved magmatic activity at 253 Ma and 215 Ma. Other plutonic bodies in the Baker terrane range in crystallization age from 279 Ma to 230 Ma; this range overlaps the age of Permian to Triassic sedimentation within the terrane. These ages are also synchronous with the age of plutonism within the Wallowa and Olds Ferry terranes (268–225 Ma), which have been interpreted as vestiges of ensimatic volcanic-plutonic complexes. Inferences drawn from geochronology, lithology, and structure of the Baker terrane suggest that it constituted the fore-arc region of a Permian-Triassic arc-type ensimatic volcanic-plutonic complex now represented by the Wallowa and Olds Ferry terranes.

INTRODUCTION

Numerous erosional inliers in the extensive Cenozoic volcanic and sedimentary blanket of northeastern Oregon and westernmost central Idaho unveil a lithologically diverse and structurally complex assemblage of late Paleozoic to late Mesozoic rocks of oceanic affinity (Vallier and others, 1977; Brooks and Vallier, 1978; Dickinson and Thayer, 1978). These rocks are exposed in a generally northeasterly trending, discontinuous belt of inliers extending approximately 350 km between the towns of Mitchell, Oreg., and Grangeville, Idaho (fig. 6.1).

This heterolithologic assemblage includes variably deformed and metamorphosed igneous rocks and sedimentary rocks derived from volcanic-plutonic complexes, ultramafic-mafic-silicic igneous rocks, chert-argillite broken formation, polymict melange tracts, and thick sequences of chiefly Upper Triassic to Upper Jurassic volcaniclastic sedimentary rocks—all of which have been intruded by numerous gabbroic to granodioritic plutons of Late Jurassic to Early Cretaceous age (Taubeneck 1957, 1958, 1964, 1967;

[1]Present address: Department of Geological Sciences, Brown University, Providence, RI 02912

Armstrong and others, 1977; Walker, 1986, 1989). The entire assemblage is regarded as allochthonous (Vallier and others, 1977; Hillhouse and others, 1982) and is among the most inboard of paleo-oceanic terranes within the Cordillera.

Rocks within this assemblage are considered to represent the five terranes distinguished by Silberling and others (1984): the Wallowa, Olds Ferry, Grindstone, Izee, and Baker terranes. These terranes, whose distribution is shown in figure 6.2, are bounded by high- to low-angle reverse faults or high-angle normal faults, commonly marked by zones of serpentinite. The terranes are crosscut by latest Jurassic to Early Cretaceous plutons (Armstrong and others, 1977, Walker, 1986, 1989). At some localities, Early Cretaceous plutons intrude interterrane boundaries (Walker, 1986, 1989). Such a relationship indicates that structural juxtaposition of terranes dates from the Early Cretaceous. After the Early Cretaceous but prior to the Eocene, the entire terrane assemblage rotated clockwise 60°±29° (Wilson and Cox, 1980).

This chapter presents U-Pb zircon geochronologic data for igneous and metaigneous components of the Baker terrane and describes the tectonic implications of these age data.

ACKNOWLEDGMENTS

James Mattinson, George Tilton, and Cliff Hopson of the University of California at Santa Barbara

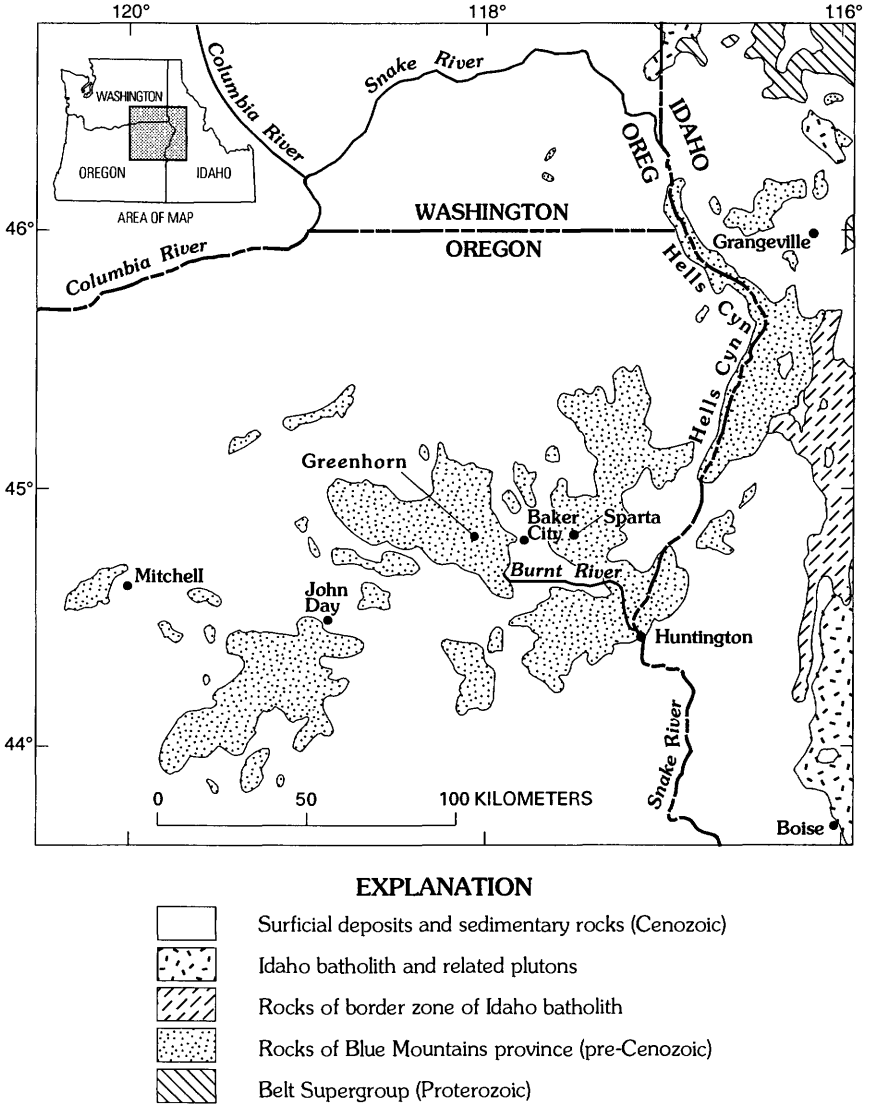

FIGURE 6.1.—Regional geologic setting of pre-Cenozoic rocks of the Blue Mountains province.

supervised the dissertation research on which this report is based. Bob Fleck and Tracy Vallier of the U.S. Geological Survey and Howard Brooks of the Oregon Department of Geology and Mineral Industries (DOGAMI) provided helpful reviews of the manuscript. Tracy Vallier, Trudy Vallier, David Scholl, and Ellery Ingall assisted in fieldwork. Tracy Vallier, Howard Brooks, and Mark Ferns (DOGAMI)

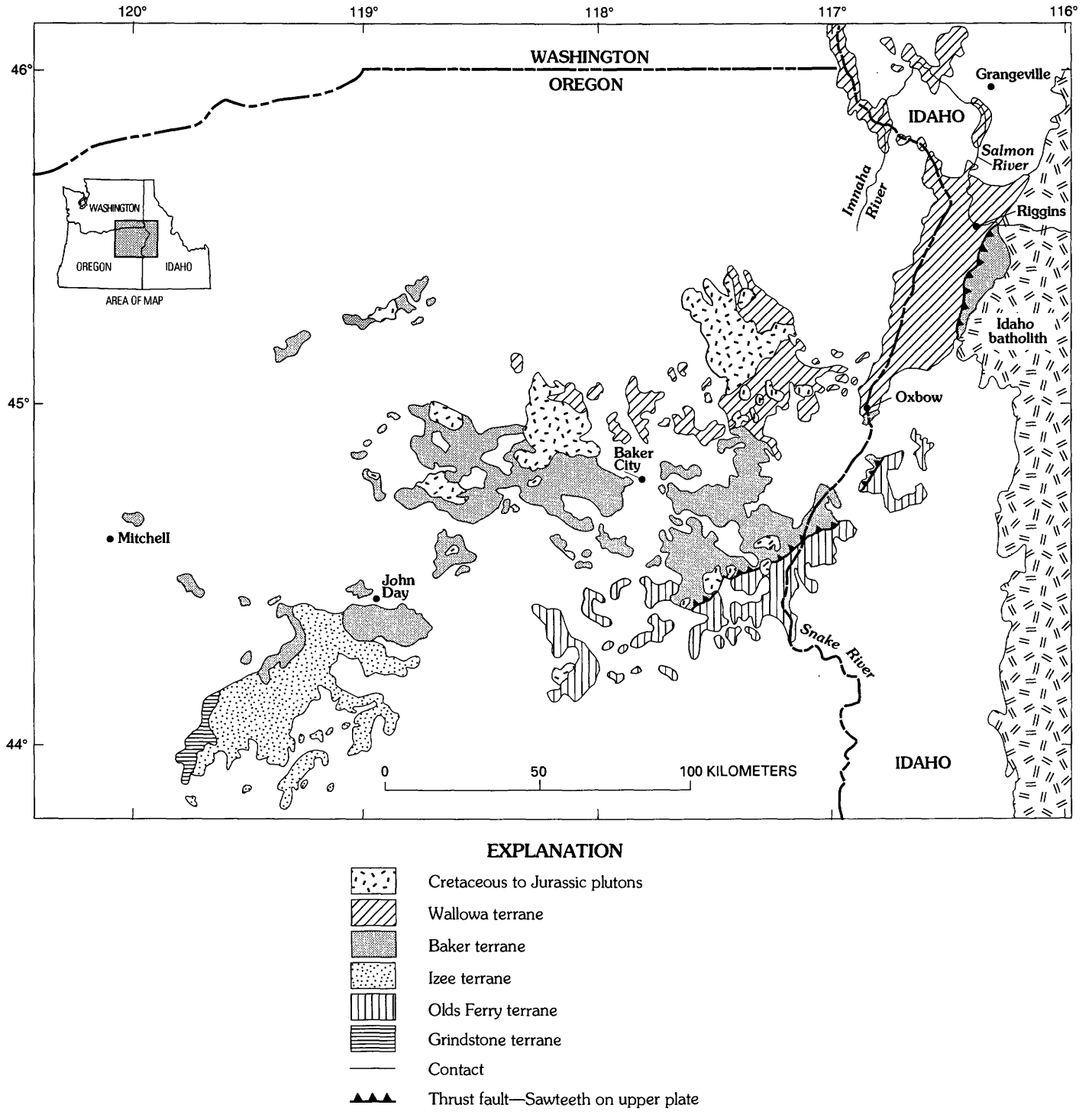

FIGURE 6.2.—Terrane map of northeastern Oregon and westernmost central Idaho (modified from Silberling and others, 1984).

led me on numerous field trips and shared their abundant knowledge of regional geologic relations in the Baker terrane and in northeastern Oregon and west-central Idaho. This research was supported by the U.S. Geological Survey, by grants from the Oregon Department of Geology and Mineral Industries, Sigma Xi, and the Penrose fund of the Geological Society of America, and by a National Science Foundation grant to James Mattinson.

DESCRIPTION OF TERRANES

The Wallowa terrane consists of a thick sequence of volcanic flows, volcaniclastic rocks, and intercalated sedimentary rocks of the Permian and Triassic Seven Devils Group (Vallier, 1977; chap. 3, this volume) which is capped by Triassic platform-carbonate and fine-grained clastic rocks of Triassic and Jurassic age. Crystalline rocks that represent the basement and plutonic infrastructure of the Seven Devils Group have magmatic ages that range from 309 Ma to 225 Ma (Walker, 1986). The Wallowa terrane is interpreted as part of an arc-type ensimatic volcanic-plutonic complex capped by intra-arc sedimentary rocks (Vallier, 1977; Vallier and others, 1977).

The Olds Ferry terrane consists of Upper Triassic volcanic and volcaniclastic rocks, intercalated sedimentary rocks, and volumetrically minor plutonic rocks; one representative pluton has yielded Middle Triassic U-Pb zircon ages (Walker, 1986). This assemblage, considered to be part of an arc-type ensimatic volcanic-plutonic complex (Vallier and others, 1977), is unconformably overlain by Lower and Middle Jurassic clastic strata of the Izee terrane, which are interpreted as fore-arc deposits by Dickinson (1979).

The Grindstone terrane is a melange tract consisting of structurally chaotic, generally lenticular blocks of silicic metavolcanic rocks, volcaniclastic greywacke, limestone, and sandstone in a matrix of deformed radiolarian chert and argillite. Although the major lithologic boundaries are faults, relatively coherent and stratigraphically distinct bodies are present. Faunal ages of these rocks range from Middle Devonian to Permian. Dickinson and Thayer (1978) suggested that the overall lithologic association and structural juxtaposition of silicic metavolcanic rocks, greywacke, and limestone in a matrix of deformed chert and argillite are evidence that this terrane represents a subduction-related complex.

The Izee terrane is a thick (locally exceeding 15 km) sequence of Upper Triassic to Upper Jurassic turbidites rich in volcanogenic components and lesser amounts of volcanic flows and tuffs. Dickinson (1979) interpreted this terrane to be of fore-arc origin.

The Baker terrane is an elongate tract with a general northeasterly trend and is exposed over a wide area (fig. 6.2). The terrane consists of a mixture of structural blocks comprising variably metamorphosed and deformed igneous suites (some of which are characteristically ophiolitic in stratigraphy), chert-argillite broken formation, polymict serpentinite-matrix melange, and limestone slabs. The southwestern part consists mainly of melange whereas more structurally coherent domains of broken formation distinguish the northeastern part. No basement to this terrane has been recognized. The overall dismembered to chaotic character of the terrane resulted from the breaking and mixing of the original plutonic and metamorphic crust upon which sedimentary and volcanic rocks had accumulated. The only likely present-day exposures of such crystalline rocks are represented by kilometer-scale slabs and blocks such as the Canyon Mountain Complex, the informally named Sparta complex of Phelps (1979), and other smaller plutonic and metamorphic fragments in melange. Considering that these plutonic rocks appear similar in the field, it is of critical importance to establish the crystallization ages of such components within the Baker terrane because their ages bear significantly on the tectonic evolution of this terrane as well as the entire pre-Tertiary terrane complex of northeastern Oregon.

U-Pb GEOCHRONOLOGY

ANALYTICAL METHODS

Isotopic analyses were conducted from 1980 through 1984 in the laboratories of J.M. Mattinson and G.R. Tilton at the University of California at Santa Barbara.

Zircon concentrates were obtained from 20 to 100 kg of sample by standard procedures of crushing and mineral separation using magnetic, heavy liquid, and Wilfley table techniques. Zircon concentrates were split into fractions on the basis of physical properties such as size and magnetic character and then hand-picked to remove impurities. Purified zircon fractions weighing from 15 to 30 mg were weighed into Teflon® dissolution capsules and given final acid washes in ultrapure 6N HCl and 7N HNO_3. Approximately 1 ml of ultrapure concentrated HF and 25 µl of concentrated HNO_3 were added to the dissolution capsule for digestion. A mixed U-Pb tracer was either delivered to a capsule that contained a representative dry split of the zircon fraction or delivered to an aliquot of the total solution following digestion. The dissolu-

tion capsules were inserted in steel jackets, sealed, and placed in a 210°C oven for four to six days. Then the HF-HNO_3 mix was evaporated and fresh acid added before an additional four-day digestion. The HF-HNO_3 was evaporated in a clean-air environment and ultrapure 3N HCl was added to prepare the zirconium salts for ion exchange chemistry. The method of chemical separation of U and Pb employed was similar to that of Krogh's (1973).

MASS SPECTROMETRY

Pb and U were loaded onto single rhenium filaments for mass spectrometry. Pb was loaded using a silica gel-phosphoric acid technique similar to that described by Cameron and others (1969); U was loaded following a phosphoric acid-graphite method similar to that of Arden and Gale's (1974).

Isotopic ratios of Pb and U were measured on a 35-cm-radius, 90°-sector, single-focusing, solid-source mass spectrometer. Within-run precision (at the two-sigma level) of the measured isotopic ratios in every analysis was better than ±0.1 percent for $^{235}U/^{238}U$, ±0.2 percent for $^{208}Pb/^{206}Pb$, ±0.15 percent for $^{207}Pb/^{206}Pb$; for $^{206}Pb/^{204}Pb$, it ranged from ±0.1 percent for low $^{206}Pb/^{204}Pb$ ratios (<1,000) to as great as ±11 percent for very high $^{206}Pb/^{204}Pb$ ratios (>17,000).

Measured U and Pb ratios are corrected for instrumental mass fractionation by replicate analyses of National Bureau of Standards (NBS) Pb standards SRM 981, SRM 982, and SRM 983, and NBS U standard SRM U500.

PROCEDURAL Pb BLANKS

Procedural Pb blanks were less than 0.3 ng whereas the total Pb concentration of individual analyzed fractions ranged from approximately 50 to 200 ng. Thus, blank Pb accounts for no more than 0.15 to 0.6 percent of the total analyzed Pb. The procedural Pb blank is therefore negligible and no blank corrections have been applied to the data.

ANALYTICAL UNCERTAINTY

Uncertainty in the calculated ages stems mainly from the precision of the within-run isotopic measurements, uncertainty in the common Pb composition (that is, blank plus initial Pb), and long-term reproducibility of analyses of NBS Pb and U standards. The combined uncertainty for individual ages reported herein was calculated on the basis of these factors.

GEOCHRONOLOGIC RESULTS

Samples used in geochronologic studies are described in table 6.1, zircon isotopic data are presented in table 6.2, and sample localities are described in figure 6.1 and figures 6.3, 6.4, and 6.6 through 6.8.

In many cases, the data presented in this chapter are slightly discordant (that is, $^{206}Pb^*$-^{238}U age ≠ $^{207}Pb^*$-^{235}U age ≠ $^{207}Pb^*$-$^{206}Pb^*$ age). Assigning precise geologic meaning to slightly discordant U-Pb ages is difficult. For geologically young zircons obtained from magmatic rocks in which there are no textural grounds for a metamorphic or thermal overprint and in which there is little cause to expect inheritance of zircons on the basis of regional geologic considerations, it is commonly observed that the $^{207}Pb^*$-$^{206}Pb^*$ ages are typically slightly older than the Pb-U ages. The cause of this age disparity may stem from one or more of the following: (1) uncertainty in the isotopic composition of common Pb used in the age calculation, (2) Pb-loss, despite the lack of textural evidence for mechanical or thermal metamorphism of the rock that houses the zircon, (3) uncertainty in the decay constants of ^{235}U and ^{238}U, and (4) volumetrically small amounts of older, entrained ("inherited") zircon around which magmatic zircon grew.

Distinguishing among the possibilities listed above is sometimes possible but was beyond the scope of this study. In no analyzed zircon fraction does strong evidence of inheritance exist and there is no evidence in the sampled rocks (other than for metagabbro of the Canyon Mountain Complex) of moderate- to high-grade metamorphism following crystallization.

Because insufficient zircon fractions were analyzed to assess the cause of the discordance, the $^{206}Pb^*$-^{238}U ages are cited as the best estimate of the crystallization ages of the sampled rocks.

ELKHORN RIDGE ARGILLITE

The most abundant supracrustal constituent of the Baker terrane is the Elkhorn Ridge Argillite (fig. 6.3), named by Gilluly (1937). The Elkhorn Ridge Argillite is mostly metamorphosed and deformed broken formation composed chiefly of chert-argillite, which locally contains crudely defined interbeds or blocks of greenstone, tuffaceous volcanic rocks, greywacke, limestone, plutonic rocks, and rare conglomerate. The stratigraphic thickness of the Elkhorn Ridge Argillite is unknown due to discontinuous exposure, structural complexity, and absence of marker horizons.

TABLE 6.1.—*Descriptions and field localities for rock samples used to obtain U-Pb zircon ages, Baker terrane, Oregon*

Sample	Locality	Field setting	Rock type, mineralogy, and texture
	Plutonic and metaplutonic rocks of the Canyon Mountain Complex		
CM79-1 -----	Canyon Mountain, Oregon, 7.5-minute quadrangle. Lat 44°18' 49" N., long 118°55'39" W.	Small pluton that intrudes cumulus gabbro.	Hornblende tonalite. Plagioclase, quartz, hornblende; secondary sericite, actinolite. Hypidiomorphic-granular texture.
CM79-3 -----	Canyon Mountain, Oregon, 7.5-minute quadrangle. Lat 44° 20'02" N., long 118°53'06" W.	Structurally concordant layer in metacumulate sequence.	Quartz-bearing gabbro. Plagioclase, orthopyroxene, clinopyroxene, magnetite, quartz; secondary serpentine, saussurite. Decussate texture.
CM79-4 -----	Canyon Mountain, Oregon, 7.5-minute quadrangle. Lat 44° 19'06" N., long 118°53'27" W.	Sample from sill complex.	Metatrondhjemite. Plagioclase, quartz; secondary epidote, saussurite. Cataclastic texture.
	Plutonic rocks of the Sparta complex		
SP-AG-81 —	Sparta, Oregon, 15-minute quadrangle. Lat 44°51'13" N., long 117°24'49" W.	Hillside exposure of silicic intrusive rocks.	Trondhjemite. Embayed quartz, plagioclase, biotite, hornblende; secondary chlorite. Porphyritic texture.
SP79-1 ------	Sparta, Oregon, 15-minute quadrangle. Lat 44°49'05" N., long 117°24'49" W.	Roadcut exposure at J.N. Bishop Spring.	Hornblende-biotite tonalite. Plagioclase, quartz, biotite, hornblende, titanite; secondary chlorite, saussurite. Hypidiomorphic-granular texture.
	Other plutonic and metaplutonic rocks of the Baker terrane		
ERA-81------	Granite, Oregon, 7.5-minute quadrangle. Lat 44°52'11" N., long 118°29'51" W.	Tectonic block within Elkhorn Ridge Argillite.	Metatrondhjemite. Plagioclase, quartz; secondary chlorite, epidote. Cataclastic texture.
OX79-1 ------	Oxman, Oregon, 7.5-minute quadrangle. Lat 43°30'42" N., long 117°31'10" W.	Tectonic block of gabbro cut by silicic dikes within Elkhorn Ridge Argillite.	Metatrondhjemite. Plagioclase, quartz, hornblende; secondary sericite, actinolite. Allotriomorphic-granular texture.
BRC79-1 ----	Lost Basin, Oregon, 7.5-minute quadrangle. Lat 44°34'47" N., long 117°33'16" W.	Small pluton cutting Burnt River Schist.	Metatrondhjemite. Plagioclase, quartz, titanite; secondary chlorite, epidote, saussurite, carbonate. Cataclastic texture.
AM80-1 -----	Aldrich Mountains Oregon, 15-minute quadrangle. Lat 45° 23'48" N., long 119°23'09" W.	Tectonic block within serpentinite-matrix melange.	Trondhjemite. Quartz, plagioclase, hornblende, titanite; secondary sericite, epidote, chlorite. Protoclastic texture.

Chert in the Elkhorn Ridge Argillite is pervasively recrystallized and, hence, radiolarians are not well preserved. Chert samples that contain identifiable radiolarian assemblages yield Permian and Late Triassic fauna (Vallier and others, 1977; Blome and others, 1986).

Middle to Late Devonian, Middle Pennsylvanian, and Early Permian fossils are reported from limestone pods (olistoliths?) within the Elkhorn Ridge Argillite (Bostwick and Koch, 1962; Brooks and others, 1976; Blome and others, 1986; Mullen-Morris and Wardlaw, 1986). Structurally separate Permian limestone blocks contain either Tethyan or North American fusulinids (Nestell, 1983). Some of the limestone blocks are recognized as allochthonous and hence at least part of the Elkhorn Ridge Argillite may be melange rather than semicoherent broken formation.

At several localities metaplutonic rocks occur as blocks within the chert-argillite matrix of the Elkhorn Ridge Argillite. These fragments range in composition

TABLE 6.2.—*Zircon isotopic data for plutonic rocks of the Baker terrane, including data for the Canyon Mountain Complex and the Sparta complex, Oregon*

Sample	Zircon fraction data[1]		Concentrations[2]		Pb isotopic composition[3]			Ages and uncertainty[4] (Ma)		
	Properties	Amount analyzed (mg)	$^{206}Pb^*$	^{238}U	$^{208}Pb/^{206}Pb$	$^{207}Pb/^{206}Pb$	$^{206}Pb/^{204}Pb$	$^{206}Pb^*/^{238}U$	$^{207}Pb^*/^{235}U$	$^{207}Pb^*/^{206}Pb^*$
Plutonic rocks of the Baker terrane										
OX79-1	c, nm, 0°	18.6	13.7	416	0.0849	0.05596	3,171	240±1	242±2	256±9
	f, nm, 0°	14.1	14.1	428	.08562	.05422	4,638	241±1	241±2	244±6
ERA-81	c, nm, 0°	18.5	6.04	180	.0869	.05220	17,752	245±1	246±2	258±4
	c, m, 0°	32.5	6.65	199	.0872	.05231	15,360	244±1	245±2	257±5
BRC79-1	c, nm, 0°	15.1	2.89	91.7	.0943	.05423	4,422	230±1	231±2	237±7
	c, m, 0°	29.1	3.06	96.2	.0879	.05238	10,558	233±1	234±2	240±5
AM80-1	bulk	23.7	9.02	236	.1971	.05365	8,170	279±1	279±2	279±6
Canyon Mountain Complex										
CM79-1	c, nm, 3°	25.5	16.6	452	0.2095	0.05464	4,832	268±1	268±1	269±4
	c, m, 0°	15.6	17.4	473	.2455	.05451	5,224	268±1	268±2	272±5
CM79-3	bulk	17.8	1.68	44.0	.2255	.09323	360	278±1	282±2	314±29
CM79-4	c, nm, 0°	18.4	1.99	52.5	.1184	.05501	4,631	276±1	278±2	278±6
	c, m, 1°	38.2	2.35	62.2	.1318	.05409	6,833	276±1	276±2	283±5
	c, m, 0°	18.0	2.58	67.5	.1224	.05467	5,197	276±1	278±2	279±5
Sparta complex										
SP-AG-81	c, nm, 0°	30.7	9.57	277	0.1180	0.05298	10,361	253±1	254±2	266±6
	f, nm, 0°	15.3	10.3	299	.1199	.05295	9,644	252±1	252±2	260±6
	c, m, 1°	31.6	16.8	484	.1243	.05288	9,552	253±1	254±2	257±5
SP79-1	c, nm, 0°	16.0	6.90	236	.0832	.05318	5,872	215±1	216±2	226±11
	c, m, 0°	24.9	6.96	237	.0918	.05439	4,028	215±1	216±2	230±8

[1]Abbreviations: c, coarse (>100 μm); f, fine (<100 μm); nm, nonmagnetic; m, magnetic. Number in degrees (°) is side tilt of Frantz magnetic separator operated at a magnet current of 1.6 amperes.

[2]Chemical processing similar to that described by Krogh (1973). Procedural Pb blanks are less than 0.3 ng. Asterisk (*) denotes radiogenic Pb corrected for blank and initial common Pb.

[3]Ratios are corrected for mass fractionation on the basis of replicate analyses of National Bureau of Standards Pb standards. Uncertainty (at the 2σ level) in the measured ratio is less than ±0.2 percent for $^{208}Pb/^{206}Pb$, less than ±0.15 percent for $^{207}Pb/^{206}Pb$, and ranges from ±0.1 to ±11 percent for $^{206}Pb/^{204}Pb$.

[4]Decay constants employed: $\lambda = 1.5513 \times e^{-10}$ for ^{238}U; $\lambda = 9.8485 \times e^{-10}$ for ^{235}U. Uncertainty in ages (stated at the 2σ level) is based on combined uncertainty in sample isotopic ratio measurements, analytical reproducibility of National Bureau of Standards Pb and U standards, uncertainty in fractionation corrections, and uncertainty in the isotopic composition of common Pb.

from serpentinized ultramafic rocks through gabbro to trondhjemite. Two such fragments were sampled (fig. 6.3) for geochronologic investigation.

In the Oxman quadrangle, east of Baker City, Oreg., a block engulfed by the Elkhorn Ridge Argillite consists of uralitized gabbro cut by dikes of trondhjemite. Two zircon fractions separated from one dike (sample OX79-1) have yielded Early Triassic $^{206}Pb^*$-^{238}U ages of 241 and 240 Ma (table 6.2).

In the Granite quadrangle (Brooks and others, 1982) metamorphosed intrusive rocks appear to be rootless fragments surrounded by Elkhorn Ridge Argillite. These metaigneous rocks consist of metamorphosed gabbro, diorite, quartz diorite, and tonalite. Two zircon fractions from tonalite (sample ERA-81) within this area have $^{206}Pb^*$-^{238}U ages of 245 and 244 Ma, indicating an Early Triassic crystallization age.

The crystallization ages for the plutonic rocks indicate that their emplacement was, at least in part, synchronous with deposition of the Elkhorn Ridge Argillite. Whether these plutons represent part of the

plutonic foundation upon which the Elkhorn Ridge Argillite was deposited or whether they are simply fragments of plutons that intruded the basin into which sedimentation was occurring remains unclear. The zircon ages, however, constrain major deformation and metamorphism of the Elkhorn Ridge Argil-

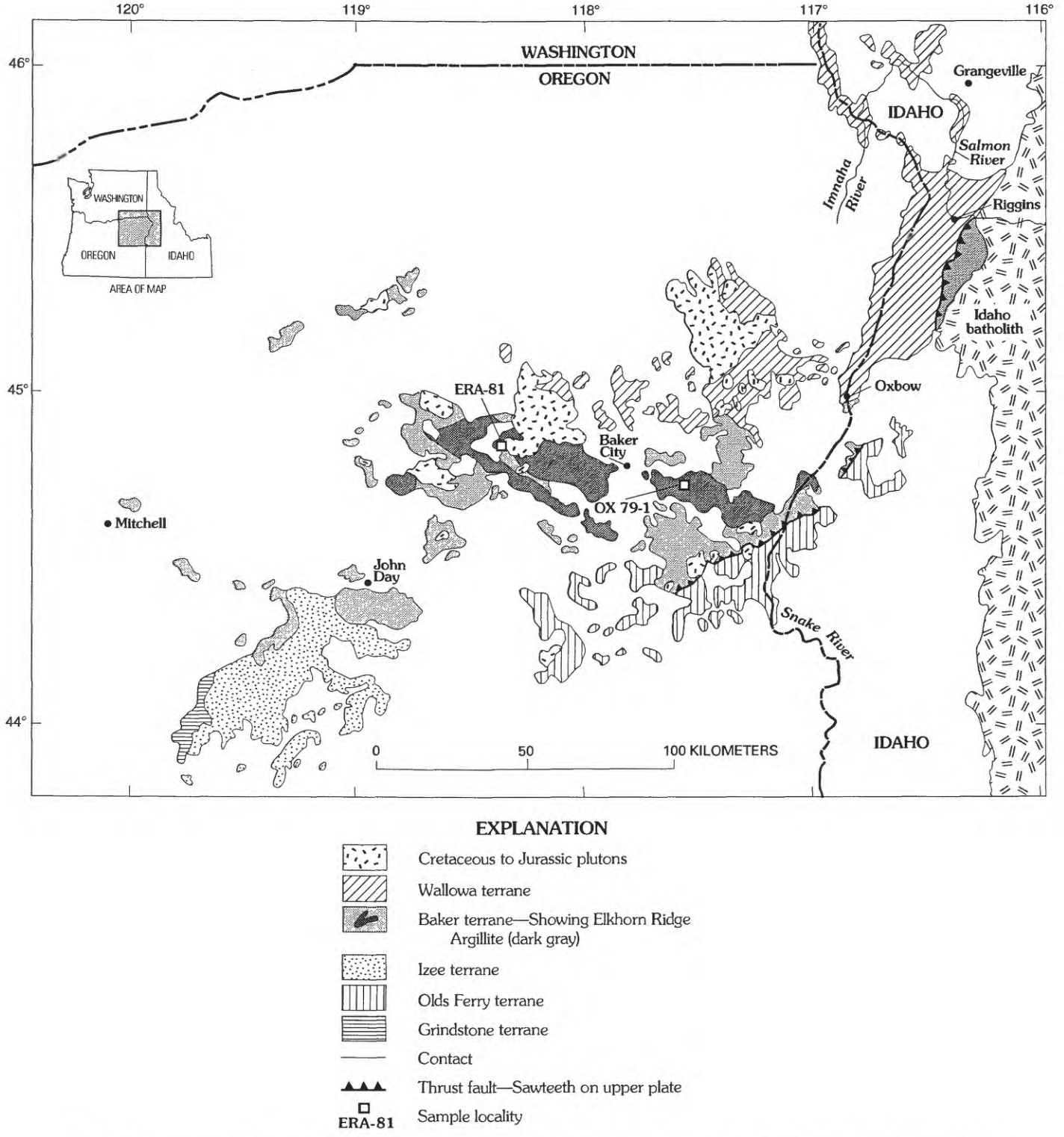

FIGURE 6.3.—Areal distribution of the Elkhorn Ridge Argillite in the Baker terrane, showing U-Pb zircon sample localities.

lite to post-240 Ma time. The formation is cut by nonmetamorphosed, undeformed Early Cretaceous plutons, the oldest of which yields U-Pb zircon ages of 144 Ma (Walker, 1989) that establish an upper limit on the time of deformation and metamorphism of the Elkhorn Ridge Argillite.

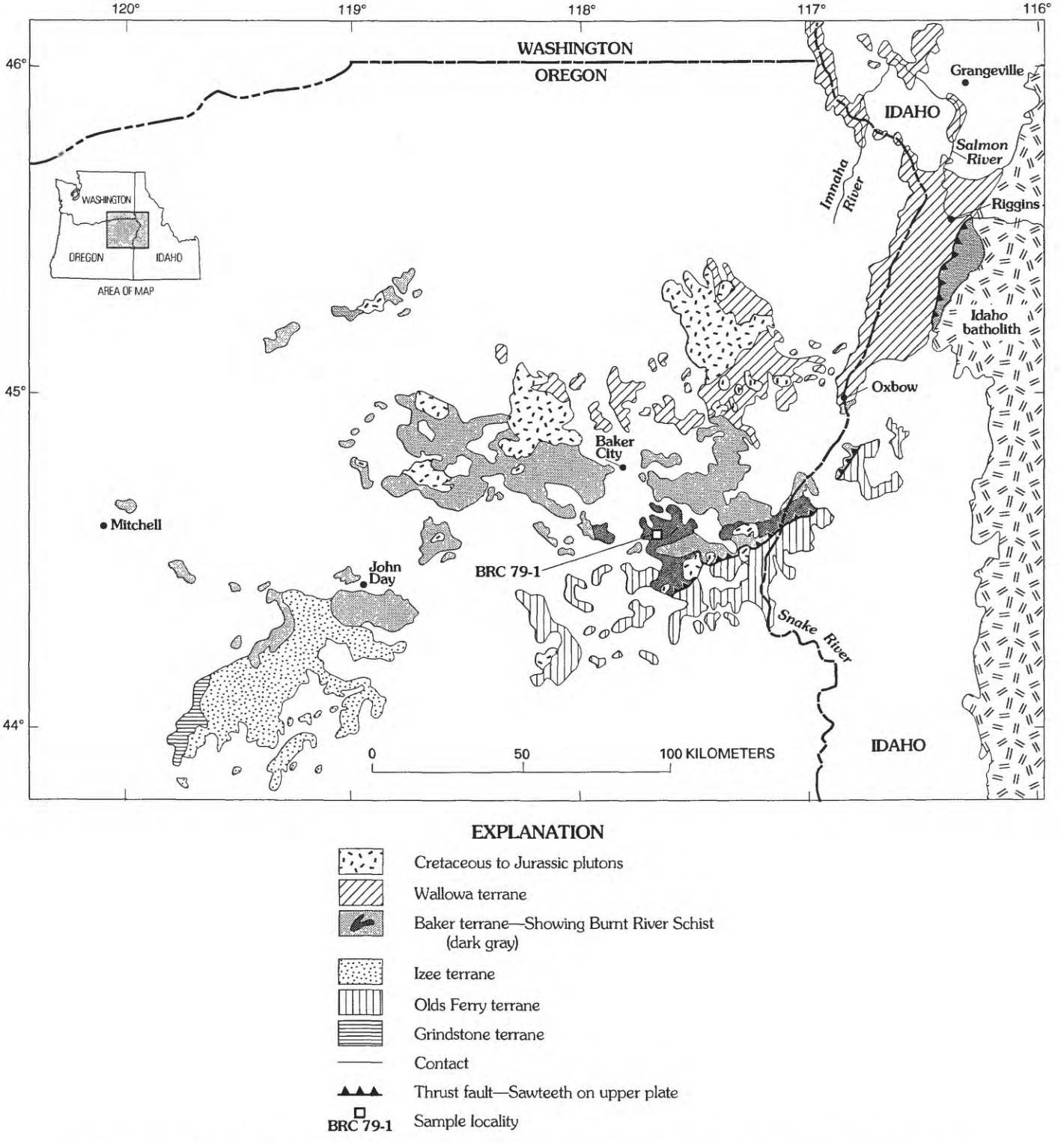

FIGURE 6.4.—Areal distribution of the Burnt River Schist in the Baker terrane, showing U-Pb zircon sample locality.

BURNT RIVER SCHIST

Another major supracrustal component of the Baker terrane is the Burnt River Schist (fig. 6.4). The Burnt River Schist is dominantly quartzose phyllite with lesser amounts of greenstone, marble, metavolcanic and metavolcaniclastic rocks, and rare metaconglomerate; these rocks have undergone greenschist- to epidote-amphibolite-facies metamorphism (Gilluly, 1937; Ashley, 1967; chap. 12, this volume). Middle to Late Triassic conodonts were recovered from marble beds (Mullen-Morris and Wardlaw, 1986) within the formation.

Several plutonic bodies that range in composition from gabbro to trondhjemite cut the protolith and were metamorphosed with it (Ashley, 1967; chap. 12, this volume). These plutons may represent exotic tectonic fragments introduced into the protolith of the Burnt River as olistostromal blocks rather than magmas that intruded the protolith. It should be noted however, that these plutons are areally extensive in outcrop (up to several square kilometers), and are the only volumetrically significant rock type enclosed by, but not considered to be part of, the formation.

A trondhjemite within the Burnt River Schist was sampled for geochronologic investigation (sample BRC79-1, fig. 6.4). Two zircon fractions from this pluton have Late Triassic $^{206}Pb^{*}$-^{238}U ages of 233 and 230 Ma. These ages set a maximum age of metamorphism of the protolith of the Burnt River Schist. Along its southern margin the Burnt River Schist is intruded by two undeformed plutons that have $^{206}Pb^{*}$-^{238}U ages of approximately 124 Ma and 120 Ma (Walker, 1986, 1989). Thus, metamorphism and deformation of the formation occurred between 230 and 124 Ma.

The Elkhorn Ridge Argillite and Burnt River Schist are lithologically similar, although the Burnt River Schist is more siliceous overall, more deformed, and metamorphosed to higher grades than the Elkhorn Ridge Argillite. On the basis of such observations, Gilluly (1937) proposed that the Burnt River is the older of the two formations. Ashley (1967), however, tentatively concluded that part of the Burnt River is correlative with the Elkhorn Ridge. Exotic or olistostromal components, which are present within the Elkhorn Ridge, have not been recognized in the Burnt River. In addition, the age of the protolith of the chert-argillite within the Elkhorn Ridge is Permian to Triassic whereas the age of deposition of the protolith to the Burnt River Schist is Triassic. It is likely therefore that the two formations represent different depositional environments, although they could be components of the same tectonic system. The original tectonic environment of the protoliths is not well established. Coward (1982) suggested that the Elkhorn Ridge Argillite represents a deformed accretionary prism, whereas Bishop (chaps. 4 and 5, this volume; Mullen, 1985) has proposed a fore-arc origin for the entire Baker terrane. This problem is considered in more detail later in this chapter.

ULTRAMAFIC-MAFIC-SILICIC OPHIOLITIC IGNEOUS SUITES

Several structural blocks of igneous and metaigneous rocks, two of which are ultramafic-mafic-silicic suites characterized by partially intact ophiolitic stratigraphy, are important constituents of the Baker terrane. Geochronologic investigation of the two most complete suites is described below.

CANYON MOUNTAIN COMPLEX

The Canyon Mountain Complex is the largest and the most structurally and lithologically coherent metaigneous suite of the Baker terrane. Structurally, the complex is a slab immersed in an extensive serpentinite-matrix melange tract in the southwestern part of the terrane (fig. 6.5). The complex is in contact with serpentinite-matrix melange on its west and northwest margins and with Quaternary sediments along its north margin, and it is faulted against Tertiary volcanic rocks on its east side. The southern extension of the complex is obscured by an unconformable cover of Tertiary volcanic rocks.

From south to north, the Canyon Mountain Complex has been divided into the following major lithologic units, each of which has a general east-west trend and steep dips (fig. 6.6; Avé Lallemant, 1976; Thayer, 1977; Himmelberg and Loney, 1980; Gerlach and others, 1981a; Leeman and others, chap. 1, this volume): tectonite harzburgite; ultramafic and gabbroic metacumulates; gabbroic cumulates with minor amounts of wehrlite and pyroxenite and isotropic hornblende gabbro; and an uppermost zone of irregular trondhjemite intrusive masses, diabase and trondhjemite sills, and keratophyre and quartz keratophyre flows.

The major part of the ultramafic unit consists of penetratively deformed tectonite composed of harzburgite, with subordinate amounts of dunite and pyroxenite, and volumetrically minor chromitite. This unit has the chemical characteristics of a refractory residuum resulting from extraction of a basaltic melt (Himmelberg and Loney, 1980).

The harzburgite tectonite is overlain by metacumulates (Himmelberg and Loney, 1980)—ultramafic and

gabbroic rocks of cumulus origin but now overprinted with metamorphic textures and a folded, penetrative foliation and (or) lineation that are shared by the underlying tectonite harzburgite. The metacumulates consist of complexly interlayered ultramafic and gabbroic rocks. Ultramafic rock types of this unit range from dunite through wehrlite to clinopyroxenite, according to their relative proportions of olivine and

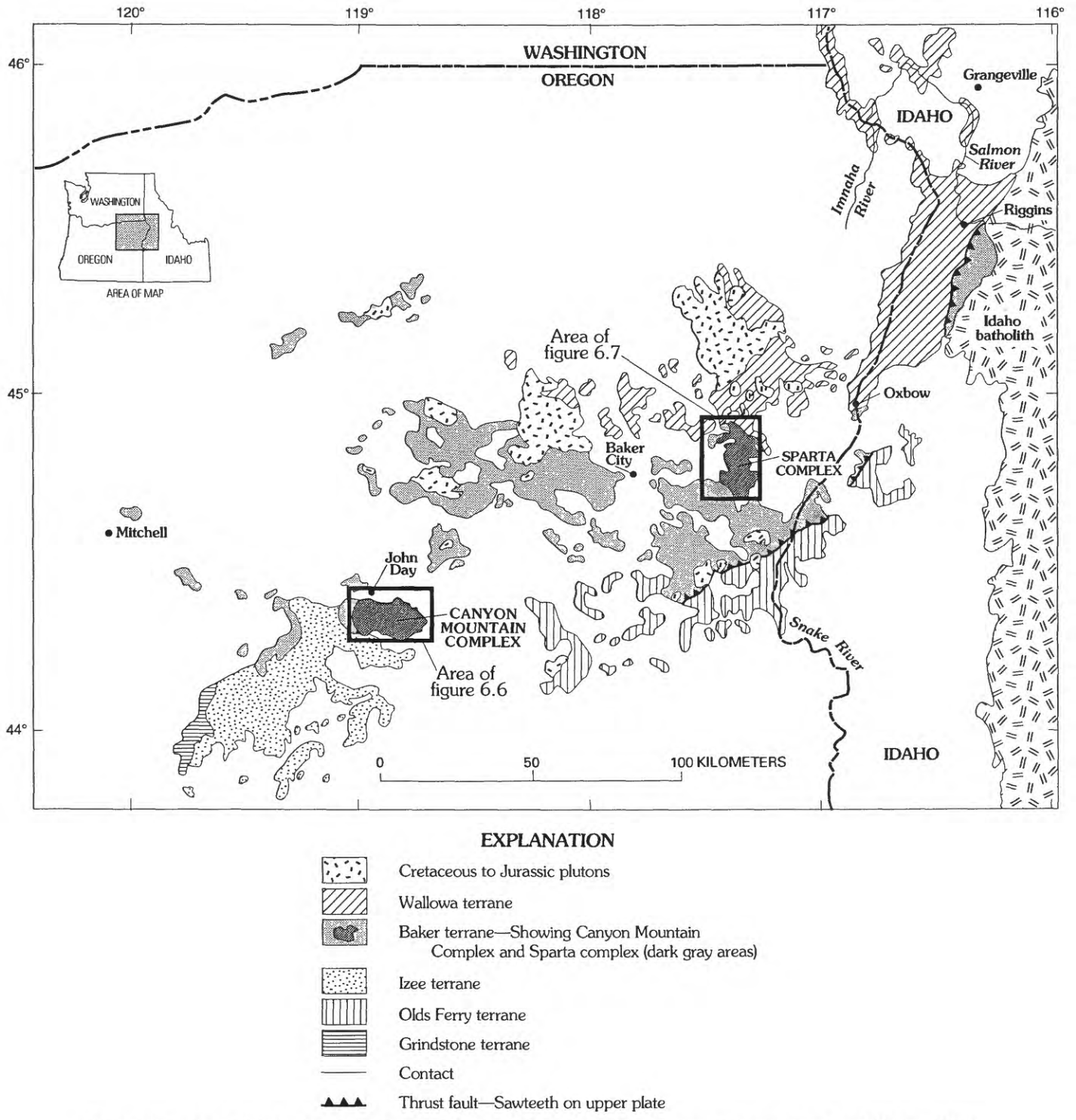

FIGURE 6.5.—Areal distribution of the Canyon Mountain Complex and the (informal) Sparta complex of Phelps (1979).

clinopyroxene. Volumetrically minor varieties of the now-metamorphosed ultramafic rocks include plagioclase-bearing varieties of those rocks named above and orthopyroxenite, lherzolite, and websterite. The metagabbroic rocks within this ophiolitic sequence formed chiefly from gabbro and gabbronorite and from minor amounts of troctolite, anorthosite, and quartz norite. The texture of the majority of the metacumulate rocks is allotriomorphic-granular, however equigranular-mosaic recrystallization textures are common as are deformation textures such as kink bands in olivine and orthopyroxene.

The metacumulate sequence is separated from overlying cumulate gabbroic rocks by a complex, interdigitating contact zone. The cumulate rocks are predominantly gabbro and gabbronorite with lenses of wehrlite and feldspathic wehrlite. Centimeter- to meter-scale layering, defined by cyclic variation in the pyroxene/plagioclase ratio, is ubiquitous in the gabbro yet absent in the enclosed ultramafic lenses. The cumulate sequence is, in part, overlain by a thin, irregular zone (not shown in fig. 6.6) of isotropic, hornblende-bearing gabbro.

The stratigraphically uppermost unit of the Canyon Mountain Complex consists of a complex zone of keratophyre and quartz keratophyre flows, irregular trondhjemite intrusive masses, and dikes and sills of diabase and trondhjemite. Gerlach and others

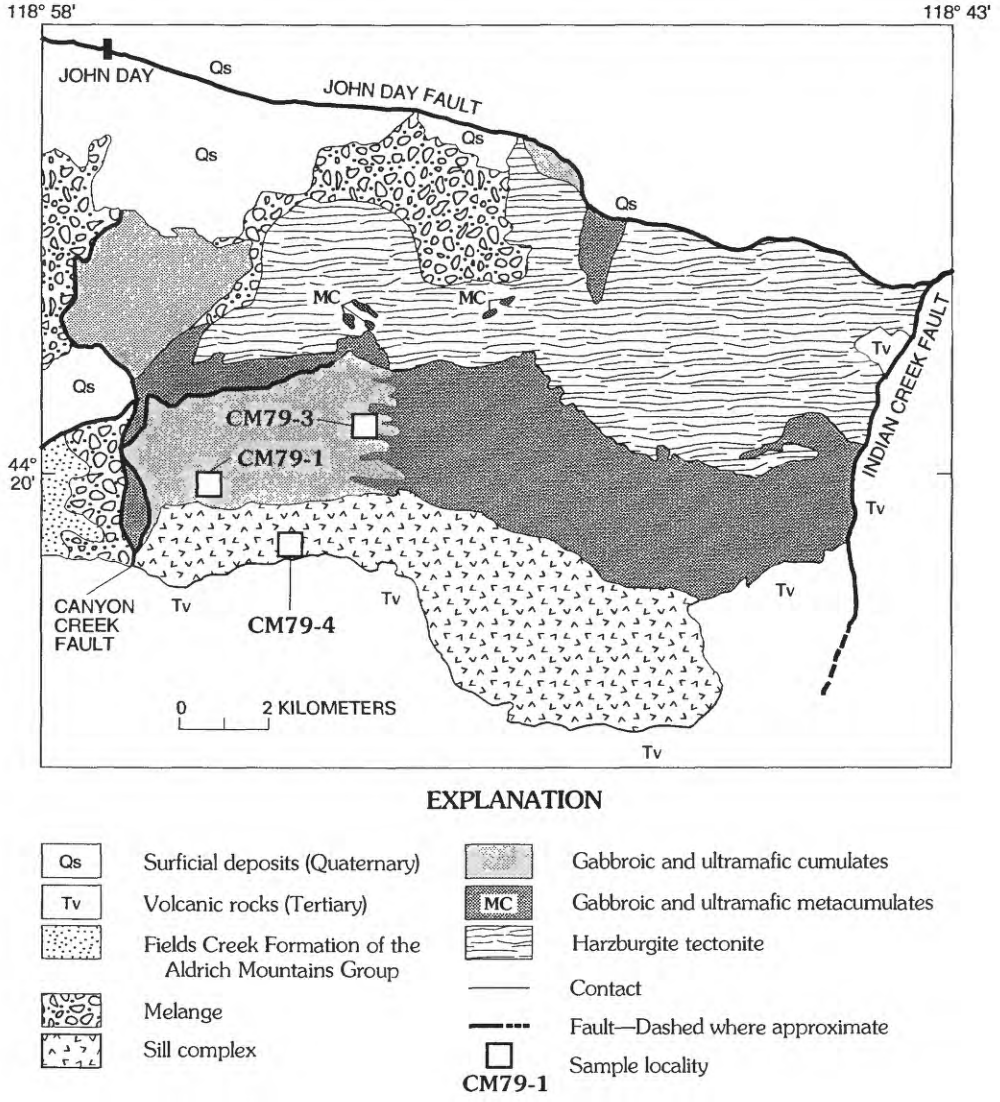

FIGURE 6.6.—Simplified geology of the Canyon Mountain Complex (modified from Himmelberg and Loney, 1980, and Gerlach and others, 1981a), showing U-Pb zircon sample localities. Area of map is shown in figure 6.5.

(1981b) interpreted this uppermost zone as representing a sill complex on the basis of the fact that the zone and lithologic contacts within it share the general east-west trend and steep dip of the underlying units.

The metamorphic textures and folded penetrative lineation and foliation developed in the basal peridotite and metacumulates were interpreted by Avé Lallemant (1976) as indicating sub-solidus flow after solidification of this part of the Canyon Mountain Complex but prior to the formation of the cumulates and sill complex, which lack such structures. Alternatively, as George (1978) suggested for the Troodos complex, the absence of such features in the gabbroic-cumulate sequence may be the result of deformation processes operative on a partially crystallized magma chamber. In his model, the metacumulate and cumulate sequences are essentially coeval. The undeformed cumulates represent a stratigraphically higher level of the chamber that remained largely liquid during deformation. Thus, if George's (1978) model is applicable to the Canyon Mountain Complex, previously crystallized magmatic rocks and the basal peridotite were overprinted by this deformation whereas crystallization of the nonmetamorphosed cumulates took place shortly after and, in part, contemporaneous with deformation.

Although the complex has been interpreted as an "ophiolite," sheeted mafic dikes, although reported from the complex (Thayer, 1977) are rare. There are domains of multiple dike and sill injection but they lack one-way chilling characteristic of sheeted complexes in ophiolites of midocean-ridge origin. In addition, as previously noted, the volcanic subunit of this complex is dominated by keratophyre and quartz keratophyre flows rather than mafic pillow lavas. Unlike most ophiolites of midocean-ridge origin, the Canyon Mountain Complex contains abundant orthopyroxene as a cumulus phase, suggesting an overall more siliceous magma composition than that of typical midocean-ridge basalt (MORB). These observations combined with mineral-chemistry data (Himmelberg and Loney, 1980; Gerlach and others, 1981a, 1981b; Leeman and others, chap. 1, this volume) have led to the interpretation that the Canyon Mountain Complex represents an arc-related magmatic complex. U-Pb geochronologic data presented herein indicate a multistage magmatic history spanning at least 8 m.y. for this complex.

PREVIOUS GEOCHRONOLOGIC INVESTIGATIONS

Previously determined isotopic ages for the Canyon Mountain Complex include 250- to 240-Ma K-Ar ages determined on hornblende from hornblende-rich pegmatite dikes cutting gabbro and 210 Ma from quartz diorite (Vallier and others, 1977). Avé Lallemant and others (1980) reported a $^{40}Ar/^{39}Ar$ age of 262 Ma from a hornblende-rich pegmatite.

U-Pb ZIRCON GEOCHRONOLOGIC RESULTS

Five samples were collected from the Canyon Mountain Complex for geochronologic investigation. Three yielded sufficient zircon for isotopic analysis. Sample localities, field occurrence, and petrographic descriptions are given in table 6.1, sample localities are shown in figure 6.6 and isotopic data are presented in table 6.2.

The oldest ages obtained for the Canyon Mountain Complex are from the metacumulate sequence. Sample CM79-3 was collected from a quartz-bearing gabbro within this sequence; its granoblastic-polygonal texture is evidence of the post-magmatic metamorphism imposed on the rock. Zircons of this sample are a deep red color and translucent to opaque. Due to low zircon yield, the bulk zircon fraction was analyzed and gave slightly discordant ages, which are interpreted to indicate a minimum age of the cumulate protolith. The $^{206}Pb^*$-^{238}U age of this fraction is 278 Ma whereas the $^{206}Pb^*$-$^{207}Pb^*$ age is 314±29 Ma. The large uncertainty in the $^{206}Pb^*$-$^{207}Pb^*$ age results from the combined effect of the very low $^{206}Pb/^{204}Pb$ ratio and the uncertainty in the $^{207}Pb/^{204}Pb$ ratio of common Pb. Interpretation of such discordant ages is difficult from a single fraction, particularly considering the large analytical uncertainty in the $^{206}Pb^*$-$^{207}Pb^*$ age. In view of this large analytical uncertainty, I interpret the 278 Ma $^{206}Pb^*$-^{238}U age as the minimum age for the protolith of the metacumulate sequence and suggest that the protolith age is no older than 314 Ma.

The zircon concentrate of this sample has low U and Pb concentrations (44 and 1.68 ppm, respectively) that may be accounted for in terms of both the composition and thermal history of the rock from which the sample was taken. The sample is from a quartz-bearing norite that is interlayered on a centimeter scale with norite and anorthosite. These rocks are interpreted to be metamorphosed fractional-crystallization products of a basaltic melt (Himmelberg and Loney, 1980); if so, they are naturally low in concentrations of large-ion-lithophile and incompatible elements such as U. As reviewed earlier, Avé Lallemant (1976) views the formation of the Canyon Mountain Complex as a two-stage process. In his model, the basal-peridotite tectonite and metacumulate sequence represent a distinctly older phase of magmatism and

deformation and metamorphism than do the overlying cumulates, sill complex, and volcanic rocks. The age discordance observed in zircons from sample CM79-3 therefore could be attributed to loss of Pb from the zircons due to metamorphism and deformation, which overprinted the original magmatic textures in the metacumulate sequence. Himmelberg and Loney (1980) have determined subsolidus reequilibration temperatures, based on pyroxene geothermometry, of approximately 880 to 975°C for the basal peridotite, metacumulates, and cumulates. Certainly, prolonged exposure to such temperatures during slow cooling or re-heating to such temperatures is sufficient to cause accelerated ionic diffusion resulting in the loss of radiogenic Pb from the zircon crystal lattice. Mattinson (1978) has empirically deduced that the blocking temperature of the U-Pb geochronometer for geologically young zircons with low U concentrations is approximately 650°C. The $^{206}Pb^{*}$-^{238}U age reported here for the metacumulate may thus represent the time at which the metacumulates cooled below the blocking temperature for zircon. The low concentration of Pb in zircons from this sample is attributed to the original low concentration of U in the melt that produced the zircon and the effects of subsolidus reequilibration that likely enhanced Pb diffusion. It is irresolvable from this single zircon fraction whether the observed discordance is a result of a dynamic metamorphic overprint, of Pb-loss related to sustained high subsolidus temperatures, or is a combination of the two processes.

Sample CM79-4 was collected from a coarse-grained trondhjemite intrusive mass that is part of the sill complex described by Gerlach and others (1981a; 1981b). This leucocratic mass, locally characterized by cataclastic domains, cuts gabbro in the southwestern part of the complex. Three zircon fractions, also characterized by low U concentrations, from this sample have yielded Early Permian $^{206}Pb^{*}$-^{238}U ages of 276 Ma. On the basis of field relations, the trondhjemite is clearly younger than the cumulates and metacumulates. However, the ages of 276 Ma for zircons from this sample are similar to the $^{206}Pb^{*}$-^{238}U age for that of sample CM79-3; this suggests either that the sill complex was affected by sustained high temperatures during sub-solidus reequilibration or that the sills intruded at this time.

The youngest age measured from the Canyon Mountain Complex is that of sample CM79-1. This sample was collected from a medium-grained, hypidiomorphic-granular hornblende tonalite that cuts gabbro near the west margin of the complex. The outcrop area of this pluton is small (<5 km^2). Zircons from this sample are characterized by distinctly higher U concentrations than those separated from samples CM79-3 and CM79-4 (table 6.2). Two zircon fractions from sample CM79-1 have yielded concordant $^{206}Pb^{*}$-^{238}U ages of 268 Ma. These ages indicate that magmatic activity in the Canyon Mountain Complex continued after emplacement of the sill complex.

The age range of magmatism within the Canyon Mountain Complex is inconsistent with geologically instantaneous generation of the complex at a mid-ocean-ridge spreading center. Rather, the geochronologic data indicate two stages of Early Permian magmatism: formation of the metacumulate and cumulate section and emplacement of trondhjemite 276 Ma (or earlier?) followed by intrusion of quartz diorite at 268 Ma.

SPARTA COMPLEX

The informally named Sparta complex, which crops out over a 70 km^2 area, is included in the Wallowa terrane by Silberling and others (1984) but had been considered by previous investigators to be part of the Baker terrane and is therefore discussed in this chapter. From north to south, the complex comprises serpentinite, cumulus clinopyroxenite, cumulus gabbroic rocks, diorite-tonalite, and trondhjemite (fig. 6.7). The south margin of the complex is in fault contact with the multiply deformed Elkhorn Ridge Argillite whereas the north margin of the complex has an uncertain contact relationship with Permian and Triassic rocks of the supracrustal Clover Creek Greenstone.

The serpentinite, whose protolith is indeterminate because of extensive serpentinization, composes a relatively small part of the complex and is locally gradational into partly serpentinized clinopyroxenite (Phelps, 1979). The clinopyroxenite is interlayered with and overlain by cumulus gabbroic rocks (chiefly gabbronorite) which become increasingly hornblende-rich near the contact with the diorite-tonalite.

The contact between the gabbroic rocks and the diorite-tonalite is marked by a zone of shearing and alteration. Locally, gabbroic xenoliths occur in the diorite-tonalite near the contact with the underlying gabbro. The contact appears intrusive at most localities although locally the contact seems gradational. Rock types within the diorite-tonalite unit grade from hornblende diorite to biotite-hornblende tonalite (Almy, 1977; Phelps 1979).

The contact between the diorite-tonalite and the trondhjemite is an indistinct zone characterized by complex contact relationships and further obscured by shearing and alteration. Thus the age of the dio-

rite-tonalite unit relative to that of the trondhjemite is not certain from field relations. Texturally, the trondhjemite is mostly massive but includes porphyritic, granophyric, hypidiomorphic-granular, and allotriomorphic granular varieties, most of which have been locally overprinted with brittle tectonite fabrics. The origin of the trondhjemite has been the subject of several studies (Gilluly, 1933; Almy, 1977; Phelps, 1979; Phelps and Avé Lallemant, 1980). Gilluly believed it to be the product of metasomatic origin, derived by Na-metasomatism of the diorite-tonalite, whereas subsequent workers considered it to be of magmatic origin. Given the variety of textures within the trondhjemite and the generally poor outcrop, it is probable that several intrusive phases are present within the area that Prostka (1962) mapped as trondhjemite.

The trondhjemite, the uppermost unit of the Sparta complex in this area, is overlain by the Clover Creek Greenstone along a poorly exposed contact. Prostka (1962) interpreted the contact to be depositional with the Clover Creek resting on the eroded surface of the trondhjemite. He based this interpretation on the occurrence of silicic plutonic clasts, which he believed to be derived from the underlying Sparta complex, in the basal part of the Clover Creek Greenstone. The Clover Creek Greenstone thickens to the northeast of the Sparta quadrangle, and therefore these clasts could have been derived from exhumed Permian plutons such as those exposed to the northeast in Hells Canyon and the Seven Devils Mountains. Locally within Hells Canyon, Middle Triassic rocks of the Seven Devils Group rest unconformably on Permian silicic plutons (Vallier, 1977); therefore, by Middle Triassic time, uplift and erosion had exhumed tonalitic-trondhjemitic plutons of the Wallowa terrane as potential contributors of clasts to the lower Clover Creek Greenstone. In an area west of the Sparta quadrangle, Brooks and others (1976) mapped trondhjemitic plutons intruding the Clover Creek Greenstone and Brooks and Vallier (1978) reported thermal alteration of the Clover Creek near trondhjemite of the Sparta complex. Almy (1977) suggested that keratophyre and quartz keratophyre of the Clover Creek Greenstone and trondhjemite of the Sparta complex are cogenetic on the basis of major-element chemical data from these rocks. Such a conclusion further implies that the contact of the trondhjemite of the Sparta complex and the Clover Creek Greenstone is intrusive.

The Clover Creek Greenstone consists of interbedded spilite, keratophyre and quartz keratophyre flows, pyroclastic rocks, volcanogenic sandstones, and volcanic breccia with minor amounts of intercalated argillite and limestone. The various rock types within the Clover Creek thicken and thin markedly along strike, and bedforms tend to be lensoid. The type locality of the Clover Creek Greenstone, originally described by Gilluly (1937), lies to the west of the Sparta complex. In the area around Sparta, Oreg., Prostka (1962) subdivided rocks correlative with the Clover Creek Greenstone into Gold Creek Greenstone and "Lower Sedimentary Series" and estimated a combined stratigraphic thickness of approximately 1,800 m for these units. Gilluly (1937) originally assigned the Clover Creek Greenstone a Permian age; however, it was demonstrated by subsequent workers (Wetherill, 1960; Bostwick and Koch, 1982; Prostka, 1962; Nolf, 1966) that the Clover Creek includes rocks as young as Late Triassic. The age of the Clover Creek in the Sparta area is uncertain but herein is considered to include rocks of Late Permian as well as Triassic age on the basis of the conformable contact relationship (Prostka, 1962) of the Clover Creek Greenstone with the Upper Triassic Martin Bridge Limestone.

The Sparta complex has been termed an "ophiolite" (Vallier and others, 1977; Phelps and Avé Lallemant, 1980) although it is lithologically unlike most well-documented ophiolites. As shown in figure 6.7, the Sparta complex includes a large volume of silicic rocks. In fact, unlike most ophiolites, the bulk of the exposed part of the complex consists of rocks of tonalitic through trondhjemitic composition. In addition, the Sparta complex lacks tectonite harzburgite, has an extremely thin exposed ultramafic component, and although numerous mafic and silicic dikes cut all lithologic units within the complex, no sheeted dike or sill complex has been recognized. The absence of a dike or sill complex strongly suggests that this igneous suite was not generated in a long-lived tensional regime such as that of an oceanic spreading center. The unconformable cover of Cenozoic volcanic rocks may mask the actual proportional distribution of the various rock types. Nevertheless, the stratigraphy and bulk composition of the Sparta complex is unlike those ophiolites, such as the Oman ophiolite and the Bay of Islands ophiolite, Newfoundland, inferred to have originated at some type of oceanic spreading center.

PREVIOUS GEOCHRONOLOGIC INVESTIGATIONS

Previous geochronologic investigation of the Sparta complex, limited to K-Ar and $^{40}Ar/^{39}Ar$ age determinations of the diorite-tonalite unit, yielded Late Triassic ages: 213 Ma K-Ar ages (reported in Vallier and others, 1977); a 223 Ma $^{40}Ar/^{39}Ar$ plateau age and a 212 Ma

total-gas age have been measured from this unit (Avé Lallemant and others, 1980). Assuming that the diorite-tonalite unit is coeval with the entire complex, the entire suite had been assigned to the Late Triassic.

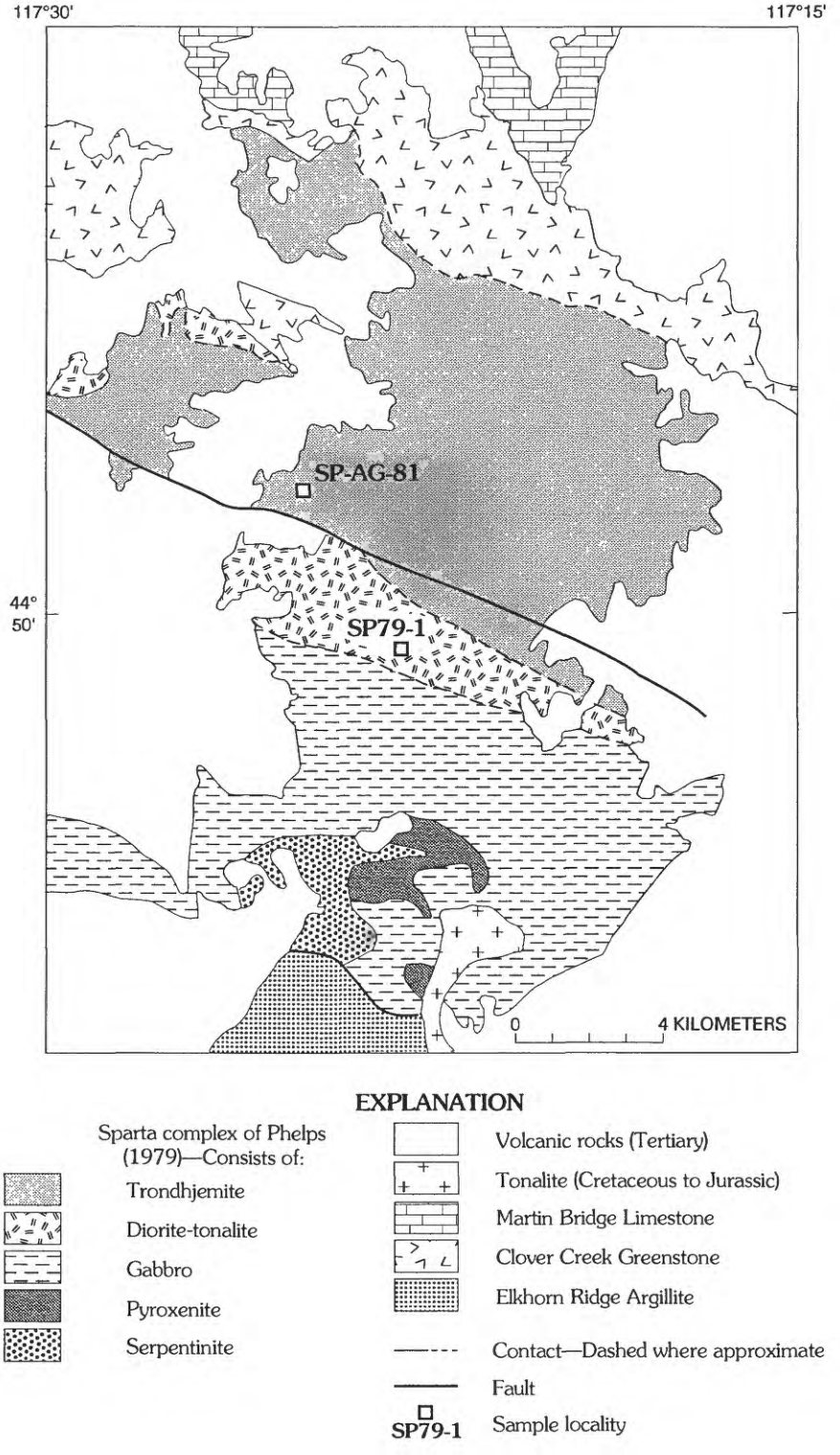

FIGURE 6.7.—Geology of the (informal) Sparta complex of Phelps (1979), showing U-Pb zircon sample localities. Geology is modified from Prostka (1962). Area of map is shown in figure 6.5.

However, as discussed herein, the geochronologic history of this igneous suite is somewhat more complex.

U-Pb ZIRCON GEOCHRONOLOGIC RESULTS

For geochronologic investigation, five samples were collected from three lithologic units within the Sparta complex—two from the cumulus gabbro, one from the diorite-tonalite unit, and two from the trondhjemite. Of these samples, only those of the diorite-tonalite unit and one of the samples of trondhjemite yielded sufficient zircon for isotopic analysis. Zircon isotopic data for the complex are presented in table 6.2.

Sample SP79-1, a hornblende-biotite tonalite, was collected at J.N. Bishop Spring in the diorite-tonalite unit. Two zircon fractions from this sample have identical Late Triassic $^{206}Pb^{*}$-^{238}U ages of 215 Ma, in good agreement with K-Ar and total-gas $^{40}Ar/^{39}Ar$ ages previously reported for this unit (Avé Lallemant and others, 1980). Inasmuch as the underlying gabbro is more altered than the diorite-tonalite and xenoliths of gabbro are locally present within the diorite-tonalite, the gabbro is therefore older than the diorite-tonalite. Gabbro of this complex is therefore at least 215 Ma in age and may be considerably older.

The oldest zircon ages measured from the complex are for the trondhjemite. The sampled trondhjemite is porphyritic and comprises phenocrysts of sodic plagioclase and rounded, embayed quartz in a fine-grained matrix of quartz, plagioclase, and minor hornblende, biotite, and titanite. The three analyzed zircon fractions from the trondhjemite yield Late Permian $^{206}Pb^{*}$-^{238}U ages of 253 Ma. Local intrusive relationships between the trondhjemite and the overlying Clover Creek Greenstone require that at least part of the Clover Creek Greenstone in the Sparta quadrangle is at least as old as Late Permian.

Phelps (1979) suggested that the trondhjemite and diorite-tonalite are cogenetic on the basis of petrologic modeling of major- and trace-element data. The U-Pb geochronologic data presented in table 6.2 and previously discussed demonstrate that the trondhjemite and the diorite-tonalite represent two distinct magmatic events separated by about 38 m.y. and preclude any likelihood that the diorite-tonalite and trondhjemite are cogenetic.

In summary, the Sparta complex comprises Late Permian and Late Triassic plutonic rocks. The trondhjemite and the diorite-tonalite unit are not coeval and represent temporally and compositionally separate intrusive events. The temporal relationship of the gabbro to the trondhjemite is not clear in the absence of field evidence such as observable contact relationships. An argument against a genetic relationship between the trondhjemite and gabbro is the tremendous volume of magma that would have had to fractionate in order to produce the large volume of trondhjemite relative to the gabbro. The Sparta complex is not the product of magmatic differentiation of a single parental magma. Rather, it represents at least two distinct magmatic events separated by some 38 m.y. Because in the Sparta quadrangle the trondhjemite of the complex locally intrudes the overlying Clover Creek Greenstone, part of the Clover Creek Greenstone is at least Late Permian.

SERPENTINITE-MATRIX MELANGE

Polymict serpentinite-matrix melange is a major component of the Baker terrane (fig. 6.8). Included tectonic blocks range from less than a meter to several kilometers in length. The blocks are compositionally as well as texturally diverse and range in degree of metamorphic grade from low greenschist to garnet amphibolite grade. Blocks of chert, greenstone (some showing pillow structure), fragmented ultramafic-mafic-silicic plutonic suites (ophiolites?), chert-argillite, foliated amphibolite, gabbro, silicic metaplutonic rocks, mafic and ultramafic plutonic rocks, mafic volcanic rocks, tuffaceous volcanic rocks, limestone, and rare blueschist are present.

The range of published isotopic ages of the tectonic blocks is Early Permian to Late Triassic. Blueschist blocks in melange near Mitchell, Oreg. (Swanson, 1969) have yielded a $^{40}Ar/^{39}Ar$ age of 223±3 Ma (Hotz and others, 1977) whereas amphibole from foliated amphibolite in serpentinite-matrix melange south of the Canyon Mountain Complex has a $^{40}Ar/^{39}Ar$ age of 255±3 Ma (Avé Lallemant and others, 1980). Carpenter and Walker (1992) reported a hornblende K-Ar age of 267 Ma for amphibolite in the Aldrich Mountains.

Early Permian fusulinids and Late Triassic radiolarians are reportedly found in melange blocks east and southwest of John Day, Oreg. (Dickinson and Thayer, 1978; Blome and others, 1986).

MELANGE IN THE ALDRICH MOUNTAINS

Serpentinite-matrix melange in the Aldrich Mountains is exposed approximately 25 km southwest of the town of John Day, Oreg. (Dickinson and Thayer, 1978). The melange matrix, composed of foliated serpentinite, engulfs blocks and slabs of heterogeneous lithology. Low-grade metavolcanic rocks, chert, amphibolite, argillite, gabbro, and peridotite are the dominant rock types that compose the blocks. Rare blocks consisting of metatrondhjemite are also present. A single zircon fraction from one such block

(sample AM80-1, fig. 6.8) yielded a concordant age of 279 Ma, which is analytically identical to the age of trondhjemite in the sill complex of the Canyon Mountain Complex. The block is therefore interpreted as a tectonic fragment of the same crust from which the Canyon Mountain Complex was derived.

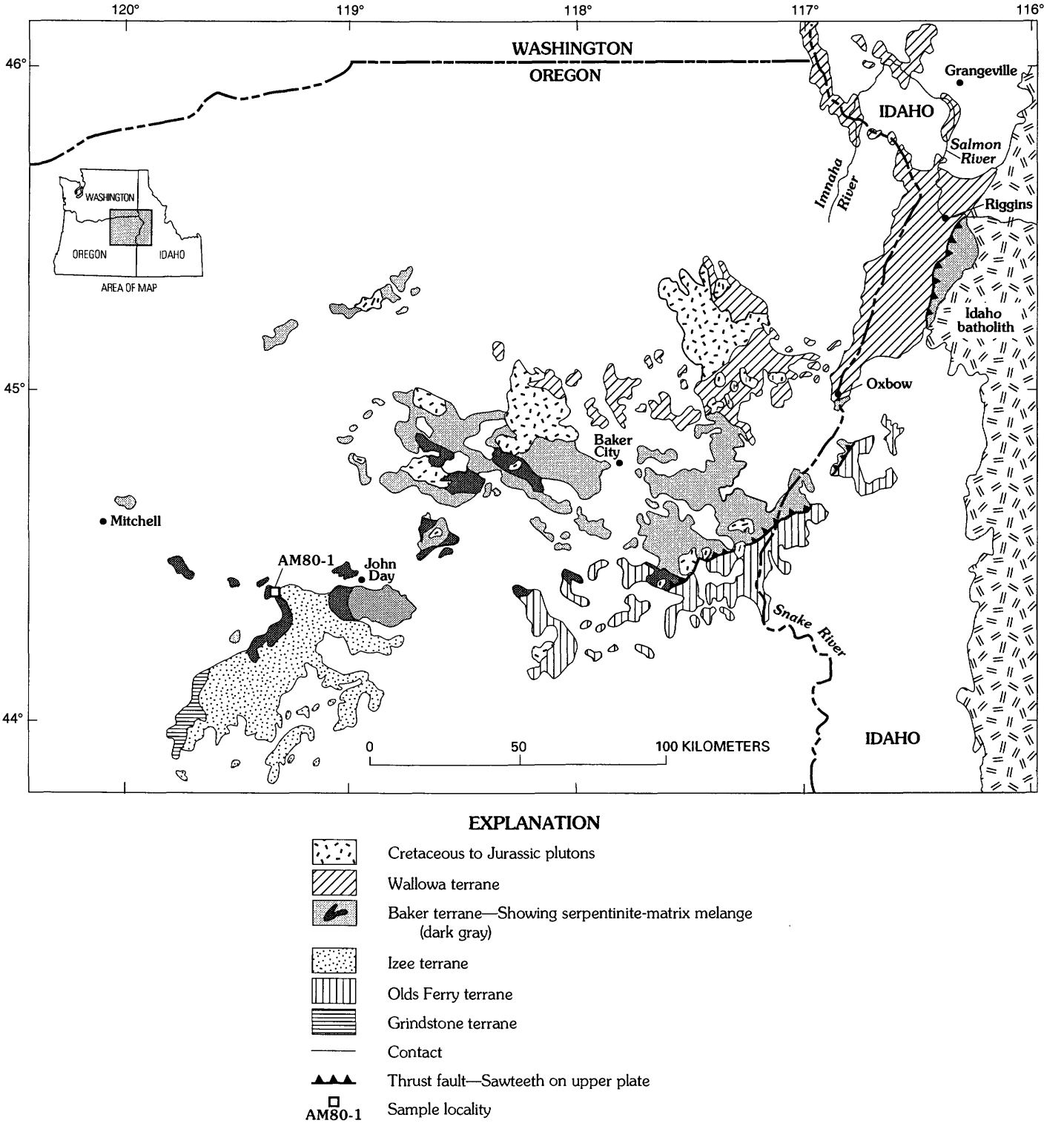

FIGURE 6.8.—Areal distribution of serpentinite-matrix melange in the Baker terrane, showing U-Pb zircon sample locality (in the Aldrich Mountains).

TIMING OF MELANGE FORMATION

In the John Day, Oreg., area, melange of the Baker terrane, which includes the Canyon Mountain Complex as a large slab, is unconformably overlain by a sequence of Upper Triassic to Upper Jurassic clastic rocks (Dickinson and Vigrass, 1965; Dickinson and Thayer, 1978). Therefore melange formation in this area is constrained to pre-Late Triassic time. However, these overlying clastic strata are deformed, numerous unconformities occur within the sequence, and the lowermost rocks of this sequence contain detritus that was most likely derived from the melange. Although intense deformation had ceased by Late Triassic time, deformation evident in this area continued until Early Jurassic time. The time of initiation of breaking and mixing that led to the development of the melange is difficult to determine. Given the abundance of Permian and Triassic faunal and isotopic ages of the blocks, it seems reasonable to infer that melange formation began no earlier than the Permian. Whether melange formation was geologically instantaneous, continuous, or episodic is not known.

Serpentinite-matrix melange in the Greenhorn area, west of Baker City, Oreg., is interpreted by Ferns and others (1983a) to be depositionally overlain by a sedimentary unit comprised of argillite and sandstone with lesser amounts of conglomerate, chert, and limestone. A similar unit mapped by Mullen (1978) has yielded both Early Permian conodonts and Early Permian fusulinids from limestone pods. As Ferns and Brooks (1983) point out, it is possible that the limestone pods represent reworked blocks from the underlying melange and therefore the depositional age of the unit could be younger than Early Permian. The minimum age of melange formation within the Elkhorn Ridge inlier is thus not well constrained.

PALEOTECTONIC SETTING OF THE BAKER TERRANE

Any interpretation regarding the paleotectonic setting for the Baker terrane must account for the following characteristics: (1) The overall character of the Baker terrane is that of a melange. (2) Rocks of different metamorphic grade, including lawsonite blueschist, are commonly juxtaposed. (3) Both Tethyan and non-Tethyan Permian fusulinids are present in structurally separate blocks. (4) Devonian conodonts and Pennsylvanian and Permian fusulinids are present in limestone olistoliths. (5) Serpentinite-matrix melange, chert-argillite broken formation, and siliceous phyllite are intermixed on a broad scale. (6) The age of plutonic rocks within the terrane ranges from about 279 to 215 Ma.

The Early Permian to Late Triassic isotopic age range coincides with that of sedimentation within the terrane as deduced from faunal ages for the Elkhorn Ridge Argillite and the Burnt River Schist. This observation suggests that the deposition of sediments and the formation of plutonic crust were largely synchronous processes. This age range is also very similar to the 264- to 225-Ma age range of plutonism within the Wallowa and Olds Ferry terranes (Walker, 1986). These terranes have been interpreted as vestiges of arc-type ensimatic volcanic-plutonic complexes. The ophiolitic ultramafic-mafic-silicic plutonic suites (such as the Canyon Mountain Complex) are characterized by a large component of silicic rocks, by the abundance of cumulus orthopyroxene in their gabbroic sections, by the rarity or complete absence of sheeted dike complexes, and by their associated keratophyric and (or) tuffaceous volcanic rocks. Features such as these however, are not characteristic of those ophiolites inferred to have originated at some type of oceanic spreading center. Rather, the Canyon Mountain Complex and the Sparta complex have features more characteristic of those ophiolites believed to have an arc-related origin (see Hawkins and Evans, 1983). Given the geologic characteristics reviewed above, only the following paleotectonic environments can reasonably account for the lithologic and structural complexity of the Baker terrane: an accretionary complex, a marginal basin, or a fore arc.

Dickinson (1979) cited the overall melange-like character of the terrane, the presence of blueschist blocks, and faunal ages as evidence that this terrane marks the existence of a former Permian to Triassic subduction zone. The juxtaposition of metamorphic rocks and tectonic blocks composed of metamorphic rocks of various grade within the terrane strongly implies that some type of mixing process has occurred. The requisite kinematic environment to accomplish such mixing may be an accretionary prism associated with an active arc-type volcanic-plutonic complex. Karig (1979), however, suggested that in active ensimatic volcanic-plutonic arc systems such admixtures of rock types may also result from strike-slip faulting along trends that are subparallel to the active magmatic-arc crest. The presence of rocks of various metamorphic grade in a melange-like setting thus is not unique to a subduction complex. The presence of both Tethyan and non-Tethyan fusulinids implies juxtaposition of different paleobiogeographic settings, but is not in and of itself evidence of a subduction complex. The ophiolitic rocks of this terrane have structural and lithologic characteristics unlike those of midocean-ridge origin (see earlier discussion) and yield U-Pb zircon ages that are synchronous with the inferred age of subduction (Permian to

Triassic). It is therefore highly unlikely that these represent obducted fragments of subducting oceanic crust. Furthermore, extensive tracts of serpentinite matrix melange, abundant in the Baker terrane, have not been reported from present-day ensimatic accretionary complexes.

Another possible paleotectonic environment for the Baker terrane is a back-arc setting between an active arc and remnant arc or a back-arc basin behind an active arc. The structural character, type of sediment, and rock types associated with such basins may be similar to those characteristic of a fore-arc setting, thus these environments can be difficult to distinguish in the rock record. Disorganized spreading in a back-arc basin (Weissel, 1981) behind an active ensimatic arc may result in the formation of oceanic crust bearing numerous fracture zones within which serpentinite diapirs could rise. These serpentinite diapirs could then mix with the overlying sediments and thereby produce such rock admixtures as are found in the Baker terrane. The main objections, however, to a marginal-basin or back-arc basin setting for the Baker terrane are the occurrence of blocks of Triassic blueschist, juxtaposed Tethyan and non-Tethyan fauna, and blocks of Devonian and Pennsylvanian limestone in a Permian to Triassic back-arc basin.

There is little supporting evidence that the Baker terrane represents either an accretionary-prism complex or a back-arc basin. Rather, the constraints just outlined are met more reasonably by a fore-arc environment of an ensimatic volcanic-plutonic arc that was tectonically and magmatically active in Permian to Triassic time—an idea first proposed by Mullen (1985).

Investigations of the fore-arc region of the active ensimatic Mariana arc in the southwestern Pacific demonstrate that it is composed of a great variety of volcanic, plutonic, sedimentary, and metamorphic rocks (Hussong and Uyeda, 1982; Bloomer, 1983). Structurally and morphologically, the Mariana fore-arc is characterized by numerous seamounts (of both volcanic and diapiric origin), horst-and-graben structures, and hummocky terrane as well as domains of relatively undisturbed volcanogenic sedimentary rocks. Lithologic components of the Mariana fore-arc reported by Bloomer and Hawkins (1982), Bloomer (1983), and Fryer and others (1985) include fragments of oceanic crust, serpentinite diapirs that have flowed laterally (some more than 10 km) upon subaqueous extrusion, alkalic basalts, siliceous tuffaceous sediments, chert, allochthonous shallow-water limestone of Cretaceous age, conglomerate, and breccia.

Some present-day fore arcs are characterized by extension-related normal faults, not uncommonly with significant vertical displacement. In the Mariana fore arc, such faults apparently have acted as conduits for protrusion of serpentinite diapirs into overlying fore-arc sediments (Fryer and others, 1985). Depending upon the depth of generation, serpentinite diapirs could entrain blocks of differing metamorphic grade during their ascent towards the surface. Such a mechanism could account for the intimate mixture of chert-argillite and serpentinite-matrix melange with blocks of varying metamorphic grade observed in the Baker terrane. The presence of limestone bearing Middle Devonian and Pennsylvanian fossils and both Tethyan and non-Tethyan fusulinids may have resulted from subduction processes welding such material to an inner trench wall. Thus, mechanisms exist by which to incorporate much older material into the fore-arc region of active arc systems.

Magmatism in fore-arc regions has been recognized in a number of volcanic-plutonic arc complexes (Gill, 1981), and ophiolitic assemblages can be generated in fore-arc settings (Leitch, 1984). In such a setting the timing of ophiolitic generation is similar to the age of magmatism in the arc with which the ophiolite is associated. Most igneous crystallization ages of ophiolite sequences and other plutonic components of the Baker terrane are synchronous with magmatic crystallization ages in the Wallowa and Olds Ferry terranes (Walker, 1986). The Wallowa and Olds Ferry terranes have been interpreted as arc-type ensimatic volcanic-plutonic arc-type complexes formed during Permian to Triassic subduction. Thus, it is possible that plutonic components of the Baker terrane are vestiges of Permian to Triassic fore-arc plutonism.

The Baker terrane is herein considered to represent the fore-arc region of an ensimatic arc-type volcanic-plutonic complex whose other components are represented by the Permian to Triassic Wallowa terrane and Triassic volcanic and plutonic rocks of the Olds Ferry terrane. The overall melange-like character of the Baker terrane may be the normal expression of tectonically active forearc environments (see fig. 1, Fryer and others, 1985). The Baker terrane, however, has been affected by post-Triassic structural modification. In the John Day, Oreg., area, rocks of the Baker terrane have been folded and faulted with overlying Triassic to Cretaceous volcanic and volcaniclastic rocks of the Izee Terrane. The Baker terrane has also been structurally telescoped against the Olds Ferry terrane along the Connor Creek fault whose age is bracketed as Late Jurassic to Early Cretaceous (Walker, 1986). Numerous Tertiary normal faults cut the terrane as well.

SUMMARY AND CONCLUSIONS

(1) Two metaplutonic fragments within the Elkhorn Ridge Argillite have crystallization ages of approximately 244 Ma and 240 Ma. These ages place lower limits on the age of deformation and metamorphism of the Elkhorn Ridge.

(2) A metamorphosed intrusive body in the Burnt River Schist has an igneous-crystallization age of approximately 233 to 230 Ma. This age represents a minimum age of deposition and maximum age of metamorphism for the Burnt River Schist.

(3) The Canyon Mountain Complex, of Early Permian age, had a protracted magmatic history spanning at least 8 m.y. The age of formation of the metacumulate sequence and cumulate sequence is at least 278 Ma, whereas the age of the sill complex is 276 Ma. A younger pluton intruded the complex at 268 Ma. The temporally protracted igneous history and lithologic characteristics are consistent with a volcanic-plutonic-arc origin for the Canyon Mountain Complex.

(4) The Sparta complex comprises rocks of Late Permian as well as Late Triassic age. The main trondhjemite unit yields U-Pb zircon ages of 253 Ma, whereas zircons from the diorite-tonalite unit are 215 Ma. The Sparta complex is the result of at least two temporally unrelated magmatic events. The complex lacks sheeted dikes or sheeted sills and is characterized by a large volume of silicic plutonic rocks, and these characteristics seem to preclude its origin in a midocean-ridge environment. Rather, it likely represents the plutonic core of a volcanic-plutonic ensimatic arc-type complex.

(5) The age of the Clover Creek Greenstone in the Sparta, Oreg., area is no younger than Late Permian on the basis of the Late Permian age for the crosscutting trondhjemite of the Sparta complex.

(6) A metatrondhjemite block in serpentinite-matrix melange in the Aldrich Mountains yielded a concordant U-Pb age of 279 Ma. Thus it appears to represent a tectonically broken fragment of crust genetically related to the Canyon Mountain Complex.

(7) The age range of magmatism recorded by U-Pb zircon ages of plutonic rocks in the Baker terrane overlap and are nearly synchronous with U-Pb ages of plutons in the Wallowa and Olds Ferry terranes.

(8) The Baker terrane probably represents the structurally telescoped fore arc of a Permian to Triassic ensimatic volcanic-plutonic arc complex.

REFERENCES CITED

Almy, R.B., 1977, Petrology and major-element geochemistry of albite granite near Sparta, Oregon: Bellingham, Western Washington University, M.S. thesis, 100 p.

Arden, J.W., and Gale, N.W., 1974, Separation of trace amounts of uranium and thorium and their determination by mass spectrometric isotope dilution: Analytical Chemistry, v. 84, p. 687–691.

Armstrong, R.L., Taubeneck, W.H., and Hales, P.O., 1977, Rb-Sr and K-Ar geochronometry of Mesozoic granitic rocks and their Sr isotopic composition, Oregon, Washington, and Idaho: Geological Society of America Bulletin, v. 88, p. 397–411.

Ashley, R.P., 1967, Metamorphic petrology and structure of the Burnt River Canyon area, northeastern Oregon: Stanford, Stanford University, Ph.D. dissertation, 193 p.

Avé Lallemant, H.G., 1976, Structure of the Canyon Mountain (Oregon) ophiolite complex and its implication for sea-floor spreading: Geological Society of America Special Paper 173, 49 p.

Avé Lallemant, H.G., Phelps, D.W., and Sutter, J.F., 1980, ^{40}Ar-^{39}Ar ages of some pre-Tertiary plutonic and metamorphic rocks of eastern Oregon and their geologic relationships: Geology, v. 8, p. 371–374.

Blome, C.D., Jones, D.L., Murchey, B.L., Lienecki, M., 1986, Geologic implications of radiolarian-bearing Paleozoic and Mesozoic rocks from the Blue Mountain province, Eastern Oregon, *in* Vallier, T.L., and Brooks, H.C., eds., Geology of the Blue Mountains Regions of Oregon, Idaho, and Washington—Geologic implications of Paleozoic and Mesozoic Paleontology and Biostratigraphy, Blue Mountains Province, Oregon and Idaho: U.S. Geological Survey Professional Paper 1435, p. 79–93.

Bloomer, S.H., 1983, Distribution and origin of igneous rocks from the landward slopes of the Mariana Trench—Implications for its structure and evolution: Journal of Geophysical Research, v. 88, no. B9, p. 7411–7428.

Bloomer, S.H., and Hawkins, J.W., 1982, Gabbroic and ultramafic rocks from the Mariana Trench—An island arc ophiolite, *in* Pt. 2 of Hayes, D.E. ed., The tectonic and geologic evolution of Southeast Asian seas and islands: Geophysical Monograph, v. 27, p. 294–317.

Bostwick, D.A., and Koch, G.S., 1962, Permian and Triassic rocks of northeastern Oregon: Geological Society of America Bulletin, v. 73, p. 419–422.

Brooks, H.C., Ferns, M.L., Coward, R.I., Paul, E.K., Nunlist, N., 1982, Geology and gold deposits of the Bourne quadrangle, Baker and Grant Counties, Oregon: Oregon Department of Geology and Mineral Industries Geologic Map, Series Map GMS-19, scale 1:24,000.

Brooks, H.C., McIntyre, J.R., Walker, G.W., 1976, Geology of the Oregon part of the Baker 1° by 2° quadrangle: Oregon Department of Geology and Mineral Industries, Map GMS-7, scale 1:250,000.

Brooks, H.C., and Vallier, T.L., 1978, Mesozoic rocks and tectonic evolution of eastern Oregon and western Idaho, *in* Howell, D.G., and McDougall, K.A., eds., Mesozoic paleogeography of the Western United States: Pacific Section, Society of Economic Paleontologists and Mineralogists, Pacific Coast Paleogeography Symposium 2, p. 133–145.

Cameron, A.E., Smith, D.H., and Walker, R.L., 1969, Mass spectrometry of nanogram-size samples of lead: Analytical Chemistry, v. 41, p. 525–526.

Carpenter, P.S., and Walker, N.W., 1992, Origin and tectonic significance of the Aldrich Mountains serpentinite-matrix melange, northeastern Oregon: Tectonics, v. 11, no. 3.

Coward, R.I., 1982, The Elkhorn Ridge Argillite—A deformed accretionary prism in northeastern Oregon [abs.]: Geological Society of America Abstracts with Programs, v. 14, no. 4, p. 157.

Dickinson, W.R., 1979, Mesozoic forearc basin in central Oregon: Geology, v. 7, p. 166-170.

Dickinson, W.R., and Thayer, T.P., 1978, Paleogeographic and paleotectonic implications of Mesozoic stratigraphy and structure in the John Day inlier of central Oregon, *in* Howell, D.G., and McDougall, K.A., eds., Mesozoic paleogeography of the Western United States, (Pacific Coast Paleogeography Symposium 2): Los Angeles, Society of Economic Paleontologists and Mineralogists, Pacific Section, p. 147–161.

Dickinson, W.R., and Vigrass, L.W., 1965, Geology of the Suplee-Izee area, Crook, Grant and Harney counties, Oregon: Oregon Department of Geology and Mineral Industries Bulletin 58, 109 p.

Ferns, M.L., and Brooks, H.C., 1983, Serpentinite-matrix melanges in parts of the Blue Mountains of northeastern Oregon [abs.]: Geological Society of America Abstracts with Programs, v. 15, no. 5, p. 371.

Ferns, M.L., Brooks, H.C., Avery, D.G., 1983, Geology and gold deposits map of the Greenhorn quadrangle, Baker and Grant Counties, Oregon: Oregon Department of Geology and Mineral Industries Geologic Map Series GMS-28, scale 1:24,000.

Fryer, P., Ambos, E.L., Hussong, D.M., 1985, Origin and emplacement of Mariana forearc seamounts: Geology, v. 13, p. 774–777.

George, R.P., Jr., 1978, Structural petrology of the Olympus ultramafic complex in the Troodos ophiolite, Cyprus: Geological Society of America Bulletin, v. 83, p. 845–865.

Gerlach, D.C., Avé Lallemant, H.G., and Leeman, W.P., 1981a, An island arc origin for the Canyon Mountain ophiolite complex, eastern Oregon, U.S.A.: Earth and Planetary Science Letters, v. 53, p. 255–265.

———1981b, Petrology and geochemistry of plagiogranite in the Canyon Mountain ophiolite, Oregon: Contributions to Mineralogy and Petrology, v. 77, p. 88–92.

Gill, J.B., 1981, Orogenic andesites and plate tectonics: New York, Springer-Verlag, 390 p.

Gilluly, J., 1933, Replacement origin of the albite granite near Sparta, Oregon: U.S. Geological Survey Professional Paper, 175-C, p. 65–81.

———1937, Geology and mineral resources of the Baker quadrangle, Oregon: U.S. Geological Survey Bulletin 879, 119 p.

Hawkins, J.W., and Evans, C.A., 1983, Geology of the Zimbales Range, Luzon, Philippine Islands—Ophiolite derived from an island arc-back arc basin pair, *in* Pt. 2 of Hayes, D.E., ed., The tectonic and geologic evolution of Southeast Asian seas and islands: Geophysical Monograph, v. 27, p. 95–123.

Hillhouse, J.W., Grommé, C.S., and Vallier, T.L., 1982, Paleomagnetism and Mesozoic tectonics of the Seven Devils arc in northeastern Oregon: Journal of Geophysical Research, v. 87, p. 3777–3794.

Himmelberg, G.R., and Loney, R.A., 1980, Petrology of ultramafic and gabbroic rocks of the Canyon Mountain ophiolite, Oregon: American Journal of Science, v. 280, p. 232–268.

Hotz, P.E., Lanphere, M.A., and Swanson, D.A., 1977, Triassic blueschists from northern California and north-central Oregon: Geology, v. 5, p. 659-663.

Hussong, D.M., and Uyeda, S., 1982, Tectonic processes and the history of the Mariana arc—A synthesis of the results of the Deep-Sea Drilling Project, Leg 60, *in* Hussong, D.M., and Uyeda, S., eds., Initial reports of the Deep-Sea Drilling Project, Leg 60.

Karig, D.E., 1979, Material transport within accretionary prisms and the "knocker" problem: Journal of Geology, v. 88, p. 27–39.

Krogh, T.E., 1973, A low contamination method for hydrothermal decomposition of zircon and extraction of U and Pb for isotopic age determination: Geochimica et Cosmochimica Acta, v. 37, p. 485–494.

Leitch, E.C., 1984, Island arc elements and arc-related ophiolites: Tectonophysics, v. 106, p. 177–203.

Mattinson, J.M., 1978, Age, origin, and thermal histories of some plutonic rocks from the Salinian block of California: Contributions to Mineralogy and Petrology, v. 67, p. 233–245.

Mullen, E.D., 1978, Geology of the Greenhorn Mountains, northeastern Oregon: Corvallis, Oregon State University, M.S. thesis, 372 p.

Mullen, E.D., 1985, Petrologic character of Permian and Triassic greenstones from the melange terrane of northeastern Oregon and their implications for terrane origin: Geology, v. 13, p. 131–134.

Mullen-Morris, E., and Wardlaw, B.R., 1986, Conodont ages for limestones of eastern Oregon and their implication for pre-Tertiary melange terranes, *in* Vallier, T.L., and Brooks, H.C., eds., Geology of the Blue Mountains Regions of Oregon, Idaho, and Washington—Geologic implications of Paleozoic and Mesozoic paleontology and biostratigraphy, Blue Mountains province, Oregon and Idaho: U.S. Geological Survey Professional Paper 1435, p. 59–63.

Nestell, M.K., 1983, Permian foraminiferal faunas of central and eastern Oregon [abs.]: Geological Society of America Abstracts with Programs, v. 45, p. 65–68.

Nolf, B., 1966, Structure and stratigraphy of part of the northern Wallowa mountains, Oregon: Princeton, Princeton University, Ph.D. dissertation, 138 p.

Phelps, D., 1979, Petrology, geochemistry, and origin of the Sparta quartz diorite-trondhjemite complex, northeastern Oregon, *in* Barker, F. ed., Trondhjemites, dacites and related rocks: Amsterdam, Elsevier, p. 547–580.

Phelps, D., and Avé Lallemant, H.G., 1980, The Sparta ophiolite complex, northeast Oregon—A plutonic equivalent to low-K_2O island-arc volcanism: American Journal of Science, v. 280-A, p. 345–358.

Prostka, H.J., 1962, Geology of the Sparta quadrangle: Oregon Department of Geology and Mineral Industries Geologic Map Series Map GMS-1, scale 1:62,500.

Silberling, N.J., Jones, D.L., Blake, M.C., Jr., and Howell, D.G., 1984, Lithotectonic terrane map of the western conterminous United States, *in* Silberling, N.J., and Jones, D.L., eds., Lithotectonic terrane maps of the North American cordillera: U.S. Geological Survey Open-File Report 84-523, p. C1–C43.

Swanson, D.A., 1969, Lawsonite blueschists from north-central Oregon, *in* Geological Survey Research 1969: U.S. Geological Survey Professional Paper 650-B, p. 8–11.

Taubeneck, W.H., 1957, Geology of the Elkhorn Mountains, northeastern Oregon—Bald Mountain batholith: Geological Society of America Bulletin, v. 68, p. 181–238.

———1958, Wallowa batholith, Wallowa Mountains, northeastern Oregon [abs.]: Geological Society of America Bulletin, v. 69, p. 1650.

———1964, Cornucopia stock, Wallowa Mountains, northeastern Oregon—Field relationships: Geological Society of America Bulletin, v. 75, p. 1093–1116.

———1967, Petrology of the Cornucopia tonalite unit, Cornucopia stock, Wallowa Mountains, northeastern Oregon: Geological Society of America Special Paper 91, 56 p.

———1969, Granitic clasts in Pennsylvanian conglomerates of central Oregon [abs.]: Geological Society of America Abstracts with Programs, Cordilleran Section, v. 1, p. 67–68.

Thayer, T.P., 1977, The Canyon Mountain Complex, Oregon, and some problems of ophiolites, *in* Coleman, R.G., and Erwin, W.P., eds., North American ophiolites: Oregon Department of Geology and Mineral Industries Bulletin 95, p. 93–106.

Thayer, T.P., and Brown, C.E., 1966, Geologic map of the Aldrich Mountain quadrangle, Grant County, Oregon: U.S. Geological Survey Geologic Quadrangle Map GQ-438.

Vallier, T.L., 1977, The Permian and Triassic Seven Devils Group, western Idaho and northeastern Oregon: U.S. Geological Survey Bulletin 1437, 58 p.

Vallier, T.L., Brooks, H.C., and Thayer, T.P., 1977, Paleozoic rocks of eastern Oregon and western Idaho, *in* Stewart, J.H., Stevens, C.H., and Fritsche, A.E., eds., Paleozoic paleogeography of the Western United States (Pacific Coast Paleogeography Symposium 1): Los Angeles, Society of Economic Paleontologists and Mineralogists, Pacific Section, p. 455–465.

Walker, N.W., 1986, U-Pb geochronologic and petrologic studies of the Blue Mountains terrane, northeastern Oregon and west-central Idaho—Implications for pre-Tertiary tectonic evolution: Santa Barbara, University of California, Ph.D. dissertation, 224 p.

———1989, Early Cretaceous initiation of post-tectonic plutonism and the age of the Connor Creek fault, northeastern Oregon [abs.]: Geological Society of America Abstracts with Programs, v. 21, no. 5, p. 155.

Weissel, J.K., 1981, Magnetic lineations in marginal basins of the western Pacific: Philosophical Transactions of the Royal Society of London, ser. A, v. 300, p. 223–247.

Wetherill, C.E., 1960, Geology of part of the southern Wallowa Mountains, northeastern Oregon: Eugene, University of Oregon, M.S. thesis, 208 p.

Wilson, D., and Cox, A., 1980, Paleomagnetic evidence for tectonic rotation of Jurassic plutons in the Blue Mountains, eastern Oregon: Journal of Geophysical Research, v. 85, no. B7, p. 3681–3689.

7. PRE-CRETACEOUS TECTONIC EVOLUTION OF THE BLUE MOUNTAINS PROVINCE, NORTHEASTERN OREGON

By HANS G. AVÉ LALLEMANT[1]

CONTENTS

	Page
Abstract	271
Introduction	272
Acknowledgments	274
Terranes of the Blue Mountains province	274
Wallowa terrane	274
Baker terrane	275
Olds Ferry terrane	275
Izee terrane	276
Early Cretaceous plutons	276
Mid-Cretaceous to Tertiary	276
Structure	277
Megascopic analysis	277
Mesoscopic analysis	277
Microscopic analysis	277
Wallowa terrane	283
D_1 deformation	283
Mesoscopic analysis	283
Microscopic analysis	283
Interpretation	285
Timing	285
D_2 deformation	285
Mesoscopic analysis	287
Microscopic analysis	287
Interpretation	287
Timing	292
D_3 deformation	292
D_4 deformation	292
Baker terrane	293
D_1 deformation	293
Mesoscopic analysis	293
Microscopic analysis	293
Interpretation	294
Timing	294
D_2 deformation	295
Mesoscopic analysis	295
Interpretation	295
Timing	295
D_3 deformation	295
Izee terrane	295
D_1 deformation	295
Structure—Continued	
Izee terrane—Continued	
D_1 deformation—Continued	
Mesoscopic analysis	295
Microscopic analysis	295
Interpretation	296
Timing	296
D_2 deformation	296
Mesoscopic analysis	296
Microscopic analysis	296
Interpretation	296
Timing	297
D_3 deformation	297
Olds Ferry terrane	297
Tectonic model	297
D_1 deformation	297
D_2 deformation	299
D_3 deformation	299
Left-oblique plate convergence	299
Post-D_3 deformation	300
Conclusions	300
References cited	301

[1] Department of Geology and Geophysics, Rice University, Houston, Texas 77251

ABSTRACT

The Blue Mountains province of northeastern Oregon has a complex tectonic history. The province consists of four major east-west-trending belts or terranes, which from north to south are the Wallowa, Baker, Izee, and Olds Ferry terranes; the small Grindstone terrane in the southwestern part of the province is not discussed here. On the basis of mesoscopic and microscopic structural analysis and previously published geologic, geochronologic, geochemical, and paleomagnetic data, a coherent although not yet completely constrained story emerges about the tectonic evolution of the province. The Olds Ferry terrane was a north-south-trending, west-facing intraoceanic volcanic island arc, active possibly from Permian but certainly from Middle Triassic to Middle Jurassic time. The Izee terrane consists of intra-arc (including fore-arc) basin deposits related to the Olds Ferry arc. The Baker terrane consists in part of melange; structures in the melange indicate that the terrane was accreted by eastward subduction underneath the Olds Ferry volcanic arc. There are indications that the convergence between the Baker oceanic terrane and the Olds Ferry arc was left-oblique. The Wallowa terrane constitutes a volcanic arc that was active during Pennsylvanian to Late Triassic time, with minor volcanism occurring until Jurassic time. The polarity of the Wallowa arc is not constrained, but it may have been west-facing. Major mylonite zones indicate that the plate convergence related

to the Wallowa arc was also left-oblique. The Wallowa arc, mostly inactive since the Late Triassic, collided with the Baker, Izee, and Olds Ferry terranes in the Late Jurassic; again, the convergence may have been left-oblique. During the collision, rocks of the Baker and Izee terranes were thrust eastward across the Olds Ferry terrane, whereas in the Wallowa terrane the Jurassic assemblage and fragments of the Permian and Triassic arc were thrust westward. After the amalgamation of all terranes, the Blue Mountains were intruded by granitic plutons during the Early Cretaceous. The collision of this amalgamated terrane with the North American craton in late Early Cretaceous time cannot be documented in Oregon, but it has been recognized in Idaho.

INTRODUCTION

The Blue Mountains province of northeastern Oregon consists of deformed pre-Cretaceous rocks, undeformed Cretaceous plutons, and Upper Cretaceous and Cenozoic sedimentary and volcanic rocks. In this chapter only the pre-Cretaceous tectonic history is described. Other names for the Blue Mountains province, as used here, are the Blue Mountains region or, for short, Blue Mountains.

All igneous rocks of the Blue Mountains province have initial Sr-isotope ratios lower than 0.704 (Armstrong and others, 1977; Fleck and Criss, 1985; Criss and Fleck, 1987). Thus, they are unrelated to the North American craton. Consequently, the entire Blue Mountains region can be called a "suspect" terrane (Coney and others, 1980) and may have traveled far before juxtaposition to the North American craton during Cretaceous time (Sutter and others, 1984; Lund and Snee, 1988; Snee and others, chap. 15, this volume). Paleomagnetic evidence suggests that, relative to the site of this juxtaposition, the Blue Mountains province was farther to the north in Permian time (Harbert and others, 1988) and farther to the south in Triassic time (Hillhouse and others, 1982).

The Blue Mountains region was subdivided into several terranes by Dickinson (1979), in part on the basis of previous work (Vallier and others, 1977; Brooks and Vallier, 1978; Dickinson and Thayer, 1978), each terrane having a distinct stratigraphy and tectonic evolution. The terranes are elongate, approximately east-west-trending belts. Boundaries between terranes are always tectonic; they may be compressional boundaries related to subduction processes or strike-slip faulting, or they may have characteristics of both. Silberling and others (1984) somewhat changed the boundaries of the terranes in the Blue Mountains and renamed them (from north to south) the "Wallowa," "Baker," "Izee," and "Olds Ferry" terranes (fig. 7.1). They also named a new terrane, the "Grindstone" terrane, which is outside the map area of figure 7.1 and about 75 km southwest of the town of John Day, Oreg.

The goal of the present study was to establish the tectonic evolution of each terrane by carrying out mesoscopic structural and strain analyses and microscopic strain and kinematic analyses. Structures common to two adjacent terranes may indicate the mechanism of juxtaposition of these terranes—whether they collided by normal convergence, oblique convergence, or strike-slip movement. Studies of recent deformation related to oblique plate convergence in New Zealand (Walcott, 1978) and Sumatra (Beck, 1983) indicate that the component of convergence normal to the plate boundary causes thrust faults and folds parallel to the boundary to form in the accretionary wedge; the component of convergence parallel to the plate boundary causes strike-slip displacements along fault zones parallel to the boundary in the accretionary wedge or the volcanic arc.

Because of the large areal extent of the Blue Mountains region, the results of the present study are clearly preliminary and the hypotheses tentative. The hypothesis proposed by Dickinson (1979) that the Baker terrane is the accretionary wedge or fore arc of the Olds Ferry volcanic-arc terrane is consistent with the structural data. The convergence may have been left-oblique; it may have started in the Permian and continued in the Late Triassic to Early Jurassic. The amalgamation of all five terranes of the Blue Mountains region took place when the Wallowa terrane collided with the amalgamated Baker-Izee-Olds Ferry terranes during Late Jurassic time. During this collision west-directed thrusting occurred in the Wallowa terrane (north-northwest-directed in present-day coordinates) and east-directed thrusting occurred in the Baker and Izee terranes (south-southeast-directed in present-day coordinates). It is possible that this convergence also had a left-lateral, strike-slip component consistent with left-oblique plate convergence elsewhere in the North American Cordilleran orogenic belt (Oldow and others, 1984, 1989; Avé Lallemant and Oldow, 1988). Collision of the Blue Mountains province with the North American craton occurred during the Cretaceous (Sutter and others, 1984; Lund and Snee, 1988; Snee and others, chap. 15, this volume), but no pervasive structures related to this collision have been identified in Oregon. Paleomagnetic evidence (Wilson and Cox, 1980; Hillhouse and others, 1982) indicates that the entire Blue Mountains province has rotated clockwise by about 65° since the intrusion of the Early Cretaceous granitic plutons. Part of the rotation may have occurred prior to or during the collision;

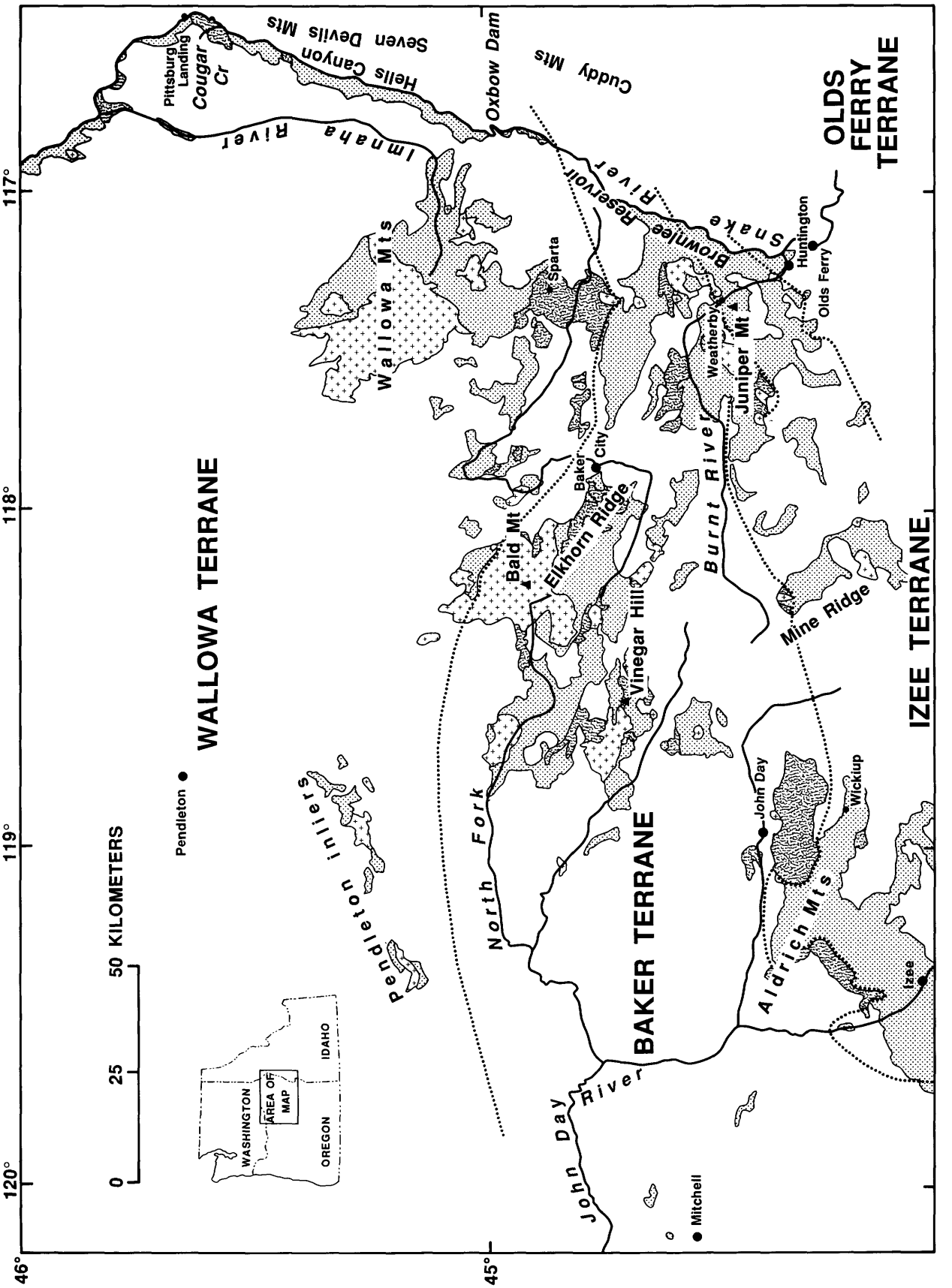

FIGURE 7.1.—Index map of Blue Mountains province, showing localities and areas mentioned in text. See figure 7.2 for explanation of map symbols and patterns.

part of it has been attributed to the post-Eocene extension of the Basin and Range province (Magill and Cox, 1981).

ACKNOWLEDGMENTS

I am grateful to Tom Thayer and Howard Brooks who introduced me to the geology of the Blue Mountains. Reviews of earlier versions of this paper by H.C. Brooks, J.G. Evans, R.L. Thiessen, T.L. Vallier, and B.P. Wernicke were very helpful. I thank Gordon and Lura Glass of John Day, who have been so hospitable and helpful through the years that I worked in Oregon. The research was primarily supported by the National Science Foundation through grants GA-25894, EAR-76-13372, EAR-79-04829, and EAR-82-06531.

TERRANES OF THE BLUE MOUNTAINS PROVINCE

WALLOWA TERRANE

The Wallowa terrane, as named by Silberling and others (1984), is identical to the Seven Devils terrane of Dickinson (1979). It underlies most of the Wallowa Mountains in Oregon and the Seven Devils Mountains in Idaho (fig. 7.1). The Wallowa terrane consists of Permian and Triassic intrusive, volcanic, and volcaniclastic rocks; Triassic and Jurassic sedimentary rocks; and Early Cretaceous plutonic rocks.

The oldest rocks of the volcanic sequence are undated quartz keratophyre flows and tuffs overlain by Lower Permian keratophyre and spilite flows interbedded with volcaniclastic rocks, and Middle to Upper Triassic (Ladinian, Carnian) andesite, keratophyre, and spilite flows interbedded with clastic rocks (Vallier, 1977). The volcanic rocks follow a low-K_2O basalt-andesite-dacite-rhyolite differentiation trend, typical of volcanic arcs (Vallier and Batiza, 1978). The main volcanic activity ceased in Carnian time (Vallier and others, 1977); sporadic volcanism continued into the Callovian (Follo, 1994; White and Vallier, 1994).

The Permian and Triassic volcanic sequence is overlain by a thick platform limestone of late Carnian to Norian age (Vallier, 1977; Newton, 1983, 1986; Follo, 1994). It is overlain by Upper Triassic (Norian) and Lower Jurassic (Toarcian) shale, thin limestone, argillite, and siltstone of the Hurwal Formation (Nolf, 1966). There is no sedimentary record between the Toarcian and Callovian. Callovian to lower Oxfordian tuff and clastic beds of the Coon Hollow Formation occur in two areas of the Snake River canyon, directly overlying Triassic and older rocks (Morrison, 1964; Vallier, 1977; Goldstrand, 1994; White and Vallier, 1994).

In the Snake River canyon are three igneous-metamorphic complexes (Vallier, 1974) consisting mostly of gabbro, amphibolite, plagiogranite, and schistose metavolcanic rocks, which Vallier and others (1977) considered to be the basement upon which the Permian and Triassic volcanic sequences were deposited. Walker (1981, 1982, 1986) obtained U-Pb zircon ages of 265 to 233 Ma for plagiogranites from all three complexes, indicating that the plagiogranites are mostly synchronous with the volcanic activity. A discordant age of 309 Ma was obtained for zircons from a gneiss (Walker, 1986). Geochemical data are consistent with a volcanic-arc environment for the formation of these complexes (Balcer, 1980; Walker, 1982; Vallier, chap. 3, this volume). Major mylonite zones that occur in all three basement complexes of the Snake River canyon formed between 262 and 218 Ma (Avé Lallemant and others, 1980; Balcer, 1980; Walker, 1986).

The (informal) Sparta complex of Phelps (1979), about 40 km east of Baker City, consists of pyroxenite, gabbro, and plagiogranite. Phelps (1979) and Phelps and Avé Lallemant (1980) have shown that this complex has volcanic-arc affinities and probably represents the root of the Wallowa volcanic arc, because there is no obvious tectonic boundary between the Sparta complex and the Triassic volcanic rocks of the Seven Devils Group (see also Brooks and Vallier, 1978). The plagiogranites were dated at 223 Ma ($^{40}Ar/^{39}Ar$: Avé Lallemant and others, 1980), and 262, 223, and 219 Ma (U-Pb: Walker, 1981, 1983, 1986); a gabbro sample yielded an age of 227 Ma ($^{40}Ar/^{39}Ar$: Avé Lallemant, 1984).

Many plate tectonic settings have been proposed for the Wallowa volcanic-arc terrane. Vallier and others (1977) and Brooks and Vallier (1978) correlated the Wallowa terrane with the Olds Ferry terrane. Silberling (1983) disagreed on the basis of stratigraphic and lithologic differences. Jones and others (1977) correlated the Wallowa terrane with the Wrangellia terrane, an exotic terrane in southeastern Alaska, Queen Charlotte Islands, and Vancouver Island, on the basis of paleomagnetic and faunal evidence. Newton (1983) agreed with the faunal correlation, but Stanley (1986) saw too many faunal differences. Sarewitz (1983) and Scheffler (1983) did not accept this correlation either, because of the large geochemical differences between the two terranes: the Upper Triassic volcanic rocks of the Wrangellia terrane are oceanic-plateau-type basalts, and those of the Wallowa terrane are calc-alkaline (Vallier and Batiza, 1978). Mortimer (1986) correlated the Wallowa ter-

rane with the Stikinia terrane in British Columbia (Monger and others, 1982; Monger and Berg, 1987). The Stikinia terrane consists of Mississippian to Jurassic arc-related volcanic and sedimentary rocks. It lies west of the Cache Creek assemblage, which is very similar in lithology and age to the Baker terrane of the Blue Mountains.

Paleomagnetic data (Harbert and others, 1988) suggest that during the Permian the Wallowa terrane resided at higher latitudes than the site of its ultimate accretion to the North American craton, and that in the Late Triassic (Hillhouse and others, 1982) it resided at lower latitudes. Thus, the Wallowa terrane may have migrated southward in post-Permian time, whereas it moved northward in post-Triassic time. This displacement history is in agreement with a model proposed by Avé Lallemant and Oldow (1988) that was based on field relationships in several Cordilleran terranes and on plate-motion reconstructions by Engebretson and others (1985). Avé Lallemant and Oldow (1988) suggested that several Cordilleran terranes, including the Wallowa terrane, moved southward along the continental margin until about 120 Ma, and northward from about 100 Ma to the present.

BAKER TERRANE

The Baker terrane lies south of the Wallowa terrane. It was previously called the Oceanic terrane (Vallier and others, 1977) and the Central Melange terrane (Dickinson and Thayer, 1978). The Central Melange terrane included Silberling and others' (1984) Grindstone terrane, an allochthonous sequence of Devonian to Lower Triassic sedimentary rocks about 75 km southwest of John Day (Blome and Nestell, 1991). The Grindstone terrane is not included in the present study.

The Baker terrane consists of large blocks that are internally coherent, separated by chaotic zones and shear zones. The main rock types are argillite and chert (of the Elkhorn Ridge Argillite), phyllite, limestone, serpentinite, gabbro, and subordinate volcanic flows and tuffs, graywacke, and conglomerate, and rare blueschists.

The ages of formation of rocks in the Baker terrane range from Devonian to Late Triassic or possibly Early Jurassic (Evans, 1986). Radiolarians in the cherts have been dated as Permian and Triassic and possibly Early Jurassic (Blome and others, 1986). Limestone blocks in the Baker terrane have Permian fusulinid faunas in some places only of Tethyan affinities, in others only of North American affinities (Nestell, 1983). Devonian through Late Triassic (Morris and Wardlaw, 1986) conodonts are present in limestone blocks throughout the Baker terrane.

The volcanic rocks of the Baker terrane have been studied in detail (Mullen, 1985; Bishop, chap. 5, this volume). Some have MORB characteristics; others are intraplate basalts. Some basalts of volcanic island arc affinities are also present.

Blueschists near Mitchell (fig. 7.1; see also fig. 7.2, area *J*) were dated by Hotz and others (1977). They yielded an age of 223 Ma ($^{40}Ar/^{39}Ar$). Amphibolites with blue amphiboles have also been described in the Vinegar Hill area (*K*, fig. 7.2; Mullen, 1978; Bishop, chap. 4, this volume).

Dickinson (1979) suggested that this terrane is a subduction complex related to the Triassic volcanic arc of the Olds Ferry terrane in the southern part of the Blue Mountains region (fig. 7.1). Structural data presented here support this hypothesis.

The Baker terrane has been correlated invariably with the Cache Creek assemblage in British Columbia (Klepacki and Wernicke, 1985; Mortimer, 1986; Monger and Berg, 1987), with the Hayfork, North Fork, and Fort Jones terranes in the Klamath Mountains, and with the Calaveras Formation in the foothills of the Sierra Nevada (Burchfiel and Davis, 1981; Mortimer, 1986). All of these rocks are lithologically very similar and are approximately of the same age as those of the Baker terrane.

OLDS FERRY TERRANE

The most southerly terrane in the study area is the Olds Ferry terrane, previously called the Juniper Mountain-Cuddy Mountain terrane by Brooks and Vallier (1978) and the Huntington terrane by Dickinson (1979). Silberling and others (1984) included the Weatherby Formation of Brooks (1979a) in the Olds Ferry terrane; the Weatherby consists of Lower Jurassic sedimentary rocks overlying the Triassic volcanic and volcaniclastic rocks. Dickinson (1979), however, put these Jurassic rocks in the Mesozoic clastic terrane, and in the present study, as well as in Vallier (chap. 3, this volume), his boundaries are used. The name Olds Ferry terrane is used here only for the Triassic volcanic and volcaniclastic rocks.

The Olds Ferry terrane is relatively small and somewhat poorly exposed. Only Middle and Upper Triassic (Carnian to Norian) rocks have been recognized. They consist of basalt, andesite, rhyolite, volcaniclastic rocks, and limestone (Brooks and Vallier, 1978; Vallier, chap. 3, this volume). It is generally accepted that these rocks formed in a volcanic-arc

environment. Quartz diorite and gabbro stocks occur throughout the terrane (Brooks and others, 1976). One pluton in Oregon has been dated at 235 Ma (U-Pb: Walker, 1986). Several plutons in the Cuddy Mountains, Idaho, were dated at 217 to 187 Ma (K-Ar: Henricksen, 1975). They are believed to have formed in an intraoceanic volcanic arc (Brooks and Vallier, 1978). Although no volcanic rocks younger than Norian are exposed, Dickinson (1979) proposed that the arc was active through the Middle Jurassic, assuming that the Callovian lavas and tuffs in the western part of the Izee terrane were derived from the Olds Ferry terrane.

In most studies, the Canyon Mountain (ophiolite) Complex near John Day is included in the Baker or Central Melange terrane. Thayer (1969) believed it to be a large fragment of oceanic crust. Avé Lallemant (1976) suggested that it had formed in a marginal basin adjacent to a volcanic island arc. On the basis of geochemical studies, Himmelberg and Loney (1980), Gerlach, Avé Lallemant, and Leeman (1981), Gerlach, Leeman, and Avé Lallemant (1981), and Mullen (1983) proposed that the complex formed in a volcanic island arc. The age of the Canyon Mountain Complex is Permian (U-Pb data: Walker and Mattinson, 1980; Walker, 1981, 1986; $^{40}Ar/^{39}Ar$ data: Avé Lallemant and others, 1980; Avé Lallemant, 1984); it is plausible that the complex represents the Permian part of the Olds Ferry volcanic island arc terrane.

Hillhouse and others (1982) have obtained paleolatitudes for the Olds Ferry terrane that are the same as those for the Wallowa. Brooks and Vallier (1978) suggested that the two terranes were fragments of the same arc. However, because the Norian limestone typical of the Wallowa terrane is absent from the Olds Ferry terrane and because the abundance of Jurassic volcanic rocks in the Izee terrane suggests that the Olds Ferry arc was active through the Middle Jurassic, Silberling (1983) concluded that the Olds Ferry terrane should not be correlated with the Wallowa terrane. Mortimer (1986) correlated the Olds Ferry terrane with the Quesnellia terrane, a Triassic to Jurassic volcanic arc terrane in British Columbia (Monger and Berg, 1987), on the basis of lithologic and age relations.

IZEE TERRANE

The Izee terrane of Silberling and others (1984) does not include the Jurassic sequence near the Snake River canyon because they assumed that the Weatherby Formation was deposited directly on the Olds Ferry terrane. Although these Jurassic sedimentary rocks most probably are related to the Olds Ferry volcanic-arc terrane (Brooks and Vallier, 1978), the contact between the two sequences is tectonic (Avé Lallemant, 1983). Furthermore, the lithologies and age of the Weatherby Formation are very similar to those of the Mesozoic clastic sedimentary rocks near John Day. Thus, these rocks are herein included in the Izee terrane.

In the John Day area the sedimentary rocks are of Late Triassic (Carnian) to Middle Jurassic (Callovian) age (Dickinson and Thayer, 1978); they are flysch-like turbidites consisting of shales and graywackes with chert, serpentinite, and volcanic-rock particles and crystal fragments of quartz, calcite, plagioclase, and spinel. Volcanic flows are ubiquitous in the lower part of the sedimentary section and become subordinate near the top. In the Snake River canyon, sedimentary rocks of similar lithology occur, but they are restricted to the Early and Middle Jurassic (Sinemurian to Bajocian), although there are Upper Jurassic (Callovian) sedimentary rocks across the Snake River in Idaho (Brooks, 1979a).

Dickinson and Thayer (1978) and Dickinson (1979) suggested that most sedimentary rocks of the Izee terrane were deposited in intra-arc basins and that the youngest Callovian sediments were deposited in a deep fore-arc basin of the Huntington or Olds Ferry volcanic arc.

EARLY CRETACEOUS PLUTONS

All four terranes of the Blue Mountains region that are discussed here were intruded post-tectonically by mostly granitic stocks and plutons. They were dated by Armstrong and others (1977) using the K-Ar and Rb-Sr methods as Late Jurassic to Early Cretaceous (160 to 95 Ma). Most of these plutonic rocks, however, have been thermally disturbed. Recent U-Pb studies (Walker, 1989) suggest that the oldest intrusions are of earliest Cretaceous age (~143 Ma); the main plutonic activity appears to have ceased at about 120 Ma (Walker, 1986, 1989). Some of the intrusions straddle the contact between terranes (Brooks and others, 1976). Paleomagnetic data (Wilson and Cox, 1980; Hillhouse and others, 1982) indicate that the granites were emplaced at the latitude of present-day Idaho but before the 65° clockwise rotation occurred.

MID-CRETACEOUS TO TERTIARY

In the western part of the Blue Mountains, Cretaceous (Albian, Cenomanian) sedimentary rocks have

been recognized; they consist of shallow-marine coarse-grained clastic rocks (Dickinson and Thayer, 1978). The remainder of the region is covered by volcanic and clastic rocks of Eocene to Pleistocene age, including the Miocene Columbia River Basalt Group.

STRUCTURE

In this chapter, structures are classified as megascopic, mesoscopic, and microscopic. Megascopic structures relate to the map scale; mesoscopic structures have a scale ranging from hand specimen to outcrop; and microscopic structures are sometimes recognized with the hand lens but generally only with the petrographic microscope.

MEGASCOPIC ANALYSIS

Megascopic folds were recognized in the Wallowa terrane by Smedes (1959), Wetherell (1960), and Vallier (1974) and in the Izee terrane by Dickinson and Vigrass (1965), Brown and Thayer (1966a, b), Thayer and Brown (1966), and W.D. Lowry and C.F. Wray (unpub. data, 1968). Because of the apparent chaotic character of the rocks, only a few megascopic folds were recognized in the Baker terrane (Gilluly, 1937; Ashley, 1966); but recently, many more megascopic folds were mapped on the basis of structural analysis of asymmetric mesoscopic folds in the Elkhorn Ridge Argillite (Coward, 1983). On the same basis, megascopic folds were recognized in the Weatherby area of the Izee terrane (Avé Lallemant, 1983). Map-scale thrust faults were observed in the Wallowa terrane by Smedes (1959) and Vallier (1974) and in the Izee terrane by Brooks and others (1976) and Avé Lallemant (1983).

MESOSCOPIC ANALYSIS

Observed mesoscopic structures include bedding planes (S_0), fold axial planes and axial-plane cleavages or foliations (S_1 to S_4), fold axes (B_1 to B_4), and lineations (L_1 to L_4) (fig. 7.2). The subscripts 1 to 4 refer to deformation phases D_1 to D_4, from the oldest to the youngest. Fold geometries are described according to the classification of Ramsay (1967). Lineations are intersection lineations (generally intersections of bedding and cleavage planes, the subscript of L corresponding to that of the cleavage involved), mineral lineations, and stretching lineations. In stretched-pebble conglomerates, the mean orientations of the three principal axes were determined. The mean short, intermediate, and long dimensions are approximately parallel, respectively, to the major principal compressive strain axis (Z), the intermediate principal strain axis (Y), and the major principal extensile strain axis (X), but exceptions are observed.

Mylonites occur in several places in the Blue Mountains province. Along fine-grained mylonitic shear zones (S_m, fig. 7.2) the cleavage or X-Y plane is subparallel to S_m, but with increasing distance from S_m the strain magnitude decreases and the angle between S_m and the X-Y plane increases. Such shear zones are called "S-C mylonites" by Berthé and others (1979). The sense of shear that caused the mylonite can be determined: The displacement is parallel to the projection of the X axis onto the S_m plane and toward the acute angle between S_m and X-Y planes.

Extension veins were recorded in several areas. The major extension axis is subperpendicular to these veins.

In each outcrop, the relative age of different structures was determined by crosscutting relationships. Locally, such as in the Canyon Mountain Complex (Avé Lallemant, 1976; Avé Lallemant and others, 1980) and in one of the basement complexes in the Snake River canyon (Walker, 1986), the oldest penetrative deformation occurred in the Permian. (These penetrative structures are not discussed in this chapter). In all other places, the first deformation (D_1) took place during Late Triassic to Early Jurassic time; the other three deformations (D_2 to D_4) appear to have occurred during the Late Jurassic.

All mesoscopic data are plotted on lower-hemisphere, equal-area stereographic projections (fig. 7.3), simplified versions of which are shown on the general map of the Blue Mountains region in figure 7.2. Axial trends of the four deformational events are also plotted in figure 7.2; these trends are based mainly on mesoscopic analysis but also on published maps by Gilluly (1937), Smedes (1959), Dickinson and Vigrass (1965), Brown and Thayer (1966a, b), Thayer and Brown (1966), Walker (1977), and Brooks (1979a).

MICROSCOPIC ANALYSIS

Several rock samples, oriented in the field, were thin-sectioned for microfabric and microtextural analysis. The word "microfabric" is used here to describe the preferred orientation of crystal lattice or optical-indicatrix axes, whereas the term "microtexture" is used to describe the spatial relationships of grains or the network of grain boundaries.

For the microfabric analysis, a four-axis universal stage was used to measure the c axes of quartz and

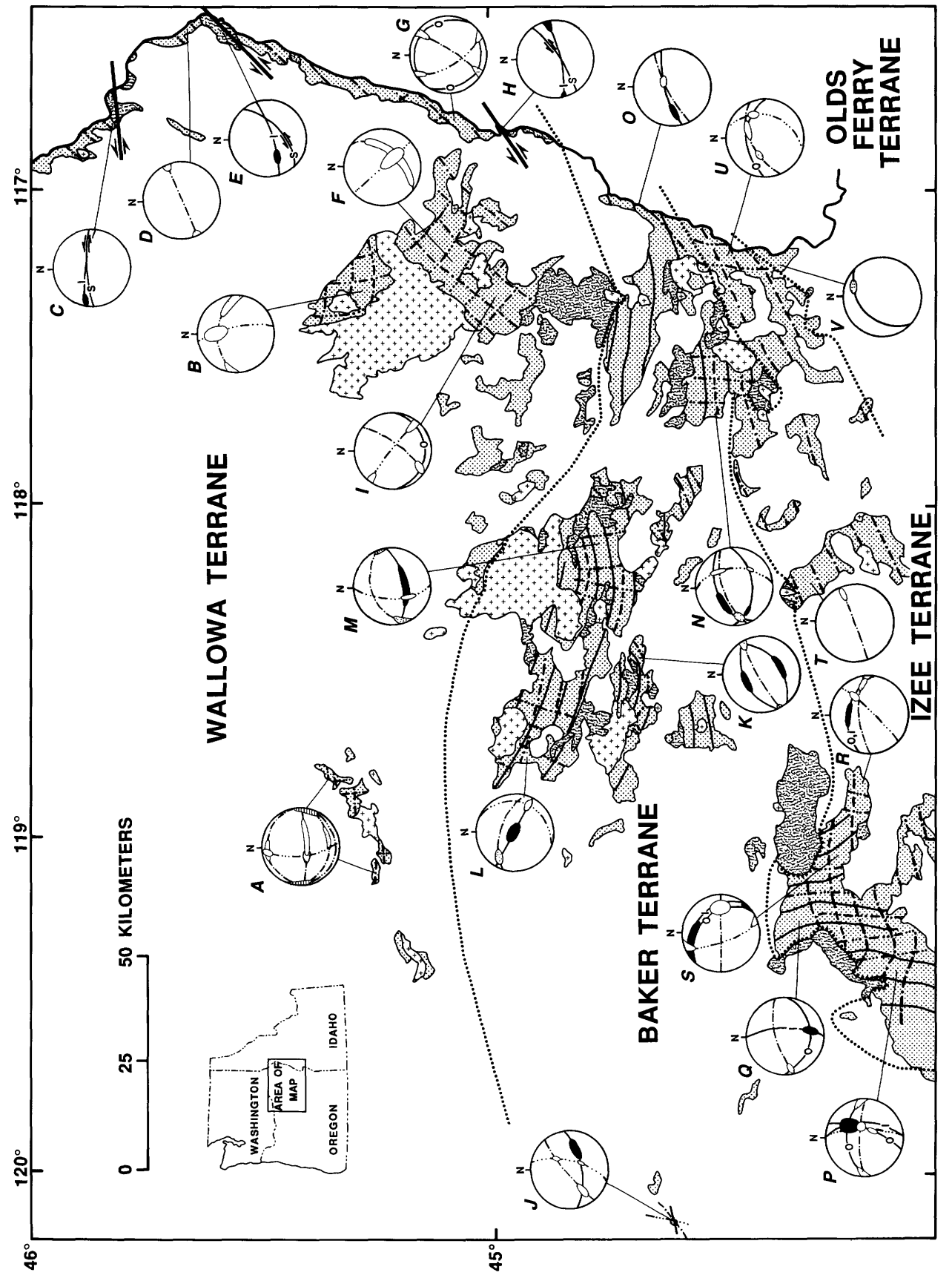

FIGURE 7.2.—Simplified geologic map of Blue Mountains province (from Walker, 1977). Lower-hemisphere, equal-area projections of average orientations of structural elements characteristic of 22 areas on the map. Mesoscopic-structure data that correspond to these 22 stereographic diagrams are shown in projections *A* through *V* on figure 7.3.

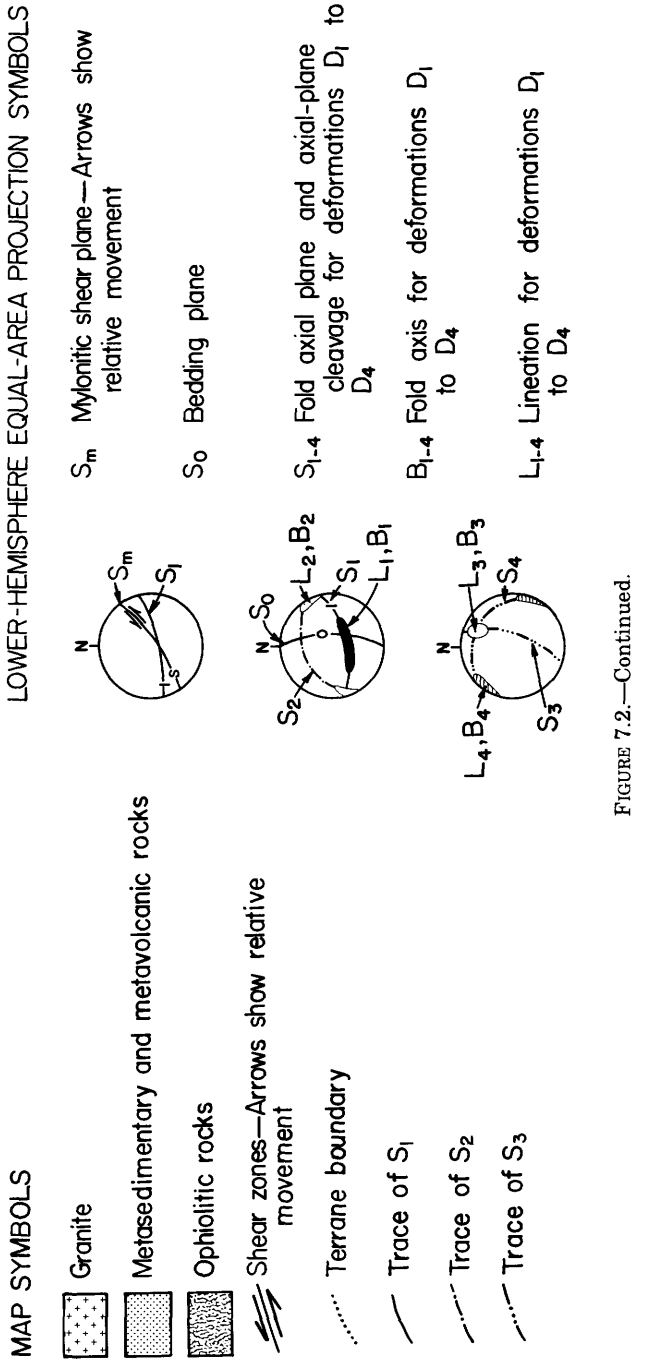

FIGURE 7.2.—Continued.

calcite, the basal plane {0001} of biotite, and the optical-indicatrix axes of amphibole and plagioclase. In biotite, the α optical-indicatrix axis that is almost perpendicular to the basal plane {0001} was measured in crystals in which {0001} made an angle of less than 45° with the thin section. Optical-indicatrix axes are symbolized by α, β, and γ instead of X, Y, and Z, because the latter symbols are used herein for the principal strain axes. In amphibole, the β axis is parallel to [010], the γ axis is inclined to [001] (the c axis) by 10° to 20°, and the α axis is almost perpendicular to (100). Because the optical-indicatrix axes approximately coincide with the crystallographic axes, the amphibole microfabrics were interpreted in terms of the lattice axes and planes. In the plagioclase (oligoclase), the α axis is inclined to [100] by 6° to 15°, the β axis is inclined to the pole of (001) by 8° to 15°, and the γ axis is inclined to the pole of (010) by 2° to 12°. Because these angles are relatively small, the plagioclase fabrics were also interpreted in terms of the lattice axes and planes.

Generally, the microfabrics have an orthorhombic symmetry. Their symmetry axes can be related to the principal strain axes on the basis of experimental work; sometimes the fabric axes were interpreted on the basis of independently determined strain axes. It has been shown that the lattice axes of minerals with only one dominant slip system rotate in such a way that the slip plane becomes parallel to the X-Y plane of the finite strain ellipsoid, and that the slip direction rotates toward the X axis.

All quartz fabrics in the present study (fig. 7.4, projections *B*, *D*, *I*, *L*, *M*; fig. 7.5, projections *B*, *C*, *D*, *G*) have the well-known cross-girdle pattern. Other researchers have recognized these fabrics elsewhere and related them to strain axes determined from other structures (for example, Sylvester and Christie, 1968). Such fabrics were produced experimentally by Green and others (1970), Tullis and others (1973), and Tullis (1977). The intersection of the two girdles is parallel to the intermediate principal strain axis, Y. The X axis is at right angles to Y, lies in the foliation or cleavage plane, and generally is at the center of the underpopulated area of the fabric diagram.

Calcite c axes tend to form a great-circle girdle (*G*, fig. 7.4; *I*, fig. 7.5) perpendicular to a mineral lineation with a weak point maximum perpendicular to the foliation plane. Such fabrics have been produced experimentally by Friedman and Higgs (1981). The girdle axis is subparallel to the X axis; thus, the mineral lineation is also subparallel to the major principal extensile-strain axis, X (see *G*, fig. 7.4). The point maximum of c axes perpendicular to the foliation is subparallel to the Z axis, the major principal compressive-strain axis.

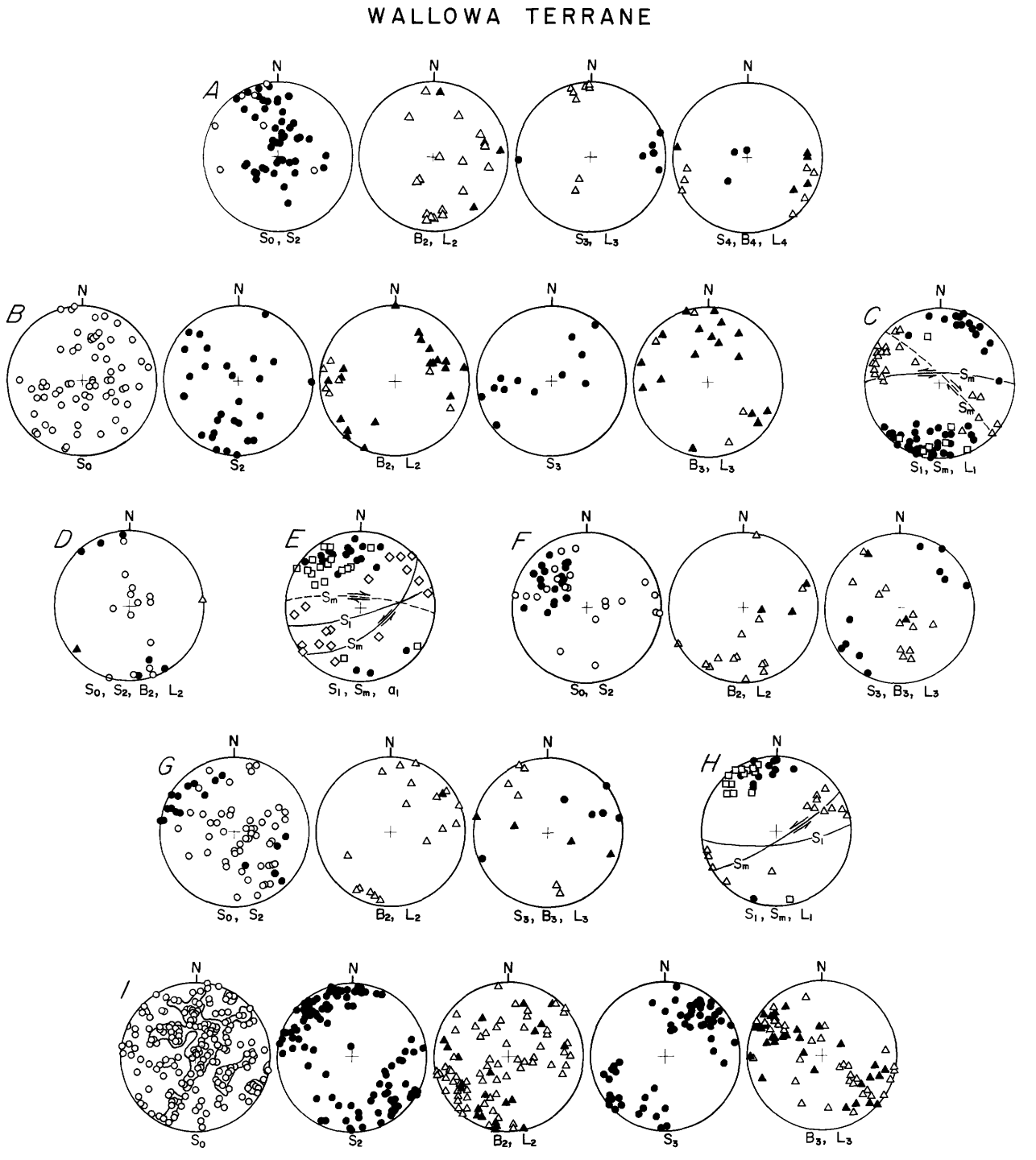

FIGURE 7.3.—Lower-hemisphere, equal-area projections of mesoscopic structural elements. Wallowa terrane: *A*, Pendleton inliers; *B*, Northern Wallowa Mountains; *C*, Confluence of Imnaha and Snake Rivers; *D*, Pittsburg Landing area; *E*, Cougar Creek area; *F*, Central Wallowa Mountains; *G*, Hells Canyon; *H*, Oxbow Dam area; *I*, Southern Wallowa Mountains. Baker terrane: *J*, Mitchell area; *K*, Vinegar Hill area; *L*, North Fork John Day River area; *M*, Elkhorn Ridge; *N*, Burnt River canyon; *O*, Brownlee Reservoir area. Izee terrane: *P*, Izee area; *Q*, Aldrich Mountains; *R*, Wickiup area; *S*, John Day area; *T*, Mine Ridge; *U*, Weatherby area. Olds Ferry terrane: *V*, Huntington area. See figure 7.2 for localities corresponding to *A* through *V*. S_0, bedding plane; S, fold axial plane and axial-plane cleavage and foliation; B, fold axis; L, lineation. Subscripts 1 to 4 refer to phase of deformation D_1 to D_4. S_m, mylonitic shear plane (arrows show relative movement; dashed great circle indicates rarer orientation); α, tectonic-transport direction; circle, pole to bedding plane; dot, pole to fold axial plane and axial-plane cleavage and foliation; solid triangle, fold axis; open triangle, lineation; diamond, tectonic-transport direction constructed from S and S_m; square, pole to mylonitic shear plane. Contour (only in *I*) drawn at 1.7 percent per 1-percent area.

Poles to {0001} of biotite form great-circle girdles perpendicular to a strong mineral lineation (*A*, *B*, and *G*, fig. 7.5) and a point maximum perpendicular to the foliation. Because of basal slip in biotite, the {0001} planes are expected to rotate during deformation into parallelism with the foliation or X-Y plane. In syntectonic-recrystallization experiments Tullis (1976) demonstrated that micas form [0001] girdles perpendicular to the X axis with a point maximum parallel to the Z axis.

Preferred orientations of amphibole (both glaucophane and green amphibole) are shown in projections

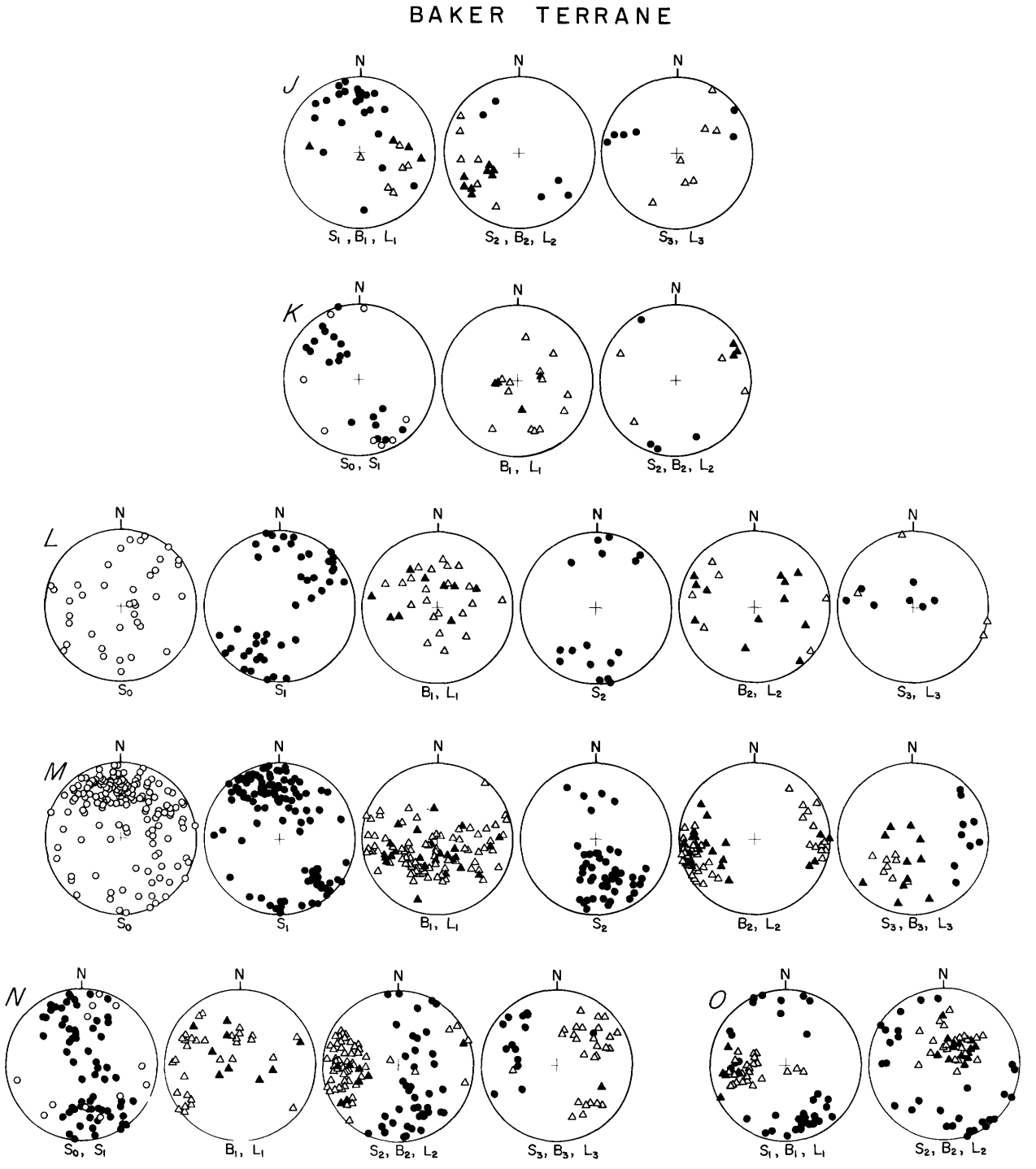

FIGURE 7.3.—Continued.

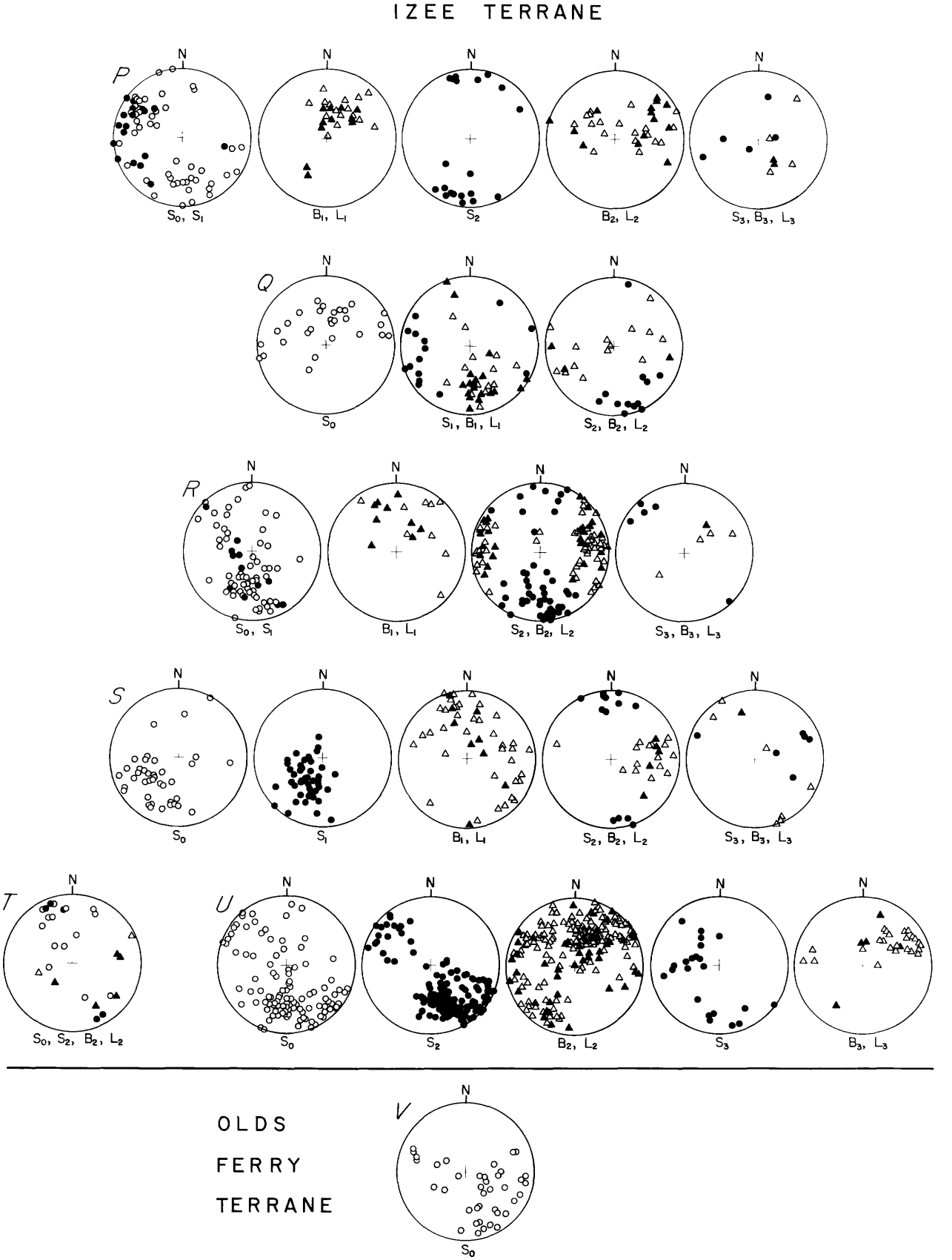

FIGURE 7.3.—Continued.

D and *F* in figure 7.4 and *C* in figure 7.5. The α axes form a point maximum perpendicular to the foliation and a γ point maximum parallel to a well-developed mineral lineation. Experimental work (Dollinger and Blacic, 1975; Nielsen and Ross, 1979) indicates that the favored slip system of amphiboles is (100)[001]. Accordingly, it is expected that during deformation the (100) planes rotate toward parallelism with the X-Y plane and the [001] axes rotate toward the X axis. The amphibole fabrics in the present study are consistent with these experimental conclusions.

Two plagioclase fabrics were determined here (*A* and *C*, fig. 7.5). Few experimental studies on plagioclase have been performed, but none of the experimentally determined slip systems are consistent with the present results. These two plagioclase fabrics can be related to the strain axes derived from the fabrics of biotite (*A*, fig. 7.5) and of quartz and amphibole (*C*, fig. 7.5). If indeed translation glide planes rotate toward the X-Y plane and the slip direction rotates toward the X axis, the required slip system for the plagioclase is (001)[100].

Only two of the microfabrics have monoclinic symmetry (*B*, *M*, fig. 7.4), and both are quartz c axis fabrics. These fabrics can be interpreted in terms of strain axes (see above) and in terms of kinematics. Studies have shown (Bouchez and Pecher, 1981) that a hypothetical shear plane can be constructed subperpendicular to the strongest of the two c axis girdles; the sense of shear or the displacement is then toward the acute angle between the shear plane and the X axis. Passchier (1983) warned, though, that this construction sometimes yields results opposite to the shear sense derived from other structural features.

All fabric diagrams in figures 7.4 and 7.5, except *B* and *M* in figure 7.4, can be considered orthorhombic. That does not necessarily mean that they formed by coaxial deformation. Orthorhombic fabrics have been produced in noncoaxial deformation experiments (see Tullis, 1977), but the sense of shear cannot be determined from the microfabric data. However, microtextural studies (figs. 7.6, 7.7) of thin sections cut parallel to the X-Z plane of samples shown in figures 7.4 and 7.5 and of several additional samples revealed the sense of displacement. The sense of shear can be determined from asymmetric pressure shadows and rotated porphyroblasts (Simpson and Schmid, 1983), curved quartz and calcite fibers in veins and pressure shadows (Ramsay and Huber, 1983), rotated chlorite flakes and quartz fibers in pressure shadows of magnetite (Spry, 1969), microscopic S-C structures (Berthé and others, 1979), and displacements along microfaults.

Directions of tectonic transport derived from these microfabric and microtextural studies and mesoscopic data are shown in figures 7.8 and 7.9. All geometric data are plotted on lower-hemisphere, equal-area stereographic projections.

WALLOWA TERRANE

D_1 DEFORMATION

The oldest penetrative deformation (D_1) structures in the Wallowa terrane occur in three so-called basement complexes exposed in the Snake River canyon (fig. 7.1; *C*, *E*, and *H*, fig. 7.2). These complexes consist of gabbro, quartz diorite, and volcanic rocks and their metamorphic and deformed equivalents. The grade of metamorphism is variable, from lowest greenschist to epidote amphibolite facies.

Both the plutonic and metavolcanic rocks are penetratively deformed in mylonitic shear zones. The Imnaha shear zone (*C*, fig. 7.2) at the confluence of the Imnaha and Snake Rivers, trends east-west and dips steeply to the north. The Cougar Creek shear zone (*E*, fig. 7.2) near Pittsburg Landing, Idaho, and the Oxbow shear zone (*H*, fig. 7.2) near the Oxbow Dam, Oregon and Idaho, strike northeast-southwest and dip steeply to the southeast.

Mesoscopic Analysis

Each of three complexes is characterized by a multitude of mesoscopic shears subparallel to the megascopic shear zone. Fine-grained ultramylonites occur along these shears. With increasing distance to the shears, the grain size of the mylonites increases, the aspect ratio of porphyroclasts decreases, and the angle between the foliation planes and the shears increases. Thus, these structures are S-C mylonites (Berthé and others, 1979). The aspect ratio of porphyroclasts is the same as the finite strain ratio X/Z (Avé Lallemant and others, 1985). In general, mineral lineations are subhorizontal. The general trend of foliations is more easterly to southeasterly than the strikes of the shears (*C*, *E*, *H*, fig. 7.3). This relationship indicates that the shears are left-lateral. Rarely, northwest-southeast- and east-west-striking shears have been recognized in the Imnaha and Cougar Creek shear zones, respectively (*C*, *E*, fig. 7.3). The foliation/shear zone relationship in these two cases is opposite to the general relationship just described and indicates right-lateral displacement.

Microscopic Analysis

Avé Lallemant and others (1985) obtained five quartz c axis microfabrics from quartz diorite mylonite

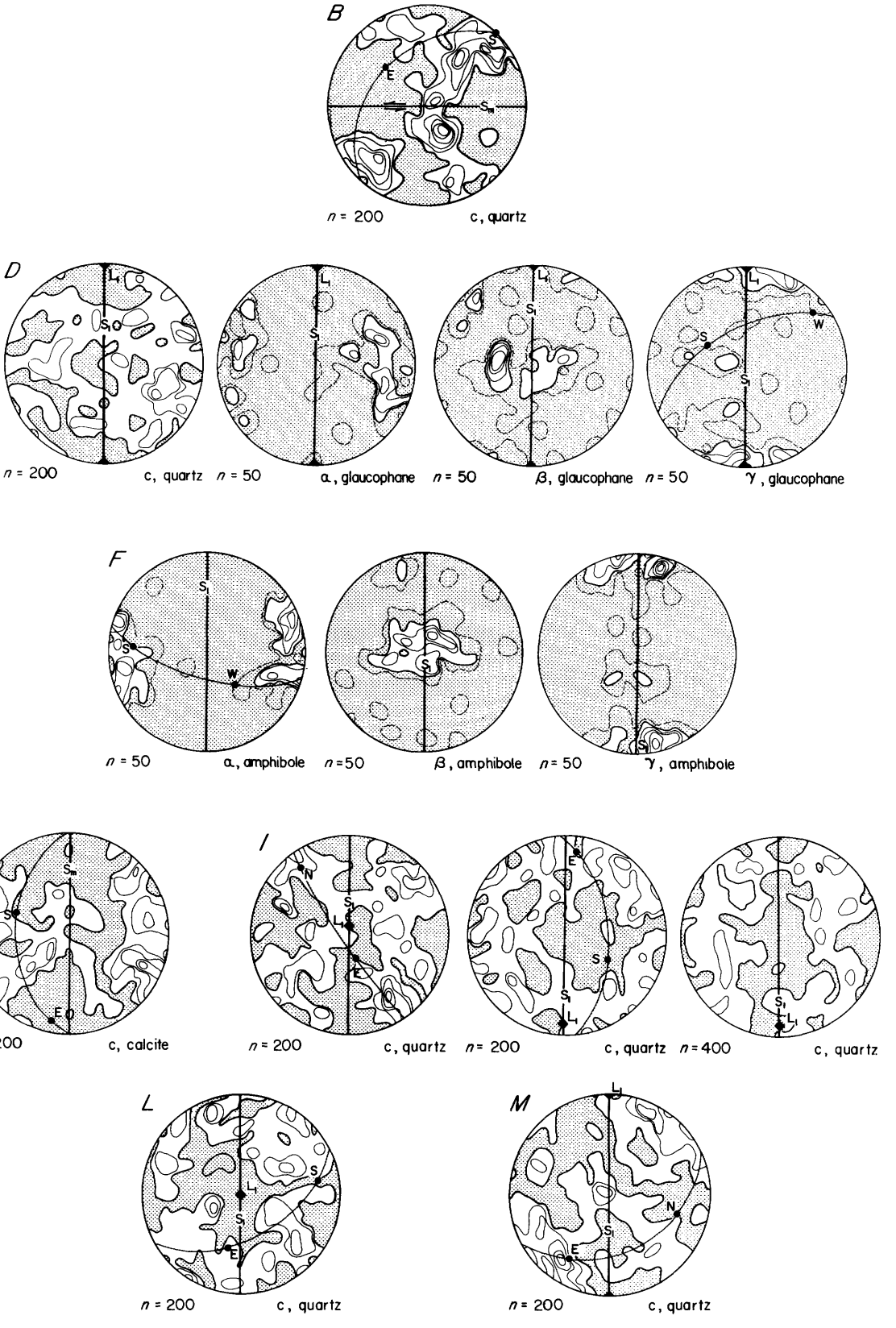
B
E
S_m
n = 200
c, quartz
D
L_1
S_1
n = 200
c, quartz
n = 50
α, glaucophane
n = 50
β, glaucophane
n = 50
γ, glaucophane
W
F
n = 50
α, amphibole
n = 50
β, amphibole
n = 50
γ, amphibole
G
S_m
E
n = 200
c, calcite
I
N
E
n = 200
c, quartz
n = 200
c, quartz
n = 400
c, quartz
L
n = 200
c, quartz
M
N
E
n = 200
c, quartz

samples from the Oxbow shear zone, and Chen (1985) obtained a large number of microfabric data from quartz diorite and granodiorite mylonites from the Imnaha shear zone: 12 quartz, 2 amphibole, and 3 plagioclase fabrics. In the present study, only one sample of quartz diorite mylonite from the Cougar Creek shear zone was analyzed; it has a very strong quartz c axis preferred orientation (*B*, fig. 7.4). This fabric and those from the other shear zones (Avé Lallemant and others, 1985; Chen, 1985) display cross-girdle patterns. Many of the fabrics have monoclinic symmetry. Microscopic S-C mylonite structures are common (*B*, fig. 7.6).

The amphibole fabrics of Chen (1985) are very well defined. They consist of an α point maximum perpendicular to the foliation, a γ point maximum subparallel to the lineation, and a β maximum perpendicular to the α and γ maxima. Some of the fabrics have monoclinic symmetry; the γ point maxima are not exactly parallel to the lineation.

The oligoclase microfabrics of Chen (1985) are also strongly defined. They consist of a γ point maximum normal to the foliation, an α maximum parallel to the lineation, and a β maximum perpendicular to α and γ.

Interpretation

The orientation of the principal finite strain axes can be derived from the quartz and amphibole microfabrics. Comparison of these strain axes and the plagioclase microfabric indicates that the plagioclase in the study area has deformed by translation glide on the (010)[001] slip system.

The orientations of the strain axes X, Y, and Z for all three shear zones are shown in projections *A* through *C* on figure 7.8. Projections *A* and *C* represent average orientations, and *B* was derived from projection *B* on figure 7.4.

The monoclinicity of some of the microfabrics in the Wallowa terrane samples and the mesoscopic relationship between foliations and shear planes indicate that all three shear zones were formed by left-lateral strike-slip motion. The rare shears oriented northwest-southeast and east-west in the Imnaha and Cougar Creek shear zones are right-lateral (*C*, *E*, fig. 7.3) and are conjugate to the major shear zones.

Avé Lallemant and others (1985) estimated that the minimum displacement along the Oxbow shear zone is 65 km. Because the other complexes are similarly deformed, the total left-lateral displacement along all three shear zones combined could easily have been 200 km or more.

Timing

The timing of the shear displacement in the Imnaha, Cougar Creek, and Oxbow areas is rather well constrained. Several $^{40}Ar/^{39}Ar$ analyses date the timing of the metamorphism that was coeval with the mylonitization at 263 to 213 Ma (Avé Lallemant and others, 1980; Balcer, 1980; Walker, 1986). An undeformed lamprophyre crosscutting the mylonites of the Oxbow shear zone has a total $^{40}Ar/^{39}Ar$ gas age of 197.4 Ma (Avé Lallemant and others, 1985).

D_2 DEFORMATION

After the Late Triassic D_1 deformation in the three basement complexes, the next major penetrative deformation in the Wallowa terrane occurred in the Late Jurassic. The associated mesoscopic deformation structures (fold axial planes, foliations, cleavages, and lineations) are plotted in figure 7.3 (projections *A*, *B*, *D*, *F*, *G*, *I*); D_2 microfabrics are shown in figure 7.5; and megascopic structural data are shown in figure 7.2 (projections *A*–*I*).

In some areas (such as Hells Canyon, *G*, fig. 7.2) the deformation is rather mild with only the development of crude cleavages subparallel to fold axial planes; in these areas, rocks have been metamorphosed only to lowest greenschist facies. In other areas (northern Wallowa Mountains, *B*, fig. 7.2, and the Pendleton inliers, *A*, fig. 7.2) the deformation is severe and the metamorphic grade is much higher. In one of the Pendleton inliers the mica schists contain sillimanite, and they are partly migmatized.

Northwest-vergent thrust faults (fig. 7.9), recognized at Pittsburg Landing (Vallier, 1974) and in the

◀ FIGURE 7.4.—Lower-hemisphere, equal-area projections of D_1-deformation microfabric elements of samples from selected areas shown in figure 7.8: *B*, Quartz diorite mylonite; *D*, blueschist; *F*, epidote amphibolite; *G*, marble; *I*, *L*, phyllites; *M*, metachert. Microfabric elements are c axes of quartz and calcite, and α, β, and γ (optical-indicatrix) axes of glaucophane and green amphibole. *n*, number of measurements. Contours drawn at intervals of 2 percent per 1-percent area where n=50, and at intervals of 1 percent per 1-percent area where $n \geq 200$. Dashed and heavy (solid) contour lines represent 2- and 4-percent contours, respectively, where n=50; heavy contour is 1-percent contour where $n \geq 200$. Great circles with dots show geographic horizontal, where N, S, E, and W represent north, south, east, and west, respectively. S_1 represents S_1 cleavage and foliation; L_1 (solid diamond) represents first (D_1-phase) lineation; S_m represents mylonitic shear plane (arrows show relative movement).

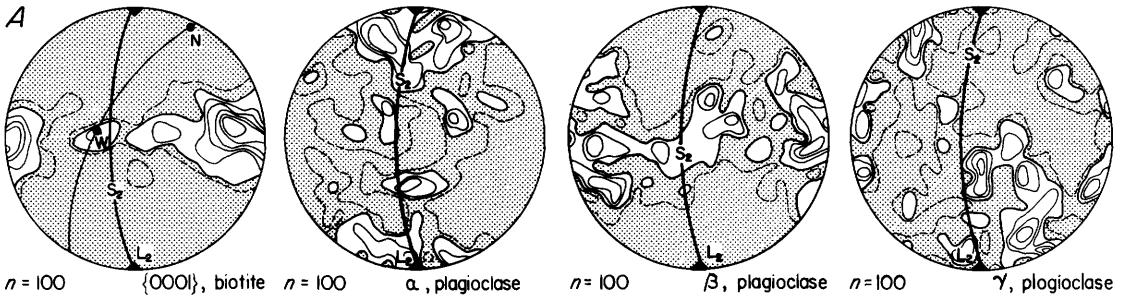
A
N
W
S_2
L_2
n = 100 {0001}, biotite
n = 100 α, plagioclase
n = 100 β, plagioclase
n = 100 γ, plagioclase

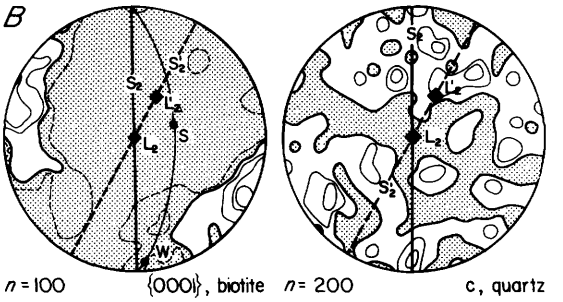
B
S_2
S_2'
L_2
S
W
n = 100 {0001}, biotite
n = 200 c, quartz

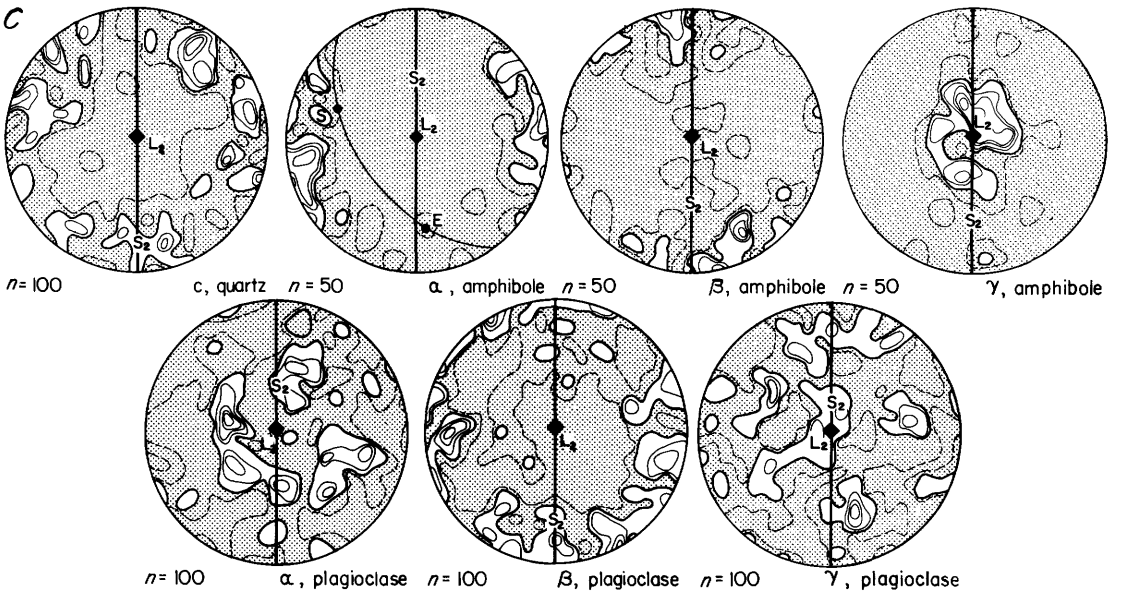
C
L_2
S_2
E
n = 100 c, quartz
n = 50 α, amphibole
n = 50 β, amphibole
n = 50 γ, amphibole
n = 100 α, plagioclase
n = 100 β, plagioclase
n = 100 γ, plagioclase

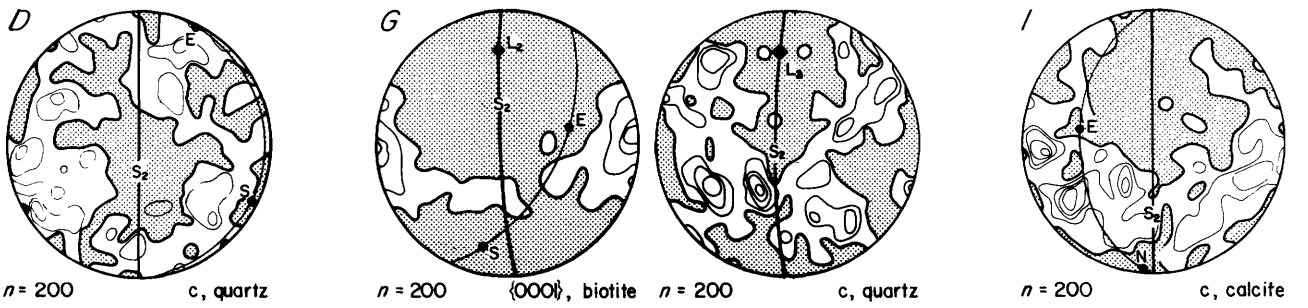
D
E
S_2
S
n = 200 c, quartz
G
L_2
S_2
E
S
n = 200 {0001}, biotite
n = 200 c, quartz
I
E
S_2
N
n = 200 c, calcite

central Wallowas (Smedes, 1959), are contemporaneous with the D_2 folding (*D*, *F*, fig. 7.2). Megascopic folds in the central and southern Wallowas are overturned to the northwest (Smedes, 1959; Mirkin, 1986).

Mesoscopic Analysis

The orientations of the mesoscopic D_2 structures are shown in figure 7.3 (projections *A*, *B*, *D*, *F*, *G*, and *I*), and average orientations are presented on figure 7.2 (projections *A*, *B*, *D*, *F*, *G*, and *I*). The style of folding strongly correlates with the metamorphic grade and is a function of the amount of strain. In Hells Canyon (*G*, fig. 7.2) and the southern Wallowas (*I*, fig. 7.2), folds are open and have a class 1b (parallel) to 1c (weakly converging dip isogons) geometry (Ramsay, 1967). In the central Wallowas (*F*, fig. 7.2), the northern Wallowas (*B*, fig. 7.2), and the Pendleton inliers (*A*, fig. 7.2), folds approach class 2 (similar-fold) geometry.

The orientation of bedding planes (S_0) is highly variable owing to the later (D_3) refolding. Two very indistinct girdles of bedding-plane poles trend northwest and northeast; the first girdle is subnormal to the B_2 fold axes (*D*, *G*, fig. 7.3); the second is related to the D_3 deformation (*B*, fig. 7.3).

Fold axial planes and axial-plane cleavages (S_2) strike generally northeast-southwest (*A*, *D*, *F*, *G*, and *I*, fig. 7.3). In the northern Wallowas (*B*, fig. 7.3) the S_2 cleavages are variable. The fold axes (B_2) and lineations (L_2) trend roughly northeast-southwest in most areas (*B*, *D*, *F*, *G*, *I*, fig. 7.3). However, in the high-grade metamorphic rocks of the Pendleton inliers (*A*, fig. 7.2; *A*, fig. 7.3) fold axes and lineations trend generally north-south; many of these lineations are mineral lineations, in particular due to parallelism of amphibole crystals.

Microscopic Analysis

Six samples were chosen for petrofabric analysis. The preferred orientations were determined for quartz (in four samples), biotite (three), plagioclase (two), amphibole (one), and calcite (one) and are presented in figure 7.5. All fabrics have orthorhombic symmetry. Quartz c axis fabrics display moderate to strong preferred orientations; each consists of two cross-girdles, the intersection of which lies in the foliation plane and is approximately 90° from a well-developed mineral lineation (*B*, *C*, *G*, fig. 7.5). Biotite [0001] axes form girdles normal to the lineation with point maxima perpendicular to the foliation (*A*, *B*, *G*, fig. 7.5). Plagioclase (oligoclase) axes show preferred orientations with an α axis small-circle girdle around the lineation; the β axes form a great circle around the lineation and have a weak point maximum normal to the foliation (*A*, *C*, fig. 7.5). Amphiboles have a strong γ point maximum parallel to the lineation and an α maximum perpendicular to the foliation (*C*, fig. 7.5). Calcite c axes are preferentially oriented in a great circle perpendicular to the lineation (*I*, fig. 7.5). Mirkin (1986) carried out microfabric analysis on ten samples from the southern Wallowas (*I*, fig. 7.2) resulting in seven quartz and three calcite fabrics. His fabric patterns are nearly identical to the quartz and calcite fabrics described above.

All these Wallowa terrane D_2 microfabrics have orthorhombic symmetry. They can be interpreted in terms of the finite-strain axes, but they do not show whether or not the deformation was coaxial. Therefore, all six samples and three additional ones were studied to find textural criteria indicating noncoaxial deformation. Criteria that were used to determine the shear sense are asymmetric pressure shadows (*A*, *B*, *J*, fig. 7.7), grain elongations at an angle to fine-grained shear zones subparallel to the foliation (*A*, *B*, fig. 7.7), rotated chlorite and quartz fibers in pressure shadows of magnetite crystals (*D*, *E*, *F*, fig. 7.7), and rotated synkinematic porphyroblasts (snowball garnet, *B*, fig. 7.7). In six of the nine samples, definite conclusions as to the sense of shear could be made.

Interpretation

The quartz, biotite, amphibole, and calcite microfabrics can be interpreted in terms of the orientation

◀ FIGURE 7.5.—Lower-hemisphere, equal-area projections of D_2-deformation microfabric elements of samples from selected areas shown in figure 7.9: *A*, Metaconglomeratic biotite-hornblende gneiss; *B*, garnet-biotite-sillimanite gneiss; *C*, garnet-biotite-hornblende gneiss; *D*, chlorite-muscovite schist; *G*, biotite gneiss; *I*, marble. Microfabric elements are c axes of quartz and calcite, poles to {0001} in biotite, and α, β, and γ (optical-indicatrix) axes of plagioclase and green amphibole. *n*, number of measurements. Contours drawn at intervals of 2 percent per 1-percent area where n=50, and at intervals of 1 percent per 1-percent area where $n \geq 100$. Biotite contours at 1, 5, 10, and 15 percent per 1-percent area in *B* and 1, 2, 5, 10, and 15 percent per 1-percent area in *G*. Dashed and heavy (solid) contour lines represent 2- and 4-percent contours, respectively, where n=50, and 1- and 2-percent contours, respectively, where n=100 (except biotite in *B*); heavy contour is 1-percent contour where n=100 (except biotite in *G*). S_2 (heavy great circle), foliation plane; S_2' (dashed great circle), rare second foliation plane; L_2 (solid diamond), mineral lineation; L_2' (solid diamond), rare second mineral lineation. Light great circle represents geographic horizontal; N, S, E, and W stand for north, south, east, and west, respectively.

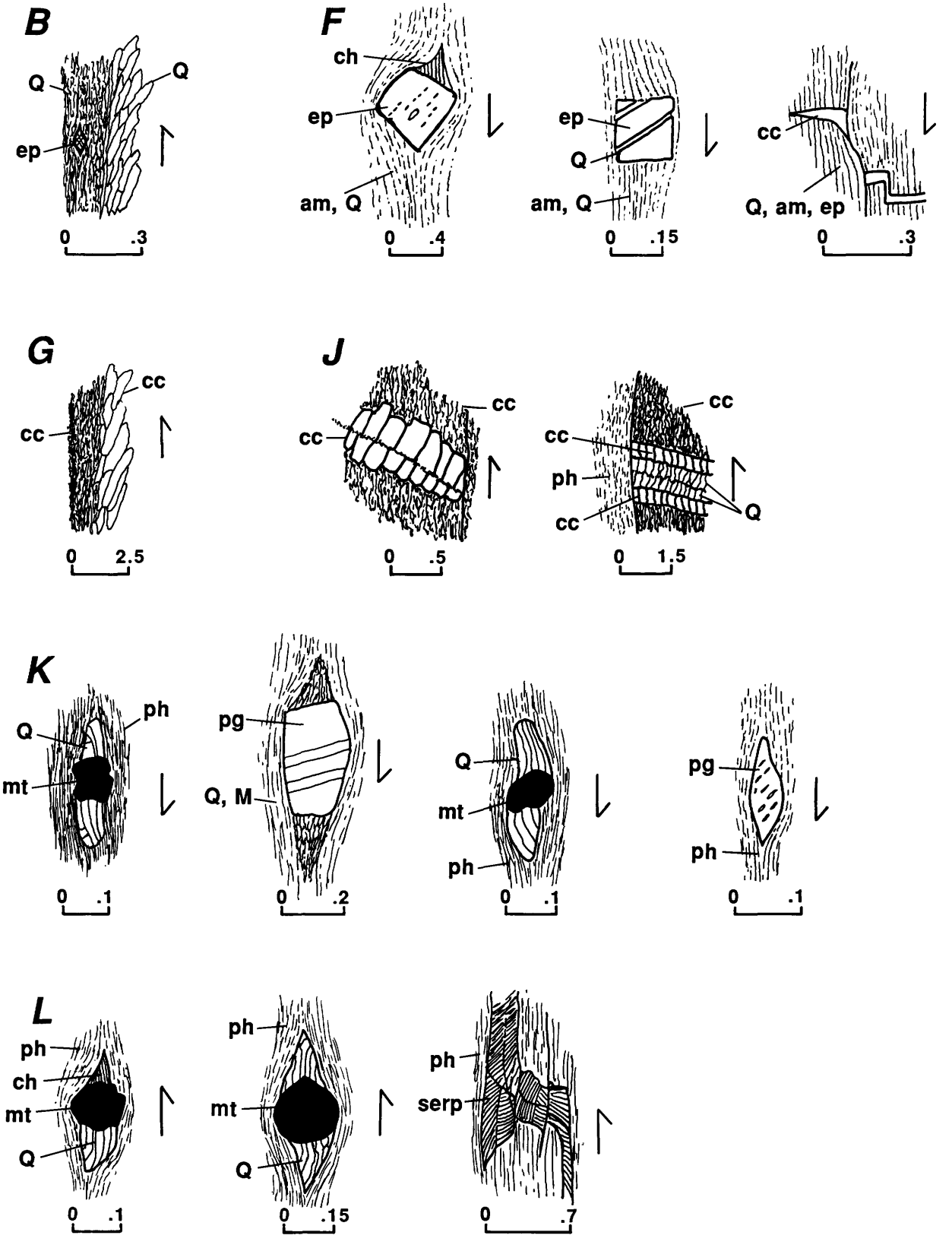

FIGURE 7.6.—Selected microtextures indicating D_1-deformation sense of shear (arrows) in thin sections cut parallel to X-Z plane from samples collected in Blue Mountains province. Letter designations *B*, *F*, *G*, *J*, *K*, and *L* refer to corresponding projections of D_1 fabrics in figure 7.8. Sample B is from Wallowa terrane; other samples from Baker terrane. *B*, Quartz diorite mylonite; *F*, epidote amphibolite; *G*, marble mylonite; *J*, calcareous phyllite; *K*, *L*, phyllite; am, amphibole; cc, calcite; ch, chlorite; ep, epidote; *M*, muscovite; mt, magnetite; pg, plagioclase; ph, phyllite; *Q*, quartz; serp, serpentine. Heavy lines (in *F*, *J*, and *L*), microfaults. All scales in millimeters.

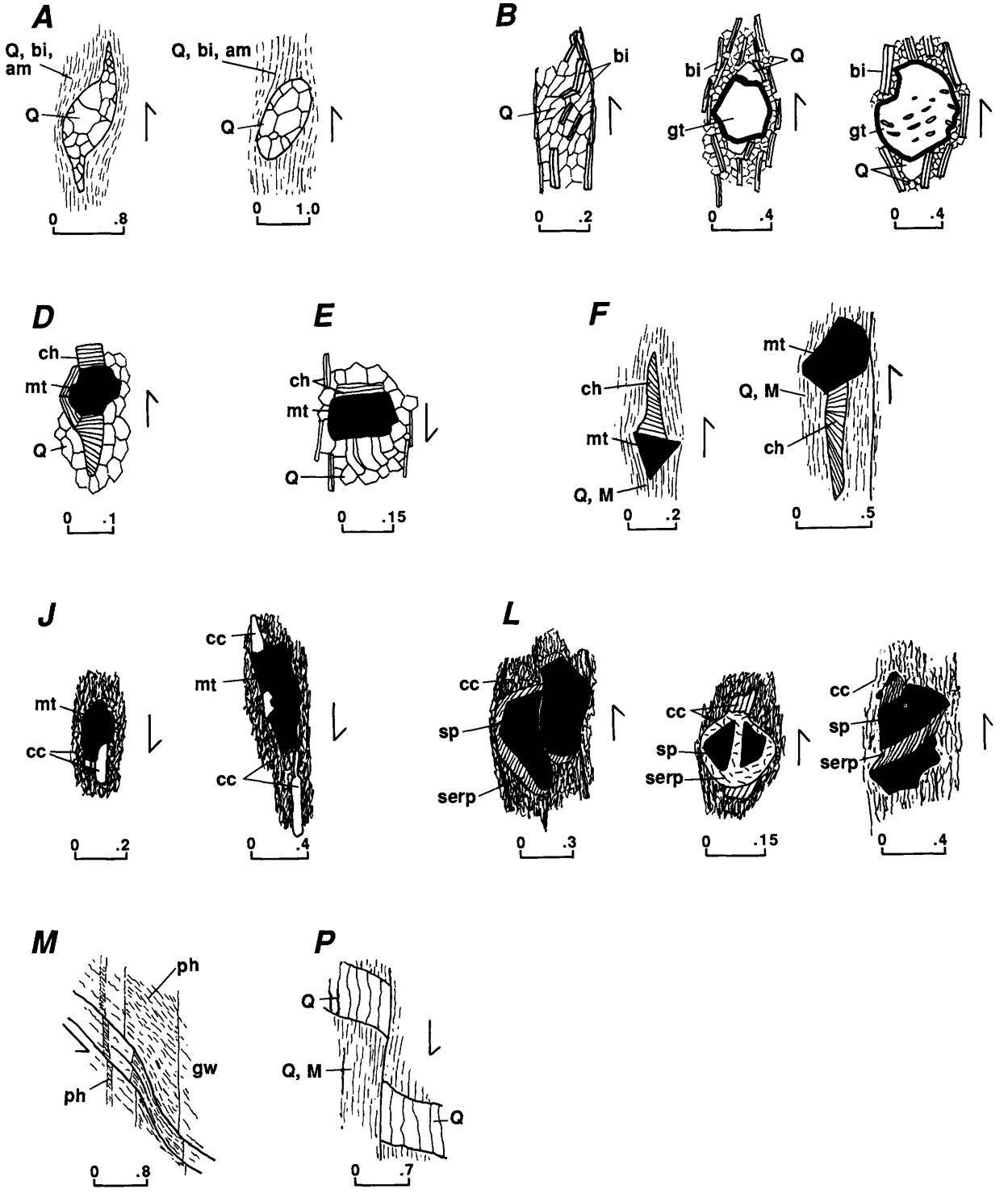

FIGURE 7.7.—Selected microtextures indicating D_2-deformation sense of shear (arrows) in thin sections cut parallel to X-Z plane from samples collected in Blue Mountains province. Letter designations *A*, *B*, *D*, *E*, *F*, *J*, *L*, *M*, and *P* refer to corresponding projections of D_2 fabrics in figure 7.9. Samples *A*, *B*, and *D* through *F*, from Wallowa terrane; samples *J*, *L*, *M*, and *P*, from Izee terrane. *A*, Metaconglomeratic biotite-hornblende gneiss; *B*, garnet-biotite-sillimanite gneiss; *D*, *E*, *F*, chlorite-muscovite schist; *J*, graphitic marble; *L*, calcareous metaconglomerate; *M*, interbedded graywacke and phyllite; *P*, metaconglomerate; am, amphibole; bi, biotite; cc, calcite; ch, chlorite; gt, garnet; gw, graywacke; *M*, muscovite; mt, magnetite; ph, phyllite; *Q*, quartz; serp, serpentine; sp, spinel. Heavy lines (in *F*, *L*, *M*, and *P*) are microfaults. All scales in millimeters.

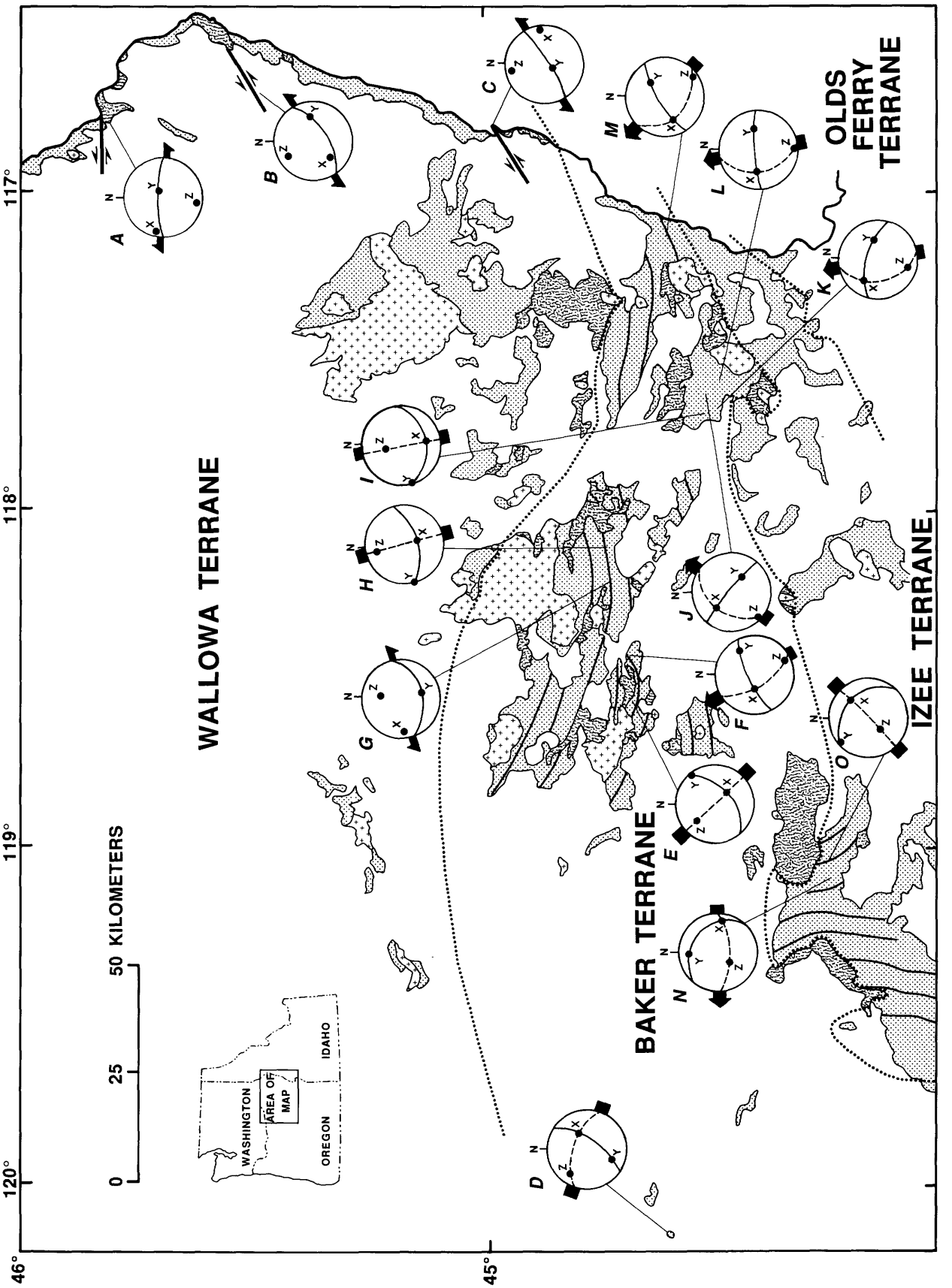

FIGURE 7.8.—Geologic map showing Late Triassic to Early Jurassic deformation (D_1) structures in Blue Mountains province. Inset diagrams A through O are lower-hemisphere, equal-area projections of principal strain axes. X, major principal extensile-strain axis; Y, intermediate principal strain axis; Z, major principal compressive-strain axis. Solid great circle, X-Y plane or cleavage plane; dashed great circle, X-Z plane or movement plane. Heavy arrow, tectonic-transport direction; double-headed arrows, left-lateral strike-slip displacement; heavy bar, strike of X-Z plane. See figure 7.2 for explanation of geologic map symbols.

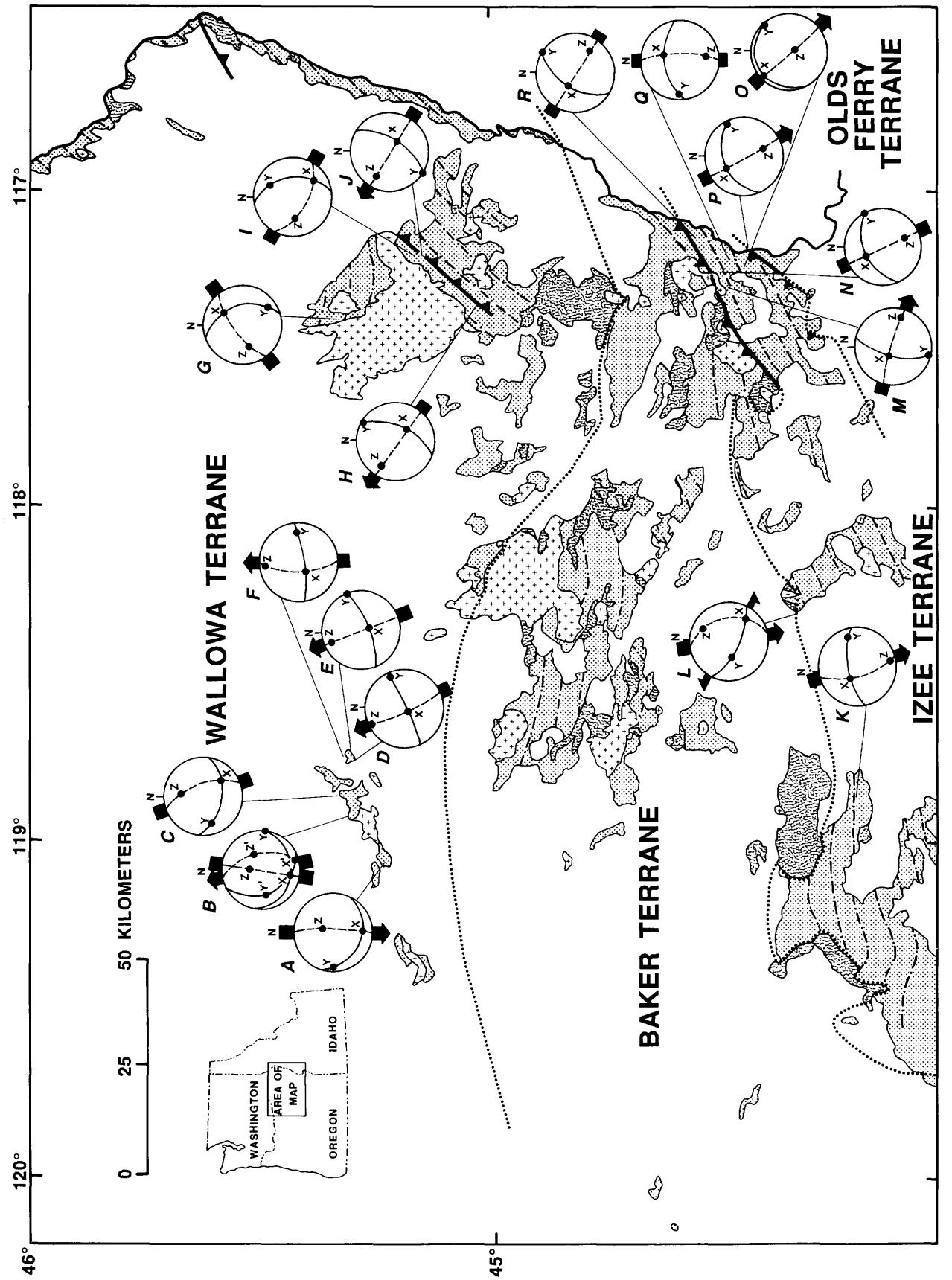

FIGURE 7.9.—Geologic map showing Late Jurassic (deformation D_2) structures in Blue Mountains province. *A–R*, lower-hemisphere, equal-area projections of principal strain axes. X, major principal extensile strain axis; Y, intermediate principal strain axis; Z, major principal compressive strain axis; X', Y', and Z', principal strain axes of rare second penetrative deformation. Solid great circle, X-Y plane or cleavage plane; dashed great circle, X-Z plane or movement plane. Heavy arrow, tectonic-transport direction; double-headed arrow (in *L*), left-lateral strike-slip displacement; heavy bar, strike of X-Z plane. Heavy barbed line, thrust fault (sawteeth on upper plate; dotted where concealed). See figure 7.2 for explanation of other geologic map symbols.

of the principal finite strain axes (see section "Structure, Microscopic Analysis"). On the basis of the deduced strain axes, the plagioclase fabrics appear to have formed by translation glide on (001)[100]. The orientation of the X, Y, and Z strain axes and the sense of shear are plotted on figure 7.9. The mean orientation of the strain axes and sense of tectonic transport as determined by Mirkin (1986) are shown in projection *H* on figure 7.9.

These results are consistent with the mesoscopic structures (*A*, *F*, fig. 7.2). Generally, the X axes are parallel to south- to southeast-plunging mineral lineations (L_2) and fold axes (B_2) (*A* and *F*, fig. 7.3), and the Z axes are perpendicular to the S_2 cleavages. The parallelism of fold axes and X axes indicates large rotations (Escher and Watterson, 1974) and thus very large strains; this is also supported by the class 2 (similar-fold) geometry (Ramsay, 1967) of the folds in the Pendleton inliers. In the southern Wallowa Mountains and in Hells Canyon, where the rocks are hardly recrystallized, fold axes trend northeast-southwest and the folds have a class 1b (parallel) to 1c (weakly converging dip isogons) geometry, indicating much lower strains and no or little strain rotations.

The strike of the X-Z planes (main planes of distortion or so-called movement planes) are accentuated in figure 7.9 with heavy bars, and where the sense of shear could be established (on the basis of microtextures or of the vergence of megascopic folds), the sense of tectonic transport is indicated. It is clear that shearing and thrusting in the Wallowa Mountains were toward the north and northwest during the D_2 deformation. The shortening direction in the northern Wallowas (*G*, fig. 7.9) is northeast-southwest; the sample from which this conclusion was drawn must have been rotated clockwise, as similarly indicated by the mesoscopic and megascopic structures. This rotation may have been produced by either the intrusion of the Wallowa batholith or younger (Tertiary) faulting (Smedes, 1959). One sample from the Pendleton inliers (*A*, fig. 7.9) shows an opposite, southerly vergence, perhaps the result of back thrusting. Another sample (*B*, fig. 7.9) shows two noncoaxial superposed strains, both probably related to the D_2 deformation.

Timing

There are not many constraints on the timing of the D_2 deformation. The youngest rocks in the Wallowa Mountains deformed during D_2 are of late Early Jurassic (Toarcian) age (Nolf, 1966). The oldest intrusives in the Wallowa terrane were dated at about 160 Ma (Armstrong and others, 1977), but, as previously mentioned, more recent work suggests that the main magmatism did not start until about 143 Ma (Walker, 1989). The plutonic rocks are all post-tectonic and cut across the D_2 structures. Thus, a Middle to Late Jurassic age for D_2 is indicated. In the Snake River canyon, Middle to Upper Jurassic (Callovian, Oxfordian) sedimentary rocks have been recognized unconformably overlying Triassic and older rocks (Morrison, 1964; Vallier, 1977; Goldstrand, 1994; White and Vallier, 1994). These Middle and Upper Jurassic rocks are folded (*D*, fig. 7.2; *D*, fig. 7.3). Fold axial planes and cleavages are steep and strike northeast-southwest; fold axes are subhorizontal. It can be argued that the deformation responsible for these folds occurred during the Cretaceous, at the same time as the major deformation in the Riggins, Idaho, area (Sutter and others, 1984), and that the unconformity is related to the post-Toarcian prebatholith deformation. However, no penetrative structures related to a Cretaceous event have been recognized elsewhere in Oregon. Thus it is suggested that the major Jurassic deformation of the Wallowa terrane occurred in the Late Jurassic, between the early Oxfordian and the time of the main batholith formation (~143 Ma).

D_3 deformation

The third penetrative deformation D_3 resulted only in small folds, kink folds, and crenulations (*A*, *B*, *F*, *G*, and *I*, fig. 7.3). It did not involve large amounts of strain. In general, folds have a class 1b (parallel) geometry (Ramsay, 1967). The axial planes are steep and strike northwest-southeast to north-south (*A*, *B*, *F*, *G*, and *I*, fig. 7.2); they are almost perpendicular to the D_2 structures.

The timing of the D_3 deformation is rather straightforward. The D_3 structures deform the older D_2 structures and are crosscut by the Wallowa batholith. Thus they may be a late expression of the same event that caused the D_2 structures. Both the D_2 folds and the D_3 cross folds may be the expression of only one displacement field. If the convergence-rate vector between two terranes is oblique to their mutual boundary, strain partitioning will occur in general: the vector component perpendicular to the boundary causes boundary-parallel thrust faults and related folds, whereas the boundary-parallel component results in boundary-parallel strike-slip faults (Oldow and others, 1990). The D_3 cross folds may be the result of restraining bends in such strike-slip faults.

D_4 deformation

A few post-D_2 deformation subhorizontal kinks with east-west-trending fold axes were identified in

the Pendleton inliers (*A*, fig. 7.3); they have been attributed to a fourth deformation (D_4). Because they have not been found elsewhere, they are considered unimportant and are not further discussed in this chapter.

BAKER TERRANE

D_1 DEFORMATION

The Permian and Triassic rocks of the Baker terrane are thought to represent a fore arc. Locally, the rocks are severely disrupted and chaotic, but in general the terrane consists of large coherent blocks in which the structures, although complex, have a certain regularity. These blocks are separated from each other by chaotic zones and shear zones. All rocks are metamorphosed, but the grade of metamorphism is extremely variable. Most of the rocks have undergone only the lowest greenschist-facies metamorphism, but amphibolites and blueschists do occur. Megascopic D_1 folds have been recognized only in the Elkhorn Ridge area (*M*, fig. 7.2); they were delineated there by mapping asymmetric mesoscopic folds and cleavage-bedding relationships (Coward, 1983).

Mesoscopic Analysis

The metasedimentary rocks are deformed into tight to isoclinal D_1 folds, which have a class 1c (weakly converging dip isogons) to class 2 (similar) geometry (Ramsay, 1967). Several generations of cleavages commonly developed (Coward, 1983) cozonally, their mutual intersections paralleling the fold axes. Apparently cleavage formation was accompanied by strong dissolution. The major trend of the axial-plane foliation and cleavage (S_1) is shown in projections *J* through *O* on figure 7.2. In the eastern part of the terrane the foliation strikes northeast-southwest; in the central and western parts it strikes approximately east-west. Fold axes (B_1) and intersection lineations (L_1) in the Baker terrane are generally steeply plunging and trend northwest-southeast. Mineral lineations in the blueschists (*J*, fig. 7.2; *J*, fig.7.3) and amphibolites (*K*, fig. 7.2; *K*, fig.7.3) also plunge steeply to the southeast. Fragments in sedimentary breccias and pebbles in conglomerates occurring in the Vinegar Hill area are flattened parallel to the foliation and have a slight elongation (parallel to the strain axis X) trending northwest-southeast (*E*, fig. 7.8). In the Elkhorn Ridge area, bedding (S_0) and foliations (S_1) are moderately to steeply dipping to the south, and fold axes (B_1) and intersection lineations (L_1) form a girdle with a south-plunging maximum (*M*, fig. 7.2; *M*, fig. 7.3). It is here that Coward (1983) discovered several generations of cleavages, all cozonal with an east-west-trending subhorizontal axis.

Also in the Elkhorn Ridge area, shear zones were identified in particular where they crosscut marble bodies. The sheared marble is strongly mylonitized and has subhorizontal, east-west-trending mineral lineations.

In the Burnt River canyon area, argillite fragments in a mud breccia are flattened and elongated. The elongations (L_1) have variable orientations: in some places they are subhorizontal and trend east-west, and in other places they plunge steeply to the south or north (*N*, fig. 7.2; *N*, fig. 7.3).

Near the Snake River canyon (*O*, fig. 7.2), chert, argillite, and limestone are exposed with steep north-dipping cleavages (S_1). Intersection lineations (L_1) plunge moderately to the west (*O*, fig. 7.3).

Microscopic Analysis

Microfabric analysis was performed on six samples from the Baker terrane. Microtextures of these and some additional samples were examined in a search for kinematic indicators.

The preferred orientation of quartz c axes and glaucophane optical-indicatrix axes in a blueschist from the Mitchell area (*D*, fig. 7.8) are shown in *D* on figure 7.4. The quartz grains are recrystallized and show poorly developed c axis cross-girdles, which intersect in the foliation plane (S_1) approximately at a right angle to the mesoscopic mineral lineation (L_1). The glaucophane crystals have an α point maximum perpendicular to S_1 and a γ point maximum parallel to L_1. No textural indicators were found to establish the shear direction.

The orientation of amphibole in an amphibolite from the Vinegar Hill area (*F*, fig. 7.8) has fabric patterns (*F*, fig. 7.4) that are nearly identical to those of the glaucophane in the blueschist. According to E.M. Bishop (Mullen, 1978; Bishop, chap. 4, this volume) these amphiboles are also sodic and thus may have formed at relatively high pressures in a subduction complex. Several kinematic indicators were found in thin sections cut parallel to the X-Z plane: rotated porphyroblasts, extension cracks, and displacements across microfaults that parallel cleavage planes (*F*, fig. 7.6).

In a marble mylonite from the Elkhorn Ridge area (*G*, fig. 7.8), the c axes of calcite lie in a girdle (*G*, fig. 7.4) perpendicular to a strong mesoscopic subhorizontal lineation trending east-west. The mylonite has a typical S-C structure indicative of the sense of

displacement: the longest dimensions of large calcite grains (subparallel to the X strain axis) are oriented at a small angle to shear zones containing fine-grained calcite (*G*, fig. 7.6).

Two phyllite samples from the Burnt River canyon yielded surprising results. These phyllites contain quartz augen and very flattened and elongate argillite pebbles that show no significant recrystallization. In one of these samples (*L*, fig. 7.8) the quartz c axes are oriented in two cross-girdles (*L*, fig. 7.4) which intersect in the foliation plane (S_1), at 90° to the lineation (L_1) that is caused by parallelism of the longest axes of the stretched argillite pebbles. Quartz fibers in pressure shadows of magnetite grains and displacements along microfaults yielded consistent shear senses (*L*, fig. 7.6). The other sample (*I*, fig. 7.8) also displays a cross-girdle pattern of quartz c axes, but the intersection of the two girdles is parallel to the lineation L_1. To verify these results, another thin section perpendicular to the first was studied, and it gave the same result (*I*, fig. 7.4).

In a sample of slightly recrystallized metachert collected in the Snake River canyon (*M*, fig. 7.8) the quartz c axes form two cross-girdles, intersecting in the S_1 plane at about 90° from a mesoscopic intersection lineation (*M*, fig. 7.4). One girdle is more strongly populated than the other, giving rise to a monoclinic symmetry which is an indicator of the shear sense.

Two other phyllite samples from the Burnt River canyon (*J*, *K*, fig. 7.8) have consistent kinematic indicators, such as rotated calcite and quartz fibers in veins (*J*, fig. 7.6), and rotated quartz fibers in pressure shadows of magnetite, asymmetric pressure shadows, and rotated porphyroclasts (*K*, fig. 7.6).

Interpretation

The microfabrics of five samples have orthorhombic symmetry, from which the orientation of the principal strains can be identified: in all instances the foliation plane S_1 coincides with the X-Y plane of the finite-strain ellipsoid. In all samples, the major principal extension axis (X) can also be identified. In four samples X is parallel to a pervasive lineation, but in one sample (*I*, fig. 7.4) X is perpendicular to the lineation. The latter situation may be the result of flattening during deposition and diagenesis, followed by tectonic deformation (see Ramsay and Wood, 1973).

The orientations of X, Y, and Z axes in the Baker terrane, as derived from microfabrics and microtextures, are shown in projections *D* through *M* on figure 7.8. These results are consistent with the mesoscopic data presented in projections *J* through *O* on figure 7.3. In all comparable instances the Z axes correspond to the maximum of poles to S_1 cleavage planes and the X axes are parallel to the maximum of B_1 fold axes (for example, compare Z and X in projection *M*, fig. 7.8, with S_1 and B_1, respectively, in projection *O*, fig. 7.3). The style of deformation (class 2, or similar-fold, geometry; Ramsay, 1967) and the parallelism of X axes and B_1 fold axes indicate large strains and large strain rotations (Escher and Watterson, 1974). Left-lateral displacement in the Elkhorn Ridge area (*G*, fig. 7.8) along a steep south-southeast-dipping shear plane is clearly different from the displacements in most other areas of the Baker terrane (*D–F* and *H–M*, fig. 7.8). The sense of shear, derived from the monoclinicity of one quartz fabric (*M*, fig. 7.4) and from several kinematic indicators (*F*, *J*, *K*, *L*, fig. 7.6), shows that most displacements in the Baker terrane are dip-slip motions related to northwest-directed thrusting or southeast-directed underthrusting. (The curved quartz fibers in the pressure shadows of drawings *K* and *L*, figure 7.6, may have formed by a small amount of simple shear followed by a large amount of pure shear; this interpretation is different from that of Etchecopar and Malavieille (1987) but is consistent with other kinematic indicators and the orthorhombic symmetry of the quartz fabrics.)

Timing

It is difficult to constrain the timing of the D_1 deformation over such a large area. It is very well possible that the deformation was diachronous, that it occurred earlier in one area and later in another, within the Baker terrane. The youngest sedimentary rocks deformed by D_1 are of Late Triassic and possibly Early Jurassic age (Blome and others, 1983, 1986). An $^{40}Ar/^{39}Ar$ age of 223 Ma (Hotz and others, 1977) for the blueschists at Mitchell indicates that the D_1 deformation at Mitchell was at least constrained to the Late Triassic. The deformation was certainly pre-Cretaceous in parts of the Baker terrane where the rocks are crosscut by Early Cretaceous granites (Armstrong and others, 1977; Walker, 1989). Although the contact between the Elkhorn Ridge Argillite and the Jurassic sedimentary rocks of the Izee terrane in the Snake River canyon—along the Brownlee Reservoir—is a tectonic contact, it is plausible that the D_2 structures in the Baker terrane (see below) were formed at the same time as the first structures (here also called D_2) in the Lower Jurassic sedimentary rocks of the Weatherby Formation; they are similar in style and orientation. The D_1 structures in the Baker terrane do not occur in the Jurassic sedimentary rocks, and thus the D_1 structures probably formed before the Early Jurassic.

D_2 DEFORMATION

Megascopic D_2 folds in the Baker terrane were recognized only in the Burnt River canyon (fig. 7.1; *N*, fig. 7.2; Ashley, 1966). Large north-dipping reverse faults were recognized along the contact of the Baker and Izee terranes (fig. 7.2 between areas *O* and *U*; Brooks, 1979a). The axial trends of the D_2 folds shown in figure 7.2 are based mainly on the mesoscopic data; these structures (B_2 and S_2) are generally subparallel to the D_1 trends. Although data on mesoscopic structure were collected and are discussed below, microscopic studies were inconclusive and are not reported in this chapter.

Mesoscopic Analysis

D_2 folds generally have a class 1b (parallel) to 1c (weakly converging dip isogons) geometry (Ramsay, 1967). They are often crenulations and kink folds involving little strain. Generally, the axial planes and cleavages dip steeply to the north and northwest (*J–O*, fig. 7.2; *J–O*, fig. 7.3). The orientations of the B_2 fold axes and L_2 lineations are variable but are often subhorizontal, trending roughly east-west.

Interpretation

Although D_2 structures are locally penetrative, no kinematic-indicator data have been gathered because microtextural features are generally reliable only in rocks deformed just once. Nonetheless, the consistent northward dip of the axial planes and cleavages in the rocks of the Baker terrane suggests a south vergence, opposite to the D_2 vergence in the Wallowa terrane but similar to the vergence of D_2 folds in the Izee terrane.

Timing

The timing of the D_2 deformation in the Baker terrane is not well constrained. This deformation postdates the D_1 deformation and certainly predates the intrusion of the granitic plutons, such as the Bald Mountain batholith, into the Elkhorn Ridge Argillite, which has been dated at about 145 Ma (Armstrong and others, 1977; Walker, 1989).

D_3 DEFORMATION

A third set of folds crosscutting the D_1 and D_2 folds is recognized almost everywhere in the Baker terrane. These D_3 folds are of only mesoscopic and microscopic size. Their geometry belongs to class 1b (parallel) to 1c (weakly converging dip isogons; Ramsay, 1967); they are generally crenulations and kink folds. Their axial planes generally are steep and strike north-south. B_3 fold axes and L_3 lineations have variable orientations (*J*, *L–N*, fig. 7.3). The general trends of D_3 structural elements are shown in projections *J* and *L* through *N* on figure 7.2.

The timing of the D_3 folding is post-D_2 deformation and prebatholith intrusion. As discussed above for the Wallowa terrane, the D_3 cross folds may have formed in response to oblique convergence.

IZEE TERRANE

D_1 DEFORMATION

The oldest structures in the Izee terrane that are ascribed to the D_1 deformation occur in the area south and southwest of the town of John Day (*P–S*, fig. 7.2). These structures are found in the oldest sedimentary rocks, which are Late Triassic (Carnian) in age, and seem to die out in rocks of Early Jurassic (Sinemurian) age. Dickinson and Vigrass (1965), Brown and Thayer (1966a, b), and Thayer and Brown (1966) recognized that the deformation was syndepositional; they mapped several north-south-trending megascopic D_1 folds.

Mesoscopic Analysis

In the Aldrich Mountains (*Q*, fig. 7.2) mesoscopic folds are open and generally of class 1b (parallel) to 1c (weakly converging dip isogons) geometry (Ramsay, 1967). Fold axes plunge to the south, and axial planes dip steeply to the east (*Q*, fig. 7.3). Elsewhere, the folds are tight to isoclinal and have class 1c to 2 (similar) geometries. Axial planes and axial-plane cleavages dip steeply eastward in the Izee area (*P*, fig. 7.2; *P*, fig. 7.3); east of Izee, in the John Day area (*S*, fig. 7.2) and the Wickiup area (*R*, fig. 7.2), the cleavages are rotated and dip moderately to the northeast (*R*, *S*, fig. 7.3).

Microscopic Analysis

None of the samples collected were suitable for petrofabric analysis. Microscopic strain analysis was performed on one graywacke sample that contained numerous fragments of chert and volcanic rocks and grains of serpentine, spinel, plagioclase, calcite, and quartz. The aspect ratio of the chert grains is about 1.5:1.0:0.5 for X:Y:Z; the orientation of these axes is shown in projection *O* on figure 7.8.

Interpretation

The asymmetry of mesoscopic folds and the general east to northeast dip of the axial planes and axial-plane cleavages suggest that the folds formed in a regime of west- to southwest-directed thrusting (*P–R*, fig. 7.2; *P–R*, fig. 7.3), although no kinematic indicators were found. The north-south to northwest-southeast trend of the D_1 structures in the Izee terrane is markedly different from the east-west to northeast-southwest trend of D_1 structures in the Baker terrane (*J–O*, fig. 7.2; *J–O*, fig. 7.3). Two factors may have been involved: (1) the ramping effect due to the rigid Canyon Mountain Complex may have caused the deviation, although this complex was itself deformed somewhat during the D_1 event (Avé Lallemant, 1976); (2) the subsequent D_2 deformation may have caused rotation of the D_1 structures.

Timing

The timing of the D_1 deformation in the Izee terrane was relatively well established by Dickinson and Vigrass (1965), Brown and Thayer (1966a, b), and Thayer and Brown (1966). The youngest sedimentary rocks deformed by D_1 are of Early Jurassic (Sinemurian) age; upper Lower Jurassic (Pliensbachian) rocks are not affected. Thayer and Brown (1966) have shown that the deformation began during the Late Triassic, because Upper Triassic rocks are more heavily strained than Lower Jurassic rocks.

D_2 Deformation

The results of the D_2 deformation are recognized in all parts of the Izee terrane. In the John Day area, D_2 structures crosscut D_1 structures; elsewhere, D_2 structures are the first penetrative structures. Megascopic folds have been recognized throughout the terrane (Dickinson and Vigrass, 1965; Brown and Thayer, 1966a, b; Thayer and Brown, 1966; Avé Lallemant, 1983). They trend generally from east-west (in the western part of the terrane) to northeast-southwest (in the eastern and central parts) (fig. 7.2). Jurassic conglomerates have been found in contact with pre-Jurassic rocks in the Mine Ridge area (*T*, fig. 7.2) and Weatherby area (*U*, fig. 7.2). These conglomerates are much more strongly deformed than the older rocks, indicating that the contact is structural. In the Weatherby area, Sinemurian sedimentary rocks overlie younger (Pliensbachian) conglomerates, suggesting a thrust relationship (Brooks and Vallier, 1978). Also in the Weatherby area (near *M*, *N*, *R*, fig. 7.9) the contact between the Baker and Izee terranes is a north-dipping reverse fault (Brooks and others, 1976) intruded by a post-tectonic stock dated at 124 Ma (Walker, 1989).

Mesoscopic Analysis

Small-scale folds in the graywackes have a class 1b (parallel) geometry and in pelitic rocks a class 1c (weakly converging dip isogons) to 2 (similar) geometry (Ramsay, 1967). In the west, fold axes (B_2) and bedding-cleavage intersection lineations (L_2) are subhorizontal and trend east-west (*P–T*, fig. 7.2; *P–T*, fig. 7.3). Near the Snake River canyon in the east, fold axes and lineations form great-circle girdles with a steep point maximum (*U*, fig. 7.2; *U*, fig. 7.3). Axial-plane cleavages (S_2) are well developed locally, in particular near the Snake River (*U*, fig. 7.3); they generally dip steeply to the north. In stretched pebble conglomerates of the Mine Ridge area (*T*, fig. 7.2), the longest pebble axes (subparallel to the strain axis X) plunge at low angles to the east-southeast. The X axes of stretched pebbles in the Weatherby area (*U*, fig. 7.2) plunge to the northwest, parallel to the dip direction of the S_2 cleavage; axial ratios X/Z are locally as large as 10.

Microscopic Analysis

Previously (Avé Lallemant, 1983), four quartz c axis fabrics were obtained from the Jurassic sedimentary sequence near Weatherby. They all display the cross-girdle pattern, and the fabrics have orthorhombic symmetry. Microtextural studies of these rocks yielded kinematic information in one sample only, in which displacements were noted along microfaults parallel to the cleavage (*M*, fig. 7.7). The Jurassic stretched-pebble conglomerates from the Mine Ridge area (*T*, fig. 7.2) and the Weatherby area (*U*, fig. 7.2) have several consistent kinematic indicators such as quartz and calcite fibers in extension veins and in pressure shadows and displacements along microfaults parallel to the cleavage plane (*L*, *P*, fig. 7.7).

Interpretation

The geometries and orientations of the D_2 folds in the Izee terrane (*P–U*, fig. 7.3) can be explained in terms of strain (see section "Structure, Microscopic Analysis"). Principal strain axes were derived from the quartz fabrics (*M*, *N*, *Q*, *R*, fig. 7.9; Avé Lallemant, 1983), and the sense of shear from microtex-

tural kinematic indicators (*L*, *M*, *P*, fig. 7.7). The shear senses in the rocks near Wickiup and Weatherby (*K*, *O*, fig. 7.9) are based on the asymmetry of the folds on all scales. All D_2 data for the Izee terrane are consistent with south- to southeast-directed thrusting during the Late Jurassic.

The kinematic results from the stretched-pebble conglomerate in the Mine Ridge area (*L*, fig. 7.9) can be interpreted in two ways. The first interpretation is that the rocks were thrust to the south and later, during the D_3 deformation, rotated into their present position. Although this interpretation is feasible, D_3 structures were not recognized in the area, and D_3 structures generally show only very minor strain. The second and preferred alternative is that these conglomerates were deformed by left-lateral strike-slip displacement along a west-northwest–east-southeast shear zone (*L*, fig. 7.9).

Timing

In the John Day area, the youngest sedimentary rocks affected by the D_2 deformation are of late Middle Jurassic (Callovian) age, whereas the oldest undeformed sedimentary rocks are of Late Cretaceous (Cenomanian) age (Dickinson and Vigrass, 1965). Small granitic plutons that intruded the Jurassic sedimentary rocks post-tectonically have not been dated but are believed to be of Early Cretaceous age (Thayer and Brown, 1966).

The youngest sedimentary rocks deformed by the D_2 deformation in the Weatherby area are of Middle Jurassic (Bajocian) age (Brooks, 1979a), but across the Snake River in Idaho lower Callovian sedimentary rocks show D_2 deformational effects (Henricksen, 1975). These rocks were intruded post-tectonically by a granitic stock, which has been dated at 124 Ma (U-Pb: Walker, 1989).

D_3 DEFORMATION

In most areas the Late Jurassic (D_2) structures have been refolded. D_3 folds are generally open and of class 1b (parallel) to 1c (weakly converging dip isogons) geometry (Ramsay, 1967). In slate and phyllite this deformation is characterized by crenulations and kink bands. Generally, the axial planes (S_3) are steep and strike north-south, whereas the fold axes (B_3) have variable orientations (*P*, *R*, *S*, *U*, fig. 7.2; *P*, *R*, *S*, *U*, fig. 7.3). The timing of the D_3 deformation is rather unconstrained. It postdates the D_2 event, but an upper age limit has not been established.

OLDS FERRY TERRANE

Although there exists a hiatus between the Upper Triassic volcanic and volcaniclastic rocks of the Huntington Formation of Brooks (1979a) and the Lower Jurassic sedimentary rocks of the Weatherby Formation, and although the lowermost rocks of the Weatherby Formation are sheared and thrust southeastward, no important deformation structures have been recognized in the Huntington Formation. No mesoscopic folds have been found, and no distinct cleavages have been observed. Poles to bedding planes have been plotted in projection *V* on figure 7.3; they form a crude girdle the normal of which plunges moderately to the northeast. On this basis it is assumed that the rocks in the Olds Ferry terrane are folded in major open folds and that this deformation took place during Late Jurassic time, although there exist no constraints on the timing.

TECTONIC MODEL

It should be reemphasized that the hypotheses proposed here are tentative and that the tectonic model is preliminary. Detailed studies should be carried out in many areas to support or reject the overall picture that emerges from the data presented here. Paleomagnetic evidence (Wilson and Cox, 1980; Hillhouse and others, 1982) indicates that the entire Blue Mountains region has to be rotated counterclockwise about 65° to place the structures within the context of regional tectonic models and pre-Cretaceous geography (fig. 7.10). Unless stated otherwise, in the following discussion of the proposed tectonic model, geographic orientations are given in terms of pre-Cretaceous coordinates.

D_1 DEFORMATION

The oldest (D_1) structures in most areas of the Baker terrane formed during the Late Triassic to Early Jurassic, probably in a subduction environment as suggested by the occurrence of 223-Ma blueschists (Hotz and others, 1977). However, a 255-Ma ($^{40}Ar/^{39}Ar$: Avé Lallemant and others, 1980) amphibolite knocker in the melange near the Canyon Mountain ophiolite suggests that the D_1 deformation may have started in the Permian. The Izee terrane was first deformed during Late Triassic to Early Jurassic time. Kinematic evidence, presented above, suggests that the D_1 deformation was caused by eastward subduction underneath the Olds Ferry volcanic-arc terrane (fig. 7.10*A*). Although the deformation appears to

have ceased in the Early Jurassic, subduction continued into Late Jurassic time as indicated by the occurrence of volcanic strata in the Izee terrane, which was interpreted as a fore-arc basin of the Olds Ferry volcanic arc (Dickinson and Vigrass, 1965). Although melange and structures related to Middle Jurassic subduction have not been recognized, they may be deeply buried or may have been removed by strike-slip displacement. A mylonitic shear zone in the Baker terrane, trending approximately north-south in the pre-Cretaceous, was formed by left-lateral slip. Thus, the convergence between an oceanic plate (part of which is preserved in the Baker terrane) and the volcanic arc (Olds Ferry) was most probably left-oblique (fig. 7.10*A*).

The most important components of the Baker terrane are the chert-argillite sequence, Permian limestone of diverse affinities (Tethyan and American), and blueschists. Very similar and coeval assemblages have been found to the south in the Klamath Mountains and the Sierra Nevada (see Schweickert and Cowan, 1975; Burchfiel and Davis, 1981; Mortimer, 1986). Thus, the Olds Ferry arc may be related to the west-facing Triassic to Early Jurassic volcanoplutonic-arc terranes in the Klamaths and Sierra Nevada. To the north, in British Columbia, the Cache Creek assemblage is virtually identical to the Baker terrane (see Monger and others, 1982; Monger and Berg, 1984). The Cache Creek assemblage lies west of the Quesnellia terrane, a volcanic-arc terrane of Triassic and Jurassic age. Thus, the Olds Ferry arc may be correlated also with the Quesnellia terrane. Mortimer (1986) made a similar correlation and, on the basis of geochemical data, suggested that the Quesnellia terrane represents a west-facing arc, which is consistent with the structural data presented herein.

The Wallowa terrane represents a volcanic arc that was active during Permian and Triassic time; volcanic activity ceased during Late Triassic (Norian) time, except for some minor enigmatic tuffs in the Middle and Upper Jurassic (Callovian to Oxfordian) Coon Hollow Formation (Goldstrand, 1994; White and Vallier, 1994). The oldest structures in the Wallowa terrane described herein are the three mylonitic shear zones (Oxbow, Cougar Creek, and Imnaha) along the Snake River. They were active during Mid-

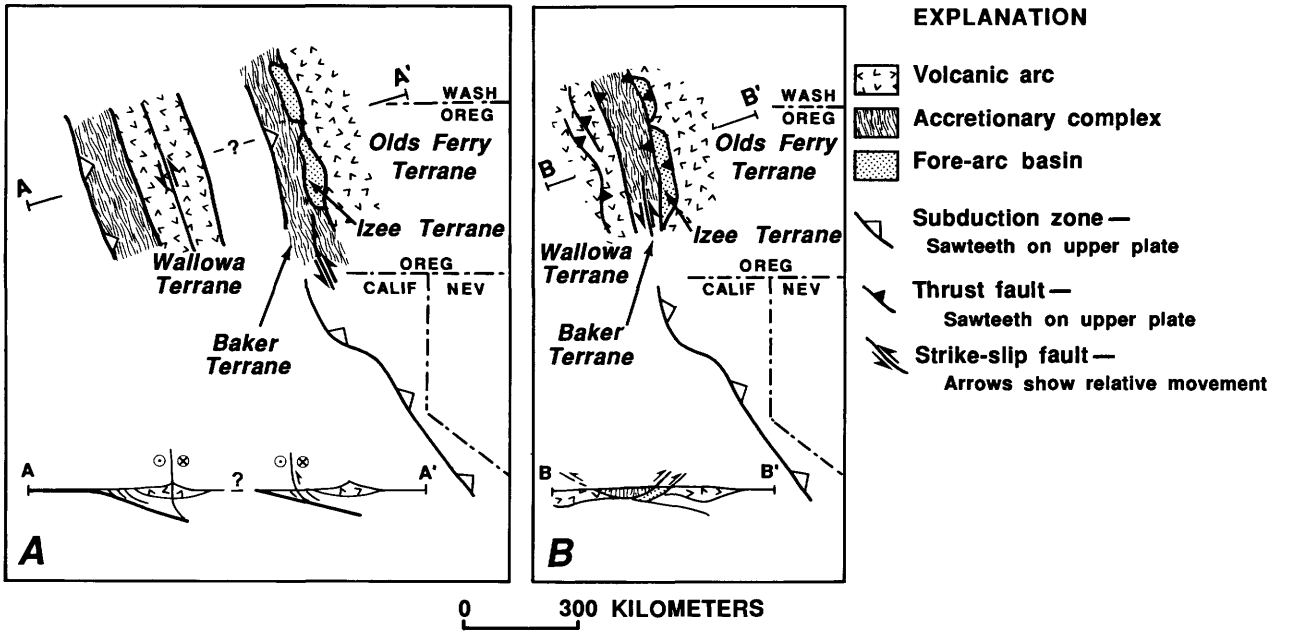

FIGURE 7.10.—Tectonic model of Blue Mountains province. *A*, Late Triassic to Early Jurassic. *B*, Late Jurassic. In *A*, Olds Ferry terrane represents a Late Triassic to Early Jurassic west-facing volcanic island arc. Concurrently, Baker terrane melange and intra- and fore-arc basin sediments of Izee terrane were underthrust eastward. Plate convergence was left-oblique; left-lateral shear zones developed in Baker terrane. Main volcanic activity in Wallowa arc ceased during Late Triassic time, when major left-lateral strike-slip zones developed. Olds Ferry volcanic arc was active until Middle Jurassic time; it may be correlated with Jurassic arc in California (Oldow and others, 1984). Collision of Wallowa terrane and the other three terranes occurred during Late Jurassic (*B*), at same time that collision apparently occurred in Sierra Nevada (Schweickert and Cowan, 1975; Oldow and others, 1984, 1989). This collision is expressed by westward thrusting in Wallowa terrane and eastward thrusting in Baker, Izee, and Olds Ferry terranes. Some left-lateral slip along north-northeast–south-southwest shear zones may have occurred. (All orientations refer to pre-Cretaceous geographic coordinates.)

dle to Late Triassic time. After applying the 65° counterclockwise rotation, their original orientation is found to be approximately north-south. All three mylonite zones were formed by left-lateral strike-slip displacement (fig. 7.10*A*). The minimum amount of displacement along the Oxbow shear zone has been estimated as 65 km by Avé Lallemant and others (1985); the aggregate displacement along all three shear zones may have been hundreds of kilometers. The displacements along the shear zones may have coincided with the end of the volcanic activity in the Wallowa volcanic arc.

The data presented herein are not sufficient to indicate the polarity of the Wallowa arc. All kinematic indicators in the Baker terrane indicate that this melange is related to the west-facing Olds Ferry arc. If the Wallowa arc was east-facing, either its accretionary wedge has not been recognized or it has been buried or completely displaced by strike-slip motion. Without evidence to the contrary, it is proposed here that the Wallowa arc was also west-facing (fig. 7.10*A*).

The Wallowa terrane has been correlated with the Wrangellia terrane (Jones and others, 1977; Newton, 1983; Klepacki and Wernicke, 1985; Wernicke and Klepacki, 1988), but this correlation has been refuted on the basis of the geochemical composition of Triassic volcanic rocks (Sarewitz, 1983; Scheffler, 1983) and of Triassic faunas (Stanley, 1986). Mortimer (1986) correlated the Wallowa terrane with the Stikinia terrane (Monger and others, 1982; Monger and Berg, 1984) in British Columbia. Monger and Berg (1984) suggested that the Cache Creek assemblage is related both to the Quesnellia terrane to the east and the Stikinia terrane to the west. A very different interpretation was favored by Klepacki and Wernicke (1985) and Wernicke and Klepacki (1988). They proposed that the Stikinia, Quesnellia, and Olds Ferry terranes are fragments of one volcanic arc terrane that was disrupted and displaced northward along right-lateral strike-slip faults resulting from the Cretaceous collision of the Wrangellia terrane (including the Wallowa terrane) with North America. Their model, while interesting and thought-provoking, is not compatible with stratigraphic and faunal data (see Oldow and others, 1989).

D_2 DEFORMATION

The D_2 deformation may have resulted from a relatively short-lived event, related to the collision of the Wallowa terrane with the amalgamated Baker-Izee-Olds Ferry terranes (fig. 7.10*A*). The youngest sedimentary rocks deformed during the D_2 event are of Oxfordian age, whereas post-tectonic plutons in all four terranes were emplaced between 143 and 120 Ma (Armstrong and others, 1977; Walker, 1989). Kinematic analysis indicates that during collision rocks in the Wallowa terrane were thrust westward, whereas the orientation of D_2 structures in the Baker and Izee terranes indicate eastward thrusting. In one area mylonites indicate left-lateral displacements along originally northeast-southwest-trending shear zones. This suggests that plate convergence during the Late Jurassic was left-oblique.

The Late Jurassic amalgamation of the Blue Mountains province is approximately coeval with probable collision in the Sierra Nevada (Schweickert and Cowan, 1975) and a back-arc basin collapse in the Klamath Mountains (Harper and Wright, 1984).

D_3 DEFORMATION

A persistent but, in terms of strain, insignificant cross-folding event occurred subsequent to the D_2 deformation. This D_3 event took place also before the emplacement of the Early Cretaceous plutons. Its origin may be related to the strike-slip component of the oblique convergence vector between the Wallowa terrane and the amalgamated Baker-Izee-Olds Ferry terranes.

LEFT-OBLIQUE PLATE CONVERGENCE

Major north-south-striking left-lateral strike-slip zones in the Blue Mountains province were active first during the Middle to Late Triassic and second during the Late Jurassic. This implies that the oceanic plates being subducted beneath the Wallowa and Olds Ferry arcs had a southward component of motion relative to the North American continent during these times. On the basis of paleomagnetic evidence, Stone and others (1982) proposed two migration models for terranes of southeastern Alaska (including the Wrangellia terrane). During the Permian, these terranes resided at high, northerly latitudes (see also Harbert and others, 1988). According to their second model, these terranes moved southward with respect to continental North America until Late Triassic time; they moved northward during the Early and Middle Jurassic, southward during the Late Jurassic and Early Cretaceous, and finally northward again from the mid-Cretaceous onward. The timing of the shearing in the Wallowas is consistent with the first southward motion of the Wrangellia terrane, and the timing of the shearing in the Izee terrane fits the second southward translation proposed by Stone and

others (1982). Left-oblique convergence during the Late Jurassic to Early Cretaceous has also been invoked to explain the structural evolution of terranes elsewhere in the North American Cordillera (Oldow and others, 1984; Avé Lallemant and Oldow, 1988).

Paleomagnetic data from the Blue Mountains province (Hillhouse and others, 1982; Harbert and others, 1988) suggest that in the Late Triassic the province was located farther south with respect to cratonic North America than at present and that it had to have moved northward again since the Late Triassic. This hypothesis is compatible with paleomagnetic data from several Cordilleran terranes which indicate that they were displaced northward since the mid-Cretaceous (see Beck, 1983; Irving and others, 1985; Hagstrum and others, 1985; Umhoefer, 1987). These data, however, were derived from igneous intrusions in which paleohorizontal is not constrained. May and Butler (1986) rightfully pointed out that the paleomagnetic data were also consistent with a systematic tilt of the terranes not necessitating any latitudinal displacements. Recently, however, Irving and Thorkelson (1990) obtained new paleomagnetic data from layered sedimentary and volcanic rocks compatible with large northward displacements. These displacements are also in accord with models of absolute plate motions based on the hot-spot model as developed by Engebretson and others (1985). Furthermore, major northward displacements of the Stikinia and Quesnellia terranes in Late Mesozoic time are required to explain the occurrence at high latitudes of Jurassic tropical fauna (Tipper, 1981; Tozer, 1982; Taylor and others, 1984).

POST-D_3 DEFORMATION

Sutter and others (1984), Lund and Snee (1988), and Snee and others (chap. 15, this volume) identified a major mid-Cretaceous to Late Cretaceous regional metamorphic event in west-central Idaho that may be related to the collision of the amalgamated Blue Mountains province with the North American craton. However, no pervasive structures related to the collision were identified in Oregon.

In eastern Oregon and western Idaho, the contours of initial Sr-isotope ratios typical of continental crust ($^{87}Sr/^{86}Sr \geq 0.706$) and typical of oceanic crust ($^{87}Sr/^{86}Sr \leq 0.704$) are very close together (Armstrong and others, 1977; Fleck and Criss, 1985; Criss and Fleck, 1987). In the same area, the Paleozoic miogeoclinal sequence, which elsewhere in the Cordillera drapes the North American continental margin, is missing. These two pieces of evidence strongly suggest that the contact between the Blue Mountains province and the craton is a strike-slip boundary. Such a boundary may have been the result of escape tectonics (Wernicke, 1984; Klepacki and Wernicke, 1985; Wernicke and Klepacki, 1988) or oblique plate convergence (Avé Lallemant and Oldow, 1988; Oldow and others, 1989). However, no evidence for mid-Cretaceous transcurrent motion along this boundary has been obtained; such structures may have been destroyed by the pervasive dip slip that constitutes the latest movement on this boundary (Strayer and others, 1989), or they may have been buried or eroded.

CONCLUSIONS

The Blue Mountains province of northeastern Oregon consists of five terranes, four of which were discussed in this chapter. These are, from north to south, the Wallowa, Baker, Izee, and Olds Ferry terranes. The pre-Cretaceous tectonic evolution of the terranes (fig. 7.10) is not easy to decipher because so much of the area is covered by Cretaceous and younger rocks and because many more detailed studies are necessary to better constrain the geologic history. Nevertheless, the following tentative conclusions are drawn (note that all geographic directions mentioned refer to pre-Cretaceous coordinates):

(1) The Baker terrane consists of a Permian and Triassic fore-arc terrane/subduction complex related to eastward subduction underneath the west-facing Olds Ferry volcanic island arc; both intra- and fore-arc-basin deposits are included in the Izee terrane (Dickinson, 1979). The Olds Ferry terrane contains only Upper Triassic island-arc deposits, but may have been active from Permian to Middle Jurassic time—if the Permian Canyon Mountain Complex is indeed part of the arc (Avé Lallemant, 1976) and if the Middle Jurassic volcanic rocks in the Izee terrane were derived from the Olds Ferry arc (Dickinson and Thayer, 1978). No melange of Jurassic age and no obvious Middle Jurassic structures related to subduction have been recognized.

(2) The simultaneous formation of north-south-trending folds and left-lateral strike-slip shear zones in the Baker terrane indicates that during the Late Triassic to Middle Jurassic, plate convergence was left-oblique, with the convergence vector partitioned into components perpendicular and parallel to the subduction zone (fig. 7.10*A*).

(3) The Wallowa terrane is a Permian and Triassic volcanic island arc. Magmatic activity virtually ceased in Late Triassic time. The polarity of the arc is unknown, but because the melanges of the Baker

terrane are probably all related to the Olds Ferry arc, it is proposed that the Wallowa arc was also west-facing (fig. 7.10*A*).

(4) North-south-striking left-lateral strike-slip shear zones in the Wallowa terrane, active in the Middle to Late Triassic, indicate left-oblique plate convergence. No coeval compressional structures were recognized however (fig. 7.10*A*).

(5) The Wallowa terrane collided with the Olds Ferry, Baker, and Izee terranes in the Late Jurassic. This collision caused east-directed thrusting and east-vergent folding in the Izee and Baker terranes and west-directed thrusting and west-vergent folding in the Wallowa terrane (fig. 7.10*B*).

(6) The mid-Cretaceous collision of the Blue Mountains province with continental North America caused no penetrative deformation of the rocks in Oregon, but intense deformation took place in Idaho (Sutter and others, 1984; Lund and Snee, 1988; Strayer and others, 1989; Snee and others, chap. 15, this volume).

REFERENCES CITED

Armstrong, R.L., Taubeneck, W.H., and Hales, P.O., 1977, Rb-Sr and K-Ar geochronometry of Mesozoic granitic rocks and their Sr isotope composition, Oregon, Washington, and Idaho: Geological Society of America Bulletin, v. 88, p. 397-411.

Ashley, R.P., 1966, Metamorphic petrology and structure of the Burnt River canyon area, northeastern Oregon: Stanford, Calif., Stanford University, Ph.D. dissertation, 193 p.

Avé Lallemant, H.G., 1976, Structure of the Canyon Mountain (ophiolite) Complex (Oregon) and its implication for sea-floor spreading: Geological Society of America Special Paper 173, 49 p.

———1983, The kinematic insignificance of mineral lineations in a Late Jurassic thrust and fold belt in eastern Oregon: Tectonophysics, v. 100, p. 389-404.

———1984, Speculations on the origin of the ophiolites of northeastern Oregon (U.S.A.): Geologie en Mijnbouw, v. 63, p. 151-158.

Avé Lallemant, H.G., and Oldow, J.S., 1988, Early Mesozoic southward migration of Cordilleran terranes: Tectonics, v. 7, p.1057-1075.

Avé Lallemant, H.G., Phelps, D.W., and Sutter, J.F., 1980, ^{40}Ar-^{39}Ar ages of some pre-Tertiary plutonic and metamorphic rocks of eastern Oregon and their tectonic relationships: Geology, v. 8, p. 371-374.

Avé Lallemant, H.G., Schmidt, W.J., and Kraft, J.L., 1985, Major Late Triassic strike-slip displacement in the Seven Devils terrane, Oregon and Idaho—A result of left-oblique plate convergence?: Tectonophysics, v. 119, p. 299-328.

Balcer, D.E., 1980, $^{40}Ar/^{39}Ar$ ages and REE geochemistry of selected basement terranes, Snake River canyon, Oregon-Idaho: Columbus, Ohio State University, M.S. thesis, 111 p.

Beck, M.E., Jr., 1983, On the mechanism of tectonic transport in zones of oblique subduction: Tectonophysics, v. 93, p. 1-11.

Berthé, D., Choukroune, P., and Jegouzo, P., 1979, Orthogneiss, mylonite, and noncoaxial deformation of granites—The example of the South Armorican shear zone: Journal of Structural Geology, v. 1, p. 31-42.

Blome, C.D., and Nestell, M.K., 1991, Evolution of a Permo-Triassic sedimentary melange, Grindstone terrane, east-central Oregon: Geological Society of America Bulletin, v. 103, p. 1280-1296.

Blome, C.D., Jones, D.L., and Murchey, B.L.,1983, Paleogeographic implications of radiolarian-rich rocks from eastern Oregon [abs.]: Geological Society of America Abstracts with Programs, v. 15, p. 371.

Blome, C.D., Jones, D.L., Murchey, B.L., and Liniecki, Margaret, 1986, Geologic implications of radiolarian-bearing Paleozoic and Mesozoic rocks from the Blue Mountains province, eastern Oregon, *in* Vallier, T.L., and Brooks, H.C., eds., Geology of the Blue Mountains region of Oregon, Idaho, and Washington—Geologic implications of Paleozoic and Mesozoic paleontology and biostratigraphy, Blue Mountains province, Oregon and Idaho: U.S. Geological Survey Professional Paper 1435, p. 79-101.

Bouchez, J.-L., and Pecher, Arnoud, 1981, The Himalayan main central thrust pile and its quartz-rich tectonites in central Nepal: Tectonophysics, v. 78, p. 23-50.

Brooks, H.C., 1979a, Geologic map of the Huntington and part of the Olds Ferry quadrangles, Baker and Malheur Counties, Oregon: Oregon Department of Geology and Mineral Industries Geologic Map Series GMS-13, scale 1:62,500.

———1979b, Plate tectonic and geologic history of the Blue Mountains: Oregon Geology, v. 41, p. 71-80.

Brooks, H.C., McIntyre, J.R., and Walker, G.W., 1976, Geology of the Oregon part of the Baker 1° by 2° quadrangle: Oregon Department of Geology and Mineral Industries Geologic Map Series GMS-7, scale 1:250,000.

Brooks, H.C., and Vallier, T. L., 1978, Mesozoic rocks and tectonic evolution of eastern Oregon and western Idaho, *in* Howell, D.G., and McDougall, K.A., eds., Mesozoic paleogeography of the Western United States (Pacific Coast Paleogeography Symposium 2): Los Angeles, Society of Economic Paleontologists and Mineralogists, Pacific Section, p. 133-145.

Brown, C.E., and Thayer, T.P., 1966a, Geologic map of the Mount Vernon quadrangle, Grant County, Oregon: U.S. Geological Survey, Geologic Quadrangle Map GQ-548, scale 1:62,500.

———1966b, Geologic map of the Canyon City quadrangle, northeastern Oregon: U.S. Geological Survey Miscellaneous Geologic Investigations Map I-447, scale 1:250,000.

Burchfiel, B.C., and Davis, G.A., 1981, Triassic and Jurassic evolution of the Klamath Mountains–Sierra Nevada geologic terrane, *in* Ernst, W.G., ed., The geotectonic development of California (Rubey volume 1): Englewood Cliffs, N.J., Prentice-Hall, p. 50-70.

Chen, S.-J., 1985, Structural geology of the Eureka complex in the Seven Devils terrane, eastern Oregon and western Idaho: Houston, Rice University, M.A. thesis, 94 p.

Coney, P.J., Jones, D.L., and Monger, J.W.H., 1980, Cordilleran suspect terranes: Nature, v. 288, p. 329-333.

Coward, R.I., 1983, Structure, stratigraphy, and petrology of the Elkhorn Ridge Argillite, Sumpter area, northeastern Oregon: Houston, Rice University, Ph.D. dissertation, 144 p.

Criss, R.E., and Fleck, R.J., 1987, Petrogenesis, geochronology, and hydrothermal systems of the northern Idaho batholith and adjacent areas based on $^{18}O/^{16}O$, D/H, $^{87}Sr/^{86}Sr$, K-Ar, and $^{40}Ar/^{39}Ar$ studies, *in* Vallier, T.L., and Brooks, H.C., eds., Geology of the Blue Mountains region of Oregon, Idaho, and Washington—The Idaho batholith and its border zone: U.S. Geological Survey Professional Paper 1436, p. 95-137.

Dickinson, W.R., 1979, Mesozoic fore-arc basin in central Oregon: Geology, v. 7, p. 166-170.

Dickinson, W.R., and Thayer, T.P., 1978, Paleogeographic and paleotectonic implications of Mesozoic stratigraphy and structure in the John Day inlier of central Oregon, *in* Howell, D.G., and McDougall, K.A., eds., Mesozoic paleogeography of the Western United States (Pacific Coast Paleogeography Symposium 2): Los Angeles, Society of Economic Paleontologists and Mineralogists, Pacific Section, p. 147-161.

Dickinson, W.R., and Vigrass, L.W., 1965, Geology of the Suplee-Izee area, Crook, Grant, and Harney Counties, Oregon: Oregon Department of Geology and Mineral Industries Bulletin 58, 109 p.

Dollinger, G.L., and Blacic, J.D., 1975, Deformation mechanisms in experimentally and naturally deformed amphiboles: Earth and Planetary Science Letters, v. 26, p. 409-416.

Engebretson, D.C., Cox, Allan, and Gordon, R.G., 1985, Relative motions between oceanic and continental plates in the Pacific Basin: Geological Society of America Special Paper 206, 59 p.

Escher, A., and Watterson, J., 1974, Stretching fabrics, folds, and crustal shortening: Tectonophysics, v. 22, p. 223-231.

Etchecopar, A., and Malavieille, J., 1987, Computer models of pressure shadows—A method for strain measurement and shear-sense determination: Journal of Structural Geology, v. 9, p. 667-677.

Evans, J.G., 1986, Geologic map of the North Fork John Day River Roadless Area, Grant County, Oregon: U.S. Geological Survey Miscellaneous Field Studies Map MF-1581-C, scale 1:48,000.

Fleck, R.J., and Criss, R.E., 1985, Strontium and oxygen isotopic variations in Mesozoic and Tertiary plutons of central Idaho: Contributions to Mineralogy and Petrology, v. 90, p. 291-308.

Follo, M.R., 1994, Sedimentology and stratigraphy of the Martin Bridge Limestone and Hurwal Formation (Upper Triassic to Lower Jurassic) from the Wallowa terrane, Oregon, *in* Vallier, T.L., and Brooks, H.C., eds., Geology of the Blue Mountains region of Oregon, Idaho, and Washington—Stratigraphy, physiography, and mineral resources of the Blue Mountains region: U.S. Geological Survey Professional Paper 1439, p. 1-27.

Friedman, Melvin, and Higgs, N.G., 1981, Calcite fabrics in experimental shear zones, *in* Carter, N.L., Friedman, Melvin, Logan, J.W., and Stearns, D.W., eds., Mechanical behavior of crustal rocks (Handin volume): American Geophysical Union Geophysical Monograph 24, p. 11-28.

Gerlach, D.C., Avé Lallemant, H.G., and Leeman, W.P., 1981, An island arc origin for the Canyon Mountain ophiolite complex, eastern Oregon, U.S.A.: Earth and Planetary Science Letters, v. 53, p. 255-265.

Gerlach, D.C., Leeman, W.P., and Avé Lallemant, H.G., 1981, Petrology and geochemistry of plagiogranite in the Canyon Mountain ophiolite, Oregon: Contributions to Mineralogy and Petrology, v. 77, p. 82-92.

Gilluly, James, 1937, Geology and mineral resources of the Baker quadrangle, Oregon: U.S. Geological Survey Bulletin 879, 119 p.

Goldstrand, P.H., 1994, The Mesozoic geologic evolution of the northern Wallowa terrane, northeastern Oregon and western Idaho, *in* Vallier, T.L., and Brooks, H.C., eds., Geology of the Blue Mountains region of Oregon, Idaho, and Washington—Stratigraphy, physiography, and mineral resources of the Blue Mountains region: U.S. Geological Survey Professional Paper 1439, p. 29-53.

Green, H.W., Griggs, D.T., and Christie, J.M., 1970, Syntectonic and annealing recrystallization of fine-grained quartz aggregates, *in* Paulitsch, Peter, ed., Experimental and natural rock deformation: New York, Springer, p. 272-335.

Hagstrum, J.T., McWilliams, Michael, Howell, D.G., and Grommé, Sherman, 1985, Mesozoic paleomagnetism and northward translation of the Baja California Peninsula: Geological Society of America Bulletin, v. 96, p. 1077-1090.

Harbert, William, Hillhouse, John, and Vallier, Tracy, 1988, Leonardian paleolatitude of Wrangellia: Eos (American Geophysical Union Transactions), v. 69, p. 1169.

Harper, G.D., and Wright, J.E., 1984, Middle to Late Jurassic tectonic evolution of the Klamath Mountains, California-Oregon: Tectonics, v. 3, p. 759-772.

Henricksen, T.A., 1975, Geology and mineral deposits of the Mineral–Iron Mountain District, Washington County, Idaho, and of a metallized zone in western Idaho and eastern Oregon: Corvallis, Oregon State University, Ph.D. dissertation, 260 p.

Hillhouse, J.W., Grommé, C.S., and Vallier, T.L., 1982, Paleomagnetism and Mesozoic tectonics of the Seven Devils volcanic arc in northeastern Oregon: Journal of Geophysical Research, v. 87, p. 3777-3794.

Himmelberg, G.R., and Loney, R.A., 1980, Petrology of ultramafic and gabbroic rocks of the Canyon Mountain ophiolite, Oregon: American Journal of Science, v. 280-A, pt. 1, p. 232-268.

Hotz, P.E., Lanphere, M.A., and Swanson, D.A., 1977, Triassic blueschist from northern California and north-central Oregon: Geology, v. 5, p. 659-663.

Irving, E., and Thorkelson, D.J., 1990, On determining paleohorizontal and latitudinal shifts—Paleomagnetism of Spences Bridge Group, British Columbia: Journal of Geophysical Research, v. 95, p. 19,213-19,234.

Irving, E., Woodsworth, G.J., Wynne, P.J., and Morrison, A., 1985, Paleomagnetic evidence for displacement from the south of the Coast Plutonic Complex, British Columbia: Canadian Journal of Earth Sciences, v. 22, p. 584-598.

Jones, D.L., Silberling, N.J., and Hillhouse, J.W., 1977, Wrangellia—A displaced continental block in northwestern North America: Canadian Journal of Earth Sciences, v. 14, p. 2565-2577.

Klepacki, D.W., and Wernicke, B.P., 1985, Escape hypothesis for the Stikine block [abs.]: Geological Society of America Abstracts with Programs, v. 17, p. 365.

Lund, Karen, and Snee, L.W., 1988, Metamorphism, structural development, and age of the continent-island arc juncture in west central Idaho, *in* Ernst, W.G., ed., Metamorphism and crustal evolution of the Western United States (Rubey volume 7): Englewood Cliffs, N.J., Prentice-Hall, p. 296-331.

Magill, J.R., and Cox, Allan, 1981, Post-Oligocene tectonic rotation of the Oregon western Cascade Range and the Klamath Mountains: Geology, v. 9, p. 127-131.

May, S.R., and Butler, R.F., 1986, North American Jurassic apparent polar wander—Implications for plate motion, paleogeography, and Cordilleran tectonics: Journal of Geophysical Research, v. 91, p. 11,519-11,544.

Mirkin, A.S., 1986, Structural analysis of the East Eagle Creek area, southern Wallowa Mountains, northeastern Oregon: Houston, Rice University, M.A. thesis, 116 p.

Monger, J.W.H., and Berg, H.C., 1987, Lithotectonic terrane map of Western Canada and southeastern Alaska, *in* Silberling, N.J., and Jones, D.L., eds., Tectonic terrane map of the northern Cordillera: U.S. Geological Survey Miscellaneous Field Studies Map MF-1874B, scale 1:2,500,000.

Monger, J.W.H., Price, R.A., and Tempelman-Kluit, D.J., 1982, Tectonic accretion and the origin of the two major metamorphic and plutonic welts in the Canadian Cordillera: Geology, v. 10, p. 70-75.

Morris, E.M., and Wardlaw, B.P., 1986, Conodont ages for limestones of eastern Oregon and their implication for pre-Tertiary me-

lange terranes, *in* Vallier, T.L., and Brooks, H.C., eds., Geology of the Blue Mountains region of Oregon, Idaho, and Washington—Geologic implications of Paleozoic and Mesozoic paleontology and biostratigraphy, Blue Mountains province, Oregon and Idaho: U.S. Geological Survey Professional Paper 1435, p. 59-63.

Morrison, R.F., 1964, Upper Jurassic mudstone unit named in Snake River canyon, Oregon-Idaho boundary: Northwest Science, v. 28, p. 83-87.

Mortimer, N., 1986, Late Triassic arc-related, potassic igneous rocks in the North American Cordillera: Geology, v. 14, p. 1035-1038.

Mullen, E.D., 1978, Geology of the Greenhorn Mountains, northeastern Oregon: Corvallis, Oregon State University, M.S. thesis, 372 p.

———1983, Petrology and regional setting of peridotite and gabbro of the Canyon Mountain Complex, northeast Oregon: Corvallis, Oregon State University, Ph.D. dissertation, 277 p.

———1985, Petrologic character of Permian and Triassic greenstones from the melange terrane of eastern Oregon and their implications for terrane origin: Geology, v. 13, p. 131-134.

Nestell, M.K., 1983, Permian foraminiferal faunas of central and eastern Oregon [abs.]: Geological Society of America Abstracts with Programs, v. 15, p. 371.

Newton, C.R., 1983, Paleozoogeographic affinities of Norian bivalves from the Wrangellian, Peninsular, and Alexander terranes, western North America, *in* Stevens, C.H., ed., Pre-Jurassic stratigraphy of western North American suspect terranes: Los Angeles, Society of Economic Paleontologists and Mineralogists, Pacific Section, p. 37-68.

———1986, Late Triassic bivalves of the Martin Bridge Limestone, Hells Canyon, Oregon—Taphonomy, paleoecology, paleozoogeography, *in* Vallier, T.L., and Brooks, H.C., eds., Geology of the Blue Mountains region of Oregon, Idaho, and Washington—Geologic implications of Paleozoic and Mesozoic paleontology and biostratigraphy, Blue Mountains province, Oregon and Idaho: U.S. Geological Survey Professional Paper 1435, p. 7-22.

Nielsen, K.C. and Ross, J.V., 1979, Deformation characteristics of calcic amphibole above .7 Tm [abs.]: Eos (American Geophysical Union Transactions), v. 60, p. 370.

Nolf, B.O., 1966, Structure and stratigraphy of part of the northern Wallowa Mountains, Oregon: Princeton, Princeton University, Ph.D. dissertation, 193 p.

Oldow, J.S., Avé Lallemant, H.G., and Schmidt, W.J., 1984, Kinematics of plate convergence deduced from Mesozoic structures in the Western Cordillera: Tectonics, v. 3, p. 201-227.

Oldow, J.S., Bally, A.W., and Avé Lallemant, H.G., 1990, Transpression, orogenic float, and lithospheric balance: Geology, v. 18, p. 991-994.

Oldow, J.S., Bally, A.W., Avé Lallemant, H.G., and Leeman, W.P., 1989, Phanerozoic evolution of the North American Cordillera, United States and Canada, *in* Bally, A.W. and Palmer, A.R., eds., The geology of North America; An overview: Geological Society of America, D.N.A.G., The geology of North America, v. A, p. 139-232.

Passchier, C.W., 1983, The reliability of asymmetric c-axis fabrics of quartz to determine sense of vorticity: Tectonophysics, v. 99, p. T9-T18.

Phelps, D.W., 1979, Petrology, geochemistry, and origin of the Sparta quartz diorite-trondhjemite complex, northeastern Oregon, *in* Barker, Fred, ed., Trondhjemites, dacites, and related rocks: New York, Elsevier, p. 547-580.

Phelps, D.W., and Avé Lallemant, H.G., 1980, The Sparta ophiolite complex, northeast Oregon—A plutonic equivalent to low-K_2O island arc volcanism: American Journal of Science, v. 280-A, pt.1, p. 345-358.

Ramsay, J.G., 1967, Folding and fracturing of rocks: New York, McGraw-Hill, 568 p.

Ramsay, J.G., and Huber, M.I., 1983, The techniques of modern structural geology—V. 1, Strain analysis: New York, Academic Press, 307 p.

Ramsay, J.G., and Wood, D.S., 1973, The geometric effects of volume change during deformation processes: Tectonophysics, v. 13, p. 263-277.

Sarewitz, Daniel, 1983, Seven Devils terrane—Is it really a piece of Wrangellia?: Geology, v. 11, p. 634-637.

Scheffler, J.M., 1983, A petrologic and tectonic comparison of the Hells Canyon area, Oregon-Idaho, and Vancouver Island, British Columbia: Pullman, Washington State University, M.S. thesis, 98 p.

Schweickert, R.A., and Cowan, D.S., 1975, Early Mesozoic tectonic evolution of the western Sierra Nevada, California: Geological Society of America Bulletin, v. 86, p. 1329-1336.

Silberling, N.J., 1983, Stratigraphic comparison of the Wallowa and Huntington terranes, northeast Oregon [abs.]: Geological Society of America Abstracts with Programs, v. 15, p. 372.

Silberling, N.J., Jones, D.L., Blake, M.C., Jr., and Howell, D.G., 1984, Lithotectonic terrane map of the western conterminous United States, Pt. C *of* Silberling, N.J., and Jones, D.L., eds., Lithotectonic terrane maps of the northern Cordillera: U.S. Geological Survey Open-File Report 84-523, 43 p.

Simpson, Carol, and Schmid, S.M., 1983, An evaluation of criteria to deduce the sense of movement in sheared rocks: Geological Society of America Bulletin 94, p. 1281-1288.

Smedes, H.W., 1959, Geology of part of the northern Wallowa Mountains, Oregon: Seattle, University of Washington, Ph.D. dissertation, 273 p.

Spry, Alan, 1969, Metamorphic textures: Oxford, U.K., Pergamon Press, 350 p.

Stanley, G.D., Jr., 1986, Late Triassic coelenterate faunas of western Idaho and northeastern Oregon—Implications for biostratigraphy and paleogeography, *in* Vallier, T.L., and Brooks, H.C., eds., Geology of the Blue Mountains region of Oregon, Idaho, and Washington—Geologic implications of Paleozoic and Mesozoic paleontology and biostratigraphy, Blue Mountains province, Oregon and Idaho: U.S. Geological Survey Professional Paper 1435, p. 23-39.

Strayer, L.M., IV, Hyndman, D.W., Sears, J.W., and Myers, P.E., 1989, Direction and shear sense of the Seven Devils–Wallowa terrane against North America in western Idaho: Geology, v. 17, p. 1025-1028.

Stone, D.B., Panuska, B.C., and Packer, D.R., 1982, Paleolatitudes versus time for southern Alaska: Journal of Geophysical Research, v. 87, p. 3697-3707.

Sutter, J.F., Snee, S.W., and Lund, Karen, 1984, Metamorphic, plutonic, and uplift history of a continent-island arc suture zone, west-central Idaho [abs.]: Geological Society of America Abstracts with Programs, v. 16, p. 670-671.

Sylvester, A.G., and Christie, J.M., 1968, The origin of crossed-girdle orientations of optic axes in deformed quartzites: Journal of Geology, v. 76, p. 571-580.

Taylor, D.G., Callomon, J.H., Smith, R., Tipper, H.W., and Westermann, G.E.G., 1984, Jurassic ammonite biogeograhy of western North America—The tectonic implications, *in* Westermann, G.E.G., ed., Jurassic-Cretaceous biochronology and paleogeography of North America: Geological Association of Canada Special Paper 27, p. 121-142.

Thayer, T.P., 1969, Peridotite-gabbro complexes as keys to petrology of mid-oceanic ridges: Geological Society of America Bulletin, v. 80, p. 1515-1522.

Thayer, T.P., and Brown, C.E., 1966, Geologic map of the Aldrich Mountain quadrangle, Grant County, Oregon: U.S. Geological Survey Geologic Quadrangle Map GQ-438, scale 1:62,500.

Tipper, H.W., 1981, Offset of an upper Pliensbachian geographic zonation in the North American Cordillera by transcurrent movement: Canadian Journal of Earth Sciences, v. 18, p. 1788-1792.

Tozer, E.T., 1982, Marine Triassic faunas of North America—Their significance for assessing plate and terrane movements: Geologische Rundschau, v. 71, p. 1077-1104.

Tullis, Jan, 1977, Preferred orientations of quartz produced by slip during plane strain: Tectonophysics, v. 39, p. 87-102.

Tullis, Jan, Christie, J.M., and Griggs, D.T., 1973, Microstructures and preferred orientation of experimentally deformed quartzites: Geological Society of America Bulletin, v. 84, p. 297-314.

Tullis, T.E., 1976, Experiments on the origin of slaty cleavage and schistosity: Geological Society of America Bulletin, v. 87, p. 745-753.

Umhoefer, P.J., 1987, Northward translation of "Baja British Columbia" along Late Cretaceous to Paleocene margin of western North America: Tectonics, v. 6, p. 377-394.

Vallier, T.L., 1974, A preliminary report on the geology of part of the Snake River canyon, Oregon and Idaho: Oregon Department of Geology and Mineral Industries Geologic Map Series GMS-6, scale 1:125,000.

———1977, The Permian and Triassic Seven Devils Group, western Idaho and northeastern Oregon: U.S. Geological Survey Bulletin 1437, 58 p.

Vallier, T.L., and Batiza, Rodey, 1978, Petrogenesis of spilite and keratophyre from a Permian and Triassic volcanic arc terrane, eastern Oregon and western Idaho, U.S.A.: Canadian Journal of Earth Sciences, v. 15, p. 1356-1369.

Vallier, T.L., Brooks, H.C., and Thayer, T.P., 1977, Paleozoic rocks of eastern Oregon and western Idaho, *in* Stewart, J.H., Stevens, C.H., and Fritsche, A.E., eds., Paleozoic paleogeography of the Western United States (Pacific Coast Paleogeography Symposium 1): Los Angeles, Society of Economic Paleontologists and Mineralogists, Pacific Section, p. 455-466.

Walcott, R.I., 1978, Geodetic strains and large earthquakes in the axial tectonic belt of North Island, New Zealand: Journal of Geophysical Research, v. 83, p. 4419-4429.

Walker, G.W., 1977, Geologic map of Oregon east of the 121st meridian: U.S. Geological Survey Miscellaneous Investigations Series Map I-902, scale 1:500,000.

Walker, N.W., 1981, U/Pb geochronology of ophiolitic and volcanic-plutonic arc terranes, northeastern Oregon and westernmost central Idaho [abs.]: Eos (American Geophysical Union Transactions), v. 62, no. 45, p. 1087.

———1982, Pre-Tertiary plutonic rocks in the Snake River canyon, Oregon/Idaho—Intrusive roots of a Permo-Triassic arc complex [abs.]: Geological Society of America Abstracts with Programs, v. 14, p. 242-243.

———1986, U/Pb geochronologic and petrologic studies in the Blue Mountains terrane, northeastern Oregon and westernmost central Idaho—Implications for pre-Tertiary tectonic evolution: Santa Barbara, University of California, Ph.D. dissertation, 224 p.

———1989, Early Cretaceous initiation of post-tectonic plutonism and the age of the Connor Creek fault, northeastern Oregon [abs.]: Geological Society of America Abstracts with Programs, v. 21, p. A-155.

Walker, N.W., and Mattinson, J.M., 1980, The Canyon Mountain Complex, Oregon: U/Pb ages of zircons and possible tectonic correlations [abs.]: Geological Society of America Abstracts with Programs, v. 12, p. 549.

Wernicke, B.P., 1984, A working hypothesis for Jurassic and Cretaceous terrane accretion in the Pacific Northwest [abs.]: Eos (American Geophysical Union Transactions), v. 65, p. 1095.

Wernicke, B.P., and Klepacki, D.W., 1988, Escape hypothesis for the Stikine block: Geology, v. 16, p. 461-464.

Wetherell, C.E., 1960, Geology of part of the southeastern Wallowa Mountains, northeastern Oregon: Corvallis, Oregon State College, M.A. thesis, 209 p.

White, D.L., and Vallier, T.L., 1994, Geologic evolution of the Pittsburg Landing area, Snake River canyon, Oregon and Idaho, *in* Vallier, T.L., and Brooks, H.C., eds., Geology of the Blue Mountains region of Oregon, Idaho, and Washington—Stratigraphy, physiography, and mineral resources of the Blue Mountains region: U.S. Geological Survey Professional Paper 1439, p. 55-73.

Wilson, Douglas, and Cox, Allan, 1980, Paleomagnetic evidence for tectonic rotation of Jurassic plutons in Blue Mountains, eastern Oregon: Journal of Geophysical Research, v. 85, p. 3681-3689.

8. PRE-TERTIARY DEFORMATION IN THE DESOLATION BUTTE QUADRANGLE, NORTHEASTERN OREGON

By JAMES G. EVANS

CONTENTS

	Page
Abstract	305
Introduction	306
Acknowledgments	306
Descriptions of the rock units	306
Elkhorn Ridge Argillite	306
Pyroclastic and volcanic rock assemblage	309
Early Triassic diorite	310
Brecciated argillite and chert unit	311
Peridotite and associated rocks assemblage	311
Andesite	313
Late Jurassic diorite	313
Quartz monzonite	313
Tertiary and Quaternary rocks and deposits	313
Genetic relations between the Elkhorn Ridge Argillite, the pyroclastic and volcanic rock assemblage, and the Early Triassic diorite	313
Metamorphism	314
Structure	317
Macroscopic structure	317
Mesoscopic structure	317
Methods	317
Elkhorn Ridge Argillite	317
Pyroclastic and volcanic rock assemblage	319
Relations among structures in the Elkhorn Ridge Argillite and the pyroclastic and volcanic rock assemblage	320
Peridotite and associated rocks assemblage	320
Relations among fabric elements in the Elkhorn Ridge Argillite and the peridotite and associated rocks assemblage	321
Deformations	323
Comparison of fabric in the Elkhorn Ridge Argillite, Desolation Butte quadrangle, with fabric in other areas	324
Discussion	326
Conclusions	328
References cited	329

ABSTRACT

Pre-Jurassic rocks of the Desolation Butte quadrangle in northeastern Oregon comprise four main assemblages: the Elkhorn Ridge Argillite (Devonian to Triassic?), a pyroclastic and volcanic rock assemblage (Lower Triassic), a brecciated argillite and chert unit (Upper Jurassic), and a peridotite and associated rocks assemblage (Late Triassic to Middle? Jurassic). The Elkhorn Ridge is most likely a tectonostratigraphic assemblage of sedimentary rocks, which, in the study area, is Paleozoic and Triassic(?) in age. The pyroclastic and volcanic rock assemblage may be partly contemporaneous with the Elkhorn Ridge Argillite or may even have been deposited on it as a developing andesitic arc. The brecciated argillite and chert may be largely equivalent to the Elkhorn Ridge Argillite but could contain additional sedimentary rocks emplaced by faulting during Late Jurassic time. The peridotite and associated rocks assemblage may represent a dismembered ophiolite-like assemblage that includes peridotite as well as gabbro, hornblende diorite, and metasedimentary and metavolcanic rocks.

Metamorphism of the Elkhorn Ridge Argillite and the pyroclastic and volcanic rock assemblage includes contact metamorphism adjacent to Triassic diorite intrusions and regional greenschist-facies metamorphism, which also affected the diorite. The peridotite and associated rocks assemblage underwent complex metamorphism in an ocean floor environment. Broad contact-metamorphic aureoles occur in all these rocks surrounding Late Jurassic diorite plutons. Narrow contact-metamorphic aureoles occur adjacent to Jurassic or Cretaceous quartz monzonite intrusions.

Deformations recorded in the rocks include pre-Mesozoic development of broken formation in the Elkhorn Ridge Argillite, Triassic imbrication of the Elkhorn Ridge Argillite, pyroclastic and volcanic rock assemblage, and Triassic diorite, and three later episodes of folding and cleavage development. The Late Triassic to Middle(?) Jurassic folding is the most widespread deformation. Folds formed during this event are subhorizontal and trend east-west. Axial planes of the folds are parallel to a generally steep cleavage. This folding event may account for the principal deformations in the Elkhorn Ridge near Baker City and in the Burnt River Schist, a possible partial lithic correlative of the Elkhorn Ridge, and may be related to the Early Triassic to Middle(?) Jurassic accretion of the Baker terrane of the Blue Mountains. Emplacement of the peridotite and associated rocks assemblage in an extensional tear in the Elkhorn Ridge may have occurred during this event. Poles of cleavages in the Elkhorn Ridge and the strike of the tear may indicate the direction of principal shortening—approximately east-west in pre-Cretaceous time. Later deformation of the peridotite and associated rocks assemblage moderately affected the Elkhorn Ridge nearby and could be related to Late Jurassic diorite emplacement that resulted in compression at right angles to the zone of peridotite and associated rocks and in widespread metamorphism that locally obliterated minor structures in the ultramafic matrix of the unit. Most deformation in the Baker terrane ceased after the Late Jurassic.

Subsequent tectonism involved rotations of large blocks that may have included the Blue Mountains.

INTRODUCTION

The Desolation Butte 15-minute quadrangle, located 55 km west of the town of Baker City, Oreg. (fig. 8.1), includes part of the melange terrane of the north-central Blue Mountains (Baker terrane of Silberling and others, 1984). This part of the Blue Mountains consists of pieces of oceanic and island arc crust and overlying sedimentary and volcanic rocks that have been greatly deformed before and during the Mesozoic, when the terrane was accreted to western North America (Brooks and others, 1976; Vallier and others, 1977; Brooks and Vallier, 1978; Dickinson and Thayer, 1978; Brooks, 1979). Stratigraphic and (or) tectonic relations between pieces of the oceanic crust and volcanic and sedimentary rock assemblages in the Blue Mountains are yet to be resolved. Stratigraphic relations between some geologic units may never be clarified because of the destruction of the evidence, presumably during subduction and pre-accretionary tectonic transport. The varied rocks in the Desolation Butte quadrangle, however, provide some clues to the geologic history of this belt of fragmented rocks.

The purpose of this chapter is to illustrate, using two geological vignettes, some of the details of the pre-Tertiary structure encountered in the Desolation Butte quadrangle (Evans, 1989) and to infer relations between the rock units. Some fabric features are revealed, although the data obtained during geologic mapping of the area are insufficient to characterize all aspects of the complex deformation these rocks have undergone.

The pre-Tertiary rocks of the Desolation Butte quadrangle, which are the chief geologic interest of this chapter, comprise four main assemblages that have had complex strain and thermal histories. Deformed and metamorphosed dioritic rocks, undeformed and metamorphosed andesite porphyry, and unaltered and unstrained diorite and granitic rocks intrude these assemblages (fig. 8.2). The main assemblages consist of the Paleozoic and Triassic(?) Elkhorn Ridge Argillite (ŘPze) that is predominantly argillite and chert, a Lower Triassic pyroclastic and volcanic rock assemblage (Řp), an Upper Jurassic brecciated argillite and chert (Jb), and a peridotite and associated rocks assemblage, including gabbro (JŘg), hornblende metadiorite (JŘm), and metamorphosed sedimentary and volcanic rocks (JŘs). Some of the components of the peridotite and associated rocks assemblage (fig. 8.2) may be as old as Paleozoic and as young as Triassic. However, in its present melange form, the unit is herein regarded as Late Triassic to Middle(?) Jurassic in age. Original relations between the Elkhorn Ridge, the pyroclastic and volcanic rock assemblage, and the peridotite and associated rocks assemblage are not known because they are in fault contact with one another (fig. 8.2). Several intrusions occur in the study area: metamorphosed and brecciated diorite (Řd) of Early Triassic age intruding the Elkhorn Ridge and the pyroclastic and volcanic rock assemblage; metamorphosed but undeformed andesite (Ja) of Jurassic age intruding the Elkhorn Ridge and the Triassic diorite; fresh Late Jurassic diorite (Jd); and fresh Jurassic or Cretaceous quartz monzonite (KJqm) (figs. 8.2, 8.3, 8.4).

ACKNOWLEDGMENTS

I wish to acknowledge the ideas, comments, and suggestions contributed during the course of this study by H.C. Brooks and M.L. Ferns of the Oregon Department of Geology and Mineral Industries and by T.L. Vallier of the U.S. Geological Survey. Brooks and Ferns visited me in the field, showed me some of the relevant geology that they had mapped in adjoining areas, and in general shared with me their expertise in the geology of northeastern Oregon. Brooks, Ferns, and Vallier suggested many improvements to the manuscript.

DESCRIPTIONS OF THE ROCK UNITS

ELKHORN RIDGE ARGILLITE

Large parts of the Desolation Butte quadrangle (fig. 8.2) and of the area shown in figure 8.3 are underlain by the black to gray argillite and chert of the Elkhorn Ridge Argillite. This formation was named by Gilluly (1937, p. 14) for exposures on Elkhorn Ridge near Sumpter, 25 km east of the Desolation Butte area. The formation contains minor amounts of other rock types: metabasalt (flows in southern part of the adjacent Trout Meadows 7.5-minute quadrangle), metatuff, limestone, and conglomerate. The conglomerate contains angular to well-rounded clasts of chert, siliceous siltstone, quartzite, argillite, granitoid rocks, and felsic volcanic rocks. Rare pods of talc-carbonate rock in the formation may be metamorphosed dolomite or could be altered ultramafic rocks that were emplaced within the argillite by faulting.

It is not clear whether the Elkhorn Ridge Argillite in the study area originally consisted of a section several thousand meters thick or whether the unit is composed of several unrelated sections assembled by accretionary processes. An unfaulted stratigraphic section is not preserved in the quadrangle, nor has the base of the formation been identified anywhere. Much of the Elkhorn Ridge has been pervasively deformed so that it is a broken formation (Hsü, 1968).

Avé Lallemant and others (1980) concluded that the Elkhorn Ridge Argillite was deposited in a volcanic-arc–back-arc-basin environment, which is at least superficially a reasonable conclusion considering the volcanic clasts in parts of the Elkhorn Ridge and the possibly large original thickness of the unit. Mullen (1985), however, concluded that a fore-arc setting is most consistent with the chemistry and petrography of the mafic metavolcanic rocks from the Baker terrane. The origin of the Elkhorn Ridge in a fore-arc setting would also be consistent with its complex internal stratigraphy. Bostwick and Nestell (1967) point out that Tethyan and American fusulinid faunas occur in separate pods of limestone in the Elkhorn Ridge. Dickinson (1979, p. 166) has interpreted these apparent faunal juxtapositions to imply tectonic juxtapositions of strata that were deposited far apart in the ancestral Pacific Ocean.

East of the Desolation Butte quadrangle, the Elkhorn Ridge Argillite has yielded Pennsylvanian and Permian fusulinids and Early to Middle Triassic pentacrinids, hydrozoans, and hexacorals (Brooks and others, 1976; Evans, 1986, table 1; Evans, 1989). A conodont fragment from a 1-m-thick limestone bed within the quadrangle (locality J299, fig. 8.3) was identified as *Polygnathus* sp., making parts of the Elkhorn Ridge in this area as old as Middle to Late Devonian in age (Morris and Wardlaw, 1986). Although regionally the Elkhorn Ridge has a Paleozoic and Triassic overall age, in the Desolation Butte quadrangle and vicinity it may be no younger than Permian. The large age range of the Elkhorn Ridge (Middle Devonian to Late Triassic, or about 150 m.y.) and its chaotic stratigraphy are consistent with the concept that the Elkhorn Ridge may have been assembled from unrelated but similar sedimentary rocks during several plate collisions, a model that Brooks (1979, p. 74) proposed for the entire oceanic-crust terrane of northeastern Oregon.

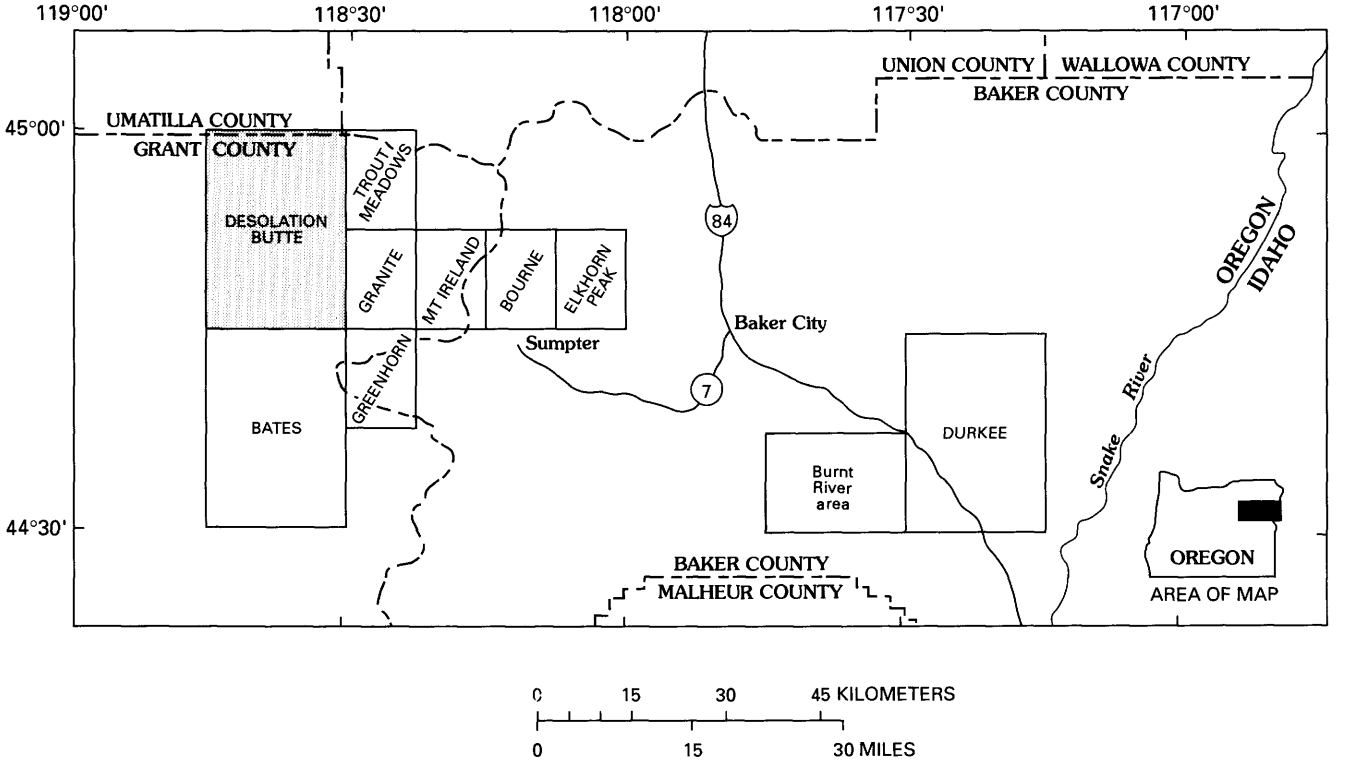

FIGURE 8.1.—Index map of northeastern Oregon, showing location of Desolation Butte (shaded) and other quadrangles mentioned in text.

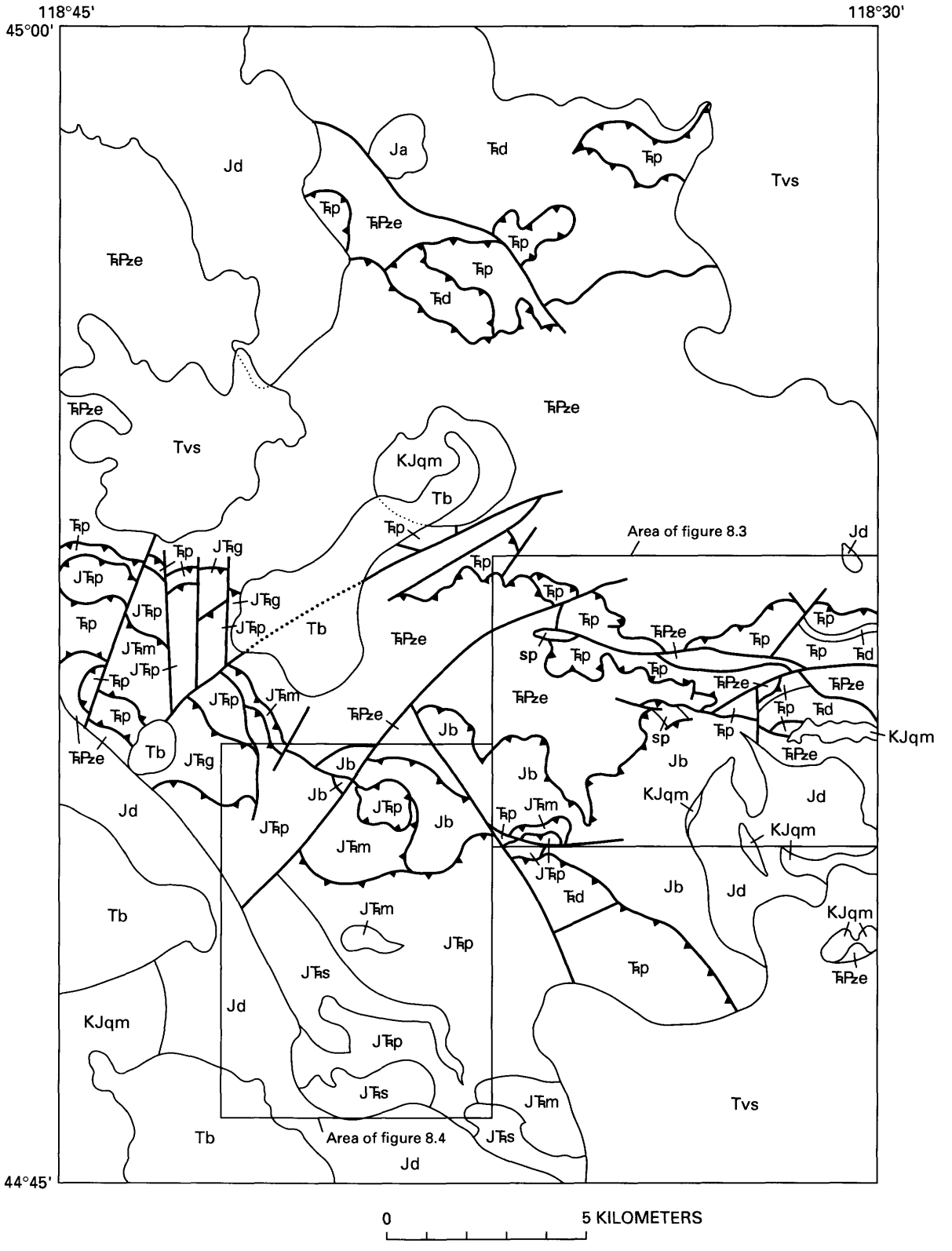

FIGURE 8.2.—Geologic sketch map of Desolation Butte quadrangle. Quaternary units not shown in this figure. Geology modified from Evans (1989).

PYROCLASTIC AND VOLCANIC ROCK ASSEMBLAGE

The pyroclastic and volcanic rock assemblage consists chiefly of tuff, some of which is clearly water-laid, lapillistone (containing fragments of andesite, tuff, and chert), and andesite flows and flow breccia. The andesite appears to have been extruded in a submarine environment because of its proximity to water-laid tuffs, but no pillows are preserved. The assemblage also includes minor siltstone, limestone, conglomerate (clasts of chert, siltstone, and tuff), and argillite. In places limestone is interbedded with tuff. The mostly angular fragments in pyroclastic and sedimentary rocks include andesite, tuff, siltstone, and chert. Estimated minimum thickness of this unit, taken from the south limb of the fold shown in cross section *B–B'* (fig. 8.5) is 850 m.

No fossils were found in the pyroclastic and volcanic rock assemblage. The unit is intruded by a diorite body dated as earliest Triassic (see section "Early Triassic Diorite"). The andesitic volcanic rocks of the pyroclastic and volcanic rock assemblage may be considered contemporaneous with the Early Triassic diorite if the diorite was the magmatic source of the

EXPLANATION FOR FIGURES 8.2 THROUGH 8.5

- Qag — Alluvium and glacial deposits (Quaternary)
- Qls — Landslide deposits (Quaternary)
- QTm — Mudflow deposits and colluvium (Quaternary and Tertiary)
- Tvs — Volcanic and sedimentary rocks (Tertiary)
- Tb — Basalt (Tertiary)
- Ta — Andesite (Tertiary)
- KJqm — Quartz monzonite (Cretaceous or Jurassic)
- Jd — Diorite (Late Jurassic)
- Jb — Brecciated argillite and chert unit (Late Jurassic)—Locally includes serpentinite (sp)
- Ja — Andesite (Jurassic)

Peridotite and associated rocks assemblage (Middle? Jurassic to Late Triassic)—Divided into:

- JTrp — Peridotite
- JTrg — Gabbro
- JTrm — Hornblende metadiorite
- JTrs — Metamorphosed sedimentary and volcanic rocks
- Trp — Pyroclastic and volcanic rock assemblage (Early Triassic)
- Trd — Diorite (Early Triassic)
- TrPze — Elkhorn Ridge Argillite (Triassic? and Paleozoic)

Contact—Dotted where concealed

Faults—Dotted where concealed. Arrows in cross sections (fig. 8.5) show displacement

Steeply dipping

Thrust—Sawteeth on upper plate

Strike and dip of beds

70 Inclined

Vertical

80 Strike and dip of foliation

Strike and dip of joints

85 Inclined

Vertical

45 Bearing and plunge of lineation

Locality J299

FIGURE 8.2.—Continued.

volcanic rocks. In this chapter the pyroclastic and volcanic rock assemblage is tentatively assigned an Early Triassic age.

The pyroclastic and volcanic rock assemblage may be a facies of the volcanic assemblage that includes the Dixie Butte Meta-andesite of Brooks and others (1984) located 15 km south of the quadrangle. The pyroclastic and volcanic rock assemblage differs from the Dixie Butte rocks in that it contains predominantly pyroclastic rocks and subordinate andesite flows. Nevertheless, the pyroclastic and volcanic rock assemblage could be a distal facies of a volcanic center located closer to or underlying the meta-andesite.

EARLY TRIASSIC DIORITE

Early Triassic dioritic rocks intrude the Elkhorn Ridge Argillite and the pyroclastic and volcanic rock assemblage; these dioritic rocks are metamorphosed to greenschist facies and brecciated. Preserved primary textures and minerals indicate that original compositions included diorite, quartz diorite, hornblende diorite, granodiorite, and quartz monzonite, but most samples are diorite. More than one episode of intrusion may have been involved, as suggested by quartz monzonite dikes cutting the diorite.

A metamorphosed and brecciated diorite in the northwest corner of the adjacent Granite 7.5-minute quadrangle (fig. 8.1) was dated as earliest Triassic (243 Ma, N.W. Walker, in Brooks and others, 1982; Palmer, 1983). This intrusion is continuous with a diorite that is shown in figure 8.2 and near the northeast corner of figure 8.3. Because of general lithologic and textural similarities, all of the metamorphosed and brecciated dioritic plutons are tentatively assigned an Early Triassic age. Such an age for this pluton would be consistent with the Devonian age for part of the Elkhorn

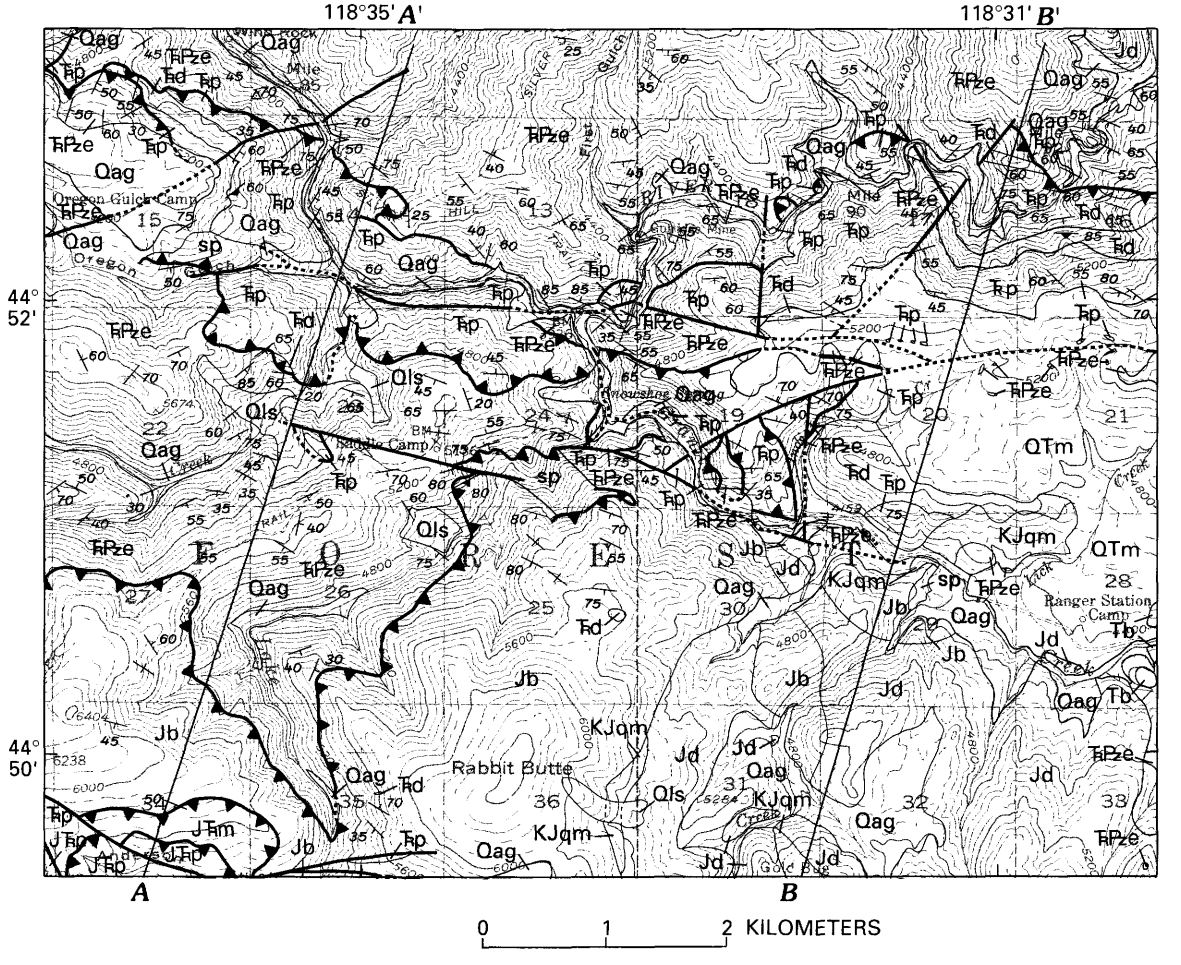

FIGURE 8.3.—Geologic map of Rabbit Butte area. See figure 8.2 for location and explanation. Base from U.S. Geological Survey 1:62,500-scale Desolation Butte quadrangle, 1950. Contour interval 80 ft. Geology from Evans (1989). See figure 8.5 for cross sections.

Ridge Argillite in the study area and with other radiometric ages in the region (Walker, 1983).

BRECCIATED ARGILLITE AND CHERT UNIT

A zone of brecciated argillite and chert as much as a few hundred meters thick is tectonically interlayered between part of the Elkhorn Ridge Argillite and the pyroclastic and volcanic rock assemblage. The breccia contains blocks of relatively undeformed chert, in which bedding is well preserved, surrounded by intensely fractured argillite and chert, in which no mesoscopic sedimentary structures are preserved due to recrystallization and later brecciation. Most of these rocks are superficially like the argillite and chert of the Elkhorn Ridge and may well have been derived from it. It is possible that the brecciated argillite and chert unit was originally part of a slope basin and that the strata were subsequently thrust over the Elkhorn Ridge rocks. Such an origin may account for some of the rock types that are found in the brecciated argillite and chert unit but are absent in the Elkhorn Ridge—such as a thin-bedded limestone lens, having outcrop dimensions of approximately 15 by 60 m, on the north slope of Rabbit Butte, and, near the mouth of Lake Creek, conglomerate containing rounded granitoid clasts (as much as 30 cm across) and sandstone. The brecciated argillite and chert unit includes serpentinite intrusions (protrusions?) (fig. 8.3, 8.4), which are common in some fore-arc environments (Bloomer, 1983; Taylor and Smoot, 1984; Fryer and others, 1985) and could have been emplaced in slope basin deposits. The brecciated argillite and chert unit also contains pods of Triassic(?) diorite. Part of the brecciated argillite and chert unit is white, suggesting bleaching of organic matter that is ordinarily abundant in the Elkhorn Ridge. Hematite and quartz veins are locally abundant in the brecciated argillite and chert unit.

The brecciated argillite and chert unit must be at least as old as Early Triassic because it contains blocks of Early Triassic diorite. A minimum age of Jurassic can be inferred from the occurrences of undeformed Jurassic andesite (see section "Andesite") in the area. This possible age range of Early Triassic to Jurassic brackets the Middle Triassic age of melange in the John Day area of central Oregon, 135 km southwest of the Desolation Butte quadrangle (Dickinson and Thayer, 1978, p. 150; Dickinson, 1979, p. 166). The brecciated argillite and chert unit, however, is tentatively assigned a Late Jurassic age because the brecciation appears to have been caused by Jurassic thrusting (see section "Structure").

PERIDOTITE AND ASSOCIATED ROCKS ASSEMBLAGE

The assemblage consisting of peridotite and associated rocks is thrust over the Elkhorn Ridge Argillite and the brecciated argillite and chert unit, and it is truncated on the southwest and south by Jurassic intrusions (figs. 8.2 and 8.4). The peridotite of this assemblage has a complex history of cataclasis, serpentinization, alteration to talc, and recrystallization of serpentine to olivine. Xenoliths in the peridotite include gabbro, hornblende diorite, and metamorphosed igneous and sedimentary rocks. The gabbro of this unit, recognized by relict textures and minerals, is mostly altered to amphibolite. The associated hornblende diorite, which may have intruded the peridotite and the metasedimentary rocks, has been recrystallized to amphibolite and, in places, is mylonitized. Some of the diorite of this unit is compositionally and texturally like the Early Triassic diorite; most of it, however, has undergone amphibolite-grade metamorphism and mylonitization in contrast to the greenschist-facies metamorphism and brecciation of the Early Triassic diorite (see section "Early Triassic Diorite"). The metasedimentary rocks of this unit consist of argillite, chert, and conglomerate containing angular to rounded clasts of chert, siltstone, quartz, sandstone, and felsic volcanic rocks. These clasts could have come from a terrane like the one that supplied clasts to the Elkhorn Ridge, suggesting the possibility that these metasedimentary rocks are related to the Elkhorn Ridge. Quartzite clasts containing recrystallized quartz grains that are sharply truncated by clast boundaries indicate that the recrystallization occurred in the source terrane. Some of the metasedimentary rocks recrystallized under nearly lithostatic conditions, as indicated by the lack of metamorphic fabric, during greenschist- to amphibolite-grade metamorphism. Some of the metasedimentary rocks have well-developed cleavage. In some pods of metasedimentary rocks that are as much as 0.5 km^2, strain intensity ranges from slightly warped bedding to isoclinally folded rocks in which bedding is transposed parallel to cleavage. Metaigneous rocks of this unit consist of amphibolite, derived from gabbro and hornblende diorite, and probable metavolcanic rocks (inferred from a few relict primary textures, high calcic plagioclase and amphibole contents, and low quartz and mica contents). A small amount of fault breccia along the contact between the peridotite and associated rocks assemblage and the brecciated

argillite and chert unit appears to be a tectonic mix of hornblende diorite and intensely brecciated chert and argillite. The clustering of small pods of metamorphosed igneous and sedimentary rocks in the peridotite suggests either that the pods are xenoliths in a peridotite intrusion (magmatic interpretation), or that they are pieces of a metamorphic, sedimentary, and igneous terrane dismembered during emplacement of a very ductile serpentinite mass (protrusion?).

One model for the peridotite and associated rocks assemblage would be a protrusion along a tear fault in an obducted plate, similar to the tectonic situation described for the Batinah melange in Oman (Robertson and Woodcock, 1983), with later structural complications (see section "Structure"). This geometry would explain why the peridotite and associated rocks assemblage is not regionally extensive. No evidence of sedimentary peridotite was found in the Desolation Butte

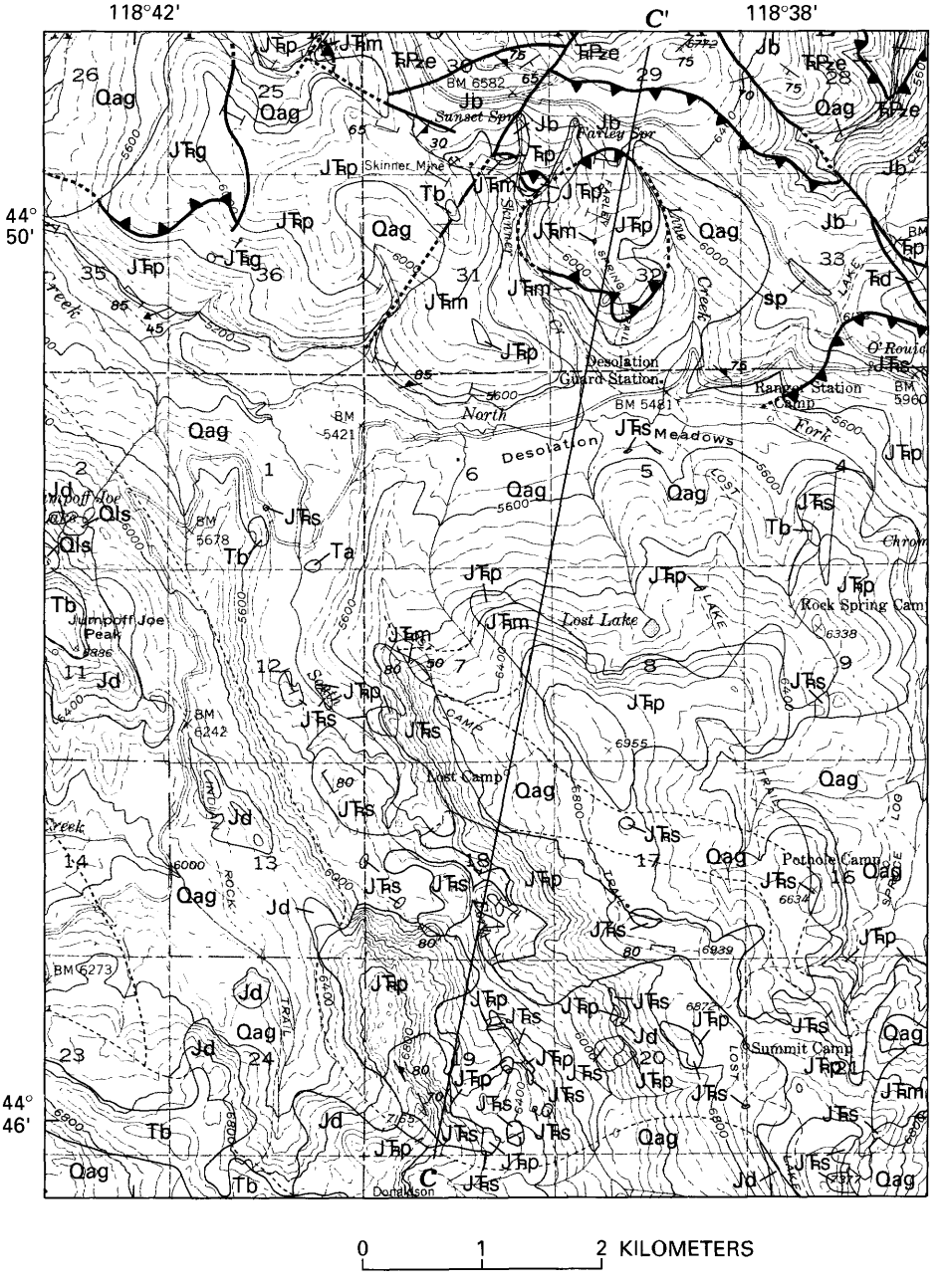

FIGURE 8.4.—Geologic map of Lost Camp area. See figure 8.2 for location and explanation. Base from U.S. Geological Survey 1:62,500-scale Desolation Butte quadrangle, 1950. Contour interval 80 ft. Geology from Evans (1989). See figure 8.5 for cross section.

quadrangle to indicate that the protrusion might have reached the sea floor, but serpentine matrix melange in the Bates quadrangle (fig. 8.1) is overlain by conglomerate containing clasts from the melange (Brooks and others, 1983). According to this model, the peridotite and associated rocks assemblage could represent basement upon which the Elkhorn Ridge Argillite was deposited or assembled, and some of the metasedimentary rocks in the peridotite and associated rocks assemblage could be fragments of the Elkhorn Ridge engulfed by the rising serpentinite protrusion.

Age of the components of the peridotite and associated rocks assemblage could be older than Devonian if the unit represents an ophiolite upon which the Elkhorn Ridge Argillite was deposited. In the dismembered-ophiolite model, the peridotite and associated rocks assemblage is presumably Late Triassic to Middle(?) Jurassic in age, on the basis of the estimated time of emplacement of the ophiolite (see section "Structure"). The emplacement age (Late Triassic to Middle? Jurassic) of the peridotite and associated rocks assemblage is the age used for this unit in this chapter.

ANDESITE

Andesite intruded the Early Triassic diorite and the Elkhorn Ridge Argillite (fig. 8.2) and was subsequently metamorphosed. The andesite in the northern part of the Desolation Butte quadrangle contains less than 5 percent metamorphic amphiboles, which are tentatively identified as actinolite and richterite. Richterite replaces actinolite locally, but calcic plagioclase has not undergone intensive alteration to epidote. Crystallization of richterite could be due to sodium metasomatism (from seawater?) or due to redistribution of sodium in the rocks during recrystallization. An andesite dike in SE1/4 sec. 13, north of North Fork John Day River, has been much altered to white mica and contains less than 1 percent brown biotite. The unstrained appearance of these intrusions suggests that they are younger than the deformations associated with the tectonic emplacement of the Triassic host rocks. The andesite, however, must have been emplaced before the unaltered Jurassic or Cretaceous plutons (see sections "Late Jurassic Diorite" and "Quartz Monzonite"). The andesite is here tentatively given a Jurassic age.

LATE JURASSIC DIORITE

Fresh or slightly altered, undeformed, mostly dioritic rocks—quartz diorite, tonalite, gabbro (Streckeisen, 1976)—compose several plutons within the Desolation Butte quadrangle (figs. 8.2–8.5). These plutons may be related to the Bald Mountain batholith exposed to the east of the quadrangle. That batholith was dated at 144±17 Ma (by the whole-rock Rb/Sr isochron method) by Armstrong and others (1977, p. 400). Although this age spans the range from Late Jurassic to Early Cretaceous (161 to 127 Ma), they postulated that the batholith was emplaced in the Late Jurassic but remained hot or was reheated during the Early Cretaceous. For this reason the diorite intrusions are here assigned a Late Jurassic emplacement age (161 Ma).

QUARTZ MONZONITE

Generally fresh quartz monzonite plutons and granite (Streckeisen, 1976) dikes intrude the Late Jurassic diorite and the Elkhorn Ridge Argillite (figs. 8.1, 8.2). Zones of greisen as much as 15 m wide occur in some of the intrusions. The spatial association of most of the quartz monzonite bodies with the Late Jurassic diorite suggests that there may be a genetic relation between the two types of intrusions. The quartz monzonite bodies may be a later product of differentiation of the magma from which the diorite plutons were derived. The age of the quartz monzonite intrusions is presumably Jurassic or Cretaceous, but a Tertiary age cannot be ruled out. In this chapter, the quartz monzonite intrusions are assigned a Jurassic or Cretaceous age.

TERTIARY AND QUATERNARY ROCKS AND DEPOSITS

Tertiary volcanic and sedimentary rocks (units Ta, Tb, and Tvs) and Tertiary and Quaternary colluvium, mudflow and landslide deposits, glacial moraine, fanglomerate, and alluvium (units QTm, Qls, and Qag) are shown on the geologic maps and cross sections (figs. 8.2–8.5) but will not be discussed here.

GENETIC RELATIONS BETWEEN THE ELKHORN RIDGE ARGILLITE, THE PYROCLASTIC AND VOLCANIC ROCK ASSEMBLAGE, AND THE EARLY TRIASSIC DIORITE

Several lines of evidence suggest but do not prove that the Elkhorn Ridge Argillite and the pyroclastic and volcanic rock assemblage were deposited at sites that may not have been very far apart: (1) The units

are imbricated; (2) Early Triassic diorite intruded both units, possibly before the imbrication (see northern part of fig. 8.2); and (3) clasts in tuff and conglomerate of the pyroclastic and volcanic rock assemblage include chert that could have been derived from the Elkhorn Ridge. The similarity in composition between the Early Triassic diorite intrusions and the andesitic volcanic rocks in the pyroclastic and volcanic rock assemblage suggests that the intrusions represent the magmatic feeders for the andesitic rocks, making at least part of the pyroclastic and volcanic rock assemblage roughly the same age as the diorite. In this case the pyroclastic and volcanic rock assemblage would appear to be younger than the Elkhorn Ridge in the study area and could have been deposited on it.

METAMORPHISM

The rocks in the Desolation Butte quadrangle record several metamorphic events, which are listed in table 8.1. Some of these events may have occurred before the Elkhorn Ridge Argillite, the pyroclastic and volcanic rock assemblage, and the peridotite and associated rocks assemblage were juxtaposed by faulting, and many of the events may have occurred before these three units were accreted to the North American continent.

The earliest metamorphic event (M1, table 8.1) for which there is evidence in the quadrangle is the recrystallization of quartzite in the Paleozoic(?) terrane that supplied clasts to the Elkhorn Ridge Argillite and possibly to the metasedimentary rocks in the peridotite and associated rocks assemblage.

The metamorphic history of the peridotite and associated rocks assemblage was already complex before the assemblage came into contact with the block composed of the Elkhorn Ridge Argillite and the pyroclastic and volcanic rock assemblage. Early contact metamorphism, (M2, table 8.1) probably to hornblende hornfels facies, affected sedimentary and volcanic rocks intruded by hornblende diorite. Evidence of this metamorphism consists of xenoliths of conglomerate (J$\overline{\text{Tr}}$s) in the diorite, and dikes of the diorite in metasedimentary rocks (J$\overline{\text{Tr}}$s) that have hornfels texture. Contact relations between the hornblende diorite and the peridotite are ambiguous. It is not clear from this evidence whether the peridotite underwent contact metamorphism from intrusion of the hornblende diorite or from another source, or whether the hornblende diorite was later engulfed by a peridotitic magma or engulfed tectonically by a serpentinized peridotite protrusion.

Gabbro and hornblende diorite in the peridotite and associated rocks assemblage have complex textural relations that could be the result of a single multistage event (M3, table 8.1) in which conditions of metamorphism—temperature, pressure, and P_{H_2O}—varied. The diorite in the southern part of the peridotite and associated rocks assemblage (fig. 8.4) is less deformed than are the diorite and gabbro close to the contact between the peridotite and associated rocks assemblage and the composite block of the Elkhorn Ridge Argillite and the pyroclastic and volcanic rock assemblage; the relatively undeformed diorite shows abundant primary igneous textures. This diorite and the amphibolites that developed from it show equilibrium relations between calcic plagioclase and actinolite and between actinolite and hornblende, and show alteration of primary ilmenite to sphene. In places, the plagioclase was altered to epidote and the hornblende to chlorite. Subsequently, hornblende crystallized from chlorite, and calcic plagioclase veins cut across the epidote. Annealing textures are developed in amphibolites that formed from the gabbro and diorite; recrystallized amphibole grains obscure a preexisting foliation. The annealing recrystallization could be due to contact metamorphism. The source of the heat could be the Late Jurassic diorite, although no firm conclusions regarding the heat source can be drawn. Late hydrothermal activity, indicated by quartz-chlorite veins in the gabbro and diorite, suggests that the Late Jurassic diorite was the heat source for the veins. However, the veins are restricted to the pods in the peridotite and thus are likely to be older than Jurassic.

A model of the kind of complex metamorphism described for the gabbro and diorite has been proposed for oceanic lithosphere at spreading centers (Bonatti and others, 1975; Elthon and Stern, 1978; Elthon, 1981), in which contact and dynamic metamorphic processes and hydrothermal alteration operate. The metamorphosed gabbro and diorite may fit into the facies scheme proposed by Elthon and Stern (1978, p. 464) and Elthon (1981, p. 286). According to their scheme, the highest metamorphic grade attained by the gabbro and diorite in the study area was the lower actinolite facies. This facies assignment is suggested by the widespread presence of calcic plagioclase in equilibrium with actinolite and by the alteration of primary ilmenite to sphene. The lower actinolite facies is approximately equivalent in temperature range (525–600°C) to the lower part of the almandine amphibolite facies of regional metamorphism and the lower hornblende hornfels facies of contact metamorphism (Turner and Verhoogen, 1960, p. 550, 552) but probably was achieved under lower

TABLE 8.1.—*Metamorphic and tectonic events in the Desolation Butte quadrangle*

[M1–M7 and D1–D7, metamorphic and tectonic events, respectively, the numbers indicating chronological order from earliest to latest event; B_1–B_4, folding events, the subscript numbers indicating relatively decreasing concentrations of fold axes]

Metamorphic event		Age	Tectonic event	
Symbol	Description		Symbol	Description
M7--------	Contact metamorphism (due to quartz monzonite intrusion) of Elkhorn Ridge Argillite and pyroclastic and volcanic rock assemblage.	Jurassic or Cretaceous.	D7 -------	Rotation, translation, and uplift of large blocks that include Blue Mountains.
M6--------	Contact metamorphism (due to diorite intrusion) of Elkhorn Ridge Argillite, pyroclastic and volcanic rock assemblage, and possibly also the peridotite and associated rocks assemblage and andesite.	Late Jurassic (161 Ma).	D6 -------	Steep faulting and minor thrusting. Thrusting of the peridotite and associated rocks assemblage over composite block of Elkhorn Ridge Argillite and pyroclastic and volcanic rock assemblage. Development of brecciated argillite and chert unit. Formation of cleavages and folds in the peridotite and associated rocks assemblage, and B_2- and B_3-type folding in Elkhorn Ridge Argillite.
M5--------	Greenschist-facies metamorphism of Elkhorn Ridge Argillite, pyroclastic and volcanic rock assemblage, and diorite.	Late Triassic to Middle(?) Jurassic.	D5 -------	B_4 folding (minor), cleavage in Elkhorn Ridge Argillite, rotation of B_1-group folds, emplacement of the peridotite and associated rocks assemblage in extensional tear.
		Early Triassic to Middle(?) Triassic.	D4 -------	B_1 folding (minor).
			D3 -------	Imbrication of Elkhorn Ridge Argillite, pyroclastic and volcanic rock assemblage, and diorite. Pervasive brecciation.
M4--------	Contact metamorphism (due to diorite intrusion).	Early Triassic.		
M3--------	Actinolite-facies metamorphism within protolith of the peridotite and associated rocks assemblage.	Devonian to Triassic ---	D2 -------	Development of broken formation in Elkhorn Ridge Argillite.
M2--------	Contact metamorphism (due to hornblende diorite intrusion) within protolith of the peridotite and associated rocks assemblage.			
M1--------	Recrystallization within source terrane of Elkhorn Ridge Argillite and metasedimentary rocks of the peridotite and associated rocks assemblage.	Pre-Devonian or Devonian.	D1 -------	Uplift and other tectonism affecting source terrane of Elkhorn Ridge Argillite and metasedimentary rocks of the peridotite and associated rocks assemblage.

pressures than would be typical for regional metamorphism (Bonatti and others, 1975, p. 67). Elthon (1981, p. 288) characterized the actinolite facies as generally undeformed, while amphibolites from oceanic fracture zones have complex strain histories. However, Bonatti and others (1975, p. 74) pointed out that dynamic metamorphism is likely during seafloor spreading and that evidence of recrystallization under directed stress was observed in metagabbros from the mid-Atlantic Ridge. Most likely the actinolite-facies metamorphism (M3, table 8.1) occurred before emplacement of the peridotite and associated rocks assemblage that is in contact with the composite block of the Elkhorn Ridge Argillite and pyroclastic and volcanic rock assemblage, and it could have occurred in the Paleozoic.

Early Triassic dioritic intrusions into this composite block were probably accompanied by contact metamorphism (M4, table 8.1); if present, the effects of such contact metamorphism would not be easily distinguished from later greenschist-facies metamorphism (M5, table 8.1) if the high-temperature parts of the aureoles had been faulted away. Greenschist-facies metamorphism (M5, table 8.1) affected the Elkhorn Ridge Argillite, the pyroclastic and volcanic rock assemblage, and the Early Triassic diorite in the Triassic, assuming that the peridotite and associated rocks assemblage and the composite block of the Elkhorn Ridge Argillite and pyroclastic and volcanic rock assemblage were already juxtaposed by the Middle Triassic. If pre-Triassic regional metamorphism occurred, it has not been distinguished from the later metamorphic events.

The peridotite component of the peridotite and associated rocks assemblage underwent a complex history of metamorphism. Stages in the development of the peridotite include recrystallization of intensely strained dunite, serpentinization, alteration to talc-carbonate rock, and recrystallization of talc and serpentine to olivine. Some of these stages may correlate with the Devonian(?) contact metamorphism and the Devonian to Triassic regional metamorphism (M2 and M3, table 8.1). Other stages may postdate these metamorphic episodes (see below, this section), and still others may have been obliterated altogether.

Recrystallization of the peridotite obliterated most evidence of the processes of emplacement. The extreme fragmentation of the metasedimentary and metavolcanic rocks in the peridotite and associated rocks assemblage, however, suggests that the peridotite engulfed these rocks either as a peridotitic magma or as a cooler ductile serpentinite possibly during diapiric emplacement in the Late Triassic to Middle(?) Jurassic. Evidence for hot emplacement of peridotite should include high-temperature metamorphic rinds on the inclusions in the peridotite. Pyroxene hornfels-facies mineral assemblages would likely characterize the rinds because the peridotite magma would have a temperature in excess of 1,000°C (Wyllie, 1971) whereas the lower temperature limit of the pyroxene hornfels facies is less than 700°C (Turner and Verhoogen, 1960, p. 520). The abundance of hornblende and muscovite throughout the metasedimentary and metavolcanic rocks that are surrounded by peridotite strongly suggests that the peridotite was not emplaced at high temperature. High-grade metamorphic rinds could conceivably have been tectonically eroded off the inclusions during postemplacement deformations. However no vestige of any high-temperature metamorphic rind was found during this study. Superficially, at least, the evidence suggests that the peridotite was emplaced as a cooler plastic serpentinite mass.

Broad contact-metamorphic aureoles as much as 1,200 m wide developed in the Elkhorn Ridge Argillite and the pyroclastic and volcanic rock assemblage in response to the Late Jurassic diorite intrusions (M6, table 8.1). The rocks in the aureoles in the northwestern and southeastern parts of the quadrangle attained hornblende hornfels-facies metamorphic grade. Intrusion of the Late Jurassic diorite also may have been responsible for some of the jackstraw-textured olivine in contact-metamorphosed peridotite of the peridotite and associated rocks assemblage. Greenschist- to amphibolite-grade metamorphism, some of it at least a thermal equivalent of the actinolite-facies metamorphism (M3, table 8.1) already discussed, accompanied development of cleavage in metasedimentary and metaigneous rocks of this assemblage (D6, table 8.1). The same metamorphic event (M6, table 8.1) may also have affected andesite in the north-central part of the quadrangle.

Contact-metamorphic aureoles up to 200 m wide occur in the composite block of the Elkhorn Ridge Argillite and the pyroclastic and volcanic rock assemblage around intrusions of Jurassic or Cretaceous quartz monzonite (M7, table 8.1). The rocks attain hornblende hornfels facies very close to the contacts with these intrusions. The outer parts of the aureoles have low-grade mineral assemblages indistinguishable from the low-grade regional-metamorphic assemblages in the host rocks but exhibit partial obliteration of sedimentary textures and bedding by recrystallization. No contact-metamorphic effects of the quartz monzonite intrusion on the Late Jurassic diorite were found.

STRUCTURE

MACROSCOPIC STRUCTURE

The cross sections (fig. 8.5) illustrate the imbricate structure of the pre-Jurassic rocks in the Desolation Butte quadrangle. Arrows on southwest-dipping faults are shown to indicate presumed relative northward displacement of the hanging walls. Folds in cross sections *A–A'* and *B–B'* were drawn assuming concentric to subconcentric form and no overturning of beds (Busk, 1929). The folds are not directly mappable because of the absence of marker beds in the Elkhorn Ridge Argillite and the pyroclastic and volcanic rock assemblage but are consistent in having their axial planes vertical or steeply dipping to the south and their subhorizontal axes trending generally west-southwest. The simplicity of the fold profiles is consistent with the absence of evidence of intricate folding on the mesoscopic scale and the uniform attitudes of bedding. The attitudes of the axial planes are consistent with assumed northward dip-slip of the upper plates of the thrusts. These relations, although resting on several assumptions, suggest that the latest movements on the thrusts between the Elkhorn Ridge Argillite and the pyroclastic and volcanic rock assemblage were synchronized with or postdated the major folding events.

The structure within the peridotite and associated rocks assemblage, shown in cross section *C–C'* (fig. 8.5), is highly conjectural. The outcrops of the metasedimentary and metavolcanic rocks in the assemblage suggest the outline of an isoclinal fold (fig. 8.5) having a subhorizontal northwest-trending axis. Continuity of the folded rocks is interrupted by peridotite. The principal fold is drawn as an antiform; to the south a less clearly defined synform is drawn, its hinge zone shown dismembered by peridotite. Exact orientation of the axis of the isoclinal fold is not clear, but it may be plunging at a low angle to the northwest. Evidence for this fold geometry is very weak; this interpretation is presented as a possible example of the kind of structural complexity one might expect within the assemblage. An alternative interpretation suggests a similar style with local large noncylindroidal folds of lenses of metamorphic rocks that are disrupted by peridotite.

MESOSCOPIC STRUCTURE

METHODS

The orientations of bedding, cleavage, fold axes, crenulations, and axes of elongate chert nodules were collected during geologic mapping in the Desolation Butte quadrangle. Although the data, especially from the peridotite and associated rocks assemblage, is scanty, it is enough to outline part of the strain history of the rocks within the quadrangle and to describe their mesoscopic fabric in a general way.

The structural data were plotted as points on the lower hemispheres of equal-area projections. Some structural data ($n \geq 25$) were contoured on equal-area lower-hemisphere projections by a method originally described by Kamb (1959) whereby a variable counting area is used. The counting area is a function of the number of data points and the frequency of significant deviations from a uniform spatial distribution. Stereograms are contoured in intervals of 2σ and 4σ, where 2σ is the expected number of data points within a counting area for a uniform distribution across the entire stereogram. A point density greater than 3σ is considered to be a significant deviation from a random distribution, while pole-free areas indicate a possibly significant absence of data points.

ELKHORN RIDGE ARGILLITE

In much of the Elkhorn Ridge Argillite, relatively well developed shear zones with a nearly penetrative shearing foliation subparallel to discontinuous bedding in broken formation surround blocks as much as 100 m long of little-sheared chert and argillite in which bedding is well preserved. Many of the unsheared blocks are elongate parallel to the shear foliation in the broken formation. In many places this shear foliation is difficult to distinguish from the bedding. Little quantitative information was gathered about this shearing deformation, but it may have caused most of the strain in the Elkhorn Ridge Argillite.

Bedding in the Elkhorn Ridge Argillite has a mean strike of N. 70° W. and dip of 52° SW. (n=303; fig. 8.6*A*). Fracture cleavage is developed locally; in places it obliterates bedding. Cleavage has an average strike of N. 75° E. and dip of 63° SE (n=56; fig. 8.6*B*). Poles to cleavage are spread along a great circle, the pole of which defines a ß-axis plunging 62°, S. 50° E.

Nearly all mesoscopic folds have a concentric form, amplitudes as much as 60 cm, and wavelengths as much as 1 m; few, seen only in float, are tight, nearly isoclinal folds. In most outcrops the folds are not penetrative.

Axes of folds and bedding crenulations plunge in many directions, mostly in the southeast quadrant (fig. 8.6*C*). The folds cluster into four populations based on relative density of fold axes; in table 8.1

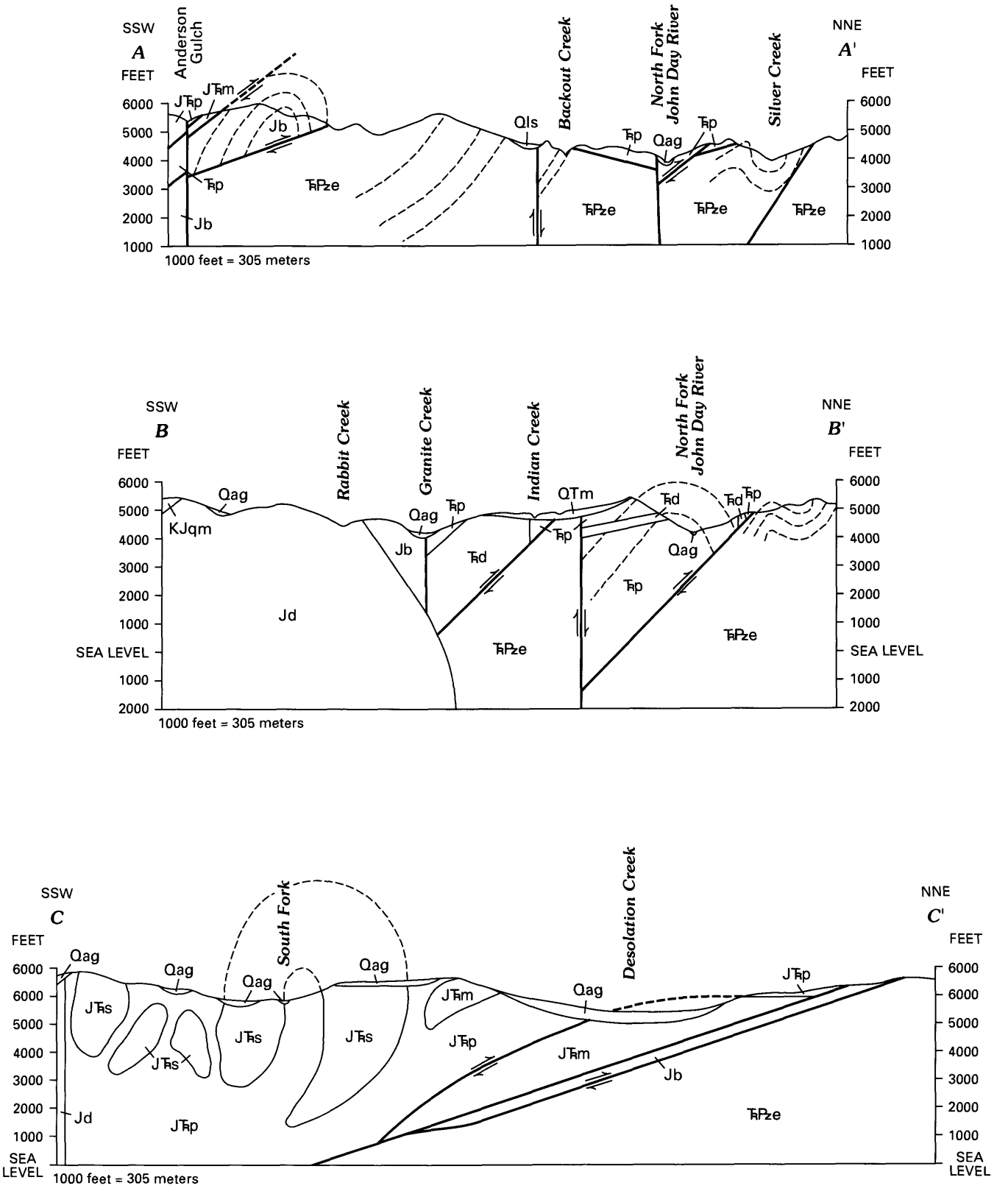

FIGURE 8.5.—Cross sections. Locations of *A–A'* and *B–B'* shown in figure 8.3; location of *C–C'* shown in figure 8.4. See figure 8.2 for explanation.

and in figures 8.6 and 8.11, these groups are represented by "B_1," "B_2," "B_3," and "B_4," ordered by decreasing concentrations of fold axes. The center of the group with the largest concentration of axes (B_1) plunges 44°, S. 22° E. These folds appear to lie along a great circle, the pole of which defines a rotation axis, R, that plunges 47°, N. 10° W., 17° from the mean of poles to cleavage. No fold axes parallel to R were measured. Also, the ß-axis of cleavage (fig. 8.6*B*) is 26° from B_1 and is on a part of the contour diagram for which concentrations of fold axes and crenulations are low (fig. 8.6*C*). Consequently, it seems unlikely that cleavage fanning was directly related to B_1-group folding. These relations suggest that the folds of the B_1 group were rotated during deformation that occurred at the same time as or later than the cleavage development, and it is possible that the rotation involved differential slip along cleavage planes.

The three other fold groups (represented by B_2, B_3, and B_4 in fig. 8.6*C*) do not appear rotated and, for that reason, are considered to be younger than B_1. Macroscopic fold axes trend northwest, subparallel to B_2.

Three of the four localities containing elongate chert nodules have nodule axes subparallel to minor B_1-group folds. At the fourth locality the nodule axes plunge steeply, closely parallel to the trend of B_3-group fold axes.

PYROCLASTIC AND VOLCANIC ROCK ASSEMBLAGE

Bedding in the pyroclastic and volcanic rock assemblage has a mean strike of N. 85° W. and a mean dip

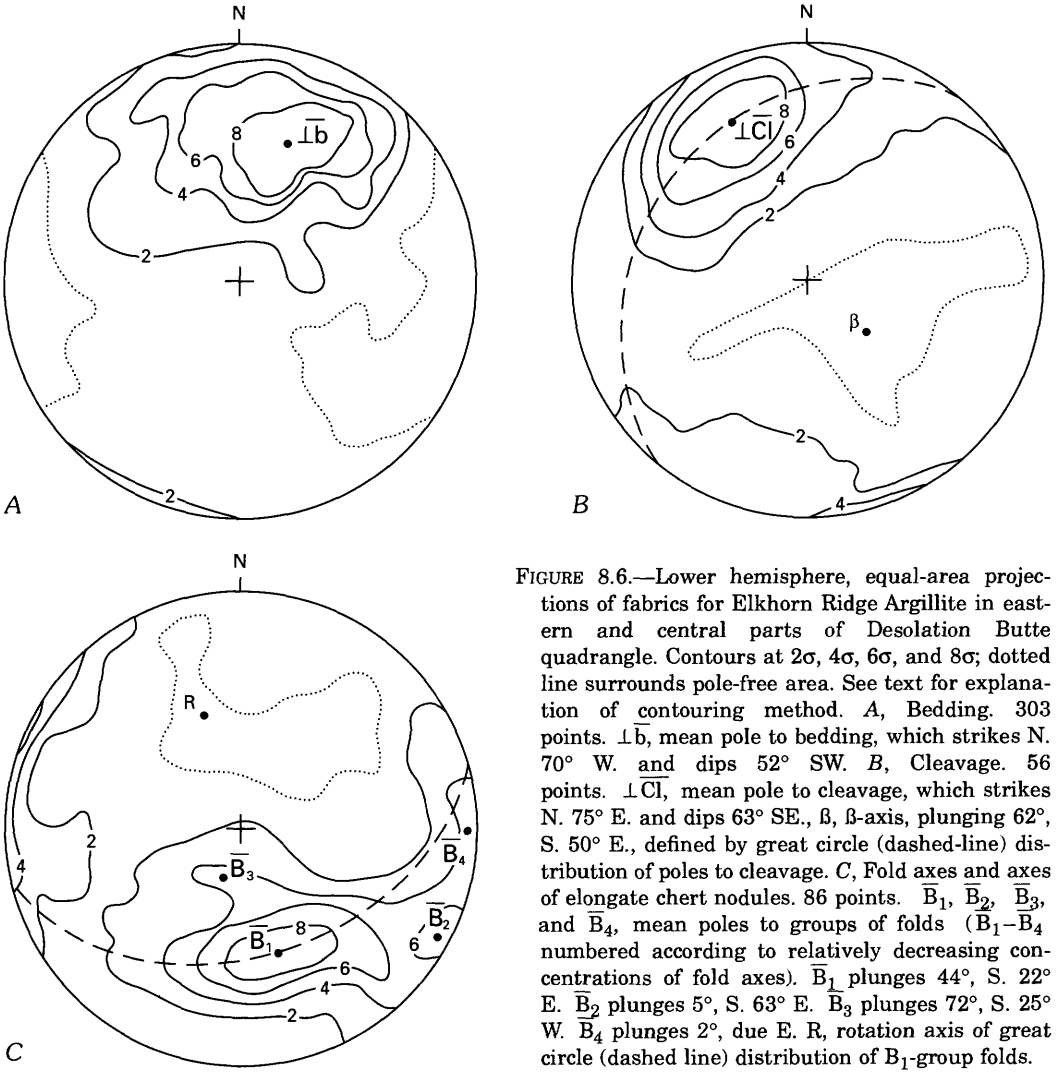

FIGURE 8.6.—Lower hemisphere, equal-area projections of fabrics for Elkhorn Ridge Argillite in eastern and central parts of Desolation Butte quadrangle. Contours at 2σ, 4σ, 6σ, and 8σ; dotted line surrounds pole-free area. See text for explanation of contouring method. *A*, Bedding. 303 points. $\perp\overline{b}$, mean pole to bedding, which strikes N. 70° W. and dips 52° SW. *B*, Cleavage. 56 points. $\perp\overline{Cl}$, mean pole to cleavage, which strikes N. 75° E. and dips 63° SE., ß, ß-axis, plunging 62°, S. 50° E., defined by great circle (dashed-line) distribution of poles to cleavage. *C*, Fold axes and axes of elongate chert nodules. 86 points. $\overline{B}_1$, $\overline{B}_2$, $\overline{B}_3$, and $\overline{B}_4$, mean poles to groups of folds ($\overline{B}_1$–$\overline{B}_4$ numbered according to relatively decreasing concentrations of fold axes). $\overline{B}_1$ plunges 44°, S. 22° E. $\overline{B}_2$ plunges 5°, S. 63° E. $\overline{B}_3$ plunges 72°, S. 25° W. $\overline{B}_4$ plunges 2°, due E. R, rotation axis of great circle (dashed line) distribution of B_1-group folds.

of 61° SW. (fig. 8.7*A*), and poles of beds appear to lie along a great circle, defining a ß-axis plunging 61°, S. 6° W. The axes of the few minor folds measured in the assemblage plunge southeast (fig. 8.7*B*).

RELATIONS AMONG STRUCTURES IN THE ELKHORN RIDGE ARGILLITE AND THE PYROCLASTIC AND VOLCANIC ROCK ASSEMBLAGE

The mean attitudes of bedding in the Elkhorn Ridge Argillite and the pyroclastic and volcanic rock assemblage are 13° apart. This angular difference could be a measure of an original angular discordance between these units. The ß-axis of bedding in the pyroclastic and volcanic rock assemblage (fig. 8.7*A*) is 22° from B_1-group folds in the Elkhorn Ridge Argillite (fig. 8.6*C*) and falls between the 4σ and 6σ contours on figure 8.6*C*—close enough to each other to suggest that the ß-axis of the pyroclastic and volcanic rock assemblage and the B_1-group folds of the Elkhorn Ridge Argillite are related. With allowances for some rotation of thrust slivers after juxtaposition, these combined similarities in orientations of structural elements in the two assemblages suggest that these units were imbricated before the earliest folding (B_1 group). The greater development of mesoscopic folds in the Elkhorn Ridge may be due to the lesser competence of the unit. The greater disruption of bedding (broken formation) in the Elkhorn Ridge, however, may be due to deformation that preceded imbrication.

PERIDOTITE AND ASSOCIATED ROCKS ASSEMBLAGE

Foliation and cleavage are present but not common in the peridotite and associated rocks assemblage. Annealing recrystallization during Late Jurassic contact metamorphism (M6, table 8.1) obliterated much of the early structure that had developed in the assemblage, especially in the peridotite. Planar structures are best preserved in some of the metasedimentary and metavolcanic rocks of the assemblage. In these rocks cleavage coincides with banding and a penetrative foliation defined by concentrations and arrays of phyllosilicate minerals and amphibole. These structural elements are steeply dipping or vertical and strike northeast to north (fig. 8.8*A*). Rotation of pods of these metasedimentary and metavolcanic rocks in the peridotitic matrix after cleavage had formed may account for some of the variation in attitude.

Planar structures are much more poorly preserved in the hornblende metadiorite and peridotite of the assemblage. In the metadiorite, cleavage mostly coincides with a foliation that is defined by arrays of long axes of amphiboles. Some of the foliation in fine-grained amphibolites that developed from the metadiorite may be mimetic after a mylonitic foliation.

Cleavage is well preserved locally in serpentinite, especially near pods of metamorphic and igneous rocks. The cleavages are developed in narrow domains (0.5 mm) of serpentine minerals (chrysotile?) showing subparallel elongation; these narrow do-

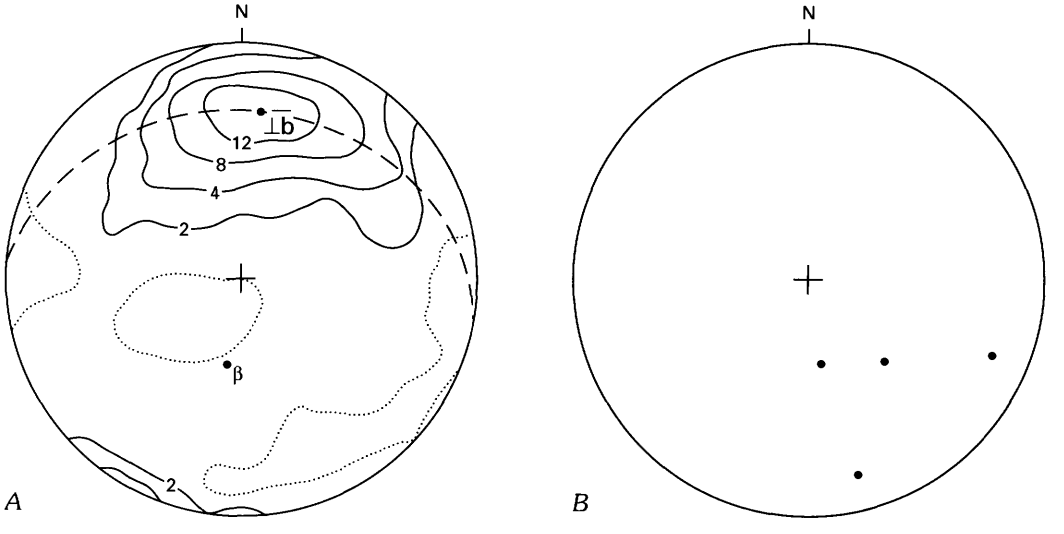

FIGURE 8.7.—Lower hemisphere, equal-area projections of fabrics for pyroclastic and volcanic rock assemblage. *A*, Bedding. 86 points. Contours at 2σ, 4σ, 8σ, and 12σ; dotted line surrounds pole-free area. See text for explanation of contouring method. ⊥ b, mean pole to bedding, which strikes N. 85° W. and dips 61° SW. ß, ß-axis, plunging 61°, S. 6° W., defined by great-circle (dashed-line) distribution of poles to bedding. *B*, Fold axes. 4 points.

mains are separated by broader domains in which serpentine minerals, talc, and carbonate are randomly oriented. Before the annealing recrystallization to form massive olivinite, most of the peridotite may have had this kind of fabric.

Attitudes of cleavages in the peridotite and hornblende metadiorite are similar and are combined in figure 8.8*B*. The cleavages are vertical to steeply dipping and strike north-northeast, similar to the cleavages in the metasedimentary and metavolcanic rocks (fig. 8.8*A*), and show less scatter than the cleavages in the metamorphic rocks.

A few crenulations and minor folds were found on cleavages and foliations in the peridotite and associated rocks assemblage (figs. 8.8*C*, 8.8*D*). The axes of minor folds and crenulations in the metasedimentary and metavolcanic rocks of the assemblage plunge at various angles in a northwest-southeast zone across the orientation diagram in figure 8.8*C*. The few linear structures in serpentinite plunge in widely varying directions at moderate to steep angles (fig. 8.8*D*). Although the linear elements in the peridotite and associated rocks assemblage do not clearly define a subfabric, they suggest the presence of sets of steep and gently plunging minor folds. These fold sets may correspond to the fold sets found in the Elkhorn Ridge Argillite (see subsection "Elkhorn Ridge Argillite" under "Mesoscopic Structure"). One group of minor folds in the peridotite and associated rocks assemblage appears to be subparallel to the northwest-trending axis of the major antiform outlined by metamorphic rocks (figs. 8.2, 8.4, 8.5; cross section *C*–*C*').

The peridotite and associated rocks assemblage would probably have had to undergo a two-stage development to explain the extensional and compressional features and the annealing textures. If the assemblage developed as a serpentine-matrix melange protrusion into a plate composed of Elkhorn Ridge Argillite, it would have been emplaced in an environment of extension at right angles to the N. 40° W. trend of the zone occupied by the assemblage. Structures developed in the assemblage at the time of protrusion should reflect the probable upward movement of the assemblage into this large extensional fracture. The thrusting and mylonitization along the northeast margin of the assemblage and the cleavage developed in it, however, reflect compression, at a high angle to the trend of the zone, rather than extension. These structures most likely resulted from a later event, possibly associated with the emplacement of Late Jurassic diorite along the southwest margin of the zone. As the dioritic magma rose preferentially along this contact, possibly to feed andesitic volcanism on the Late Jurassic surface, the peridotite and associated rocks assemblage was pushed aside, with the resulting development of the compressional structures. Heat from the diorite caused widespread recrystallization of deformed serpentinite to a massive olivinite and also affected the metamorphic rocks of the assemblage, including the mylonite. Most of the minor structures in the serpentinite were obliterated during recrystallization.

RELATIONS AMONG FABRIC ELEMENTS IN THE ELKHORN RIDGE ARGILLITE AND THE PERIDOTITE AND ASSOCIATED ROCKS ASSEMBLAGE

Part of the Elkhorn Ridge Argillite in the western part of the Desolation Butte quadrangle (fig. 8.2) has a subfabric that may bear on the relative timing of the development of fabric elements in the Elkhorn Ridge and in the peridotite and associated rocks assemblage. Cleavage there cuts intercalated chert and argillite. Beds are disrupted along cleavages, and cleavage-bound chert fragments are flattened perpendicular to cleavage. Long axes of chert fragments parallel minor folds and crenulations. Attitudes of cleavages vary widely (fig. 8.8*E*), but many resemble those in the peridotite and associated rocks assemblage (figs. 8.8*A*, 8.8*B*) more than those in the Elkhorn Ridge Argillite in the eastern and central parts of the Desolation Butte quadrangle (fig. 8.6*B*). In the western part of the quadrangle minor folds and elongate chert nodules in the Elkhorn Ridge plunge steeply or gently (fig. 8.8*F*). Many of these linear elements have attitudes like the ones in the peridotite and associated rocks assemblage (figs. 8.8*C*, 8.8*D*). These similarities in fabric between the part of the Elkhorn Ridge in the western part of the quadrangle and the peridotite and associated rocks assemblage suggest that the fabric in the assemblage developed during or after juxtaposition of the assemblage and the composite block of the Elkhorn Ridge and the pyroclastic and volcanic rock assemblage. The steep and gently plunging folds in the peridotite and associated rocks assemblage (figs. 8.6*C*, 8.6*D*) may correspond to the B_2- and B_3-group folds in the Elkhorn Ridge. If these correlations are correct, then B_1- and B_4-group folds in the Elkhorn Ridge most likely formed before the peridotite and associated rocks assemblage was juxtaposed with the composite block of the Elkhorn Ridge and the pyroclastic and volcanic rock assemblage, because folds with the B_1- and B_4-type orientations appear to be lacking in the fabric of the peridotite and associated rocks assemblage.

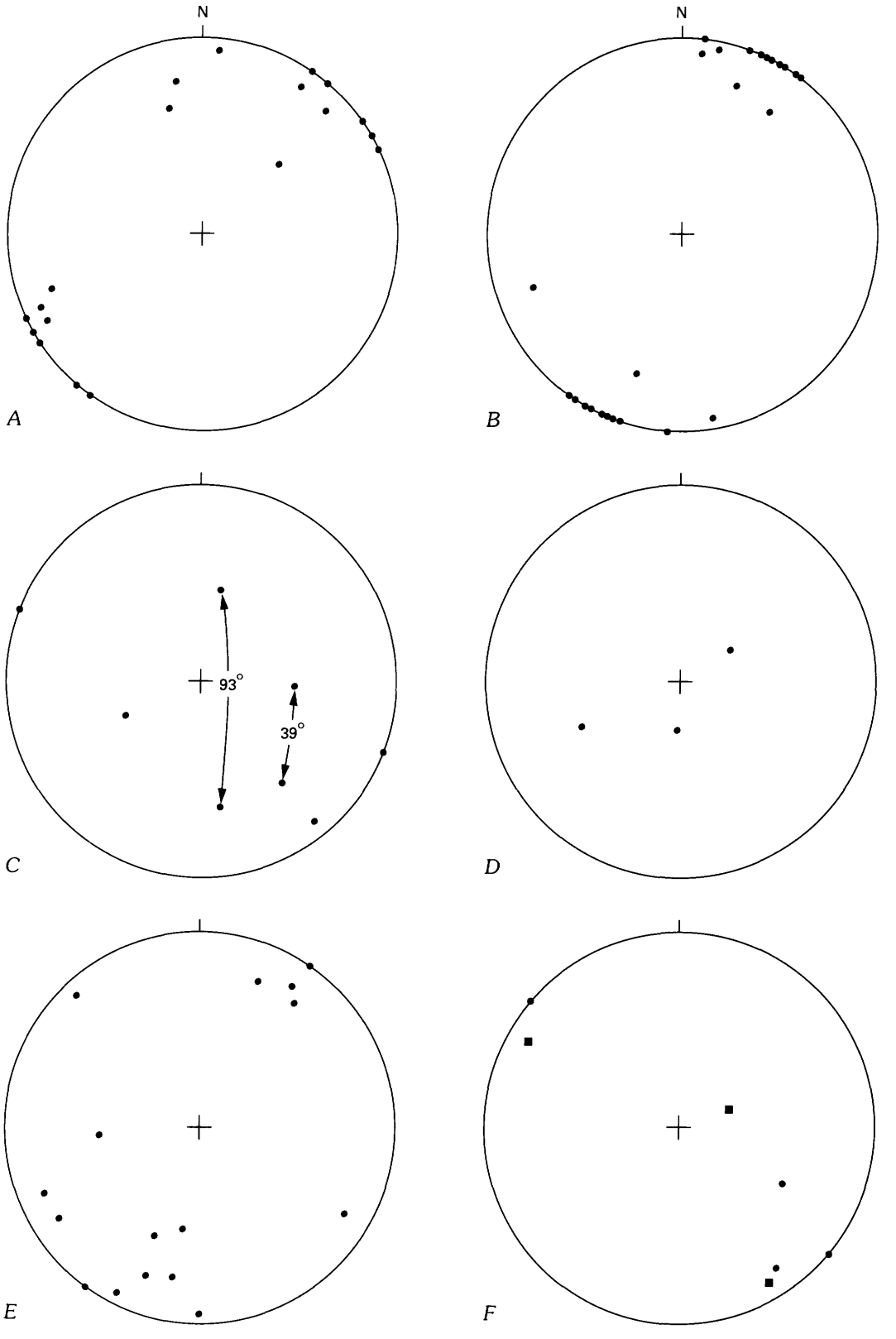
N
A
N
B
93°
39°
C
D
E
F

DEFORMATIONS

Rocks of the Desolation Butte quadrangle have undergone several deformations (D1 to D7, table 8.1). Like the metamorphic events, some of the deformations occurred before the peridotite and associated rocks assemblage and the composite block of the Elkhorn Ridge Argillite and the pyroclastic and volcanic rock assemblage were juxtaposed by faulting. Other deformations may have occurred jointly in both blocks before the rocks arrived in their present location.

The earliest deformation (D1, table 8.1) recorded is uplift of the terrane that supplied sediment to the Elkhorn Ridge Argillite, to the pyroclastic and volcanic rock assemblage, and possibly to the metasedimentary rocks in the peridotite and associated rocks assemblage. Some of this uplift may date from pre-Devonian time.

The Elkhorn Ridge Argillite developed broken formation during Devonian to Triassic time (D2, table 1). This event probably occurred before the Elkhorn Ridge and the pyroclastic and volcanic rock assemblage were imbricated, because the assemblage does not have the appearance of broken formation. Alternatively, the absence of broken formation in the assemblage could be due to the greater competence of the assemblage, but this explanation would be more convincing if the pyroclastic and volcanic rock assemblage consisted entirely of volcanic flows or of flows and thick-bedded well-cemented volcaniclastic rocks. The thick zones of thin-bedded or laminated tuff and argillite in the assemblage most likely would not have remained intact if the development of a broken formation had occurred after the imbrication (D3, table 8.1). Possibly some of the Elkhorn Ridge was not completely lithified before the development of broken formation, whereas the pyroclastic and volcanic rocks assemblage had a greater bulk competence than the Elkhorn Ridge had during that event (D2, table 8.1). If the Elkhorn Ridge (Paleozoic and Triassic?) within the study area is older than the pyroclastic and volcanic rock assemblage (Early Triassic), the Elkhorn Ridge was probably well lithified by Triassic time and had existed in the paleo-oceanic (Pacific) crust for about 125 m.y., long enough to have developed complex internal structure before imbricate thrusting with (or even before the deposition of) the pyroclastic and volcanic rock assemblage. The development of broken formation (D2, table 8.1) can be given a tentative age of Devonian to Triassic assuming that broken formation in the Elkhorn Ridge records a structurally distinct strain event that is not shown in other rocks of the study area.

Evidence of deformation of the peridotite and associated rocks assemblage, especially the peridotite, during the Triassic and perhaps even pre-Mesozoic time, was largely obliterated during subsequent recrystallization. If this assemblage was once an ophiolite, disruption of the original, lithologically varied stratigraphy has resulted in the present-day nearly chaotic outcrop pattern of lithologic components.

Early Triassic to Middle(?) Jurassic imbrication of the Elkhorn Ridge Argillite, the pyroclastic and volcanic rock assemblage, and the Triassic diorite (D3, table 8.1) occurred after intrusion of the Triassic diorite.

Mesoscopic folds (B_1, fig. 8.6*C* and table 8.1; D4, table 8.1) appear to have developed during or after imbrication of the Elkhorn Ridge Argillite and the pyroclastic and volcanic rock assemblage, on the basis of similarities between the fabric of the assemblage and a subfabric of the Elkhorn Ridge, especially the orientations of certain linear elements (fig. 8.9*A*). The B_1-folding event (D4, table 8.1) probably occurred during the interval from the Early Triassic to the Middle(?) Triassic.

Southeast-dipping cleavage developed in the Elkhorn Ridge during an event (D5, table 8.1) that may also have resulted in rotation of B_1-group folds. Minor B_4-group folds as well as some macroscopic folds (such as are shown in cross sections *A–A'* and *B–B'*, fig. 8.5) may have formed during this same event. The peridotite and associated rocks assemblage is presumed to have been emplaced at about this time (Late Triassic to Middle? Jurassic).

During a later event (D6, table 8.1), the peridotite and associated rocks assemblage was thrust over the composite block of the Elkhorn Ridge Argillite and pyroclastic and volcanic rock assemblage, and the brecciated argillite and chert unit formed and was thrust into contact with part of the composite unit. At this time new cleavage formed in serpentinite and metamorphic rocks of the peridotite and associated rocks assemblage, and mylonite zones developed in

◀

FIGURE 8.8.—Lower hemisphere, equal-area projections of fabrics for the peridotite and associated rocks assemblage and for Elkhorn Ridge Argillite in northwestern and western parts of Desolation Butte quadrangle. *A*, Poles to cleavage and foliation in metamorphic rocks of the peridotite and associated rocks assemblage (n=14). *B*, Poles to cleavage in peridotite and associated hornblende metadiorite (n=16). *C*, Fold axes in metamorphic rocks of the peridotite and associated rocks assemblage (n=7). Double-headed arrows show angles between intersecting fold axes. *D*, Fold axes in peridotite (n=3). *E*, Poles to cleavage in Elkhorn Ridge Argillite in northwestern part of quadrangle (n=15). *F*, Fold axes and elongate chert nodules in Elkhorn Ridge Argillite in western part of quadrangle (n=6). Dots, fold axes; squares, axes of elongate chert nodules.

the hornblende diorite in response to emplacement of the Late Jurassic diorite.

B_2- and B_3-group folds in the Elkhorn Ridge Argillite, folds in the peridotite and associated rocks assemblage, and steeply dipping to vertical northwest-striking cleavage and foliation in the peridotite and associated rocks assemblage and in part of the Elkhorn Ridge may have formed when the peridotite and associated rocks assemblage was thrust over the composite block of the Elkhorn Ridge Argillite and pyroclastic and volcanic rock assemblage (D6, table 8.1). It is not clear whether these structures formed during the same 161-Ma tectonic events, dated by Oldow and others (1984, p. 214) that resulted in penetrative deformation in the Blue Mountains. They suggested that three generalized episodes of Mesozoic deformation affected the Blue Mountains: Triassic to Early Jurassic, Late Jurassic, and Cretaceous. The two earlier deformations were penetrative and may correspond to deformations D5 and D6 (table 8.1). No evidence was found for Cretaceous deformation in the Desolation Butte quadrangle.

Steep northwest- and northeast-striking faults cut the imbricated assemblages—the peridotite and associated rocks assemblage and the (composite) Elkhorn Ridge Argillite-pyroclastic and volcanic rock assemblage-brecciated argillite and chert unit—before emplacement of the Late Jurassic diorite. These faults could be tear faults in thrust sheets developed during imbrication (D3, table 8.1), but movement on some of them may have continued until long after D6 (table 8.1).

Avé Lallemant and others (1980, p. 374) concluded that the Blue Mountains may have been accreted to the continent in the Late Jurassic. If so, D6 may be related to accretionary processes.

Post-accretionary deformation in the Jurassic or Cretaceous (D7, table 8.1) included rotation, translation, and uplift of large blocks that include the Blue Mountains.

COMPARISON OF FABRIC IN THE ELKHORN RIDGE ARGILLITE, DESOLATION BUTTE QUADRANGLE, WITH FABRIC IN OTHER AREAS

The fabric of the Elkhorn Ridge Argillite in the Desolation Butte quadrangle (hereinafter referred to as "Elkhorn Ridge Argillite-DB" for the sake of convenience) is similar to the fabric of the Elkhorn

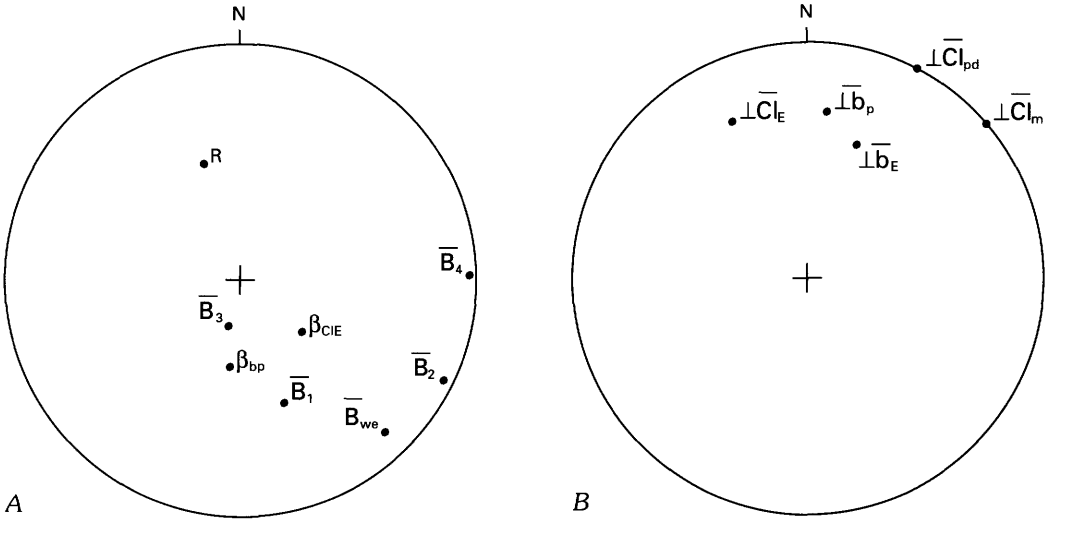

FIGURE 8.9.—Lower hemisphere equal-area summary projections for assemblages in Desolation Butte quadrangle. *A*, Linear elements. $\overline{B}_1$, $\overline{B}_2$, $\overline{B}_3$, and $\overline{B}_4$, mean orientations of fold groups from figure 8.6*C*. R, rotation of axis of $\overline{B}_1$-group folds. β_{bp}, ß-axis of poles to bedding, pyroclastic and volcanic rock assemblage; β_{CIE}, ß-axis of poles to cleavage, Elkhorn Ridge Argillite; $\overline{B}_{WE}$, mean orientation of subhorizontal folds in Elkhorn Ridge Argillite in western part of Desolation Butte quadrangle. *B*, Planar elements. $\perp\overline{b}_E$, mean pole to bedding, Elkhorn Ridge Argillite. $\perp\overline{b}_p$, mean pole to bedding, pyroclastic and volcanic rock assemblage. $\perp\overline{Cl}_E$, mean pole to cleavage, Elkhorn Ridge Argillite. $\perp\overline{Cl}_{pd}$, mean pole to cleavage, peridotite and diorite. $\perp\overline{Cl}_m$, mean pole to cleavage, metasedimentary and metavolcanic rocks of the peridotite and associated rocks assemblage.

Ridge Argillite in the Elkhorn Peak quadrangle (hereinafter referred to as "Elkhorn Ridge Argillite-EP") west of Baker City (fig. 8.1; Coward, 1983) and to that of the Burnt River Schist (Ashley, 1966), a possible correlative of part of the Elkhorn Ridge Argillite (Gilluly, 1937, p. 13). The Elkhorn Ridge Argillite-EP and the Burnt River Schist have undergone compound, nearly coaxial deformations in which at least two similar cleavages, and two sets of subparallel fold axes formed. Orientations of corresponding fabric elements (bedding, cleavages, and fold axes) are similar for the two areas (fig. 8.10). The deformation in the Burnt River Schist seems to be more intense than in the Elkhorn Ridge Argillite-EP, and bedding and cleavages in the Burnt River tend to have great-circle pole distributions defining ß-axes.

Ages of the deformations in the Elkhorn Ridge Argillite-EP and the Burnt River Schist may be similar. Ashley (chap. 12, this volume) considers the age of deformation in the Burnt River Schist to be no older than Middle Triassic and no younger than Early Cretaceous. Coward (1983, p. 109–110) concluded that the main deformation in the Elkhorn Ridge Argillite-EP occurred in Late Triassic to earliest Jurassic time, apparently on the basis of Late Triassic to Early Jurassic radiolarians from a locality several kilometers south of Sumpter (fig. 8.1). Brooks and Ferns (1986) reported Late Triassic (early Norian) conodonts in the Elkhorn Ridge Argillite-EP, indicating post-early Norian deformation. If the deformations in the Elkhorn Ridge Argillite-EP and Burnt River Schist are correlative, as suggested by similarities in rock fabric, the main deformation must have occurred in the Late Triassic or Jurassic and possibly no later than the Middle Jurassic.

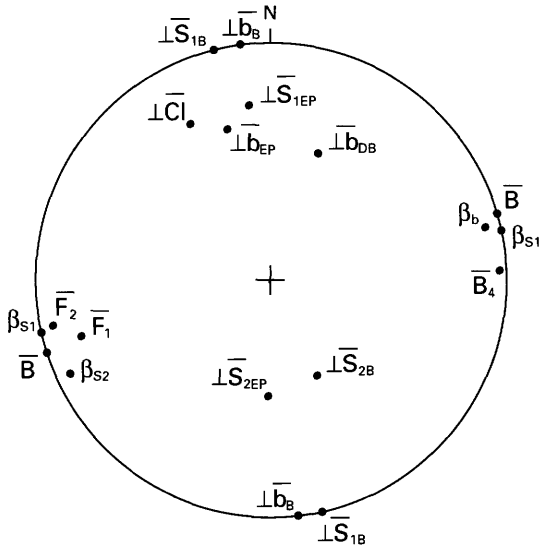

FIGURE 8.10.—Lower hemisphere, equal-area summary projection for fabrics in Desolation Butte quadrangle, Elkhorn Peak quadrangle, and Burnt River area. Fabric elements from Desolation Butte quadrangle: $\perp\bar{b}_{DB}$, pole to average bedding; $\perp\bar{Cl}$, pole to average cleavage; $\bar{B}_4$, average of group of east-west-trending folds. Elements from Elkhorn Peak quadrangle: $\perp\bar{b}_{EP}$, pole to average bedding; $\perp\bar{S}_{1EP}$ and $\perp\bar{S}_{2EP}$, poles to average cleavages; $\bar{B}$, average of minor-fold axes. Elements from Burnt River area: $\perp\bar{b}_B$, pole to average bedding; $\perp\bar{S}_{1B}$ and $\perp\bar{S}_{2B}$, poles to average cleavages; $\bar{F}_1$ and $\bar{F}_2$, average minor-fold axes; $ß_b$, ß-axis of bedding; $ß_{S1}$, ß-axis of S_1 cleavage; $ß_{S2}$, ß-axis of S_2 cleavage.

The average attitude of bedding in the Elkhorn Ridge Argillite-DB is not close to that of either the Elkhorn Ridge Argillite-EP or the Burnt River Schist, although data points overlap considerably. The orientations in the subfabric that includes B_4-group folds and cleavage in the Elkhorn Ridge Argillite-DB resemble those of folds and early cleavage in the Elkhorn Ridge Argillite-EP and the Burnt River Schist (fig. 8.10); this similarity further supports a Late Triassic or Jurassic age for the D5 deformation in the Elkhorn Ridge Argillite-DB. However, these fabric elements do not seem as strongly developed in the Elkhorn Ridge Argillite-DB as they are in the Elkhorn Ridge Argillite-EP.

The B_1-group of folds in the Elkhorn Ridge Argillite-DB does not have counterparts in the fabrics of the Elkhorn Ridge Argillite-EP and the Burnt River Schist. Because the Elkhorn Ridge Argillite-DB may be much older (Devonian, in part) than the Elkhorn Ridge Argillite-EP and the Burnt River Schist, it may have undergone several deformations before the Paleozoic sedimentary rocks were gathered into the Elkhorn Ridge tectonostratigraphic package. If B_4-group folds and correlative fabric elements in the Elkhorn Ridge Argillite-EP and the Burnt River Schist correspond to Late Triassic or Jurassic deformations, then B_1 folding may have occurred in the Early to Middle(?) Triassic.

Folds with attitudes like those of the B_2 and B_3 groups are not common in the Elkhorn Ridge Argillite-EP and the Burnt River Schist. In the Elkhorn Ridge Argillite-DB, B_2- and B_3-type folding may have been associated with the Late Jurassic diorite intrusion. Structures correlative with this event would probably be uncommon in the Elkhorn Ridge Argillite-EP and absent in the Burnt River Schist. Present evidence suggests that B_2- and B_3-type folds and cleavage in the western part of the Elkhorn Ridge Argillite-DB and in the peridotite and associated rocks assemblage represent local strain.

DISCUSSION

The history of the rocks in the Desolation Butte quadrangle reveals the long time involved in the structural development of the rock units, about 200 m.y. from the end of the Devonian to the intrusion of the Late Jurassic diorite. The structural and metamorphic complexity of these rocks is consistent with a history spanning several geologic periods and with assembly from a variety of rock types that may have originated in widely separated and different environments. More than one subduction-obduction event can be postulated to explain the heterogeneous nature of the rocks. It is not clear how much of the rock fabric is a result of accretionary processes or is due to later tectonism. Regional foliation, mesoscopic folds, and coaxially refolded folds, such as in the Elkhorn Ridge Argillite-EP and the Burnt River Schist, can all be produced in accretionary wedges (Moore and Wheeler, 1978; Moore and Karig, 1980; Speed, 1983; Cloos, 1984) as well as in nonobduction environments; the rock fabric by itself is unlikely to provide enough clues to the tectonic environment.

Geologic relations point to nonpenetrative deformation occurring before the earliest (Triassic) folding. With regard to the total strain in the Elkhorn Ridge Argillite, the broken formation that developed during the Devonian to Triassic in the Elkhorn Ridge (D2, table 8.1) may have been the most significant deformation. Unfortunately, it is also the least studied or understood of the deformations. During the Early to Middle(?) Triassic, the Elkhorn Ridge Argillite may have been uplifted and eroded to supply chert clasts to the pyroclastic and volcanic rock assemblage. Later, the Elkhorn Ridge, the pyroclastic and volcanic rock assemblage, and the Early Triassic diorite were imbricated (D3, table 8.1).

The nearly penetrative deformations (D4 through D6, table 8.1) occurred over the time interval Early Triassic to Late Jurassic in a series of intermittent events, the last of which may have been regionally unimportant.

Before drawing conclusions about structural history from the fabric data, the 60° clockwise post-Jurassic rotation postulated for the Blue Mountains (Wilson and Cox, 1980) should be removed from the fabric orientation. The pre-Cretaceous orientations of the main fabric features of the Desolation Butte quadrangle are shown in figure 8.11, after 60° counterclockwise rotation about a vertical axis.

The oldest and best represented group of folds (B_1-type; D4, table 8.1) plunged on the average approximately 45°, S. 78° E. during the Early to Middle(?) Triassic (fig. 8.11*A*); later (Late Triassic to Middle? Jurassic) they were rotated during B_4-type folding (D5, table 8.1). Orientations of B_1-type axial surfaces as well as later linear elements within the study area are difficult to measure because the structures are mostly crenulations and open concentric folds in which the axial surfaces are not precisely determinable. The general impression is, however, that in pre-Cretaceous time axial planes were at large angles to bedding and were vertical or steeply dipping and west-northwest striking. If axial planes of concentric folds are expected to be approximately perpendicular to the greatest total compressive strain in the rocks (Dieterich and Carter, 1969; Dieterich, 1969, 1970), then B_1 folding may be due to shortening along an Early to Middle(?) Triassic axis oriented north-northeast–south-southwest.

If cleavage is a shortening phenomenon (Ramsay, 1967, p. 180; Siddans, 1972, p. 219; Wood, 1974, p. 398–399; Hobbs and others, 1976, p. 252), then cleavages in the Elkhorn Ridge Argillite in the Desolation Butte and Elkhorn Peak quadrangles and in the Burnt River Schist give clues to the directions of principal shortening during Late Triassic to Late Jurassic deformations. During the Late Triassic to Middle(?) Jurassic tectonism (D5, table 8.1) in the Desolation Butte quadrangle, the direction of shortening was oriented approximately east-west (fig. 8.11*A*). Equivalent shortening in the Elkhorn Peak quadrangle and the Burnt River area (fig. 8.1) was oriented about west-northwest (fig. 8.11*B*). This cleavage-forming event is correlative with tectonic shortening described by Oldow and others (1984, D1 in fig. 2), whose data suggest that this deformation in northeastern Oregon was part of a regional tectonic episode that also affected the northern Sierra Nevada. Associated fold axes in the northern Sierra Nevada, however, range in orientation from gently to steeply plunging, indicating that the total movement picture there is complex and probably differs appreciably in detail from the movement picture in the Desolation Butte quadrangle–Elkhorn Peak quadrangle–Burnt River area.

If the peridotite and associated rocks assemblage was emplaced along a tear in an obducted plate, as occurred in the Batinah melange (Robertson and Woodcock, 1983), the long axis of the tear could be an extension fracture oriented at a low angle to the local movement direction of the plate. Corrected for post-Jurassic rotation, this direction would have been approximately N. 80° E. (fig. 8.11), which is close to the orientation of the Late Triassic to Middle(?) Jurassic shortening in the Desolation Butte quadrangle–Elkhorn Peak quadrangle–Burnt River area. During this event the ultramafic component of the peridotite

and associated rocks assemblage was most likely largely serpentinite.

After its development, the tear occupied by the peridotite and associated rocks assemblage remained a zone of weakness that was used during intrusion of the Late Jurassic diorite. The greatest principal strain, oriented north-northwest in the Late Jurassic (fig. 8.7) and arising from the diorite's pushing aside the peridotite and associated rocks assemblage, resulted in a cleavage in the serpentinite and metasedimentary rocks of the assemblage and in mylonitization of the unit. In addition, the peridotite and associated rocks assemblage was thrust over the block composed of the Elkhorn Ridge Argillite and the pyroclastic and volcanic rock assemblage along the northern (Late Jurassic) border of the extensional tear zone (D6, table 8.1). Thrust faulting brought rocks (brecciated argillite and chert unit) that are somewhat different from the Elkhorn Ridge Argillite into the area and caused moderate nearly penetrative disruption of the earlier fabric of the Elkhorn Ridge Argillite in the western Desolation Butte quadrangle. The fabric resulting from the 161-Ma tectonism (D6, table 8.1) does not appear to be of regional extent like the fabric that was produced by Late Triassic to Middle(?) Jurassic events (D5, table 8.1), because the younger (D6-type) fabric is not developed in either the Elkhorn Peak quadrangle (Coward, 1983) or the Burnt River Schist (Ashley, 1966). Also, the orientations of axial planes of possibly geometrically and temporally equivalent folds in the northern Sierra Nevada (Oldow and others, 1984, fig. 3) are different from D6-type cleavages.

As the diorite was emplaced, possibly feeding andesitic extrusions on the Late Jurassic surface, heat and possibly fluids penetrated and generally recrystallized the peridotite and associated rocks; this widespread recrystallization nearly obliterated cleavage and other D6-type structural elements in the ultramafic matrix of the unit.

The presence of the peridotite and associated rocks assemblage and similar serpentine-matrix melanges in the Desolation Butte quadrangle and vicinity implies the existence, at least in the past, of an ophiolitic layer below the Elkhorn Ridge Argillite. One can only speculate whether the ophiolitic layer was basement rock on which the Elkhorn Ridge was deposited or whether the peridotite and associated rocks assemblage was part of a regional ultramafic plate over which the Elkhorn Ridge was tectonically emplaced.

Dickinson (1981) showed northeastern Oregon as an extension of the Late Jurassic to middle Tertiary zone of the Franciscan Complex. This view is partly consistent with the Late Jurassic deformational ages inferred by Avé Lallemant and others (1980) and Coward (1983) for the Blue Mountains. However,

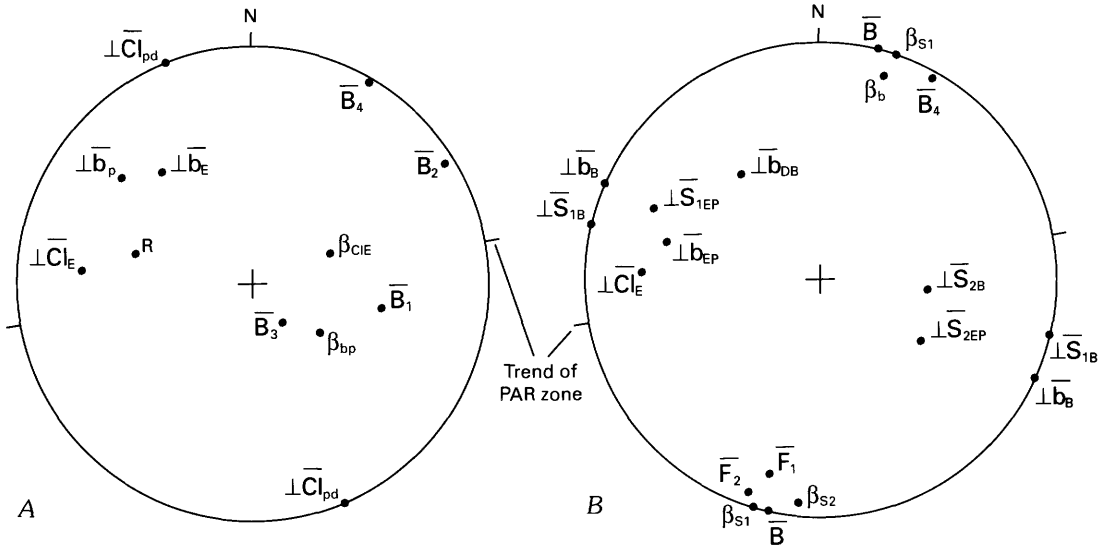

FIGURE 8.11.—Lower hemisphere, equal-area summary projections for fabrics of rocks in Desolation Butte quadrangle, Elkhorn Peak quadrangle, and Burnt River area. Fabric rotated 60° counterclockwise about a vertical axis to remove post-Jurassic rotation of Blue Mountains. PAR, peridotite and associated rocks assemblage, possibly emplaced along tear in an obducted plate (see section "Discussion"). See figures 8.9 and 8.10 for explanation of symbols. *A*, Desolation Butte quadrangle. *B*, Fabric resulting from 161-Ma tectonism (D6, table 8.1) for area comprising the Desolation Butte quadrangle-Elkhorn Peak quadrangle-Burnt River area.

penetrative deformation in the Desolation Butte quadrangle and possibly in other parts of the oceanic terrane of northeastern Oregon must have largely ceased after the intrusion of the Bald Mountain batholith and its satellitic plutons in the early Late Jurassic, about 161 Ma (Armstrong and others, 1977). By this time the accreting oceanic terrane had ceased deforming internally, but may not yet have firmly docked at the continental margin. Post-Jurassic deformations involved rotation, translation, and uplift of large blocks that include the Blue Mountains.

CONCLUSIONS

1. Pre-Jurassic rocks of the Desolation Butte quadrangle are divided into four main assemblages: the Elkhorn Ridge Argillite, a pyroclastic and volcanic rock assemblage, a brecciated argillite and chert unit, and a peridotite and associated rocks assemblage.
2. The Elkhorn Ridge Argillite contains Devonian fossils in the Desolation Butte quadrangle but ranges to Late Triassic (and may possibly range to Early Jurassic) age in areas to the south and east. It is apparently a tectonostratigraphic unit with a 200-m.y. history and was assembled from unrelated packets of oceanic sedimentary and volcanic rocks.
3. The pyroclastic and volcanic rock assemblage, presumably Early Triassic in age, may represent an andesitic-arc environment that was not far from or was on top of the Elkhorn Ridge Argillite. The Triassic dioritic rocks in the area may have fed the vents from which the extrusive rocks originated.
4. The brecciated argillite and chert unit may consist mostly of brecciated fragments derived from the Elkhorn Ridge Argillite, although sedimentary rocks derived from other sources, including fore-arc basins, may have been emplaced by thrust faulting during Late Jurassic time.
5. The peridotite and associated rocks assemblage, possibly in part a dismembered ophiolite, contains rocks that may have undergone complex metamorphism in an oceanic crustal environment before juxtaposition with the composite block of Elkhorn Ridge Argillite, pyroclastic and volcanic rock assemblage, and brecciated argillite and chert unit. Part of the metasedimentary rock component of the peridotite and associated rocks assemblage may be related to the Elkhorn Ridge Argillite. The emplacement of the peridotite and associated rocks assemblage may have been by local protrusion from a peridotite-rich basement during the Late Triassic to Middle(?) Jurassic.
6. Pre-Jurassic metamorphism in the study area includes low-grade regional and contact metamorphism of the Elkhorn Ridge Argillite, the pyroclastic and volcanic rock assemblage, and the Triassic diorite, as well as complex metamorphism of the peridotite and associated rocks assemblage. All these rocks were affected by widespread contact metamorphism as a result of intrusion of the Late Jurassic diorite and minor contact metamorphism around intrusions of Jurassic or Cretaceous quartz monzonite.
7. Tectonism in the study area includes possibly Paleozoic development of broken formation, Triassic thrusting, Triassic and Jurassic folding and cleavage-formation, and Late Jurassic thrusting and folding caused by emplacement of a diorite pluton. Most deformation within the Baker terrane ceased by the end of the Jurassic. Subsequent tectonism involved movements of large crustal blocks that may have included the rest of the Blue Mountains.
8. The most widespread deformation in the oceanic terrane in the Desolation Butte quadrangle–Elkhorn Peak quadrangle–Burnt River area seems to be east-west folding with subhorizontal axes and a steep cleavage developed approximately parallel to axial planes of the folds. Structures related to this deformation are less developed in the Desolation Butte quadrangle than in areas to the east and are most abundant in the Burnt River Schist, a possible partial lithic correlative of the Elkhorn Ridge Argillite. This deformation may be a result of Early Triassic to Middle(?) Jurassic oceanic crust–island arc convergence with its resultant obduction-subduction. The peridotite and associated rocks assemblage may have been emplaced as a protrusion along an extensional tear in the obducted plate. The orientation of pre-Cretaceous shortening was approximately east-west.
9. Deformation in the Desolation Butte quadrangle occurred during the Late Jurassic intrusion of diorite alongside the peridotite and associated rocks assemblage. Emplacement of the diorite forced aside the peridotite and associated rocks assemblage, resulting in northward (pre-Cretaceous) thrusting of this unit, development of steep east-west cleavage in the ser-

pentinite-matrix melange, mylonitization of mafic igneous rocks in this unit, and moderate disruption of the earlier fabric of part of the Elkhorn Ridge Argillite. Heat and possibly fluids from the intrusion later resulted in widespread recrystallization of the peridotite and associated rocks assemblage.

10. The rocks of the Desolation Butte quadrangle were rotated, translated, and uplifted in the Jurassic and (or) Cretaceous.

REFERENCES CITED

Armstrong, R.L., Taubeneck, W.H., and Hales, P.O., 1977, Rb-Sr and K-Ar geochronometry of Mesozoic granitic rocks and their Sr isotopic composition, Oregon, Washington, and Idaho: Geological Society of America Bulletin, v. 88, p. 397–411.

Ashley, R.P., 1966, Metamorphic petrology and structure of the Burnt River Canyon area, northeastern Oregon: Stanford, Calif., Stanford University, Ph.D. dissertation, 193 p.

Avé Lallemant, H.G., Phelps, D.W., and Sutter, J.F., 1980, ^{40}Ar-^{39}Ar ages of some pre-Tertiary plutonic and metamorphic rocks of eastern Oregon and their geologic relationships: Geology, v. 8, p. 371–374.

Bloomer, S.H., 1983, Distribution and origin of igneous rocks from the landward slopes of the Mariana Trench—Implications for its structure and evolution: Journal of Geophysical Research, v. 88, no. B9, p. 7411–7428.

Bonatti, Enrico, Honnorez, Jose, Kirst, Paul, and Radicati, Filippo, 1975, Metagabbros from the Mid-Atlantic Ridge at 06°N.—Contact-hydrothermal-dynamic metamorphism beneath the axial valley: Journal of Geology, v. 83, no. 1, p. 61–78.

Bostwick, D.A., and Nestell, M.K., 1967, Permian Tethyan fusulinid faunas of the northwestern United States: Systematics Association Publication 7, p. 93–102.

Brooks, H.C., 1979, Plate tectonics and the geologic history of the Blue Mountains: Oregon Geology, v. 41, no. 5, p. 71–80.

Brooks, H.C., and Ferns, M.L., 1986, Geology and gold deposits map of the Elkhorn Peak quadrangle, Baker County, Oregon: Oregon Department of Geology and Mineral Industries GMS–41, scale 1:24,000.

Brooks, H.C., Ferns, M.L., and Avery, D.G., 1984, Geology and gold deposits map of the southeast quarter of the Bates quadrangle, Grant County, Oregon: Oregon Department of Geology and Mineral Industries GMS–35, scale 1:24,000.

Brooks, H.C., Ferns, M.L., and Mullen, E.D., 1982, Geology and gold deposits map of the Granite quadrangle, Grant County, Oregon: Oregon Department of Geology and Mineral Industries, Map GMS–25, scale 1:24,000.

Brooks, H.C., Ferns, M.L., Wheeler, G.R., and Avery, D.G., 1983, Geology and gold deposits of the northeast quarter of the Bates quadrangle, Baker and Grant Counties, Oregon: Oregon Department of Geology and Mineral Industries, Map GMS–29, scale 1:24,000.

Brooks, H.C., McIntyre, J.R., and Walker, G.W., 1976, Geology of the Oregon part of the Baker 1° by 2° quadrangle: Oregon Department of Geology and Mineral Industries, Map GMS–7, scale 1:250,000.

Brooks, H.C., and Vallier, T.L., 1978, Mesozoic rocks and tectonic evolution of eastern Oregon and western Idaho, *in* Howell, D.G., and McDougall, K.A., eds., Mesozoic paleogeography of the Western United States (Pacific Coast Paleogeography Symposium 2): Los Angeles, Society of Economic Paleontologists and Mineralogists, Pacific Section, p. 133–146.

Busk, H.G., 1929, Earth flexures: London, Cambridge University Press, 106 p.

Cloos, Mark, 1984, Landward-dipping reflectors in accretionary wedges—Active dewatering conduits?: Geology, v. 12, p. 519–522.

Coward, R.I., 1983, Structural geology, stratigraphy, and petrology of the Elkhorn Ridge Argillite in the Sumpter area, northeastern Oregon: Houston, Tex., Rice University, Ph.D. dissertation, 144 p.

Dickinson, W.R., 1979, Mesozoic fore-arc basin in central Oregon: Geology, v. 7, p. 166–170.

———1981, Plate tectonics and the continental margin of California, *in* Ernst, W.G, ed., The geotectonic development of California: Rubey Volume I, Englewood Cliffs, N.J., Prentice-Hall, p. 1–28.

Dickinson, W.R., and Thayer, T.P., 1978, Paleogeographic and paleotectonic implications of Mesozoic stratigraphy and structure in the John Day inlier of central Oregon, *in* Howell, D.G., and McDougall, K.A., eds., Mesozoic paleogeography of the Western United States (Pacific Coast Paleogeography Symposium 2): Los Angeles, Society of Economic Paleontologists and Mineralogists, Pacific Section, p. 147–161.

Dieterich, J.H., 1969, Origin of cleavage in folded rocks: American Journal of Science, v. 267, no. 2, p. 155–165.

———1970, Computer experiments on mechanics of finite-amplitude folds: Canadian Journal of Earth Sciences, v. 7, no. 2, pt. 1, p. 467–476.

Dieterich, J.H., and Carter, N.L., 1969, Stress history of folding: American Journal of Science, v. 267, no. 2, p. 129–154.

Elthon, Don, 1981, Metamorphism in oceanic spreading centers, *in* The oceanic lithosphere, v. 7, *of* Emiliani, Cesare, ed., The seas: New York, John Wiley, p. 185–203.

Elthon, Don, and Stern, C.W., 1978, Metamorphic petrology of the Sarmiento ophiolite complex, Chile: Geology, v. 6, p. 464–468.

Evans, J.G., 1986, Geologic map of the North Fork John Day River Roadless Area, Grant County, Oregon: U.S. Geological Survey Miscellaneous Field Studies Map MF 1581–C, scale 1:48,000.

———1989, Geologic map of the Desolation Butte quadrangle, Grant and Umatilla Counties, Oregon: U.S. Geological Survey Quadrangle Map GQ–1654, scale 1:62,500.

Fryer, Patricia, Ambos, E.L., and Hussong, D.M., 1985, Origin and emplacement of Mariana fore-arc seamounts: Geology, v. 13, no. 11, p. 774–777.

Gilluly, James, 1937, Geology and mineral resources of the Baker quadrangle, Oregon: U.S. Geological Survey Bulletin 879, 109 p.

Hobbs, B.E., Means, W.D., and Williams, P.F., 1976, An outline of structural geology: New York, John Wiley and Sons, 571 p.

Hsü, K.J., 1968, Principles of melanges and their bearing on the Franciscan-Knoxville Paradox: Geological Society of America Bulletin, v. 79, p. 1063–1074.

Kamb, W.B., 1959, Ice petrofabric observations from Blue Glacier, Washington, in relation to theory and experiment: Journal of Geophysical Research, v. 4, p. 1891–1909.

Moore, G.F., and Karig, D.E., 1980, Structural geology of Nias Island, Indonesia—Implications for subduction zone tectonics: American Journal of Science, v. 280, no. 3, p. 193–223.

Moore, J.C., and Wheeler, R.L., 1978, Structural fabric of a melange, Kodiak Islands, Alaska: American Journal of Science, v. 278, no. 5, p. 739–765.

Morris, E.M., and Wardlaw, B.R., 1986, Conodont ages for limestones of eastern Oregon and their implication for pre-Tertiary melange terranes: U.S. Geological Survey Professional Paper 1435, p. 59–63.

Mullen, E.D., 1985, Petrologic character of Permian and Triassic greenstones from the melange terrane of eastern Oregon and their implications for terrane origin: Geology, v. 13, no. 2, p. 131–134.

Oldow, J.S., Avé Lallemant, H.G., and Schmidt, W.J., 1984, Kinematics of plate convergence deduced from Mesozoic structures in the Western Cordillera: Tectonics, v. 3, no. 2, p. 201–227.

Palmer, A.R., 1983, The Decade of North American Geology 1983 geologic time scale: Geology, v. 11, no. 9, p. 503–504.

Ramsay, J.G., 1967, Folding and fracturing of rocks: New York, McGraw-Hill, 568 p.

Robertson, A.H.F., and Woodcock, N.H., 1983, Genesis of the Batinah melange above the Semail ophiolite, Oman: Journal of Structural Geology, v. 5, no. 1, p. 1–17.

Siddans, A.W.B, 1972, Slaty cleavage—A review of research since 1815: Earth Science Reviews, v. 8, p. 205–232.

Silberling, N.J., Jones, D.L., Blake, M.C., Jr., and Howell, D.G., 1984, Lithotectonic terrane map of the western conterminous United States, Pt. C *of* Silberling, N.J., and Jones, D.L., eds., Lithotectonic terrane maps of the North American Cordillera: U.S. Geological Survey Open-File Report 84–523, 43 p.

Speed, R.C., 1983, Structure of the accretionary complex of Barbados—Pt. 1, Chalky Mount: Geological Society of America Bulletin, v. 94, no. 1, p. 92–116.

Streckeisen, A.L., 1976, To each plutonic rock its proper name: Earth Science Reviews 12, p. 1–33.

Taylor, Brian, and Smoot, N.C., 1984, Morphology of Bonin fore-arc submarine canyons: Geology, v. 12, no. 12, p. 724–727.

Turner, F.J., and Verhoogen, John, 1960, Igneous and metamorphic petrology (2d ed.): New York, McGraw-Hill, 694 p.

Vallier, T.L., Brooks, H.C., and Thayer, T.P., 1977, Paleozoic rocks of eastern Oregon and western Idaho, *in* Stewart, J.H, Stevens, C.H., and Fritsche, A.E., eds., Paleozoic paleogeography of the Western United States (Pacific Coast Paleogeography Symposium 1): Los Angeles, Society of Economic paleontologists and Mineralogists, Pacific Section, p. 455–466.

Walker, N.W., 1983, Pre-Tertiary tectonic evolution of northeastern Oregon and west-central Idaho—Constraints based on U/Pb ages of zircons: Geological Society of America Abstracts with Program, v. 15, no. 5, p. 371.

Wilson, Douglas, and Cox, Allen, 1980, Paleomagnetic evidence for tectonic rotation of Jurassic plutons in Blue Mountains, eastern Oregon: Journal of Geophysical Research, v. 85, no. B7, p. 3681–3689.

Wood, D.S., 1974, Current views of the development of slaty cleavage: Annual Review of Earth and Planetary Science, v. 2, p. 369–401.

Wyllie, P.J., 1971, Experimental limits for melting in the Earth's crust and upper mantle, *in* The structure and physical properties of the Earth's crust: American Geophysical Union Geophysical Monograph, no. 14, p. 279–301.

9. THE BOURNE AND GREENHORN SUBTERRANES OF THE BAKER TERRANE, NORTHEASTERN OREGON: IMPLICATIONS FOR THE EVOLUTION OF THE BLUE MOUNTAINS ISLAND-ARC SYSTEM

By MARK L. FERNS[1] and HOWARD C. BROOKS[1,2]

CONTENTS

Abstract ---- 331
Introduction ---- 331
Bourne subterrane ---- 334
  Elkhorn Ridge Argillite ---- 335
  Goodrich Creek and North Fork units ---- 337
  Olive Creek unit ---- 339
  Mixed-rock zones ---- 340
Greenhorn subterrane ---- 342
  Badger Creek unit ---- 342
  Melange of Vinegar Hill ---- 343
  Dixie Butte Meta-andesite ---- 346
Structure ---- 347
  Planar elements ---- 347
  Folds ---- 349
  Structure summary ---- 350
Summary ---- 350
Discussion ---- 353
References cited ---- 356

ABSTRACT

The central part of the Baker terrane in northeastern Oregon is made up of two lithologically distinctive belts of late Paleozoic and early Mesozoic age. The northernmost belt, herein informally referred to as the Bourne subterrane, consists of slabs and blocks of argillaceous broken formation (Elkhorn Ridge Argillite) that are tectonically intercalated with stratally disrupted slabs and blocks of island-arc rocks and oceanic rocks and chaotic mixed-rock zones. The Elkhorn Ridge Argillite contains limestone olistoliths of Devonian, Pennsylvanian, and Permian age, and ribbon cherts of Permian and Late Triassic (Karnian) age. Permian fusulinids in limestone blocks are mostly of Tethyan affinity. The association of presumably deepwater chert and siliceous argillite with alkalic pillow basalt and ophiolitic mixed-rock zones suggests ocean-floor (nonvolcanic arc) origins for parts of the Bourne subterrane. Intercalated low-K diorite and quartz diorite intrusions, basalt and andesite flows and breccias, tuffs, epiclastic sandstones, and Late Triassic (Norian) bedded limestones are interpreted to be volcanic-arc fragments. The Bourne subterrane includes severely deformed zones similar in appearance to type II and type IV melanges described by Cowan (1985). Deformational style and rock types are consistent with an accretionary wedge setting, as suggested by Coward (1983).

The southern belt, herein informally named the Greenhorn subterrane, is composed mainly of serpentinite-matrix melange that resembles the type III melange described by Cowan (1985). Other components include late Paleozoic clastic sedimentary rocks and basaltic andesite and andesite flows and tuffs. Blocks incorporated within the melanges include both oceanic and island-arc volcanic rocks as well as epidote amphibolites that contain blue amphibole. Permian fusulinids are similar to fusulinids from the Grindstone terrane to the south and the McCloud area in the Klamath Mountains of northern California. The close association of serpentinite-matrix melanges with coarse clastic sedimentary rocks suggests that the Greenhorn subterrane may be part of the outer high of a fore-arc basin as suggested by Mullen (1985).

Lithodemic units in both assemblages are cut by a prominent south-dipping fracture cleavage that apparently developed in conjunction with high-angle reverse and thrust faults. Both the fracture cleavage and the faults appear to have formed during an intense, short-lived period of penetrative deformation that was followed by post-orogenic emplacement of Late Jurassic batholiths and stocks.

INTRODUCTION

The Baker terrane is an eastward-tapering tectonostratigraphic terrane (fig. 9.1) that separates the Grindstone, Izee, and Olds Ferry terranes on the south from the Wallowa terrane on the northeast (Silberling and others, 1984). The Baker terrane includes extensively disrupted late Paleozoic and early Mesozoic ocean-floor (non-arc) and island-arc material that separates the Permian and Late Triassic island-arc volcanic rocks (Brooks and others, 1976; Brooks and Vallier, 1978) of the Wallowa terrane on the northeast from the Late Triassic volcanic rocks and Late Triassic to Late Jurassic clastic sedimentary rocks of the Olds Ferry and Izee terranes on the south (Silberling and

[1]Oregon Dept. of Geology and Mineral Industries, Baker City Field Office, 1831 First Street, Baker City, OR 97814
[2]Present address: 950 11th Street, Baker City, OR 97814

others, 1984). Previous workers suggested that the Baker terrane is part of a paleosuture zone between two separate and distinct volcanic arcs now represented by the Wallowa and Olds Ferry terranes (Dickinson, 1979; Hietanen, 1981; Mortimer, 1986; Blome and Nestell, 1991). These workers generally agree that the Grindstone, Olds Ferry, and Izee terranes represent part of an island-arc system that bordered the continental margin, and that the Baker and Wallowa terranes are more "exotic" ocean-floor and island-arc material initially formed at some distance from the continent. Other workers (including Vallier, chap. 3, this volume) suggest that the Baker terrane is part of a marginal basin developed within a single complex island-arc system.

Detailed mapping (fig. 9.2; see Mullen, 1978; Brooks, Ferns, Coward, and others, 1982; Brooks, Ferns, and Mullen, 1982; Ferns and others, 1987; and Evans, 1988), coupled with geochemical analyses of volcanic rocks (samples and locations listed in table 9.1), faunal

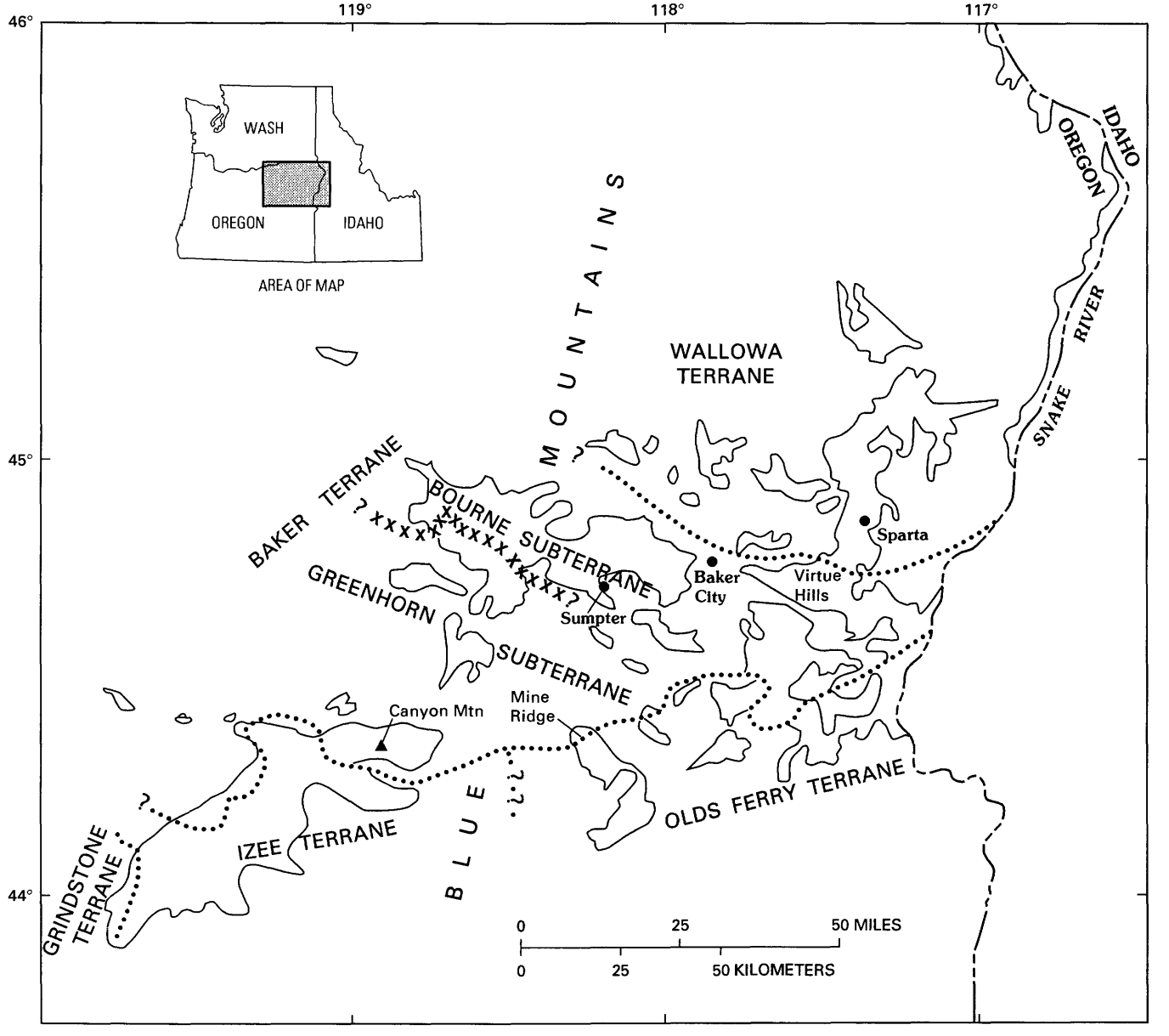

FIGURE 9.1.—Pre-Tertiary terranes in the Blue Mountains province. Terrane names are modified from Silberling and others (1984). Dotted lines, queried where uncertain, are terrane boundaries modified from Silberling and others (1984). Line of x's, queried where uncertain, marks boundary between the Bourne and Greenhorn subterranes (of the Baker terrane) discussed in text. Solid lines outline areas of exposure of pre-Tertiary rocks.

TABLE 9.1.—*Location of samples used for geochemical analyses*

Sample	Subterrane	Unit	1/4	1/4	Section	Township	Range	Elevation (ft)	Quadrangle
EP-105	Bourne	Goodrich Creek unit	NE	NW	28	8 S.	38 E.	6,360	Elkhorn Peak
B-125	Bourne	Goodrich Creek unit	NE	NW	33	8 S.	38 E.	6,600	Elkhorn Peak
B-57	Bourne	Goodrich Creek unit	NE	SE	33	8 S.	38 E.	7,000	Elkhorn Peak
EP-89	Bourne	Goodrich Creek unit	NE	NE	10	9 S.	38 E.	6,500	Elkhorn Peak
EP-102	Bourne	Goodrich Creek unit	NW	NW	19	9 S.	38 E.	5,500	Elkhorn Peak
EP-38	Bourne	Goodrich Creek unit	NE	SW	22	9 S.	38 E.	7,700	Elkhorn Peak
B-27	Bourne	Goodrich Creek unit	SW	NE	23	9 S.	38 E.	7,400	Elkhorn Peak
EP-52	Bourne	Goodrich Creek unit	SE	SE	30	8 S.	38 E.	8,700	Elkhorn Peak
B-90	Bourne	Goodrich Creek unit	NW	NW	1	9 S.	38 E.	4,400	Elkhorn Peak
EP-48	Bourne	Goodrich Creek unit	SW	NE	28	9 S.	38 E.	7,000	Elkhorn Peak
B-261	Bourne	North Fork unit	SW	SW	15	8 S.	35 E.	6,000	Granite
B-259A	Bourne	North Fork unit	SE	SW	15	8 S.	35 E.	5,760	Granite
B-259B	Bourne	North Fork unit	SE	SW	15	8 S.	35 E.	5,760	Granite
153	Bourne	North Fork unit	NE	NW	22	8 S.	35 E.	5,440	Granite
B-289	Bourne	North Fork unit	NE	SE	16	8 S.	35 E.	5,900	Granite
77	Bourne	McCully Fork mixed-rock zone	SW	SW	5	9 S.	36 E.	5,800	Mt. Ireland
MB-45	Bourne	McCully Fork mixed-rock zone	NE	NE	28	9 S.	37 E.	5,000	Bourne
BB-133	Bourne	McCully Fork mixed-rock zone	SE	NW	29	10 S.	39 E.	3,840	Blue Canyon
B-133A	Bourne	McCully Fork mixed-rock zone	SE	NW	29	10 S.	39 E.	3,840	Blue Canyon
B-135B	Bourne	McCully Fork mixed-rock zone	SE	SE	24	10 S.	38 E.	4,160	Blue Canyon
74	Bourne	Olive Creek unit	SW	SE	34	9 S.	35 E.	5,600	Greenhorn
B-364	Greenhorn	Melange of Vinegar Hill	NW	NE	5	10 S.	35 E.	6,320	Bates NE
55	Greenhorn	Melange of Vinegar Hill	SW	SW	5	10 S.	35 E.	7,320	Bates NE
V-1	Greenhorn	Melange of Vinegar Hill	SW	NE	12	10 S.	34 E.	8,000	Bates NE
V-2	Greenhorn	Melange of Vinegar Hill	SW	NE	12	10 S.	34 E.	8,000	Bates NE
V-3	Greenhorn	Melange of Vinegar Hill	SW	NE	12	10 S.	34 E.	8,000	Bates NE
60A	Greenhorn	Melange of Vinegar Hill	SW	NE	16	10 S.	35 E.	6,200	Bates NE
60B	Greenhorn	Melange of Vinegar Hill	NW	NE	16	10 S.	35 E.	6,400	Bates NE
63A	Greenhorn	Melange of Vinegar Hill	SW	SW	9	10 S.	35 E.	6,800	Bates NE
B-372	Greenhorn	Melange of Vinegar Hill	SW	SW	12	10 S.	35 E.	5,600	Greenhorn
185	Greenhorn	Dixie Butte Meta-andesite	NW	NW	35	11 S.	33 E.	4,900	Bates SW
DBV	Greenhorn	Dixie Butte Meta-andesite	NW	NW	33	11 S.	34 E.	6,700	Bates SW
VDB-1	Greenhorn	Dixie Butte Meta-andesite	NE	SW	28	11 S.	34 E.	7,400	Bates SW
VDB-2	Greenhorn	Dixie Butte Meta-andesite	NE	SW	28	11 S.	34 E.	7,400	Bates SW

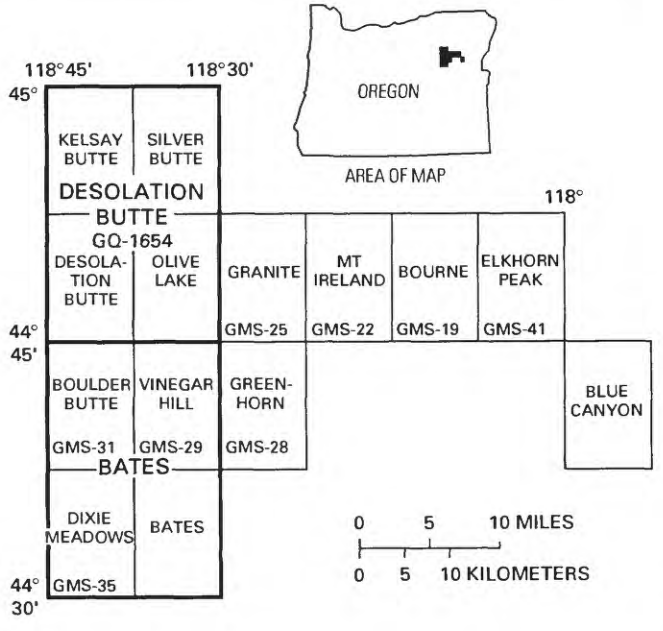

FIGURE 9.2.—Quadrangles mentioned in text, and recently published geologic maps covering central part of Baker terrane. GMS-19, Brooks, Ferns, Coward, and others (1982); GMS-22, Ferns and others (1982); GMS-25, Brooks, Ferns, and Mullen (1982); GMS-28, Ferns and others (1983); GMS-29, Brooks and others (1983); GMS-31, Ferns and others (1984); GMS-35, Brooks and others (1984); GMS-41, Ferns and others (1987); GQ-1654, Evans (1988). Generalized geology of all but Blue Canyon and Bates 7½-minute quadrangles is shown in figure 9.3.

and radiometric ages, and sparse structural data, indicates to us that the Baker terrane consists of two distinct subterranes, herein referred to as the Bourne and Greenhorn subterranes (fig. 9.3). The configuration and composition of the subterranes indicate that the Baker terrane may be a paleosuture zone that contains part of an accretionary wedge (represented by the Bourne subterrane) and a fore-arc high (represented by the Greenhorn subterrane).

BOURNE SUBTERRANE

The main lithologic unit in the Bourne subterrane is the Elkhorn Ridge Argillite (Gilluly, 1937), which is

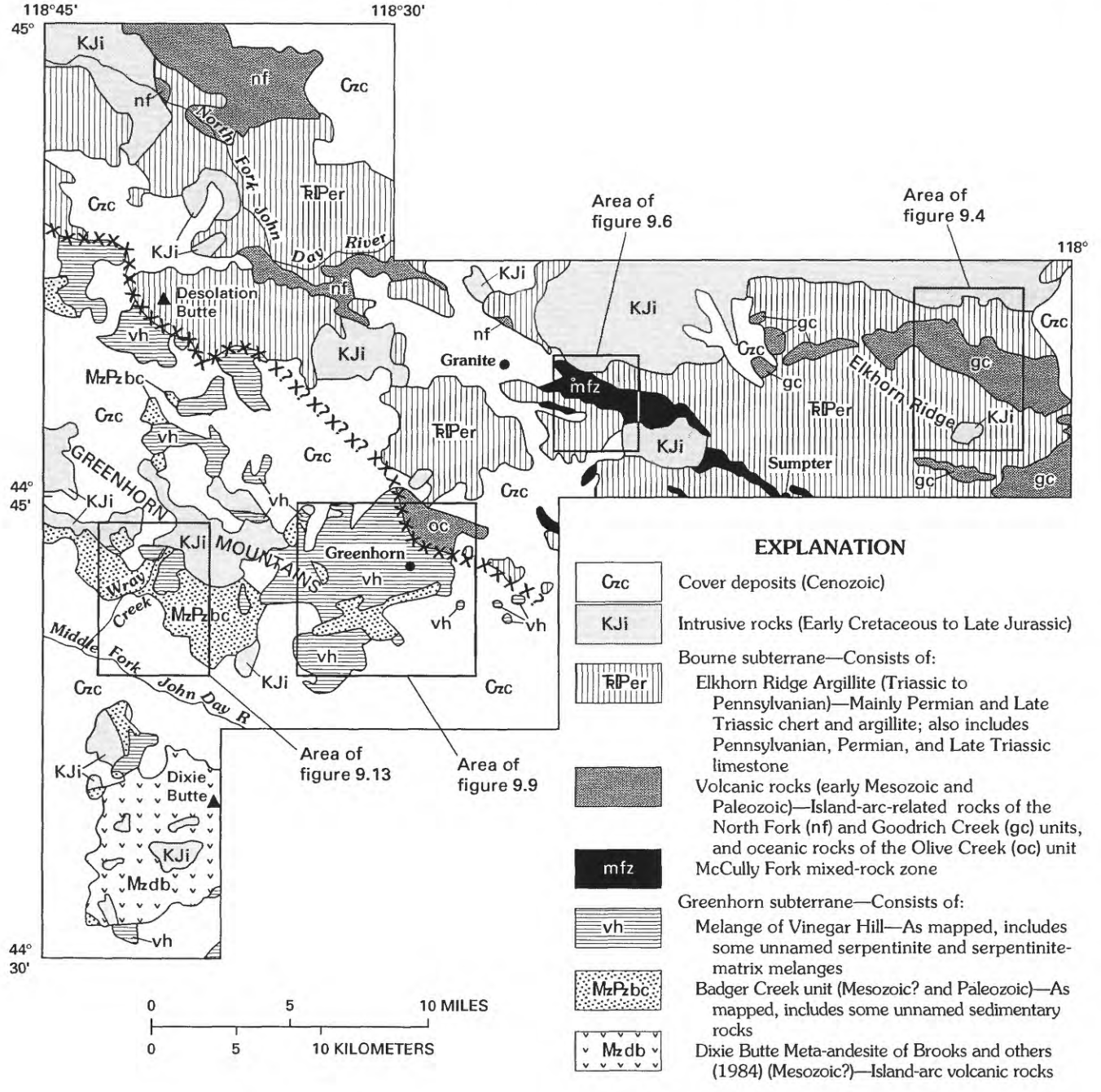

FIGURE 9.3.—Simplified geologic map of central part of Baker terrane. Line of x's, queried where uncertain, marks boundary between the Bourne and Greenhorn subterranes.

TABLE 9.2.—*Melange types and characteristics in the central part of the Baker terrane*

[Modified from Cowan, 1985]

Melange type	Description	Process of formation	Baker terrane examples
Type I ------Stratified sandstone and mudstone sequences.	Broken zones with elongate and lenticular sedimentary blocks formed by layer-parallel extension.	In situ disruption of layered sediments by gravity slides or thrust faults in accretionary prisms.	No examples known.
Type II -----Progressively disrupted sequences of mudstone, tuff, chert, and sandstone.	Grossly layered, stratally disrupted zones subparallel to originally stratigraphic layering formed by layer-parallel extension with local zones of folding and transposition.	Progressive disruption of layered sediments by gravity slides or thrust faults in accretionary prisms.	Elkhorn Ridge(?) Argillite.
Type III ----Block-in-matrix mudstone chaos.	Polymict, chaotically disposed blocks in massive, weakly fissile, or scaly matrix.	Incorporation of exotic blocks in a remobilized matrix as submarine debris flows or as diapirs.	Melange of Vinegar Hill.
Type IV ----Mudstone-dominated brittle fault zones.	Semipenetrative foliation defined by myriad anastomosing subparallel slip surfaces that envelop lenticular tectonic inclusions.	Progressive dismemberment in large fault zones.	McCully Fork mixed-rock zone.

best described as argillaceous broken formation. Discrete, mappable zones of oceanic volcanic rocks (mainly alkalic pillow basalts) and island-arc and intrusive rocks, including low-K tholeiites, calc-alkaline basalts, andesites, dacites, diorites and albite granites, are locally interleaved as tectonic slabs within the Elkhorn Ridge Argillite (see Brooks, Ferns, and Mullen, 1982; Ferns and others, 1987). In this chapter, we use the term "slab" for a coherent, tabular-shaped body of rock and the term "block" for a coherent, equidimensional body of rock.

ELKHORN RIDGE ARGILLITE

The Elkhorn Ridge Argillite (Gilluly, 1937) consists mainly of stratally disrupted, fine-grained siliceous sedimentary rocks (argillite, massive chert, and ribbon chert). On Elkhorn Ridge (fig. 9.3), the unit occurs in thick, southward-dipping fault-bounded packets of pervasively cleaved, dark-colored argillite and chert that contain only minor amounts of intercalated limestone, tuff, sandstone, and conglomerate. Individual packets of the Elkhorn Ridge Argillite are generally coherent, lithologically homogeneous rock masses that are cut by a pervasive fracture cleavage (Coward, 1983). The northernmost exposures form generally coherent rock masses that are considerably less disrupted than exposures to the south and west, where Evans (1986, 1988) recognized a wide crushed area interpreted as a megabreccia zone along the southernmost exposures of the Elkhorn Ridge Argillite. Internal chert and argillite fabrics are nearly obliterated within this and a similar zone mapped in the Granite quadrangle to the east (Brooks, Ferns, and Mullen, 1982).

In gross aspect, the Elkhorn Ridge Argillite is best described as broken formation (after Hsü, 1968). Much of the Elkhorn Ridge Argillite also fits the description of a type II melange (table 9.2; Cowan, 1985), consisting of stratigraphically continuous zones of isoclinally folded chert and argillite that are bounded by either faults or cataclasite zones (Coward, 1983).

ROCK TYPES

The Elkhorn Ridge Argillite consists mainly of dark-colored siliceous argillite, argillite, and chert. Carbonaceous argillite, feldspar-bearing tuffaceous argillite, and ribbon chert are locally abundant, whereas sandstone and conglomerate are rare. Most of the Elkhorn Ridge Argillite consists of massive, homogeneous outcrops of blocky argillite in which bedding features are generally absent. Chert and metachert are present as

both coherent and dismembered strata, with individual chert beds 5 to 10 cm thick. Chert boudins and pseudoconglomerates, that is, broken elongate lenses of chert in sheared dark argillite (Pardee and Hewett, 1914), are present where chert and argillite are interbedded.

Limestone is generally not common in the central part of the Baker terrane; however, large elongate limestone masses up to 1,000 m in length are present in several limestone-rich zones in the Elkhorn Peak quadrangle (Ferns and others, 1987). Both individual limestone pods and limestone-rich zones parallel the regional strike of the enclosing fault-bounded chert and argillite packages (fig. 9.4). Very little limestone is associated with the Elkhorn Ridge Argillite west of Elkhorn Ridge. Margins of some limestone lenses on Elkhorn Ridge are marked by limestone-clast breccias. Oolites, peloids, and fossil detritus in some of the limestone masses indicate shallow-water deposition (Coward, 1983). Because the limestones are now enclosed in presumably deepwater siliceous sediments, the limestones are interpreted as olistoliths that formed as shallow-water bioherms and were subsequently transported with the limestone breccias as carbonate slide blocks into the enclosing deepwater sediments (Coward, 1983).

AGE

Devonian, Pennsylvanian, and Permian limestones are enclosed within the Elkhorn Ridge Argillite. Evans (1988) and Morris and Wardlaw (1986) reported a Devonian conodont from a small limestone block in the Desolation Butte area. According to Coward (1983), the limestone masses on the east end of Elkhorn Ridge are Pennsylvanian and Permian in age. Permian fusulinids include *Yabeina* sp., *Cuseneallа* sp., *Neoschwagerina* sp., and *Pseudoliolina* sp. and are considered to be a Tethyan fauna (Coward, 1983; Nestell, 1983). Similar Tethyan fusulinids are reported from the Virtue Hills area east of Baker City, Oreg. (fig. 9.1), where limestone of Pennsylvanian, Permian, and Late Triassic ages have been identified (C.D. Blome and M.K. Nestell, written commun., 1987), whereas a fusulinid assemblage similar to those in the Grindstone terrane and the McCloud area in northern California is reported south of Sumpter, Oreg. (Bostwick and Koch, 1962).

Recent collections by C.D. Blome (Ferns and others, 1987) indicate that cherts in the Bourne subterrane are Permian and Late Triassic in age, although Coward (1983) reported radiolarians (*Canoptum* sp.) possibly as young as Early Jurassic from cherts south of Elkhorn Ridge. Blome has identified six localities in the Elkhorn Peak quadrangle (Ferns and

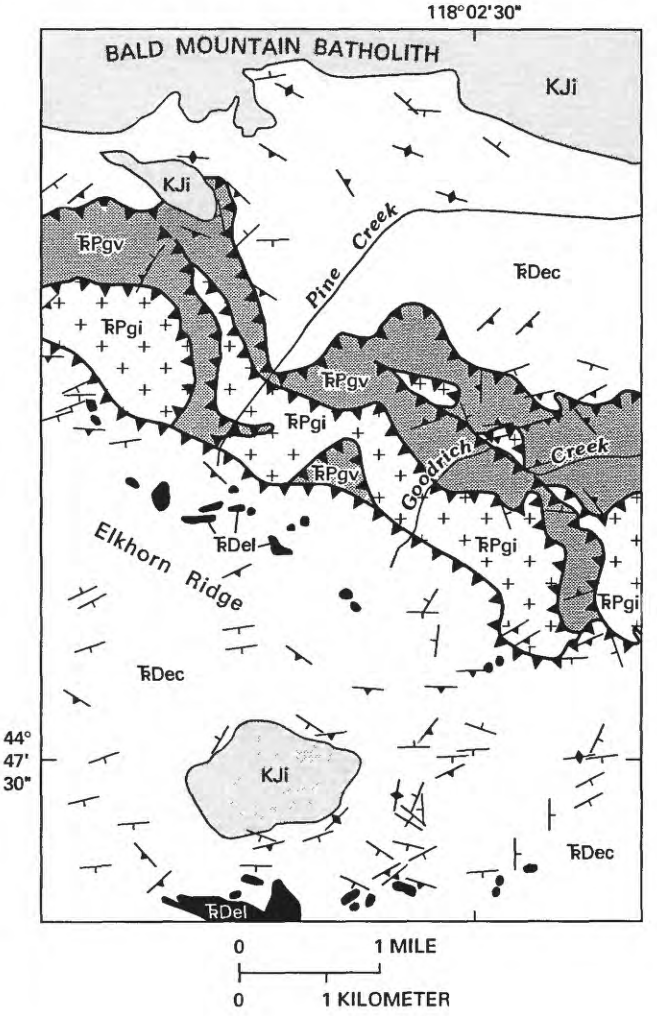

FIGURE 9.4.—Geologic map of the Elkhorn Ridge area. Shows contact relations between the Elkhorn Ridge Argillite and intrusive and volcanic and sedimentary rocks on Goodrich Creek. Note imbricate thrust faults separating rock types on Goodrich Creek (modified from Ferns and others, 1987).

others, 1987) that contain Late Triassic (Karnian) radiolarians, including one locality adjacent to a Permian fusulinid-bearing limestone lens; he has also identified one locality that contains late Paleozoic radiolarians. Similar chert outcrops east of Baker City also are Permian and Late Triassic in age (Blome and others, 1986).

METAMORPHISM, STRUCTURE, AND CONTACT RELATIONSHIPS

Metamorphic mineral assemblages are not easily recognized in the fine-grained argillite and chert. Coarser grained clastic rocks contain low-grade mineral assemblages typical of greenschist-facies conditions, including biotite+chlorite+white mica (Evans, 1986) and white mica+chlorite+quartz (Kays and others, 1987). Argillite and chert have locally been converted to coarser grained biotite and biotite-garnet schists within thermal aureoles of Late Jurassic and Early Cretaceous intrusions.

GOODRICH CREEK AND NORTH FORK UNITS

Disrupted, southward-dipping masses of metamorphosed intrusive, extrusive, and sedimentary rocks of probable island-arc origin are tectonically intercalated with the Elkhorn Ridge Argillite in the northernmost exposures of the Bourne subterrane (Stimson, 1980; Brooks, Ferns, Coward, and others, 1982; Brooks, Ferns, and Mullen, 1982; Evans, 1986, 1988; Ferns and others, 1987). The two main areas of island-arc volcanic rocks are herein referred to as the North Fork and Goodrich Creek units. The North Fork unit consists of andesitic flows and volcaniclastic rocks and intrusive rocks that crop out along the North Fork of the John Day River west of Granite, Oreg. (fig. 9.3) (Brooks, Ferns, and Mullen, 1982; Evans, 1986). Similar volcaniclastic rocks, siliceous tuffs, lava flows, and intrusive rocks are tectonically intercalated with slabs of the Elkhorn Ridge Argillite on Elkhorn Ridge and are well exposed along Goodrich Creek (fig. 9.4) (Stimson, 1980; Brooks, Ferns, Coward, and others, 1982; Coward, 1983; Ferns and others, 1987). Both the North Fork and the Goodrich Creek units are separated from adjacent overlying and underlying slabs of Elkhorn Ridge Argillite by generally low-angle, southward-dipping reverse or thrust faults.

ROCK TYPES

Gray calcareous argillite, sandstone, dark-gray impure argillaceous limestone, and white and blue keratophyre tuff and tuff breccia are complexly interlayered with limestone, argillite, basalt, and andesite flows, all of which are in thrust contact with intrusive rocks. The volcaniclastic rocks include siliceous tuff, quartz keratophyre, tuff, and calcareous wacke. Intrusive rocks include mainly equigranular diorite and subordinate quartz diorite, albite granite, and foliated hornblende gabbro, all of which are similar to the intrusions described by Gilluly (1937). Coarse-grained pyroxenite and hornblende pegmatite are rare. Serpentinite and its metamorphic derivatives are notably scarce, present only as widely separated, narrow serpentinitic or talcose selvages along faults and within narrow, discontinuous mixed-rock or brittle fault zones similar to type IV melanges (table 9.2; Cowan, 1985). Individual beds cannot be traced for more than 100 m. Unlike the argillites in the Elkhorn Ridge Argillite, the sediments in the Goodrich Creek unit locally preserve sedimentary structures, including graded bedding and flame structures. Much of the Goodrich Creek unit consists of widespread, apparently randomly oriented cataclasite zones.

Cataclasite zones generally obscure contacts between intrusive and volcanic or volcaniclastic rocks; however, small exposures of amphibolite along contacts in the Goodrich Creek area may be relicts of contact aureoles between greenstones and diorite intrusions. Strongly deformed hornblende gabbros are cut by equigranular hornblende diorites that are in turn cut by quartz diorite and albite granite masses. The quartz diorite and albite granite masses locally intrude volcanic and sedimentary rocks.

Intrusive rocks are separated by faults from the volcanic and volcaniclastic rocks. The imbricate nature of these faults is well demonstrated on the high ridge northwest of Pine Creek (fig. 9.4) where a 400-m-thick sequence of tuff breccia, argillite, and argillaceous limestone is tectonically overlain and underlain by southward-dipping fault slices of diorite (Ferns and others, 1987).

GEOCHEMISTRY

Andesite is the most abundant volcanic rock type on the North Fork of the John Day River. Major-element geochemistry (table 9.3) suggests that most if not all of the Goodrich Creek and North Fork volcanic flow rocks formed in an island-arc environment. Generally, the basaltic rocks have low TiO_2 contents and low K_2O contents (table 9.3) typical of low-K tholeiites. Mullen (1985) concluded that North Fork rocks have an island-arc origin on the basis of their relatively high SiO_2 contents (53–55 percent), low TiO_2 contents, depleted light rare-earth elements, and position within the destructive margin field on the Hf/3-Th-Ta plot of Wood and others (1979). Calder (1986)

TABLE 9.3.—*Major-element data for greenstones from the Bourne subterrane*

[Values in weight percent. All analyses recalculated to 100 percent on a volatile-free basis. n.d., not determined]

Unit	Volcanic rocks										
	Olive Creek unit	McCully Fork mixed-rock zone					Goodrich Creek unit				
Sample	[1]74	[2]B-135B	[3]BB-133	[3]MB-45	[1]77	[2]B-133A	[1]B-57	[1]EP-105	[1]EP-89	[1]B-27	[1]EP-38
SiO_2	46.27	51.39	51.63	52.14	53.18	53.50	49.66	49.76	51.92	50.32	53.40
Al_2O_3	16.00	17.55	16.52	17.18	16.45	14.14	18.24	16.63	14.18	18.22	17.54
TiO_2	1.75	1.43	1.30	0.84	1.00	1.11	1.19	1.70	1.67	1.22	1.16
FeO*	10.22	7.12	5.45	8.95	9.20	6.93	10.23	10.36	11.21	10.21	9.35
MnO	0.13	0.16	0.15	0.15	0.16	0.13	0.17	0.18	0.18	0.15	0.19
CaO	15.30	11.95	14.69	10.37	8.54	13.95	11.37	12.31	10.49	9.97	9.37
MgO	4.88	6.80	6.69	6.78	7.39	6.19	6.51	6.52	7.46	4.26	4.45
K_2O	0.38	0.25	0.17	0.10	0.02	0.29	0.14	0.06	0.02	1.57	0.00
Na_2O	4.80	3.27	3.26	3.36	3.95	3.64	2.30	2.31	2.69	3.38	4.33
P_2O_5	0.30	0.18	0.13	0.11	0.10	0.12	0.19	0.17	0.18	0.70	0.21
H_2O^+	n.d.	2.35	n.d.	n.d.	n.d.	2.13	n.d.	n.d.	n.d.	n.d.	n.d.
H_2O^-	n.d.	0.38	n.d.	n.d.	n.d.	0.12	n.d.	n.d.	n.d.	n.d.	n.d.
CO_2	n.d.	0.17	n.d.	n.d.	n.d.	1.51	n.d.	n.d.	n.d.	n.d.	n.d.

Unit	Volcanic rocks—Continued						Plutonic rocks			
	Goodrich Creek unit—Continued		North Fork unit				Goodrich Creek unit			North Fork unit
Sample	[1]EP-102	[1]B-125	[1]B-259A	[1]B-259B	[1]153	[1]B-261	[1]B-90	[1]EP-52	[1]EP-48	[1]B-289
SiO_2	55.19	57.30	58.29	62.28	74.07	75.63	55.87	58.80	74.07	64.48
Al_2O_3	14.20	18.64	18.33	15.66	14.75	14.15	15.16	20.05	13.81	16.62
TiO_2	0.96	1.01	1.27	0.93	0.36	0.43	0.70	0.93	0.61	0.67
FeO*	9.49	7.54	10.74	9.02	2.46	2.25	9.07	6.57	3.52	5.99
MnO	0.17	0.13	0.06	0.06	0.04	.05	0.18	0.10	0.07	0.13
CaO	10.64	6.27	2.23	4.72	2.22	0.15	7.97	4.90	2.56	6.52
MgO	6.59	3.97	5.73	4.20	1.35	1.53	7.32	2.88	0.65	2.24
K_2O	0.04	1.75	0.27	0.15	1.19	3.52	0.49	0.79	0.10	0.03
Na_2O	2.61	3.23	2.80	2.70	3.47	2.23	3.17	4.73	4.49	3.22
P_2O_5	0.10	0.18	0.17	0.26	0.08	0.03	0.07	0.24	0.11	0.10
H_2O^+	n.d.	n.d.	n.d.	n.d.	n.d.	n.d.	n.d.	n.d.	n.d.	n.d.
H_2O^-	n.d.	n.d.	n.d.	n.d.	n.d.	n.d.	n.d.	n.d.	n.d.	n.d.
CO_2	n.d.	n.d.	n.d.	n.d.	n.d.	n.d.	n.d.	n.d.	n.d.	n.d.

[1]Sample analyzed by X-ray fluorescence at Washington State University, Pullman, Wash.
[2]Sample analyzed by X-ray fluorescence at U.S. Geological Survey, Menlo Park, Calif.
[3]Sample analyzed by atomic absorption at University of Oregon, Eugene, Oreg.

presented trace-element data that suggest that Goodrich Creek greenstones also include low-K island-arc tholeiites.

Coarse-grained plutonic rocks have major-element contents (table 9.3) similar to those of rocks in the (informal) Sparta complex of Phelps (1979) (fig. 9.5), which are considered to be genetically related to the overlying volcanic rocks of the Wallowa arc (Almy, 1977; Phelps, 1979; Avé Lallemant and others, 1980). Analyzed flows from both the Goodrich Creek and the North Fork units are similar to Wallowa arc rocks in that they have low amounts of K_2O and TiO_2. High-

silica intrusive rocks in the North Fork and Goodrich Creek units are high in Na_2O and low in K_2O content, which in part may reflect mobilization of these oxides during metamorphism.

AGE AND CORRELATIONS

Available radiometric data indicate that the volcanic-arc rocks are about the same age, Permian and Late Triassic, as the adjoining fine-grained siliceous sedimentary rocks of the Elkhorn Ridge Argillite. An Early Triassic low-K quartz diorite intrusion from the North Fork of the John Day River has yielded a U-Pb zircon age of 243 Ma (Brooks, Ferns, and Mullen, 1982; Walker, 1983). Intruded greenstones are therefore earliest Triassic or older in age. Limestones interbedded with pyroclastic rocks on Goodrich Creek contain Late Triassic (Norian) conodonts (Wardlaw, written commun., 1986; Ferns and others, 1987). These data, although sparse, suggest earliest Triassic or older volcanism, followed by emplacement of earliest Triassic plutons, in turn followed by renewed pyroclastic volcanism and limestone deposition in the Norian.

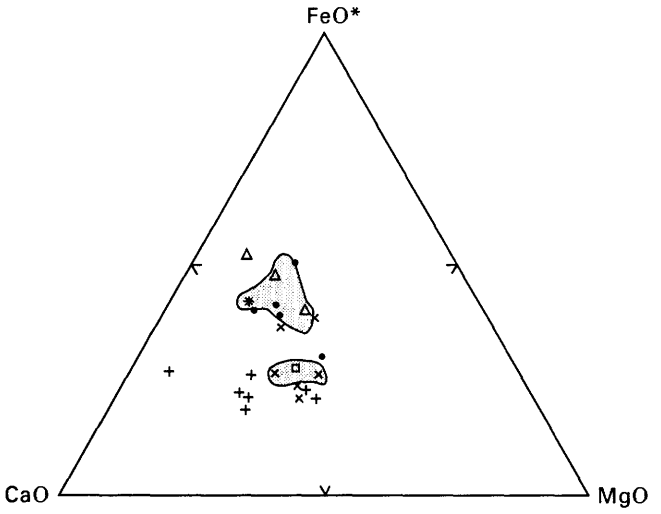

EXPLANATION

Baker terrane—
Bourne subterrane—
Goodrich Creek unit
△ 3 ODGMI analyses
• 5 analyses by Stimson (1980)
North Fork unit
✱ 1 ODGMI analysis
Greenhorn subterrane—
Melange of Vinegar Hill
▫ 1 ODGMI analysis
× 6 analyses by Hunt (1985)
+ 7 analyses by Mullen (1978)

FIGURE 9.5.—FeO*-CaO-MgO diagram of analyzed metamorphosed intrusive rocks from central part of Baker terrane. Shaded fields are from 24 analyses by Almy (1977) and Phelps (1978, 1979) of the (informal) Sparta complex of Phelps (1979). Baker terrane data are from table 9.4 and from master's theses by Mullen (1978), Hunt (1985), and Stimson (1980). ODGMI, Oregon Department of Geology and Mineral Industries.

METAMORPHISM

Mineral assemblages outside the thermal aureoles of the Late Jurassic intrusions are generally typical of greenschist-facies conditions. In the greenstones, metamorphic assemblages include actinolite+albite+epidote+chlorite+calcite, epidote+albite+chlorite+calcite, and chlorite+actinolite+albite+calcite. One foliated sample from a fault zone on the east end of Elkhorn Ridge contains stilpnomelane.

OLIVE CREEK UNIT

Alkalic pillow basalt (Mullen, 1982, 1985) and intercalated felsic tuff, volcanic breccia, limestone lenses, and contorted ribbon chert are exposed along Olive Creek about 2 km north of Greenhorn, Oreg. (figs. 9.3, 9.9). The volcanic rocks are tectonically interleaved with slices and slivers of metamorphosed intrusive rocks and chert and argillite of the Elkhorn Ridge Argillite (Ferns and others, 1983) near what we interpret as the southern margin of the Bourne subterrane. The Olive Creek volcanic rocks and the cherts and intrusive rocks appear to be components of a slab melange in which little or no matrix is present. Individual slabs are large elongate masses, as much as 2,400 m in length.

PILLOW LAVA GEOCHEMISTRY

Mullen (1978, 1982, 1985) identified relict titaniferous clinopyroxenes in the Olive Creek pillow lavas; such clinopyroxenes are typical of alkalic basalts. The pillow lavas' major-element contents, including high TiO_2 contents (table 9.3), are also indicative of alkalic basalts (Mullen, 1978, 1982; Ferns and others, 1983). Rare-earth-element data presented by Mullen (1985) are consistent with the pillow lavas originating in an intra-plate or seamount setting.

AGE

Rocks of the Olive Creek unit are apparently Permian and Late Triassic in age. Dickinson and Thayer (1978) reported Permian conodonts from ribbon chert in the Olive Creek area. C.D. Blome (written commun., 1987) identified Late Triassic radiolarians from contorted ribbon chert exposed along Olive Creek. Early Permian (Leonardian) conodonts were reported by Mullen (1978) from a limestone lens encased in mafic tuff and pillow lava exposed in a small pre-Tertiary inlier east of Olive Creek.

METAMORPHISM

Pillow lava samples usually retain relict igneous textures. Massive greenstones are nonschistose and contain typical greenschist-facies mineral assemblages. Mafic phenocrysts are partially replaced by felted mats of chlorite, epidote, and (or) actinolite (Mullen, 1978). Regional metamorphic mineral assemblages include chlorite+albite+epidote and chlorite+albite+actinolite.

MIXED-ROCK ZONES

The term "mixed-rock zone" is used (Brooks, Ferns, Coward, and others, 1982; Ferns and others, 1982, 1983; Ferns and Ramp, 1988) to describe mappable lithodemic units in which individually unmappable (at a reasonable scale) slabs and slices of diverse rock types are juxtaposed. These zones often contain relatively small slices and anastomosing lenses of intervening serpentinite-matrix melange and are similar in overall appearance to the slab melange described by Robertson and Woodcock (1983) in the Batinah melange in Oman. The mixed-rock zones are analogous to the brittle fault zones or type IV melanges of Cowan (1985; table 9.2). The zones are composed of elongate, lensoid slices of diverse rock types such as argillite, greenstone, serpentinite, and metaserpentinite, all of which are bounded by faults generally parallel to the dominant foliation or cleavage.

The McCully Fork mixed-rock zone (figs. 9.3, 9.6) is the largest mixed-rock zone in the Bourne subterrane. This northwest-trending zone is traceable for about 18 km along strike and ranges from a few hundred meters to 3,200 m in width. It is composed of randomly juxtaposed slices and blocks of argillite, serpentinite, pyroxenite, gabbro, diorite, quartz diorite, basalt, volcaniclastic breccia and conglomerate, limestone, and chert that are locally separated by ultramafic melange zones containing from about 10 to 70 percent matrix (Ferns and Ramp, 1988). Individual slices outside the melange zones are elongate parallel to the northwesterly strike of the McCully Fork mixed-rock zone and seldom reach more than 150 m in width and 1,000 m in length. Blocks within the melange zones are equidimensional, ranging from 1

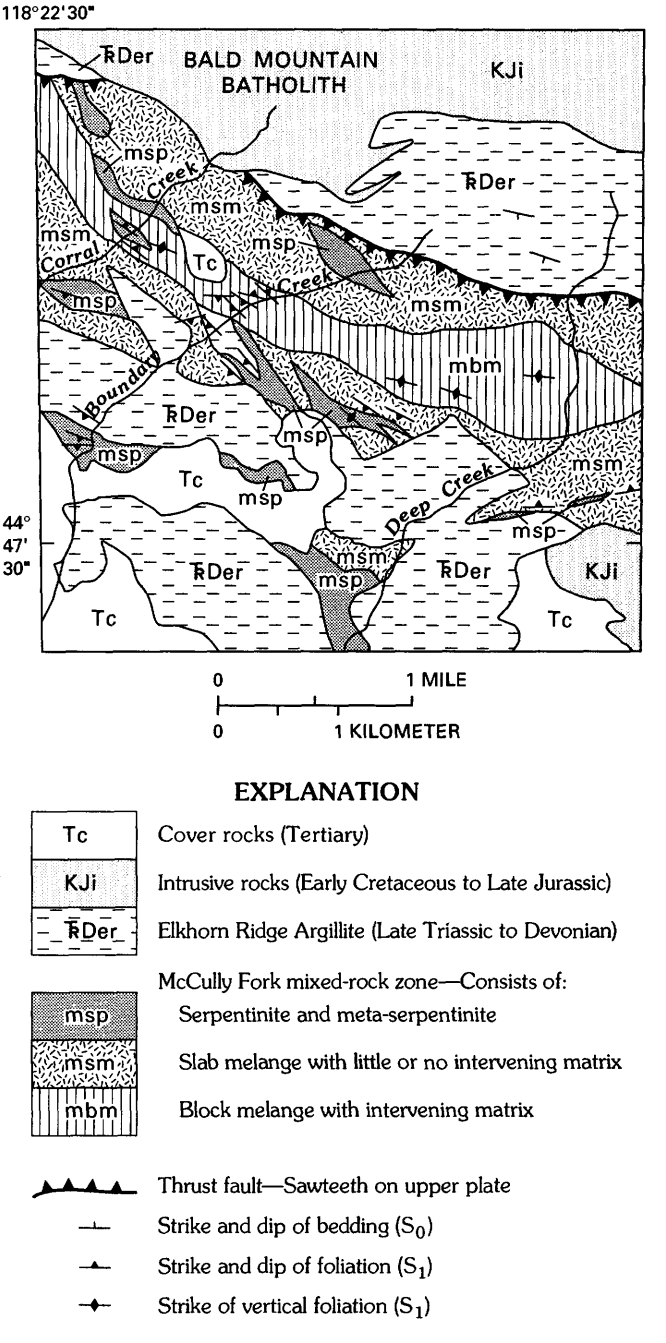

FIGURE 9.6.—Geologic map of McCully Fork mixed-rock zone east of Sumpter, Oreg. (modified from Ferns and others, 1982, and Ferns and Ramp, 1988).

TABLE 9.4.—*Trace-element data for greenstones from the central part of the Baker terrane*

[Values in parts per million. All samples analyzed at U.S. Geological Survey, Menlo Park, Calif. Samples VDB-1 and VDB-2 analyzed by X-ray fluorescence, all others by instrumental neutron activation analysis. ---, not determined or below instrumental detection limit]

	Bourne subterrane		Greenhorn subterrane				
Unit	McCully Fork mixed-rock zone		Melange of Vinegar Hill			Dixie Butte Meta-andesite	
Sample	B-133A	B-135B	V-1	V-2	V-3	VDB-1	VDB-2
Rb	2	4	13	10	21	20	20
Sr	223	162	373	172	188	230	230
Ba	32	56	677	189	99	320	60
Th	0.5	0.9	2.61	0.50	0.96	---	---
U	---	---	0.73	0.45	0.59	---	---
La	7	11	22.5	3.54	10.4	20	20
Ce	15	20	44.7	.0	1.6	5	0
Sm	---	---	6.3	---	4.0	---	---
Eu	1.04	1.17	1.70	0.89	1.31	---	---
Gd	3.2	3.9	5.5	---	---	---	---
Tb	0.71	0.65	0.85	0.70	0.70	---	---
Tm	---	---	0.42	---	--	---	----
Yb	2.5	2.1	2.26	3.42	2.41	---	---
Lu	0.41	0.32	0.33	0.52	0.37	---	---
Y	23	22	27	30	26	15	25
Zr	95	97	212	60	133	110	170
Hf	2.3	2.2	4.74	1.54	2.89	---	---
Ta	0.48	0.84	1.75	---	0.72	---	---
Nb	7	13	25	9	16	<10	10
Ni	96	73	---	---	---	---	---
Co	37	36	47	57	66	---	---
Cr	310	121	295	320	679	---	---
Sc	34.8	33.9	20.8	61.6	32.6	---	---
Zn	72	75	100	134	104	---	---

to 40 m in diameter, and consist mainly of greenstone, but also include basalt, pyroclastic breccias, metagabbro, and metadiorite.

Serpentinite- and metaserpentinite-matrix melanges are best developed in the center of the McCully Fork mixed-rock zone where it widens east of Granite, Oreg. A high-angle reverse fault separates the mixed-rock zone from the structurally underlying Elkhorn Ridge Argillite to the north (Brooks, Ferns, Coward, and others, 1982; Ferns and others, 1982). Thin mylonite zones in the underlying Elkhorn Ridge Argillite strike parallel to the faults. The contact between the McCully Fork mixed-rock zone and the overlying Elkhorn Ridge Argillite to the south is a diffuse zone of intercalated slices of argillite and serpentinite. Unusually coarse grained sedimentary rocks, including chert-pebble conglomerate and graywacke interbedded with small limestone lenses, locally crop out along the southern contact zone. The Late Jurassic Bald Mountain batholith intrudes the contact and has converted the serpentinite matrix of the melange zones to a variety of metaserpentinites, including talc- and enstatite-olivinites (Ferns and Ramp, 1988).

GEOCHEMISTRY

Ophiolitic components of the mixed-rock zones include serpentinite, gabbro, basalt, and chert. Basalts (table 9.3) are low-K tholeiites that are slightly enriched in light rare-earth elements (table 9.4). Some basalts are similar to the low-K tholeiites of the Goodrich Creek unit (low K_2O and moderate Na_2O contents). The mixed-rock-zone basalts have generally lower FeO* (total iron as FeO) contents than the Goodrich Creek and North Fork rocks. Oceanic affinities are suggested by various trace-element plots, including the Ti-Zr-Y plot (fig. 9.7) and the Hf-Ta-Th plot (fig. 9.8).

METAMORPHISM

Most of the rocks within the mixed-rock zones have been recrystallized by Late Jurassic intrusions. Metamorphic zonation around the Bald Mountain batholith is well evidenced in the metaserpentinites that grade from enstatite-olivine rock outward through talc-amphibole and talc-carbonate rock into antigorite-carbonate rock (Ferns and Ramp, 1988). Metamorphic mineral assemblages in greenstones outside the thermal aureoles are typical albite-epidote facies assemblages (epidote + chlorite + albite + calcite and epidote + chlorite + albite + actinolite + calcite).

GREENHORN SUBTERRANE

Serpentinite-matrix melange, best exposed at Vinegar Hill (see fig. 9.9), is the main unit in the Greenhorn subterrane. Other major Greenhorn subterrane units include the clastic-rich Badger Creek unit and volcanic rocks of the Dixie Butte Meta-andesite of Brooks and others (1984) (fig. 9.3).

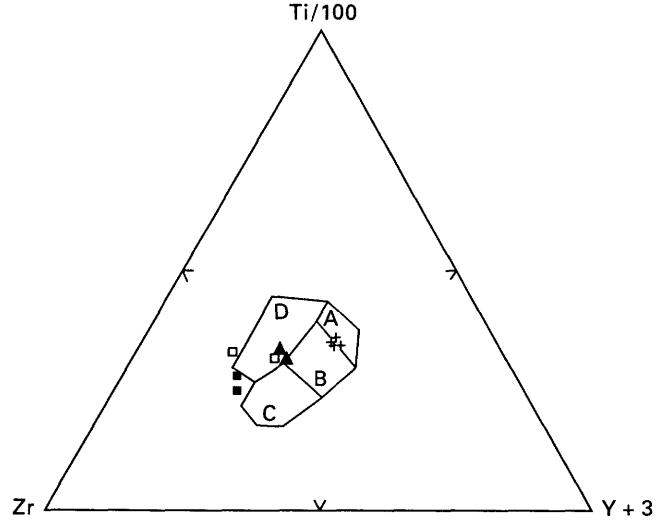

FIGURE 9.7.—Triangular diagram of Ti-Zr-Y contents in greenstones from central part of Baker terrane. Bourne subterrane samples include samples of Goodrich Creek unit (crosses) from Calder (1986) and samples from McCully Fork mixed-rock zone (triangles). Greenhorn subterrane samples are from the melange of Vinegar Hill (open squares) and from the Dixie Butte Meta-andesite of Brooks and others (1984) (solid squares). Fields from Pearce and Cann (1973): A, ocean-island and continental basalts; B, calc-alkaline basalts; C, ocean-floor basalts, low-K tholeiites, and calc-alkaline basalts; D, low-K tholeiites.

BADGER CREEK UNIT

Greenhorn subterrane supracrustal rocks include Paleozoic and possibly Mesozoic clastic sedimentary rocks previously informally referred to as undivided sedimentary rocks (JPu) by Brown and Thayer (1966), the Badger Creek unit by Wheeler (1976) and Mullen (1978), and clastic sedimentary rocks (PPa) by Ferns and others, (1983). In this chapter, we use the name "Badger Creek unit" (Wheeler, 1976; Mullen, 1978).

ROCK TYPES

The Badger Creek unit includes sedimentary rocks made up chiefly of fine- to medium-grained calcareous sandstone, chert-pebble conglomerate, tuff, limestone lenses, argillite, and polymict breccia that have been folded and pervasively sheared. Although the Badger Creek unit is discontinuously exposed over an area of about 155 km^2, extensive Tertiary cover has prevented the determination of its stratigraphic relationships.

Sedimentary features such as graded bedding and flame structures are locally preserved in fine-grained calcareous sandstone and argillite. In some places inverted graded bedding suggests that the sandstones are locally overturned. Conglomerate units contain well-rounded clasts of sandstone, chert, argillite, and andesite, as well as detrital quartz and feldspar grains. Chert-pebble conglomerates locally fill channels cut down into argillite and sandstone. Chert pebbles are

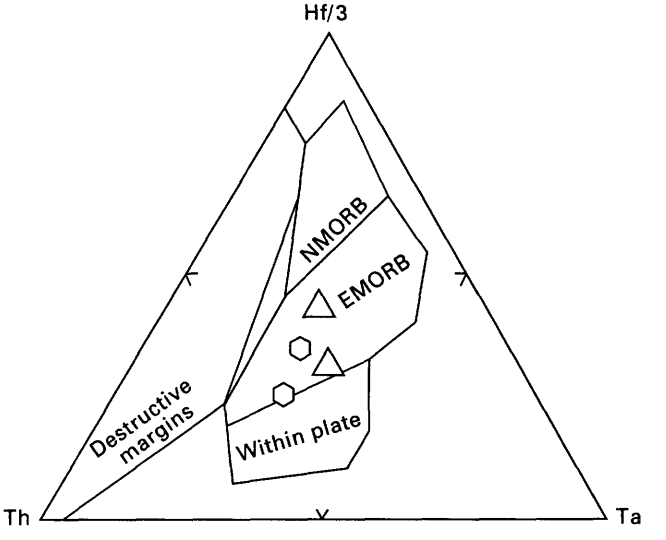

FIGURE 9.8.—Triangular diagram of Hf/3-Ta-Th contents in greenstones from central part of Baker terrane. Bourne subterrane (triangles) and Greenhorn subterrane (hexagons) samples and localities listed in tables 9.1 and 9.4. Fields from Wood and others (1979). NMORB, normal midocean-ridge basalts; EMORB, evolved midocean-ridge basalts.

well rounded and typically range from 1 to 5 cm in diameter. In some areas, such as east of Vinegar Hill (Brooks and others, 1983), conglomerate beds are carbonate cemented and contain crinoidal debris. These chert-pebble conglomerate beds are interbedded with 1- to 25-m-thick fossiliferous limestone lenses, which, at Vinegar Hill, contain Pennsylvanian conodonts (Morris and Wardlaw, 1986).

Polymict breccias occur in the Badger Creek unit near its contact with the underlying melange of Vinegar Hill. Clasts are subangular to subrounded and include metamorphosed intrusive rocks, greenstones, and chert. Clasts are up to 12 cm in diameter and occur in both argillaceous matrix-supported and clast-supported breccias. Distinctive lineated gabbro clasts appear to be derived from immediately adjacent gabbro blocks within the underlying melange. Serpentinite-matrix and talc-matrix sedimentary breccias (Ferns and Ramp, 1988), although rare, are important because they indicate sporadic introduction of ultramafic olistostromes as the Badger Creek unit was being deposited.

AGE AND FAUNAL CORRELATIONS

Pennsylvanian, Permian, and Late Triassic(?) faunas have been reported from the Badger Creek unit. Pennsylvanian (Desmoinesian) conodonts were identified from a limestone pod interbedded with chert-pebble conglomerate on the east flank of Vinegar Hill (Morris and Wardlaw, 1986). Both Permian conodonts and fusulinids have been identified in a limestone pod west of Granite Boulder Creek (see fig. 9.13) (Mullen, 1978). Permian (Guadalupian) radiolarians have been found in siliceous interbeds in sandstone and siltstone on Granite Boulder Creek near the fusulinid locality (Ferns and others, 1984; Blome and others, 1986), indicating that the limestones here are not olistoliths of older Paleozoic material incorporated into a younger Mesozoic strata.

Fusulinids include *Pseudofusulinella* and *Schwagerina* (Mullen, 1978). Nestell (oral commun., 1986) suggested that the fusulinid assemblage of the Badger Creek unit is similar to those from the McCloud area in the Klamath Mountains of northern California and is different from most of the Tethyan fusulinid assemblages found in similar-aged limestones in the Elkhorn Ridge Argillite in the Bourne subterrane.

The Badger Creek unit may include Mesozoic (Late Triassic?) sediments as evidenced by poorly preserved cone-shaped radiolarians (Blome, oral commun., 1983) collected from green chert beds along a depositional contact with underlying melange south of the town of Greenhorn (Ferns and others, 1982). This chert separates the melange of Vinegar Hill from a coarse polymict breccia that contains clasts derived from blocks within the melange.

METAMORPHISM

Most of the outcrop area of the Badger Creek unit lies within thermal aureoles of Late Jurassic to Early Cretaceous intrusions. Sedimentary rocks outside of the aureoles are poorly recrystallized and lack recognizable metamorphic fabrics. The typically observed metamorphic mineral assemblage of epidote+actinolite+chlorite+ albite would be characteristic of either low-grade regional or low-grade contact metamorphism.

MELANGE OF VINEGAR HILL

The northernmost unit of the Greenhorn subterrane is the serpentinite-matrix melange of Vinegar Hill (fig. 9.9). This melange is exposed over an area of about 180 km^2 in the Greenhorn Mountains and is separated from units of the Bourne subterrane by a major, southward-dipping high-angle reverse or thrust fault (Ferns and others, 1983; Evans, 1988). The melange of Vinegar Hill is composed of mafic plutonic and volcanic rocks, silicic volcanic rocks, chert, and argillite in irregularly shaped blocks ranging from 2 m to more than 3 km in length, which are encased in a serpentinite matrix that makes up over 50 percent of the unit. Blocks include monolithologic greenstone, gabbro, and argillite and heterolithologic blocks made up of intrusive, extrusive, and sedimentary rocks that occasionally retain primary depositional and (or) intrusive contacts. The melange of Vinegar Hill is analogous to the type III melange of Cowan (1985) in that diverse rock types are apparently randomly arrayed as blocks in a chaotic, fine-grained matrix. Some of the blocks are cut by narrow schistose serpentinite veins that appear similar to those described in the Kaweah belt in California by Saleeby (1979), which document the rafting apart of the greenstones as serpentinite was injected. Metasomatic reaction rinds (rodingite) occur only along the margins of the gabbro blocks. Since rodingites form during serpentinization (Coleman, 1963), the lack of metasomatic reaction rinds in the greenstones suggests that the greenstones were incorporated into the melange after initial serpentinization, presumably as the serpentinite was injected along fractures.

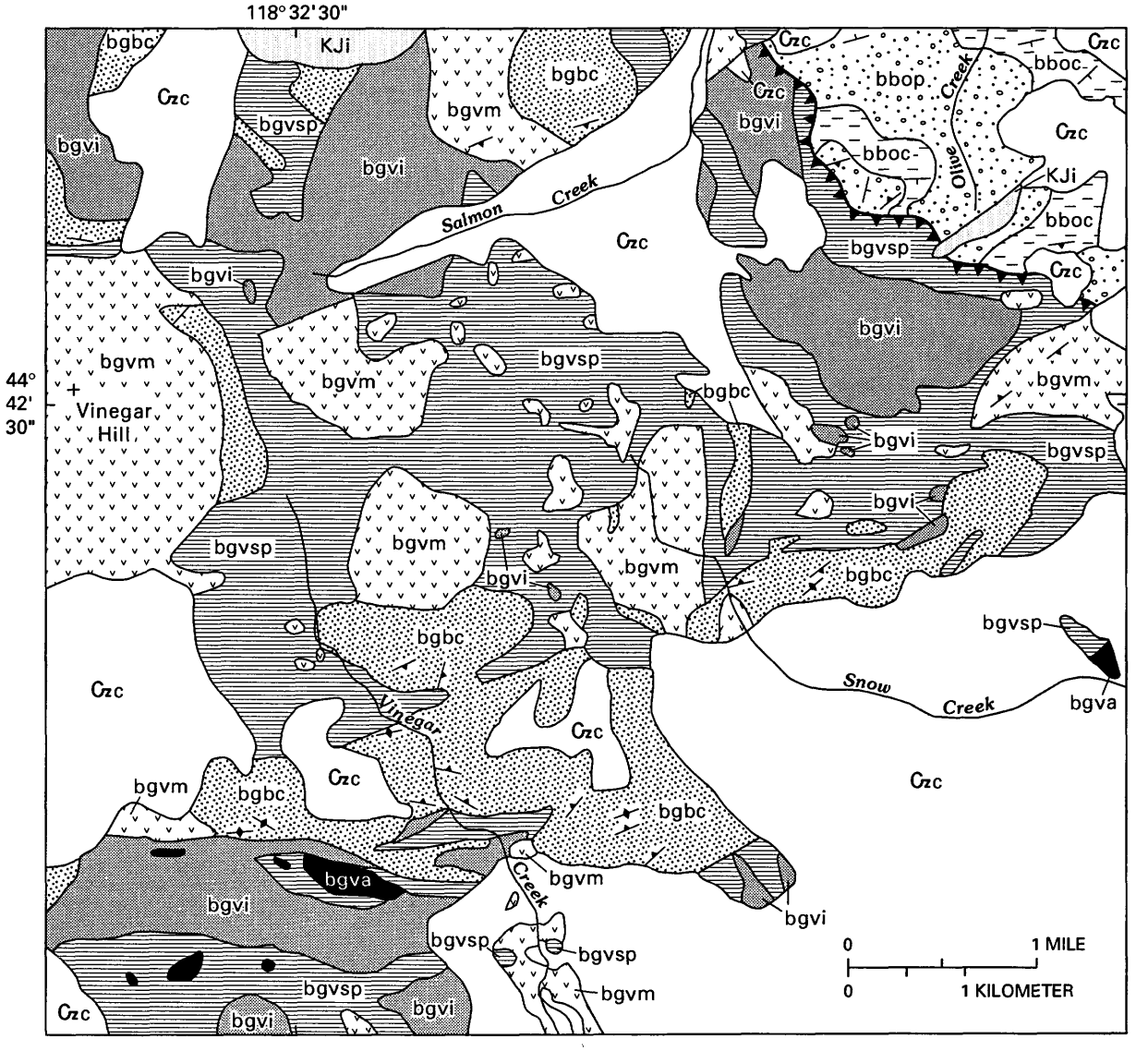

EXPLANATION

Czc — Cover deposits (Cenozoic)

KJi — Intrusive rocks (Early Cretaceous and Late Jurassic)

Baker terrane—Divided into:

Bourne subterrane—Consists of:

Olive Creek unit—Divided into:

bboc — Ribbon chert and argillite

bbop — Alkalic pillow basalts and volcaniclastic rocks

Greenhorn subterrane—Consists of:

bgbc — Badger Creek unit

Melange of Vinegar Hill—Divided into:

bgvsp — Serpentinite

bgvm — Metavolcanic rocks

bgvi — Meta-intrusive rocks

bgva — Foliated amphibolite

Thrust fault and subterrane boundary—Sawteeth on upper plate

Strike and dip of bedding (S_0)

Strike and dip of foliation (S_1)

Strike of vertical foliation (S_1)

FIGURE 9.9.—Geologic map of melange of Vinegar Hill showing boundary thrust fault between Greenhorn and Bourne subterranes (modified from Ferns and others, 1983, and Brooks and others, 1983).

TABLE 9.5.—*Major-element data for greenstones from the Greenhorn subterrane*

[All samples normalized to 100 percent on a volatile-free basis. n.d., not determined]

Unit -------	Melange of Vinegar Hill									Dixie Butte Meta-andesite			
Sample ---	[2]B-372	[1]V-3	[2]63A	[2]B-364	[1]V-2	[1]V-1	[2]60A	[2]60B	[2]55	[2]185	[2]VDB-1	[2]VDB-2	[2]DBV
SiO_2 ------	44.14	45.75	46.12	47.07	47.18	49.75	50.51	70.85	49.17	53.37	53.61	55.04	55.46
Al_2O_3 -----	16.62	15.62	19.40	16.60	15.22	15.05	16.43	14.56	19.82	15.68	16.16	16.45	18.94
TiO_2 -------	1.49	1.77	0.63	1.84	1.01	2.43	0.79	0.35	0.44	0.85	1.00	1.36	1.52
FeO* -----	15.67	11.88	9.64	10.34	13.80	11.98	9.18	4.22	7.19	7.72	8.50	8.73	7.56
MnO ------	0.29	0.20	0.17	0.12	0.20	0.20	0.15	0.09	0.14	0.15	0.16	0.14	0.14
CaO--------	11.29	10.44	12.22	11.85	11.61	9.02	9.74	1.57	11.19	10.27	8.56	8.48	6.82
MgO-------	7.73	9.02	9.24	4.95	8.54	8.29	9.18	2.56	8.57	8.93	7.96	5.61	3.31
K_2O--------	0.26	1.58	0.20	1.29	0.36	0.35	0.16	0.60	0.17	0.74	1.00	1.01	2.22
Na_2O------	2.37	3.47	2.34	5.30	2.36	2.54	3.69	5.13	3.27	2.22	2.85	2.93	3.74
P_2O_5 -------	0.14	0.28	0.03	0.64	0.16	0.39	0.15	0.07	0.04	0.14	0.18	0.25	0.30
H_2O^+ ------	n.d.	4.10	n.d.	n.d.	2.23	2.25	n.d.	n.d.	n.d.	n.d.	n.d.	n.d.	n.d.
H_2O^- ------	n.d.	0.27	n.d.	n.d.	0.17	0.38	n.d.	n.d.	n.d.	n.d.	n.d.	n.d.	n.d.
C_2O--------	n.d.	4.79	n.d.	n.d.	0.08	0.01	n.d.	n.d.	n.d.	n.d.	n.d.	n.d.	n.d.

[1]Analyzed at U.S. Geological Survey, Menlo Park, Calif.
[2]Analyzed at Washington State University, Pullman, Wash.

GEOCHEMISTRY

Major- and trace-element contents (tables 9.4, 9.5) indicate that greenstone blocks within the melange include both oceanic and island-arc-related material. The large heterolithologic block south of Greenhorn includes island-arc basalts (Mullen, 1978, 1982) and dacite (Ferns and others, 1983). Both alkalic and low-K tholeiitic basalts (tables 9.4, 9.5) occur in the large heterolithologic block that culminates in the summit of Vinegar Hill. This block, which is made up of interlayered pillow lava and banded chert intruded by narrow diorite dikes, is apparently a fragment of oceanic crust. It contains a low-K tholeiite geochemically similar to the Bourne subterrane mixed-rock-zone rocks that plots within the evolved-midocean-ridge-basalt (E-MORB) field on the Hf/3-Th-Ta diagram (fig. 9.8). The one Vinegar Hill low-K tholeiite has a flatter rare-earth-element pattern than the Bourne subterrane mixed-rock-zone low-K tholeiites (fig. 9.10).

Work by E.M. Bishop (Mullen, 1985) indicates that Vinegar Hill gabbros are tholeiitic in character and may have more oceanic affinities than the gabbros in the Canyon Mountain Complex. Major-element abundances (table 9.5) show that the Vinegar Hill intrusive blocks are chemically distinct from the Bourne subterrane island-arc intrusive rocks. Vinegar Hill blocks are enriched in CaO and MgO and depleted in TiO_2 and FeO* as compared to Bourne subterrane intrusive rocks of similar silica content (fig. 9.5).

METAMORPHISM

Blocks in the melange of Vinegar Hill range from prehnite-pumpellyite to epidote-amphibolite in metamorphic grade. Igneous textures in the lower grade rocks are obscured by felted masses of chlorite, albite, and epidote. Epidote amphibolites are typically tightly crenulated foliated rocks either associated with sheared serpentinite along major fault zones or

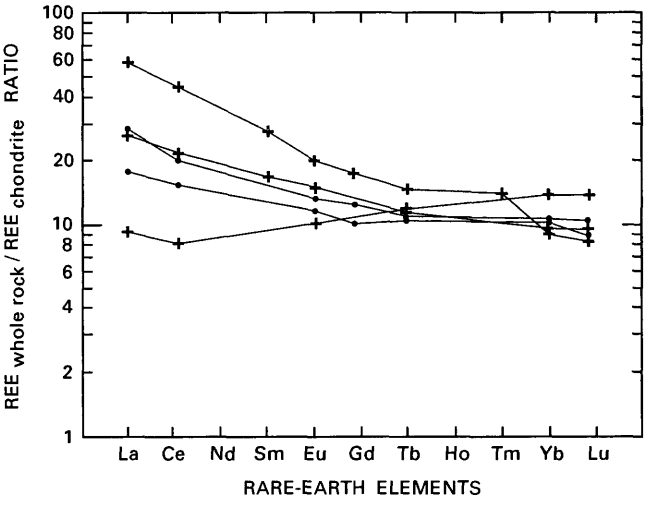

FIGURE 9.10.—Rare-earth-element (REE) plot for greenstones from Baker terrane. Dots, basalts from mixed-rock zones in Bourne subterrane; crosses, basalts of the melange of Vinegar Hill (Greenhorn subterrane). Data are listed in table 9.4 and Vallier (1985 and chap. 3, this volume).

along the outer margins of metagabbro blocks. Metamorphic minerals include greenish-brown hornblende, epidote, sodic plagioclase, and quartz.

Blue amphiboles occur in foliated metamorphic rocks encased in melange in small inliers southeast of the main exposures of the melange of Vinegar Hill (Mullen, 1978, 1980; Ferns and others, 1983). Associated minerals include chlorite, epidote, albite, quartz, white mica, and garnet. Mullen (1978, 1980) reported that the amphiboles recorded two periods of metamorphism. An early low-temperature/high-pressure event (about 350°C and 6.5 kb) is indicated by barroisitic amphibole cores. A later, moderate-temperature/moderate-pressure event (400–450°C and 3–5 kb) is indicated by more calcic amphibole rims.

ORIGIN AND AGE

Fossil data pertaining to the age of the melange of Vinegar Hill are fragmentary and contradictory. Ages are based mainly on the overlying Badger Creek unit, which contains Pennsylvanian, Permian, and Late Triassic fossils. Morris and Wardlaw (1986) reported Pennsylvanian conodonts from a limestone lens interbedded with chert-pebble conglomerate and calcareous sandstone and siltstone in apparent depositional contact with the Vinegar Hill block. The sediments were considered by Brooks and others (1983) to be part of the depositionally overlying Badger Creek unit. Provided that the limestone is not an exotic clast in the overlying sediments, the underlying block in the melange of Vinegar Hill must be Pennsylvanian or older in age. However Blome (oral commun., 1983) reported that radiolarians from green cherts near the base of the Badger Creek unit near Greenhorn and from a bedded chert block encased within the melange south of Greenhorn, although poorly preserved, were cone-shaped and likely Mesozoic in age.

The apparent wide range of faunal ages in the overlying Badger Creek unit sediments suggests that the melange of Vinegar Hill may be polygenetic, that is, it may have developed over a period of time under changing tectonic conditions. Scattered exposures of overlying polymict sedimentary breccia and conglomerate that contain clasts locally derived from blocks within the melange, along with rare exposures of overlying serpentinite-matrix and talc-matrix sedimentary breccias, indicate that the melange of Vinegar Hill locally shed olistostromal debris into flanking sedimentary basins. Many of the smaller sedimentary blocks are completely engulfed by serpentinite and now compose part of the melange, indicating that melange continued to develop after deposition of the sediments began. The elongate slices of foliated epidote amphibolite and sheared serpentinite that are tectonically interleaved with sheared sedimentary rock in fault zones along the contact between the melange and the Badger Creek unit (Brooks and others, 1983) indicate that tectonic mixing continued after the sediments were initially deposited.

Small patches of serpentinite-matrix sedimentary breccias south of Greenhorn that locally overlie the melange of Vinegar Hill do not appear to be as intensely deformed as the rest of the Badger Creek unit, indicating that serpentinite did not breach the oceanic floor until later stages of basin development. Late-stage breaching by serpentinite is supported also by Hunt (1985), who reported deformation of melange blocks prior to serpentinite injection. Widespread introduction of ultramafic rocks may not have occurred until the late stages of melange evolution, as suggested by the general absence of ultramafic detritus in Mesozoic polymict breccias that contain abundant block-derived detritus in the form of gabbro and greenstone clasts.

Earlier periods of serpentinite emplacement may be evidenced by local ophicarbonate (talc-carbonate) beds within the central part of the Badger Creek unit in the Granite Boulder Creek area (see fig. 9.13; Ferns and Ramp, 1988). Permian fusulinid and radiolarian localities occur in the immediate vicinity of the ophicarbonate bed.

The melange of Vinegar Hill may have begun to form in a fore-arc setting as a rising serpentinite diapir similar to those reported in the Mariana and Bonin arcs in the western Pacific Ocean (Bloomer, 1983; Taylor and Smoot, 1984). Serpentinites apparently form from fluxing of ultramafic rocks at the base of the outer wall of the fore arc by waters derived from the underlying subducted slab. Presumably, the decrease in specific gravity during conversion of ultramafic rock to serpentinite would allow for diapiric injection of serpentinite into a fracturing cover of overlying, foundering oceanic and island-arc crust in the fore-arc wall. Olistostromal debris derived from the rising diapir and fractured cover could then be shed as gravity slides into flanking basins. Blue-amphibole-bearing epidote amphibolites and disrupted intrusive rocks may be fragments of the underlying crust which were later incorporated into the diapir.

DIXIE BUTTE META-ANDESITE

The southernmost major lithologic unit mapped in the central part of the Baker terrane is the volcanic-arc-related Dixie Butte Meta-andesite of Brooks and others (1984). These volcanic rocks crop out over an

area of about 80 km^2 and are mainly massive plagiophyric andesite and basaltic andesite flows that are interbedded with island-arc basalts (Mullen, 1982).

ROCK TYPES

Major rock types are pyroxene basalts and plagiophyric basaltic andesites that contain feldspar phenocrysts up to 5 cm in length. The Dixie Butte Meta-andesite is estimated to be about 2,100 m thick, with the lowermost 600 m being mainly thick-bedded andesitic lithic tuff, tuff breccia, and coarse tuffaceous sedimentary rocks (Brooks and others, 1984). Scattered round chert clasts in the basal sedimentary rocks indicate that the Dixie Butte Meta-andesite is depositional onto older ocean-floor material made up of chert and argillite. Melange with chert and argillite is exposed along the eastern and southern flanks of Dixie Butte (see fig. 9.3; Brooks and others, 1984).

GEOCHEMISTRY

Dixie Butte basalts and basaltic andesites are calc-alkaline (table 9.5) and have volcanic-arc affinities (Mullen, 1982). They differ from the Bourne subterrane volcanic-arc rocks in that the Dixie Butte rocks have considerably higher abundances of K_2O and Zr (tables 9.3–9.5).

AGE AND REGIONAL CORRELATIONS

The eastern exposures of the Dixie Butte Meta-andesite are in high-angle contact with a serpentinite-matrix melange similar in appearance to the melange of Vinegar Hill. This melange contains diverse lithologic blocks whose compositions range from greenschist to foliated epidote amphibolite. The melange also contains porphyritic andesite blocks and Permian (Guadalupian) ribbon cherts (Brooks and others, 1984; Blome and others, 1986).

Chert clasts presumably derived from the underlying Permian ribbon cherts are present in tuffaceous sedimentary rocks exposed near the base of Dixie Butte. The rounded chert clasts indicate that the Dixie Butte flows and tuffs were emplaced after the cherts were eroded, rounded, and redeposited, and are evidence that the Dixie Butte is younger than Guadalupian in age.

The low metamorphic rank and absence of S_1 cleavage further suggest that the Dixie Butte Meta-andesite may be younger than all the other Paleozoic and Triassic components of the Baker terrane and may be one of the postulated northern volcanic sources for andesitic tuffs and lava flows in the Late Triassic Fields Creek Formation in the Izee terrane to the south (Brown and Thayer, 1966). High K_2O contents suggest that the Dixie Butte rocks are not related to the Wallowa terrane (Mortimer, 1986).

METAMORPHISM

Metamorphic recrystallization and hydrothermal alteration due to emplacement of numerous small Late Jurassic and early Tertiary intrusions (Brooks and others, 1984) have generally obscured early metamorphic mineral assemblages at Dixie Butte. Regional metamorphic assemblages include chlorite+albite+calcite+zeolite and chlorite+albite+actinolite.

STRUCTURE

Major structural characteristics of the Bourne and Greenhorn subterranes are summarized below. For a more detailed treatment of structural development in the Baker terrane, the reader is referred to Coward (1983), Evans (chap. 8, this volume), and Hunt (1985).

Four major structural events can be recognized: (1) early disruption with development of type II melanges and cataclasite zones in the Bourne subterrane and development of serpentinite-matrix melange and ophicarbonates in the Greenhorn subterrane, (2) folding of Bourne and Greenhorn subterrane units about north- and northeast-trending fold axes without development of penetrative cleavages, (3) later development of penetrative and subpenetrative fracture cleavages (S_1) axial planar to east-west-trending folds in both subterranes, and (4) local development of penetrative and spaced cleavages (S_2), mainly in the matrixes of melange zones in both subterranes.

PLANAR ELEMENTS

Bedding is preserved only locally in large Bourne subterrane blocks where bedded sequences are separated by cataclasite or shear zones. Both Coward (1983) and Evans (chap. 8, this volume) describe the Elkhorn Ridge Argillite as a broken formation whose initial fragmentation predated development of penetrative and subpenetrative cleavages. Bedding (S_0) in the Bourne subterrane is most common in the layered cherts of the Elkhorn Ridge Argillite and lay-

ered cherts in the Olive Creek area; bedding is only rarely preserved in argillites of the Elkhorn Ridge Argillite and finer grained sedimentary facies of the Goodrich Creek and North Fork units. Inverted graded beds on the east end of Elkhorn Ridge indicate at least local overturning of units in the Goodrich Creek area (Ferns and others, 1987). Attitudes of bedding planes in the greenstones are more varied than those of bedding planes in the adjacent Elkhorn Ridge Argillite, which generally strike east-west and dip steeply to the south.

Bedding is only locally apparent in Greenhorn subterrane units. Inverted graded beds and flame structures in the Badger Creek unit suggest some overturning of units. Bedding-plane relationships are difficult to determine in the Dixie Butte Metaandesite, owing to the massive nature of flow units. Vhay (1960) notes that steeply dipping and locally overturned tuff beds indicate extensive folding of the Dixie Butte. Basal tuffs at Dixie Butte generally strike to the north and dip to the east and west.

FAULTS, MICROBRECCIAS, AND CATACLASITE ZONES

Pervasive, apparently randomly oriented, anastomosing microbreccia zones as much as 1 cm in width cut all rock types in the Goodrich Creek unit. Microbreccia zones are made up of angular and flattened porphyroclasts arranged in an isotropic groundmass. Extensive areas of protocataclasites mark contacts within the Goodrich Creek between metamorphosed intrusive rocks and all other rock types. The protocataclasites are zones as much as a hundred meters wide in which protoliths are difficult to distinguish. The protocataclasite zones contain granular pophyroclasts in an isotropic matrix.

Narrow cataclasite zones, with partially recrystallized matrix, and microbreccias also cut across the Elkhorn Ridge Argillite, which bears a strong resemblance to Cowan's (1985) type II melange. Coward (1983) noted that bedding and folds were transposed by movement along shear planes that are subparallel or at low angles (<45°) to bedding or axial-plane surfaces. Evans (chap 8, this volume) notes that the shear zones surround unsheared blocks that are generally elongate parallel to both bedding (S_0) and cleavage (S_1).

The shear planes and cataclasite zones apparently parallel S_0 in the Elkhorn Ridge Argillite. Orientation and distribution of the Goodrich Creek cataclasite zones have not been determined. In outcrop, multiple generations of apparently randomly oriented shears may indicate progressive rotation or grinding of blocks within the Goodrich Creek cataclasite zones.

Cataclasites comparable to those in the Bourne subterrane have not been recognized in the Greenhorn subterrane. Mullen (1978) noted cataclasites in metagabbros along the boundary fault separating the subterranes, whereas Hunt (1985) noted a lack of cataclasites in blocks of the melange of Vinegar Hill, about 5 km to the south.

CLEAVAGES

The most prominent structural element in nearly all the units of the Baker terrane is a generally east-west-striking, south-dipping spaced fracture cleavage (S_1). S_1 is best developed in the finer grained argillites of the Elkhorn Ridge Argillite and the Goodrich Creek unit in the Bourne subterrane and the Badger Creek unit in the Greenhorn subterrane.

S_1 in stratigraphically coherent ribbon-chert blocks of the Elkhorn Ridge Argillite generally parallel the narrow microbreccia and cataclasite zones that bound the blocks. Similarities in orientation of S_0 and S_1 in the Elkhorn Ridge Argillite suggest that bedding may be transposed or that S_1 is axial planar to east-west-trending folds in the Elkhorn Ridge (F_2 of Avé Lallemant and others, 1980). S_1 cuts across cataclasite zones in the Goodrich Creek unit and tends to parallel the trend of the faults that separate the Goodrich Creek unit from overlying and underlying slabs of Elkhorn Ridge Argillite. S_1 attitudes in the Goodrich Creek unit, although varied, generally parallel the east-west striking and south-dipping S_1 of the Elkhorn Ridge. Superposition of S_1 on the cataclasite zones in the Goodrich Creek unit indicates that the greenstone cleavage developed after formation of the cataclasite zones. S_1 fracture cleavage in the Olive Creek rocks is poorly developed in comparison to S_1 in the Elkhorn Ridge Argillite. S_1 in the Olive Creek unit appears to be axial planar to east-west-trending fold axes and parallels the strike of the thrust faults that separate the Elkhorn Ridge slices from enclosed Goodrich Creek and North Fork slices (see Ferns and others, 1987). Steep S_1 cleavages in greenstone units also generally parallel the predominantly east-west regional strike of the faults.

S_1 in the Greenhorn subterrane is best developed in argillites of the Badger Creek unit as a penetrative slaty cleavage. S_1 in coarser grained Badger Creek conglomerates is defined by subparallel alignment of anastomosing stringers of sheet silicates (Hunt, 1985). S_1 generally cuts bedding in the Badger Creek rocks and strikes east-west. The general

east-west strike of S_1 in the Greenhorn subterrane is similar to that of S_1 fracture cleavage in the Bourne subterrane, and the two sets of cleavage are presumed to be of the same age. Steep northerly dips are more common in the Greenhorn subterrane units, and the average dip of S_1 is closer to vertical in the Greenhorn than in the Bourne subterrane units (fig. 9.11). S_1 is poorly developed in greenstones, is defined by widely spaced fracture cleavage in blocks of the melange of Vinegar Hill (Hunt, 1985), and has not been recognized in the Dixie Butte Meta-andesite. The intervening serpentinite matrix of the melange of Vinegar Hill apparently lacks the S_1 cleavage and is cut by a younger, phacoidal cleavage (S_2). Hunt (1985) suggested that the similarity in S_1 orientation in different Vinegar Hill blocks indicates that serpentinite was injected after development of S_1 with little or no rotation of individual blocks. Alternatively, early S_1 fabrics in the serpentinite matrix may have been destroyed by serpentinite flowage during subsequent deformation.

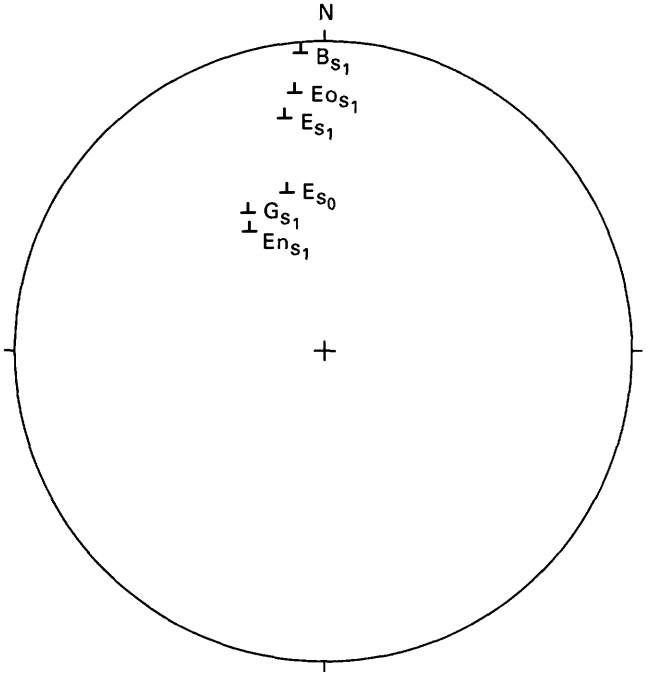

FIGURE 9.11.—Lower-hemisphere, equal-area plot comparing visually determined mean poles to bedding (S_0) and cleavage (S_1). En_{S_1}, S_1 cleavages from outcrops of the Elkhorn Ridge Argillite north of the Goodrich Creek unit (number of data points (n)=36); E_{S_1}, S_1 cleavages from outcrops of Elkhorn Ridge Argillite in area between the Goodrich Creek unit and McCully Fork mixed-rock zone (n=108); Eo_{S_1}, S_1 cleavages from outcrops in the Elkhorn Ridge Argillite and Olive Creek unit south of the McCully Fork mixed-rock zone (n=40); E_{S_0}, bedding-plane orientations in Elkhorn Ridge Argillite (n=157); G_{S_1}, S_1 cleavages from the Goodrich Creek unit (n=31); B_{S_1}, S_1 cleavages from the Badger Creek unit (n=48). Note the progressive steepening of cleavage from northern to southern parts of the study area.

Evans (chap. 8, this volume) notes that the shear zones surround unsheared blocks that are generally elongate parallel to bedding (S_0) and fracture cleavage (S_1). Coward (written commun., 1993) suggested that these features indicate isoclinal folding and brittle shortening that has formed a type II melange (Cowan, 1985) in which stratigraphically continuous zones of isoclinally folded chert and argillite are bounded by either faults or cataclasite zones.

A younger cleavage (S_2) affects some Baker terrane units. Coward (1983) noted a northerly dipping spaced cleavage that cuts S_1 of the Elkhorn Ridge Argillite; the spaced cleavage is defined by alignment of fine-grained phyllosilicates. S_2 postdates the S_1 fracture cleavage and may have formed in response to emplacement of the Late Jurassic to Early Cretaceous intrusions.

A phacoidal cleavage defined by augen of unsheared serpentinite in intensely sheared serpentinite was recognized by Hunt (1985) in the melange of Vinegar Hill. The strike of the cleavage parallels that of contacts between matrix and blocks in the melange of Vinegar Hill and appears randomly oriented (Hunt, 1985). Serpentinite injected along fault zones south of Hunt's area exhibits a strongly developed shear foliation that parallels both the direction of elongation of metamorphic and sedimentary blocks and the S_1 fracture cleavage within the blocks (Brooks and others, 1983). A similar matrix cleavage (herein defined as S_2) is developed in the McCully Fork mixed-rock zone and parallels the regional strike of the zone and the direction of elongation of included slabs. S_2 occurs in talc-amphibole hornfels within the contact aureole of the Bald Mountain batholith and apparently developed in conjunction with recrystallization of serpentinite matrix in the McCully Fork mixed-rock zone during batholith emplacement. Late development of the McCully Fork mixed-rock zone is suggested by Coward (1983) and supported by narrow cataclasite zones in the underlying Elkhorn Ridge Argillite that parallel the fault contact between the Elkhorn Ridge Argillite and the McCully Fork mixed-rock zone, and cut across S_1 of the Elkhorn Ridge Argillite.

FOLDS

Mesoscopic folds are relatively uncommon in all Bourne subterrane units. Two sets of fold axes (fig. 9.12) have been identified in the Elkhorn Ridge Argillite: a steeply plunging north-south-trending set

(F_1) and a more gently plunging east-west-trending set (F_2) (Avé Lallemant and others, 1980).

F_1 includes rare open folds in the Goodrich Creek unit and tight isoclinal folds in Elkhorn Ridge and Olive Creek cherts. F_1 axes plunge 30° to 35° to the south and parallel the southeast-plunging outcrop pattern of metamorphosed intrusive rocks of the Goodrich Creek unit on the east end of Elkhorn Ridge (Ferns and others, 1987).

F_2 fold axes are nearly horizontal and trend east-west. Coward (1983) noted two varieties: prelithification folds that lack axial-planar cleavage (his F_{1nc}), and folds with axial-planar cleavage (his F_{1wc}). Fold axes of both varieties are oriented east-west with southerly dipping axial planes and are herein designated F_2. Similarly oriented F_2 folds that occur in the Goodrich Creek unit include small folds with 5-cm wavelengths in contorted limestones and folded contacts between Goodrich Creek rock types.

Mesoscopic F_1 folds have not been identified in Greenhorn subterrane units. Possible north- to northeast-trending F_1 axes are suggested by overturning of S_0 in the Badger Creek unit and the Dixie Butte Meta-andesite. A thrust fault separating the Badger Creek unit from ultramafic rocks on Badger Creek (fig. 9.13) may also be folded about a northeast-trending axis (Ferns and others, 1983).

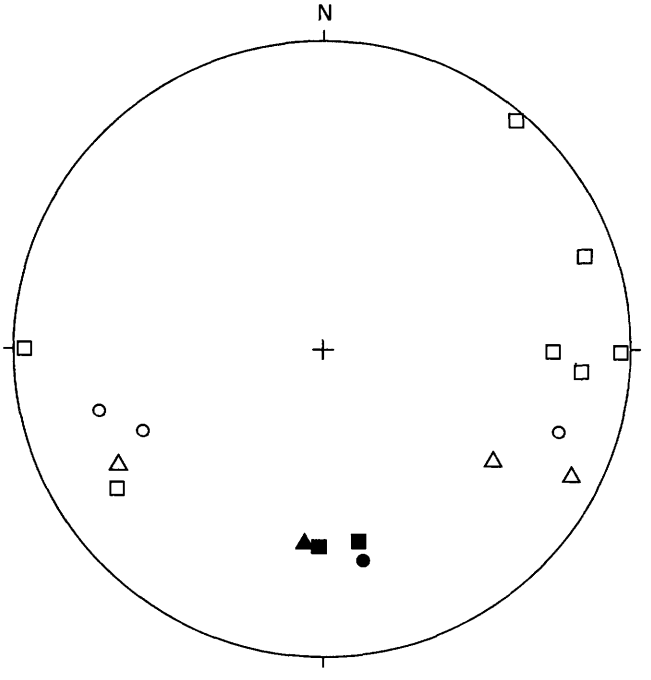

FIGURE 9.12.—Lower-hemisphere, equal-area plot of fold axes. Filled symbols represent F_1 axes; open symbols, F_2 axes. Squares represent data from Elkhorn Ridge Argillite; circles, data from Olive Creek unit; triangles, data from Goodrich Creek unit.

F_2 folds related to an axial-planar cleavage have been recognized by Hunt (1985) in the Badger Creek unit along Snow Creek (fig. 9.9). Axial planes of tight, upright symmetrical folds parallel the northeast strike and near-vertical dip of the cleavage here (Hunt, 1985).

Mullen (1978) recognized a later folding event (herein referred to as F_3) affecting the amphibolitic blocks of the melange of Vinegar Hill. Axial planes to F_3, which consists of small isoclinal folds and crenulations in foliated metamorphic rocks, apparently strike northwest (Mullen, 1978), parallel to the subterrane boundary.

STRUCTURE SUMMARY

While gross similarities in late structural styles and fracture cleavages in the Bourne and Greenhorn subterranes indicate contemporaneous late deformation, distinctly different styles of early deformation indicate separate early-deformation paths for the subterranes. Early deformation in the Bourne subterrane was characterized by severe internal disruption of units, including the development of type II melange in the Elkhorn Ridge Argillite and the development of cataclasite zones in the Goodrich Creek unit. Later structures include poorly preserved folds about north-trending fold axes (F_1), thrust faults, and axial-planar cleavage (S_1) about east-west-trending F_2 fold axes. In the Greenhorn subterrane, development of serpentinite-matrix melanges was followed by clastic basinal sedimentation prior to thrust faulting and folding about north- to northeast-trending F_1 axes. The folds are cut by the penetrative S_1 cleavage in some but not all Greenhorn subterrane units. A later cleavage (S_2) is locally developed in melange matrixes in both subterranes and is apparently related to remobilization and recrystallization of serpentinite accompanying Late Jurassic plutonism.

SUMMARY

The Bourne subterrane of the Baker terrane is composed mainly of southward-dipping, fault-bounded packages of the Elkhorn Ridge Argillite, a sedimentary sequence made up chiefly of deepwater chert and siliceous argillites of Permian and Late Triassic (Karnian) age. These deepwater cherts and argillites enclose olistoliths of shallow-water limestones that range from Devonian to Permian in age (fig. 9.14). Although most of the known Permian fusulinid locali-

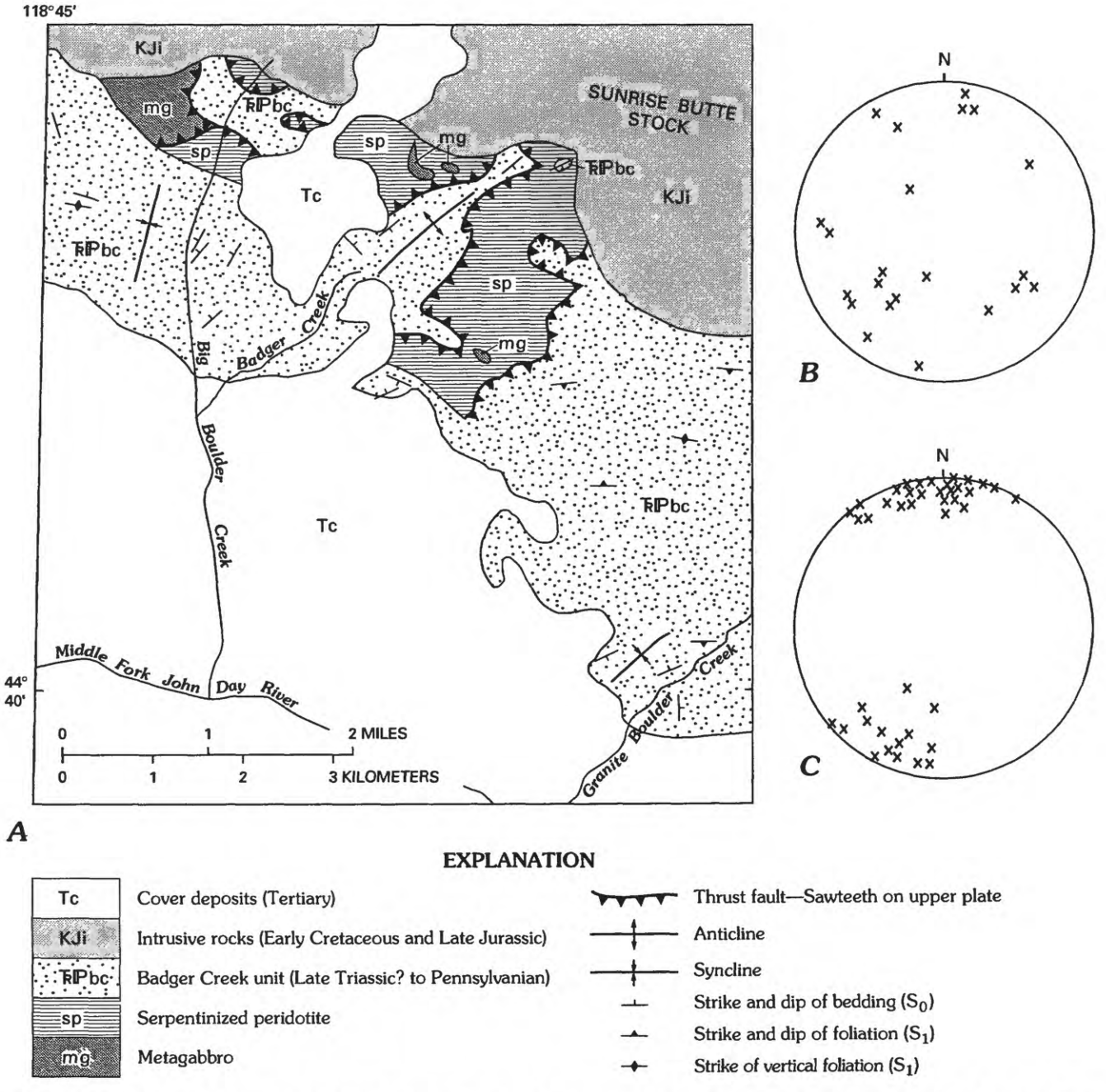

FIGURE 9.13.—Relations between bedding (S_0), cleavage (S_1), and intercalated ultramafic sheets in the Badger Creek unit. *A*, Geologic map. *B*, Lower-hemisphere, equal-area projection of poles to bedding (S_0) in the Badger Creek unit. *C*, Lower-hemisphere, equal-area projection of poles to cleavage (S_1) in the Badger Creek unit.

ties yielded fusulinids of Tethyan affinities, one locality with fusulinids similar to those of the McCloud Limestone in northern California has been described in the literature. Slices of disrupted volcanic rocks of island-arc affinities are intercalated with the Elkhorn Ridge Argillite along southward-dipping high-angle reverse and thrust faults along the northern margin of the Bourne subterrane. The island-arc packages consist of Late Permian to Early Triassic intrusive and extrusive rocks and Late Triassic (Norian) sedimentary rocks. Alkalic pillow basalts are intercalated with Permian and Triassic cherts along the southern margin of the subterrane.

Bourne subterrane rocks are strongly faulted, locally brecciated, and cataclasized, and they generally correspond to the type II melanges of Cowan (1985)

(tables 9.2, 9.6). Strongly disrupted mixed-rock zones resembling the type IV melanges of Cowan (1985) cut across the central and southern parts of the Bourne subterrane. The Elkhorn Ridge Argillite along the southern margin of the Bourne subterrane has locally been converted to large megabreccia zones. A generally south-dipping fracture cleavage (S_1) affects all Bourne subterrane units.

The Greenhorn subterrane of the Baker terrane is composed mainly of serpentinite-matrix melange that

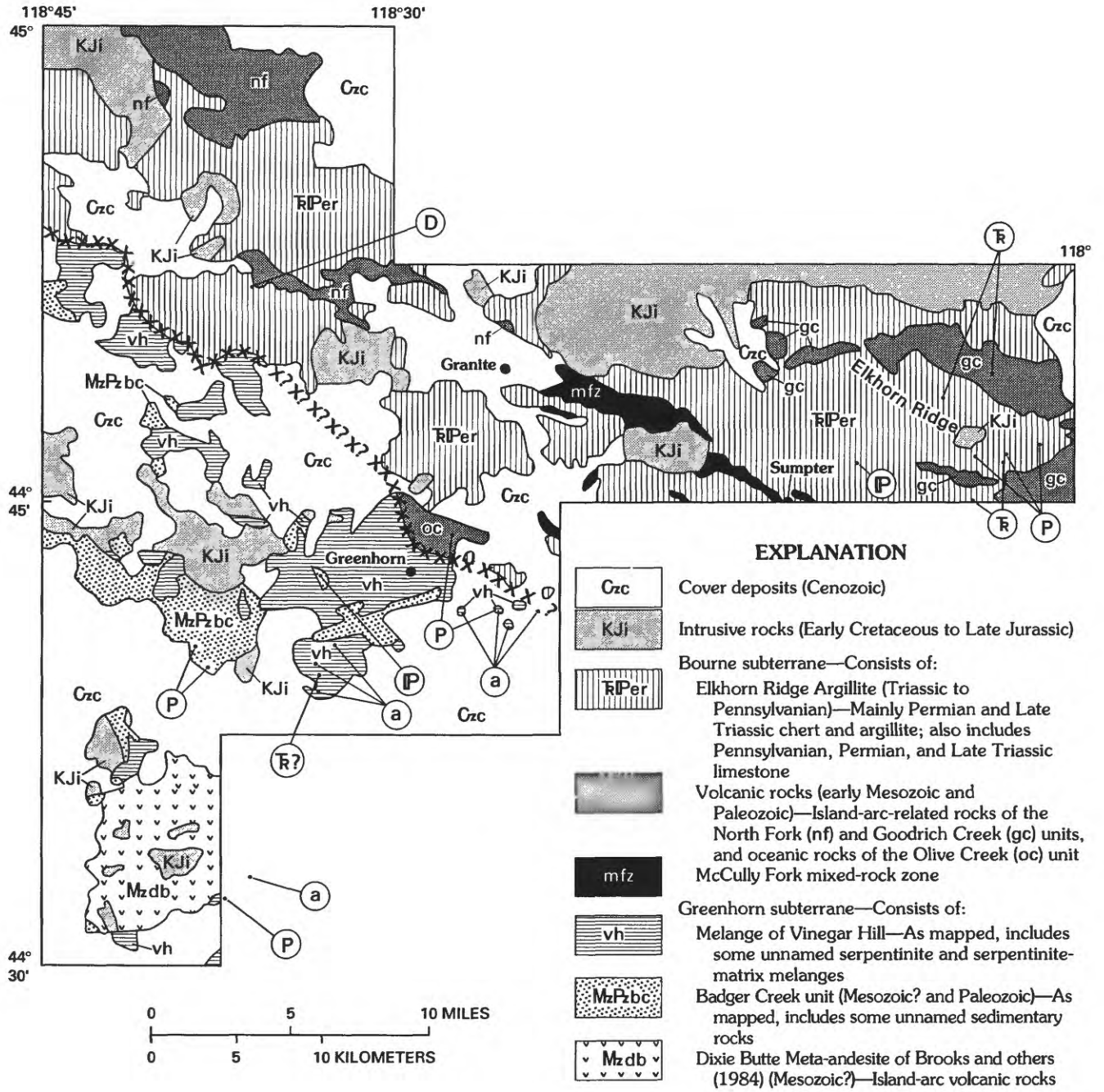

FIGURE 9.14.—Fossil and amphibolite localities in central part of Baker terrane. Fossil localities: D, Devonian; IP, Pennsylvanian; P, Permian; Tr, Triassic, queried where uncertain. Paleontological ages are from Blome and others (1986), Morris and Wardlaw (1986), Ferns and others (1987), C.D. Blome (written commun., 1987), and M.K. Nestell, (oral commun., 1986). a, foliated amphibolite localities.

TABLE 9.6.—*Comparison of lithologic, structural, and paleontologic characteristics of the Greenhorn and Bourne subterranes*

	Greenhorn subterrane	Bourne subterrane
Main lithologic unit	Serpentinite-matrix melange (melange of Vinegar Hill).	Chert and argillite (Elkhorn Ridge Argillite).
Volcanic rock types	High-K calc-alkaline volcanic rocks (Dixie Butte Meta-andesite); calc-alkaline, alkalic, and oceanic melange blocks (melange of Vinegar Hill).	High-Na calc-alkaline volcanic rocks (Goodrich Creek and North Fork units); alkalic pillow lavas (Olive Creek unit); ocean-floor(?) tholeiites (McCully Fork mixed-rock zone).
Intrusive rock types	Mafic gabbros, minor pyroxenites and harzburgites (melange of Vinegar Hill).	Low-K diorites, quartz diorites, and gabbros similar to the Sparta complex (Goodrich Creek and North Fork units).
Melange types (see table 9.2)	Serpentinite-matrix block-in-matrix, analogous to type III.	Type IV, brittle fault zones (McCully Fork mixed-rock zone); type II, disrupted chert and argillite sequences (Elkhorn Ridge Argillite).
Faunal ages	Pennsylvanian, Permian, and early Mesozoic(?) (Badger Creek unit); Permian and early Mesozoic(?) blocks (melange of Vinegar Hill).	Devonian, Pennsylvanian, Permian, and Late Triassic limestone blocks and Permian and Late Triassic cherts (Elkhorn Ridge Agillite); Late Triassic limestones (Goodrich Creek unit).
Faunal affinities	McCloud, Calif., area (Badger Creek unit).	Separate blocks withTethyan and McCloud (Calif.) area affinities (Elkhorn Ridge Argillite).
Metamorphism	Epidote-amphibolite blocks with blue amphibole (melange of Vinegar Hill).	Greenschist facies in all units.
Sedimentary rocks	Interbedded sandstone, siltstone, and limestone (Badger Creek unit).	Chert and argillite with limestone olistoliths (Elkhorn Ridge Argillite), tuffaceous siltstones and limestones interbedded with tuffs and volcaniclastic rocks (Goodrich Creek unit).
Proposed tectonic environment	Fore arc	Accretionary wedge/marginal basin.

contains a wide variety of metamorphic and igneous rocks, including blue-amphibole-bearing epidote amphibolites (fig. 9.14), lower greenschist and greenschist facies greenstones, and a variety of island-arc, oceanic-island (seamount?), and tholeiitic pillow basalts. Associated Paleozoic and Mesozoic(?) clastic sedimentary rocks include coarse polymict breccias derived from blocks within the melange, and limestone lenses containing Permian fusulinids with affinities to those of the McCloud Limestone of northern California. Overall, the Greenhorn subterrane bears a strong resemblance to modern fore-arc zones in the Marianas and Bonin arcs, where various island-arc and oceanic volcanic rocks are intimately associated with serpentinite diapirs, polymict breccias, and clastic basinal sediments.

DISCUSSION

Previous workers (Dickinson and Thayer, 1978; Brooks, 1979; Hietanen, 1981), citing the blueschist blocks at Mitchell, Oreg., and the mixed Tethyan and non-Tethyan fusulinid faunas, suggested that the Baker terrane represents a paleosuture zone. Dickinson and Thayer (1978) postulated that the suture is the product of subduction that lasted until at least Middle Triassic time. Hietanen (1981) noted that

long-lasting subduction during late Paleozoic to early Mesozoic time also occurred in the Sierra Nevada and Klamath Mountains in northern California and southwestern Oregon, and she suggested that rocks of the Baker terrane are an extension of the Sierra Nevada-Klamath suture system.

Our work, in conjunction with that of Mullen (1978), Evans (chap. 8, this volume), and Coward (1983) leads us to suggest that the Bourne and Greenhorn subterranes evolved along separate early-deformation paths and represent different tectonic environments within the suture zone. The Greenhorn subterrane appears to have been a fore-arc high (Mullen, 1985), as evidenced by serpentinite-matrix melanges, clastic basinal sedimentary rocks, mixed island-arc and oceanic volcanic rocks, and moderately high pressure/low temperature foliated metamorphic rocks. Permian fusulinid assemblages are similar to those of the Coyote Butte area in the Grindstone terrane to the southwest (fig. 9.1) and the McCloud area in the eastern Klamath Mountains in northern California, and may indicate a link between the Grindstone terrane and the Greenhorn subterrane. The apparent age range of the basinal supracrustal rocks of the Badger Creek unit—from Pennsylvanian to possibly Triassic time—suggests that the Greenhorn subterrane was a site of active sedimentation over a long time period.

Intercalation of Permian to Late Triassic deepwater chert and siliceous argillite packages with Permian to Late Triassic island-arc packages in the Bourne subterrane suggests significant post-Late Triassic crustal shortening during tectonic mixing of coeval island-arc and oceanic material. The Permian to Late Triassic island-arc packages may correlate with the Wallowa terrane now exposed immediately to the north. Volcanic rocks exposed in the central and southern portions of the Bourne subterrane have oceanic characteristics and may represent oceanic-island or ocean-floor material peripheral to the island-arc rocks of the Wallowa terrane.

Cowan (1985) noted that type II and type IV melanges might develop in an accretionary wedge setting above a subduction zone. Assuming that boundary faults separating lithologic units within the Bourne subterrane dip toward the subduction zone, then the sense of subduction, discounting postsuture rotation, would have been roughly from the north down to the south. The present distribution of intercalated island-arc slabs in the north and oceanic slabs in the south may record the impingement of a Permian to Late Triassic island-arc system (Wallowa terrane?) on a southward-dipping subduction zone in the post-Late Triassic (fig. 9.15).

Evans (chap. 8, this volume) and Coward (1983) recognize early, nonpenetrative deformations in the Bourne subterrane that may record early development of argillaceous broken formation (type II melange of Cowan, 1985) in an accretionary wedge setting. Tethyan Permian fusulinids in the Bourne subterrane indicate an environmental or paleogeographic setting distinct from that of the Greenhorn subterrane. Evans (chap. 8, this volume) indicates that rocks which constitute the Bourne and Greenhorn subterranes in the Desolation Butte quadrangle underwent separate deformations prior to their juxtaposition in Late Triassic or Early Jurassic time. The presence of Late Triassic cherts in the Elkhorn Ridge Argillite and Late Triassic limestones in Bourne subterrane island-arc packages indicates that nonpenetrative deformation continued through the Late Triassic as the Bourne subterrane rocks were tectonically intercalated within the suture zone.

Other workers (Evans, chap. 8, this volume; Avé Lallemant and others, 1980) have recognized an early, locally penetrative deformation that affected some Bourne subterrane components in the Baker terrane and is apparently related to a regionally extensive Late Triassic to Early Jurassic orogenic event (Dickinson and Thayer, 1978; Avé Lallemant and others, 1980). We suggest that this event *may* represent the cessation of subduction within the suture zone due to the incomplete consumption of the lighter (as compared to oceanic) island-arc material now preserved on the North Fork of the John Day River and on Elkhorn Ridge. This interpretation is suggested by extensive cataclasite zones in the Bourne subterrane. The Late Triassic to Early Jurassic event may be recorded in the Greenhorn subterrane by the poorly documented north- to northeast-trending fold axes in the Badger Creek unit and the Dixie Butte Meta-andesite of Brooks and others (1984). The northerly trending Greenhorn subterrane fold axes are similar in orientation to northerly trending fold axes identified by Dickinson and Thayer (1978) and Avé Lallemant and others (1980) in Late Triassic and Early Jurassic clastic sedimentary rocks in the Izee terrane to the south. Cessation of subduction at about this time may be marked by the 225-Ma blueschist block near Mitchell, Oreg. (Hotz and others, 1977).

The readily apparent, widespread, southerly dipping S_1 cleavage records a regional, short-lived, penetrative deformation event in the Late Jurassic. S_1 cleavage is apparent in most of the Baker terrane components as well as the overlying Jurassic clastic basinal sediments of the Olds Ferry terrane to the south. S_1 apparently developed in conjunction with the thrust and high-angle reverse faults that now

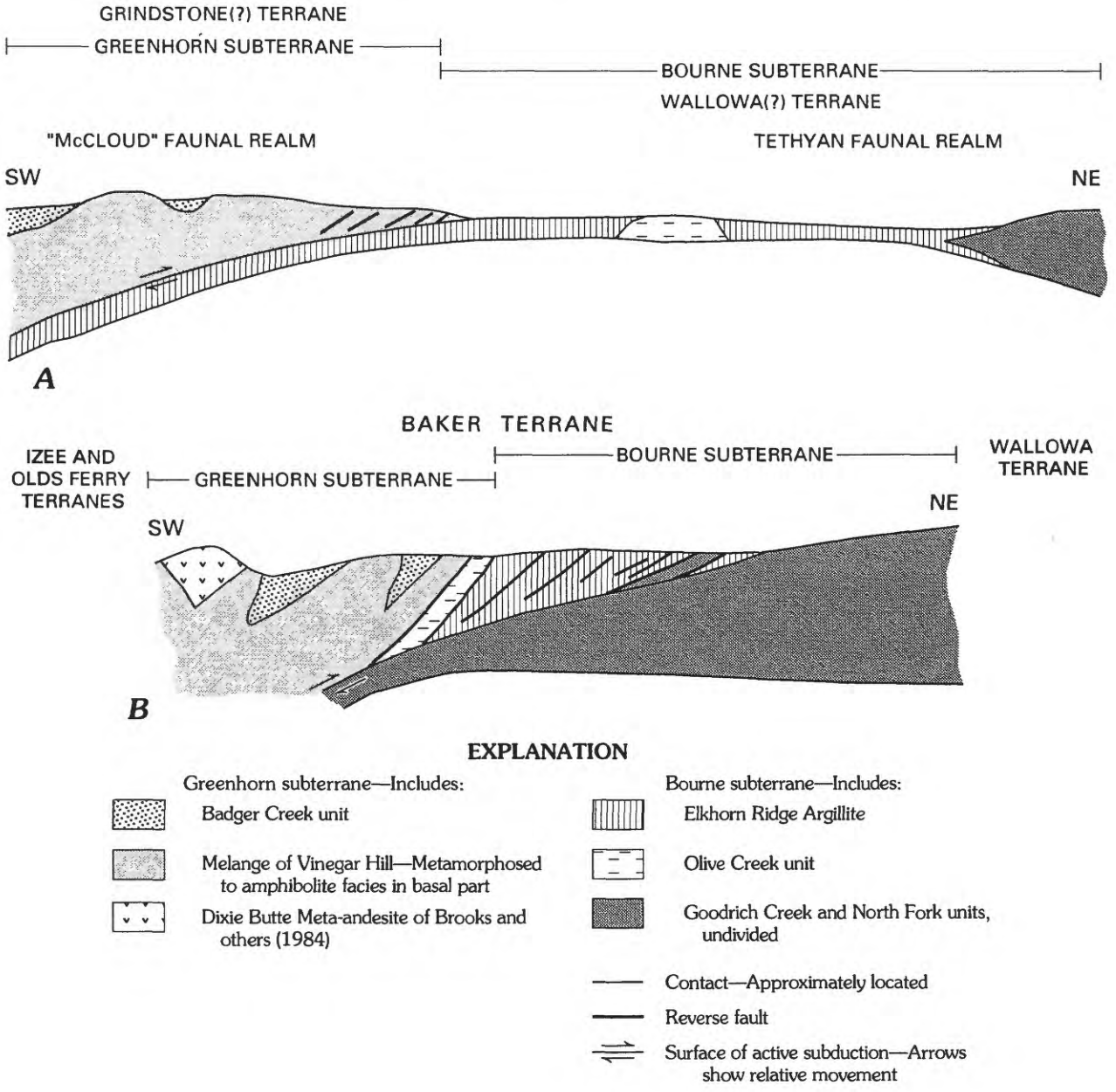

FIGURE 9.15.—Schematic diagram showing possible evolutionary path for development of Baker terrane. Compass directions, on diagrams and in caption, are approximate and are in present-day coordinates. *A*, The Pennsylvanian to the Late Triassic was a time of active subduction of open-ocean and (or) Wallowa terrane back-arc basin material beneath a volcanic arc southwest of the Greenhorn subterrane. Significant events in formation of Greenhorn subterrane units include deposition of Badger Creek unit as basinal sediments in a faunal realm similar to that of the McCloud Limestone, initial protrusion of serpentinite diapirs in the melange of Vinegar Hill, initial formation of high-pressure metamorphic rocks beneath the melange of Vinegar Hill, and (not shown on this diagram) eruption of the Dixie Butte Meta-andesite of Brooks and others (1984). Significant events in formation of Bourne subterrane units include deposition and soft-sediment deformation of Elkhorn Ridge Argillite, incorporation of Tethyan limestone olistoliths into Elkhorn Ridge Argillite, formation of alkalic seamounts of the Olive Creek unit in the open ocean, and formation of volcanic and sedimentary rocks of the Goodrich Creek and North Fork units as parts of the Wallowa arc. *B*, In Late Triassic to Early Jurassic time, units of the Bourne and Greenhorn subterranes were amalgamated into the Baker terrane owing to clogging of the subduction zone by the Wallowa terrane. Important events include incorporation of fragments of Wallowa terrane (Goodrich Creek and North Fork units) into the Bourne subterrane, initial development of cataclasite zones within Goodrich Creek unit, folding of all Baker terrane units about north-south and northeast-southwest fold axes, cessation of deposition of basinal sediments of Badger Creek unit, and shifting of depocenters to Izee and Olds Ferry terranes to the southwest.

separate lithic packages in the central part of the Baker terrane (Avé Lallemant and others, 1980; Engh, 1984).

In conclusion, there is evidence for four separate periods and (or) styles of deformation within the suture zone. (1) Early, long-lasting subduction-related deformations were marked by soft-sediment deformation, incorporation of limestone olistoliths, and development of type II melange in the Elkhorn Ridge Argillite of the Bourne subterrane and by development of polymict breccias in the Badger Creek unit of the Greenhorn subterrane. Subduction-related deformation may have started as early as the Pennsylvanian. (2) A later, locally penetrative deformation in the Late Triassic to Early Jurassic was related to incomplete subduction of the Bourne subterrane island-arc rocks, as evidenced by development and folding of cataclasite zones in the island-arc packages, development of mixed-rock zones (type IV melanges) in the Bourne subterrane, and development of north-trending fold axes in the Greenhorn subterrane. (3) Imposition of regionally extensive fracture cleavage took place in conjunction with development of major thrust and high-angle reverse faults in the Late Jurassic. (4) Melange matrixes were recrystallized and remobilized during emplacement of Late Jurassic intrusions.

The above discussion does not take into account the 60°+ postaccretion clockwise rotation of the Blue Mountains region identified by Wilson and Cox (1980). Assuming no significant rotation of the Baker terrane components during amalgamation from Late Triassic to Jurassic time, the original tectonic configuration would have placed an island arc (Wallowa terrane) to the northwest of the Bourne subterrane. The sense of subduction would have been from west to east, with the Wallowa terrane and intervening Bourne subterrane collapsing against the Olds Ferry terrane and flooring the Greenhorn subterrane to the east in the Late Triassic (see Dickinson, 1979; Hietanen, 1981).

REFERENCES CITED

Almy, R., III, 1977, Petrology and major element geochemistry of albite granite near Sparta, Oregon: Bellingham, Western Washington University M.S. thesis, 100 p.

Avé Lallemant, H.G., Phelps, D.W., and Sutter, J.F., 1980, $^{40}Ar/^{39}Ar$ ages of some pre-Tertiary plutonic and metamorphic rocks of eastern Oregon and their geologic relationships: Geology, v. 8, p. 371–374.

Blome, C.D., Jones, D.L., Murchey, B.L., and Lienecki, Margaret, 1986, Geologic implications of radiolarian-bearing Paleozoic and Mesozoic rocks from the Blue Mountains province, eastern Oregon, *in* Vallier, T.L., and Brooks, H.C., eds., Geology of the Blue Mountains region of Oregon, Idaho and Washington—Geologic implications of Paleozoic and Mesozoic paleontology and biostratigraphy, Blue Mountains province, Oregon and Idaho: U.S. Geological Survey Professional Paper 1435, p. 79–93.

Blome, C.D., and Nestell, M.K., 1991, Evolution of a Permo-Triassic sedimentary melange, Grindstone terrane, east-central Oregon: Geological Society of America Bulletin, v. 103, p. 1280–1296

Bloomer, S.H., 1983, Distribution and origin of igneous rocks from the landward slopes of the Mariana Trench—Implications for its structure and evolution: Journal of Geophysical Research, v. 88, p. 7411–7428.

Bostwick, D.L., and Koch, G.S., 1962, Permian and Triassic rocks of northeastern Oregon: Geological Society of America Bulletin, v. 73, p. 419–422.

Brooks, H.C., 1979, Plate tectonics and the geologic history of the Blue Mountains: Oregon Geology, v. 41, no. 5, p. 71–80.

Brooks, H.C., Ferns, M.L., and Avery, D.G., 1984, Geology and gold deposits map of the southwest quarter of the Bates quadrangle, Grant County, Oregon: Oregon Department of Geology and Mineral Industries Geologic Map Series GMS-35, scale 1:24,000.

Brooks, H.C., Ferns, M.L., Coward, R.I., Paul, K.K., and Nunlist, M., 1982, Geology and gold deposits map of the Bourne quadrangle, Oregon: Oregon Department of Geology and Mineral Industries Geologic Map Series GMS-19, scale 1:24,000.

Brooks, H.C., Ferns, M.L., and Mullen, E.D., 1982, Geology and gold deposits map of the Granite quadrangle, Oregon: Oregon Department of Geology and Mineral Industries Geologic Map Series GMS-25, scale 1:24,000.

Brooks, H.C., Ferns, M.L., Wheeler, G.R., and Avery, D.G., 1983, Geology and gold deposits map of the northeast quarter of the Bates quadrangle, Baker and Grant Counties, Oregon: Oregon Department of Geology and Mineral Industries Geologic Map Series GMS-29, scale 1:24,000.

Brooks, H.C., McIntyre, J.R., and Walker, G.W., 1976, Geology of the Oregon part of the Baker 1° by 2° quadrangle: Oregon Department of Geology and Mineral Industries Geological Map Series GMS-7, scale 1:250,000.

Brooks, H.C., and Vallier, T.L., 1978, Mesozoic rocks and tectonic evolution of eastern Oregon and western Idaho, *in* Howell, D.G., and McDougall, K.A., eds., Mesozoic paleogeography of the western United States (Pacific Coast Paleogeography Symposium 2, Sacramento, Calif.): Los Angeles, Society of Economic Paleontologists and Mineralogists, Pacific Section, p. 133–146.

Brown, C.E., and Thayer, T.P., 1966, Geologic map of the Canyon City quadrangle, northeastern Oregon: U.S. Geological Survey Miscellaneous Geologic Investigations Map I-447, scale 1:24,000.

Calder, C.P., 1986, Geochemistry of the Eureka-Excelsior gold-lode deposit and associated greenstones and metasedimentary rocks, Cracker Creek District, Baker County, Oregon: Cheney, Eastern Washington University, M.S. thesis, 82 p.

Coleman, R.G., 1963, Serpentinites, rodingites, and tectonic inclusions in alpine-type mountain chains: Geological Society of America Special Paper 73, 130 p.

Cowan, D.S., 1985, Structural styles in Mesozoic and Cenozoic melanges in the western Cordillera of North America: Geological Society of America Bulletin, v. 96, no. 4, p. 451–462.

Coward, R.I., 1983, Structural geology, stratigraphy and petrology of the Elkhorn Ridge Argillite, Sumpter area, northeastern Oregon: Houston, Rice University, Ph.D. dissertation, 144 p.

Dickinson, W.R., 1979, Mesozoic fore-arc basin in central Oregon: Geology, v. 7, p. 166–170.

Dickinson, W.R., and Thayer, T.P., 1978, Paleogeographic and paleotectonic implications of Mesozoic stratigraphy and structure in the John Day inlier in central Oregon, *in* Howell, D.G., and McDougall, K.A., eds., Mesozoic paleogeography of the Western United States (Pacific Coast Paleogeography Symposium 2, Sacramento, Calif.): Society of Economic Paleontologists and Mineralogists, Pacific Section, p. 147–161.

Engh, K.R., 1984, Structural geology of the Rastus Mountain area, east-central Oregon: Pullman, Washington State University, M.S. thesis, 78 p.

Evans, J.G., 1986, Geologic map of the North Fork John Day River roadless area, Grant County, Oregon: U.S. Geological Survey Miscellaneous Field Studies Map MF-1581-C, scale 1:48,000.

———1988, Geologic map of the Desolation Butte quadrangle, Grant and Umatilla Counties, Oregon: U.S. Geological Survey Geologic Quadrangle Map GQ-1654, scale 1:62,500.

Ferns, M.L., and Brooks, H.C., 1983, Serpentinite-matrix melanges in parts of the Blue Mountains of northeast Oregon: Geological Society of America Abstracts with Programs, v. 15, no. 5, p. 371.

Ferns, M.L., Brooks, H.C., and Avery, D.G., 1983, Geology and gold deposits map of the Greenhorn quadrangle, Baker and Grant Counties, Oregon: Oregon Department of Geology and Mineral Industries Geologic Map Series GMS-28, scale 1:24,000.

———1987, Geology and gold deposits map of the Elkhorn Peak quadrangle, Baker County, Oregon: Oregon Department of Geology and Mineral Industries Geologic Map Series GMS-41, scale 1:24,000.

Ferns, M.L., Brooks, H.C., and Ducette, J., 1982, Geology and mineral deposits of the Mt. Ireland quadrangle, Baker and Grant Counties, Oregon: Oregon Department of Geology and Mineral Industries Geologic Map Series GMS-22, scale 1:24,000.

Ferns, M.L., Brooks, H.C., and Wheeler, G.R., 1984, Geology and gold deposits map of the northwest quarter of the Bates quadrangle, Grant County, Oregon: Oregon Department of Geology and Mineral Industries Geologic Map Series GMS-31, scale 1:24,000.

Ferns, M.L., and Ramp, Len, 1988, Investigations of talc in Oregon: Oregon Department of Geology and Mineral Industries Special Paper 18, 52 p.

Gilluly, James, 1937, Geology and mineral resources of the Baker quadrangle, Oregon: U.S. Geological Survey Bulletin 879, 119 p.

Hietanen, Anna, 1981, Petrologic and structural studies in the northwestern Sierra Nevada, California—Extension of Sierra Nevada-Klamath suture system into eastern Oregon and western Idaho: U.S. Geological Survey Professional Paper 1226-C, 11 p.

Hotz, P.E., Lanphere, M.A., and Swanson, D.A., 1977, Triassic blueschist from California and north-central Oregon: Geology, v. 5, p. 659–663.

Hsü, K.J., 1968, Principles of melange and their bearing on the Franciscan-Knoxville paradox: Geological Society of America Bulletin, v. 79, p. 1063–1074.

Hunt, P.T., 1985, The metamorphic petrology and structural geology of the serpentinite-matrix melange in the Greenhorn Mountains: Eugene, University of Oregon, M.S. thesis, 127 p.

Kays, M.A., Ferns, M.L., and Brooks, H.C., 1987, Metamorphism of Triassic-Paleozoic belt rocks—A guide to field and petrologic relations in the oceanic melange, Klamath and Blue Mountains, California and Oregon, *in* Ernst, W.G., ed., Metamorphism and crustal evolution of the Western United States (Rubey Volume VII): Englewood, Cliffs, N.J., Prentice-Hall, p. 1098–1120.

Morris, E.M., and Wardlaw, B.R., 1986, Conodont ages for limestone of eastern Oregon and their implication for pre-Tertiary melange terranes, *in* Vallier, T.L., and Brooks, H.C., eds., Geology of the Blue Mountains region of Oregon, Idaho, and Washington—Geologic implications of Paleozoic and Mesozoic paleontology and biostratigraphy, Blue Mountains province, Oregon and Idaho: U.S. Geological Survey Professional Paper 1435, p. 59–63.

Mortimer, N., 1986, Late Triassic, arc-related, potassic igneous rocks in the North American Cordillera: Geology, v. 14, p. 1035–1038.

Mullen, E.D., 1978, Geology of the Greenhorn Mountains, northeastern Oregon: Corvallis, Oregon State University, M.S. thesis, 372 p.

———1980, Temperature-pressure progression in high-pressure Permo-Triassic metamorphic rocks of northeast Oregon [abs.]: EOS (American Geophysical Union Transactions), v. 61, p. 70.

———1982, Permian and Triassic forearc terrane of the Blue Mountains, northeast Oregon—Geochemical and other evidence [abs.]: Geological Society of America Abstracts with Programs, v. 14, p. 573.

———1985, Petrologic character of Permian and Triassic greenstones from the melange terrane of eastern Oregon and their implications for terrane origin: Geology v. 13, p. 131–134.

Nestell, M.K., 1983, Permian foraminiferal faunas of central and eastern Oregon [abs.]: Geological Society of America Abstracts with Programs, v. 15, p. 372.

Pardee, J.T., and Hewett, D.F., 1914, Geology and mineral resources of the Sumpter quadrangle, Oregon: Oregon Bureau of Mines and Geology, Mineral Resources of Oregon, v. 1, no. 6, p. 3–128.

Pardee, J.T., Hewett, D.F., Rosenkranz, T.H., Katz, F.J., and Calkins, F.C., 1941, Preliminary geologic map of the Sumpter quadrangle: Oregon Department of Geology and Mineral Industries geologic map, scale 1:96,000.

Pearce, J.A., and Cann, J.R., 1973, Tectonic setting of basic volcanic rocks determined using trace element analyses: Earth and Planetary Science Letters, v. 19, p. 290–300.

Phelps, D.W., 1978, Petrology, geochemistry, and structural geology of Mesozoic rocks in the Sparta quadrangle and Oxbow and Brownlee Reservoir areas, eastern Oregon and western Idaho: Houston, Rice University, Ph.D. dissertation, 241 p.

———1979, Petrology, geochemistry, and origin of the Sparta quartz diorite-trondhjemite complex, northeastern Oregon, *in* Barker, Fred, ed., Trondhjemites, dacites, and related rocks: New York, Elsevier, p. 547–580.

Robertson, A.H.F., and Woodcock, N.H., 1983, Genesis of the Batinah melange above the Semail ophiolite, Oman: Journal of Structural Geology, v. 5, no. 1, p. 1–17.

Saleeby, J.B., 1979, Kaweah serpentinite melange, southwest Sierra Nevada foothills, California: Geological Society of America Bulletin, v. 90, no. 1, p. 29–46.

Silberling, N.J., Jones, D.L., Blake, M.C., Jr., and Howell, D.G., 1984, Lithotectonic terrane map of the western conterminous United States, *in* Silberling, N.J., and Jones, D.L., eds., Lithotectonic terrane maps of the North American Cordillera: U.S. Geological Survey Open-File Report 84-523, 43 p.

Stimson, E.J., 1980, Geology and metamorphic petrology of the Elkhorn Ridge area, northeastern Oregon: Eugene, University of Oregon, M.S. thesis, 123 p.

Taylor, B., and Smoot, N.C., 1984, Morphology of Bonin forearc submarine canyons: Geology, v. 12, p. 724–727.

Vallier, T.L., 1985, Petrologic implications for the tectonic evolution of the Blue Mountains island arc, eastern Oregon and western Idaho [abs.]: Geologic Society of America Abstracts with Programs, v. 17, p. 269.

Vhay, J.S., 1960, A preliminary report on the copper-cobalt deposits of the Quartzburg district: U. S. Geological Survey Open-File Report 60-143, 20 p.

Walker, N.W., 1983, Pre-Tertiary tectonic evolution of northeastern Oregon and west-central Idaho—constraints based on U/Pb ages of zircons [abs.]: Geological Society of America Abstracts with Programs, v. 15, no. 5, p. 371.

Wheeler, G.R., 1976, Geology of the Vinegar Hill area, Grant County, Oregon: Seattle, University of Washington Ph.D. dissertation, 94 p.

Wilson, Douglas, and Cox, Allan, 1980, Paleomagnetic evidence for tectonic rotation of Jurassic plutons in the Blue Mountains, eastern Oregon: Journal of Geophysical Research, v. 85, p. 3681-3689.

Wood, D.A., Jordon, J.L., and Treuil, M., 1979, A re-appraisal of the usage of trace elements to classify and discriminate between magma series erupted at different tectonic settings: Earth and Planetary Science Letters, v. 45, p. 326-336.

10. AN $^{40}Ar/^{39}Ar$ CHRONICLE OF THE TECTONIC DEVELOPMENT OF THE SALMON RIVER SUTURE ZONE, WESTERN IDAHO

By LAWRENCE W. SNEE, KAREN LUND, JOHN F. SUTTER, DAVID E. BALCER,[1] *and* KARL V. EVANS

CONTENTS

	Page
Abstract	359
Introduction	359
Acknowledgments	360
Geologic setting	360
Analytical methods	366
$^{40}Ar/^{39}Ar$ techniques	366
U-Pb techniques	368
Sample distribution and isotopic data	369
Interpretation	369
Basement rocks of the Snake River canyon area and associated plutons of island-arc affinity	369
Metamorphic rocks of the Riggins Group and Seven Devils island arc	385
Deformed plutons of the Salmon River suture zone	396
Undeformed plutons of the Idaho batholith	398
Discussion	402
Metamorphism and plutonism in eastern Oregon and western Idaho	403
Cooling and uplift history of the area east of the Salmon River suture zone	406
Depth of emplacement of muscovite-biotite granite	407
Erosion and Cretaceous sedimentation	408
Summary of Cretaceous tectonic history—central Idaho and southwestern Montana	409
Conclusion	409
References cited	411

ABSTRACT

In west-central Idaho, rocks of island-arc origin are in sharp contact with North American continental rocks. The contact, called the Salmon River suture zone, is marked by lithologic and chemical differences, and rocks directly adjacent to the suture zone are characterized by high-grade metamorphism and structural complexity. The origin and age of the suture zone have been the subject of debate. $^{40}Ar/^{39}Ar$ age-spectrum data for hornblende, biotite, muscovite, and microcline from 48 samples of metamorphic and plutonic rocks in both island-arc and continental settings, and U-Pb data for one sample of continental plutonic rock, record the geologic development of this area between 244 and 55 Ma. Rocks of island-arc origin, which include the Riggins and Seven Devils Groups, contain evidence for a period of metamorphism at about 244 Ma and two periods of plutonism at about 227 and 145 Ma, all of which occurred before the island-arc rocks were accreted to the North American continent. Accretion of the island-arc terrane took place along the Salmon River suture zone in western Idaho and is recorded by at least four episodes of metamorphism at 130, 118, 109, and 101 Ma. Minor plutonism took place within this interval; the most extensive of this plutonism has been dated at about 115 Ma. The island-arc terrane was stitched to the North American continent at 93 Ma by the emplacement of tonalitic plutons, some of which were emplaced as deep as 20 km or more. These plutons are the first intrusions of the Idaho batholith, and chemically similar rocks were emplaced up to 139 km east of the suture zone until about 86 Ma. Porphyry mineralization is associated with this stage of plutonic emplacement. At or before 88 Ma, rapid uplift of continental rocks at rates greater than 3 mm/yr began along high-angle structures within and adjacent to the suture zone; this rapid uplift moved eastward about 3 m.y. later. Postdeformational cooling or uplift continued in some places along the suture zone until 79 Ma. More than 15 km of uplift affected a region extending at least 50 km eastward from the suture zone during a 10-m.y. period from about 88 to 78 Ma; no plutonic activity during this uplift is recorded by the argon data. Beginning at about 78 Ma, muscovite-biotite granites of the Idaho batholith were emplaced at depths less than 9 km; the granites cooled below 300°C by 70 Ma. From 78 to 68 Ma, mineralized quartz veins filled fractures and faults in roof pendants of the granites and are apparently genetically related to the granites. By 55 Ma, a large part of the presently exposed Cretaceous plutons of the Idaho batholith was at a crustal depth of about 5 km or less and had cooled to less than 130°C. The sedimentary record to the east and west of the Salmon River suture zone reflects this complex history of metamorphism, deformation, plutonism, and uplift that took place between 130 and 55 Ma.

INTRODUCTION

In western Idaho, oceanic rocks of island-arc origin are in sharp contact with continental units (Hamilton, 1963; Lund, 1984); the contact is north-trending and is thought to be the western extent of North American sialic crust (Criss and Fleck, 1987; Lund and Snee, 1988). Nonplutonic rocks west of this boundary, which was named the Salmon River suture zone by Lund and Snee (1988), consist mainly of volcanic and metavolcanic rocks of the Seven Devils and

[1]Chevron, USA, 935 Gravier St., Rm. 910, New Orleans, LA 70112

Riggins Groups (Hamilton, 1963; Vallier, 1977). To the east, the metasedimentary rocks are correlative with Belt Supergroup and pre-Belt units of Proterozoic age and with continental sedimentary units of uncertain, but probable Late Proterozoic or Paleozoic, age (fig. 10.1).

Although there is a clear difference in lithology across the boundary, the exact location of the lithologic change is generally obscured by high-grade metamorphism and by younger deformed and undeformed plutons that clearly crosscut the regional metamorphic fabric. However, within the plutonic rocks, the boundary is sharply defined by a major discontinuity in initial $^{87}Sr/^{86}Sr$ ratios. To the west, initial $^{87}Sr/^{86}Sr$ ratios are 0.704 or less; to the east, initial $^{87}Sr/^{86}Sr$ ratios are 0.706 or greater (Armstrong and others, 1977; Fleck and Criss, 1985; Davidson, 1989). In some ways, the discontinuity in initial $^{87}Sr/^{86}Sr$ ratios is the easiest way to trace the boundary because the discontinuity is sharply defined within the younger, crosscutting plutons. The discontinuity trends northward in Idaho from near McCall to Orofino where it abruptly swings westward (Armstrong and others, 1977; Fleck and Criss, 1985). To the south, the discontinuity is covered by Cenozoic rocks.

Even though a major suture zone has been suspected in this area since 1976 (Hamilton, 1976; Onasch, 1976; Hyndman and Talbot, 1976), its tectonic origin remains obscure. In an attempt to provide some regional time and temperature constraints on the formation of this unusual crustal boundary in west-central Idaho, we have studied $^{40}Ar/^{39}Ar$ age spectra of hornblende, biotite, muscovite, and microcline from metamorphic and plutonic rocks within a large area extending from eastern Oregon to western Montana and straddling the suture zone. U-Pb data for zircon and sphene from one sample of tonalite from the Idaho batholith are also included. The purpose of our work is to determine the age of metamorphism, deformation, plutonism, cooling, and uplift of this large area and to use these data to unravel its tectonic evolution during the Cretaceous. In addition, we investigate whether a temporal relationship exists between the Cretaceous tectonic development of this area and the structural activity along the suture zone between the island-arc terranes and the North American continent. This project has been done in conjunction with a mapping study of the suture zone; the results of the mapping study are presented in Lund (1984; chap. 14, this volume), and an interpretation of the tectonic development of the suture zone is discussed within the framework of the mapping and $^{40}Ar/^{39}Ar$ thermochronologic study in Lund and Snee (1988). In the following discussion, some of the details from previously published works are summarized and placed within the context of this study.

ACKNOWLEDGMENTS

The authors have benefited from the insight and ideas of E-an Zen, Tracy Vallier, Jane Selverstone, Robert Scholten, Cathy Manduca, Mel Kuntz, Anna Hietanen, Jane Hammarstrom, Warren Hamilton, Jad D'Allura, Gary Davidson, and Howard Brooks. Earl Bennett, Wayne Hall, Chris Gammons, and Thor Kiilsgaard kindly provided some samples from the Idaho batholith. Special thanks go to George Simmons for spectacular helicopter rides to remote sample sites in the Snake River canyon. Careful reviews of the manuscript were provided by Tracy Vallier and Howard Brooks.

GEOLOGIC SETTING

In the Riggins-Slate Creek area of west-central Idaho (fig. 10.2), pre-Cretaceous rocks east of the Salmon River suture zone are metasedimentary rocks whose protoliths were derived from terrigenous sources. These rocks have been divided into five tectonostratigraphic packages by Lund (1984). The metamorphic rocks are preserved as roof pendants and xenoliths in the Idaho batholith. The structurally lowest and probably oldest tectonostratigraphic unit is composed of mica schist and feldspathic gneiss with interleaved calcsilicate and quartzitic gneiss; it was intruded by igneous rocks that predate the Idaho batholith and are now amphibolite and augen gneiss (Lund, 1984). This lowermost unit is probably Middle Proterozoic in age on the basis of an inferred U-Pb zircon crystallization age of the augen gneiss of about 1,370 Ma (Evans and Fischer, 1986). Above this unit lie two Middle Proterozoic(?) tectonostratigraphic units composed of calcsilicate gneiss and quartzite with a combined thickness of about 3,000 m. The uppermost two tectonostratigraphic units are probably either Late Proterozoic or Paleozoic in age and form

FIGURE 10.1.—Index maps of region discussed in text. *A*, General geology and location map. Numbered areas are 1, Bald Mountain batholith; 2, Wallowa batholith; 3, The Oxbow on the Snake River; 4, Pittsburg Landing; 5, confluence of Imnaha and Snake Rivers; 6, Round Valley; 7, Riggins; 8, Slate Creek; 9, Orofino; 10, McCall; 11, Buffalo Hump area; 12, Yellow Pine; 13, Stanley; 14, Thompson Creek; 15, Warm Spring Forest Service Station; 16, Warm Lake; 17, Pioneer Mountains; and 18, Hailey. *B*, Areas of figures 10.2 through 10.6, 10.21, and 10.23.

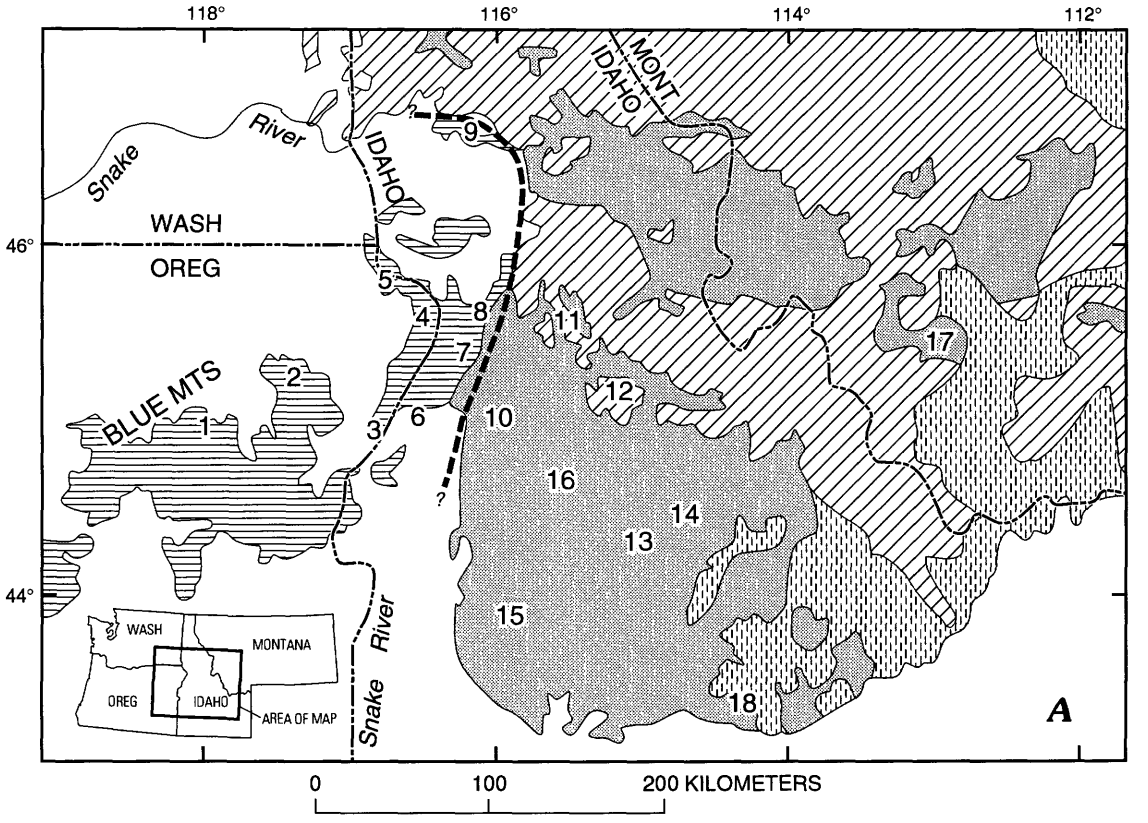

EXPLANATION

- Cenozoic volcanic and sedimentary rocks
- Tertiary and Mesozoic igneous rocks
- Mesozoic and Paleozoic oceanic and island-arc volcanic, plutonic, and sedimentary rocks
- Mesozoic and Paleozoic sedimentary rocks
- Precambrian sedimentary, plutonic, and sedimentary rocks
- Salmon River suture zone—Queried where covered by younger rocks

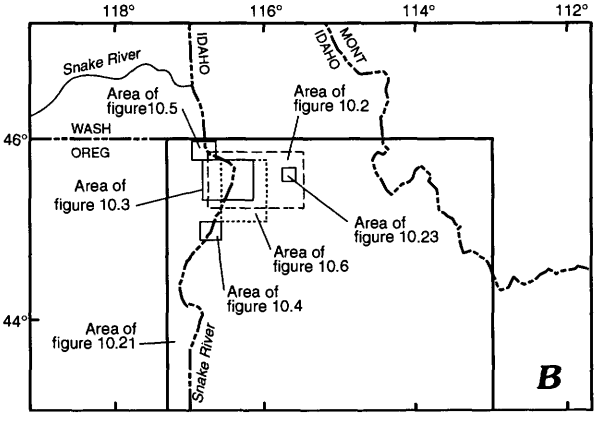

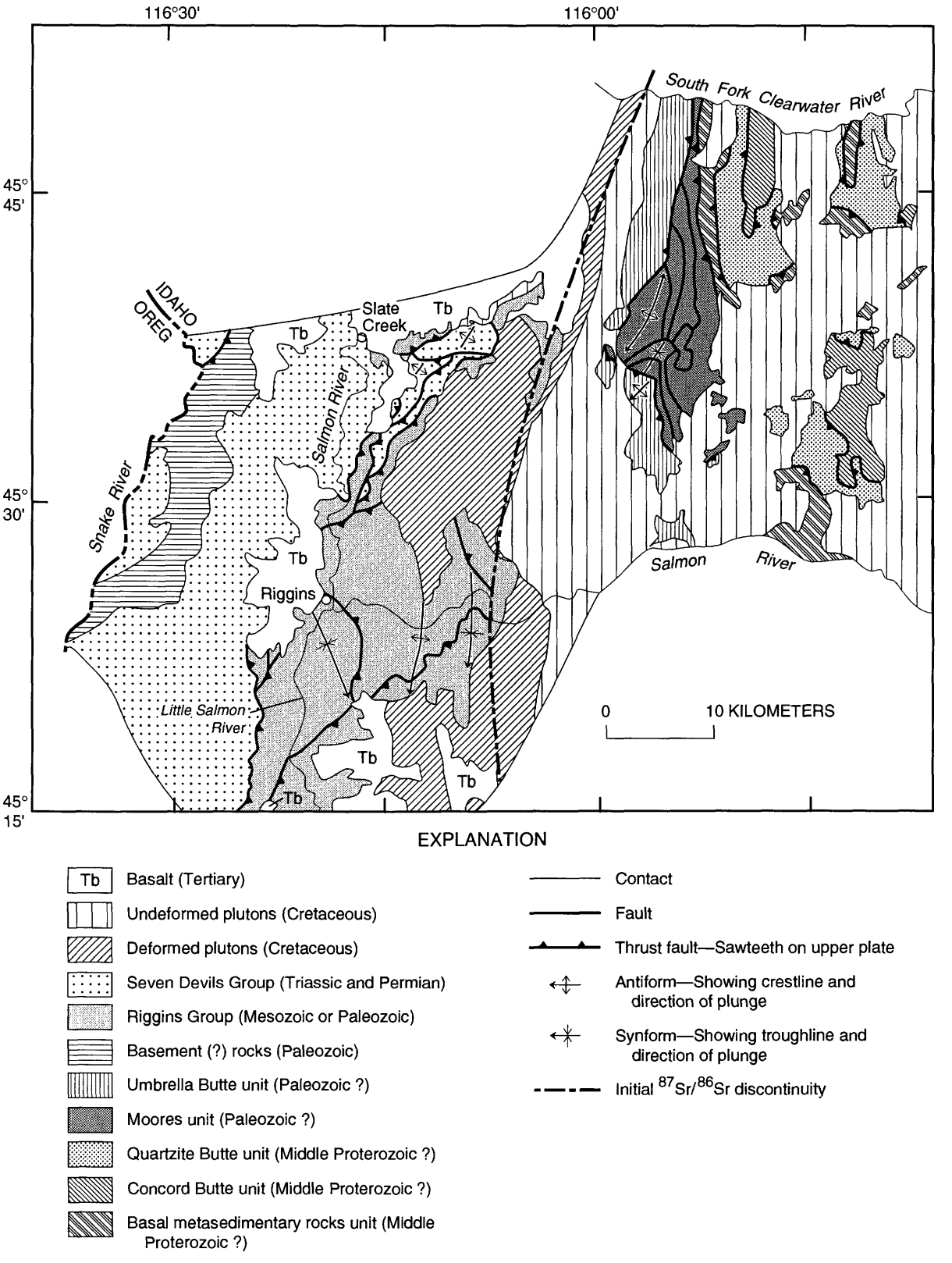

FIGURE 10.2.—Geologic map of study area along Salmon River suture zone in west-central Idaho. Geology modified from Lund and Snee (1988); stratigraphic nomenclature directly from Lund and Snee (1988, fig. 11-2). Salmon River suture zone marked by discontinuity in initial $^{87}Sr/^{86}Sr$ ratio is shown as dot-and-dashed line. Geology of unpatterned areas is not compiled.

a distinctive multilithologic sequence composed of quartzite, quartzite-pebble quartzose conglomerate, calcsilicate gneiss, mica schist, and marble.

West of the suture zone, the metamorphic country rocks consist of felsic to mafic volcanic, volcaniclastic, intrusive, volcanogenic-sedimentary, and calcareous rocks (Hietanen, 1962: Hamilton, 1963; Onasch, 1977; Vallier, 1977; Myers, 1982; Lund, 1984). Nearest the suture zone, units of pre-Tertiary age are of low, middle, and high metamorphic grade and were named the Riggins Group by Hamilton (1963). The Riggins Group consists of two lower units composed of volcanic rocks and a structurally higher unit composed of carbonaceous and calcareous phyllite to schist and minor carbonate rocks. Some sheared serpentinite bodies are present along faults (Hamilton, 1963; Onasch, 1977).

The Riggins Group structurally overlies more extensive Permian and Middle and Upper Triassic rocks of the Seven Devils island-arc sequence of Dickinson (1979) (also known as the Wallowa terrane of Silberling and others, 1984). In the vicinity of Snake River canyon, rocks of the Seven Devils Group (Vallier, 1977) are predominantly very low grade to medium-grade metamorphosed volcanic rocks with minor interbedded volcaniclastic conglomerate and sedimentary rocks. Stratigraphically overlying the Seven Devils Group is a sequence of interfingered volcaniclastic, carbonate, and minor volcanic rocks (Lund and others, 1983a; Lund, 1984 and chap. 14, this volume). A similar sequence overlies the Seven Devils Group in northeastern Oregon (Follo and Sievers, 1984; Follo, 1992, 1994). This similarity suggests that the change upward in the stratigraphic section from volcanic units of the Seven Devils Group to carbonaceous and calcareous shale and carbonate rocks (and in eastern Oregon, younger noncalcareous shale and conglomerate) is of regional extent.

Metamorphic grade both east and west of the Salmon River suture zone decreases away from the suture zone. East of the suture zone in the Riggins and Slate Creek areas the highest grade rocks are of upper amphibolite facies and occur in a band about 6 km wide adjacent to the suture zone. The rocks of this band include sillimanite-bearing metapsammitic rocks, garnet- and sillimanite-bearing metapelitic rocks, and diopside-bearing calcsilicate gneiss. Because of stacking by thrust faulting, metamorphic facies are inverted to the east, where higher grade rocks structurally overlie lower grade rocks (Lund and Snee, 1988).

Metamorphic grade in the Riggins Group and Seven Devils island-arc sequence decreases westward from the suture zone. The three formations of the Riggins Group are at lowest metamorphic grade near Riggins and increase in grade toward the northeast, east, and south (Hamilton, 1963; Onasch, 1977, 1987). At lowest grades, greenschist-facies rocks are muscovite and (or) chlorite schist, with plagioclase, quartz, and epidote in the groundmass and, at slightly higher grade, with porphyroblasts of biotite flakes, unoriented hornblende needles, and carbonate rhombs (Hamilton, 1963). Closer to the Salmon River suture zone, the rocks are garnet-muscovite schist, biotite schist, garnet-hornblende-biotite schist, and garnet-amphibolite gneiss, depending on original composition. Along a narrow belt adjacent to the suture zone in this area, the rocks of the Riggins Group contain clear evidence of more than one dynamothermal event. This high-grade overprinted zone is about 10 km wide, but it widens south of the Salmon River. In these rocks, garnet, hornblende, and other porphyroblasts were rolled during formation of a secondary schistosity (Lund and Snee, 1988; see also figs. 10.15 and 10.16); growth of new minerals is indicated in many places by the presence of two generations of the same phase that have different orientations and (or) fabric characteristics. In some areas, fabric and complex crosscutting relations are consistent with emplacement of some dikes and small plutonic bodies between metamorphic pulses.

Along the Snake River (Vallier, 1977) and near Riggins (Hamilton, 1963), the Seven Devils Group is mostly metamorphosed volcanic and volcaniclastic rocks. Metamorphic grade in these rocks increases to the northeast from the Riggins area. In the Slate Creek area, the Seven Devils Group is at greenschist facies and includes rocks containing metavolcanic clasts in a metatuffaceous matrix (Lund, 1984). Recrystallized quartz, untwinned plagioclase, chlorite, tremolite, epidote, biotite, and muscovite constitute the mineralogically variable groundmass. Plagioclase, garnet, and chlorite porphyroblasts are common.

The stratigraphic section of the Seven Devils island-arc sequence reflects a complex history of volcanic-island-arc formation through late-stage quiescence (Lund and others, 1983a; Follo and Sievers, 1984; Lund, chap. 14, this volume; Follo, 1992, 1994). Chemistry of the Riggins Group was described by Hamilton (1963) as "similar in many respects to the Seven Devils volcanics"; in addition, he noted that "the distribution of minor elements [in the Seven Devils Group] is *** identical with that in the metavolcanic rocks of the Riggins Group." Furthermore, detailed mapping by Onasch (1977, 1987), Lund (1984 and chap. 14, this volume), and McCollough (1984) has shown that units of the Riggins Group are traceable northward along strike and across meta-

morphic isograds into rocks earlier mapped as part of the Seven Devils island-arc sequence by Hamilton (1963).

Hamilton (1963) named the Riggins Group as a separate stratigraphic unit from the Seven Devils Group on the basis of differences in metamorphic grade and the presence of a separating structure. However, the metamorphic grade of the Seven Devils Group clearly increases to upper greenschist or amphibolite facies near its eastern extent where it is in thrust contact with the Riggins Group of similar grade (Lund, 1984; Onasch, 1987). The structure that separates these two sequences was named the Rapid River thrust fault by Hamilton (1963), who later stated that it is the suture that marks the collision of the Seven Devils ensimatic island arc with the continent during Late Permian or Triassic time (Hamilton, 1976). In contrast, Lund and Snee (1988) have suggested that there is no direct evidence that the Seven Devils and Riggins Groups represent different units or terranes; instead, the Riggins Group is simply the more highly metamorphosed equivalent of the Seven Devils Group. The Rapid River thrust fault, then, is not a suture between two different terranes but is one of a group of structures of similar age within a single package of rocks. In fact, the Rapid River thrust fault and other associated structures commonly place higher grade metamorphic rocks over their lower grade metamorphic equivalents; this type of structural stacking is probably related to development of the Salmon River suture zone (Lund, 1984 and chap. 14, this volume; Lund and Snee, 1988).

Within the Snake River canyon, Vallier (1974, 1977) mapped and described three areas of basement rocks (Cougar Creek Complex of Vallier, 1968) underlying units of the Seven Devils Group (see figs. 10.3, 10.4, and 10.5). From north to south, these areas are the confluence of the Imnaha and Snake Rivers, the Pittsburg Landing area, and the area of The Oxbow. The exposures of basement rocks were mapped in part as shear zones that include crushed and recrystallized breccia, schist, mylonite, gneissic mylonite, amphibolite, metadiorite, metagabbro, and metatrondhjemite (Vallier, 1974). The rocks are generally metamorphosed to amphibolite facies, but retrograde chlorite, especially after biotite, is common. In the Imnaha River and Pittsburg Landing areas, younger plutons and dikes of tonalite and quartz diorite intruded the metamorphic units; these relatively unmetamorphosed intrusive rocks commonly also contain chloritized biotite. Ages of metamorphosed rocks and unmetamorphosed plutonic rocks in the basement complexes, based on U-Pb isotopic ages on zircons, range from 266 to 145 Ma (Walker, 1986).

The relation between the basement complexes and the Seven Devils Group has been the subject of speculation but is becoming clarified (White and Vallier, in press). The basement rocks are generally amphibolite facies gneisses and highly deformed. In contrast, nearby rocks of the Seven Devils Group are low grade to unmetamorphosed and exhibit primary volcanic and sedimentary textures. Plutons are common in both the basement rocks and the Seven Devils Group. Some of the plutons were emplaced before metamorphism of the basement complex; others were emplaced after metamorphism of the basement rocks; still others were emplaced after metamorphism of the Seven Devils Group. Wherever in contact, the basement rocks and the Seven Devils Group are separated by faults. Generally these are high-angle structures, but at Pittsburg Landing, Vallier (1968, 1977; White and Vallier, in press) mapped a thrust fault separating lower-plate Middle Jurassic (Bajocian to Callovian) strata from the overriding metamorphic and plutonic rocks of the Permian Cougar Creek (basement) Complex and an unnamed member of the Wild Sheep Creek Formation, a unit of the Seven Devils Group and Middle Triassic (Ladinian; between about 235 and 230 Ma) in age. This thrust fault, therefore, must be younger than Middle Jurassic. In contrast, other structures, such as the ductile shear zones developed in rocks at the confluence of the Imnaha and Snake Rivers (fig. 10.5) and the area of The Oxbow (fig. 10.4), are likely older. Therefore isotopic age constraints are needed for several important questions, such as, what is the age of metamorphism of the Cougar Creek (basement) Complex, what is the age of the various plutonic rocks, and when did the thrusts, high-angle faults, and shear zones form?

Postmetamorphic plutonic rocks intrude the Seven Devils and Riggins Groups or correlative units in numerous places in the region in addition to Snake River canyon. Two of the largest of these plutons are the Wallowa and Bald Mountain batholiths (Taubeneck, chap. 2, this volume), which intrude units correlative with the Seven Devils Group in northeastern Oregon (fig. 10.1). Previously published Rb-Sr and K-Ar dates for these intrusive bodies (Armstrong and others, 1977) are widely discordant but generally bracket emplacement within the Jurassic to the Cretaceous. In addition, stocks that were emplaced after metamorphism of the basement rocks are exposed east of Snake River canyon near the Rapid River thrust fault. Several small plutons along the Rapid River southwest of Riggins are crosscut by structures like the Rapid River thrust fault but appear to intrude mylonites and faults (Sarewitz, 1982) that are apparently older than the Rapid River

thrust fault. These plutons along the Rapid River exhibit metamorphic effects similar in grade to that displayed by the surrounding Seven Devils Group. This similarity in metamorphic grade indicates that the plutons were emplaced after regional metamorphism of the Cougar Creek (basement) Complex but prior to metamorphism of the Seven Devils Group, which has been attributed to activity on the Salmon River suture zone (Lund and Snee, 1988).

Within the highest grade and most deformed rocks of some parts of the Salmon River suture zone are large areas of strongly deformed plutons of tonalitic and trondhjemitic compositions. The most extensive exposures of these plutons are near McCall and near Orofino, Idaho. Although some of these plutons are about 90 Ma (see next paragraph), an increasing amount of isotopic data indicate that some are about 115 Ma (Davidson, 1990; C.A. Manduca, California Institute of Technology, unpub. data, 1990; Snee and others, in press). The 115-Ma plutons are of island-arc chemical affinity (Davidson, 1990) and generally have initial $^{87}Sr/^{86}Sr$ ratios of less than 0.704 (Armstrong and others, 1977; Criss and Fleck, 1987; Snee and others, in press). Temporal and spatial relations indicate that these plutons were emplaced during the period of metamorphism that affected Riggins Group rocks (Onasch, 1987).

A younger group of hornblende-biotite tonalite and granodiorite plutons (about 95 to 90 Ma; Lund and Snee, 1988), some of which contain magmatic epidote, intruded along the Salmon River suture zone after the youngest metamorphism and deformation affecting the Riggins Group and Seven Devils island arc had taken place (fig. 10.2). These plutons cut rocks of both island-arc and North American continental affinities. Where primary epidote is present, petrologic evidence indicates depths of emplacement greater than 25 km (Zen and Hammarstrom, 1984); however, not all tonalites contain epidote and, as is argued below, this structurally complex zone may juxtapose various levels of the same pluton. These plutons are the first-phase intrusions of the Idaho batholith, and their emplacement occurred after the island-arc terrane(s) finally accreted to the North American continent (Lund, 1984; Lund and Snee, 1988). The plutons and roof pendants within them and nearby metamorphic rocks of the Riggins Group were deformed together by one or more postemplacement events that were confined to a zone about 5 km wide along the suture zone. The fabrics that formed during this deformation are manifested by steep schistosity that parallels the suture zone and by steep southeast-plunging mineral lineations that dominate the fabric in plutonic rocks on the west side of the suture zone (Lund, 1984).

Away from the suture zone, hornblende-biotite tonalite and biotite granodiorite plutons intruded both terranes (fig. 10.2). Epidote is present as a primary magmatic mineral in some of the undeformed tonalites (Hammarstrom and Zen, 1988). The rocks are mostly homogeneous in texture, although a foliation is present in some places. The magmas intruded by magmatic stoping (Lund, 1984). These plutonic rocks may be undeformed equivalents of, or cogenetic with, tonalitic rocks that were emplaced into and deformed along the suture zone. They may also be laterally equivalent to similar plutons along the east side of the Idaho batholith near Thompson Creek, Hailey, and Stanley (fig. 10.1; see also fig. 10.21).

In the eastern, continental terrane, the tonalite, granodiorite, and metamorphic country rocks were intruded by biotite granite to granodiorite and muscovite-biotite granite plutons with peraluminous to near-peraluminous chemical compositions. Muscovite is primary in the muscovite-biotite granites and is a common deuteric or hydrothermal alteration phase in the biotite granite to granodiorite. These plutons have no directional fabric (Lund and others, 1986) and, like the tonalite, intruded passively by magmatic stoping. Country-rock xenoliths, which are prevalent in the upper parts of the plutons, were not rotated during stoping (Lund, 1984). Some workers (for example, Hyndman, 1981; W.B. Hamilton, U.S. Geological Survey, oral commun., 1988) have argued that because the muscovite-biotite granite plutons contain magmatic muscovite, they must have been emplaced at depths greater than 17 km. Lund and Snee (1988) and Lund and others (1986) presented evidence, based on cooling calculations, that the granites must have been emplaced at depths *less than* 9 km (see below).

The ages of emplacement of plutons within the Idaho batholith have been difficult to define despite the numerous attempts at isotopic dating that have been made. The earliest numerical ages on the plutons were Pb-alpha determinations by Larsen and Schmidt (1958) that ranged between 90 and 135 Ma. This method has since been shown to provide unreliable results, and in the case of the Idaho batholith, the Pb-alpha dates are at least 20 percent too old. The vast majority of isotopic dates for Idaho batholith plutons have been determined by the conventional K-Ar method, but the complex subsolidus thermal and tectonic history of the batholith has caused inconsistent results which range from 117 to about 50 Ma (for example, Armstrong, 1975; Armstrong and others, 1977; Criss and others, 1982). Many of these dates are geologically meaningless when they are

carefully evaluated. Because more accurate and precise results are now available, these earlier dates are not used in this paper for evaluating ages of intrusion of plutons of the Idaho batholith.

ANALYTICAL METHODS

$^{40}Ar/^{39}Ar$ TECHNIQUES

The $^{40}Ar/^{39}Ar$ dating technique is a variant of the conventional K-Ar method. To obtain a date by this technique, the sample of unknown age and a standard of known age are irradiated together in a nuclear reactor to produce ^{39}Ar from ^{39}K by fast-neutron bombardment. After irradiation, the $^{40}Ar/^{39}Ar$ ratios of sample and standard are measured. The date of a sample can be calculated from its $^{40}Ar/^{39}Ar$ ratio in comparison with the $^{40}Ar/^{39}Ar$ ratio of the standard. Only the isotopic composition of the argon of the sample and standard need be measured and this is done by gas-source mass spectrometry, potentially a very precise analytical technique. In contrast, for a conventional K-Ar date, both ^{40}K and ^{40}Ar must be measured quantitatively. To do this, argon (a gas) in one aliquot of sample is measured by isotope-dilution, gas-source mass spectrometry. Potassium (a solid) in a different aliquot of sample is determined by some other analytical method such as flame photometry, X-ray fluorescence, or isotope-dilution, solid-source mass spectrometry. Thus, one inherent problem of the conventional K-Ar technique is the necessity of measuring isotopic abundances for separate aliquots of the same sample. This poses the danger that, because of sample inhomogeneity, different potassium and (or) argon contents may exist in each aliquot. Two major advantages of the $^{40}Ar/^{39}Ar$ dating method are (1) only isotopic ratios of argon need be determined, and (2) all measurements are made on the same sample aliquot, thus avoiding the question of inhomogeneity. In addition, by the $^{40}Ar/^{39}Ar$ method, it is possible to obtain a series of dates from a single sample when argon is extracted by step-heating. The combination of these advantages potentially increases both the accuracy and precision of the $^{40}Ar/^{39}Ar$ method over the conventional K-Ar technique. However, the $^{40}Ar/^{39}Ar$ technique will suffer if proper corrections are not made for interfering radiation-induced isotopes; these corrections are well known and routinely made.

Details of the $^{40}Ar/^{39}Ar$ dating technique have been discussed by Dalrymple and others (1981). The procedures specific to our study are described in Snee and others (1985, 1987b, 1988). To place the data of this paper in the proper perspective, however, a summary of the formulation of the age equation, a discussion of mineral argon-retention temperatures, and an evaluation of various types of age spectra are presented.

The $^{40}Ar/^{39}Ar$ date of a sample is calculated according to the age equation,

$$t_u=(1/\lambda)\ln(JF+1),$$

where t_u is the calculated date of the "unknown" sample, λ is the decay constant for decay of ^{40}K to ^{40}Ar and ^{40}Ca, J is related to neutron flux during irradiation, and F is the ratio of $^{40}Ar_R$ (radiogenic ^{40}Ar) to $^{39}Ar_K$ (potassium-derived ^{39}Ar) of the sample. The decay constants used in this study are those recommended by Steiger and Jäger (1977), that is, $\lambda_\varepsilon=0.581\times10^{-10}$/yr, $\lambda_{B-}=4.962\times10^{-10}$/yr, and $\lambda=\lambda_\varepsilon+\lambda_{B-}=5.543\times10^{-10}$/yr. The flux parameter, J, is calculated according to the relationship

$$J=(e^{\lambda t_m}-1)/(^{40}Ar_R/^{39}Ar_K)_m,$$

where e is a constant, t_m is the age of the primary flux "monitor" (that is, standard), and $(^{40}Ar_R/^{39}Ar_K)_m$ is the measured ratio of the standard. The standard for this experiment is hornblende MMhb-1 with percent K=1.555, $^{40}Ar_R=1.624\times10^{-9}$ mol/g, and K-Ar age=519.4 Ma (Alexander and others, 1978; Dalrymple and others, 1981). F is calculated from the measured argon isotopic abundances by mass spectrometry. In order to determine the actual F, that is, $^{40}Ar_R/^{39}Ar_K$ ratio, of a sample or standard, it is necessary to correct for the presence of atmospheric ^{40}Ar and irradiation-produced interfering isotopes such as ^{40}Ar (from ^{40}K), ^{39}Ar (from ^{42}Ca), and ^{36}Ar (from ^{40}Ca and ^{35}Cl). These corrections are well defined and were all made on the data used in this study. Because the mathematical formulation for F is complex, it is not presented here.

$^{40}Ar/^{39}Ar$ age-spectrum dating of hornblende, muscovite, biotite, and microcline, which formed during metamorphism or crystallization from a magma, is currently the best method for determining thermal history and age of complex metamorphic and plutonic terranes. Ideally, a mineral date determined by this method marks the time when that mineral became closed to the diffusion of argon. Closure of a particular mineral to diffusion is controlled chiefly by temperature, to a smaller extent by cooling rate (Dodson, 1973), and possibly by chemical compositional variation, structural-state variation, or grain-size variation within a particular kind of mineral. Each mineral that is appropriate for argon dating has a characteristic closure temperature (or argon-retention temperature) that is known with a precision of about ±20°C. The closure temperature is higher for minerals that

cooled rapidly and lower for minerals that cooled slowly. Commonly accepted closure temperatures that span a range from rapid cooling (1,000°C/m.y.) to slow cooling (5°C/m.y.) are 580–480°C for hornblende (Harrison, 1981), 325–270°C for muscovite (Snee and others, 1988), 300–260°C for biotite (Harrison and McDougall, 1980; Snee, 1982), and 160–100°C for microcline (Harrison and McDougall, 1982). For simplicity, intermediate closure temperatures, that is, closure temperatures for intermediate cooling rates of 500–100°C/m.y., are assumed for most of this study: 530°C, 300°C, 280°C, and 130°C for hornblende, muscovite, biotite, and microcline, respectively.

The $^{40}Ar/^{39}Ar$ method was first used in "total-fusion" experiments in which an irradiated sample was completely melted and all isotopes of argon measured in a single analysis to calculate a date for the sample. This total-fusion date is roughly analogous to a conventional K-Ar date for the sample except that no isotopic concentration measurements are required. Very soon after the first uses of the $^{40}Ar/^{39}Ar$ method, it was realized that a sample could be progressively degassed in temperature increments (Merrihue and Turner, 1966). A date can be calculated for each increment of gas released, and the dates can be plotted against percent of released argon to form an age spectrum. The character of the spectrum can be evaluated within a theoretical framework to interpret the apparent distribution of potassium and argon within the sample.

Turner (1968) showed that the dates for the temperature increments of some meteorites were identical within analytical precision and that when plotted on an age-spectrum diagram, which shows date of each temperature increment as a function of percent ^{39}Ar released during the experiment, the spectra formed "plateaus." In contrast, some age spectra exhibit a distinct increase in dates for the temperature increments from low-temperature to high-temperature extraction-steps in the experiment. Turner showed theoretically that an age spectrum will exhibit a step-up in dates if argon was lost from the sample in the geologic environment by thermally activated volume diffusion. The age spectrum will exhibit a plateau if the sample had never been disturbed after formation or if the sample had been completely reset by a younger event. Depending on the amount of thermal disturbance, that is, the percentage of argon lost, the date of the younger, low-temperature fractions will be equal to, or older than, the age of the thermal disturbance that affected the sample, whereas the date of the older, high-temperature fractions will be equal to, or younger than, the original age of closure. This step-up in dates exhibited by an age spectrum and apparently resulting from argon loss due to geologic activity has been experimentally reproduced by Harrison (1981) from hornblende and has been observed by numerous investigators in data from hornblende, muscovite, and K-feldspar (see below and, for example, Snee and others, 1988, and Harrison, 1982).

Recently, the reliability of hornblende and other minerals, including muscovite and K-feldspar, as recorders of geologically induced, thermally activated argon loss in an age spectrum produced during experimental degassing in the laboratory has been challenged by Lee and others (1991). Their contention is that hydrous minerals in particular, but also K-feldspar, undergo changes—including dehydration, melting, and phase conversions—during heating under vacuum that prevent release of argon by thermally-activated volume diffusion from the mineral. Thus, according to Lee and others (1991), experimental reproduction of the geologic phenomenon of argon loss is impossible.

Although the mechanism responsible for the development of apparent argon-loss age spectra from some hornblendes, K-feldspars, and muscovites may not be completely understood, there is no question that this pattern is exhibited by many, if not most, of these minerals after they undergo partial argon loss due to reheating by later thermal activity. Besides thermally activated volume diffusion, several other possible mechanisms can explain apparent argon-loss spectra. For example, two or more phases with different closure ages may coexist in one rock. If these phases of different age are similar enough in physical character to coexist in a mineral separate (for example, if one is phengite, a white mica formed under high-pressure metamorphic conditions, and the other is muscovite, a white mica formed under high-temperature conditions), and if each phase degasses under vacuum over different temperature ranges, then the resultant age spectrum will represent a mixture of the age spectra for both samples and will resemble an argon-loss spectrum (Roeske and others, 1995). Similarly, a single-phase mineral separate that has several grain sizes or structural types that degas at different temperatures under vacuum can produce the same result (Cosca and others, 1992). In both of these examples, the apparent argon-loss spectrum can be interpreted as if it had resulted from thermally activated volume diffusion. That is, the apparent age of the younger, lower temperature fractions is approximately the age of, or older than, the thermal disturbance, and the apparent age of the older, higher temperature fractions is approximately the age of, or younger than, the original closure. Therefore, apparent argon-loss spectra can be potentially very

useful for understanding the thermal histories of complex geologic environments. However, caution must be taken when interpreting apparent argon-loss spectra because other, nongeologic factors, such as extraction-system blanks and sample impurity, can affect the age spectra.

Besides argon loss, excess ^{40}Ar can be detected in a sample. Excess ^{40}Ar is incorporated into rocks and minerals by processes other than in situ decay of ^{40}K. The mechanism for the incorporation of excess ^{40}Ar into a rock or mineral is unknown, but several possible explanations exist. If a rock or mineral crystallizes in an environment that contains argon with an $^{40}Ar/^{36}Ar$ ratio greater than 295.5 (present-day ratio for atmospheric argon), the extra ^{40}Ar is "excess." Similarly, hydrothermal fluids are known to carry argon that commonly has an $^{40}Ar/^{36}Ar$ ratio composition greater than 295.5, perhaps due to their interaction with rocks containing radiogenic argon. If these fluids alter or become incorporated in a rock or mineral, excess ^{40}Ar can be added to that rock or mineral. Several studies (for example, Lanphere and Dalrymple, 1971, 1976; Kaneoka, 1974) have documented that large quantities of excess ^{40}Ar in a sample will produce a saddle-shaped $^{40}Ar/^{39}Ar$ age spectrum with anomalously old dates for the low-temperature and high-temperature extraction steps. Small quantities of excess ^{40}Ar commonly only affect the low-temperature steps and form an L-shaped spectrum.

Many studies have shown that meaningful ages of samples could be determined by the age-spectrum technique even though some loss or gain of ^{40}Ar had occurred during the geologic history of the sample. However, loss or gain of ^{40}Ar by a sample will result in an erroneous conventional K-Ar date, and because loss or gain of ^{40}Ar by a sample is primarily thermally controlled, samples from thermally complex areas such as metamorphic and plutonic complexes should by analyzed by the $^{40}Ar/^{39}Ar$ age-spectrum technique. Similarly, conventional K-Ar data from these geologic settings should be viewed with caution.

Ideally a sample dated by the $^{40}Ar/^{39}Ar$ age-spectrum technique will yield concordant dates for all temperature steps. If a sample's age spectrum is 100 percent concordant, that is, if all temperature steps yield identical dates within 2 standard deviations (2σ) of the weighted mean date for all temperature steps, then clearly the best date for the sample is a weighted mean of the dates of all temperature steps. The geologic significance of the resultant date must then be evaluated using geologic or other independent constraints. (In this paper, "date," "apparent age," or "numerical age" is used to refer to the analytical number determined by solution of the age equation using isotopic data produced for a sample in the laboratory. In contrast, "age" or a specific type of "age," such as "emplacement age," "cooling age," or "age of metamorphism," refers to a date that has been constrained by geologic data and is interpreted to have geologic meaning.)

In reality most dated samples display some discordancy in their age spectra, either because of a physical or chemical disturbance, because of ^{40}Ar not derived from in situ decay of ^{40}K, or because of loss of some ^{40}Ar after the original closure of the samples to ^{40}Ar diffusion. Even if discordancy exists in an age spectrum, the interpreted date may still hold geologic significance. Some terms for interpreted dates that are used in this paper include "total-gas date," "plateau date," and "preferred date." The "total-gas date" of an age spectrum results from weight-averaging dates of all temperature steps for a sample; the total-gas date is comparable to a conventional K-Ar date but is more precise and more accurate. The "plateau date" is that part of an age-spectrum diagram composed of contiguous gas fractions that together represent more than 50 percent of the total ^{39}Ar released from the sample and for which no difference in date can be detected between any two temperature fractions at the 95-percent confidence level (Fleck and others, 1977). The term "plateau date" has been used by others (for example, Lanphere and Dalrymple, 1971; Dalrymple and Lanphere, 1974) to refer to a "high-temperature segment" of an age spectrum over which the dates of the plateau-defining steps are concordant at the 95-percent confidence level. In some cases, by this usage, a single temperature step may define a plateau. In this paper, we use the definition for plateau of Fleck and others (1977). Finally, some age spectra show near-concordancy and yield weight-average dates of the near-concordant parts of the spectra that seem to have geologic meaning. We refer to these dates as "preferred dates," which either consist of an apparent plateau with less than 50 percent of the released ^{39}Ar or consist of fractions of gas whose dates overlap within 3 standard deviations (3σ) of the weighted mean.

U-Pb TECHNIQUES

Dissolution and chemical preparation of zircon and sphene samples were accomplished using a procedure slightly modified from Krogh (1973). Samples of approximately 10 to 20 mg were dissolved in hydrofluoric acid in Teflon bombs at 200°C, followed by Pb purification on a bromide-form anion-exchange column. Lead content was determined by isotope dilution on an ali-

quot of the dissolved sample. A combined ^{235}U and ^{230}Th spike was added to the sample before dissolution, and eluate off the bromide-form column was passed through a nitrate-form anion-exchange column to isolate uranium and thorium. Isotopic ratios were determined using a 15-cm (U, Th) or 30-cm (Pb) automated solid-source mass spectrometer.

Uranium, thorium, and lead contents are considered accurate to ±1 percent (2σ). Lead concentration ratios have uncertainties of ±0.1 percent (2σ), except $^{206}Pb/^{204}Pb$ ratios greater than 1,000, which probably have uncertainties of 1–3 percent. A common lead correction was made by first subtracting lead equal in amount and composition to the analytical blank, which over the course of this study was about 0.7 ng. The remaining ^{204}Pb was assumed to be 100-Ma-model lead with the composition $^{204}Pb:^{206}Pb:^{207}Pb:^{208}Pb=1:18.55:15.62:38.45$. Model lead compositions are from Stacey and Kramers (1975); all constants are from Steiger and Jäger (1977). Uncertainty of the lower-intercept date is the 95-percent confidence limit calculation according to Ludwig (1980, 1982).

SAMPLE DISTRIBUTION AND ISOTOPIC DATA

To evaluate the age of metamorphism, deformation, plutonism, cooling, and uplift of rocks in the vicinity of the suture zone in western Idaho, this paper synthesizes the argon data for 48 samples—from which we analyzed 34 hornblendes, 12 biotites, 11 muscovites, and 5 microclines—that were collected in an area extending from the Snake River canyon in Oregon and Idaho eastward to Thompson Creek near Stanley, Idaho. U-Pb dates on one sample of plutonic rock from the west side of the Idaho batholith are also included. Preliminary argon data for five additional samples of the Bald Mountain batholith are discussed. The data for this paper are synthesized from studies of several areas which include (1) the Bald Mountain batholith in the Blue Mountains, Oregon (L.W. Snee and W.H. Taubeneck, unpub. data, 1987), (2) the basement metamorphic and plutonic rocks of the Cougar Creek Complex in the Wallowa terrane in the Snake River canyon area between the confluence of the Imnaha and Snake Rivers and The Oxbow, Oregon (Balcer, 1980), (3) metamorphic rocks of the Riggins Group and Seven Devils island arc, and deformed and undeformed plutons and dikes from the Slate Creek-Riggins-Round Valley area, Idaho (Lund and Snee, 1988), (4) plutonic rocks of the Idaho batholith and metasedimentary roof pendants in the Buffalo Hump area, Idaho (Lund and others, 1986), and (5) plutonic rocks of the Idaho batholith near Stanley, Warm Lake, and Warm Springs Forest Service Station, Idaho, and alteration associated with the Thompson Creek porphyry molybdenum deposit (L.W. Snee, unpub. data, 1987). Distribution of these samples is shown on figures 10.3 through 10.6, 10.21, and 10.23, and locations are listed in table 10.1. Argon data are summarized in table 10.2, and detailed data are listed in table 10.3. U-Pb data are listed in table 10.4, and a Concordia diagram of the U-Pb data is plotted on figure 10.20.

INTERPRETATION

Because of the diversity of these data, the following discussion is divided into four sections: (1) basement rocks of the Snake River canyon area and associated plutons of island-arc affinity, (2) metamorphic rocks of the Riggins Group and Seven Devils island arc, (3) deformed plutons of the Salmon River suture zone, and (4) undeformed plutons elsewhere in the Idaho batholith.

BASEMENT ROCKS OF THE SNAKE RIVER CANYON AREA AND ASSOCIATED PLUTONS OF ISLAND-ARC AFFINITY

In an attempt to determine age of the metamorphism, shearing, and later plutonism that affected the basement rocks in the Snake River canyon area, we used the $^{40}Ar/^{39}Ar$ age-spectrum technique to analyze samples from the three areas of exposure: Pittsburg Landing, The Oxbow, and the confluence of the Imnaha and Snake Rivers (fig. 10.1). Balcer (1980) analyzed five hornblende and two biotite samples from amphibolite and gneiss near Pittsburg Landing, and two hornblende samples from two sheared amphibolites formed from metamorphism of mafic dikes, one intrusive into the basement rocks and the other intrusive into the Windy Ridge Formation near The Oxbow. Balcer also analyzed four hornblende samples from unmetamorphosed plutons that intruded the basement rocks near the confluence of the Imnaha and Snake Rivers, and Snee and others (1987b) dated hornblende from unmetamorphosed tonalitic dikes that intruded the basement complex about 8 km east of Pittsburg Landing. In addition, a hornblende sample from a pluton that intruded the Seven Devils Group along the Rapid River and later underwent greenschist-facies metamorphism along with the Seven Devils Group was also dated. The sample locations for each area are shown on figures 10.3 through 10.6, and a summary of the dates is given in table

TABLE 10.1.—*Sample locations*

[Mineral abbreviations: bi, biotite; hb, hornblende; mi, microcline; mu, muscovite. All quadrangles are 7.5-minute quadrangles, except Burgdorf, Copperfield, and Warm Lake, which are 15-minute quadrangles]

Sample	Mineral	Quadrangle	Location
R3	mu	Kessler Creek	45°23'26" N., 116°25'14" W., SE1/4 sec. 26, T.24N., R.1E., Idaho County, Idaho.
R7	bi, hb	Riggins	45°24'30" N., 116°20'13" W., NE1/4 sec. 21, T.24N., R.1E., Idaho County, Idaho.
R8a	bi, mi, mu	Burgdorf	45°27'30" N., 115°54'29" W., not surveyed, Idaho County, Idaho.
R10	mu	Kelly Mountain	45°25'23" N., 116°01'55" W, NE1/4 sec. 13, T.24N., R.3E., Idaho County, Idaho.
R11	hb	Riggins Hot Springs	45°24'35" N., 116°07'34" W., NE1/4 sec. 19, T.24N., R.3E., Idaho County, Idaho.
R12	bi, hb	Riggins Hot Springs	45°25'43" N, 116°08'34" W, SW1/4 sec. 7, T.24N., R.3E., Idaho County, Idaho.
R14	hb	Riggins Hot Springs	45°24'02" N., 116°12'51" W., SE1/4 sec. 21, T.24N., R.2E., Idaho County, Idaho
R16	bi, hb	Riggins	45°24'46" N., 116°15'18" W., SE1/4 sec. 18, T.24N., R.2E., Idaho County, Idaho.
R17	hb	Riggins	45°25'15" N., 116°16'48" W., NW1/4 sec. 13, T.24N., R.1E., Idaho County, Idaho.
R18	hb	Riggins	45°24'38" N., 116°18'24" W., NW1/4 sec. 23, T.24N., R.1E., Idaho County, Idaho.
R20	hb	Grave Point	45°39'25" N., 116°23'54" W., SE1/4 sec. 24, T.24N., R.1W., Idaho County, Idaho.
R21	bi, hb, mi	Dairy Mountain	45°37'58" N., 116°00'45" W., not surveyed, Idaho County, Idaho.
R22	hb	Florence	45°37'22" N., 116°03'43" W., NE1/4 sec. 3, T.26N., R.3E., Idaho County, Idaho.
R23	hb	Dairy Mountain	45°38'14" N., 116°06'14" W., NE1/4 sec. 32, T.27N., R.3E., Idaho County, Idaho.
R24	hb, mi, mu	Dairy Mountain	45°38'25" N., 116°07'18" W., NE1/4 sec. 31, T.27N., R.3E., Idaho County, Idaho.
R25	bi	McKinzie Creek	45°38'09" N., 116°08'31" W., NE1/4 sec. 36, T.27N., R.2E., Idaho County, Idaho.
R26	bi, hb	McKinzie Creek	45°38'08" N., 116°11'36" W., NW1/4 sec. 34, T.27N., R.2E., Idaho County, Idaho.
R27	hb	McKinzie Creek	45°38'07" N., 116°14'12" W., NW1/4 sec. 32, T.27N., R.2E., Idaho County, Idaho.
R28	hb	Bally Mountain	45°07'28" N., 116°17'40" W., SE1/4 sec. 26, T.21N., R.1E., Adams County, Idaho.
R29	hb	Indian Mountain	45°09'43" N., 116°17'54" W., NE1/4 sec. 14, T.21N., R.1E. Idaho County, Idaho.
R30	hb	Pollock	45°15'10" N., 116°20'5" W., NE1/4 sec. 16, T.22N., R.1E., Adams County, Idaho.
R34	hb	Riggins	45°27'41" N., 116°18'26" W., SW1/4 sec. 35, T.25N., R.1E., Idaho County, Idaho.
R35	mu	Riggins	45°29'17" N., 116°18'05" W., NW1/4 sec. 23, T.25N., R.1E., Idaho County, Idaho.
R36	bi	Riggins Hot Springs	45°24'35" N., 116°07'34" W., NE1/4 sec. 19, T.24N., R.3E., Idaho County, Idaho.

TABLE 10.1.—*Sample locations* —Continued

Sample	Mineral	Quadrangle	Location
7-30-5	hb	Indian Mountain	45°08'05" N., 116°16'56" W, NW1/4 sec. 25, T.21N., R.1E., Adams County, Idaho.
Hcm-23	hb	Cactus Mountain	45°49'26" N., 116°41'46" W., NE1/4 sec. 28, T.29N., R.3W., Idaho County, Idaho.
Hdh-24	hb	Deadhouse Ridge	45°49'00" N., 116°45'45" W., not surveyed, Wallows County, Oregon.
Hdh-25	hb	Deadhouse Ridge	45°49'25" N., 116°46'31" W., not surveyed, Wallows County, Oregon.
Hdh-27	hb	Deadhouse Ridge	45°49'00" N., 116°45'48" W., not surveyed, Wallows County, Oregon.
Hkc-29	bi	Kirkwood Creek	45°36'48" N., 116°27'35" W., S1/2 sec. 4, T.26N., R.1W., Idaho County, Idaho.
Hkc-32	hb	Kirkwood Creek	45°36'46" N., 116°27"35" W., S1/2 sec. 4, T.26N., R.1W., Idaho County, Idaho.
Hkc-34	hb	Kirkwood Creek	45°36'25" N., 116°27'35" W., N1/2 sec. 9, T.26N., R.1W., Idaho County, Idaho.
Hkc-35	hb	Kirkwood Creek	45°36'25" N., 116°27'35" W., N1/2 sec. 9, T.26N., R.1W., Idaho County, Idaho.
Hkc-36	bi, hb	Kirkwood Creek	45°36'36" N., 116°27'35" W., N1/2 sec. 9, T.26N., R.1W., Idaho County, Idaho.
Hkc-37	hb	Kirkwood Creek	45°36'36" N., 116°27'35" W., N1/2 sec. 9, T.26N., R.1W., Idaho County, Idaho.
Hcop-39	hb	Copperfield	44°58'45" N., 116°51'30" W., SE1/4 sec. 17, T.19N., R.4W., Adams County, Idaho.
Hcop-40	hb	Copperfield	44°56'55" N., 116°50'45" W., NE1/4 sec. 21, T.5S., R.48E., Baker County, Oregon.
D81-1	hb	Heavens Gate	45°19' N., 116°25' W., NE1/4 sec. 23,T.23N., R.1W., Idaho County, Idaho.
1KE052	mi, mu	Buffalo Hump	5°32'24" N., 115°40'10" W., not surveyed, Idaho County, Idaho.
2KE080	hb, bi	Buffalo Hump	45°31'50" N., 115°43'11" W., not surveyed, Idaho County, Idaho.
2KE086	hb	Buffalo Hump	45°33'10" N., 115°41'38" W., not surveyed, Idaho County, Idaho.
2KE087	mu	Buffalo Hump	45°35'14" N., 115°40'53" W., not surveyed, Idaho County, Idaho.
MP201	hb	East Basin Creek	44°20' N., 114°50' W., sec. 24, T.11N., R.14E., Custer County, Idaho.
TC-S-41-16	mu	Thompson Creek	44°19'00" N., 114°33'45" W., SE1/4 sec. 34, T.12N., R.16E., drill hole S41, 495.4-ft depth, Custer County, Idaho.
TC-S-124-23	mu	Thompson Creek	44°19'00" N., 114°33'45" W., SE1/4 sec.34, T.12N., R.16E., drill hole S124, 1606.5-ft depth, Custer County, Idaho.
D3113M	mu	Warm Lake	44°38'44" N., 115°36'33" W., SW1/4, sec. 9, T.15N., R.7E., Valley County, Idaho.
B12178201	mu	Teapot Mountain	44°57'25" N., 115°38'00" W., NE1/4, sec. 29, T.19N., R.7W., Valley County, Idaho.
B12198202	bi, mi	Eightmile Mountain	44°08'09" N., 115°18'53" W., sec. 7, T.9N., R.10E., Boise County, Idaho.

TABLE 10.2.—*Summary of $^{40}Ar/^{39}Ar$ age-spectrum data*

[Mineral abbreviations: bi, biotite; hb, hornblende; mi, microcline; mu, muscovite. Metamorphic-zone abbreviations: An, andesine; Bi, biotite; Ch, chlorite; Gt, garnet; (Hi), upper amphibolite facies or higher; Ol, oligoclase; Si, sillimanite; ---, unmetamorphosed. Other abbreviations: Ar loss, apparent argon loss; do, ditto; Tmp, preferred age of sample; T_p, plateau age. All errors are 1 standard deviation from mean. Decay constants and isotopic abundances are those recommended by Steiger and Jäger (1977)]

Sample	Mineral	Metamorphic zone	Unit or rock type	Age, and characteristics of $^{40}Ar/^{39}Ar$ spectrum
Basement rocks and associated plutons				
Hdh-24	hb	---	Tonalite	T_p=215.6±3.6 Ma; Ar loss from 220 Ma.
Hdh-25	hb	---	do	T_p=213.0±2.0 Ma.
Hdh-27	hb	---	do	T_p=225.0±2.3 Ma.
Hcm-23	hb	---	Tonalite inclusion in mafic dike.	T_p=223.3±5.9 Ma.
Hkc-29	bi	(Hi)	Deformed plagiogranite	T_p=233.5±2.5 Ma; disturbed.
Hkc-32	hb	(Hi)	Amphibolite	T_p=229.3±2.6 Ma; Ar loss from 232 Ma.
Hkc-34	hb	(Hi)	do	T_p=225.8±6.7 Ma; Ar loss? from 229 Ma.
Hkc-35	hb	(Hi)	do	T_p=239.2±7.6 Ma; Ar loss from 243 Ma.
Hkc-36	hb	(Hi)	do	T_p=238.6±3.4 Ma; Ar loss from 244 Ma.
do	bi	(Hi)	do	Disturbed.
Hkc-37	hb	(Hi)	do	T_p=235.0±3.5 Ma; disturbed.
Hcop-39	hb	(Hi)	do	T_p=227.8±5.3 Ma.
Hcop-40	hb	(Hi)	do	T_p=219.2±7.6 Ma; Ar loss from 224 Ma.
R20	hb	---	Tonalite	T_p=227.1±1.2 Ma.
D81-1	hb	Ch	do	T_p=145.1±1.5 Ma.
Rocks near the suture zone				
R7	hb	Gt	Riggins Group	T_{mp}=117.0±0.6 Ma; minor excess argon.
do	bi	do	do	T_p=116.1±0.6 Ma.
R30	hb	(Hi)	Riggins(?) Group	T_p=118.1±0.6 Ma; Ar loss to 114 Ma.
R3	mu	Ch	Seven Devils island arc	Ar loss: 105–100 Ma.

TABLE 10.2.—*Summary of $^{40}Ar/^{39}Ar$ age-spectrum data* —Continued

Sample	Mineral	Metamorphic zone	Unit or rock type	Age, and characteristics of $^{40}Ar/^{39}Ar$ spectrum
		Rocks near the suture zone—Continued		
R28	hb	(Hi)	Riggins(?) Group	T_p=107.7±0.5 Ma ; Ar loss: 108–100 Ma.
R29	hb	(Hi)	Riggins(?) Group	T_p=108.1±0.5 Ma; Ar loss to 107 Ma.
R18	hb	Ol	Riggins Group	T_{mp}=106.5±1.4 Ma; disturbed.
R17	hb	Ol	----- do	T_p=106.8±0.5 Ma; Ar loss: 107–105 Ma.
R34	hb	Gt	----- do	T_p=109.1±0.5 Ma.
R27	hb	Ol	----- do	T_{mp}=108.9±0.6 Ma; minor excess Ar.
R26	hb	An	----- do	Ar loss: 109–94 Ma.
--- do -------	bi	-- do --------	----- do	T_p=89.9±0.6 Ma.
R35	mu	Bi	----- do	T_p=98.3±0.2 Ma; Ar loss: 101–97 Ma.
R16	hb	An	----- do	Ar loss: 100.5–93 Ma.
--- do -------	bi	-- do --------	----- do	T_p=87.9±0.4 Ma.
R14	hb	Si	----- do	Ar loss: 101–89 Ma.
R25	bi	An	Seven Devils island arc	T_p=84.1±0.4 Ma.
7-30-5	hb	---	Tonalite	T_p=112.0±0.7 Ma.
		Suture-zone rocks		
R24	hb	(Hi)	Riggins(?) Group	Ar loss: 92.5–88 Ma.
--- do -------	mu	-- do --------	Deformed pegmatite in R24 gneiss.	T_p=83.4±0.4 Ma.
--- do -------	mi	-- do --------	----- do	Ar loss: 79–69.5 Ma.
R23	hb	(Hi)	Riggins(?) Group inclusion	Ar loss: 99.5–93 Ma.
R22	hb	(Hi)	----- do	T_p=89.3±0.6 Ma.
R12	hb	---	Riggins(?) Group	Ar loss: 93.5–88 Ma.
--- do -------	bi	---	----- do	T_p=82.6±0.4 Ma.

10.2 under the heading "Basement Rocks and Associated Plutons." Samples from plutons of the Bald Mountain batholith (L.W. Snee and W.H. Taubeneck, unpub. data, 1987) have also been analyzed.

The $^{40}Ar/^{39}Ar$ age spectra of the five hornblende samples from metamorphic rocks near Pittsburg Landing (Hkc-32, Hkc-34, Hkc-35, Hkc-36, and Hkc-37; fig. 10.3) show variable amounts of discordance.

TABLE 10.2.—*Summary of $^{40}Ar/^{39}Ar$ age-spectrum data* —Continued

Sample	Mineral	Metamorphic zone	Unit or rock type	Age, and characteristics of $^{40}Ar/^{39}Ar$ spectrum
			Suture-zone rocks—Continued	
R11	hb	---	Deformed tonalite	T_p=84.9±0.3 Ma.
R36	bi	---	Deformed granodiorite	T_p=80.5±0.4 Ma.
			Undeformed plutons and associated rocks	
R21	hb	---	Tonalite	T_p=83.9±0.4 Ma.
--- do -------	bi	---	----- do	T_p=81.1±0.4 Ma.
--- do -------	mi	---	----- do	Ar loss: 78–75 Ma.
R10	mu	---	Pegmatite in tonalite	T_p=76.7±0.4 Ma.
R8a	mu	---	Muscovite-biotite granite	T_p=75.3±0.4 Ma.
--- do -------	bi	---	----- do	T_p=74.7±0.4 Ma.
--- do -------	mi	---	----- do	Ar loss: 69–47 Ma.
2KE080	hb	(Hi)	Country rock (amphibolite)	T_p=81.2±0.4 Ma.
--- do -------	bi	-- do --------	----- do	T_p=78.2±0.4 Ma.
2KE086	hb	(Hi)	----- do	T_p=80.5±0.6 Ma.
1KE052	mu	---	Muscovite-biotite granite	T_p=73.8±0.4 Ma.
--- do -------	mi	---	----- do	Ar loss: 67–55 Ma.
2KE087	mu	---	Quartz vein	T_p=71.0±0.4 Ma.
MP201	hb	---	Hornblende-biotite granodiorite.	T_p=86.3±0.4 Ma.
TC-S-41-16	mu	---	Molybdenum porphyry	T_p=87.4±0.4 Ma.
TC-S-124-23	mu	---	----- do	T_p=87.6±0.4 Ma.
D3113M	mu	---	Muscovite-biotite granite	T_p=72.4±0.4 Ma.
B12178201	mu	---	----- do	T_p=70.1±0.4 Ma.
B12198202	bi	---	Leucogranite	Disturbed.
--- do -------	mi	---	----- do	Ar loss: 66–55 Ma.

Even though the analytical precision for these analyses is relatively large (ranging from 3 to 8 m.y.) compared to that of our other data, the data are precise enough to show that each of the samples has lost some argon over geologic time. Because the hornblendes define the metamorphic foliation of the amphibolites, their plateau dates should be minimum estimates for the age of metamorphism. However, the superposed argon loss probably occurred during a thermal event, such as heat flow associated with later plutonism,

TABLE 10.3.—*$^{40}Ar/^{39}Ar$ age-spectrum data for samples from west-central Idaho and eastern Oregon*

[All errors are 1 standard deviation from mean. Italic entries indicate data used to calculate plateau dates. J, flux parameter (see text); mol, mole; pct, percent; wt., weight; ---, not determined]

Temperature (°C)	$^{40}Ar/^{39}Ar$	$^{37}Ar/^{39}Ar$	$^{36}Ar/^{39}Ar$	^{39}Ar (pct of total)	pct $^{40}Ar_R$	^{39}Ar (mol x10^{-13})	Apparent K/Ca (mol/mol)	Apparent age and error (Ma)
R3, MUSCOVITE								
Total-gas date: 102.0 Ma; no plateau; J=0.007387; wt., 0.0226 g								
750	9.403	0.5345	0.0110	3.9	65.7	0.129	0.97	80.6±0.5
875	8.512	.0266	.0027	13.3	90.7	.449	19.5	100.1±0.7
925	8.415	.0070	.0015	38.1	94.7	1.29	74.8	103.2±0.5
975	8.569	.0079	.0017	21.8	94.2	.737	66.0	104.5±0.5
1,000	10.75	.2273	.0089	4.4	75.7	.148	22.9	105.3±0.6
1,050	10.61	.8400	.0109	3.6	70.3	.121	.62	96.7±0.6
Fuse	9.82	.3253	.0064	15.2	81.1	.514	1.60	103.1±0.5
R7, HORNBLENDE								
Total-gas date: 133.7 Ma; no plateau; J=0.007083; wt.,0.7261 g								
850	112.45	2.826	0.1420	1.5	63.0	0.067	0.18	733.7±4.1
950	51.49	7.399	.0902	1.0	49.4	.045	.07	298.6±2.7
1,000	29.67	9.483	.0639	1.1	38.8	.049	.06	141.3±0.9
1,050	24.76	10.85	.0443	2.7	50.6	.122	.05	153.2±0.8
1,100	19.85	12.84	.0301	5.2	60.2	.235	.04	146.5±0.7
1,125	15.69	13.80	.0217	8.4	66.0	.375	.04	127.6±0.7
1,150	15.43	14.04	.0225	9.0	64.0	.402	.04	121.8±0.6
1,175	16.20	14.25	.0255	7.2	60.3	.320	.04	120.5±0.6
1,200	12.11	14.45	.0133	16.0	76.8	.714	.04	115.0±0.6
1,250	10.95	14.43	.0088	39.5	86.5	1.76	.04	117.0±0.6
Fuse	15.98	14.29	.0261	8.5	58.8	.380	.04	116.0±0.6
R7, BIOTITE								
Total-gas date: 115.7 Ma; plateau date: 116.1±0.6 Ma; J=0.007272; wt., 0.0712 g								
850	10.03	0.0127	0.0038	11.6	88.9	1.35	40.9	113.4±0.6
1,000	10.01	.0118	.0027	30.5	91.9	3.55	44.2	116.9±0.6
1,050	10.08	.0217	.0032	21.8	90.6	2.54	24.0	116.0±0.6
1,100	10.43	.1098	.0045	20.7	87.2	2.41	4.74	115.5±0.6
1,200	12.19	.0792	.0104	13.5	74.8	6.56	6.56	115.9±0.6
Fuse	53.29	.2905	.1510	1.8	16.3	.215	1.79	110.5±0.9
R8a, MUSCOVITE								
Total-gas date: 75.1 Ma; plateau date: 75.3±0.4 Ma; J=0.007296; wt. 0.0642 g								
750	32.87	0.9163	0.094	40.3	15.3	0.035	0.57	65.0±2.2
875	10.45	.0143	.0167	.8	52.8	.111	36.4	71.1±0.4
925	8.386	.0086	.0089	2.0	68.6	.256	60.7	74.1±0.4
975	6.622	.0003	.0026	13.6	88.5	1.78	1,750.0	75.5±0.4
1,015	6.191	.0006	.0011	32.1	94.5	4.20	845.0	75.4±0.4
1,050	6.471	.0007	.0022	16.1	90.1	2.11	73.0	75.2±0.4
1,200	7.285	.0004	.0050	16.8	79.5	2.20	116.0	74.7±0.4
Fuse	8.363	.0005	.0086	18.4	69.5	2.40	95.1	74.9±0.4

younger than the metamorphism. Therefore, the minimum cooling age of the metamorphic event is best represented by the highest temperature, oldest step of the oldest spectrum. The age spectra for samples Hkc-35 and Hkc-36 show relatively little disturbance and step up to 242.4±4.2 and 243.8±3.7 Ma, respectively. Therefore, we interpret the cooling age of the metamorphism that affected the basement rocks of the Pittsburg Landing area to be about 244 Ma. Because this is a cooling age that represents the time when the rocks cooled below 530°C (hornblende argon-closure temperature) and because these rocks were affected

TABLE 10.3.—*$^{40}Ar/^{39}Ar$ age-spectrum data for samples from west-central Idaho and eastern Oregon*—Continued

Temperature (°C)	$^{40}Ar/^{39}Ar$	$^{37}Ar/^{39}Ar$	$^{36}Ar/^{39}Ar$	^{39}Ar (pct of total)	pct $^{40}Ar_R$	^{39}Ar (mol x10^{-13})	Apparent K/Ca (mol/mol)	Apparent age and error (Ma)
R8a, BIOTITE								
Total-gas date: 74.3 Ma; plateau date: 74.7±0.4 Ma; J=0.007309; wt., 0.0630 g								
650	21.24	1.036	0.0615	0.4	14.8	0.047	0.50	41.1±1.0
850	7.164	.0168	.0056	6.9	77.0	.849	30.9	71.3±0.4
1,000	6.174	.0017	.0013	38.8	93.9	4.78	304.0	74.9±0.4
1,050	7.083	.0420	.0044	7.8	81.5	.965	12.4	74.6±0.4
1,125	6.613	.0178	.0028	16.4	87.3	2.03	29.2	74.6±0.4
1,200	7.156	.0134	.0047	25.0	80.6	3.08	38.8	74.6±0.4
Fuse	13.41	.0713	.0262	4.7	42.3	.574	7.29	73.3±0.4
R8a, MICROCLINE								
Total-gas date: 67.4 Ma; no plateau; J=0.007244; wt. 0.0938 g								
600	22.90	0.3228	0.0495	0.2	36.2	0.049	1.61	105.2±1.2
700	9.724	.0465	.0206	.5	37.4	.126	11.2	46.9±0.7
800	5.203	.0147	.0031	1.7	82.2	.427	35.5	55.0±0.3
900	5.538	.0168	.0018	4.3	90.2	1.09	31.0	64.1±0.3
1,000	5.299	.0118	.0005	16.4	96.9	4.11	43.9	65.9±0.3
1,050	5.361	.0057	.0005	16.9	97.0	4.23	91.3	66.7±0.3
1,100	5.476	.0042	.0007	14.1	95.9	3.51	124.0	67.4±0.4
1,150	5.796	.0098	.0017	7.9	91.3	1.98	52.9	67.8±0.3
1,250	6.075	.0182	.0024	10.7	88.4	2.67	28.6	68.9±0.4
Fuse	5.928	.0057	.0017	27.3	91.4	6.82	90.7	69.4±0.4
R10, MUSCOVITE								
Total-gas date: 76.8 Ma; plateau date: 76.7±0.4 Ma; J=0.007333; wt., 0.0630 g								
750	10.85	0.2755	0.0179	1.0	51.4	0.128	1.89	72.3±0.6
875	7.093	.2519	.0037	4.2	84.9	.539	2.06	78.0±0.4
925	6.613	.0273	.0021	6.5	90.4	.833	19.0	77.4±0.4
975	6.477	.0192	.0019	11.8	91.4	1.51	27.0	76.7±0.4
1,000	6.367	.0134	.0015	23.2	93.0	2.67	38.7	76.7±0.4
1,050	6.343	.0144	.0015	20.0	93.2	2.56	36.2	76.6±0.4
Fuse	6.303	.0104	.0012	33.4	94.2	4.28	50.2	76.9±0.4
R11, HORNBLENDE								
Total-gas date: 85.3 Ma; plateau date: 84.9±0.3 Ma; J=0.007156; wt., 0.7533 g								
850	28.22	5.812	0.0613	0.2	37.4	0.051	0.09	131.2±0.9
1,000	17.17	2.094	.0347	.6	41.3	.126	.25	89.2±0.9
1,050	21.92	2.490	.0497	.5	33.8	.110	.21	93.2±0.5
1,100	9.478	3.533	.0101	5.1	71.4	1.07	.15	85.3±0.4
1,125	7.926	3.656	.0051	9.9	84.6	2.10	.14	84.5±0.4
1,150	7.632	3.656	.0041	12.9	87.8	2.74	.14	84.5±0.4
1,175	7.420	3.635	.0032	22.4	90.9	4.75	.14	85.0±0.4
1,200	7.448	3.622	.0033	21.4	90.0	4.54	.14	85.1±0.4
1,250	7.805	3.612	.0045	14.5	86.6	3.06	.14	85.1±0.4
Fuse	8.841	3.918	.0076	12.4	77.9	2.63	.13	86.8±0.5

by later thermal activity, 244 Ma is a minimum estimate of the age of the oldest metamorphism that is preserved in argon systematics of these rocks. The age spectra of the two biotite samples from the Pittsburg Landing area (Hkc-29 and Hkc-36) are disturbed and corroborate the interpretation that these rocks were thermally or chemically affected after metamorphism.

The age spectra for two hornblende samples from sheared amphibolites near The Oxbow (Hcop-39 and Hcop-40; fig. 10.4) also show variable discordance, but sample Hcop-39 yields a plateau date of 227.8±5.3 Ma with some apparent argon loss. This date may represent cooling after the 244-Ma metamorphism, a later metamorphic event (that is, after

TABLE 10.3.—*$^{40}Ar/^{39}Ar$ age-spectrum data for samples from west-central Idaho and eastern Oregon*—Continued

Temperature (°C)	$^{40}Ar/^{39}Ar$	$^{37}Ar/^{39}Ar$	$^{36}Ar/^{39}Ar$	^{39}Ar (pct of total)	pct $^{40}Ar_R$	^{39}Ar (mol x10^{-13})	Apparent K/Ca (mol/mol)	Apparent age and error (Ma)
R12, HORNBLENDE								
Total-gas date: 92.0 Ma; no plateau; J=0.007363; wt., 0.8408 g								
850	33.43	1.789	0.0855	0.2	24.8	0.038	0.29	106.9±1.8
950	42.14	1.635	.1170	.3	18.2	.058	.32	99.2±1.4
1,000	72.72	2.636	.2220	.2	10.0	.034	.20	94.1±2.2
1,050	20.58	4.333	.0477	1.5	33.1	.265	.12	88.3±0.5
1,100	9.647	4.545	.0102	11.7	72.4	2.10	.11	90.4±0.4
1,125	8.616	4.520	.0064	22.6	82.0	4.05	.11	91.5±0.5
1,150	8.471	4.573	.0056	30.0	84.8	5.38	.11	92.9±0.5
1,175	10.80	4.577	.0133	9.1	66.8	1.64	.11	93.4±0.5
1,200	9.99	4.462	.0110	13.6	71.0	2.45	.11	91.8±0.5
1,250	12.84	4.432	.0207	8.2	55.1	1.47	.11	91.5±0.5
Fuse	34.45	4.403	.0944	2.7	20.0	4.76	.11	89.1±0.6
R12, BIOTITE								
Total-gas date: 80.3 Ma; plateau date: 82.6±0.4 Ma; J=0.007332; wt., 0.0680 g								
650	13.73	0.0164	0.0366	1.52	1.2	0.187	31.7	38.1±0.4
850	6.876	.0042	.0030	26.8	86.9	3.25	123.0	77.3±0.4
1,000	6.887	.0045	.0016	27.3	92.9	3.31	117.0	82.7±0.4
1,050	7.155	.0065	.0026	13.3	89.2	1.61	80.4	82.5±0.4
1,125	7.469	.0080	.0037	11.7	85.2	1.43	65.4	82.3±0.4
1,200	7.914	.0173	.0054	12.2	79.8	1.48	30.0	81.7±0.4
Fuse	10.50	.0194	.0143	7.2	59.7	.875	26.8	81.1±0.4
R14, HORNBLENDE								
Total-gas date: 97.9 Ma; no plateau; J=0.007400; wt., 0.7880 g								
850	47.81	3.512	0.129	2.3	20.6	0.098	0.14	126.7±2.0
1,000	30.33	7.545	.0804	3.2	23.6	.135	.07	93.1±0.7
1,050	22.03	13.65	.0551	3.1	30.9	.130	.04	88.5±0.6
1,100	14.98	16.36	.0303	10.9	48.7	.451	.03	94.8±0.5
1,125	16.49	16.77	.0347	7.0	45.7	.290	.03	97.8±0.6
1,150	15.07	16.96	.0301	11.8	49.7	.488	.03	97.1±0.6
1,175	14.80	17.26	.0291	13.6	51.0	.564	.03	97.8±0.5
1,200	14.50	17.54	.0286	14.0	51.1	.578	.03	96.2±0.5
1,250	14.00	17.47	.0265	16.3	58.7	.674	.03	97.6±0.5
Fuse	22.27	17.16	.0536	17.7	34.9	.732	.03	100.7±0.6
R16, HORNBLENDE								
Total-gas date: 99.7 Ma; no plateau; J=0.007254; wt., 0.7839 g								
850	46.42	2.390	0.116	0.8	26.2	0.061	0.22	152.5±1.0
1,000	31.54	3.964	.0811	1.7	24.9	.132	.13	100.1±0.7
1,050	20.71	8.198	.0476	2.4	35.2	.186	.06	92.8±0.6
1,100	11.84	9.259	.0164	10.5	65.1	.822	.06	98.1±0.5
1,125	15.37	9.373	.0280	12.1	50.8	.949	.06	99.4±0.5
1,150	14.06	9.186	.0235	6.1	55.7	.475	.06	99.7±0.5
1,175	16.86	9.326	.0335	3.4	45.6	.265	.06	97.7±0.5
1,200	14.77	9.683	.0266	7.3	51.9	.569	.05	97.5±0.5
1,250	10.60	9.538	.0121	16.9	73.2	1.33	.05	98.6±0.5
Fuse	10.01	9.266	.0096	39.0	79.0	3.06	.06	100.6±0.5

244 Ma), complete resetting by postmetamorphic thermal activity or shearing, or time of emplacement of the dikes. Considering the data from postmetamorphic igneous rocks, below, we suggest that 227 Ma may be the age of emplacement and (or) shearing of these rocks.

TABLE 10.3.—*$^{40}Ar/^{39}Ar$ age-spectrum data for samples from west-central Idaho and eastern Oregon*—Continued

Temperature (°C)	$^{40}Ar/^{39}Ar$	$^{37}Ar/^{39}Ar$	$^{36}Ar/^{39}Ar$	^{39}Ar (pct of total)	pct $^{40}Ar_R$	^{39}Ar (mol x10^{-13})	Apparent K/Ca (mol/mol)	Apparent age and error (Ma)
R16, BIOTITE								
Total-gas date: 83.8 Ma; plateau date: 87.9±0.4 Ma; J=0.006750; wt., 0.0609 g								
650	5.955	0.0262	0.0103	3.8	48.9	0.347	19.8	35.1±0.4
850	7.926	.0067	.0045	21.9	83.3	1.99	77.4	78.6±0.4
1,000	8.151	.0077	.0024	31.7	91.1	2.88	67.3	88.2±0.4
1,050	8.224	.0160	.0027	23.2	90.1	2.11	32.5	88.1±0.4
1,125	8.300	.0375	.0032	14.3	88.7	1.30	13.5	87.4±0.4
1,200	11.19	.0663	.0131	4.6	65.3	.420	7.85	86.9±0.4
Fuse	58.42	.5734	.1770	.5	10.4	.048	.91	72.2±2.7
R17, HORNBLENDE								
Total-gas date: 121.1 Ma; plateau date: 106.8±0.5 Ma; J=0.007350; wt., 0.7460 g								
850	73.67	9.917	0.1050	0.8	58.9	0.056	0.05	499.7±3.2
1,000	48.67	5.095	.0580	1.6	65.6	.112	.10	380.5±1.8
1,050	26.44	8.583	.0342	3.6	64.3	.243	.06	212.4±1.0
1,100	13.25	9.668	.0147	10.4	72.9	.708	.05	123.6±0.6
1,125	12.01	9.918	.0142	11.8	71.4	.808	.05	110.1±0.6
1,150	12.17	9.904	.0156	8.0	68.3	.546	.05	107.0±0.5
1,175	11.12	10.16	.0127	8.6	73.3	.584	.05	104.9±0.6
1,200	10.09	10.28	.0088	15.1	82.0	1.03	.05	106.4±0.5
1,250	10.14	10.31	.0088	23.5	82.3	1.60	.05	107.3±0.5
Fuse	12.14	10.24	.0157	16.7	68.3	1.14	.05	106.6±0.5
R18, HORNBLENDE								
Total-gas date: 110.5 Ma; no plateau; J=0.007200; wt., 0.7413 g								
900	38.09	4.151	0.0680	0.7	48.1	0.033	0.13	223.5±2.2
1,000	25.57	8.557	.0536	3.2	40.7	.146	.06	130.2±0.7
1,050	20.11	10.54	.0398	4.2	45.6	.192	.05	115.1±1.7
1,100	12.80	13.12	.0164	21.5	70.0	.981	.04	112.7±0.6
1,125	13.32	13.31	.0187	13.0	66.2	.595	.04	111.1±0.6
1,150	11.22	13.22	.0130	17.8	74.9	.811	.04	105.9±0.5
1,175	11.12	12.96	.0121	6.9	77.0	.315	.04	107.9±0.6
1,200	11.11	13.48	.0128	11.3	75.3	.517	.04	105.4±0.6
1,250	11.83	13.31	.0145	16.8	72.6	.765	.04	108.2±0.6
Fuse	18.83	13.31	.0389	4.6	44.5	.210	.04	105.2±0.6
R20, HORNBLENDE								
Total-gas date: 227.5 Ma; plateau date: 227.1±1.2 Ma; J=0.007210; wt., 0.8099 g								
850	69.45	6.893	0.1620	0.4	31.8	0.032	0.08	266.7±4.1
950	59.35	9.580	.1430	.6	30.1	.048	.05	218.6±3.8
1,000	56.01	10.42	.1330	.4	31.4	.033	.05	215.1±1.7
1,050	42.17	10.36	.0790	1.4	46.6	.106	.05	238.8±1.5
1,100	34.14	9.420	.0532	2.1	56.1	.165	.06	233.2±1.3
1,125	31.37	8.953	.0447	2.9	60.1	.223	.06	229.8±1.2
1,150	23.89	8.612	.0195	7.7	78.7	.602	.06	229.1±1.1
1,175	22.07	8.523	.0136	14.7	84.8	1.15	.06	228.3±1.1
1,200	21.36	8.478	.0118	20.6	86.8	1.61	.06	226.3±1.3
1,250	21.23	8.475	.0115	25.8	87.1	2.02	.06	225.8±1.1
Fuse	22.54	8.834	.1540	23.4	82.9	1.83	.06	227.9±1.1

Age spectra for hornblendes from postmetamorphic plutons at the confluence of the Imnaha and Snake Rivers (Hcm-23, Hdh-24, Hdh-25, and Hdh-27; fig. 10.5) and near Pittsburg Landing (R20; fig. 10.6) are less complicated and generally display plateaus that represent the time when these rocks cooled below 530°C. At the Imnaha and Snake River confluence, the dates range from 213.0±2.0 to 225.0±5.3 Ma. This dispersion

TABLE 10.3.—*$^{40}Ar/^{39}Ar$ age-spectrum data for samples from west-central Idaho and eastern Oregon*—Continued

Temperature (°C)	$^{40}Ar/^{39}Ar$	$^{37}Ar/^{39}Ar$	$^{36}Ar/^{39}Ar$	^{39}Ar (pct of total)	pct $^{40}Ar_R$	^{39}Ar (mol x10^{-13})	Apparent K/Ca (mol/mol)	Apparent age and error (Ma)
R21, HORNBLENDE								
Total-gas date: 83.9 Ma; plateau date: 83.9±0.4 Ma; J=0.006690; wt., 0.7187 g								
850	41.19	2.472	0.1120	0.9	19.8	0.165	0.21	96.9±1.0
950	16.72	1.181	.0338	1.1	40.8	.187	.44	80.5±0.5
1,000	22.87	2.449	.0533	.5	31.9	.086	.21	86.0±0.9
1,050	15.85	3.403	.0304	1.1	44.9	.96	.15	83.8±0.5
1,100	9.506	3.694	.0090	7.0	74.9	1.23	.14	83.9±0.4
1,125	8.918	3.695	.0070	8.5	79.9	1.51	.14	84.0±0.4
1,150	8.725	3.700	.0064	13.7	81.6	2.42	.14	83.9±0.4
1,175	8.695	3.702	.0063	16.6	81.8	2.93	.14	83.8±0.4
1,200	8.184	3.700	.0046	24.8	86.8	4.39	.14	83.7±0.4
1,250	8.412	3.767	.0053	23.9	84.9	4.23	.14	84.2±0.4
Fuse	39.13	3.855	.1110	1.9	17.2	3.40	.14	79.4±0.5
R21, BIOTITE								
Total-gas date: 80.5 Ma; plateau date: 81.1±0.4 Ma; J=0.007000; wt., 0.0698 g								
850	7.113	0.0040	0.0024	21.2	89.9	2.60	131.0	79.1±0.4
1,000	6.895	.0045	.0011	32.6	95.4	4.01	115.0	81.3±0.4
1,050	6.998	.0081	.0014	20.1	93.9	2.47	63.9	81.1±0.4
1,100	7.292	.0128	.0025	16.6	89.9	2.03	40.5	81.1±0.4
1,250	10.22	.0448	.0126	8.4	63.6	1.03	11.6	80.5±0.4
Fuse	55.45	.2324	.1680	1.1	10.4	.140	2.24	71.6±0.3
R21, MICROCLINE								
Total-gas date: 76.8 Ma; no plateau; J=0.007313; wt., 0.0823 g								
600	33.85	0.0047	0.0882	0.1	23.0	0.025	111	99.7±2.1
700	7.964	.0014	.0073	.5	72.9	.109	365	75.0±0.6
800	6.153	.0014	.0013	3.8	93.9	.809	380	74.7±0.7
900	5.943	.0008	.0004	11.2	97.7	2.41	651	75.0±0.4
1,000	6.031	.0007	.0006	24.2	97.2	5.21	790	75.7±0.4
1,050	6.261	.0004	.0015	8.0	93.0	1.72	1360	75.2±0.4
1,100	6.705	.0004	.0025	8.6	88.9	1.85	1210	77.0±0.4
1,150	7.469	.0004	.0047	19.9	81.5	4.29	1430	78.6±0.4
Fuse	8.209	.0002	.0073	16.8	73.6	3.62	2220	78.0±0.4
R22, HORNBLENDE								
Total-gas date: 89.2 Ma; plateau date: 89.3±0.6 Ma ; J=0.007373; wt., 0.8212 g								
850	33.35	2.632	0.0848	0.5	25.5	0.089	0.20	109.7±1.0
950	20.98	3.023	.0481	.7	33.4	.131	.17	90.7±0.7
1,000	14.87	3.844	.0277	.9	47.0	.170	.14	90.6±0.5
1,050	8.267	4.180	.0058	7.5	83.3	1.42	.12	89.3±0.5
1,100	8.317	4.270	.0061	5.3	82.2	.994	.12	88.7±0.5
1,125	13.30	4.225	.0233	1.6	50.8	.297	.12	87.6±0.5
1,150	10.59	4.285	.0138	3.8	64.7	.720	.12	88.8±0.4
1,175	9.021	4.335	.0087	5.3	75.3	.989	.12	88.1±0.4
1,200	8.662	4.338	.0074	12.8	78.6	2.41	.12	88.3±0.4
1,250	7.909	4.585	.0048	24.6	86.6	4.63	.11	88.9±0.4
Fuse	8.055	4.495	.0050	37.0	85.9	6.97	.12	89.7±0.4

in dates may be due to analytical error, differential cooling of the pluton, or later thermal effects. Sample R20 was analyzed by higher precision methods and yielded a date of 226.7±1.1 Ma. We interpret this date to record a period of postmetamorphic plutonism that occurred at about 227 Ma and after the metamorphic rocks had cooled below 280°C (argon-retention temperature of biotite). The thermal effect of this plutonism was large enough to cause partial to complete argon loss from some of the hornblendes in the metamorphic

TABLE 10.3.—*$^{40}Ar/^{39}Ar$ age-spectrum data for samples from west-central Idaho and eastern Oregon*—Continued

Temperature (°C)	$^{40}Ar/^{39}Ar$	$^{37}Ar/^{39}Ar$	$^{36}Ar/^{39}Ar$	^{39}Ar (pct of total)	pct $^{40}Ar_R$	^{39}Ar (mol x10^{-13})	Apparent K/Ca (mol/mol)	Apparent age and error (Ma)
R23, HORNBLENDE								
Total-gas date: 96.9 Ma; no plateau; J=0.006873; wt., 0.7618 g								
850	41.74	3.891	0.1200	0.3	15.6	0.038	0.13	79.0±2.1
950	30.64	2.846	.0827	.3	20.9	.046	.18	77.8±1.2
1,000	40.32	3.806	.1120	.2	18.3	.031	.14	89.4±2.2
1,050	36.57	5.822	.0997	.4	20.7	.058	.09	91.5±1.2
1,100	15.02	6.494	.0265	2.3	51.1	.312	.08	92.8±0.5
1,125	10.65	5.547	.0114	4.6	72.5	.643	.09	93.2±0.5
1,150	9.471	5.491	.0072	10.6	82.2	1.47	.09	94.0±0.5
1,175	9.209	5.304	.0059	18.0	85.6	2.50	.10	95.1±0.5
1,200	9.261	5.105	.0052	21.0	87.5	2.91	.10	97.8±0.5
1,250	9.505	5.045	.0058	19.7	86.0	2.73	.10	98.6±0.5
Fuse	10.09	5.087	.0076	22.6	81.7	3.13	.10	99.4±0.5
R24, HORNBLENDE								
Total-gas date: 91.8 Ma; no plateau; J=0.006832; wt., 0.8055 g								
850	53.59	2.530	0.140	1.1	23.1	0.057	0.21	146.3±4.3
950	31.43	1.839	.0797	1.4	25.5	.071	.28	96.2±0.7
1,000	41.07	4.490	.118	1.1	16.1	.057	.12	79.7±1.7
1,050	49.52	8.973	.148	1.3	13.2	.068	.06	78.5±0.9
1,100	31.95	12.35	.0866	3.2	22.9	.160	.05	88.0±0.8
1,125	20.89	13.26	.0486	4.3	36.2	.218	.04	90.8±0.5
1,150	14.74	13.56	.0275	11.1	52.0	.556	.04	91.9±0.5
1,175	12.42	13.63	.0197	26.6	61.6	1.33	.04	91.9±0.5
1,200	19.19	13.67	.0432	8.8	39.1	.442	.04	90.1±0.5
1,250	13.97	13.65	.0248	19.2	55.2	.963	.04	92.6±0.5
Fuse	15.61	13.56	.0308	21.9	48.5	1.10	.04	90.8±0.5
R24, MUSCOVITE								
Total-gas date; 83.4 Ma: plateau date: 83.4±0.4 Ma; J=0.007107; wt., 0.580 g								
750	15.95	0.0350	0.0342	0.7	36.6	0.095	14.9	73.3±1.2
875	8.797	.0117	.0068	2.0	77.2	.252	44.4	85.0±0.5
925	7.856	.0016	.0037	3.6	86.1	.465	333.0	84.7±0.4
975	7.749	.0007	.0037	5.7	85.9	.731	743.0	83.8±0.4
1,050	7.711	.0	.0035	12.6	86.4	1.61	.0	83.5±0.4
1,150	7.235	.0	.0019	23.3	92.0	2.98	.0	83.4±0.4
1,200	7.374	.0004	.0024	42.4	90.4	5.42	1160.0	83.5±0.4
Fuse	11.76	.0026	.0174	9.6	56.2	1.23	196.0	82.7±0.4
R24, MICROCLINE								
Total-gas date: 77.8 Ma; no plateau; J=0.007168; wt., 0.0713 g								
600	22.35	0.0344	0.0343	0.6	54.7	0.097	15.1	151.5±0.8
700	6.470	.0273	.0033	1.3	84.7	.225	19.1	69.5±0.4
800	6.118	.0207	.0011	4.7	94.5	.793	25.1	73.3±0.4
900	6.141	.0073	.0005	12.6	97.4	2.15	71.6	75.8±0.4
1,000	6.245	.0097	.0006	13.4	96.9	2.28	53.8	76.6±0.4
1,050	6.611	.0091	.0017	10.6	92.2	1.81	57.2	77.2±0.4
1,100	6.967	.0094	.0029	10.0	87.7	1.71	55.3	77.3±0.4
1,100	7.426	.0127	.0043	12.9	82.9	2.19	41.0	77.9±0.4
1,250	7.669	.0118	.0071	15.8	81.2	2.69	44.1	78.8±0.4
Fuse	8.346	.0062	.0071	18.0	74.8	3.06	83.9	79.0±0.4

TABLE 10.3.—*$^{40}Ar/^{39}Ar$ age-spectrum data for samples from west-central Idaho and eastern Oregon*—Continued

Temperature (°C)	$^{40}Ar/^{39}Ar$	$^{37}Ar/^{39}Ar$	$^{36}Ar/^{39}Ar$	^{39}Ar (pct of total)	pct $^{40}Ar_R$	^{39}Ar (mol x10^{-13})	Apparent K/Ca (mol/mol)	Apparent age and error (Ma)
R25, BIOTITE								
Total-gas date: 83.7 Ma; plateau date: 84.1±0.4 Ma; J=0.007340; wt., 0.0628 g								
650	23.95	0.2735	0.0674	0.3	16.9	0.034	1.90	52.8±0.7
850	7.834	.1717	.0054	5.8	79.8	.646	3.03	81.0±0.4
1,000	7.024	.0105	.0018	27.0	92.5	2.99	49.5	84.0±0.4
1,050	7.110	.0080	.0021	16.0	91.4	1.77	65.3	84.0±0.4
1,125	7.052	.0105	.0019	35.0	92.2	3.87	49.5	84.1±0.4
1,200	8.109	.0975	.0054	14.3	80.3	.58	36.1	84.2±0.4
Fuse	29.95	.0975	.0809	1.7	20.2	.183	5.34	78.3±0.7
R26, HORNBLENDE								
Total-gas date: 107.5 Ma; no plateau; J=0.006691; wt., 0.7132 g								
850	36.21	3.767	0.0903	2.3	27.1	0.223	0.14	114.6±0.8
950	17.82	3.902	.0343	2.1	44.7	.199	.13	93.7±0.5
1,000	17.45	5.923	.0329	1.6	46.8	.151	.09	96.0±0.5
1,050	11.75	6.486	.0118	6.3	74.6	.605	.08	102.8±0.5
1,100	10.57	6.172	.0065	22.3	86.3	2.15	.08	106.8±0.5
1,125	11.06	6.127	.0076	14.7	84.8	1.42	.09	108.8±0.5
1,150	11.73	6.201	.0100	7.1	79.0	.684	.08	108.5±0.5
1,175	18.81	6.099	.0341	2.0	49.0	.192	.09	107.8±0.6
1,200	17.77	6.254	.0310	2.8	51.2	.783	.08	106.7±0.6
1,250	13.53	6.337	.0162	8.1	68.2	.783	.08	108.0±0.6
Fuse	11.75	6.281	.0099	30.9	79.3	2.98	.08	109.0±0.6
R26, BIOTITE								
Total-gas date: 89.0 Ma; plateau date: 89.9±0.6; J=0.007327; wt., 0.0697 g								
650	9.944	0.0634	0.0217	0.8	35.5	0.093	8.20	46.1±0.7
850	7.476	.0133	.0028	13.8	89.1	1.59	39.0	85.9±0.4
1,000	7.423	.0099	.0015	35.4	93.9	4.07	52.7	89.9±0.4
1,050	7.440	.0211	.0015	21.6	94.1	2.49	24.7	90.8±0.5
1,125	7.549	.0257	.0020	23.1	92.3	2.67	20.2	89.8±0.5
1,200	10.84	.0775	.0132	4.6	64.1	.529	6.71	89.7±0.5
Fuse	49.72	.1644	.1480	.6	11.9	.074	3.16	76.8±0.8
R27, HORNBLENDE								
Total-gas date: 111.8 Ma; no plateau; J=0.007171; wt., 0.7382 g								
850	47.94	5.651	0.1280	2.0	21.9	0.099	0.09	130.8±1.6
950	31.97	6.827	.0723	1.6	34.8	.078	.08	138.4±1.0
1,000	26.49	8.640	.0634	1.5	31.8	.074	.06	105.7±0.7
1,050	19.93	14.02	.0400	4.1	46.2	.199	.04	115.2±0.6
1,100	18.00	15.19	.0344	8.5	50.0	.409	.03	112.8±0.6
1,125	17.27	14.51	.032	9.0	51.6	.436	.04	111.6±0.6
1,150	18.86	15.44	.0383	7.3	46.4	.350	.03	109.7±0.6
1,175	14.09	15.09	.0226	14.3	61.6	.689	.03	108.9±0.6
1,200	18.51	15.19	.0371	9.8	47.2	.472	.03	109.5±0.6
1,250	14.13	15.20	.0220	16.7	62.4	.805	.03	110.6±0.6
Fuse	15.17	15.30	.0251	25.2	59.0	1.21	.03	112.1±0.6

rocks and to disturb the argon age spectra of metamorphic biotite.

Preliminary age-spectrum data for seven samples from plutons in the Bald Mountain batholith (fig. 10.1; five biotites and two hornblendes; L.W. Snee and W.H. Taubeneck, unpub. data, 1987) range from 142.3±0.8 to 144.6±1.0 Ma. This narrow range in dates recorded by both hornblende and biotite within five distinct plutons of the batholith suggests rapid cooling, which in turn indicates emplacement over a very short period of time and at high crustal levels. This period of intrusive activity was apparently regional in scope as

TABLE 10.3.—*$^{40}Ar/^{39}Ar$ age-spectrum data for samples from west-central Idaho and eastern Oregon*—Continued

Temperature (°C)	$^{40}Ar/^{39}Ar$	$^{37}Ar/^{39}Ar$	$^{36}Ar/^{39}Ar$	^{39}Ar (pct of total)	pct $^{40}Ar_R$	^{39}Ar (mol x10^{-13})	Apparent K/Ca (mol/mol)	Apparent age and error (Ma)
R28, HORNBLENDE								
Total-gas date: 107.0 Ma; plateau date: 107.7±0.5 Ma; J=0.007334; wt., 0.7885 g								
850	13.40	1.383	0.0187	1.3	59.5	0.232	0.38	102.4±0.6
1,000	9.694	.2511	.0065	3.8	80.3	.664	2.07	100.1±0.5
1,050	12.61	1.384	.0164	1.9	62.4	.332	.38	101.3±0.5
1,100	10.57	3.429	.0089	6.2	77.7	1.10	.15	105.5±0.5
1,125	9.608	4.211	.0055	10.4	86.5	1.83	.12	106.7±0.5
1,150	9.457	4.454	.0050	9.5	88.1	1.67	.12	107.0±0.5
1,175	9.301	4.538	.0045	13.2	89.6	2.31	.11	107.9±0.5
1,200	9.451	4.582	.0049	8.8	88.5	1.55	.11	107.4±0.5
1,250	8.882	4.737	.0027	20.6	95.1	3.62	.11	108.4±0.5
Fuse	9.043	4.755	.0034	24.2	93.1	4.24	.11	108.0±0.5
R29, HORNBLENDE								
Total-gas date: 107.8 Ma; plateau date: 108.1±0.5 Ma; J=0.007326; wt., 0.7110 g								
850	37.06	1.997	0.0974	0.5	22.8	0.0634	0.26	108.3±1.0
1,000	26.75	2.067	.0671	.6	26.4	.0753	.25	91.0±0.7
1,050	25.30	4.713	.0622	.7	28.8	.0902	.11	93.9±0.7
1,100	11.08	5.556	.0107	6.7	75.4	.847	.09	107.1±0.6
1,125	9.86	5.528	.0064	12.0	85.2	1.52	.09	107.7±0.5
1,150	9.86	5.524	.0064	12.2	85.3	1.55	.09	108.0±0.5
1,175	9.68	5.469	.0057	16.9	87.1	2.14	.09	108.1±0.5
1,200	9.17	5.486	.0039	29.0	92.0	3.67	.09	108.2±0.6
1,250	11.76	5.495	.0126	6.8	71.8	.860	.09	108.3±0.6
Fuse	11.00	5.439	.0101	14.6	76.8	1.85	.09	108.3±0.6
R30, HORNBLENDE								
Total-gas date: 118.8 Ma; plateau date: 118.1±0.6 Ma; J=0.007093; wt., 0.7041 g								
850	32.43	4.138	0.0394	0.6	65.1	0.0737	0.13	251.7±1.3
1,000	34.83	2.530	.0802	.0	32.5	.0051	.21	139.3±2.6
1,050	21.03	4.717	.0412	1.1	43.8	.135	.11	114.2±0.6
1,100	12.58	5.424	.0124	4.6	74.5	.545	.10	116.2±0.6
1,125	11.19	5.471	.0070	6.7	85.2	.797	.10	118.0±0.6
1,150	16.73	5.416	.0054	11.2	89.1	1.34	.10	118.4±0.6
1,200	10.65	5.376	.0051	28.7	87.7	1.44	.10	118.5±0.6
1,250	10.80	5.386	.0059	12.2	87.7	1.44	.10	117.3±0.6
Fuse	10.31	5.353	.0041	34.8	92.4	4.13	.10	117.9±0.6
R34, HORNBLENDE								
Total-gas date: 109.2 Ma; plateau date: 109.1±0.5 Ma; J=0.007270; wt., 0.8333 g								
850	42.59	2.597	0.116	1.9	19.7	0.105	0.20	106.6±1.7
950	20.31	12.60	.0428	3.5	42.6	.188	.04	109.9±0.6
1,000	18.02	13.72	.0354	3.8	47.8	.208	.04	109.5±0.6
1,050	13.97	13.57	.0214	8.1	62.3	.438	.04	110.5±0.6
1,100	12.28	13.39	.0159	16.6	70.1	.902	.04	109.5±0.6
1,125	11.69	13.42	.0142	16.2	73.1	.881	.04	108.7±0.6
1,150	11.87	13.55	.0146	14.1	72.5	.765	.04	109.3±0.6
1,175	12.55	13.61	.0170	8.7	68.5	.470	.04	109.3±0.6
1,200	13.44	13.65	.0202	9.3	63.4	.503	.04	108.3±0.6
1,250	14.54	13.56	.0238	9.6	58.9	.519	.04	108.8±0.6
Fuse	18.87	13.52	.0382	8.3	45.7	.453	.04	109.5±0.6

TABLE 10.3.—*$^{40}Ar/^{39}Ar$ age-spectrum data for samples from west-central Idaho and eastern Oregon*—Continued

Temperature (°C)	$^{40}Ar/^{39}Ar$	$^{37}Ar/^{39}Ar$	$^{36}Ar/^{39}Ar$	^{39}Ar (pct of total)	pct $^{40}Ar_R$	^{39}Ar (mol x10^{-13})	Apparent K/Ca (mol/mol)	Apparent age and error (Ma)
R35, MUSCOVITE								
Total-gas date: 98.6 Ma; plateau date: 98.3±0.2 Ma; J=0.007340; wt., 0.0628 g								
750	12.49	0.8865	0.0205	0.6	51.9	0.069	0.59	84.4±0.7
875	9.735	.6722	.0077	2.0	77.3	.216	.77	97.5±0.5
925	8.667	.0384	.0041	4.6	86.0	.506	13.6	96.7±0.5
975	8.195	.0112	.0021	13.6	92.4	1.49	46.5	98.2±0.5
1,015	7.959	.0010	.0012	25.4	95.3	2.79	53.4	98.4±0.5
1,200	8.062	.0023	.0011	36.2	95.8	3.98	23.0	99.4±0.5
Fuse	10.36	.2632	.0088	4.3	75.1	.475	1.98	100.9±0.5
R36, BIOTITE								
Total-gas date: 80.1 Ma; plateau date: 80.5±0.4 Ma; J=0.007174; wt., 0.1243 g								
500	8.568	---	0.0094	6.0	67.6	3.72	---	73.5±0.4
650	6.861	---	.0017	14.7	92.5	9.06	---	80.3±0.4
850	6.570	---	.0007	25.5	96.7	15.7	---	80.4±0.4
1,050	6.615	---	.0008	29.3	96.4	18.0	---	80.7±0.4
1,250	6.549	---	.0006	20.9	97.0	12.8	---	80.4±0.4
Fuse	6.882	---	.0014	3.6	94.0	2.18	---	81.8±0.8
7-30-5, HORNBLENDE								
Total-gas date: 115.4 Ma; plateau date: 112.0±0.7 Ma; J=0.005480; wt., 1.1493g								
650	204.1	5.543	0.3470	0.4	50.0	0.821	0.09	801.8±4.2
850	44.28	3.574	.1020	.8	32.7	1.84	.15	137.8±0.8
950	15.08	3.792	.0124	6.0	77.7	13.2	.14	112.2±0.6
1,000	15.26	3.804	.0130	4.6	76.7	10.1	.14	112.1±0.7
1,050	13.78	3.789	.0084	8.4	84.0	18.5	.14	111.0±0.6
1,100	12.72	3.774	.0046	26.4	91.5	57.9	.14	111.5±0.5
1,150	12.54	3.784	.0039	25.3	93.0	55.6	.14	111.8±0.6
1,200	12.52	3.823	.0035	21.9	94.1	48.0	.14	112.8±0.6
1,250	16.17	3.791	.0156	2.8	73.2	6.15	.14	113.4±0.6
1,350	17.16	3.782	.0193	2.7	68.5	6.02	.14	112.5±0.6
1,450	49.32	3.781	.1270	.4	24.4	.862	.14	115.4±1.2
Fuse	81.01	3.790	.2330	.2	15.3	.419	.14	118.3±3.6
Hcm-23, HORNBLENDE								
Total-gas date: 224.5 Ma; plateau date: 223.3±5.9 Ma; J=0.004577; wt., approx. 1.5 g								
900	789.8	39.78	2.579	3.53	3.9	1.5	0.01	246.6±214.7
1,000	198.1	17.02	.5702	2.44	15.7	1.0	.03	242.7±96.9
1,050	61.22	19.60	.1165	16.44	46.4	6.9	.03	223.5±11.4
1,120	38.29	16.40	.0380	24.35	74.2	10.2	.03	223.1±6.1
Fuse	51.16	16.78	.0816	53.24	55.6	22.3	.03	223.2±5.8
Hdh-24, HORNBLENDE								
Total-gas date: 214.7 Ma; plateau date: 215.6±3.6 Ma; J=0.005570; approx. 1.5 g								
800	99.97	13.86	0.2784	2.48	18.9	4.1	0.04	181.8±22.4
1,000	66.40	14.48	.1543	2.76	33.1	4.6	.04	210.7±18.1
1,050	51.58	12.02	.1007	2.60	44.3	4.3	.04	217.7±14.6
1,150	38.58	7.96	.5670	69.05	58.3	114.1	.07	214.1±3.2
Fuse	35.38	11.74	.0448	23.11	65.3	38.2	.04	220.1±3.8

TABLE 10.3.—*$^{40}Ar/^{39}Ar$ age-spectrum data for samples from west-central Idaho and eastern Oregon*—Continued

Temperature (°C)	$^{40}Ar/^{39}Ar$	$^{37}Ar/^{39}Ar$	$^{36}Ar/^{39}Ar$	^{39}Ar (pct of total)	pct $^{40}Ar_R$	^{39}Ar (mol x10^{-13})	Apparent K/Ca (mol/mol)	Apparent age and error (Ma)
Hdh-25, HORNBLENDE								
Total-gas date: 213.0 Ma; plateau date: 213.0±2.0 Ma; J=0.005570; wt., approx. 1.5 g								
1,025	33.34	7.68	0.0386	18.28	67.7	39.4	0.07	214.8±3.5
1,075	24.39	7.64	.0089	54.25	91.8	116.8	.07	213.2±2.5
1,150	24.88	7.79	.0112	11.91	89.2	25.6	.07	211.4±3.1
Fuse	24.92	7.96	.0115	15.57	89.0	33.5	.07	211.3±2.9
Hdh-27, HORNBLENDE								
Total-gas date: 225.5 Ma; plateau date: 225.0±2.3 Ma; J=0.005570; wt., approx. 1.5 g								
900	171.3	13.19	0.4985	2.26	14.6	3.6	0.04	238.0±33.1
1,025	27.54	9.94	.0153	40.60	86.6	64.3	.05	226.5±2.9
1,075	25.35	9.80	.0089	35.14	92.8	55.6	.05	223.7±2.8
1,100	28.20	10.65	.0181	7.35	84.2	11.6	.05	225.6±4.1
Fuse	26.95	11.25	.0142	14.65	87.9	23.2	.05	225.3±3.6
HKc-29, BIOTITE								
Total-gas date: 218.3 Ma; plateau date: 233.5±2.5 Ma; J=0.003578: wt., approx. .25 g								
600	16.68	---	0.0202	7.22	64.2	11.5	---	67.8±2.5
800	38.32	---	.0057	32.41	95.6	51.5	---	222.2±2.6
900	40.73	---	.0078	13.39	94.3	21.3	---	232.4±3.1
1,025	40.28	---	.0036	27.89	97.3	44.3	---	236.8±2.8
Fuse	41.25	---	.0114	19.09	91.8	30.3	---	229.3±2.8
Hkc-32, HORNBLENDE								
Total-gas date: 225.8 Ma; plateau date: 229.3±2.6 Ma; J=0.005570; wt., approx. 1.5 g								
900	32.33	5.45	0.0345	9.33	69.9	21.7	0.10	214.6±4.1
1,025	27.05	6.61	.0137	36.40	87.0	84.6	.08	223.3±2.8
1,075	29.12	6.51	.0188	10.14	82.7	23.6	.08	228.2±3.7
1,100	25.78	6.49	.0078	21.45	93.1	49.9	.08	227.5±2.8
Fuse	26.76	6.69	.0096	22.68	91.5	52.7	.08	231.6±2.9
Hkc-34, HORNBLENDE								
Total-gas date: 224.6 Ma; plateau date 225.8±6.7 Ma; J=0.005570; wt., approx. 1.5g								
900	211.8	29.78	0.6497	2.02	10.5	0.9	0.02	215.4±103.1
1,025	298.4	28.81	.9512	2.97	6.6	1.3	.02	191.9±112.8
1,075	59.33	30.56	.1318	12.02	38.6	5.1	.02	221.4±15.3
1,100	36.56	29.54	.0534	40.63	63.5	17.3	.02	224.0±5.4
Fuse	63.50	31.20	.1433	42.36	37.4	18.1	.02	228.9±7.8
Hkc-35, HORNBLENDE								
Total-gas date: 241.1 Ma; plateau date: 239.2±7.6 Ma; J=0.005570; wt., approx. 1.5 g								
900	154.8	23.87	0.4253	2.84	20.1	1.3	0.02	293.3±60.9
1,025	75.12	32.31	.1802	17.82	32.7	8.1	.02	236.4±11.8
1,075	36.01	31.56	.0474	31.31	68.4	14.3	.02	236.9±6.0
Fuse	32.65	33.51	.0346	48.04	77.2	21.9	.02	242.4±4.2
Hkc-36, HORNBLENDE								
Total-gas date: 231.0 Ma; plateau date: 238.6±3.4 Ma; J=0.003585; wt., approx. 1.5 g								
800	53.83	4.64	0.0935	10.31	49.4	8.6	0.11	164.8±5.8
1,025	44.59	24.60	.0275	35.09	86.3	29.4	.02	237.2±3.1
1,070	42.50	26.51	.0217	24.28	90.1	20.3	.02	236.4±3.2
1,100	43.68	27.47	.0243	11.17	88.8	9.4	.02	239.2±3.9
Fuse	45.07	27.11	.0262	19.15	87.8	16.0	.02	243.8±3.7

TABLE 10.3.—*$^{40}Ar/^{39}Ar$ age-spectrum data for samples from west-central Idaho and eastern Oregon*—Continued

Temperature (°C)	$^{40}Ar/^{39}Ar$	$^{37}Ar/^{39}Ar$	$^{36}Ar/^{39}Ar$	^{39}Ar (pct of total)	pct $^{40}Ar_R$	^{39}Ar (mol x10^{-13})	Apparent K/Ca (mol/mol)	Apparent age and error (Ma)
Hkc-36, BIOTITE								
Total-gas date: 216.8 Ma; no plateau; J=0.003578; wt., approx. .25 g								
600	65.10	---	0.1944	8.64	11.8	8.9	---	48.8±8.3
800	50.52	---	.0459	34.66	73.1	35.7	---	223.9±3.3
900	73.23	---	.1140	15.06	54.0	15.5	---	238.7±5.6
1,025	59.43	---	.0649	24.10	67.7	24.8	---	242.6±3.9
Fuse	73.24	---	.1209	17.53	51.2	18.1	---	227.3±5.1
Hkc-37, HORNBLENDE								
Total-gas date: 239.1; plateau date: 235.0±3.5 Ma; J=0.004577; wt., approx. 1.5 g								
950	55.11	9.60	0.0859	7.29	55.4	6.7	0.05	237.4±10.6
1,025	43.41	16.08	.0450	11.85	72.4	10.9	.03	245.3±6.8
1,070	37.68	14.23	.0253	28.25	83.3	25.9	.04	244.4±4.1
1,125	33.17	11.93	.0143	26.85	90.2	24.6	.04	233.5±3.4
Fuse	34.07	13.44	.0164	25.77	89.0	23.6	.04	236.6±3.6
Hcop-39, HORNBLENDE								
Total-gas date: 224.9 Ma; plateau date: 227.8±5.3 Ma; J=0.004577; wt., approx. 1.5 g								
900	307.1	20.32	0.9538	7.35	8.8	3.1	0.03	212.8±74.2
1,000	274.7	11.73	.8461	3.02	9.3	1.3	.04	201.7±99.7
1,050	129.9	19.28	.3603	3.23	19.3	1.4	.03	198.6±56.8
1,100	43.43	31.73	.0554	44.42	66.4	18.9	.02	227.1±4.9
Fuse	43.92	20.92	.0562	41.97	66.1	17.9	.02	228.4±5.9
Hcop-40, HORNBLENDE								
Total-gas date: 215.4 Ma; plateau date; 219.2±7.6 Ma; J=0.005570; wt., approx. 1.5 g								
900	29.29	14.01	0.0302	29.72	73.5	28.9	0.04	206.4±3.6
1,000	23.20	14.75	.0090	41.14	94.1	40.0	.04	217.5±2.9
1,050	34.28	14.55	.0414	3.66	67.9	3.6	.04	221.9±13.7
1,100	32.66	14.23	.0396	4.34	67.8	4.2	.04	211.8±13.2
Fuse	28.75	15.29	.0223	21.15	81.4	20.6	.03	223.5±4.1
D81-1, HORNBLENDE								
Total-gas date: 148.5 Ma; plateau date: 145.1±1.5 Ma; J=0.004290; wt. 1.1024 g								
850	87.20	5.808	0.2214	2.3	25.5	0.544	0.09	164.2±6.5
975	67.87	3.541	.1583	2.5	31.5	.598	.15	158.1±5.2
1,075	57.72	23.22	.1280	8.2	37.6	1.96	.02	160.4±2.0
1,175	37.43	23.81	.0645	27.8	54.0	6.64	.02	150.0±1.3
1,275	32.99	23.75	.0522	43.0	58.8	10.3	.02	144.2±1.2
Fuse	55.65	24.68	.1276	16.2	35.7	3.87	.02	147.5±1.8

indicated by the hornblende plateau date of 145.1±1.5 Ma for slightly metamorphosed tonalite that intruded the Seven Devils Group along Rapid River southwest of Riggins (sample D81-1; fig. 10.6) and by an $^{40}Ar/^{39}Ar$ date of about 145 Ma on hornblende from pre-accretionary quartz diorite near Orofino (fig. 10.1; Fleck and Criss, 1987; Davidson and Snee, 1989; Davidson, 1990).

METAMORPHIC ROCKS OF THE RIGGINS GROUP AND SEVEN DEVILS ISLAND ARC

In an attempt to determine the age of metamorphism and deformation that affected the island-arc rocks near the Salmon River suture zone, 15 samples were analyzed by the $^{40}Ar/^{39}Ar$ method. Rocks from the Riggins Group and Seven Devils island arc were

TABLE 10.3.—*$^{40}Ar/^{39}Ar$ age-spectrum data for samples from west-central Idaho and eastern Oregon*—Continued

Temperature (°C)	$^{40}Ar/^{39}Ar$	$^{37}Ar/^{39}Ar$	$^{36}Ar/^{39}Ar$	^{39}Ar (pct of total)	pct $^{40}Ar_R$	^{39}Ar (mol x10^{-13})	Apparent K/Ca (mol/mol)	Apparent age and error (Ma)
2KE080, HORNBLENDE								
Total-gas date: 80.9 Ma; plateau date: 81.2±0.4 Ma; J=0.008163; wt., 1.0388 g								
550	66.33	5.629	0.2184	0.0	3.4	0.0418	0.09	32.5±29.8
700	50.94	3.856	.1575	.1	9.2	.0867	.13	68.0±7.4
800	115.9	4.291	.3708	.1	5.7	.123	.12	95.4±19.9
900	63.77	6.187	.1964	.2	9.7	.216	.08	89.0±3.2
950	45.93	7.441	.1386	.5	12.1	.667	.07	79.9±1.8
1,000	7.256	5.468	.0073	10.5	76.2	14.3	.09	79.6±0.4
1,025	6.650	5.102	.0049	15.7	84.2	21.3	.10	80.6±0.4
1,050	7.131	4.914	.0066	9.3	78.1	12.6	.10	80.2±0.4
1,075	7.855	4.850	.0088	6.0	71.6	8.19	.11	80.9±0.4
1,100	7.478	4.794	.0074	6.5	75.5	8.89	.11	81.2±0.4
1,125	6.881	4.849	.0055	9.8	81.8	13.4	.11	81.0±0.4
1,150	6.479	4.849	.0041	15.1	87.3	20.6	.11	81.3±0.4
1,200	6.503	4.835	.0041	23.2	87.2	31.6	.11	81.6±0.5
Fuse	21.21	4.803	.0544	3.0	26.0	4.01	.11	79.4±0.7
2KE080, BIOTITE								
Total-gas date: 78.2 Ma; plateau date: 78.2±0.4 Ma; J=0.007930; wt., 0.0446 g								
750	23.175	8.719	0.0606	1.8	25.7	0.523	0.0593	83.2±1.0
1,050	6.491	.02527	.0030	65.2	86.4	18.5	20.7	78.5±0.4
1,100	7.718	.2476	.0074	21.9	71.7	6.21	2.10	77.5±0.4
Fuse	10.272	.8158	.0163	11.1	53.6	3.16	.637	77.2±0.4
2KE086, HORNBLENDE								
Total-gas date: 80.4 Ma; plateau date: 80.5±0.6 Ma; J=0.008190; wt., 0.9842 g								
550	142.0	9.144	0.4356	0.0	9.9	0.0381	0.06	195.9±62.2
700	100.2	5.191	.3118	.1	8.5	.0607	.10	121.0±30.9
800	114.6	4.785	.3800	.1	2.3	.0910	.11	39.1±12.8
900	71.34	4.220	.2256	.5	7.0	.384	.12	72.4±5.3
950	60.74	8.194	.1897	.2	8.8	.199	.06	77.0±6.8
975	91.15	10.97	.2968	.2	4.7	.137	.05	62.4±17.3
1,000	32.49	11.29	.0939	.6	17.3	.437	.05	81.0±0.8
1,025	15.30	9.169	.0354	2.4	36.2	1.95	.06	79.9±0.5
1,050	9.167	8.443	.0146	5.7	60.1	4.55	.06	79.5±0.4
1,075	7.388	8.190	.0083	16.1	75.2	12.9	.06	80.2±0.5
1,100	7.936	8.253	.0103	17.7	69.8	14.2	.06	80.0±1.0
1,125	11.99	8.235	.0238	2.9	46.5	2.34	.06	80.5±0.5
1,150	12.37	8.159	.0249	3.1	45.7	2.48	.06	81.5±0.5
1,175	8.667	8.061	.0127	8.2	63.8	6.58	.06	79.8±0.4
1,225	8.725	8.208	.0128	13.9	63.8	11.2	.06	80.4±0.5
Fuse	8.557	8.387	.0121	28.2	65.7	22.6	.06	81.1±0.4
1KE052, MUSCOVITE								
Total-gas date: 73.7 Ma; plateau date: 73.8±0.4 Ma; J=0.008244; wt., 0.1812 g								
750	6.193	0.0035	0.0040	5.4	80.7	5.70	149	72.9±0.4
875	5.597	.0016	.0018	16.9	90.4	18.0	328	73.8±0.4
925	5.563	.0012	.0017	27.2	90.9	29.0	434	73.7±0.4
975	5.738	.0042	.0024	10.3	87.7	11.0	122	73.3±0.4
1,015	5.600	.0015	.0018	13.9	90.2	14.8	351	73.6±0.4
1,050	5.582	.0009	.0017	17.2	91.0	18.3	554	74.0±0.4
1,100	6.189	.0051	.0037	9.0	82.4	9.62	102	74.3±0.4
Fuse	113.488	.1614	.3750	.1	2.4	.133	3.22	39.6±13.2

TABLE 10.3.—*$^{40}Ar/^{39}Ar$ age-spectrum data for samples from west-central Idaho and eastern Oregon*—Continued

Temperature (°C)	$^{40}Ar/^{39}Ar$	$^{37}Ar/^{39}Ar$	$^{36}Ar/^{39}Ar$	^{39}Ar (pct of total)	pct $^{40}Ar_R$	^{39}Ar (mol x10^{-13})	Apparent K/Ca (mol/mol)	Apparent age and error (Ma)
1KE052, MICROCLINE								
Total-gas date: 63.5 Ma; no plateau; J=0.007990; wt., 0.0785 g								
400	23.500	0.0025	0.0627	0.1	21.2	0.0414	20.9	70.4±3.8
500	34.384	.0068	.0794	.1	31.8	.0485	7.63	151.1±5.5
600	11.282	.0025	.0113	.6	70.4	.295	21.0	111.0±0.7
700	4.656	.0028	.0027	1.4	82.5	.763	18.3	54.5±0.4
800	4.661	.0030	.0026	3.8	83.4	2.00	17.5	55.2±0.3
900	4.422	.0037	.0013	5.3	91.1	2.82	14.2	57.1±0.3
1,000	4.506	.0049	.0011	13.4	93.0	7.09	10.6	59.4±0.3
1,050	4.938	.0042	.0021	9.7	87.5	5.17	12.5	61.2±0.3
1,100	5.632	.0024	.0042	7.8	77.8	4.13	21.7	62.0±0.3
1,150	6.253	.0018	.0050	7.3	71.6	3.85	28.1	63.4±0.4
1,200	7.336	.0019	.0097	6.9	61.0	3.67	27.3	63.3±0.3
1,260	7.425	.0028	.0096	9.1	61.9	4.82	18.7	65.0±0.4
1,300	6.785	.0017	.0069	19.6	69.8	10.40	30.1	67.0±0.4
Fuse	6.938	.0010	.0074	15.0	68.2	7.94	51.6	67.0±0.3
2KE087, MUSCOVITE								
Total-gas date: 70.7 Ma; plateau date: 71.0±0.4 Ma; J=0.008244; wt., 0.1946 g								
750	5.405	0.0024	0.0024	11.2	86.8	9.87	219	68.4±0.3
875	5.208	---	.0012	25.5	93.0	22.3	---	70.7±0.4
925	5.149	---	.0009	25.7	94.5	22.5	---	71.0±0.4
975	5.184	---	.0011	18.3	93.8	16.1	---	70.9±0.4
1,050	5.404	.0001	.0016	14.4	91.0	12.7	5400	71.7±0.4
1,100	7.066	.0017	.0074	4.5	69.0	3.99	312	71.1±0.4
Fuse	38.81	.0197	.0117	0.3	10.9	.303	26.4	61.7±0.9
MP201, HORNBLENDE								
Total-gas date: 86.6 Ma; plateau date: 86.3±0.4 Ma; J=0.006390; wt., 0.5054 g								
850	0.75	2.405	0.0740	2.2	29.5	2.05	0.22	101.5±0.6
950	10.52	4.575	.0107	10.0	73.2	9.33	.11	86.6±0.5
1,000	9.281	4.829	.0067	8.3	82.7	7.79	.11	86.4±0.4
1,050	9.058	4.881	.0060	7.2	84.7	6.75	.11	86.3±0.5
1,100	8.718	4.916	.0047	9.3	88.3	8.73	.11	86.6±0.4
1,150	8.442	4.987	.0040	14.2	90.7	13.3	.10	86.1±0.5
1,200	8.286	5.003	.0035	17.4	92.1	16.3	.10	85.9±0.5
1,250	8.465	5.019	.0039	13.8	91.0	12.9	.10	86.7±0.4
1,450	8.434	5.166	.0040	12.8	90.7	12.0	.10	86.1±0.4
Fuse	10.93	5.240	.0125	4.8	69.9	4.49	.10	86.0±0.5
TC-S-41-16, MUSCOVITE								
Total-gas date: 87.4 Ma; plateau date: 87.4±0.4 Ma; J=0.006400; wt., 0.1094 g								
550	22.72	0.0880	0.0509	2.2	33.8	4.27	5.91	86.5±0.5
650	10.65	.0057	.0093	3.4	74.2	6.53	91.5	89.0±0.4
800	8.237	.0013	.0014	7.8	94.8	15.1	396	88.0±0.4
900	8.003	.0006	.0008	15.7	96.9	30.6	817	87.4±0.4
1,000	8.010	.0021	.0010	11.2	96.2	21.9	252	86.8±0.5
1,125	7.898	.0014	.0005	33.4	97.9	65.0	360	87.2±0.4
Fuse	8.102	.0079	.0011	26.4	95.9	51.5	66.1	87.6±0.4

collected from an area extending from Slate Creek in the north to Round Valley in the south, and from 7 mi west of Riggins on Papoose Creek to the easternmost exposures of the Riggins Group or correlative rocks on the Salmon River (fig. 10.6). Samples of hornblende, muscovite, and biotite from all metamorphic grades were dated. The argon age spectra are simple for some of these samples and complex for

TABLE 10.3.—*$^{40}Ar/^{39}Ar$ age-spectrum data for samples from west-central Idaho and eastern Oregon*—Continued

Temperature (°C)	$^{40}Ar/^{39}Ar$	$^{37}Ar/^{39}Ar$	$^{36}Ar/^{39}Ar$	^{39}Ar (pct of total)	pct $^{40}Ar_R$	^{39}Ar (mol x10^{-13})	Apparent K/Ca (mol/mol)	Apparent age and error (Ma)
TC-S-124-23, MUSCOVITE								
Total-gas date: 87.6 Ma; plateau date: 87.6±0.4 Ma; J=0.006400; wt., 0.1194 g								
550	10.06	0.1233	0.0083	3.6	75.8	7.64	4.22	86.0±0.4
650	8.736	.0079	.0026	3.1	91.1	6.75	65.6	89.6±0.4
800	8.207	.0037	.0012	4.8	95.6	10.4	139	88.4±0.4
900	8.100	.0014	.0011	13.9	96.1	29.9	367	87.7±0.4
1,000	7.989	.0010	.0008	24.3	97.0	52.2	519	87.3±0.4
1,125	7.879	.0004	.0003	25.0	98.6	53.6	1480	87.6±0.4
Fuse	7.930	.0012	.0004	25.3	98.3	54.2	436	87.8±0.5
D3113M, MUSCOVITE								
Total-gas date: 72.5 Ma; plateau date: 72.4±0.4 Ma; J=0.004750; wt., 0.1019 g								
550	16.04	0.2556	0.0237	1.5	56.4	2.07	2.04	75.9±0.5
650	12.33	.0968	.0121	1.6	70.9	2.21	5.37	73.4±0.4
800	9.941	.0233	.0044	3.9	86.9	5.38	22.4	72.5±0.4
900	9.970	.0107	.0045	12.2	86.6	16.6	48.5	72.5±0.4
1,000	9.392	.0139	.0026	20.6	91.7	28.1	37.4	72.3±0.4
Fuse	9.121	.0115	.0017	60.2	94.6	82.1	45.3	72.4±0.4
B12178201, MUSCOVITE								
Total-gas date: 70.5 Ma; plateau date: 70.1±0.4 Ma; J=0.004897; wt., 0.1012 g								
550	23.57	0.0338	0.0539	1.3	32.4	1.66	15.4	66.3±0.4
650	9.757	.0032	.0055	7.7	83.1	10.1	160	70.3±0.4
900	8.886	.0009	.0023	29.2	92.3	38.5	592	71.0±0.4
950	8.618	.0007	.0018	19.8	93.6	26.1	695	69.9±0.3
1,000	8.566	.0018	.0017	12.5	94.0	16.5	294	69.8±0.3
1,125	8.414	.0020	.0010	19.7	96.6	26.0	264	70.4±0.4
Fuse	8.567	.0069	.0011	10.0	96.3	13.2	75.4	71.4±0.4
B12198202, BIOTITE								
Total-gas date: 68.7 Ma; no plateau; J=0.004445; wt., 0.1012 g								
550	10.24	0.0503	0.0098	5.9	71.7	4.44	10.3	57.9±0.3
750	10.03	.0159	.0042	27.4	87.7	20.6	32.7	69.2±0.4
850	12.34	.0209	.0060	10.1	85.6	7.58	24.9	82.8±0.4
950	12.04	.0240	.0042	11.2	89.8	8.41	21.7	84.6±0.4
1,050	10.92	.0271	.0059	6.7	83.9	5.03	19.2	72.0±0.4
1,150	8.662	.0256	.0030	11.4	89.6	8.57	20.3	61.2±0.3
Fuse	8.810	.0561	.0036	27.3	88.0	20.5	9.27	61.1±0.3
B12198202, MICROCLINE								
Total-gas date: 60.5 Ma; no plateau; J=0.004695; wt., 0.1042 g								
600	9.132	0.0038	0.0085	6.0	72.5	5.89	138	55.2±0.3
700	7.801	.0030	.0031	7.3	88.1	7.14	175	57.3±0.3
800	7.469	.0023	.0019	5.1	92.3	5.02	225	57.5±0.3
900	7.304	.0026	.0012	8.5	94.9	8.35	197	57.8±0.3
1,000	7.374	.0025	.0009	12.3	96.4	12.1	208	59.2±0.3
1,050	7.578	.0028	.0012	10.3	95.3	10.1	186	60.2±0.3
1,100	7.791	.0043	.0017	10.5	93.5	10.4	121	60.7±0.3
1,200	8.005	.0054	.0022	12.7	91.9	12.5	95.4	61.3±0.3
1,300	8.511	.0049	.0033	13.0	88.4	12.8	106	62.7±0.3
Fuse	8.741	.0017	.0028	14.4	90.3	14.2	300	65.7±0.4

others; many exhibit argon loss. A brief summary is presented in table 10.2 under the heading "Rocks Near the Suture Zone."

Even though $^{40}Ar/^{39}Ar$ age spectra of metamorphic minerals from the Riggins Group and Seven Devils island arc are complex (figs. 10.7, 10.10, 10.14, 10.19, and 10.25), some general observations are evident. Age spectra of 7 of the 12 dated hornblendes exhibit plateaus or near-plateaus (figs. 10.7, 10.10, and 10.17); five of these display minor argon loss, indicated by progressively increasing dates from left to right on the age-spectrum diagrams (figs. 10.7, 10.10, and 10.17). Two of the five age spectra that do not exhibit plateaus display argon loss (figs. 10.10 and 10.17). Hornblende dates form at least three statistically distinct groups at about 118, 109, and 101 Ma (fig. 10.25); a younger 93-Ma thermal event is documented by the $^{40}Ar/^{39}Ar$ dates of hornblende from suture-zone plutons (see below). These groups of dates show a clear geographical

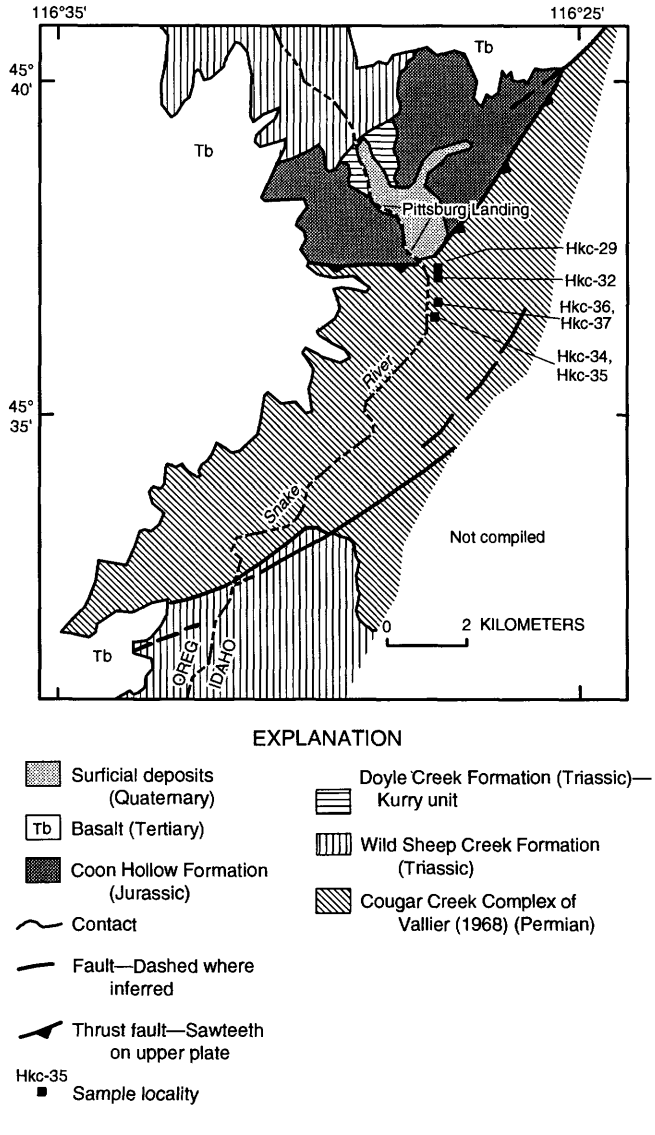

FIGURE 10.3.—Sample locality map for Pittsburg Landing area on Snake River. Geologic base from Vallier (1974 and written commun., 1987) and White and Vallier (1994).

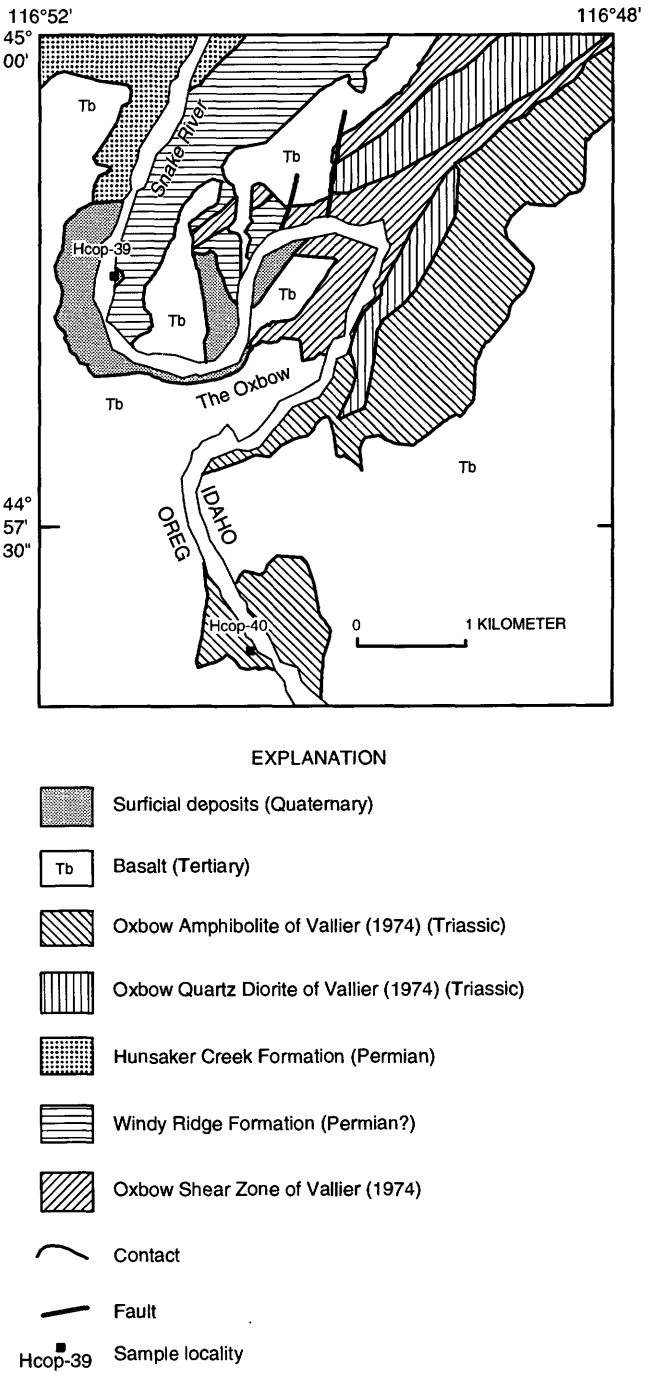

FIGURE 10.4.—Sample locality map for area of The Oxbow on Snake River. Geologic base modified from Vallier (1974).

distribution: the 118-Ma group is located south and west of Riggins; the 109-Ma group forms an apparent belt to the north, east, and south of the 118-Ma group; and the 101-Ma group is located farther east along the west side of the suture zone. This geographic distribution is schematically shown on figure 10.6. The groups of dates also exhibit a relation, albeit less clearly defined, to the metamorphic grade described by Hamilton (1963), Onasch (1977, 1987), and Lund (1984). The 118-Ma group occurs not only in greenschist-facies, garnet-zone rocks but also in upper-amphibolite-facies rocks in this region; the 109-Ma group occurs in amphibolite-facies, oligoclase- and andesine-zone rocks; and the 101-Ma group occurs in upper-amphibolite-facies, sillimanite-zone rocks. Although argon loss from hornblende is present in all age groups, it is found only in rocks of oligoclase-zone or higher grade metamorphism. Argon loss is most severe where textural evidence shows that the rock contains hornblende of two different ages or has undergone multiple deformations. The dates of muscovites and biotites are generally younger than the dates of hornblendes from any particular group. One biotite preserves a cooling age that is statistically identical to the date of a coexisting hornblende that records the oldest metamorphic event. Two dated muscovites from biotite-zone rocks exhibit argon loss. Three biotites from andesine-zone rocks display significantly younger dates than coexisting hornblendes.

An important conclusion from these data is that the oldest metamorphism associated with the Salmon River suture zone in the Riggins-Slate Creek area occurred at 116 to 118 Ma. One sample (R7), which yielded this date (116.5±0.6 Ma), is a garnet-zone rock containing hornblende crystals that define a single foliation but no lineation (figs. 10.7, 10.8). The mineral assemblage indicates that the hornblende formed within the lower limits of the stability field of hornblende and probably at a temperature of 500°C or

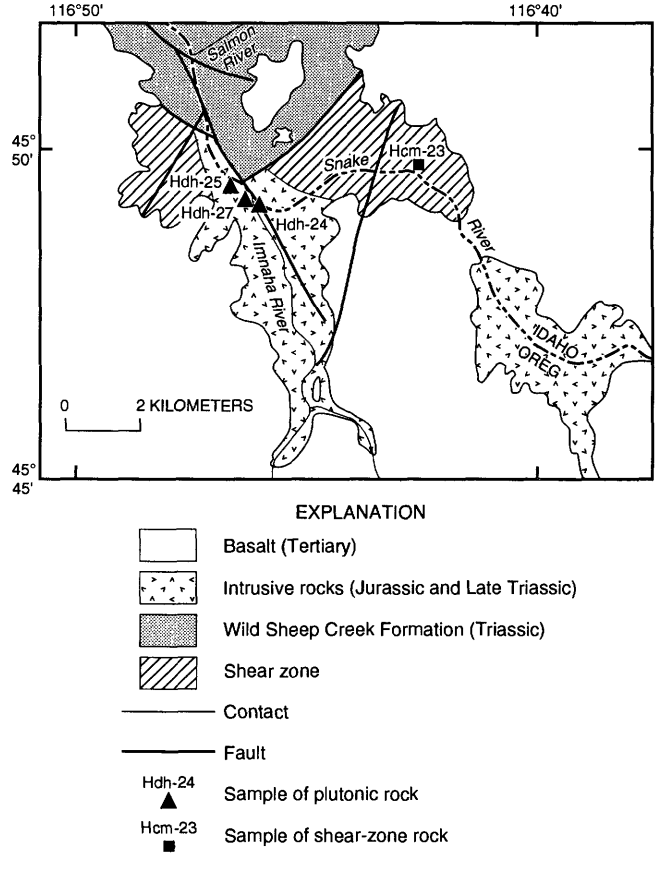

FIGURE 10.5.—Sample locality map for area at confluence of Imnaha and Snake Rivers. Geologic base modified from Vallier (1974).

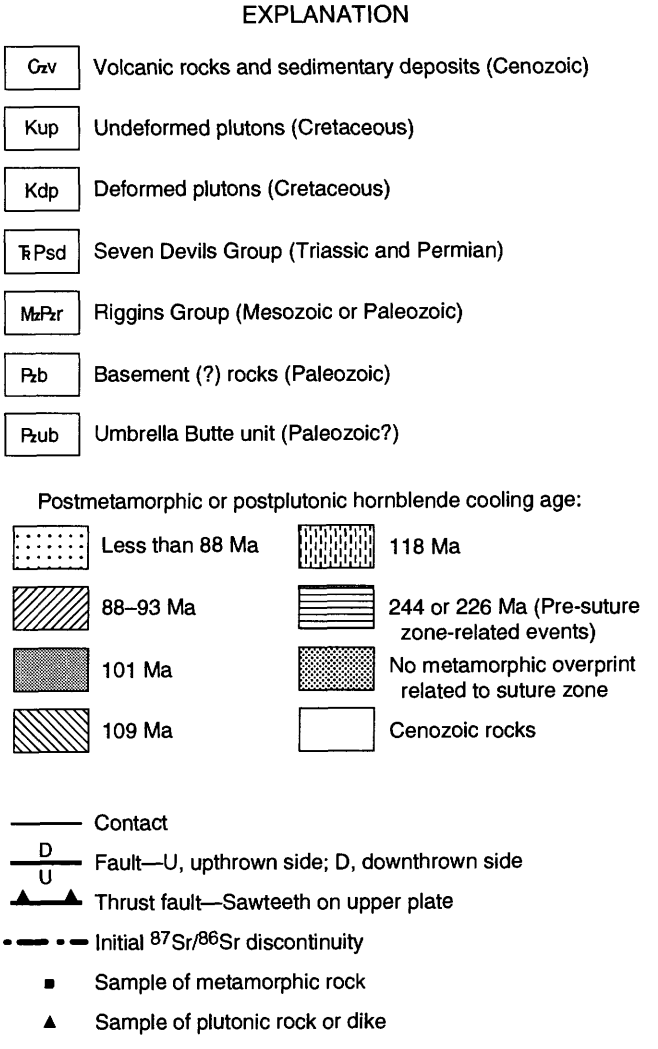

FIGURE 10.6.—Explanation.

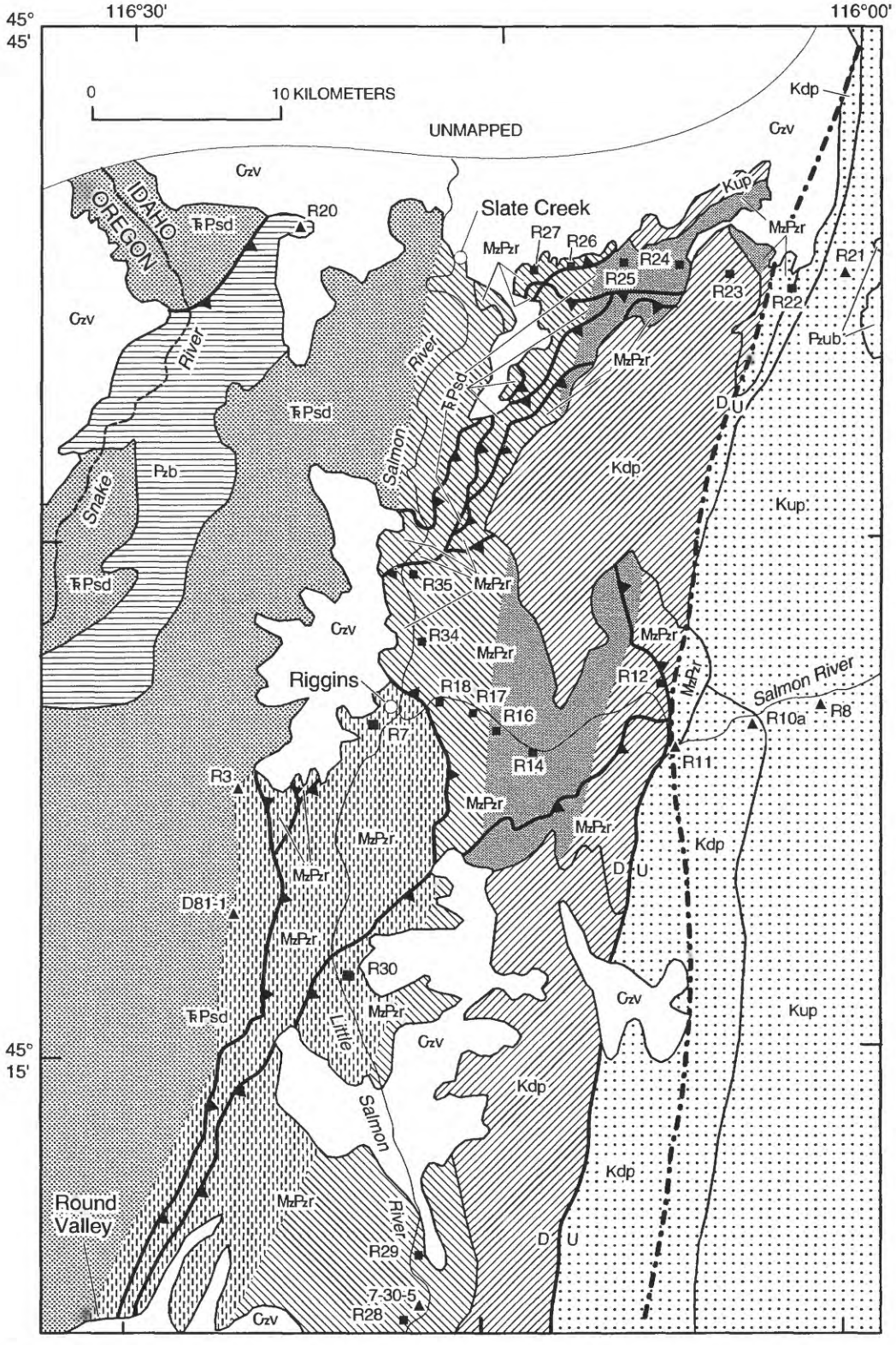

FIGURE 10.6.—Sample locality map for Riggins, Idaho, area. Age-distribution pattern is based on hornblende $^{40}Ar/^{39}Ar$ dates and is highly generalized. Geology is modified from Lund and Snee (1988). See also figure 10.2, which covers part of the same area. Geology of unpatterned area is not compiled.

lower (upper greenschist facies; Winkler, 1979). Because the argon closure-temperature of hornblende is over 500°C even at slow cooling rates, this hornblende probably closed to diffusion of argon upon formation, that is, this age does not reflect any significant period of cooling. The coexisting biotite of this sample (R7) yielded a plateau date of 115.8±0.3 Ma, indicating that this rock cooled very quickly after metamorphism to a temperature lower than 280°C (biotite argon-retention temperature). Hornblende (R30) from amphibolite-facies rocks also has a single hornblende-defined foliation (figs. 10.7, 10.9); this sample, which probably formed at about 600°C (above the hornblende argon-closure temperature), also gives an age of 118 Ma. Therefore, it is unlikely that an extended period of cooling could have occurred after metamorphism in either upper-amphibolite-facies or greenschist-facies rocks of this age. In fact, sample R30 preserves evidence for a second period of metamorphism that caused the formation of symplectic epidote and hornblende at the expense of grossular garnet. Thermodynamically, this reaction indicates an increase in pressure from the conditions of the first metamorphism when the garnet formed (A.B. Till, U.S. Geological Survey, written commun., 1989); however, the temperature of this reaction is not well constrained. The argon spectrum for this sample displays argon loss, which we interpret to have occurred during the second, higher pressure metamorphic episode. If our interpretation is correct, the temperature of this second event must have been close to but lower than about 530°C, the argon closure-temperature of hornblende, because the argon loss was minor. This conclusion is consistent with geobarometry data (Selverstone and others, 1992) that indicate that the metamorphic rocks of the area of sample R30 and southward underwent an increase in pressure after the higher temperature metamorphic event. We suggest that this increase in pressure occurred after 118 Ma and possibly is our 109-Ma metamorphic event (see below).

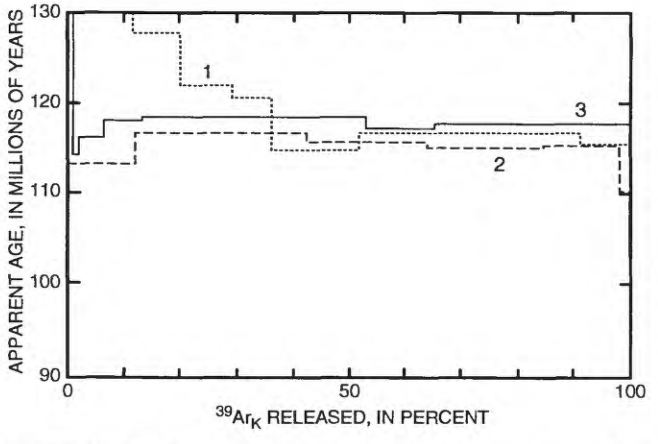

FIGURE 10.7.—Composite $^{40}Ar/^{39}Ar$ age-spectrum diagram for 118-Ma metamorphic rocks from Riggins Group. 1, Hornblende from sample R7; T_{mp} (preferred date)=116.5±0.6 Ma (preferred date defined by 48 percent of total $^{39}Ar_K$ released). 2, Biotite sample from R7; T_p (plateau date)=116.1±0.6 Ma (plateau date defined by 87 percent of total $^{39}Ar_K$ released). 3, Hornblende sample from R30; T_p=118.0±0.5 Ma (plateau date defined by 94 percent of total $^{39}Ar_K$ released; minor argon loss to 114 Ma). See text for discussion of plateau date, preferred date, and argon loss.

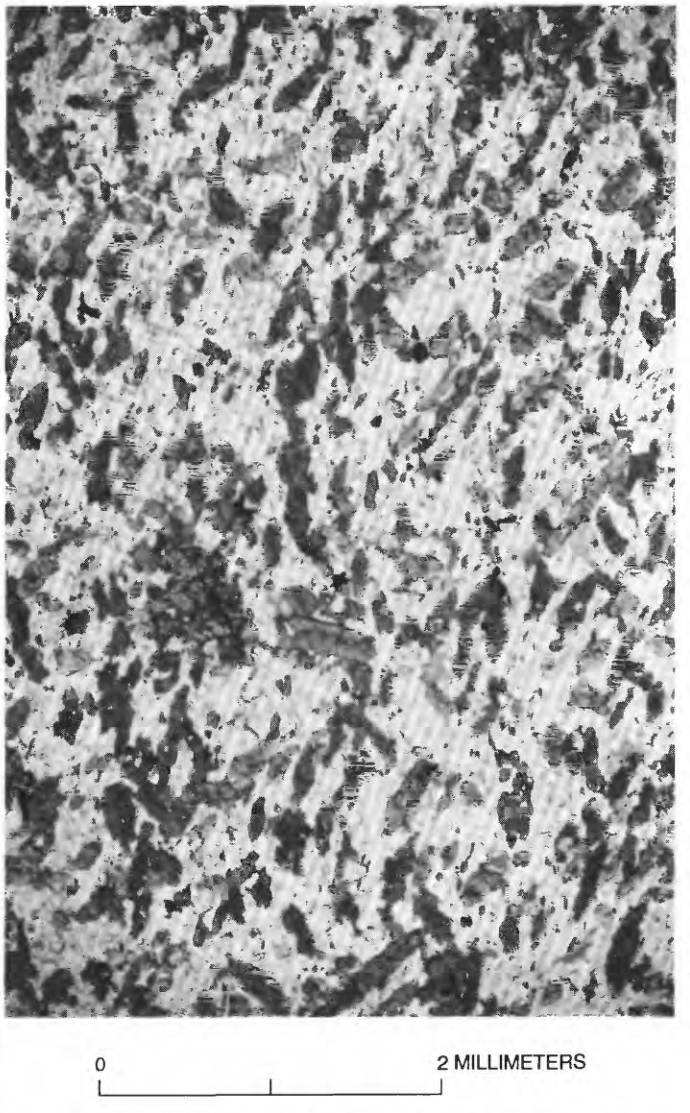

FIGURE 10.8.—Photomicrograph of sample R7: non-lineated, garnet-zone amphibolite from the Riggins Group. Hornblende (darker prismatic mineral among lighter colored feldspar and quartz) is randomly to weakly oriented, but rock has moderately defined foliation in hand specimen. Garnet (dark, poorly defined grain in left center of photomicrograph) is uncommon; biotite is common in other layers. Plane light.

Formerly, the oldest documented metamorphic event associated with tectonic activity along the Salmon River suture zone was the 118-Ma metamorphism described above. But recently Davidson and Snee (1989, 1990), Davidson (1990), and Snee and others (in press) have demonstrated that regional dynamothermal metamorphism along the Salmon River suture zone in the Orofino, Idaho, area began at 130 Ma. This period of metamorphism is preserved in $^{40}Ar/^{39}Ar$ age spectra for hornblendes from upper-greenschist-facies metamorphic rocks adjacent to the suture zone. If metamorphism as old as 130 Ma affected rocks in the Riggins-Slate Creek area, no argon isotopic record is preserved. It is possible that metamorphism associated with the suture zone was diachronous. It is equally possible, however, that 130-Ma metamorphic rocks in the Riggins-Slate Creek area were tectonically removed by right-slip movement along the suture or were structurally buried and(or) thermally overprinted during overthrusting of higher grade, younger metamorphic rocks.

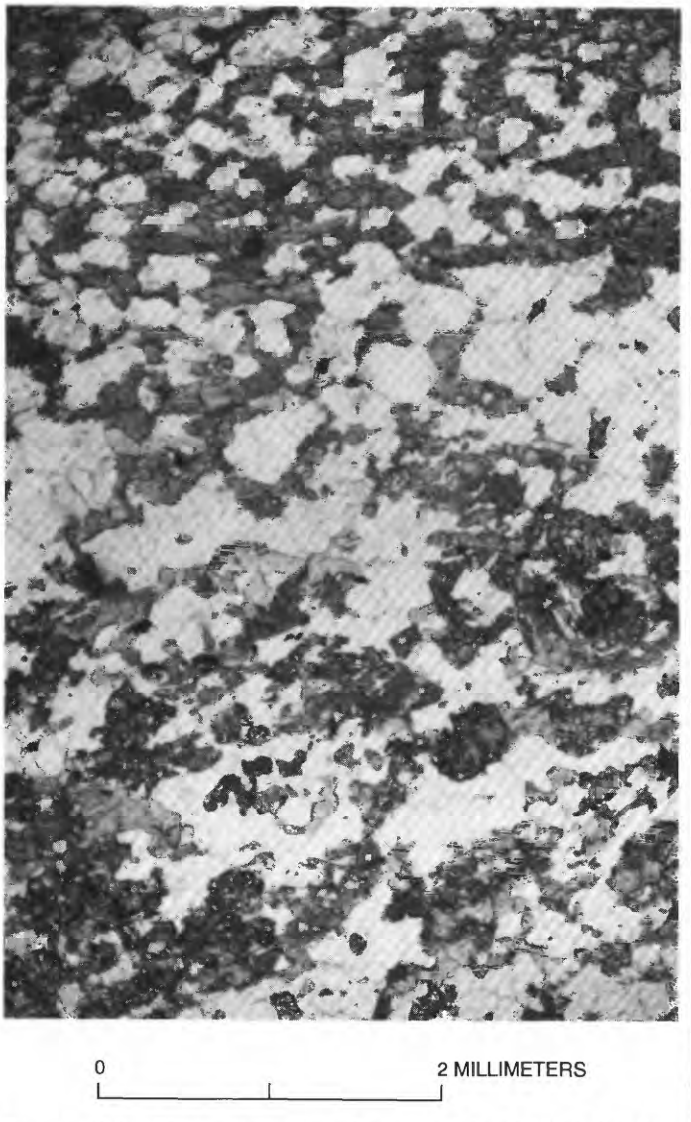

FIGURE 10.9.—Photomicrograph of sample R30: foliated, banded, non-lineated amphibolite from the Riggins Group. Band in upper half of photomicrograph is unoriented hornblende (darker mineral) and quartz and feldspar (lighter minerals). Band in lower half consists of unoriented symplectic epidote, symplectic hornblende, and altered grossular garnet (darker minerals) and quartz, feldspar, and calcite (lighter minerals). Mineral assemblage in lower band formed during a second, higher pressure metamorphic event than that forming the assemblage in the upper band. Plane light.

The $^{40}Ar/^{39}Ar$ age-spectrum data for metamorphic rocks from the Riggins-Slate Creek area reveal a second period of hornblende growth and argon closure that occurred at about 109 Ma. Samples that best show this are two postkinematic hornblendes (samples R27 and R34; figs. 10.10–10.12); these hornblendes formed after deformation that produced strong foliation in garnet-zone rocks. No argon loss is exhibited by either spectrum, and sample R34 has a well-defined plateau. Like the 118-Ma garnet-zone sample, these younger garnet-zone hornblendes probably formed at a temperature below that for hornblende argon closure. Thus, the dates closely approximate the age of static hornblende formation. That this thermal activity was accompanied in places by deformation is supported by data from five other synkinematic hornblendes from middle- to upper-amphibolite-facies rocks (samples R17, R18, R26, R28, and R29; figs. 10.10 and 10.13),

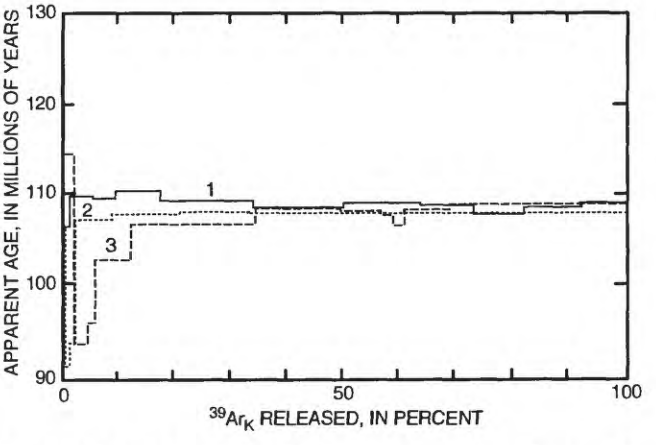

FIGURE 10.10.—Composite $^{40}Ar/^{39}Ar$ age-spectrum diagram for 109-Ma metamorphic rocks from Riggins Group. 1, Hornblende from sample R34; T_p (plateau age)=109.1±0.5 Ma (plateau defined by 83 percent of $^{39}Ar_K$ released). 2, Hornblende from sample R29; T_p=108.1±0.7 Ma (plateau defined by 98 percent of $^{39}Ar_K$ released). 3, Hornblende from sample R26; argon loss; T_{max} (maximum date)=109.0±0.6 Ma; T_{min} (minimum date)=93.7±0.5 Ma. Omitted from this diagram for clarity but of the same group are hornblende samples R17, R18, R27, and R28.

which show variable amounts of argon loss superposed on a maximum age of about 109 Ma. Argon loss recorded by these five hornblende samples probably resulted from one or more overprinting events.

Sillimanite-zone samples (R14, R16, and R23)—which clearly show two foliations, a lineation-dominated fabric, or two different episodes of hornblende growth (figs. 10.14–10.16)—have age spectra with minor argon loss from high-temperature ages of 99.5–101 Ma to low-temperature ages of 89–93 Ma (fig. 10.17). Although it is difficult to confidently interpret the high-temperature ages of these three samples, these data indicate another pulse of thermal activity at about 101 Ma. Argon loss exhibited by the low-temperature ages of these three samples probably resulted during emplacement and deformation of the suture-zone plutons.

Argon age-spectrum data also constrain the timing of deformation. Primary foliation, which in places partially transposes bedding (fig. 10.18), is defined (in the appropriate rock types) by 118-Ma hornblende

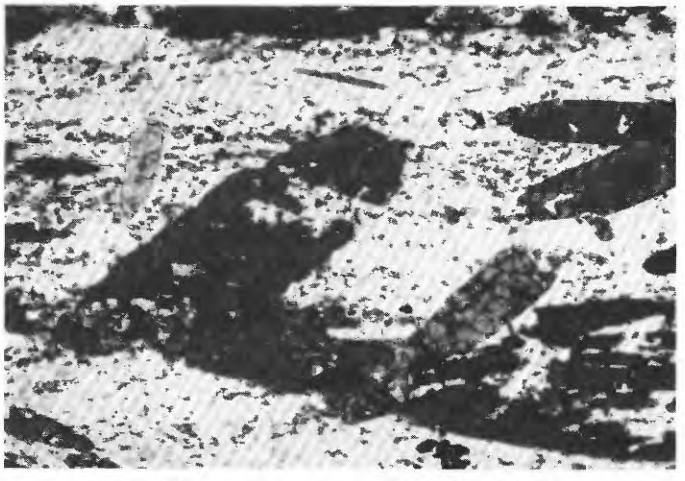

FIGURE 10.11.—Photomicrograph of sample R34: garnet-zone gneiss from Riggins Group. Foliation is defined by oriented biotite (uncommon planar minerals) and layers rich in epidote (small, clear, high-relief minerals) alternating with layers rich in quartz and feldspar. Hornblende (large, dark crystals) is unoriented and postkinematic. Plane light.

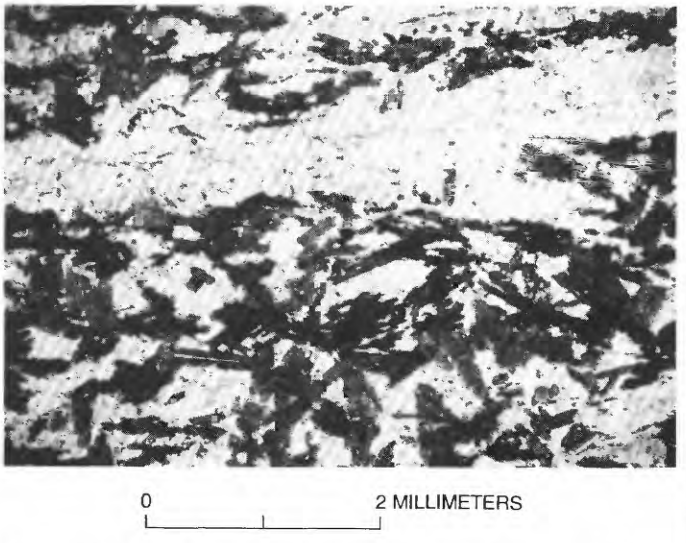

FIGURE 10.12.—Photomicrograph of sample R27: garnet-zone gneiss from Riggins Group. Unoriented, postkinematic amphibole (dark, prismatic crystals) formed over compositional banding that defines an earlier foliation. Plane light.

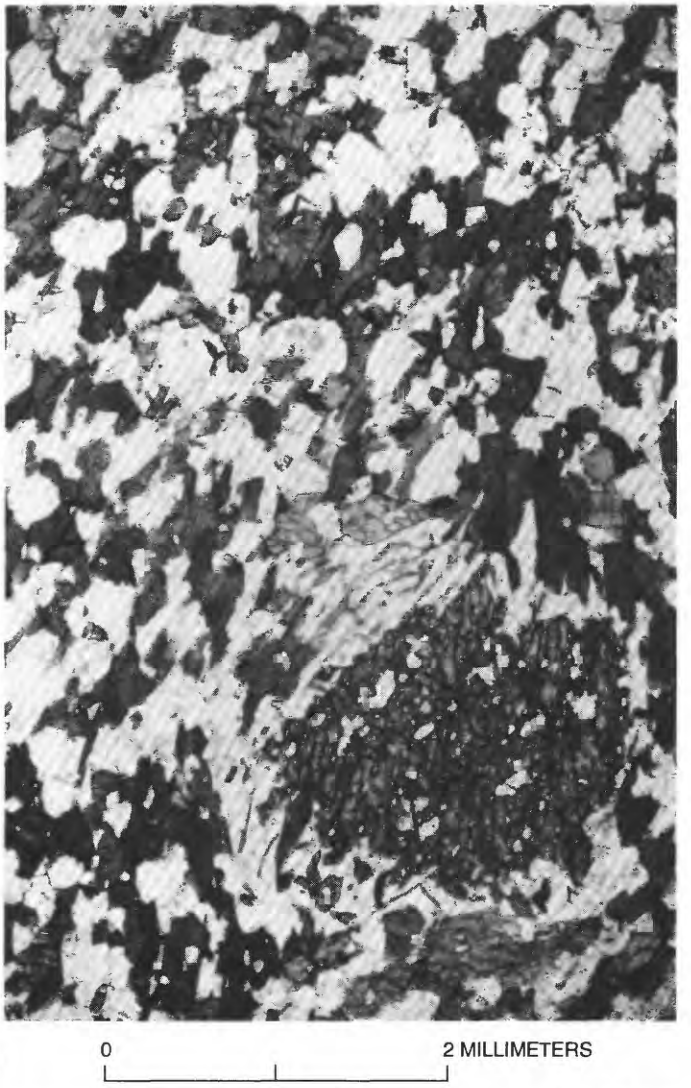

FIGURE 10.13.—Photomicrograph of sample R29: amphibolite from Riggins Group. Unoriented amphibole (dark minerals) and quartz and feldspar (light minerals) in a strongly banded gneiss. Earlier, deformed garnet (large grain in lower right) is partly altered to chlorite. Plane light.

that is associated with the onset of metamorphism. Thus, structures that deform metamorphic fabric in these rocks are all 118 Ma or younger. Although we feel that the Rapid River thrust fault is only one of several important postmetamorphic fault systems within the Riggins Group and Seven Devils island arc, it is a well-known feature for which an age can be derived from the argon data. Because this fault system cuts 118- and 109-Ma metamorphic rocks that have short cooling histories, it must have formed after 109 Ma. (As discussed below, it must be older than 93 Ma because it is intruded by 93-Ma plutons.) This conclusion is corroborated by the age spectrum for muscovite sample R3, which displays argon loss from 105 to 100 Ma. Sample R3 was collected from a pegmatite that intruded Seven Devils island-arc rocks near the Rapid River thrust fault on Papoose Creek (fig. 10.6) and was later deformed by boudinage. Both the pegmatite's emplacement and its later deformation may have been related to activity on the Rapid River thrust fault.

Within the island-arc metamorphic rocks of the Riggins Group, small bodies of deformed to undeformed tonalite and leucotonalite are exposed in places, and pegmatites are also present in both the Riggins Group and Seven Devils island-arc rocks. Whether these bodies are pre- or synmetamorphic has been an important question. Hornblende from a weakly foliated tonalite that intruded the Riggins(?) Group near Round Valley (sample 7-30-5) was dated (fig. 10.6) and yielded a plateau date of 112.0±0.7 Ma. This date, as well as the sample R3 muscovite date from pegmatite on Papoose Creek, provides evidence that pluton emplacement, albeit apparently minor in the Riggins area, occurred during the period of metamorphism and deformation, that is, 101–118 Ma. Additional data from other locations within the suture zone, such as Orofino, Idaho (fig. 10.1; Snee and others, 1987a; Davidson and Snee, 1989; Davidson, 1990; Snee and others, in press), suggest that magmatic activity occurred after both the 118-Ma and the 109-Ma metamorphic events and that later deformation commonly did not entirely reset the mineral argon systems. Preliminary results of U-Pb zircon dating (C.A. Manduca, California Institute of Technology, unpub.

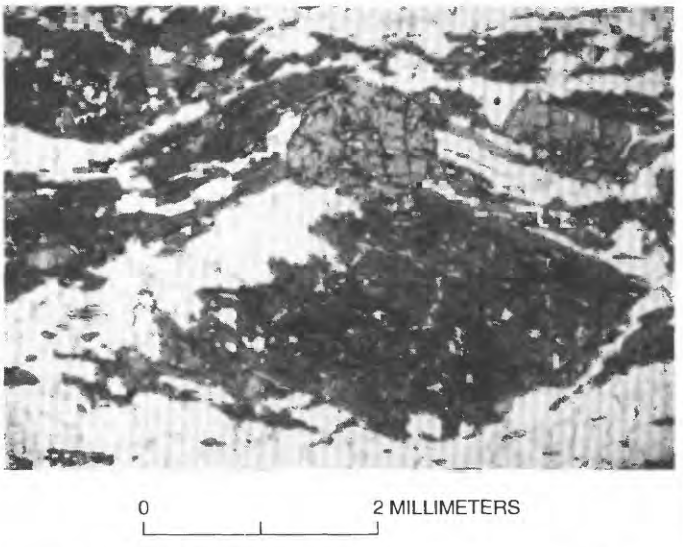

FIGURE 10.14.—Photomicrograph of sample R16: anorthite-zone amphibolite from Riggins Group. Foliation is well defined by younger generation of hornblende, which can be seen here wrapping around older hornblende microaugen. Fractured, postkinematic garnets (gray mineral in upper center) overgrew hornblende foliation. Plane light.

FIGURE 10.15.—Photomicrograph of sample R14: anorthite-zone amphibolite from Riggins Group. Foliation is well defined by bands rich in hornblende (dark minerals) and bands rich in quartz and feldspar (light minerals). Older hornblende microaugen (for example, large grain in center) are wrapped by the compositional bands. Plane light.

data, 1990; Snee and others, in press) indicate that some deformed plutons with island-arc chemical affinities located west of the suture zone were emplaced at 115 Ma. Current work is attempting to determine the extent of these plutons.

DEFORMED PLUTONS OF THE SALMON RIVER SUTURE ZONE

Determination of the age of tonalitic plutons within the suture zone by the $^{40}Ar/^{39}Ar$ age-spectrum technique is difficult because minerals may remain open to argon diffusion during postcrystallization cooling and deformation. (Age spectra for suture-zone plutons are summarized in table 10.2 under "Suture-zone Rocks.") Because the emplacement temperature of tonalite is about 850°C (Naney, 1983) and because the argon-closure temperature for hornblende is about 530°C, hornblende dates should provide a minimum estimate that, unless the plutons had an extended early cooling history, should be close to the age of crystallization.

The $^{40}Ar/^{39}Ar$ age spectrum for a sample of hornblende taken from a metasedimentary xenolith (sample R23; figs. 10.16, 10.19) in a suture-zone pluton provides important constraints on the emplacement history of the enclosing pluton. This age spectrum shows argon loss superposed on an earlier cooling age. The cooling age indicates that the metamorphic rock from which the hornblende was taken had cooled below the hornblende argon-closure temperature at or before 99.5 Ma; thus, this hornblende formed during a metamorphic event that preceded emplacement of the enveloping tonalite. Argon loss at about 91.5 Ma, which is preserved in the spectrum, probably resulted from emplacement of the tonalite. Because this hornblende was not completely reset during pluton emplacement, it seems likely that the heat of the pluton was lost quickly. Quick loss of heat suggests a short cooling history and implies a high crustal emplacement level for this tonalite at some time after 99.5 Ma. Therefore, the date of 91.5 Ma,

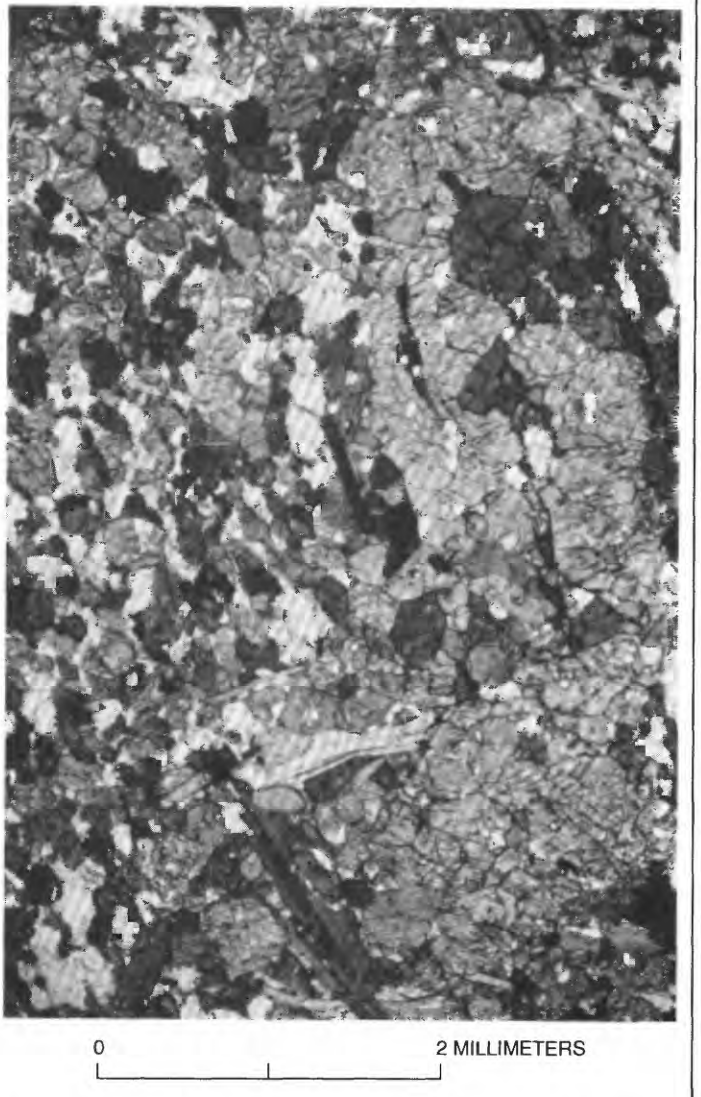

FIGURE 10.16.—Photomicrograph of sample R23: amphibolite roof pendant in foliated tonalite of suture zone. Older, coarse-grained hornblende (see right half of photo) has been partly replaced by finer grained hornblende (see left half of photo) that forms lineation perpendicular to plane of photo. Plane light.

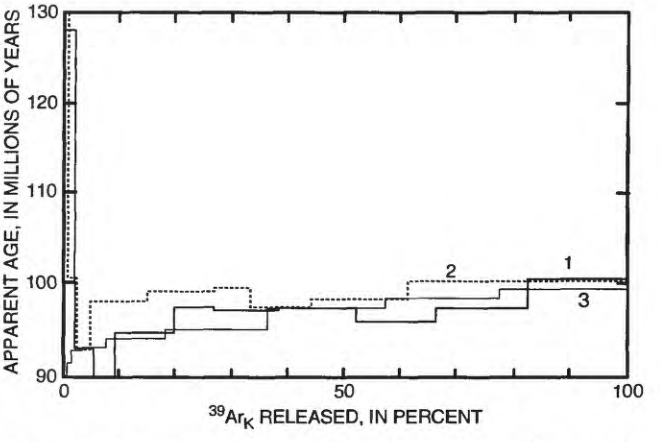

FIGURE 10.17.—Composite $^{40}Ar/^{39}Ar$ age-spectrum diagram for 101-Ma metamorphic rocks from Riggins Group. 1, Hornblende from sample R14; complex age spectrum showing argon loss from T_{max} (maximum date)=100.7±0.6 Ma to T_{min} (minimum date)=88.5±0.6 Ma. 2, Hornblende from sample R16; complex age spectrum showing argon loss from T_{max}=100.6±0.5 Ma to T_{min}=92.8±0.6 Ma. 3, Hornblende from sample R23; argon-loss spectrum showing consecutively increasing date, with T_{max}=99.4±0.5 Ma and T_{min}=91.5±1.2 Ma. T_{min} is chosen according to apparent K/Ca ratio that is consistent with higher temperature steps.

an estimate of the time of the argon loss from the metamorphic hornblende, may be close to the age of emplacement of the suture-zone tonalite.

The age spectrum of hornblende sample R12 (fig. 10.19) from suture-zone tonalite supports the interpretation that plutons were emplaced within the suture zone at or before about 91.5 Ma. Hornblende in this sample, which contains no epidote, was deformed by a strong postemplacement event that produced a steep southeast-plunging lineation defined by the deformed hornblende crystals. Argon loss exhibited by the age spectrum apparently occurred at 88 Ma, probably during deformation; the date of 93.5 Ma for the highest temperature extraction step is a minimum estimate of the age of emplacement of the tonalite. The virtually identical data of hornblende samples R24 and R22 (fig. 10.19), which were collected from the suture zone more than 25 km north of the location of sample R12, lend additional support to the interpretation that at least some tonalites within the suture zone were emplaced at a relatively shallow level at or before 93.5 Ma and that a major episode of deformation caused argon loss at about 88 Ma.

The ages of emplacement and deformation of the suture-zone plutons provide additional constraints on the age of the Rapid River thrust fault. In the Slate Creek area, as mentioned above, the Rapid River thrust fault cuts 118-Ma and 109-Ma metamorphic rocks that had short cooling histories; therefore the thrust fault is younger than 109 Ma. The Rapid River thrust fault in the Slate Creek area is folded and cut by later thrust faults (Lund, 1984), and all of the thrust faults are intruded by the 93.5-Ma or older suture-zone plutons. Thus the original Rapid River thrust-faulting event, plus the later folding and rethrusting, all occurred between 109 and 93.5 Ma. Finally, after the emplacement of the suture-zone plutons, high-angle deformation occurred at about 88

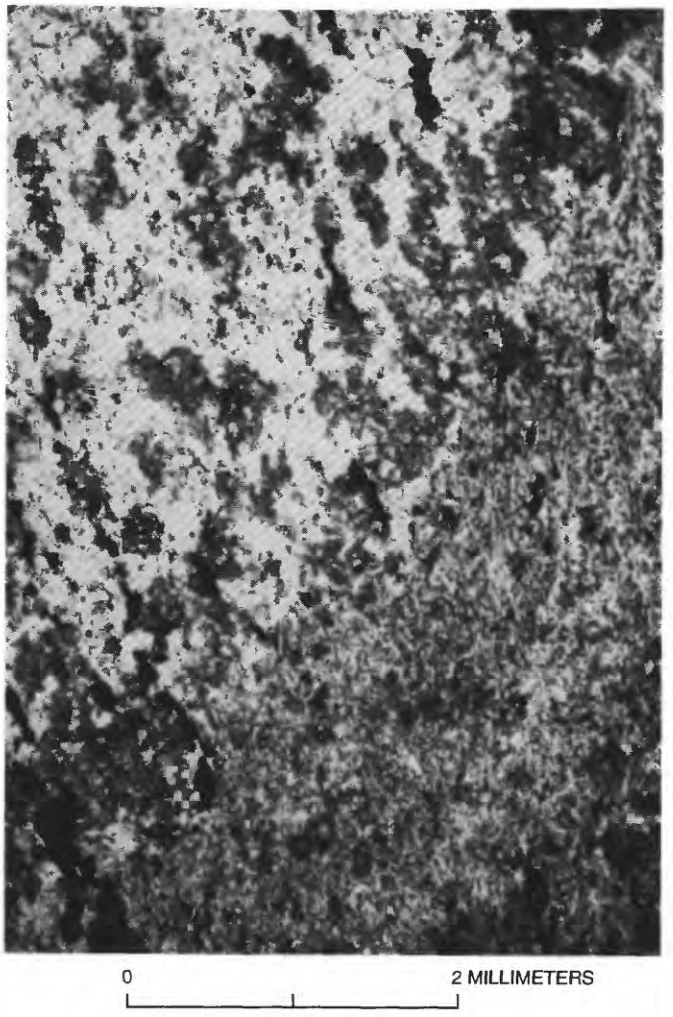

FIGURE 10.18.—Photomicrograph of sample R6: garnet-zone gneiss from Riggins Group, collected near sample R7. Contact between compositional layers extends from upper right to lower left corner of photo. Incipient transposition of compositional layering to an orientation extending from top to bottom is evident in hornblende and biotite crystals (dark minerals) and iron oxide minerals (opaque grains) along the contact. Plane light.

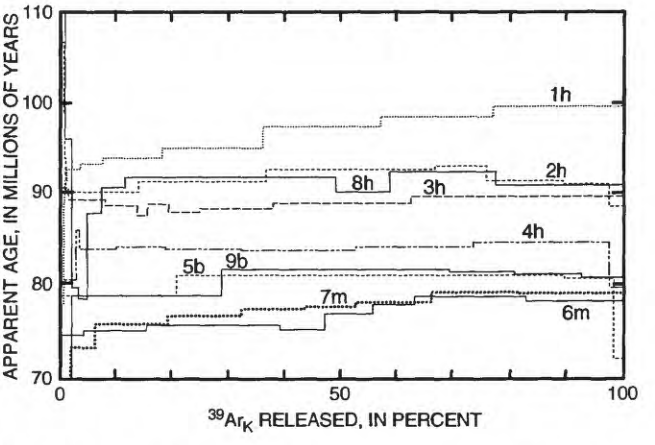

FIGURE 10.19.—Composite $^{40}Ar/^{39}Ar$ age-spectrum diagram for 93-Ma plutonic rocks from suture zone in Riggins area. 1h, Hornblende from sample R23; same spectrum as shown in figure 10.17. 2h, Hornblende from sample R24; disturbed spectrum; T_{mp} (preferred date)=92.6±0.5 Ma. 3h, Hornblende from sample R22; T_p (plateau date)=89.3±0.6 Ma (plateau date defined by 62 percent of $^{39}Ar_K$ released). 4h, Hornblende from sample R21; T_p=83.9±0.4 Ma (plateau date defined by 96 percent of $^{39}Ar_K$ released). 5b, Biotite from sample R21; T_p=81.1±0.4 Ma (plateau date defined by 69 percent of $^{39}Ar_K$ released). 6m, Microcline from sample R21; disturbed spectrum; T_{max} (maximum date)=78.6±0.4 Ma. 7m, Microcline from sample R24; argon loss from T_{max}=79.0±0.4 Ma to T_{min} (minimum date)=69.5±0.4 Ma. 8h, Hornblende from sample R12; argon loss from T_{max}= 93.4±0.5 Ma to T_{min}=88.3±0.5 Ma. 9b, Biotite from sample R12; T_p=82.6±0.4 Ma.

Ma. This 88-Ma fabric is most strongly developed in the suture-zone plutons, but this high-angle fabric also cuts off the 118- and 109-Ma metamorphic fabric near the suture zone.

Regionally, the younger, steeply plunging, lineation-dominated fabric is well-developed in a narrow belt of highly deformed rocks straddling the suture zone and in many places completely transposes any older fabrics. For example, sample R11, collected near the location of sample R12, is, like sample R12, from deformed plutonic rock on the Salmon River (fig. 10.6) and on structural trend with samples R24 and R22 from the Slate Creek area to the north. A plateau date of 85.1±0.4 Ma for deformed hornblende from this sample is evidence that deformation or cooling affected this area after 88 Ma. Furthermore, hornblende plateau dates from similarly deformed tonalites on structural trend about 50 km south of the location of sample R11 range from 81 to 79 Ma (L.W. Snee, unpub. data, 1990); for similarly deformed rocks in the McCall area, hornblende plateau dates range from 79 to 88 Ma (L.W. Snee and M.A. Kuntz, U.S. Geological Survey, unpub. data, 1990). For samples of similarly deformed plutonic rocks on structural trend in the suture zone to the north near Orofino (fig. 10.1), plateau dates for hornblendes range from 83 to 81 Ma (Snee and others, 1987a; Davidson and Snee, 1989; Davidson, 1990); U-Pb zircon dates indicate that some of these plutons were emplaced at 115 Ma (Snee and others, in press). Furthermore, long periods of cooling after deformation along parts of the suture zone, such as at Orofino, are supported by the coexistence of 74-Ma biotite with 83- to 81-Ma hornblende (Snee and others, 1987a; Davidson and Snee, 1989; Davidson, 1990; Snee and others, in press) and 115-Ma zircon. In summary, cooling ages for hornblendes from this fabric throughout the region range from 88 to 79 Ma and indicate the regional extent of the vertical movement that affected a narrow belt of rocks near the suture zone. The complex and large-magnitude character of deformation in this narrow belt is confirmed by the juxtaposition of epidote-free (that is, shallow) and epidote-bearing (that is, deep-seated) plutons as well as plutons of different ages within this belt.

UNDEFORMED PLUTONS OF THE IDAHO BATHOLITH

$^{40}Ar/^{39}Ar$ age-spectrum data for undeformed plutons east of the suture zone are summarized in table 10.2 under the heading "Undeformed Plutons and Associated Rocks." Sample R21, tonalite that contains magmatic epidote (fig. 10.6), is from the oldest undeformed phase of the Idaho batholith. Hornblende geobarometry (Hammarstrom and Zen, 1988), as well as the presence of magmatic epidote, indicates that this tonalite was emplaced at a depth of about 20 km. The $^{40}Ar/^{39}Ar$ age spectra for hornblende, biotite, and microcline define the cooling history of this sample from about 530°C at 84 Ma, to 280°C at 81 Ma, to 130°C at 78 Ma (fig. 10.19). The hornblende plateau date of 83.9±0.4 Ma is a minimum estimate for the age of emplacement. U-Th-Pb isotopic analyses of five zircon fractions and one sphene fraction from sample R21 yield a lower-intercept date of 90±3 Ma (mean square of weighted deviates=7.4; fig. 10.20; table 10.4). The lower-intercept date is interpreted to be the best estimate for age of emplacement of the tonalite pluton. Using U-Pb zircon data, C.A. Manduca (California Institute of Technology, unpub. data, 1992) has determined an identical emplacement age for similar undeformed tonalite in the McCall area, east of the Salmon River suture zone.

On the east side of the Idaho batholith, metaluminous granodiorite and tonalite were emplaced earlier than the extensive muscovite-biotite granites that are typical of the central part of the batholith (Hall, 1985; Kiilsgaard and Lewis, 1985; Lewis and others, 1987; fig. 10.21). Sample MP201 of hornblende-biotite porphyritic granodiorite from 15 km east of Stanley, Idaho, on the Salmon River yielded a hornblende plateau date of 86.3±0.5 Ma (fig. 10.22; table 10.3). (An unpublished U-Pb zircon date from the same outcrop of 88±6 Ma by Lynn Fischer, U.S. Geological Survey,

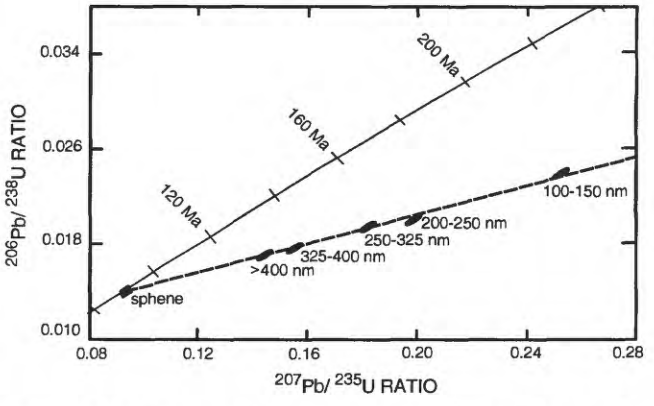

FIGURE 10.20.—Concordia diagram for sample R21, from undeformed pluton east of Salmon River suture zone. Solid line (concordia) is time curve that is the locus of all concordant U-Pb dates. Dashed line (discordia) is defined by U-Pb dates on minerals from sample R21. Five discordant dates are from five size fractions of zircon; one concordant date is from sphene. Error envelopes for each date are defined by symbols. Discordia intercepts concordia at 90.4±3 Ma (see diagram) and at 1,932±150 Ma (not shown). Best estimate of crystallization age is lower intercept date, 90.4±3 Ma. Mean square of weighted deviates (MSWD)=7.4.

TABLE 10.4.—*U, Th, and Pb analytical data and dates for sample R21*

[Size-fraction ranges listed for zircon; sphene separate was not sized]

Size fraction (nm)	Concentration (ppm)			Measured ratio	Isotopic composition of lead (atom percent)				Dates (Ma)			
	U	Th	Pb	$\frac{^{206}Pb}{^{204}Pb}$	^{204}Pb	^{206}Pb	^{207}Pb	^{208}Pb	$\frac{^{206}Pb}{^{238}U}$	$\frac{^{207}Pb}{^{235}U}$	$\frac{^{207}Pb}{^{206}Pb}$	$\frac{^{208}Pb}{^{232}Th}$
100–150	413	145	10.4	2,146	0.0312	82.17	6.740	11.06	152	228	1,111	160
200–250	412	154	8.7	1,932	.0275	82.79	6.295	10.89	130	185	965	126
250–325	408	165	8.3	4,462	.0110	83.32	5.793	10.87	125	170	857	118
325–400	402	179	7.6	1,786	.0359	81.79	5.716	12.46	114	147	726	107
>400	416	195	10.7	155	.4164	65.32	10.020	24.24	110	138	641	102
Sphene	120	166	3.8	79.5	.5688	49.29	10.744	39.40	91	91	99	91

1985, and cited in Lewis and others, 1987, is statistically identical to the hornblende date.) Approximately 25 km farther east, the Thompson Creek porphyry molybdenum deposit formed during emplacement of a stock composed of biotite granodiorite and biotite granite of Cretaceous age (Hall and others, 1984). Two muscovite samples (TC-S-41-16 and TC-S-124-23) from a drill core of alteration assemblages associated with the molybdenite have plateau dates of 87.4±0.4 and 87.6±0.4 Ma, respectively (fig. 10.22; table 10.3). These muscovite dates indicate that the minimum age of the associated plutons is about 87.5 Ma. Numerous additional hornblende $^{40}Ar/^{39}Ar$ cooling ages for metaluminous plutons in the southern part of the Idaho batholith range from 93 to 88 Ma (L.W. Snee, unpub. data, 1991). Thus, on the basis of all the ages for metaluminous plutons of the Idaho batholith, an area extending from the Salmon River suture zone up to 139 km to the east was affected by this period of metaluminous magmatism.

Sample R8 is a representative sample of the voluminous muscovite-biotite granites of the Idaho batholith from a few miles east of the suture zone (fig. 10.6). Muscovite and biotite plateau dates of 75.3±0.4 and 74.7±0.4 Ma, respectively (tables 10.2, 10.3), are statistically indistinguishable and mark the time when this pluton cooled through 325°C and 280°C, the argon-closure temperatures of muscovite and biotite, respectively. Whether approximately 75 Ma is the age of emplacement of the muscovite-biotite granite depends upon how rapidly the granite cooled from its emplacement temperature of about 650–750°C to below 300°C. This cooling rate is controlled in part by the temperature of the country rocks at the time of emplacement of the granite and the depth of emplacement. The argon age spectrum of the microcline from sample R21, a sample from one of the metaluminous plutons discussed above, indicates that the country rocks, including the metaluminous plutons, of the muscovite-biotite granite had cooled below about 130°C by 78 Ma. Using this temperature as a maximum for the country rocks of the muscovite-biotite granite at the time of its emplacement and assuming a minimum geothermal gradient of 25°C/km at the time of emplacement (see below), the maximum depth of emplacement of muscovite-biotite granite near the suture zone was about 5 km (that is, 130°C, microcline argon-closure temperature, divided by 25°C/km). Both the low temperature of the country rocks and the relatively shallow depth support the contention that the muscovite-biotite granite cooled rapidly upon emplacement. The contention that the granites were emplaced about 75 Ma also is supported by the date of 76.7±0.4 Ma from muscovite sample R10 (fig. 10.6; tables 10.2, 10.3), from a pegmatite dike that intruded undeformed tonalite and may be part of the same granitic intrusive episode.

Additional $^{40}Ar/^{39}Ar$ muscovite dates from muscovite-biotite granite throughout the southern part of the Idaho batholith range from 70.1±0.3 to 76.7±0.4 Ma (table 10.3). Muscovite sample 1KE052 from muscovite-biotite granite of the Buffalo Hump area (fig. 10.23) yields the best constrained of these cooling ages. Lund and others (1986) dated six mineral separates from this area (fig. 10.24): two hornblendes and one biotite from two amphibolites within a metasedimentary roof pendant (samples 2KE080 and 2KE086), muscovite and microcline from muscovite-biotite granite (sample 1KE052), and muscovite from a younger gold-bearing quartz vein (sample 2KE087). These data indicate that the amphibolite and surrounding metasedimentary rocks cooled below 280°C by 78 Ma, that the granite intruded the metasedimentary roof at about 74 Ma, and that all rocks cooled below about 100°C by 55 Ma. (Lund and others, 1986, used a multidomainal diffusion model for interpretation of the microcline data in this study. This model recognizes the probable existence in any

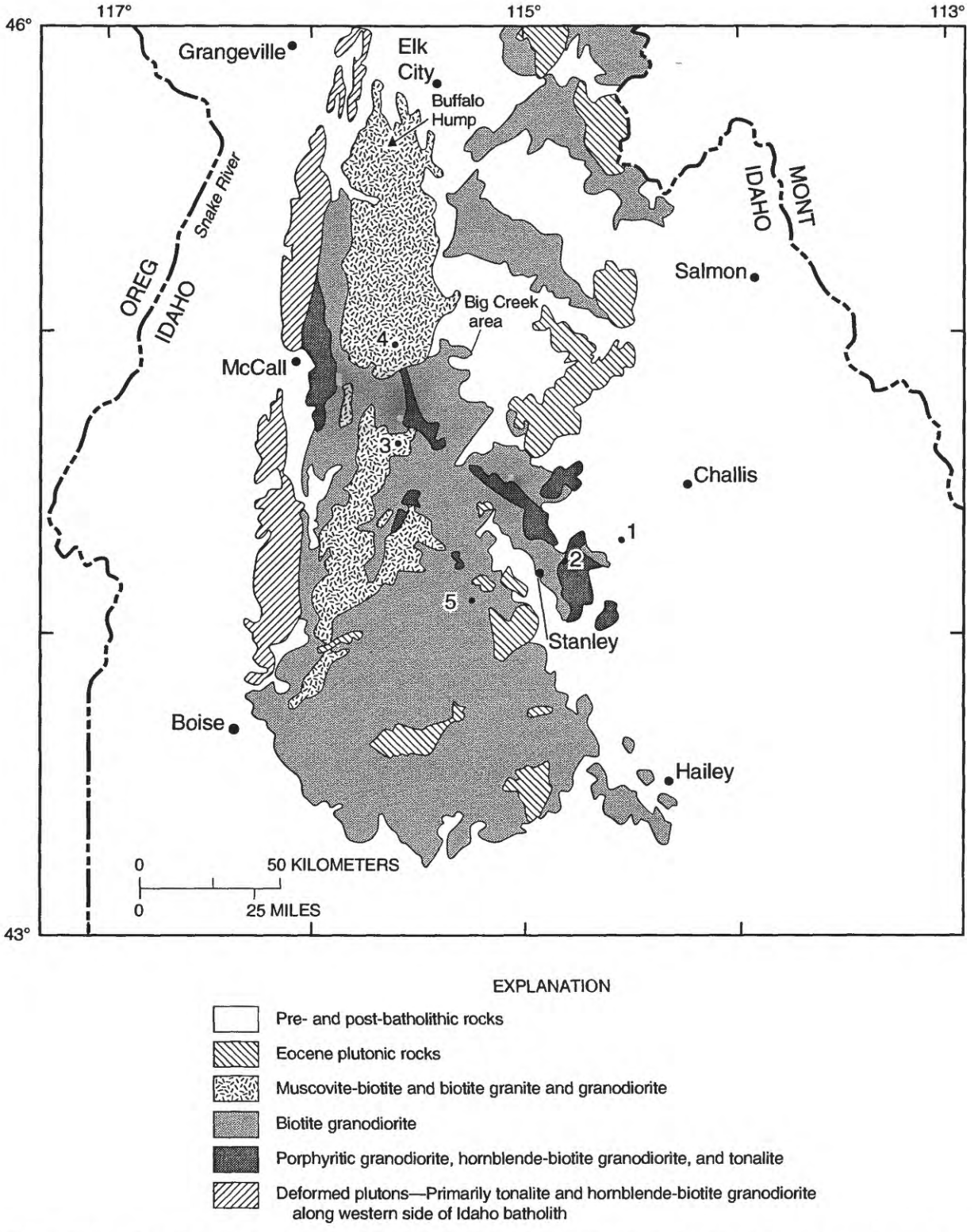

FIGURE 10.21.—Sample locality map for central part of Idaho batholith. Geologic base modified from Kiilsgaard and Lewis (1985), Lund and others (1989), and Worl and others (1991). 1, Molybdenite porphyry (samples TC-S-41-16 and TC-S-124-23); 2, Hornblende-biotite granodiorite (sample MP201); 3, Muscovite-biotite granite (sample D3113M); 4, Muscovite-biotite granite (sample B12178201); 5, Leucogranite (sample B12198202).

potassium feldspar of at least two argon diffusion domains with different closure temperatures, in this case, 150° and 100°C.) Interpolating the cooling history of these rocks from the biotite cooling age through the microcline cooling age and using a geothermal gradient of 25°C/km, the maximum depth of emplacement of the granite was less than 9 km (fig. 10.27), which is in agreement with the conclusion above about depth of emplacement of muscovite-biotite granite near the suture zone. In addition, gold-bearing quartz veins were formed at 71 Ma within fractures that had cut the already cool (less than 280°C) granite and roof pendants.

The low-temperature cooling history preserved in the microcline sample from Buffalo Hump is nearly identical to that of a microcline sample (B12198202; fig. 10.21; table 10.3) from leucogranite near the Warm Springs Forest Service Station on the South Fork of the Payette River, which is almost 160 km south of Buffalo Hump (fig. 10.1). Although more than two samples are necessary to draw detailed conclusions about the cooling history of the central part of the Idaho batholith, these nearly identical age spectra indicate that a large part of the central Idaho batholith had cooled below 130°C by 67–55 Ma and was not affected by any later thermal activity.

Sample B12198202 (fig. 10.21) is also important because the biotite separate yielded a highly discordant, "hump-shaped" pattern (table 10.3) that is typical for slightly altered biotite (Kunk, 1982; Hess and Lippolt, 1986). No single temperature step from this sample yielded a geologically meaningful age, and the total-gas date, which is a weight-averaged date including all data and is comparable to a conventional K-Ar date, also has no geologic meaning. Because the total-gas date is within the realm of reasonable geologic ages, it exemplifies the danger of dating biotites from complex areas by the conventional K-Ar method. As pointed out by Lewis and others (1987), most cited

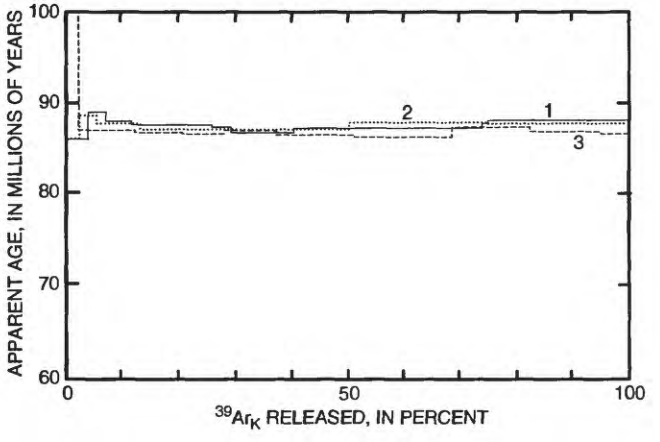

FIGURE 10.22.—Composite age-spectrum diagram for Thompson Creek porphyry molybdenum deposit and for hornblende-biotite granodiorite near Stanley, Idaho. Numbers refer to specific samples: 1, Muscovite sample TC-S-124-23 from Thompson Creek porphyry molybdenum deposit; T_p (plateau date)=87.6±0.4 Ma (plateau date defined by 88 percent of $^{39}Ar_K$ released). 2, muscovite sample TC-S-41-16 from Thompson Creek porphyry molybdenum deposit; T_p=87.4±0.4 Ma (plateau date defined by 94 percent of $^{39}Ar_K$ released). 3, Hornblende sample MP201 from hornblende-biotite granodiorite near Stanley, Idaho; T_p=86.3±0.4 Ma (plateau date defined by 98 percent of $^{39}Ar_K$ released).

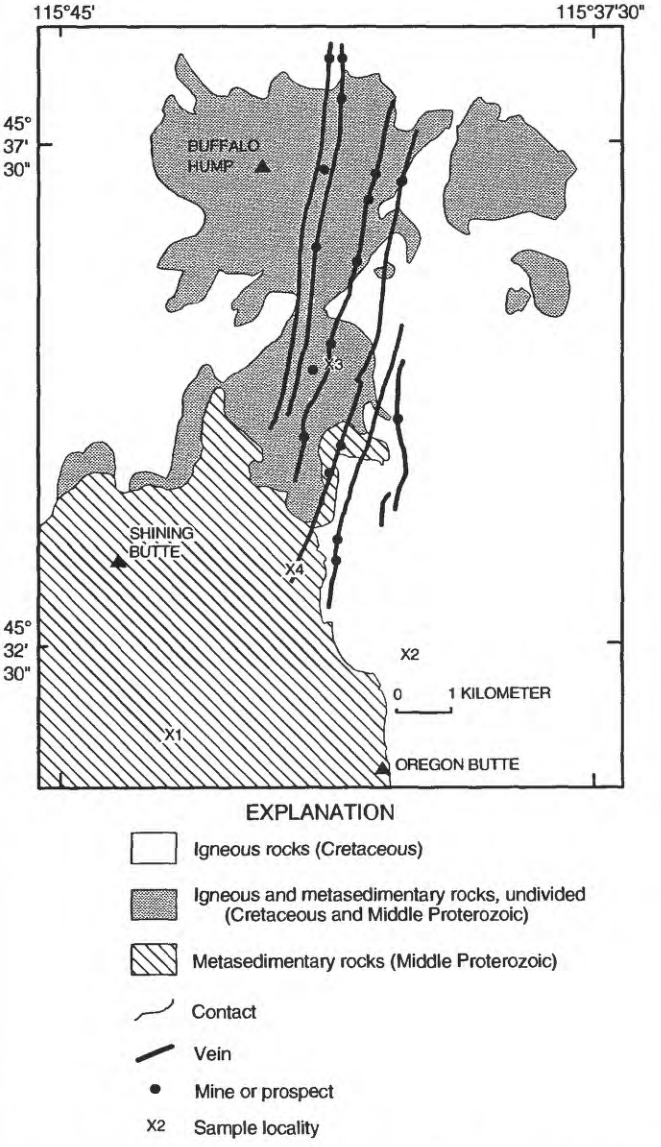

FIGURE 10.23.—Geology and sample locality map of Buffalo Hump area modified from Lund and others (1986). 1, Amphibolite (sample 2KE080); 2, Muscovite-biotite granite (sample 1KE052); 3, Quartz vein from Mother Lode mine (sample 2KE087); 4, Amphibolite (sample 2KE086).

geochronologic data for the Idaho batholith are conventional K-Ar dates on biotite (or even less reliable Pb-alpha numerical ages on zircon). Scatter in the conventional K-Ar dates has led to much confusion about the actual age of the Idaho batholith and even has been used to construct elaborate uplift histories that have no basis in geologic reality (see, for example, Criss and others, 1982). However, Snee (1982), Lund and others (1986), Criss and Fleck (1987), and Meen and others (1988), among others, have demonstrated that $^{40}Ar/^{39}Ar$ age-spectrum analyses of hornblende, biotite, muscovite, and potassium feldspar yield useful data that are providing an understanding of the age and extent of Cretaceous magmatism in the northwestern United States.

Other muscovite dates for granite, which are as young as 72.4±0.4 and 70.1±0.3 Ma (samples D3113M from near Warm Lake and B12178201 from north of Warm Lake and east of McCall, respectively; table 10.3), were obtained from samples collected near the center of a large area of muscovite-biotite granite (fig. 10.21); muscovite dates from the center of the granite area tend to be younger than muscovite dates from the outer parts of the granite, as described above. This trend may be a result of multiple intrusive pulses, differential cooling, or exposure of different emplacement levels.

In addition to dates obtained directly from samples of the muscovite-biotite granites, muscovites from mineral deposits throughout the central part of the batholith and near roof zones of the muscovite-biotite granites yield dates ranging from about 78 to 68 Ma (Snee and others, 1985; Gammons and others, 1985; Gammons, 1986; Lund and others, 1986; Snee, 1987; and Snee and Kunk, 1989). These muscovites are generally from quartz veins that were emplaced in fractures and fault zones near or within roof pendants in the biotite and muscovite-biotite granite. This range in dates is consistent with the data for the granites and supports the conclusions that the deposits are genetically related to the granites and that granite emplacement and quartz vein formation spanned this time period.

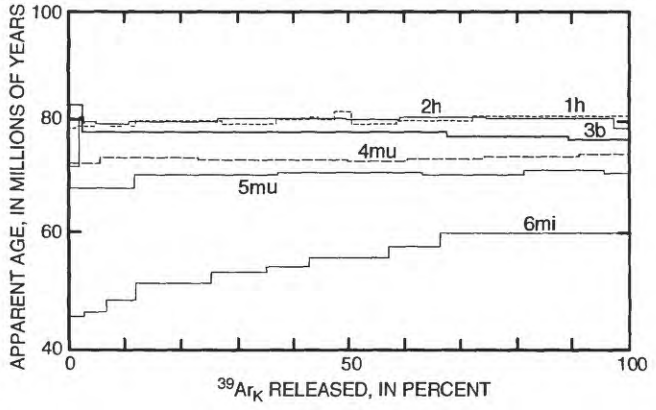

FIGURE 10.24.—Composite age-spectrum diagram for Buffalo Hump district and Mother Lode mine. 1h, Hornblende sample 2KE086 from amphibolite; T_p (plateau date)=80.5±0.6 Ma (plateau date defined by 90 percent of $^{39}Ar_K$ released). 2h, Hornblende sample 2KE080 from amphibolite; T_p=81.2±0.4 Ma (plateau date defined by 61 percent of $^{39}Ar_K$ released). 3b, Biotite sample 2KE080 from amphibolite; T_p=78.2±0.4 Ma (plateau date defined by 88 percent of $^{39}Ar_K$ released). 4mu, Muscovite sample 1KE052 from muscovite-biotite granite; T_p=73.8±0.4 Ma (plateau date defined by 95 percent of $^{39}Ar_K$ released). 5mu, Muscovite sample 2KE087 from quartz vein at Mother Lode mine; T_p=71.0±0.4 Ma (plateau date defined by 89 percent of $^{39}Ar_K$ released). 6mi, Microcline sample 1KE052 from muscovite-biotite granite; apparent argon loss from T_{max} (maximum date)=67.0±0.3 Ma to T_{min} (minimum date)=54.5±0.4 Ma.

DISCUSSION

The $^{40}Ar/^{39}Ar$ age-spectrum data of this study provide time constraints on several metamorphic and plutonic events in western Idaho and eastern Oregon. These data can be used to reconstruct the geologic development of a large area straddling the Salmon River suture zone between accreted island-arc terranes and the pre-Cretaceous North American continent. The available argon data include (1) the age of one of the latest pre-accretion metamorphic events and two periods of subsequent pre-accretion plutonism within the accreted island-arc terranes; (2) the age of metamorphism that occurred during accretion (Lund and Snee, 1988) of previously amalgamated allochthonous island-arc terranes (Vallier and Engebretson, 1983; Hillhouse and others, 1982) to the North American continent along the Salmon River suture zone; (3) the time of final stitching of the island-arc terranes to the North American continent marked by emplacement of plutons along the Salmon River suture zone; (4) the age of postaccretion deformation caused by vertical movement along the suture zone; (5) the age of emplacement of metaluminous plutons of the Idaho batholith and the age of apparently associated porphyry deposits; and (6) the age of emplacement of the large bodies of muscovite-biotite granite of the Idaho batholith and associated mineral deposits. In addition to direct ages for these events, the $^{40}Ar/^{39}Ar$ age-spectrum mineral dates used within a time-temperature framework provide information about depth of emplacement of plutons, cooling, and uplift.

METAMORPHISM AND PLUTONISM IN EASTERN OREGON AND WESTERN IDAHO

Our $^{40}Ar/^{39}Ar$ age-spectrum data record several periods of metamorphism and plutonism that affected island-arc rocks in west-central Idaho and eastern Oregon. The oldest metamorphism documented by this study took place at or before 244 Ma and affected basement rocks now exposed in Snake River canyon. This age of metamorphism is consistent with ages reported by numerous studies (for example, Walker, 1981, 1983, 1986; Avé Lallemant and others, 1980, 1985) for plutonism and shearing within the allochthonous island-arc terranes and, on the basis of current data, is likely the youngest dynamothermal metamorphic event that took place during proposed amalgamation of separate island-arc terranes and associated shearing (Avé Lallemant and others, 1980; Lund and Snee, 1988) before the terranes were accreted to the North American continent.

At about 227 Ma, tonalite and quartz diorite plutons and dikes intruded the 244-Ma metamorphic rocks after the metamorphic rocks had cooled below 280°C, the argon-closure temperature of biotite. T.L. Vallier (oral commun., 1988) regards these igneous rocks as part of magmatic roots of volcanoes that were active during the deposition of the contemporaneous volcanic rocks of the Wild Sheep Creek Formation. In turn, this age is very important for understanding the timing of pre-accretionary structural events within the island-arc terrane because, on the basis of the mapping of Vallier (1974) and White and Vallier (1994), the Triassic Wild Sheep Creek Formation of the Seven Devils Group was deposited on basement rocks metamorphosed during the 244-Ma event and subsequently intruded by these 227-Ma plutons. Thus, the cooling after metamorphism of the basement rocks and the deposition of the Wild Sheep Creek Formation, which is Middle Triassic (Ladinian; between 235 and 230 Ma), is bracketed between 244 and 227 Ma. Therefore, the age of the plutons is consistent with the interpretation that their emplacement is temporally close to the beginning of Seven Devils Group deposition. Other studies (Hotz and others, 1977; Avé Lallemant and others, 1980, 1985; Walker, 1981, 1983, 1986) have recorded additional events, including structural emplacement of blueschist, ductile shearing, and plutonism, within the island-arc terranes at about 227 Ma.

On the basis of zircon U-Pb dates, Walker (1981, 1983, 1986) has shown that several periods of plutonism occurred in the island-arc terranes between 266 and 145 Ma. His data were derived from samples of deformed and metamorphosed as well as unmetamorphosed plutons. The argon data for rocks of Snake River canyon clarify and provide some constraints with respect to tectonic interpretation of the zircon U-Pb data. Metamorphism at 244 Ma was a major event that affected preexisting plutons and volcanic rocks, and plutonism and volcanism seem to have resumed almost immediately after metamorphism. High-grade metamorphism, like that of the 244-Ma event, is not generally associated with the numerous plutonic episodes documented by the U-Pb data. Thus, the 244-Ma metamorphism represents a singular dynamothermal event that dates the construction and (or) amalgamation of the island-arc terrane. Subsequent to this major amalgamation event, plutonism, blueschist emplacement, and ductile shearing affected the amalgamated rocks at 227 Ma and mark the reorganization of the terranes and resumption of island-arc volcanism.

At about 145 Ma, plutons with island-arc chemical affinity and compositions ranging from tonalite to granite (Armstrong and others, 1977) were emplaced into the Seven Devils island-arc terrane in several areas in the Blue Mountains and along the Rapid River, west of Riggins. Plutons of the Wallowa batholith of northeastern Oregon were emplaced into the Seven Devils island arc at about the same time (Armstrong and others, 1977; L.W. Snee and W.H. Taubeneck, unpub. data, 1987) and were possibly part of the same magmatic event. The 145-Ma tonalite pluton along the Rapid River, southwest of Riggins, which we dated, was later metamorphosed to greenschist facies by the events that affected rocks along the Salmon River suture zone to the east. Because some of these plutons were affected by metamorphism associated with Salmon River suture zone activity, their 145-Ma age provides the maximum age for accretion of the island-arc terranes to the North American continent.

Low- to high-grade metamorphism affected a belt of rocks along the Salmon River suture zone beginning about 130 Ma. At least four groups of metamorphic and deformational ages (130, 118, 109, and 101 Ma; fig. 10.25) are documented in the Riggins Group and Seven Devils island-arc rocks near the suture zone. A summary of the thermal history is displayed on a time-temperature diagram (fig. 10.26). The oldest metamorphic event associated with accretion along the Salmon River suture zone is documented in rocks of the Orofino area and occurred at 130 Ma. The oldest documented event in the Riggins-Slate Creek area occurred at about 118 Ma. Both the 130- and 118-Ma events were dynamothermal and were marked by a rapid rise to maximum metamorphic conditions followed by rapid cooling. The next two

events also may have been dynamothermal, or their ages may reflect nonthermal deformation that exposed two deeper, hotter crustal levels to cooling at 109 and 101 Ma, respectively. Subsequent cooling after each event is constrained by only a few samples, as shown on figure 10.26, but the data suggest that the island-arc rocks cooled below about 300°C after the third and fourth metamorphic pulses. Al-

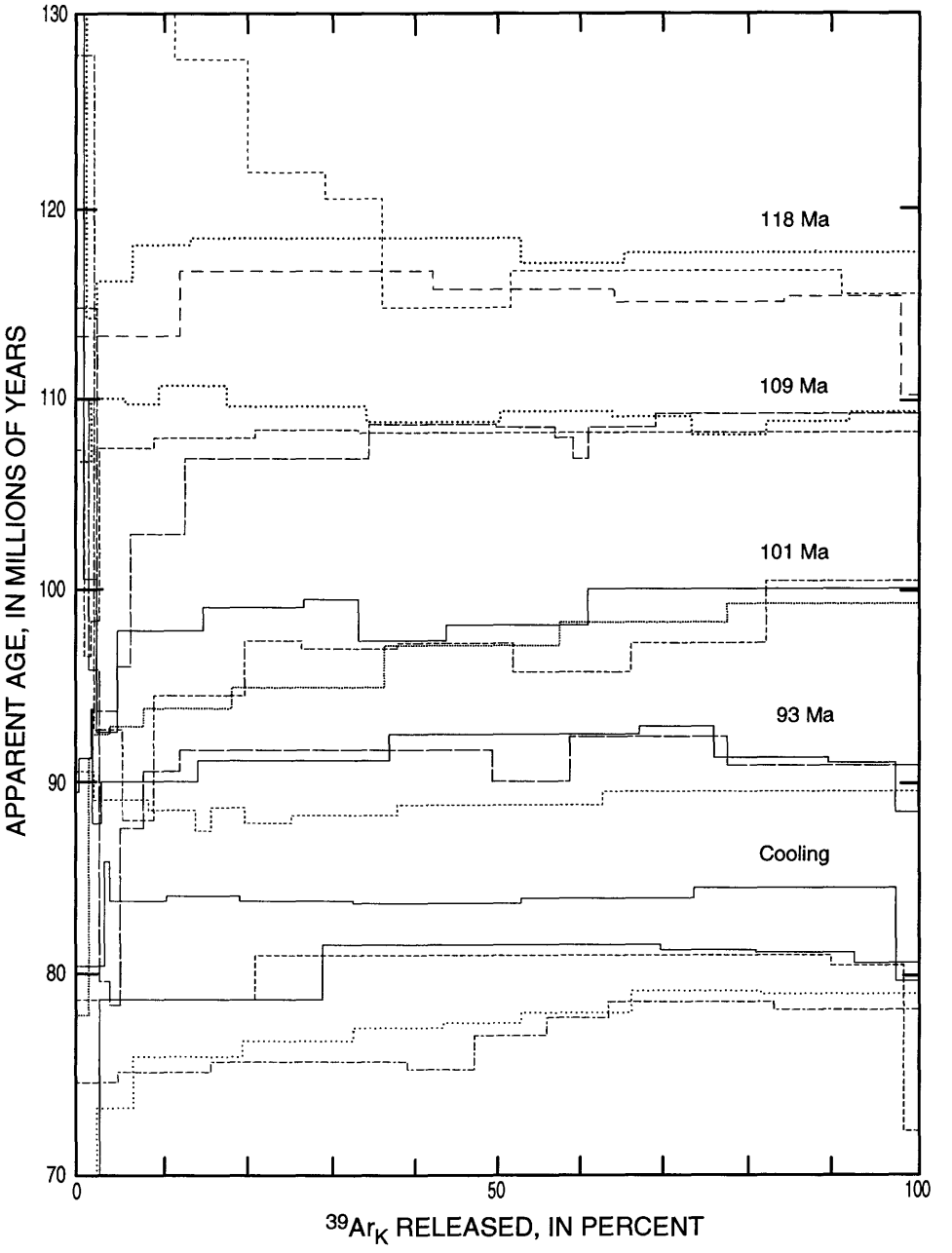

FIGURE 10.25.—Composite age-spectrum diagram including all spectra from metamorphic and plutonic rocks of Salmon River suture zone shown on figures 10.7, 10.10, 10.17, and 10.19. Grouping of hornblende age spectra clearly shows four thermal events at about 118, 109, 101, and 93 Ma, as well as post-93-Ma cooling of undeformed plutonic rocks east of, but near to, the suture zone. These groups would be preserved even if hornblende age spectra of excluded samples of Riggins Group were added to the diagram. Data for 88-Ma and younger hornblendes that define late uplift of continental block along high-angle fault parallel to suture zone are omitted for clarity.

though some tonalitic magma with island-arc affinity was emplaced into the metamorphic rocks during the 118- to 101-Ma interval, plutonism did not cause the dynamothermal metamorphism exhibited within the Salmon River suture zone. Instead, plutonism trailed metamorphism by a few million years and was more likely an effect of the tectonic activity that caused the metamorphism.

At about 93 to 90 Ma, the Salmon River suture zone was the site of a fifth period of metamorphism and deformation that was accompanied by emplacement of plutons with compositions ranging from tonalite to granodiorite (figs. 10.25, 10.26); these plutons reheated adjacent island-arc metamorphic rocks, which had cooled below 280°C before the 93- to 90-Ma event. Emplacement of the tonalitic plutons stitched the island-arc terranes and the North American continent together, and the island-arc terranes became part of the stable North American continent. Beginning at or before 88 Ma and extending to at least 79 Ma, deformation resulting from vertical movement affected the Salmon River suture zone.

The emplacement of these 93-Ma tonalitic plutons marked the initiation of magmatism that formed the Idaho batholith. These plutons were emplaced into island-arc and North American continental rocks that had been juxtaposed along the Salmon River suture zone. The preservation of the initial $^{87}Sr/^{86}Sr$ ratio discontinuity in these plutons is conclusive evidence that both the island-arc and continental terranes influenced the composition of the magmas. Undeformed metaluminous plutons in the vicinity of the suture zone were emplaced at the same time as some of the deformed tonalitic plutons within the suture zone. Until about 86 Ma, metaluminous magmatism affected an area extending up to 139 km east of the suture zone, where plutons of the Idaho batholith with similar compositions were emplaced. The 87.5-Ma porphyry

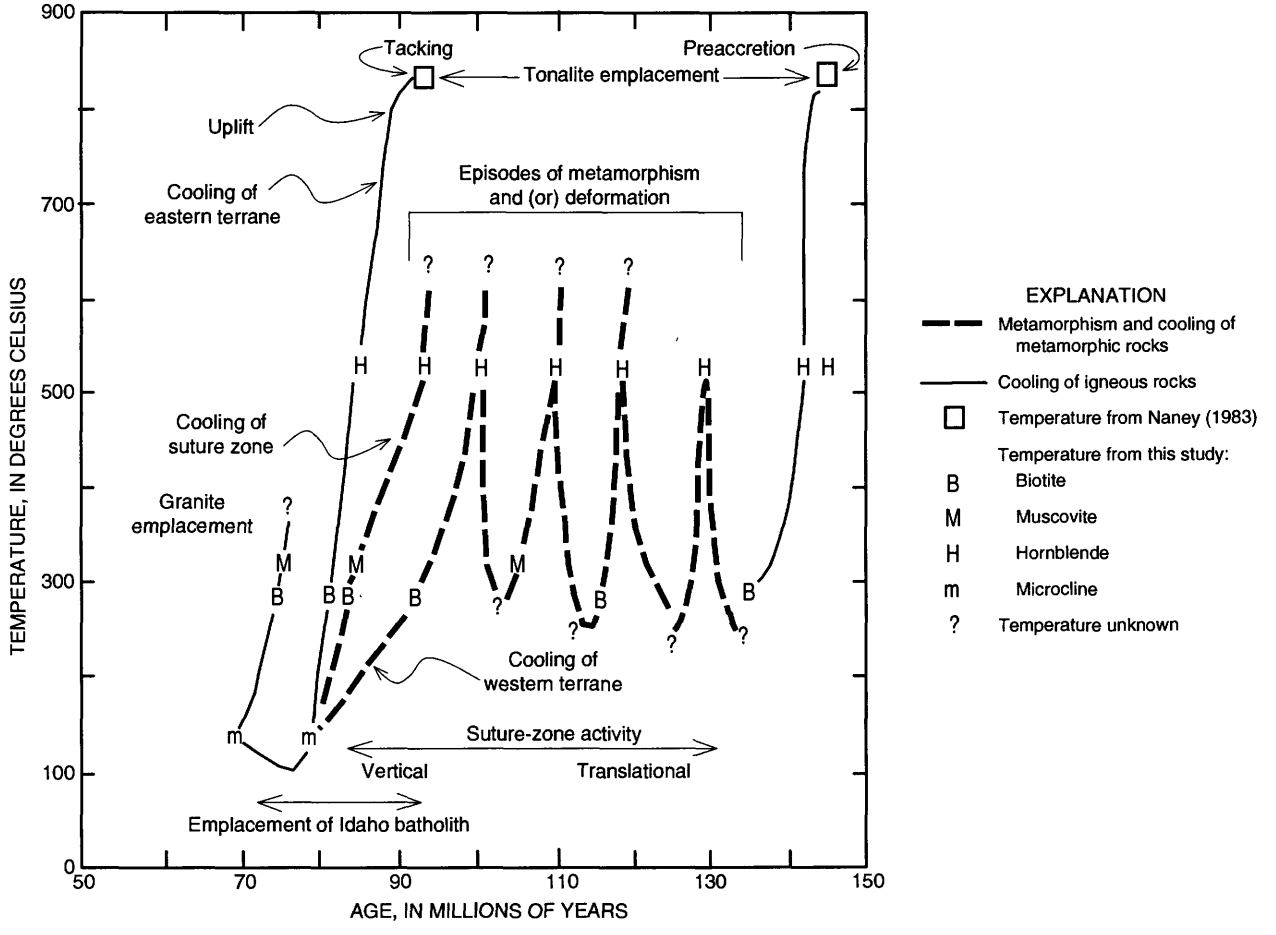

FIGURE 10.26.—Thermal history of Salmon River suture zone, Idaho, based on time and temperature relations derived from $^{40}Ar/^{39}Ar$ age-spectrum data (from Lund and Snee, 1988). Cooling of 115-Ma suture-zone plutons omitted for clarity. The metamorphic episode at 130 Ma is recorded in rocks near Orofino, Idaho, but not in rocks of the Riggins, Idaho, area.

molybdenum deposit at Thompson Creek is a vestige of the mineralization that accompanied this period of igneous activity.

Beginning about 78 Ma, after an apparent 10-m.y. lull in plutonic activity, the voluminous muscovite-biotite granites, which are characteristic of the central part of the Idaho batholith, were emplaced. Muscovite dates indicate that emplacement of the granites and that cooling of the rocks to below 300°C were completed by 70 Ma. Many gold-bearing quartz veins that are within fractures and fault zones primarily in roof pendants of the muscovite-biotite granites were emplaced from 78 to 68 Ma during several stages of mineralization.

An important result of our study is the discovery that the Idaho batholith is younger than the metamorphism of the rocks within the Salmon River suture zone. Thus, even though the batholith is adjacent to and in some places cross-cuts the suture, its emplacement did not cause the metamorphism. Instead, it is reasonable to conclude that metamorphism and possibly plutonism along the suture zone were in response to events that occurred during accretion of the island-arc terrane to North America.

COOLING AND UPLIFT HISTORY OF THE AREA EAST OF THE SALMON RIVER SUTURE ZONE

The last structural event in the region before the onset of extension and basaltic magmatism in the Miocene is manifested by sets of north-northeast-trending, high-angle normal faults that are parallel to the Salmon River suture zone and along which uplift occurred. In some places (see fig. 10.6) the high-angle faults coincide with the initial $^{87}Sr/^{86}Sr$ ratio discontinuity that marks the Salmon River suture zone and apparently truncate the suture zone. The uplift event began during or immediately before emplacement of the unfoliated tonalitic plutons of the Cretaceous Idaho batholith (Lund and others, 1986) and continued at least until after emplacement of Eocene epizonal granitic magmas in the same region (Lund and others, 1983b).

The rate of this uplift for the suture zone area can be calculated from cooling rates derived directly from the argon data plotted on figure 10.26. The cooling rate for the undeformed tonalite during the interval from 84 to 81 Ma is 95°C/m.y., and the cooling rate from 81 to 78 Ma is about 45°C/m.y. This rapid cooling rate is consistent either with high-level emplacement or with rapid uplift following an unknown period of slow cooling after deep emplacement. The presence of magmatic epidote suggests emplacement at a depth of greater than 25 km (Zen and Hammarstrom, 1984) if the epidote crystallized at the level of pluton emplacement (Evans and Vance, 1985). Additional study of the Rocky Bluff pluton by Hammarstrom and Zen (1988) indicates a depth of emplacement of about 20 km based on hornblende geobarometry. Assuming that the tonalite was emplaced at a depth of 20 km or deeper and assuming a closure temperature of 530°C for diffusion of argon from hornblende, a geothermal gradient of about 27°C/km is derived. This value is similar to, but slightly larger than, that resulting from a synthesis of studies by Carmichael (1978), Hyndman and others (1979), Hollister (1982), and Zen (1985). Using a geothermal gradient of 25°C/km, the average uplift rate from 84 to 81 Ma was 3 mm/yr; the average rate from 81 to 78 Ma was about 2 mm/yr. If a higher geothermal gradient or greater depth of emplacement of the tonalite were assumed, the uplift would have been faster. These rates are less than, but on the same order as, the rapid recent uplift of 5 mm/yr for the Nanga Parbat massif in the Himalaya (Zeitler, 1985) and the 2.5 to 14 mm/yr uplift along the Alpine fault in New Zealand (Adams, 1981).

In the Buffalo Hump area, located about 50 km east of the suture zone (fig. 10.1), cooling rates can be determined from figure 10.27 (Lund and others,

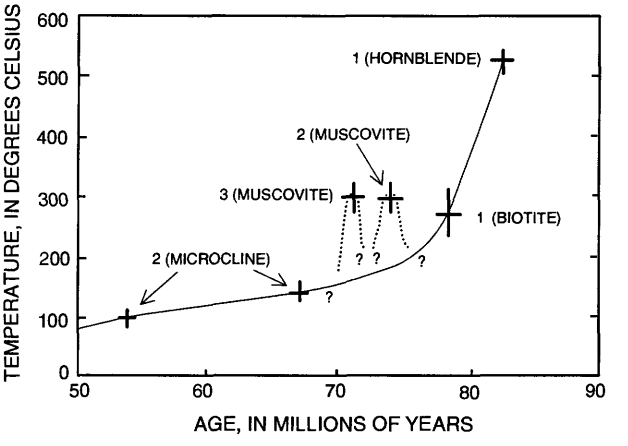

FIGURE 10.27.—Cooling curve for Buffalo Hump area from Lund and others (1986). Numbers indicate the following rock types: 1, amphibolite; 2, muscovite-biotite granite; 3, quartz vein. Name of dated mineral is shown in parentheses. Two-domain diffusion model was used for microcline date, with closure temperature of most retentive domain equal to 130°C and closure temperature for least retentive domain equal to 100°C. Vertical bar in each cross shows approximate error estimate in selected closure temperatures; horizontal bar shows one-sigma analytical error of each date. Dotted lines indicate hypothesized local temperature increases during emplacement of muscovite-biotite granite and quartz veins. Queries indicate that relation between local temperature increases and regional cooling curve is unknown.

1986). The cooling rate for the metasedimentary roof pendant at Buffalo Hump from about 81 to 78 Ma, before emplacement of muscovite-biotite granite, was about 85°C/m.y. This rapid cooling was taking place during the same time that the cooling to the west along the suture zone had slowed to about 45°C/m.y. In the Buffalo Hump area, cooling from 78 Ma to the time of emplacement of muscovite-biotite granite at 74 Ma cannot be directly calculated, but it must have been slower than 85°C/m.y. and probably closer to 45°C/m.y. on the basis of interpolation between biotite and microcline cooling ages. Assuming a geothermal gradient of 25°C/km, the rate of uplift of rocks in the Buffalo Hump area was probably similar to that near the suture zone, but the time of uplift of rocks of the Buffalo Hump area lagged behind that of rocks of the suture zone by about 3 m.y. The nearly identical age spectra for microcline from muscovite-biotite granite at Buffalo Hump and microcline from leucogranite near the Warm Springs Forest Service Station provide constraints on cooling of the central part of the Idaho batholith: By 55 Ma, this part of the batholith had cooled below 130°C, the argon-closure temperature for microcline, and therefore must have been no deeper than 5 km. Fluid-inclusion data from quartz in gold-bearing quartz veins emplaced at 71 Ma in the Buffalo Hump area (Muniz and Brown, 1984) and between 74 and 71 Ma in the Big Creek area (fig. 10.21; Gammons and others, 1985; Gammons, 1986) suggest that the depth to the granite was less than 4 km.

DEPTH OF EMPLACEMENT OF MUSCOVITE-BIOTITE GRANITE

Much petrologic debate has focused recently on the depth of emplacement of plutons containing magmatic muscovite. The $^{40}Ar/^{39}Ar$ age-spectrum data of this study provide some independent control on the depth of emplacement of muscovite-biotite granites in the Idaho batholith. Muscovite-biotite granite near the Salmon River suture zone was emplaced after 76 Ma into country rock that had already cooled below 130°C (microcline argon-closure temperature; fig. 10.26). The emplacement of muscovite-biotite granite had little or no effect on the age-spectrum of a sample of microcline (sample R21, which cooled below about 130°C at 78 Ma) collected from nonfoliated tonalitic plutons only a few hundred yards from the granite contact. Assuming a reasonable minimum geothermal gradient of 25°C/km, the depth of emplacement of the granite must have been less than 6 km. Lund and others (1986) used the cooling history shown on figure 10.27 to derive a similar estimate (less than 9 km) for depth of emplacement of muscovite-biotite granite in the Buffalo Hump area. Thus, in general, the argon data support contentions of Miller and others (1981) and Anderson and Rowley (1981) that primary muscovite of non-endmember composition can form at relatively low pressure.

An apparent discrepancy exists when the 20-km minimum depth of emplacement for the epidote-bearing tonalite of the suture zone is compared to our less-than-9-km depth-of-emplacement estimate for muscovite-biotite granite of the Idaho batholith. However, the existing $^{40}Ar/^{39}Ar$ age-spectrum data reveal a gap of about 8 to 10 m.y. between the end of emplacement of metaluminous tonalites and granodiorites and the beginning of emplacement of biotite and muscovite-biotite granites. During this time gap, our cooling data indicate that more than 10 km of uplift affected the region of the Idaho batholith. We contend that the time gap and the large amount of uplift that occurred during this gap not only explain the difference in depth of emplacement but also are important clues that directly bear on the abrupt change during the Cretaceous in the Idaho batholith from metaluminous tonalitic magmatism to the voluminous muscovite-biotite (peraluminous) granitic magmatism.

This change in composition of magma and the intervening time gap were a direct result of progressive tectonic events along the Salmon River suture zone. These progressive events include accretion, tectonically driven crustal thickening, increasing crustal temperatures, buoyancy contrast between thickened continental crust and underlying mantle, uplift, depressurization melting, and granitic magmatism. During accretion, thrust plates moved both to the west and to the east away from the zone of convergence that is now the Salmon River suture zone. The degree of tectonic thickening to the east of the suture zone was 20 km or more on the basis of the hornblende geobarometry of Zen and Hammarstrom (1984) for tonalite along the eastern side of the suture zone. Roof pendants exposed in these plutons preserve some of the thrust plates that are evidence of this crustal thickening (see fig. 10.2). The greatly thickened crust east of the suture zone plus the emplacement of tonalitic magmas raised the geothermal gradient. This hot, thickened crust was of pelitic and psammitic composition and more buoyant than less thickened crust farther east within the craton, creating a buoyancy contrast in the underlying mantle. Uplift of the buoyant crust would have resulted. Our argon data indicate that this uplift began at about 88 Ma. With the onset of uplift, pressure in the lower part of the structurally thickened pelitic rocks would have quickly been

reduced and the trapped heat would have been sufficient to cause melting and the production of peraluminous magma. These magmas in turn were lighter than their surrounding source region and rose to less than 9 km before freezing. These peraluminous magmas derived abundant volatiles from their hydrated source rocks—volatiles that were effective in transport of metals that now form important mineral deposits associated with the muscovite-biotite granites. Our cooling age constraints indicate that about 10 m.y. elapsed between last emplacement of metaluminous magma and first emplacement of peraluminous magma. Peraluminous magma emplacement and associated mineral deposit formation took place over an additional 10-m.y. period.

EROSION AND CRETACEOUS SEDIMENTATION

The onset of orogeny along the Salmon River suture zone caused by accretion of island-arc terranes to the North American continent occurred approximately 130 Ma; this is the earliest time that significant amounts of coarse continental sediments would have been deposited as an onlapping sequence on the island-arc rocks. Furthermore, on the basis of the cooling histories derived from the argon data, rapid erosional unroofing in the area would have occurred when 15 km of rapid uplift and erosion of parts of the Idaho batholith began about 90 Ma; the rate of uplift slowed somewhat by 76 Ma, but uplift certainly continued, albeit more slowly, until the Eocene. By 55 Ma, much of the Idaho batholith was within a few kilometers of the present-day erosion level. The sedimentary record both to the east and to the west reflects these events.

In central Oregon, conglomeratic rocks of the Albian to Cenomanian (113 to 91 Ma) Gable Creek Formation of Wilkinson and Oles (1968) crop out in the Mitchell inlier. Partly correlative conglomeratic rocks of the Cenomanian Bernard Formation of Dickinson and others (1979) crop out in the John Day inlier. Detrital grains in sandstone layers include quartz, mica, and potassium feldspar. Conglomeratic layers include granitic and metaquartzite clasts as well as more common greenstone, volcanic, and phyllitic clasts. The clasts in these sedimentary rocks reflect a mixed provenance of metamorphic, plutonic, and volcanic rocks that is thought to have been a "mature and dissected arc terrane" (Dickinson and others, 1979).

To the east, a major angular unconformity in southwestern Montana is located at the base of the Cretaceous Kootenai Formation and exhibits a discordance of up to 40° (for example, Myers, 1952; Snee, 1982; Zen, 1988). The erosion surface defining this unconformity is developed on rocks as young as the Jurassic Morrison Formation; however, Jurassic rocks are generally thin (a few tens of meters; Perry, 1986) or absent, and commonly the youngest rocks below the unconformity are Triassic in age. Basal conglomerate of the Kootenai marks a resumption of deposition after a major period of erosion. The age of the oldest Kootenai sedimentary rocks in Montana is poorly constrained, but is thought to be earliest Aptian (118 Ma; Schwartz and DeCelles, 1988). In southwestern Montana the oldest Cretaceous sediments represented by the Kootenai Formation are generally only 200 m thick (Zen, 1988).

Major sedimentation began in early Albian time (about 113 Ma) and extended to the end of the Cretaceous (66 Ma). It produced a very thick sequence consisting of graywacke, sandstone, volcanogenic sandstone, ash, and conglomerate that was deposited conformably on the Kootenai Formation (Schwartz and DeCelles, 1988). In the Pioneer Mountains, Montana (fig. 10.1), more than 2,000 m of this sequence, the Colorado Group, was derived from the west and deposited in a fluvial environment (Snee, 1982; Zen, 1988). Recent U-Pb dating of zircon from porcellanite beds in the upper, volcaniclastic Vaughn Member of the Blackleaf Formation within the Colorado Group from the eastern Pioneer Mountains, Montana (fig. 10.1), yielded dates ranging from 97 to 93 Ma (Zartman and others, 1995). Although slightly older than our oldest dates for Idaho batholith magmatism, these zircon dates are reasonably consistent with an interpretation that the volcanic beds of the Vaughn Member were derived during earliest Idaho batholith magmatism.

The origin of Aptian through Upper Cretaceous sedimentary rocks both to the east and to the west of the Salmon River suture zone is thus directly linked in time to metamorphic, deformational, plutonic, and uplift events along the suture zone and within the area of the Idaho batholith. In fact, Schwartz and DeCelles (1988) have demonstrated a genetic relation between sedimentation in the Cretaceous and the timing of tectonism established by Lund and Snee (1988) along the Salmon River suture zone. According to Schwartz and DeCelles (1988), coarse sediments were deposited in the Cretaceous in three intervals at 118, 109, and 101-99 Ma, corresponding to three periods of metamorphism and deformation along the Salmon River suture zone. On a more regional scale, Heller and others (1986) concluded that thrusting during the Sevier orogeny began in the early Aptian; this conclusion was

reached by evaluating synorogenic conglomerates in Wyoming, Utah, and Colorado. In addition to the link between metamorphic and deformational events and the deposition of coarse sediments from 118 to 99 Ma, we suggest that the thick sequence of Cretaceous sedimentary rocks now exposed in western Montana reflects the more than 15 km of uplift that occurred between about 90 and 75 Ma. The lack of significant amounts of Paleocene and Eocene sedimentary rocks in southwestern Montana probably reflects the decrease of uplift and erosion in the area of the Idaho batholith.

SUMMARY OF CRETACEOUS TECTONIC HISTORY—CENTRAL IDAHO AND SOUTHWESTERN MONTANA

The Cretaceous tectonic history of central Idaho and southwestern Montana from 130 to 75 Ma is summarized in figure 10.28—a series of hypothetical cross sections from the Snake River canyon to the Pioneer Mountains along a line at latitude 45°30′ N. These cross sections are intended to generally represent (and in some cases exaggerate) the major activity along the line of section during each of five time periods: 130–100 Ma, 95–90 Ma, 85 Ma, 80 Ma, and 75 Ma. Important events portrayed on the figure are summarized below.

From 130 to 100 Ma, the Salmon River suture zone was the locus of right-slip transpressive movement between island-arc terranes and North America. Associated with this transpression were dynamothermal metamorphism, regional thrust faulting that verged both to the east and west away from the suture zone, and local pluton emplacement. Transpression caused thickening of the crust at the suture zone. Thrusting was assymetrical with the largest area affected lying to the east of the suture zone. The thickened crust west of the suture zone underwent partial melting at the crust-mantle boundary to form tonalitic magmas. Erosion driven by orogenesis resulted in sediments that were deposited in southwestern Montana.

From 95 to 90 Ma, right-slip transpression was virtually complete, and the sense of movement within the suture zone changed to predominantly vertical. This was a period of major metaluminous magmatism marking the beginning of Idaho batholith plutonism. Plutons were emplaced as far as 139 km to the east. These magmas were likely derived from the base of the thickened crust as a result of partial melting of material of intermediate composition at the crust-mantle boundary. The resultant magmas were buoyant, and their rise drove uplift of blocks within the suture zone and to the east. In southwestern Montana, volcaniclastic rocks derived from the region of the Idaho batholith were deposited during continued sedimentation.

At about 85 Ma, uplift along high-angle faults within the Salmon River suture zone was well underway. Metaluminous magmatism of the Idaho batholith was nearing completion. The area influenced by thrust faulting extended into southwestern Montana where some of the thrust sheets overrode the recently deposited Cretaceous sediments (Snee, 1982; Zen, 1988).

At about 80 Ma, uplift along high-angle faults in the Salmon River suture zone had decreased. Rapid uplift was underway in the central part of the Idaho batholith. Magmatism within the area of the Idaho batholith was in a lull, but the earliest mafic magmas were emplaced in southwestern Montana (Snee, 1982). Andesitic volcanism had begun in southwestern Montana (Snee, 1982).

At about 75 Ma, peraluminous magmatism affected a large area within the Idaho batholith. These magmas were likely derived from the partial melting of pelitic rocks at midcrustal levels within the thrust-thickened crust. Gold-bearing quartz veins were emplaced in fractures in roof pendants of these granites. In southwestern Montana, this was the predominant period of metaluminous magmatism (Snee, 1982; Zen, 1988). Some dacitic volcanism was still active (Snee, 1982).

After 70 Ma, igneous and hydrothermal activity in the region of the Idaho batholith was nearly complete. Uplift also was nearly complete. In southwestern Montana, magmatism, faulting, uplift, mineral-deposit emplacement, and erosion continued until about 60 Ma (Snee, 1982).

CONCLUSION

The Salmon River suture zone marks an area of multiple metamorphic events, complex structure, and several periods of intrusion. It also marks a sharp lithologic and chemical break between younger island-arc rocks to the west and older continental rocks to the east. Lund (1984) and Lund and Snee (1988) have proposed that the Salmon River suture zone is a right-lateral transpressive fault along which exotic island-arc terranes were accreted to the North American continent. If this proposal is correct, transpression along the suture zone caused some, if not all, of the prograde metamorphism that affected the Riggins Group and Seven Devils island arc, as well as rocks of the North American continent in cen-

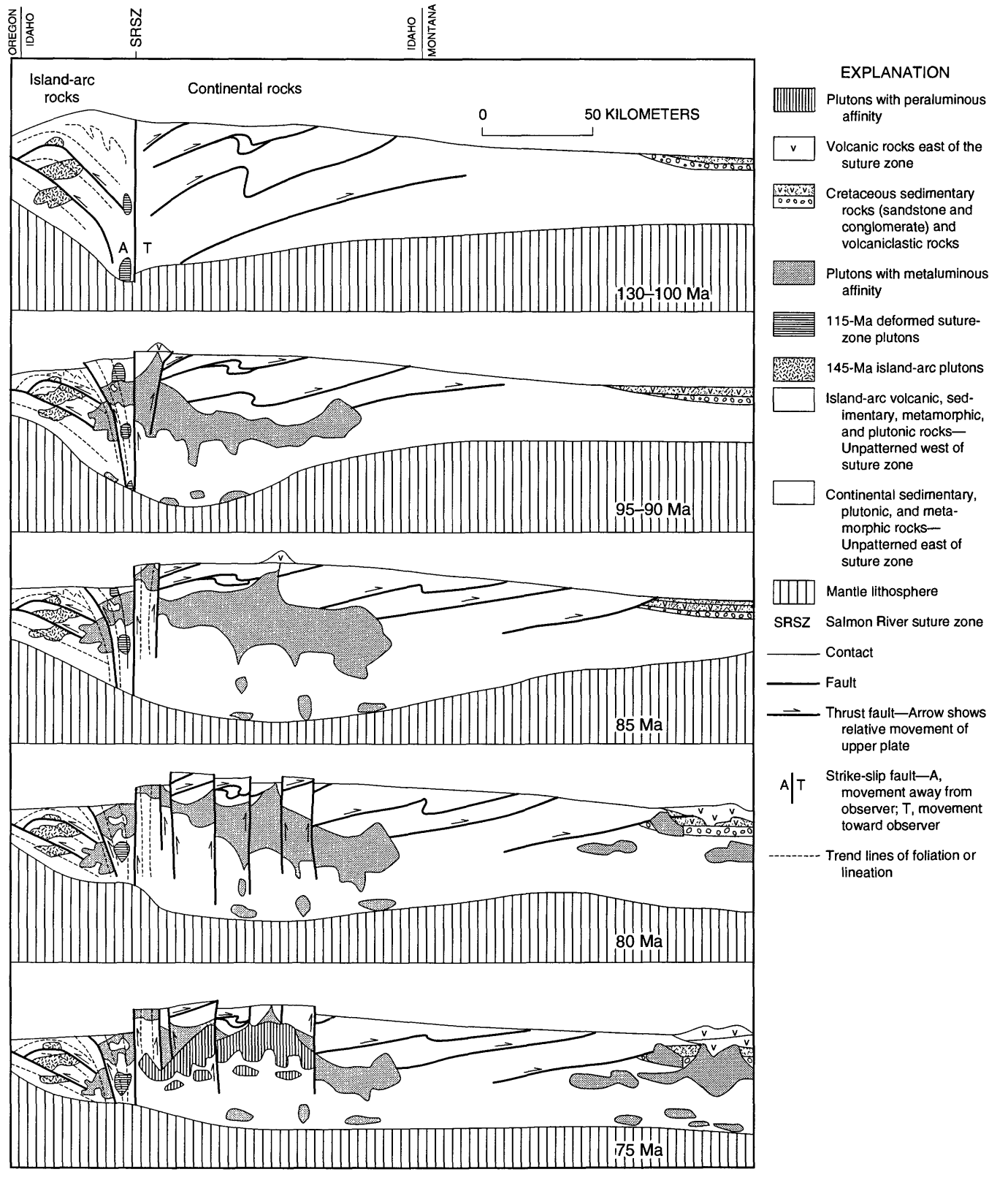

FIGURE 10.28.—Hypothetical cross sections from Snake River canyon, at the boundary between Oregon and Idaho, to Pioneer Mountains, Montana, at latitude 45°30′ N. From top to bottom, cross sections show tectonic development of central Idaho and southwestern Montana from 130 to 75 Ma. (See text for explanation.) No vertical exaggeration. Some features are exaggerated to emphasize process.

tral Idaho. This metamorphism began at about 130 Ma and continued until 93 Ma, when the terranes were stitched by the emplacement of plutons of the suture zone. If the Salmon River suture zone is the structure along which the island-arc terranes were accreted to North America, then events prior to 93 Ma, which are preserved in rocks west of the suture zone, occurred when the island-arc terranes were not attached to this part of North America. These events include the 244-Ma metamorphism and 227- and 145-Ma plutonism documented by argon dating in this report, and the 266- to 145-Ma plutonism demonstrated by the U-Pb dating of Walker (1981, 1983, 1986).

The emplacement of the Idaho batholith did not cause the regional metamorphism exhibited by the rocks within the Salmon River suture zone. Indeed, emplacement of the Idaho batholith began with the intrusion of tonalitic plutons at about 93 to 90 Ma within the suture zone and as far away as 139 km to the east. The oldest plutons of the eastern part of the Idaho batholith thus far identified were emplaced at 91 Ma, virtually simultaneously with tonalites of the suture zone. Some of the suture-zone plutons were emplaced at depths of 20 km or more; others were emplaced at relatively high crustal levels and were associated with porphyry mineralization. At or before 88 Ma, uplift at the rate of 3 mm/yr or more began along the suture zone; it spread eastward about 3 m.y. later. An apparent interval of 10 m.y. elapsed between metaluminous and peraluminous plutonism. Beginning at 78 Ma, muscovite-biotite granites were emplaced at depths of less than 9 km after some of the terrain east of the suture zone had experienced more than 10 km of uplift. Quartz-vein mineralization accompanied granite emplacement at relatively shallow depths. By 55 Ma, much of the central part of the Idaho batholith had been uplifted to upper crustal levels where the temperature was less than 130°C. As much as 20 km of uplift (and overburden removal) are recorded in the cooling histories of some rocks east of the suture zone and in the sedimentary record observed both to the east and to the west of the suture zone.

REFERENCES CITED

Adams, D.J., 1981, Uplift rates and thermal structure in the Alpine Fault Zone and Alpine schists, southern Alps, New Zealand, *in* McClay, K.R., and Price, N.J., eds., Thrust and nappe tectonics: Boston, Blackwell Scientific Publications, p. 211–222.

Alexander, E.C., Jr., Michelson, G.M., and Lanphere, M.A., 1978, MMhb-1: A new ^{40}Ar-^{39}Ar dating standard, *in* Zartman, R.E., ed., Short papers of the Fourth International Conference, Geochronology, Cosmochronology, Isotope Geology; Snowmass-at-Aspen, Colo., Aug. 20-25, 1978: U.S. Geological Survey Open-File Report 78-701, p. 6-8.

Anderson, J.L., and Rowley, M.C., 1981, Synkinematic intrusion of peraluminous and associated metaluminous granitic magmas, Whipple Mountains, California: Canadian Mineralogist, v. 19, p. 83-101.

Armstrong, R.L., 1975, The geochronometry of Idaho: Isochron West, v. 14, p. 1-50.

Armstrong, R.L., Taubeneck, W.H., and Hales, P.O., 1977, Rb-Sr and K-Ar geochronometry of Mesozoic granitic rocks and their Sr isotopic composition, Oregon, Washington, and Idaho: Geological Society of America Bulletin, v. 88, p. 397-411.

Avé Lallemant, H.G., Phelps, D.W., and Sutter, J.F., 1980, $^{40}Ar/^{39}Ar$ ages of some pre-Tertiary plutonic and metamorphic rocks of eastern Oregon and their geologic relationships: Geology, v. 8, p. 371-374.

Avé Lallemant, H.G., Schmidt, W.J., and Kraft, J.L., 1985, Major Late Triassic strike-slip displacement in the Seven Devils terrane, Oregon and Idaho—A result of left-oblique plate convergence?: Tectonophysics, v. 119, p. 299-328.

Balcer, D.E., 1980, $^{40}Ar/^{39}Ar$ ages and REE geochemistry of basement terranes in the Snake River Canyon, northeastern Oregon-western Idaho: Columbus, The Ohio State University, M.S. thesis, 111 p.

Carmichael, D.M., 1978, Metamorphic bathozones and bathograds—A measure of the depth of post-metamorphic uplift and erosion on the regional scale: American Journal of Science, v. 278, p. 769-797.

Cosca, M.A., Hunziker, J.C., Huon, S., and Masson, H., 1992, Radiometric age constraints on mineral growth, metmorphism, and tectonism of the Gummfluh klippe, Brianconnais domain of the Prealps, Switzerland: Contributions to Mineralogy and Petrology, v. 112, p. 439-449.

Criss, R.E., and Fleck, R.J., 1987, Petrogenesis, geochronology, and hydrothermal systems of the northern Idaho batholith and adjacent areas based on $^{18}O/^{16}O$, D/H, $^{87}Sr/^{86}Sr$, K-Ar, and $^{40}Ar/^{39}Ar$ studies, *in* Vallier, T.L., and Brooks, H.C., eds., Geology of the Blue Mountains region of Oregon, Idaho, and Washington—The Idaho batholith and its border zone: U.S. Geological Survey Professional Paper 1436, p. 95-137.

Criss, R.E., Lanphere, M.A., and Taylor, H.P., Jr., 1982, Effects of regional uplift, deformation, and meteoric-hydrothermal metamorphism on K-Ar ages of biotites in the southern half of the Idaho batholith: Journal of Geophysical Research, v. 87, p. 7029-7046.

Dalrymple, G.B., Alexander, E.C., Jr., Lanphere, M.A., and Kraker, G.P., 1981, Irradiation of samples for $^{40}Ar/^{39}Ar$ dating using the Geological Survey TRIGA reactor: U.S. Geological Survey Professional Paper 1176, 56 p.

Dalrymple, G.B., and Lanphere, M.A., 1974, $^{40}Ar/^{39}Ar$ age spectra of some undisturbed terrestrial samples: Geochimica et Cosmochimica Acta, v. 38, p. 715-738.

Davidson, G.F., 1989, Southwest-vergent thrusting and metamorphism along the northern margin of the Wallowa terrane near Orofino, Idaho: Geological Society of America Abstracts with Programs, v. 21, p. A89.

———1990, Cretaceous tectonic history along the Salmon River suture zone near Orofino, Idaho—Metamorphic, structural, and $^{40}Ar/^{39}Ar$ thermochronologic constraints: Corvallis, Oregon State University, M.S. thesis, 143 p.

Davidson, G.F., and Snee, L.W., 1989, Cretaceous tectonic history along the Salmon River suture near Orofino, Idaho—$^{40}Ar/^{39}Ar$ constraints: EOS, v. 70, p. 1310.

Davidson, G.F., and Snee, L.W., 1990, Resetting of the hornblende K-Ar isotopic system during mylonitization—Implications for direct dating of ductile shear zones: EOS, v. 71, p. 1662.

Dickinson, W.R., 1979, Mesozoic forearc basin in central Oregon: Geology, v. 7, p. 166-170.

Dickinson, W.R., Helmod, K.P., and Stein, J.A., 1979, Mesozoic lithic sandstones in central Oregon: Journal of Sedimentary Petrology, v. 49, p. 501-516.

Dodson, M.H., 1973, Closure temperature in cooling geochronological and petrological systems: Contributions to Mineralogy and Petrology, v. 40, p. 259-274.

Evans, B.W., and Vance, J.A., 1985, Properties of truly magmatic epidote: Geological Society of America Abstracts with Programs, v. 17, p. 576.

Evans, K.V., and Fischer, L.B., 1986, U-Pb geochronology of two augen gneiss terranes, Idaho—New data and tectonic implications: Canadian Journal of Earth Sciences, v. 23, 1919-1927.

Fleck, R.J., and Criss, R.E., 1985, Strontium and oxygen isotopic variation in Mesozoic and Cenozoic plutons of central Idaho: Contributions to Mineralogy and Petrology, v. 90, p. 291-308.

Fleck, R.J., Sutter, J.F., and Elliot, D.H., 1977, Interpretation of discordant $^{40}Ar/^{39}Ar$ age spectra of Mesozoic tholeiites from Antarctica: Geochimica et Cosmochimica Acta, v. 38, p. 15-32.

Follo, M.F., 1992, Conglomerates as clues to the sedimentary and tectonic evolution of a suspect terrane—Wallowa Mountains, Oregon: Geological Society of America Bulletin, v. 104, p. 1561-1576.

———1994, Sedimentology and stratigraphy of the Martin Bridge Limestone and Hurwal Formation (Upper Triassic to Lower Jurassic) from the Wallowa terrane, Oregon, *in* Vallier, T.L., and Brooks, H.C., eds., Geology of the Blue Mountains region of Oregon, Idaho, and Washington—Stratigraphy, physiography, and mineral resources: U.S. Geological Survey Professional Paper 1439, p. 1-27.

Follo, M.F., and Siever, Raymond, 1984, Conglomerates as clues to the evolution of a suspect terrane—Wallowa Mountains, Oregon: Geological Society of America Abstracts with Programs, v. 16, p. 510.

Gammons, C.H., 1986, A paragenetic and fluid inclusion study of polymetallic vein mineralization in the Big Creek mining district, Valley County, Idaho: State College, Pennsylvania State University, M.S. thesis, 273 p.

Gammons, C.H., Rose, A.W., Snee, L.W., and Lund, Karen, 1985, Paragenesis, fluid inclusions, and Ar-dating of the Big Creek mining district, Valley County, central Idaho: Geological Society of America Abstracts with Programs, v. 17, p. 588.

Hall, W.E., 1985, Stratigraphy of and mineral deposits in middle and upper Paleozoic rocks of the black-shale mineral belt, central Idaho, *in* McIntyre, D.H., ed., Symposium on the geology and mineral deposits of the Challis 1°×2° quadrangle, Idaho: U.S. Geological Survey Bulletin 1658, p. 117-131.

Hall, W.E., Schmidt, E.A., Howe, S.S., and Broch, M.J., 1984, The Thompson Creek, Idaho, porphyry molybdenum deposit—An example of a fluorine-deficient molybdenum granodiorite system, *in* Sixth Quadrennial International Association on the Genesis of Ore Deposits, Tbilisi, USSR, 1982, Proceedings: Stuttgart, E. Schweizerbart'sche Verlagsbuchhandlung, v. 1, p.349-358.

Hamilton, W.R., 1963, Metamorphism in the Riggins region, western Idaho: U.S. Geological Survey Professional Paper 436, 95 p.

———1976, Tectonic history of west-central Idaho: Geological Society of America Abstracts with Programs, v. 8, p. 378.

Hammarstrom, J.M., and Zen, E-an, 1988, Petrology and mineral chemistry of magmatic epidote-bearing rocks from the suture zone near Round Valley, western Idaho: Geological Society of America Abstracts with Programs, v. 20, p. 419.

Harrison, T.M., 1981, Diffusion of ^{40}Ar in hornblende: Contributions to Mineralogy and Petrology, v. 78, p. 324-331.

Harrison, T.M., and McDougall, Ian, 1980, Investigations of an intrusive contact, northwest Nelson, New Zealand—1. Thermal, chronological, and isotopic constraints: Geochimica et Cosmochimica Acta, v. 46, p. 1811-1820.

———1982, The thermal significance of potassium feldspar K-Ar ages inferred from $^{40}Ar/^{39}Ar$ age spectrum results: Geochimica et Cosmochimica Acta, v. 46, p. 1811-1820.

Heller, P.L., Bowdler, S.S., Chambers, H.P., Coogan, J.C., Hagen, E.S., Shuster, M.W., Winslow, N.S., and Lawton, T.F., 1986, Time of initial thrusting in the Sevier orogenic belt, Idaho-Wyoming and Utah: Geology, v. 14, p. 388-391.

Hess, J.C., and Lippolt, H.J., 1986, Kinetics of Ar isotopes during neutron irradiation—^{39}Ar loss from minerals as a source of error in $^{40}Ar/^{39}Ar$ dating: Chemical Geology, v. 59, p. 223-236.

Hietanen, Anna, 1962, Metasomatic metamorphism in western Clearwater County, Idaho: U.S. Geological Society Professional Paper 344-A, 116 p.

Hillhouse, J.W., Gromme, C.S., and Vallier, T.L., 1982, Paleomagnetism and Mesozoic tectonics of the Seven Devils volcanic arc in northeastern Oregon: Journal of Geophysical Research, v. 87, p. 3777-3794.

Hollister, L.S., 1982, Metamorphic evidence for rapid (2 mm/yr) uplift of a portion of the Central Gneiss Complex, Coast Mountains, B.C.: Canadian Mineralogist, v. 20, p. 319-332.

Hotz, P.E., Lanphere, M.A., and Swanson, D.A., 1977, Triassic blueschist from northern California and north-central Oregon: Geology, v. 5, p. 659-663.

Hyndman, D.W., 1981, Controls on source and depth of emplacement of granitic magma: Geology, v. 9, p. 244-249.

Hyndman, D.W., and Talbot, J.L., 1976, The Idaho batholith and related subduction complex: Geological Society of America, Cordilleran Section, Field Guide 4, 15 p.

Hyndman, R.D., Jessop, A.M., Judge, A.S., and Rankin, D.S., 1979, Heat flow in the Maritime Provinces of Canada: Canadian Journal of Earth Science, v. 16, p. 1154-1165.

Kaneoka, Ichiro, 1974, Investigations of excess argon in ultramafic rocks from the Kola Peninsula by the $^{40}Ar/^{39}Ar$ method: Earth and Planetary Science Letters, v. 22, p. 145-156.

Kiilsgaard, T.H., and Lewis, R.S., 1985, Plutonic rocks of Cretaceous age and faults in the Atlanta Lobe of the Idaho batholith, Challis quadrangle, *in* McIntyre, D.H., ed., Symposium on the geology and mineral deposits of the Challis 1°×2° quadrangle, Idaho: U. S. Geological Survey Bulletin 1658, p. 29-42.

Krogh, T.E., 1973, A low-contamination method for hydrothermal decomposition of zircon and extraction of U and Pb for isotopic age determination: Geochimica et Cosmochimica Acta, v. 37, p. 485-494.

Kunk, M.J., 1982, Application of the $^{40}Ar/^{39}Ar$ age spectrum technique to the dating of biotite from Middle Ordovician bentonites, eastern North America: Columbus, The Ohio State University, M.S. thesis, 137 p.

Lanphere, M.A., and Dalrymple, G.B., 1971, A test of the $^{40}Ar/^{39}Ar$ age spectrum technique on some terrestrial materials: Earth and Planetary Science Letters, v. 12, p. 359-372.

———1976, Identification of excess ^{40}Ar by the $^{40}Ar/^{39}Ar$ age spectrum technique: Earth and Planetary Science Letters, v. 32, p. 141-148.

Larson, E.S., Jr., and Schmidt, R.G., 1958, A reconnaissance of the Idaho batholith and comparison with the southern California batholith: U.S. Geological Survey Bulletin 1070B, p. 35-62.

Lee, J.K.W., Onstott, T.C., Cashman, K.V., Cumbest, R.J., and Johnson, D., 1991, Incremental heating of hornblende in vacuo—Implications for $^{40}Ar/^{39}Ar$ geochronology and the interpretation of thermal histories: Geology, v. 19, p.872-876.

Lewis, R.S., Kiilsgaard, T.H., Bennett, E.H., and Hall, W.E., 1987, Lithologic and chemical characteristics of the central and southeastern part of the southern lobe of the Idaho batholith, *in* Vallier, T.L., and Brooks, H.C., eds., Geology of the Blue Mountains region of Oregon, Idaho, and Washington—The Idaho batholith and its border zone: U.S. Geological Survey Professional Paper 1436, p. 171-196.

Ludwig, K.R., 1980, Calculation of uncertainties of U-Pb isotopic data: Earth and Planetary Science Letters, v. 46, p. 212-220.

———1982, Programs for filing and plotting U-Pb isotopic data for concordia diagrams, using an HP-p830 computer and HP-p862 plotter: U.S. Geological Survey Open-File Report 82-386, 22 p.

Lund, Karen, 1984, Tectonic history of a continent-island arc boundary—West-central Idaho: State College, Pennsylvania State University, Ph.D. dissertation, 207 p.

Lund, Karen, Alminas, H.V., Kleinkopf, M.D., Ehmann, W.J., and Bliss, J.D., 1989, Preliminary mineral resource assessment of the Elk City 1°×2° quadrangle, Idaho and Montana: U.S. Geological Survey Open-File Report 89-16, 180 p., 14 maps, scale: 1:250,000.

Lund, Karen, Rehn, W.M., and Holloway, C.D., 1983b, Geologic map of the Blue Joint wilderness study area, Ravalli County, Montana, and the Blue Joint roadless area, Lemhi County, Idaho: U.S. Geological Survey Miscellaneous Field Studies Map MF-1557-B, scale 1:50,000.

Lund, Karen, Scholten, Robert, and McCollough, F.M., 1983a, Consequences of interfingered lithologies in the Seven Devils island arc: Geological Society of America Abstracts with Programs, v. 15, p. 284.

Lund, Karen, and Snee, L.W., 1988, Metamorphism, structural development, and age of the continent-island arc juncture in west-central Idaho, *in* Ernst, W.G., ed., Metamorphism and crustal evolution in the western conterminous U.S.: Englewood Cliffs, N.J., Prentice Hall, p. 296-331.

Lund, Karen, Snee, L.W., and Evans, K.V., 1986, Age and genesis of precious-metals deposits, Buffalo Hump district, central Idaho—Implications for depth of emplacement of quartz veins: Economic Geology, v. 81, p. 990-996.

McCollough, W.F., 1984, Stratigraphy, structure, and metamorphism of Permo-Triassic rocks along the western margin of the Idaho batholith, John Day Creek, Idaho: State College, Pennsylvania State University, M.S. thesis, 141 p.

Meen, J.K., Snee, L.W., Lund, Karen, and Eggler, D.H., 1988, Cretaceous volcanism from Idaho to Wyoming: Geological Society of America Abstracts with Programs, v. 20, p. 432.

Merrihue, Craig, and Turner, Granville, 1966, Potassium-argon dating by activation with fast neutrons: Journal of Geophysical Research, v. 71, p. 2852-2857.

Miller, C.F., Stoddard, E.F., Bradfish, L.J., and Dollase, W.A., 1981, Composition of plutonic muscovite—Genetic implications: Canadian Mineralogist, v. 19, p. 25-34.

Muniz, P.F., and Brown, P.E., 1984, Au-Ag mineralization in the Buffalo Hump district, central Idaho: Geological Society of America Abstracts with Programs, v. 16, p. 604.

Myers, P.E., 1982, Geology of the Harpster area, Idaho County, Idaho: Idaho Bureau of Mines and Geology Bulletin 25, 46 p.

Myers, W.B., 1952, Geology and mineral deposits of the northwest quarter of the Willis quadrangle and adjacent Brown's Lake area, Beaverhead County, Montana: U.S. Geological Survey Open-File Report 147, 46 p.

Naney, M.T., 1983, Phase equilibria of rock-forming ferromagnesian silicates in granitic systems: American Journal of Science, v. 283, p. 993-1033.

Onasch, C.M., 1976, Infrastructure-suprastructure relations and structural mechanics along the western margin of the Idaho batholith: Geological Society of America Abstracts with Programs, v. 8, p. 402.

———1977, Structural evolution of the western margin of the Idaho batholith in the Riggins, Idaho area: State College, Pennsylvania State University, Ph.D. dissertation, 196 p.

———1987, Temporal and spatial relations between folding, intrusion, metamorphism, and thrust faulting in the Riggins area, west-central Idaho, *in* Vallier, T.L., and Brooks, H.C., eds., Geology of the Blue Mountains region of Oregon, Idaho, and Washington—The Idaho batholith and its border zone: U.S. Geological Survey Professional Paper 1436, p. 139-149.

Perry, W.J., 1986, Critical deep drillholes and indicated Paleozoic paleotectonic features north of the Snake River downwarp in southern Beaverhead County, Montana, and adjacent Idaho: U.S. Geological Survey Open-File Report 86-413, 16 p.

Roeske, S.M., Dusel-Bacon, Cynthia, Aleinikopf, J.N., and Snee, L.W., 1995, Metamorphic and structural history of continental crust at a Mesozoic collisional margin, central Alaska: Journal of Metamorphic Geology, v. 13, p. 25-40.

Sarewitz, Daniel, 1982, Geology of a part of the Heavens Gate quadrangle, Seven Devils Mountains, western Idaho: Corvallis, Oregon State University, M.S. thesis, 144 p.

Schwartz, R.K., and DeCelles, P.G., 1988, Cordilleran foreland basin evolution in response to interactive Cretaceous thrusting and foreland partitioning, southwestern Montana, *in* Schmidt, C.J., and Perry, W.J., eds., Interaction of the Rocky Mountain foreland and the Cordilleran thrust belt: Geological Society of America Special Paper 171, p. 489-513.

Selverstone, Jane, Wernicke, B.P., and Aliberti, E.A., 1992, Intracontinental subduction and hinged unroofing along the Salmon River suture zone, west central Idaho: Tectonics, v. 11, p. 124-144.

Silberling, N.J., Jones, D.L., Jones, M.C., Jr., and Howell, D.G., 1984, Lithotectonic terrane map of the western conterminous United States, Part C *of* Silberling, N.J., and Jones, D.L., eds., Lithotectonic terrane maps of the North American Cordillera: U.S. Geological Survey Open-File Report 84-523, 43 p.

Snee, L.W., 1982, Emplacement and cooling of the Pioneer batholith, southwestern Montana: Columbus, The Ohio State University, Ph.D. dissertation, 320 p.

———1987, $^{40}Ar/^{39}Ar$ thermochronology of mineral deposits—Information on age, duration, number of episodes, and temperature of mineralization, *in* Sachs, J.S., ed., USGS research on mineral deposits, 1987; Program and abstracts; Third annual V.E. McKelvey Forum on Mineral and Energy Resources: U.S. Geological Survey Circular 995, p. 67-68.

Snee, L.W., Davidson, G.F., and Unruh, D.M., in press, Geologic, geochemical, and $^{40}Ar/^{39}Ar$ and U-Pb thermochronologic constraints for the tectonic development of the Salmon River suture zone near Orofino, Idaho: GSA Special Paper.

Snee, L.W., and Kunk, M.J., 1989, $^{40}Ar/^{39}Ar$ thermochronology of mineral deposits in the southern part of the Idaho batholith: U.S. Geological Survey Open-File Report 89-639, p. 37-38.

Snee, L.W., Lund, Karen, and Davidson, Gary, 1987a, Ages of metamorphism, deformation, and cooling of juxtaposed oceanic and continental rocks near Orofino, Idaho: Geological Society of America Abstracts with Programs, v. 19, p. 335.

Snee, L.W., Lund, Karen, and Evans, K.V., 1985, $^{40}Ar/^{39}Ar$ age-spectrum data for the Buffalo Hump mining district,

Clearwater Mountains, central Idaho: U.S. Geological Survey Open-File Report 85-0102, 10 p.

Snee, L.W., Sutter, J.F., and Kelly, W.C., 1988, Thermochronology of economic mineral deposits—Dating the stages of mineralization at Panasqueira, Portugal, by high-precision $^{40}Ar/^{39}Ar$ age-spectrum techniques on muscovite: Economic Geology, v. 83, p. 335-354.

Snee, L.W., Sutter, J.F., Lund, Karen, Balcer, D.E., and Evans, K.V., 1987b, $^{40}Ar/^{39}Ar$ age-spectrum data for metamorphic and plutonic rocks from west-central Idaho: U.S. Geological Survey Open-File Report 87-052, 20 p.

Stacey, J.S., and Kramers, J.D., 1975, Approximation of terrestrial leadisotope evolution by a two-stage model: Earth and Planetary Science Letters, v. 26, p. 207-221.

Steiger, R.H., and Jäger, Emilie, 1977, Subcommission on geochronology—Convention on the use of decay constants in geo- and cosmo-chronology: Earth and Planetary Science Letters, v. 36, p. 359-362.

Turner, Granville, 1968, The distribution of potassium and argon in chrondites, *in* Ahrens, L.H., ed., Origin and distribution of the elements: New York, Pergamon Press, p. 387-398.

Vallier, T.L., 1968, Reconnaissance geology of the Snake River Canyon between Granite Creek and Pittsburg Landing, Oregon and Idaho: The Ore Bin, v. 30, p. 233-252.

———1974, Preliminary report on the geology of part of the Snake River Canyon: Oregon Department of Geology and Mining Industries Map GMS-6, 28 p.

———1977, The Permian and Triassic Seven Devils Group, western Idaho and northeastern Oregon: U.S. Geological Survey Bulletin 1437, 58 p.

Vallier, T.L., and Engebretson, D.C., 1983, The Blue Mountains island arc of Oregon, Idaho, and Washington—An allochthonous coherent terrane from the ancestral western Pacific Ocean, *in* Howell, D.G., Jones, D.L., Cox, Allan, and Nur, Amos, eds., Proceedings of the Circum-Pacific Terrane Conference: Stanford, California, Stanford University Publications, v. 18, p. 197-199.

Wagner, W.R., 1945, Geological reconnaissance between the Snake and Salmon Rivers north of Riggins: Idaho Bureau of Mines and Geology Pamphlet 74, 16 p.

Walker, N.W., 1981, U-Pb geochronology of ophiolitic and volcanic-plutonic arc terranes, northeastern Oregon and westernmost-central Idaho: American Geophysical Union Transactions, v. 62, p. 1087.

———1983, Pre-Tertiary evolution of northeastern Oregon and west-central Idaho—Constraints based on U/Pb ages of zircons: Geological Society of America Abstracts with Programs, v. 15, p. 371.

———1986, U/Pb geochronologic and petrologic studies in the Blue Mountains terrane, northeastern Oregon and westernmost-central Idaho—Implications for pre-Tertiary tectonic evolution: Santa Barbara, University of California, Ph.D. dissertation, 214 p.

White, D.L., and Vallier, T.L., 1994, Geologic evolution of the Pittsburg Landing area, Snake River canyon, Oregon and Idaho, *in* Vallier, T.L., and Brooks, H.C., eds., Geology of the Blue Mountains region of Oregon, Idaho, and Washington—Stratigraphy, physiography, and mineral resources: U.S. Geological Survey Professional Paper 1439, p. 55-73.

Wilkinson, W.D., and Oles, K.F., 1968, Stratigraphy and paleoenvironments of Cretaceous rocks, Mitchell quadrangle, Oregon: American Association of Petroleum Geologists Bulletin, v. 52, p. 129-161.

Winkler, H.G.F., 1979, Petrogenesis of metamorphic rocks: New York, Springer-Verlag, 348 p.

Worl, R.G., Kiilsgaard, T.H., Bennett, E.H., Link, P.K., Lewis, R.S., Mitchell, V.E., Johnson, K.M., and Snyder, L.R., 1991, Geologic map of the Hailey 1°×2° quadrangle, Idaho: Idaho Geological Survey Open-File Report 91-340.

Zartman, R.E., Dyman, T.S., Tysdal, R.G., and Pearson, R.C., 1995, U-Pb ages of volcanogenic zircon from porcellanite beds in the Vaughn Member of the mid-Cretaceous Blackleaf Formation, southwestern Montana: U.S. Geological Survey Bulletin 2113–B, 16 p.

Zeitler, P.K., 1985, Cooling history of the NW Himalaya, Pakistan: Tectonics, v. 4, p. 127-151.

Zen, E-an, 1985, Implications of magmatic epidote-bearing plutons on crustal evolution in the accreted terranes of northwestern North America: Geology, v. 13, p. 266-269.

———1988, Bedrock geology of the Vipond Park 15-minute, Stine Mountain 7½-minute, and Maurice Mountain 7½-minute quadrangles, Pioneer Mountains, Beaverhead County, Montana: U.S. Geological Survey Bulletin 1625, 49 p., 2 pls.

Zen, E-an, and Hammarstrom, J.M., 1984, Magmatic epidote and its petrologic significance: Geology, v. 12, p. 515-518.

11. GEOLOGY OF THE NORTHERN PART OF THE IRONSIDE MOUNTAIN INLIER, NORTHEASTERN OREGON

By PETER R. HOOPER, MICHEL D. HOUSEMAN, JOHN E. BEANE, GREGORY M. CAFFREY, KENNETH R. ENGH, JAMES V. SCRIVNER, and A. JOHN WATKINSON[1]

CONTENTS

Abstract ---- 415
Introduction ---- 416
Acknowledgments ---- 416
Analytical methods ---- 417
Rocks of the Baker terrane ---- 418
  Peridotite of Bullrun Mountain ---- 418
  Serpentinite ---- 418
  Chemical composition of peridotite and serpentinite ---- 422
  Melange of Mine Ridge ---- 423
    Metamorphosed gabbro and basalt ---- 424
    Plagiogranite ---- 426
    Schistose rocks of Mine Ridge ---- 427
    Ribbon chert ---- 429
    Pre-Jurassic volcanic rocks ---- 431
  Origin of the rocks of the Baker terrane, Ironside Mountain inlier ---- 432
  Correlation and timing of the deformation of the schistose rocks of Mine Ridge ---- 433
Fore-arc basin deposits: the Weatherby Formation ---- 433
  Provenance ---- 434
  Deformation of the Weatherby Formation ---- 437
Post-Jurassic igneous rocks ---- 437
  Granodiorite of Bullrun Creek ---- 440
  Granodiorite of Grouse Creek and related minor intrusions ---- 441
  Late-stage porphyritic dikes ---- 442
  Chemical composition of the Oligocene intrusions ---- 443
Alteration and mineralization ---- 444
  Granodiorite of Bullrun Creek—Record Mine ---- 444
  Granodiorite of Grouse Creek ---- 445
Discussion and conclusions ---- 449
References cited ---- 453

ABSTRACT

The Ironside Mountain inlier exposes Permian and Triassic ophiolitic rocks along the southern margin of the Baker terrane at the center of the Blue Mountains province. Lying between the Canyon Mountain Complex and the (informal) Sparta complex, rocks of the Ironside Mountain inlier consist of dunite, harzburgite, and a serpentinized melange containing knockers of peridotite, metagabbro, plagiogranite, schist, ribbon chert, and pre-Jurassic andesite. The peridotite has a high-temperature mineralogy and an equivalent bulk chemical composition depleted in Al_2O_3 and CaO. Its coarse metamorphic fabric predates two stages of serpentinization, the second of which may have been associated with the intrusion of the peridotite into the crust. These properties are consistent with an origin as the residuum of partial melting in the mantle.

The knockers of the schistose rocks of Mine Ridge include three fold phases. F_1 folds are isoclinal folds whose axes plunge down the dip of a steep east-northeast-striking penetrative foliation (S_1 parallel to S_0, henceforth referred to as S_0-S_1) associated with epidote amphibolite-facies metamorphism. The hornblende lies parallel to the F_1 fold axes and has been dated at 260 Ma. F_2 fold axes also plunge down the dip of the S_0-S_1 plane, but the F_2 fold axes have varied axial surfaces that are at high angles to the foliation and are not associated with a new metamorphic fabric. F_3 folds are a younger set of crenulations. All three fold phases are correlated with the regional D_1 deformation event, which is interpreted as a result of the subduction process. In this model the original fold axes were formed horizontally in the subduction plane perpendicular to the direction of subduction, but were then steepened and reoriented into parallelism with the direction of subduction by extensive transport down the subduction plane.

Rare-earth-element patterns, the presence of large andesite blocks in the melange, and the near coincidence between the age of crystallization of the ophiolitic rocks and the age of their first major metamorphism all support the hypotheses that (1) the rocks of the Ironside Mountain inlier are similar in composition and age to the rocks of the Canyon Mountain Complex, and (2) each of these ophiolitic sequences represents the root zones of neighboring island arcs, rather than the remains of midocean ridge-rift systems that were transported large distances to their present positions.

The Permian and Triassic rocks are overlain by calcareous wackes of the Jurassic Weatherby Formation, a part of the Izee terrane. The wackes were derived in large part from the Permian and Triassic rocks, on which they appear to lie unconformably, although observed contacts are now faulted. The Weatherby is deformed into tight chevron folds with horizontal axes and steep east-northeast-striking axial surfaces that parallel the S_0-S_1 plane of the older rocks. These folds represent approximately horizontal north-northwest/south-southeast compression and are correlated with the regional D_2 event of Jurassic age that others have associated with the accretion of these rocks to the North American plate in the Late Jurassic. Failure to recognize the D_2 event in the fabric of the knockers of the schistose rocks of Mine Ridge is attributed to the incompetency of the serpentinite matrix of the melange;

[1]All at Department of Geology, Washington State University, Pullman, WA 99164-2812

the matrix apparently absorbed the strain so that the D_2 compression resulted only in the reorientation of the long axes of the knockers into the steep east-northeast-striking D_2 axial surface.

Undeformed granitic bodies of Late Jurassic, Cretaceous, and Oligocene age intrude the Blue Mountains province. Two large igneous bodies and numerous dikes and sills (36 to 34 Ma) intrude the Weatherby Formation at the north end of the Ironside Mountain inlier. All have a very similar tonalitic composition but are distinguished by texture and degree of alteration. The well-developed hydrothermal alteration associated with the younger intrusion caused Cu-Au-Ag and associated base-metal enrichment and is the first Tertiary porphyry to be documented in northeastern Oregon.

Interpretation of the Permian and Triassic rocks as the roots of the primitive island-arc systems and the derivation of the Jurassic Weatherby Formation from these older oceanic rocks imply that the various "terranes" of the Blue Mountains province were in close proximity to each other at the time of their formation. To this extent the term "terrane" may not be entirely appropriate. The varied "terranes" appear to represent a complex system of primitive oceanic island arcs formed by subduction off the western edge of the North American plate at a latitude relative to the North American plate equivalent to that observed today. These terranes suffered compression during both the subduction (Permian, D_1) and the accretion (Jurassic to Cretaceous, D_2) processes.

INTRODUCTION

Ironside Mountain is one of many inliers of pre-Tertiary rocks exposed through the cover of Tertiary volcanic and sedimentary rocks of northeastern Oregon (Thayer and Brown, 1973). The inlier forms a north-northwest-trending faulted anticlinal ridge of Tertiary age immediately west and south of Unity on Highway 26, approximately 60 km southwest of Baker City (fig. 11.1, inset). The anticlinal ridge has a core of Tertiary granitic intrusions.

An important boundary between the Baker (oceanic) terrane to the north and the Izee (fore-arc basin) terrane to the south runs east-west across the northern part of the inlier. The Baker and Izee terranes are two of the four allochthonous Mesozoic terranes recognized in northeastern Oregon (Brooks and Vallier, 1978; Dickinson and Thayer, 1978; Brooks, 1979a; Silberling and others, 1984). The other two are the Wallowa (Seven Devils arc) terrane and the Olds Ferry (Huntington arc) terrane (fig. 11.1). The four terranes were welded together by Middle Jurassic time and subsequently accreted to the western edge of the North American craton, a process completed in the Late Cretaceous (75–65 Ma) (Fleck and Criss, 1985).

The two northern spurs of the inlier, Mine Ridge and Bullrun Mountain (fig. 11.1), are formed by rocks of the Baker terrane. The north end of Bullrun Mountain is a large fault-bounded peridotite body. Mine Ridge is composed of a serpentinite melange with blocks (knockers) of peridotite, gabbro, plagiogranite, and basalt of ophiolite affinity. The knockers are intermixed with ribbon cherts, relatively fresh massive blocks of pre-Jurassic andesite, and various schistose units (the schistose rocks of Mine Ridge), which include hornblende schist, mica schist, and quartzite. The units of the melange are of mid-Permian to Triassic age (Lowry, 1968; Brooks and Ferns, 1979; Brooks and others, 1979), are metamorphosed to the epidote amphibolite facies, and are complexly folded. The peridotite of Bullrun Mountain and the melange of Mine Ridge are separated by the Oligocene granodiorite of Bullrun Creek (fig. 11.1).

The Izee terrane is represented by the Jurassic Weatherby Formation of Brooks (1979b), which consists of calcareous graywacke and siltstone with minor horizons of conglomerate, tuff, limestone, arkosic sandstone, and shale. All exposed contacts between the Jurassic Weatherby Formation and the Permian and Triassic melange are faulted, but an originally unconformable contact is suggested both by the presence of the graywacke north and south of the older units and by conglomeratic horizons close to the contact containing clasts apparently derived from the melange (Lowry, 1968; Brooks and Ferns, 1979; Brooks and others, 1979). The Weatherby has been folded in a single episode of deformation.

Many dikes, sills, and stocks of fine-grained granodiorite intrude the Weatherby along the axis of the anticlinal ridge and are now known to be of Oligocene age (34–36 Ma) (N.W. Walker, oral commun., 1986; Manville Products Corporation, oral commun., 1986). To the south of the mapped area, however, the diorite of Tureman Ranch intruded the Weatherby in the Early Cretaceous (Brown and Thayer, 1966; Lowry, 1968; Thayer and Brown, 1973). Mild deformation of the inlier continued into the Holocene, as fault-controlled basins were filled with fluvial and lacustrine Pliocene to Holocene sediments that have steep faulted contacts against the older rocks (Brooks and Ferns, 1979; Brooks and others, 1979).

The northern part of the Ironside Mountain inlier is a microcosm of the complex geology of the accreted terranes of the Blue Mountains province in northeastern Oregon. Over several years the authors have mapped critical parts of the inlier with the purpose of clarifying the structural relations between the units, correlating them with similar units exposed elsewhere in northeastern Oregon, and so gaining a better understanding of the origin of the various rocks represented.

ACKNOWLEDGMENTS

Study of the Ironside Mountain inlier was originally suggested, encouraged, and subsequently supported by Howard Brooks and Mark Ferns of the Oregon

Department of Mines and Geology, Baker City office. We greatly appreciate their continuing support. Particular aspects of the study were also supported by the Washington Mining and Mineral Resources Research Institute, Manville Corporation, and the Ladies Auxiliary to the American Institute of Mining, Metallurgical, and Petroleum Engineers. Peter Hooper acknowledges the kind cooperation of J.N. Walsh, Kings College, London, in making his inductively coupled plasma laboratory available for trace- and rare-earth-element analyses. Detailed reviews by Mark Ferns, James Evans, and Tracy Vallier added significantly to the clarity of the paper and are gratefully acknowledged.

ANALYTICAL METHODS

Samples were analyzed for major elements on a manual Philips 1410 X-ray spectrometer using 2:1

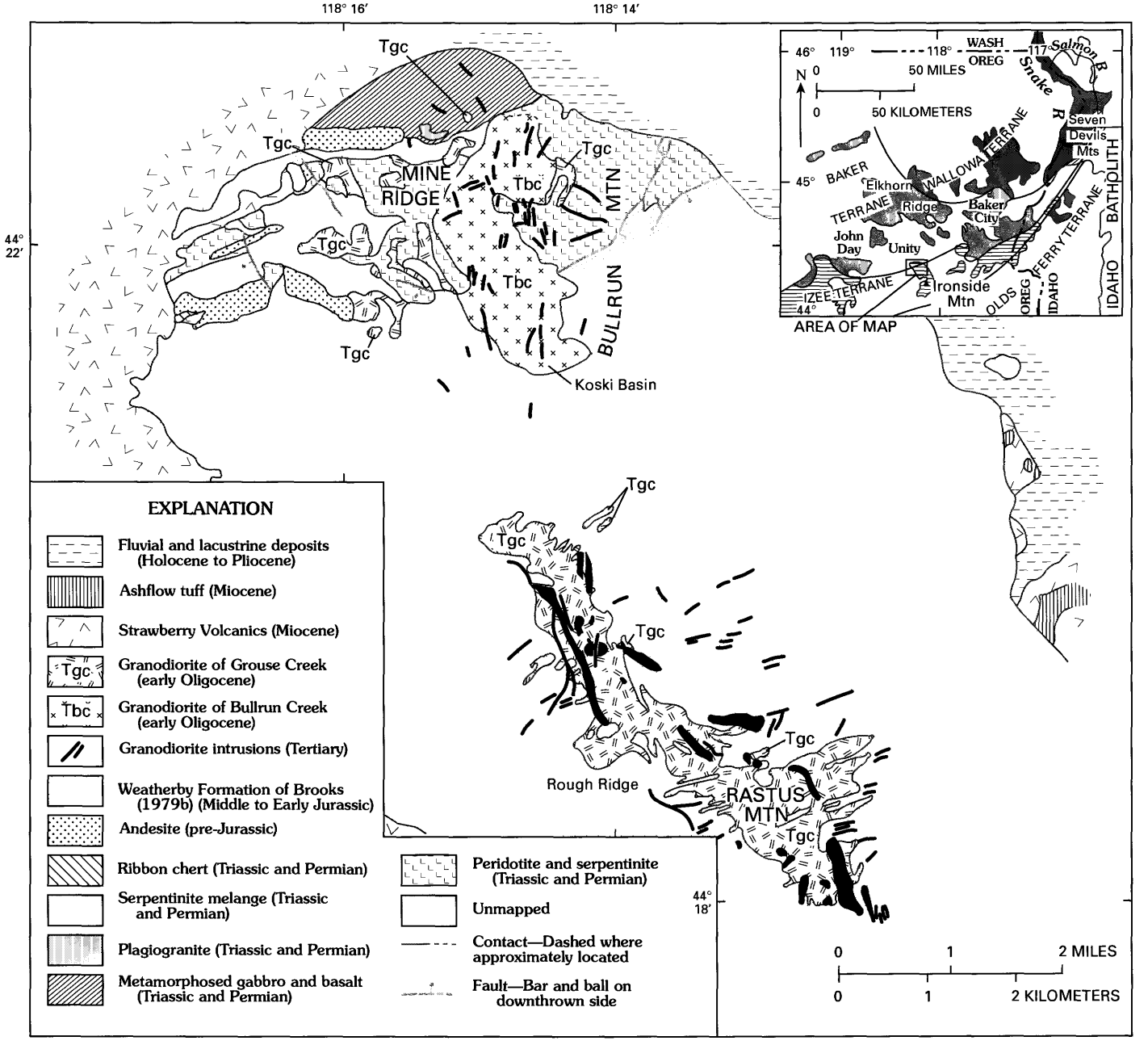

FIGURE 11.1.—Simplified geologic map of north end of Ironside Mountain inlier. Inset shows position of inlier in relation to the four major allochthonous terranes recognized in northeastern Oregon. Patterns in inset map show outcrop areas in the four terranes.

$Li_2B_4O_7$:rock powder fused disks (Hooper and Atkins, 1969; Hooper and others, 1976). Trace elements, including rare-earth elements, were analyzed on an automated Philips inductively coupled plasma spectrometer by the senior author at Kings College, London (Thompson and Walsh, 1983). The compositions of olivines and orthopyroxenes in the peridotite were determined on an automatic Cameca electron microprobe. X-ray diffraction analysis of four samples was used to verify the optical identification of serpentine polymorphs.

ROCKS OF THE BAKER TERRANE

PERIDOTITE OF BULLRUN MOUNTAIN

A large body of peridotite which is here called the peridotite of Bullrun Mountain covers an area of about 4 km^2 at the northeast end of the Ironside Mountain inlier (figs. 11.1, 11.2). Smaller bodies of ultramafic rock, most totally serpentinized, form pods and the matrix of the melange on Mine Ridge to the west. The main peridotite body forms bold rounded cliffs on Bullrun Mountain, broken by more easily eroded serpentinized zones. It is separated from the younger Weatherby Formation to the south by serpentinized fault zones intruded by younger granodiorite dikes. In the valley of Bullrun Creek the peridotite is intruded by, and occurs as inclusions in, the granodiorite of Bullrun Creek (fig. 11.2). To the north and northeast the ultramafic rocks are onlapped by the Pliocene to Holocene fluvial and lacustrine sediments of Unity basin. The covered contact between the inlier and the basin is assumed to be faulted (Thayer and Brown, 1973).

The peridotite is everywhere partially serpentinized (30–90 percent serpentine with an average of 60 percent; Caffrey, 1982), but in the main peridotite body the original mineralogy is generally apparent. It is restricted to the three phases olivine, orthopyroxene, and chromite. The rocks range from dunite (0–10 percent orthopyroxene) to harzburgite (10–25 percent orthopyroxene) (Streckeisen and others, 1973). Vague and irregular compositional banding is present locally (fig. 11.3). Only one crystal of clinopyroxene has been observed, and the orthopyroxene lacks exsolution lamellae. Plagioclase is absent.

The olivine forms small 0.5–1.0 mm grains separated by a mesh of serpentine. The small grains occur in optically continuous groups as much as 10.0 mm in diameter. The groups are elongate parallel to each other and represent primary olivine crystals. Deformation lamellae and, less commonly, kink bands are visible in approximately 60 percent of the primary crystals; irregular shadowy extinction is present in most others. Kink bands may be traced across many smaller grains of a single primary crystal and demonstrate that serpentinization postdates the deformation that produced the kink bands (fig. 11.4). The olivine grains have optic angles close to 90° ($2V\gamma$=89° to 93°, estimated), and electron microprobe analyses indicate compositions ranging from $Fo_{90.7}$ to $Fo_{92.4}$ (table 11.1).

Orthopyroxene crystals are as much as 8.0 mm in length, enclose small grains of chromite, and tend to poikilitically enclose olivine. Crystals are commonly bent, and kink bands are developed in many. Orthopyroxene has been altered to anthophyllite or Mg-rich cummingtonite along its cleavage and rims, and may have been completely pseudomorphed in the more highly serpentinized rocks. Most crystals are optically positive ($2V\gamma$=87° to 93°±5°), and electron microprobe analyses give a compositional range of $En_{91.0}$ to $En_{95.3}$, well within the enstatite range (table 11.1).

Chromite is ubiquitous in both the dunite and harzburgite in modal proportions varying from 1 percent to 4 percent. It appears as scattered brown or red-brown isotropic grains with both embayed and euhedral shapes. It alters to magnetite on rims and along fractures.

The primary-phase assemblage of the ultramafic rocks (olivine+orthopyroxene+spinel) is typical of mantle, not crustal, conditions. The coarse grain size, the lack of zoning in both olivine and orthopyroxene, the lack of significant rhythmic layering, and in particular the lack of either plagioclase- or clinopyroxene-bearing layers suggest that the peridotite of Bullrun Mountain is a residue of partial melting in the mantle. However, the nonmetamorphic poikilitic relations between olivine and orthopyroxene are a common feature of cumulate rocks.

Similar cumulate-like textures are common in alpine peridotites and other ultramafic assemblages that are associated with ophiolite complexes and have generally been interpreted as residual mantle (Moores, 1969; England and Davies, 1973; Jackson and others, 1975; Coleman, 1977; Evarts, 1977; Malpas, 1977). The olivine alignment seen in the peridotite of Bullrun Mountain is typical of mantle metamorphic fabrics (Coleman, 1977), and the embayed shape of many chromite grains in the peridotite mirrors those reported by Augustithis (1979) from mantle xenoliths in Ethiopian basalt and from mantle diapirs in Greece. The experimental work by Avé Lallemant and Carter (1968, 1970) indicates that recrystallization in the upper mantle can yield all of these typical alpine peridotite fabrics.

SERPENTINITE

Samples of peridotite described above have retained their primary structure and enough of their

primary mineralogy to permit unequivocal identification as peridotite. Elsewhere on Bullrun Mountain the olivine has been completely serpentinized, and for these rocks the term serpentinite is used.

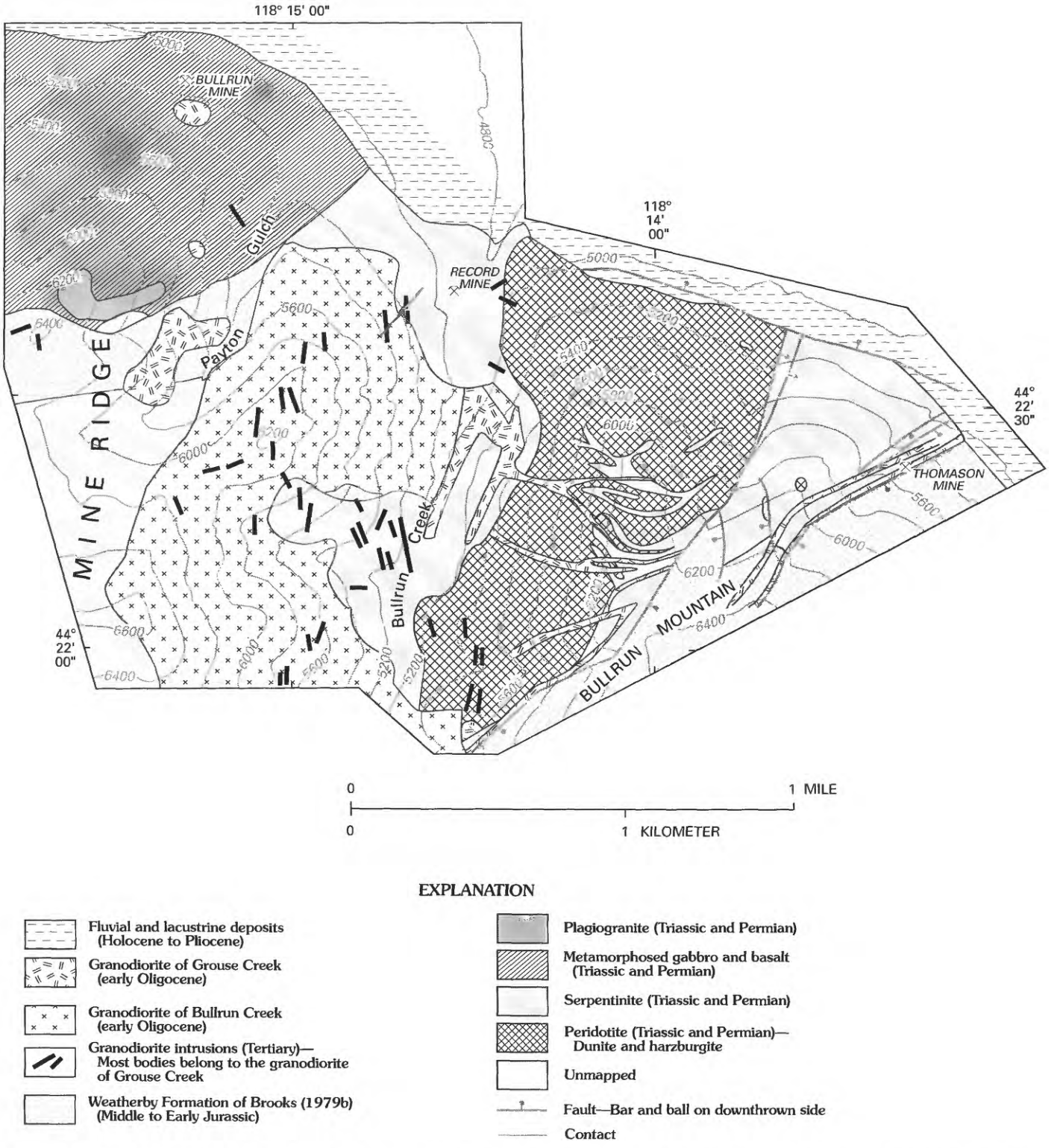

FIGURE 11.2.—Geologic map of Bullrun Creek and north end of Bullrun Mountain. Contour interval, 200 ft. Base from U.S. Geological Survey 1:24,000-scale quadrangles: Bullrun Rock, 1972 (photorevised 1983); Rail Gulch, Rastus Mountain, and Unity, 1972 (photorevised 1984).

TABLE 11.1.—*Compositions of olivine and orthopyroxene in peridotite from Bullrun Mountain*

[ppm, parts per million; tr, trace; ---, not determined]

Sample	Rock type	Olivine			Orthopyroxene		
		Forsterite (percent)	Ni (ppm)	Cr (ppm)	Enstatite (percent)	Ni (ppm)	Cr (ppm)
GC-81-126G	Dunite	91.9–92.4	1,070–1,100	tr	---	---	---
GC-81-139B	Dunite	90.8–91.8	1,070–1,130	tr	---	---	---
GC-81-6	Harzburgite	90.7–91.2	1,040–1,150	tr	91.0–95.3	220–260	1,840–1,960
GC-81-107	Harzburgite	90.8–91.4	900–1,050	tr	91.2–91.6	130–150	1,350–1,460

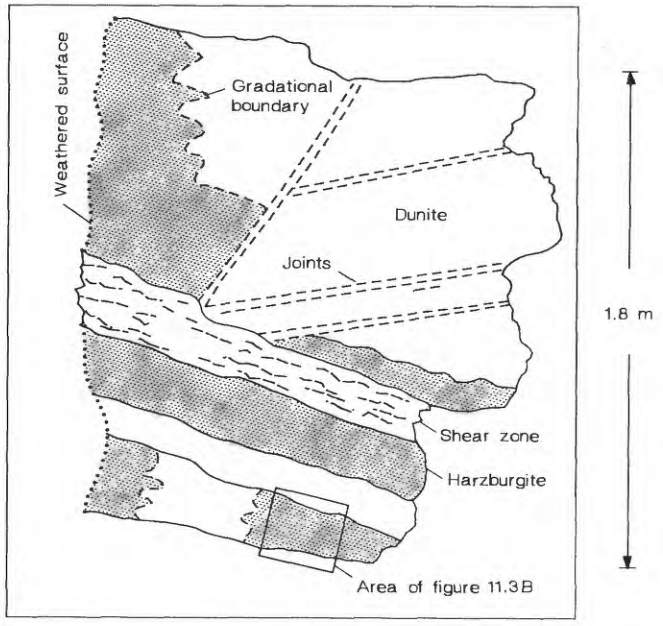

A

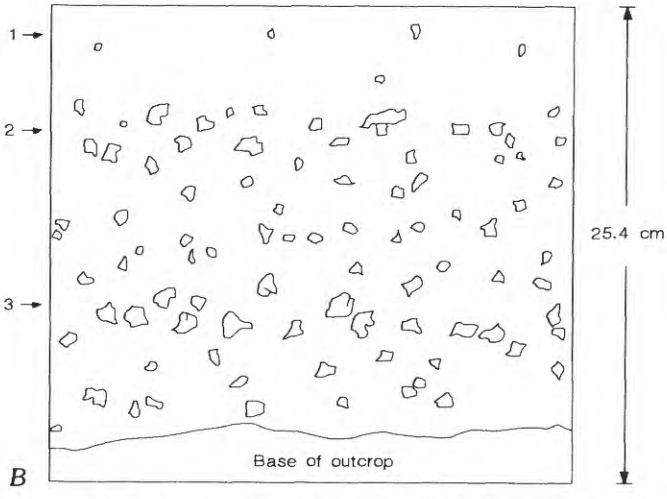

B

FIGURE 11.3.—Compositional banding in peridotite of Bullrun Mountain. *A*, Sketch of peridotite outcrop showing banding and shearing. *B*, Detail from figure 11.3*A*. 1, dunite; 2, 3, harzburgite. Large crystals shown are orthopyroxene; they lie in matrix of partially serpentinized olivine grains.

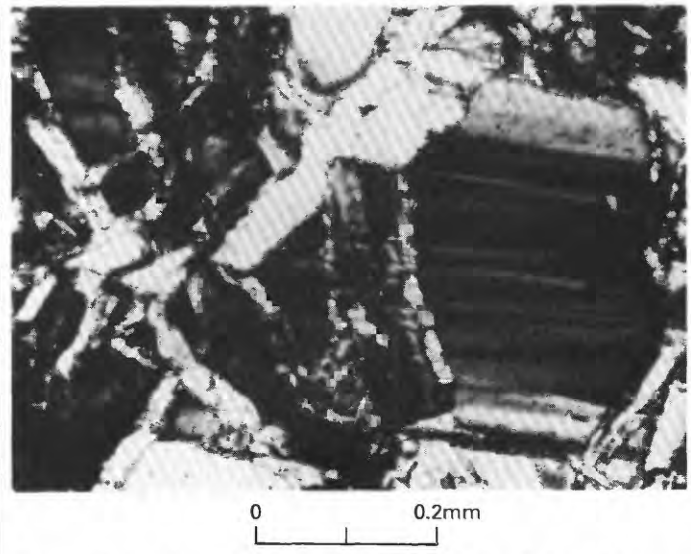

FIGURE 11.4.—Photomicrograph of kink bands in olivine. Note continuity from grain to grain across serpentine veinlets. Rock is dunite, viewed in crossed nicols.

Serpentinite is less resistant to erosion than the peridotite and forms a more subdued outcrop pattern; it often is seen only as loose debris on the ground surface. Various textural types of serpentinite may be correlated in a general way with the serpentinite's position relative to the main peridotite body (fig. 11.2). Most common is a distinctive banded serpentinite (fig. 11.5*A*) that forms broad zones striking east-west and dipping steeply northward in the peridotite of Bullrun Mountain. The banded serpentinite is also exposed over large areas to the east and west of the peridotite body (fig. 11.2). Brecciation, slickensides, and other evidence of shearing are generally absent in the banded serpentinite, which is composed of black bands of magnetite with a roughly planar orientation in a matrix of olive-green lizardite associated with some brucite (fig. 11.5*A*). Pseudomorphs of anthophyllite after orthopyroxene are present, and primary chromite remains, altered to magnetite around its margins. Locally, the banded serpentinite grades into a variety

that has a radiating acicular (felted) texture crosscut by trains of tiny magnetite grains.

Near the faulted southeastern margin of the peridotite body (fig. 11.2), the banded serpentinite grades into a mottled variety whose appearance is due to the accumulation of magnetite into irregular, slightly elongate clots (fig. 11.5*B*). Near the Thomason Mine (fig. 11.2), the mottled serpentinite is severely sheared and has a matrix of antigorite (Caffrey, 1982). Primary chromite is present, and some talc has formed; a small volume of a chlorite phase appears to be pseudomorphing orthopyroxene.

Talc-bearing serpentinite breccia is restricted to the faulted and hydrothermally altered southeastern mar-gin of the peridotite body, near the Thomason Mine (fig. 11.2). It contains cryptocrystalline silica derived from hydrothermal activity and talc derived from the silicic alteration of serpentine (Caffrey, 1982). An iron oxide stain and slickensides are common. An oval outcrop of serpentinite breccia about 50 ft long within the main body of peridotite, unrelated to faulting and containing fragments coated with cryptocrystalline magnesite and (or) dolomite, is suggestive of a breccia pipe.

A narrow zone of intensely sheared and fractured serpentinite is present along the poorly exposed intrusive contact with the granodiorite of Bullrun Creek and is believed to have resulted from contact metamorphism and faulting (Caffrey, 1982).

Timing of serpentinization relative to the peridotite emplacement remains elusive. The mottled and sheared serpentinite along the southeastern margin of the peridotite body is associated, at least in part,

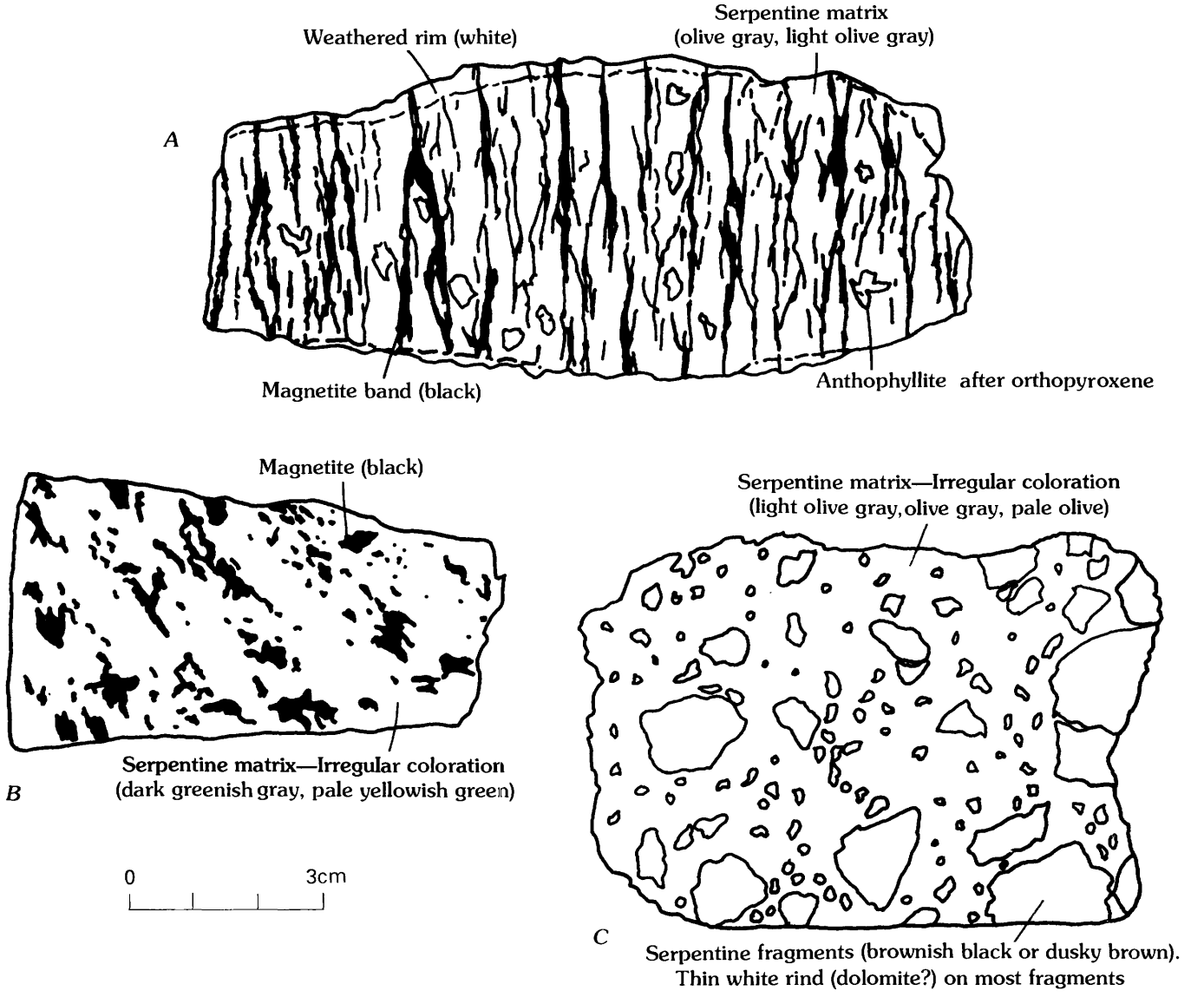

FIGURE 11.5.—Three main varieties of serpentinite. *A*, Banded serpentinite; *B*, mottled serpentinite; *C*, serpentinite breccia.

TABLE 11.2.—*Major- and trace-element analyses of peridotite from Bullrun Mountain and Mine Ridge*

[Analyses by X-ray-fluorescence spectroscopy, Washington State University (Hooper and Johnson, 1989). Major elements normalized on a volatile-free basis with 0.9 Fe expressed as FeO, 0.1 Fe expressed as Fe_2O_3, and Fe* equal to $FeO+Fe_2O_3$. ---, not determined]

	Dunite, Bullrun Mountain					Harzburgite, Bullrun Mountain									Mine Ridge		
Sample------	GC-1	TC-5	GC-7	BRUM-A	JB-81-34	GC-2	GC-3	GC-4	GC-6	GC-10	GC-12	BRUM-B	BRUM-E	BRUM-F	A15B	R-68	R-84
Major elements (weight percent)																	
SiO_2--------	44.88	44.29	46.48	43.01	45.69	47.56	46.61	45.94	46.45	46.51	46.68	47.92	46.72	48.93	48.52	46.44	50.58
Al_2O_3-------	.00	.01	.00	.00	.00	1.18	.63	.72	.23	.70	.51	.40	.50	.35	.19	.22	.36
TiO_2--------	.02	.02	.02	.02	.02	.02	.02	.02	.01	.02	.02	.03	.03	.03	.03	.02	.03
Fe*----------	9.78	9.53	9.25	9.39	10.10	9.01	10.04	9.78	9.46	9.53	10.02	9.54	9.70	9.76	11.04	9.99	10.21
MnO--------	.17	.16	.17	.15	.17	.15	.15	.16	.15	.15	.19	.15	.16	.15	.13	.17	.14
CaO --------	.08	.08	.64	.10	.67	1.03	.64	.36	.45	.55	.61	.59	1.10	.22	.07	.17	.10
MgO--------	45.03	45.89	43.38	47.31	43.30	41.01	41.89	43.01	43.23	42.49	41.92	41.34	41.77	40.54	40.01	42.94	38.56
K_2O --------	.04	.02	.04	.03	.03	.03	.02	.02	.01	.05	.05	.02	.02	.02	.01	.05	.02
Na_2O -------	.00	.00	.03	.00	.00	.01	.00	.00	.00	.00	.00	.00	.00	.00	.00	.00	.00
P_2O_5--------	.00	.00	.00	.00	.00	.00	.00	.00	.00	.00	.00	.00	.00	.00	.00	.00	.00
Trace elements (parts per million)																	
Ba----------	--	--	--	10	--	--	--	--	--	--	--	6	26	2	4	7	8
Cr----------	--	--	--	300	--	--	--	--	--	--	--	774	1,370	1,061	1,008	1,442	1,388
Cu----------	--	--	--	11	--	--	--	--	--	--	--	11	12	15	9	40	17
Nb----------	--	--	--	6	--	--	--	--	--	--	--	5	6	6	4	4	4
Ni----------	--	--	--	2,120	--	--	--	--	--	--	--	1,938	1,875	1,900	2,196	1,962	2,069
Sc----------	--	--	--	4	--	--	--	--	--	--	--	10	9	9	9	8	8
Sr----------	--	--	--	3	--	--	--	--	--	--	--	2	4	5	2	2	2
V----------	--	--	--	27	--	--	--	--	--	--	--	50	51	48	47	51	47
Y----------	--	--	--	1	--	--	--	--	--	--	--	1	1	1	1	1	1
Zn----------	--	--	--	70	--	--	--	--	--	--	--	70	68	70	69	101	93
Zr----------	--	--	--	4	--	--	--	--	--	--	--	4	4	4	4	4	4

with marginal faults and was probably formed during the tectonic emplacement of the peridotite body into the upper crust, or during the reactivation of those faults at a later period, or both. The presence of antigorite rather than lizardite in the mottled and sheared serpentinite also implies shear stress during formation of the mottled and sheared serpentinite and probably a higher metamorphic grade than that of the lizardite-bearing banded serpentinite (Coleman, 1977; Evans, 1977). We conclude that the mottled and sheared serpentinite was formed during peridotite emplacement at considerable depth by the recrystallization of the banded lizardite serpentinite. The banded serpentinite predates emplacement and was formed at considerable depths in an environment of low directed stress. This early serpentinization affected rocks that already possessed a metamorphic fabric and well-developed kink bands.

CHEMICAL COMPOSITION OF PERIDOTITE AND SERPENTINITE

Seventeen peridotite samples (dunites and harzburgites) and 20 serpentinite samples have been analyzed for major elements (tables 11.2 and 11.3). Seven peridotite samples were also analyzed for trace elements (table 11.2). The very low concentrations of Al_2O_3 and CaO in the peridotite samples reflect the almost total absence of clinopyroxene and plagioclase and place these rocks firmly in the MgO corner of the $MgO-CaO-Al_2O_3$ diagram, in the "metamorphic ultramafic rocks" field of Coleman (1977, p. 45). On an AFM diagram (fig. 11.6) the peridotite samples plot on the edge of the "metamorphic ultramafic rocks" field of Coleman (1977). The analyses support the mineralogical and textural evidence that the peridotite of Bullrun Mountain is residual mantle material formed by partial melting. The chemical composition of the peridotite body is similar to that of peridotites from Vourinos, Greece (Moores, 1969), Burro Mountain, Calif. (Coleman and Keith, 1971; Loney and others, 1971), Del Puerto, Calif. (Himmelberg and Coleman, 1968), and Point Sal, Calif. (Hopson and Frano, 1977). The peridotite of Bullrun Mountain has significantly less CaO than the clinopyroxene-bearing harzburgite of the Canyon Mountain Complex in the John Day basin about 70 km west of the Ironside Mountain inlier (Thayer, 1977).

Banded and mottled serpentinites (table 11.3) have Al_2O_3 values that imply they were derived from both

TABLE 11.3.—*Major-element analyses of serpentinite from Bullrun Mountain and Mine Ridge*

[All values in weight percent. Analyses by X-ray fluorescence spectroscopy, Washington State University (Hooper and Johnson, 1989). Major elements normalized on a volatile-free basis with 0.9 Fe expressed as FeO, 0.1 Fe expressed as Fe_2O_3, and Fe* equal to $FeO+Fe_2O_3$]

	Banded and mottled serpentinite							Contact-metamorphic serpentinite		
Sample	GC-11	JB-81-74	GC-8	GC-9	JB-81-32	JB-81-45	GC-150	GC-14	GC-15	GC-16
SiO_2	49.15	48.22	49.74	48.60	46.66	52.18	46.15	50.19	48.72	49.35
Al_2O_3	.49	.01	.86	.81	.74	.00	.00	.27	.00	.38
TiO_2	.02	.02	.02	.02	.02	.02	.02	.02	.02	.02
Fe*	9.25	11.01	9.74	11.11	9.76	10.88	8.42	8.74	10.22	10.21
MnO	.13	.15	.10	.07	.24	.19	.14	.12	.17	.14
CaO	.09	.08	.03	.06	.59	.33	4.65	1.39	.38	.85
MgO	40.84	40.44	39.49	39.31	41.98	36.28	40.46	39.28	40.47	38.91
K_2O	.03	.02	.02	.02	.01	.03	.01	.02	.02	.04
Na_2O	.00	.05	.00	.00	.00	.08	.14	.00	.00	.10
P_2O_5	.00	.00	.00	.00	.00	.00	.00	.00	.00	.00

	Contact-metamorphic serpentinite—Continued		Sheared talc-bearing serpentinite							
Sample	GC-17	GC-18	JB-81-33	GC-31	GC-28	GC-29	A-24	A-15a	R-03	R-61
SiO_2	48.42	48.67	49.43	59.53	68.11	61.54	58.44	50.37	49.98	47.99
Al_2O_3	.00	.00	.81	.33	.00	.28	.05	.76	.76	.46
TiO_2	.01	.02	.02	.02	.01	.02	.04	.03	.04	.02
Fe*	10.73	10.00	8.90	7.15	11.31	12.51	6.90	9.44	10.23	9.89
MnO	.09	.18	.10	.05	.01	.02	.10	.13	.14	.12
CaO	.15	.07	.05	7.15	.10	.13	.16	.05	.09	.06
MgO	40.59	41.05	40.67	25.35	20.43	25.45	34.27	39.21	38.7	41.40
K_2O	.01	.02	.01	.02	.01	.01	.04	.01	.05	.04
Na_2O	.00	.00	.00	.38	.02	.02	.00	.00	.00	.00
P_2O_5	.00	.00	.00	.02	.00	.02	.00	.00	.00	.00

dunite and harzburgite. In the less serpentinized peridotites, CaO abundances are generally lower and FeO/MgO and SiO_2/MgO values are significantly higher, suggesting loss of Ca and gain of Fe and Si relative to Mg in the serpentinization process (Barnes and O'Neill, 1969; Coleman, 1977). Most serpentinite from Mine Ridge is similar to the banded and mottled serpentinite from Bullrun Mountain. Sheared, talc-bearing varieties occur in fault zones, and the more brecciated varieties tend to have higher SiO_2 and lower MgO concentrations than do the unbrecciated varieties.

The narrow zone of serpentinized peridotite adjacent to the granodiorite intrusion is not noticeably different in chemical composition from the banded and mottled serpentinite varieties.

The serpentinization process that formed the banded and mottled serpentinite appears to have occurred at constant volume with loss of MgO, because SiO_2/MgO is generally higher in the serpentinite than in the peridotite whereas SiO_2/FeO is about the same in both rock types (fig. 11.7). These relations imply that MgO has decreased and SiO_2 and FeO have remained unchanged during serpentinization. We conclude that water was added and MgO removed according to the following reaction:

$$2Mg_2SiO_4 + 2H_2O \rightarrow Mg_3Si_2O_5(OH)_4 + MgO$$
(olivine) (added) (serpentine) (removed)

The scarcity of brucite in the serpentinite supports this conclusion, implying that the following reaction, which requires an increase in volume (Hostetler and others, 1966; Thayer, 1966), is not pertinent:

$$2Mg_2SiO_2 + 3H_2O \rightarrow Mg_3Si_2O_5(OH)_4 + Mg(OH)_2$$
(olivine) (added) (serpentine) (brucite)

MELANGE OF MINE RIDGE

West of the granodiorite of Bullrun Creek (fig. 11.2) the ultramafic rocks form the eastern slopes of Mine

Ridge. From the crest of the ridge westward they are increasingly serpentinized, dismembered into smaller pods, and mixed with numerous pods of the more resistant ribbon chert, schists, and andesitic "knockers." We here refer to this assemblage as the melange of Mine Ridge (fig. 11.8). The ultramafic rocks of the melange (dunite, harzburgite, and serpentinite) are similar to, and an obvious continuation of, the main peridotite body to the east. But they are extensively sheared, a process accompanied by the formation of talc and substantial amounts of cryptocrystalline silica and magnetite. Serpentinite veins are locally tightly folded.

METAMORPHOSED GABBRO AND BASALT

Metamorphosed gabbro, basalt, and plagiogranite have been collected from poor exposures on the northeastern slopes of Mine Ridge (fig. 11.2; Beane, 1984). Metamorphosed basalt was found only as loose samples. The metamorphosed gabbro forms rounded boulder ledges that have a weak foliation and are elongate in an east-northeast direction. This direction is approximately parallel to the long axes of the knockers in the melange and many of the more obvious joints and fracture planes. Compositional layering was not observed in the gabbro, but wide variations in modal mineral proportions in samples from the same outcrop imply its presence. Many samples of both gabbro and basalt retain their igneous texture; others have been partly converted to a metamorphic fabric.

Primary mineralogy still recognizable in the metamorphosed gabbro includes cloudy plagioclase feldspar (40–60 modal percent) and augite (20–30 modal percent). Augite is partially replaced by green hornblende along margins and cleavages. Primary hornblende, subordinate to augite, occurs in some samples. Chlorite is rare. Serpentine minerals are commonly intergrown with tremolite and clinozoisite, the last replacing plagioclase. Opaque minerals or their alteration products are rare to absent. Poikilitic textures were not observed. Both mineralogy and texture suggest that the metamorphosed gabbro originated as an adcumulate.

Basaltic rocks are scarcer than gabbro, and pillow structures have not been observed. One sample has an aphyric plagioclase-hornblende composition; its original intergranular to subophitic igneous texture is still apparent, although the pyroxene has been pseudomorphed by blue-green hornblende. The metamorphic mineral assemblage is dominated by horn-

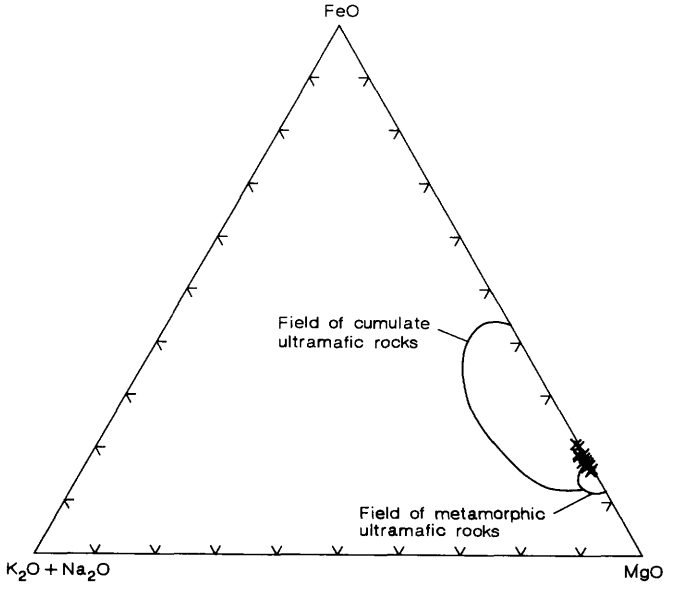

FIGURE 11.6.—Alkali (Na_2O+K_2O)-FeO-MgO diagram of peridotite at Bullrun Mountain and Mine Ridge. Cumulate and metamorphic fields from Coleman (1977).

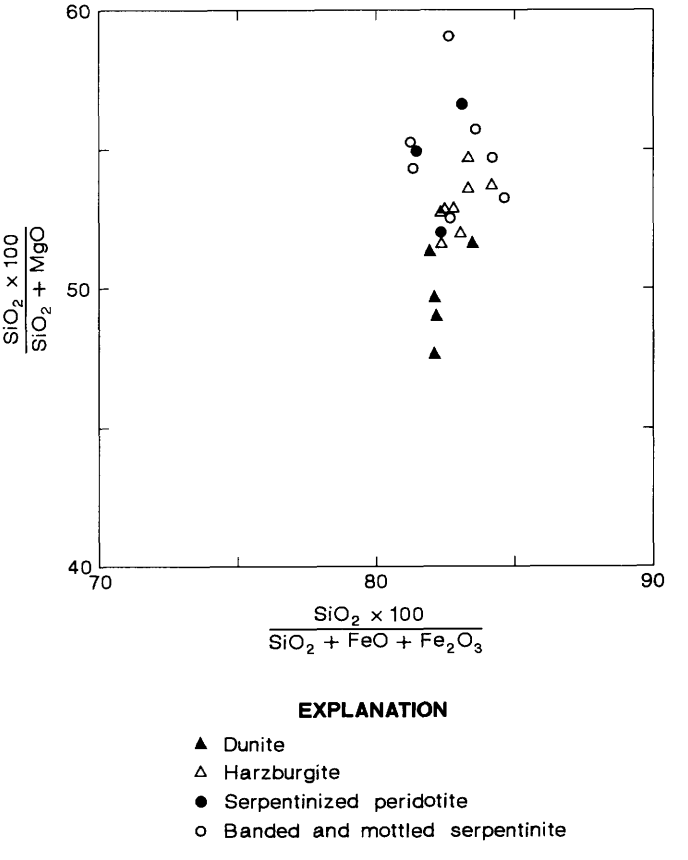

FIGURE 11.7.—Silicon-magnesium and silicon-iron variation in peridotite and serpentinite of Ironside Mountain inlier.

blende, sodic andesine, and opaque minerals, and also contains epidote, chlorite, and calcite.

Major- and trace-element analyses of gabbro and basalt samples are listed in table 11.4. The adcumulate nature of the gabbro samples is reflected in the exceptionally low and variable concentrations of incompatible elements (TiO_2, K_2O, P_2O_5, Rb, Y, and Zr) in contrast to the high but equally variable abundances

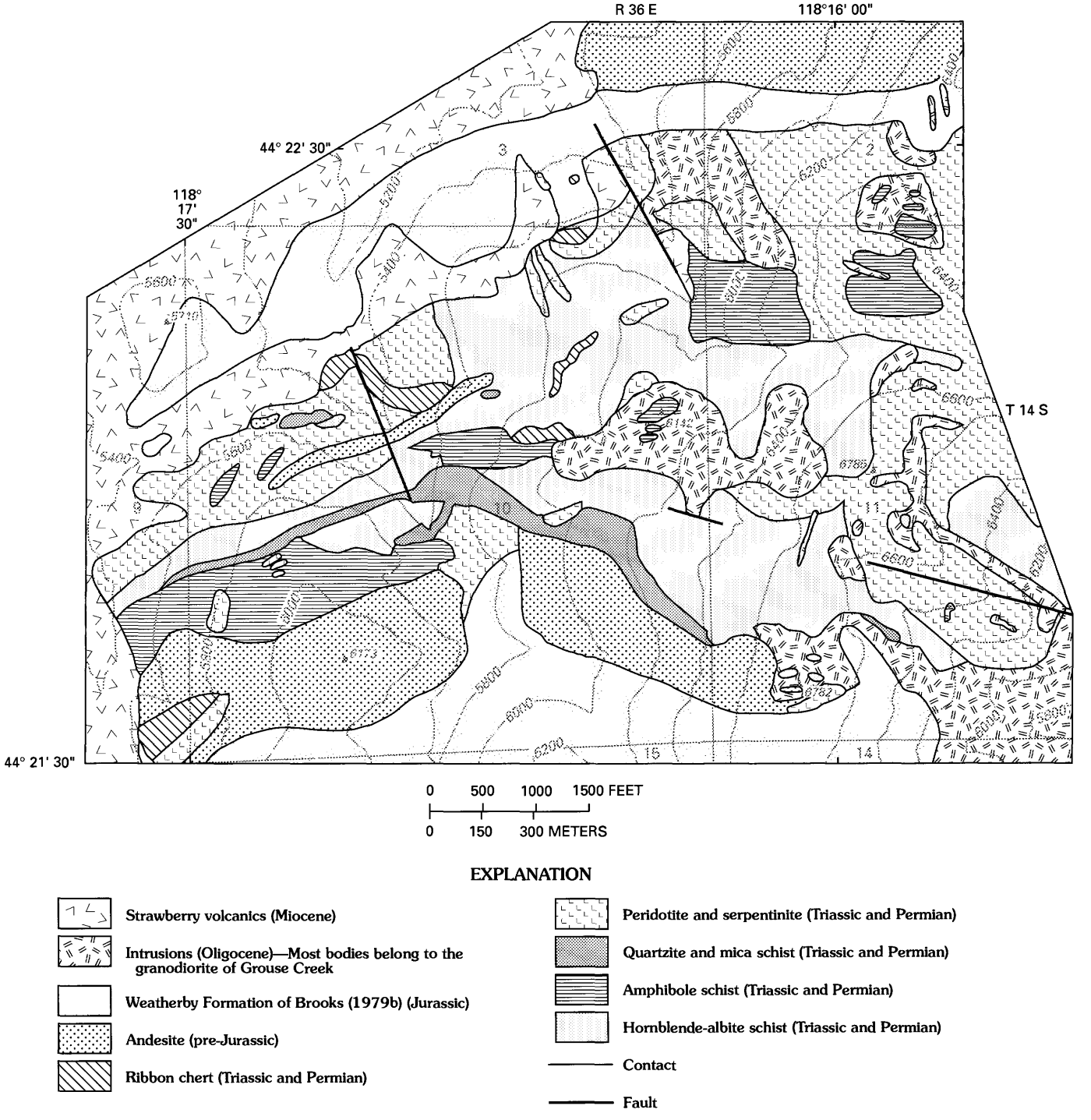

FIGURE 11.8.—Geologic map of melange of Mine Ridge and adjacent units. Melange of Mine Ridge includes the andesite, ribbon chert, quartzite and mica schist, amphibole schist, and hornblende-albite schist units, and the part of the peridotite-and-serpentinite unit that lies west of Mine Ridge. Contour interval, 200 ft. Section numbers for township and range are shown within map area. Base from U.S. Geological Survey 1:24,000-scale quadrangles: Bullrun Rock, 1972 (photorevised 1983), and Rail Gulch, 1972 (photorevised 1984).

TABLE 11.4.—*Major- and trace-element analyses of gabbro, basalt, plagiogranite, and related schists of the melange of Mine Ridge*

[Analyses by X-ray-fluorescence spectroscopy, Washington State University (Hooper and Johnson, 1989). Major elements normalized on a volatile-free basis with 0.9 Fe expressed as FeO, 0.1 Fe expressed as Fe_2O_3, and Fe* equal to FeO+Fe_2O_3. ---, not determined]

	Metamorphosed gabbro				Metamorphosed basalt and andesite			Hornblende schist		Plagiogranite	
Sample ---	JB-81-03	JB-81-42A	JB-81-42B	JB-81-82	JB-81-BR1	JB-82-120	JB-81-86B	A-31	A-52	JB-81-83B	JB-81-84
Major elements (weight percent)											
SiO_2 -------	48.21	44.39	47.68	47.94	51.22	50.51	58.41	49.79	49.57	75.10	66.89
Al_2O_3 -----	16.40	26.13	16.91	17.49	15.17	16.24	17.88	13.12	16.04	13.15	13.87
TiO_2 -------	.24	.13	.32	.89	1.67	.96	1.43	1.84	1.55	.27	.46
Fe*---------	5.50	3.71	7.66	9.29	11.20	10.63	6.56	13.29	10.72	3.36	6.31
MnO -------	.15	.09	.16	.20	.21	.19	.08	.23	.17	.09	.12
CaO--------	14.46	17.95	14.04	12.02	10.01	11.79	7.29	11.08	10.68	1.19	5.43
MgO -------	11.62	5.49	10.27	9.31	7.33	6.28	3.40	7.68	8.24	.66	3.09
K_2O--------	.29	.09	.32	.10	.11	.35	.76	.52	.44	.19	.14
Na_2O------	3.08	1.97	2.59	2.73	2.94	2.98	3.89	1.66	2.40	5.94	3.61
P_2O_5-------	.04	.06	.03	.03	.14	.09	.30	.16	.15	.06	.09
Trace elements (parts per million)											
Ba ----------	---	---	---	---	---	---	---	21	67	40	43
Cr ----------	209	---	---	---	62	---	---	133	169	1	61
Cu ----------	14	---	---	---	56	---	---	79	17	6	14
Nb----------	6	---	---	---	18	---	---	21	17	2	4
Ni ----------	117	---	---	---	66	---	---	110	138	13	39
Sc ----------	52	---	---	---	40	---	---	46	40	12	14
Sr ----------	182	---	---	---	110	---	---	103	158	65	203
V ----------	176	---	---	---	286	---	---	404	294	16	85
Y ----------	7	---	---	---	37	---	---	48	32	74	62
Zn ----------	69	---	---	---	86	---	---	110	79	67	66
Zr----------	8	---	---	---	30	---	---	20	18	(10)	(9)
Rb----------	7	---	---	---	6	---	---	---	---	5	6

of such oxides as Al_2O_3, CaO, and MgO, which are concentrated in the cumulate phases plagioclase and augite. The basalt samples have higher concentrations of incompatible elements than the gabbros and presumably have compositions closer to the original liquid from which the gabbro cumulates were derived. Both basaltic rocks analyzed are quartz normative. It may be noted in passing that the two hornblende schist samples of the schistose rocks of Mine Ridge (see below) have major- and trace-element compositions similar to those of the basalt (table 11.4).

PLAGIOGRANITE

A minor summit on the north spur of Mine Ridge is underlain by medium- to coarse-grained, equigranular, quartz-rich intrusive rock (fig. 11.2). Most outcrops are deeply weathered. Samples contain equal amounts of quartz and albite in which opaque minerals, biotite, chlorite, muscovite, and zircon are present as accessories. Primary ferromagnesian minerals have been largely replaced, but a single crystal of augite, rimmed by biotite, was noted. Zones where this plagiogranite is composed of finer grained quartz and albite surrounded by mafic alteration minerals are interpreted as due to cataclastic shear. Bent albite twin lamellae and strain-induced extinction in quartz grains attest to the deformation of these rocks.

Two analyses of plagiogranite are listed in table 11.4. The analyses reflect the samples' low K_2O and high Na_2O concentrations and so emphasize their tonalitic (trondhjemitic) affinities. Their rare-earth elements (REEs) (table 11.5; fig. 11.9*A*) are depleted in light rare-earth elements (LREEs) and have chondrite-normalized patterns similar to those of the basic rocks of Mine Ridge and the basic and silicic

TABLE 11.5.—*Abundances of rare-earth elements in rocks of the Ironside Mountain inlier*

[All values in parts per million. Analyses by inductively coupled plasma spectrometry, Kings College, London. Analyst, P.R. Hooper]

Rock type	Peridotite	Hornblende schist	Quartz-mica schist	Plagiogranite		Pre-Jurassic andesite	Strawberry Volcanics	Granodiorite of Grouse Creek
Sample	Brum-A	A-31	A-02	JB-8183B	JB-8184	A-33a	A-28	MH-51
La	<0.3	4.45	18.89	2.05	3.72	23.09	43.69	13.10
Ce	<.5	11.97	43.73	6.40	9.78	42.80	84.91	23.97
Pr	<.5	2.12	4.91	1.29	1.96	5.77	10.63	3.27
Nd	<.2	11.68	21.95	8.27	11.46	23.07	43.79	13.07
Sm	<.1	4.16	4.86	4.09	4.51	4.30	7.51	2.45
Eu	<.05	1.44	1.17	1.64	2.09	1.37	2.12	.79
Gd	<.2	5.74	4.77	7.57	6.87	3.76	5.62	2.30
Dy	<.1	7.06	4.90	9.95	7.01	3.04	3.69	2.19
Ho	<.05	1.51	.96	2.30	1.58	.71	.86	.56
Er	<.5	4.51	2.93	6.59	4.14	1.72	1.93	1.36
Yb	<.1	4.32	2.86	5.33	3.25	1.36	1.43	1.26
Lu	<.02	.67	.45	.83	.54	.20	.20	.18

rocks of Canyon Mountain (lat 44°20' N., long 118°53' W.; Gerlach and others, 1981).

SCHISTOSE ROCKS OF MINE RIDGE

The schistose rocks of Mine Ridge include four dominant rock types: hornblende-garnet schist, hornblende-albite schist, quartz-mica-garnet schist, and quartzite. Of these the hornblende schist is by far the most abundant. All these rock types are poorly exposed and form isolated pods in the serpentinite matrix of the melange (fig. 11.8). Some pods include more than one rock type; consistent lithologic relations in the pods, together with the direction in which beds young as defined by graded beds in the quartzite, suggest an original stratigraphic sequence (Scrivner, 1983). At the base, overlying the ultramafic materials, is the hornblende-garnet schist; it is overlain by hornblende-albite schist, quartz-mica-garnet schist, and quartzite on top. Contacts, where observed, are typically steep and strike east-northeast; the whole sequence apparently is overturned to the north.

The modal mineralogy of the schists is listed in table 11.6. The hornblende-garnet schist is a dense dark-green rock containing aligned elongate hornblende crystals and conspicuous equant garnet porphyroblasts. Sphene is present as inclusions in both the major phases. Primary sphene forms fractured euhedral prismatic grains with metamorphic euhedral overgrowths. Quartz and epidote fill fractures in the garnet.

Hornblende-albite schist contains green layers of fine- to medium-grained hornblende alternating with white albite layers 2±1 mm thick. The layers are clearly metamorphic, paralleling a penetrative cleavage that includes the orientation of white mica in other lithologies. Where the boundaries between rock units (S_0) are observed, the layering and cleavage (S_1) are essentially parallel to them. Hornblende grains are also aligned in this plane (S_0-S_1). Garnet is absent, and the albite has a dusting of sericite and inclusions of epidote.

The quartz-mica-garnet schist and the quartzite tend to occur together with gradational contacts. The schist is a well-foliated, buff-colored rock in which orientated muscovite grains cause the penetrative cleavage (S_1). Quartz forms layers (S_0-S_1) that pinch and swell between muscovite layers, the latter including pale pink garnet porphyroblasts (table 11.6). Epidote porphyroblasts and elongate grains of euhedral zircon are associated with mica-garnet-hornblende layers.

The quartzite is 95 percent quartz with wavy extinction and ragged crystal margins. Muscovite, sphene, and garnet occur as accessories closely associated with each other; the mica defines a cleavage cut at a high angle by quartz veins.

The quartzite contains graded beds and clearly had a sedimentary origin. The hornblende schists, in contrast, have basaltic compositions (table 11.4), and these rocks probably represent highly metamorphosed and deformed igneous rocks, rather than calcareous sediments as suggested by Lowry (1968). The quartz-mica-garnet schist has an intermediate composition that

may reflect an origin from more evolved igneous rocks or, conceivably, from physical mixing between the basaltic units and the overlying psammitic material during intense metamorphism and deformation.

The various schistose units are tightly folded, and three fold phases are apparent in some outcrops (fig. 11.10). The metamorphic foliation and associated mineral alignment represent the earliest penetrative

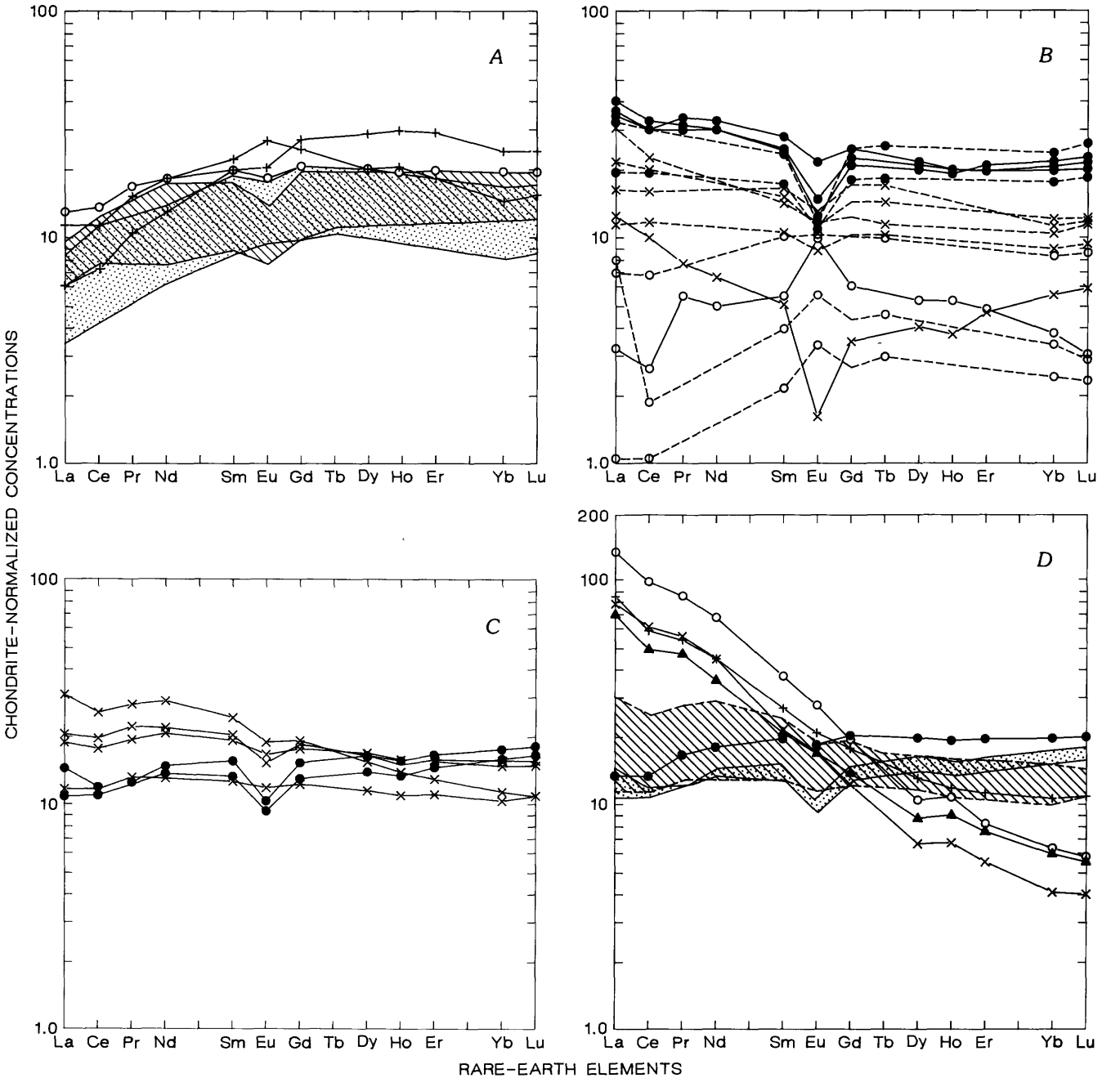

FIGURE 11.9.—Chondrite-normalized rare-earth-element (REE) concentrations in igneous rocks of Blue Mountains province. *A*, Basic (open circles) and granitic (crosses) rocks of melange of Mine Ridge. Basic rocks (shaded area) and plagiogranite and keratophyre (diagonal lines) from Canyon Mountain Complex (Gerlach and others, 1981). *B*, Sparta complex of Phelps (1979). Solid lines, this paper; dashed lines, Phelps (1978). Dots, plagiogranite; x's, diorite; open circles, gabbro. *C*, Representative samples from Seven Devils Group (Hooper and Scheffler, unpub. data, 1983). Dots, Permian; x's, Triassic. *D*, REE concentrations in pre-Jurassic andesite of melange of Mine Ridge (triangles) and other calc-alkaline volcanic rocks of eastern Oregon. Open circles, andesite of Strawberry Volcanics, Mine Ridge; x's, Permian Hunsaker Creek Formation, Seven Devils Group; crosses, andesite of Strawberry Volcanics near Baker City, Oreg.; dots, hornblende schist of melange of Mine Ridge; diagonal lines, Triassic rocks of Seven Devils Group; vertical lines, Permian rocks of Seven Devils Group (fig. 11.9*C*).

TABLE 11.6.—*Modal mineralogy of the schistose rocks of Mine Ridge*

[All values in volume percent. tr, trace; ---, not observed]

	Hornblende-garnet schist	Hornblende-albite schist		Quartz-mica-garnet schist
	Sample A-31	Sample A-52	Average (9 samples)	Average (2 samples)
Quartz	tr	tr	0–35	5–40
Plagioclase	tr	[1]30	[1]10–40	0–10
Hornblende	80	50	35–70	0–25
Orthoclase	---	---	0–5	---
Muscovite	---	tr	0–5	20–30
Almandine	5	---	---	5–20
Zircon	tr	---	---	0–10
Sphene	tr	tr	0–1	tr
Allanite	---	---	tr	---
Pyrite	---	tr	0–10	---
Serpentine	tr	---	0–1	---
Chlorite	tr	tr	0–30	---
Epidote	15	20	0–20	0–15
Opaque minerals	tr	tr	tr	tr
Goethite	---	---	0–5	tr

[1]All plagioclase in these samples is albite.

fabric (S_1), with which the original premetamorphic lithologic boundaries (S_0) have been brought into parallelism (S_0-S_1). The earliest folds recognized in outcrop (F_1) have a steeply dipping, predominantly east-northeast-striking penetrative axial-planar cleavage (S_1). The F_1 folds are isoclinal with axes (L_1) approximately parallel to the dip of the axial planes (figs. 11.11, 11.12*A*). The steep S_0-S_1 plane is ubiquitous throughout the schistose rocks of Mine Ridge.

Folds of the second phase (F_2) vary in style from tight folds with thickening of layers around the hinge zones (fig. 11.10) to open box folds with steep but variable S_2 (fig. 11.11). S_2 normally cuts across S_0-S_1 at moderate to large angles, but L_1 and L_2 are approximately parallel (fig. 11.12*C*). The typical interference pattern of F_2 and F_1 is shown in fig. 11.11*C*. The main fabric (S_0-S_1) is also crenulated by F_3 folds (fig. 11.12*D*) whose axial planes lie at a high angle to S_0-S_1. In thin section, most minerals are seen to be bent by F_3. Chlorite fills fractures in epidote perpendicular to the S_0-S_1 surface and is orientated parallel to S_3. Evidence of slip along some S_3 surfaces includes fracturing of pyrite developed in the slip planes where the pyrite crystals are also flattened and partly altered to goethite.

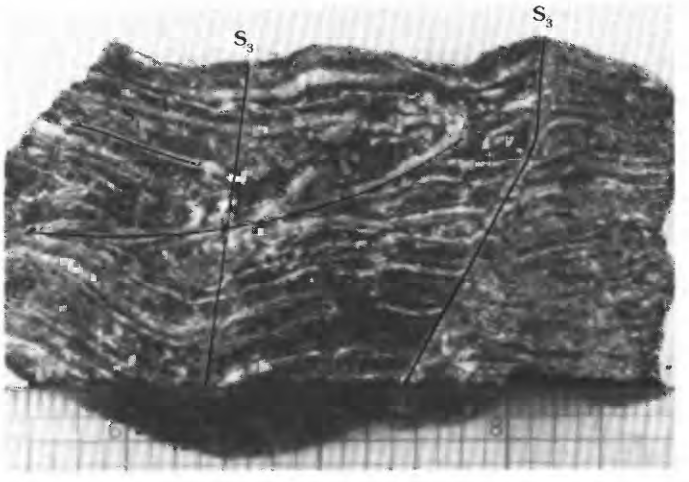

FIGURE 11.10.—Three fold phases in hornblende-albite schist from melange of Mine Ridge. S_1, S_2, and S_3 are axial-planar surfaces produced, respectively, by F_1, F_2, and F_3. S_1 (to which S_0 is now parallel) is tightly folded by F_2 and crenulated by an irregularly oriented F_3. Scale in inches.

RIBBON CHERT

If the apparent stratigraphic sequence of the schistose rocks of Mine Ridge, discussed above, is real, then the ribbon chert lies above the schists, but

the nature of the melange prevents this relationship from being demonstrated unequivocally. The chert is composed of alternating layers of fine-grained chocolate-brown chert and argillite, 1–3 cm thick. Fine-grained quartz forms about 95 percent of the chert, and carbonate forms up to 5 percent. Despite careful search no radiolarians have been found. The cherts are similar to those described from other parts of the central melange terrane of northeastern Oregon (Elkhorn Ridge Argillite, cherts of Vinegar Hill, and so on; Gilluly, 1937; Ashley, 1966; Mullen, 1979).

The layers are folded by a single set of overturned, moderately open to close, asymmetric chevron folds. Axial planes strike east-northeast and dip south at moderate angles; the fold axes plunge southeast at moderate angles.

The single set of folds lacks an axial-planar cleavage. The folds in the chert differ in style from both

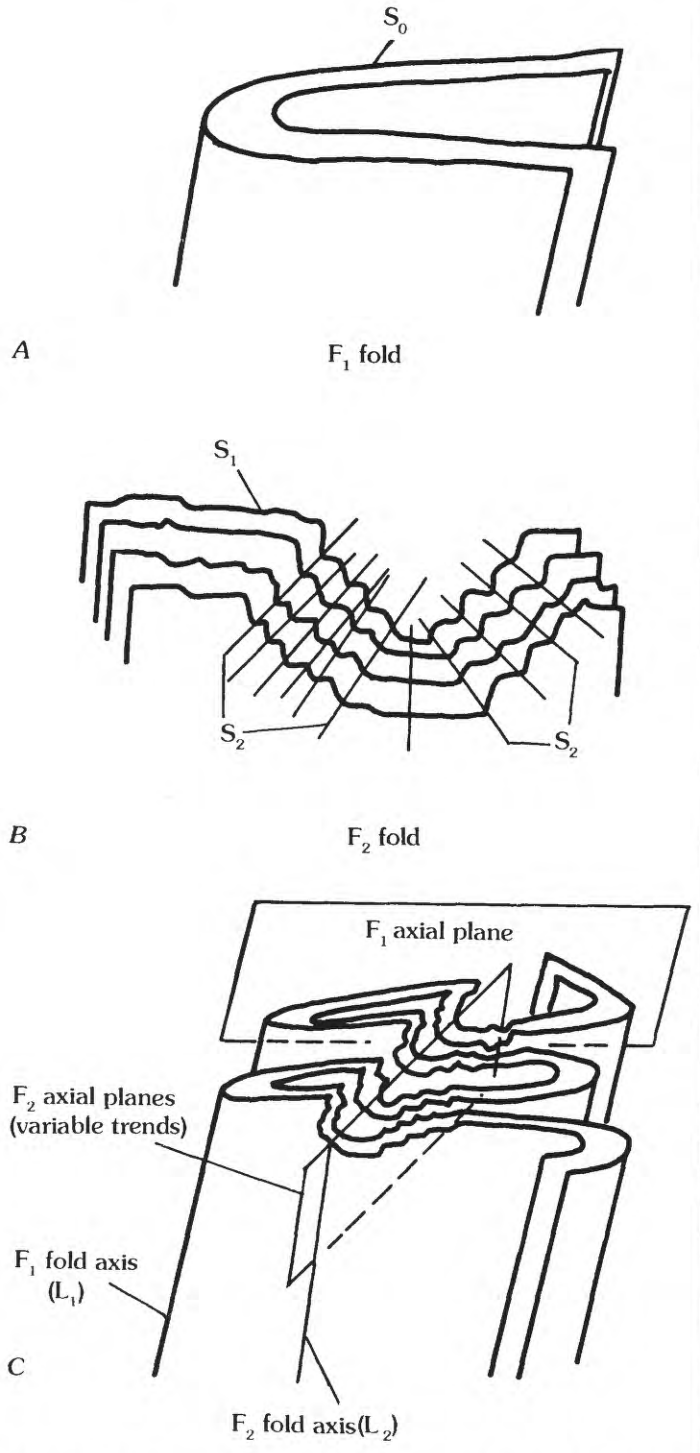

FIGURE 11.11.—Diagram to illustrate relations between F_1 and F_2 folds in melange of Mine Ridge. *A*, Bedding (S_0) folded by F_1. *B*, S_1 axial-planar surfaces folded by F_2. S_2 axial-planar surfaces have variable orientations. *C*, Although F_1 and F_2 axial planes generally intersect at moderate to large angles, F_1 and F_2 fold axes are approximately parallel.

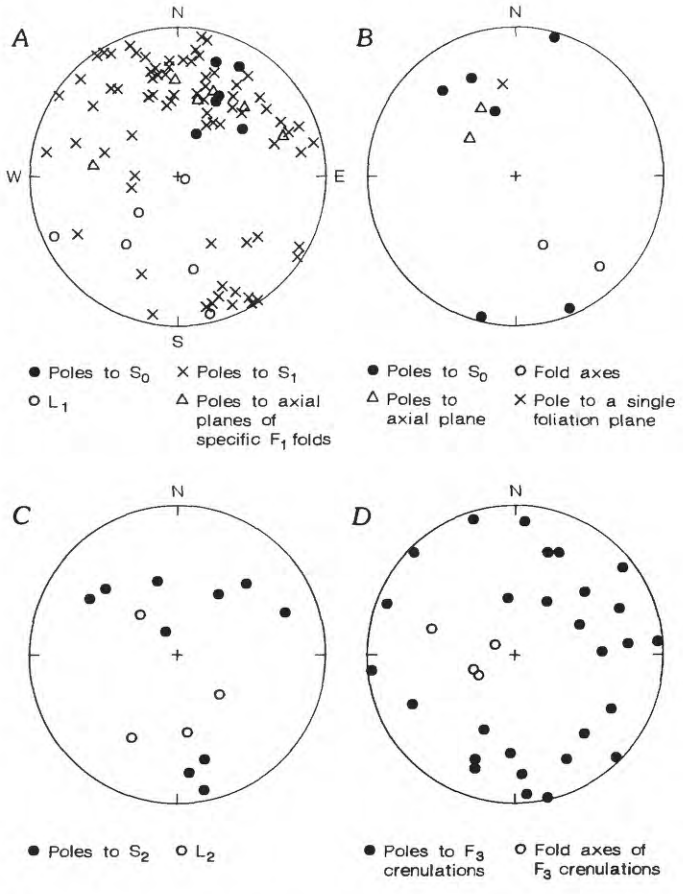

FIGURE 11.12.—Lower-hemisphere, equal-area projections of structural data for the schistose rocks of Mine Ridge. S_0, bedding planes; S_1, foliations axial planar to first-generation folds (F_1); L_1, F_1 fold axes; B1, poles to axial planes of specific F_1 folds; S_2, axial planes to second-generation folds (F_2); L_2, F_2 fold axes; F_3, third-generation folds. *A*, Bedding planes and F_1 folds in schistose rocks of Mine Ridge. *B*, Single fold set in ribbon chert. *C*, F_2 folds in schistose rocks of Mine Ridge. *D*, Crenulations (F_3) in schistose rocks of Mine Ridge.

TABLE 11.7.—*Major- and trace-element analyses of pre-Jurassic volcanic rocks, quartz-mica-garnet schist, chlorite schist, and ribbon chert from the melange of Mine Ridge*

[Analyses by X-ray fluorescence, Washington State University (Hooper and Johnson, 1989). Major elements normalized on a volatile-free basis with 0.9 Fe expressed as FeO, 0.1 Fe expressed as Fe_2O_3, and Fe* equal to $FeO+Fe_2O_3$]

	Pre-Jurassic volcanic rocks				Quartz-mica-garnet schist	Chlorite schist	Ribbon chert
Sample	A-15	AD-01	AD-04	A-33a	A-02	A-08a	RC
Major elements (weight percent)							
SiO_2	47.93	59.35	69.31	55.98	73.08	52.43	96.01
Al_2O_3	15.36	17.37	11.20	16.75	11.24	6.06	2.13
TiO_2	.63	.89	.69	1.31	.71	.50	.09
Fe*	9.33	9.54	8.08	7.15	7.11	8.75	.41
MnO	.14	.17	.16	.12	.32	.28	.07
CaO	11.18	5.63	6.84	7.51	2.21	9.32	.00
MgO	12.24	3.42	2.50	5.83	2.48	21.83	.44
K_2O	1.11	1.29	.20	1.34	1.71	.04	.67
Na_2O	1.78	2.21	.89	3.66	1.02	.75	.17
P_2O_5	.29	.19	.12	.35	.13	.04	.01
Trace elements (parts per million)							
Ba	486	852	480	499	364	10	134
Cr	499	68	56	104	66	630	34
Cu	127	74	91	61	96	30	23
Nb	15	14	12	30	10	9	2
Ni	356	55	54	87	87	826	19
Sc	37	36	28	23	22	20	3
Sr	591	90	38	1,132	73	9	11
V	204	240	209	204	144	176	19
Y	17	28	24	20	32	12	4
Zn	70	100	78	84	95	70	19
Zr	50	51	34	118	26	11	16

F_1 and F_2 folds in the schists; these differences probably reflect the chert's thin alternating layers of contrasting competence rather than a different stress regime.

PRE-JURASSIC VOLCANIC ROCKS

The melange of Mine Ridge also includes large, relatively coherent blocks of massive, dark-green, fine-grained volcanic rocks. The blocks are elongated east-west to northeast-southwest, parallel to the gross structural trend of the melange. Most are aphyric flows, although some phenocrysts of olivine and augite, and more rarely plagioclase, are present. In the stratigraphic framework described above, these rocks appear to lie stratigraphically above the schists, but their age relative to the ribbon cherts is obscure.

These predominantly andesitic volcanic rocks are surprisingly fresh. They lack the penetrative deformation of the schistose rocks of Mine Ridge, but contain many discrete shear planes. Original textures are generally well preserved but are modified locally by a metamorphic fabric that includes mortar textures and triple junctions between grains. Plagioclase ($An_{50\pm10}$) is bent and altered to sericite and epidote.

Chemical analyses (table 11.7) show that the volcanic rocks range in composition from olivine basalt, through andesite, to (rare) rhyolite. Up to 30 modal percent hypersthene may be present. Olivine and augite dominate in some samples, hypersthene and pigeonite in

others. Opaque minerals are relatively scarce. Secondary minerals include quartz, epidote, and hornblende, and traces of chlorite, sericite, sphene, calcite, and goethite. The rhyolite has a cataclastic texture and may have formed from a silicic protolith or may be derived from a more mafic parent silicified in the metamorphic process.

It is not clear whether these volcanic rocks have suffered less deformation than the schistose rocks of Mine Ridge, or whether they have been shielded from the same deformation by their more massive form. The number of analyses available is not adequate to fully characterize the group, but the wide range in major- and trace-element compositions, their LREE enrichment (fig. 11.9*D*), and their original mineralogy suggest a calc-alkaline affinity.

ORIGIN OF THE ROCKS OF THE BAKER TERRANE, IRONSIDE MOUNTAIN INLIER

The chemical composition, the mineralogy, and the texture of the dunite and harzburgite that constitute the peridotite body forming the north end of Bullrun Mountain all support the thesis that these rocks represent the residuum of partial melting in the mantle. Serpentinization of the peridotite to form banded and mottled serpentinite occurred without production of significant brucite, but with loss of magnesium and consequently little change in volume. This process occurred at depth in peridotite that had already been deformed. Subsequent injection of the partially serpentinized body into the upper crust along major fault planes and the formation of the melange were accompanied by additional serpentinization involving severe shear and an increase in SiO_2.

The much smaller volumes of cumulate gabbro, basalt, and plagiogranite are best explained as crystallization products derived from the melt produced in the same partial melting process. Pillow basalts and a basic dike swarm are missing from the complex, as they are from both the Canyon Mountain Complex (Thayer, 1977) and the (informal) Sparta complex of Phelps (1979) and Almy (1977). Their absence from all three complexes probably means that they were never formed. Earlier workers (for example, Gerlach and others, 1981) use the absence of pillow basalts and basic dike swarms as evidence that the ophiolitic rocks of northeastern Oregon originated at the base of an island-arc system rather than at a midocean ridge. This argument is equally applicable to the rocks of the Ironside Mountain inlier.

Chondrite-normalized patterns of the rare-earth elements (REEs) of the Ironside Mountain ophiolitic rocks are particularly revealing when compared to those of the Canyon Mountain Complex and the Sparta complex (fig. 11.9). The REE patterns for these two complexes are fundamentally different from each other. All samples from the Canyon Mountain Complex, gabbro through basalt to plagiogranite and keratophyre, have essentially similar patterns of light-rare-earth-element (LREE) depletion, usually accompanied by a well-marked negative europium anomaly (fig. 11.9*A*).

The REE data from the Sparta complex (Phelps, 1978; P.R. Hooper, unpub. data, 1984; fig. 11.9*B*) appear to divide these rocks into two groups: (1) gabbro with LREE depletion and a positive europium anomaly and (2) diorite and plagiogranite with mild LREE enrichment and a strong negative europium anomaly. It is possible that the two patterns represent cumulates and residual magmas of a parent with an almost flat REE pattern at a value ten times the chondrite value. Alternatively, the two patterns may represent the products of two mantle sources with different degrees of LREE depletion. Whichever interpretation is favored, both patterns are distinct from the single pattern displayed by the rocks of the Canyon Mountain Complex. Three chondrite-normalized REE profiles from Mine Ridge, one for a basic rock and two for plagiogranite, clearly resemble the pattern from the Canyon Mountain Complex (fig. 11.9*A*). We conclude that the ophiolitic rocks of the Ironside Mountain inlier are most likely the lateral equivalents of the Canyon Mountain Complex and may, therefore, be assumed to have the same Late Permian age.

The schistose rocks of Mine Ridge include rocks of basic igneous origin, comparable to nonschistose metamorphic basalts of the ophiolite complex, and rocks of sedimentary origin such as the quartzites and probably the muscovite schists. The relationship between these metamorphic rocks and the less metamorphosed and deformed chert and andesite of the melange of Mine Ridge is not clear. The ribbon chert requires a relatively deep oceanic environment remote from a clastic source for its formation. The andesite has a LREE-enriched, typically calc-alkaline REE pattern (fig. 11.9*D*) similar to patterns observed in the Strawberry Volcanics and in a few samples of the Seven Devils Group. This pattern is distinct from the relatively flat REE pattern of the majority of both Permian and Triassic Seven Devils rocks, which closely resembles the pattern of the ophiolitic rocks of Mine Ridge (figs. 11.9*C*, 11.9*D*). Rare-earth-element patterns for island-arc suites vary from LREE-depleted in the earlier, more primitive island-arc tholeiites to LREE-enriched in the more typical calc-alkaline suites, so the striking differences in pattern observed in figure 11.9*D* need not imply two distinct tectonic settings. Indeed all these rocks have characteristics of

rocks found in primitive volcanic island arcs. But the REE differences, when added to the different degrees of deformation observed, reinforce the possibility that the coherent blocks of andesite and the ophiolites represent two suites of rocks of different age.

CORRELATION AND TIMING OF THE DEFORMATION OF THE SCHISTOSE ROCKS OF MINE RIDGE

All mesoscopic structures observed in the blocks of schist within the melange on Mine Ridge are correlated with the earlier (D_1) of two major deformations recognized throughout the Baker and Izee terranes by Avé Lallemant and others (1980). D_1 on Mine Ridge, as elsewhere, is a relatively high grade metamorphic event (epidote amphibolite facies) that developed a strong axial-planar foliation (S_1) with isoclinal folds (F_1) whose axes plunge steeply downdip. The isoclinal folds bring bedding planes (S_0) into parallelism with S_1 (S_0-S_1) except at fold hinges. S_0-S_1 is characterized by oriented mica plates and elongate hornblende crystals aligned within S_0-S_1 and parallel to the F_1 fold axes. On Mine Ridge S_0-S_1 strikes east to northeast, and the fold axes (L_1) plunge steeply south (fig. 11.12).

The second phase of more open, commonly box-shaped folds is approximately coaxial with the first phase, but the second-phase folds have steep axial planes at a high angle to S_0-S_1. A third fold phase within the D_1 event formed crenulation cleavage. The sequence of fold phases can be interpreted as progressive, noncoaxial shear deformation that occurred during, and subsequent to, the development of the dominant metamorphic fabric (S_1).

The F_1 folds and associated mineral fabrics must have developed prior to the formation of the serpentinite melange matrix. Once the matrix formed, subsequent strain would be absorbed by the incompetent envelope—the matrix—leaving the more competent blocks of the schistose rocks of Mine Ridge to react only passively. If deformation developed on shear planes parallel to the plane of subduction (Dickinson and Thayer, 1978), then horizontal fold axes would develop about axial surfaces parallel to the subduction plane, at lower dips than are now seen. Thus, reorientation of the F_1 folds is required to achieve the present uniformly steep plunge of the F_1 fold axes down the dip of the F_1 axial surfaces. In a subduction zone, in which extension parallel to the direction of subduction is likely to be extreme on the upper surface of the subducting slab, rotation of early folds is not only feasible but almost unavoidable. All early fold axes would be transposed into the direction of maximum extension, down the dip of their axial surfaces. Transposition of this type would be greatly facilitated as serpentinites were incorporated into the shear system to form a melange. This is the model outlined by Avé Lallemant and others (1980).

The east-to-northeast strike of S_0-S_1 on Mine Ridge and elsewhere in the Baker terrane parallels the terrane boundaries, and the associated F_1 fold axes, which plunge down the dip of these nearly vertical axial surfaces, are also similar to the regional pattern. The pattern implies a subduction zone striking approximately east-west with subduction either toward the north, under the arc rocks of the Wallowa terrane, or toward the south, under the arc rocks of the Olds Ferry terrane. Wilson and Cox (1980) postulated 60° clockwise rotation of the Wallowa terrane in post-Jurassic time; if this rotation extended as far south as Ironside Mountain, then the direction of subduction would have been N. 60° W. or S. 60° E. These subduction directions, however, assume that the D_1 structures were not reoriented during the D_2 event. As discussed later in the section "Deformation of the Weatherby Formation," reorientation during D_2 is probable, so these apparent directions of subduction may have little meaning.

The present attitude of S_0-S_1 and the F_1 fold axes is steeper than is required in a subduction model, but is readily explained by the reorientation that appears to have accompanied the second regional deformation (D_2).

A recent K-Ar age on hornblende from the schistose rocks of Mine Ridge is 260 Ma (N.W. Walker, oral. commun., 1987). The D_1 event is, therefore, Late Permian rather than Late Triassic in age (Avé Lallemant and others, 1980). This age is similar to the 262-Ma age determined for the Canyon Mountain Complex by Avé Lallemant and others (1980) and precludes the possibility of that ophiolite complex forming in an oceanic ridge-rift system far from the subduction zone.

FORE-ARC BASIN DEPOSITS: THE WEATHERBY FORMATION

A broad east-west zone of Paleozoic to Mesozoic clastic sedimentary deposits, the Izee terrane, lies across northeastern Oregon, south of the Baker terrane and northwest of the Olds Ferry terrane (Huntington arc; fig. 11.1; Brooks and Vallier, 1978; Dickinson and Thayer, 1978). Dickinson (1979) suggests that these sedimentary materials were deposited in a fore-arc basin between a ridge of ocean-floor melange (Baker terrane) to the northwest and a rising volcanic arc (the Huntington arc of the Olds Ferry terrane) to the southeast.

In the John Day basin on the west end of the zone (fig. 11.1), Dickinson (1979) and Dickinson and others (1979) have described a series of clastic units that range in age from Karnian (Late Triassic) to Cretaceous. Farther east, from Strawberry Mountain (about 20 km southeast of the town of John Day; Robyn, 1977) to the Snake and Salmon River canyons of western Idaho, a less well known but apparently similar sequence of metasedimentary turbidites is exposed. These constitute the Weatherby Formation of Brooks (1979b). Crinoids, brachiopods, molluscs and ammonites distributed sparsely throughout these rocks date them as Early (Sinemurian) to Middle (late Bajocian) Jurassic (200–170 Ma) in age (Brooks and Vallier, 1978). In the Snake River area the Weatherby includes clasts apparently derived from the Huntington arc (Olds Ferry terrane, fig. 11.1, inset), which the Weatherby appears to overlie unconformably (Brooks, 1979b). Farther north near the Snake River the Weatherby is in fault contact with rocks of the Baker terrane (Connor Creek fault; see Brooks and Vallier, 1978).

The Weatherby Formation is the most extensive unit of the Ironside Mountain inlier (Lowry, 1968; Brooks and Ferns, 1979; Brooks and others, 1979). It is strongly folded and is intruded by a series of Cretaceous to Oligocene diorite to granodiorite stocks along the anticlinal axis of the inlier.

The Weatherby Formation in the inlier consists of olive-gray to gray-brown lithic wacke, lithic arenite, brown-gray slate, light-brown-gray silty limestone, and limey siltstone (Engh, 1984). Typically, its beds range in thickness from 25 cm in the coarser units to 5 cm in the finest pelitic units. Close to the Permian and Triassic rocks of the Baker terrane at the north end of the inlier, wacke, siltstone, and conglomerate predominate; minor horizons of arkose and breccia are also present. Large angular chert fragments up to 4.0 cm across occur in the breccias in a chert matrix. The conglomerate contains smaller angular fragments of chert, volcanic rock, and serpentinite. The Weatherby is in fault contact with the rocks of the melange of Mine Ridge, but the conglomeratic horizons and clasts derived from the melange and the presence of the Weatherby on both the north and south sides of the melange (fig. 11.1) suggest that its sediments were originally laid down unconformably on, and were largely derived from, rocks of the melange. No useful fossils have been found in the Weatherby Formation during the present study, but H.C. Brooks (oral. commun., 1983) has observed limestone pods with abundant but poorly preserved fossils that are tentatively assigned a Jurassic age.

Sedimentary structures are well developed in the turbidites. Among these structures are graded bedding (including some reverse grading), small ripples, load casts and flame structures, and wavy or convolute laminae. Rip-up clasts are common. Together the structures provide abundant evidence for identifying facing directions, that is, the directions in which beds young. In general, the beds fit the Bouma sequence model (Middleton and Hampton, 1976), although a complete Bouma sequence is rare.

The Weatherby Formation is strongly folded about a single axial-planar surface represented by a penetrative cleavage striking east-northeast and dipping steeply south. The consistent relations between facing directions and fold limbs, as defined by the cleavage-bedding relationship, and the lack of interference structures imply that the folds belong to a single episode of deformation. The effects of low-grade regional metamorphism are apparent throughout the formation. Chlorite, stilpnomelane, and quartz form pressure shadows. Calcite and albite are also present. Absent are zeolites, prehnite, pumpellyite, lawsonite, and any amphibole or pyroxene.

Contact metamorphism and mineralization occurred around the granodiorite of Grouse Creek. These processes obscured the cleavage in some areas and obliterated it in others, and they were accompanied by the formation of calc-silicate minerals. Close to the granodiorite body, garnet and epidote are present, disappearing approximately 450 m from the contact. Outside the garnet-epidote zone a spotted cordierite hornfels is found locally; the hornfels contains up to 30 percent radiating cordierite crystals in a matrix that appears to contain both andalusite and anthophyllite.

PROVENANCE

Lithic arenite and lithic wacke make up approximately 75 percent of the Weatherby section in the Rastus Mountain area. They contain 10–60 percent volcanic rock fragments (average 45 percent). Feldspar, quartz, chert, and detrital quartzite grains are the other major components, forming about 10 percent each. The lithic wacke contains greater than 15 percent of very fine grained matrix, but matrix estimates are complicated by the low-grade metamorphism.

Pelitic layers are composed of 45 percent sheet silicates, commonly stilpnomelane, and 30 percent or more very fine grained microcrystalline quartz. The remaining 25 percent consists primarily of lithic fragments and feldspar. The silty limestone has an average composition of 75 percent calcite, 7 percent volcanic rock fragments, 3 percent mica and chlorite, and about 15 percent organic material and fine clay minerals. The

TABLE 11.8.—*Petrographic analyses of the Weatherby Formation*

[All values except "Average grain size" and "Total framework grains counted" are in volume percent. ---, not observed; tr, trace; n.d., not determined]

Sample	KE-29	KE-290	KE-2	KE-30	KE-3	KE-14	KE-7	KE-6	RR	RR-100	LR-207	KE-207B
Volcanic fragments	32	22	25	12	52	30	58	10	10	55	---	20
Chert and quartzite	14	5	2	---	12	10	5	---	10	3	30	---
Calcite	35	52	20	80	17	40	5	70	60	6	---	---
Quartz	1	5	2	8	---	10	6	10	7	6	20	40
Sedimentary rock fragments	1	1	---	---	---	---	---	---	---	3	---	---
Feldspar	---	7	10	---	---	4	4	---	4	14	2	---
Micas	2	---	1	---	12	3	2	3	1	13	48	40
Matrix	15	8	30	tr	7	4	10	7	7	---	---	---
Average grain size (μm)	<1	<1	<1	0.5	1	1	1.5	3	2	2	>4	>4
Proportions used in figure 11.13												
Quartz (Q)	24	20	21	n.d.	5	12	8	n.d.	31	n.d.	n.d.	n.d.
Feldspar (F)	9	29	5	n.d.	4	19	7	n.d.	10	n.d.	n.d.	n.d.
Lithic fragments (L)	67	51	74	n.d.	91	69	84	n.d.	58	n.d.	n.d.	n.d.
Monocrystalline quartz (Qm)	5	7	1	n.d.	1	3	1	n.d.	4	n.d.	n.d.	n.d.
Feldspar (F)	9	29	5	n.d.	19	19	7	n.d.	10	n.d.	n.d.	n.d.
Total lithic fragments (Lt=Qp+Lv+Ls)	86	64	95	n.d.	80	78	92	n.d.	86	n.d.	n.d.	n.d.
Polycrystalline quartz (Qp)	22	19	22	n.d.	4	11	8	n.d.	32	n.d.	n.d.	n.d.
Lithic volcanic fragments (Lv)	56	75	59	n.d.	91	80	88	n.d.	52	n.d.	n.d.	n.d.
Lithic sedimentary fragments (Ls)	22	6	20	n.d.	5	9	4	n.d.	16	n.d.	n.d.	n.d.
Total framework grains counted	308	232	253	n.d.	307	233	327	n.d.	178	n.d.	n.d.	n.d.

lithology is summarized in table 11.8 and plotted in figure 11.13.

On the quartz-feldspar-lithic (QFL) diagram (fig. 11.13*A*) all the Weatherby rocks plot near the lithic pole; they are fairly similar to the clastic sediments of the John Day inlier (Dickinson and others, 1979), but have less feldspar. Plots of the Weatherby rocks lie within the transitional arc and undissected arc provenance fields as defined by Dickinson and others (1983). The inferred main source for these sediments is a volcanic arc; subordinate debris was derived from flanking metamorphic rocks and their sedimentary cover.

The monocrystalline quartz-feldspar-total lithic (QmFLt) diagram (fig. 11.13*C*) emphasizes provenance. Samples of the Weatherby Formation plot near the lithic pole (Lt) within the field of a melange source, similar to samples from the Vester Formation of the John Day inlier (Dickinson and others, 1979). A single exception falls within the volcanic source field. On the polycrystalline quartz-lithic volcanic-lithic sedimentary (Qp-Lv-Ls) diagram (fig. 11.13*B*), which includes only polycrystalline grains, most samples plot near the volcanic pole in the magmatic-arc source field (Dickinson and Suczek, 1979).

Some limitations in the application of these diagrams to the determination of the provenance of the Weatherby Formation need to be stressed. Both chert and quartzite fragments are recorded together as a polycrystalline quartz. Quartzite makes up 50 percent or more of these fragments in some samples. Quartzite is one of the components of the older melange of

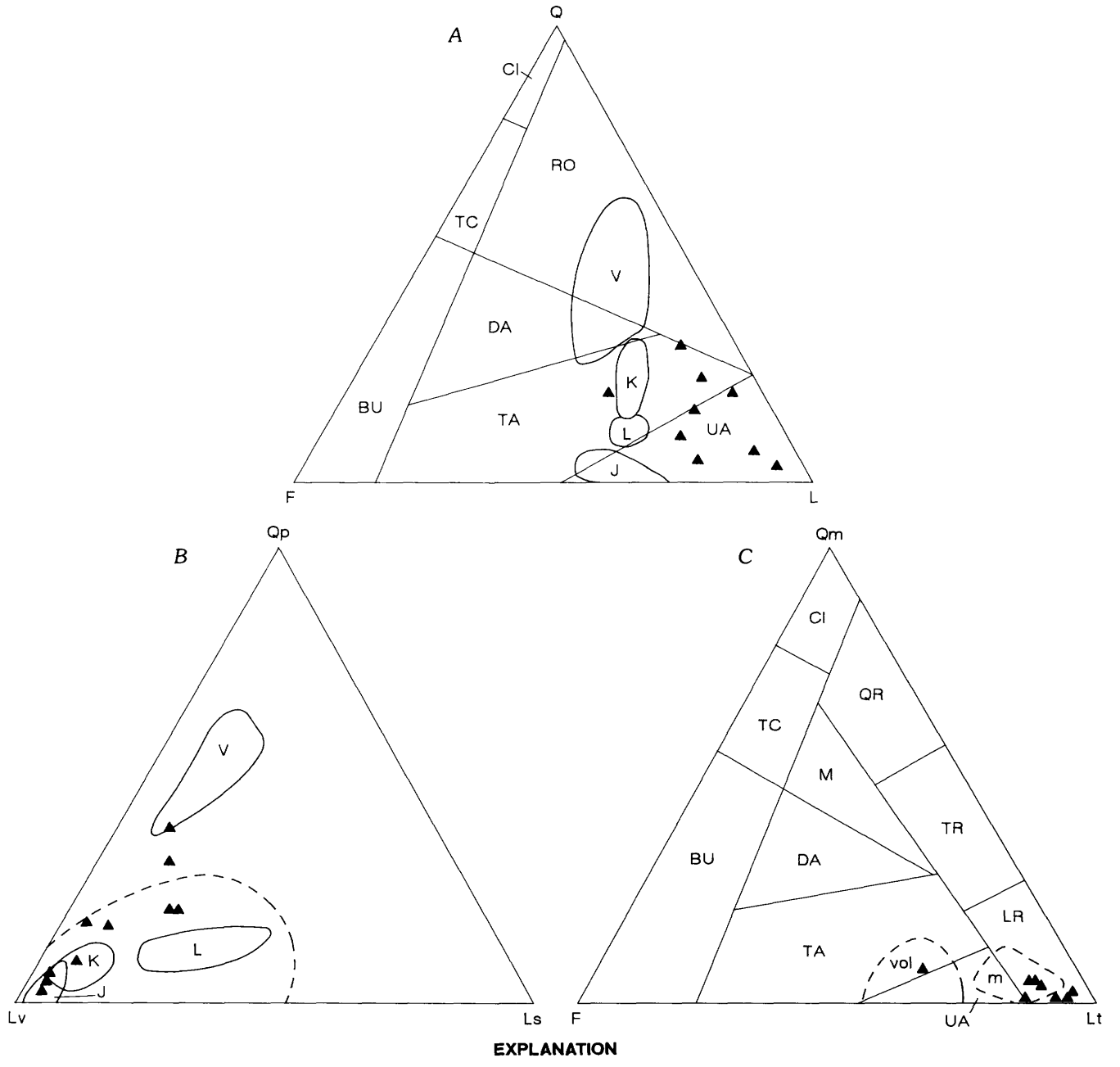

FIGURE 11.13.—Composition and provenance of Weatherby Formation of Brooks (1979b), Ironside Mountain inlier. *A*, Ternary plot of quartz (Q), feldspar (F), and lithic (L) components. *B*, Ternary plot of polycrystalline quartz (Qp), volcanic lithic (Lv), and sedimentary lithic (Ls) components. Dashed line surrounds field of arc-orogen sources of Dickinson and Suczek (1979). *C*, Ternary plot of monocrystalline quartz (Qm), feldspar (F), and total lithic (Lt) components. Ten samples plotted in each diagram; some samples overlap in figures 11.13*A* and 11.13*C*.

Mine Ridge, but the relative abundance of quartzite fragments in the Weatherby could be construed as evidence of another, more continental source component.

The low-grade metamorphism may also bias the interpretation of these diagrams by altering grain size and mineralogy. Such alteration may explain in part the low feldspar count. Small feldspar grains are commonly corroded and replaced by calcite and clay minerals, resulting in original feldspar grains being counted as matrix. Despite these limitations, the rocks of the Weatherby Formation appear to have been derived from sources whose origin and tectonic setting are similar to those of the John Day inlier. The Weatherby was probably deposited in an arc-trench gap or fore-arc basin; the sediments were most likely derived from a volcanic arc underlain by metamorphic terrane, although some material (quartzite) may have been derived from a continental source.

DEFORMATION OF THE WEATHERBY FORMATION

The Weatherby Formation of the Ironside Mountain inlier is dominated by a well-developed penetrative cleavage striking east-northeast. Bedding is preserved in many places but is less evident than cleavage. Use of cleavage/bedding relations permits an accurate reconstruction of minor and major folds (figs. 11.14–11.16), although actual folds are rarely seen in outcrop.

Critical structural data are plotted in figure 11.15. The poles to the cleavage surface (fig. 11.15*C*) are more scattered than might be expected from a single strong episode of folding in a relatively homogeneous lithology. This scattering is due to refraction of the cleavage across beds of varying competence; dips of cleavage planes around a single fold vary by as much as 20°. Only the cleavage in the pelitic horizons is truly axial planar.

Fold style is illustrated in figure 11.16. One of the rare folds observed in the field is shown in figure 11.16*A*. A reconstruction of the fold style based on cleavage/bedding relations and facing-direction data is shown in figure 11.16*B*. The folds are strongly asymmetric and have a similar or chevron style. The axial plane lies close to the more southerly limb, and beds thicken over the fold hinges.

The axial-planar cleavage and the two fold limbs maintain relatively constant orientations across the mapped area, but the sense of asymmetry, or the relative length of one limb compared to the other, varies systematically and permits the identification of major fold hinges (fig. 11.14).

An analysis of strain in the Weatherby Formation using elliptical microlitic glass grains (Dunnet, 1969; Dunnet and Siddans, 1971) is shown in figure 11.17. The strain occupies the oblate field of a Flinn diagram (fig. 11.17*B*). Some volume loss could well have occurred, as evidenced by pressure-solution features in the cleavage planes, and the strain shape may, therefore, reflect components of both tectonic strain and volume loss. The flattening occurs with maximum shortening perpendicular to the axial surface and maximum elongation down the dip of the axial surface; the intermediate axis lies approximately parallel to the fold axis. Boudinage structures and crinoid fragments in suitably oriented two-dimensional sections (Engh, 1984) suggest a maximum extension of 35 percent down the dip of the axial plane and maximum shortening of 50 percent perpendicular to that plane.

Joints, dikes, and veins show little evidence of preferred orientations, but slickensides on a number of small faults, which dip at a slightly lower angle to the south-southeast than the fold axial planes, indicate oblique slip toward the southeast.

We consider the post-Jurassic folds in the Weatherby Formation to be the products of the second (D_2) episode of regional deformation recognized by Avé Lallemant and others (1980). The lack of evidence of the D_2 deformation within the much older competent blocks of the schistose rocks of Mine Ridge is surprising, although it is possible that the F_3 crenulation cleavage reflects the Late Jurassic (D_2) event. The explanation, we assume, lies in the concept that once the melange was formed, all subsequent strain suffered by the melange, including that undergone during D_2, was taken up by the incompetent matrix of serpentinite. The competent blocks only rotated passively, undergoing little internal deformation, but the D_2 rotation brought the S_0-S_1 surfaces into near parallelism with the D_2 axial surface and steepened the axes of the F_1 folds.

The predominantly upright orientation of the major folds in the Weatherby Formation and their near-symmetrical form suggest that the older Permian and the younger Jurassic rocks were flattened against each other so that the direction of maximum extension was close to vertical. Some small component of thrusting toward the northwest may have been the cause of the asymmetric distribution of the cleavage surfaces in the Weatherby folds of the D_2 deformation (fig. 11.16*B*).

POST-JURASSIC IGNEOUS ROCKS

South of Ironside Mountain the diorite of Tureman Ranch intruded the Weatherby Formation in the Cretaceous (about 120 Ma) (Thayer and Brown, 1964). Within the mapped area of the inlier (fig. 11.1), early Oligocene intrusions were emplaced over a period of

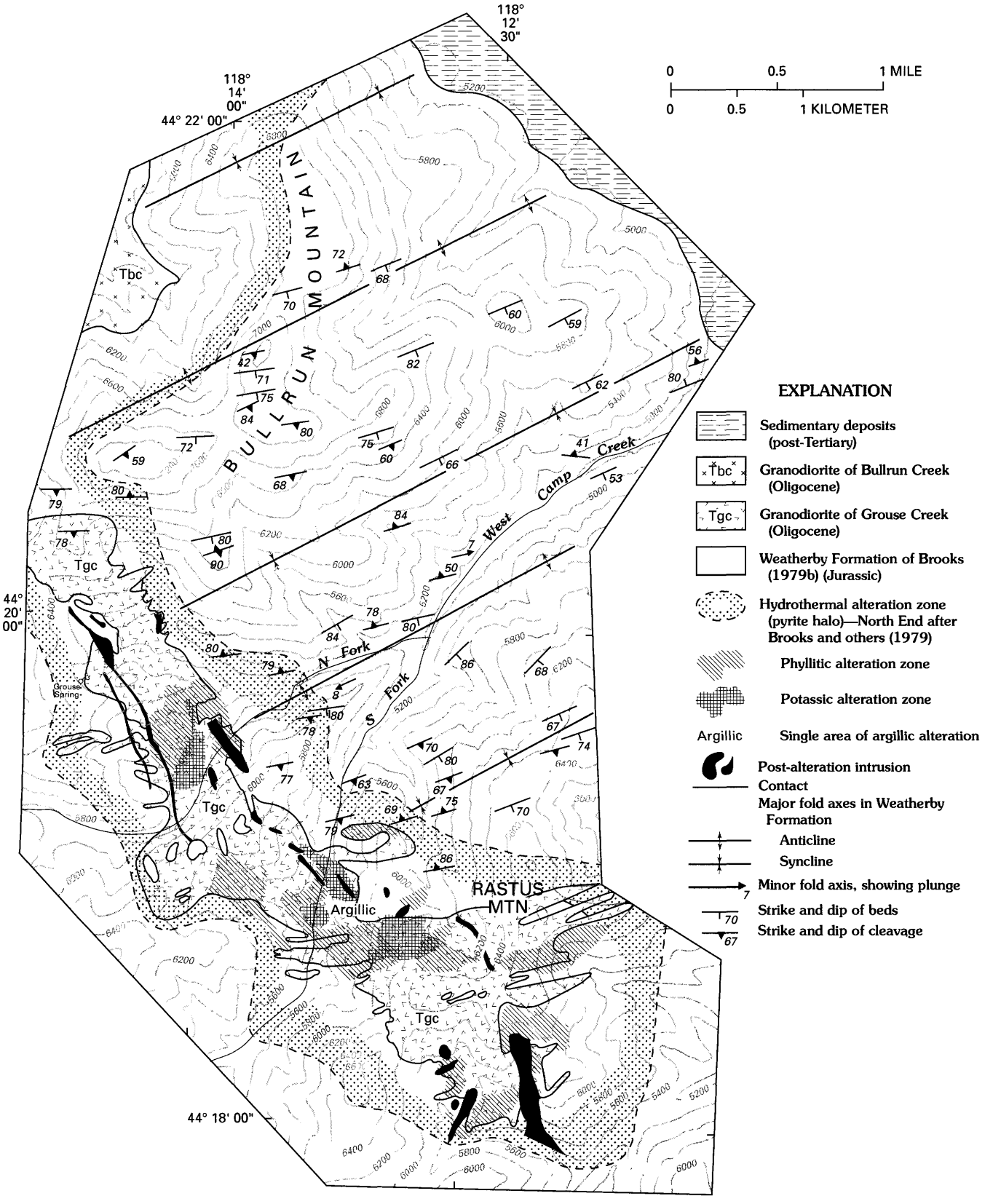

FIGURE 11.14.—Map of Ironside Mountain inlier, showing bedding/cleavage relations and major fold hinges in Weatherby Formation, and zones of hydrothermal alteration in and around granodiorite of Grouse Creek. Contour interval, 200 ft. Base from U.S. Geological Survey 1:24,000, Rastus Mountain quadrangle, 1972 (photorevised 1984).

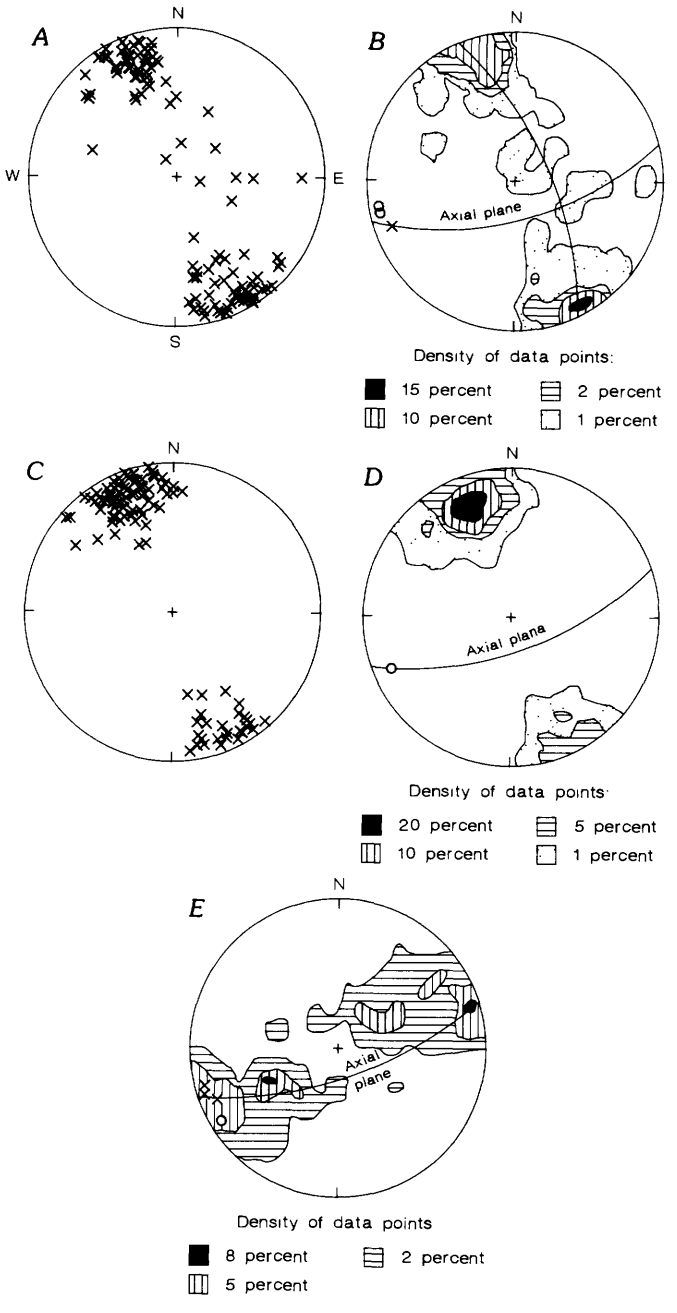

FIGURE 11.15.—Lower-hemisphere, equal-area projections of structural data for Weatherby Formation of Brooks (1979b). *A*, Poles to bedding. Number of data points (n)=115. *B*, Contour diagram of poles to bedding. Density reported in percentage of total data points per 1-percent area of diagram. Open circle, minor fold axis (measured); x, fold axis (estimated). *C*, Poles to cleavage (n=117). *D*, Contour diagram of poles to cleavage. Density and symbols as in figure 11.15*B*. *E*, Contour diagram of bedding/cleavage intersections (n=60). Density as in figure 11.15*B*. x, fold axis (measured); open circle, bedding/cleavage intersection (measured).

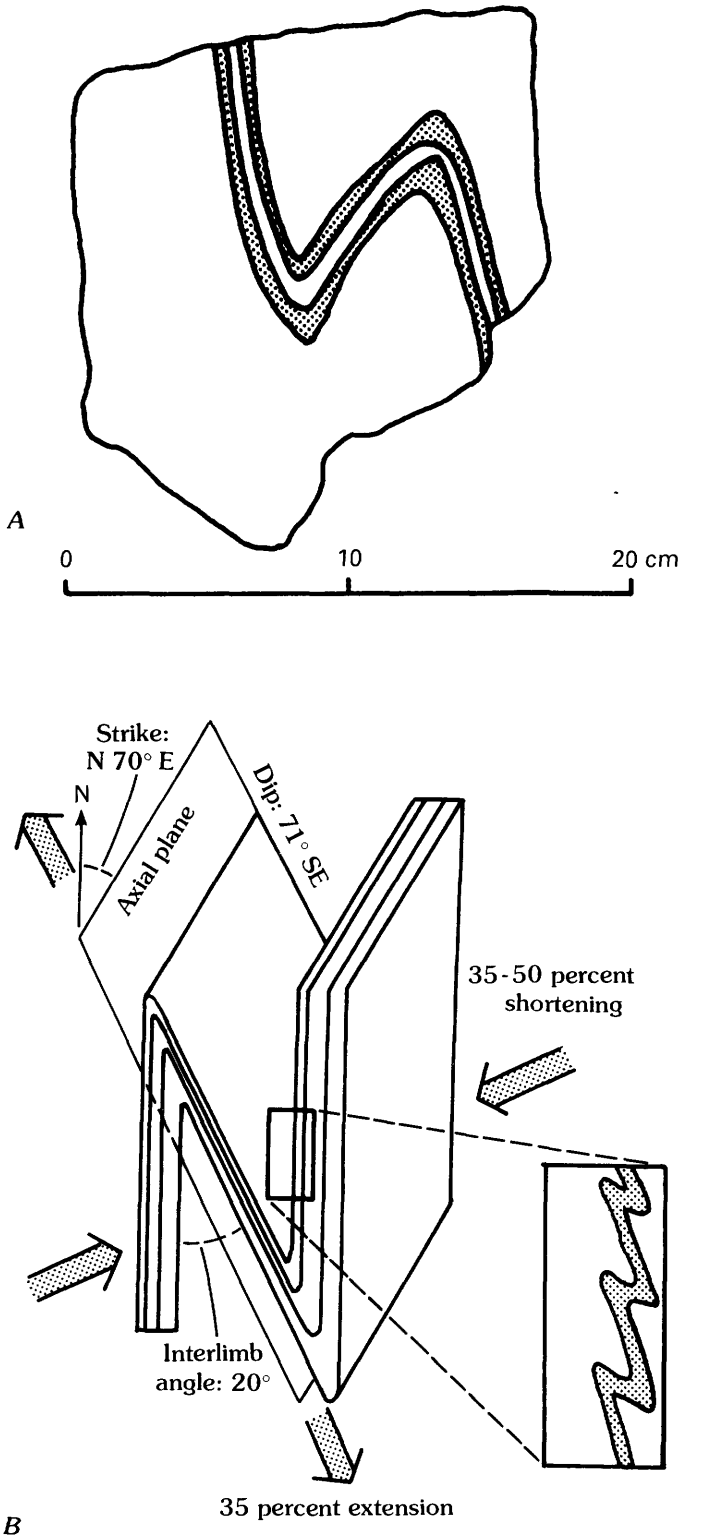

FIGURE 11.16.—Fold style in Weatherby Formation of Brooks (1979b). *A*, Minor fold traced from field photograph. *B*, Diagram of fold style as determined from observed folds and cleavage/bedding relations. Large arrows indicate directions of principal strain.

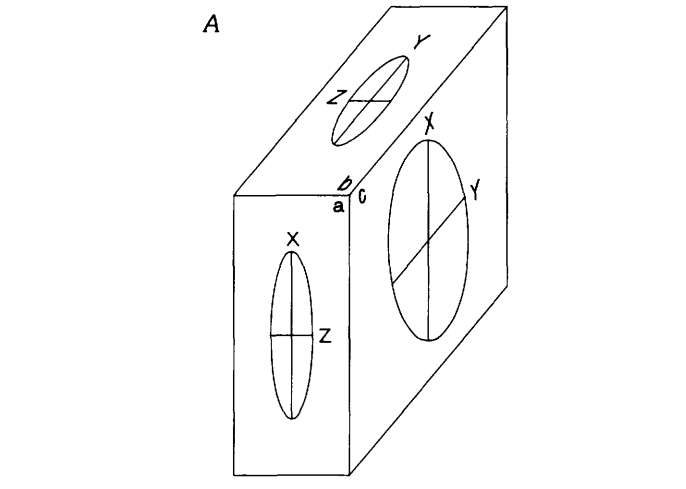

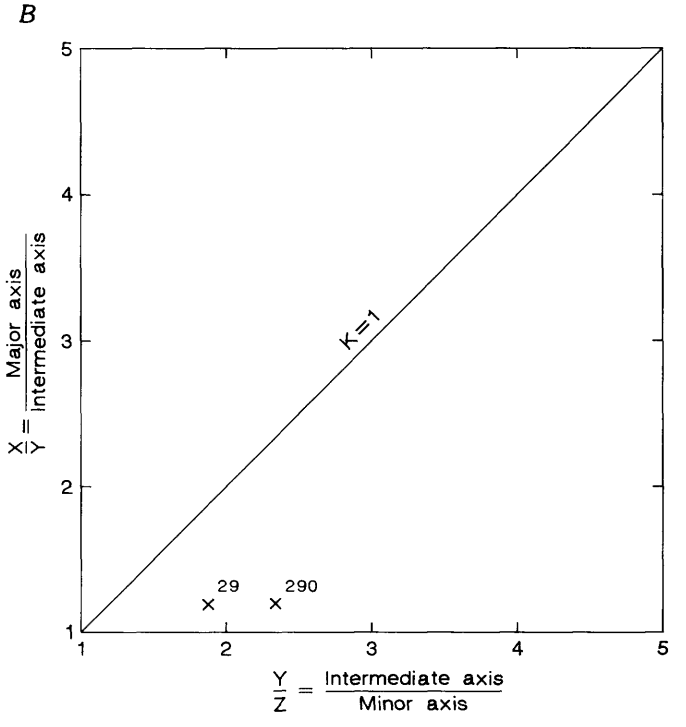

C

Sample number	Strain ratios X/Z	Y/Z	X/Y	Stretching (percent) X	Y	Z
29 -----	2.5	1.9	1.2	40	7	-33
290 ----	2.9	2.3	1.2	45	15	-40

FIGURE 11.17.—Orientation and degree of strain in Weatherby Formation of Brooks (1979b). *A*, Strain ellipsoid. X, major axis; Y, intermediate axis; Z, minor axis. Strain ellipse ratio X/Z on face a is greater than ratio Y/Z on face b, which is greater than ratio X/Y on face c. *B*, Flinn diagram. K=(X/Y–1)/(Y/Z–1). Line K=1 separates field of apparent flattening (K<1) from field of apparent constriction (K>1). 29 and 290 are sample numbers. *C*, Strain ratios and stretching values for samples 29 and 290. X, Y, and Z are axes shown in figure 11.17*A*. Stretching values assume there was no change in volume during or after deformation.

at least 2 m.y. (36 to 34 Ma) (N.W. Walker, oral commun., 1986; Manville Products Corp., oral commun., 1986) at the beginning of the Oligocene. The Tertiary intrusive activity can be divided into three periods: (1) emplacement of the granodiorite of Bullrun Creek between Mine Ridge and Bullrun Mountain (fig. 11.1), associated with a few late-stage biotite-bearing dikes, at 36 Ma; (2) emplacement of the porphyritic granodiorite of Grouse Creek along the axis of the inlier to the south of Bullrun Mountain (fig. 11.1), accompanied by many minor intrusions and associated with extensive hydrothermal alteration and mineralization, at 34 Ma; (3) emplacement of several types of post-hydrothermal minor intrusions concentrated immediately southeast of Bullrun Mountain (fig. 11.14). Volcanic rocks of Tertiary age dip off the inlier to east and west and are described by Walker (1990).

GRANODIORITE OF BULLRUN CREEK

The intrusion that is here called the granodiorite of Bullrun Creek (hereafter also referred to as the Bullrun Creek stock) is a kidney-shaped stock 2.0×0.7 km that occupies the east side of Mine Ridge, crosses Bullrun Creek, and extends south into Koski Basin (figs. 11.1, 11.2).

The main phase of the stock is a massive, medium-grained, gray granodiorite that contains plagioclase, K-feldspar, quartz, biotite, and hornblende in modal proportions that span the tonalite-granodiorite boundary (table 11.9; fig. 11.18; Houseman, 1983). Inclusions are rare but are occasionally found near metasedimentary contacts. A seriate porphyritic border phase occurs in Payton Gulch, and a dark, slightly mafic-rich tonalitic border phase is found on the lower, eastern slope of Mine Ridge. Both variants grade into the main body of the stock. Late aplite veins and dikes from 1 to 50 cm wide, with minor green amphibole in a feldspar-rich matrix, are common within the stock.

The border zone is poorly exposed, but the contact against hornfelsed metasedimentary rocks can be observed in both Koski Basin and Payton Gulch where small-scale forked and braided dikes penetrate a few meters into the hornfels. The contact between the granodiorite and serpentinite is exposed underground in the Record Mine, where it dips 60° NE but is modified by faulting. Discontinuous shear zones containing lensoid slivers of serpentinite within argillized granodiorite parallel the contact and are cut by northeast-striking en echelon fractures and faults that dip steeply northwest. This latter set, although displaying only limited offsets, has strongly influenced later vein and dike orientations. In undisturbed granodiorite/serpentinite contacts, chill zones in the granodiorite are limited to 0.5 to 1.0 m in width.

TABLE 11.9.—*Estimated modal mineralogy of the granodiorite of Bullrun Creek*

[All values in volume percent. Traces of apatite and zircon were detected in all samples. Epidote and muscovite are present in JB-81-18E, and significant calcite occurs in JB-81-59A. tr, trace; ---, not observed]

Sample	JB-81-18E	JB-81-35	JB-81-59A	JB-81-59C	JB-81-61	JB-81-63	JB-81-71
Plagioclase	55	53	60	58	61	50	60
K-feldspar	7	5	6	5	5	10	5
Quartz	15	30	20	25	20	20	20
Hornblende	15	5	7	5	7	15	7
Biotite	---	3	3	5	5	1	3
Chlorite	5	1	1	---	1	---	2
Opaque minerals	3	1	3	3	2	4	3
Sphene	tr	tr	tr	---	tr	tr	---

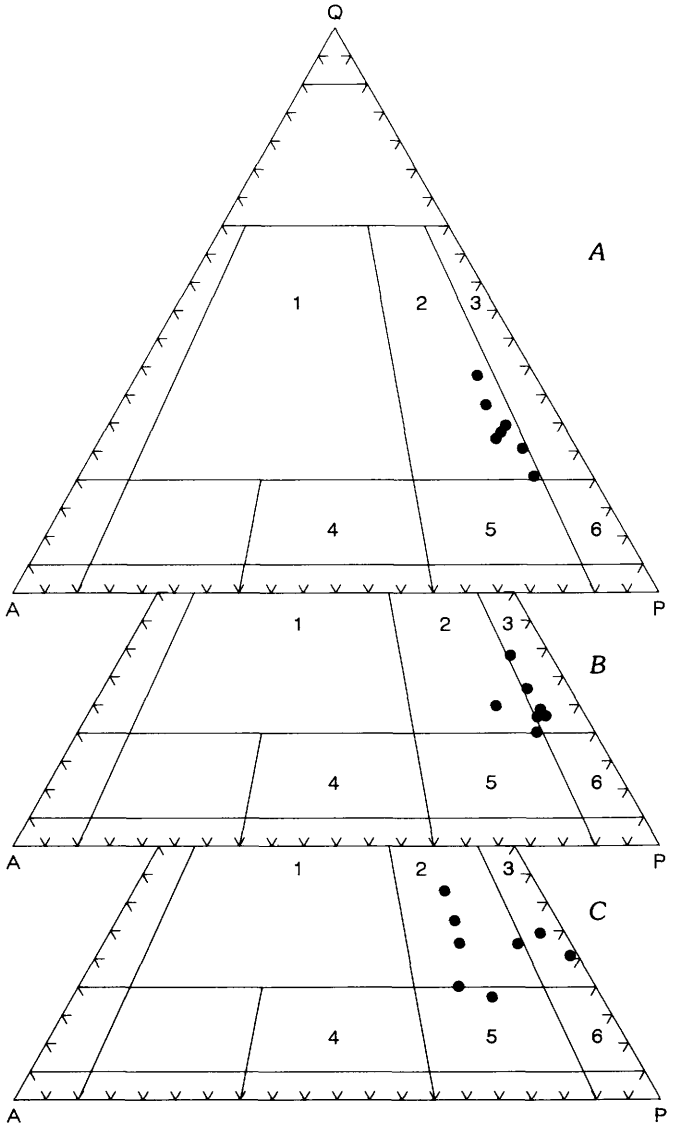

Fine-grained biotite tonalite dikes cut the granodiorite of Bullrun Creek at the Record Mine and to the south in Koski Basin. These dikes are cut by younger porphyritic dikes at both localities. The biotite tonalite dikes are quartzofeldspathic and equigranular, and are believed to represent a late phase of the Bullrun Creek stock.

Hydrothermal alteration associated with the emplacement of the granodiorite of Bullrun Creek is minimal. Amphibole-apatite-sulfide veins and quartz-albite-carbonate alteration is present along the eastern margins of the stock at the Record Mine and at least intermittently along the serpentinite contact to the south. The veins represent later infilling of northeast-striking en echelon fractures.

GRANODIORITE OF GROUSE CREEK AND RELATED MINOR INTRUSIONS

The main stock that is here called the granodiorite of Grouse Creek (hereafter also referred to as the Grouse Creek stock) is elongated northwest and is 4.25 km long and 0.75 km wide (figs. 11.1, 11.14). It is a pale, medium- to fine-grained rock with phenocrysts (1–4 mm) of plagioclase, hornblende, and, in some areas, quartz. The groundmass of plagioclase,

◀ FIGURE 11.18.—Streckeisen diagram of samples of the equigranular granodiorite of Bullrun Creek. Q, quartz; A, alkali feldspar; P, plagioclase. Fields 1 through 6 (from Streckeisen and others, 1973): 1, granite; 2, granodiorite; 3, tonalite; 4, quartz monzonite; 5, quartz monzodiorite and quartz monzogabbro; 6, quartz diorite, quartz gabbro, and quartz anorthosite. *A*, Normative values with normative albite and anorthite summed to create total normative plagioclase. *B*, Modal values. *C*, Normative values with plagioclase calculated to An_{40} and remaining albite placed in alkali-feldspar component.

hornblende, quartz, and opaque minerals, with traces of K-feldspar and biotite and secondary chlorite and sericite, is too fine grained for modal analysis, but a normative plot (fig. 11.19) indicates a granodiorite composition. The main stock and the many associated dikes, sills, and breccias are pervasively altered and lie in the central part of a larger alteration halo that overprints all pre-Tertiary rocks. Alteration assemblages and copper mineralization (Houseman, 1983) imply that a copper porphyry system is associated with the intrusion.

The complex border zone is composed of alternating slivers of calc-silicate hornfels and porphyritic dikes and sills (Houseman, 1983). On a large scale, porphyritic dike orientation corresponds to the prevailing east-northeast strike of the axial-planar cleavage in the country rock (Weatherby Formation). In detail, dike margins are irregular and accompanied by conspicuous brecciation. Breccia zones range from a few meters to several hundred meters across and consist of metasedimentary clasts from 1 cm to 1 m in size in an igneous matrix. Large metasedimentary roof pendants are common and typically haloed by breccia. Smaller sedimentary inclusions occur throughout the stock. Breccias also occur within the main stock as dikes and pipes a few centimeters to a few hundred meters across. Simple breccia zones contain monolithologic assemblages of porphyritic granodiorite fragments, whereas the more complex zones contain fragments of both granodiorite and metasedimentary rock. In the latter the clasts are more obviously abraided and show evidence of multiple brecciation. Many breccia zones have a northwest to north-northwest orientation. The breccia matrix is typically aplitic, altered to a felty aggregate of chlorite, epidote, and clinozoisite.

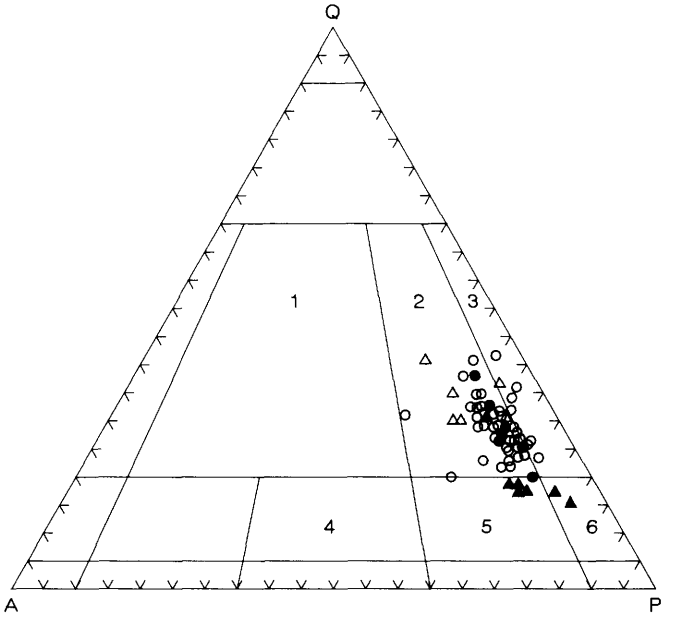

FIGURE 11.19.—Normative values of all analyses of Oligocene intrusive rocks of Ironside Mountain inlier plotted on Streckeisen diagram (Streckeisen and others, 1973) with normative albite and anorthite summed to create total normative plagioclase. Endpoints and fields as in figure 11.18.

Several northwest-striking fracture zones cross the stock northwest of Rough Ridge (figs. 11.1, 11.14). These appear to represent major zones of weakness and host one or more late-stage intrusive phases. Movement along the fractures does not appear to have been significant.

Numerous, apparently co-magmatic, porphyritic dikes associated with propylitic alteration crop out on Mine Ridge and on Bullrun Mountain. Chilling of the porphyritic dikes against the granodiorite of Bullrun Creek indicates that at least a brief period of cooling separated the two intrusive events. Dikes intruding along the eastern margins of the Bullrun Creek stock are commonly quartz-albite-carbonate altered. Along Bullrun Creek, the dikes tend to strike north-northwest. To the east, within the ultramafic rocks, the dikes tend to strike more northeasterly. These latter dikes intrude along faults that are parallel to, or form the contact between, the Weatherby Formation and ultramafic rocks (fig. 11.2).

LATE-STAGE PORPHYRITIC DIKES

Several phases of porphyritic dikes postdate the granodiorite of Grouse Creek. Some are texturally and mineralogically similar to the stock and are distinguished only by their lack of hydrothermal alteration. Relative ages of the younger dikes are determined by their mutual crosscutting relations, and the increasingly younger dikes are progressively more distinct in appearance and texture from the granodiorite.

Plagioclase and hornblende phyric granodiorite dikes cut the granodiorite of Grouse Creek on the southeast side of Rough Ridge (fig. 11.1) and cut the granodiorite of Bullrun Creek and adjacent peridotite near the Record Mine (fig. 11.2). The dikes are elon-

gate, irregular bodies as much as 150 m long. One large body near the Record Mine is 100×30 m. These dikes resemble the rocks of the granodiorite of Grouse Creek but lack the alteration and are chilled against altered granodiorite.

Chemically similar dikes that postdate the hydrothermal alteration intrude both the granodiorite of Grouse Creek and its country rock near Rastus Mountain. These are aphyric to weakly phyric and contain biotite as the dominant phase. They have variable widths and are as much as 700 m long in a north-northwest direction. Some are circular-shaped bodies chilled against the granodiorite.

Another, younger group of post-hydrothermal plagioclase-hornblende-biotite-phyric dikes form a north-northwest-oriented group that dips 30°–85° northeast between Rough Ridge and Bullrun Mountain. The dikes are 3–15 m wide and 50–1,500 m long. Some pinch and swell and appear to have intruded along prominent north-northeast-striking fracture zones that cut the Grouse Creek stock and the adjacent Weatherby Formation.

CHEMICAL COMPOSITION OF THE OLIGOCENE INTRUSIONS

The Bullrun Creek and the Grouse Creek stocks are readily distinguished in the field by texture and degree of hydrothermal alteration. Differences in bulk chemical composition are small.

Classification of coarse-grained calc-alkaline rocks is normally based on the relative proportions of modal quartz, alkali feldspar, and plagioclase (Streckeisen and others, 1973). Modal analysis of the fine-grained and altered porphyritic rocks of the granodiorite of Grouse Creek is impractical, and the bulk chemical composition provides a better means of recording and comparing their compositions. Superimposing normative values derived from chemical analyses on a Streckeisen modal diagram results in some distortion. Various methods for converting from modal to normative data have been attempted (Le Maitre, 1976).

Figure 11.18 shows the modal compositions of the equigranular Bullrun Creek stock plotted directly on a Streckeisen diagram (fig. 11.18*B*). It also shows the differences produced by plotting the normative values of the same samples on the same diagram, first, with normative albite and anorthite summed to create a total normative plagioclase (fig. 11.18*A*), and second, with normative plagioclase calculated assuming a plagioclase composition of An_{40} (judged the average plagioclase composition), the remaining normative albite being added to the alkali feldspar component (fig. 11.18*C*). Le Maitre's calculations were tested but not used because the results were at greater variance with the modal plots than were the results of the two methods described above. We conclude from figure 11.18 that a straightforward normative plot (fig. 11.18*A*) shows the least divergence from the true modal plot, although it results in a slight bias toward the alkali feldspar side of the diagram. Plots of the normative values of all the analyzed samples of the various Oligocene intrusions (tables 11.10–11.12) are shown in figure 11.19.

Figures 11.18 and 11.19 demonstrate that all the Oligocene intrusive rocks from the north end of the Ironside Mountain inlier have compositions close to the tonalite-granodiorite boundary and that they are not obviously distinguishable one from another on the basis of major-element composition. Nor do the relatively few trace-element analyses provide an obvious means of distinguishing the rocks (table 11.13). The low-K tonalitic aspect of these rocks is further emphasized in Barker's (1979) diagram (fig. 11.20) in which the great majority of samples fall within Barker's tonalite field, some in the trondhjemite field, and only a few in the granodiorite field. While clearly calc-alkaline in character (fig. 11.21), all these rocks belong to a low-K calc-alkaline suite (Barker and Arth, 1976).

The analyses are displayed in a Harker variation diagram in figure 11.22. Although some scatter is apparent, most obviously in the CaO, K_2O, and Na_2O concentrations of the hydrothermally altered Grouse Creek rocks, the overall trends are typical of calc-alkaline suites, with the exception that there is little evidence of the expected positive correlation between K_2O and SiO_2 concentrations.

Potassium-poor salic magmas similar to those of the Ironside Mountain inlier have been interpreted by Ewart (1979) as indicative of subcontinental or young continental crust, whereas Barker (1979) suggested that such tonalite-trondhjemite suites are frequently found within Mesozoic to Cenozoic continental margins and typically on the ocean side of large calc-alkaline batholiths. The Oligocene intrusions of the Ironside Mountain inlier were emplaced into recently accreted Permian and Triassic ophiolites and Mesozoic volcaniclastic rocks. During the Oligocene these terranes lay marginal to the continent, outboard (west) of the broad calc-alkaline Challis-Absaroka arc (which extends from northern Washington through central Idaho and into northwestern Wyoming) and the Cretaceous to Tertiary intrusions associated with the Idaho batholith. The age of the Ironside Mountain intrusions suggests that they were emplaced during the abrupt westward migration of calc-alkaline volcanism from the Challis-Absaroka arc into central and western Oregon and are best regarded as intrusive equivalents of the Clarno Formation of northeastern Oregon.

TABLE 11.10.—*Chemical analyses of the granodiorite of Bullrun Creek and related dike and aplite*

[All values in weight percent. Major-element analyses and Cross, Iddings, Pirsson, and Washington (CIPW) norms by X-ray-fluorescence spectroscopy, Washington State University (Hooper and Johnson, 1989). Major elements normalized on a volatile-free basis with 0.9 Fe expressed as FeO, 0.1 Fe expressed as Fe_2O_3, and Fe* equal to FeO+Fe_2O_3. ---, not present]

Sample	JB-81-62	JB-82-133	JB-81-36	JB-81-55	JB-81-59	JB-82-157	JB-82-162	GCA	JB-82-295	JB-82-332
Major elements										
SiO_2	66.84	63.34	68.60	65.28	63.46	68.10	66.11	67.14	69.55	79.30
Al_2O_3	16.71	16.69	16.54	17.07	18.01	15.98	16.12	15.83	16.48	12.16
TiO_2	.65	.85	.63	.84	.84	.69	.68	.66	.43	.18
Fe*	3.35	5.04	3.54	4.15	4.34	3.58	4.38	3.87	2.68	.00
MnO	.05	.10	.05	.07	.08	.06	.08	.06	.03	.00
CaO	4.27	5.16	3.61	4.83	5.56	4.09	5.13	4.20	3.63	.89
MgO	2.28	2.58	2.21	2.41	2.60	2.07	2.48	2.04	1.19	.08
K_2O	1.57	1.37	1.33	1.43	1.18	1.58	1.25	1.76	.95	2.61
Na_2O	4.10	4.64	3.33	3.72	3.71	3.68	3.60	4.43	4.91	4.75
P_2O_5	.17	.23	.15	.22	.22	.18	.19	.19	.15	.04
CIPW norms										
Quartz	24.45	16.68	33.01	24.30	21.59	28.80	25.51	22.90	27.80	39.77
Corundum	.91	---	3.42	1.15	1.05	1.21	---	---	1.13	---
Orthoclase	9.28	8.10	7.86	8.45	6.97	9.34	7.39	10.60	5.60	15.42
Albite	34.70	39.26	28.18	31.47	31.40	31.14	30.46	37.20	41.55	40.19
Anorthite	20.07	20.67	16.93	22.52	26.15	19.11	24.13	18.10	17.03	4.15
Wollastonite	---	1.43	---	---	---	---	.03	.80	---	---
Enstatite	5.68	6.43	5.50	6.00	6.48	5.15	6.18	5.10	2.96	.20
Ferrosillite	1.02	1.78	1.16	1.21	1.33	1.10	1.62	1.20	.94	---
Magnetite	2.26	3.41	2.39	2.80	2.93	2.42	2.96	2.60	1.81	---
Ilmenite	1.23	1.61	1.20	1.60	1.59	1.31	1.29	1.20	.82	---
Rutile	---	---	---	---	---	---	---	---	---	.18
Apatite	.40	.54	.35	.52	.52	.43	.45	.30	.35	.09

ALTERATION AND MINERALIZATION

The emplacement of the granodiorite of Grouse Creek was accompanied by extensive hydrothermal alteration that caused Cu-Au-Ag and associated base-metal enrichment. Within the vicinity of the Grouse Creek stock, this alteration was responsible for silver and base-metal enrichment. To the north, within the granodiorite of Bullrun Creek and the ultramafic rocks, porphyritic dike emplacement was associated with widespread gold and base-metal mineralization.

GRANODIORITE OF BULLRUN CREEK—RECORD MINE

Gold mineralization occurred within amphibole stockwork zones in the granodiorite of Bullrun Creek (Record Mine, fig. 11.2) and within sheared, talc-carbonate-altered ultramafic rocks on Bullrun Mountain (Thomason Mine, fig. 11.2) and Mine Ridge (Bullrun Mine, fig. 11.2; Orion Mine, lat 44°20'40" N., long 118°16'47" W.). These mines form the old Bullrun Mining District. The Record Mine, the largest mine in the district, is thought to have produced about $103,000, mainly during the 1930's (Brooks and Ramp, 1968).

Gold mineralization at the Record Mine is in northeast-striking amphibole veins and stockwork zones along the northeast margin of the Bullrun Creek stock. The veins extend 100–200 m into the stock away from the ultramafic contact, but few veins extend beyond the contact into the ultramafic rocks. Within the stock, vein densities and gold mineralization appear to increase outward toward the ultramafic contact. The veins consist of a dark-green coarse-bladed amphibole, coarse-grained apatite, magnetite, sulfides, and occa-

sional pyroxene or albite intergrowths. Sulfide minerals include molybdenite, pyrrhotite and lesser pyrite, chalcopyrite, and cobaltite. Molybdenite-cobaltite concentrations may locally reach several percent. Very fine to coarse free gold is present as intergrowths with amphibole, apatite, magnetite, or molybdenite, and as very fine inclusions in most sulfides. Actinolite, biotite, and chlorite replace amphibole and pyroxene, and, along with rare quartz, form late, crosscutting veins. These late veins also contain pyrrhotite, pyrite, and chalcopyrite and some free gold. Albite encloses most amphibole veins and locally replaces the equigranular wall rock. Within albitic zones, primary hornblende is replaced by a secondary pale or light-green amphibole.

Alteration and vein formation must have occurred when the Bullrun Creek stock was cool enough to sustain brittle fracture. Mineralized veins cut both the stock and later biotite-tonalite dikes, but few veins are found crosscutting porphyritic dikes. Instead, many of the porphyritic dikes (associated with the Grouse Creek stock) in the vicinity of the Record Mine are pervasively altered to secondary amphibole and albite, suggesting alteration may have accompanied, or closely followed, the emplacement of the porphyritic dikes. These porphyritic dikes may contain several percent disseminated pyrrhotite, chalcopyrite, and pyrite, and many are gold-bearing.

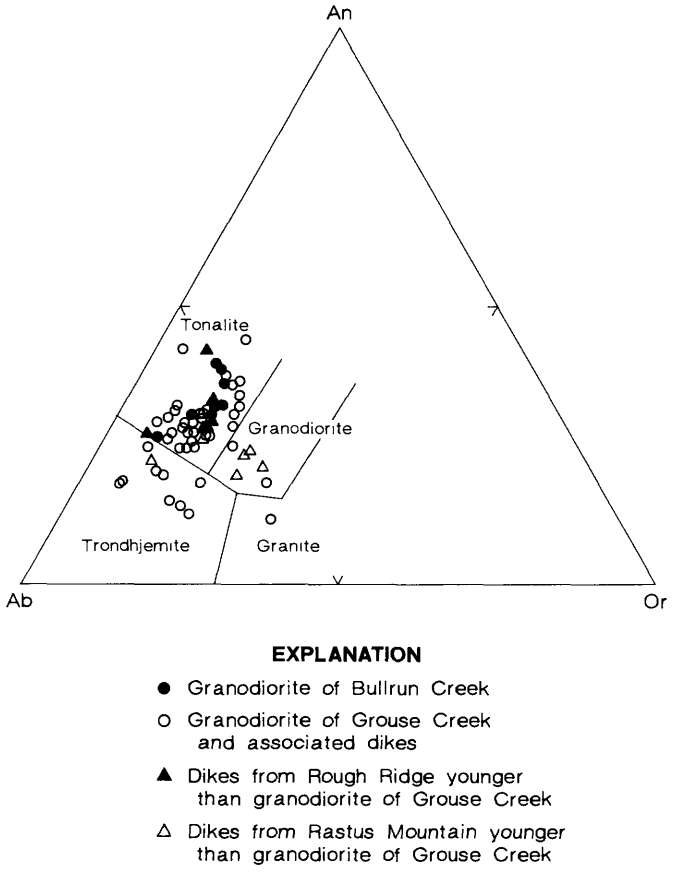

FIGURE 11.20.—Normative anorthite(An)-albite(Ab)-orthoclase(Or) diagram (Barker, 1979) of all analyses of Oligocene intrusive rocks of north end of Ironside Mountain inlier.

GRANODIORITE OF GROUSE CREEK

The granodiorite of Grouse Creek forms the core of a large, elongate hydrothermal alteration zone (fig. 11.14), or pyrite halo, that extends from the south end of Mine Ridge 13–14 km southeast toward Ironside Mountain (figs. 11.1, 11.14). The zone is formed mainly within the Weatherby Formation, but in Koski Basin it cuts the south end of the Bullrun Creek stock. Altered metasedimentary rock within the zone typically contains secondary pyrite in amounts ranging from trace to several percent; in addition the rock may be weakly silicified. Calcareous beds near the margins of the Grouse Creek stock contain minor skarn. Porphyritic dikes within the alteration zone are propylitically altered.

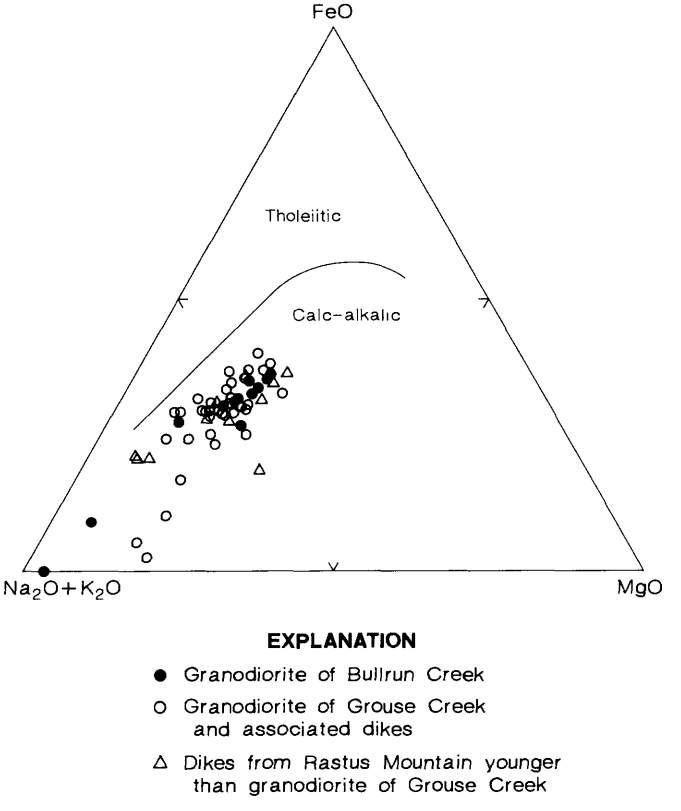

FIGURE 11.21.—Alkali (Na_2O+K_2O)-FeO-MgO diagram of all Oligocene intrusive rocks of north end of Ironside Mountain inlier. Tholeiitic and calc-alkalic fields from Kuno (1968).

TABLE 11.11.—*Chemical analyses of*

[All values in weight percent. Major-element analyses and Cross, Iddings, Pirsson, and Washington (CIPW) norms by X-ray-fluorescence spectroscopy, Washington State University

Sample	MH2	MH11	MH36	MH49A	MH51	MH65	MH101A	MH140	MH165	MH174
										Major
SiO_2	69.65	66.45	66.52	68.03	67.99	66.89	68.04	67.27	66.35	66.90
Al_2O_3	16.26	17.13	17.04	17.14	16.27	17.42	16.73	17.03	16.43	17.31
Fe*	2.60	3.20	3.39	2.98	3.27	2.55	.75	2.77	3.74	3.61
MgO	1.02	1.99	1.86	2.01	1.61	1.69	1.84	1.85	2.07	1.98
CaO	4.95	4.51	3.88	3.86	3.56	4.48	3.18	4.30	4.27	4.14
Na_2O	3.32	5.07	5.17	3.43	5.24	4.41	5.15	4.52	4.87	3.88
K_2O	1.61	.90	1.26	1.74	1.31	1.78	3.57	1.51	1.44	1.38
TiO_2	.34	.52	.62	.53	.46	.57	.54	.60	.59	.56
P_2O_5	.10	.15	.19	.16	.16	.15	.15	.19	.19	.17
MnO	.06	.08	.07	.13	.13	.05	.04	.03	.07	.07
										CIPW
Quartz	30.27	23.64	23.52	28.71	25.56	23.53	18.26	23.72	21.06	26.76
Corundum	---	.60	1.18	2.43	.93	.47	---	.67	---	2.08
Orthoclase	9.99	5.56	7.86	10.82	8.21	11.17	21.80	9.40	8.92	8.57
Albite	29.79	38.42	39.27	30.13	39.26	35.54	39.26	37.23	39.69	32.75
Anorthite	23.52	21.84	18.46	18.45	17.09	21.63	14.00	20.04	19.21	19.66
Wollastoite	.24	---	---	---	---	---	.43	---	.43	---
Enstatite	2.39	6.42	4.66	4.96	4.01	3.81	4.49	4.78	5.23	4.91
Ferrosilite	1.13	5.23	1.12	1.13	1.43	.65	---	.71	2.60	1.35
Magnetite	1.80	2.18	2.31	2.00	2.23	1.73	---	1.86	2.52	2.44
Hematite	---	---	---	---	---	---	.33	---	---	---
Ilmenite	.65	1.01	1.20	1.01	.89	1.10	.91	1.16	1.14	1.08
Sphene	---	---	---	---	---	---	.17	---	---	---
Apatite	.24	.36	.45	.38	.40	.38	.36	.45	.45	.43

Sample	JB-81-25	JB-81-26	JB-81-40	JB-81-48	JB-82-154	JB-82-156	JB-82-163	JB-81-JM1	GCB	GCC
										Major
SiO_2	66.30	66.48	66.59	65.36	67.88	67.21	66.52	67.89	65.17	69.00
Al_2O_3	16.02	16.08	17.35	17.76	16.22	16.12	16.31	17.30	16.54	15.98
Fe*	3.65	3.74	3.69	4.39	3.52	4.23	4.39	2.89	4.38	3.07
MgO	2.34	2.04	2.54	2.33	1.87	1.95	2.22	.89	2.61	2.59
CaO	4.10	5.33	3.88	4.63	3.78	3.86	3.58	5.18	3.84	1.70
Na_2O	4.88	4.49	3.88	3.33	4.77	3.91	4.80	3.12	4.50	3.80
K_2O	1.71	1.00	1.39	1.28	1.24	1.98	1.26	1.49	1.98	3.35
TiO_2	.78	.63	.48	.71	.52	.55	.64	.43	.88	.47
P_2O_5	.19	.17	.14	.18	.14	.16	.17	.13	.26	.13
MnO	.04	.05	.06	.02	.06	.03	.11	.07	.05	.05
										CIPW
Quartz	19.70	22.96	26.31	27.54	24.29	25.40	22.48	30.11	19.30	26.90
Corundum	---	---	2.74	2.91	0.49	0.91	0.95	0.30	0.50	3.40
Orthoclase	10.19	5.91	8.21	7.56	7.33	11.70	7.45	8.80	11.70	20.00
Albite	41.30	37.99	32.83	28.18	40.37	33.08	40.62	26.40	38.30	32.00
Anorthite	16.75	20.77	18.33	21.80	17.84	18.10	16.65	27.97	17.50	7.50
Wollastoite	0.98	1.91	---	---	---	---	---	---	---	---
Enstatite	5.83	5.08	6.33	5.80	4.66	4.86	5.53	2.22	6.50	6.50
Ferrosilite	0.96	1.27	1.52	1.47	1.33	1.67	1.76	1.14	1.20	0.10
Magnetite	2.46	2.52	2.49	2.97	2.38	2.86	2.96	1.94	2.80	1.80
Hematite	---	---	---	---	---	---	---	---	---	---
Ilmenite	1.48	1.20	0.91	1.35	0.99	1.04	1.22	0.82	1.70	2.00
Sphene	---	---	---	---	---	---	---	---	---	---
Apatite	0.45	0.40	0.33	0.43	0.33	0.38	0.40	0.31	0.60	0.30

the granodiorite of Grouse Creek

(Hooper and Johnson, 1989). Major elements normalized on a volatile-free basis with 0.9 Fe expressed as FeO, 0.1 Fe expressed as Fe_2O_3, and Fe* equal to FeO+Fe_2O_3. ---, not present]

MH178C	MH179	MH180	MH189	MH191	MH196A	MH198B	MH204	MH208	MH219	MH221	MH226
elements											
67.64	69.21	66.97	66.09	66.51	68.35	68.16	66.40	68.91	69.30	69.83	64.43
17.02	17.28	16.71	17.31	17.21	16.84	16.48	17.13	16.64	17.31	17.08	17.62
3.70	3.26	5.07	3.92	3.52	1.23	3.56	3.88	3.13	1.71	3.29	4.82
2.15	2.27	2.23	2.41	1.81	1.98	2.14	2.03	1.61	1.71	1.66	1.84
3.24	2.17	2.37	3.55	3.82	3.69	4.88	3.93	3.14	3.12	1.75	4.16
3.95	3.95	4.08	4.33	4.79	4.72	3.48	4.50	4.39	4.81	4.23	4.62
1.50	1.07	1.68	1.52	1.55	2.45	.46	1.31	1.50	1.40	1.50	1.37
.55	.56	.63	.59	.54	.52	.61	.60	.46	.50	.48	.77
.17	.18	.19	.21	.19	.14	.15	.16	.13	.13	.13	.27
.07	.05	.08	.07	.07	.07	.07	.07	.07	.03	.05	.10
norms											
28.15	33.87	27.66	23.79	22.18	21.28	32.00	23.61	28.14	27.48	32.95	20.61
3.21	6.01	4.21	2.43	1.18	.01	1.65	1.49	2.33	2.58	5.59	1.62
9.34	6.56	10.46	9.52	9.63	15.19	2.54	8.16	9.34	8.75	9.34	8.10
33.25	33.26	34.02	25.88	39.09	38.84	29.79	36.98	36.39	39.35	35.37	39.09
15.19	9.74	10.65	16.54	17.94	17.67	23.31	18.70	15.03	14.91	7.87	18.87
---	---	---	---	---	---	---	---	---	---	---	---
5.48	5.78	5.80	6.08	4.81	4.88	5.53	5.48	4.26	4.28	4.16	4.58
1.42	1.09	2.09	1.48	1.28	---	1.22	1.43	1.22	.24	1.24	1.78
2.49	2.20	3.44	2.65	2.38	.72	2.41	2.62	2.12	1.13	2.23	3.26
---	---	---	---	---	.05	---	---	---	---	---	---
1.06	1.08	1.22	1.14	1.05	1.01	1.18	1.16	.89	.95	.95	1.46
---	---	---	---	---	---	---	---	---	---	---	---
.43	.38	.47	.50	.47	.36	.38	.38	.31	.33	.33	.64

GCD	GCE	GCG	GCH	KEBR7	KEX9	KE9	KE17	KE19	KE95	KE113	KE214
elements											
68.49	65.76	68.84	68.53	64.17	70.48	68.40	67.48	69.53	68.21	66.41	67.98
16.62	17.58	16.98	17.37	18.47	16.46	16.75	16.56	16.62	15.98	17.63	16.36
3.83	3.14	3.34	3.91	4.74	1.98	3.28	4.18	3.11	.30	4.89	3.41
1.84	2.67	1.88	3.02	2.07	1.08	1.64	2.05	1.29	1.77	2.57	1.63
1.76	4.03	3.12	1.99	4.60	4.39	2.93	3.71	1.96	6.19	1.81	4.14
4.90	4.98	4.52	4.08	3.50	3.48	5.12	4.28	5.57	4.85	4.21	4.36
2.03	.81	.76	.47	1.50	1.74	1.19	.94	1.27	1.89	1.41	1.47
.53	.92	.54	.59	.69	.27	.49	.57	.47	.49	.74	.51
.15	.22	.16	.16	.17	.08	.15	.16	.14	.13	.24	.15
.04	.03	.02	.06	.07	.04	.07	.06	.06	.05	.08	.06
norms											
25.40	21.20	30.00	34.00	24.90	33.20	25.00	22.70	26.20	20.00	28.20	24.90
3.50	1.40	3.30	6.80	3.10	1.20	1.90	2.00	2.90	---	6.20	---
12.20	5.00	4.40	2.80	8.90	10.00	7.20	5.60	7.20	11.10	8.30	8.90
41.40	41.90	38.30	34.60	29.30	29.30	43.50	36.20	47.20	41.40	35.60	36.70
7.80	19.20	14.70	8.90	22.00	20.80	13.60	17.50	8.90	16.10	8.10	20.60
---	---	---	---	---	---	---	---	---	5.10	---	---
4.60	.40	4.70	7.60	5.20	0.40	4.00	5.10	3.10	4.40	6.60	3.90
1.30	6.70	1.10	1.30	1.70	2.60	1.20	1.70	1.20	---	1.80	1.50
2.60	2.10	2.10	2.60	3.20	2.10	2.30	2.80	2.10	---	3.20	2.30
---	---	---	---	---	---	---	---	---	.20	---	---
1.10	1.70	1.10	1.10	1.40	.50	.90	1.10	.90	.50	1.40	.90
---	---	---	---	---	---	---	---	---	.60	---	---
0.30	.60	.30	.30	.30	.30	.30	.30	.30	.30	.60	.30

TABLE 11.12.—*Chemical analyses of dikes that postdate hydrothermal alteration*

[All values in weight percent. Major-element analyses and Cross, Iddings, Pirsson, and Washington (CIPW) norms by X-ray fluorescence spectroscopy, Washington State University (Hooper and Johnson, 1989). Major elements normalized on a volatile-free basis with 0.9 Fe expressed as FeO, 0.1 Fe expressed as Fe_2O_3, and Fe* equal to $FeO+Fe_2O_3$. ---, not present]

Sample	MH89[1]	MH216[1]	JB81-6[1]	GCF[1]	KEX10[1]	KE26[1]	MH5[2]	MH188[2]	MH53[3]	MH199[3]	MH32[4]	MH184[4]	MH211[4]
Major elements													
SiO_2	61.77	62.73	60.69	63.75	59.73	63.00	66.81	67.11	68.43	68.68	71.66	73.60	71.45
Al_2O_3	16.27	16.86	17.84	17.61	18.07	16.87	17.63	17.18	17.08	16.82	16.08	15.73	16.56
TiO_2	.93	.89	1.29	2.40	.88	.79	.58	.54	.40	.43	.27	.27	.27
Fe*	5.58	5.13	5.71	3.63	6.67	5.13	3.65	3.00	2.92	3.20	1.93	1.78	1.97
MnO	.10	.08	.07	4.77	.10	.07	.07	.07	.06	.05	.03	.03	.04
CaO	4.78	4.62	4.78	5.71	5.92	5.23	2.64	4.25	3.19	3.36	3.22	2.45	2.85
MgO	3.53	2.82	3.50	.82	3.61	2.57	2.06	2.08	1.78	1.72	.95	.45	.80
K_2O	1.71	1.85	1.58	1.06	.92	1.82	2.30	1.30	1.64	1.46	2.19	2.36	2.18
Na_2O	4.98	4.67	4.30	.21	3.96	4.63	4.08	4.33	4.38	4.14	3.57	3.25	3.79
P_2O_5	.36	.33	.25	.04	.16	.30	.18	.15	.12	.13	.09	.09	.09
CIPW norms													
Quartz	13.93	15.09	14.24	12.70	13.90	15.10	25.62	24.81	27.84	28.82	32.84	37.97	32.96
Corundum	---	---	---	.96	---	.10	---	3.87	1.18	2.66	2.46	.60	3.36	2.77
Orthoclase	10.64	11.47	9.34	5.00	5.60	10.60	14.30	8.04	10.28	15.19	5.56	14.59	13.59
Albite	38.00	38.00	36.38	48.20	33.50	38.80	33.76	35.97	35.28	34.69	38.42	28.09	32.32
Anorthite	18.76	19.77	22.08	20.00	28.40	18.90	12.15	16.54	15.37	16.17	12.15	11.75	13.83
Wollastonite	1.18	.47	---	1.20	---	2.20	---	---	---	---	---	---	---
Enstatite	9.12	7.55	8.72	9.10	2.80	6.70	4.93	5.18	4.33	4.18	2.07	1.67	1.69
Ferrosilite	1.95	1.70	1.40	---	9.40	2.20	1.32	1.03	1.18	1.29	.75	.65	.80
Magnetite	3.79	3.47	3.86	1.20	4.40	3.50	2.48	2.02	1.97	2.16	1.29	1.17	1.31
Haematite	---	---	---	.30	---	---	---	---	---	---	---	---	---
Ilmenite	1.79	1.71	2.40	2.00	1.70	1.50	1.12	1.03	.78	.82	1.01	.51	.51
Apatite	.88	.81	.59	.30	.30	.60	.45	.38	.31	.31	.21	.24	.24

[1]Porphyritic quartz monzodiorite.
[2]Porphyritic granodiorite, Rough Ridge.
[3]Bullrun Mountain granodiorite dikes.
[4]Rastus Mountain granodiorite dikes.

At the core of the pyrite halo, within the Grouse Creek stock, porphyritic granodiorite is altered to propylitic, phyllitic, argillic, and potassic alteration assemblages. These assemblages form complex, overlapping alteration zones that pervasively alter the stock (fig. 11.14; propylitic zone not shown). Typically, zones of early propylitic and potassic alteration are partially or completely overprinted by later phyllitic or argillic alteration.

The zone of potassic alteration in the granodiorite, characterized by the replacement of hornblende by secondary biotite, crops out in topographically low-lying areas along the north and south forks of West Camp Creek. Exploratory drilling in these areas encountered well-developed potassic alteration at depth. Throughout the Grouse Creek stock, the potassic alteration zone apparently forms a deeper alteration assemblage exposed only in eroded, low-lying valleys. Geochemical sampling and drilling in the potassic zone encountered significant enrichment in disseminated chalcopyrite and molybdenite.

The most widespread alteration within the Grouse Creek stock is propylitic alteration (not shown in fig. 11.14) formed at the same time as the potassic alteration. The propylitic alteration is characterized by the formation of secondary epidote, chlorite, calcite, and pyrite, as well as minor clinozoisite, sphalerite, and galena. Both the potassic and propylitic zones are partially overprinted by the younger quartz-sericite-pyrite assemblage of the phyllitic alteration. This younger phyllitic-alteration assemblage forms widespread, geometrically complex zones around the margins of the Grouse Creek stock, as well as blanket-like zones on Rough Ridge and Rastus Mountain. Porphyritic granodiorite within the phyllitic alteration zone is strongly silicified and pyritized. Plagioclase is typically altered

TABLE 11.13.—*Trace-element analyses of Oligocene intrusions, Ironside Mountain inlier*

[All values in parts per million. Analyses by inductively coupled plasma spectrometry, Kings College, London; analyst, P.R. Hooper. ---, not determined]

	Granodiorite of Bullrun Creek		Granodiorite of Grouse Creek				Postalteration dikes	
Sample	JB-81-55	JB-82-295	MH-51[1]	MH-55	MH-89	JB-81-48	MH-5	MH-53
Ba	---	738	783	763	797	---	761	966
Cr	27	13	39	27	63	21	35	35
Cu	20	11	13	42	43	29	21	16
Nb	24	12	13	13	20	16	13	11
Ni	31	18	32	37	68	30	34	29
Sc	10	6	8	9	14	10	10	8
Sr	655	456	632	675	755	632	643	686
V	97	48	61	73	123	87	82	62
Y	18	13	15	15	21	16	13	11
Zn	63	28	83	125	125	33	67	50
Rb	34	26	---	---	---	39	---	---

[1]Rare-earth-element data (in parts per million) for sample MH-51: La, 3.10; Ce, 23.97; Pr, 3.27; Nd, 13.07; Sm, 2.45; Eu, 0.79; Gd, 2.30; Dy, 2.19; Ho, 0.56; E, 1.36; Yb, 1.26; Lu, 0.18.

to sericite, and hornblende is altered to a sericite-chlorite aggregate.

Late-stage argillic alteration overprints propylitic, potassic, and phyllitic alteration zones on the lower western slopes of Rastus Mountain. The irregularly shaped argillic zone appears to represent the youngest alteration event in the Rastus Mountain area, and is characterized by intense acid-leaching of the porphyritic granodiorite. The rock's primary texture has been destroyed and altered to an aggregate of quartz, sericite, clay, and limonite. The late-stage argillic alteration zone contains anomalously high amounts of mercury and antimony. Coarse bladed stibnite is exposed locally in a roadcut in intensely acid-leached porphyritic granodiorite.

On the ridge west of Grouse Spring, younger hydrothermal breccias crosscut the Grouse Creek stock. Though exposures are poor, results of exploratory drilling in the area suggest the presence of an irregularly shaped, shallow, northeast-plunging hydrothermal breccia zone or pipe. Within the pipe, porphyritic granodiorite and metasedimentary fragments are cemented by chlorite, quartz, calcite, epidote, clinozoisite, pyrite, and chalcopyrite. Intergrowths of fine- to coarse-grained chalcopyrite with chlorite, quartz, and calcite have partially replaced earlier epidote and clinozoisite. Drilling within the breccia reveals copper mineralization averaging as much as 1 percent Cu, with locally higher grades with as much as 4 percent Cu. Mineralized zones are silver enriched, and their Cu:Ag ratios average around 1:1 (Manville Products Corporation, oral commun., 1986).

Hydrothermal breccias in the Grouse Spring area display a close spatial and temporal relation to aplite-cemented intrusion breccias cropping out on the same ridge. In drill core, hydrothermal breccias are both superimposed upon and crosscut by aplitic intrusion breccias. Both breccia types contain a variety of porphyritic fragments with different alteration assemblages. Both of these breccias may be related to deeper, late-stage magmatic activity. The alteration zones associated with the Grouse Creek stock constitute the first Tertiary porphyry system documented in northeastern Oregon.

DISCUSSION AND CONCLUSIONS

The pre-Jurassic rocks of the Ironside Mountain inlier include serpentinized peridotite, gabbro, and plagiogranite as well as some basalt, ribbon chert, and various schistose units that vary from crossbedded quartzite through mica- to hornblende-schist. All but the massive peridotite of Bullrun Mountain occur as oriented blocks in a melange with a highly sheared, serpentinized matrix. The melange also contains large blocks of calc-alkaline andesite. The association of rock types is similar to that of an ophiolite assemblage (Coleman, 1977), although the andesite is anomalous, and neither pillow basalt nor a basic dike complex is present.

Ironside Mountain lies between two larger and better exposed inliers of ophiolitic rocks within the Baker terrane: the Canyon Mountain Complex 50 km to the

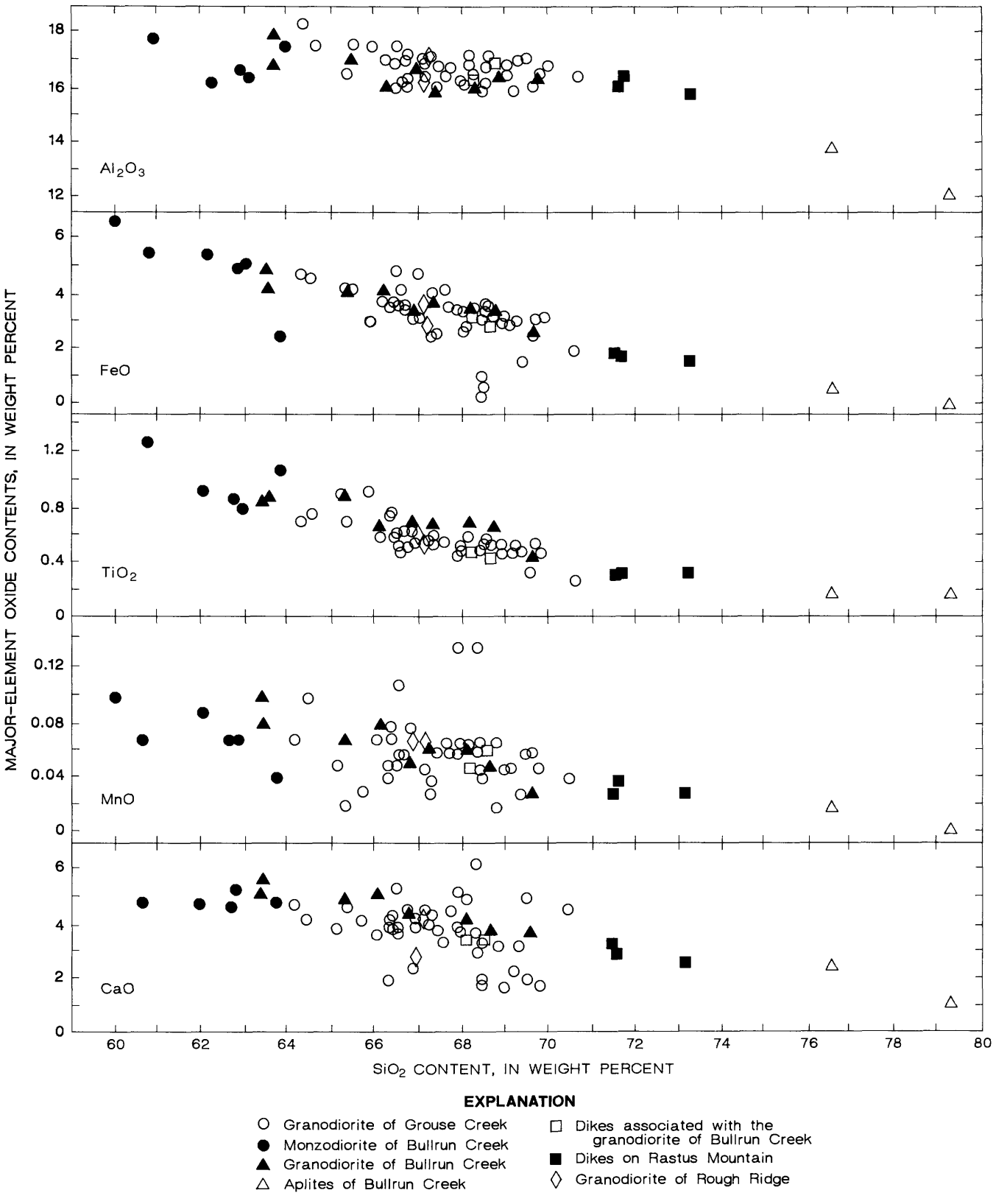

FIGURE 11.22.—Major-element-oxide concentrations plotted against SiO_2 concentrations for samples of Oligocene intrusions from north end of Ironside Mountain inlier.

west and the Sparta complex almost 100 km to the northeast (Thayer, 1977; Gerlach and others, 1979; Phelps, 1979; Phelps and Avé Lallemant, 1980). These two complexes have different ages (approximately 260 Ma and 230 Ma, respectively) (Avé Lallemant and others, 1980) and have distinctive REE patterns (fig. 11.9). The rock associations of both complexes are broadly similar to those of the Ironside Mountain inlier, but the Ironside Mountain rocks correspond in age and in their more depleted LREE patterns to those of the Canyon Mountain Complex. All three inliers lack a basic dike complex, posses little if any pillow basalt, and include relatively large proportions of plagiogranite and keratophyre; these characteristics, taken together with their geochemical signatures, have led previous authors to postulate that the Sparta complex and the Canyon Mountain Complex originated as the residual roots of an island-arc system (Phelps and Avé Lallemant, 1980; Gerlach and others, 1981) rather than as a section of mantle and oceanic crust formed at some distant midoceanic ridge-rift system (Coleman, 1977). The same arguments apply to the rocks of the Ironside Mountain inlier, where they are supported by the date of the first major (D_1) deformation, which is almost coincident with the formation of the ophiolitic rocks of the Canyon Mountain Complex. These rocks were formed and then deformed (presumably in the subduction process, see below) within a short period, permitting no time for their transport from some distant midoceanic ridge-rift system to the

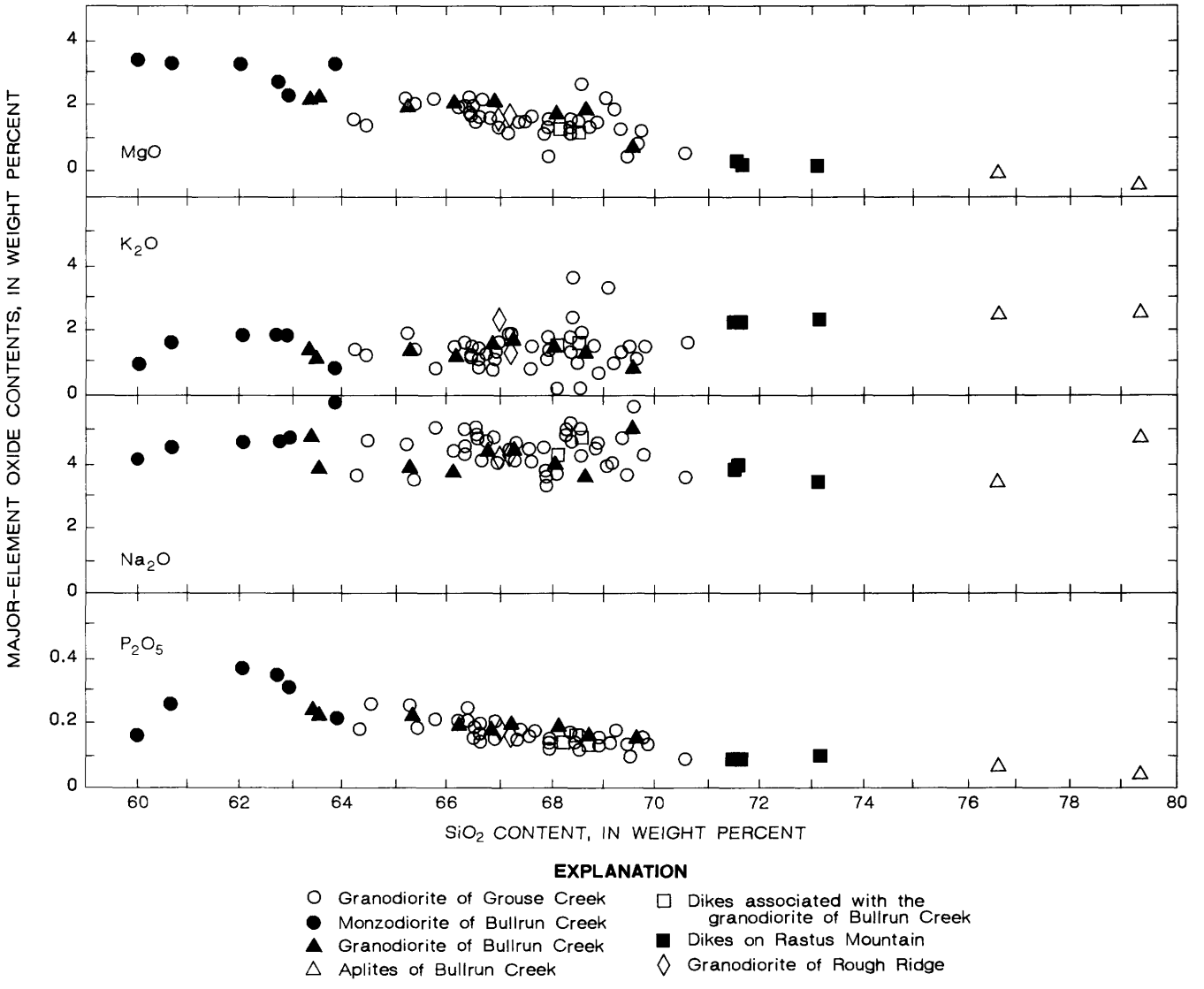

FIGURE 11.22.—Continued.

site of subduction. As argued by Gerlach and others (1979) for the Canyon Mountain Complex, the ophiolitic rocks of the Ironside Mountain inlier probably represent the roots of a primitive island-arc system, an environment in which the large blocks of calc-alkaline andesite are less anomalous than they would be in a midocean setting.

The peridotite of Bullrun Mountain and Mine Ridge has a restricted dunite-harzburgite mineralogy, conspicuously lacking in the plagioclase and well-developed phase layering that would be expected of a cumulate formed from a basaltic magma within the crust. This mineralogy, reflected in the low CaO and Al_2O_3 concentrations, taken together with the coarse fabric of elongate refractory (Fo_{90-92}) olivine grains, indicates that the peridotite formed as the residuum of partial melting in the mantle, not as a crustal cumulate. As in a more typical ophiolitic complex, the closely associated basalt, gabbro, and plagiogranite are interpreted as the fractionated derivatives of the basaltic melt crystallizing within the overlying crust.

The peridotite has undergone at least two distinguishable phases of serpentinization. The first phase bears no evidence of slickensides or brecciation, and the serpentinite assemblage includes lizardite, normally associated with a low shear-stress environment. This event postdates formation of the metamorphic fabric of the peridotite, including kink bands. It appears to have occurred at depth and to predate emplacement of the peridotite into the crust. The second phase of serpentinization includes the formation of talc associated with slickensiding and brecciation, in addition to the formation of antigorite, all of which imply an environment of considerable shear stress. This phase is most obviously associated with the emplacement of the peridotite into the crust, an event that culminated in the formation of the melange of Mine Ridge.

The three fold phases present in the schistose rocks of Mine Ridge are interpreted as the result of progressive, noncoaxial shear deformation and are correlated with the D_1 deformation recognized throughout the Baker terrane by Avé Lallemant and others (1980). The isoclinal F_1 folds are associated with a relatively high grade (epidote amphibolite facies) metamorphic fabric dated at 260 Ma and characterized by a penetrative, near-vertical east- to northeast-striking foliation plane within which the fold axes plunge steeply to the north or south. The two later fold phases are nonpenetrative and have variable axial planes.

The geometry of isoclinal F_1 folds whose axes plunge consistently down the dip of their axial surfaces is consistent with the model advocated by Avé Lallemant and others (1980). In this model, folds develop whose axes are originally horizontal and perpendicular to the direction of transport in the planes of variable shear parallel to the plane of subduction. These early folds are subsequently tightened by flattening and, as the degree of extension increases down the subduction plane, have their axes rotated into the direction of maximum extension (parallel to the direction of subduction). Rotation would be greatly facilitated by the incorporation into the shear system of incompetent serpentinite between the more competent blocks to create the melange of Mine Ridge.

Once the serpentinite was in place, subsequent deformation would be largely absorbed by the serpentinite, the blocks acting only passively as the whole melange changed shape. The blocks would rotate but would carry little or no internal record of any later regional strain. Avé Lallemant and others (1980) demonstrated the regionally consistent north-south trend of the F_1 fold axes (and east-striking axial surfaces), which implies a north-south direction of subduction. However, the original direction of subduction could have been very different. First, if the area of 60° clockwise Tertiary rotation of the Wallowa Mountains block (Wilson and Cox, 1980) extended as far as the Mine Ridge area, then the original direction of compression and subduction resulting in the D_1 strain pattern would have been N. 60° W. Second, the S_0-S_1 plane appears to have been rotated subsequently into parallelism with the Late Jurassic (D_2) deformation.

The second (D_2) episode of regional deformation recognized by Avé Lallemant and others (1980) occurred in the Late Jurassic. D_2 is responsible for the tight chevron folds in the bedded turbidites of the Weatherby Formation. The D_2 folds have steep east- to northeast-striking axial surfaces and horizontal fold axes. Using the asymmetry of the minor folds, the bedding/cleavage relations, and the abundant sedimentary structures that indicate tops and bottoms of beds, larger fold closures can be recognized (fig. 11.14). The D_2 deformation appears to represent north-south to northwest-southeast shortening with maximum extension in a vertical direction.

Although the D_2 deformation is relatively severe in the Jurassic sedimentary rocks, no trace of it is recognized in the Permian blocks of schistose rocks in the melange of Mine Ridge (although it is possible that the F_3 crenulation folds in these schists are associated with the D_2 event). It is assumed that the D_2 strain was absorbed by the incompetent serpentinite matrix of the melange, passively rotating the blocks to produce steeper S_1 axial surfaces and F_1 fold axes.

The contact between the Jurassic Weatherby Formation and the older Permian rocks is also the

boundary between the Baker terrane and the Izee terrane. All exposures of this boundary appear to be faulted, and the original relations must remain somewhat speculative. But as noted by Brooks and Ferns (1979) the Weatherby Formation adjacent to the older rocks is often much coarser grained than elsewhere, containing large clasts of serpentinite, chert, quartzite, and other rock types clearly derived from the adjacent melange. A thin strip of the Weatherby Formation also lies along the northern side of the melange (fig. 11.1). We conclude that the Weatherby was deposited unconformably on the exposed Permian melange and that the contact has been only slightly modified by faulting. A significant degree of thrusting is not apparent, but the slight asymmetry of the cleavage with respect to the fold limbs of the D_2 folds may imply some small component of thrusting to the northwest.

The source of the Weatherby Formation exposed in the Ironside Mountain inlier is predominantly the ophiolitic melange and island-arc rocks. To the south the Weatherby is derived from the similar island-arc rocks of the Olds Ferry terrane (Huntington arc; Brooks, 1979b). If the ophiolitic rocks represent the roots of the primitive island-arc systems associated with the subduction zone that created the melange, and the younger Jurassic sediments are derived from the same older units, then it is probable that each of the four "terranes" of the Blue Mountains province were formed in proximity to each other, although compressed by the subduction and subsequent accretion processes. Hillhouse and others (1982) demonstrate that the Wallowa terrane was formed offshore but in approximately the same latitude relative to the North American craton as at present. We can, therefore, surmise that the Blue Mountains province originated as a complex series of island-arc systems lying off the western coast of North America and that these were compressed by inter-arc subduction from the Permian through the Triassic (D_1) and subsequently by accretion to the craton in the Jurassic through the Early Cretaceous (D_2) (Fleck and Criss, 1985). Use of the term "terrane" for these various units may be criticized in that although each unit does possess discrete stratigraphic sequences, the units originated in proximity to each other and are not wholly unrelated.

The D_2 deformation is cut by undeformed intrusions of Late Jurassic to Cretaceous age (Armstrong and others, 1977; Fleck and Criss, 1985). The Late Jurassic intrusions often lie across contacts between the various "terranes," which must, therefore, have been in their present relative positions by the end of the Jurassic. Calc-alkaline igneous activity continued intermittently in northeastern Oregon through the Miocene. The Ironside Mountain inlier contains a Cretaceous (approximately 120 Ma) intrusion at its south end (Thayer and Brown, 1964). At its north end are the granodiorites of Bullrun Creek and Grouse Creek; their ages—36 to 34 Ma—are similar to those of the calc-alkaline volcanic rocks of the eastern part of the Clarno Formation (Urbanczyk and Lilligren, 1990; Walker, 1990), which flank the inlier on either side. The eastern part of the Clarno Formation is overlain by the Miocene calc-alkaline Strawberry Volcanics (Robyn, 1977).

The northern part of the Ironside Mountain inlier is intruded by two main stocks—the granodiorites of Bullrun Creek and Grouse Creek—and numerous associated smaller intrusive bodies dated at between 36 Ma and 34 Ma. The various intrusions are distinguished by their textures and associated hydrothermal activity but are mineralogically and chemically very similar. Their low-K tonalite-trondhjemite composition is cited by Barker (1979) as typical of intrusions in accreted terranes on the oceanic side of large calc-alkaline batholiths emplaced along cratonic margins. The chemical signature of these early Oligocene intrusions is similar in some critical respects to the older Permian and Triassic igneous rocks of the inlier, and it is possible that they were generated, at least in part, by the partial melting of the older accreted rocks.

The younger of the two large stocks and the porphyritic dikes related to it are associated with gold and base-metal mineralization in the vicinity of the peridotite of Bullrun Creek. The main stock, intruding the Weatherby Formation farther south, forms the core of a large northwest-elongated alteration zone that is associated with a silver and base-metal enrichment. This alteration zone is the first Tertiary porphyry system documented in northeastern Oregon.

REFERENCES CITED

Almy, R.B., III, 1977, Petrology and major element geochemistry of albite granite near Sparta, Oregon: Bellingham, Western Washington State College, M.S. thesis, 100 p.

Armstrong, R.L., Taubeneck, W.H., and Hales, P.O., 1977, Rb-Sr and K-Ar geochronometry of Mesozoic granitic rocks and their Sr isotopic composition, Oregon, Washington, and Idaho: Geological Society of America Bulletin, v. 88, p. 397-411.

Ashley, R.P., 1966, Metamorphic petrology and structure of the Burnt River Canyon area, northeastern Oregon: Stanford, Calif., Stanford University, Ph.D. dissertation, 193 p.

Augustithis, S.S., 1979, Atlas of the textural patterns of basic and ultrabasic rocks and their genetic significance: Berlin, Walter de Grayter, 393 p.

Avé Lallemant, H.G., and Carter, N.L., 1968, Upper mantle origin of Alpine-type peridotites: Geological Society of America Special Paper 121, 12 p.

———1970, Syntectonic recrystallization of olivine and modes of flow in the upper mantle: Geological Society of America Bulletin, v. 81, p. 2203-2220.

Avé Lallemant, H.G., Phelps, D.W., and Sutter, J.F., 1980, $^{40}Ar^{39}Ar$ ages of some pre-Tertiary plutonic and metamorphic rocks of eastern Oregon and their geologic relationships: Geology, v. 8, p. 371-374.

Barker, F., 1979, Trondhjemite—Definition, environment and hypothesis of origin, *in* Barker, F., ed., Trondhjemites, dacites, and related rocks: New York, Elsevier, p. 1-12.

Barker, F., and Arth, J.C., 1976, Generation of trondhjemites-tonalitic liquids and Archaen bimodal trondhjemite-basalt suites: Geology, v. 4, p. 596-600.

Barnes, I., and O'Neill, J.R., 1969, The relationship between fluids in some fresh Alpine-type ultramafics and possible modern serpentinization, western United States: Geological Society of America Bulletin, v. 80, p. 1947-1960.

Beane, J.E., 1984, The petrology of ophiolitic and dioritic rocks from Mine Ridge and the Bullrun Creek Valley, Baker County, Oregon: Pullman, Washington State University, M.S. thesis, 123 p.

Brooks, H.C., 1979a, Plate tectonics and the geologic history of the Blue Mountains: Oregon Geology, v. 41, p. 71-80.

———1979b, Geologic map of Huntington and part of Olds Ferry quadrangles, Oregon: Oregon Department of Geology and Mineral Industries Geologic Map Series GMS-13, scale 1:62,500.

Brooks, H.C., and Ferns, M.L., 1979, Geologic map of the Bullrun Rock quadrangle, Oregon: Oregon Department of Geology and Mineral Industries Geologic Map 0-79-6, scale 1:24,000.

Brooks, H.C., Ferns, M.L., Nusbaum, R.W., and Kovich, P.M., 1979, Geologic map of the Rastus Mountain quadrangle, Oregon: Oregon Department of Geology and Mineral Industries Geologic Map 0-79-7, scale 1:24,000.

Brooks, H.C., and Ramp, L., 1968, Gold and silver in Oregon: Oregon Department of Geology and Mineral Industries Bulletin G1, 337 p.

Brooks, H.C., and Vallier, T.L., 1978, Mesozoic rocks and tectonic evolution of eastern Oregon and western Idaho, *in* Howell, D.G., and McDougall, K.A., eds., Mesozoic paleogeography of the Western United States (Pacific Coast Paleogeography Symposium 2, Sacramento, Calif.): Los Angeles, Society of Economic Paleontologists and Mineralogists, Pacific Section, p. 133-145.

Brown, C.E., and Thayer, T.P., 1966, Geologic map of the Canyon City quadrangle, northeastern Oregon: U.S. Geological Survey Miscellaneous Geologic Investigations Map I-447, scale 1:250,000.

Caffrey, G.M., 1982, Petrology and alteration of ultramafic rocks of Bullrun Mountain, Baker County, Oregon: Pullman, Washington State University, M.S. thesis, 130 p.

Coleman, R.G., 1977, Ophiolites—Ancient oceanic lithosphere?, v. 12 *of* Minerals, Rocks, and Organic Materials Series: New York, Springer-Verlag, 229 p.

Coleman, R.G., and Keith, T.E., 1971, A chemical study of serpentinization, Burro Mountain, California: Journal of Petrology, v. 12, p. 311-328.

Dickinson, W.R., 1979, Mesozoic forearc basin in central Oregon: Geology, v. 7, p. 166-170.

Dickinson, W.R., Beard, L.S., Brakenridge, G.R., Erjavec, J.L., Ferguson, R.C., Inman, K.F., Knapp, R.A., Lindberg, F.A., and Ryberg, P.T., 1983, Provenance of North American Phanerozoic sandstones in relation to tectonic setting: Geological Society of America Bulletin, v. 94, p. 222-235.

Dickinson, W.R., Helmold, K.P., and Stein, J.A., 1979, Mesozoic lithic sandstones in central Oregon: Journal of Sedimentary Petrology, v. 49, p. 501-516.

Dickinson, W.R., and Suczek, C.A., 1979, Plate tectonics and sandstone compositions: American Association of Petroleum Geologists Bulletin, v. 63, p. 2164-2182.

Dickinson, W.R., and Thayer, T.P., 1978, Paleogeographic and paleotectonic implications of Mesozoic stratigraphy and structure in the John Day inlier of central Oregon, *in* Howell, D.G., and McDougall, K.A., eds., Mesozoic paleogeography of the Western United States (Pacific Coast Paleogeography Symposium 2, Sacramento, Calif.): Los Angeles, Society of Economic Paleontologists and Mineralogists, Pacific Section, p. 147-161.

Dunnet, D., 1969, A technique of finite strain analysis using elliptical particles: Tectonophysics, v. 7, p. 117-136.

Dunnet, D., and Siddans, A., 1971, Non-random sedimentary fabrics and their modification by strain: Tectonophysics, v. 12, p. 307-325.

Engh, K.R., 1984, Structural geology of the Rastus Mountain area, east-central Oregon: Pullman, Washington State University, M.S. thesis, 78 p.

England, R.N., and Davies, H.L., 1973, Mineralogy of ultramafic cumulates and tectonites from Eastern Papua: Earth and Planetary Science Letters, v. 17, p. 416-425.

Evans, B.W., 1977, Metamorphism of alpine peridotite and serpentinite: Annual Review of Earth and Planetary Science, v. 5, p. 397-447.

Evarts, R.C., 1977, The geology and petrology of the Del Puerto ophiolite, Diablo Range, central California Coast Ranges, *in* Coleman, R.G., and Irwin, W.P., eds., North American ophiolites: Oregon Department of Geology and Mineral Industries Bulletin 95, p. 121-140.

Ewart, A., 1979, A review of the mineralogy and chemistry of Tertiary-Recent dacitic, latitic, rhyolitic, and related salic volcanic rocks, *in* Barker, F., ed., Trondhjemites, dacites and related rocks: New York, Elsevier, p. 13-121.

Fleck, R.J., and Criss, R.E., 1985, Strontium and oxygen isotopic variations in Mesozoic and Tertiary plutons of central Idaho: Contributions to Mineralogy and Petrology, v. 90, p. 291-308.

Gerlach, D.C., Leeman, W.P., and Avé Lallemant, H.G., 1979, Petrology and geochemistry of silicic rocks in the Canyon Mountain ophiolite, northeastern Oregon: Geological Society of America Abstracts with Programs, v. 11, p. 79.

Gerlach, D.C., Avé Lallemant, H.G., and Leeman, W.P., 1981, An island arc origin for the Canyon Mountain ophiolite complex, eastern Oregon, U.S.A.: Earth and Planetary Science Letters, v. 53, p. 255-265.

Gilluly, James, 1937, Geology and mineral resources of the Baker quadrangle, Oregon: U.S. Geological Survey Bulletin 879, 119 p.

Hillhouse, J.W., Grommé, C.S., and Vallier, T.L., 1982, Paleomagnetism and tectonics of the Seven Devils volcanic arc in northeastern Oregon: Journal of Geophysical Research, v. 87, p. 3777-3794.

Himmelberg, G.R., and Coleman, R.G., 1968, Chemistry of primary minerals and rocks from the Red Mountain-Del Puerto ultramafic mass, California: U.S. Geological Survey Professional Paper 600-C, p. C18-C26.

Hooper, P.R., and Atkins, L., 1969, The preparation of fused samples in X-ray fluorescence analysis: Mineralogical Magazine, v. 37, p. 409-413.

Hooper, P.R., and Johnson, D., 1989, Major and trace element analyses of rocks and minerals by automatic X-ray spectrometry: Washington State University Geology Department Open-File Report, 17 p.

Hooper, P.R., Reidel, S.P., Brown, J.C., Holden, G.S., Kleck, W.D., Sundstrom, C.E., Taylor, T.L., 1976, Major element analyses of Columbia River Basalt, Part I: Washington State University Geology Department Open File Report, 59 p.

Hopson, C.A., and Frano, C.J., 1977, Igneous history of the Point Sal ophiolite, southern California, *in* Coleman, R.G., and Irwin, W.A., eds., North American ophiolites: Oregon Department of Geology and Mineral Industries Bulletin 95, p. 161-183.

Hostetler, P.B., Coleman, R.G., and Evans, B.W., 1966, Brucite in alpine serpentinites: American Mineralogist, v. 51, p. 75-98.

Houseman, M.D., 1983, Petrology and alteration of the Grouse Creek granodiorite porphyry: Pullman, Washington State University, M.S. thesis, 166 p.

Jackson, E.D., Green, H.W., II, and Moores, E.M., 1975, The Vourinos ophiolite, Greece—Cyclic units of lineated cumulates overlying harzburgite cumulates: Geological Society of America Bulletin, v. 86, p. 390-398.

Kuno, Hisashi, 1968, Differentiation of basaltic magmas, *in* Hess, H.H., and Poldervaart, Arie, eds., Basalts, v. 2: New York, John Wiley and Sons, p. 623-689.

Le Maitre, R.W., 1976, A new approach to the classification of igneous rocks using the basalt-andesite-dacite-rhyolite suite as an example: Contributions to Mineralogy and Petrology, v. 56, p. 191-203.

Loney, R.A., Himmelberg, G.R., and Coleman, R.G., 1971, Structure and petrology of the Alpine-type peridotite at Burro Mountain, California, U.S.A.: Journal of Petrology, v. 12, p. 245-309.

Lowry, W.D., 1968, Geology of the Ironside Mountain quadrangle: Oregon Department of Geology and Mineral Industries open file report (never published), 76 p., scale 1:125,000.

Malpas, J., 1977, Petrology and tectonic significance of Newfoundland ophiolites, with examples from Bay of Islands, *in* Coleman, R.G., and Irwin, W.P., eds., North American ophiolites: Oregon Department of Geology and Mineral Industries Bulletin 95, p. 13-24.

Middleton, G.V., and Hampton, M.A., 1976, Subaqueous transport and deposition by sediment gravity flows, *in* Stanley, D.J., and Swift, D.J.P., eds., Marine sediment transport and environmental management: New York, John Wiley and Sons, p. 197-218.

Moores, E.M., 1969, Petrology and structure of the Vourinos ophiolitic complex, northern Greece: Geological Society of America Special Paper 118, 74 p.

Mullen, E.P., 1979, Geology of the Greenhorn Mountains, northeastern Oregon: Corvallis, Oregon State University, M.S. thesis, 175 p.

Phelps, D.W., 1978, Petrology, geochemistry, and structural geology of Mesozoic rocks in the Sparta quadrangle and Oxbow and Brownlee Reservoir areas, eastern Oregon and western Idaho: Houston, Rice University, Ph.D. dissertation, 229 p.

———1979, Petrology, geochemistry and origin of the Sparta quartz diorite-trondhjemite complex, northeastern Oregon, *in* Barker, F., ed., Trondhjemites, dacites, and related rocks: New York, Elsevier, p. 547-579.

Phelps, D.W., and Avé Lallemant, H.G., 1980, The Sparta ophiolite complex, northeast Oregon—Plutonic equivalent to low K_2O island-arc volcanism: American Journal of Science, v. 280-A, p. 345-358.

Robyn, T.L., 1977, Geology and petrology of the Strawberry Volcanics, northeast Oregon: Eugene, University of Oregon, Ph.D. dissertation,197 p.

Scrivner, J.V., 1983, The geology of Mine Ridge, Baker County, Oregon: Pullman, Washington State University, M.S. thesis, 114 p.

Silberling, N.J., Jones, D.L., Blake, M.C., Howell, D.G., 1984, Lithotectonic terrane map of the western conterminous United States, *in* Silberling, N.J., and Jones, D.L., eds., Tectonic terrane map of the northern Cordillera: U.S. Geological Survey Open-File Report OF-84-523, Pt. C, p. C1-C43.

Streckeisen, A.L., and others, 1973, Plutonic rocks —Classification and nomenclature recommended by the IUGS Subcommission on the Systematics of Igneous Rocks: Geotimes, v. 18, no. 10, p. 26-30.

Thayer, T.P., 1966, Serpentinization considered as a constant volume process: American Mineralogist, v. 51, p. 685-710.

———1977, The Canyon Mountain complex, Oregon, and some problems of ophiolites, *in* Coleman, R.G., and Irwin, W.P., eds., North American ophiolites: Oregon Department of Geology and Mineral Industries Bulletin 95, p. 93-105.

Thayer, T.P., and Brown, C.E., 1964, Pre-Tertiary orogenic and plutonic intrusive activity in central and northeastern Oregon: Geological Society of America Bulletin, v. 75, p. 1255-1261.

———1973, Ironside Mountain, Oregon—A Late Tertiary volcanic and structural enigma: Geological Society of America Bulletin, v. 84, p. 489-498.

Thompson, M., and Walsh, J.N., 1983, A handbook of inductively coupled plasma spectrometry: Glasgow, Blackie and Son, 273 p.

Urbanczyk, K.M., and Lilligren, S.P., 1990, Geology and geochemistry of the eastern Clarno Formation, Grant County, Oregon, U.S.A. [abs.]: Geological Association of Canada and Mineralogical Association of Canada Annual Meeting, Vancouver, British Columbia, May 1990, Programs with Abstracts, v. 15, p. A133.

Vallier, T.L., and Batiza, Rodey, 1978, Petrogenesis of spilite and keratophyre from a Permian and Triassic volcanic arc terrane, eastern Oregon and western Idaho, U.S.A.: Canadian Journal of Earth Sciences, v. 15, p. 1356-1369.

Walker, G.W., ed., 1990, Geology of the Blue Mountains region of Oregon, Idaho, and Washington—Cenozoic geology of the Blue Mountains region: U.S. Geological Survey Professional Paper 1437, 135 p.

Wilson, Douglas, and Cox, Allan, 1980, Paleomagnetic evidence for the tectonic rotation of Jurassic plutons in the Blue Mountains, Oregon: Journal of Geophysical Research, v. 85, p. 3681-3689.

12. PETROLOGY AND DEFORMATION HISTORY OF THE BURNT RIVER SCHIST AND ASSOCIATED PLUTONIC ROCKS IN THE BURNT RIVER CANYON AREA, NORTHEASTERN OREGON

By ROGER P. ASHLEY

CONTENTS

	Page
Abstract	457
Introduction	458
General geology	459
Lithology	461
Deer Creek phyllite unit	461
Metasedimentary rocks	461
Metamorphosed volcanic and volcaniclastic rocks	463
Conditions of deposition, age, and correlation	463
Campbell Gulch phyllite unit	467
Phyllitic rocks and quartzite	467
Marble	467
Metavolcanic rocks	467
Conditions of deposition, age, and correlation	469
Intrusive rocks	469
Blue Spring Gulch pluton	469
Other metamorphosed intrusions in the Deer Creek phyllite unit	470
Metamorphosed intrusions and serpentinite in the Campbell Gulch phyllite unit	471
Altered mafic dikes	471
Lamprophyre dikes	471
Pedro Mountain stock	472
Igneous petrology	473
Metavolcanic rocks	473
Blue Spring Gulch pluton	474
Metamorphic petrology	475
Structural geology	477
Mesoscopic structural features	477
Deer Creek phyllite unit	477
Blue Spring Gulch pluton and other deformed intrusive rocks	480
Altered mafic dikes	481
Campbell Gulch phyllite unit	481
Country rocks of the Pedro Mountain stock	482
Macroscopic structure	483
Deer Creek phyllite unit	483
Campbell Gulch phyllite unit	485
Regional distribution and relations of the Burnt River Schist	486
Cave Creek fault and distribution of the units of the Burnt River Schist	486
Relation of the Burnt River Schist to surrounding units	489
Discussion and conclusions	490
References cited	493

ABSTRACT

The Burnt River Schist is a lithodemic unit that constitutes the southeastern part of the Baker terrane in the Blue Mountains region of Oregon. The Burnt River Schist forms an east-northeast-trending belt 6 to 22 km wide that extends for almost 90 km from Bald Mountain through Burnt River Canyon into western Idaho. The Burnt River Schist in Burnt River Canyon consists of two mappable metamorphic rock units that are separated by a high-angle fault of pre-Tertiary age that trends east-west through the center of the area.

The metasedimentary rocks on the north side of the high-angle fault, called the Deer Creek phyllite unit, are thinly layered phyllitic quartzite and quartz phyllite, locally interbedded with tuffs and flows of intermediate to mafic composition. Mineral assemblages reflect conditions of low-grade metamorphism. Structural analysis of the phyllitic rocks reveals two fold systems. The tight folds of the earlier system trend east-northeast and plunge at low angles to the west; axial-plane cleavage dips steeply. The later fold system is nearly coaxial with the earlier one, but axial surfaces dip at low to high angles to the north. Concordant and discordant metamorphosed bodies of hornblende gabbro, diorite, quartz diorite, and leucotonalite of Middle Triassic age intrude these metamorphic rocks. North of Burnt River Canyon, numerous intrusions form a composite plutonic mass, herein called the Blue Spring Gulch pluton, that separates the Burnt River Canyon metamorphic rocks from the Elkhorn Ridge Argillite. The Deer Creek phyllite unit is lithologically similar to parts of the Elkhorn Ridge Argillite.

The metamorphic rocks on the south side of the high-angle fault, called the Campbell Gulch phyllite unit, are mainly pelitic phyllite, greenstone (metamorphosed mafic lavas), and marble. Mineral assemblages generally reflect conditions of moderately high pressure low-grade metamorphism. Structural analysis reveals two deformations. The folds of the earlier deformation are tight to isoclinal and plunge at low to moderate angles to the west. Axial-plane cleavage generally dips at high to low angles to the south. Effects of the second deformation are limited to local small folds accompanied by a crenulation axial-plane cleavage.

The central part of the exposure area of the Burnt River Schist is intruded by several unmetamorphosed quartz diorite stocks of inferred Late Jurassic to Early Cretaceous age. In the southeastern part of the Burnt River Canyon area, adjacent to the Pedro Mountain stock, metabasalt and phyllite have been thermally metamorphosed to amphibolite and schist containing mineral assemblages characteristic of medium-grade metamorphism. The foliation planes of the schist are refolded, and veinlets and segregations in the amphibolite

are microfolded around steeply plunging axes. These effects postdate the two deformations of the Campbell Gulch phyllite unit of the Burnt River Schist.

Both phyllite units contain arc-related volcanic rocks, and the rocks of these units could have formed in either a fore-arc or an intra-arc depositional environment. The Blue Spring Gulch pluton and associated predeformation intrusive rocks form an arc-related calc-alkaline suite that dates deformation and metamorphism of the Deer Creek phyllite unit as younger than Middle Triassic. Middle and Late Triassic faunal ages for the Campbell Gulch phyllite unit date its deformation and metamorphism as younger than Late Triassic. Contact metamorphism and local deformation around the Pedro Mountain stock show that regional metamorphism and both regional deformations affecting the Campbell Gulch phyllite unit are older than middle Early Cretaceous.

Most exposures of the Burnt River Schist to the west of Burnt River Canyon are assigned to the Deer Creek phyllite unit, whereas most exposures of the Burnt River Schist to the east of Burnt River Canyon are assigned to the Campbell Gulch phyllite unit. The Burnt River Schist exposure area, as currently recognized, does not include any rocks that cannot be correlated with one of these two phyllite units. Thus the Burnt River Schist is composed of two metamorphic belts. These belts probably represent different parts of a subduction complex, on the basis of conditions of metamorphism and character of deformation of the rocks of each unit.

INTRODUCTION

The Baker terrane is a belt of deformed and metamorphosed sedimentary, volcanic, and plutonic rocks of late Paleozoic and early Mesozoic age that trends eastward through the center of the Blue Mountains region (fig. 12.1; Silberling and others, 1987). The most extensive formation in the eastern half of the Baker terrane, east of Elkhorn Ridge, is the Elkhorn Ridge Argillite (Gilluly, 1937). The most common rock types in the Elkhorn Ridge Argillite are argillite, chert, tuff, and lava flows. Limestone pods are common and widespread but not abundant. The metasedimentary rocks that constitute the southern part of the Baker terrane east of Elkhorn Ridge, although lithologically similar to the Elkhorn Ridge Argillite, have better developed schistosity and appear to be more strongly metamorphosed than any other rocks in the region. Gilluly (1937) named these rocks the Burnt River Schist for exposures in Burnt River Canyon and suggested that they might be older than the

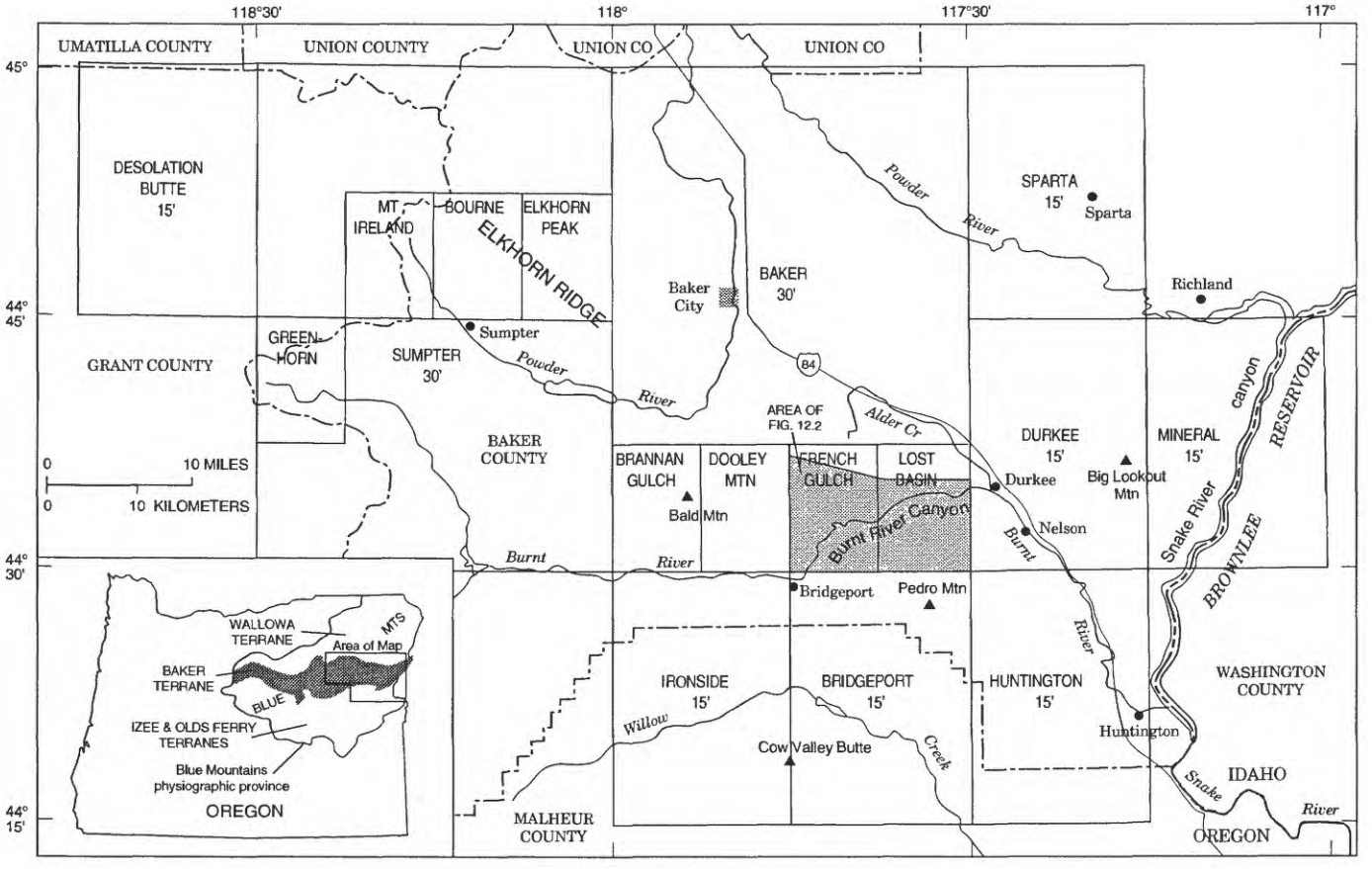

FIGURE 12.1.—Location of study area, quadrangles, and geographic features referred to in text. Study area, which is also the area of figure 12.2, is shaded. Shading on inset map shows area of outcrops of the Baker terrane, modified from Silberling and others, 1987. Outline of Blue Mountains physiographic province from Dicken, 1965.

Elkhorn Ridge Argillite, which was then thought to be of Pennsylvanian age. The Burnt River Schist has been geographically extended to the south and east of Burnt River Canyon as a result of subsequent investigations (Wolff, 1965; Prostka, 1967; Brooks, 1978); as currently recognized, it makes up the southeastern part of the Baker terrane, forming a belt that extends northeastward from Burnt River Canyon to the Snake River canyon, and westward from Burnt River Canyon to at least Bald Mountain, about 22 km south of Baker City.

In the last 20 years several authors have attempted to synthesize the pre-Tertiary tectonic and orogenic history of northeastern Oregon and western Idaho by incorporating modern concepts of plate tectonics and tectonostratigraphic terranes (Vallier and others, 1977; Jones and others, 1977; Brooks and Vallier, 1978; Brooks, 1979a; Dickinson, 1979; Coward, 1983; Mullen, 1985; Silberling and others, 1987; White and others, 1992). In these syntheses, the Burnt River Schist and Elkhorn Ridge Argillite together have been interpreted in various ways. Some investigators consider the two units to be oceanic crust terrane; others consider them to be fore-arc terrane. Some propose the two units originated a great distance from the North American continent, and others believe they originated near their present locations. Regarding regional structural features, the two formations have been interpreted by some as parts of a subduction zone complex, and by others as parts of a fold and thrust belt unrelated to subduction.

In this paper I summarize petrographic and structural information from an earlier detailed study (Ashley, 1966), incorporate petrologic and geochronologic information from subsequent regional studies (Mullen, 1985; Morris and Wardlaw, 1986; Walker, 1981, 1986), and present some new analytical data for metamorphosed igneous rocks from the Burnt River Canyon area. I discuss the possible depositional setting, tectonic setting, and tectonic history of the Burnt River Schist, incorporating all information available for the area for which it was named (T. 11 and 12 S., R. 41 and 42 E., French Gulch and Lost Basin quadrangles, Baker County, Oreg.). I also attempt to clarify regional relations and distribution of the unit.

GENERAL GEOLOGY

The Burnt River Schist exposed in Burnt River Canyon consists of two informal units separated by a high-angle fault that trends approximately east-west across the study area and crosses Burnt River midway between the east and west ends of the canyon (fig. 12.2). This structure is called the Cave Creek fault. Topographic depressions, springs, and zones of hydrothermal alteration mark the fault zone where it crosses the valley of Cave Creek about 1 km south of Burnt River. Minor movement occurred on this fault during late Tertiary time, when the rocks on the south side were downthrown. The amount and direction of movement prior to late Tertiary time is unknown.

The northernmost unit of the Burnt River Schist is here called the Deer Creek phyllite unit. Typical exposures of this unit can be seen in the canyon of Deer Creek, a prominent tributary on the north side of Burnt River Canyon (fig. 12.2). Quartz phyllite, which is the most common rock type in the unit, is well exposed along a secondary road that extends northwestward up Deer Creek from Burnt River Canyon. The southernmost unit of the Burnt River Schist is here called the Campbell Gulch phyllite unit; it is named for good exposures of phyllite and interbedded metavolcanic rocks and marble in Campbell Gulch, a short, high-gradient tributary on the south side of Burnt River (fig. 12.2). Campbell Gulch is accessible by unmaintained jeep trails extending westward from Cave Creek and southward from Burnt River Canyon.

Although phyllite is the most common rock type in both units, the Deer Creek and Campbell Gulch phyllite units differ significantly in lithology and metamorphic grade. They both show evidence of two deformations, but no deformation is closely similar between the two units. In both units the first folding is the major folding, primarily responsible for the distribution of rock types. The east-northeast trends and westerly plunges of the first-deformation fold axes are roughly similar in both units, but the orientations of the second-deformation folds differ greatly between the two units.

The Deer Creek phyllite unit is intruded by metamorphosed plutonic rocks. The largest intrusive body, which bounds the study area on the north (fig. 12.2), is here called the Blue Spring Gulch pluton, for good exposures in Blue Spring Gulch, a tributary of Deer Creek. Mafic dikes cut both the phyllite units. A quartz diorite body called the Pedro Mountain stock by Wolff (1965) intruded the Campbell Gulch phyllite unit and metamorphosed and deformed the metavolcanic rock and phyllite around its periphery. The stock belongs to the Late Jurassic to Early Cretaceous plutonic suite that includes the Wallowa and Bald Mountain batholiths (Armstrong and others, 1977).

Large continuous exposures of Tertiary rocks border the study area on the west and northeast (Brooks and others, 1976). All Tertiary exposures within the area,

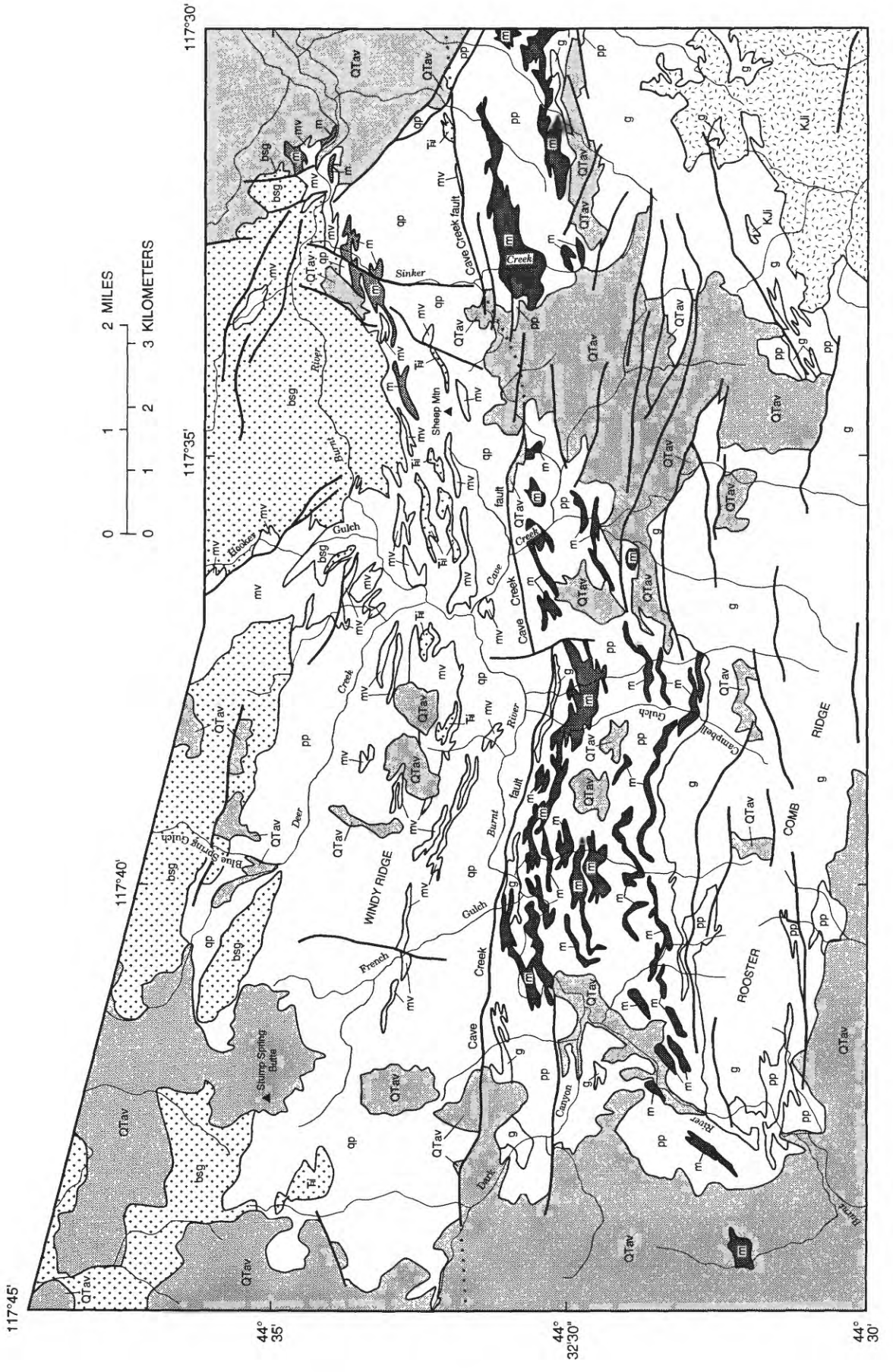
117°45'
117°40'
117°35'
117°30'
44° 35'
44° 32'30"
44° 30'
0 1 2 MILES
0 1 2 3 KILOMETERS
WINDY RIDGE
COMB RIDGE
ROOSTER
Sheep Mtn
Sinker Creek
Cave Creek fault
Burnt fault
Deer Creek
Blue Spring Gulch
Stump Spring Butte
French Gulch
Campbell Gulch
Canyon
Burnt River
QTav
mv
Ti
qp
bsg
pp
g
m
KJ

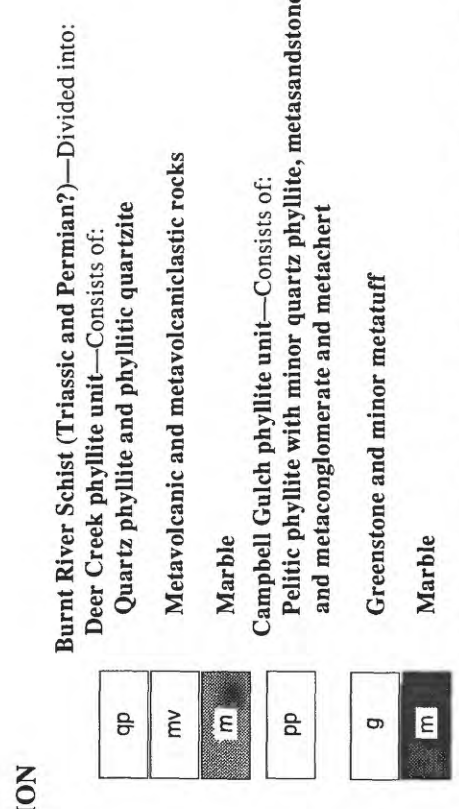

Note: Rocks of unit m exposed east of area of figure 12.2 have been mapped as the informally named Nelson marble by Prostka (1967), Brooks and others (1976), and Brooks (1978).

FIGURE 12.2.—Geologic map of the Burnt River Canyon area, northeastern Oregon. See figure 12.1 for location.

except those in the vicinity of the Cave Creek drainage, are small and isolated (fig. 12.2). The oldest Tertiary materials consist of fluvial sedimentary deposits in the vicinity of Cave Creek and on the spurs 2 to 3 km south of Burnt River, and an andesitic tuff breccia exposed mainly along the southern boundary of the study area. Geologic units of Miocene age include the Dooley Volcanics (previously called the Dooley Rhyolite Breccia by Gilluly, 1937), which is exposed on the north and west sides of the study area, and overlying porphyritic olivine basalt, which is exposed mainly on the north side of the study area. The Dooley Volcanics consists mainly of rhyolitic welded ash-flow tuff and rhyolite domes and related flows (Evans, 1992).

The Tertiary beds strike approximately east-west and dip south at low angles. Most of the numerous Tertiary faults trend east-west, with south sides downthrown. In the vicinity of Sinker Creek, the Cave Creek fault trends east-northeast under a mantle of Tertiary fluvial sedimentary deposits, and several east-west Tertiary faults follow this older fault zone in an en echelon pattern. In the Durkee and Bridgeport Valleys, bordering the study area on the northeast and southwest sides, respectively, the pre-Tertiary rocks have been downfaulted and covered with sedimentary deposits of late Miocene and Pliocene age (Brooks and others, 1976).

The most important Quaternary deposits are gravels on the south side of Burnt River Canyon up to 100 m above present river level. These deposits appear to occupy former river channels rather than bedrock terraces. Both the Tertiary gravel and the Quaternary gravel that overlie bedrock south of Burnt River are auriferous.

LITHOLOGY

DEER CREEK PHYLLITE UNIT

METASEDIMENTARY ROCKS

Metasedimentary rocks of the Deer Creek phyllite unit consist of phyllitic quartzite, quartz phyllite, quartzofeldspathic phyllite, pelitic phyllite, calc-phyllite, and marble. Phyllitic quartzite and quartz phyllite, intergradational rock types, are the most abundant. They consist of quartzite or quartz phyllite beds, 1 to 5 cm thick, separated by pelitic phyllite partings as much as 3 mm thick. The quartz-rich layers are 85 to 95 percent quartz that has been recrystallized to an interlocking aggregate of grains 5 to 20 μm in diameter. The phyllosilicate minerals that form the

pelitic partings and the remaining 5 to 15 percent of the quartz-rich layers are mainly muscovite and less abundant chlorite and biotite (fig. 12.3). The phyllosilicate flakes within the quartz-rich layers are arranged in thin folia spaced 20 to 200 μm apart, producing slaty cleavage. Microporphyroblasts of clinozoisite, biotite, chlorite, and garnet are sparse constituents of the quartz phyllite. Vestiges of radiolarian tests occur in a few samples. Before regional metamorphism, the phyllitic quartzite and quartz phyllite were likely thinly bedded chert and siliceous mudstone with shale partings.

Phyllitic quartzite and quartz phyllite grade into pelitic phyllite with few quartzose interbeds. Pelitic phyllite is composed mainly of quartz, muscovite, albite, chlorite, and minor biotite and clinozoisite, with locally abundant fine-grained carbonaceous material. The original rocks were probably mudstone or claystone.

Quartzofeldspathic phyllite beds show relict clastic texture, with monocrystalline grains of quartz and albite ranging from silt size to fine sand size. These feldspathic siltstones and sandstones are poorly bedded and have moderately developed slaty cleavage. Clinozoisite is an important constituent, forming idioblastic microporphyroblasts. Chlorite is more abundant, and muscovite and biotite less abundant, than in pelitic phyllite. Polycrystalline clasts, probably originally metachert and fine-grained sedimentary or felsic volcanic grains, are prominent in some sandstone beds. Both the monocrystalline and polycrystalline clasts are probably recrystallized.

Calcareous rocks occur as thin beds that do not extend for more than 1 km along strike. They range from pure calcite marble with less than 1 percent impurities (carbonaceous material, muscovite, and quartz) to quartz marble with as much as 50 percent quartz, to calc-phyllite with much quartz and carbo-

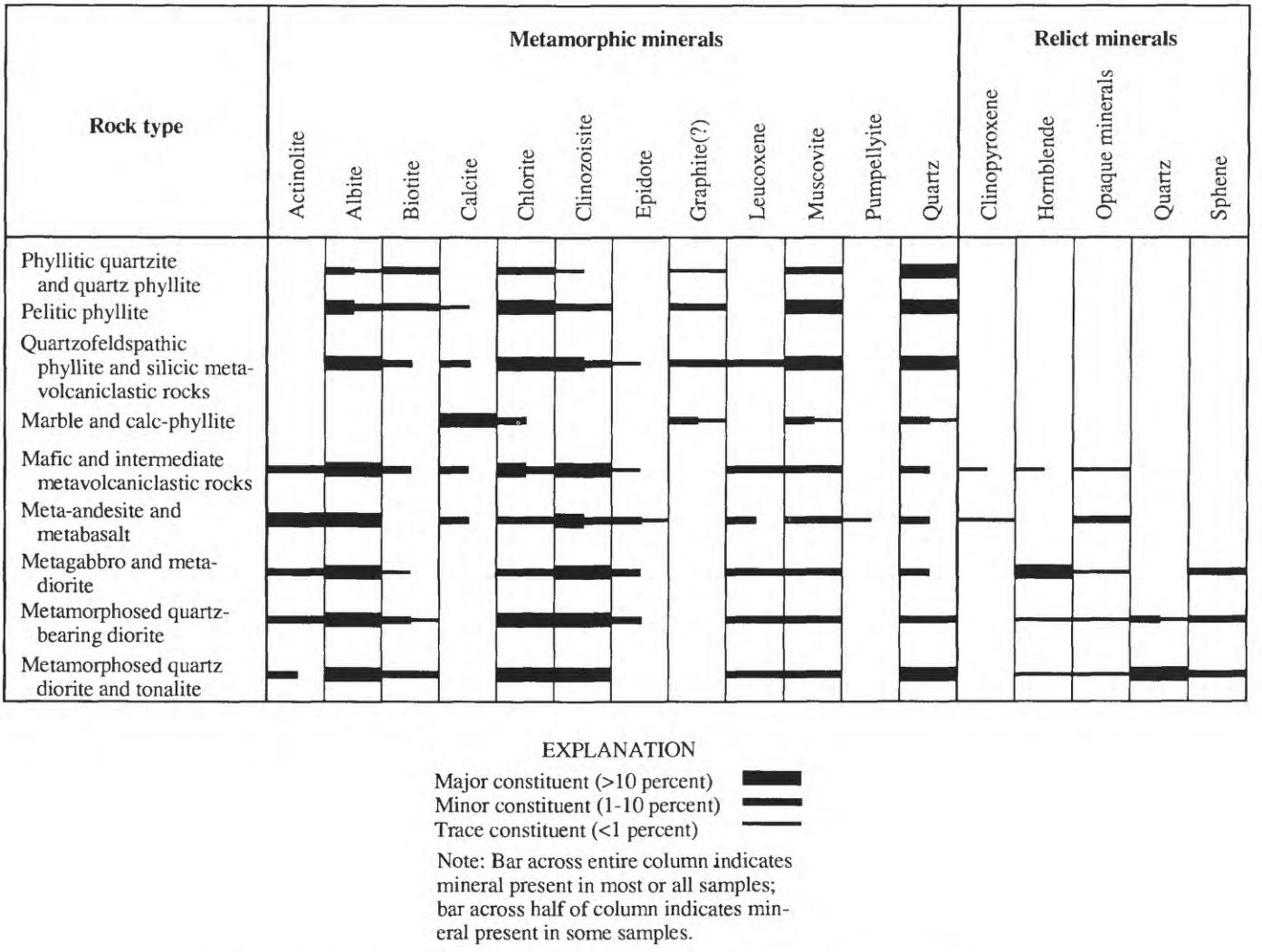

FIGURE 12.3.—Mineral assemblages of Deer Creek phyllite unit of Burnt River Schist.

naceous material. Calc-phyllite bears thin laminae of carbonaceous pelitic phyllite and is easily weathered. Pure marble forms massive light-gray or bluish-gray outcrops.

METAMORPHOSED VOLCANIC AND VOLCANICLASTIC ROCKS

Rocks of volcanic origin form numerous bodies that lie mainly in a belt extending from French Gulch to the east end of Burnt River Canyon (fig. 12.2). The larger bodies are particularly varied and include massive lavas, schistose to semi-schistose volcaniclastic rocks, and minor interbedded metasedimentary rocks; flows and volcaniclastic rocks also coexist in many of the smaller bodies.

The most common rock types are metamorphosed coarse andesitic or basaltic tuff and lithic lapilli tuff. Larger clasts in the tuffs show original porphyritic textures: the phenocrysts are plagioclase that has been replaced by albite containing minor muscovite and clinozoisite; the matrix consists of fine-grained crystalloblastic albite, muscovite, and actinolite, and smaller amounts of chlorite, biotite, clinozoisite, leucoxene (fine-grained anatase, rutile, or sphene), and quartz (fig. 12.3). A few clasts contain small ragged hornblende relics and a very few contain partly altered clinopyroxene. Metamorphosed dacitic volcaniclastic rocks are also abundant. They lack actinolite and have more chlorite and muscovite than the andesitic and basaltic rocks. Non-volcanic clasts, including quartz, chert, calcite, and fine-grained sedimentary rocks, do not total more than 10 percent by volume of any rock examined. The material between clasts is a crystalloblastic aggregate of 5- to 20-μm clinozoisite, albite, muscovite, chlorite, and biotite grains, concentrated in irregular folia that produce a semischistose texture.

Fine-grained metamorphosed tuffs are crystalloblastic aggregates of albite and quartz and lesser amounts of other metamorphic minerals, including the assemblages clinozoisite-actinolite-chlorite-biotite, actinolite-chlorite-biotite, and muscovite-chlorite-biotite(-clinozoisite). The mineral assemblages suggest that the protoliths of these rocks were andesitic and dacitic tuffs.

The protoliths of the metamorphosed lavas were basalt, basaltic andesite, and andesite flows and flow breccias. Most are porphyritic, containing abundant euhedral plagioclase phenocrysts as much as 2 mm long, which now consist of secondary albite with abundant inclusions of clinozoisite, muscovite, and chlorite. The porphyritic rocks have a few pseudomorphs of actinolite after clinopyroxene phenocrysts, and their groundmasses are composed of fine-grained albite, sphene, actinolite, epidote, and chlorite. A few flows show intergranular or intersertal texture, consisting of small plagioclase laths with interstitial aggregates of actinolite, epidote, chlorite, and opaque minerals. Some rocks contain relics of pumpellyite partly replaced by clinozoisite. Some fragments in flow breccia have abundant tiny albite amygdules or varioles of leucoxene and actinolite.

Chemical analyses and norms of metamorphosed and altered igneous rocks from the Burnt River Canyon area are shown in tables 12.1 and 12.2, and sample site locations and descriptions are shown in table 12.3. The weight percentages of major-element oxides have been recalculated to 100 percent volatile-free (normalized) to facilitate comparison with unmetamorphosed igneous rocks, but the total volatile content is also shown to indicate the degree to which the rocks have been converted to hydroxyl- and carbonate-bearing mineral phases. Samples 14-6B and 77-1A are typical metamorphosed lapilli tuffs from the Deer Creek phyllite unit. The composition of sample 14-6B is that of a basalt or basaltic andesite. Sample 77-1A contains significant amounts of both modal and normative quartz. If the silica content represents that of the protolith, it is best classified as a dacite (Peccerillo and Taylor, 1976). If the potassium content were also representative of the protolith the rock would be a low-potassium dacite, but movement of alkalis likely occurred during diagenesis and low-grade metamorphism.

Chemical analyses for Deer Creek metalavas include samples 76-2, 155-3, 15-22, 78-1B, and 76-3 (table 12.1). Protoliths of all these rocks except sample 76-3 could be classified either as basalt or basaltic andesite on the basis of their silica contents. They are probably best classified as basalt, because they contain significant amounts of normative olivine, and 76-2 contains normative nepheline. Sample 76-3 is best classified as an andesite rather than a dacite, because it lacks modal quartz. Six of the seven metavolcanic rock samples from the Deer Creek phyllite unit have relatively high Na_2O and low K_2O values. Sample 155-3, however, has nearly equal amounts of Na_2O and K_2O; both the altered plagioclase phenocrysts and groundmass of this rock contain abundant muscovite. The presence of abundant muscovite and normative corundum indicate that potassium metasomatism affected this rock.

CONDITIONS OF DEPOSITION, AGE, AND CORRELATION

The siliceous character of the Deer Creek phyllite unit and the lack of shallow-water sedimentological

or faunal features indicate that the depositional environment was most likely hemipelagic, as noted by Coward (1983) for the Elkhorn Ridge Argillite. Limestone bodies in the Elkhorn Ridge area, which are not completely recrystallized, show shallow-water features and were interpreted by Coward as olistostromes. In the Burnt River Canyon study area, however, the limestones of the Deer Creek phyllite unit

TABLE 12.1.—*Chemical analyses of metavolcanic rocks, Burnt River Canyon area*

[Major-element oxide contents are in weight percent, recalculated to 100 percent, volatile-free. FeO* is total iron calculated as FeO. Σ volatiles is the sum of H_2O^+, H_2O^-, and CO_2, in weight percent. Total is the sum of major-element oxides and volatiles before recalculation. CIPW (Cross, Iddings, Pirsson, and Washington) norms were calculated from the major-element oxides normalized on a volatile-free basis. Major-element oxide contents for samples 76-2, 155-3, 15-22, 14-6B, 78-1B, 76-3, 77-1A, 37-1, and 35-2 were determined in USGS laboratories by wavelength-dispersive X-ray spectroscopy; analysts, A.J. Bartel, D.F. Siems, K.C. Stewart, J.E. Taggart, Jr. FeO, H_2O^+, H_2O^-, and CO_2 contents were determined by various conventional analytical methods; analysts, E.L. Brandt, H.G. Neiman, S.T. Pribble. Trace-element contents, in parts per million, were determined by energy-dispersive X-ray spectroscopy; analysts, B.-S. W. King, K.O. Dennen, R.G. Johnson. Data for sample BR-59 from Mullen (1985). Data for samples BR-49, BR-52, and BR-59A from E.M. Bishop (written commun., 1983). BR-series samples analyzed by P.R. Hooper, Washington State University, Pullman, Wash. For sample locations and descriptions, see table 12.3. n.d., not determined; – – –, absent or value less than 0.01 weight percent]

	Deer Creek phyllite unit							Campbell Gulch phyllite unit					
Sample	76-2	155-3	15-22	14-6B	78-1B	76-3	77-1A	37-1	35-2	BR-49	BR-59	BR-52	BR-59A
Major-element oxides (weight percent)													
SiO_2	51.8	52.3	52.8	52.3	52.8	62.0	64.3	54.0	54.3	51.3	52.5	53.8	56.6
Al_2O_3	16.6	21.5	17.6	16.6	16.9	16.7	15.4	15.9	14.9	18.6	17.8	16.5	16.5
Fe_2O_3	1.54	1.45	1.25	1.85	2.83	1.28	1.90	1.05	1.43	4.11	4.22	4.63	4.21
FeO	8.86	6.73	9.20	8.27	6.62	5.57	3.94	7.53	6.06	4.71	4.82	5.54	4.82
FeO*	10.25	8.04	10.32	9.93	9.17	6.71	5.65	8.47	7.35	8.40	8.61	9.71	8.61
MgO	5.62	4.65	6.47	7.86	5.82	3.23	2.75	7.04	7.89	5.81	6.62	5.84	5.72
CaO	8.76	4.96	5.35	7.04	8.97	3.54	6.78	8.33	12.07	11.21	9.84	8.76	6.92
Na_2O	5.04	3.45	5.15	4.75	4.22	5.61	3.65	4.02	2.53	3.20	3.21	3.73	4.11
K_2O	.35	3.56	.63	.03	.63	.88	.27	1.19	.09	.01	.02	.02	.03
TiO_2	1.18	1.03	1.12	1.09	.93	.82	.79	.79	.58	.70	.80	.91	.90
P_2O_5	.14	.15	.15	.10	.11	.19	.17	.07	.05	.11	.09	.09	.08
MnO	.17	.19	.23	.18	.17	.16	.13	.14	.14	.25	.13	.18	.14
Σ volatiles	5.41	4.98	5.49	4.18	2.93	2.74	3.55	3.28	4.31	n.d.	n.d.	n.d.	n.d.
Total[1]	102.6	101.9	100.6	102.9	103.7	101.6	99.7	99.9	100.2	99.9	99.6	99.3	99.7
Normative minerals (weight percent)[2]													
Quartz	– – –	– – –	– – –	– – –	– – –	10.5	23.5	– – –	4.1	– – –	2.0	3.1	7.1
Corundum	– – –	3.3	– – –	– – –	– – –	.5	– – –	– – –	– – –	– – –	– – –	– – –	– – –
Orthoclase	2.1	21.1	3.7	0.2	3.7	5.2	1.6	7.0	.6	0.1	.1	.1	.2
Albite	37.8	29.2	43.6	40.2	35.7	47.4	30.9	34.0	21.4	27.2	27.2	31.6	34.9
Anorthite	21.5	23.6	23.1	23.8	25.2	16.3	24.7	21.7	29.0	36.5	34.1	28.3	26.4
Nepheline	2.6	– – –	– – –	– – –	– – –	– – –	– – –	– – –	– – –	– – –	– – –	– – –	– – –
Diopside	17.4	– – –	2.0	8.5	15.1	– – –	6.4	15.6	24.6	15.1	11.6	12.0	6.1
Hypersthene	– – –	10.2	5.8	8.3	9.4	16.1	8.3	9.3	17.0	16.4	19.9	19.4	19.9
Olivine	13.8	8.2	17.5	14.1	5.3	– – –	– – –	9.1	– – –	.02	– – –	– – –	– – –
Magnetite	2.2	2.1	1.8	2.7	3.6	1.9	2.8	1.5	2.1	3.2	3.4	3.5	3.5
Hematite	– – –	– – –	– – –	– – –	– – –	– – –	– – –	– – –	– – –	– – –	– – –	– – –	– – –
Ilmenite	2.2	2.0	2.1	2.1	1.8	1.6	1.6	1.5	1.1	1.3	1.5	1.7	1.7
Apatite	.3	.3	.3	.2	.3	.4	.4	.2	.1	.3	.2	.2	.2
Trace elements (parts per million)													
Ba	75	740	101	50	170	270	76	141	109	n.d.	n.d.	n.d.	n.d.
Rb	<10	45	6	<10	<10	<10	7	26	<5	n.d.	n.d.	n.d.	n.d.
Sr	105	135	106	225	255	200	345	125	58	n.d.	n.d.	n.d.	n.d.
Nb	<10	<10	6	<10	<10	<10	6	5	9	n.d.	n.d.	n.d.	n.d.
Y	22	14	20	21	<10	23	31	22	20	n.d.	n.d.	n.d.	n.d.
Zr	65	60	62	70	46	100	184	57	51	n.d.	n.d.	n.d.	n.d.

[1]Total is the sum of major-element oxides and volatiles before normalization; it is not the sum of the calculated values that precede it in each column.
[2]Based on major-element analyses recalculated to 100-percent volatile-free oxides.

are completely recrystallized to marble and no original textural features are preserved.

No datable fauna have been recovered from the Deer Creek phyllite unit. A metadiorite sample collected from the eastern part of the Blue Spring Gulch pluton (same locality as sample 105-15, table 12.2) yielded a zircon U-Pb age of about 230 Ma (Walker, 1986). If this determination represents a crystallization age, the host metasedimentary rocks can be no younger than Middle Triassic.

The rock types and their relative abundances in the Deer Creek phyllite unit are similar to those described in the Elkhorn Ridge Argillite by Gilluly (1937), Pardee and Hewett (1914), Brooks and others (1976), Coward (1983), and Ferns and others (1987), with the possible exception that chert is more abundant and argillite

TABLE 12.2.—*Chemical analyses of meta-intrusive rocks, Burnt River Canyon area*

[All samples determined in USGS laboratories; for methods, analysts, and explanation of symbols, see table 12.1. For sample locations and descriptions, see table 12.3]

	Blue Spring Gulch pluton							Other meta-intrusive rocks			Dikes	
Sample	16-3	106-14	16-4	105-15	106-13B	105-22	77-22	78-10	78-3B	14-17C	78-2	14-29B
Major-element oxides (weight percent)												
SiO_2	46.6	48.9	48.5	58.3	59.9	62.1	70.4	60.7	64.6	68.0	53.5	54.0
Al_2O_3	17.0	14.8	14.2	19.4	18.9	18.2	16.0	19.4	17.5	15.3	16.5	17.7
Fe_2O_3	3.05	1.45	1.93	1.01	1.41	4.13	.18	1.76	1.29	2.12	2.83	1.89
FeO	7.49	8.83	8.38	5.02	3.77	0.92	.51	3.14	3.30	1.93	4.82	4.95
FeO*	10.23	10.13	10.12	5.93	5.04	4.96	.67	4.72	4.47	3.84	7.37	6.64
MgO	9.12	10.84	11.77	2.87	2.50	2.68	1.22	2.35	2.94	1.53	9.29	6.57
CaO	13.34	11.89	11.05	6.60	6.08	5.64	4.30	5.94	3.65	5.61	7.25	8.91
Na_2O	1.93	1.91	2.11	5.57	6.39	4.96	6.16	5.39	5.79	4.15	3.46	3.80
K_2O	.14	.17	.61	.11	.08	.36	.48	.30	.37	.48	1.37	1.13
TiO_2	1.05	.82	1.02	.82	.70	.77	.61	.65	.36	.58	.72	.81
P_2O_5	.09	.09	.15	.26	.20	.22	.19	.20	.10	.16	.17	.17
MnO	.18	.21	.20	.09	.08	.08	.04	.08	.09	.07	.14	.13
Σ volatiles	3.75	4.45	3.49	3.53	3.28	2.92	1.36	3.21	1.77	1.54	4.15	4.12
Total[1]	104.2	101.8	103.1	101.0	100.7	100.6	99.4	100.9	99.6	101.7	103.2	102.0
Normative minerals (weight percent)[2]												
Quartz	---	---	---	5.2	5.3	13.8	23.4	11.0	15.6	28.9	---	---
Corundum	---	---	---	---	---	---	---	---	1.1	---	---	---
Orthoclase	0.9	1.0	3.6	.7	.5	2.1	2.8	1.8	2.2	2.8	8.1	6.7
Albite	16.4	16.1	17.8	47.1	54.1	42.0	52.1	45.6	49.0	35.1	29.3	32.1
Anorthite	37.2	31.4	27.6	27.5	22.7	26.2	14.5	27.9	17.4	21.8	25.5	27.9
Nepheline	---	---	---	---	---	---	---	---	---	---	---	---
Diopside	23.0	21.8	21.1	2.9	5.1	.3	4.4	.2	---	4.0	7.5	12.3
Hypersthene	1.1	13.2	6.9	12.9	8.5	12.2	1.0	9.2	11.9	2.9	19.8	15.2
Olivine	15.5	12.5	17.8	---	---	---	---	---	---	---	4.8	1.2
Magnetite	3.8	2.1	2.8	1.5	2.0	1.3	.003	2.6	1.9	3.1	3.3	2.7
Hematite	---	---	---	---	---	---	.2	---	---	---	---	---
Ilmenite	2.0	1.6	1.9	1.6	1.3	1.5	1.2	1.2	.7	1.1	1.4	1.5
Apatite	.2	.2	.4	.6	.5	.5	.4	.5	.2	.4	.4	.4
Trace elements (parts per million)												
Ba	50	78	235	86	35	278	310	127	311	176	730	660
Rb	<10	<5	<10	8	11	6	6	<5	7	17	20	<10
Sr	235	93	80	325	490	323	202	231	140	556	570	305
Nb	<10	6	<10	6	6	5	9	<5	9	6	<10	<10
Y	12	15	11	14	9	13	31	11	16	13	12	14
Zr	32	46	50	78	56	85	185	50	89	88	100	95

[1]Total is the sum of major-element oxides and volatiles before normalization; it is not the sum of the calculated values that precede it in each column.
[2]Based on major-element analyses recalculated to 100-percent volatile-free oxides.

TABLE 12.3.—*Locations and site descriptions of analyzed samples, Burnt River Canyon area*

[Locations can be found on U.S. Geological Survey 7½-minute topographic quadrangles: French Gulch, Oreg.; and Lost Basin, Oreg. For analyses, see tables 12.1 and 12.2]

Sample	Protolith composition	Latitude (N.)	Longitude (W.)	Site description
76-2	Basalt	44°34.9'	117°36.9'	Large metavolcanic body comprising mostly flows, crest of ridge west of Hooker Gulch, Deer Creek phyllite unit, sec. 30 (unsurveyed), T. 11 S., R. 42 E.
155-3	Basalt	44°34.6'	117°32.1'	Metavolcanic rock adjacent to Blue Spring Gulch pluton, exposed along Burnt River Canyon road near east end of canyon, Deer Creek phyllite unit, sec. 26 (unsurveyed), T. 11 S., R. 42 E.
15-22	Basalt	44°33.9'	117°37.3'	Metavolcanic body exposed on south side of Deer Creek canyon 1 km west-northwest of confluence of Deer Creek and Burnt River, Deer Creek phyllite unit, sec. 31 (unsurveyed), T. 11 S., R. 41 E.
14-6B	Basalt tuff	44°33.3'	117°39.1'	Metavolcaniclastic body, south side of Windy Ridge 1.6 km east of French Gulch, Deer Creek phyllite unit, NE1/4NE1/4 sec. 2, T. 12 S., R. 41 E.
78-1B	Basalt	44°33.2'	117°36.8'	Small metavolcaniclastic and metavolcanic body, west side of Cave Creek canyon near confluence of Cave Creek and Burnt River, Deer Creek phyllite unit, NE1/4NE1/4 sec. 6, T. 12 S., R. 42 E.
76-3	Andesite	44°35.2'	117°36.6'	Large metavolcanic body comprising mostly flows, crest of ridge west of Hooker Gulch, Deer Creek phyllite unit, sec. 19 (unsurveyed), T. 11 S., R. 42 E.
77-1A	Dacite tuff	44°34.0'	117°36.9'	Small metavolcanic body, north side of Deer Creek canyon near confluence of Deer Creek and Burnt River, Deer Creek phyllite unit, sec. 3 (unsurveyed), T. 11 S., R. 42 E.
37-1	Basaltic andesite	44°31.2'	117°42.7'	Greenstone belt, Burnt River Canyon road near west end of canyon, Campbell Gulch phyllite unit, NE1/4SE1/4 sec. 17, T. 12 S., R. 41 E.
35-2	Basaltic andesite	44°32.8'	117°43.0'	Moderately large metavolcanic body, east side of Dark Canyon, Campbell Gulch phyllite unit, SW1/4SE1/4 sec. 5, T. 12 S., 41 E.
BR-49	Basaltic andesite	44°31.0'	117°41.0'	Greenstone belt, road along crest of Rooster Comb Ridge, Campbell Gulch phyllite unit, SE1/4SW1/4 sec. 15, T. 12 S., R. 41 E.
BR-59, 59A	Basaltic andesite	44°31.4'	117°41.0'	Greenstone belt, north side of Rooster Comb Ridge, Campbell Gulch phyllite unit, SE1/4NW1/4 sec. 15, T. 12 S., R. 41 E.
BR-52	Basaltic andesite	44°31.2'	117°41.0'	Greenstone belt, north side of Rooster Comb Ridge, Campbell Gulch phyllite unit, NE1/4SW1/4 sec. 15, T. 12 S., R. 41 E.
16-3	Gabbro	44°35.6'	117°39.4'	Blue Spring Gulch pluton, Blue Spring Gulch, SW1/4NE1/4 sec. 23, T. 11 S., R. 41 E.
106-14	Gabbro	44°34.8'	117°33.0'	Blue Spring Gulch pluton, Burnt River Canyon road near east end of canyon, sec. 27 (unsurveyed), T. 11 S., R. 42 E.
16-4	Gabbro	44°35.4'	117°38.4'	Blue Spring Gulch pluton, ridge crest north of Deer Creek and east of Blue Spring Gulch, NE1/4SW1/4 sec. 24, T. 11 S., R. 41 E.
105-15	Leucodiorite	44°34.5'	117°33.7'	Blue Spring Gulch pluton, Burnt River Canyon road near east end of canyon, sec. 27 (unsurveyed), T. 11 S., R. 42 E.
106-13B	Leuco-quartz diorite	44°34.8'	117°33.2'	Blue Spring Gulch pluton, Burnt River Canyon road near east end of canyon, sec. 27 (unsurveyed), T. 11 S., R. 42 E.
105-22	Leuco-quartz diorite	44°34.5'	117°33.8'	Blue Spring Gulch pluton, Burnt River Canyon road near east end of canyon, 150 m west of locality 105-15, sec. 28 (unsurveyed), T. 11 S., R. 42 E.
77-22	Leucotonalite	44°34.3'	117°35.2'	Blue Spring Gulch pluton, north side of Burnt River Canyon, 2.3 km east-northeast of confluence of Deer Creek and Burnt River, sec. 29 (unsurveyed), T. 11 S., R. 42 E.
78-10	Leuco-quartz diorite	44°33.5'	117°35.4'	Small intrusive body in phyllite, ridge crest 1.1 km west of summit of Sheep Mountain, sec. 32 (unsurveyed), T. 11 S., R. 42 E.
78-3B	Leuco-quartz diorite	44°33.2'	117°34.9'	Small intrusive body in phyllite, road to Sheep Mountain manganese prospect, south side of Sheep Mountain, NE1/4NW1/4 sec. 4, T. 12 S., R. 42 E.
14-17C	Tonalite	44°33.6'	117°37.2'	Small intrusive body in metavolcanic and metavolcaniclastic rocks, northwest side of Burnt River Canyon at confluence of Deer Creek and Burnt River, sec. 31 (unsurveyed), T. 11 S., R. 42 E.
78-2	Basaltic andesite	44°33.0'	117°36.2'	Hornblende lamprophyre dike in phyllite, northeast side of Cave Creek canyon, SE1/4NW1/4 sec. 5, T. 12 S., R. 42 E.
14-29B	Basaltic andesite	44°33.3'	117°36.9'	Hornblende lamprophyre dike in phyllite, Burnt River Canyon road at confluence of Burnt River and Cave Creek, NW1/4NE1/4 sec. 6, T. 12 S., R. 42 E.

less abundant in the Burnt River Canyon area than in most parts of the Elkhorn Ridge Argillite. I concluded earlier (Ashley, 1966) that the Deer Creek phyllite unit could be included as part of the Elkhorn Ridge Argillite on the basis of similar lithology. More recent detailed mapping has shown, however, that the Elkhorn Ridge Argillite is not a simple stratigraphic unit, but it is a composite unit consisting of blocks that have different lithologic and structural characteristics (see Coward, 1983; Ferns and others, 1982; Ferns and others, 1983; Evans, chap. 8, this volume). In some places these blocks are clearly fault- or melange-bounded. Thus the Deer Creek phyllite unit cannot be correlated with the entire Elkhorn Ridge Argillite. Whether the Deer Creek phyllite unit is correlative with a specific subterrane or block within the Elkhorn Ridge cannot be considered until the entire Elkhorn Ridge has been mapped in more detail and more age data are available for the Deer Creek phyllite unit.

CAMPBELL GULCH PHYLLITE UNIT

PHYLLITIC ROCKS AND QUARTZITE

Pelitic phyllite is an abundant rock type of the Campbell Gulch phyllite unit (fig. 12.2). This rock type is poorly exposed, and thin interbeds of other rock types are relatively scarce; bedding is seen at few outcrops.

The pelitic phyllite was originally claystone or shale and is now composed of 30 to 50 percent or more fine-grained muscovite and chlorite in about equal proportions (fig. 12.4). The phyllosilicates are strongly aligned, resulting in slaty cleavage. Most of the remaining material is crystalloblastic quartz in grains smaller than 20 μm in diameter. Some carbonaceous material is everywhere present, as are scattered silt-size detrital quartz grains that are probably recrystallized. Silty varieties contain as much as 30 percent silt-size quartz grains. Minor minerals include very fine grained crystalloblastic albite and clinozoisite.

Thin lenses of quartzofeldspathic phyllite are found throughout the pelitic phyllite, but their aggregate volume is very small. They were originally beds of sandstone and, less commonly, conglomerate. Most of these lenses are in the vicinity of the large U-shaped bend in Burnt River, east of Dark Canyon (fig. 12.2). The clasts of the conglomerates are as much as 5 cm long and are mostly mafic and intermediate volcanic rocks, mudstone, and chert. Albite grains appear in most samples and form as much as 25 percent of some of the metasandstones. Lenses with volcanic clasts contain minor actinolite.

Phyllitic quartzite is abundant in a few places, for example, in the lower part of Dark Canyon. It is lithologically similar to phyllitic quartzite of the Deer Creek phyllite unit, containing more than 90 percent quartz, numerous quartz veinlets, and scarce relict outlines of recrystallized radiolarians.

A few massive quartzite bodies as much 30 m thick and 600 m long form prominent exposures in a small area on the east side of Cave Creek. Elsewhere, quartzite beds generally less than 3 m thick and 30 m long are scattered throughout the phyllite. Their uniform fine grain size and xenoblastic texture indicate that these rocks are metachert.

MARBLE

Marble forms numerous prominently exposed bodies aligned in belts that trend approximately parallel to the foliation of the phyllite. Most marble bodies are almost entirely calcite, generally with a grain size of about 1 mm. Minor quartz and carbonaceous material were the only impurities observed (fig. 12.4). At some localities there are quartzite interbeds 1 to 3 cm thick, spaced 5 to 15 cm apart. The fine-grained quartz of these interbeds contains minor muscovite and scattered rhombs of ferroan carbonate that are pigmented with limonite on the weathered surface, giving the interbeds a distinctive pale-brown weathered color. A few calcareous quartzite beds containing as much as 30 percent calcite are scattered through the phyllite.

METAVOLCANIC ROCKS

Greenstone (metamorphosed mafic lava) with minor phyllite forms a broad belt that is adjacent to the southern boundary of the study area and encompasses Rooster Comb Ridge ("g," fig. 12.2, hereafter referred to as the "greenstone belt"). This belt crosses the western part of Burnt River Canyon, where it interfingers with phyllite and marble. Relict textures and structures are rare, but pillow structures with variolitic rims, tuff breccia, and flow breccia are present locally. Schistose metatuff is widespread and is locally interlayered with greenstone. The pillow structures and associated sedimentary rocks indicate that the volcanic accumulation is submarine.

Most samples of greenstone are composed of dense aggregates of actinolite, albite, pumpellyite, chlorite, leucoxene, and minor quartz and muscovite (fig. 12.4). Scattered through this crystalloblastic groundmass are subhedral relict clinopyroxene phenocrysts

as much as 1 mm long, which form as much as 20 percent of the rock. Most rocks contain patches and folded, disrupted veinlets of fine-grained pumpellyite. In a few rocks, minor granular clinozoisite coexists with pumpellyite, and in a very few, subidioblastic clinozoisite grains occur instead of pumpellyite in the groundmass, accompanied by clinozoisite-albite veinlets instead of pumpellyite veinlets.

The pillows have massive cores with compositions and textures like those described above. The pillow margins have variolitic rinds as much as several centimeters thick. Individual varioles consist of crudely radial bundles of actinolite, dusty granular leucoxene, and minor albite and pumpellyite. Between the varioles are actinolite sheaves, patches and stringers of fibrous-appearing pumpellyite, and minor albite.

Porphyritic greenstone with as much as 10 percent altered plagioclase phenocrysts is another common rock type. In some of these rocks the phenocrysts are replaced only by twinned albite, but generally they are replaced by albite, pumpellyite, minor muscovite, and minor calcite. Groundmass textures and mineral assemblages are like those of rocks without plagioclase phenocrysts. Porphyritic greenstone also contains slightly altered clinopyroxene phenocrysts. Stilpnomelane is largely restricted to these porphyritic rocks; it forms sprays and matted aggregates in veins with albite or calcite, and also forms scattered plates in the groundmass. The varioles that rim pillows in these rocks are radiating clusters of albite laths, with leucoxene granules and tiny chlorite and muscovite flakes; the interstices between the varioles

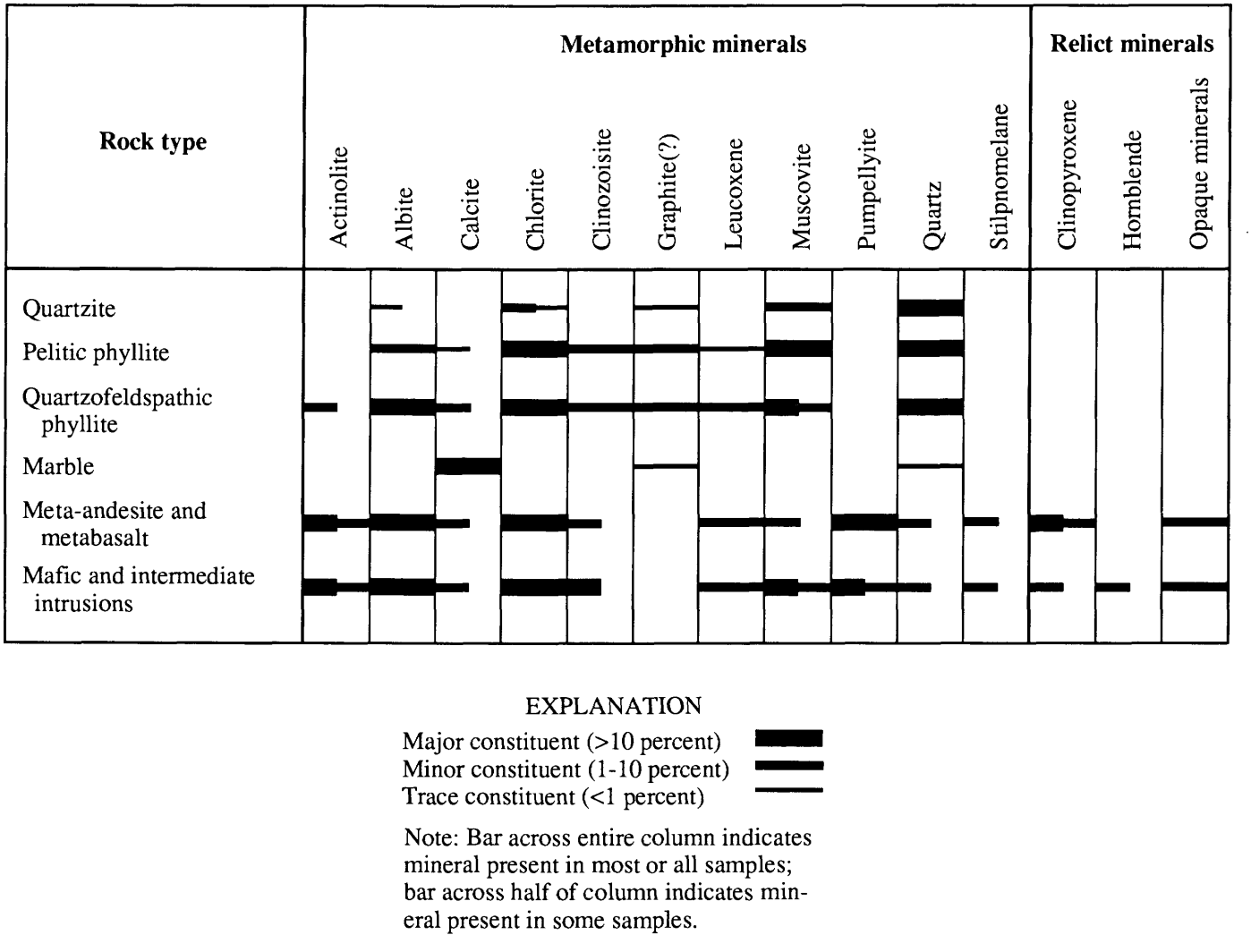

FIGURE 12.4.—Mineral assemblages of Campbell Gulch phyllite unit of Burnt River Schist.

contain albite, muscovite, chlorite, and minor pumpellyite and sphene. The protoliths of these porphyritic rocks were more felsic than those of the rocks free of plagioclase phenocrysts.

The metatuffs range from actinolite-rich to chlorite-muscovite-rich varieties and thus have a range of compositions. Some contain scattered clinopyroxene crystals. Actinolite and all phyllosilicates are strongly oriented, producing slaty cleavage.

Six chemical analyses for greenstones exposed on Rooster Comb Ridge and at the west end of Burnt River Canyon are shown in table 12.1. The greenstones are derived from basaltic andesites, on the basis of silica contents of about 51 to 57 percent and small to moderate amounts of normative quartz or normative olivine. As is the case with the Deer Creek phyllite unit, primary alkali contents probably have been modified by secondary processes. K_2O contents for the BR sample series (last four columns in table 12.1) seem anomalously low, suggesting possible analytical bias toward low values. Nevertheless, the rocks are likely generally low in K_2O. Na_2O was probably added to some rocks during recrystallization under very low grade metamorphic conditions.

CONDITIONS OF DEPOSITION, AGE, AND CORRELATION

The fine-grained clastic rocks that dominate the Campbell Gulch phyllite unit represent terrigenous debris deposited in moderately deep water. Although the phyllite is locally siliceous, chert beds are scarce. The relatively coarse clastic interbeds may represent shallow-water deposits or turbidites or both. The sandstones and conglomerates are immature, containing abundant feldspar and volcanic fragments. The metavolcanic rocks are derived mainly from basaltic andesite, locally pillowed, and minor tuff. They represent products of arc-related submarine volcanism (see section "Igneous Petrology"). Recrystallization has mostly destroyed original textures in the marble bodies, but rarely preserved shallow-water fauna suggest these were reefal limestones. Whether they were formed in shallow water, then transported and deposited in deeper water, is problematic.

All the fossils yet recovered from the Burnt River Schist are from the Campbell Gulch phyllite unit. A bryozoan collected from a marble pod in SW1/4 sec. 10, T. 12 S., R. 41 E., French Gulch quadrangle, yielded a questionable Permian age (Ashley, 1966), whereas marble collected by D.A. Bostwick from the same or a nearby pod yielded a pentacrinid columnal that he considered to be probably Late Triassic in age (Brooks and others, 1976). The belt containing abundant marble bodies narrows and continues eastward into the Durkee quadrangle, where it was called the (informal) Nelson marble by Prostka (1967). Conodonts from a marble pod in lower French Gulch and from the Nelson marble near Durkee are of Middle to Late Triassic age at both localities (Morris and Wardlaw, 1986).

Faunal ages from the Campbell Gulch phyllite unit overlap those of the Wild Sheep Creek and Doyle Creek Formations in the Snake River canyon area (Vallier, 1977); the Martin Bridge Limestone, Hurwal Formation, and parts of the Clover Creek Greenstone (Gilluly, 1937) and Lower Sedimentary Series of Smith and Allen (1941) in the Wallowa Mountains (Brooks and others, 1976); the Elkhorn Ridge Argillite (Brooks and others, 1976; Blome and others, 1986); and volcanic rocks exposed near Huntington, Oreg. (fig. 12.1; Brooks and others, 1976; Brooks, 1979b; Silberling, 1983). Owing to structural complexity, it is not possible to define a stratigraphic succession for the Campbell Gulch phyllite unit (see section "Regional Distribution and Relations of the Burnt River Schist") or to correlate it directly with any other stratigraphic unit in the region.

INTRUSIVE ROCKS

BLUE SPRING GULCH PLUTON

Numerous intrusions into the Deer Creek phyllite unit consist of concordant and discordant bodies ranging in areal extent from a few hundred square meters to several square kilometers. The largest intrusion, a composite body, bounds the mapped area on the north (fig. 12.2). Extensive exposures of this body continue northward for about 5 km to Alder Creek (fig. 12.1; Brooks and others, 1976). This intrusive mass is here called the Blue Spring Gulch pluton. In addition to this pluton, many other small bodies occur in a belt extending from Sinker Creek westward across Sheep Mountain to Windy Ridge (fig. 12.2).

North of Deer Creek and northwest of Stump Spring Butte, the Blue Spring Gulch pluton consists mainly of metamorphosed hornblende diorite and gabbro (IUGS modal classification, Streckeisen, 1976). East of Hooker Gulch, it includes much metamorphosed quartz diorite, leuco-quartz diorite, and leucodiorite, as well as metamorphosed diorite and gabbro. The rocks are medium-grained, consisting mainly of hornblende and plagioclase, with hypidiomorphic-granular texture. In some of the more mafic varieties hornblende is sub-

poikilitic around plagioclase laths. The hornblende is bluish- to brownish-green, possibly of pargasitic composition, and shows only minor alteration to chlorite and clinozoisite or epidote (fig. 12.3). The chief mafic mineral in the metamorphosed quartz diorite is also hornblende, but it is extensively altered to aggregates of Fe-Mg chlorite, and chlorite with minor olive-green to olive-brown metamorphic biotite replaces scarce primary biotite. Plagioclase in all rocks is completely recrystallized to albite with variable amounts of clinozoisite-epidote minerals and muscovite. Metamorphosed quartz diorite has interstitial quartz, and all rocks have minor interstitial sphene.

Metamorphosed gabbro and diorite of the Blue Spring Gulch pluton locally show mineral lineation defined by long axes of hornblende grains. The strength and attitude of this lineation both vary markedly within tens of meters. The abrupt changes in mineral lineation suggest that the lineation is of magmatic origin and the pluton is a dike-and-sill complex.

The least abundant rocks of the Blue Spring Gulch pluton are metamorphosed leucotonalite (also called trondhjemite; Streckeisen, 1976) and quartz-albite pegmatite (albite granite and silicified gabbro of Gilluly, 1937). A large number of small metamorphosed leucotonalite dikes and plugs intrude metamorphosed quartz diorite, leuco-quartz diorite, diorite, and gabbro on the north side of Burnt River Canyon east of Hooker Gulch, locally forming as much as 20 percent of the exposed intrusive rocks. Individual dikes are less than 100 m long and 10 m wide. Modal compositions are 40 to 50 percent quartz and 35 to 55 percent albite; other minerals total 5 to 15 percent. Albite crystals 1 to 4 mm long are set in a matrix of quartz grains 0.5 to 1 mm in diameter. Albite crystals are serrate to embayed on contacts with quartz. Muscovite and clinozoisite-epidote minerals form inclusions in the albite crystals. Chlorite, biotite, sphene, and scarce opaque minerals form scattered grains and patches within the quartz aggregates. The CaO content of the only analyzed metamorphosed leucotonalite sample (77-22, table 12.2), and the presence of clinozoisite-epidote inclusions in albite in all the leucotonalite samples indicate that the primary plagioclase was oligoclase. The FeO* (total iron calculated as FeO) content of sample 77-22 is relatively low and the MgO content is relatively high compared to those of most trondhjemites (Barker, 1979), possibly as a result of metamorphism. The sharp contacts, lack of mafic or intermediate-rock relics, and lack of any transitional rock type suggest that the protoliths of the leucotonalite bodies were of magmatic origin and were not a product of soda-silica metasomatism of mafic rocks.

Metamorphosed quartz-albite pegmatites with a wide range of quartz content (10 to 60 percent) form patches as much as 50 m in diameter scattered widely within metamorphosed diorite and gabbro. These patches consist of web-like networks apparently filling fractures. In specimens with low quartz percentage, the quartz is restricted to veinlets. Relatively quartz-rich rocks have subhedral albite crystals 5 mm to 2 cm in diameter surrounded by fine-grained quartz and cut by many tiny quartz veinlets.

A small, poorly exposed serpentinite body occurs within the metamorphosed gabbro and diorite mass located south of upper Deer Creek, which is included in the Blue Spring Gulch pluton. The serpentinite body is penetratively foliated, possibly as a result of shearing. It consists of well-oriented chrysotile partly recrystallized to randomly oriented chrysotile, and 1 percent chromite grains surrounded by thin patchy halos of fine-grained talc. The shearing and recrystallization have obliterated relict textures, but the presence of chromite suggests that the protolith was an olivine-bearing ultramafic rock. This serpentinite body is not obviously associated with a fault. It may be a small intrusion, on the basis of its metamorphic mineral assemblage, which is lower grade than that of the surrounding metamorphosed gabbro and diorite (Evans, 1977).

Observed contacts of the Blue Spring Gulch pluton are sharp, generally discordant with the foliation of metasedimentary host rocks, and devoid of obvious contact metamorphic effects. Within the metamorphosed pluton, intrusions of diorite and quartz diorite, including leucocratic varieties, are generally younger than gabbro intrusions, and leucotonalite dikes and plugs intrude all other plutonic rock types.

Walker (1986) obtained slightly discordant U-Pb ages of 230±1 and 233±1 Ma on two zircon fractions from a metamorphosed trondhjemite (sample BR-79-1; see Vallier, chap. 3, this volume) collected at the same locality as sample 105-15 (leucodiorite; tables 12.2 and 12.3). These are the only radiometric age data available for the Blue Spring Gulch pluton.

OTHER METAMORPHOSED INTRUSIONS IN THE DEER CREEK PHYLLITE UNIT

Metamorphosed phaneritic intrusive rocks of intermediate composition make up the small bodies exposed on Sheep Mountain, on Windy Ridge, and 1.5 km southwest of Stump Spring Butte (fig. 12.2). These rocks are medium-grained and hypidiomorphic-granular in texture. Their protolith compositions are biotite-hornblende diorite, leucodiorite, and tonal-

ite, and biotite quartz diorite and leuco-quartz diorite; their color indices range from 10 to 30. Quartz, in polycrystalline patches and veinlets that locally replace plagioclase, forms as much as 25 percent of the rocks. Even the smallest bodies show internal variations in color index, hornblende-biotite ratio, and quartz content. Alteration of hornblende and biotite is similar to that in the metamorphosed quartz diorite of the Blue Spring Gulch pluton.

METAMORPHOSED INTRUSIONS AND SERPENTINITE IN THE CAMPBELL GULCH PHYLLITE UNIT

Some small intrusions are located within or near greenstone bodies. The sizes and shapes of the intrusions within the greenstones are difficult to determine, but they are probably dikes. Those in phyllite near the greenstones appear to be sills as much as 30 m long. These intrusions have ophitic to subophitic textures, with as much as 40 percent clinopyroxene or hornblende partly altered to chlorite or actinolite (fig. 12.4). The remainder is albite with abundant inclusions of pumpellyite or clinozoisite and flakes of white mica. These dikes and sills are probably subvolcanic intrusions associated with the lavas and tuffs of the Campbell Gulch phyllite unit.

Five serpentinite bodies were mapped in the Campbell Gulch phyllite unit, none more than 150 m long. The serpentine minerals are chrysotile and lizardite, accompanied by minor magnetite. Several bodies contain talc and chalcedony veinlets. One body shows subhedral serpentine pseudomorphs with mesh structure, about 10 percent poikilitic orange-brown hornblende partly altered to Fe-Mg chlorite, and the remainder interstitial chlorite, fine-grained serpentine, and talc(?). The original rock probably contained subhedral olivine and was a hornblende-bearing peridotite. All of these bodies are located in fault zones. They probably represent small ultramafic masses that were intruded along the faults or tectonically emplaced, or both.

At many localities south and east of Burnt River Canyon, the Campbell Gulch phyllite unit hosts mafic and ultramafic intrusive bodies clearly older than the Jurassic to Cretaceous plutons (Wolff, 1965; Brooks, 1978). These intrusive rocks have not been radiometrically dated. Unlike the Blue Spring Gulch pluton, they commonly contain pyroxene and olivine.

ALTERED MAFIC DIKES

Altered mafic dikes intrude the Deer Creek phyllite unit within 1.5 km of the Cave Creek fault. They range from less than 1 m to as much as 3 m in width and are less than 50 m long. Even the widest of the dikes appears to be homogeneous, and they show no recognizable external contact effects. They are concordant with slaty cleavage of phyllitic host rocks, but are deformed (see section "Structural Geology").

The dikes contain as much as 50 percent Mg chlorite, which forms relatively coarse-grained patchy networks. Other constituents are anhedral quartz and albite, radiating sprays of clinozoisite prisms, and scattered sphene granules (fig. 12.5). Chlorite is the only constituent abundant in all specimens; percentages of the others vary greatly. Calcite is a minor constituent in some samples, as is white mica in samples with more than 20 percent albite.

All the constituent minerals are typical of low-grade metamorphic rocks; however, they are coarse-grained compared to those of the surrounding metamorphic rocks. The dikes do not have recognizable relict magmatic textures. They probably represent basalt that reacted with hydrothermal fluid after crystallization and was completely altered to hydrous low-grade assemblages.

LAMPROPHYRE DIKES

Lamprophyre dikes, which are much more abundant than the altered mafic dikes, contain 40 to 45 percent hornblende and are characterized by panidiomorphic-granular texture. They are widely scattered through the Deer Creek phyllite unit and occur in the Blue Spring Gulch pluton. They also cut the Campbell Gulch phyllite unit at five scattered localities. Individual dikes are either concordant or discordant with the slaty cleavage of phyllitic wallrocks and are undeformed. Dike margins show relatively fine-grained chilled zones, but there are no visible contact effects in adjacent wallrocks. Several well-exposed dikes are banded parallel to wallrock contacts. Internal bands with either sharp or gradational contacts are marked by relatively large numbers of chlorite amygdules, whereas outer bands generally have no amygdules.

The main constituents of these dikes are olive-green hornblende crystals, as much as 2 mm long, and strongly saussuritized subhedral plagioclase laths (30 to 40 percent) with irregular overgrowths of clear albite (fig. 12.5). Of the 15 dikes examined in detail, 5 have former olivine phenocrysts completely replaced by smectite and clinopyroxene phenocrysts partly to completely replaced by smectite or epidote. Interstitial materials besides albite are potassium feldspar (1 to 15 percent), quartz (5 to 15 percent),

and in some specimens, radiating aggregates of epidote or prehnite. All specimens contain scattered euhedral opaque granules. Small amygdules (2 mm or less in diameter) composed of Fe-Mg or Fe chlorite occupy as much as 15 percent of the rock.

In some of the hornblende lamprophyre dikes, the plagioclase has been altered to nearly clear albite rather than saussurite. Interstitial material includes quartz, sometimes in myrmekitic intergrowths with albite, radiating growths of matted chlorite (Fe-Mg, Mg-Fe, and, rarely, Mg types), radiating sprays of clinozoisite, and minor muscovite. In one dike, relatively abundant Mg chlorite not only forms interstitial aggregates but extensively replaces hornblende. Thus these mafic dikes show various degrees of alteration to hydrous mineral assemblages.

Before alteration the dikes probably ranged in composition from basalt to andesite. The two analyzed samples (78-2 and 14-29B, table 12.2) are basaltic andesite, on the basis of silica contents and the presence of small amounts of normative olivine. Barium, strontium, and zirconium are more abundant in these two samples than in samples of metamorphosed basalt and basaltic andesite from the Deer Creek and Campbell Gulch phyllite units and metamorphosed gabbro and diorite from the Blue Spring Gulch pluton.

PEDRO MOUNTAIN STOCK

The metamorphic rocks in the study area are cut by an unmetamorphosed medium-grained biotite- and hornblende-bearing quartz diorite intrusion (fig. 12.2). The main mass of the intrusion lies south of the area of figure 12.2, and a smaller exposure area extends to the east. Various parts of the intrusion were mapped by Wolff (1965), Prostka (1967), and Kennedy (1956). Wolff (1965) referred to it as the Pedro Mountain stock. The entire pluton is delineated on the regional geologic map of Brooks and others (1976). This regional map shows that the Pedro Mountain stock is the largest of a group of Jurassic to Cretaceous plutons that form a 55-km-long northeast-trending belt extending from Cow Valley Butte on the southwest to Big Lookout Mountain on the northeast (fig. 12.1). These masses belong to a plutonic suite of quartz dioritic and granodioritic composition that is widely exposed in northeastern Oregon and includes the Wallowa and Bald Mountain batholiths. Radiometric ages of these plutons range from about 120 to 160 Ma (Armstrong and others, 1977; Marvin and Dobson, 1979; Walker, 1986). Walker (1986) obtained U-Pb ages of 119±1, 120±1, and 122±1 Ma on three zircon fractions from a tonalite sample collected from the southern part of the Pedro

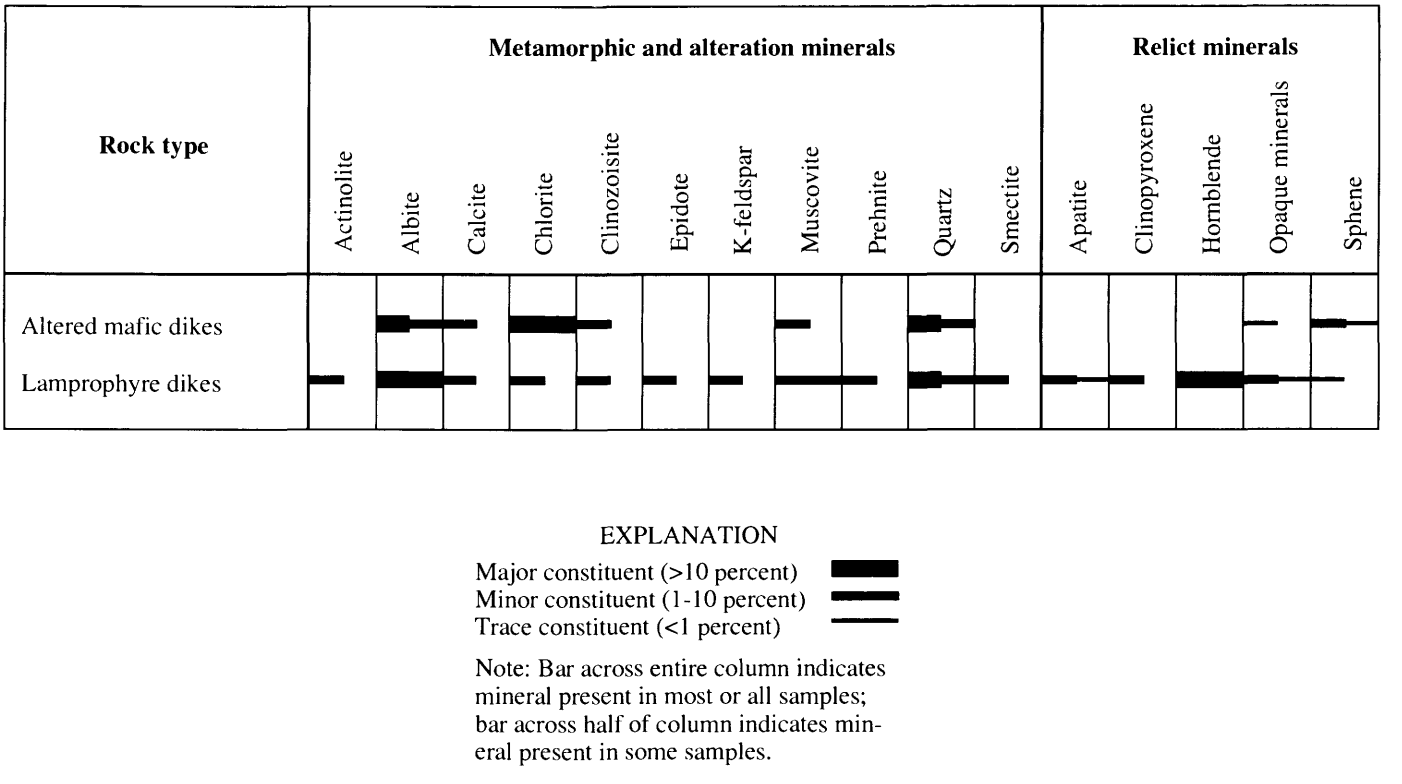

FIGURE 12.5.—Mineral assemblages of altered mafic dikes and lamprophyre dikes in Burnt River Canyon area.

Mountain stock, in the northeast corner of the Bridgeport quadrangle (fig. 12.1).

On the west and south sides of the Pedro Mountain stock, the intrusive contact has a simple arcuate outline and the foliation in the wallrocks is strongly deflected around the intrusion, parallel to the contact (Wolff, 1965). In contrast, the wallrock foliation on the north side of the intrusion is not strongly deflected, and the steeply dipping contact there has a complex outline with several large reentrants (fig. 12.2). The wallrock foliation parallels large segments of the contact, and mineral foliation in the intrusion, produced by oriented biotite, shows orientations similar to those of nearby wallrock foliation. Mineral lineation in the intrusion, produced by oriented hornblende, is generally steeply plunging. These features suggest that the northern part of the intrusion, although modally nearly homogeneous, is probably a series of connected semiconcordant sheets or lobes that pushed upward into the greenstone belt of the Campbell Gulch phyllite unit, guided by wallrock foliation.

IGNEOUS PETROLOGY

METAVOLCANIC ROCKS

Because the alkali contents of the metamorphosed igneous rocks have probably been modified, alkali-silica variation and the alkali-lime index cannot be used to characterize these rocks. Instead variation diagrams of SiO_2 versus FeO*/MgO and FeO* versus FeO*/MgO can be used to distinguish rocks with affinities to calc-alkaline series from those with affinities to tholeiitic series (Miyashiro, 1975). Analytical data for metamorphosed volcanic and intrusive rocks from the study area are plotted on an SiO_2-versus-FeO*/MgO variation diagram in figure 12.6, with a reference line dividing calc-alkaline and tholeiitic series. Below FeO*/MgO=2, trends for calc-alkaline and tholeiitic series converge, so the cluster of analyses for metamorphosed basalt and basaltic andesite of the Campbell Gulch and Deer Creek phyllite units cannot be classified as calc-alkaline or tholeiitic.

Titanium, zirconium, niobium, and yttrium are thought to be relatively immobile during low-grade alteration and metamorphism (Cann, 1970) and can provide insight into the tectonic environment in which mafic volcanic rocks formed (Pearce and Cann, 1973). On both Ti-Zr-Y and Ti-Zr discriminant diagrams (fig. 12.7), data for mafic metavolcanic rocks from the Deer Creek and Campbell Gulch phyllite units plot in the field where data from ocean-floor basalts, low-potassium tholeiites, and calc-alkaline basalts overlap (Pearce and Cann, 1973). On Y-Zr, Ti-Zr, and Nb-Zr variation diagrams (not shown; see Pearce and Norry, 1979), the data fall close to trend lines for various volcanic arcs rather than trend lines for within-plate volcanoes. The metavolcanic rocks contain moderate amounts of titanium and relatively small amounts of zirconium, falling within the compositional range for these elements in island-arc tholeiites (Baker, 1982; Jakeš and White, 1971; see table 12.1 for data). Most analyses fall in the island-arc tholeiite field on a TiO_2-MnO-P_2O_5 discriminant diagram (Mullen, 1983a), as shown on figure 12.8. I conclude that the metavolcanic rocks of both the Deer Creek and Campbell Gulch phyllite units are derived from arc rocks, but whether either group clearly fol-

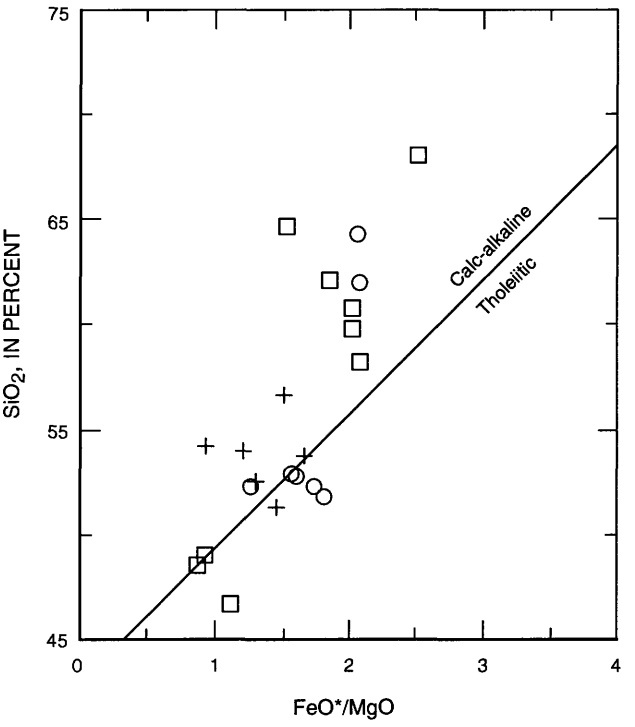

FIGURE 12.6.—SiO_2 versus FeO*/MgO variation diagram for metavolcanic and meta-intrusive rocks of the Burnt River Canyon area. FeO* is total iron calculated as FeO. Boundary between calc-alkaline and tholeiitic fields is from Miyashiro (1975).

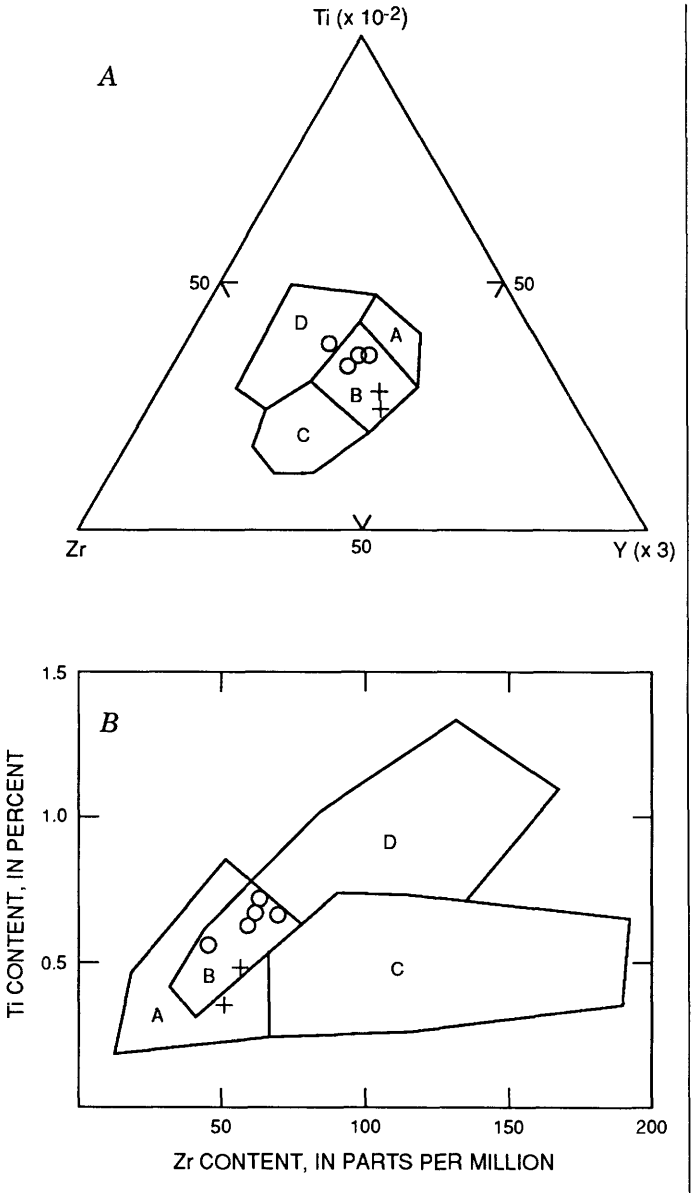

FIGURE 12.7.—Ti, Zr, and Y discriminant diagrams after Pearce and Cann (1973) for mafic metavolcanic rocks (45–54 percent SiO_2) of Burnt River canyon area. *A*, Ti-Zr-Y discriminant diagram. Scaling factors ($Ti \times 10^{-2}$, $Y \times 3$) used to bring points into center of diagram without altering relative positions. Low-K tholeiites plot in fields A and B, calc-alkaline basalts in fields B and C, ocean-floor basalts in field B, and oceanic-island and continental basalts in field D. *B*, Ti-Zr discriminant diagram. Low-K tholeiites plot in fields A and B, calc-alkaline basalts in fields B and C, and ocean-floor basalts in fields B and D.

lows a tholeiitic or a calc-alkaline differentiation trend is indeterminate with present data. Mullen (1985) also proposed an arc origin for metabasalt probably obtained from the Campbell Gulch phyllite unit.

BLUE SPRING GULCH PLUTON

Analyses for the Blue Spring Gulch pluton and other meta-intrusive rocks that cut the Deer Creek phyllite unit (table 12.2) are also shown on the variation diagram (figure 12.6). The six analyses for metamorphosed diorite, quartz diorite, and tonalite samples show a calc-alkaline trend. The analysis for sample 77-22, a metamorphosed leucotonalite, is not included because its FeO*/MgO is anomalously low. The fact that original biotite in metamorphosed quartz diorite sam-

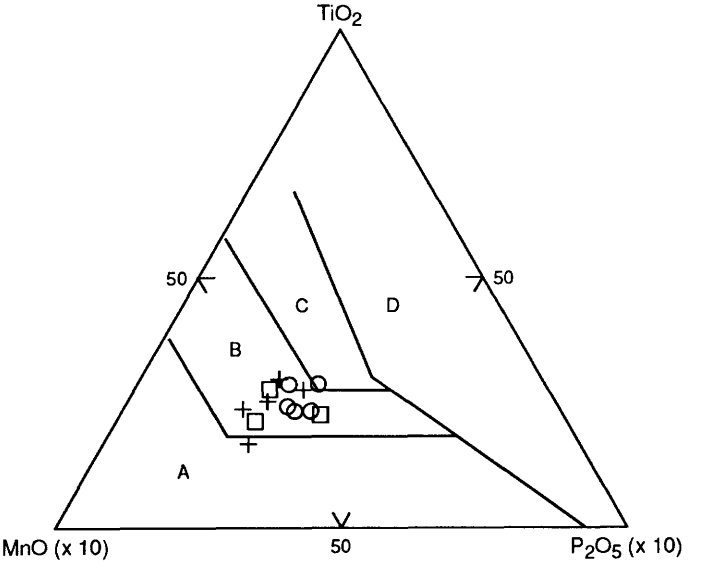

FIGURE 12.8.—MnO-TiO_2-P_2O_5 discriminant diagram for mafic metavolcanic and meta-intrusive rocks (45–54 percent SiO_2) of Burnt River Canyon area. Scaling factors ($Mn \times 10$, $P_2O_5 \times 10$) used to bring points into center of diagram without altering relative positions. Calc-alkaline basalts plot in field A, island-arc tholeiites in field B, midocean-ridge basalts in field C, and seamount alkalic basalts and tholeiites in field D. Diagram from Mullen (1983a).

ples is altered to chlorite suggests that potassium may be somewhat depleted in these rocks owing to alteration and metamorphism. One metamorphosed leucoquartz diorite sample (78-3B) shows normative corundum, likely the result of alkali depletion and possibly calcium depletion as well. All analyzed samples in the intrusive series are metaluminous, with the exception of sample 78-3B, which is peraluminous. Rocks of basic to intermediate calc-alkaline and tholeiitic arc suites are typically metaluminous (Brown, 1982).

The mafic minerals in the more felsic members of this intrusive series are hornblende and biotite, which are typical of calc-alkaline plutonic rocks. The only mafic mineral in the metamorphosed diorite and gabbro samples, however, is hornblende. Yoder and Tilley (1962) showed that magmas of basaltic composition crystallize to form amphibolites at P_{H_2O} greater than 1.4 kbar. Thus these intrusions crystallized from hydrous magmas at a minimum depth of about 5 km. The lack of contact effects indicates that the terrane was at elevated temperatures and fluid pressures at the time of intrusion.

Ba, Rb, and Sr contents vary in the analyzed suite of intermediate and felsic intrusive rock samples (table 12.2), probably as a result of secondary processes. Ba and Sr contents, nevertheless, generally are similar to those found in calc-alkaline andesite and dacite, and island-arc intrusive suites (Jakeš and White, 1972; Mason and McDonald, 1978; Baker, 1982). Rb contents are low, providing supporting evidence for K depletion. Zr, which should be relatively immobile in secondary processes, is present in the intermediate to felsic intrusive rocks in amounts more typical of arc tholeiites than calc-alkaline arc rocks (Jakeš and White, 1972; Baker, 1982). Nb, which also should be relatively immobile, is present in amounts characteristic of volcanic-arc magmas (Pearce and Gale, 1976; Pearce and Norry, 1979).

Rocks of the Blue Spring Gulch pluton show many similarities to intermediate and silicic rocks of the (informal) Sparta complex, about 30 km northeast of Burnt River Canyon. Metamorphosed diorite and quartz diorite samples from the Burnt River area (table 12.2) are chemically similar to quartz diorite from the Sparta complex (Phelps, 1979), except that Na_2O content is higher in the Burnt River rocks. The metamorphosed leucotonalite of the Burnt River area (sample 77-22, table 12.2) is similar in occurrence, texture, and composition to fine-grained low-K_2O trondhjemite at Sparta described by Phelps (1979), but the Burnt River sample has anomalously low FeO* content. The southern part of the Sparta complex, consisting of two-pyroxene gabbro, hornblende-bearing two-pyroxene gabbro, pyroxenite, and peridotite (Prostka, 1962), has no counterpart in the Blue Spring Gulch pluton. The Sparta complex has yielded ages ranging from 213 Ma (Vallier and others, 1977) to 253 Ma (Walker, 1981, and this volume); this range includes the U-Pb age of approximately 230 Ma determined for a sample from the Blue Spring Gulch pluton (Walker, 1986).

The Canyon Mountain Complex consists of harzburgite tectonite overlain successively by plagiogranite intrusions and interlayered variably altered basalt, diabase, and keratophyre (Thayer, 1977; Gerlach and others, 1981). The only rocks in the Canyon Mountain Complex similar to those of the Blue Spring Gulch pluton are those of the plagiogranite suite, which includes diorite, quartz diorite, tonalite, and trondhjemite (Gerlach and others, 1981). Thayer (1977) proposed that the Canyon Mountain Complex is an ophiolite of oceanic-ridge origin. Himmelberg and Loney (1980) and Gerlach and others (1981), however, concluded that it is of island-arc origin. Vallier and others (1977) suggested that the complex forms the basement for supracrustal sedimentary rocks of the Baker terrane. U-Pb ages of 279 to 268 Ma for Canyon Mountain intrusive rocks (Walker, 1983) indicate that all parts of the Canyon Mountain Complex are significantly older than the Blue Spring Gulch pluton.

The Blue Spring Gulch pluton is here interpreted as an intrusive phase of Middle Triassic arc-related calc-alkaline magmatism. Similarly, Phelps and Avé Lallemant (1980) concluded that the Sparta complex is an intrusive phase of Late Triassic arc-related magmatism, on the basis of age data then available, which gave an age range of 219 to 213 Ma. Arc magmatism of Middle and Late Triassic age produced the younger volcanic-rock-dominated sequences of the Wallowa terrane (the upper part of the Clover Creek Greenstone (Gilluly, 1937), the informally named Gold Creek greenstone of Prostka (1962), the Wild Sheep Creek Formation, and the Doyle Creek Formation) and the volcanic rocks of the Huntington Formation of Brooks (1979b) of the Olds Ferry terrane (see "Discussion and Conclusions" section; Vallier and others, 1977; Brooks and Vallier, 1978; Silberling and others, 1987).

METAMORPHIC PETROLOGY

The mineral assemblages of metamorphosed and altered rocks of the Burnt River Canyon area are summarized in figures 12.3 through 12.5, and 12.9. The assemblages for all common rock types of the Deer Creek and Campbell Gulch phyllite units are summarized in figures 12.3 and 12.4, respectively.

Mineral assemblages in altered mafic dikes and lamprophyre dikes are summarized in figure 12.5. The assemblages for five contact metamorphic zones delineated in Campbell Gulch greenstones are summarized in figure 12.9.

Mineral phases were identified mainly by transmitted-light optical microscopy and whole-rock X-ray diffraction. A few mineral separates were prepared from metamorphic segregation veinlets and identified by powder-camera X-ray diffraction. Several serpentine samples were investigated by differential thermal analysis. Microanalysis of individual mineral phases has not been performed, but the available optical and X-ray diffraction data are adequate to define the general conditions of metamorphism.

Mineral assemblages in the Deer Creek phyllite unit and in the plutonic rocks that intrude it largely reflect conditions of greenschist-facies metamorphism, as shown by the presence of actinolite in all mafic and intermediate metavolcanic rocks and most meta-intrusive rocks and the common occurrence of the biotite-muscovite assemblage in pelitic rocks (Winkler, 1979; Liou and others, 1985). In the meta-intrusive rocks, the only prominent relict magmatic minerals are hornblende and quartz. In the metamorphosed mafic and intermediate volcanic and volcaniclastic rocks, relict phases include minor clinopyroxene, hornblende, and opaque minerals. Pumpellyite, largely replaced by clinozoisite, was observed in metabasalt samples from two localities. It is probably a relict of lower-temperature metamorphic conditions (prehnite-pumpellyite or pumpellyite-actinolite facies) that the Deer Creek phyllite unit passed through during prograde metamorphism. Garnet present in some quartz phyllite samples in trace amounts is probably spessartine formed under low-grade conditions. The pressure

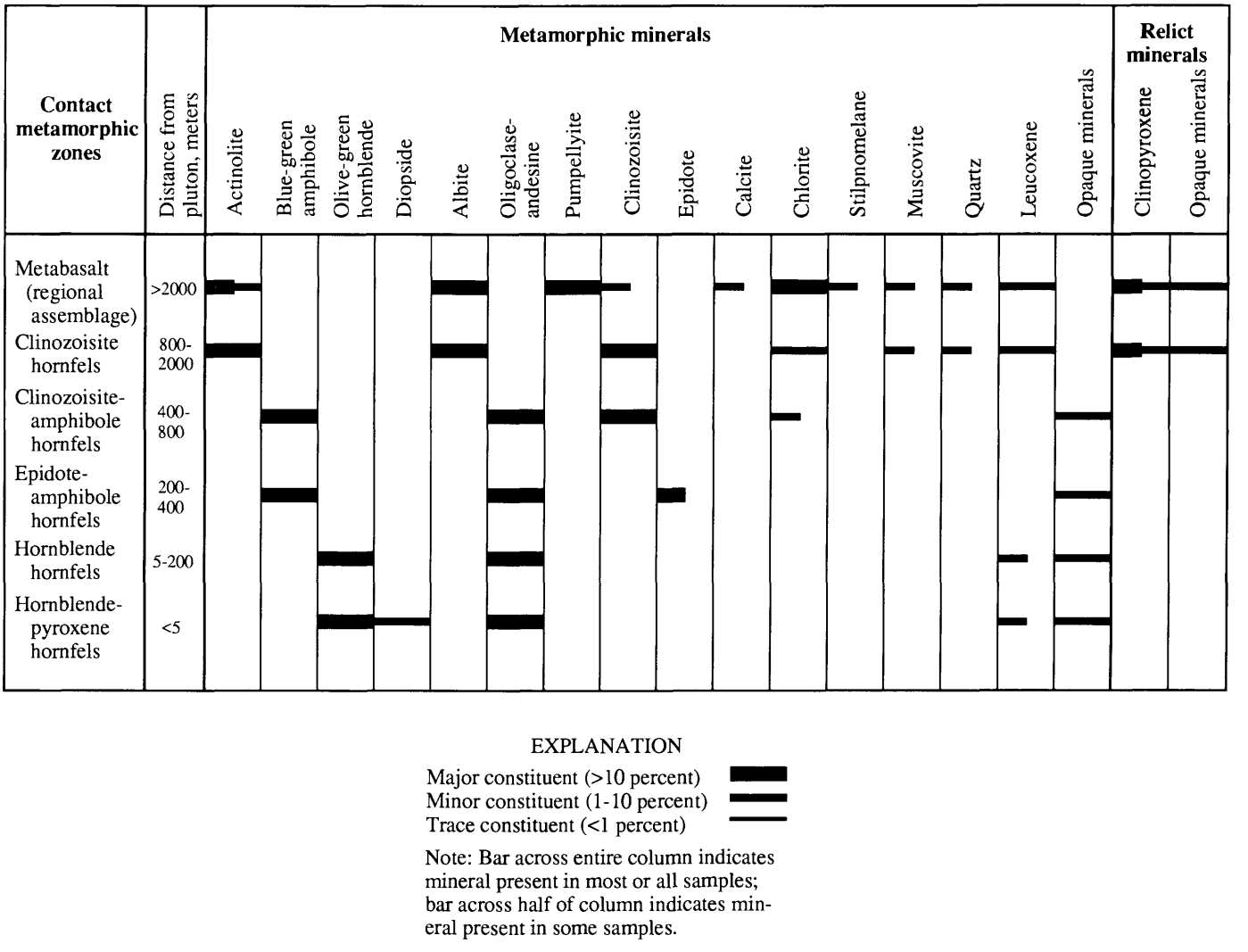

FIGURE 12.9.—Mineral assemblages of contact-metamorphosed greenstones in the Campbell Gulch phyllite unit of Burnt River Schist.

range for the greenschist facies is from about 2 kbar or less to about 8 kbar, and the temperature range is about 320 to 450°C (Liou and others, 1985).

The common presence of pumpellyite and actinolite in mafic metavolcanic rocks of the Campbell Gulch phyllite unit (fig. 12.4) indicates that mineral assemblages here adjusted to conditions of the pumpellyite-actinolite facies (Liou and others, 1985) and that maximum regional temperatures were not as high as in the Deer Creek phyllite unit. Lack of reaction of stilpnomelane to biotite also indicates lower temperatures of metamorphism in the Campbell Gulch phyllite unit. Relict magmatic clinopyroxene, hornblende, and opaque minerals persist in metamorphosed volcanic and intrusive rocks of the Campbell Gulch phyllite unit. The pressure range for the pumpellyite-actinolite facies is approximately 3 to 8 kbar, and the temperature range is approximately 250 to 350°C.

The regional metamorphic mineral assemblages of the Campbell Gulch phyllite unit have been overprinted by contact metamorphic effects of the Pedro Mountain stock (fig. 12.9). In greenstone 2 km from the intrusive contact, pumpellyite is replaced by clinozoisite, a zone boundary readily seen in the field because the characteristic dark green pumpellyite veinlets disappear. At about 800 m from the intrusive contact, the rocks contain oligoclase instead of albite, and all relict clinopyroxene is converted to bluish-green amphibole, which also replaces fine-grained actinolite in the groundmass. These changes are not obvious in the field, but oligoclase-bearing rocks have veinlets of plagioclase and clinozoisite that are visible in outcrop. At 600 to 800 m, plagioclase, clinozoisite, and idioblastic bluish-green amphibole begin to segregate into lensoid domains parallel to the foliation. Amphibole becomes coarser and more deeply colored toward the stock; at about 300 m the rocks are gneissose amphibolites with visible amphibole grains and abundant plagioclase segregations and folded veinlets. Epidote takes the place of clinozoisite in these rocks and is prominent to within about 200 m of the contact, where it disappears and olive-green hornblende replaces the blue-green amphibole. A few meters from the contact, hornblende is accompanied by scattered grains of diopside. The epidote amphibolite- and amphibolite-facies assemblages that occur within 800 m of the stock formed at pressures greater than about 2 kbar and temperatures greater than about 400°C (Liou and others, 1985).

Pelitic rocks from 1 km to within 300 m of the Pedro Mountain stock are mainly muscovite-biotite-quartz schists. Spotted schists occur locally within 300 m of the contact. The spots, composed of muscovite and graphite(?), probably represent altered andalusite.

Serpentinite bodies in both the Campbell Gulch phyllite unit and the Blue Spring Gulch pluton are composed mainly of chrysotile or lizardite or both. Chrysotile and lizardite are stable only under conditions of very low grade metamorphism (Evans, 1977). Absence of antigorite suggests that these serpentinized ultramafic bodies postdate the main thermal metamorphic event(s).

Altered mafic dikes, although unusual in that they contain abundant chlorite and only minor actinolite, have low-grade metamorphic mineral assemblages that must have formed under temperature and pressure conditions similar to those that affected their host rocks (fig. 12.5).

Lamprophyre dikes show little or no alteration of apatite, sphene, and opaque minerals, partial alteration of hornblende, partial to complete alteration of clinopyroxene, and complete alteration of plagioclase and olivine. Although the extent of hydration and recrystallization is variable, alteration assemblages suggest that the lamprophyre dikes were exposed to conditions of the prehnite-actinolite facies. The temperature range for the prehnite-actinolite facies is approximately 250 to 350°C, and the pressure range is less than 1 kbar to approximately 2 kbar (Liou and others, 1985). Clays in these rocks may have formed at temperatures less than 200°C.

STRUCTURAL GEOLOGY

Structural data were collected at a density of 3 or 4 field stations per square kilometer, for a total of 676 stations in the study area. For each station, a stereogram was prepared to check the geometric relations of the structural data against the relations observed in the field.

The notation used here is from Freedman and others (1964): S denotes a planar element, L denotes a linear element, F is any fold involving any S as form surface, A is a fold axis, and D is a single deformation defined by a set of contemporaneous tectonic structural elements. S_0 designates bedding, and S_n, L_n, F_n, and A_n refer to planar surfaces, lineations, folds, and fold axes related to D_n.

MESOSCOPIC STRUCTURAL FEATURES

DEER CREEK PHYLLITE UNIT

Slaty cleavage (S_1) is the dominant S-surface in most phyllitic rocks, but bedding (S_0) is dominant in

rocks such as phyllitic quartzites that have interbeds with strongly contrasting properties (fig. 12.10*A*). S_1 is obvious in all rock types except massive metavolcanic and intrusive bodies. It did not form in the Blue Spring Gulch pluton, which responded to deformation by irregularly distributed shearing and crushing. A later cleavage (S_2) varies greatly in strength from place to place, on a scale of tens of meters (fig. 12.10*B*). Where S_2 is well developed in pelitic phyllite, it is a slaty cleavage, but S_2 is never visible in quartzite layers. S_2 is moderately strong in quartzofeldspathic phyllites and metavolcaniclastic rocks, but weak or absent in metalavas.

A strong microcrenulation lineation (L_2) pervades phyllitic rocks, metavolcaniclastic rocks, and marble (fig. 12.10*C*). It is always parallel to the S_1-S_2 intersection line and to the axes of minor (F_2) folds whose axial surfaces are nearly parallel to S_2 and whose form sur-

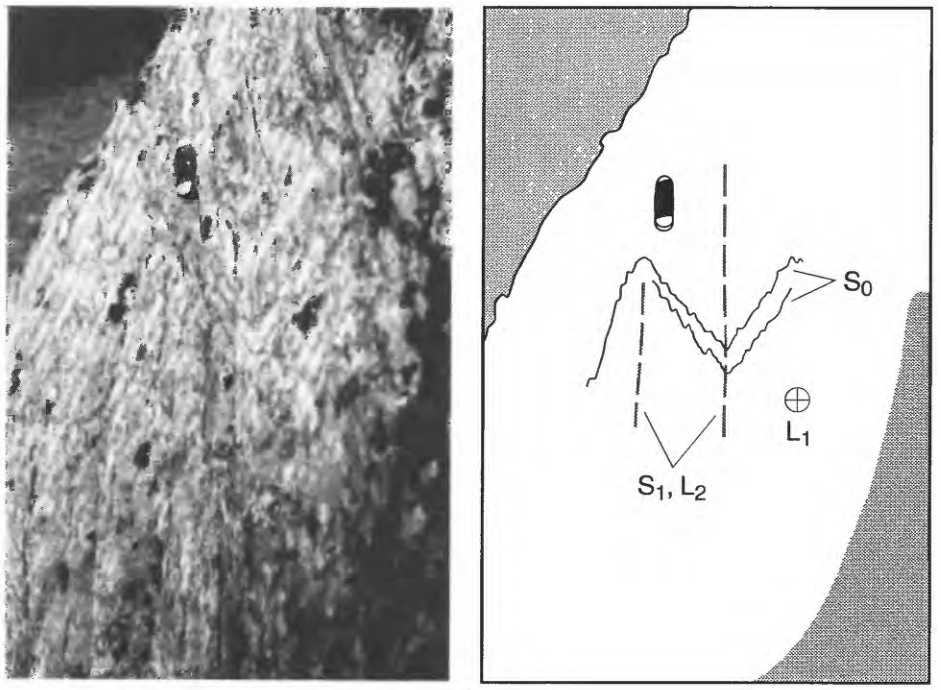

A

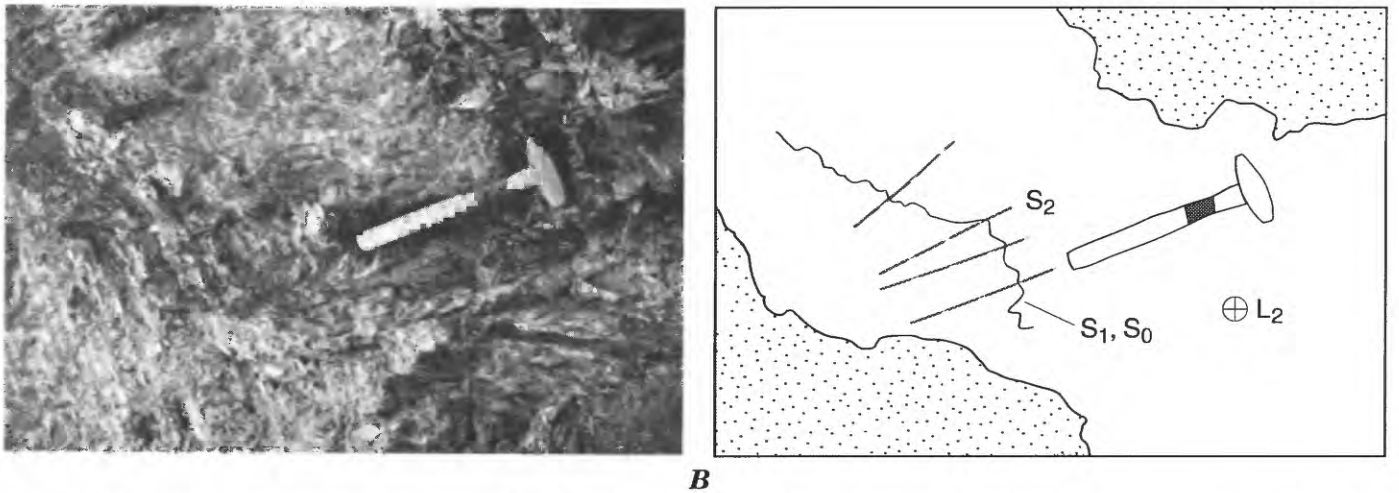

B

FIGURE 12.10.—Mesoscopic structural features of Deer Creek phyllite unit. *A*, Outcrop of phyllitic quartzite with thin pelitic phyllite interbeds, viewed parallel to L_1 and S_1, showing F_1 folds. Sketch shows trace of bedding (S_0), which defines F_1 folds. L_2 is inclined toward observer, and trace of S_1 is parallel to L_2. Knife is 8 cm long. *B*, Outcrop of thinly laminated quartz phyllite, phyllitic quartzite, and pelitic phyllite, viewed parallel to L_2, showing F_2 folds. Sketch shows traces of S_1 cleavage, which defines F_2 folds, and S_2 cleavage. Bedding is parallel to S_1. Note fanning of S_2. Hammer is 40 cm long.

faces are S_1. The S_0-S_1 intersection forms a lineation (L_1) that is older than the strong crenulation lineation. Wherever S_0 is a strong feature, L_1 can be distinguished from L_2 by careful observation.

F_1 folds are visible at a few outcrops. Pelitic beds show similar-type folds with amplitudes of 15 to 70 cm, having subsidiary folds with amplitudes as small as 1 mm (fig. 12.10*A*). Folds with amplitudes from 70 cm to 5 m are visible in rocks with strong bedding features, particularly phyllitic quartzites. Folds are tight, with amplitudes ranging from one to four times wavelength, and nearly always asymmetrical. Exposures oriented approximately perpendicular to F_1 axes commonly show many small folds with the same sense of asymmetry.

F_2 folds are locally well developed (fig. 12.10*B*). Amplitudes range from a few millimeters to 60 m, but for most folds, amplitudes do not exceed 1 m, and are generally smaller than wavelengths, so the folds are open, with no thickening in the axial regions. Locally, where F_2 folding is very strong, amplitudes exceed wavelengths and the folds are similar folds with strong S_2 cleavage in fans opening outward from fold cores. The angle between S_2 and the average S_1 attitude varies within the area and controls the shapes of F_2 folds; the smaller the angle between S_2 and average S_1, the more asymmetrical the fold. Average S_1 is the attitude of an envelope containing a given F_2-folded S_1 surface (Turner and Weiss, 1963).

The metavolcaniclastic rocks show moderately to well-developed S_1, much like that of the quartzofeldspathic phyllites. S_2 is weaker than S_1, and locally it is absent. Phyllosilicates in the crystalloblastic matrix between clasts are concentrated in folia that form S_1 and S_2. The folia are very poorly developed within the clasts, so rocks with coarse protolith textures are semischistose. L_2 is well developed, but L_1 is difficult to observe in most exposures because these rocks are poorly bedded, and consequently the line of intersection between S_0 and S_1 cannot be seen.

C

FIGURE 12.10.—Continued. *C*, Outcrop of quartz phyllite, showing strong mullion structure produced by L_2 microcrenulation and intersecting S_1 and S_2 cleavages, parallel to L_2. Note well-developed cross joints. Hammer, at top of outcrop, is 40 cm long.

Axial ratios of the clasts indicate the amount of apparent strain produced by D_1 and D_2 combined. Where L_1 and L_2 are nearly parallel (the angle between them less than 20–25°), it is not possible to distinguish whether the longest axes of the clasts are parallel to L_1 or L_2. The intermediate axes of the clasts lie within S_1 approximately perpendicular to the average of L_1 and L_2, and the short axes are perpendicular to S_1. Axial ratios range from 8:2:1 to 3:1.5:1. Where L_1 and L_2 are at a high angle (60° or more), the longest axes of the clasts are clearly parallel to L_1, the intermediate axes perpendicular to L_1 within S_1, and the short axes perpendicular to S_1, but the long axes of the clasts have been shortened and the short axes lengthened by D_2 strain, resulting in axial ratios of about 2:1.5:1. Since the L_1-L_2 angle is generally small and L_2 is the most prominent lineation throughout the area, the clasts at many localities appear to be strongly extended parallel to L_2 and the apparent strain they record seems to be the result of D_2. D_1, however, produced much of the strain.

The metalavas are generally massive, and they show all tectonic structures poorly. Only the originally fine-grained or glassy parts of flow breccias associated with the flows show strongly oriented chlorite fabrics that produce conspicuous S_1. Actinolite is nearly randomly oriented throughout the rocks.

In phyllitic rocks with weak S_2 and no mesoscopic F_2 folds, marble interbeds are massive, with weak S_1. Where S_2 is strong and accompanies mesoscopic F_2 folds in phyllitic rocks, marble beds have an S_2 fabric of flattened calcite grains. L_2 is visible only in impure marble and calc-phyllite.

Observations of microscopic fabrics, particularly in the phyllite and quartz phyllite, show that metamorphic recrystallization continued throughout both D_1 and D_2 deformations. Reorientation of phyllosilicate grains from S_0 to S_1 folia and from both S_0 and S_1 to S_2 folia was accomplished by recrystallization. Throughout the rocks, few phyllosilicate flakes are even slightly bent. Biotite microporphyroblasts, seen in a few quartz phyllite samples, show weak preferred orientation parallel to S_1, weak to strong preferred orientation parallel to S_2, and other orientations not clearly related to D_1 or D_2. All biotite microporphyroblasts are unstrained, regardless of size or habit. (See Ashley, 1966, for details of microfabric features.)

All the quartzose and quartzofeldspathic rocks contain four generations of quartz(-albite) veinlets. Pre-D_1 veinlets are parallel to or at various angles to S_0 and show tight F_1 microfolds and refolded fold forms produced by D_2 (fig. 12.11*A*). Late-D_1 veinlets cut the rocks at various angles, are gently microfolded with axial planes parallel to S_1, and show effects of D_2 folding. Post-D_1, pre-D_2 veinlets are mostly parallel to S_0 or S_1, and they show only F_2 microfolds. Post-D_2 veinlets are parallel to S_0, S_1, or S_2, or have apparently random orientations. They are not folded but locally show small offsets along S_1 or S_2 surfaces.

BLUE SPRING GULCH PLUTON AND OTHER DEFORMED INTRUSIVE ROCKS

The intrusive rocks are penetratively fractured and brecciated. Plagioclase and hornblende show bent and broken twin lamellae and deformed cleavage surfaces on the microscopic scale throughout the intrusive bodies. Cataclasite and microbreccia sheets (nomenclature of Higgins, 1971) are the only mesoscopic tectonic features visible in the metamorphosed intrusions (fig. 12.11*B*). Individual sheets are typically several millimeters thick, spaced several centimeters apart, and do not persist for more than 3 m. They cut and offset early epidote veinlets as much as 10 cm. The finely crushed matrix of the sheets is completely recrystallized to crystalloblastic aggregates of clinozoisite or epidote, albite, chlorite, actinolite, and leucoxene. Most exposures show one or two sets of parallel cataclasite sheets, but as many as four sets may be visible in a single outcrop. At many localities one or two sets of cataclasite sheets strike east to northeast and dip steeply, generally similar to S_1 in the metasedimentary rocks, but direct correlation of these shear surfaces with S-surfaces in the phyllite is not possible because no suitable metasedimentary rock exposures were found at the external contacts of the large intrusive bodies.

At the margins of the small metamorphosed diorite and quartz diorite bodies exposed on Sheep Mountain and Windy Ridge, intense pervasive cataclasis was followed by development of phyllosilicates, which form wispy, irregular folia within the cataclasite sheets and have a common orientation throughout the rock that may diverge from the orientations of the sheets. Near the margins of these intrusive bodies, extremely strong cataclasis plus recrystallization of phyllosilicates into folia produced a semischistose texture parallel to the slaty cleavage (S_1) of the surrounding metasedimentary rocks. F_2 microfolds are weakly developed in the semischistose quartz diorites, but no other feature in the metamorphosed intrusions can be definitely attributed to D_2.

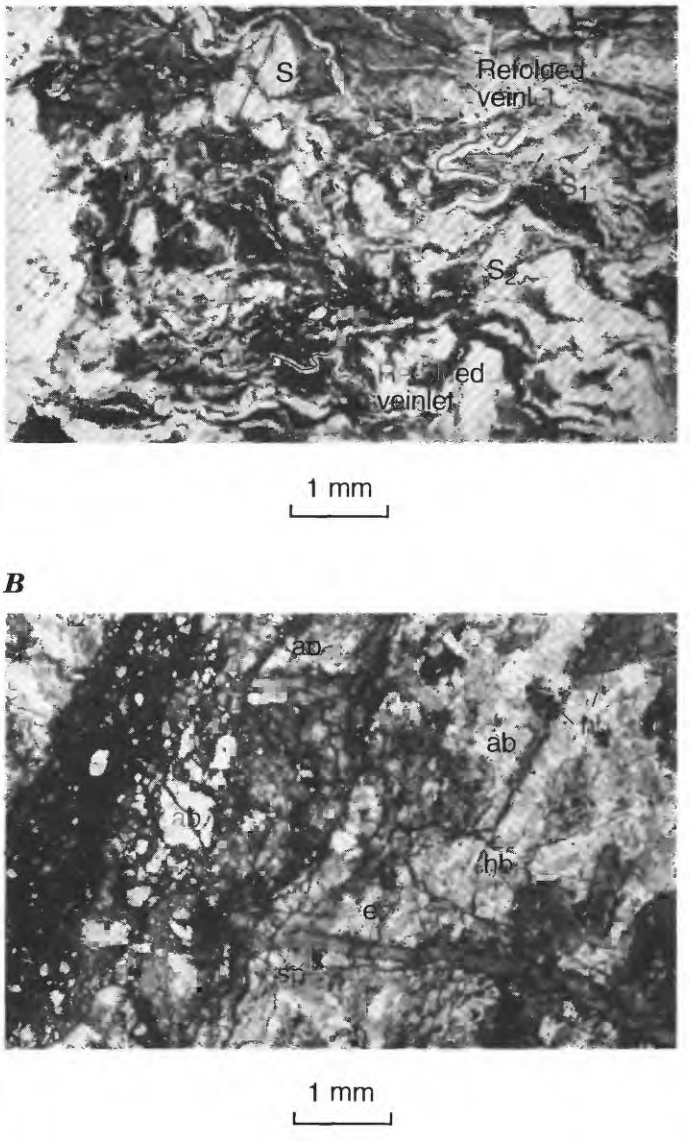

FIGURE 12.11.—Photomicrographs showing structural features. *A*, Pelitic phyllite of the Deer Creek phyllite unit showing both F_1 and F_2 microfolds. White bands are quartz veinlets, many of which pre-date D_1 and show refolded fold forms, with folds symmetrical to S_1 planes refolded about axial planes parallel to S_2. Traces of S_1 and S_2 and examples of refolded quartz veinlets are shown. *B*, Metamorphosed leucogabbro. Main constituent is albite with muscovite inclusions (ab); also contains hornblende grains (hb), sphene (sp), and epidote veinlets (ep). Intensity of deformation increases from right side of view area to the left. To right of center, albite and hornblende are fractured; to the left, they are crushed, with a matrix of crystalloblastic epidote, actinolite, and albite. On the extreme left is a cataclasite band consisting of fine-grained crystalloblastic epidote, albite, actinolite, and leucoxene, with scattered albite and hornblende porphyroclasts.

ALTERED MAFIC DIKES

The altered mafic dikes are always concordant with the slaty cleavage (S_1) of their host rocks. The thinner dikes and the margins of the thicker ones have weak schistosity parallel to S_1, produced by preferred orientation of chlorite. Where S_1 in the host rocks forms F_2 folds, the dikes are also folded and S_1 in the dikes remains parallel to the dike margins and to S_1 of the host rocks. Thus the dikes were emplaced before D_2. Although they could be pre-D_1 sills, more likely they were emplaced after S_1 formed in the metasedimentary rocks, then were foliated by renewed compressive stress before D_1 ended.

CAMPBELL GULCH PHYLLITE UNIT

The phyllitic rocks have a well-developed slaty cleavage, S_1, generally parallel to bedding. At a few outcrops of pelitic phyllite, thin marble or quartzite (metasandstone) beds outline F_1 folds that show greatly thickened hinges and pinched-out limbs (fig. 12.12*A*). The F_1 folds are tight to isoclinal, and S_1 is an axial-plane cleavage. Phyllosilicates strongly aligned parallel to S_1 are evenly distributed through most phyllite, which lacks strong bedding features. Quartz and plagioclase grains in metamorphosed conglomerate and lithic sandstone beds form domains nearly free of cleavage folia. Feldspathic metasandstone, which contains abundant quartz and plagioclase grains, is semischistose.

L_1 is well defined in some exposures by one of several features, including intersection of prominent interbeds with S_1, boudinage structure in thin marble beds interlayered with phyllite, quartz rods that are probably remnants of disrupted folded veinlets, stretched clasts and calcareous concretions, and crenulations developed near fold hinges in competent beds. More commonly, poorly developed spaced cleavages intersect S_1 at low angles to produce L_1. The origin of these spaced cleavages is unknown. In some cases they may be parallel to subtle bedding features.

The long axes of stretched clasts are parallel to L_1, their intermediate axes are perpendicular to L_1 in the plane of S_1, and their short axes are perpendicular to S_1. Stretching ratios in the plane of S_1 are 1.5:1 to 3:1, indicating moderate apparent stretching parallel to L_1, and flattening ratios are 2:1 to 15:1, indicating strong apparent flattening in S_1.

Adjacent to the southern boundary of the study area, a second lineation, L_2, is strongly developed in the phyllitic rocks and rarely developed in metatuff. S_1 is folded to form F_2 folds that have a new axial-plane cleavage, S_2, which intersects S_1 to form L_2 (fig. 12.12*B*). S_2 is a spaced crenulation cleavage produced by thin bands of aligned phyllosilicates (fig. 12.12*C*). Both zonal and discrete cleavages are seen in individual samples, but discrete cleavages are more common where S_2 is relatively well developed (nomenclature of Gray, 1979). Because the zonal type of S_2 crenulation cleavage is most common, the rock usually breaks along S_1 folia, and L_2 thus appears as a series of strongly asymmetric wrinkles on S_1 surfaces. Mesoscopic F_2 folds are open flexural folds with amplitudes less than wavelengths (fig. 12.12*B*). Apparent offsets on S_2 surfaces consistently move the fold limbs away from the hinges enough to produce slight thinning of the limbs and thickening of the hinges. These apparent offsets are probably the result of dissolution and removal of quartz and feldspar from the phyllosilicate domains (Gray, 1979).

North of the greenstone belt ("g," fig. 12.2), no mesoscopic F_2 folds exist and no S_2 is present, but L_2 persists. S_1 surfaces are deformed into microcrenulations with a consistent sense of asymmetry. Near the Cave Creek fault, D_2 features are absent. In general, within the Campbell Gulch phyllite unit, rocks with F_2 and S_2 grade northward into rocks with only L_2, and these in turn grade into rocks with no D_2 features.

Marble bodies generally show vague foliation. Very small bodies and the margins of larger bodies are moderately to strongly foliated, and the foliation is parallel to S_1 in the surrounding phyllite. The degree to which the constituent calcite grains are flattened controls the strength of the foliation. The smaller, more highly foliated bodies have an L_1 lineation produced by elongation of the grains. The extremely tight F_1 folding and moderate apparent stretching parallel to L_1 observed in the phyllite suggest that the podlike and lensoid shapes of the marble bodies are at least partly tectonic features rather than entirely original sedimentary features.

The more quartz-rich rocks, including phyllitic quartzite and massive metasandstone, contain many quartz veinlets, including strongly folded pre-D_1 veinlets, weakly folded late-D_1 veinlets, and post-D_1, pre-D_2 veinlets.

Strength of S_1 varies greatly in the metavolcanic rocks. This variation is related primarily to original differences in texture. L_1 is generally weak. It results from small-scale folding of pre-D_1 veinlets and of primary structures such as flow layering. L_1 is not visible in the most massive metalava, whereas in the metatuff it is as strongly developed as it is in the phyllite. L_2 in metalava is very rare, even though F_2 affects phyllite interbedded with greenstone on the south side of the greenstone belt.

COUNTRY ROCKS OF THE PEDRO MOUNTAIN STOCK

In addition to thermal contact effects, the Pedro Mountain stock produced wallrock structures that postdate all structural features associated with regional deformation and metamorphism. The most commonly observed structural effect is folding of veinlets and segregations in the amphibolite of the contact

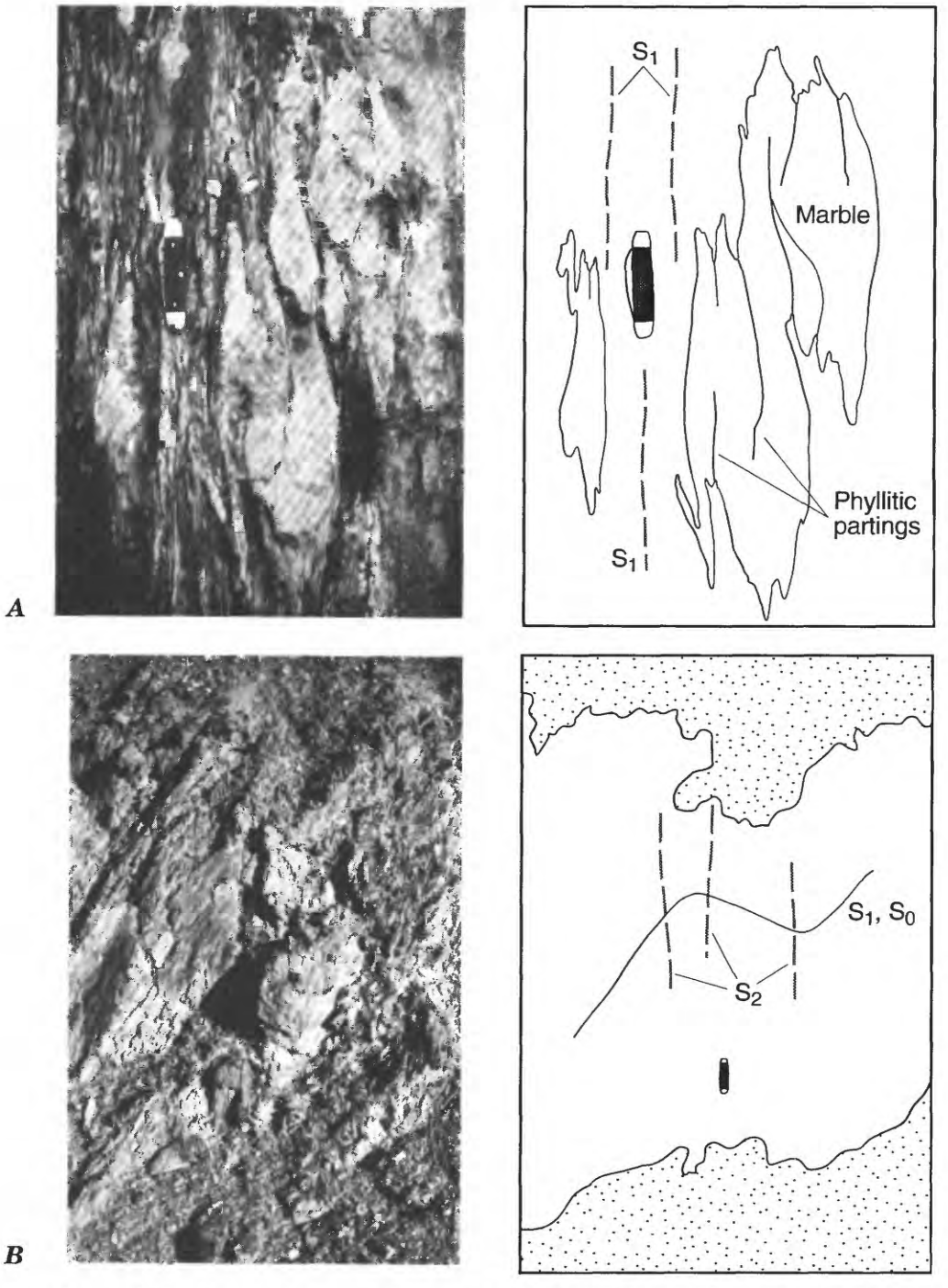

FIGURE 12.12.—Mesoscopic structural features of Campbell Gulch phyllite unit. *A*, Small isoclinal F_1 folds shown by marble beds in phyllite. Sketch shows contact between marble and phyllite, trace of S_1, and phyllitic partings within marble. Partings mark cores of F_1 folds, or in some cases bound sheared-off fold limbs. Knife is 8 cm long. *B*, F_2 folds with S_2 axial-plane cleavage. Sketch shows traces of S_1 and S_2. Bedding (S_0) is parallel to S_1. Knife at lower center is 8 cm long.

aureole. Networks of post-D_1 veinlets appear in greenstone about 1 km from the intrusion. At 600 to 800 m the veinlets are microfolded strongly enough to form a new lineation. Since the veinlets are segregation features that resulted from heating by the intrusion, this lineation must have been produced by mechanical effects of the intruding mass. The lineation persists in gneissose amphibolite close to the stock and generally plunges steeply.

Biotite-muscovite schist 600 to 800 m from the intrusion has a weak spaced S_3 cleavage produced by discontinuous mica folia. S_1 in schist less than 300 m from the intrusion is minutely folded. Much of the biotite and muscovite in these rocks is reoriented to form S_3, a closely spaced discrete crenulation cleavage parallel to the axial planes of the new folds. The intersection of S_1 and the new axial-plane cleavage (S_3) forms a new lineation (L_3). Locally the schist has three lineations; two of the lineations, interpreted as L_1 and L_2, are folded around late mesoscopic folds (F_3) with axes equivalent to the new lineation (L_3). Thus the intrusion locally produced a third deformation as it was emplaced.

MACROSCOPIC STRUCTURE

DEER CREEK PHYLLITE UNIT

Orientations of S_1, S_2, L_1, L_2, and L_3 in the study area are shown in figure 12.13. In the Deer Creek phyllite unit (subareas 2 and 3, fig. 12.13), S_1 generally strikes east-northeast and dips steeply. From west to east S_1 changes from mainly south dips through vertical to north dips, and back to south dips; the area with north dips overlaps subareas 2 and 3. L_1 plunges west to west-southwest at low to moderate angles throughout the area, generally steepening from west to east.

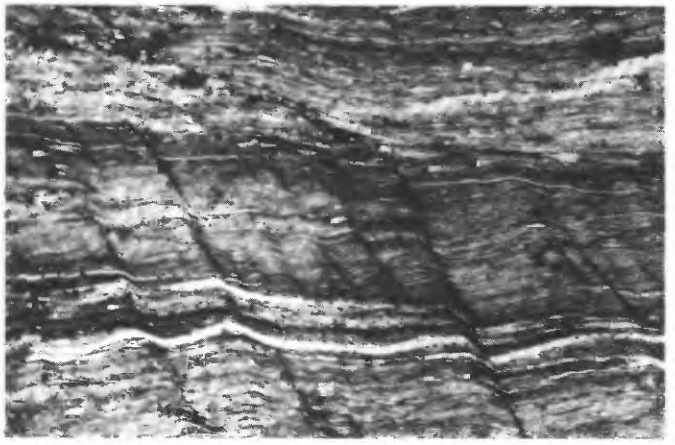

C

FIGURE 12.12.—Continued. *C*, Photomicrograph of pelitic phyllite showing spaced S_2 cleavage consisting of asymmetric microcrenulations confined to phyllosilicate-rich layers. Thin section is perpendicular to L_2.

F_1 folding is characterized throughout the unit by tight, upright folds. Because S_1 is an axial-plane cleavage and L_1 is parallel to F_1 fold axes, the attitudes of S_1 and L_1 together show the attitudes of F_1 folds. At many outcrops F_1 folds are asymmetric and the enveloping surface enclosing S_0 forms a small angle with S_1. Average orientations of S_0 and S_1, however, are not significantly different throughout the Deer Creek phyllite unit. Observations of relatively well exposed areas in the lower part of French Gulch and the central part of Deer Creek suggest that most macroscopic F_1 folds have wavelengths from 15 to 300 m. Judging from the size and geometry of the F_1 folds, the distribution of metavolcaniclastic beds within the Deer Creek phyllite unit must primarily reflect stratigraphic variations rather than repetition of beds by macroscopic F_1 folds (fig. 12.2). In restricted areas, however, there may be some repetition of units owing to F_1 folding. Neither S_1 nor S_2 shows significant postfolding shearing, and there is no evidence of penetrative post-D_2 shearing, so F_1 folds are not significantly disrupted.

S_2 in the Deer Creek phyllite unit is quite variable, but it generally dips to the north (subareas 2 and 3, fig. 12.13). Locally in the center of the study area, S_2 shows horizontal to low dips to the south. At the west edge of the area, L_2 is approximately horizontal, shown by the point density contours on the subarea 2 diagram of figure 12.13. To the east it becomes steeper, locally dipping as much as 40° W. (subarea 3, fig. 12.13). F_2 folds are not large enough (wavelengths generally less than 60 m) to affect the distribution of lithologic units depicted at the scale of figure 12.2. L_1 orientation is generally near that of L_2 throughout the Deer Creek phyllite unit, but tends to plunge more steeply to the west (fig. 12.13). Because the angle between L_1 and L_2 is generally relatively small and L_2 is parallel to F_2 fold axes, the geometry of S_0 approaches that of two coaxially superposed fold systems (Turner and Weiss, 1963).

Variations in the angles between all the S-surfaces produce differences in the appearance of outcrops in different parts of the area, even in a single rock type. Where S_0 and S_1 are nearly parallel and at a high angle to S_2, a strong cleavage-mullion structure results (the "pencil" structure described by Gilluly, 1937; fig. 12.14*A*). Where bedding in thinly-bedded rocks diverges notably from S_1, the mullions have

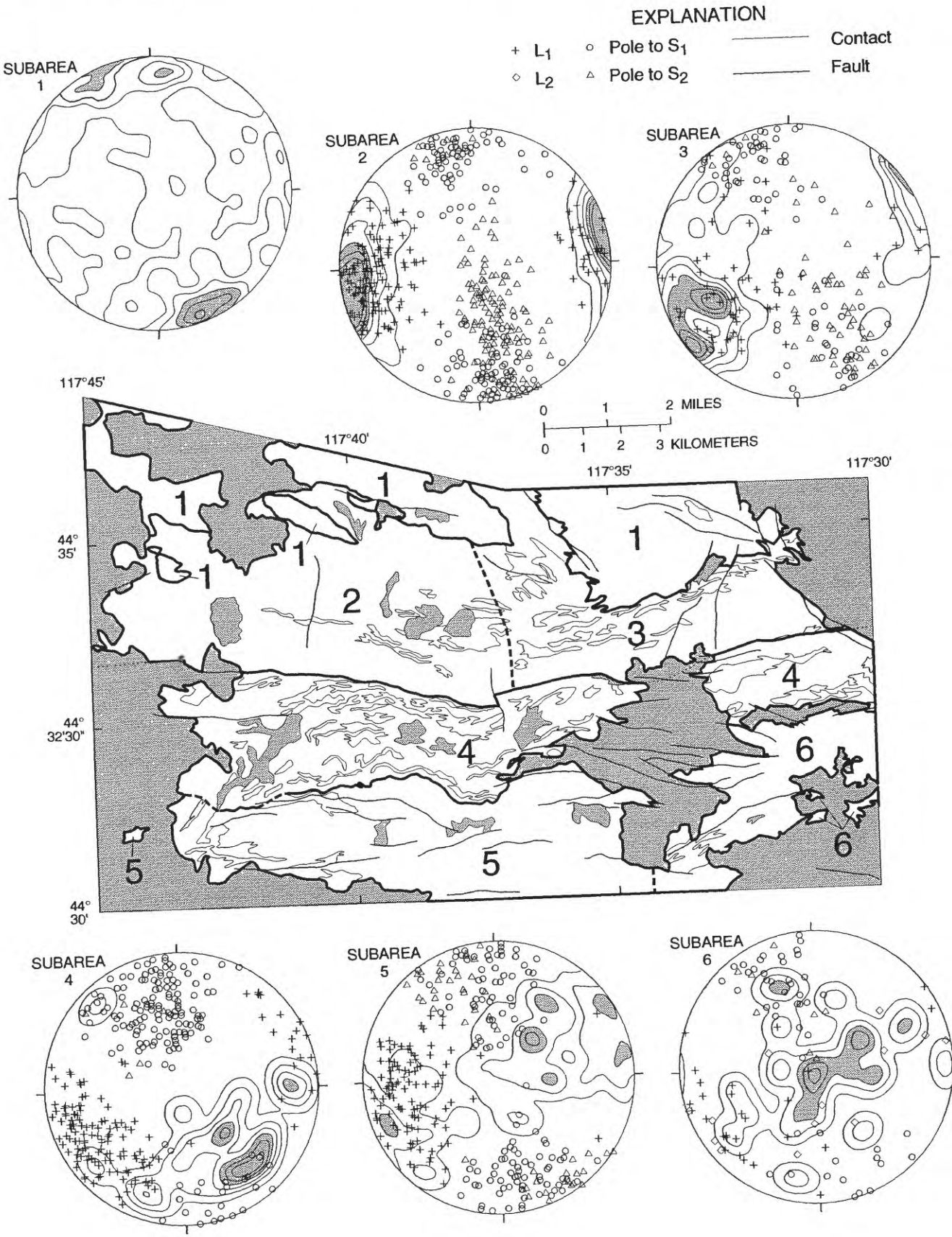
EXPLANATION
+ L_1
◇ L_2
○ Pole to S_1
△ Pole to S_2
Contact
Fault
SUBAREA 1
SUBAREA 2
SUBAREA 3
SUBAREA 4
SUBAREA 5
SUBAREA 6
117°45'
117°40'
117°35'
117°30'
44° 35'
44° 32'30"
44° 30'
0 1 2 MILES
0 1 2 3 KILOMETERS
1
2
3
4
5
6

oblique terminations, forming "torpedo" shapes (Gilluly, 1937; fig. 12.14*B*). Where S_1 and S_2 are relatively close together but S_0 and S_1 diverge, so that phyllitic quartzite beds with pelitic phyllite interlayers are cut obliquely by strong cleavage, the rocks resemble those in the vicinity of Sumpter called "pseudoconglomerates" by Pardee and Hewett (1914; fig. 12.14*C*). They attribute this structure to extensive shearing of fragments of competent beds into incompetent layers, and Coward (1983) states that it results from cataclastic deformation where shear zones cut thick chert sequences. Rocks in both areas consist of rhomboid quartz-rich microlithons bounded by phyllitic partings, but observations in the Burnt River Canyon area indicate that such rocks can form without notable shearing. All prominent S-surfaces and lineations show local variations in orientation that result from multiple folding. Detailed structural analysis by Ashley (1966) shows that all geometrical relations can be explained by D_1 and D_2, and there is no evidence for significant subsequent penetrative deformation.

CAMPBELL GULCH PHYLLITE UNIT

In the Campbell Gulch phyllite unit, S_1 strikes east to northeast and dips mainly south at moderate to steep angles throughout the area north of the greenstone belt (subarea 4, fig. 12.13). On the south side of the greenstone belt (southern parts of subareas 5 and 6, fig. 12.13), dips are generally to the north. L_1 generally plunges west to southwest at low to moderate angles, with little change along strike from one end of the study area to the other. Detailed structural analysis (Ashley, 1966) shows that bedding is generally parallel to S_1, as anticipated from the isoclinal style of F_1 folding commonly observed at mesoscopic scale. Structural analysis also indicates that fanning of S_1 related to F_1 folding is important on the macroscopic scale. The wide greenstone belt may be a complex west-plunging antiform with S_1 fanning upward and outward from its core (subarea 5, fig. 12.13).

Many marble exposures in the steep-walled valleys of tributaries entering Burnt River from the south outline the noses of mesoscopic and macroscopic isoclinal folds. It is clear from the outcrop pattern, however, that the marble horizons are discontinuous along strike, probably owing both to depositional variations and tectonic stretching. The exposures of marble in the walls of Burnt River Canyon just west of the confluence of French Gulch and Burnt River reveal a westward-plunging complex antiform that repeats one or two marble-bearing horizons. At many localities, however, it is impossible to determine whether numerous marble pods reflect different marble-bearing stratigraphic intervals, or structural repetition of one or a few marble beds.

Along the south side of the area, S_2, although visible only in phyllite outcrops, consistently strikes about N. 60° E. and dips steeply (subarea 5, fig. 12.13). Mesoscopic F_2 folds are found only in this part of the area, also restricted to the patches of phyllite. In the northern part of the Campbell Gulch phyllite unit (subarea 4, fig. 12.13), S_2 is developed at only a few localities but L_2 is visible at many localities. L_2 here has various orientations that tend to lie in a plane that strikes east-northeast to northeast and dips at a low angle to the southeast, shown by the girdle pattern of L_2 point density contours on the subarea 4 diagram (fig. 12.13). This plane is interpreted to represent an average S_2 plane for that part of the Campbell Gulch phyllite unit north of the greenstone belt. Structural analysis indicates that D_2 had only minor geometric effects on D_1 features, as might be expected from the restricted occurrence of F_2 folds (Ashley, 1966).

L_3, seen around the Pedro Mountain stock, varies greatly in orientation, but generally plunges moderately to steeply (see point density contours on subarea 6 diagram, fig. 12.13).

◀

FIGURE 12.13.—Orientations of structural features of Burnt River Canyon area, shown by summary structural diagrams. Map shows boundaries of numbered subareas as heavy lines, solid where they follow lithologic contacts, dashed within lithologic units. Shaded areas of the map are post-deformation cover rocks and intrusive rocks. Diagram for subarea 1 shows contoured density of poles to 162 sets of cataclasite and microbreccia bands in Blue Spring Gulch pluton; contours at point densities of 0.5, 1.5, 2.5, 3.5, 4.5, and 5.5 percent. Areas having point densities greater than 3.5 percent are shaded. Diagrams for subareas 2, 3, and 4 show contoured densities of 147, 61, and 35 orientation measurements of L_2, respectively; contours at point densities of 0.5, 2.0, 4.0, 6.0, 8.0, and 10.0 percent. Areas having L_2 point densities greater than 6.0 percent are shaded. Measurements for other structural elements shown by symbols. Diagram for subarea 5 shows contoured density of 55 measurements of L_2, contours at point densities of 0.5, 2.0, 4.0, and 6.0 percent. Areas having L_2 point densities greater than 4.0 percent are shaded. Diagram for subarea 6 shows contoured density of 29 measurements of L_3, contours at point densities of 0.5, 2.0, 4.0, 6.0, and 8.0 percent. Areas having L_3 point densities greater than 4.0 percent are shaded. All diagrams are lower-hemisphere Schmidt equal-area projections oriented with north at the top. Point densities for contouring were calculated using a spherical Gaussian weighting function (Robin and Jowett, 1986).

REGIONAL DISTRIBUTION AND RELATIONS OF THE BURNT RIVER SCHIST

CAVE CREEK FAULT AND DISTRIBUTION OF THE UNITS OF THE BURNT RIVER SCHIST

The Cave Creek fault marks a discontinuity in lithology, metamorphic grade, and style and orientation of structural elements, although not all these features appear different everywhere along the fault. Although the fault is nowhere well exposed, field work has shown that it is a narrow zone with no known associated mylonitization or retrograde alteration.

Thermal metamorphism persisted through D_1 and D_2 in both the Deer Creek and Campbell Gulch phyllite units, and involved higher temperatures during both D_1 and D_2 in the Deer Creek phyllite unit than in the Campbell Gulch phyllite unit, as described earlier. The difference in metamorphic grade across the fault is visible in the field only in greenstone outcrops, where it is indicated by the presence of pumpellyite in mafic and intermediate rocks of the Campbell Gulch phyllite unit.

The strike of S_1 and the plunge of L_1 are generally similar on both sides of the fault, but locally there is an abrupt change in the dip of S_1. D_2 features in the Deer Creek phyllite unit are truncated by the fault, but D_2 features in the Campbell Gulch phyllite unit die out south of the fault. Local D_3 features produced by the Pedro Mountain stock also die out south of the fault, so in the Burnt River Canyon area the age of displacement cannot be fixed relative to the Jurassic to Cretaceous plutonism. Wherever Tertiary rocks of Miocene age or older cover the fault zone, they show small displacements, generally south side down. Northwest-trending Tertiary faults truncate the Cave Creek fault at the west edge of Durkee Valley (fig. 12.15), and the Pliocene sedimentary rocks of Durkee Valley completely cover the fault zone.

An interpretation of (1) the geographic distribution of the two units of the Burnt River Schist in the eastern part of the Baker terrane and (2) the location of the Cave Creek fault to the east and west of the

A

B

FIGURE 12.14.—Effects of variations in relative orientations of S-surfaces, Deer Creek phyllite unit. *A*, Debris from outcrop of phyllite, fragments showing strong cleavage-mullion or "pencil" structure, produced by S_2 at a high angle to S_1, and S_0 nearly parallel to S_1. Hammer is 40 cm long. See also figure 12.10*C*. *B*, Outcrop of quartz phyllite showing obliquely terminated mullions bounded by S_1 and S_0 surfaces, or "torpedo" structure, produced by S_2 at a high angle to S_1, and S_0 at a moderate angle to S_1. Sketch shows traces of S_0 and S_1. Surface of outcrop is approximately parallel to S_2. Knife is 8 cm long.

Burnt River Canyon area is shown in figure 12.15. Tracing the Cave Creek fault along strike to the east is made difficult by lack of marker rock types and detailed structural information. Existing information from the geologic maps of Prostka (1967) and Brooks (1978) is not adequate to detect discontinuities in S_1 or L_1 attitudes or various D_2 features.

In the Durkee quadrangle, between the Burnt River Canyon area and Big Lookout Mountain (fig. 12.1), relations are obscured by Jurassic to Cretaceous intrusive bodies and extensive cover of Tertiary sedimentary and volcanic rocks. Prostka (1967) states that the southwest-trending lobe of the Big Lookout Mountain pluton invades a major northeast-trending fault zone. I infer that this zone is the eastward extension of the Cave Creek fault. If this inference is correct, juxtaposition of the Deer Creek and Campbell Gulch phyllite units along the Cave Creek fault predates the Big Lookout Mountain pluton, dated at about 124 Ma (Walker, 1986). The area of the Deer Creek phyllite unit shown north of this fault on figure 12.15 is mapped by Prostka (1967) as his greenschist unit. Rock types described by Prostka for this map unit match closely those seen in the Deer Creek phyllite unit at the east end of Burnt River Canyon, between Sheep Mountain and Durkee Valley.

East of the study area, the marble bodies of the Campbell Gulch phyllite unit form a single belt that is easily traced eastward across Burnt River at Nelson, south of Durkee Valley (equivalent to the informally named Nelson marble of Prostka, 1967), and thence east-northeast to the Snake River canyon (Brooks and others, 1976; Brooks, 1978). The Nelson marble and the phyllite and greenschist associated with it in the Durkee and Mineral quadrangles constitute the eastern extension of the Campbell Gulch phyllite unit from the Burnt River Canyon area.

East of Big Lookout Mountain and west of the Snake River, Brooks (1978) did not find any well-defined subunit in the Burnt River Schist other than the Nelson marble, and he did not recognize any major fault within the Burnt River Schist such as the Cave Creek fault. Mitchell and Bennett (1979) do not show any internal subdivisions or structures in the Burnt River Schist on the east side of the Snake River. The Deer Creek phyllite unit, therefore, is not recognized and may not exist east of Big Lookout Mountain. The Burnt River Schist is covered by flows of the Columbia River Basalt Group 8 to 12 km east of the Snake River.

South of Burnt River Canyon, Wolff (1965) described the Burnt River Schist as a northeast-dipping block that was pushed upward and southwestward by the Pedro Mountain stock. In this area, S_1 generally strikes west-northwest and dips north-northeast, and L_1 plunges to the northwest. Major rock types of the Burnt River Schist west of Pedro Mountain (fig. 12.15) consist of metamorphosed sedimentary and volcanic rocks in about equal proportions. Metasedimentary rocks include quartz phyllite, pelitic phyllite and schist, quartzite (metachert), and minor marble. Metavolcanic rocks include metalava and metatuff; flows are locally pillowed. On the basis of similar lithology, structural style, and orientation of structures, I conclude that the Campbell Gulch phyllite unit continues south into the Bridgeport quadrangle, around the south side of the Pedro Mountain stock (fig. 12.15; Brooks and others, 1976). In the Bridgeport quadrangle, the metamorphic grade of the Burnt River Schist is generally higher than it is in the Burnt River Canyon area, owing to thermal contact metamorphism by the Pedro Mountain stock and other intrusions southwest of Pedro Mountain.

To the west of Burnt River Canyon, extensive Tertiary rocks of the Dooley Volcanics cover the Cave Creek fault. Exposures in the southeastern part of the Dooley Mountain quadrangle include slate, metamorphosed andesitic tuff and flows, and minor marble (Evans, 1992) that I interpret as part of the Campbell Gulch phyllite unit. Exposures extending westward from the west-central part of the Dooley Mountain quadrangle to the vicinity of Bald Mountain in the Brannan Gulch quadrangle are mainly quartz phyllite, phyllite, argillite, and minor marble. On the basis of mapping by Evans (1994) and reconnaissance examination of mesoscopic structural fea-

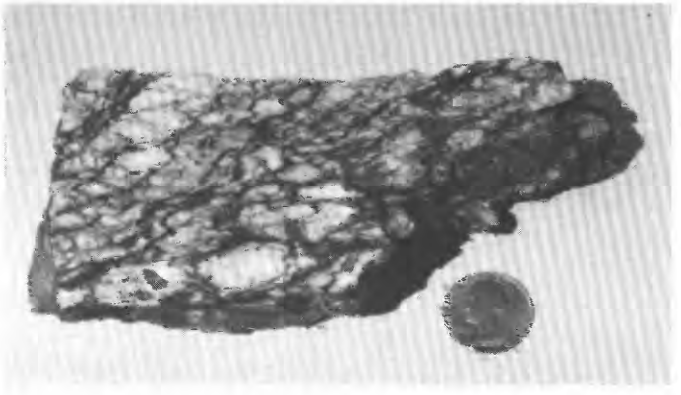

C

FIGURE 12.14.—Continued. *C*, Hand specimen of interbedded phyllitic quartzite and pelitic phyllite cut approximately perpendicular to S_1 and S_2, which are nearly parallel. Shows "pseudoconglomerate" structure, produced by phyllitic quartzite beds (S_0) cut obliquely by strong combined S_1 and S_2 cleavages, which form phyllitic partings.

117°45'
117°30'
117°15'
117°00'
44°45'
44°30'
Reservoir
Brownlee
Connor Creek fault
Big Lookout Mtn.
Sheep Mtn.
Pedro Mtn.
Durkee Valley
Bridgeport Valley
AREA OF FIG. 12.2
5 MILES
5 KILOMETERS
QTav
JTrlw
KJl
TrPze
Trov
Tri
pg
m
p
bsg
sc

Notes: Rocks of unit m exposed east of area of figure 12.2 have been mapped as the informally named Nelson marble by Prostka (1967), Brooks and others (1976), and Brooks (1978). Rocks of unit JTRiw have been included in the Olds Ferry terrane by Silberling and others (1987).

FIGURE 12.15.—Regional map showing distribution of Burnt River Schist in eastern part of Baker terrane. Compiled from Ashley (1966), Brooks and others (1976), Brooks and Vallier (1967), Gilluly (1937), Mitchell and Bennett (1979), and Wolff (1965).

tures, I include these exposures in the Deer Creek phyllite unit. The Cave Creek fault must continue westward under Tertiary rocks, passing south of the Bald Mountain area. Farther west, Pardee (1941) mapped metasedimentary rocks on strike with the Deer Creek phyllite unit of the Brannan Gulch quadrangle and included them in the Elkhorn Ridge Argillite. The western limit of the Burnt River Schist cannot be defined with the geologic information that is currently available.

Geologic maps of the Durkee quadrangle (Prostka, 1967), the Oregon part of the Mineral quadrangle (Brooks, 1978), and the Bridgeport quadrangle (Wolff, 1965) show that bedding and S_1 in the Campbell Gulch phyllite unit generally dip steeply to the north. The Campbell Gulch exposures in Burnt River Canyon and the Dooley Mountain quadrangle (Evans, 1992), however, include an appreciable area with southerly dips, and therefore one cannot assume that stratigraphic tops are to the north. The tight to isoclinal folding and lack of indicators of stratigraphic tops in the Burnt River Canyon area appear to be characteristic of all rocks of the Burnt River Schist that are assigned to the Campbell Gulch phyllite unit. Consequently, there is no basis for a consistent interpretation of the internal stratigraphy of the Campbell Gulch phyllite unit, and correlations with specific units elsewhere in the region are not possible.

RELATION OF THE BURNT RIVER SCHIST TO SURROUNDING UNITS

Structural and stratigraphic relations between the Deer Creek phyllite unit of Burnt River Canyon and exposures of the Elkhorn Ridge Argillite to the northwest, north, and northeast are obscured by intrusive rocks of the Blue Spring Gulch pluton and Tertiary volcanic and sedimentary cover rocks. East of Durkee Valley, the exposures of Prostka's (1967) greenschist unit that I consider to be part of the Deer Creek phyllite unit are separated from the Elkhorn Ridge Argillite to the north by a mass of metagabbro (fig. 12.15).

Between the Big Lookout Mountain pluton and the Snake River, the contact between the Burnt River Schist and the Elkhorn Ridge Argillite shown on figure 12.15 is that of Brooks and others (1976). In the center of the Mineral quadrangle, Brooks (1978) shows a fault at this boundary and shows the same fault cutting and displacing Tertiary basalt. Elsewhere in the Mineral quadrangle the boundary is shown as a depositional contact. In the Snake River canyon the contact is located between a section of quartz phyllite with interbedded metavolcaniclastic

rocks and pillowed greenstone to the north and a section of interbedded pelitic phyllite and quartz phyllite to the south. The schistosity consistently dips steeply northward throughout both sections. Mullen (1983b) stated that the contact here is gradational. Whether the contact is affected only by minor faulting of Tertiary age or whether significant pre-Tertiary shear displacement is distributed through the gradational zone is unknown. On the east side of the Snake River, Mitchell and Bennett (1979) show the contact between the Elkhorn Ridge Argillite and the Burnt River Schist as a high-angle fault (fig. 12.15).

The south side of the exposure belt of the Burnt River Schist is in contact with volcanic sandstone and siltstone of the Weatherby Formation of Brooks (1979b), which is included in the Olds Ferry terrane by Silberling and others (1987) and in the Izee terrane by Vallier (chap. 3, this volume) and Avé Lallemant (chap. 7, this volume). These rocks are much less strongly folded and metamorphosed than are the rocks of the Burnt River Schist, and they are of Early and Middle Jurassic age (Brooks and others, 1976; Brooks, 1979b). Between Burnt River and the Snake River canyon, the contact is a north-dipping high-angle reverse fault locally called the Connor Creek fault (Brooks, 1978, 1979a, 1979b; Roure, 1982). In the vicinity of Pedro Mountain and south of Bridgeport, Wolff (1965) shows the contact as a series of high-angle faults with various orientations (fig. 12.15). West of Bridgeport, the contact is obscured by Tertiary deposits. Because the Connor Creek fault is cut by a quartz diorite mass that is probably related to the Big Lookout Mountain pluton (Prostka, 1967; Brooks and others, 1976), the Burnt River Schist and the Weatherby Formation must have been juxtaposed between Middle Jurassic and Early Cretaceous time.

DISCUSSION AND CONCLUSIONS

The Blue Mountains region has been rotated approximately 60° clockwise since Early Cretaceous time (Wilson and Cox, 1980), so the present east to northeast trends of the pre-Tertiary formations of the region were originally northeast to north. In the following discussion, regional tectonic features are described in their original orientations. Local features are described in their present orientations, and their original orientations are also indicated.

The available minor-element data show that both the Deer Creek and Campbell Gulch phyllite units contain arc-related volcanic rocks. Both units could have formed in either a fore-arc or an intra-arc depositional environment. The Deer Creek phyllite unit, which contains abundant siliceous sedimentary materials, more likely formed in a fore-arc environment, as Mullen (1985) suggested for the lithologically similar Elkhorn Ridge Argillite. Deposition of the Deer Creek phyllite unit in a fore-arc setting is also compatible with the idea presented by White and others (1992) that the Wallowa and Baker terranes formed as an arc/fore-arc pair over a west-dipping subduction zone (fig. 12.1). The only volcanic rocks in northeastern Oregon that could be contemporaneous with the Deer Creek phyllite unit are those in the Windy Ridge and Hunsaker Creek Formations of Permian age (Vallier, 1977) and the Cougar Creek Complex of Vallier (1968) of late Paleozoic age (see Vallier, chap. 3, this volume; fig. 12.16). All these units are found in the Wallowa terrane.

The Campbell Gulch phyllite unit, which contains abundant clastic and volcanic rocks, more likely formed in an intra-arc rather than a fore-arc environment, as Mullen (1985) suggested for the Burnt River Schist (undivided). White and others (1992) proposed that westward subduction continued into Middle Triassic time, followed by possibly eastward subduction in Late Triassic to Early Jurassic time. The Late Triassic to Early Jurassic subduction produced the arc-related volcanic rocks of the Olds Ferry terrane. Based on the Middle and Late Triassic faunal ages for the Campbell Gulch phyllite unit, Campbell Gulch volcanism could be contemporaneous with the Wild Sheep Creek Formation, Doyle Creek Formation, upper part of the Clover Creek Greenstone, or Gold Creek greenstone of the Wallowa terrane, or the Huntington Formation of the Olds Ferry terrane (fig. 12.16). It could therefore be related either to westward or eastward subduction, or both, and its apparent intra-arc setting is explained by its position between the volcanic belts of the Wallowa and Olds Ferry terranes, even though arc volcanism may not have occurred simultaneously both to the east and west (Silberling, 1983).

The Blue Spring Gulch pluton and associated rocks form an arc-related calc-alkaline suite; they intrude the Deer Creek phyllite unit and do not represent ophiolitic basement rocks of oceanic origin. The Sparta complex is also an arc-related pluton rather than an inlier of oceanic basement (Phelps, 1979). The late Paleozoic through Late Triassic age span of volcanic rocks in the Wallowa terrane and the range of age determinations for arc-related plutons in the Wallowa terrane (265–225 Ma) are similar to the range of age determinations for plutons in the eastern part of the Baker terrane (277–213 Ma; Vallier and others, 1977; Avé Lallemant and others, 1980; Walker, 1981, 1982, 1983, 1986, chap. 6 of this volume), whereas the age

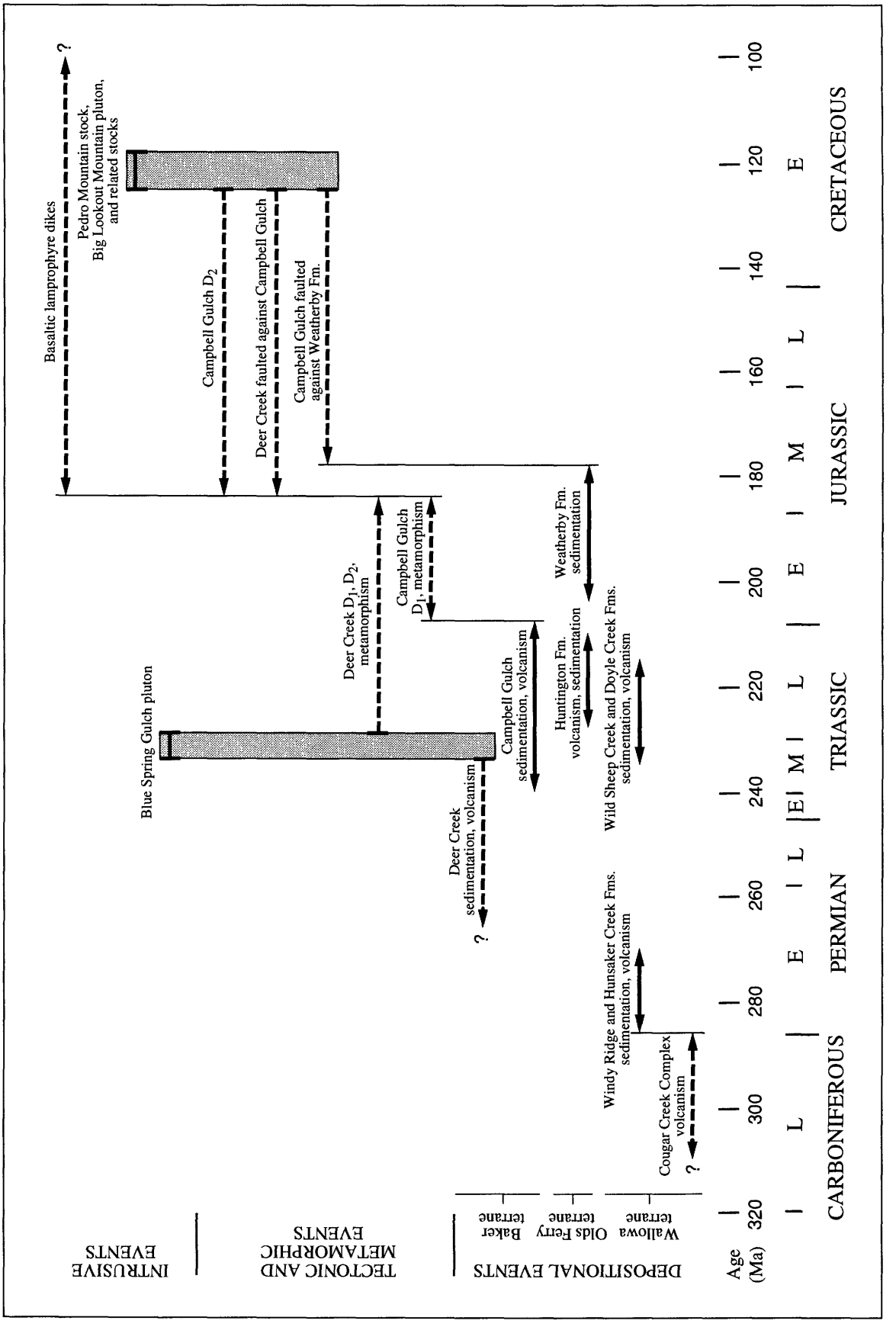

FIGURE 12.16.—Chronology of selected late Paleozoic and Mesozoic geologic events in the Blue Mountains region, northeastern Oregon, showing age relations of events recorded in the Burnt River Canyon area. Solid horizontal lines indicate direct paleontologic or radiometric evidence for age within range shown; dashed lines indicate indirect evidence for age within range shown. Heavy vertical bar indicates age limit constrained by radiometric data. Arrow indicates approximate or poorly constrained age limit; arrow with query indicates age limit unknown. Sequential events that share a mutual age limit are connected by a light vertical line. Analytical ranges of radiometric age determinations are shown by shaded boxes. Unit terminology shown in figure includes the following: Deer Creek, Deer Creek phyllite unit (of Burnt River Schist); Campbell Gulch, Campbell Gulch phyllite unit (of Burnt River Schist); Weatherby Formation of Brooks (1979b); Cougar Creek Complex of Vallier (1968); Huntington Formation of Brooks (1979b). Data sources include Brooks (1979b), Brooks and others (1976), Imlay (1986), Vallier (1977), and Walker (1986). Geologic time scale is from Palmer (1983). E, Early; M, Middle; L, Late.

span of volcanic rocks in the Olds Ferry terrane is much more restricted (fig. 12.16). It therefore seems likely that the plutons of the eastern part of the Baker terrane, including the Sparta complex and Blue Spring Gulch pluton, are related to arc magmatism of the Wallowa terrane.

The extension parallel to fold axes that is associated with D_1 and D_2 deformations in the Deer Creek phyllite unit and D_1 deformation in the Campbell Gulch phyllite unit probably represents approximately orogen-parallel extension. Such extension is a feature commonly seen in belts of deformed low- to medium-grade metamorphic rocks (Hobbs and others, 1976). The relation between stretching lineations and relative plate motions in subduction orogens, however, is not necessarily simple (Ellis and Watkinson, 1987).

If the Deer Creek phyllite unit is part of a fold belt deformed as a result of simple regional compression, the entire exposure area of the Deer Creek phyllite unit studied here constitutes the south (originally southeast) side of a major F_1 antiform. Alternatively, if it is part of a fold-and-thrust belt, north- (originally northwest-) directed overthrusting could account for the asymmetric folding. Avé Lallemant (chap. 7, this volume), infers a major northwest-directed component of tectonic transport for all penetratively deformed rocks in the eastern part of the Baker terrane, on the basis of microfabric and microtextural kinematic indicators. The greatly varied dips of axial planes of F_2 folds in the Deer Creek phyllite unit probably cannot be reliably interpreted as related to any simple regime of thrust faulting.

Mesoscopic and inferred macroscopic D_1 structures in the part of the Campbell Gulch phyllite unit in the Burnt River Canyon area are not consistently compatible with any simple structural regime involving regional thrusting. D_1 fabric elements in the Campbell Gulch phyllite unit do not show a consistent direction of rotation or asymmetry. The northwest-directed thrusting inferred by Avé Lallemant (chap. 7, this volume) for D_1 in the eastern part of the Baker terrane thus best applies to the Elkhorn Ridge Argillite and the Deer Creek phyllite unit. As in the Deer Creek phyllite unit, the varied dips of axial planes of F_2 folds in the Campbell Gulch phyllite unit are not easily related to regional thrusting.

The ages of the deformations in both units of the Burnt River Schist are not closely constrained, but deformation could have begun earlier in the Deer Creek phyllite unit (fig. 12.16). Deformation in the Blue Spring Gulch pluton is correlative with D_1 in the Deer Creek phyllite unit, so the age of the pluton dates D_1 in the Deer Creek phyllite unit as late Middle Triassic at the earliest. Similarly, faunal ages for the Campbell Gulch phyllite unit constrain the time of deformation there to later than Late Triassic. The ages of undeformed plutons of the Pedro Mountain-Big Lookout Mountain belt (about 125–120 Ma; Walker, 1986) provide evidence that no regional deformation seen in the Burnt River Canyon area is younger than Early Cretaceous, because structures and contact metamorphism around the Pedro Mountain stock postdate D_2 in the Campbell Gulch phyllite unit, and contact metamorphism around the Big Lookout Mountain pluton probably postdates D_2 in the Deer Creek phyllite unit. Avé Lallemant (chap. 7, this volume) concludes that D_1 in the Baker terrane is probably pre-Early Jurassic in age.

The actinolite- and biotite-bearing greenschist mineral assemblages of the Deer Creek phyllite unit show the highest temperatures (350–450°C) of regional metamorphism yet recognized in the eastern part of the Baker terrane, whereas the pumpellyite-actinolite assemblage of the Campbell Gulch phyllite unit records relatively high pressures at relatively low temperatures (about 3–8 kbar at 250–350°C; Liou and others, 1985). High-pressure/low-temperature metamorphic assemblages are most easily formed in subduction zones (Coleman, 1972). Although the greenschist-facies metamorphism of the Deer Creek phyllite unit is not diagnostic of tectonic environment, presence of pumpellyite relicts in the Deer Creek rocks suggests that the prograde pressure-temperature path included a pumpellyite-bearing facies and thus may have involved moderately high pressures. Models of thermal relaxation accompanying uplift and erosion of subducted sediment wedges predict that high-pressure assemblages can be destroyed by retrograde reactions under conditions of the greenschist facies (England and Richardson, 1977). Ernst (1988) showed that the majority of exposed blueschist metamorphic belts have undergone pervasive retrograde reaction to greenschist- and amphibolite-facies assemblages, but some have retained high-pressure assemblages because they migrated slowly back up near their subduction zones, retracing their prograde pressure-temperature paths. Therefore the prograde metamorphism of both the Deer Creek and Campbell Gulch phyllite units probably occurred in a subduction environment, but because the Deer Creek rocks underwent extensive retrograde alteration to greenschist-facies assemblages, whereas the Campbell Gulch rocks did not, the retrograde metamorphic history of each unit is significantly different.

Differences in style of D_1 and D_2 deformation and metamorphic history suggest that the Deer Creek and Campbell Gulch phyllite units were deformed in

different orogenic episodes, or if they were deformed in the same orogenic episode(s), they must have been located in different parts of the deformation zone. The older age of the Deer Creek rocks permits the speculation that the Deer Creek phyllite unit was metamorphosed and deformed (D_1 and possibly also D_2) during Late Triassic subduction, possibly subjacent to Campbell Gulch strata accumulating at the same time (fig. 12.16). Just as it is not possible to determine whether volcanic rocks of the Campbell Gulch phyllite unit are related to Wallowa terrane subduction or Olds Ferry terrane subduction, it is not possible to determine whether deformation of the Deer Creek phyllite unit, if indeed it occurred in Late Triassic time, is related to Wallowa terrane or Olds Ferry terrane subduction. The fact that Deer Creek D_1 structures are compatible with north (originally northwest)-directed overthrusting or south (originally southeast)-directed underthrusting favors eastward subduction related to Olds Ferry terrane arc volcanism (White and others, 1992).

The Campbell Gulch phyllite unit was metamorphosed and deformed in Early to Middle Jurassic time, probably subjacent to the northwestern (originally western) part of the Weatherby Formation, which was accumulating at the same time (fig. 12.16). This metamorphism and deformation could have been produced by eastward subduction related to Olds Ferry terrane arc volcanism, especially if the subduction zone migrated eastward. However, the retrograde metamorphism of the Deer Creek phyllite unit, which implies relatively rapid uplift, could better be accommodated by westward subduction beneath the Baker terrane. White and others (1992) suggested that westward subduction occurred in Middle Jurassic time, producing renewed arc volcanism in the Wallowa terrane.

The Deer Creek phyllite unit was faulted against the Campbell Gulch phyllite unit on the Cave Creek fault and the Campbell Gulch phyllite unit was faulted against the Weatherby Formation on the Connor Creek fault between Middle Jurassic and Early Cretaceous time (fig. 12.16). The maximum age of faulting of the Deer Creek phyllite unit against the Campbell Gulch phyllite unit is shown on fig. 12.16 as somewhat greater than the maximum age of faulting of the Campbell Gulch phyllite unit against the Weatherby Formation, mainly to indicate that the Connor Creek and Cave Creek faults are not necessarily the same age. Although the upper age limit of the Connor Creek fault is constrained by the age of the Weatherby Formation, the age of the Cave Creek fault is not similarly constrained, and it could be older or younger than the Connor Creek fault. The fact that the Connor Creek fault is a high-angle reverse fault suggests that compressive deformation occurred during the Middle Jurassic to Early Cretaceous.

The lamprophyre dikes of basaltic composition in the Burnt River Canyon area were emplaced after D_1 in the Campbell Gulch phyllite unit, but were subjected to conditions of the prehnite-actinolite facies, suggesting that they were emplaced before Tertiary uplift. Thus extension must have occurred at some time between the Middle Jurassic and the early Tertiary. Since the Middle Jurassic, serpentinite has been intruded locally along faults in the Baker terrane, including faults that may be of Tertiary age.

REFERENCES CITED

Armstrong, R.L., Taubeneck, W.H., and Hales, P.O., 1977, Rb-Sr and K-Ar geochronometry of Mesozoic granitic rocks and their Sr isotopic composition, Oregon, Washington, and Idaho: Geological Society of America Bulletin, v. 88, p. 397-411.

Ashley, R.P., 1966, Metamorphic petrology and structure of the Burnt River Canyon area, northeastern Oregon: Stanford, Calif., Stanford University, Ph.D. dissertation, 193 p.

Avé Lallemant, H.G., Phelps, D.W., and Sutter, J.F., 1980, ^{40}Ar-^{39}Ar ages of some pre-Tertiary plutonic and metamorphic rocks of eastern Oregon and their geologic relationships: Geology, v. 8, p. 371-374.

Baker, P.E., 1982, Evolution and classification of orogenic volcanic rocks, *in* Thorpe, R.S., ed., Andesites—Orogenic andesites and related rocks: Chichester, John Wiley & Sons, p. 11-24.

Barker, Fred, 1979, Trondhjemite—Definition, environment and hypotheses of origin, *in* Barker, Fred, ed., Trondhjemites, dacites, and related rocks: Amsterdam, Elsevier, p. 1-12.

Blome, C.D., Jones, D.L., Murchey, B.L., and Liniecki, Margaret, 1986, Geologic implications of radiolarian-bearing Paleozoic and Mesozoic rocks from the Blue Mountains Province, eastern Oregon, *in* Vallier, T.L., and Brooks, H.C., eds., Geology of the Blue Mountains region of Oregon, Idaho, and Washington—Geologic implications of Paleozoic and Mesozoic paleontology and biostratigraphy, Blue Mountains Province, Oregon and Idaho: U.S. Geological Survey Professional Paper 1435, p. 79-101.

Brooks, H.C., 1978, Geologic map of the Oregon part of the Mineral quadrangle: Oregon Department of Geology and Mineral Industries Geological Map Series GMS-12, scale 1:62,500.

———1979a, Plate tectonics and the geologic history of the Blue Mountains: Oregon Geology, v. 41, p. 71-80.

———1979b, Geologic map of the Huntington and part of the Olds Ferry quadrangles, Baker and Malheur Counties, Oregon: Oregon Department of Geology and Mineral Industries Geological Map Series GMS-13, scale 1:62,500.

Brooks, H.C., McIntyre, J.R., and Walker, G.W., 1976, Geology of the Oregon part of the Baker 1° by 2° quadrangle: Oregon Department of Geology and Mineral Industries Geological Map Series GMS-7, scale 1:250,000.

Brooks, H.C., and Vallier, T.L., 1967, Progress report on the geology of part of the Snake River Canyon, Oregon and Idaho: The Ore Bin, v. 29, p. 233-262.

———1978, Mesozoic rocks and tectonic evolution of eastern Oregon and western Idaho, *in* Howell, D.G., and McDougall, K.A., eds., Mesozoic paleogeography of the Western United States

(Pacific Coast Paleogeography Symposium 2, Sacramento, Calif.): Los Angeles, Society of Economic Paleontologists and Mineralogists, Pacific Section, p. 133-145.

Brown, G.C., 1982, Calc-alkaline intrusive rocks—Their diversity, evolution, and relation to volcanic arcs, *in* Thorpe, R.S., ed., Andesites—Orogenic andesites and related rocks: Chichester, John Wiley & Sons, p. 437-464.

Cann, J.R., 1970, Rb, Sr, Y, Zr and Nb in some ocean floor basaltic rocks: Earth and Planetary Science Letters, v. 10, p. 7-11.

Coleman, R.G., 1972, Blueschist metamorphism and plate tectonics: Twenty-fourth International Geological Congress Proceedings Reports, Section 2, Petrology, p. 19-26.

Coward, R.I., 1983, Structure, stratigraphy, and petrology of the Elkhorn Ridge Argillite, Sumpter area, northeastern Oregon: Houston, Tex., Rice University, Ph.D. dissertation, 144 p.

Dicken, S.N., 1965, Oregon geography (4th ed.): Eugene, Oregon, 127 p.

Dickinson, W.R., 1979, Mesozoic forearc basin in central Oregon: Geology, v. 7, p. 166-170.

Dickinson, W.R., and Thayer, T.P., 1978, Paleogeographic and paleotectonic implications of Mesozoic stratigraphy and structure in the John Day inlier of central Oregon, *in* Howell, D.G., and McDougall, K.A., eds., Mesozoic paleogeography of the western United States (Pacific Coast Paleogeography Symposium 2, Sacramento, Calif.): Los Angeles, Society of Economic Paleontologists and Mineralogists, Pacific Section, p. 147-161.

Ellis, Michael, and Watkinson, A.J., 1987, Orogen-parallel extension and oblique tectonics—The relation between stretching lineations and relative plate motions: Geology, v. 15, p. 1022-1026.

England, P.C., and Richardson, S.W., 1977, The influence of erosion upon the mineral facies of rocks from different metamorphic environments: Geological Society of London Journal, v. 134, p. 201-213.

Ernst, W.G., 1988, Tectonic history of subduction zones inferred from retrograde blueschist P-T paths: Geology, v. 16, p. 1081-1084.

Evans, B.W., 1977, Metamorphism of alpine peridotite and serpentinite: Annual Review of Earth and Planetary Sciences, v. 5, p. 397-447.

Evans, J.G., 1992, Geologic map of the Dooley Mountain 7½' quadrangle, Baker County, Oregon: U.S. Geological Survey Geologic Quadrangle Map GQ-1694, scale 1:24,000.

———1994, Geologic map of the Brannan Gulch 7½' quadrangle, Baker County, Oregon: U.S. Geological Survey Quadrangle Map GQ-1744, scale 1:24,000.

Ferns, M.L., Brooks, H.C., and Avery, D.G., 1983, Geology and gold deposits map of the Greenhorn quadrangle, Baker and Grant Counties, Oregon: Oregon Department of Geology and Mineral Industries Geological Map Series GMS-28, scale 1:24,000.

Ferns, M.L., Brooks, H.C., Avery, D.G., and Blome, C.D., 1987, Geology and mineral resources map of the Elkhorn Peak quadrangle, Baker County, Oregon: Oregon Department of Geology and Mineral Industries Geological Map Series GMS-41, scale 1:24,000.

Ferns, M.L., Brooks, H.C., and Ducette, J., 1982, Geology and mineral resources map of the Mt. Ireland quadrangle, Baker and Grant Counties, Oregon: Oregon Department of Geology and Mineral Industries Geological Map Series GMS-22, scale 1:24,000.

Freedman, Jacob, Wise, D.U., and Bentley, R.D., 1964, Pattern of folded folds in the Appalachian Piedmont along Susquehanna River: Geological Society of America Bulletin, v. 75, p. 621-638.

Gerlach, D.C., Avé Lallemant, H.G., and Leeman, W.P., 1981, An island arc origin for the Canyon Mountain ophiolite complex, eastern Oregon, U.S.A.: Earth and Planetary Science Letters, v. 53, p. 255-265.

Gilluly, James, 1937, Geology and mineral resources of the Baker quadrangle, Oregon: U.S. Geological Survey Bulletin 879, 119 p.

Gray, D.R., 1979, Microstructure of crenulation cleavages—An indicator of cleavage origin: American Journal of Science, v. 279, p. 97-128.

Higgins, M.W., 1971, Cataclastic rocks: U.S. Geological Survey Professional Paper 687, 97 p.

Himmelberg, G.R., and Loney, R.A., 1980, Petrology of ultramafic and gabbroic rocks of the Canyon Mountain ophiolite, Oregon: American Journal of Science, v. 280-A, p. 232-268.

Hobbs, B.E., Means, W.D., and Williams, P.F., 1976, An outline of structural geology: New York, John Wiley & Sons, 571 p.

Imlay, R.W., 1986, Jurassic ammonites and biostratigraphy of eastern Oregon and western Idaho, *in* Vallier, T.L., and Brooks, H.C., eds., Geology of the Blue Mountains region of Oregon, Idaho, and Washington—Geologic implications of Paleozoic and Mesozoic paleontology and biostratigraphy, Blue Mountains Province, Oregon and Idaho: U.S. Geological Survey Professional Paper 1435, p. 53-57.

Jakeš, Petr, and White, A.J.R., 1971, Composition of island arcs and continental growth: Earth and Planetary Science Letters, v. 12, p. 224-230.

———1972, Major and trace element abundances in volcanic rocks of orogenic areas: Geological Society of America Bulletin, v. 83, p. 29-40.

Jones, D.L., Silberling, N.J., and Hillhouse, John, 1977, Wrangellia—A displaced terrane in northwestern North America: Canadian Journal of Earth Science, v. 14, p. 2565-2577.

Kennedy, J.M., 1956, The geology of the northwest quarter of the Huntington quadrangle, Oregon: Eugene, University of Oregon, M.S. thesis, 91 p.

Liou, J.G., Maruyama, Shigenori, and Cho, Moonsup, 1985, Phase equilibria and mineral parageneses of metabasites in low-grade metamorphism: Mineralogical Magazine, v. 49, p. 321-333.

Marvin, R.F., and Dobson, S.W., 1979, Radiometric ages—Compilation B, U.S. Geological Survey: Isochron/West, no. 26, p. 3-32.

Mason, D.R., and McDonald, J.A., 1978, Intrusive rocks and porphyry copper occurrences of the Papua New Guinea-Solomon Islands region—A reconnaissance study: Economic Geology, v. 73, p. 857-877.

Mitchell, V.E., and Bennett, E.H., 1979, Geologic map of the Baker quadrangle, Idaho: Idaho Bureau of Mines and Geology Geologic Map Series, Baker 2° quadrangle, scale 1:250,000.

Miyashiro, Akiho, 1975, Volcanic rock series and tectonic setting: Annual Review of Earth and Planetary Sciences, v. 3, p. 251-269.

Morris, E.M., and Wardlaw, B.R., 1986, Conodont ages for limestones of eastern Oregon and their implication for pre-Tertiary melange terranes, *in* Vallier, T.L., and Brooks, H.C., eds., Geology of the Blue Mountains region of Oregon, Idaho, and Washington—Geologic implications of Paleozoic and Mesozoic paleontology and biostratigraphy, Blue Mountains Province, Oregon and Idaho: U.S. Geological Survey Professional Paper 1435, p. 59-63.

Mullen, E.D., 1983a, $MnO/TiO_2/P_2O_5$—A minor element discriminant for basaltic rocks of oceanic environments and its implications for petrogenesis: Earth and Planetary Science Letters, v. 62, p. 53-62.

———1983b, Paleozoic and Triassic terranes of the Blue Mountains, northeast Oregon; Discussion and field trip guide—Part II. Road log and commentary: Oregon Geology, v. 45, p. 75-82.

———1985, Petrologic character of Permian and Triassic greenstones from the melange terrane of eastern Oregon and their implications for terrane origin: Geology, v. 13, p. 131-134.

Palmer, A.R., 1983, The Decade of North American Geology 1983 geologic time scale: Geology, v. 11, p. 503-504.

Pardee, J.T., 1941, Preliminary geologic map of the Sumpter quadrangle, Oregon: Oregon Department of Geology and Mineral Industries map, scale 1:125,000.

Pardee, J.T., and Hewett, D.F., 1914, Geology and mineral resources of the Sumpter quadrangle, Oregon: Oregon Bureau of Mines and Geology, The Mineral Resources of Oregon, v. 1, no. 6, p. 4-128.

Pearce, J.A., and Cann, J.R., 1973, Tectonic setting of basic volcanic rocks determined using trace element analyses: Earth and Planetary Science Letters, v. 19, p. 290-300.

Pearce, J.A., and Gale, G.H., 1976, Identification of ore-deposition environment from trace-element geochemistry of associated igneous host rocks, *in* Volcanic processes in ore genesis: Proceedings of joint meeting of the Volcanic Studies Group of the Geological Society of London and the Institution of Mining and Metallurgy, London, Jan. 21 and 22, 1976, p. 14-24.

Pearce, J.A., and Norry, M.J., 1979, Petrogenetic implications of Ti, Zr, Y, and Nb variations in volcanic rocks: Contributions to Mineralogy and Petrology, v. 69, p. 33-47.

Peccerillo, Angelo, and Taylor, S.R., 1976, Geochemistry of Eocene calc-alkaline volcanic rocks from the Kastamonu area, northern Turkey: Contributions to Mineralogy and Petrology, v. 58, p. 63-81.

Phelps, David, 1979, Petrology, geochemistry and origin of the Sparta quartz diorite-trondhjemite complex, northeastern Oregon, *in* Barker, Fred, ed., Trondhjemites, dacites, and related rocks: Amsterdam, Elsevier, p. 547-580.

Phelps, David, and Avé Lallemant, H.G., 1980, The Sparta ophiolite complex, northeast Oregon—A plutonic equivalent to low K_2O island-arc volcanism, *in* Irving, A.J., and Dungan, M.A., eds., The Jackson volume: American Journal of Science, v. 280-A, p. 345-358.

Prostka, H.J., 1962, Geology of the Sparta quadrangle, Oregon: Oregon Department of Geology and Mineral Industries Geological Map Series GMS-1, scale 1:62,500.

———1967, Preliminary geologic map of the Durkee quadrangle, Oregon: Oregon Department of Geology and Mineral Industries Geological Map Series GMS-3, scale 1:62,500.

Robin, P.-Y.F., and Jowett, E.C., 1986, Computerized density contouring and statistical evaluation of orientation data using counting circles and continuous weighting functions: Tectonophysics, v. 121, p. 207-223.

Roure, François, 1982, Mise en évidence d'une tectonique majeure du Jurassique supérieur (phase névadienne) dans le Nord-Est de l'Orégon (secteur d'Huntington): Comptes Rendus des Séances de le Académie des Sciences, Paris, t. 294, p. 921-926.

Silberling, N.J., 1983, Stratigraphic comparison of the Wallowa and Huntington terranes, northeast Oregon: Geological Society of America Abstracts with Programs, v. 15, p. 372.

Silberling, N.J., Jones, D.L., Blake, M.C., Jr., and Howell, D.G., 1987, Lithotectonic terrane map of the western conterminous United States: U.S. Geological Survey Miscellaneous Field Studies Map MF-1874-C, scale 1:2,500,000.

Smith, W.D., and Allen, J.E., 1941, Geology and physiography of the northern Wallowa Mountains, Oregon: Oregon Department of Geology and Mineral Industries Bulletin 12, 65 p.

Streckeisen, A.L., 1976, To each plutonic rock its proper name: Earth-Science Reviews, v. 12, p. 1-33.

Thayer, T.P., 1977, The Canyon Mountain complex, Oregon, and some problems of ophiolites, *in* Coleman, R.G., and Irwin, W.P., eds., North American ophiolites: Oregon Department of Geology and Mineral Industries Bulletin 95, p. 93-106.

Turner, F.J., and Weiss, L.E., 1963, Structural analysis of metamorphic tectonites: New York, McGraw-Hill, 545 p.

Vallier, T.L., 1968, Reconnaissance geology of the Snake River Canyon between Granite Creek and Pittsburg Landing, Oregon and Idaho: The Ore Bin, v. 30, no. 12, p. 233-252.

———1977, The Permian and Triassic Seven Devils Group, western Idaho and northeastern Oregon: U.S. Geological Survey Bulletin 1437, 58 p.

Vallier, T.L., Brooks, H.C., and Thayer, T.P., 1977, Paleozoic rocks of eastern Oregon and western Idaho, *in* Stewart, J.H., Stevens, C.H., and Fritsche, A.E., eds., Paleozoic paleogeography of the Western United States (Pacific Coast Paleogeography Symposium 1, Bakersfield, Calif.): Los Angeles, Society of Economic Paleontologists and Mineralogists, Pacific Section, p. 455-466.

Walker, Nicholas, 1982, Pre-Tertiary plutonic rocks in the Snake River Canyon, Oregon/Idaho—Intrusive roots of a Permo-Triassic arc complex: Geological Society of America Abstracts with Programs, v. 14, p. 242-243.

Walker, N.W., 1981, U-Pb geochronology of ophiolitic and volcanic-plutonic arc terranes, northeastern Oregon and westernmost-central Idaho [abs.]: Eos (American Geophysical Union Transactions), v. 62, p. 1087.

———1983, Pre-Tertiary tectonic evolution of northeastern Oregon and west-central Idaho—Constraints based on U/Pb ages of zircons: Geological Society of America Abstracts with Programs, v. 15, p. 371.

———1986, U/Pb geochronologic and petrologic studies in the Blue Mountains terrane, northeastern Oregon and westernmost-central Idaho—Implications for pre-Tertiary tectonic evolution: Santa Barbara, University of California, Ph.D. dissertation, 224 p.

White, J.D.L., White, D.L., Vallier, Tracy, Stanley, G.D., Jr., and Ash, S.R., 1992, Middle Jurassic strata link Wallowa, Olds Ferry, and Izee terranes in the accreted Blue Mountains island arc, northeastern Oregon: Geology, v. 20, p. 729-732.

Wilson, Douglas, and Cox, Allan, 1980, Paleomagnetic evidence for tectonic rotation of Jurassic plutons in Blue Mountains, eastern Oregon: Journal of Geophysical Research, v. 85, no. B7, p. 3681-3689.

Winkler, H.G.F., 1979, Petrogenesis of metamorphic rocks (5th ed.): New York, Springer-Verlag, 348 p.

Wolff, E.N., 1965, Geology of the northern half of the Caviness quadrangle, Oregon: Eugene, University of Oregon, Ph.D. dissertation, 214 p.

Yoder, H.S., Jr., and Tilley, C.E., 1962, Origin of basalt magmas—An experimental study of natural and synthetic rock systems: Journal of Petrology, v. 3, p. 342-532.

13. GRAVITY STUDIES OF AN ISLAND-ARC/CONTINENT SUTURE ZONE IN WEST-CENTRAL IDAHO AND SOUTHEASTERN WASHINGTON

By GREGORY B. MOHL[1,2] and RICHARD L. THIESSEN[1]

CONTENTS

	Page
Abstract	497
Introduction	497
Acknowledgments	499
Methods	499
Geologic and tectonic elements	501
North American assemblage	501
Accreted-terrane assemblage	501
Boundary zone	501
Columbia River Basalt Group	502
Gravity signature	502
West-central Idaho	504
Southeastern Washington	504
Gravity modeling	508
Interpretation	511
Conclusions	512
References cited	513

ABSTRACT

Gravity anomalies in west-central Idaho and southeastern Washington correlate well with an island-arc/continent suture zone previously defined by initial $^{87}Sr/^{86}Sr$ ratios and detailed field mapping. Using a regional compilation of gravity data supplemented with data collected in southeastern Washington, we correlated the observed anomalies with geologic and tectonic elements associated with the suture zone. These correlations are supported by theoretical models that establish the gravity signature of geologic elements suspected to be causing anomalies in the study area.

The character of the observed gravity anomalies varies within the study area. In the northern part, the gravity signature consists of a regional high-low paired anomaly with local highs superimposed near the suture zone. In the central part, this signature does not correlate well with the suture zone defined by initial $^{87}Sr/^{86}Sr$ ratios, and the locally superimposed highs are absent. The gravity signature observed in the southern part of the study area returns to the regional paired anomaly with a broad gradient that steepens in the suture zone. Isolated highs outboard of the suture zone were also observed.

Correlation of these anomalies to geologic features, magnetic anomalies, and theoretical models indicates that the primary source of the lows in the northern part of the study area is probably the Idaho batholith. The highs are likely to be related to near-surface mafic and ultramafic bodies caught in or near the suture zone. The lack of correlation between gravity anomalies and initial $^{87}Sr/^{86}Sr$ ratios in the central part of the study area may be due to the relativity coarse level of gravity data available, or it may be related to geologic elements that are not reflected in the isotopic analyses. Gravity anomalies in the southern part of the study area appear to be related to differences in crustal composition or thickness that have been overprinted by the effects of the Idaho batholith.

In Washington, geologic control is limited to a few isolated exposures, but detailed gravity data closely define the suture zone by extending the anomaly signature observed in Idaho. This investigation provides a basis for better understanding the geometry of the suture zone and accurately delineating its location to the west where thick sections of the Columbia River Basalt Group prevent detection by traditional geochemical and field-mapping techniques.

INTRODUCTION

The recognition of exotic terranes in the northwestern United States has led to the definition of a suture zone between these terranes and the North American craton. Where exposed in west-central Idaho, the suture zone is characterized by a steep gradient in initial $^{87}Sr/^{86}Sr$ ratios (Armstrong and others, 1977; Fleck and Criss, 1985; Criss and Fleck, 1987) (fig. 13.1) and discontinuities in petrologic, metamorphic, and structural features (Hamilton, 1963; Myers, 1982; Onasch, 1979, 1987; Aliberti and Manduca, 1988a, b; Davidson, 1988; Lund, 1988; Lund and Snee, 1988; Strayer, 1988; Strayer and others, 1989, 1990; Lund and others, 1990; Blake, 1991; Selverstone and others, 1992; Manduca and others, 1992, 1993; Blake and Thiessen, in press). In adjacent Washington, westward-thickening flood basalts of the Columbia River Basalt Group obscure the suture zone's surface expression, and the currently used techniques are of little value in defining its subsurface location. Accurately locating the suture zone

[1]Washington State University, Pullman, WA 99164-2812
[2]Present address: Conoco, Inc., Casper, WY 82601

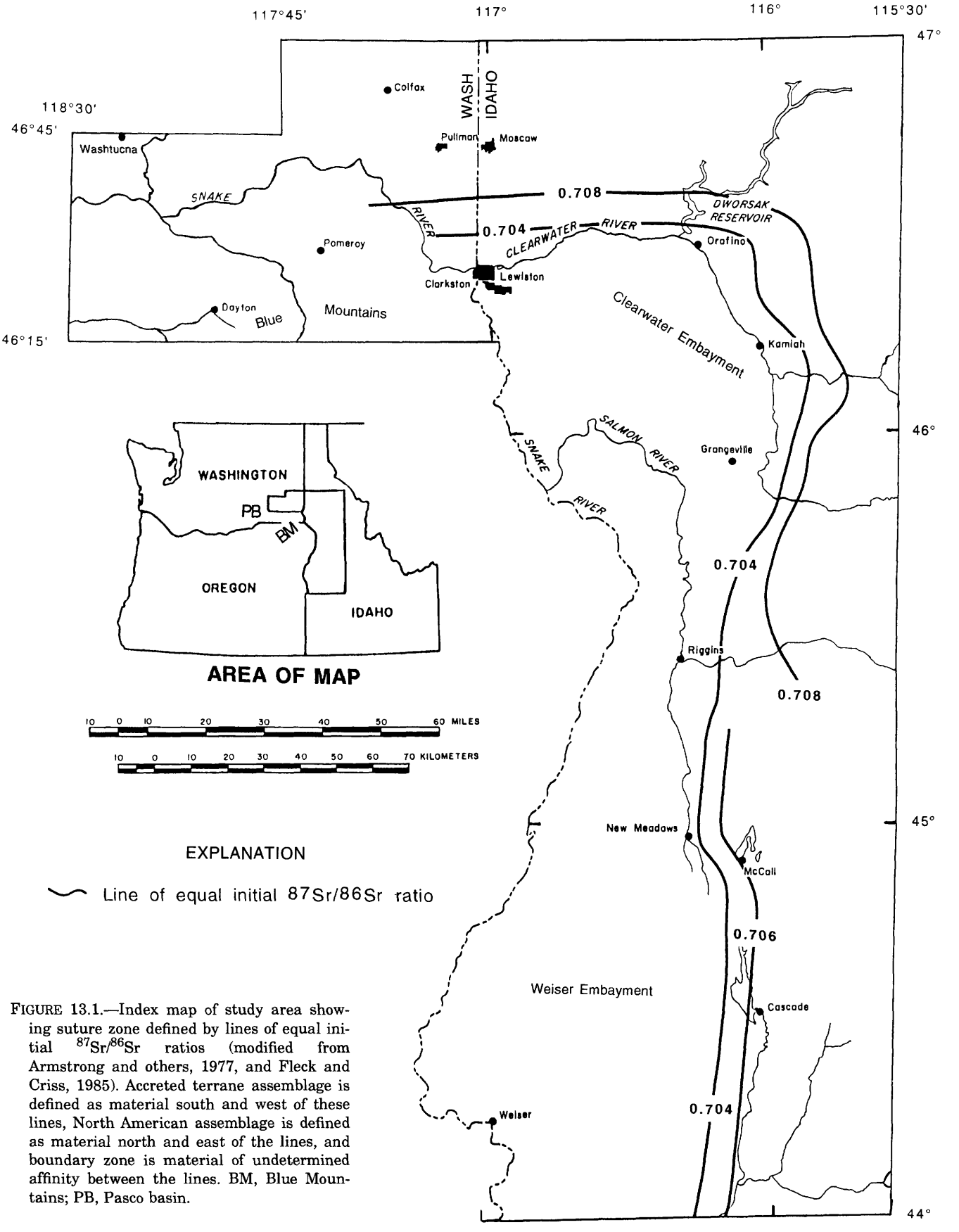

FIGURE 13.1.—Index map of study area showing suture zone defined by lines of equal initial $^{87}Sr/^{86}Sr$ ratios (modified from Armstrong and others, 1977, and Fleck and Criss, 1985). Accreted terrane assemblage is defined as material south and west of these lines, North American assemblage is defined as material north and east of the lines, and boundary zone is material of undetermined affinity between the lines. BM, Blue Mountains; PB, Pasco basin.

under the basalt is essential to understanding the geometry of the suture zone as well as to developing models that explain accretion of exotic terranes.

Detailed mapping of gravity variations is one method by which the suture zone in southeastern Washington may be defined. This approach utilizes differences in bulk density that result from juxtaposition of crust of differing composition and thickness across the suture zone. The purpose of this paper is to use geologic and tectonic elements associated with the suture zone to define its gravity signature in west-central Idaho. This signature is then used to delineate the suture zone in southeastern Washington where the suture zone's location is poorly constrained by exposures of rock underlying the basalt.

ACKNOWLEDGMENTS

We are grateful for critical reviews by Peter Hooper and John Watkinson as well as helpful discussions with Paul Myers, David Blake, and Kent Johnson.

METHODS

From various published sources we compiled information about geologic and tectonic elements in the study area that may affect gravity measurements. Then we correlated these elements with the suture zone in west-central Idaho that had been defined previously by geologic and geochemical analyses (Armstrong and others, 1977; Vallier, 1977; Vallier and others, 1977; Brooks and Vallier, 1978; Brooks, 1979; Myers, 1982; Fleck and Criss, 1985; Criss and Fleck, 1987; Onasch, 1987; Aliberti and Manduca, 1988a, b; Davidson, 1988; Lund, 1988; Lund and Snee, 1988; Strayer, 1988; Strayer and others, 1989, 1990; Lund and others, 1990; Blake, 1991; Selverstone and others, 1992; Manduca and others, 1992, 1993; Blake and Thiessen, in press). These correlations were supplemented with observations of aeromagnetic data (Zietz and others, 1971, 1978). Due to the regional nature of this investigation, the geology of the study area has been simplified to four lithotectonic assemblages: the North American assemblage, the accreted-terranes assemblage, the boundary zone, and the Columbia River Basalt Group.

A gravity signature of the suture zone in west-central Idaho was defined by comparing available gravity data (Bankey and others, 1984) with the geologic and tectonic elements and magnetic anomalies observed in the area. This comparison was supplemented with numeric models generated to examine the gravity signature of the various tectonic elements observed in the region. The data are directly from Bankey and others (1984) and were collected from approximately 1,000 stations distributed as shown in figure 13.2. Also shown in figure 13.2 are approximately 900 additional stations where data were collected in southeastern Washington by Mohl, 1987. Bankey and others (1984) used the International Gravity Standardization Net 1971 (IGSN 71) datum (Morelli, 1974), the 1967 gravity formula (International Association of Geodesy, 1967), and a Bouguer reduction density of 2.67 g/cm^3. Terrain corrections were applied radially from each station to a distance of 167 km (Bankey and others, 1984).

When we began this study, gravity data in southeastern Washington were insufficient to define the suture zone. The thick basalt cover in southeastern Washington made it necessary to use a higher density of gravity stations there than in Idaho to determine the location of the suture zone. Approximately 900 stations were added to the existing network in the Washington portion of the study area by Mohl (1987; fig. 13.2). Additional stations where Phole (1979) collected data were added to the network, as were stations where Gregory and Jackson (1976) took measurements. The data gathered by Mohl (1987) were collected with a Worden gravimeter at bench marks, triangulation stations, and other points of known elevation. All the measurements were tied to the IGSN 71 datum and corrected for drift, latitude (formula from International Association of Geodesy, 1967), free air, and a Bouguer anomaly (density of 2.67 g/cm^3) (Mohl, 1987). The data are currently on file with the Defense Mapping Agency (U.S. Department of Defense), which has recalculated them using a 1984 latitude-correction formula. Differences between the 1967 and 1984 formulas are slight and result in changes that are well within the accuracy of the investigation. Terrain corrections were not applied to these data because the amount of correction that would result is not significant on the scale of the anomalies observed.

This report discusses the regional map patterns of gravity anomalies in the western Idaho suture zone (WISZ) in western Idaho and southeastern Washington as first defined in print by Strayer and others (1987, 1989, 1990), Strayer (1988), and Fleck and Criss (1988). Subsequent publications by Lund (1988 and chap. 14, this volume), Lund and Snee (1988), Lund and others (1990), and Snee and others (chap. 10, this volume) called the western Idaho suture zone the "Salmon River suture zone" (see discussion and reply in Lund and others, 1990, and Strayer and others, 1990). In a companion study (Johnson and others, 1988; Mohl, 1989), we collected detailed data

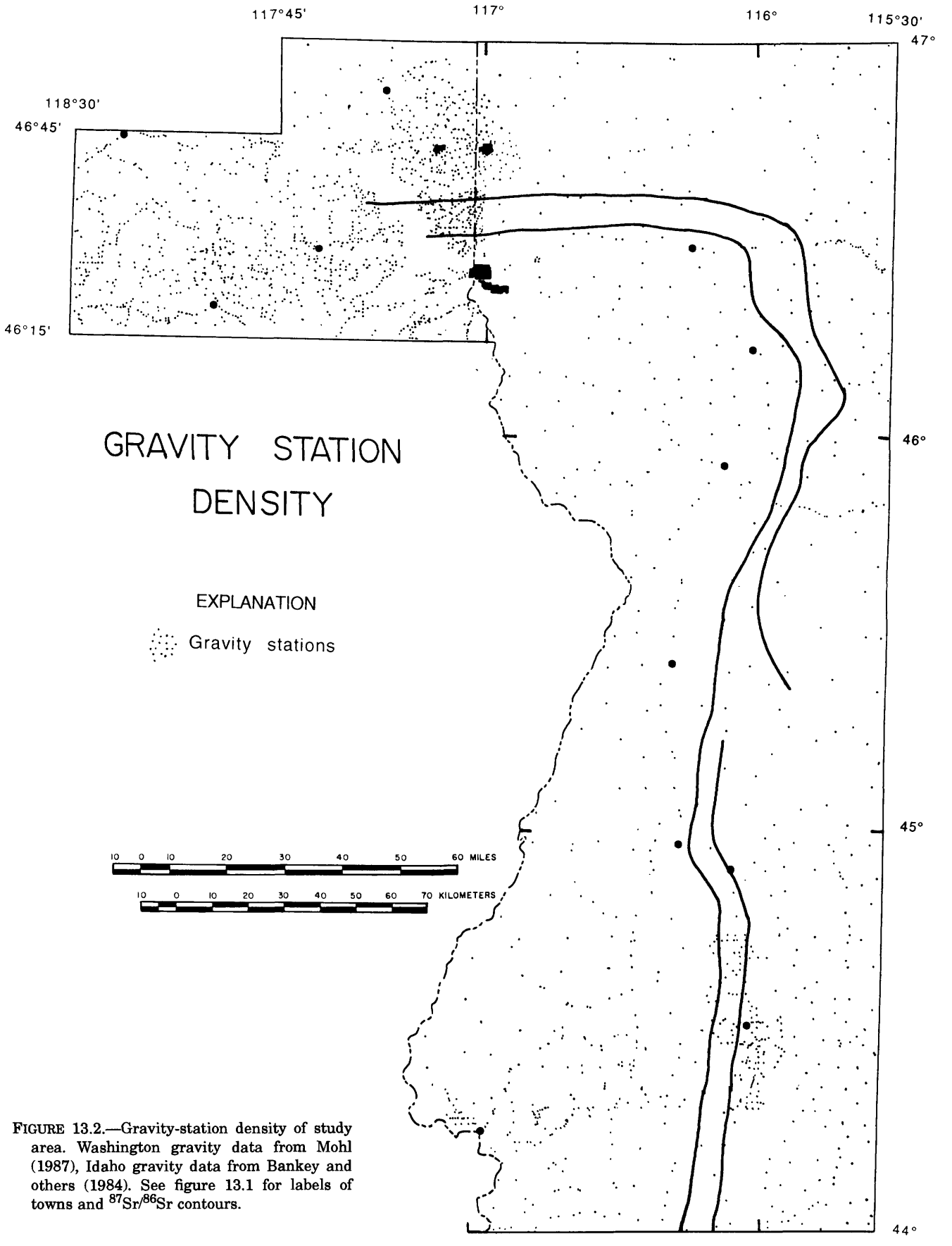

FIGURE 13.2.—Gravity-station density of study area. Washington gravity data from Mohl (1987), Idaho gravity data from Bankey and others (1984). See figure 13.1 for labels of towns and $^{87}Sr/^{86}Sr$ contours.

along a series of four gravity traverses across the western Idaho suture zone straddling the major bend in the suture zone near Orofino, Idaho. Detailed gravity models were prepared for these traverses on the basis of local geologic and density observations.

GEOLOGIC AND TECTONIC ELEMENTS

The geologic and tectonic units associated with the western margin of the North American craton and the accreted terranes are well studied. Significant works include, but are not limited to, Armstrong and others (1977), Vallier (1977), Vallier and others (1977), Bond and Wood (1978), Brooks and Vallier (1978), Brooks (1979), Hyndman (1979, 1983), Myers (1982), Fleck and Criss (1985), Criss and Fleck (1987), Onasch (1987), Wiswal and Hyndman (1987), Aliberti and Manduca (1988a, b), Davidson (1988), Lund (1988), Strayer (1988), Strayer and others (1989, 1990), Lund and others (1990), Blake (1991), Selverstone and others (1992), Manduca and others (1992, 1993), and Blake and Thiessen (in press). The generalized assemblages presented herein are based on the work of these and other investigators.

NORTH AMERICAN ASSEMBLAGE

The North American assemblage is defined as the suite of rocks exposed north and east of the $^{87}Sr/^{86}Sr=0.708$ and $^{87}Sr/^{86}Sr=0.706$ lines (fig. 13.1; Armstrong and others, 1977; Fleck and Criss, 1985). Termed the "Belt-Yellowjacket terrane" by Fleck and Criss (1985) and Criss and Fleck (1987), this assemblage consists of granodiorite and monzogranite of the Idaho batholith, Proterozoic metasedimentary rocks of the Belt Supergroup (Hyndman, 1979), and granitic-gneissic pre-Belt basement rocks (Armstrong, 1975; Fleck and Criss, 1985). Seismic-refraction studies (Smith, 1978; Allenby and Schnetzler, 1983; Sheriff and Stickney, 1984) indicate that the crust in central Idaho is between 33 and 45 km thick.

The dominant quartzofeldspathic composition and relative thickness of the crust formed by the North American assemblage result in smooth and consistent long-wavelength gravity anomalies. Density measurements (Criss and Champion, 1984; Mohl, 1989) indicate that the densities of the batholith and later epithermal plutons range from 2.43 to 2.81 g/cm^3 and average 2.56 g/cm^3 and 2.58 g/cm^3, respectively. The Precambrian units have average densities of 2.67 g/cm^3 for gneissic units, 2.71 g/cm^3 for schists and marbles, and 2.56 g/cm^3 for quartzites (Mohl, 1989). These densities are all within the published ranges for metasedimentary rocks (Sharma, 1976; Telford and others, 1976). The density of possible pre-Belt basement rocks (Armstrong, 1975) averages 2.66 g/cm^3, which is approximately the often quoted value of 2.67 g/cm^3 for continental crust. Magnetic anomalies observed over the North American assemblage are also relatively smooth and consistent (Mabey and others, 1978).

ACCRETED-TERRANE ASSEMBLAGE

The accreted-terrane assemblage consists of the material south and west of the $^{87}Sr/^{86}Sr=0.704$ line (fig. 13.1). More diverse and structurally complex than the North American assemblage, this suite of rocks includes thick clastic and carbonate sequences, island-arc volcanic rocks, dismembered oceanic crust, and granitic plutons. Basement rocks include quartz diorite, plagiogranite, gabbro, and pyroxenite (Brooks, 1979; Hyndman, 1979). Seismic-refraction and other studies indicate that the crust is 20 to 25 km thick in central Washington and 25 to 30 km thick in the area of this assemblage (Hill, 1972, 1978; Smith, 1978; Allenby and Schnetzler, 1983; Zervas and Crosson, 1986; Catchings and Mooney, 1988; Sobczyk, 1994).

Geophysical characteristics of the accreted-terrane assemblage are not as well defined as their counterparts in the North American assemblage. The magnetic signature is chaotic and typified by relatively short-wavelength anomalies (Mabey and others, 1978). Gravity anomalies are similar owing to the relatively thin crust and disjointed nature of the assemblage. Densities of the island-arc volcanic rocks (Mohl, 1989) average 2.72 g/cm^3. Basement rocks, as well as overlying clastic and carbonate rocks, were poorly exposed in Mohl's (1989) study area and so were not sampled for density measurements. Characterization based on lithologic association indicates that the densities of the basement rocks in the accreted-terrane assemblage are generally higher than those observed in the North American assemblage, owing to the higher proportion of denser mafic components.

BOUNDARY ZONE

The width and limits of the boundary zone between the accreted-terrane and North American assemblages are different depending the data used to define them. Locations of suture-zone plutons, deformation, metamorphism, lithologic changes, isotopic changes, and geophysical characteristics all define somewhat

different boundary zones. However, the limits of the boundary zone are best defined by the $^{87}Sr/^{86}Sr=0.708$ and $^{87}Sr/^{86}Sr=0.706$ lines on the north and east and by the $^{87}Sr/^{86}Sr=0.704$ line on the south and west. The boundary zone consists of a series of geochemically and mineralogically distinct lens-shaped plutons (Kuntz, M.A., Allen, C.C., and LaFortune, J.R., unpub. data, 1984; Fleck and Criss, 1985; Criss and Fleck, 1987; Aliberti and Manduca, 1988a, b; Lund, 1988), ultramafic pods (Hietanen, 1962; Hamilton, 1963; Bonnichsen, 1987), and highly deformed schistose metasedimentary rocks (Hamilton, 1963, 1969; Myers, 1982; Onasch, 1979, 1987; Aliberti and Manduca, 1988a, b; Davidson, 1988; Lund, 1988; Lund and Snee, 1988; Strayer, 1988; Strayer and others, 1989, 1990; Lund and others, 1990; Blake, 1991; Selverstone and others, 1992; Manduca and others, 1992, 1993; Blake and Thiessen, in press). This zone ranges from 5 to 25 km wide (Criss and Fleck, 1987) in west-central Idaho and is of undefined dimensions in southeastern Washington. Plutons of the boundary zone contain material derived from both the accreted-terrane and the North American assemblages (Criss and Fleck, 1987), and they tend to be compositionally and texturally similar to the plutons of the accreted-terrane assemblage (Fleck and Criss, 1985).

Geophysical characteristics of this assemblage vary with the width and lithology of the boundary zone itself. Ultramafic pods or mafic plutons composed of large percentages of ferromagnesian minerals have relatively high densities that result in gravity highs. Conversely, absence of these ferromagnesian minerals in the metasedimentary rocks results in gravity lows. Anomalies associated with this assemblage are likely to be isolated due to the discontinuous nature of the bodies observed. Detailed analysis of the gravity anomalies within the boundary zone must be done with much higher resolution gravity data sets than those currently available (Mohl, 1989), particularly because over part of its length, the boundary zone is covered with basalt.

COLUMBIA RIVER BASALT GROUP

The Columbia River Basalt Group covers much of the surface expression of the suture zone. This sequence of tholeiitic basalts originated in a series of dike swarms near the western Idaho border (Hooper, 1982). In the Idaho part of the study area, the Clearwater and Weiser embayments represent the eastern limit of the basalt (fig. 13.1; Swanson and others, 1980). In these areas, deep drainages were invaded and filled with as much as 100 m of basalt (P.R. Hooper, oral commun., 1988). Near the margins, nonmarine clastic sediments shed from the surrounding highlands intertongue with the basalt flows to create a complex stratigraphic sequence (Cavin, 1964; Lin, 1967; Myers and Price, 1979). In south-central Washington, the basalt thickens to the west to more than 3,000 m in the central part of the Pasco basin (PB on fig. 13.1; Hooper, 1982), and the relative proportion of interbedded sedimentary rocks diminishes (Cavin, 1964).

The problem of defining the gravity signature of the Columbia River Basalt Group is in determining the density and thickness of the basalt section. Near the margins, interbedded sedimentary rocks of varying proportions could reduce the density of the basalt stratigraphic section to below that of the surrounding country rocks. This would result in a gravity low of varying proportion. Toward the center of the basin the interbedded sedimentary rocks thin, but the relative proportion of highly fractured and vesicular basalt, which also would reduce the density of the section, is unknown. Furthermore, the basalt is known to have inundated a deeply dissected preexisting topographic surface that is poorly defined (P.R. Hooper, oral commun., 1988), resulting in highly variable thickness. Where measured from basalt samples taken across the plateau (Yost and Steele, 1978; Robbins and others, 1979; Smith, 1979; Schmidt and others, 1980), densities range from 1.8 g/cm^3 to 2.8 g/cm^3 as a function of vesicularity and degree of fracturing in a given sample. Samples from west-central Idaho (Mohl, 1989) range from 2.49 g/cm^3 to 2.91 g/cm^3 with an average of 2.74 g/cm^3. These measured densities are significantly lower than those commonly reported for basalts (Sharma, 1976; Telford and others, 1976), probably because textbook examples do not take into account the vesicularity and fracturing observed. Near the margins of the basins, the overall density of the basalt section is further reduced by the interbedded sedimentary rocks, whose densities range from 0.95 to 2.4 g/cm^3 (Yost and Steele, 1978; Mohl, 1989).

GRAVITY SIGNATURE

Gravity studies over several suture zones exposed elsewhere in the world imply that suture zones are characterized by a paired high-low gravity anomaly (Gibb and Thomas, 1976; Fountain and Salisbury, 1981; Hutchinson and others, 1983; Karner and Watts, 1983; Price and Hatcher, 1983; Thomas, 1983; Cook, 1984; Dainty and Frazier, 1984; Fisher and von

Huene, 1984; Johnson and others, 1984; Keller and others, 1985; Thomas and others, 1988). In most of these studies, a regional high is observed over the accreted terranes and a regional low over the continental material. The suture zone itself is often characterized by isolated highs either in the suture zone or just outboard, and a steep gradient that marks the change from the regional high of the accreted terranes to the regional low of the continent. As shown in figure 13.3, the total difference in gravity values and the distance between the regional high and low anomalies vary from suture zone to suture zone. Relatively few models have been developed to explain the attributes of the paired anomalies. In these investigations most of the regional high and low gravity anomalies have been conceptually modeled as products of either obduction of oceanic crust (fig. 13.3, models A and B) or crustal thickening (model C). Local anomalies, such as the highs directly associated with the suture zone and those produced by relatively light upper-crustal bodies, are shown in models D and E.

Report	Region	Δ Grav. (milligals)	Dist. (kilometers)	Model
Gibb and Thomas (1976)	Canadian Shield	66	80	A
Fountain and Salisbury (1981)	5 around world	30-140	30-60	B
Hutchinson and others (1983)	Southern Appl.	60-150	60-120	C, D
Thomas (1983)	Southern Appl.	60-150	80	A
Karner and Watts (1983)	Alps, Appl.	80-200	70-200	F
Johnson and others (1984)	Wyoming	50-100	90	C, D, E
Cook (1984)	Southern Appl.	60-140	50-140	C
Dainty and Frasier (1984)	Southern Appl.	60	60	C, D
Fisher and von Huene (1984)	Southern Alaska	60-70	50	B
Keller and others (1985)	Virginia	<15	40	C, D, E

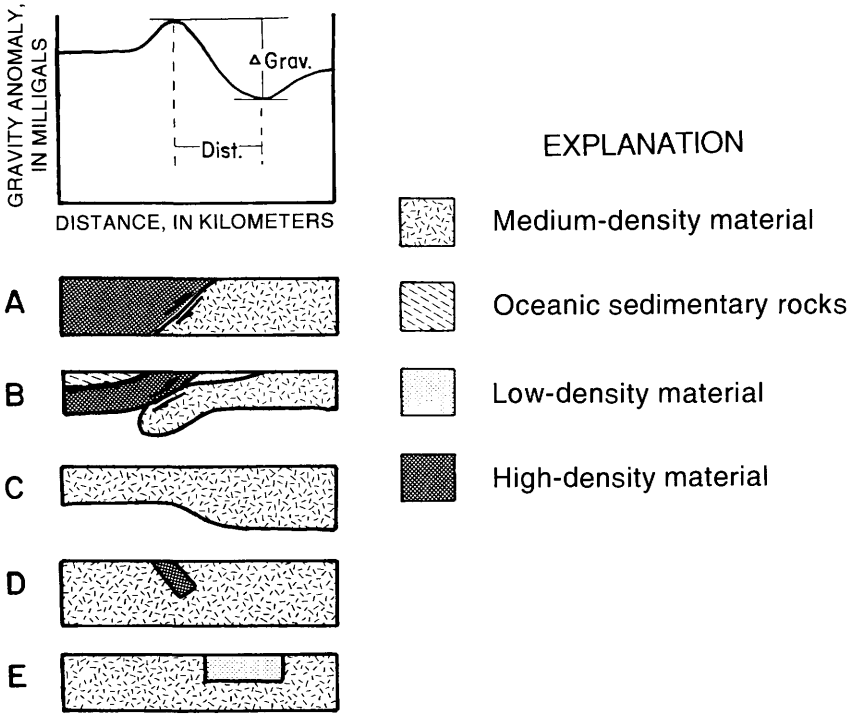

FIGURE 13.3.—Gravity anomalies and conceptual models (cross sections A–E) for suture zones in various regions. Graph shows general shape of all anomalies; specific values given in table. Appl., Appalachian Mountains in North America; Dist., distance; Δ Grav., total change in gravity over specified distance. Arrows in models A and B show direction of relative movement.

WEST-CENTRAL IDAHO

West-central Idaho gravity data (Bankey and others, 1984) display a paired high-low anomaly that is similar to the signature observed in other suture zones (fig. 13.4). Gravity values in the accreted-terrane assemblage tend to be relatively higher than their continental counterparts. With respect to the anomalies that characterize the suture zone itself, a series of isolated highs are observed immediately south and west of the $^{87}Sr/^{86}Sr=0.704$ line. A gradient with gravity values decreasing to the north and east is also seen. The relative magnitude of the gradient is 25 to 80 mGal over a distance of 15 to 70 km. The highs are smaller (5–15 mGal) and of much more limited extent.

In the northern part of the study area, lat 46°–47° N., the suture zone appears to have two distinct anomaly signatures. The east-west segment from Orofino, Idaho, to the Washington border is typified by a small but uniform gradient with gravity values decreasing to the north and by well-defined highs outboard of the $^{87}Sr/^{86}Sr=.704$ line. In this area, highs appear to coincide with local mafic Mesozoic intrusions emplaced near the suture zone. The north-south segment displays a steep gradient with gravity values decreasing to the east. The gradient and paired anomaly have higher amplitudes than in the east-west segment, and highs are poorly defined. On the whole the gradient defines the northern and eastern extent of the Columbia River Basalt Group in the Clearwater embayment (fig. 13.1). It also approximately coincides with the western edge of the Idaho batholith.

In the central part of the study area, lat 45°–46° N., the gradient swings to the west and crosses the suture zone defined by $^{87}Sr/^{86}Sr$ ratios. The gradient also crosses the southern limit of the Clearwater embayment (fig. 13.1) and places metasedimentary rocks of the Riggins Group (Hamilton, 1963; Myers, 1982) as well as at least one major boundary pluton on the east side of the gradient (see area A, fig. 13.4). In the area of the (informal) Little Goose Creek and Hazard Creek complexes of Aliberti and Manduca (1988a, b) and Manduca and others (1993), indicated with the letter B on fig. 13.4, the gradient appears to diverge and surround these plutonic bodies. The local highs are absent in this part of the study area.

In the southern part of the study area, lat 44°–45° N., the gravity contours once again form a single, steep gradient. The gradient is steep in the vicinity of the $^{87}Sr/^{86}Sr=0.706$ line and roughly coincides with the western border of the Idaho batholith, or the eastern limit of the Columbia River Basalt Group in the Weiser embayment (fig. 13.1). Several poorly defined highs are present outboard of the suture zone, but these, unlike those found in the northern part of the study area, do not appear to be related to exposures of Mesozoic intrusive rocks.

Comparison of the gravity signatures with aeromagnetic data from the study area (Mabey and others, 1978; Zietz and others, 1978) shows that several of the gravity features appear to be associated with magnetic anomalies (fig. 13.5). The magnetic anomalies exhibit a major change in character from relatively smooth, long-wavelength anomalies over the North American assemblage to more chaotic, short-wavelength anomalies over the accreted-terrane assemblage (Mabey and others, 1978). In the northern part of the study area, this change in character corresponds with the line of gravity highs observed at the suture zone. Near Grangeville, Idaho, the gravity gradient that crosses from east to west of the suture zone is reflected by a similar magnetic gradient. In the southern part of the study area, the change in character of the magnetic anomalies coincides with the steep slope of the gravity gradient as well as the suture zone defined by $^{87}Sr/^{86}Sr$ ratios.

SOUTHEASTERN WASHINGTON

Increased detail afforded by the higher density of gravity stations in southeastern Washington (Mohl, 1987) permits more accurate definition of gravity anomalies there than in the Idaho portion of the study area. Contoured on an interval of 2 mGal rather than the interval of 5 mGal used in Idaho, the Washington data accurately define several major gravity features that may be associated with the suture zone. Correlation of these detailed gravity anomalies to geologic and tectonic features is difficult, because outcrops of pre-basalt rocks are limited to a few isolated exposures near the Idaho-Washington border and in the northern Blue Mountains south of Pomeroy, Wash. (fig. 13.1). Given this lack of exposure, extrapolation of the geologic and tectonic associations expressed in Idaho and correlation with structures within the basalt and with physiographic features provide the primary means of interpreting the data.

Gravity anomalies observed in southeastern Washington are labeled A through F on figure 13.6. The regional paired anomaly signature observed in Idaho is not as strongly defined in these data. However, the signature observed from Orofino, Idaho, to the Washington border (fig. 13.4) does extend into southeastern Washington, where it is expressed as an east-west-trending series of highs (B1, B2, B3 on fig. 13.6)

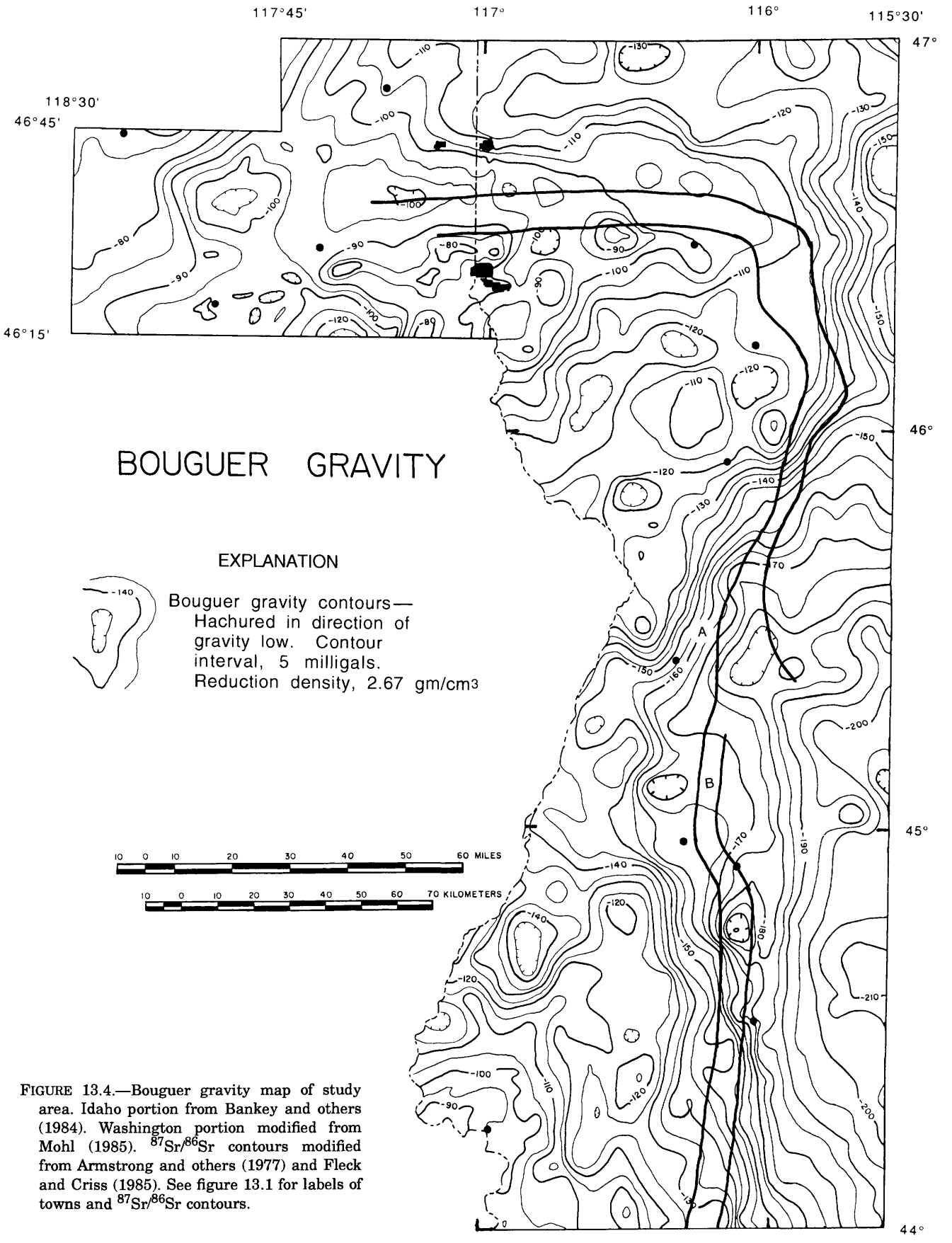

FIGURE 13.4.—Bouguer gravity map of study area. Idaho portion from Bankey and others (1984). Washington portion modified from Mohl (1985). $^{87}Sr/^{86}Sr$ contours modified from Armstrong and others (1977) and Fleck and Criss (1985). See figure 13.1 for labels of towns and $^{87}Sr/^{86}Sr$ contours.

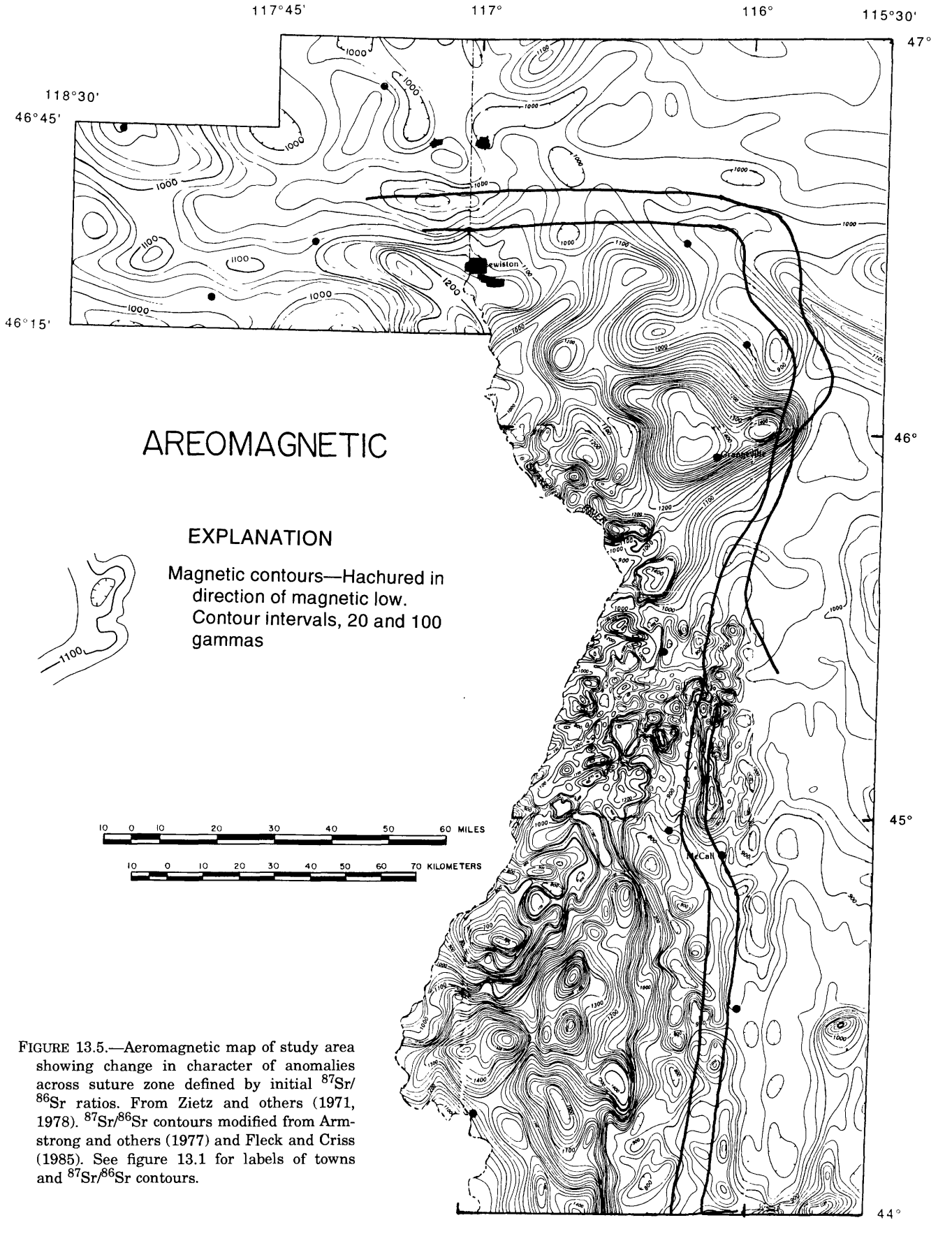

FIGURE 13.5.—Aeromagnetic map of study area showing change in character of anomalies across suture zone defined by initial $^{87}Sr/^{86}Sr$ ratios. From Zietz and others (1971, 1978). $^{87}Sr/^{86}Sr$ contours modified from Armstrong and others (1977) and Fleck and Criss (1985). See figure 13.1 for labels of towns and $^{87}Sr/^{86}Sr$ contours.

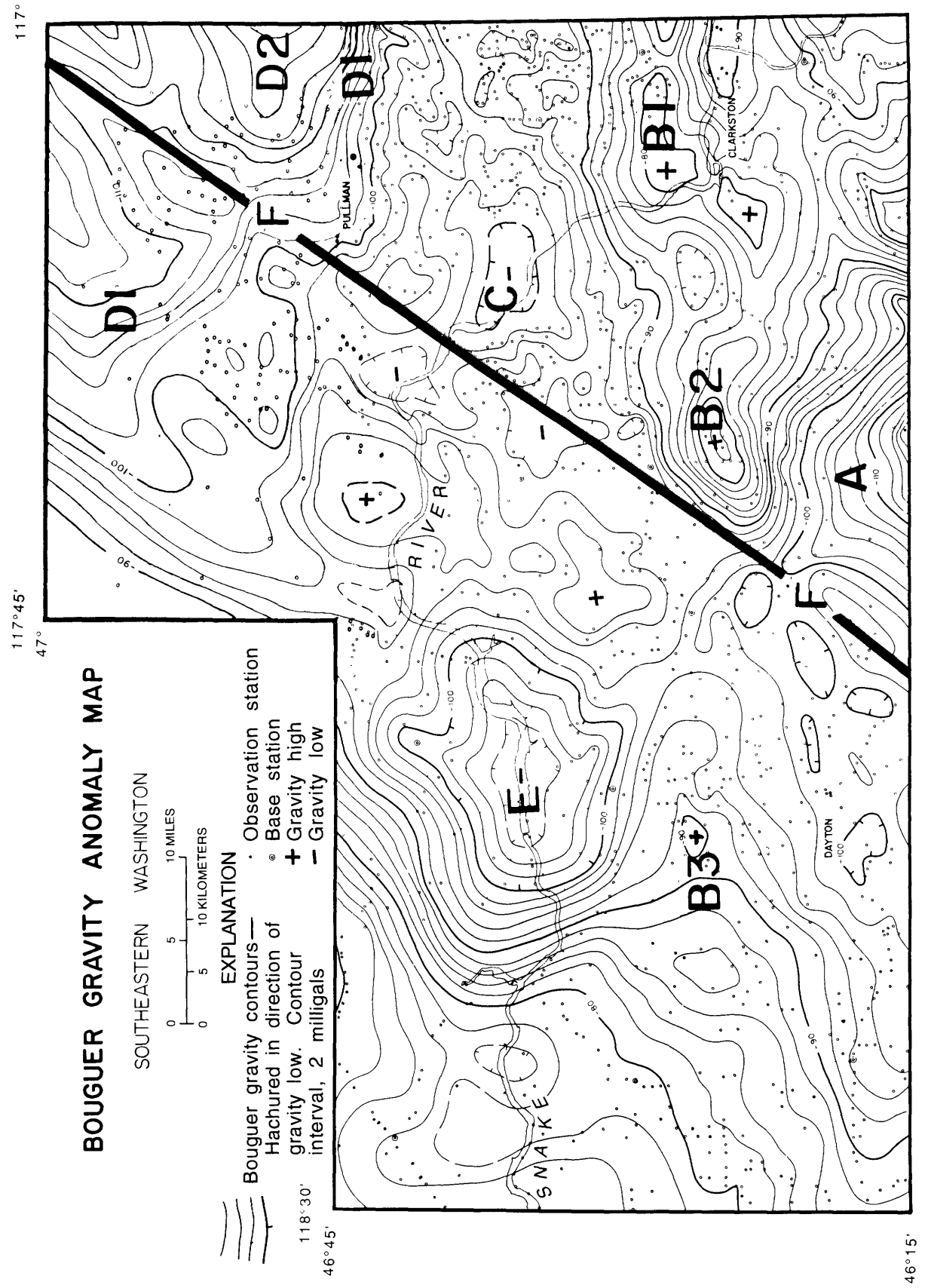

FIGURE 13.6.—Detailed Bouguer gravity map of Washington portion of study area showing relative location and magnitude of anomalies observed. See text for description of origin of anomalies A through F. Modified from Mohl (1985).

and a parallel gradient sloping down to the north and northeast (D1). This signature is complicated by a crosscutting linear feature (F) and two subcircular features (A, E). An isolated subcircular feature (C) corresponds to the westernmost exposure of the North American assemblage in southeastern Washington (Armstrong and others, 1977).

The east-west-trending series of highs (B1, B2, B3) correlates to several local geologic and physiographic features shown on regional maps by Myers and Price (1979) and Swanson and others (1980). Anomaly B1 coincides with a complex set of folds, faults, and faulted folds called the Lewiston structure (Camp, 1976). This structure is characterized by anomalous paleomagnetic rotations of basalts (Lim, 1986; Thiessen and others, 1986). The gravity anomaly corresponds to the structure for several kilometers, then continues to the west (B2), following a series of small monoclines along the northern edge of the Blue Mountains near Pomeroy (fig. 13.1). Near the northwest corner of the Blue Mountains, the folds die out, and the anomaly abruptly changes character from a high-amplitude feature (B2) to a more subdued, low-amplitude feature (B3). This series of highs is approximately 5 to 10 km south of the extrapolated location of the $^{87}Sr/^{86}Sr=0.704$ line and is on the accreted-terrane assemblage side of the suture zone.

The gradient (D1) and low (D2) also correlate to local geologic and physiographic features. The gradient roughly defines the southern extent of the Palouse ridge, which is a quartzitic and granitic topographic high buried beneath the Columbia River Basalt Group (Strand, 1949; Cavin, 1964; Lin, 1967). North and west of Pullman the gradient weakens, possibly divides, then joins a major regional northeast-trending gradient discussed by Cady and Fox (1984), Johnson and others (1989), and Thiessen and others (1992). The subcircular low (C) located between the gradient and the high trend appears to be related to a subbasalt ridge similar to that correlated with the D1 and D2 set of anomalies. On the basis of $^{87}Sr/^{86}Sr$ ratios, this material is unquestionably of North American assemblage affinity (Armstrong and others, 1977).

Other significant gravity features include subcircular lows (A and E) and a linear anomaly (F). Anomaly A corresponds to the Blue Mountains highland, which includes several isolated exposures that resemble the rocks of the accreted-terrane assemblage (Armstrong and others, 1977; Swanson and others, 1980). The other subcircular anomaly, E, does not correlate to any surface geologic or physiographic element. However, it does correlate to a zone of anomalous paleomagnetic rotations as observed in a late-stage basalt flow (Lim, 1986; Thiessen and others, 1986). The linear anomaly, F, is tentatively correlated to an extension of Riddihough and others' (1986) Klamath-Blue Mountain lineament (Mohl and Thiessen, 1985; Mohl, 1985). This feature truncates the high-amplitude high (B2), changing the character of the anomaly to a much more subdued feature. It aligns with the Hite Fault, a normal fault that drops the basalt down to the west. It also correlates with a major break in the gradient (D1) and forms the western edge of anomaly A.

When compared with aeromagnetic anomalies observed in southeastern Washington (Zietz and others, 1978), three of the gravity features are seen to have corresponding magnetic expressions. These features include the east-west-trending series of gravity highs (B1, B2, B3) that corresponds to a similar series of magnetic highs, and gravity lows (A and C) that coincide with magnetic lows. The linear gravity anomaly (F) coincides with a reduction of the magnetic intensities from relatively high-magnitude features on the east side to more subdued features on the west side.

GRAVITY MODELING

The origin and significance of gravity anomalies observed in this investigation may be addressed with simple two-dimensional computer models. The program used in this analysis (Thiessen, 1986) is based on Talwani and others' (1959) algorithm, which determines the expected gravity signature of isolated geologic elements of known dimension and density.

The effects of crustal differences on gravity anomalies were modeled on the basis of three variables: crustal thickness, crustal composition, and suture-zone geometry (fig. 13.7*A*). In models A through G on figure 13.7, the density of cratonic crust was assumed to be 2.67 g/cm^3, on the basis of the limited samples of Criss and Champion (1984) and Mohl (1989). This is the density commonly assumed for continental crust. The density of the accreted block was assumed in models B, D, and F to be equal to that of the continental block, reflecting an assumption that the two blocks are of similar composition. In models C, E, and G, the density of the accreted block was assumed to be 2.70 g/cm^3, 0.03 g/cm^3 denser than the continental block, reflecting an assumption that the accreted block consists of slightly more mafic rocks. The effect of varying this density contrast by various intervals, from 0.02 to 0.1 g/cm^3, is indicated by dashed lines in the graph at the upper left of figure 13.7*A*. The density of the upper mantle is assumed to be 3.0 g/cm^3. The geometry of the suture zone was varied to simulate a vertical con-

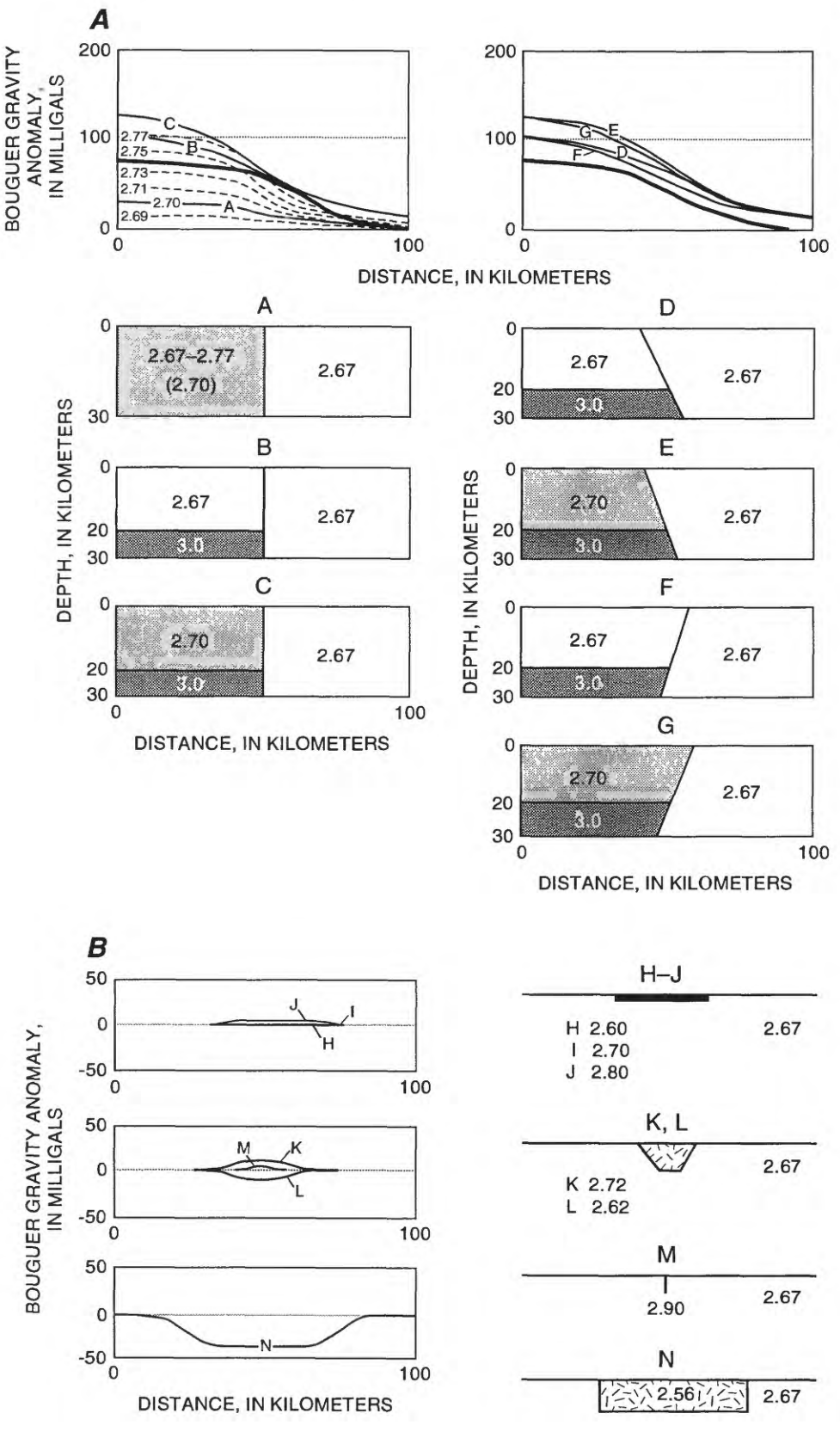

FIGURE 13.7.—Generalized models of Bouguer gravity anomalies produced by various geologic elements observed or inferred in study area. Numbers to two decimal places are densities in g/cm^3. *A*, Models showing effects of variations in crustal thickness, crustal density, and suture-zone orientation. Accreted crust shown on left, continental crust on right. In two graphs at top of figure 13.7*A*, solid lines labeled with letters show anomalies that correspond to lettered cross sections. Dashed lines are anomalies produced by varying differences in density between accreted crust and continental crust in model A; dashed lines are labeled with densities postulated for accreted crust. Heavy solid line in each graph shows representative anomaly across suture zone in west-central Idaho. *B*, Models showing effects of near-surface geologic bodies. Models H through J show effects of variations in density of slab of Columbia River Basalt Group 30 km wide by 1 km thick. Models K and L represent suture-zone plutons of same size (20 km wide at top, 10 km wide at bottom, and 8 km thick) but different densities. Model M represents vertical high-density body such as sliver of mafic rocks 1 km wide by 5 km deep; model N represents low-density body 50 km wide by 10 km thick emplaced in upper crust, such as Idaho batholith. In cross sections, density values on left are for near-surface geologic bodies and those on right for enclosing continental crust.

tact (models A–C), inclined subduction (models D and E), and inclined obduction (models F and G). The heavy line on each of the two graphs at the top of figure 13.7*A* shows a representative section across the suture zone in west-central Idaho. The effects of an abrupt contrast in crustal thickness across the suture zone were studied on all three geometries using crustal thicknesses as indicated in seismic-refraction studies (Smith, 1978; Allenby and Schnetzler, 1983; Sheriff and Stickney, 1984): 20 km for the accreted-terrane assemblage and 30 km for the continent. As summarized in figure 13.7*A*, the overall shape of the gravity anomaly varies with each change in variables, but the long wavelength and the total change in gravity remain similar. If a simple density contrast of 0.03 g/cm^3 is applied (model A), the resulting anomaly is about 30 mGal with a wavelength of more than 50 km. If a corresponding 10-km change in crustal thickness is applied (model C), the magnitude of the gradient is increased to approximately 100 mGal and the wavelength to 80 km. Increasing either the density contrast between the two blocks to 0.1 g/cm^3 or the density of the upper mantle component to 3.4 g/cm^3 (simulating more mafic mantle) causes the anomaly to increase by another 100 mGal. Reducing the thickness contrast across the suture would reduce the gravity anomaly accordingly.

This series of models demonstrates that several combinations of differences in crustal composition and thickness and in underlying components associated with the suture zone will result in gravity anomalies that are about 100 mGal or greater. Such configurations are characterized by the long wavelength of the anomalies observed in the study area.

Near-surface geologic bodies are characterized by sharp, short-wavelength anomalies whose magnitude is directly proportional to the density contrast between the body and the surrounding background material. Near-surface geologic bodies in west-central Idaho include the Columbia River Basalt Group, suture-zone plutons, and the Idaho batholith; models of these bodies are shown in figure 13.7*B*.

Several models were developed to estimate the influence of the rocks of the Columbia River Basalt Group in the study area. For these models, H through J on figure 7.13*B*, we assumed the presence of a tabular basalt body 1,000 m thick and varied the density of the body to examine the influence of changes in density in the basalt section. Three densities were used for the basalt body: 2.60 g/cm^3 (model H) to simulate basalt with numerous, less dense sedimentary interbeds; 2.70 g/cm^3 (model I) to simulate basalt with a few sedimentary interbeds; and 2.80 g/cm^3 (model J) to simulate basalt with no sedimentary interbeds. A density of 2.67 g/cm^3 was assumed for the surrounding rock. As shown in figure 13.7*B*, gravity anomalies generated by these parameters are of negligible significance on the scale of the anomalies observed in this study. If the basalt body is assumed to be wedge-shaped the generated anomaly is even less significant.

Suture-zone plutons, such as the Kamiah pluton or Blacktail stock, are represented by models K and L on figure 13.7*B*. The sign of the anomaly is positive if the body is more dense and negative if the body is less dense than the background material. These models assume that the suture-zone pluton is limited in lateral and vertical extent and that the background material has a density of 2.67 g/cm^3. The gravity anomaly produced by a body that is 0.05 g/cm^3 more dense (2.72 g/cm^3) or 0.05 g/cm^3 less dense (2.62 g/cm^3) than the background material has a magnitude of about 10 mGal.

Pods of mafic or ultramafic rocks caught in the accreted-terrane assemblage, or in the suture zone itself, may be responsible for some of the gravity highs outboard of the suture zone. Such a feature is represented by model M on figure 13.7*B*, where the pod is assumed to be a body 1 km wide by 5 km deep with a density of 2.90 g/cm^3 set in a matrix of country rock with a density of 2.67 g/cm^3. This configuration produces a very sharp gravity anomaly of 8 mGal, which is very similar to the anomalies observed in the northern portion of the study area. This anomaly is much sharper than those produced by the deeper crustal differences across the suture zone (fig. 13.7*A*).

Anomalies generated by relatively thick upper-crustal bodies of low-density material, such as the Idaho batholith, are more like the anomalies observed in west-central Idaho. A model of such an anomaly, N on figure 13.7*B*, assumes the same background density as continental crust (2.67 g/cm^3), and places a body 10 km thick and 0.11 g/cm^3 less dense (2.56 g/cm^3) into the upper crust. The geometry of the lighter body was not varied because such variation would only affect the shape of the anomaly, and not its magnitude. The importance of this model is that it might explain why the gradient observed in west-central Idaho follows the western margin of the Idaho batholith. It does not, however, explain why the gradient crosses to the west of the suture zone as defined by strontium ratios in the central part of the study area. This model also does not explain the magnitude of the anomaly in the southern part of the study area unless one assumes an unrealistically thick batholith.

The approach of identifying possible anomaly sources is appropriate for areas where the gravity data are relatively coarse and there is geologic con-

trol to guide the interpretation. As applied to the anomalies observed in the study area, these models represent a qualitative analysis of the relation between the anomalies and the geologic elements to which they are tentatively correlated. Where gravity anomalies are more tightly constrained, the general models may be supplemented with a specific model generated to match the anomalies in the field data. Johnson and others (1988) and Mohl (1989) generated such models for four detailed traverses in the north-central portion of the study area.

A detailed model (fig. 13.8) developed on a north-south profile at a longitude of 117° W. near the Idaho-Washington border utilizes the high-resolution Washington gravity data. The geology of the model is constrained by exposures of the Idaho batholith at the north end of the profile and the Columbia River Basalt Group in the central and southern parts. It is also weakly constrained by the projection, near the center of the profile, of the suture zone delineated by initial $^{87}Sr/^{86}Sr$ ratios. The anomalies observed along this profile may be generated with the combination of a relatively light body (model N, fig. 13.7) and two north-dipping dense bodies (model M, fig. 13.7). Variations in crustal thickness or composition are poorly constrained and not consistent with the gravity anomalies observed. Thus, they are not included in this model. The basalt section was not included due to the relative insignificance of the anomaly it generates. Note that any gravity model matched to field data, such as that shown in figure 13.8, provides only a first approximation of the anomaly-producing bodies and is not a unique solution.

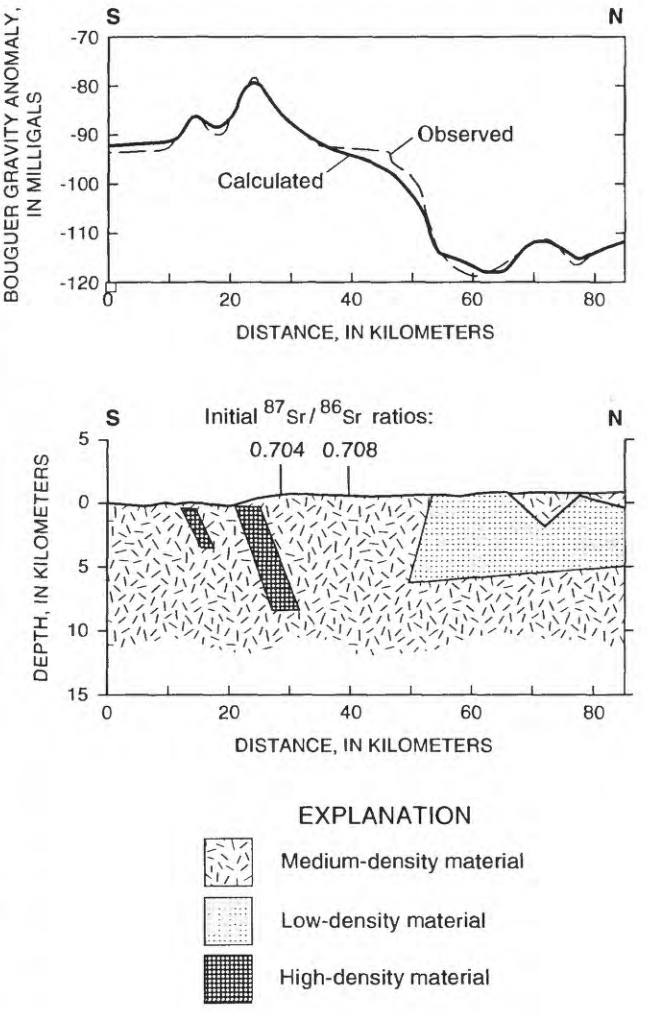

FIGURE 13.8.—Model of Bouguer gravity along Idaho-Washington border. Field observations shown with dashed line; calculated gravity anomaly with solid line. The model includes high- and medium-density slivers along the boundary zone, which lies between the initial $^{87}Sr/^{86}Sr$ ratio values of 0.704 and 0.708 near the center of the profile. It also includes a less dense body in the upper crust associated with outlier plutons of the Idaho batholith.

INTERPRETATION

The models in figure 13.7 indicate that there are two general classes of gravity anomalies that may be associated with the geologic features of the suture zone. The first group consists of relatively narrow and sharp anomalies that are limited to less than 30 mGal (fig. 13.7*B*). These types of anomalies can only be created by near-surface bodies that are isolated and have distinctly different densities than the surrounding country rock. The second group consists of broad, long-wavelength anomalies that may display a total change in gravity of greater than 30 mGal (fig. 13.7*A*). The magnitude of the anomaly produced by this type of feature depends on the size of the density contrast, the difference in crustal thickness, and the density of the underlying crustal material.

The suture zone in the northern part of the study area is characterized by two distinct regional gravity signatures: (1) a relatively steep gradient of 20 mGal in the east-west part of the suture zone west of Orofino, Idaho, and (2) a true paired-anomaly gravity signature with a regional high and a regional low separated by a gradient in the north-south part of the suture zone immediately south of Orofino. The location, wavelength, and magnitude of the gradient between the regional high and low suggest that this gradient is due in part to differences in composition and (or) thickness of the crust on either side of the suture zone. The gradient is also due in part to large-scale, near-surface features such as the Idaho batholith. Several anomalies superimposed on the gradient

appear to originate in the near surface on the basis of their relatively small size and sharp features. They are explained as representing isolated bodies of rock emplaced in the upper part of the crust within or near the suture zone, such as the Kamiah pluton and amphibole-rich plutons. The relatively steep gradient of 20 mGal in the east-west part of the suture zone west of Orofino appears to be due entirely to near-surface bodies. The magnitude and shape of this anomaly indicate that it does not represent differences on the crustal scale, unless those differences are offset by other geologic effects such as crustal thinning of continental North America, as discussed by Mohl (1989).

Interpretation of the gravity signature of the central part of the study area is difficult because the gradient crosses the suture zone defined by initial $^{87}Sr/^{86}Sr$ ratios. This apparent lack of correlation between the gravity signature and the suture zone leads to several possible interpretations: (1) geologic elements overprint the signature of the suture zone, (2) the geometry of the suture zone changes at depth, (3) the geophysical characteristics of the material within the suture zone vary along the suture zone, or (4) the apparent intersection of gradient and suture zone is simply a relict of the relatively coarse level of data available for this area. The magnitude and shape of the gradient suggest that the gravity signature is due at least in part to crustal differences on either side of the gradient. However, the complex geology that has been observed on the surface in this part of the study area indicates that contributions from near-surface elements are to be expected. Significantly more geophysical and density data are needed to evaluate interpretations.

The gravity signature in the southern part of the study area is a long-wavelength anomaly overprinted by a sharper gradient near the suture zone defined by initial $^{87}Sr/^{86}Sr$ ratios. The long wavelength and large magnitude of the gradient indicate a significant contribution from crustal-scale anomaly sources as demonstrated by the theoretical models in figure 13.7*A*. Probable upper-crustal sources include contrasts in thickness and density that are larger than the gravity data indicate farther to the north. The superimposed gradient is most likely related to the western edge of the Idaho batholith. This sharper anomaly also coincides with the abrupt change in character of the magnetic anomalies. To the west, several isolated gravity highs that do not correlate with any surface features probably define other near-surface elements, but more detailed gravity data are needed before these highs can be adequately analyzed.

CONCLUSIONS

Gravity studies in west-central Idaho and southeastern Washington delineate the suture zone between an assemblage of accreted terranes and continental North America as a marked change in regional gravity values and closely associated suture-zone anomalies. The character of the observed gravity anomalies varies within the study area. In the northern part, the signature is a classic regional high-low paired anomaly with local highs superimposed near the suture zone. The gradient between the regional high and low does not always coincide with the suture zone defined by initial $^{87}Sr/^{86}Sr$ ratios, as is evident in the central part of the study area where the gradient crosses the suture zone. In the southern part of the study area, the broad gradient that separates the high and low in the regional paired anomaly does coincide with the suture zone and steepens there. Isolated highs outboard of the suture zone are also observed in this part of the study area.

Correlation of these anomalies to geologic features, magnetic anomalies, and theoretical models indicates that the primary source of the lows in the northern part of the study area is probably the Idaho batholith, whose effects are superimposed on contrasts in crustal thickness and (or) composition. The highs are probably related to near-surface mafic and ultramafic bodies caught in or near the suture zone. Lack of correlation in the central part of the study area may be due simply to the relatively coarse level of gravity data available, or it may be related to geologic elements that are not reflected in the Sr analyses. Gravity anomalies in the southern part of the study area appear to be related to differences in crustal composition or thickness that have been overprinted by the effects of the Idaho batholith.

In southeastern Washington, geologic control is limited to a few isolated exposures, but detailed gravity data closely define the suture zone by extending the anomaly signature observed in Idaho. This signature can be traced approximately 60 km west of the Idaho-Washington border, where it becomes more poorly defined due to thicker basalt cover. It is still identifiable to the north in the east-central Columbia plateau, approximately 25 to 35 km north of Washtucna (fig. 13.1; Johnson and others, 1989, Thiessen and others, 1992). However, rocks that appear to have a continental affinity have been sampled with a drill hole 23 km west of the southwest corner of figure 13.6 (Reidel and others, 1994; Sobczyk, 1994), indicating that the boundary zone may extend to the southwest from anomaly B2 through the southern

anomaly F (fig. 13.6). In northeastern Washington and British Columbia, accreted terranes are thought to have been thrust over a wedge of continental material. This relationship may extend directly to the south under the Columbia River Basalt Group. The gravity anomaly discussed by Johnson and others (1989) and Thiessen and others (1992) aligns with the eastern limit of the accreted terranes in northeastern Washington and British Columbia. The cratonic margin defined by Reidel and others (1994) and Sobczyk (1994) corresponds to the western limit of the wedge of continental crust.

Further definition of the tectonic significance of these gravity anomalies in west-central Idaho and southeastern Washington requires that significantly higher resolution data be acquired. In west-central Idaho, detailed gravity traverses across the suture zone have been studied and modelled (Mohl, 1989) in order to more accurately define the signature where it is constrained by better exposure. In Washington, higher resolution gravity data are needed to further define the westward extension of the suture zone (Johnson and others, 1989; Thiessen and others, 1992). This definition is particularly crucial for determining the point where the suture zone returns to a north-south orientation; such a determination is vital to tectonic models developed for the region.

REFERENCES CITED

Aliberti, E.A., and Manduca, C.A., 1988a, Field guide to a transect across an island arc-continent boundary in west-central Idaho: Montana Bureau of Mines and Geology Special Publication 96, p. 181-189.

———1988b, A transect across an island arc-continent boundary in west-central Idaho: Idaho Geologic Survey Bulletin 27, p. 99-107.

Allenby, R.J., and Schnetzler, C.C., 1983, United States crustal thickness: Tectonophysics, v. 93, p. 13-31.

Armstrong, R.L., 1975, Precambrian (1,500-m.y. old) rocks of central Idaho—The Salmon River Arch and its role in Cordilleran sedimentation and tectonics: American Journal of Science, v. 275-A, p. 437-467.

Armstrong, R.L., Taubeneck, W.H., and Hales, P.O., 1977, Rb-Sr and K-Ar geochronometry of Mesozoic granitic rocks and their Sr isotopic composition, Oregon, Washington, and Idaho: Geologic Society of America Bulletin, v. 88, p. 397-411.

Bankey, V., Webring, M., Mabey, D.R., and Kleinkopf, D., 1984, Complete Bouguer gravity anomaly map of Idaho: Idaho Bureau of Mines and Geology, scale, 1:500,000.

Blake, D.E., 1991, Geology of the western Idaho suture zone in the Salmon River Gorge, west-central Idaho: Pullman, Washington State University, Ph.D. dissertation, 330 p.

Blake, D.E., and Thiessen, R.L., in press, Tectonic implications of flattening fabrics in the western Idaho suture zone along the Salmon River gorge near Riggins, Idaho: Geologic Society of America special paper.

Bond, J.G., and Wood, C.H., 1978, Geologic map of Idaho: Idaho Bureau of Mines and Geology, scale, 1:500,000.

Bonnichsen, B., 1987, Pre-Cenozoic geology of the West Mountain-Council Mountain-New Meadows area, west-central Idaho: U.S. Geological Survey Professional Paper 1436, p. 151-170.

Brooks, H.C., 1979, Plate tectonics and the geologic history of the Blue Mountains: Oregon Geology, v. 41, no. 5, p. 71-80.

Brooks, H.C., and Vallier, T.L., 1978, Mesozoic rocks and tectonic evolution of eastern Oregon and western Idaho, *in* Howell, D.G., and McDougall, K.A., eds., Mesozoic paleogeography of the Western United States (Pacific Coast Paleogeography Symposium 2): Los Angeles, Society of Economic Paleontologists and Mineralogists, Pacific Section, p. 133-146.

Cady, J.W., and Fox, K.F., 1984, Geophysical interpretation of the gneiss terrane of northern Washington and southern British Columbia, and its implications for uranium exploration: U.S. Geological Survey Professional Paper 1260, 29 p.

Camp, V.W., 1976, Petrochemical stratigraphy and structure of the Columbia River Basalt, Lewiston Basin area, Idaho-Washington: Pullman, Washington State University, Ph.D. dissertation, 201 p.

Cavin, R.E., 1964, Significance of the intrabasalt sediments in the Moscow Basin, Idaho: Pullman, Washington State University, M.S. thesis, 91 p.

Catchings, R.D., and Mooney, W.D., 1988, Crustal structure of the Columbia plateau: Evidence for continental rifting: Journal of Geophysical Research, v. 93, no. B1, p. 459-474.

Cook, F.A., 1984, Towards an understanding of the southern Appalachian Piedmont crustal transition: A multidisciplinary approach: Tectonophysics, v. 109, p. 77-92.

Criss, R.E., and Champion, D.E., 1984, Magnetic properties of granitic rocks from the southern half of the Idaho batholith: Influences on hydrothermal alteration and implications for aeromagnetic interpretation: Journal of Geophysical Research, v. 89, p. 7061-7076.

Criss, R.E., and Fleck, R.J., 1987, Petrogenesis, geochronology, and hydrothermal systems of the northern Idaho batholith and adjacent areas based on $^{18}O/^{16}O$, D/H, $^{87}Sr/^{86}Sr$, K-Ar, and $^{40}Ar/^{39}Ar$ studies: U.S. Geological Survey Professional Paper 1436, p. 95-137.

Dainty, A.M., and Frazier, J.E., 1984, Bouguer gravity in northeastern Georgia: A buried suture, a surface suture, and granites: Geological Society of America Bulletin, v. 95, p. 1168-1175.

Davidson, G.F., 1988, Field guide to mylonitic rocks west of Orofino, Idaho: Montana Bureau of Mines and Geology Special Publication 96, p. 171-174.

Fisher, M.A., and von Huene, Roland, 1984, Geophysical investigation of a suture zone: The Border Ranges fault of southern Alaska: Journal of Geophysical Research, v. 89, p. 11,333-11,351.

Fleck, R.J., and Criss, R.E., 1985, Strontium and oxygen isotopic variations in Mesozoic and Tertiary plutons of central Idaho: Contributions to Mineralogy and Petrology, v. 90, p. 291-308.

———1988, Location, age and tectonic significance of the western Idaho suture zone (WISZ) and its relation to the Idaho batholith [abs.]: Geologic Society of America Abstracts with Programs, v. 20, p. 414.

Fountain, D.M., and Salisbury, M.H., 1981, Exposed cross-sections through the continental crust: Implications for crustal structure, petrology, and evolution: Earth and Planetary Science Letters, v. 56, p. 263-277.

Gibb, R.A., and Thomas, M.D., 1976, Gravity signature of fossil plate boundaries in the Canadian shield: Nature, v. 262, p. 199-200.

Gregory, D.I., and Jackson, D.B., 1976, Bouguer gravity map of Moscow, Idaho-Pullman, Washington area: U.S. Geological Survey Open-File Report 76-280, scale 1:62,500.

Hamilton, W.B., 1963, Metamorphism in the Riggins region, western Idaho: U.S. Geological Survey Professional Paper 436, 95 p.

———1969, Reconnaissance geologic map of the Riggins quadrangle, west-central Idaho: U.S. Geological Survey Map I-579.

Hietanen, Anna, 1962, Metasomatic metamorphism in western Clearwater County, Idaho: U.S. Geological Survey Professional Paper 344-A, 116 P.

Hill, D.P., 1972, Crustal and upper-mantle structure of the Columbia plateau from long-range seismic-refraction measurements: Geological Society of America Bulletin, v. 83, p. 1639-1648.

———1978, Seismic evidence for the structure and Cenozoic tectonics of the Pacific coast states: Geological Society of America Memoir, v. 152, p. 145-174.

Hooper, P.R., 1982, The Columbia River Basalts: Science, v. 215, p. 1463-1468.

Hutchinson, D.R., Grow, J.A., and Klitgord, K.D., 1983, Crustal structure beneath the southern Appalachians: Nonuniqueness of gravity modeling: Geology, v. 11, p. 611-615.

Hyndman, D.W., 1979, Major tectonic elements and tectonic problems along the line of section from northeastern Oregon to west-central Montana—Map summary: Geological Society of America Bulletin, Part 1, v. 90, p. 715-718.

———1983, The Idaho batholith and associated plutons, Idaho and western Montana: Geological Society of America Memoir 159, p. 213-240.

International Association of Geodesy, 1967, Systeme geodesique de reference 1967: International Association of Geodesy Special Publication No. 3, 115 p.

Johnson, K.R., Mohl, G.B., and Thiessen, R.L., 1988, Gravity signatures of suture zones: A comparison between the island arc-continent boundary in Idaho and the Montagua suture of Guatemala [abs.]: Geologic Society of America Abstracts with Programs, v. 20, p. 423.

Johnson, K.R., Thiessen, R.L., and Parodi, M.R., 1989, Geophysical constraints on the location of the cratonic margin beneath the Columbia plateau [abs.]: Geologic Society of America Abstracts with Programs, v. 21, p. 98.

Johnson, R.A., Karlstron, K.E., Smithson, S.B., and Houston, R.S., 1984, Gravity profiles across the Cheyenne belt, a Precambrian crustal suture in southeastern Wyoming: Journal of Geodynamics, v. 1, p. 445-472.

Karner, G.D., and Watts, A.B., 1983, Gravity anomalies and flexure of the lithosphere at mountain ranges: Journal of Geophysical Research, v. 88, p. 10,449-10,477

Keller, M.R., Robinson, E.S., and Glover, L., 1985, Seismicity, seismic refraction, gravity, and geology of the central Virginia seismic zone—Part 3. Gravity: Geological Society of America Bulletin, v. 96, p. 1580-1584.

Lim, J.B., 1986, Structural relationship between paleomagnetic trends and remote sensing data on the Pomona Basalt flow: Pullman, Washington State University, M.S. thesis, 144 p.

Lin, C.L., 1967, Factors affecting ground-water recharge in the Moscow Basin, Latah County, Idaho: Pullman, Washington State University, M.S. thesis, 86 p.

Lund, Karen, 1988, The Salmon River suture, western Idaho: An island arc-continent boundary: Montana Bureau of Mines and Geology Special Publication 96, p. 103-110.

Lund, Karen, and Snee, L.W., 1988, Metamorphism, structural development, and age of the continent island arc juncture in west-central Idaho, *in* Ernst, W.G., ed., Metamorphism and crustal evolution, western conterminous United States (Rubey Volume VII): Englewood Cliffs, New Jersey, Prentice Hall, p. 296-331.

Lund, Karen, Snee, L.W., and Davidson, G.F., 1990, Comment on "Direction and shear sense during suturing of the Seven Devils-Wallowa terrane against North America in western Idaho": Geology, v. 18, p. 1031.

Mabey, D.R., Zietz, I., Eaton, G.P., and Kleinkopf, M.D., 1978, Regional magnetic patterns in part of the Cordillera in the western United States: Geological Society of America Memoir 152, p. 93-106.

Manduca, C.A., Kuntz, M.A., and Silver, L.T., 1993, Emplacement and deformation history of the western margin of the Idaho batholith near McCall, Idaho: Influence of a major terrane boundary: Geological Society of America Bulletin, v. 105, p. 749-765.

Manduca, C.A., Silver, L.T., and Taylor, H.P., 1992, $^{87}Sr/^{86}Sr$ and $^{18}O/^{16}O$ isotopic systematics and geochemistry of granitoid plutons across a steeply dipping boundary between contrasting lithospheric blocks in western Idaho: Contributions to Mineralogy and Petrology, v. 109, p. 355-372.

Mohl, G.B., 1985, Bouguer gravity investigation of the cratonic margin—Southeastern Washington: Pullman, Washington State University, M.S. thesis, 67 p.

———1987, Land gravity data, southeast Washington State Source no. 7564: Defense Mapping Agency, Gravity Library Services, St. Louis, MO 63118-3399.

———1989, Gravity expression of the west Idaho suture zone: West central Idaho: Pullman, Washington State University, Ph.D. dissertation, 107 p.

Mohl, G.B., and Thiessen, R.L., 1985, Subsurface structure in southeastern Washington as defined by Bouguer gravity measurements [abs]: Geological Society of America Abstracts with Programs, v. 17, p. 370.

Morelli, C., ed., 1974, The International Gravity Standardization Net 1971: International Association of Geodesy Special Publication No. 4, 194 p.

Myers, C.W., and Price, S.M., 1979, Geologic studies of the Columbia plateau: A status report: Rockwell Hanford Operations, RHO-BWI-ST-4.

Myers, P.E., 1982, Geology of the Harpster area, Idaho County, Idaho: Idaho Bureau of Mines Geology Bulletin, v. 27, 46 p.

Onasch, C.M., 1979, Multiple folding along the western margin of the Idaho batholith in the Riggins, Idaho, area: Northwest Geology, v. 8, p. 94-100.

———1987, Temporal and spatial relations between folding, intrusion, metamorphism, and thrust faulting in the Riggins area, west-central Idaho: U.S. Geological Survey Professional Paper 1436, p. 139-149.

Phole, J.A., 1979, Geophysical investigation of the Uniontown Plateau, Washington: Pullman, Washington State University, M.S. thesis, Pullman, 130 p.

Price, R.A., and Hatcher, R.D., Jr., 1983, Tectonic significance of similarities in the evolution of the Alabama-Pennsylvania Appalachians and the Alberta-British Columbia Canadian Cordillera: Geological Society of America Memoir 158, p. 149-160.

Reidel, S.P., Campbell, N.P., Fecht, K.R., and Lindsey, K.A., 1994, Late Cenozoic structure and stratigraphy of south-central Washington: Washington Division of Geology and Earth Resources Bulletin 80, p. 159-180.

Riddihough, R.P., Finn, C., and Couch, R., 1986, Klamath-Blue Mountain lineament, Oregon: Geology, v. 14, p. 528-531.

Robbins, S.L., Martinez, R.J., and Smith, D.L., 1979, Principal facts for borehole gravity stations in wells DC-3, DC-5, DC-7 at the Hanford Site, Washington, and in well RSH #1 Rattle-

snake Hills, Washington: U.S. Geological Survey Open-File Report 79-849.

Schmidt, B., Daly, W.F., Bradley, S.W., and Squire, P.R., 1980, Thermal and mechanical properties of Hanford basalts—Compilation and analysis: Rockwell Hanford Operations RHO-BWI-C-90.

Selverstone, J., Wernicke, B.P., and Aliberti, E.A., 1992, Intracontinental subduction and hinged unroofing along the Salmon River suture zone, west central Idaho: Tectonics, v. 11, p. 124-144.

Sharma, P.V., 1976, Geophysical methods in geology: New York, Elsevier, 428 p.

Sheriff, S.D., and Stickney, M.G., 1984, Crustal structure of southwestern Montana and east-central Idaho—Results of a reversed seismic refraction line: Geophysical Research Letters, v. 11, no. 4, p. 299-302.

Smith, B.J., 1979, Geophysical investigations in the Moscow-Troy area, Idaho: Pullman, Washington State University, M.S. thesis, 246 p.

Smith, R.B., 1978, Seismicity, crustal structure, and intraplate tectonics of the interior of the Western Cordillera: Geological Society of America Memoir 152, p. 111-144.

Sobczyk, S.M., 1994, The structures of the upper crust and crustal thicknesses of the Columbia plateau: Inferred from selected geophysical studies: Pullman, Washington State University, Ph.D. dissertation, 220 p.

Strand, J.R., 1949, Structural geology of pre-Tertiary rocks in southeastern Washington and adjacent portions of Idaho: Pullman, Washington State University, M.S. thesis, 25 p.

Strayer, L.M., IV, 1988, Field guide to deformation and sense of displacement in mylonitic rocks near Orofino, Idaho: Montana Bureau of Mines and Geology Special Publication 96, p. 165-169.

Strayer, L.M., IV, Hyndman, D.W., and Sears, J.W., 1987, Movement direction and displacement estimate in the western Idaho suture zone mylonite: Dworshak Dam/Orofino area, west central Idaho [abs.]: Geologic Society of America Abstracts with Programs, v. 19, p. 857.

Strayer, L.M., IV, Hyndman, D.W., Sears, J.W., and Myers, P.E., 1989, Direction and shear sense during suturing of the Seven Devils-Wallowa terrane against North America in western Idaho: Geology, v. 17, p. 1025-1028.

———1990, Reply on "Direction and shear sense during suturing of the Seven Devils-Wallowa terrane against North America in western Idaho": Geology, v. 18, p. 1031-1032.

Swanson, D.A., Wright, T.L., Camp, V.E., Gardner, J.N., Heltz, R.T, Price, S.M., Reidel, S.P., and Ross, M.E., 1980, Reconnaissance geologic map of the Columbia River Basalt Group, Pullman and Walla Walla quadrangles, southeast Washington and adjacent Idaho: U.S. Geological Survey Miscellaneous Investigations Map I-1139, scale 1:250,000.

Talwani, M., Worzel, J.L., and Landisman, M., 1959, Rapid gravity computations for two-dimensional bodies with application to the Mendocino submarine fracture zones: Journal of Geophysical Research, v. 64, p. 49-59.

Telford, W.M., Geldart, L.P., Sheriff, R.E., and Keys, D.A., 1976, Applied geophysics: New York, Cambridge University Press, 859 p.

Thiessen, R.L., 1986, GRVPRF—Gravity profiles on an HP9845, *in* National Association of Geology Teachers Special Publication, Computer software designed for use in undergraduate geologic education: p. 171-177.

Thiessen, R.L., Johnson, K.R., and Mohl, G.B., 1992, Geophysical investigations of the cratonic margin in the Pacific Northwest *in* Bartholomew, M.J., Hyndman, D.W., Mogk, D.W., and Mason, R., eds., Basement tectonics 8: Characterization and comparison of ancient and Mesozoic continental margins: Boston, Kluwer Academic Publishers, p. 231-240.

Thiessen, R.L., Mohl, G.B., and Lim, J.B., 1986, Geophysical investigations of southeastern Washington [abs.]: Tobacco Root Geological Society Abstracts with Programs, p. 17-18.

Thomas, M.D., 1983, Tectonic significance of paired gravity anomalies in the southern and central Appalachians: Geological Society of America Memoir 158, p. 113-124.

Thomas, M.D., Grieve, R.A.F., and Sharpton, V.L., 1988, Gravity domains and assembly of the North American continent by collisional tectonics: Nature, v. 331, p. 333-334.

Vallier, T.L., 1977, The Permian and Triassic Seven Devils Group: U.S. Geological Survey Bulletin 1437, 58 p.

Vallier, T.L., Brooks, H.C., and Thayer, T.P., 1977, Paleozoic rocks of eastern Oregon and western Idaho, *in* Stewart, J.H., Stevens, C.H., and Fritsche, A.E., eds., Paleozoic paleogeography of the Western United States (Pacific Coast Paleogeography Symposium 1): Los Angeles, Society of Economic Paleontologists and Mineralogists, Pacific Section, p. 455-466.

Wiswal, C.G., and Hyndman, D.W., 1987, Emplacement of the Bitterroot lobe of the Idaho batholith: U.S. Geological Survey Professional Paper 1436, p. 59-72.

Yost, C.R., and Steele, W.K., 1978, Gravity survey of the Cheney quadrangle, Washington: Northwest Science, v. 52, p. 250-260.

Zervas, C.E., and Crosson, R.S., 1986, Pn observation and interpretation in Washington: Bulletin of the Seismological Society of America, v. 76, p. 521-546.

Zietz, I., Gilbert, F.P., and Kirby, J.R., 1978, Aeromagnetic map of Idaho: U.S. Geological Survey Geophysical Investigations Map GP-919, scale 1:500,000.

Zietz, I., Hearn, B.C., Jr., Higgins, M.W., Robinson, G.D., and Swanson, D.A., 1971, Interpretation of an aeromagnetic strip across the northwestern United States: Geological Society of America Bulletin, v. 82, p. 3347-3372.

14. METAMORPHIC AND STRUCTURAL DEVELOPMENT OF ISLAND-ARC ROCKS IN THE SLATE CREEK-JOHN DAY CREEK AREA, WEST-CENTRAL IDAHO

By KAREN LUND

CONTENTS

Abstract ---- 517
Introduction ---- 517
Acknowledgment ---- 519
Rocks of the Blue Mountains island arc ---- 519
  Rocks of the Wallowa terrane ---- 521
    Seven Devils Group ---- 521
    Upper Triassic Martin Bridge Formation ---- 521
      Stratigraphy ---- 521
      Correlation ---- 523
    Metamorphosed rocks of uncertain age ---- 525
      Rapid River plate ---- 525
        Description of rocks ---- 525
        Proposed correlation ---- 526
      North Fork block ---- 526
        Description of rocks ---- 526
        Proposed correlation ---- 527
Late Cretaceous crosscutting plutonic rocks ---- 527
  Rock units ---- 528
  Isotopic ages ---- 528
Metamorphic history ---- 528
  Description ---- 529
  Ages of metamorphism ---- 530
Structure ---- 530
  Fabrics and geometries ---- 530
  Ages ---- 534
Discussion ---- 535
Conclusions ---- 536
References cited ---- 538

ABSTRACT

Metamorphosed volcanic island-arc rocks of the Slate Creek-John Day Creek area of western Idaho are bounded on the east by the Salmon River suture, the structure that separates these oceanic rocks from North American continental rocks to the east. The island-arc rocks are characterized by multiple overprints of medium- to high-grade metamorphism and multiple phases of deformation, all of which were caused by late Early to Late Cretaceous movement along the Salmon River suture as the oceanic rocks were being accreted to the North American continent. The island-arc rocks occur as three imbricated tectonostratigraphic units that probably originated as part of the Blue Mountains island arc but are now part of a complex, inverted metamorphic sequence. At the bottom of the sequence are the lowest grade metamorphic rocks in the study area; these are part of the Wallowa terrane (the lower plate). This lower plate is composed of Lower Permian and Upper Triassic rocks of the Seven Devils Group as well as the Upper Triassic Martin Bridge Formation (here made up primarily of calcareous slate to schist containing marble lenses, minor metavolcanic rocks, and possible marble clast conglomerate). The middle tectonostratigraphic unit or plate, which is herein also called the Rapid River plate, generally is correlative with rocks previously called the Riggins Group; in this paper, rocks of the Rapid River plate are tentatively considered to be a tectonic slice of the Wallowa terrane. The uppermost tectonostratigraphic unit or plate, herein called the North Fork block, is multiply metamorphosed, deformed, and intruded and cannot definitely be correlated with known units.

Metamorphism of rocks in the study area began about 120 Ma and continued during deformation until about 90 Ma. Rocks in the North Fork block show conclusive evidence of overprinting amphibolite-facies events. The earliest observed deformation, which produced foliation, occurred with metamorphism about 120 Ma; multiple phases of megascopic deformation, which imbricated and folded the rocks, occurred from 109 to 90 Ma. A 90-Ma dynamothermal event caused the last observed metamorphic/deformational fabric in rocks in the North Fork block and juxtaposed the deep-seated rocks of this upper plate against shallower, earlier metamorphosed and deformed rocks of other plates. The earliest nonallochthonous plutons intruded across the Salmon River suture starting 93 m.y. ago; these are the first plutons of the Idaho batholith. Plutonic rocks in the North Fork block were strongly deformed together with the older wallrocks during the 90 Ma event; away from the Salmon River suture, these plutons (as well as younger plutons) are not strongly deformed.

INTRODUCTION

As recognized early (Lindgren, 1904), west-central Idaho is underlain by metamorphosed oceanic volcanic and volcaniclastic rocks that are directly juxtaposed against metamorphosed older terrigenous metasedimentary rocks. The Salmon River suture between these crustal blocks is everywhere intruded by Late Cretaceous plutons of the Idaho batholith and is covered by Miocene basalt along much of its length (fig. 14.1).

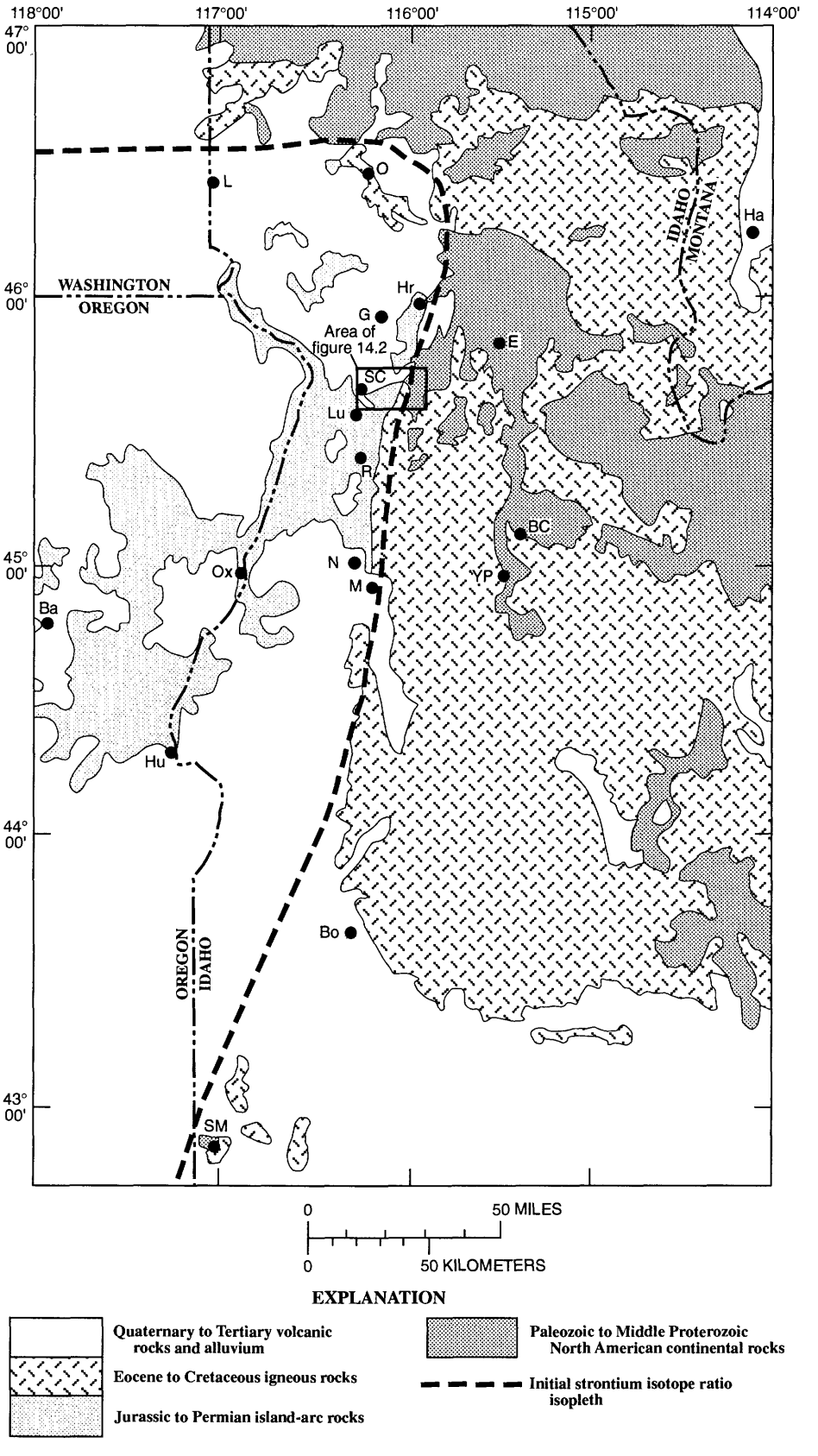
118°00'
117°00'
116°00'
115°00'
114°00'
47° 00'
46° 00'
45° 00'
44° 00'
43° 00'
WASHINGTON
OREGON
IDAHO
MONTANA
OREGON
IDAHO
L
O
Ha
Hr
G
Area of figure 14.2
E
SC
Lu
R
BC
N
Ox
YP
M
Ba
Hu
Bo
SM
0
50 MILES
0
50 KILOMETERS
EXPLANATION
Quaternary to Tertiary volcanic rocks and alluvium
Eocene to Cretaceous igneous rocks
Jurassic to Permian island-arc rocks
Paleozoic to Middle Proterozoic North American continental rocks
Initial strontium isotope ratio isopleth

The Slate Creek-John Day Creek area of western Idaho (fig. 14.2) is underlain by oceanic rocks west of an exposed segment of the Salmon River suture zone. This area contains the major rock types and deformational features commonly found along the suture. It has been mapped in detail (Lund, 1984; McCollough, 1984; Lund and others, 1993) and has been the subject of detailed dating studies (Snee and others, 1985; Snee and others, 1987; Snee and others, chap. 10, this volume). Data from these studies are the basis for this paper and the reader is referred to them for further details. Tectonic models to explain the metamorphic and structural geometry on both sides of the Salmon River suture (Lund, 1984) and the timing of these events were published by Lund and Snee (1988).

Several mechanisms for accretion of the oceanic rocks to North American continental rocks have been proposed: (1) subduction (Hamilton, 1976; Hyndman and Talbot, 1976; Onasch, 1977; Davis and others, 1978; Hillhouse and others, 1982), (2) dextral transpression along the Salmon River suture involving no subduction at this site of final suturing (Lund, 1984; Lund and Snee, 1988), and (3) collision penetration with subduction in western Idaho and tectonic escape to north (Wernicke and Klepacki, 1988; Selverstone and others, 1992). Prior to isotopic dating studies, estimates for the time of accretion were based on geologic constraints and range from Triassic to Cretaceous (Hamilton, 1963a; Brooks and Vallier, 1978; Dickinson and Thayer, 1978; Hillhouse and others, 1982; Lund, 1984; Wernicke and Klepacki, 1988). Dating of minerals from metamorphic rocks, which formed during suturing, indicates that orogenic events in the Salmon River suture zone occurred during the interval from 130 to 75 Ma (Sutter and others, 1984; Lund and Snee, 1988; Davidson, 1990; Getty and others, 1991).

ACKNOWLEDGMENT

This work was possible because of the guidance and inspiration of W.R. Greenwood, Robert Scholten, and Anna Hietanen.

◀ FIGURE 14.1.—General geology of Salmon River suture zone. Geology modified from Bond (1978), Brooks and Vallier (1978), Lund (1984), and McCollough (1984). Initial strontium isotope ratio line divides oceanic values of <0.704 (generally west of line) from continental values of >0.706 (generally east of line); isopleth was approximated from data published by Armstrong and others (1977) and by Fleck and Criss (1985). Ba, Baker City; BC, Big Creek; Bo, Boise; E, Elk City; G, Grangeville; Ha, Hamilton; Hr, Harpster; Hu, Huntington; L, Lewiston; Lu, Lucile; M, McCall; N, New Meadows; O, Orofino; Ox, Oxbow; R, Riggins; SC, Slate Creek; SM, South Mountain; YP, Yellow Pine.

ROCKS OF THE BLUE MOUNTAINS ISLAND ARC

Hamilton (1963a, 1969) provided the first comprehensive study of the oceanic rocks in western Idaho. He subdivided oceanic rocks near Riggins (fig. 14.1) into three stratigraphic sequences similar to the three tectonostratigraphic units used in the present study (fig. 14.3). The metamorphic, structural, and intrusive history of the tectonostratigraphic units is different enough to make it difficult to correlate map units among the three. The structurally lowest tectonostratigraphic unit is in stratigraphic continuity with Permian and Triassic rocks of the Wallowa terrane (Silberling and others, 1992) that is equivalent to the so-called Seven Devils island arc (Brooks and Vallier, 1978; Dickinson, 1979; Hillhouse and others, 1982) and that is one of four terranes grouped together and named the Blue Mountains island arc (Vallier and Brooks, 1986) of eastern Oregon and western Idaho. Thus, a large portion of the island-arc rocks of western Idaho are known to be part of the Wallowa terrane. The middle tectonostratigraphic unit is herein called the Rapid River plate; it contains rocks that are along strike with the Riggins Group (Hamilton, 1963a). The structurally uppermost tectonostratigraphic unit, herein called the North Fork block, consists of a complex of metavolcanic, metavolcaniclastic, and plutonic rocks; the premetamorphic-predeformation stratigraphy is not well preserved.

Rocks of the Riggins Group have been correlated in the past with rocks of the Baker and Izee terranes (Brooks and Vallier, 1978; Silberling and others, 1992) or with the Olds Ferry terrane (White and others, 1992), which are all part of the Blue Mountains island arc of eastern Oregon and westernmost Idaho. Rocks of the North Fork block have not been previously correlated with any particular terrane of eastern Oregon because these metavolcanic rocks were not previously mapped separately from younger plutonic rock (Hamilton, 1963a, c; 1969). These two structurally highest tectonostratigraphic units were also tentatively correlated to the Wallowa terrane (Lund, 1984; Lund and Snee, 1988; Lund and others, 1993) on the basis of the model that these metamorphosed and deformed rocks were the leading edge of the Wallowa terrane that underwent the most severe effects of accretion to North America. This correlation with the Wallowa terrane was also suggested by Onasch (1977) and Vallier (1977).

The oceanic terranes in Oregon and Idaho have been variously correlated to regional superterranes. In particular, the Wallowa terrane first was suggested to be a piece of the western British Columbian Wrangellia terrane (Jones and others, 1977; Hillhouse and

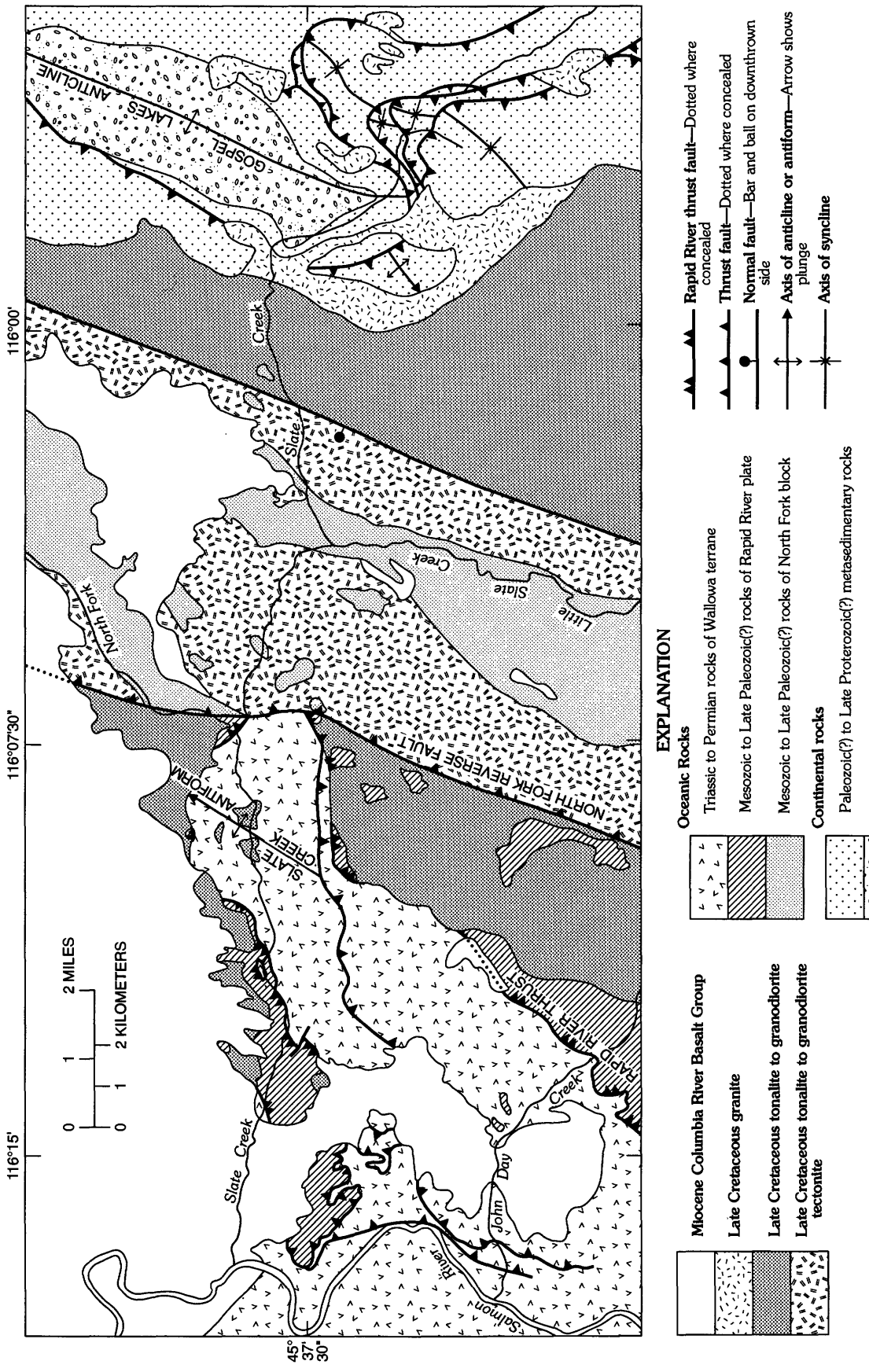

FIGURE 14.2.—Simplified geology of Slate Creek-John Day Creek area (modified from Lund, 1984; McCollough, 1984; Lund and others, 1993).

others, 1982) but more recently was argued to be correlative with the eastern British Columbian Stikinia terrane (Mortimer, 1986).

ROCKS OF THE WALLOWA TERRANE

SEVEN DEVILS GROUP

Volcanic rocks of the Seven Devils Group (included in "Triassic and Permian rocks of Wallowa terrane" unit in fig. 14.2; Vallier, 1977) crop out along the Salmon River near the mouth of John Day Creek and possibly as a small klippe in the Slate Creek drainage (Lund and others, 1993). Lithologically, these rocks consist of orange-weathering (green where fresh), massive metamorphosed tuffs and flows and metamorphosed volcanic conglomerate that consists of stretched volcanic clasts in a tuffaceous matrix. Recrystallized quartz, untwinned plagioclase, chlorite, tremolite, epidote, biotite, and muscovite make up the mineralogically variable fine-grained groundmass. Garnet and chlorite porphyroblasts are common; plagioclase occurs as both relict phenocrysts and metamorphic porphyroblasts. Marble layers less than 10 m thick in the upper part of the Seven Devils Group are known both in this area and in the Riggins area to the south (Hamilton, 1963a; Onasch, 1977).

A tonalitic to quartz dioritic pluton crops out in the Salmon River canyon (Hamilton, 1963a; McCollough, 1984; Lund and others, 1993). The mineralogy of the pluton is plagioclase, quartz, altered hornblende, and chloritized biotite. The isotopic age of the pluton is about 259 Ma as determined by U-Pb zircon methods on two splits (Walker, 1986). Foliations in the pluton and in the metavolcanic country rock are parallel, but the contact between the two units is discordant to the foliation. This pluton is therefore interpreted to have intruded one of the two Permian units of the Seven Devils Group prior to the metamorphic event that formed the foliation—probably during construction of the Blue Mountains island arc.

Although all of the four formations, which make up the Seven Devils Group elsewhere (fig. 14.3), have not been mapped in the Slate Creek-John Day Creek area, both the lower and upper parts of the group presumably crop out in the area. Because of the 259-Ma (Permian) age for the crosscutting pluton, the rocks of the Seven Devils Group that crop out along the Salmon River in this area (fig. 14.2) are presumably Early Permian. Either the Hunsaker Creek or Windy Ridge Formation could have been intruded by a 259-Ma pluton. Gradational stratigraphic contacts between the Seven Devils Group and the overlying calcareous phyllite (see section "Upper Triassic Martin Bridge Formation") indicate that the uppermost unit of the Seven Devils Group, the Upper Triassic Doyle Creek Formation, is also present in the study area. Others have reported a gradational upper contact for the Doyle Creek Formation in the Wallowa Mountains of eastern Oregon (Follo, 1994) and along the Snake River on the Oregon-Idaho boundary (fig. 14.1; Vallier, 1977). The base of the Seven Devils Group is not exposed in the study area.

UPPER TRIASSIC MARTIN BRIDGE FORMATION

About one-third of the Slate Creek-John Day Creek area is underlain by a sequence of Upper Triassic metasedimentary rocks. The top of this sequence, which is truncated by faulting, is not known to crop out in western Idaho. The lower part of the section crops out between Slate Creek and John Day Creek; here greenschist-facies metasedimentary rocks grade into the underlying metavolcanic rocks of the Seven Devils Group. Also included in this unit are amphibolite-facies rocks in the core of the northeast-plunging Slate Creek antiform that crosses Slate Creek in the study area (fig. 14.2).

STRATIGRAPHY

There are two major and two minor rock types in this metasedimentary section. The most common rock type is calcareous phyllite to schist with which the less common rock types are interbedded. The calcareous phyllite to schist is composed of calcite, plagioclase, biotite or phlogopite, muscovite, chlorite, rounded fine-grained quartz, epidote, and siderite cubes. It also contains disseminated fine graphite grains. At higher metamorphic grades, the schist contains abundant sphene, amphibole, and garnet; in the John Day Creek drainage, andalusite, kyanite, sillimanite, chloritoid, staurolite, and prochlorite are reported (E.H. Price, 1985, written commun.). Gray and white, fine- to coarse-grained calcite marble, which forms layers from 5 to 500 m thick, is the second most common lithology. At high metamorphic grade, the marble usually contains a few percent phlogopite and a trace of fine-grained graphite.

The two minor rock types are metavolcanic and conglomeratic rocks. Green, chloritic metavolcanic layers occur at several stratigraphic horizons and are composed of fine, interlocking grains of plagioclase that form the groundmass for porphyroblastic intergrowths of actinolite and chlorite. Fine grains of opaque minerals, quartz, sphene, and apatite are also present. Lenses of calcareous schist containing

multilithologic clasts (fig. 14.4) crop out in a few places. Although first interpreted to be fault breccia (Lund, 1984), the presence of more than one carbonate-clast rock type suggests that these diamictites were originally limestone-conglomerate lenses similar to those found in the Martin Bridge Limestone in the Wallowa Mountains, eastern Oregon (Follo, 1994).

As seen between the mouth of Slate Creek and the mouth of John Day Creek, the lower contact between the Upper Triassic metasedimentary section and the metavolcanic rocks of the Seven Devils Group is interbedded through about 10 m of stratigraphic section (fig. 14.5). This contact zone is characterized by centimeter-scale interfingering among layers of finely laminated tuffaceous chloritic greenstone, layers of laminated gray calcareous phyllite, and lenses of quartz-carbonate rock (McCollough, 1984); phyllite predominates upward. Marble layers or lenses 5 to 500 m thick occur at several stratigraphic horizons in the calcareous phyllite to schist section (fig. 14.6). At the intraformational contacts with the marble, interbedding of phyllitic and marble layers or gradation from calcareous phyllite to graphitic-quartzitic-micaceous marble to fairly pure marble occurs across about 2 m. A thick marble band (possibly as much as 1000 m thick, probably tectonically thickened) forms the structurally truncated top of the Upper Triassic metasedimentary section from south of John Day

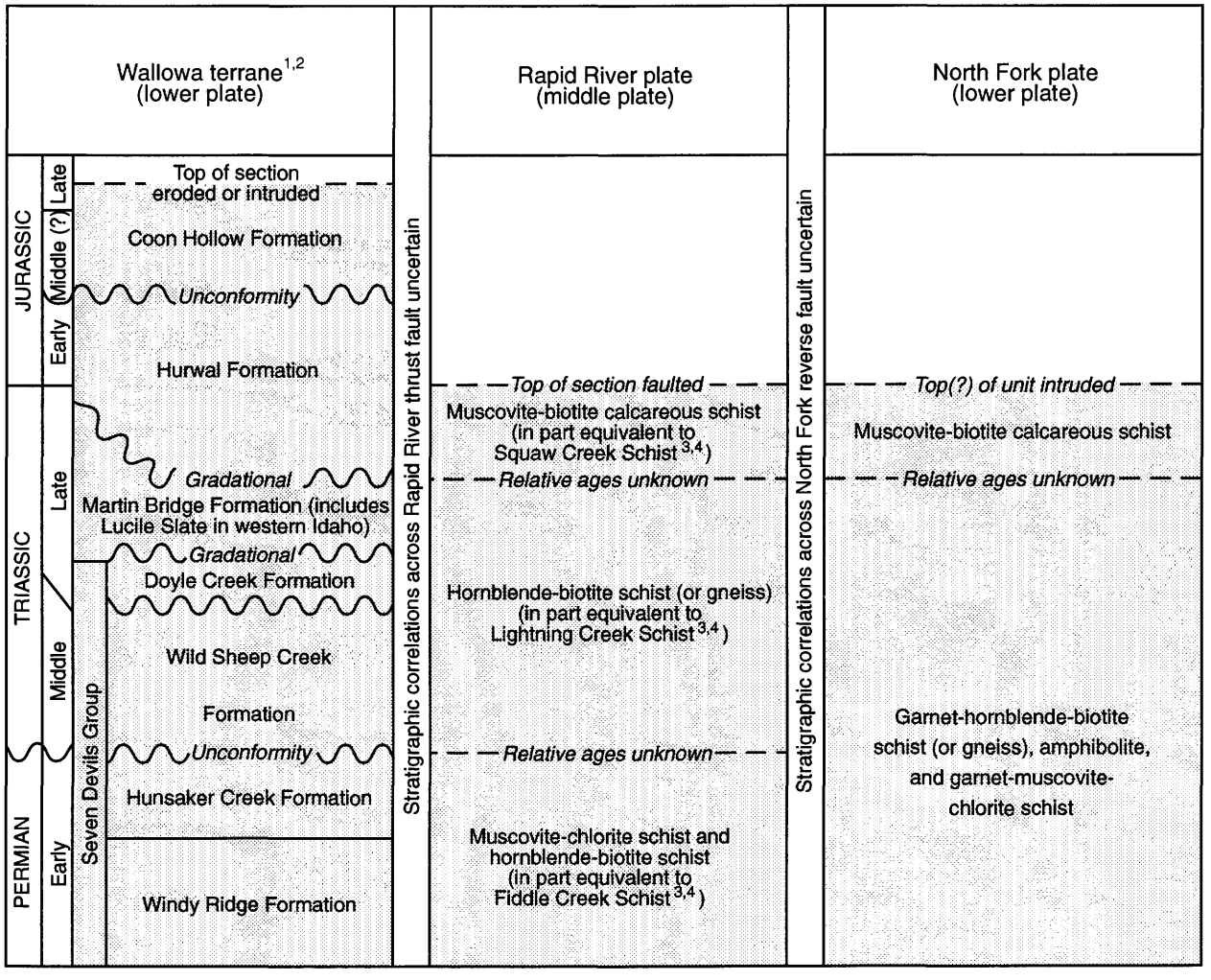

[1] Vallier, 1977.
[2] Follo, 1994.
[3] Hamilton, 1963a.
[4] Onasch, 1977.

FIGURE 14.3.—Generalized correlation diagram for oceanic rocks of western Idaho.

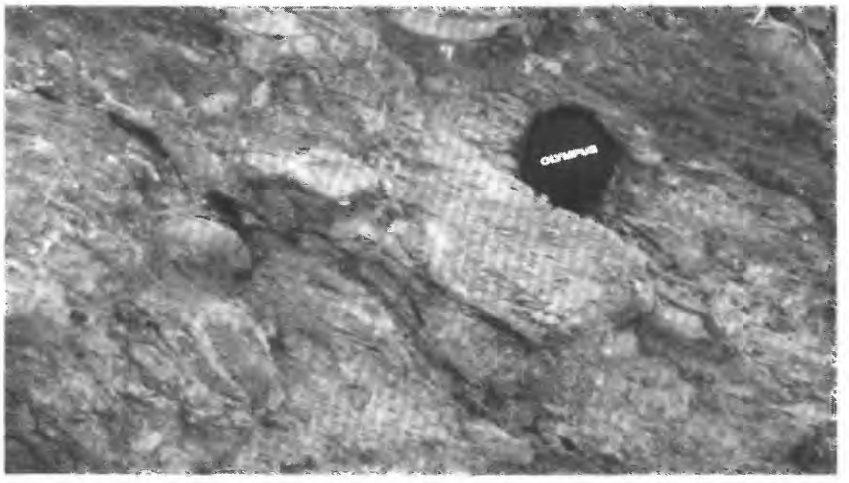

FIGURE 14.4.—Multilithologic, calcareous-cobble conglomerate with calcareous-schist matrix in amphibolite-facies Upper Triassic Martin Bridge Formation. Lens cap is 5.25 cm in diameter.

FIGURE 14.5.—Detail of interbedding between metavolcanic-rock (light) and calcareous-shale (dark) layers at gradational top of greenschist-facies rocks of the Seven Devils Group. Lens cap is 5.25 cm in diameter.

Creek to Slate Creek (Onasch, 1977). Toward the north and west, this single, thick marble unit splits into several thinner marble layers that gradually rejoin to form a single layer again near the mouth of Slate Creek.

Stratigraphic relationships such as interbedding are difficult to recognize in the deformed, medium- to high-grade metamorphic rocks along Slate Creek and upper John Day Creek; commonly, stratigraphic layering cannot be distinguished from structural intercalation. In addition, transposition of bedding can be observed in the low-grade rocks (McCollough, 1984) but is difficult to identify in higher grade, multiply deformed rocks. However, despite local structural complexities, the majority of foliation measurements are consistently parallel to lithologic contacts. This parallelism, together with the apparently gradational contacts, indicates that the major lithologic contacts are original stratigraphic features.

CORRELATION

Correlation of the metasedimentary rocks is problematic. On the basis of reconnaissance mapping between the Snake and Salmon Rivers, the name "Lucile Series" (Wagner, 1945) was first applied to a sequence of metasedimentary and subordinate metavolcanic rocks near the Slate Creek-John Day Creek area. Because probable Triassic fossils were found in marble beds within metasedimentary rocks continuous with rocks of the "Lucile Series" near Riggins, Idaho, and because of metamorphic and structural complexity within the upper part of the "Lucile Series," Hamilton (1963a) reevaluated the stratigraphy

of these rocks. Along the east flank of the Seven Devils Mountains southwest of the study area, a thick marble layer that overlies the Seven Devils Group was correlated with the Martin Bridge Formation of the Wallowa Mountains and named the "Martin Bridge Limestone" (Hamilton,1963a). South of Riggins, Hamilton (1963a) thought that the lower contact with the volcanic rocks was depositional—although he cited no supporting evidence—whereas north of Riggins, the contact was described as tectonic (Hamilton, 1963a). Calcareous slate to schist, which overlies the marble layer along the east flank of the Seven Devils Mountains, was named the "Lucile Slate" (Hamilton, 1963a). Although Hamilton did not do detailed mapping of the type locality of the "Lucile Slate" north of Riggins near the town of Lucile, Idaho, he described lithologic and structural characteristics of rocks between the town of Lucile and the mouth of Slate Creek: "Near Lucile, the [Lucile] slate is repeated structurally several times and lies between sheets of Martin Bridge Limestone and Seven Devils" Group (Hamilton, 1963a). The calcareous schist described at Hamilton's type locality for the "Lucile Slate" is in the present study area. This calcareous schist is less than 5 km south of and along strike (in continuously exposed outcrops) with the calcareous phyllite in this study area that has gradational contacts with both the underlying Seven Devils Group and the interbedded and overlying marble layers (Onasch, 1977; McCollough; 1984; Lund and others, 1993). Much of the complexity that Hamilton (1963a) described previously as structural is due to stratigraphic interfingering (McCollough, 1984).

Follo (1986, 1994) has described complex meter-scale interfingering of limestone, organic-rich calcareous and noncalcareous shale, and argillite in the Upper Triassic Martin Bridge Formation (Limestone) where it was originally described in the southern Wallowa Mountains of Oregon (Ross, 1938). The Martin Bridge Formation is in gradational contact with and laterally interfingers with the overlying argillaceous sedimentary rocks, graywacke, calcareous argillite, and limestone of the Upper Triassic and Lower Jurassic Hurwal Formation (fig. 14.3; Follo, 1986, 1992).

Detailed studies of unmetamorphosed and only slightly deformed rocks in the Wallowa Mountains indicate that interfingered units and limestone lenses in the Slate Creek-John Day Creek area of western Idaho are common in this complex island-arc setting. Although inadequate fossil control makes correlation difficult, the probable Triassic fossils found in the section south of Riggins, Idaho (Hamilton, 1963a), and mapping completed in other parts of the region

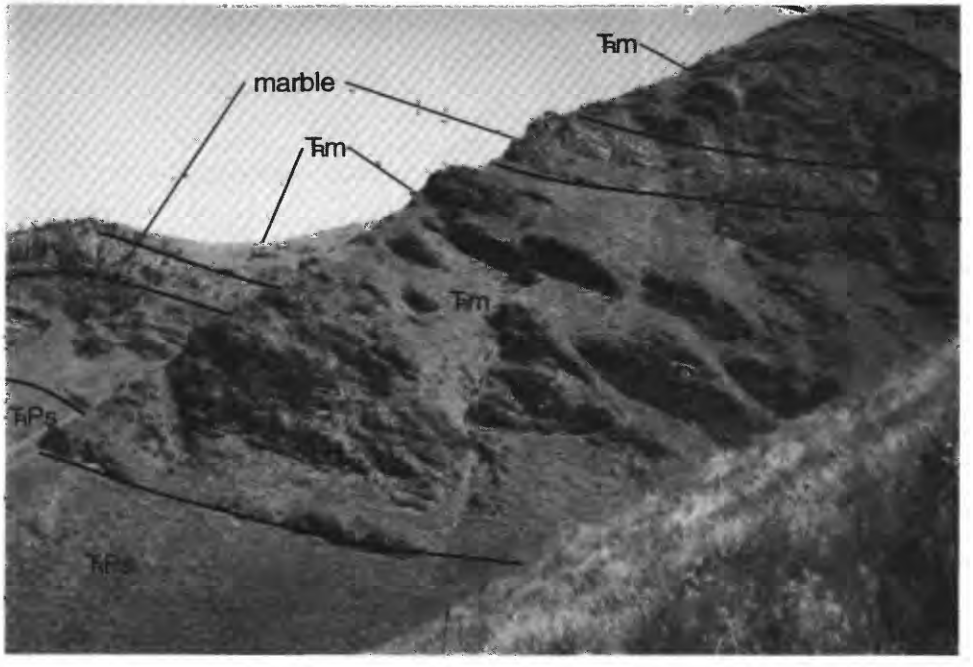

FIGURE 14.6.—Marble layers and lenses interbedded with calcareous phyllite in greenschist-facies rocks of the Martin Bridge Formation. Intraformational marble layer outlined in photograph is 10 to 20 m thick. Trm, Upper Triassic Martin Bridge Formation; TrPs, Permian and Triassic Seven Devils Group.

(Vallier, 1977) confirms Hamilton's (1963a) conclusion that the metasedimentary section that overlies the Seven Devils Group in western Idaho is Upper Triassic. However, the entire metasedimentary section is most probably correlative with the Upper Triassic Martin Bridge Limestone of the Wallowa Mountains. Herein the unit is called the Martin Bridge Formation both because of prior use of this name for the unit in Oregon (Ross, 1936) and along the Snake River in Oregon and Idaho (Vallier, 1977) and because "limestone" describes neither the stratigraphic nor metamorphic character of the unit in western Idaho.

METAMORPHOSED ROCKS OF UNCERTAIN AGE

RAPID RIVER PLATE

Structurally overlying the rocks that are known to be part of the Wallowa terrane is a group of rocks that had both volcanic and volcaniclastic-sedimentary protoliths (fig. 14.3). Hamilton (1963a) described these rocks near Riggins, named them the Riggins Group, and subdivided them into formations (Fiddle Creek Schist, Lightning Creek Schist, Berg Creek Amphibolite, and Squaw Creek Schist); many aspects of the stratigraphy and structure of the Riggins Group near Riggins were refined by Onasch (1977, 1987). These rocks are also found along strike in the Slate Creek-John Day Creek area, where metamorphic grade is generally higher than in the Riggins area. Metamorphic grade also increases eastward across the Slate Creek-John Day Creek area. Metamorphic variation across the study area complicates description of the formations of the Riggins Group; likewise, metamorphic variation across the region complicates correlations. Both the base and top of the Rapid River plate are faulted contacts. Therefore, rocks in the same structural position and along strike with the Riggins Group are herein treated as a single lithodemic unit and referred to as the Rapid River plate. Rocks of the Rapid River plate in the Slate Creek-John Day Creek area are named according to their lithology; problems and possible correlations are discussed separately.

Description of Rocks

The dominant rock type in the Rapid River plate is green-gray to dark-gray chlorite-biotite schist and hornblende-biotite gneiss (fig. 14.3). The mineralogy of these metavolcanic rocks changes with metamorphic grade. Plagioclase and subequal amounts of quartz are the most abundant minerals. Chlorite and biotite are the most common mafic minerals in greenschist- to lower-amphibolite-facies metamorphic rocks on the western side of the area, whereas biotite and hornblende are the mafic minerals in the amphibolite-facies metamorphic rocks on the east side of the Rapid River plate. Retrograde chlorite is found in some of the hornblende-biotite gneiss in the Rapid River plate. The common accessory minerals throughout are garnet, opaque minerals, epidote, muscovite, and apatite. Interlayered in the chlorite-biotite schist and hornblende-biotite gneiss unit are two minor rock types of special note. A subordinate but important rock type is hornblende-biotite conglomeratic gneiss that has relatively felsic multilithologic clasts; this gneiss forms layers that probably represent metamorphosed volcaniclastic conglomerate beds. Another minor rock type is a more feldspathic gneiss with fine-grained plagioclase, quartz, and biotite as the common minerals. The protolith for this gneiss may have been fine-grained plutonic rocks or a more felsic volcanic flow.

The second most common metavolcanic rock type in the Rapid River plate is greenish muscovite-chlorite schist or orange-weathering muscovite schist (fig. 14.3). The major minerals in the groundmass are muscovite, plagioclase, quartz, and chlorite. These schists commonly contain porphyroblastic garnet, chlorite, biotite, or quartz; many of the garnet porphyroblasts have chloritic rims (McCollough, 1984). Accessory minerals include common plagioclase, epidote, and opaque grains as well as sparse carbonate minerals.

Epidote-garnet-muscovite-biotite leucotonalite to quartz diorite in the chlorite-biotite schist and biotite gneiss unit along lower and middle Slate Creek (Lund and others, 1993) is metamorphosed and deformed. Plagioclase is the most common mineral in the felsic metaplutonic rocks; it forms untwinned, sericitized intergrowths with other minerals. Other primary minerals in these rocks are fine-grained and strained quartz, chloritized biotite, and accessory apatite. As much as 5 percent of fine- to medium-grained secondary pyrite and calcite are present; garnet, muscovite, and epidote are metamorphic minerals. Although no radiometric ages are available for these rocks, foliation in the pluton and associated dikes is concordant with that in the metavolcanic country rocks whereas the contact between the rocks is commonly discordant to the foliation. The metamorphic overprint on the pluton and the parallel foliation in the two rock types indicate that, although possibly the pluton intruded the volcanic host rocks during formation of the island arc and may be Permian to Triassic, (see "Proposed Correlation" section under "Rapid River Plate"), the

pluton was definitely emplaced prior to the metamorphic event that formed the foliation.

Garnet-muscovite-chlorite schist or muscovite schist (depending on metamorphic grade) is commonly found near the structural base of the plate. In upper John Day Creek, the thickness of this schist is estimated to be 2,700 m (McCollough, 1984), whereas in Slate Creek, it is common to have less than 50 m preserved at the base of the Rapid River plate. Chlorite-biotite schist and hornblende-biotite gneiss compose the structurally upper unit (fig. 14.3). The original contact between these rock types was not observed; the type of contact and the relative age of these units are unknown. The only evidence of primary depositional features in the metavolcanic rocks is volcaniclastic conglomerate that forms layers in the hornblende-biotite gneiss. In general, the foliation parallels the major lithologic breaks and relict conglomeratic layers. Therefore, except in areas of local structural disturbance, foliation in these rocks generally parallels bedding.

Proposed Correlation

Physical continuity indicates that garnet-muscovite-chlorite schist and muscovite schist in the John Day Creek drainage (McCollough, 1984) are equivalent to the Fiddle Creek Schist (the lowest Riggins Group unit, fig. 14.3) that has been traced into the south side of John Day Creek (Onasch, 1977, 1987). On the basis of mineralogy and chemistry of rocks of the Riggins Group south of this area (Hamilton, 1963a), muscovite schist in the Slate Creek area is probably also part of the Fiddle Creek Schist. However, direct tracing of the Lightning Creek Schist, the lowest unit of the Riggins Group, into the Slate Creek-John Day Creek area is not possible and the mafic schist and gneiss in the study area cannot be confidently correlated because rocks of this composition are found in both the Fiddle Creek and Lightning Creek Schists (Hamilton, 1963a; Onasch, 1977). Metavolcaniclastic rocks similar to the Squaw Creek Schist of the upper Riggins Group do not form part of the Rapid River plate in the Slate Creek-John Day Creek area.

No direct age information is available for rocks of the Rapid River plate. Although undated rocks that are part of the Rapid River plate in the John Day Creek drainage were previously considered to be correlative, in part, with the undivided Riggins Group (Hamilton, 1963a), and physical connection between one formation of the Riggins Group (Fiddle Creek Schist) and schists of the Rapid River plate is documented on the south side of John Day Creek (Onasch, 1977, 1987; McCollough, 1984), the age of the Riggins Group is also uncertain (Hamilton, 1963a). In light of suggestions that the Riggins Group is possibly a higher grade, more deformed equivalent of part of the Wallowa terrane (Onasch, 1977; Vallier, 1977; Lund, 1984; also see "Discussion" section), rocks of the Rapid River plate are also probably Triassic to Permian. If the Riggins Group is correlative with units in the Baker terrane of eastern Oregon (Elkhorn Ridge Argillite and Burnt River Schist) as has also been suggested (Vallier, 1977; Brooks and Vallier, 1978), the age is still uncertain.

North Fork Block

The North Fork reverse fault separates multiply deformed, complexly intruded amphibolite-facies metavolcanic rocks of the North Fork block from rocks of the Rapid River plate that lie structurally below and to the west; the Salmon River suture forms the east boundary of the plate (fig. 14.2). Metavolcanic rocks of the North Fork block are preserved as screens, roof pendants, and xenoliths within deformed plutonic rocks. Because of this, previous workers generally did not differentiate between the metamorphic and igneous rocks that crop out in this complex structural position. However, it is generally accepted that the metamorphic rocks had an island-arc protolith, and some workers have suggested that similar rocks to the south may be equivalent to the Riggins Group (Hamilton, 1963a, b; Onasch, 1977, 1987) and therefore equivalent to rocks of the Rapid River plate.

Description of Rocks

The primary rock type in the North Fork block is garnet-biotite-hornblende feldspathic gneiss and garnet amphibolite gneiss. Most of the rocks contain distinct mafic and quartzofeldspathic layers. Rolled porphyroblasts of garnet and hornblende are common. A complex paragenetic sequence of metamorphic minerals is preserved. In many places, two phases of the same mineral with different orientations and (or) characteristics are present; for instance, early formed hornblende porphyroblasts are wrapped by oriented, medium-grained hornblende grains (fig. 14.7). A less common rock type in the North Fork block is biotite-calc-silicate gneiss; centimeter-scale quartz-rich layers are common and marble was noted in this plate near the headwaters of John Day Creek (E.H. Price, oral commun., 1987). These calc-silicate gneiss and calcareous rocks occur along the east side of the North Fork block. An uncommon rock type is garnet-muscovite-biotite schist that is in a few isolated localities near the west edge of the North Fork block.

Rocks in the North Fork block contain no known original sedimentary features. They are structurally discontinuous with rocks in the Wallowa terrane or Rapid River plate; the rocks are multiply deformed and complexly intruded by tonalite plutons. Exposures of the metamorphic rock are isolated in the dominant plutonic rock, and, after intrusion, metamorphic and plutonic rock were concordantly deformed. As a result, lithologic units commonly lack mappable continuity. For rocks of the North Fork block, layering probably does not parallel bedding and original stratigraphic relationships among lithologic units are unknown.

Proposed Correlation

The metavolcanic rocks in the North Fork block previously were not separately mapped or correlated to specific units mapped elsewhere. This igneous-metamorphic complex (or "gneiss complex" of Hamilton, 1963a) was referred to as the "western border zone of the Idaho batholith" (Hamilton, 1963b, c; Vallier and Brooks, 1987). Hamilton (1963a) suggested that metamorphic rocks within the complex are at least partly correlative with the Riggins Group (fig. 14.3).

There is no direct information available on the age of metamorphic rocks in the North Fork block. Based on the Slate Creek area, it is apparent from both structural studies and dating of the metamorphic rocks (Lund, 1984; Lund and Snee, 1988) that there is no direct stratigraphic continuity between the Rapid River and North Fork blocks. Therefore, all that can be concluded about the correlation of these rocks is that they are metavolcanic and metavolcaniclastic rocks of probable island-arc origin (Hamilton, 1963a; Fleck and Criss, 1985) and that, on the basis of lithology, they are probably higher grade, structurally more complex equivalents of rocks in the Wallowa terrane and (or) the Rapid River plate (fig. 14.3). Accordingly, garnet-biotite-hornblende gneiss and garnet amphibolite gneiss are possibly equivalent to metavolcanic rocks of the Fiddle Creek and Lightning Creek Schists of the Riggins Group (see Hamilton, 1963a) and (or) to metavolcanic rocks of the Seven Devils Group. The rocks with calc-silicate- and quartz-bearing layers are possibly equivalent to the Squaw Creek Schist of the Riggins Group described by Hamilton (1963a) and (or) to the Martin Bridge Formation.

LATE CRETACEOUS CROSSCUTTING PLUTONIC ROCKS

Quartz diorite, tonalite, and granodiorite plutons intruded metamorphosed and deformed rocks of the

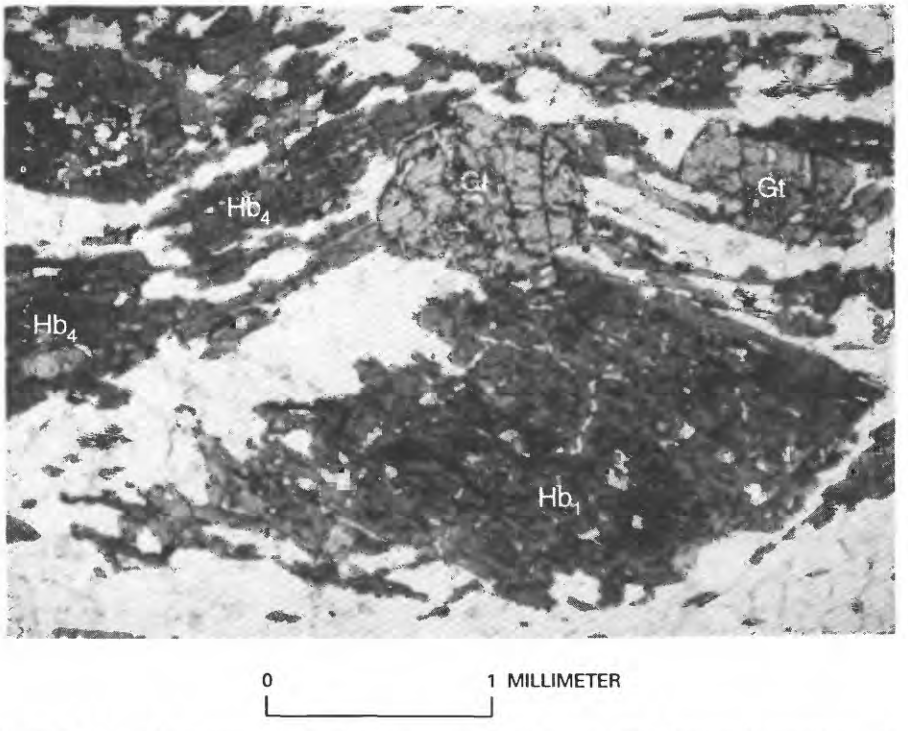

FIGURE 14.7.—Photomicrograph showing evidence of overprinted dynamothermal events in hornblende gneiss from the North Fork plate. Hornblende porphyroblast of S_1 fabric is wrapped by hornblende of S_4 fabric; postkinematic garnet postdates both. Hb_1, earlier hornblende; Hb_4, later hornblende; Gt, garnet.

Wallowa terrane, Rapid River plate, and North Fork block as well as the North American continent to the east; these plutonic rocks are the early phases of the Idaho batholith and are undivided on figure 14.2, where plutonic rocks of Late Cretaceous through Eocene age are shown as one unit. These rocks are progressively more common eastward across the area; they occur over only a small part of the middle of the area, whereas the eastern part of the area is dominated by these plutonic rocks. Thus, in the North Fork block, metamorphic rocks are found primarily as roof pendants and xenoliths within these plutonic rocks (fig. 14.2). These plutonic rocks are grouped separately from those thought to be island-arc related or premetamorphic because they (1) do not contain retrograde-metamorphic mineral assemblages, (2) cut metamorphic fabrics and postmetamorphic structures, (3) are affected by late deformation that cuts earlier features, (4) have isotopic ages that are younger than ages of metamorphism affecting other plutonic rocks (see "Isotopic Ages" section and Snee and others, chap. 10, this volume), and (or) (5) can be shown to stitch island arc to continental rocks by intruding across the Salmon River suture. In this chapter, only these and younger, autochthonous or semiautochthonous plutons are considered part of the Idaho batholith.

ROCK UNITS

The prevalent postmetamorphic plutonic rocks in Slate Creek-John Day Creek area are hornblende-biotite and biotite tonalite. Primary epidote (Zen and Hammarstom, 1984; Zen, 1985) and sphene are common accessory minerals and, if present, are usually coarse enough to be seen in hand specimen. Textures vary according to structural position across the area but generally may be divided into three major textural groups: (1) Plutonic rocks that cut continental rocks to the east (Lund, 1984) are mostly homogeneous in texture although faint, inconsistently oriented foliation is present in places. (2) Plutonic rocks that intruded Wallowa terrane and Rapid River plate rocks in the center of the Slate Creek-John Day Creek area cut metamorphic fabric, the Rapid river thrust fault, and the Slate Creek antiform but were intruded into and deformed along reverse faults related to pervasive deformation and emplacement of the North Fork block. These plutonic rocks are in places foliated and contain secondary muscovite. (3) Plutonic rocks that intruded the North Fork block have ubiquitous strong fabrics wherein postplutonic foliation and lineation have been superimposed on both the plutonic rocks and the metamorphic country rocks (see "Structure" section). Foliation, where present, is defined by biotite; lineation is defined by hornblende. Quartz grains are strained.

Less dominant quartz diorites and granodiorites that are similar in mineralogy and texture have been noted in the field but not mapped separately. It is not known if these are local phases of one pluton or if several different plutons are present. Plutonic boundaries have not been found, and any that existed may have been obscured by subsequent deformation.

ISOTOPIC AGES

Age information for these plutonic rocks comes from field relationships and from dating of both metamorphic events and plutonic rocks. In the central part of the area, these intrusive rocks cut across the metamorphic fabric and postmetamorphic structures that deform rocks of the Wallowa terrane and Rapid River plate (Lund, 1984). $^{40}Ar/^{39}Ar$-age-spectrum analysis indicates that metamorphic events in rocks of the Wallowa terrane and Rapid River plate occurred before 101 Ma. Radiometric dates for the crosscutting plutonic rocks are 93 to 85 Ma. In addition, U-Pb data for sphene-epidote-hornblende-biotite tonalite on the east side of the area give a concordant age (on four zircon splits and one sphene split) of 90.4±3.0 Ma (Snee and others, chap. 10, this volume). In the North Fork block, $^{40}Ar/^{39}Ar$ data shows that the record of an approximately 100-Ma event was destroyed by another event that caused argon loss and reequilibration about 90 Ma.

Because these Late Cretaceous plutons intruded across the suture and are unmetamorphosed, they are considered to be the earliest plutons of the Idaho batholith; some workers have even referred to them as a specific compositional phase of the Idaho batholith that occupies a peculiar structural setting and have called them the "western border zone of the Idaho batholith" (Hamilton, 1963a; Vallier and Brooks, 1987). However, chemically identical plutons of the same age can be found across the top and on the east side of the central Idaho batholith (Lund, 1984; Lund and others, 1986; Lewis and others, 1987; Toth, 1987). These tonalitic plutons seem to have been widespread across the area of the batholith rather than limited to the west side.

METAMORPHIC HISTORY

The Slate Creek-John Day Creek area has a complex metamorphic history involving several apparent

episodes of metamorphism and disruption of metamorphic patterns caused both by overlapping metamorphic events and by deformation. The pervasive, prograde metamorphic events, which are very strongly represented in the Slate Creek-John Day Creek area, are younger than metamorphic events documented in the island-arc rocks about 35 km outboard from the suture (Hotz and others, 1977; Avé Lallemant and others, 1980, 1985). Information from outside of the study area provides the only evidence of earlier metamorphic history in these rocks because, near the Salmon river suture, evidence of earlier events has been largely obliterated by complex higher grade metamorphism.

Although not manifested in the Slate Creek-John Day Creek area, the island-arc rocks apparently underwent low-grade metamorphism and reaction to seawater during and immediately following deposition or emplacement. The resulting spilite, keratophyre, and slate are preserved in parts of the Wallowa terrane that crop out in the Seven Devils Mountains and along the Snake River in Idaho as well as in Oregon (Hamilton, 1963a; Vallier, 1977).

It is probable that earlier Mesozoic metamorphism and deformation affected rocks in the Slate Creek-John Day Creek area because outboard rocks exhibit effects of several earlier dynamothermal events: (1) The Baker terrane (Silberling and others, 1992), which is one suggested correlative for metavolcanic rocks of the Rapid River plate (Brooks and Vallier, 1978), underwent Triassic metamorphism and deformation (Hotz and others, 1977; Avé Lallemant and others, 1980, 1985). (2) Rocks of the Wallowa terrane in the Wallowa Mountains of Oregon (probable correlatives of most metamorphic rocks in the study area) underwent pre-Late Jurassic deformation (Prostka, 1962; Follo, 1986). (3) On the basis of tectonic models, it is possible that rocks along the leading edge of the oceanic terrane underwent metamorphism and deformation related to collision with North America at some other location prior to final accretion in what is now western Idaho. What is inferred about the early Mesozoic history depends on the preferred correlation between high-grade rocks of the Rapid River plate and North Fork block, on how widespread earlier orogenic activity was, as well as on tectonic models for accretion of these rocks to the continent.

DESCRIPTION

In the Slate Creek-John Day Creek area, earlier metamorphic effects are overprinted and, in most cases, obliterated by prograde regional metamorphism. As elsewhere in western Idaho (Hamilton, 1963a; Onasch, 1977, 1987; Myers, 1982), metamorphic grade and complexity increase toward the Salmon River suture—from greenschist facies on the west side of the area (fig. 14.2) to upper amphibolite facies near the Salmon River suture on the east. This occurs mostly by means of structural shortening whereby several major thrust or reverse faults juxtapose rocks having different metamorphic histories and bring higher grade rocks over lower grade rocks.

Rocks of the Wallowa terrane generally record a fairly simple metamorphic history. Only one foliation is seen in these rocks. At low metamorphic grade, porphyroblasts (especially hornblende) are randomly oriented in the plane of foliation; at higher metamorphic grades, porphyroblasts are well aligned within the single foliation. These single fabric rocks contain evidence for only a single dynamothermal event. Mineral growth after the metamorphic peak or related to a late-stage, nondeformational metamorphic event is indicated by common unoriented biotite grains in the lower- to middle-amphibolite-facies rocks.

Fabrics in rocks of the Rapid River plate are more complex. Along upper John Day Creek, garnet- and biotite-porphyroblastic muscovite schists contain evidence of two high-grade events. In the first event, helicitic-garnet and biotite porphyroblasts were formed and the muscovite-rich fabric was wrapped around the porphyroblasts; after deformation, euhedral rims grew over the syntectonic-garnet cores (McCollough, 1984). A lower grade dynamothermal overprint in these rocks is demonstrated by deformed chlorite porphyroblasts that grew across the preexisting fabric (McCollough, 1984). In addition, evidence of low-grade metamorphic overprinting of higher grade events is found near Riggins south of this study area, where oriented chlorite flakes grew in the axial-planar cleavage of a postmetamorphic megascopic fold in middle-amphibolite-facies rocks (Onasch, 1977, 1987).

Metavolcanic rocks of the North Fork block contain clear evidence of more than one dynamothermal event. Two nearly equal magnitude metamorphic events are indicated in many places by the presence of two generations of the same mineral that have different orientations and characteristics. In some of these rocks, deformed metamorphic hornblende porphyroblasts form augen; these augen are wrapped by a finer grained groundmass that has a secondary schistosity containing a second-growth hornblende. Postkinematic garnets commonly overprint these oriented fabrics (fig. 14.7).

AGES OF METAMORPHISM

As just described, it is common, except in the lowest grade rocks, to observe evidence of two or more metamorphic events in most rocks in the region. This preserved overprinting is characterized by (1) common unoriented biotite flakes superimposed on the earlier upper-greenschist- to lower-amphibolite-facies directional fabric; (2) garnet porphyroblasts, formed in response to prograde dynamothermal amphibolite-facies metamorphism and subsequently cut by a metamorphic fabric of slightly lower grade; and (3) in most middle to upper amphibolite-facies rocks along the east side of the area, multiple generations of amphibole growth punctuated by episodes of deformation. Detailed $^{40}Ar/^{39}Ar$-age-spectrum dating of metamorphism in these rocks (Snee and others, 1987, chap. 10, this volume; Lund and Snee, 1988) revealed additional information on the metamorphic history. Where the appropriate mineralogy is present, it is possible to date either the prograde metamorphic event or the retrograde metamorphic event, and, in some cases it is even possible to date both the major metamorphic event and the overprinting event.

$^{40}Ar/^{39}Ar$-age-spectrum dating of metamorphic minerals from the lowest grade, simplest island-arc metamorphic rocks shows that the closest approximation of time of formation of foliation in the greenschist-facies rocks is about 120 Ma. This age is constrained by data from foliated but nonlineated hornblende at its lower stability limit in greenschist-facies metavolcanic rocks (Snee and others, chap. 10, this volume). This is the best information on the onset of metamorphism and deformation that can be gained from rocks in the study area. An apparent age for the overprinting, randomly oriented biotite porphyroblasts from lower-amphibolite-facies calcareous schist of the Martin Bridge Formation (Wallowa terrane) of about 84 Ma indicates local late reheating at that time.

Metamorphic ages of hornblende from higher grade, more complex rocks of the Rapid River plate form two age groups about 109 and 101 Ma. Age data for some of the rock samples, which contain overprinting chlorite porphyroblasts, indicate initial cooling at about 109 Ma and also an argon-loss event at about 94 Ma (Snee and others, chap. 10, this volume); these ages represent both cooling after prograde metamorphism that formed the hornblende fabric and a later reheating event that caused the growth of overprinting chlorite porphyroblasts.

$^{40}Ar/^{39}Ar$-age-spectrum data for hornblende from the paragenetically complex metavolcanic rocks of the North Fork block commonly exhibit hybrid age spectra indicating argon loss from about 101 to 90 Ma or reset ages of about 90 Ma. These data indicate that the metavolcanic rocks cooled to below 530°C by 101 Ma and were subsequently reheated and deformed before final cooling about 90 Ma.

The age data show clearly that metamorphism spanned from about 120 to 90 Ma. Careful age-spectrum work documents the eastward-increasing complexities of the paragenetic sequences and metamorphic overprinting as well as documenting the timing of events. The apparent eastward decrease in metamorphic ages may be in part related to simple cooling of rocks at deeper levels within the orogenic belt or to greater eastward structural disruption that brought deeper rocks up (from the east) to cool at later times. However, on the basis of age data and the mineralogic and deformational overprinting revealed by examination of the metamorphic textures, it is apparent that some aspects of the eastward increasing complexity of metamorphic fabrics and eastward-decreasing ages are due to distinct cycles of metamorphism and deformation.

STRUCTURE

Deformation as well as metamorphism becomes more intense to the east across the Slate Creek-John Day Creek area, and structural features differ accordingly. For this reason, mesoscopic (outcrop-scale) structures described in low-grade rocks to the south (Onasch, 1977, 1987) and on the west side of this study area commonly take a different form from and are difficult to correlate with mesoscopic structures in the high-grade rocks in eastern John Day Creek or along Slate Creek. In addition, there are many structural domains caused by overprinting events in these rocks as well as several structural plates, and same-age features commonly have different orientations. Tracing macroscopic (map-scale) structures from area to area and interpreting the associated local mesoscopic structures in terms of the macroscopic structures are the best ways to piece together the deformational history of this area.

FABRICS AND GEOMETRIES

According to McCollough (1984), the low-grade calcareous slate to schist of the Wallowa terrane near the mouth of John Day Creek contains evidence of folding that produced schistosity. The regional foliation (S_1), which is a demonstrable axial-planar schistosity or cleavage in this part of the study area, is

defined by the preferred orientation of muscovite or chlorite in pelitic rocks and of carbonate grains in calcareous rocks where pressure solution may have been the major process in forming directional fabric. Except in fold hinges, the axial-planar fabric (S_1) parallels bedding (S_0; McCollough, 1984). The first generation folds (F_1), in bedding (S_0), are tight to isoclinal folds that plunge shallowly to the north, south, and east. Upper-greenschist- to amphibolite-facies rocks along Slate Creek and upper John Day Creek do not retain details of S_0 (bedding), and F_1 (early folds) that produced S_1 (foliation) are not found because of more intense dynamothermal processes.

The low-grade calcareous slate to phyllite of the Martin Bridge Formation contains a particularly spectacular array of mesoscopic structures presumably because the composition and grade are conducive to the formation and preservation of minor local structures that cannot be identified in the massive metavolcanic rocks or marble that make up the rest of the section. Although these structures attest to the complexity of the structural history, they commonly cannot be correlated with macroscopic features. In this greenschist-facies calcareous slate to phyllite, the S_1 foliation is locally deformed by later northwest-verging asymmetric folds of variable orientation, and these as well as the early isoclinal F_1 folds are locally overprinted by northeast-plunging open folds with northwest-dipping closely spaced fracture cleavage (McCollough, 1984). The higher grade rocks of the Wallowa terrane and Rapid River plate contain evidence for only one phase of early folding F_2 (figs. 14.8 and 14.9) that deforms the foliation. In the higher grade rocks, the F_2 folds are tight to isoclinal folds of S_1, the principle schistosity. F_2 fold axes plunge at a low angle toward the northeast or southwest, but the dip of axial planes varies from place to place.

A thrust fault juxtaposes amphibolite-facies rocks of the Rapid River plate over upper-greenschist- to amphibolite-facies rocks of the Wallowa terrane (fig. 14.10). This fault can be traced discontinuously across the Slate Creek-John Day Creek area. In the John Day Creek area, the trace of this fault connects with the Rapid River thrust fault (Onasch, 1977, 1987; McCollough, 1984). Mesoscopic structures in the narrow Rapid River thrust fault zone verge west-

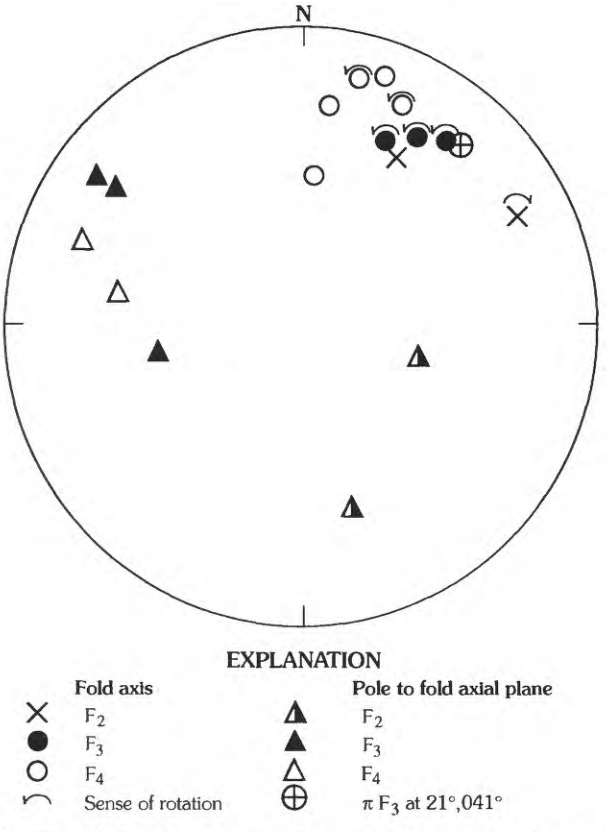

FIGURE 14.8.—Lower-hemisphere, equal-area projection of mesoscopic structures in rocks of the Wallowa terrane in Slate Creek area. π pole (⊕) is fold axis of F_3 fold determined from fig. 14.11.

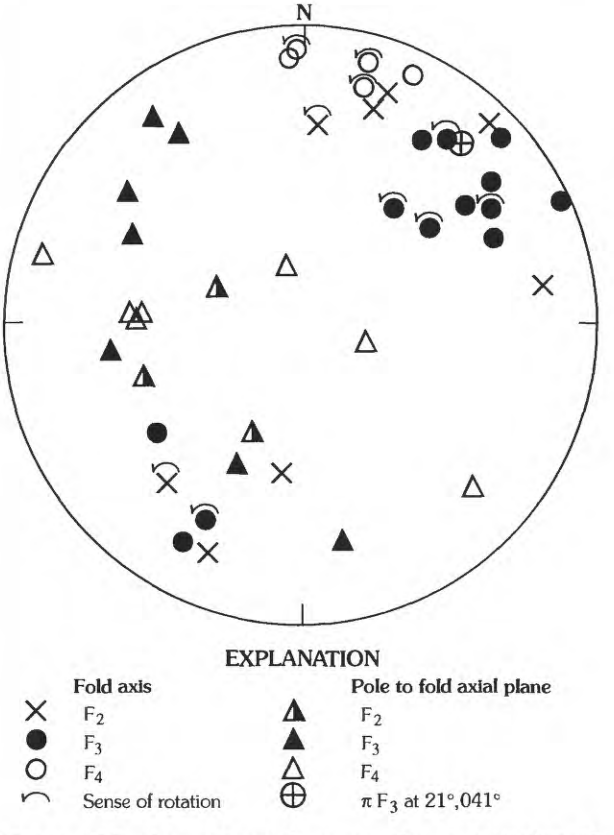

FIGURE 14.9.—Lower-hemisphere, equal-area projection of mesoscopic structures in rocks from the Rapid River plate in Slate Creek area. π pole (⊕) is fold axis of F_3 fold determined from fig. 14.11.

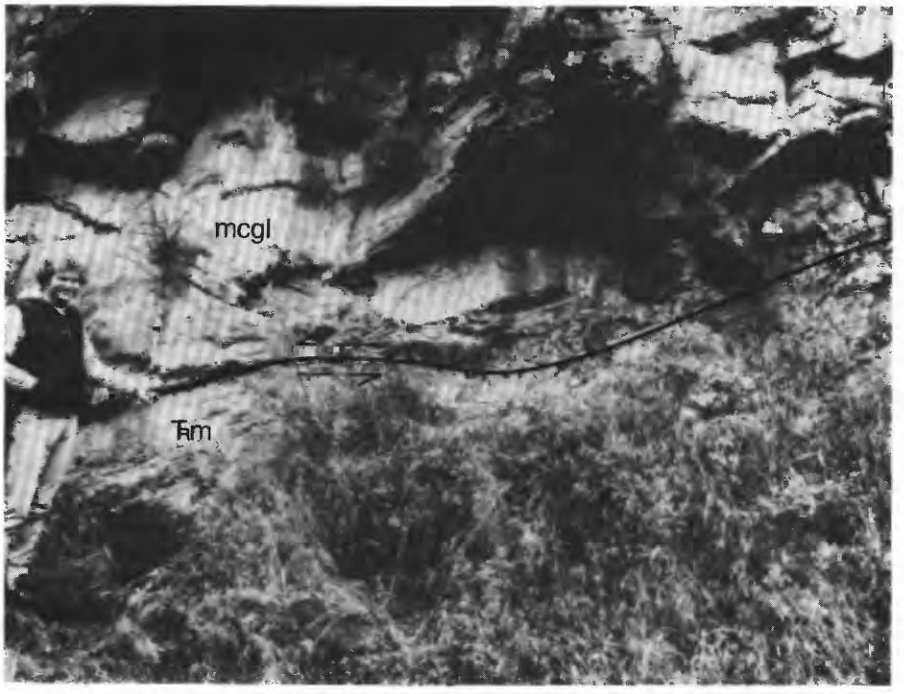

FIGURE 14.10.—Rapid River thrust fault along Slate Creek. Geologist is pointing to fault surface. Hanging wall consists of middle-amphibolite-facies metavolcaniclastic conglomerate of Rapid River plate (mcgl); footwall consists of lower-amphibolite-facies calcareous schist of the Upper Triassic Martin Bridge Formation (Trm) of the Wallowa terrane.

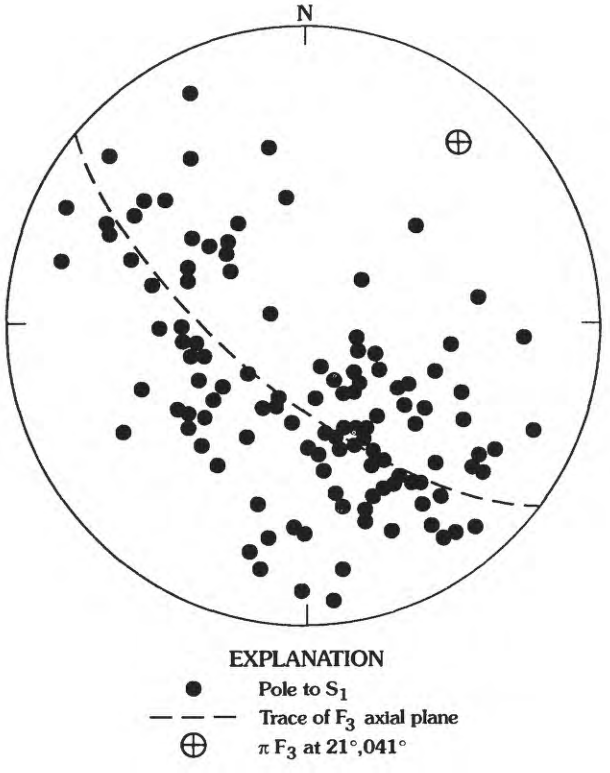

FIGURE 14.11.—Lower-hemisphere, equal-area projection showing poles to S_1 foliation in rocks of the Wallowa terrane and Rapid River plate. Girdle represents axial plane to F_3 fold. π is pole to F_3 axial plane.

northwest. The tight F_2 folds of foliation (figs. 14.8 and 14.9) may have formed during movement along the thrust fault.

On a macroscopic scale, the Rapid River thrust fault is folded into the gently northeast-plunging Slate Creek antiform (figs. 14.2 and 14.11) that has been subsequently deformed on the east limb. Related mesoscopic symmetric and asymmetric F_3 folds (figs. 14.8 and 14.9) that refold earlier mesoscopic folds are found throughout the area. These folds plunge consistently northeast at a low angle. Folds on the east limb are commonly asymmetric with an west-verging sense of rotation.

Evidence of the presumably latest phase of folding is found in the high-grade rocks on the east limb of the Slate Creek antiform. Macroscopic reverse faults disrupt the trace of the Rapid River thrust fault and the Slate Creek antiform (fig. 14.2). These faults cut the core of the Slate Creek antiform and rotated the east limb to vertical or overturned. Klippen of higher grade rocks on lower grade rocks along lower John Day and Slate Creeks may also be the result of the same deformation. Additionally this event is manifested by F_4 upright, open mesoscopic folds and crenulations that plunge north-northeast at a low angle with steeply dipping axial planes and consistent west-vergent rotation (figs. 14.8 and 14.9). The synclines are commonly cut out by steep reverse

faults that formed during the late stages of F_4 folding. Boudinage structures formed along many of the exposed faults by the deformation of minor leucocratic tonalite dikes that were emplaced along the faults (fig. 14.12). Thus, this complex stage of deformation began with ductile folding and continued into brittle faulting, then magma was emplaced and the resulting dikes were deformed during the last stages of the brittle faulting.

Rocks of the Wallowa terrane and Rapid River plate that contain sequential evidence of (1) early folding, (2) west-directed movement along the Rapid River thrust fault, (3) folding of the Slate Creek antiform, and (4) west-vergent folding and reverse faulting form the footwall to the steeply east-dipping North Fork reverse fault. These lower-plate rocks, which retain evidence of multiple deformations of the primary schistosity (S_1), are juxtaposed against deformed metamorphic and plutonic rocks of the North Fork block (upper plate). Metavolcanic rocks of the North Fork block retain only vestiges of the earlier fabric and amphibolite-facies mineralogy but are almost completely transformed by younger amphibolite-facies minerals of an overprinted younger fabric. The paragenetic sequence of metamorphic minerals and their structural characteristics (described earlier in this section) indicates that the early amphibolite-facies minerals, which are probably contemporaneous with the primary schistosity (still preserved in less complex rocks of the footwall), were deformed prior to the growth of younger amphibolite-facies minerals (fig. 14.7). Second-stage hornblendes are within a younger foliation (S_4) or define a secondary lineation (L_4) that has an orientation markedly different from the orientation of earlier hornblendes. The dominant fabric in both the deformed metamorphic and igneous rocks of the North Fork block is characterized by steeply inclined north-northeast-trending S_4 foliation and (or) steeply southeast-plunging L_4 mineral lineation (fig. 14.13). The fabric is steepest along the suture and becomes more shallow at higher elevations on the west side of the North Fork block (Lund and others, 1993). Although most of the rocks are L- and (or) S-tectonites indicative of plane strain, the occur-

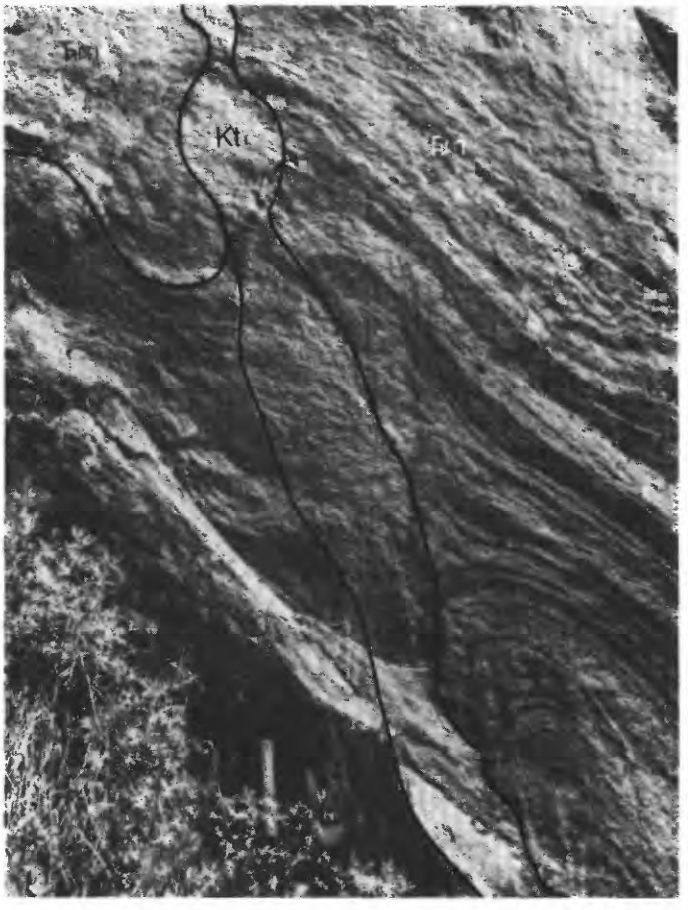

FIGURE 14.12.—Detail of F_4 folds in calcareous schist of the Upper Triassic Martin Bridge Formation (Trm) of the Wallowa terrane. East-vergent, mesoscopic folds were faulted and intruded by Late Cretaceous tonalite (Kt); tonalite shows boudinage structure, which formed along fault during final movement. Shaft of hammer is approximately 27 cm long.

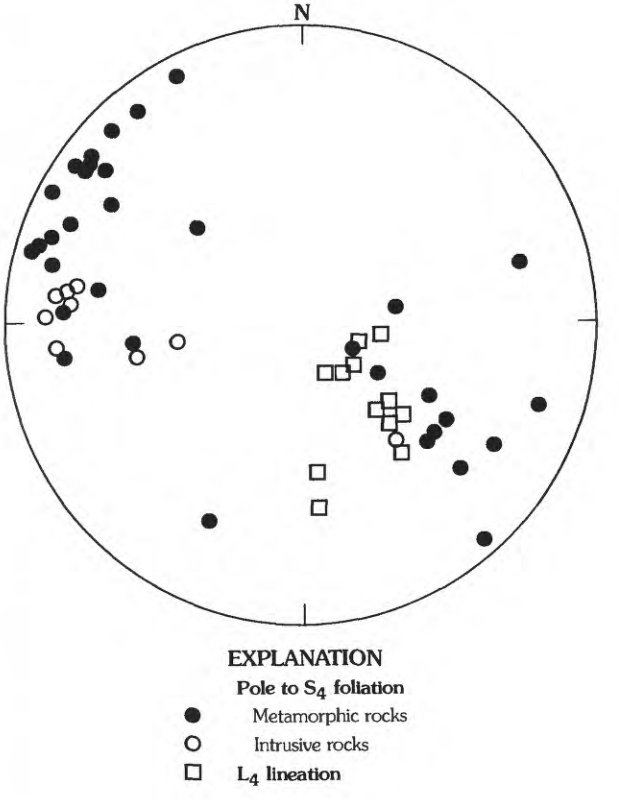

FIGURE 14.13.—Lower-hemisphere, equal-area projection showing poles to S_4 foliation and L_4 lineation in rocks of North Fork block.

rence of L-tectonites indicates a component of intense unidirectional vertical flow (pure shear) during deformation. Evidence for rotational deformation (simple shear) has not been found in the North Fork block in the Slate Creek-John Day Creek area.

Although obscured by intrusive rocks, the North Fork reverse fault cuts off the Rapid River thrust fault and the nose of the Slate Creek antiform and is therefore younger (fig. 14.2; Lund and others, 1993). The pervasive S_4 schistosity and L_4 lineation in the North Fork block formed in response to extreme strain. Formation of the new fabric destroyed evidence of bedding and transposed lithologic and plutonic contacts. Also, the imposed changes in mineralogy and fabric effectively cut off or transposed early structures. However, the multiple generations of some minerals and the microfabrics are good evidence of earlier metamorphic and structural events. Therefore, the overprinting fabric in rocks of the North Fork block is younger than both the regional S_1 foliation and the F_2 and F_3 structures in the Wallowa terrane and Rapid River plate. Movement along the North Fork reverse fault and the young deformation (S_4 and L_4) in the North Fork block are probably contemporaneous with (1) formation of the F_4 west-vergent folds and reverse faults that are on the east side of the lower plate (Martin Bridge Formation) near the North Fork reverse fault and (2) formation of late, moderately plunging crenulation lineations in rocks of upper John Day Creek (McCollough, 1984).

Crosscutting structures and metamorphic-mineral paragenesis evident in the regional-metamorphic fabrics indicate progressively younger deformation toward the Salmon River suture. Characteristically, the younger deformation in the higher grade rocks is more pervasive than older deformation in lower grade rocks and resulted in virtual obliteration of early structures.

AGES

A $^{40}Ar/^{39}Ar$-age-spectrum study of metamorphic rocks in the Salmon River suture zone provides information on the age of specific structures and of the duration and complexity of dynamothermal processes in the area. A minimum of four important successive deformational events are recognized from progressive overprinting in rocks of the Slate Creek-John Day Creek area: (1) formation of the S_1 primary regional foliation, (2) regional juxtaposition of higher grade rocks over lower grade rocks along the Rapid River thrust fault and simultaneous formation of F_2 folds, (3) macroscopic F_3 folding of the regionally juxtaposed rocks represented by the Slate Creek antiform (Lund, 1984) and possibly the Riggins synform and Lake Creek antiform (Hamilton, 1963a; Onasch, 1977), and (4) initiation of the North Fork reverse fault, dynamothermal overprinting S_4 schistosity and L_4 lineation in rocks of the North Fork block, and disruption of the Slate Creek antiform by reverse faulting coincident with F_4 folding.

Dating of poorly formed, nonlineated, metamorphic hornblende in greenschist-facies, foliated metavolcanic rocks shows that the S_1 foliation formed about 120 Ma, and this age dates the beginning of dynamothermal metamorphism. Metamorphic ages for minerals that delineate the S_1 foliation in amphibolite-facies rocks of the Wallowa terrane and Rapid River plate form two groups, about 109 and 101 Ma, and indicate either that these higher grade rocks cooled more slowly from the foliation-forming event that began about 120 Ma or that these ages represent successive dynamothermal events. Metamorphic ages that date foliation in the North Fork block are complex. Some hornblende samples have age spectra that indicate minor argon loss; compared to primary cooling ages of about 100 Ma, reset ages are 89 and 93 Ma, most samples having been completely reset to about 90 Ma. Therefore, the pervasively overprinting S_4 and L_4 fabric in rocks of the North Fork block formed during a dynamothermal event about 90 Ma.

The Rapid River thrust fault cuts rocks having metamorphic ages in the range of 118 through 109 Ma, and the Slate Creek antiform folds foliation that is of the same age. Therefore, the best estimate for the maximum age of these structures is 109 Ma. The minimum age for the thrust and antiform is approximately 93 Ma, the age of crosscutting tonalitic rocks. Thus, the Rapid River thrust fault and the Slate Creek antiform formed between 109 and 93 Ma. The age of the North Fork reverse fault that cuts both the Rapid River thrust fault and the Slate Creek antiform is also a limiting factor in determining relative ages of structures.

Because the North Fork reverse fault cuts approximately 93-Ma plutonic rocks and cuts off rocks in the North Fork block that have an approximately 90 Ma metamorphic overprint the fault probably formed no earlier than about 90 Ma. The 90-Ma metamorphic fabric in the North Fork block formed during a dynamothermal event that was distinct from earlier events and was restricted to a narrow zone along the Salmon River suture. It is not known whether the steep to vertical tectonic flow that formed this fabric was caused by a distinctly, late-stage transpressional event along the suture or whether the ductile effects constitute an early nonbrittle response of deep-seated rock to uplift parallel to the suture.

DISCUSSION

The general structural geometry of the Slate Creek-John Day Creek area is that of stacked thrust plates. In each successively higher and more easterly plate, the stratigraphy is less well understood because of eastward-increasing complexity of metamorphic overprinting and structure; this gives rise to several major, interrelated problems. First, it is unclear how many stratigraphically distinct allochthons (terranes) occur in this area; there may be as many as three such terranes, or a single terrane may have been imbricated. Secondly, the mechanism for the eastward-increasing complexity of metamorphism and deformation is problematic; causes that have been suggested include plate interactions or dynamic emplacement of the Idaho batholith.

Questions about the correlation of stratigraphically coherent sequences arise from the absence of dates on the units, medium- to high-grade metamorphism of the rocks, and transposition of bedding. Physical continuity between dated rocks along the Snake River and rocks along the Salmon River makes it possible to correlate rocks of the Wallowa terrane of Oregon with exposures in the western part of the Slate Creek-John Day Creek area. However, the sedimentology and stratigraphy of the Martin Bridge Formation in western Idaho is not well documented because of metamorphism and deformation.

The progressive increase in metamorphic grade is also a problem in correlation of rocks of the Rapid River plate. Greenschist-facies rocks are found near Riggins, where these rocks were first described (Hamilton, 1963a), whereas in the Slate Creek-John Day Creek area, rocks thought to be along strike are of the upper amphibolite facies (Onasch, 1977; Lund, 1984; McCollough, 1984). Therefore it is difficult to correlate units of this plate across structural breaks. Most importantly, because there is little lithologic or chemical difference between units of the Wallowa terrane and Rapid River plate (Hamilton, 1963a), it is virtually impossible to distinguish them at like metamorphic grades if the units cannot be traced along strike.

This problem is even more significant for rocks of the North Fork block where even the gross lithologic boundaries between units have been transposed and intruded. Furthermore, no known differences in composition or previous history conclusively separate these rocks from either the Wallowa terrane or the Rapid River plate.

Probably only through detailed chemical studies or through dating the extrusive age of the volcanic protolith can any differences among these allochthonous sequences be conclusively determined. Because all the rock sequences are compositionally similar and the only known differences among them were superimposed during Cretaceous orogenic events, it seems most plausible to consider these rocks to be imbricated parts of a single island-arc terrane.

On the basis of successively overprinting fabrics and of age data, deformation of the rocks in the Slate Creek-John Day Creek area apparently occurred in several discrete steps. At least two stages of metamorphism are documented: Early low-grade metamorphism was associated with dynamic processes that produced a foliation, and the latest high-grade metamorphism was associated with processes that formed a pervasive, crosscutting foliation in rocks of the North Fork block (including Late Cretaceous tonalite of the Idaho batholith). Age data indicate several additional groupings among the medium- to high-grade rocks. These groupings of the data may be related to multiple discrete thermal pulses and (or) to intermittent nonthermal tectonism that periodically exposed hotter rocks from deeper crustal levels to cooling.

The earliest plutonic rocks of the Idaho batholith intruded both island-arc and continental rocks and were involved in the deformation that affected the North Fork block. A zone of intense deformation clearly crosscuts earlier dynamothermal fabrics and structures. Analyzing this same structural zone east of Riggins and south of the Slate Creek-John Day Creek area, Hamilton (1963b, c) interpreted this complex mixture of deformed metamorphic and plutonic rocks as a zone of vertical "plutonic flow" and called it part of "the western border zone of the Idaho batholith." He concluded that deformation and metamorphism in western Idaho were the result of westward thrusting of the Idaho batholith over the low-grade metavolcanic rocks of the Wallowa terrane; that the area of the North Fork block was the zone of movement between the batholithic rocks and the island-arc rocks; and that the metamorphism and deformation to the west of the zone were caused by the same event, thought to have occurred in the middle Cretaceous.

However, evidence that strain was greater toward the Salmon River suture is found in the increasingly complex dynamothermal overprinting in island-arc rocks all along the oceanic-continental boundary from north of Harpster to near Riggins as one approaches the suture (fig. 14.1; Hamilton, 1963a; Myers, 1968, 1982; Onasch, 1977). In addition, the metamorphic intensity and amount of strain recorded in continental rocks are also greater toward the boundary irrespective of the relative amount of plutonic rock present. Except for the zone within 5 km of the suture, plutonic rocks cut earlier dynamothermal fabrics. Therefore, metamorphism and deformation in the Slate Creek-

John Day Creek area predated most plutonic rocks of the Idaho batholith, dynamothermal processes were localized along the Salmon River suture and were independent of intrusive boundaries, and the earliest plutons were deformed in the last stages of the late Early to Late Cretaceous regional dynamothermal event. This orogenic event that formed the Salmon River suture and caused the associated metamorphism and deformation was probably also responsible for formation of the Idaho batholith.

Age data show that metamorphic and deformational features described herein and in mapping of nearby areas (Hamilton, 1963a; Onasch, 1977, 1987; McCollough, 1984) are all Cretaceous. The dynamothermal events lasted about 30 Ma and included several major stages. In amphibolite-facies rocks, any record of possible earlier (preCretaceous) dynamothermal events was destroyed by the >500°C temperatures and high strains associated with the late Early to Late Cretaceous deformation. In addition, the area affected by any earlier event localized along the east edge of these island-arc rocks apparently was no wider than the present orogenic belt because the only record of dynamothermal events in the lower-greenschist-facies rocks indicates that deformation in them also dates from the Cretaceous.

CONCLUSIONS

Even in the lowest grade metamorphic rocks of the Wallowa terrane in west-central Idaho, the stratigraphy is not adequately established. Metamorphic complications, structural complexity, and lack of isotopic age data all contribute to the problem. In spite of generally inadequate stratigraphic data, detailed study of the Slate Creek-John Day Creek area has provided new information on and insight into the stratigraphy of the Wallowa terrane in western Idaho. Although formations have not been delineated for all such rocks in the study area, both Permian metavolcanic rocks (either Hunsaker Creek or Windy Ridge Formation) and the Triassic Doyle Creek Formation of the Seven Devils Group are in this area (Lund and others, 1993). Detailed stratigraphic observations indicate that the upper part of the Seven Devils Group is gradational with overlying calcareous slate to phyllite, which is in turn interfingered with marble lenses. Stratigraphic data from the Slate Creek-John Day Creek area and from the Riggins area to the south show that the Triassic rocks of the Wallowa terrane are composed of irregularly stacked lithologic lenses and should not be divided into lithostratigraphic units and that the Triassic rocks are remarkably like the sequence of unmetamorphosed rocks in the type section in the Wallowa Mountains (Follo, 1992, 1994). Therefore, probably all the metasedimentary rocks of the Wallowa terrane in western Idaho are correlative with the Triassic Martin Bridge Limestone (Vallier, 1977; Follo, 1994). The name "Lucile Slate" is thought to be inappropriate for stratigraphic reasons and its use should be discontinued; the name Martin Bridge Formation should be adopted for the Triassic section of interfingered calcareous phyllite-schist, biotite-chlorite schist, calc-silicate gneiss, and marble gradationally overlying the Seven Devils Group (Lund and others, 1993).

Despite the fact that rocks on the south side of John Day Creek are along strike and in physical continuity with units of the Rapid River plate (the Riggins Group as defined by Hamilton, 1963a), lateral tracing of the units across structures and metamorphic-facies boundaries has proven to be impossible in many places. Where rocks of the Wallowa terrane consist of medium-grade metamorphic rocks, the rock types are identical to those originally described in medium-grade rocks of the Rapid River plate. Likewise, amphibolite-facies rocks of the North Fork block are lithologically similar to those of amphibolite-facies Rapid River plate. Rocks of the Rapid River plate were originally separated from metavolcanic rocks of the Wallowa terrane because of higher metamorphic grade, because distinct map units had been recognized in these rocks but not (at that time) in the lower grade volcanic rocks, and despite chemical similarity (Hamilton, 1963a). It is now known that distinct units exist in the Seven Devils Group of the Wallowa terrane (Vallier, 1977) and that, at like grades of metamorphism, there are more similarities than differences among rocks of the three main structural units that are described in this study.

The combination of similar stratigraphy in all three plates, characteristically complex original stratigraphy, changes in metamorphic grade, and complexly overprinted macroscopic structures makes it difficult to separate rocks of the different plates on a regional basis. Additionally, because the stacked plates had similar histories throughout the metamorphic and deformational events that affected them and because the structures that juxtaposed the plates are late Early to Late Cretaceous, it is proposed that rocks of the Rapid River plate (previously called Riggins Group) and the North Fork block might best be considered the leading edge of the Wallowa terrane. These rocks may be high-grade, multiply deformed portions of the Wallowa terrane that were more strongly affected by dynamothermal processes with their increasing involvement

in the suturing process and that were ultimately imbricated. Correlation of all three tectonic slices with the Wallowa terrane simplifies regional stratigraphic problems as well as models for the structural and microplate tectonic histories.

Metamorphic grade increases eastward across the Slate Creek-John Day Creek area. The simplest metamorphic fabrics are found in the lowest grade rocks in the west part of the area; complex, multiple metamorphic overgrowths and complications from later cycles of deformation occur farther east in the study area. Onset of prograde metamorphism occurred about 120 Ma in the study area and as early as 130 Ma in other parts of the suture (Davidson, 1990). A separate 90-Ma event recorded in high-grade metamorphic rocks within 5 km of the suture is the youngest dynamothermal stage. Intermediate ages of 109 and 101 Ma in medium- to high-grade rocks resulted either from separate cycles of metamorphism or from disruption of metamorphic patterns by macroscopic structures that juxtaposed higher grade rocks over lower grade rocks and thus produced the regional inverted metamorphic gradient.

Structural complexity also increases eastward. Evidence of early phases of mesoscopic deformation is found in lower grade rocks in the west side of the area. In eastern parts of the area, intense metamorphism and deformation obliterated most early mesoscopic features. The earliest preserved mesoscopic structures formed in the Wallowa terrane during prograde regional metamorphism about 120 Ma. Early structures in rocks of the Rapid River plate cannot be directly correlated with those in Wallowa terrane rocks because early phases are not consistent in style, appression, or orientation. However, mesoscopic features that formed in the juxtaposed Rapid River plate and Wallowa terrane after movement on the Rapid River thrust fault are correlative. After formation of the Rapid River thrust fault, both the thrust fault and rocks of the Wallowa terrane and Rapid River plate were folded together to form the Slate Creek antiform. The best limits on the timing of Rapid River thrust faulting and formation of the Slate Creek antiform range between 109 and 93 Ma. The first postmetamorphic plutons were emplaced at 93 Ma. The last pervasive deformation event at 90 Ma formed the North Fork reverse fault and a steep L- and (or) S-tectonite fabric in plutonic and metamorphic rocks of the North Fork block; this 90 Ma event cut off and (or) overprinted earlier structures in the North Fork block.

The best estimate for direction of relative movement of the upper plate along the Rapid River thrust fault is west-northwest (Lund, 1984); this is in agreement with that determined on the same fault near Riggins (Hamilton, 1963a; Onasch, 1977, 1987). The fold axes of the Slate Creek antiform and associated mesoscopic folds are perpendicular to the determined direction of movement along the Rapid River thrust fault. Folds in late reverse faults, which formed after the Slate Creek antiform and may signify the lower plate's response to deformation in the North Fork block, are coaxial with the Slate Creek antiform and indicate that movement along the thrust faults was westward, generally parallel to movement directions determined for the Rapid River thrust fault. Thus, regional stresses seem to have maintained a consistent orientation for several discrete events related to and following formation of the Rapid River thrust fault.

Prograde metamorphic fabric in the island-arc metamorphic rocks of the Slate Creek-John Day Creek area developed and was multiply deformed between 120 and 93 Ma—prior to intrusion of earliest plutons of the Idaho batholith. These plutons intruded both island-arc and continental rocks after 93 Ma and thereby sealed the join between the North American continent and the accreted island-arc rocks. Although metamorphic grade increases eastward toward the main mass of plutonic rocks, pluton contacts regionally crosscut metamorphic patterns. More importantly, in continental metamorphic rocks that form roof pendants in the main mass of the Idaho batholith, metamorphic grade also increases westward into the suture zone; metamorphic patterns and structures in continental metamorphic rocks also are cut by plutonic rocks (Lund, 1984). The age information confirms this time gap between metamorphism and plutonism. The only deformed Idaho batholith plutonic rocks are the 93 to 85 Ma tonalite suite, where emplaced along the suture. Therefore instead of causing the regional dynamothermal events, the Idaho batholith probably formed as a result of the same processes that caused the Salmon River suture.

On basis of this work on island-arc rocks of the Slate Creek-John Day Creek area and of work on continental rocks in the upper Slate Creek drainage and to the east, metamorphism and deformation of rocks in the vicinity of the Salmon River suture apparently occurred during formation of and movement along the accretionary boundary. Age data indicate that the metamorphism and deformation occurred from 120 to 88 Ma. Geochemical data (Armstrong and others, 1977; Fleck and Criss, 1985; Hoover, 1986), geophysical data (Bankey, 1992; McCafferty, 1992), and geological constraints (Lund, 1984; Hoover, 1986; Manduca, 1988) indicate that the suture is steep to vertical. The structural geometry fits

best with a model of transpressive (oblique-transcurrent) movement (Lund, 1984). The contact between island-arc and continental rocks is obscured by post-accretionary plutons, and the evidence for timing of motion between them indicates that the motion was late-stage and postplutonic (after 93 Ma). Additionally, and as expected from models (Wilcox and others, 1973; Harding, 1976; Sylvester and Smith, 1976; Odonne and Vialon, 1983; Sylvester, 1988), shear indicators show the rock underwent dominantly pure shear resulting in vertical motion—up and out of the suture. However, during the part of the Cretaceous when transpressive movement was occurring along the Salmon River suture, displacement of the Farallon plate with respect to North America had a major right-lateral component (Engebretson and others, 1985; Mammerickx and others, 1988) and major contemporaneous transcurrent faults in Washington and Canada were also right lateral (Monger, 1984; Gabrielse, 1985). Thus, metamorphism and deformation in the Slate Creek-John Day Creek area as well as along both sides of the rest of the Salmon River suture occurred during the interval 120 to 88 Ma and was probably due to right-lateral transpressive motion that juxtaposed island-arc rocks against continental rocks.

REFERENCES CITED

Armstrong, R.L., Taubeneck, W.H., and Hales, P.L., 1977, Rb/Sr and K/Ar geochronometry of Mesozoic granitic rocks and their Sr isotopic composition, Oregon, Washington, and Idaho: Geological Society of America Bulletin, v. 88, p. 397–411.

Avé Lallemant, H.G., Phelps, D.W., and Sutter, J.F., 1980, $^{40}Ar/^{39}Ar$ ages of some pre-Tertiary plutonic and metamorphic rocks of eastern Oregon and their geologic relationships: Geology, v. 8, p. 371–374.

Avé Lallemant, H.G., Schmidt, W.J., and Kraft, J.L., 1985, Major Late Triassic strike-slip displacement in the Seven Devils terrane, Oregon and Idaho—A result of left-oblique plate convergence?: Tectonophysics, v. 119, p. 299–328.

Bankey, Viki, 1992, Complete Bouguer gravity, isostatic residual gravity, and related geophysical maps centered on the Idaho batholith and Challis volcanic field, northwestern United States: U.S. Geological Survey Geophysical Investigations Map GP-995, 2 sheets, scale 1:1,000,000.

Brooks, H.C., and Vallier, T.L., 1978, Mesozoic rocks and tectonic evolution of eastern Oregon and western Idaho, *in* Howell, D.G., and McDougall, K.A., eds., Mesozoic Paleogeography of the Western United States (Pacific Coast Paleogeography Symposium 2): Los Angeles, California, Society of Economic Paleontologists and Mineralogists, Pacific Section, p. 133–145.

Davidson, G.F., 1990, Cretaceous tectonic history along the Salmon River suture zone near Orofino, Idaho: Metamorphic, structural and $^{40}Ar/^{39}Ar$ constraints: Corvallis, Oregon, Oregon State University, M.S. thesis, 143 p.

Davis, G.A., Monger, J.W.H., and Burchfiel, B.C., 1978, Mesozoic construction of the Cordilleran "collage," central British Columbia to central California, *in* Howell, D.G., and McDougall, K.A., eds., Mesozoic Paleogeography of the Western United States (Pacific Coast Paleogeography Symposium 2): Los Angeles, California, Society of Economic Paleontologists and Mineralogists, Pacific Section, p. 1–32.

Dickinson, W.R., 1979, Mesozoic fore-arc basin in central Oregon: Geology, v. 7, p. 166–170.

Dickinson, W.R., and Thayer, T.P., 1978, Paleogeographic and paleotectonic implications of Mesozoic stratigraphy and structure in the John Day inlier of central Oregon, *in* Howell, D.G., and McDougall, K.A., eds., Mesozoic Paleogeography of the Western United States (Pacific Coast Paleogeography Symposium 2): Los Angeles, California, Society of Economic Paleontologists and Mineralogists, Pacific Section, p. 147–161.

Engebretson, D.C., Allan, C., and Gordon, R.G., 1985, Relative motions between oceanic and continental plates in the Pacific Basin: Geological Society of America Special Paper 206, 59 p.

Fleck, R.J., and Criss, R.E., 1985, Strontium and oxygen isotopic variations in Mesozoic and Tertiary plutons of central Idaho: Contributions to Mineralogy and Petrology, v. 90, p. 291–308.

Follo, M.F., 1986, Sedimentology of the Wallowa terrane, northeastern Oregon: Cambridge, Massachusetts, Harvard University, Ph.D. dissertation, 292 p.

———1992, Conglomerates as clues to the sedimentary and tectonic evolution of a suspect terrane: Wallowa Mountain, Oregon: Geological Society of America Bulletin, v. 104, p. 1561–1576.

———1994, Sedimentology and stratigraphy of the Martin Bridge Limestone and Hurwal Formation (Upper Triassic to Lower Jurassic) from the Wallowa terrane, Oregon, *in* Vallier, T.L., and Brooks, H.C., eds., Geology of the Blue Mountains region of Oregon, Idaho, and Washington—Stratigraphy, physiography, and mineral resources of the Blue Mountains region: U.S. Geological Survey Professional Paper 1439, p. 1–27.

Gabrielse, Hugh, 1985, Major dextral transcurrent displacements along the northern Rocky Mountain trench and related lineaments in north-central British Columbia: Geological Society of America Bulletin, v. 96, p. 1–14.

Getty, S.R., Selverstone, Jane, Wernicke, B.P., and Jacobsen, S.B., 1991, Sm-Nd dating of multiple garnet growth events and arc-continent collision, Salmon River suture zone, western Idaho: Geological Society of America Abstracts with Programs, v. 23, p. 191.

Hamilton, W.B., 1963a, Metamorphism in the Riggins region, western Idaho: U.S. Geological Survey Professional Paper 436, 95 p.

———1963b, Overlapping of late Mesozoic orogens in western Idaho: Geological Society of America Bulletin, v. 74, p. 779–788.

———1963c, Trondhjemite in the Riggins quadrangle, western Idaho, *in* Geological Survey Research 1962: U.S. Geological Survey Professional Paper 450, p. E98–E101.

———1969, Reconnaissance geologic map of the Riggins quadrangle, west-central Idaho: U.S. Geological Survey Miscellaneous Geologic Investigations Map I-579,1 map sheet, scale 1:125,000.

———1976, Tectonic history of west-central Idaho: Geological Society of America Abstracts with Programs, v. 8, p. 378.

Harding, T.P., 1976, Tectonic significance and hydrocarbon trapping consequences of sequential folding synchronous with San Andreas faulting, San Joaquin Valley, California: American Association of Petroleum Geologists Bulletin, v. 60, p. 356–378.

Hillhouse, J.W., Grommé, C.S., and Vallier, T.L., 1982, Paleomagnetism and Mesozoic tectonics of the Seven Devils volcanic arc in northeastern Oregon: Journal of Geophysical Research, v. 87, p. 3777–3794.

Hoover, A.L., 1986, Transect across the Salmon River suture, South Fork of the Salmon River, western Idaho: Rare-earth

element, geochemical, structural, and metamorphic study: Corvallis, Oregon, Oregon State University, M.S. thesis, 138 p.

Hotz, P.E., Lanphere, M.A., and Swanson, C.A., 1977, Triassic blueschist from northern California and north-central Oregon: Geology, v. 5, p. 659–663.

Hyndman, D.W., and Talbot, J.L., 1976, The Idaho batholith and related subduction complex, *in* Field Guide 4: Washington State University, p. 15.

Jones, D.L., Silberling, N.J., and Hillhouse, J., 1977, Wrangellia—A displaced terrane in northwestern America: Canadian Journal of Earth Sciences, v. 14, p. 2565–2577.

Lewis, R.S., Kiilsgaard, T.H., Bennett, E.H., and Hall, W.E., 1987, Lithologic and chemical characteristics of the central and southeastern part of the southern lobe of the Idaho batholith, *in* Vallier, T.L., and Brooks, H.C., eds., Geology of the Blue Mountains region of Oregon, Idaho, and Washington—The Idaho batholith and its border zone: U.S. Geological Survey Professional Paper 1436 p. 171–196.

Lindgren, Waldemar, 1904, A geological reconnaissance across the Bitterroot Range and Clearwater Mountains in Montana and Idaho: U.S. Geological Survey Professional Paper 27, 123 p.

Lund, Karen, 1984, Tectonic history of a continent-island arc boundary: west-central Idaho: University Park, Pennsylvania, The University of Pennsylvania, Ph.D dissertation, 210 p.

Lund, Karen, McCollough, W.F., and Price, E.H., 1993, Geologic map of the Slate Creek-John Day Creek area, Idaho County, Idaho: U.S. Geological Survey Miscellaneous Investigations Map I-2299, scale 1:50,000.

Lund, Karen, and Snee, L.W., 1988, Metamorphism, structural development, and age of the continent-island arc juncture in west-central Idaho, *in* Ernst, W.G., ed., Metamorphism and Crustal Evolution in the Western Coterminous U.S.: Englewood Cliffs, New Jersey, Prentice-Hall, Rubey Volume VII, p. 296–331.

Lund, Karen, Snee, L.W., and Evans, K.V., 1986, Age and genesis of precious metals deposits, Buffalo Hump district, central Idaho: Implications for depth of emplacement of quartz veins: Economic Geology, v. 81, p. 990–996.

Mammerickx, J., and Sharman, G.F., 1988, Tectonic evolution of the North Pacific during the Cretaceous quiet period: Journal of Geophysical Research, v. 93, p. 3009–3024.

McCafferty, A.E., 1992, Aeromagnetic maps and terrace-magnetization map centered on the Idaho batholith and Challis volcanic field, northwestern United States: U.S. Geological Survey Geophysical Investigations Map GP-994, 2 sheets, scale 1:1,000,000.

McCollough, W.F., 1984, Stratigraphy, structure, and metamorphism of Permo-Triassic rocks along the western margin of the Idaho batholith, John Day Creek, Idaho: University Park, Pennsylvania, The Pennsylvania State University, M.S. thesis, 141 p.

Monger, J.W.H., 1984, Cordilleran tectonism—A Canadian perspective: Bulletin de la Societe Geologique de France, v. 27, p. 255–278.

Mortimer, Nick, 1986, Later Triassic, arc-related, potassic igneous rocks in the North American Cordillera: Geology, v. 14, p. 1035–1038.

Myers, P.E., 1982, Geology of the Harpster area, Idaho County, Idaho: Idaho Bureau of Mines and Geology Bulletin 25, 46 p.

Odonne, F., and Vialon, P., 1983, Analogue models of folds above a wrench fault: Tectonophysics, v. 99, p. 31–46.

Onasch, C.M., 1977, Structural evolution of the western margin of the Idaho batholith in the Riggins, Idaho, area: University Park, Pennsylvania, The Pennsylvania State University, Ph.D. dissertation, 196 p.

———1987, Temporal and spatial relations between folding, intrusion, metamorphism, and thrust faulting in the Riggins area, west-central Idaho, *in* Vallier, T.L., and Brooks, H.C., eds., Geology of the Blue Mountains region of Oregon, Idaho, and Washington—The Idaho batholith and its border zone: U.S. Geological Survey Professional Paper 1436, p. 139–150.

Prostka, H.J., 1962, Geology of the Sparta quadrangle, Oregon: Oregon Department of Geology and Mineral Industries Geologic Map Series GMS-1, scale 1:62:500.

Ross, C.P., 1938, The geology of part of the Wallowa Mountains: Oregon Department of Geology and Mineral Industries Bulletin 3, 74 p.

Selverstone, Jane, Wernicke, B.P., and Aliberti, E.A., 1992, Intracontinental subduction and hinged unroofing along the Salmon River suture zone, west central Idaho: Tectonics, v. 11, p. 124–144.

Silberling, N.J., Jones, D.L., Monger, J.W.H., and Coney, P.J., 1992, Lithotectonic terrane map of the North American Cordillera: U.S. Geological Survey Miscellaneous Investigations Map I-2176, 2 sheets, scale 1:5,000,000.

Snee, L.W., Lund, Karen, and Evans, K.V., 1985, $^{40}Ar/^{39}Ar$-age-spectrum data for the Buffalo Hump mining district, Clearwater Mountains, central Idaho: U.S. Geological Survey Open-File Report 85-102, 10 p.

Snee, L.W., Sutter, J.F., Lund, Karen, Balcer, D.E., and Evans, K.V., 1987, $^{40}Ar/^{39}Ar$-age-spectrum data for metamorphic and plutonic rocks from west-central Idaho: U.S. Geological Survey Open-File Report 87-52, 19 p.

Sutter, J.F., Snee, L.W., and Lund, Karen, 1984, Metamorphic, plutonic, and uplift history of a continent-island arc suture zone, west-central Idaho: Geological Society of America Abstracts with Programs, v. 16, p. 670–671.

Sylvester, A.G., and Smith, R.R., 1976, Tectonic transpression and basement-controlled deformation in San Andreas fault zone, Salton trough, California: American Association of Petroleum Geologists Bulletin, v. 60, p. 2081–2102.

Sylvester, S.G., 1988, Strike-slip faults: Geological Society of America Bulletin, v. 100, p. 1666–1703.

Toth, M.I., 1987, Petrology and origin of the Bitterroot lobe of the Idaho batholith, *in* Vallier, T.L., and Brooks, H.C., eds., Geology of the Blue Mountains region of Oregon, Idaho, and Washington—The Idaho batholith and its border zone: U.S. Geological Survey Professional Paper 1436, p. 9–36.

Vallier, T.L., and Brooks, H.C., 1987, Geology of the Blue Mountains region of Oregon, Idaho, and Washington: The Idaho batholith and its border zone: U.S. Geological Survey Professional Paper 1436, 196 p.

Vallier, T.L., and Brooks, H.C., 1986, Paleozoic and Mesozoic faunas of the Blue Mountains province: A review of their geologic implications and comments on papers in the volume, *in* Vallier, T.L., and Brooks, H.C., eds., Geology of the Blue Mountains region of Oregon, Idaho and Washington—Geologic implications of Paleozoic and Mesozoic paleontology and biostratigraphy, Blue Mountains province, Oregon and Idaho: U.S. Geological Survey Professional Paper 1435, p. 1–6.

Wagner, W.F., 1945, A geological reconnaissance between the Snake and Salmon Rivers north of Riggins, Idaho: Idaho Bureau of Mines and Geology Pamphlet 74, 16 p.

Walker, N.W., 1986, U/Pb geochronologic and pertologic studies in the Blue Mountains terrane, northeastern Oregon and westernmost-central Idaho—Implications for pre-Teriary tectonic evolution: Santa Barbara, California, University of California, 214 p.

Wernicke, B.P., and Klepacki, D.W., 1988, Escape hypothesis for the Stikine block: Geology, v. 16, p. 461–464.

White, J.D.L., White, D.L., Vallier, T., Stanley, G.D., Jr., and Ash, S.R., 1992, Middle Jurassic strata link Wallowa, Olds Ferry,

and Izee terranes in the accreted Blue Mountains island arc, northeastern Oregon: Geology, v. 20, p. 729–732.

Wilcox, R.E., Harding, T.P., and Seely, D.R., 1973, Basic wrench tectonics: American Association Petroleum Geologists Bulletin, v. 57, p. 74–96.

Zen, E-an, 1985, Implications of magmatic epidote-bearing plutons on crustal evolution in the accreted terranes of northwestern North America: Geology, v. 13, p. 266–269.

Zen, E-an, and Hammarstom, J.M., 1984, Magmatic epidote and its petrologic significance: Geology, v. 12, p. 515–518.

☆ U.S. GOVERNMENT PRINTING OFFICE: 1995 - 673-046 / 20010 REGION NO. 8

SELECTED SERIES OF U.S. GEOLOGICAL SURVEY PUBLICATIONS

Periodicals

Earthquakes & Volcanoes (issued bimonthly).
Preliminary Determination of Epicenters (issued monthly).

Technical Books and Reports

Professional Papers are mainly comprehensive scientific reports of wide and lasting interest and importance to professional scientists and engineers. Included are reports on the results of resource studies and of topographic, hydrologic, and geologic investigations. They also include collections of related papers addressing different aspects of a single scientific topic.

Bulletins contain significant data and interpretations that are of lasting scientific interest but are generally more limited in scope or geographic coverage than Professional Papers. They include the results of resource studies and of geologic and topographic investigations, as well as collections of short papers related to a specific topic.

Water-Supply Papers are comprehensive reports that present significant interpretive results of hydrologic investigations of wide interest to professional geologists, hydrologists, and engineers. The series covers investigations in all phases of hydrology, including hydrogeology, availability of water, quality of water, and use of water.

Circulars present administrative information or important scientific information of wide popular interest in a format designed for distribution at no cost to the public. Information is usually of short-term interest.

Water-Resource Investigations Reports are papers of an interpretive nature made available to the public outside the formal USGS publications series. Copies are reproduced on request unlike formal USGS publications, and they are also available for public inspection at depositories indicated in USGS catalogs.

Open-File Reports include unpublished manuscript reports, maps, and other material that are made available for public consultation at depositories. They are a nonpermanent form of publication that may be cited in other publications as sources of information.

Maps

Geologic Quadrangle Maps are multicolor geologic maps on topographic bases in 7 ½- or 15-minute quadrangle formats (scales mainly 1:24,000 or 1:62,500) showing bedrock, surficial, or engineering geology. Maps generally include brief texts; some maps include structure and columnar sections only.

Geophysical Investigations Maps are on topographic or planimetric bases at various scales; they show results of surveys using geophysical techniques, such as gravity, magnetic, seismic, or radioactivity, which reflect subsurface structures that are of economic or geologic significance. Many maps include correlations with the geology.

Miscellaneous Investigations Series Maps are on planimetric or topographic bases of regular and irregular areas at various scales; they present a wide variety of format and subject matter. The series also includes 7 ½-minute quadrangle photogeologic maps on planimetric bases that show geology as interpreted from aerial photographs. Series also includes maps of Mars and the Moon.

Coal Investigations Maps are geologic maps on topographic or planimetric bases at various scales showing bedrock or surficial geology, stratigraphy, and structural relations in certain coal-resource areas.

Oil and Gas Investigations Charts show stratigraphic information for certain oil and gas fields and other areas having petroleum potential.

Miscellaneous Field Studies Maps are multicolor or black-and-white maps on topographic or planimetric bases on quadrangle or irregular areas at various scales. Pre-1971 maps show bedrock geology in relation to specific mining or mineral-deposit problems; post-1971 maps are primarily black-and-white maps on various subjects, such as environmental studies or wilderness mineral investigations.

Hydrologic Investigations Atlases are multicolor or black-and-white maps on topographic or planimetric bases presenting a wide range of geohydrologic data of both regular and irregular areas; principal scale is 1:24,000, and regional studies are at 1:250,000 scale or smaller.

Catalogs

Permanent catalogs, as well as some others, giving comprehensive listings of U.S. Geological Survey publications are available under the conditions indicated below from the U.S. Geological Survey, Books and Open-File Reports Sales, Federal Center, Box 25286, Denver, CO 80225. (See latest Price and Availability List.)

"Publications of the Geological Survey, 1879–1961" may be purchased by mail and over the counter in paperback book form and as a set of microfiche.

"Publications of the Geological Survey, 1962–1970" may be purchased by mail and over the counter in paperback book form and as a set of microfiche.

"Publications of the Geological Survey, 1971–1981" may be purchased by mail and over the counter in paperback book form (two volumes, publications listing and index) and as a set of microfiche.

Supplements for 1982, 1983, 1984, 1985, 1986, and for subsequent years since the last permanent catalog may be purchased by mail and over the counter in paperback book form.

State catalogs, "List of U.S. Geological Survey Geologic and Water-Supply Reports and Maps For (State)," may be purchased by mail and over the counter in paperback booklet form only.

"Price and Availability List of U.S. Geological Survey Publications," issued annually, is available free of charge in paperback booklet form only.

Selected copies of a monthly catalog "New Publications of the U.S. Geological Survey" are available free of charge by mail or may be obtained over the counter in paperback booklet form only. Those wishing a free subscription to the monthly catalog "New Publications of the U.S. Geological Survey" should write to the U.S. Geological Survey, 582 National Center, Reston, VA 22092.

Note.—Prices of Government publications listed in older catalogs, announcements, and publications may be incorrect. Therefore, the prices charged may differ from the prices in catalogs, announcements, and publications.

U.S. DEPARTMENT OF THE INTERIOR
MARCH 3, 1849